frontiers | Research Topics

Targeting neuroinflammation for novel therapeutics in neurodegenerative diseases

Edited by
Pukar Khanal, Jatin Machhi and Rupesh V. Chikhale

Published in
Frontiers in Pharmacology
Frontiers in Neuroscience



FRONTIERS EBOOK COPYRIGHT STATEMENT

The copyright in the text of individual articles in this ebook is the property of their respective authors or their respective institutions or funders. The copyright in graphics and images within each article may be subject to copyright of other parties. In both cases this is subject to a license granted to Frontiers.

The compilation of articles constituting this ebook is the property of Frontiers.

Each article within this ebook, and the ebook itself, are published under the most recent version of the Creative Commons CC-BY licence. The version current at the date of publication of this ebook is CC-BY 4.0. If the CC-BY licence is updated, the licence granted by Frontiers is automatically updated to the new version.

When exercising any right under the CC-BY licence, Frontiers must be attributed as the original publisher of the article or ebook, as applicable.

Authors have the responsibility of ensuring that any graphics or other materials which are the property of others may be included in the CC-BY licence, but this should be checked before relying on the CC-BY licence to reproduce those materials. Any copyright notices relating to those materials must be complied with.

Copyright and source acknowledgement notices may not be removed and must be displayed in any copy, derivative work or partial copy which includes the elements in question.

All copyright, and all rights therein, are protected by national and international copyright laws. The above represents a summary only. For further information please read Frontiers' Conditions for Website Use and Copyright Statement, and the applicable CC-BY licence.

ISSN 1664-8714
ISBN 978-2-8325-6416-5
DOI 10.3389/978-2-8325-6416-5

About Frontiers

Frontiers is more than just an open access publisher of scholarly articles: it is a pioneering approach to the world of academia, radically improving the way scholarly research is managed. The grand vision of Frontiers is a world where all people have an equal opportunity to seek, share and generate knowledge. Frontiers provides immediate and permanent online open access to all its publications, but this alone is not enough to realize our grand goals.

Frontiers journal series

The Frontiers journal series is a multi-tier and interdisciplinary set of open-access, online journals, promising a paradigm shift from the current review, selection and dissemination processes in academic publishing. All Frontiers journals are driven by researchers for researchers; therefore, they constitute a service to the scholarly community. At the same time, the *Frontiers journal series* operates on a revolutionary invention, the tiered publishing system, initially addressing specific communities of scholars, and gradually climbing up to broader public understanding, thus serving the interests of the lay society, too.

Dedication to quality

Each Frontiers article is a landmark of the highest quality, thanks to genuinely collaborative interactions between authors and review editors, who include some of the world's best academicians. Research must be certified by peers before entering a stream of knowledge that may eventually reach the public - and shape society; therefore, Frontiers only applies the most rigorous and unbiased reviews. Frontiers revolutionizes research publishing by freely delivering the most outstanding research, evaluated with no bias from both the academic and social point of view. By applying the most advanced information technologies, Frontiers is catapulting scholarly publishing into a new generation.

What are Frontiers Research Topics?

Frontiers Research Topics are very popular trademarks of the *Frontiers journals series*: they are collections of at least ten articles, all centered on a particular subject. With their unique mix of varied contributions from Original Research to Review Articles, Frontiers Research Topics unify the most influential researchers, the latest key findings and historical advances in a hot research area.

Find out more on how to host your own Frontiers Research Topic or contribute to one as an author by contacting the Frontiers editorial office: frontiersin.org/about/contact

Targeting neuroinflammation for novel therapeutics in neurodegenerative diseases

Topic editors

Pukar Khanal — Emory University, United States

Jatin Machhi — University of Nebraska Medical Center, United States

Rupesh V. Chikhale — University College London, United Kingdom

Citation

Khanal, P., Machhi, J., Chikhale, R. V., eds. (2025). *Targeting neuroinflammation for novel therapeutics in neurodegenerative diseases*. Lausanne: Frontiers Media SA. doi: 10.3389/978-2-8325-6416-5

Table of contents

05 Editorial: Targeting neuroinflammation for novel therapeutics in neurodegenerative diseases
Pukar Khanal, Rupesh Chikhale and Jatin Machhi

09 Comprehensive spectroscopic and computational insight into the binding of vanillin with human transferrin: targeting neuroinflammation in Alzheimer's disease therapeutics
Mohammed Alrouji, Sabina Yasmin, Fahad A. Alhumaydhi, Sharaf E. Sharaf, Moyad Shahwan, Mohammad Furkan, Rizwan Hasan Khan and Anas Shamsi

18 Melatonin modulates neuroinflammatory response and microglial activation in mice exposed to dim blue light at night
Chao Song, Zhaotaize Suo, Zixu Wang, Jing Cao, Yulan Dong and Yaoxing Chen

30 The role of statins in amyotrophic lateral sclerosis: protective or not?
Hayder M. Al-kuraishy, Majid S. Jabir, Ghassan M. Sulaiman, Hamdoon A. Mohammed, Ali I. Al-Gareeb, Ali K. Albuhadily, Sabrean F. Jawad, Ayman A. Swelum and Mosleh M. Abomughaid

45 Gasdermin D could be lost in the brain parenchyma infarct core and a pyroptosis-autophagy inhibition effect of Jie-Du-Huo-Xue decoction after stroke
Chang Zhou, Shi-wei Qiu, Feng-ming Wang, Yu-chen Liu, Wei Hu, Mei-lan Yang, Wang-hua Liu and Hua Li

66 Melatonin improves cognitive dysfunction and decreases gliosis in the streptozotocin-induced rat model of sporadic Alzheimer's disease
Zsolt Gáll, Bernadett Boros, Krisztina Kelemen, Melinda Urkon, István Zolcseak, Kincső Márton and Melinda Kolcsar

80 The relation between Parkinson's disease and non-steroidal anti-inflammatories; a systematic review and meta-analysis
Amal Mohammad Badawoud, Lashin Saad Ali, Mahmoud S. Abdallah, Ramy M. El Sabaa, Mostafa M. Bahaa, Thanaa A. Elmasry, Eman Wahsh, Mohamed Yasser, Nashwa Eltantawy, Mamdouh Eldesoqui and Manal A. Hamouda

91 Polydatin attenuated neuropathic pain and motor dysfunction following spinal cord injury in rats by employing its anti-inflammatory and antioxidant effects
Faezeh Sadat Bagheri Bavandpouri, Atefeh Azizi, Fatemeh Abbaszadeh, Amir Kiani, Mohammad Hosein Farzaei, Ehsan Mohammadi-Noori, Sajad Fakhri and Javier Echeverría

102 Neuroprotective effects of *Gastrodia elata* Blume on promoting M2 microglial polarization by inhibiting JNK/TLR4/T3JAM/NF-κB signaling after transient ischemic stroke in rats
Shang-Chih Huang, Hui-Chi Huang, Wen-Ling Liao, Shung-Te Kao and Chin-Yi Cheng

118 Exploring novel natural compound-based therapies for Duchenne muscular dystrophy management: insights from network pharmacology, QSAR modeling, molecular dynamics, and free energy calculations
Mohd Saeed, Ashanul Haque, Ambreen Shoaib and Syed Mohd Danish Rizvi

136 Combined administration of catalpol, puerarin, gastrodin, and borneol modulates the Tlr4/Myd88/NF-κB signaling pathway and alleviates microglia inflammation in Alzheimer's disease
Huijing Ren, Ling Tang, Zhiying Yuan, Yang Liu, Xuejiao Zhou, Xiao Xiao, Xingyu Wu, Weihai Chen, Yi Chen, Hongjin Wang, Qiang Xue and Xiaoyu Xu

155 (+)-Borneol inhibits neuroinflammation and M1 phenotype polarization of microglia in epileptogenesis through the TLR4-NFκB signaling pathway
Shuo Li, Alhamdu Adamu, Yucai Ye, Fankai Gao, Rulin Mi, Guofang Xue and Zhaojun Wang

169 Xixin Decoction's novel mechanism for alleviating Alzheimer's disease cognitive dysfunction by modulating amyloid-β transport across the blood–brain barrier to reduce neuroinflammation
Chaokai Yang, Enlong Zhao, Hu Zhang, Liqi Duan, Xinyue Han, Hongli Ding, Yan Cheng, Dengkun Wang, Xiaojing Lei and Yongchang Diwu

190 Mechanistic insight of curcumin: a potential pharmacological candidate for epilepsy
Saima Khatoon and Nida Kalam

219 Pirfenidone regulates seizures through the HMGB1/TLR4 axis to improve cognitive functions and modulate oxidative stress and neurotransmitters in PTZ-induced kindling in mice
Mansi Dahalia, Sparsh Gupta, Haya Majid, Divya Vohora and Nidhi

238 Enhanced bioavailability of Quercetin-loaded niosomal in situ gel for the management of Parkinson's disease
Abhishek A. Revankar, Archana S. Patil, Reshma Karishetti, Krutuja R. Chougule, Priyanka Patil and Abhijit Salokhe

255 Acetate and propionate vs. iTBS as a novel method for cognitive dysfunction and anxiety symptoms in delayed encephalopathy after acute carbon monoxide poisoning rat
Tianyu Meng, Xin Zhang, Jili Zhao, Hui Xue and Lehua Yu

266 Evaluating the anti-neuropathic effects of the thymol-loaded nanofibrous scaffold in a rat model of spinal cord injury
Roshanak Amirian, Pardis Mohammadi Pour, Hassan Maleki, Sajad Fakhri, Sedigheh Asgary, Mohammad Hossein Farzaei and Javier Echeverría

frontiers | Frontiers in Pharmacology

TYPE Editorial
PUBLISHED 25 April 2025
DOI 10.3389/fphar.2025.1602495

Check for updates

OPEN ACCESS

EDITED AND REVIEWED BY
Dieter Steinhilber,
Goethe University Frankfurt, Germany

*CORRESPONDENCE
Pukar Khanal,
pukarkhanal58@gmail.com
Rupesh Chikhale,
rupeshchikhale7@gmail.com

RECEIVED 29 March 2025
ACCEPTED 01 April 2025
PUBLISHED 25 April 2025

CITATION
Khanal P, Chikhale R and Machhi J (2025) Editorial: Targeting neuroinflammation for novel therapeutics in neurodegenerative diseases.
Front. Pharmacol. 16:1602495.
doi: 10.3389/fphar.2025.1602495

COPYRIGHT
© 2025 Khanal, Chikhale and Machhi. This is an open-access article distributed under the terms of the Creative Commons Attribution License (CC BY). The use, distribution or reproduction in other forums is permitted, provided the original author(s) and the copyright owner(s) are credited and that the original publication in this journal is cited, in accordance with accepted academic practice. No use, distribution or reproduction is permitted which does not comply with these terms.

Editorial: Targeting neuroinflammation for novel therapeutics in neurodegenerative diseases

Pukar Khanal[1]*, Rupesh Chikhale[2]* and Jatin Machhi[3]

[1]Emory University, Atlanta, GA, United States, [2]Department of Pharmaceutical and Biological Chemistry, School of Pharmacy, University College London, London, United Kingdom, [3]University of Nebraska Medical Center, Omaha, NE, United States

KEYWORDS

Amyotrophic Lateral Sclerosis, Alzheimer's disease, computational pharmacology, nanoengineering, Parkinson's disease, ethnopharmacology

Editorial on the Research Topic
Targeting neuroinflammation for novel therapeutics in neurodegenerative diseases

Introduction

Neuroinflammation has emerged as a pivotal driver in the initiation and advancement of neurodegenerative disorders, including Alzheimer's (AD) and Parkinson's disease (PD). Historically, anti-inflammatory therapies faced critical hurdles in clinical translation which were limited by challenges such as blood-brain barrier (BBB) penetration, off-target effects, and the complex, multi-faceted nature of neuroimmune signaling. However, recent breakthroughs are reshaping this landscape. Advances in decoding inflammatory cascades and innovations in drug delivery systems enable precise modulation of brain immunity. Concurrently, the field is shifting from single-target drugs to integrative strategies, e.g., repurposed immunomodulators, synergistic natural compounds, and computational models that predict multi-target drug interactions. This Research Topic reflects a transformative focus—moving beyond palliative care to address the root causes of neurodegeneration. By harmonizing cutting-edge technology, cross-disciplinary research, and patient-specific biomarker profiling, these approaches aim to achieve durable disease modification, heralding a new era in neurodegenerative disease therapeutics.

Bridging acute and chronic neurological disorders through non-invasive and metabolic interventions

The non-invasive neuromodulation has gained traction as an essential pillar for neuroprotection, offering distinct yet complementary mechanisms to combat neuroinflammation. In a pioneering study by Meng et al., the therapeutic potential of short-chain fatty acids (SCFAs) is contrasted with intermittent theta burst

stimulation (iTBS) in treating delayed encephalopathy following acute carbon monoxide poisoning. Their work reveals a temporal dichotomy—iTBS elicits immediate cognitive improvements and synaptic plasticity, while SCFAs exert sustained neuroprotection by dampening pro-inflammatory cytokines and restoring glutamatergic/GABAergic balance. This dichotomy provokes a critical hypothesis—Could sequential or combined application of iTBS and SCFAs harmonize acute functional recovery with long-term anti-inflammatory resilience, optimizing outcomes in time-sensitive neuropathologies? Shifting focus to chronic neurodegeneration, Yang et al. explore the broad effects of a traditional herbal formulation, Xixin Decoction (XXD) in AD. Their findings extend beyond conventional amyloid-beta (Aβ) targeting, demonstrating XXD efficacy to repair BBB integrity by upregulating tight junction proteins (claudin-5, occludin)—and rebalancing the RAGE/LRP1 axis. By concurrently mitigating neurovascular dysfunction, suppressing NLRP3 inflammasome activation, and enhancing glymphatic drainage, XXD addresses AD multifactorial etiology. This polypharmacological approach underscores the XXD value in tackling complex neuroinflammatory cascades, positioning it as a viable adjunct to monoclonal antibody therapies, which often lack BBB penetrance or holistic immunomodulation.

Together, these studies highlight the evolving landscape of neuroinflammation therapeutics, where metabolic interventions and neuromodulation offer stratified benefits. Future research may prioritize combinatorial trials—e.g., pairing iTBS with SCFA supplementation in acute brain injury or integrating XXD with anti-Aβ immunotherapies to test for synergistic efficacy in AD. As the field advances, personalized sequencing of these modalities may emerge as a paradigm for bridging acute recovery and chronic disease modification.

Harnessing nature's pharmacy: innovations in bioactive compounds for neuroprotection

The resurgence of natural compounds as multi-targeted neurotherapeutics reflects a paradigm shift toward harmonizing traditional medicine with cutting-edge delivery technologies. Revankar et al. exemplifies this synergy by engineering an intranasal quercetin-loaded niosomal gel to surmount the flavonoid's notorious bioavailability challenges in PD. The formulation not only enhances brain delivery but also demonstrates striking motor recovery and attenuation of oxidative stress, underscoring how advanced drug delivery systems can resurrect poorly bioavailable phytochemicals. In cerebral ischemia-reperfusion injury, Zhou et al. redefine neuroprotection with Jie-Du-Huo-Xue decoction (JDHXD). By independently suppressing both pyroptosis and autophagy, JDHXD uniquely disrupts the pathological interplay between inflammatory cell death and dysregulated protein clearance. The discovery of compartment-specific GSDMD localization in infarcted tissue not only challenges dogma but also opens avenues for spatially targeted stroke therapies. Next, epilepsy research illustrates the transformative potential of bioenhancement strategies. A review by Khatoon and Kalam delineates curcumin dual blockade of NF-κB-driven neuroinflammation and Nrf2-mediated antioxidant defenses, yet its clinical utility has long been hamstrung by rapid hepatic metabolism. Khatoon and Kalam further highlight nanocarriers enhance curcumin brain bioavailability, positioning it as a viable alternative to conventional antiepileptics. Parallel work by Li et al. on (+)-borneol reveals a microglial reprogramming mechanism—TLR4-NFκB axis inhibition coupled with M1-to-M2 polarization shifts, mirroring Huang et al. findings with Gastrodia elata Blume extract in ischemia. Both studies highlight conserved anti-inflammatory pathways across distinct neuropathologies, suggesting broad applicability for terpenoid-rich botanicals. The frontier of neuroprotection embraces polyherbal strategies that mimic nature's combinatorial logic. Next, Ren et al. pioneer a quadra-compound formulation (borneol, gastrodin, catalpol, and puerarin) for AD, achieving synergistic suppression of microglial hyperactivation and amyloid burden via TLR4/MyD88/NF-κB silencing. This phytochemical cocktail approach, leveraging additive pharmacokinetics and complementary targets, outperforms single-agent therapies and aligns with the multi-system etiology of neurodegeneration.

These advances underscore three pillars of progress—(1) Delivery innovation (intranasal niosomes, nanocarriers) to unlock the potential of poorly soluble phytochemicals; (2) Pathway convergence (NF-κB, Nrf2, TLR4) as a blueprint for target selection; and (3) Polypharmacology through rational multi-compound design. Future research may prioritize clinical translation of these platforms while exploring artificial intelligence-driven phytochemical screening and biomarker-guided personalized herbal regimens. By bridging ancient pharmacopeias with modern neurobiology, we may inch closer to therapies that are as complex and adaptive as the diseases they aim to treat.

Nanotechnology and biomaterial-based approaches in neuroinflammation to engineer spinal cord injury

The fusion of nanotechnology and neurobiology is redefining regenerative medicine, offering precision-engineered solutions to combat neuroinflammation and neural degeneration. Amirian et al. pioneered this frontier with thymol-loaded poly (vinyl alcohol)/chitosan nanofibrous scaffolds for spinal cord injury (SCI) and strategically delivered Thymol *via* a biocompatible scaffold. The electrospun nanofibers provided structural support to bridge lesion gaps and also created a neurodegenerative niche. Their results underscore how biomaterial design can synergize with bioactive compounds to address SCI-related challenges such as physical disruption and chronic inflammation. Next, Bavandpouri et al. complement this approach by leveraging polydatin, to tackle its biochemical cascade.

Together, these studies exemplify two pillars of next-gen neurotherapy— (1) biomaterial scaffolds that remodel injury sites, and (2) small-molecule bioactives that quell inflammation. Future directions could integrate these strategies—e.g., embedding

polydatin within nanofibrous matrices to achieve spatiotemporal control over drug release and tissue remodeling. Additionally, leveraging functionalized nanoparticles to target specific cell populations (e.g., reactive microglia) could amplify therapeutic precision. As the field evolves, combinatorial platforms that merge material science with immunometabolic modulation may hold the key to unlocking full functional recovery in SCI and beyond.

Repurposing pharmaceuticals for neurodegenerative disorders: navigating promise and pitfalls

The repurposing of existing drugs for neurodegenerative diseases offers a pragmatic yet intricate path forward, demanding a balance between mechanistic insight and clinical nuance. A meta-analysis by Badawoud et al. reveals a critical divide—non-aspirin NSAIDs, with their COX-2 selectivity, may lower PD risk by tempering neuroinflammation, while aspirin and ibuprofen—agents with broader COX inhibition—fail to show benefit. This divergence underscores the importance of dissecting drug mechanisms beyond class-wide assumptions, emphasizing that even subtle differences in molecular targeting (e.g., COX-2 vs COX-1) can yield starkly divergent outcomes in neurodegeneration. A review of controversy around statins in Amyotrophic Lateral Sclerosis (ALS) is highlighted by Al-Kuraishy et al. to illustrate the precarious nature of repurposing. Statins' dual role—neuroprotective in early stages *via* anti-inflammatory and lipid-lowering effects, yet potentially detrimental in advanced disease by impairing cholesterol-dependent repair—exposes the temporal fragility of therapeutic interventions. This paradox calls for a dynamic approach to treatment, where timing and genetic context (e.g., SOD1 mutations) dictate therapeutic candidacy, rather than a blanket application. Meanwhile, Dahalia et al. work with pirfenidone in epilepsy exemplifies the strategic repurposing by targeting the HMGB1/TLR4 axis (shared pathway in neuroinflammation and fibrosis), pirfenidone bridges disparate disease mechanisms, offering a blueprint for cross-disciplinary drug discovery. Such efforts highlight the value of prioritizing agents with pleiotropic anti-inflammatory or antioxidant properties that intersect with neurodegeneration's multifactorial roots.

Here, the path forward lies in marrying mechanistic rigor with clinical adaptability. First, agents like pirfenidone, which act on convergent inflammatory nodes (e.g., DAMPs, TLR4), should be prioritized for their ability to disrupt multiple disease pathways. Second, therapies must be tailored to disease stages—statins may stabilize early ALS but harm late-stage patients, necessitating biomarker-guided timelines. Finally, patient stratification through genetic, metabolic, or inflammatory profiling could resolve conflicting trial outcomes, transforming repurposing from a gamble into a precision tool. Future studies should explore combinatorial regimens (e.g., COX-2 inhibitors paired with HMGB1 blockers) and leverage artificial intelligence to map off-target drug effects against neuroinflammatory networks, ensuring repurposed therapies are as nuanced as the diseases they aim to treat.

Computational and mechanistic insights into targeted treatment

The integration of computational biology and mechanistic studies may revolutionize our ability to dissect neuroinflammatory cascades and pinpoint actionable therapeutic nodes. Saeed et al. explore network pharmacology and molecular dynamics simulations to unravel the fibro-inflammatory axis in Duchenne muscular dystrophy, identifying SMAD3 (transcriptional regulator of TGF-β signaling) as a central orchestrator of muscle-brain crosstalk. Their multimodal approach not only maps fibrosis-related pathways but also screens compounds for SMAD3 binding, offering a blueprint for repurposing pleiotropic phytochemicals against neuroinflammation-associated fibrosis. Further, in AD, Alrouji et al. employ a hybrid in silico-in vitro strategy to decode vanillin anti-inflammatory potential. Molecular docking and spectroscopic analyses reveal vanillin efficacy in stabilizing human transferrin by binding to its apically charged cleft. This structural stabilization can mitigate iron-mediated neurotoxicity and oxidative stress, while circular dichroism and *in vitro* assays confirm vanillin role in preserving transferrin functionality.

These studies underscore the transformative potential of merging computational rigor with mechanistic inquiry. Saeed et al. systems-level mapping of SMAD3-driven networks highlights the utility of multi-omics integration to identify upstream regulators of neuroinflammation. Meanwhile, Alrouji et al. focus on transferrin-vanillin interactions to illustrate how atomistic simulations can guide the rational design of small molecules to stabilize critical proteins in neurodegenerative milieus. Future efforts may explore molecular generative platforms to accelerate the discovery of SMAD3 inhibitors or transferrin-stabilizing agents while advancing digital twin models of neuroinflammatory cascades to predict therapeutic synergies. As computational tools evolve, their seamless integration with wet lab experimentation can be pivotal in translating mechanistic insights into therapies that disrupt neuroinflammation at its roots.

Melatonin exerts neuroprotective effects by regulating circadian rhythms and neuroinflammation

Melatonin is emerging as a versatile modulator of neuroinflammatory cascades, offering therapeutic promise across neurodegenerative and environmental contexts. Gáll et al. illuminate its potential in AD, demonstrating that melatonin not only rescues cognitive deficits in rodent models but also dampens microglial hyperactivation. Although the precise mechanisms remain elusive, melatonin pleiotropic effects likely stem from its ability to scavenge reactive oxygen species, inhibit NLRP3 inflammasome assembly, and suppress pro-inflammatory cytokines. These actions position melatonin as a compelling adjunct to amyloid- or tau-targeted therapies by addressing both pathology and symptom burden. Further, Song et al. extend this narrative into the realm of environmental neurotoxicity, revealing how melatonin mitigates dim blue light-induced neuroinflammation which is a growing concern in our screen-saturated world. Their investigation uncovers a receptor-dependent mechanism, i.e., activation of

MT2 receptors with melatonin suppresses NF-κB translocation, thereby blocking downstream inflammatory gene expression. This finding not only underscores melatonin role as a circadian synchronizer but also highlights its capacity to counteract externally triggered neuroinflammatory insults (e.g., light pollution). The study raises critical questions about modern environmental exposures and their disruption of endogenous neuroprotective rhythms.

Together, these studies reframe melatonin as a dual-axis therapeutic by balancing intrinsic circadian rhythms with extrinsic anti-inflammatory defenses. Findings from Gáll et al. suggest its utility in chronic neurodegeneration, while Song et al. emphasize its relevance in acute, environmentally driven inflammation. Future research can explore receptor-specific agonists (e.g., MT2-targeted compounds) to enhance precision, minimizing off-target effects linked to broad receptor affinity. Next, clinical trials may investigate melatonin synergy with lifestyle interventions (e.g., light exposure regulation) to amplify its circadian benefits. As the boundaries between environmental stressors and neurodegenerative processes blur, the multifaceted actions of melatonin offer a template for therapies that harmonize biological rhythms with neuroimmune resilience.

Convergent innovation in neuroinflammation therapeutics

The rapidly expanding toolkit against neuroinflammation—spanning phytochemical pool bioenhancement, biomaterial engineering, drug repurposing, computational deconvolution, and circadian modulation—reflects a paradigm shift toward precision, synergy, and systems-level intervention. Natural compounds like quercetin and curcumin, once limited by bioavailability, now thrive through nanotechnology, while repurposed agents such as pirfenidone and statins are being recontextualized through biomarker-guided stratification. Computational platforms, exemplified by network mapping and compound(s)-protein(s) interaction modeling, are no longer auxiliary tools but drivers of mechanistic discovery, accelerating the transition from serendipity to rational design. Yet challenges persist—the duality of therapies like statins in ALS underscores the non-linear biology of neuroinflammation, demanding temporal precision and patient-specific adaptation. Similarly, the dual role of melatonin as a chronobiotic and NF-κB antagonist highlights the underappreciated interplay between environmental stressors and endogenous neuroprotection which is a frontier ripe for exploration. Now, the path forward lies in orchestrating these advances into context-aware therapeutic ecosystems. Imagine artificial intelligence-optimized polypharmacy regimens delivered via intranasal nanocarriers, timed to circadian peaks in neuroinflammation, while biomaterial scaffolds release polydatin at injury sites in response to real-time inflammatory biosensors. Such integration of computation, material science, and chronobiology could transform neuroprotection from reactive to proactive, targeting diseases at their inflammatory roots. Success will hinge on dismantling disciplinary silos, fostering partnerships between pharmacologists, computational biologists, and circadian neuroscientists to pioneer therapies as dynamic and resilient as the brain itself.

Author contributions

PK: Writing – original draft, Writing – review and editing. RC: Writing – review and editing. JM: Writing – review and editing.

Funding

The author(s) declare that no financial support was received for the research and/or publication of this article.

Conflict of interest

The authors declare that the research was conducted in the absence of any commercial or financial relationships that could be construed as a potential conflict of interest.

Generative AI statement

The author(s) declare that no Generative AI was used in the creation of this manuscript.

Publisher's note

All claims expressed in this article are solely those of the authors and do not necessarily represent those of their affiliated organizations, or those of the publisher, the editors and the reviewers. Any product that may be evaluated in this article, or claim that may be made by its manufacturer, is not guaranteed or endorsed by the publisher.

Author Disclaimer

All the editors involved in this research topic was served in their personal interest and do not represent the views/positions of their affiliations.

frontiers | Frontiers in Pharmacology

TYPE Original Research
PUBLISHED 10 May 2024
DOI 10.3389/fphar.2024.1397332

Check for updates

OPEN ACCESS

EDITED BY
Pukar Khanal,
Emory University, United States

REVIEWED BY
Pankaj Kumar,
Nitte Gulabi Shetty Memorial Institute of Pharmaceutical Sciences, India
Vishal Patil,
KLE College of Pharmacy, India

*CORRESPONDENCE
Anas Shamsi,
anas.shamsi18@gmail.com

RECEIVED 07 March 2024
ACCEPTED 25 April 2024
PUBLISHED 10 May 2024

CITATION
Alrouji M, Yasmin S, Alhumaydhi FA, Sharaf SE, Shahwan M, Furkan M, Khan RH and Shamsi A (2024), Comprehensive spectroscopic and computational insight into the binding of vanillin with human transferrin: targeting neuroinflammation in Alzheimer's disease therapeutics.
Front. Pharmacol. 15:1397332.
doi: 10.3389/fphar.2024.1397332

COPYRIGHT
© 2024 Alrouji, Yasmin, Alhumaydhi, Sharaf, Shahwan, Furkan, Khan and Shamsi. This is an open-access article distributed under the terms of the Creative Commons Attribution License (CC BY). The use, distribution or reproduction in other forums is permitted, provided the original author(s) and the copyright owner(s) are credited and that the original publication in this journal is cited, in accordance with accepted academic practice. No use, distribution or reproduction is permitted which does not comply with these terms.

Comprehensive spectroscopic and computational insight into the binding of vanillin with human transferrin: targeting neuroinflammation in Alzheimer's disease therapeutics

Mohammed Alrouji[1], Sabina Yasmin[2], Fahad A. Alhumaydhi[3], Sharaf E. Sharaf[4], Moyad Shahwan[5,6], Mohammad Furkan[7], Rizwan Hasan Khan[8] and Anas Shamsi[6]*

[1]Department of Medical Laboratories, College of Applied Medical Sciences, Shaqra University, Shaqra, Saudi Arabia, [2]Department of Pharmaceutical Chemistry, College of Pharmacy, King Khalid University, Abha, Saudi Arabia, [3]Department of Medical Laboratories, College of Applied Medical Sciences, Qassim University, Buraydah, Saudi Arabia, [4]Pharmaceutical Sciences Department, College of Pharmacy, Umm Al-Qura University, Makkah, Saudi Arabia, [5]Department of Clinical Sciences, College of Pharmacy and Health Sciences, Ajman University, Ajman, United Arab Emirates, [6]Center of Medical and Bio-Allied Health Sciences Research (CMBHSR), Ajman University, Ajman, United Arab Emirates, [7]Department of Biochemistry, Aligarh Muslim University, Aligarh, India, [8]Interdisciplinary Biotechnology Unit, Aligarh Muslim University, Aligarh, India

In present times, vanillin stands out as a promising therapeutic molecule that can be implicated in the treatment of neurodegenerative disorders (NDs), notably Alzheimer's disease (AD). This can be attributed to the highly potent scavenging activity of vanillin against reactive oxygen species (ROS). Oxidative stress leads to generation of ROS that serves a critical role in AD's pathological progression. It is apparent from various studies that diets rich in polyphenols prevent oxidative stress associated with AD development, implying the crucial role of vanillin in AD therapeutics. It is crucial to maintain iron balance to manage AD associated oxidative stress, unveiling the significance of human transferrin (hTf) that maintains iron homeostasis. Here, we have performed an integrated study of spectroscopic and computational approaches to get insight into the binding mechanism of vanillin with hTf. In the preliminary study, molecular docking deciphered that vanillin primarily occupies the hTf binding pocket, forming multiple interactions with its key residues. Moreover, the binding mechanism was evaluated at an atomistic level employing comprehensive molecular dynamic (MD) simulation. MD analysis demonstrated that binding of vanillin to hTf stabilizes its structure, without inducing any significant alterations in its native conformation. The docked complex was maintained throughout the simulations without changing its original conformation. Essential dynamics analysis further confirms that hTf achieved a stable conformation with vanillin. The outcomes were further supplemented by fluorescence spectroscopy which confirms the

formation of stable hTf-vanillin complex. Taken together, the current study unveils the interaction mechanism of vanillin with hTf and providing a platform to use vanillin in AD therapeutics in the context of iron homeostasis.

KEYWORDS

oxidative stress, molecular dynamic simulation, fluorescence spectroscopy, Alzheimer's disease, vanillin

1 Introduction

Presently, bioactive natural products are vital in drug development due to their favorable safety profile and potent antioxidant capabilities along with their broad therapeutic potentials and minimal side effects. All these characteristics make them a vital cog in disease therapeutics, highlighting their importance in the current disease era. Vanillin, a natural phenolic compound plentiful in various vanilla beans, is extensively employed in the food, cosmetic, and pharmaceutical industries (Arya et al., 2021). Apart from its industrial usage, vanillin offers several health benefits, namely, antioxidant properties, anti-inflammatory, anti-mutagenic, anti-metastatic, and anti-depressant effects (Bezerra-Filho et al., 2019; Costantini et al., 2021). Vanillin serves as the principal and highly stable curcumin degradation product, a natural polyphenol (Wang et al., 1997). In recent times, studies have reported neuroprotective and anticancer effect of vanillin, implying its therapeutic potential (Li et al., 2018; Rakoczy et al., 2021; Yousuf et al., 2021; Iannuzzi et al., 2023). Neuroinflammation stands out as a prevalent pathological process in various neurological diseases, intricately linked to the fundamental mechanisms of neurodegenerative disorders (NDs). The primary hallmarks of neurodegeneration are Neuroinflammation and oxidative stress (Singh et al., 2019; Teleanu et al., 2022). Alzheimer's disease (AD), an age-related ND, is a complex multifactorial disease (Lane et al., 2018). The primary neuropathological indicators of AD encompass the development of "neurofibrillary tangles" (NFTs) and accumulation of "amyloid beta" (Aβ) plaques within the brain (Iannuzzi et al., 2023). Additionally, cholinergic deficit, along with oxidative stress and neuroinflammation, plays a vital role in processes that lead to neuronal death (Butterfield and Halliwell, 2019; Guo et al., 2020). A recent study established that vanillin decreased the Aβ effects on learning and memory by suppressing oxidative stress. Another research stated that vanillin showed an acetylcholinesterase inhibitory activity *in vitro*, implying vanillin to be safe and effective natural drug candidate offering enormous promise for AD management.

Presently, the precise cause of AD remains poorly understood with age recognized as the primary risk factor for AD (Imtiaz et al., 2014). The major problem associated with AD therapeutics is that no disease-modifying drugs are currently available and moreover, clinical trials have highest failure rates in any therapeutic area (Yiannopoulou and Papageorgiou, 2013; Chen and Pan, 2015). Oxidative stress plays a vital role in the pathological progression of AD, along with various other diseases such as cancer, diabetes, and neurological disorders (Markesbery, 1997). Many studies have reported that consuming diets abundant in polyphenols prevent the oxidative stress associated with the AD pathogenesis (Kundu and Mitra, 2013; Cremonini et al., 2019; Salau et al., 2020; Ahammed et al., 2021). Various studies have reported vanillin's anti-inflammatory effects and its anti-oxidant activity (Zhao et al., 2017; Gu et al., 2019). Given its strong scavenging activity against reactive oxygen species (ROS) and its ability to inhibit inflammatory pathway activation, vanillin emerges as a promising therapeutic molecule for the prevention of AD and other NDs. Studies have reported that vanillin shows "AChE inhibitory activity", *in vitro* and *in vivo*, hinders amyloid aggregation, and provides protection against neuronal oxidative damage (Ahammed et al., 2021). Vanillin has been reported to not only inhibit AChE activity but also restore oxidative balance in Fe^{2+}-induced brain tissue damage (Salau et al., 2020). All these studies highlight the importance of vanillin in providing protection against neuronal oxidative damage observed in AD and other NDs conditions.

Free iron serves as a potent neurotoxin capable of triggering the generation of ROS, creating an environment of oxidative stress. In its unbound state, iron functions as a formidable neurotoxin, possessing the potential to induce oxidative stress (Shahwan et al., 2023). The production of ROS and Reactive nitrogen species (RNS), directly implicated in the inflammatory process, can markedly impact iron metabolism by interacting with iron-regulatory proteins (IRPs). Thus, maintaining proper iron levels is vital and human transferrin (hTf) plays a key role in iron homeostasis along with ferritin. Iron homeostasis plays a vital role in AD associated oxidative stress, thus implying the significant role played by hTf in AD therapeutics. Owing to pivotal role of vanillin and hTf, the present study encompasses a combination of experimental and computational approaches to delineate the atomistic insights into the binding of vanillin with hTf.

2 Materials and Methods

2.1 Materials

Human transferrin (hTf) and vanillin were bought from Sigma Aldrich (St. Louis, USA). For buffer preparations, all the chemicals were of the best quality purchased from HiMedia. All the buffers were filtered before use and for spectroscopic assays, corresponding blanks were taken.

2.2 Molecular docking

Molecular docking studies were conducted on a DELL® workstation to elucidate the interactions between Vanillin and hTf. Computational tools were used to optimize visualization, evaluation, and analysis of the docking results. We obtained three-dimensional configuration of hTf (PDB ID: 3V83) and PubChem database (PubChem CID: 1183) was used to obtain vanillin structure. We prepared vanillin structure using MGL

AutoDock tools (Huey et al., 2012). Further, docking simulations were carried out using AutoDock Vina (Trott and Olson, 2010). We employed PLIP to explore the intricate ligand-receptor interactions between vanillin and hTf (Salentin et al., 2015). To gain an in-depth understanding of the binding conformation and the nature of interactions between vanillin and hTf, PyMOL (DeLano, 2002) and Discovery Studio Visualizer (Biovia, 2017) were used.

2.3 MD simulations

MD simulations were conducted to explore the dynamic behavior of hTf and hTf-vanillin complex. We performed a simulation at 300 K temperature, using charmm36-jul2022 force field (Huang and MacKerell, 2013), implemented within GROMACS version 2020 (Van Der Spoel et al., 2005). The topology for vanillin was generated using CHARMM CGenFF program, using a Python script. hTf and hTf-Vanillin were later solvated in cubic boxes with 1 nm dimensions in the SPC216 water model using *GROMACS gmx solvate* tool (Glättli et al., 2002). Both systems were neutralized by adding suitable quantities of counterions to achieve a concentration of 0.15 M. Equilibration processes in the NVT and NPT ensembles were conducted, where the systems were slowly heated to 300 K over 1000 ps. Subsequently, solvent molecules were allowed to relax in the NPT ensemble for an additional 1000 ps without any restraints, while maintaining a pressure of 1 bar using the Berendsen Barostat method. To constrain bond lengths, the LINCS algorithm was applied, while SETTLE restrained water molecules. The system's energy was minimized with 1500 iterations of the steepest descent approach. We employed a range of tools provided by GROMACS to analyze trajectories generated during MD simulations. The results obtained from the MD simulations were presented graphically using the XMGrace software (Turner, 2005). Graphs and figures were created to illustrate key findings, aiding in a clear and concise explanation of the obtained results.

2.4 Principal component analysis and free energy landscapes

Principal component analysis (PCA) is an essential tool for understanding the primary motions and conformational sampling of proteins in MD simulations. The MD trajectories of hTf and hTf-vanillin underwent PCA to explore their predominant modes of motion. This involved diagonalizing the covariance matrix to derive the first two eigenvectors (EVs), which depict the primary motions of the protein or protein-ligand complex. Additionally, we generated free energy landscapes (FELs) to assess the stability and folding dynamics of hTf and its complex with vanillin. Conformational sampling techniques were employed to construct FELs, enabling the visualization of energy landscapes and the identification of stable conformations or metastable states.

2.5 Fluorescence spectroscopy

We performed fluorescence spectroscopy on Shimadzu (RF 6000) spectrofluorometer. The concentration of hTf was fixed at 4 μM and vanillin was varied in a range of "0–5 μM". The quenching data was analyzed using "Modified Stern–Volmer" equation (MSV) to compute binding parameters of hTf-vanillin complex.

3 Result and discussion

3.1 Molecular docking

Vanillin showed remarkable interactions towards hTf, resulting in a highly favorable binding affinity in triplicate dodcking experiments. Vanillin binds to hTf with an average binding affinity of −5.8 kcal/mol, implying vanillin's potential as a potent hTf binding partner. Vanillin is predicted to primarily interact with the hTf binding pocket (Figure 1A). Notably, vanillin forms three hydrogen bonds with key residues, *viz.* Ser409, Arg475, and Leu649 (Figure 1B; Supplementary Table S1). Tyr536 is a vital active site residue that plays a key role for iron (Fe^{3+}) binding in hTf, which plays a key role in forming these interactions (Noinaj et al., 2012). Tyr536 forms a hydrophobic bond with vanillin, further stabilizing the complex (Figure 1B). The 2D and surface plots further shed light on other interactions playing a key role in stabilizing the hTf-vanillin complex. Arg475 is another active site residuewhich is responsible to bind with hydrogencarbonate. The surface representation of the docked complex further revealed that vanillin fits into the internal cavity of hTf (Figures 1C, D). Earlier studies have also reported iron binding to hTf showing similar interactions, thereby validating our findings (Noinaj et al., 2012; Ghanbari et al., 2017). Overall, it is indicated that vanillin binds to the hTf binding pocket.

3.2 MD simulation analysis

MD simulations are a widely adopted computational technique for unraveling the underlying dynamics and structural alterations of proteins and protein-ligand complexes (Shukla and Tripathi, 2020). MD simulation serves as a valuable tool for probing the biomolecular interactions within a defined time frame (Mohammad et al., 2020). In this specific investigation, we conducted a comprehensive MD simulation spanning 200 nanoseconds, encompassing hTf and the hTf-vanillin docked complex. Our key goal was to scrutinize changes in conformation, assess stability, and unravel the fundamental mechanisms governing the interaction between vanillin and hTf. First, to evaluate the structural changes, we employed the root mean square deviation (RMSD) on the simulated trajectory. Our findings reveal that vanillin binding leads to the stabilization of hTf without inducing any significant alterations in its inherent configuration, as clearly depicted in Figure 2A. However, during the initial phase, the RMSD showed intermittent fluctuations, primarily attributable to the accommodation of vanillin within hTf's binding site.

To delve into local structural changes and residue flexibility, we calculated and visually represented the root-mean-square fluctuation (RMSF) of the simulated systems (Figure 2B). The RMSF plot highlights varying levels of residue fluctuations across different zones of the hTf structure. Intriguingly, the overall average RMSF of hTf and hTf-vanillin exhibited a consistent pattern. Importantly, the introduction of vanillin resulted in heightened

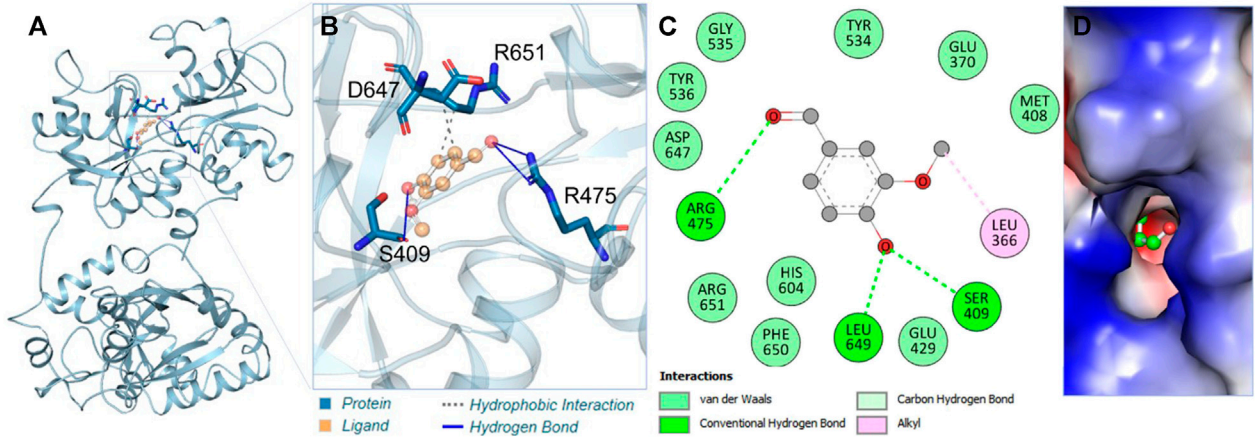


FIGURE 1
Interaction analysis. **(A)** Illustration of vanillin binding with hTf. **(B)** Ribbon representation depicting the docking of vanillin. **(C)** Two-dimensional interaction plot illustrating vanillin's binding interactions with hTf. **(D)** Visualization of the surface potential in the hTf binding pocket occupied by vanillin.

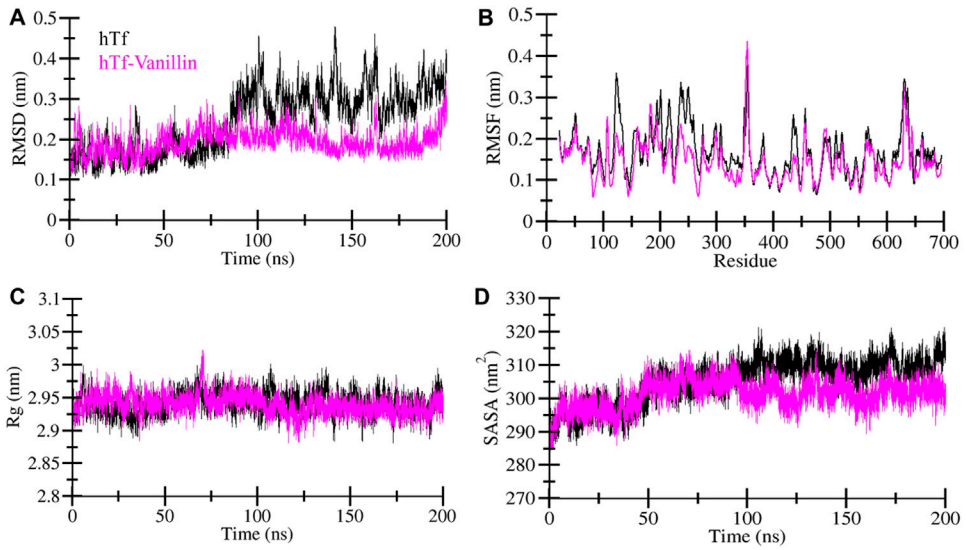


FIGURE 2
Exploring the structural dynamics of hTf in the presence of vanillin **(A)** RMSD **(B)** RMSF **(C)** Rg, and **(D)** SASA plots.

residue fluctuations, indicative of increased system dynamics. These enhanced fluctuations may be attributed to residual vibrations during the simulation process.

The radius of gyration (*Rg*) is a commonly utilized measure to glean insights into the folding and structural conformation of the proteins. A higher *Rg* typically implies a less condensed conformation. In the case of the hTf-vanillin, our observations indicate a minor decrease in *Rg* compared to the unbound hTf, signifying that the structure maintains compactness throughout the simulation, as illustrated in Figure 2C. Despite slight variations in *Rg*, there are no significant alterations in the packing of hTf following the binding of vanillin. These findings underscore that vanillin induces minimal structural deviations in hTf.

The solvent-accessible surface area (SASA) represents the fraction of a protein's surface directly exposed to the adjacent solvent and is closely associated with the *Rg*. We calculated and visually depicted the average SASA for hTf and hTf-vanillin from the simulated trajectory. In the instance of the hTf-vanillin complex, we observed a minor decrease in SASA compared to the free hTf, implying the maintenance of structural compactness during the simulation. Despite minimal variations in SASA, no significant alterations in the packing of hTf were discernible following the binding of vanillin (Figure 2D).

Moreover, by employing MD simulation trajectories, we have successfully depicted the conformational snapshots showcasing the binding interactions between vanillin and hTf. This analysis enabled us to monitor the temporal evolution of the binding prototype. Structural assessments were performed at five distinct time intervals: 1, 50, 100, 150, and 200 ns, as illustrated in Figure 3. Notably, our investigation

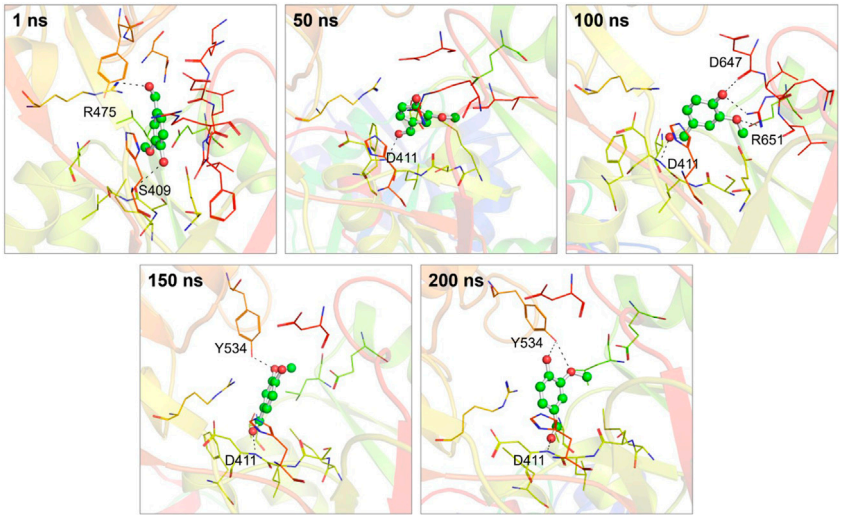


FIGURE 3
Conformational dynamics of the hTf-vanillin complex at different time intervals during 200 ns. The binding conformations showing hTf-vanillin interactions at 1, 50, 100, 150, and 200 ns, respectively.

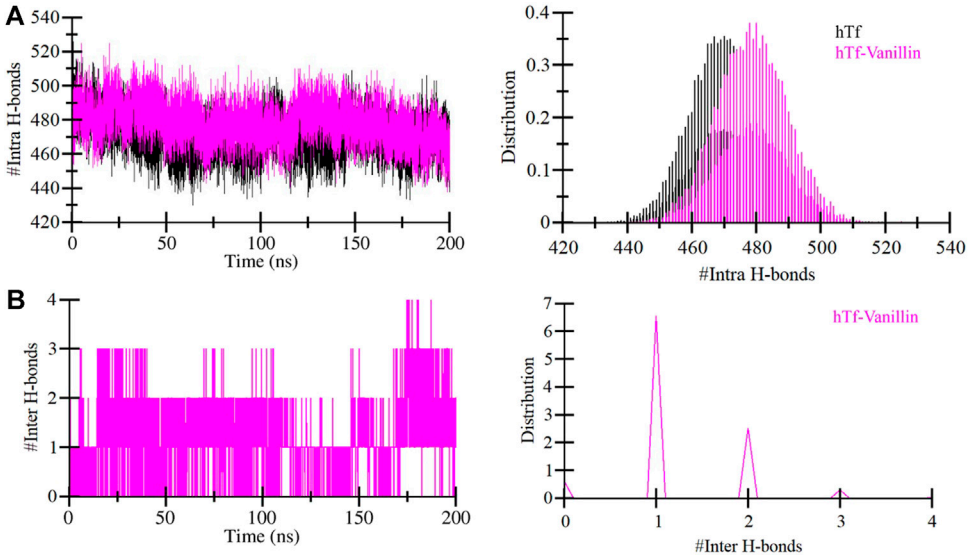


FIGURE 4
Temporal development of hydrogen bonds established **(A)** Within hTf, and **(B)** Hydrogen bonds between vanillin and hTf.

unveiled that vanillin maintained its initial docking positions consistently throughout the simulation, indicating minimal conformational alterations.

3.3 Stabilization of hTf-Vanillin complex

Evaluating the dynamics of hydrogen bonding is crucial for assessing the stability of the proteins and protein-ligand complexes. In this investigation, we quantified and explored the dynamics of hydrogen bonds intramolecularly within hTf and intermolecularly between hTf and vanillin (Figure 4). Upon the vanillin binding to hTf, we observed a minor increase in the number of intramolecular hydrogen bonds within hTf due to the higher compactness of the protein (Figure 4A). We also calculated the intermolecular hydrogen bonds formed between hTf and vanillin. Our analysis revealed the presence of up to 4 hydrogen bonds within the protein-ligand complex. We also observed that vanillin effectively nestled within hTf's iron-binding pocket, forming 3-4 hydrogen bonds with some fluctuation and 1-2 hydrogen bonds with higher stability (Figure 4B). This thorough analysis provides additional supportive evidence for the stable binding of hTf and vanillin.

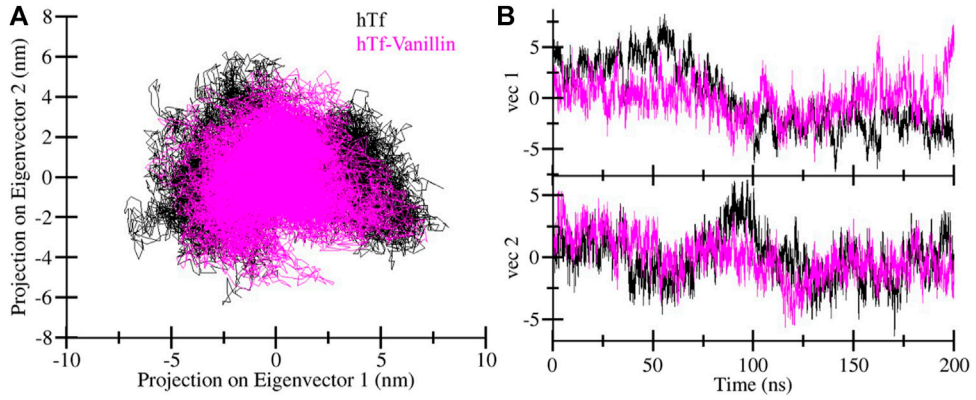


FIGURE 5
Principal component analysis. **(A)** Two-dimensional projections of hTf conformation, and **(B)** Temporal evolution of trajectory projections.

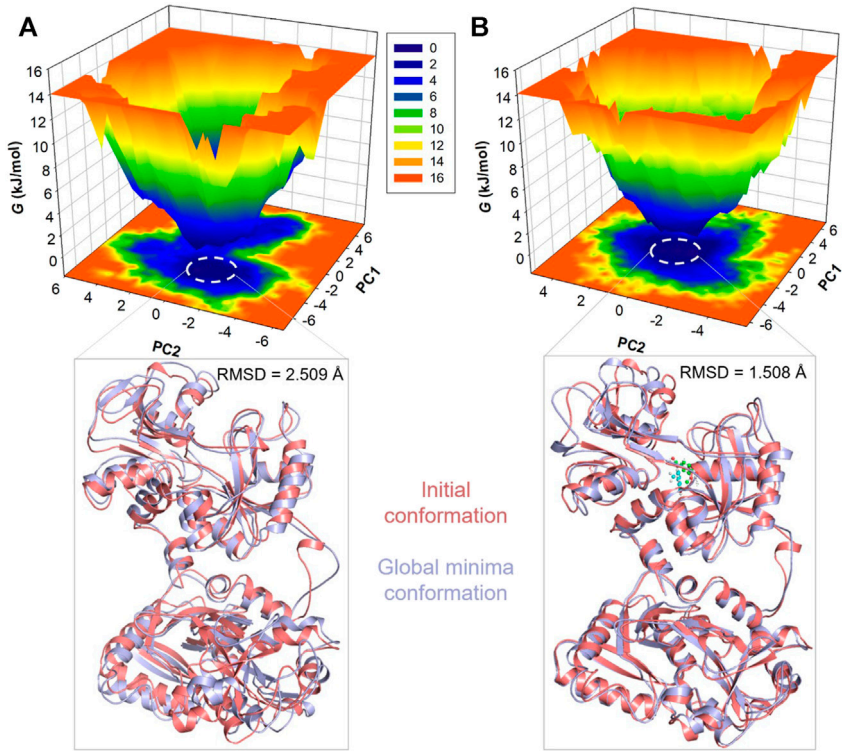


FIGURE 6
Free energy landscape plots for **(A)** Unbound hTf and **(B)** The hTf-Vanillin complex. Lower panels showed the global minima conformations of hTf in comparison to the initial conformations.

3.4 Principal component analysis

Principal component analysis (PCA) offers valuable insights into protein stability and conformational landscape (Stein et al., 2006). Here, we employed PCA to investigate the conformational dynamics of hTf and hTf-vanillin from the simulated trajectory. Figure 5 demonstrates the conformational dynamics of these systems along eigenvector 1 and eigenvector 2. The PCA plot indicates that in the presence of vanillin, hTf explores a more confined range of phase spaces (Figure 5A). We did not observe any significant overarching transitions or major conformational changes in the motion of hTf following vanillin binding (Figure 5B). This implies that the vanillin binding does not cause substantial conformational changes in hTf.

3.5 Free energy landscape analysis

To gain deeper insights into the folding landscape of the systems, we delved into the free energy landscapes (FELs)

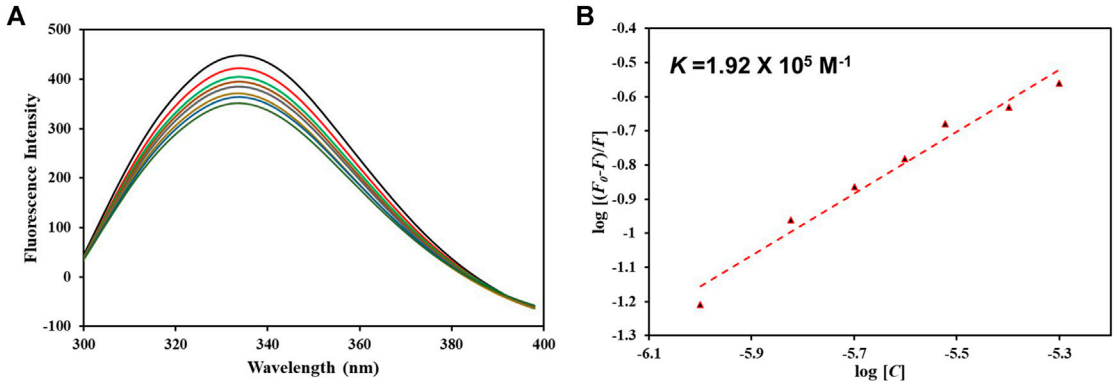


FIGURE 7
(A) Fluorescence emission spectra of free hTf and hTf with different vanillin concentrations (0–5 μM). **(B)** MSV plot of hTf-vanillin interaction.

generated through the simulated trajectories. Figure 6 presents a visual representation of the FELs for hTf and hTf-vanillin. In hTf's FEL, it is indicated that hTf explores two distinct energy minima confined within 2-3 basins (Figure 6A). Conversely, when vanillin is introduced, a noticeable feature is a prominent single global minimum, mainly concentrated within a single basin, as illustrated in Figure 6B. Importantly, no significant or drastic conformational rearrangements are observed due to this binding event. This observation implies that vanillin binding introduces novel conformational states and influences hTf's energy landscape. Examining these FELs provides valuable details about the conformational stability of hTf and hTf-vanillin.

3.6 Fluorescence binding

After confirming hTf-vanillin complex formation through computational approaches, we used fluorescence binding to validate the obtained results. It is a powerful technique to study protein-ligand interactions, ascertaining the actual affinity of a ligand with the protein. Figure 7A shows the fluorescence emission spectra of hTf without vanillin and in the presence of varying vanillin concentrations (0–5 μM). It is apparent that with increasing vanillin concentrations, a decrease in the fluorescence intensity of hTf was apparent. The obtained quenching data was fitted into MSV equation as per earlier reports (Shamsi et al., 2020) with intercept of the obtained MSV plot (Figure 7B) giving the binding constant (K) of hTf-vanillin complex. Vanillin binds to hTf with a significant affinity forming a stable hTf-vanillin complex; evident from the obtained K of $1.92 \times 10^5\ M^{-1}$, suggestive of strong binding between vanillin and hTf.

4 Conclusion

Collectively, this investigation implies that vanillin possesses the capability to impede hTf's function through strong and persistent interactions, predominantly characterized by hydrogen bonds with crucial amino acids. Our molecular docking simulations unveiled strong and favorable interactions between vanillin and hTf, with vanillin predominantly occupying the hTf binding pocket. Notably, vanillin formed multiple hydrogen bonds with key residues of hTf, indicative of stable binding. MD simulations further corroborated these findings by demonstrating that the binding of vanillin to hTf stabilizes the protein structure without inducing significant conformational alterations. Analysis of hydrogen bonding dynamics, radius of gyration, and solvent-accessible surface area supported the stability of the hTf-vanillin complex throughout the simulation. Furthermore, fluorescence spectroscopy provided experimental validation of the hTf-vanillin interaction, confirming the formation of a stable complex with significant binding affinity. The blend of molecular docking, MD simulations, and diverse analytical approaches along with spectroscopic approach yields a holistic comprehension of the interaction between hTf and vanillin. While our study contributes valuable insights into the potential therapeutic role of vanillin in AD by targeting iron homeostasis through hTf binding, it is not without limitations. Conducting longer simulations, *in vivo* studies, elucidating high-resolution structures, and exploring combination therapies represent promising avenues for advancing the development of vanillin-based interventions for AD and other NDs.

Data availability statement

The original contributions presented in the study are included in the article/Supplementary Material, further inquiries can be directed to the corresponding author.

Author contributions

MA: Data curation, Investigation, Methodology, Validation, Writing–original draft. SY: Data curation, Formal Analysis,

Investigation, Validation, Visualization, Writing–original draft. FA: Data curation, Investigation, Software, Writing–review and editing. SS: Methodology, Software, Validation, Writing–review and editing. MS: Formal Analysis, Investigation, Methodology, Writing–original draft. MF: Data curation, Investigation, Visualization, Writing–review and editing. RK: Data curation, Methodology, Supervision, Writing–review and editing. AS: Conceptualization, Funding acquisition, Investigation, Methodology, Project administration, Writing–original draft.

Funding

The author(s) declare financial support was received for the research, authorship, and/or publication of this article. The authors extend their appreciation to the Deanship of Scientific Research at King Khalid University for funding this work through a small research group program under grant number RGP. 1/219/44. MA would like to thank the Deanship of Scientific Research at Shaqra University for supporting this work. AS is grateful to Ajman University for supporting this publication.

Conflict of interest

The authors declare that the research was conducted in the absence of any commercial or financial relationships that could be construed as a potential conflict of interest.

Publisher's note

All claims expressed in this article are solely those of the authors and do not necessarily represent those of their affiliated organizations, or those of the publisher, the editors and the reviewers. Any product that may be evaluated in this article, or claim that may be made by its manufacturer, is not guaranteed or endorsed by the publisher.

Supplementary material

The Supplementary Material for this article can be found online at: https://www.frontiersin.org/articles/10.3389/fphar.2024.1397332/full#supplementary-material

References

Ahammed, S., Afrin, R., Uddin, N., Al-Amin, Y., Hasan, K., Haque, U., et al. (2021). Acetylcholinesterase inhibitory and antioxidant activity of the compounds isolated from vanda roxburghii. *Adv. Pharmacol. Pharm. Sci.* 2021, 5569054. doi:10.1155/2021/5569054

Arya, S. S., Rookes, J. E., Cahill, D. M., and Lenka, S. K. (2021). Vanillin: a review on the therapeutic prospects of a popular flavouring molecule. *Adv. traditional Med.* 21, 1–17. doi:10.1007/s13596-020-00531-w

Bezerra-Filho, C. S., Barboza, J. N., Souza, M. T., Sabry, P., Ismail, N. S., and De Sousa, D. P. (2019). Therapeutic potential of vanillin and its main metabolites to regulate the inflammatory response and oxidative stress. *Mini Rev. Med. Chem.* 19, 1681–1693. doi:10.2174/1389557519666190312164355

Biovia Dassault Systèmes (2017) *Discovery studio visualizer*. San Diego, CA, USA: Biovia, 936.

Butterfield, D. A., and Halliwell, B. (2019). Oxidative stress, dysfunctional glucose metabolism and Alzheimer disease. *Nat. Rev. Neurosci.* 20, 148–160. doi:10.1038/s41583-019-0132-6

Chen, X., and Pan, W. (2015). The treatment strategies for neurodegenerative diseases by integrative medicine. *Integr. Med. Int.* 1, 223–225. doi:10.1159/000381546

Costantini, E., Sinjari, B., Falasca, K., Reale, M., Caputi, S., Jagarlapodii, S., et al. (2021). Assessment of the vanillin anti-inflammatory and regenerative potentials in inflamed primary human gingival fibroblast. *Mediat. Inflamm.* 2021, 5562340. doi:10.1155/2021/5562340

Cremonini, A. L., Caffa, I., Cea, M., Nencioni, A., Odetti, P., and Monacelli, F. (2019). Nutrients in the prevention of Alzheimer's disease. *Oxidative Med. Cell. Longev.* 2019, 1–20. doi:10.1155/2019/9874159

Delano, W. L. (2002). Pymol: an open-source molecular graphics tool. *CCP4 Newsl. Protein Crystallogr.* 40, 82–92.

Ghanbari, Z., Housaindokht, M. R., Bozorgmehr, M., and Izadyar, M. (2017). Effects of synergistic and non-synergistic anions on the iron binding site from serum transferrin: a molecular dynamic simulation analysis. *J. Mol. Graph. Model.* 78, 176–186. doi:10.1016/j.jmgm.2017.10.013

Glättli, A., Daura, X., and Van Gunsteren, W. F. (2002). Derivation of an improved simple point charge model for liquid water: SPC/A and SPC/L. *J. Chem. Phys.* 116, 9811–9828. doi:10.1063/1.1476316

Gu, X., Chen, J., Zhang, Y., Guan, M., Li, X., Zhou, Q., et al. (2019). Synthesis and assessment of phenylacrylamide derivatives as potential anti-oxidant and anti-inflammatory agents. *Eur. J. Med. Chem.* 180, 62–71. doi:10.1016/j.ejmech.2019.07.020

Guo, T., Zhang, D., Zeng, Y., Huang, T. Y., Xu, H., and Zhao, Y. (2020). Molecular and cellular mechanisms underlying the pathogenesis of Alzheimer's disease. *Mol. Neurodegener.* 15, 40–37. doi:10.1186/s13024-020-00391-7

Huang, J., and Mackerell, A. D. (2013). CHARMM36 all-atom additive protein force field: validation based on comparison to NMR data. *J. Comput. Chem.* 34, 2135–2145. doi:10.1002/jcc.23354

Huey, R., Morris, G. M., and Forli, S. (2012). Using AutoDock 4 and AutoDock vina with AutoDockTools: a tutorial. *Scripps Res. Inst. Mol. Graph. Laboratory* 10550, 1000.

Iannuzzi, C., Liccardo, M., and Sirangelo, I. (2023). Overview of the role of vanillin in neurodegenerative diseases and neuropathophysiological conditions. *Int. J. Mol. Sci.* 24, 1817. doi:10.3390/ijms24031817

Imtiaz, B., Tolppanen, A.-M., Kivipelto, M., and Soininen, H. (2014). Future directions in Alzheimer's disease from risk factors to prevention. *Biochem. Pharmacol.* 88, 661–670. doi:10.1016/j.bcp.2014.01.003

Kundu, A., and Mitra, A. (2013). Flavoring extracts of Hemidesmus indicus roots and Vanilla planifolia pods exhibit *in vitro* acetylcholinesterase inhibitory activities. *Plant foods Hum. Nutr.* 68, 247–253. doi:10.1007/s11130-013-0363-z

Lane, C. A., Hardy, J., and Schott, J. M. (2018). Alzheimer's disease. *Eur. J. neurology* 25, 59–70. doi:10.1111/ene.13439

Li, J.-M., Lee, Y.-C., Li, C.-C., Lo, H.-Y., Chen, F.-Y., Chen, Y.-S., et al. (2018). Vanillin-ameliorated development of azoxymethane/dextran sodium sulfate-induced murine colorectal cancer: the involvement of proteasome/nuclear factor-κB/mitogen-activated protein kinase pathways. *J. Agric. food Chem.* 66, 5563–5573. doi:10.1021/acs.jafc.8b01582

Markesbery, W. R. (1997). Oxidative stress hypothesis in Alzheimer's disease. *Free Radic. Biol. Med.* 23, 134–147. doi:10.1016/s0891-5849(96)00629-6

Mohammad, T., Siddiqui, S., Shamsi, A., Alajmi, M. F., Hussain, A., Islam, A., et al. (2020). Virtual screening approach to identify high-affinity inhibitors of serum and glucocorticoid-regulated kinase 1 among bioactive natural products: combined molecular docking and simulation studies. *Molecules* 25, 823. doi:10.3390/molecules25040823

Noinaj, N., Easley, N. C., Oke, M., Mizuno, N., Gumbart, J., Boura, E., et al. (2012). Structural basis for iron piracy by pathogenic Neisseria. *Nature* 483, 53–58. doi:10.1038/nature10823

Rakoczy, K., Szlasa, W., Saczko, J., and Kulbacka, J. (2021). Therapeutic role of vanillin receptors in cancer. *Adv. Clin. Exp. Med.* 30, 1293–1301. doi:10.17219/acem/139398

Salau, V. F., Erukainure, O. L., Ibeji, C. U., Olasehinde, T. A., Koorbanally, N. A., and Islam, M. S. (2020). Vanillin and vanillic acid modulate antioxidant defense system via amelioration of metabolic complications linked to Fe 2+-induced brain tissues damage. *Metab. brain Dis.* 35, 727–738. doi:10.1007/s11011-020-00545-y

Salentin, S., Schreiber, S., Haupt, V. J., Adasme, M. F., and Schroeder, M. (2015). PLIP: fully automated protein–ligand interaction profiler. *Nucleic acids Res.* 43, W443–W447. doi:10.1093/nar/gkv315

Shahwan, M., Anwar, S., Yadav, D. K., Khan, M. S., and Shamsi, A. (2023). Experimental and computational insights into the molecular interactions between human transferrin and apigenin: implications of natural compounds in targeting neuroinflammation. *ACS omega* 8, 46967–46976. doi:10.1021/acsomega.3c06799

Shamsi, A., Anwar, S., Mohammad, T., Alajmi, M. F., Hussain, A., Rehman, M. T., et al. (2020). MARK4 inhibited by AChE inhibitors, donepezil and Rivastigmine tartrate: insights into Alzheimer's disease therapy. *Biomolecules* 10, 789. doi:10.3390/biom10050789

Shukla, R., and Tripathi, T. (2020). Molecular dynamics simulation of protein and protein–ligand complexes. *Computer-aided drug Des.*, 133–161. doi:10.1007/978-981-15-6815-2_7

Singh, A., Kukreti, R., Saso, L., and Kukreti, S. (2019). Oxidative stress: a key modulator in neurodegenerative diseases. *Molecules* 24, 1583. doi:10.3390/molecules24081583

Stein, S. a.M., Loccisano, A. E., Firestine, S. M., and Evanseck, J. D. (2006). Principal components analysis: a review of its application on molecular dynamics data. *Annu. Rep. Comput. Chem.* 2, 233–261.

Teleanu, D. M., Niculescu, A.-G., Lungu, I. I., Radu, C. I., Vladâcenco, O., Roza, E., et al. (2022). An overview of oxidative stress, neuroinflammation, and neurodegenerative diseases. *Int. J. Mol. Sci.* 23, 5938. doi:10.3390/ijms23115938

Trott, O., and Olson, A. J. (2010). AutoDock Vina: improving the speed and accuracy of docking with a new scoring function, efficient optimization, and multithreading. *J. Comput. Chem.* 31, 455–461. doi:10.1002/jcc.21334

Turner, P. (2005) *XMGRACE, version 5.1. 19. Center for coastal and land-margin research*. Beaverton, OR 2: Oregon Graduate Institute of Science and Technology.

Van Der Spoel, D., Lindahl, E., Hess, B., Groenhof, G., Mark, A. E., and Berendsen, H. J. (2005). GROMACS: fast, flexible, and free. *J. Comput. Chem.* 26, 1701–1718. doi:10.1002/jcc.20291

Wang, Y.-J., Pan, M.-H., Cheng, A.-L., Lin, L.-I., Ho, Y.-S., Hsieh, C.-Y., et al. (1997). Stability of curcumin in buffer solutions and characterization of its degradation products. *J. Pharm. Biomed. analysis* 15, 1867–1876. doi:10.1016/s0731-7085(96)02024-9

Yiannopoulou, K. G., and Papageorgiou, S. G. (2013). Current and future treatments for Alzheimer's disease. *Ther. Adv. neurological Disord.* 6, 19–33. doi:10.1177/1756285612461679

Yousuf, M., Shamsi, A., Queen, A., Shahbaaz, M., Khan, P., Hussain, A., et al. (2021). Targeting cyclin-dependent kinase 6 by vanillin inhibits proliferation of breast and lung cancer cells: combined computational and biochemical studies. *J. Cell. Biochem.* 122, 897–910. doi:10.1002/jcb.29921

Zhao, D., Sun, J., Sun, B., Zhao, M., Zheng, F., Huang, M., et al. (2017). Intracellular antioxidant effect of vanillin, 4-methylguaiacol and 4-ethylguaiacol: three components in Chinese Baijiu. *RSC Adv.* 7, 46395–46405. doi:10.1039/c7ra09302k

frontiers | Frontiers in Pharmacology

TYPE Original Research
PUBLISHED 30 May 2024
DOI 10.3389/fphar.2024.1416350

Check for updates

OPEN ACCESS

EDITED BY
Pukar Khanal,
Emory University, United States

REVIEWED BY
Bijendra Mandar,
Sopan Pharmaceutical Pvt Ltd., Nepal
Prarambh S. R. Dwivedi,
Nitte Gulabi Shetty Memorial Institute of Pharmaceutical Sciences, India

*CORRESPONDENCE
Yaoxing Chen,
yxchen@cau.edu.cn

†These authors have contributed equally to this work and share first authorship

RECEIVED 12 April 2024
ACCEPTED 02 May 2024
PUBLISHED 30 May 2024

CITATION
Song C, Suo Z, Wang Z, Cao J, Dong Y and Chen Y (2024), Melatonin modulates neuroinflammatory response and microglial activation in mice exposed to dim blue light at night.
Front. Pharmacol. 15:1416350.
doi: 10.3389/fphar.2024.1416350

COPYRIGHT
© 2024 Song, Suo, Wang, Cao, Dong and Chen. This is an open-access article distributed under the terms of the Creative Commons Attribution License (CC BY). The use, distribution or reproduction in other forums is permitted, provided the original author(s) and the copyright owner(s) are credited and that the original publication in this journal is cited, in accordance with accepted academic practice. No use, distribution or reproduction is permitted which does not comply with these terms.

Melatonin modulates neuroinflammatory response and microglial activation in mice exposed to dim blue light at night

Chao Song[1†], Zhaotaize Suo[2†], Zixu Wang[1], Jing Cao[1], Yulan Dong[1] and Yaoxing Chen[1*]

[1]College of Veterinary Medicine, China Agricultural University, Beijing, China, [2]The High School Affiliated to Renmin University of China, Beijing, China

Objectives: Dim light at night contributes to neurodegenerative diseases by causing neuroinflammation. In the central nervous system, the activation of microglia is a significant contributor to neuroinflammation. Therefore, there is an urgent need to find an intervention to treat the neuroinflammatory response caused by dim light at night. Melatonin is a rhythmic hormone whose synthesis is suppressed during the day. In this study, we attempt to explore whether and how melatonin improves hippocampal neuroinflammation in mice exposed to dim blue light at night.

Materials and Methods: *In vivo*, a total of 36 male C57BL6/J mice that exposed to no light at night, dim blue light at night, and dim blue light at night with melatonin treatment. *In vitro*, the corticosterone-induced BV2 cells with or without melatonin treatment were used.

Results: Both *in vivo* and *in vitro* experiments showed melatonin treatment significantly reduced dim blue light -induced hippocampal microglial activation and the expression of inflammatory factors IL-1β and TNF-α. This improved effect of melatonin is related to its receptor MT2 rather than MT1. The MT2 blockers significantly increased mRNA levels of M1-type activation marker CD86 and inflammatory cytokines IL-1β and TNF-α in melatonin-treated BV2 cells. Binding of melatonin to its receptor MT2 downregulated the expression of inflammatory proteins P-P65 and NLRP3, consequently inhibited the CD80 expression and M1-type activation in microglia. Furthermore, consistent with the decrease in microglial activation and inflammatory response after melatonin treatment, we also observed a reduction in hippocampal neuron loss and damage to the HT22 cells.

Conclusion: Our findings suggested that melatonin may regulate microglial polarization through MT2/NF-kB-NLRP3 pathway and improves dim blue light -induced hippocampal neuroinflammation in mice.

KEYWORDS

d-BL, melatonin, MT2, microglia, neuroinflammation

1 Introduction

The term "blue light" refers to the type of light emitted by mobile phones, computers, and other electronic devices, which falls within a potent spectrum on the light spectrum (Zhao et al., 2018; Calvo-Sanz and Tapia-Ayuga, 2020). Despite its dim appearance in dark environments or during nighttime use, screen light can profoundly affect human health and wellbeing (Silvani et al., 2022). As artificial lighting becomes increasingly prevalent, extensive research has delved into its health implications, especially focusing on the neurophysiological effects of dim blue light at night (dBL). Liu et al. (2022) have highlighted the capacity of dBL to induce spatial memory impairment in mice, an effect mediated by neuroinflammation and oxidative stress within the hippocampus, underscoring the vulnerability of this brain region to light-induced perturbations. The significance of these findings is echoed by González (2018) and Fonken et al. (2012; 2013b), who have documented the broad physiological and cognitive disruptions caused by dBL, including exacerbated inflammatory responses and adverse metabolic effects, thus providing a compelling narrative on the health risks associated with night-time exposure to artificial lighting.

In this context, melatonin is highlighted as a compound with significant potential for therapeutic applications due to its potent antioxidative, anti-inflammatory, and neuroprotective properties. Studies by Xu et al. (2020) and Ali et al. (2020) illustrate melatonin's efficacy in modulating immune responses, particularly in attenuating neuroinflammation by regulating microglial activity, a mechanism critical for mitigating the adverse effects of environmental stressors like dBL. These investigations align with broader research efforts, such as those by Zheng et al. (2021) and Wang et al. (2021), which further elucidate melatonin's role in downregulating inflammatory pathways and protecting against cognitive deficits.

The intricate interplay between melatonin and microglial activation (Hardeland R, 2021; Guo er al., 2023). Through an integrative analysis, we explore the neuroprotective effects of melatonin against dBL-induced hippocampal inflammation and microglial activation, drawing upon the foundational work of Gao et al. (2023), which underscore the hormone's capacity to modulate neuroinflammatory responses. Moreover, the study by Wongprayoon and Govitrapong (2015) highlights melatonin's ability to counteract neuroinflammation through receptor-mediated pathways, providing a molecular basis for its therapeutic potential. Our investigation provides a comprehensive understanding of how melatonin interacts with the neuroinflammatory cascade triggered by dBL and elucidates the underlying mechanisms of its protective effects.

2 Materials and methods

2.1 Treatment of laboratory animals

In order to replicate a typical daytime environment, a total of 36 male C57BL6/J mice (Vitonglihua, Beijing) were exposed to white LEDs (150 lux) during the day. The mice were exposed to low levels of blue light (5 lux, peak wavelength: 444 nm) all night long throughout the night phase. After the 10th week of exposure to evening light, a 4-week intraperitoneal injection of melatonin (20 mg/kg body weight with melatonin dissolved in anhydrous ethanol) was given. After a 1-week adaptation period, the mice were randomly divided into three groups: (1) LD group: n = 12; a light (~150 lux)/dark (0 lux) cycle, (2) dBL group: n = 12; a light (~150 lux)/dim blue light (~5 lux) cycle, (3) dBL + Melatonin group: n = 12; a light (~150 lux)/dim blue light (~5 lux) cycle, melatonin: 20 mg/kg body weight. The experiment was conducted according to the Guide for the Care and Use of Experimental Animals published by the Animal Welfare Committee of the Agricultural Research Organization of China Agricultural University (Approval number: AW92303202-2-2).

2.2 Immunohistochemical staining

Iba1 antibody that was resistant to rabbits was incubated overnight on paraffin slices of the mouse hippocampus (1:500, ab178846, Abcam). On the second day, the sections were cleaned with PBS and incubated for 2 hours with biotinylated goat anti-rabbit immunoglobulin G (IgG, 1:100, A0277, Beyotime, Shanghai, China). Following washing, the tissue would be processed for 1.5 h at room temperature using streptavidin-horseradish peroxidase (1:300, A0303. Beyotime in Shanghai, China). Finally, DAB was used to observe the color development. A termination reaction was triggered by a positive signal. The slide was then sealed and the nucleus stained with hematoxylin. Utilizing a microscope (BX51, Olympus, Tokyo, Japan), the location and distribution of immunoreactive chemicals inside the hippocampal region were observed.

2.3 Real-time reverse transcription-polymerase chain reaction (RT-PCR)

The TRIzol reagent (CW0580; Vazyme, Nanjing, China) was used to extract total mRNA from liver tissues and HepG2. RevertAid First Strand cDNA Synthesis Kit (R312-01; Vazyme, Nanjing, China) was used to perform reverse transcription on the total mRNA in order to produce cDNA. AceQ qPCR SYBR Green premix (Q111-02, Vazyme, Nanjing, China) was used to perform RT-PCR amplification with chosen gene primers. The relative mRNA level of each sample was standardized to the expression level of the reference gene Gapdh after each sample was examined in triplicate. Table 1 contains a list of the RT-PCR primers.

2.4 Western blot assay

RIPA lysate (CW2333S, CWBIO) with 1% phosphatase inhibitor (CW2383S, CWBIO) and 1% protease inhibitor (CW2200S, CWBIO) was used to lyse the liver tissues and BV2 cells. The lysate was centrifuged at 12,000 g for 15 min at 4°C. Using a protein assay kit (CW0014, CWBIO), the supernatant's protein concentration was measured. Subsequently, the proteins were loaded onto an 8%–12% gradient polyacrylamide gel, electrophoretically transferred to a PVDF membrane (Millipore, Billerica, MA, United States), and primed for incubation with

TABLE 1 Primers used for real-time PCR analysis and expected product length.

Gene	Accession no.	Primer sequence (5′to 3′)		Length (bp)
mIl-1β	NM_008361.4	F: TGCCACCTTTTGACAGTGATG	R: TGATGTGCTGCTGCGAGATT	138
mTnf-a	NM_013693.3	F: CCACGTCGTAGCAAACCAC	R: TTGAGATCCATGCCGTTGGC	90
mIl-4	NM_021283.2	F: CTCGAATGTACCAGGAGCCAT	R: ACTCTCTGTGGTGTTCTTCGTT	153
mIl-10	NM_009716.3	F: GCATGGCCCAGAAATCAAGG	R: ACACCTTGGTCTTGGAGCTTATTA	226
mCd86	NM_019388.3	F: ATGGACCCCAGATGCACCAT	R: CCAGCTCACTCAGGCTTATGT	260
mCd206	NM_008625.2	F: TCAGCTATTGGACGCGAGG	R: TGAGAATCTGACACCCAGCG	144
mCxcl1	NM_008176.3	F: ACTGCACCCAAACCGAAGTC	R: TGGGGACACCTTTTAGCATCTT	114
mCxcl2	NM_009140.2	F: TGCCGGCTCCTCAGTGCT	R: GCCTTGCCTTTGTTCAGTATCTTTTG	281
mGapdh	NM_001289726.2	F: ACTCAGGAGAGTGTTTCCTCG	R: TGAAGGGGTCGTTGATGGC	140

F = forward primer; R = reverse primer.

primary antibodies (P-P65, 1:1,000, TP56372, Abmart; CD80, 1:1,000, 66406-1-Ig, Proteintech; NLRP3, 1:1,000, TD7438, Abmart; β-actin, 1:8,000, 66009-1-Ig, Proteintech). The membranes were rinsed with TBST and treated for 1.5 h with horseradish peroxidase-conjugated goat anti-rabbit IgG (1:8,000; CW0103, COWIN) or goat anti-mouse IgG (1:8,000; CW0102, COWIN). The embossed bands were scanned and examined, and the IOD was calculated using ImageJ (Scion Corp., Frederick, MD, United States). The relative protein level in the Ctrl group *in vivo* or in the control cells *in vitro* was defined as 100%. The protein level was adjusted to the density ratio of β-actin.

2.5 Double labeling immunofluorescence

Primary antibody against CD80 (1:500, 66406-1-IG, Proteintech) was incubated overnight at 4°C on paraffin slices of the hippocampus and BV2 cell slides. After rinsing the slices in PBS, they were incubated for 2 hours at room temperature with anti-mouse Alexa Fluor 488 (1:300, P0188, Beyotime). After 30 min of room temperature incubation with 5% goat serum, sections were left overnight at 4°C to be exposed to rabbit Iba1 primary antibody (1:1,000, ab178846, Abcam). After that, the slices were cleaned in PBS and left to incubate for 2 hours at room temperature with the anti-rabbit Alexa Fluor 594 (1:300, P0179, Beyotime). Finally, DAPI (1 μg/mL, C0065, Solarbio, Beijing, China) is used to stain the nuclei for 15 min. Utilizing a microscope (BX51, Olympus, Tokyo, Japan), the distribution and position of immunoreactive materials in microglia were examined.

2.6 Cell culture and treatment

The BV2 cells were grown at 37°C with 5% CO2 in high-glucose DMEM supplemented with 10% fetal bovine serum (FBS) and 1% penicillin/streptomycin. Prior to receiving medication, the cells were cultured for 6 hours in complete culture medium (DMEM) containing 10% FBS after being injected into either six- or 96-well plates. Following that, the cells were cultured for 12 h in DMEM (base medium) without FBS. The MT1-selective melatonin receptor antagonist Luzindole (HY-101254; MCE, China), the MT2-selective melatonin receptor antagonist 4P-PDOT (HY-100609; MCE, China), and the corticosterone (HY-B1618; MCE, China) were all individually dissolved in DMSO. Melatonin (M5250; Sigma, United States) should be dissolved in anhydrous ethanol. The cells were treated with corticosterone (5 μM) for 12 h, then pretreated with Luzindole (1 μM) and 4P-PDOT (1 μM) for 30 min, respectively, and then treated with Melatonin (200 nM) for 12 h. The protein content was evaluated on a 6-well plate. HT22 cell activity was measured with CCK8. First, for a whole day, BV2 cells were treated to 200 nM melatonin and 5 μM corticosterone. After centrifuging the cells for 10 min at 1,000 rpm to eliminate cell precipitation, HT22 cells were treated with the culture media that was left over. After being injected into 96-well plates, the HT22 cells were grown for 6 hours in complete media and 12 hours in basic medium. The HT22 cells were then given a 24-h treatment with BV2 media. Lastly, the CCK8 assay was used to evaluate cell viability.

2.7 Statistical analysis

SPSS version 25.0 (IBM Corp., Armonk, NY, United States) was used to analyze the data, and the results were presented as means ± standard errors. To statistically analyze the group differences, One-way ANOVA was employed. A criterion of $p < 0.05$ was established for statistical significance.

3 Results

3.1 Melatonin can reduce hippocampal neuroinflammation in mice exposed to dim blue light at night

First, to examine the potential impact of melatonin on hippocampal neuroinflammation induced by dim light at night, we quantified the number of CA1, CA3, and DG microglia in the hippocampus of mice across various groups (LD, dBL, and dBL + Melatonin groups). The results showed that the number of microglia

10.3389/fphar.2024.1416350

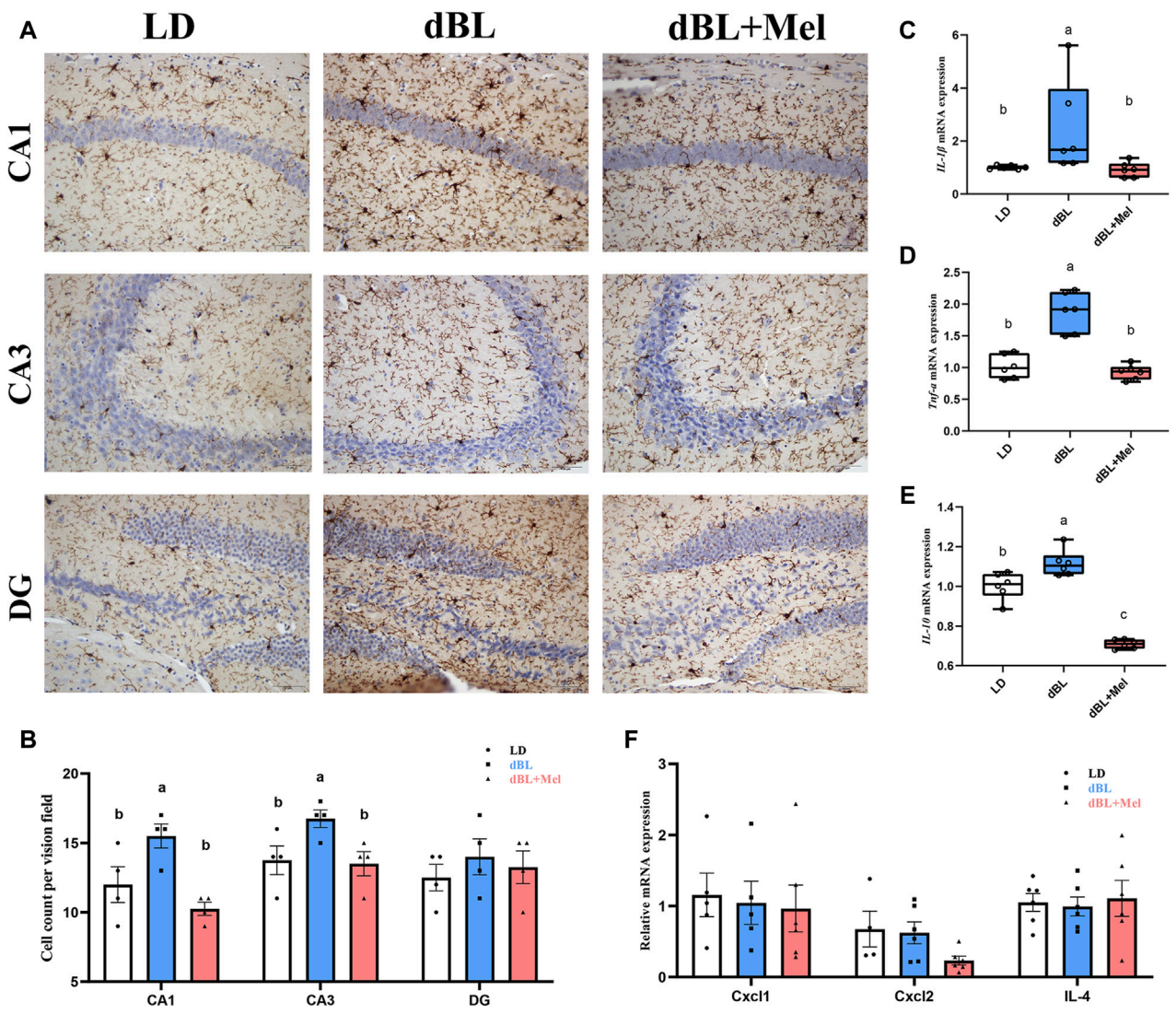


FIGURE 1
Melatonin can reduce hippocampal neuroinflammation in mice exposed to dim blue light at night. **(A)** Immunohistochemistry of mouse hippocampal microglia in different groups. **(B)** The number of microglia in CA1, CA3 and DG regions of mouse hippocampus. **(C–F)** The mRNA levels of IL-1β, TNF-α, Il-10, Cxcl1, Cxcl2, and Il-4 (n = 6). The outcome is the mean ± standard error of the mean. Values (a,b,c and d) without a common superscript letter differ significantly at $p < 0.05$, but values (a,b and c) with the same letter do not differ significantly at $p \geq 0.05$. LD, dark at night; dBL, dim blue light at night; Mel, Melatonin.

in CA1 and CA3 regions of hippocampus in melatonin group was significantly reduced by 23.87% (p = 0.002) and 19.40% (p = 0.023), respectively, compared with dBL group (Figure 1B). The occurrence of inflammation is often accompanied by the release of inflammatory factors. Therefore, we detected changes in the mRNA levels of IL-1β, TNF-α, IL-4, and IL-10 in the hippocampus of mice. The results showed that the mRNA expression levels of IL-1β, TNFα, and IL-10 were significantly increased by 423% (p = 0.041), 118% (p = 0.001), and 39.3% (p = 0.008), respectively, compared with the LD group (Figures 1C–E). After melatonin treatment, the increase in inflammatory factors induced by blue light was significantly inhibited. Specifically, IL-1β, TNFα, and IL-10 were reduced by 75.7% (p = 0.044), 50.9% ($p < 0.001$), and 40.7% ($p < 0.001$), respectively (Figures 1C–E). The mRNA levels of Cxcl1, Cxcl2, and IL4 did not show significant differences between the groups (Figure 1F).

3.2 Melatonin improved the loss of hippocampal neurons in mice exposed to dim blue light

The hippocampus is a crucial structural component for learning and memory functions in mice, and the decline in these functions is frequently linked to neuronal loss. Overactivation of microglia impairs the morphology and function of neurons. Next, we examined the effects of melatonin on hippocampal neuron density in mice. Mouse Nissl staining is shown in Figure 2A. Compared with the LD group, the density of neurons in the hippocampal CA3 region decreased by 10.60% (p = 0.001) in the dBL group. The loss of hippocampal neurons in the dBL group may be the result of overactivation of microglia. The neuronal density in the CA1 and CA3 regions of the hippocampus in the melatonin

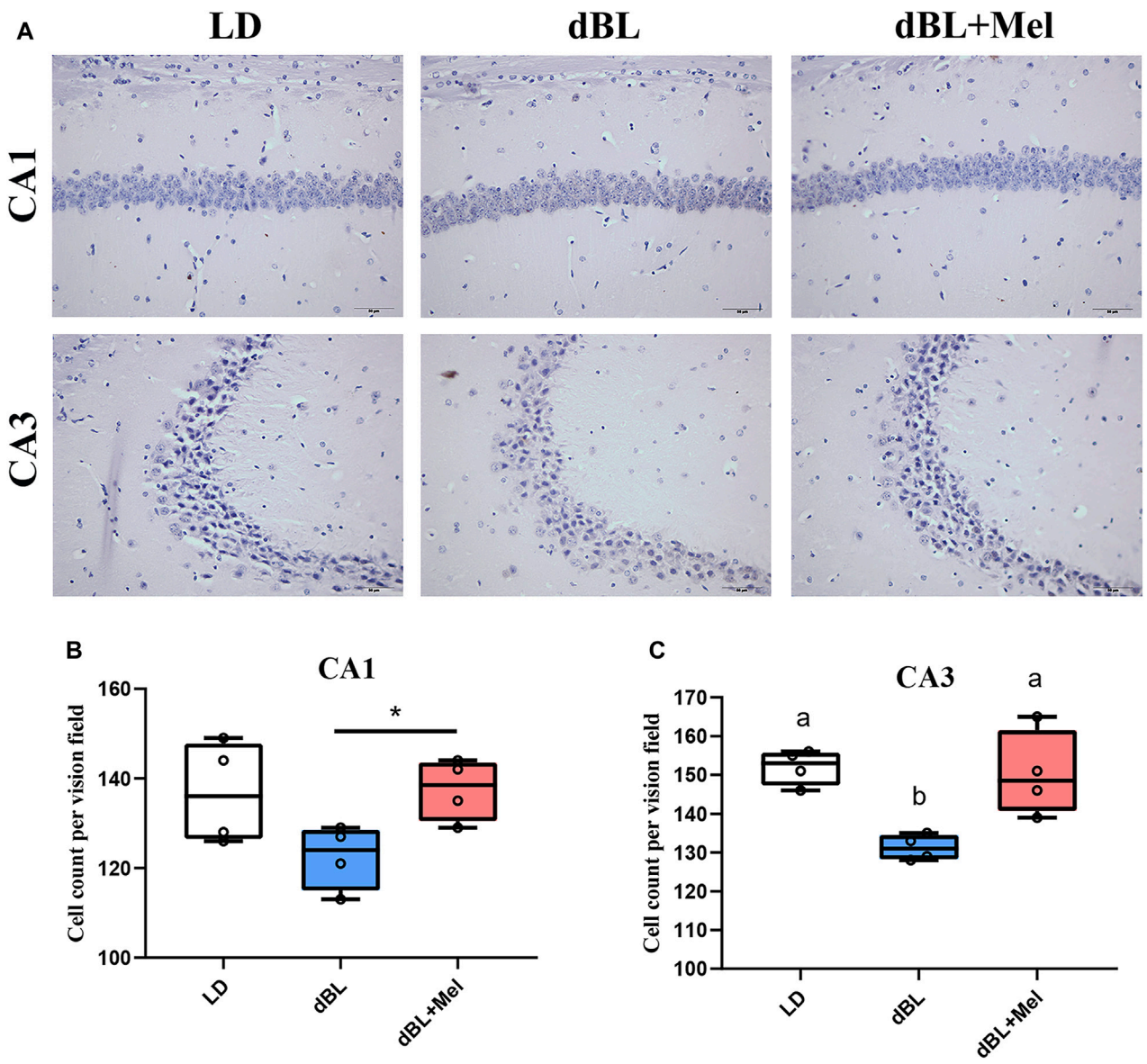


FIGURE 2
Melatonin improved the loss of hippocampal neurons in mice exposed to dim blue light. **(A)** Nith staining of mouse hippocampus. **(B)** Neuron density in the CA1 region of the mouse hippocampus. **(C)** Neuron density in the CA3 region of the mouse hippocampus. The outcome is the mean ± standard error of the mean. Values (a,b,c and d) without a common superscript letter differ significantly at $p < 0.05$, but values (a,b and c) with the same letter do not differ significantly at $p \geq 0.05$. LD, dark at night; dBL, dim blue light at night; Mel, Melatonin.

treatment group was significantly increased by 11.57% ($p = 0.023$) and 13.53% ($p = 0.016$), respectively, compared with the dBL group.

3.3 Melatonin regulates hippocampal inflammation by inhibiting the activation of microglia

As the primary line of immune defense in the central nervous system, microglia play a crucial role in the inflammatory response. The activation of microglia *in vivo* is accompanied by significant morphological changes. Our staining results revealed that the cell bodies of hippocampal microglia in the dBL group were enlarged, and the number of branches was significantly reduced. This suggests that exposure to dark blue light at night significantly enhances the activation of hippocampal microglia. However, melatonin supplementation significantly mitigated the blue light-induced morphological changes in microglia (Figure 3A). In addition, we demonstrated the expression of the M1-type marker CD80 on hippocampal microglia using dual immunofluorescence labeling. Immunofluorescence results showed that the expression of CD80 in the microglia of the mouse hippocampus was significantly increased in the blue light group (Figure 3B). Melatonin supplementation reversed the expression of CD80 on microglia, suggesting that melatonin could effectively inhibit the activation of microglia caused by blue light, thereby reducing the level of inflammation in the hippocampus of mice.

10.3389/fphar.2024.1416350

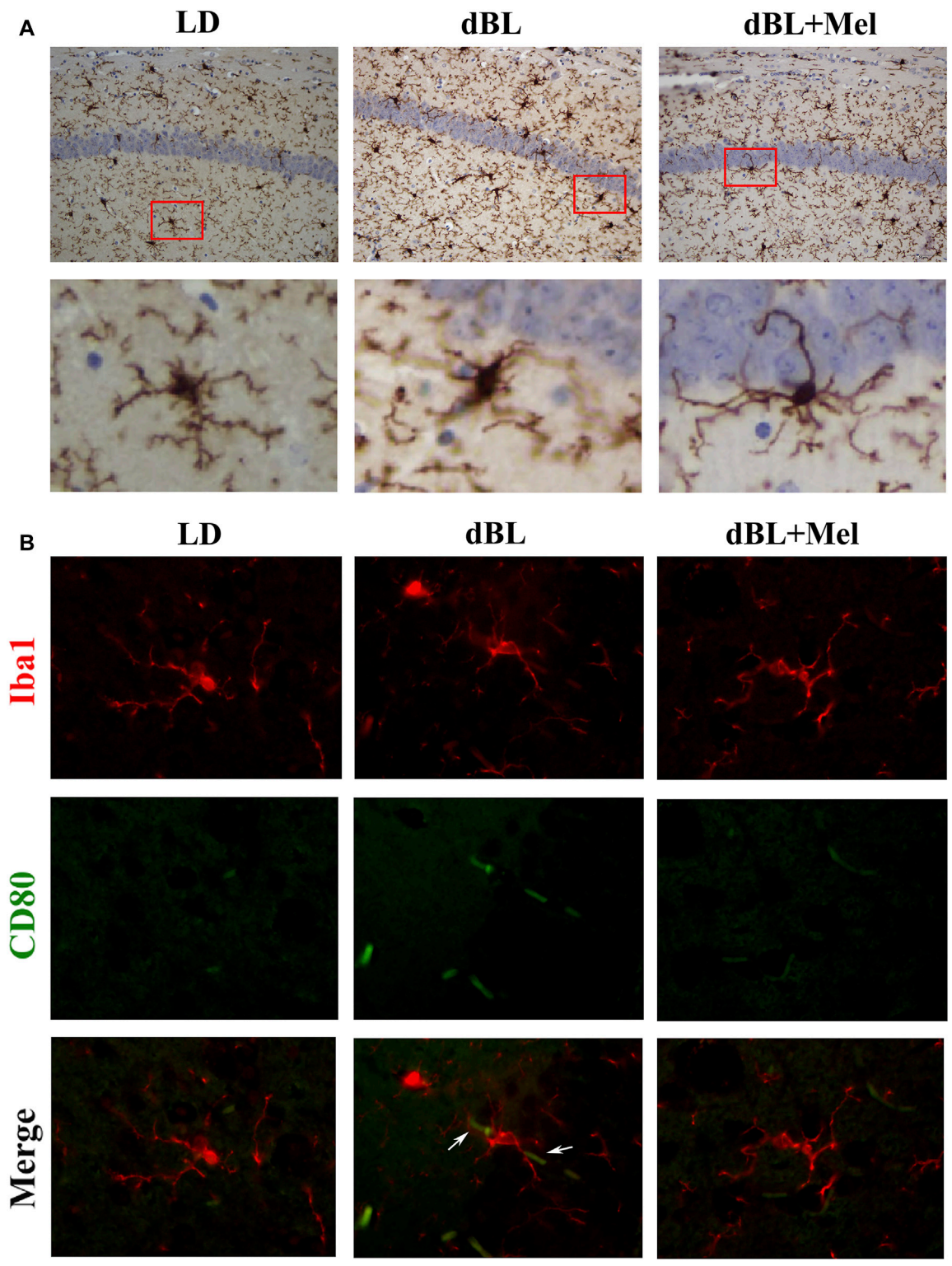


FIGURE 3
Melatonin regulates hippocampal inflammation by inhibiting the activation of microglia. **(A)** Immunohistochemical diagram of microglia in different groups. **(B–G)** Fluorescence colocalization of CD80 and Iba1 in the mouse hippocampus. Red fluorescent label Iba1 (594 nm) and green fluorescent label CD80 (488 nm). LD, dark at night; dBL, dim blue light at night; Mel, Melatonin.

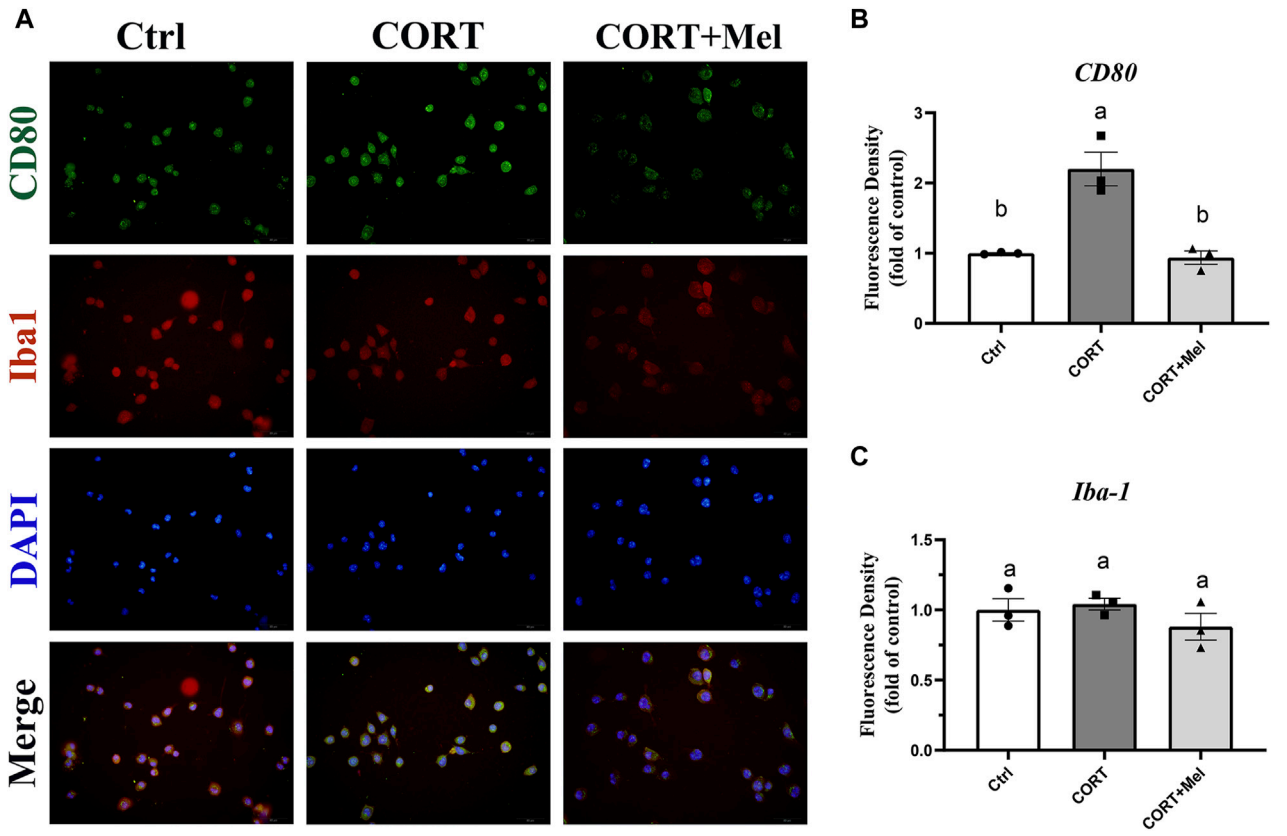


FIGURE 4
Melatonin inhibits the M1-type activation of BV2 cells induced by corticosterone. **(A)** Immunofluorescence localization of Iba1 and CD80 in BV2 cells, red fluorescence labeled Iba1 (594 nm), green fluorescence labeled CD80 (488 nm), and DAPI labeled nucleus. **(B,C)** Fluorescence intensity analysis of CD80 and Iba1 (n = 3). The outcome is the mean ± standard error of the mean. Values (a,b,c and d) without a common superscript letter differ significantly at $p < 0.05$, but values (a,b and c) with the same letter do not differ significantly at $p \geq 0.05$. CORT, corticosterone; Mel, Melatonin.

3.4 Melatonin inhibits the M1-type activation of BV2 by inhibiting the activation of NF-kB and NLRP3

After determining the regulatory effect of melatonin on microglia in mice, we continued our investigation of melatonin's role using the BV2 cell line. We simulated the effects of blue light on microglia by stimulating BV2 cells with corticosterone. Our previous results showed that exposure to dim blue light at night significantly increased plasma corticosterone levels and activated hippocampal microglia (Liu et al., 2022). BV2 cells were labeled with Iba1, and then the expression of CD80 was quantified after various treatments (Figure 4A). The results showed that corticosterone and melatonin treatment had no significant effect on the fluorescence intensity of Iba1 in BV2 cells (Figure 4C). However, the fluorescence intensity of CD80 was significantly enhanced after corticosterone treatment, indicating that corticosterone promoted the activation of BV2 cells to the M1 type (Figure 4B). After melatonin supplementation, the expression of CD80 was significantly reduced. This suggests that melatonin may regulate corticosterone-induced BV2 cell inflammation by decreasing the M1-type activation of microglia. We treated BV2 cells with corticosterone and melatonin, as shown in Figure 5A, and then detected the protein expression of CD80, p-P65, and NLRP3. The results showed that the expression of CD80 (56%, $p = 0.018$), PP65 (96.6%, $p = 0.026$), and NLRP3 (43.6%, $p = 0.036$) in BV2 cells significantly increased after corticosterone stimulation (Figures 5B–E). Melatonin can significantly inhibit the activation of NF-kB/NLRP3. The protein levels of p-p65 and NLRP3 in BV2 cells supplemented with melatonin are significantly downregulated compared to the corticosterone group (Figures 5B–E).

3.5 The viability of HT22 cells was significantly improved by adding BV2 culture medium exposed to melatonin

The interaction between microglia and neurons plays a key role in maintaining brain health. Therefore, we proceeded to culture HT22 cells in BV2's medium to investigate the various effects of microglia on neurons (Figure 6A). First, the results of the CCK-8 assay showed that the cell activity of HT22 was significantly inhibited (29.16%, $p < 0.001$) in BV2 culture containing corticosterone (Figure 6B). In addition, the number of HT22 cells attached to the wall was significantly reduced in the corticosterone group (Figure 6C). The activity of HT22 cells in the melatonin treatment group significantly increased by 30.27% ($p < 0.001$) compared to the cells in the CORT group (Figure 6B).

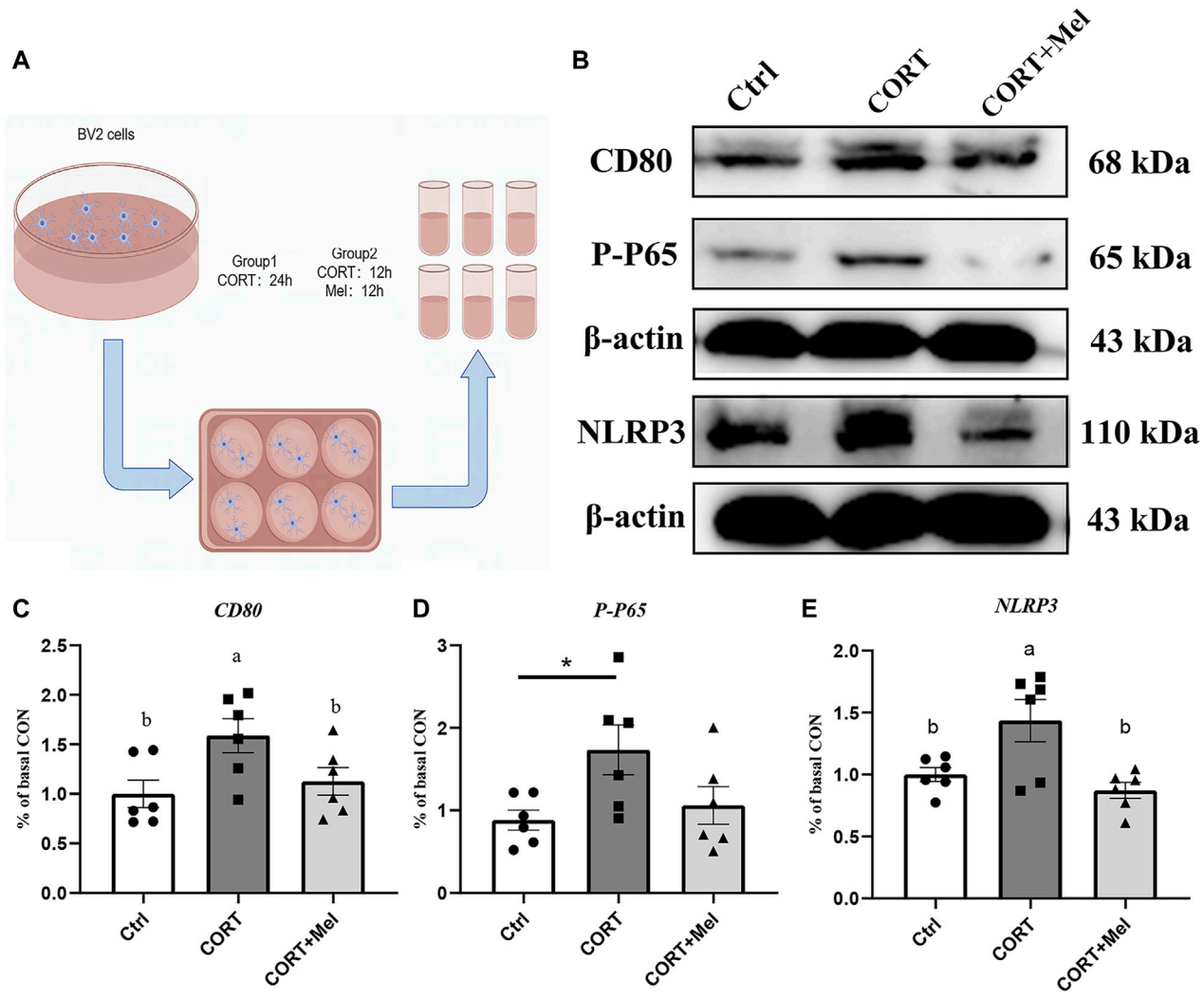


FIGURE 5
Melatonin reduces M1-type activation of BV2 by inhibiting the activation of NF-kB and NLRP3. **(A)** Schematic diagram of *in vitro* test. **(B–E)** Relative protein levels of CD80, P-P65, and NLRP3 in hippocampus (n = 6). The outcome is the mean ± standard error of the mean. Values (a,b,c and d) without a common superscript letter differ significantly at $p < 0.05$, but values (a,b and c) with the same letter do not differ significantly at $p \geq 0.05$. CORT, corticosterone; Mel, Melatonin.

3.6 Melatonin inhibits the activation of BV2 through MT2 and reduces the occurrence of inflammation

To explore the pathway of melatonin action, we added MT1 and MT2 receptor blockers, Luzindole and 4-P-PDOT, to BV2 cells, respectively. First, mRNA levels of IL-1β, TNF-α, and CD86 in BV2 cells were significantly reduced, and mRNA expression of IL-10 was significantly increased after melatonin treatment compared with the corticosterone-stimulated group (IL-1β, 44.25%, $p = 0.006$; TNF-α, 27.54%, $p < 0.001$; Cd86, 47.56%, $p = 0.001$; IL-10, 36.05%, $p = 0.018$; Figures 7A–D). The mRNA levels of IL-1β and Cd86 significantly increased after 4-P-PDOT was added to BV2 cells compared to the melatonin treatment group (IL-1β, 64.95%, $p = 0.013$; Cd86, 76.16%, $p = 0.001$). When luzindole was added to BV2 cells, there was no significant effect on the action of melatonin. This suggests that melatonin can influence the activation of microglia to M1 type through MT2 receptors.

4 Discussion

Nighttime exposure to artificial lighting (Dim Light at Night) and shift work have been shown to disrupt normal physiological activities in the brain and body (González, 2018). The study discovered that dLAN of 5 lux influences neuronal dendritic shape in the CA1 and DG areas of the hippocampus, influencing learning and memory function (Fonken et al., 2012). Recent studies have shown that dim light at night can trigger an inflammatory response in the central nervous system (Chen et al., 2021; Liu et al., 2022). Microglia are a type of glial cell, which constitutes the central nervous system's most crucial immune defense line. Microglia perform essential functions, such as environmental perception and protection against internal and external stimuli. Thus, microglia play an important role in maintaining brain homeostasis and synaptic function, depending on the balance between the M1 and M2 phenotypes of microglia (Rasia-Filho

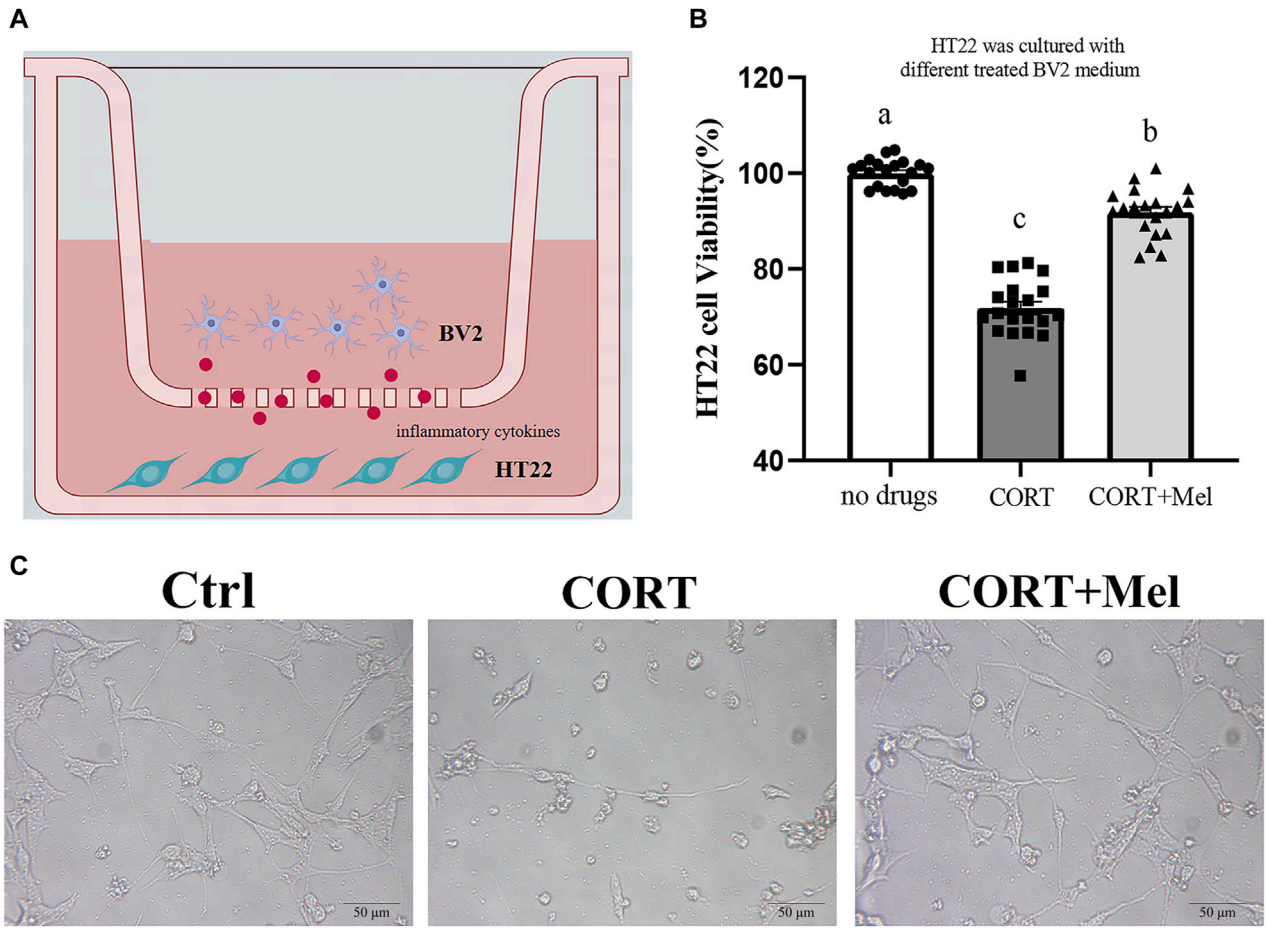


FIGURE 6
The viability of HT22 cells was significantly improved by adding BV2 culture medium exposed to melatonin. **(A)** Schematic diagram of *in vitro* test. **(B)** The CCK8 method was used to detect the activity of HT22 cells exposed to different BV2 medium (n = 20). **(C)** Photomicrograph of HT22 cells treated with different BV2 medium. The outcome is the mean ± standard error of the mean. Values (a,b,c and d) without a common superscript letter differ significantly at $p < 0.05$, but values (a,b and c) with the same letter do not differ significantly at $p \geq 0.05$. CORT, corticosterone; Mel, Melatonin.

et al., 2023). Overactivation of microglia can lead to dysregulation of synaptic plasticity and neurotoxicity. Age and sex factors also appear to influence the effects of nighttime dim light on the neuroinflammation. Chen et al.'s study showed that adolescent mice exposed to nighttime light exhibited higher levels of pro-inflammatory factors in the hippocampus. Female mice were found to be more susceptible to nighttime dim light than male mice (Chen et al., 2021). Light information includes light intensity, duration, and wavelength. Our previous studies demonstrated the influence of light wavelength factors on the hippocampal inflammatory response in mice. Under dWL and dBL conditions, the density of CA3 and CA1 neurons in the mice hippocampus significantly decreased, while the number and activation of microglia in the hippocampus significantly increased, leading to oxidative stress and neuroinflammation (Liu et al., 2022). Furthermore, several studies have indicated that Dim Light at Night changes the inflammatory response in mice, particularly by boosting the expression of pro-inflammatory cytokines in microglia (Fonken et al., 2013a; Fonken et al., 2013b). Given the exacerbating effect of dim light on neuroinflammation at night, it is critical to find a solution. Melatonin, which is secreted by the pineal gland, has anti-inflammatory, antioxidant, and antidepressant effects, making it thought to offer significant therapeutic potential for neurodegenerative illnesses (Xu et al., 2020). Melatonin is an essential regulator of neuroinflammation. Tahir Ali et al. found that melatonin reduces LPS-induced activation of astrocytes and microglia while improving neuroinflammation (Ali et al., 2020). Our study discovered that melatonin can reduce the level of hippocampal inflammation caused by dBL, diminish the expression of CD80 in microglia, and block the activation of microglia.

Corticosterone is a hormone that is secreted rhythmically and is easily influenced by light. The Dim Light at Night can affect corticosterone secretion, and this effect is related to the species and the lighting conditions used, such as light wavelength, light intensity, etc (Rumanova et al., 2020). In previous studies, plasma corticosterone levels in mice were significantly increased under constant light at night with white light (dWL) and constant light at night with blue light (dBL). Corticosterone was found to activate BV2 cells, leading to the expression of pro-inflammatory cytokines and proteins (Liu et al., 2022). Recent studies have confirmed that corticosterone is involved in stress-induced neuroinflammatory responses, thus playing a significant role in the pathogenesis of

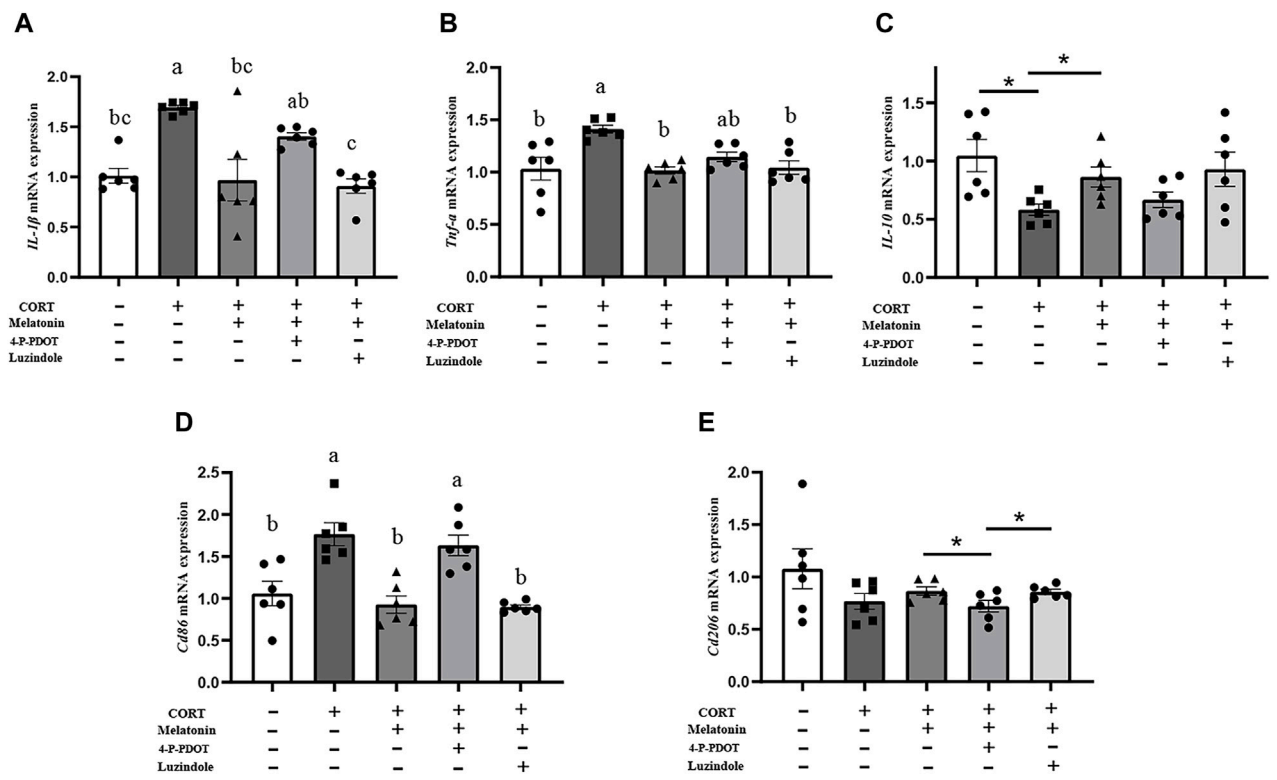


FIGURE 7
Melatonin inhibits the activation of BV2 through MT2 and reduces the occurrence of inflammation. **(A–E)** The mRNA levels of IL-1β, TNF-α, IL-10, Cd86, and Cd206 in BV2 cells treated with CORT, Meltonin, Luzindole, and 4-P-PDOT (n = 6). The outcome is the mean ± standard error of the mean. Values (a,b,c and d) without a common superscript letter differ significantly at $p < 0.05$, but values (a,b and c) with the same letter do not differ significantly at $p \geq 0.05$. CORT, corticosterone, Mel, Melatonin; Luzindole, MT1 receptor blockers; 4-P-PDOT, MT2 receptor blockers.

diseases like depression and post-traumatic stress disorder. For example, Bin Xu et al. demonstrated that corticosterone can activate the MAPK signaling pathway in microglia in the dentate gyrus (DG) region of the hippocampus in mice, promoting the pro-inflammatory activation of microglia (Xu et al., 2019). Nod-like receptor protein 3 (NLRP3) inflammasome is expressed in microglia and plays a crucial role in the release of proinflammatory factors from microglia. It is able to activate caspase-1 to produce inflammatory factors such as IL-1β (Dong et al., 2020). Feng et al. found that glucocorticoids can increase NF-kB nuclear transcription in hippocampal microglia, which then activates the NLRP3 inflammasome, disrupting the homeostasis of hippocampal microglia (Feng et al., 2019). Therefore, *in vitro* experiments, we used corticosterone to stimulate BV2 cells to mimic the effects of dark blue light at night on hippocampal microglia. The results showed that the expressions of CD80, pp65, and NLRP3 in BV2 cells significantly increased after corticosterone treatment. This indicates that corticosterone effectively stimulated the activation of microglia by activating the NLRP3 inflammasome through NF-kB signaling. This indicates that our method of modeling BV2 cells with corticosterone stimulation *in vitro* is feasible. It has been reported that microglial activation induces neuronal cell death through the overexpression of pro-inflammatory mediators, leading to neuronal disorder and death (Jebelli et al., 2014). Melatonin regulates the state of microglia to protect hippocampal neurons, a finding that was also confirmed in our study. We found that treating the BV2 cell culture medium with melatonin significantly increased the cell viability of HT22 cells. Unfortunately, we did not detect the expression of inflammatory factors in the BV2 cell culture.

The regulatory effect of melatonin on NF-kB and NLRP3 in BV2 cells has been confirmed in several studies. For example, melatonin preconditioning attenuates manganese and LPS-induced NF-kB activation and reduces the expression of iNOS and nitric oxide (NO) in BV2 cells (Park and Chun, 2017). Tang et al. showed that melatonin therapy improved the activation of the NLRP3 inflammasome in thrombine-induced activated BV2 cells, and that this improvement was associated with a reduction in ROS production (Tang et al., 2020). We investigated the impact of melatonin on corticosterone-induced microglia activation and observed that the inclusion of melatonin in BV2 cells significantly decreased corticosterone-induced inflammation. This reduction was evident in the decreased expression of inflammatory proteins PP65, NLRP3, and the M1 marker CD80 in microglia. This suggests that melatonin may reduce NF-kB transcription and control the activation of the NLRP3 inflammasome to improve the overactivation of microglia by corticosterone. In addition, Zheng Ran et al. reported that melatonin can reduce MPTP-induced microglial activation, inhibit the activity of the NLRP3 inflammasome, and suppress IL-1β secretion (Zheng et al., 2021). Melatonin treatment significantly inhibited sleep deprivation (SD)-induced hippocampal NF-κB activation and the

production of pro-inflammatory cytokines, demonstrating anti-inflammatory effects (Wang et al., 2021). These studies suggest that melatonin is involved in the activation of microglia NF-kB signaling pathway and NLRP3, influencing microglia polarization to control brain inflammation.

At present, there are few reports on how melatonin regulates microglia. Melatonin is a pleiotropic molecule that exerts various physiological effects primarily through receptor-dependent signaling cascades. The main membrane receptors for melatonin are MT1 and MT2, which are G-protein-coupled receptors. Gao Yuan et al. indicated that melatonin alleviates inflammation-mediated brain edema and neurological deficits by activating the MT2/IL-33/*F*th pathway (Gao et al., 2023). In another study, pretreatment with 100 nM melatonin prevented the overexpression of TNF-α induced by methamphetamine exposure. Conversely, the anti-inflammatory effects of melatonin were eliminated when MT2 was knocked down using siRNA (Wongprayoon and Govitrapong, 2015). Our results showed that melatonin could significantly improve the secretion of corticosterone-induced inflammatory factors in BV2 cells. However, the beneficial effect of melatonin was no longer observed after the addition of the MT2 receptor blocker 4-P-PDOT. This suggests that melatonin alleviated corticosterone-induced activation of BV2 cells primarily through MT2 receptors. A study has also shown that the effects of melatonin on microglia are primarily receptor-mediated and partly dependent on SIRT1 activation (Merlo et al., 2023). It can be seen that the receptor action pathway of melatonin is crucial for regulating microglia polarization.

In summary, this study showed that melatonin alleviates nocturnal blue-induced hippocampal neuroinflammation by modifying phenotypic markers of microglia, thereby reducing neuronal damage. Melatonin regulates microglial activation towards the M1 proinflammatory type through the NF-kB - NLRP3 pathway, and MT2 plays a crucial role in the modulation of microglial polarization. This finding reflects the beneficial role of Mel-MT2 in regulating microglia polarization, offering new insights into the management of nerve disorders triggered by light pollution, such as dim light at night. However, there are also limitations in this study. First, we only analyzed the role of melatonin from the perspective of the receptor pathway. Whether the non-receptor pathway of melatonin also has the ability to regulate microglia polarization remains to be clarified. Second, this study only investigated the effects of melatonin on microglia in the hippocampus. Studies have shown that light not only affects the activation of microglia in the hippocampus but also has an effect on microglia in the basolateral amygdala (BLA), anterior cingulate cortex (ACC), and other brain regions (Costello A et al., 2023). Therefore, whether melatonin can improve neuroinflammation in these brain regions remains to be studied. Third, this experiment uses rodents as test models, and it is important to consider species differences when translating *in vivo* and *in vitro* test results to humans.

Data availability statement

The raw data supporting the conclusion of this article will be made available by the authors, without undue reservation.

Ethics statement

The animal study was approved by Animal Welfare Committee of the Agricultural Research Organization of China Agricultural University (Approval number: AW92303202-2-2). The study was conducted in accordance with the local legislation and institutional requirements.

Author contributions

CS: Writing–original draft, Validation, Methodology, Data curation, Conceptualization. ZS: Methodology, Writing–original draft, Validation, Data curation, Conceptualization. ZW: Supervision, Resources, Project administration, Writing–original draft. JC: Writing–original draft, Supervision. YD: Writing–original draft, Supervision. YC: Writing–original draft, Validation, Funding acquisition, Data curation, Conceptualization.

Funding

The author(s) declare that financial support was received for the research, authorship, and/or publication of this article. This work was supported by the Chinese National Natural Science Foundation (32372954, 32172801) and the Beijing Natural Science Foundation (6222019).

Conflict of interest

The authors declare that the research was conducted in the absence of any commercial or financial relationships that could be construed as a potential conflict of interest.

Publisher's note

All claims expressed in this article are solely those of the authors and do not necessarily represent those of their affiliated organizations, or those of the publisher, the editors and the reviewers. Any product that may be evaluated in this article, or claim that may be made by its manufacturer, is not guaranteed or endorsed by the publisher.

References

Ali, T., Rahman, S. U., Hao, Q., Li, W., Liu, Z., Ali Shah, F., et al. (2020). Melatonin prevents neuroinflammation and relieves depression by attenuating autophagy impairment through FOXO3a regulation. *J. Pineal Res.* 69, e12667. doi:10.1111/jpi.12667

Calvo-Sanz, J. A., and Tapia-Ayuga, C. E. (2020). Blue light emission spectra of popular mobile devices: the extent of user protection against melatonin suppression by built-in screen technology and light filtering software systems. *Chronobiol Int.* 37, 1016–1022. doi:10.1080/07420528.2020.1781149

Chen, R., Weitzner, A. S., McKennon, L. A., and Fonken, L. K. (2021). Light at night during development in mice has modest effects on adulthood behavior and neuroimmune activation. *Behav. Brain Res.* 405, 113171. doi:10.1016/j.bbr.2021.113171

Costello, A., Linning-Duffy, K., Vandenbrook, C., Lonstein, J. S., and Yan, L. (2023). Daytime light deficiency leads to sex- and brain region-specific neuroinflammatory responses in a diurnal rodent. *Cell Mol. Neurobiol.* 43, 1369–1384. doi:10.1007/s10571-022-01256-x

Dong, Y., Li, S., Lu, Y., Li, X., Liao, Y., Peng, Z., et al. (2020). Stress-induced NLRP3 inflammasome activation negatively regulates fear memory in mice. *J. Neuroinflammation* 17, 205. doi:10.1186/s12974-020-01842-0

Feng, X., Zhao, Y., Yang, T., Song, M., Wang, C., Yao, Y., et al. (2019). Glucocorticoid-driven NLRP3 inflammasome activation in hippocampal microglia mediates chronic stress-induced depressive-like behaviors. *Front. Mol. Neurosci.* 12, 210. doi:10.3389/fnmol.2019.00210

Fonken, L. K., Kitsmiller, E., Smale, L., and Nelson, R. J. (2012). Dim nighttime light impairs cognition and provokes depressive-like responses in a diurnal rodent. *J. Biol. Rhythms* 27, 319–327. doi:10.1177/0748730412448324

Fonken, L. K., Lieberman, R. A., Weil, Z. M., and Nelson, R. J. (2013a). Dim light at night exaggerates weight gain and inflammation associated with a high-fat diet in male mice. *Endocrinology* 154, 3817–3825. doi:10.1210/en.2013-1121

Fonken, L. K., Weil, Z. M., and Nelson, R. J. (2013b). Mice exposed to dim light at night exaggerate inflammatory responses to lipopolysaccharide. *Brain Behav. Immun.* 34, 159–163. doi:10.1016/j.bbi.2013.08.011

Gao, Y., Wang, T., Cheng, Y., Wu, Y., Zhu, L., Gu, Z., et al. (2023). Melatonin ameliorates neurological deficits through MT2/IL-33/ferritin H signaling-mediated inhibition of neuroinflammation and ferroptosis after traumatic brain injury. *Free Radic. Biol. Med.* 199, 97–112. doi:10.1016/j.freeradbiomed.2023.02.014

González, M. M. C. (2018). Dim light at night and constant darkness: two frequently used lighting conditions that jeopardize the health and well-being of laboratory rodents. *Front. Neurol.* 9, 609. doi:10.3389/fneur.2018.00609

Guo, Y. L., Wei, X. J., Zhang, T., and Sun, T. (2023). Molecular mechanisms of melatonin-induced alleviation of synaptic dysfunction and neuroinflammation in Parkinson's disease: a review. *Eur. Rev. Med. Pharmacol. Sci.* 27 (11), 5070–5082. doi:10.26355/eurrev_202306_32624

Hardeland, R. (2021). Melatonin and microglia. *Int. J. Mol. Sci.* 22 (15), 8296. doi:10.3390/ijms22158296

Jebelli, J., Hooper, C., and Pocock, J. M. (2014). Microglial p53 activation is detrimental to neuronal synapses during activation-induced inflammation: implications for neurodegeneration. *Neurosci. Lett.* 583, 92–97. doi:10.1016/j.neulet.2014.08.049

Liu, Q., Wang, Z., Cao, J., Dong, Y., and Chen, Y. (2022). Dim blue light at night induces spatial memory impairment in mice by hippocampal neuroinflammation and oxidative stress. *Antioxidants (Basel)* 11, 1218. doi:10.3390/antiox11071218

Merlo, S., Caruso, G. I., Korde, D. S., Khodorovska, A., Humpel, C., and Sortino, M. A. (2023). Melatonin activates anti-inflammatory features in microglia in a multicellular context: evidence from organotypic brain slices and HMC3 cells. *Biomolecules* 13, 373. doi:10.3390/biom13020373

Park, E., and Chun, H. S. (2017). Melatonin attenuates manganese and lipopolysaccharide-induced inflammatory activation of BV2 microglia. *Neurochem. Res.* 42, 656–666. doi:10.1007/s11064-016-2122-7

Rasia-Filho, A. A., Calcagnotto, M. E., and von Bohlen Und Halbach, O. (2023). Glial cell modulation of dendritic spine structure and synaptic function. *Adv. Neurobiol.* 34, 255–310. doi:10.1007/978-3-031-36159-3_6

Rumanova, V. S., Okuliarova, M., and Zeman, M. (2020). Differential effects of constant light and dim light at night on the circadian control of metabolism and behavior. *Int. J. Mol. Sci.* 21, 5478. doi:10.3390/ijms21155478

Silvani, M. I., Werder, R., and Perret, C. (2022). The influence of blue light on sleep, performance and wellbeing in young adults: a systematic review. *Front. Physiol.* 13, 943108. doi:10.3389/fphys.2022.943108

Tang, J., Chen, R., Wang, L., Yu, L., Zuo, D., Cui, G., et al. (2020). Melatonin attenuates thrombin-induced inflammation in BV2 cells and then protects HT22 cells from apoptosis. *Inflammation* 43, 1959–1970. doi:10.1007/s10753-020-01270-5

Wang, X., Wang, Z., Cao, J., Dong, Y., and Chen, Y. (2021). Melatonin ameliorates anxiety-like behaviors induced by sleep deprivation in mice: role of oxidative stress, neuroinflammation, autophagy and apoptosis. *Brain Res. Bull.* 174, 161–172. doi:10.1016/j.brainresbull.2021.06.010

Wongprayoon, P., and Govitrapong, P. (2015). Melatonin attenuates methamphetamine-induced neuroinflammation through the melatonin receptor in the SH-SY5Y cell line. *Neurotoxicology* 50, 122–130. doi:10.1016/j.neuro.2015.08.008

Xu, B., Lang, L. M., Li, S. Z., Guo, J. R., Wang, J. F., Yang, H. M., et al. (2019). Microglia activated by excess cortisol induce HMGB1 acetylation and neuroinflammation in the hippocampal DG region of mice following cold exposure. *Biomolecules* 9, 426. doi:10.3390/biom9090426

Xu, Y., Cui, K., Li, J., Tang, X., Lin, J., Lu, X., et al. (2020). Melatonin attenuates choroidal neovascularization by regulating macrophage/microglia polarization via inhibition of RhoA/ROCK signaling pathway. *J. Pineal Res.* 69, e12660. doi:10.1111/jpi.12660

Zhao, Z. C., Zhou, Y., Tan, G., and Li, J. (2018). Research progress about the effect and prevention of blue light on eyes. *Int. J. Ophthalmol.* 11, 1999–2003. doi:10.18240/ijo.2018.12.20

Zheng, R., Ruan, Y., Yan, Y., Lin, Z., Xue, N., Yan, Y., et al. (2021). Melatonin attenuates neuroinflammation by down-regulating NLRP3 inflammasome via a SIRT1-dependent pathway in MPTP-induced models of Parkinson's disease. *J. Inflamm. Res.* 14, 3063–3075. doi:10.2147/JIR.S317672

frontiers | Frontiers in Neuroscience

TYPE Review
PUBLISHED 05 June 2024
DOI 10.3389/fnins.2024.1422912

Check for updates

OPEN ACCESS

EDITED BY
Pukar Khanal,
Emory University, United States

REVIEWED BY
Prarambh S. R. Dwivedi,
Nitte Gulabi Shetty Memorial Institute of Pharmaceutical Sciences, India
Raushan Kumar Chaudhary,
Nitte Gulabi Shetty Memorial Institute of Pharmaceutical Sciences, India

*CORRESPONDENCE
Majid S. Jabir
✉ 100131@uotechnology.edu.iq
Ghassan M. Sulaiman
✉ ghassan.m.sulaiman@uotechnology.edu.iq

RECEIVED 24 April 2024
ACCEPTED 23 May 2024
PUBLISHED 05 June 2024

CITATION
Al-kuraishy HM, Jabir MS, Sulaiman GM, Mohammed HA, Al-Gareeb AI, Albuhadily AK, Jawad SF, Swelum AA and Abomughaid MM (2024) The role of statins in amyotrophic lateral sclerosis: protective or not? *Front. Neurosci.* 18:1422912. doi: 10.3389/fnins.2024.1422912

COPYRIGHT
© 2024 Al-kuraishy, Jabir, Sulaiman, Mohammed, Al-Gareeb, Albuhadily, Jawad, Swelum and Abomughaid. This is an open-access article distributed under the terms of the Creative Commons Attribution License (CC BY). The use, distribution or reproduction in other forums is permitted, provided the original author(s) and the copyright owner(s) are credited and that the original publication in this journal is cited, in accordance with accepted academic practice. No use, distribution or reproduction is permitted which does not comply with these terms.

The role of statins in amyotrophic lateral sclerosis: protective or not?

Hayder M. Al-kuraishy[1], Majid S. Jabir[2]*, Ghassan M. Sulaiman[2]*, Hamdoon A. Mohammed[3,4], Ali I. Al-Gareeb[5], Ali K. Albuhadily[1], Sabrean F. Jawad[6], Ayman A. Swelum[7] and Mosleh M. Abomughaid[8]

[1]Department of Clinical Pharmacology and Medicine, College of Medicine, Mustansiriyah University, Baghdad, Iraq, [2]Department of Applied Sciences, University of Technology, Baghdad, Iraq, [3]Department of Medicinal Chemistry and Pharmacognosy, College of Pharmacy, Qassim University, Qassim, Saudi Arabia, [4]Department of Pharmacognosy and Medicinal Plants, Faculty of Pharmacy, Al-Azhar University, Cairo, Egypt, [5]Department of Clinical Pharmacology and Medicine, College of Medicine, Jabir Ibn Hayyan Medical University, Kufa, Iraq, [6]Department of Pharmacy, Al-Mustaqbal University College, Hillah, Iraq, [7]Department of Animal Production, King Saud University, Riyadh, Saudi Arabia, [8]Department of Medical Laboratory Sciences, College of Applied Medical Sciences, University of Bisha, Bisha, Saudi Arabia

Amyotrophic lateral sclerosis (ALS) is a progressive neurodegenerative disease of motor neurons characterized by muscle weakness, muscle twitching, and muscle wasting. ALS is regarded as the third-most frequent neurodegenerative disease, subsequent to Alzheimer's disease (AD) and Parkinson's disease (PD). The World Health Organization (WHO) in 2007 declared that prolonged use of statins may induce development of ALS-like syndrome and may increase ALS risk. Subsequently, different studies have implicated statins in the pathogenesis of ALS. In contrast, results from preclinical and clinical studies highlighted the protective role of statins against ALS neuropathology. Recently, meta-analyses and systematic reviews illustrated no association between long-term use of statins and ALS risk. These findings highlighted controversial points regarding the effects of statins on ALS pathogenesis and risk. The neuroprotective effects of statins against the development and progression of ALS may be mediated by regulating dyslipidemia and inflammatory changes. However, the mechanism for induction of ALS neuropathology by statins may be related to the dysregulation of liver X receptor signaling (LXR) signaling in the motor neurons and reduction of cholesterol, which has a neuroprotective effect against ALS neuropathology. Nevertheless, the exact role of statins on the pathogenesis of ALS was not fully elucidated. Therefore, this narrative review aims to discuss the role of statins in ALS neuropathology.

KEYWORDS

Amyotrophic lateral sclerosis, neurodegenerative diseases, pathogenesis, statins, aging

1 Introduction

Amyotrophic lateral sclerosis (ALS), also known as Lou Gehrig's disease, is a progressive neurodegenerative disease among motor neuron diseases (Verber et al., 2019; Feldman et al., 2022). Other motor neuron diseases include primary lateral sclerosis, progressive muscle atrophy, progressive bulbar palsy, monometic amyotrophy, and pseudobulbar palsy (Verber et al., 2019). ALS was first described by Charles Bell in 1824; subsequently, in 1869, Jean-Martin Charcot explained the association between

neurological disorders and the presenting feature of ALS; and the term ALS was first used by Jean-Martin Charcot in 1874 (Cho and Shukla, 2020).

ALS is the most common type of motor neuron diseases and is the third-most frequent neurodegenerative disease subsequent to Alzheimer's disease (AD) and Parkinson's disease (PD) (Bennett et al., 2019; Masrori and Van Damme, 2020). The incidence of ALS is more common in men of White race and those with age >60 (Mehta et al., 2022). It has been reported that ALS prevalence is 50–100 times higher in the Western Pacific regions than other regions in the world (Mehta et al., 2022). ALS can occur at any age, but its peak incidence is between 50 and 75 years and sharply decreases after 80 years (Vinceti et al., 2019). Moreover, sporadic ALS is more common in people aged 58–63 years. ALS cases are expected to reach 300,000 in 2040 worldwide (Vinceti et al., 2019; Mehta et al., 2022).

ALS is characterized by muscle weakness, muscle twitching, and muscle wasting. In limb-onset ALS, the muscle weakness starts in the arms or legs in 50% of patients. The weakness most commonly starts in the limb muscles, more often in distal muscles than in proximal muscles (Bennett et al., 2019; Masrori and Van Damme, 2020). In bulbar-onset ALS, there are difficulties in swallowing and speaking, which are present in 25%−30% of ALS patients (Bennett et al., 2019). Approximately 50% of patients will suffer from extra-motor manifestations to some degree in addition to their motor problems (Masrori and Van Damme, 2020). It has been observed that 15% of ALS patients develop frontotemporal dementia and cognitive impairments (Masrori and Van Damme, 2020). According to the etiopathological factors, there are two types of ALS: 95% is idiopathic (sporadic) ALS and 5% is familial ALS (Delpont et al., 2019; Masrori and Van Damme, 2020).

Classical ALS involves both upper and lower motor neurons, leading to spasticity and muscle weakness, respectively. Classical ALS contributes to 70% of all ALS cases classified as limb-onset ALS and bulbar-onset ALS. Some ALS variants present limited symptoms due to localized neuronal injury that progresses slower than classical ALS, such as flail arm syndrome, caused by damage to motor neurons in arm muscles (Masrori and Van Damme, 2020). In addition, isolated bulbar palsy is caused by damage to motor neurons in the bulbar region, leading to dysarthria and dysphagia (Delpont et al., 2019; Masrori and Van Damme, 2020; Goutman et al., 2022). The diagnosis of ALS is based on clinical manifestations and neuroimaging findings (Goutman et al., 2022).

ALS is an incurable disease, and the treatment is mainly symptomatic. Median survival time is 2–4 years from onset; only 5%−10% of patients survive beyond 10 years (Chiò et al., 2013). The ALS mortality rate was 1.70 per 100,000 in the United States. Similarly, other studies have also found lower ALS mortality rates among Hispanics. Lower incidence and mortality among non-Whites and Hispanics may reflect less detection among non-Whites or a genetic factor predisposing Whites to ALS (Goutman et al., 2022). However, slowing the progression of the disease is the main goal in ALS management by using riluzole and sodium phenylbutyrate, which extend the life only by several months (Chiò et al., 2013; Andrews et al., 2020).

The causes of ALS are not fully known; however, environmental and genetic factors contribute equally to the pathogenesis of ALS (Feldman et al., 2022; Hartmann et al., 2022). Genetic alterations, together with environmental factors, promote the development of ALS (Motataianu et al., 2022). ALS below the age of 70 is more common in men by 20%, but sex differences are not observed above the age of 70 years (Borghero et al., 2023). ALS neuropathology is characterized by neuronal lesions located in the brain motor cortex for the upper motor neurons, the brain stem, and spinal cord for the lower motor neurons (Del Tredici and Braak, 2022). The pathognomonic pathological feature of ALS is the presence of specific inclusion bodies called Bunina bodies in the cytoplasm of motor neurons (Bede et al., 2021).

The constituents of Bunina bodies are TAR DNA-binding protein 43 (TDP-43), which is present in 97% of ALS patients (Mori et al., 2019). However, in ALS, superoxide dismutase 1 (SOD1) is the main constituent of Bunina bodies, which is due to a gene mutation (Wright et al., 2019). These inclusion bodies have the ability to transport from cell to cell in a prion disease-like manner (Mori et al., 2019; Wright et al., 2019). Mutant SOD1 proteins have the ability to accumulate intracellularly and inhibit protein degradation (Berdyński et al., 2022). Inclusion bodies in ALS induce glutamate neurotransmission, leading to excessive intracellular calcium accumulation and excitotoxicity (Diana and Bongioanni, 2022). It has been shown that motor neurons are highly sensitive to the effect of excitotoxicity due to their low calcium buffering capacity (Tedeschi et al., 2021).

In ALS, excitatory amino acid transporter 2 (EAAT2), which is responsible for the transport of synaptic glutamate, is significantly downregulated (Fontana et al., 2023). Therefore, dysregulation of glutamate neurotransmission is regarded as the main pathophysiological mechanism intricate in ALS neuropathology. Hence, riluzole, which inhibits presynaptic glutamate release, can attenuate the pathogenesis of ALS (Chen et al., 2020). Interestingly, environmental factors such as toxins, viruses, and metals, together with SOD-1 mutation, trigger excitotoxicity, mitochondrial dysfunction, oxidative stress, neuroinflammation, and aggregation of abnormal proteins, leading to impairment of axonal transport and neuronal apoptosis (Mori et al., 2019; Bede et al., 2021; Del Tredici and Braak, 2022) .

According to the genetic base, TDP-43 and SOD-1 genetic mutations are the main mutations involved in the pathogenesis of ALS (Farina et al., 2021; Brenner and Freischmidt, 2022). Other mutated genes involved in ALS are listed as follows (Renton et al., 2014; Gregory et al., 2020) (Table 1).

The underlying causes of cell deaths in ALS are development of mitochondrial dysfunction, impairment of nucleocytoplasmic transport, and ROS production due to progressive accumulation of mutant TDP-43 (Davis et al., 2018). TDP-43 interferes with mitochondrial respiratory complex I proteins (Wang et al., 2016), leading to mitochondrial dysfunction and loss of motor neurons in ALS. Interestingly, loss of motor neurons in ALS is mainly through induction of the apoptotic pathway (Vogt et al., 2018).

Originally, it was established that mutant TDP-43 triggers the expression of pro-apoptotic proteins in a p53-dependent manner (Vogt et al., 2018). However, neuronal death in ALS is independent of caspase-3 activation, and inhibition of caspase-3 does not affect the percentage of neuronal loss (Re et al., 2014). In addition, co-cultured astrocytes derived from ALS patients with human

TABLE 1 Genes involved in ALS.

Gene	Location	Inheritance	Function	% in familial ALS	% in sporadic ALS
SQSTM1	1q35	AD	Autophagy	1	<1
TARDBP	1p36	AD	RNA metabolism	4	1
VCP	9p13	AD	Proteasome	1	1
C9ORF72	9p21	AD	DENN protein	40	1
OPTN	10p13	AD	Vesicle trafficking	<1	<1
FUS	16p11	AD	RNA metabolism	4	1
PFN1	17p13	AD	Cytoskeleton	<1	<1
UBQLN2	Xp11	XD	Proteasome	<1	<1

AD, autosomal-dominant; XD, X-linked dominant.

motor neurons led to high neuronal loss. Similarly, necroptosis is implicated in the progression of neuronal loss in ALS. The application of the necroptosis inhibitor necrostatin-1 prevents neuronal loss in ALS, which substantiates the aforementioned (Re et al., 2014). Therefore, both apoptosis and necroptosis pathways are intricately involved in neuronal loss in ALS.

Furthermore, derangement of RNA metabolism in ALS is evident in the majority of familial ALS due to alteration of RNA translocation, RNA degradation, pre-mRNA splicing, and the formation of a ribonucleoprotein complex by mutant genes (Strong, 2010). The mutant TDP-43 and SOD1 proteins can form cytosolic aggregates, which affect the stability of mRNA through an interaction with mRNA species in ALS (Strong, 2010). Therefore, ALS is regarded as a disorder of RNA metabolism, and alteration of RNA metabolism appears central to the pathogenesis of ALS. In addition, microRNA (miRNA) is a noncoding RNA that is involved in substantial control of gene expression and has a critical role in cell death. Importantly, miRNA controls apoptosis, programmed cell death, and necroptosis in ALS (Gagliardi et al., 2019). Deregulation of miRNA has been observed in the brain, spinal cord, blood, and CSF of ALS patients (Gagliardi et al., 2019). Downregulation of miRNA was observed mainly in the motor neurons (Gagliardi et al., 2019), suggesting the protective role of miRNA against ALS neuropathology.

Moreover, noncoding genomes such as long noncoding RNA (IncRNA) are highly expressed in spinal motor neurons in the early stages of the ALS pathological process (Gagliardi et al., 2018a, 2019). IncRNA acts as an epigenetic regulator of the target gene by controlling the interaction between miRNA and mRNA. It has been observed that IncRNA is upregulated in the peripheral blood mononuclear cells of sporadic ALS but deregulated in familial ALS (Gagliardi et al., 2018b). Notably, degeneration of motor neurons is caused by a combination of intrinsic neuronal defects and extrinsic factors such as astrocyte-mediated toxicity (Del Tredici and Braak, 2022). In ALS, the astrocytes are activated to release pro-inflammatory cytokines and chemokines, causing sustained neurotoxic effects and neuronal apoptosis (Bede et al., 2021), as illustrated in Figure 1.

As ALS is more common in older age groups having comorbidities such as diabetes, hypertension, and dyslipidemia, the use of lipid-lowering agents such as statins is more frequent in those patients (Hu and Ji, 2022). It has been demonstrated that statins may have beneficial or detrimental effects on the pathogenesis of ALS (Nabizadeh et al., 2022; Wang et al., 2023). Thus, this review aims to discuss the potential effects of statins on ALS neuropathology.

2 Method and search strategy

In this review, a systematic literature search of the Web of Science, Scopus, PubMed, Cochrane Library, ProQuest, ISI Processing, and OpenGray databases was performed to recognize the relevant literature. Additional records were obtained through a manual search. Two authors assessed the eligibility by checking the title and abstract and checking the full articles. The search was conducted by using relevant keywords [Amyotrophic lateral sclerosis AND Statins], [Amyotrophic lateral sclerosis AND Neuronal apoptosis], [Amyotrophic lateral sclerosis AND Oxidative stress], [Amyotrophic lateral sclerosis AND Neuroinflammation], [Statins AND Oxidative stress], and [Statins AND Neuroinflammation]. The quality of the studies was estimated by the authors for compatibility with the present review. The included studies are original studies, retrospective studies, and prospective studies. However, a case report study, a review study, and articles published in languages other than English were excluded from this review.

3 Pharmacology of statins

Statins are cholesterol-lowering drugs that inhibit *de novo* hepatic cholesterol biosynthesis through suppression of a rate-limiting hydroxyl-methyl-glutaryl Coenzyme A (HMG-CoA) reductase (Al-Kuraishy et al., 2020b; Alromi et al., 2021). Figure 2 shows the mechanisms of statins.

Reduction of circulating cholesterol by statins triggers the expression of low-density lipoprotein (LDL) receptors, subsequently increasing the uptake of LDL-c (Al-Kuraishy and Al-Gareeb, 2017). In addition, statins promote the expression of high-density lipoprotein (HDL), which removes cholesterol from the tissues to the liver (Al-Kuraishy et al., 2020b). In addition, statins have potential pleiotropic effects, including antioxidant, anti-inflammatory, antiatherogenic, and antiplatelet

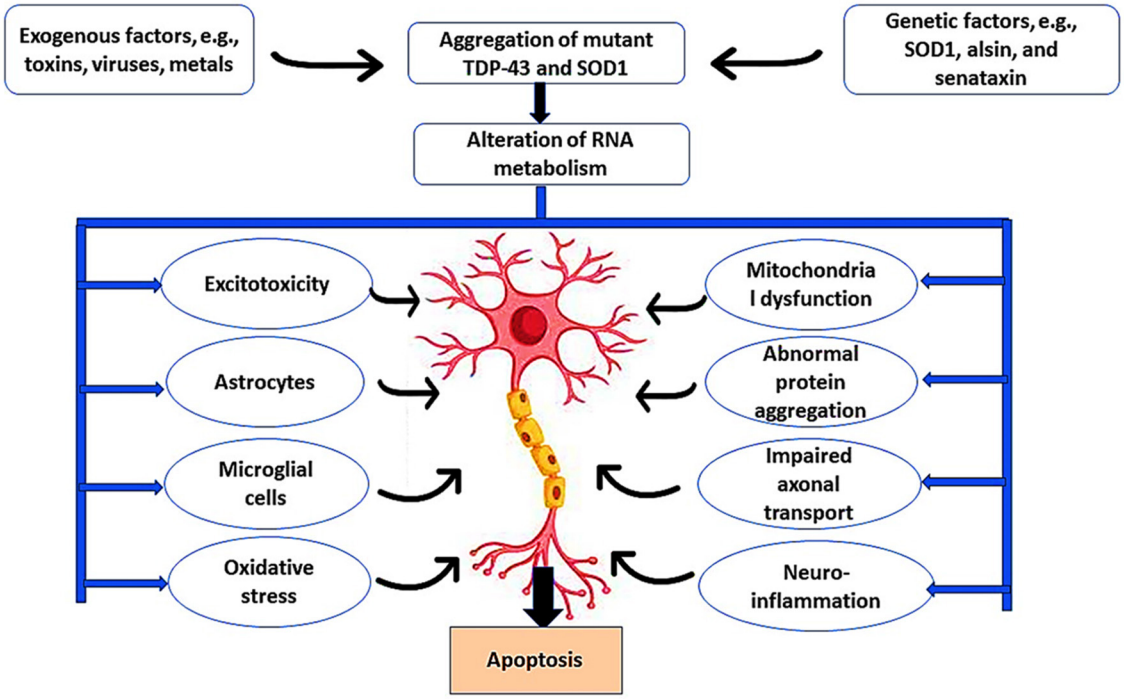


FIGURE 1
Pathophysiology of ALS. Exogenous factors such as toxins, viruses, and metals induce ALS neuropathology through the induction of microglia and astrocytes that cause excitotoxicity and oxidative stress. In addition, genetic risk factors such as mutations in the *SOD1* gene promote ALS neuropathology by inducing mitochondrial dysfunction, abnormal protein aggregation, impaired abnormal axonal transport, and development of neuroinflammation. These changes trigger the apoptosis of motor neurons.

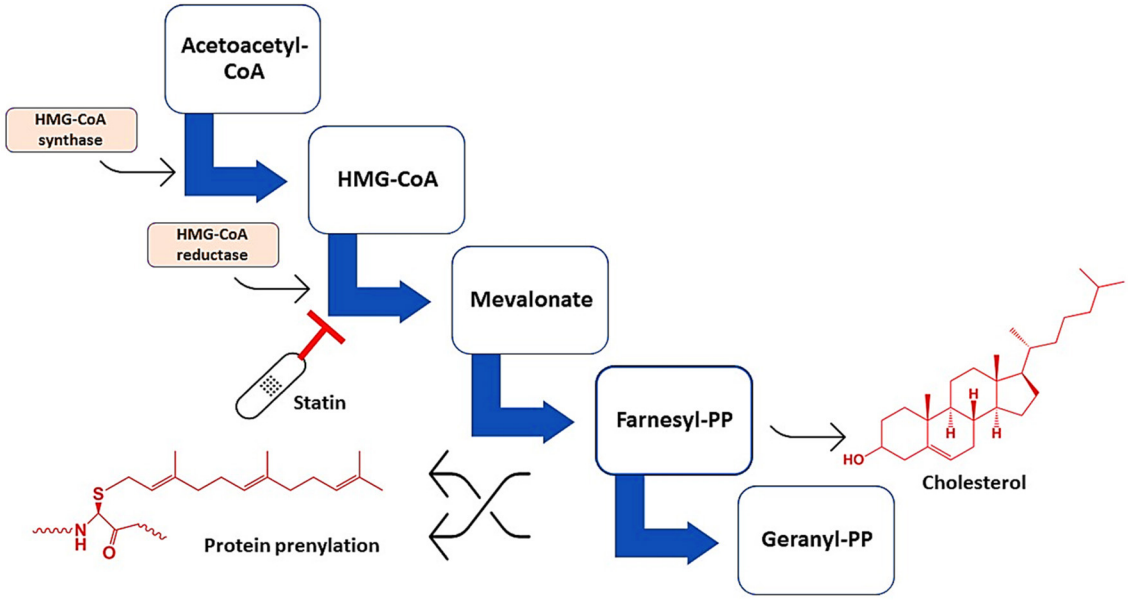


FIGURE 2
Mechanisms of action of statins. Statins inhibit HMG-CoA reductase, leading to the formation of mevalonate, farnesyl pyrophosphate, and geranyl pyrophosphate, which are essential for the synthesis of cholesterol and involved in protein prenylation.

effects (Kadhim et al., 2019; Al-Rubiay et al., 2021). Therefore, statins are used in the management of hypercholesterolemia, dyslipidemia, and as primary and secondary preventive therapy against cardiovascular diseases. According to their lipid solubility, statins are classified into lipophilic statins, such as simvastatin and atorvastatin, and hydrophilic statins, such as rosuvastatin

(Al-Kuraishy et al., 2020c). Lipophilic statins can cross the blood–brain barrier (BBB) causing inhibition of brain cholesterol by suppressing the activity of brain HMG-CoA reductase (Al-Kuraishy and Al-Gareeb, 2016; Al-Kuraishy et al., 2018a).

Lipophilic statins have more central effects compared to hydrophilic statins (Simon et al., 2019; Climent et al., 2021); therefore, lipophilic statins may affect neurocognitive functions in a dual role that could be detrimental or beneficial (Jamshidnejad-Tosaramandani et al., 2022). Regarding the pharmacokinetics of statins, they are absorbed orally and may be affected by food. For example, pravastatin absorption is reduced by 35% when administrated with food, while food increases the absorption of lovastatin by 50% (Al-Kuraishy et al., 2018b). However, the absorption of rosuvastatin and pitavastatin is not affected by food (Al-Kuraishy et al., 2019). Statins have a plasma protein-binding capacity of 95%, with the exception of pravastatin, which has a plasma protein-binding capacity of 50%. Some statins can inhibit P-glycoprotein, leading to drug–drug interactions with P-glycoprotein substrates such as verapamil (Al-Kuraishy et al., 2019).

Statins are mainly metabolized by CYP450 isoenzymes, though pravastatin is metabolized by the cytosolic sulfation pathway (Filppula et al., 2021). Enzyme inducer drugs such as rifampicin increase statin metabolism, while enzyme inhibitors such as macrolides increase the risk of statin toxicity (Filppula et al., 2021). However, pitavastatin and rosuvastatin are less metabolized by CYP450 isoenzymes, so they are less subjected to drug–drug interactions (Hirota et al., 2020). In addition, P-glycoprotein is concerned with the biliary and intestinal elimination of rosuvastatin and pravastatin (Liu, 2019). Statins are mainly excreted by urine, with the exception of atorvastatin, which is eliminated through bile. The most common adverse effects linked with prolonged use of statins are gastrointestinal discomfort, myopathy, cognitive dysfunction, elevation of liver enzymes, an increased risk of diabetes, and peripheral neuropathy (Deng et al., 2021). The pharmacokinetic effects of statins are unique, intestinal SLCO2B1 protein mediates the absorption of statins, which, through the intestinal CYP3A4 enzyme, are converted to active and inactive metabolites. Statin metabolites produced by the hepatic CYP3A4 enzyme are processed and eliminated from the circulation (Hirota et al., 2020; Filppula et al., 2021).

4 Statins role in neurodegenerative diseases

Neurodegenerative diseases are a group of diseases caused by progressive degeneration of neurons with subsequent neuronal deaths (Hansson, 2021). Neuroinflammation, oxidative stress, and mitochondrial dysfunction are the most common mechanisms sharing an intricate link in the neurodegenerative process (Elfawy and Das, 2019). The underlying causes for development of neuroinflammation, oxidative stress, and mitochondrial dysfunction are progressive accumulation of misfolded proteins such as amyloid beta (Aβ) in Alzheimer's disease (AD) and alpha synuclein (α-Syn) in Parkinson's disease (PD) (Kabir et al., 2020). The etiopathological causes of neurodegenerative diseases are chiefly unknown; however, environmental factors in genetically susceptible subjects may be the most proposed mechanism (Al-Kuraishy et al., 2020a). AD is the most common neurodegenerative disease and represents two-thirds of dementia cases (Alromi et al., 2021; Al-Kuraishy et al., 2023b). AD is characterized by intracellular accumulation of neurofibrillary tangles (NFTs) and extracellular accumulation of non-soluble Aβ (Alsubaie et al., 2022). AD is most common in individuals aged >65 years, leading to cognitive dysfunction and progressive memory loss (Ali et al., 2024).

It has been shown that prolonged use of statins, mainly in elderly patients, may adversely affect cognitive function. Statins can induce cognitive decline in healthy subjects and in AD patients (Alsubaie et al., 2022). However, observational and prospective studies did not provide a clinical clue regarding the harmful and beneficial effects of statins on AD neuropathology (Group, 2002; McGuinness et al., 2009). Interestingly, users of statins such as simvastatin and atorvastatin experience reversible cognitive impairment within 2 months (Wagstaff et al., 2003). It has been illustrated that lipophilic statins trigger the development of cognitive impairment through inhibition of brain cholesterol, which is necessary for neuronal integrity and synaptic plasticity (Schultz et al., 2018). Inhibition of brain cholesterol by lovastatin promotes Aβ formation and development of AD in mice (Strandberg et al., 1999). Inhibition of brain cholesterol by statins attenuates neuronal myelination, causing worsening of AD neuropathology (Alsubaie et al., 2022). In addition, prolonged use of statins reduces the neuroprotective CQ10, leading to mitochondrial dysfunction, oxidative stress, and enhancement in Aβ formation (Alsubaie et al., 2022). Therefore, prolonged use of statins is implicated in the pathogenesis of AD by different mechanisms, as shown in Figure 3.

In contrast, long-term use of statins may have beneficial effects on AD neuropathology through modulation of ApoE. Thus, early treatment with statins could be therapeutically effective against AD neuropathology (Prince et al., 2014). Evidence from clinical studies confirmed the protective role of statins against the development and progression of AD (Haag et al., 2009; Lin et al., 2015). The fundamental mechanism for the protective effects of statins against AD development is linked to the inhibition of Aβ formation by suppressing ApoE4 (Bagheri et al., 2020). In addition, statins improve α-secretase activity, which enhances the production of neuroprotective soluble Aβ with subsequent reduction in neurotoxic Aβ. Statins have direct neuroprotective effects through inhibition of brain HMG-CoA reductase, reduction of platelet activity in the cerebral vasculature, stabilization of atherosclerotic plaques, and modulation of Rho GPTase activity. In addition, statins have indirect neuroprotective effects against AD neuropathology by targeting Aβ (Haag et al., 2009; Lin et al., 2015; Bagheri et al., 2020), as shown in Figure 4. These findings indicated a potential controversy regarding statin use and AD risk.

PD is the second-most common progressive neurodegenerative disease caused by degeneration of dopaminergic neurons in the substantia nigra (Al-Kuraishy et al., 2023c). PD is more frequent in subjects aged >65 years with specific classical features including bradykinesia, resting tremor, rigidity, and postural instability (Alrouji et al., 2024). It has been reported that long-term use of statins for prevention of primary and secondary outcomes in

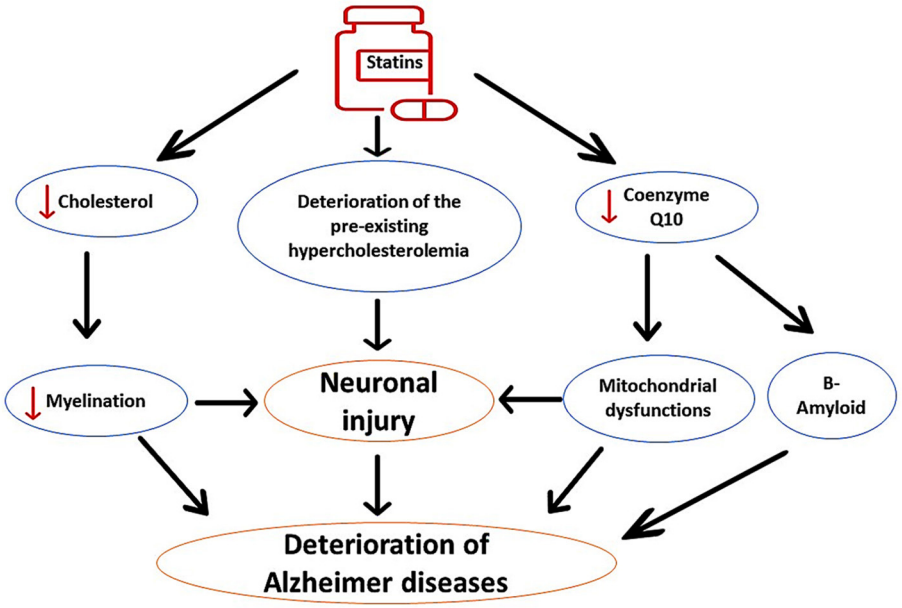


FIGURE 3
The detrimental effects of statins on AD neuropathology. Statins impair neuronal myelination through inhibition of neuronal cholesterol; therefore; statins worsen preexistent cholesterol aberrations. In addition, statins inhibit mitochondrial CoQ10, leading to oxidative stress, neuronal injury, and acceleration of Aβ aggregation. These changes induced by the use of statins exacerbate AD neuropathology.

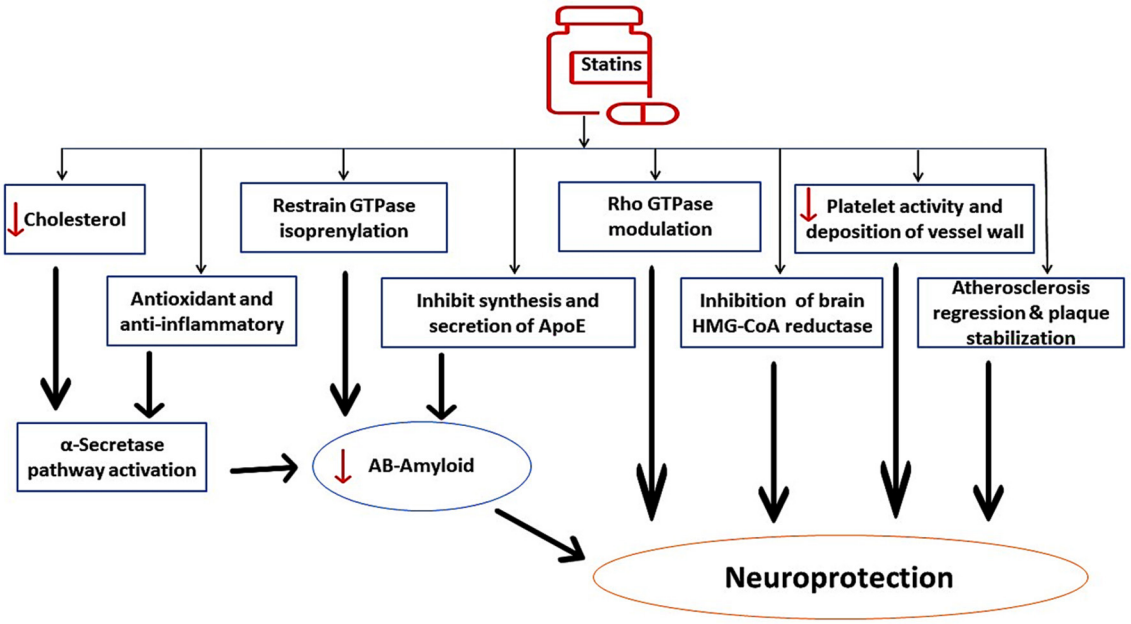


FIGURE 4
The beneficial role of statins against AD neuropathology. Statins improve α-secretase activity, which enhances the production of neuroprotective soluble Aβ with subsequent reduction in neurotoxic Aβ. Statins inhibit brain HMG-CoA reductase, reduce platelet activity in the cerebral vasculature, stabilize atherosclerotic plaques, and modulate Rho GPTase activity. Statins have indirect neuroprotective effects against AD neuropathology by targeting Aβ.

patients with cardiovascular diseases may affect the pathogenesis of PD in a bidirectional way and could be advantageous or disadvantageous (Al-Kuraishy et al., 2023a). These findings raise a conflicting role for statins in PD neuropathology. Different studies have highlighted that statins have protective effects against PD incidence, independent of cholesterol-lowering effects (Roy and Pahan, 2011). Findings from preclinical studies revealed that lipophilic simvastatin attenuates PD development in mice (Tang

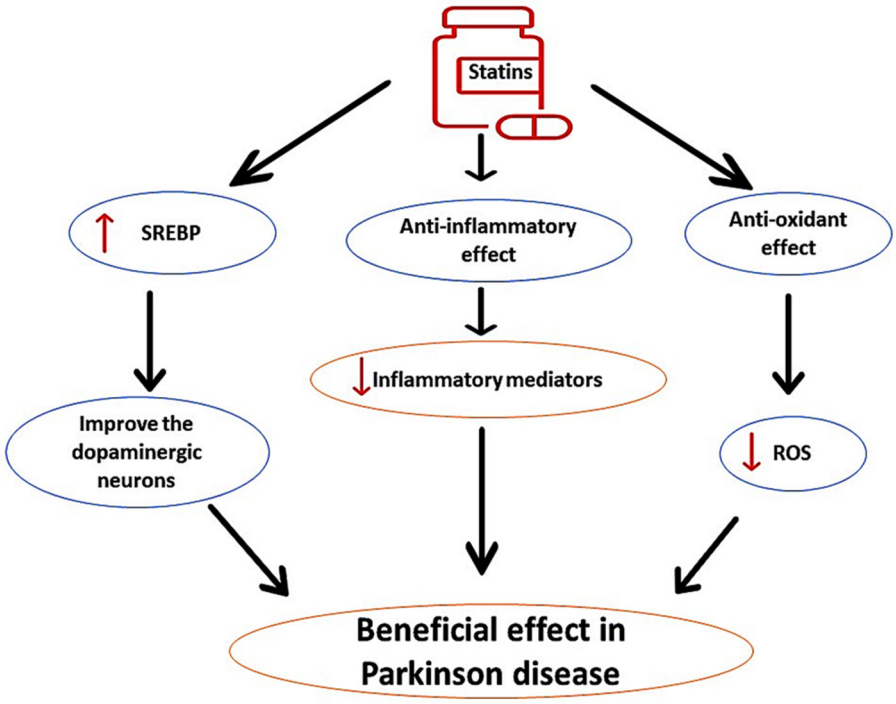


FIGURE 5
The protective role of statins in PD. Statins, through their anti-inflammatory and antioxidant effects, as well as by increasing sterol regulatory element-binding protein (SREBP), improve the activity of dopaminergic neurons, can reduce the pathogenesis of PD.

et al., 2019). Clinically, prolonged use of statins reduces PD risk (Wahner et al., 2008). It has been shown that statins through their anti-inflammatory and antioxidant effects as well as by increasing sterol regulatory element-binding protein (SREBP), improve the activity of dopaminergic neurons (Wahner et al., 2008), as shown in Figure 5.

In contrast, lipophilic statins may increase PD risk within 2.5 years by reducing the neuroprotective effect of cholesterol (Liu et al., 2017). Interestingly, short-term use of statins for <1 year augments PD risk in a dose-dependent manner by inhibiting dopamine transporters, though long-term use of statins did not have this effect (Jeong et al., 2019). Therefore, the effects of statins on and PD risk and neuropathology depend on the stage of PD and the duration of statin therapy. In a similar manner, statins affect other neurodegenerative diseases.

Taken together, the effects of statins on the most common neurodegenerative diseases, including AD and PD, appear conflicting. The underlying causes of the conflicting effects of statins on AD and PD need to be addressed by prospective studies.

5 Role of statins in ALS

5.1 Protective effects

Many studies have highlighted the protective effects of statins against ALS risk (Weisskopf et al., 2022; Kreple et al., 2023). Lovastatin 40 mg/kg attenuates ALS risk in a mouse model by 28% (Kreple et al., 2023). Lovastatin has an inverse relationship in a dose-dependent manner with the risk of motor neuron disease and delays the onset of ALS in transgenic mice (Kreple et al., 2023). A longitudinal case–control study observed that prolonged use of statins >3 years reduces ALS risk (Weisskopf et al., 2022), suggesting that long-term use of statins had a protective role against the development and progression of ALS.

Preclinical findings showed that simvastatin can reduce the activation of astrocytes and microglia and inhibit the release of pro-inflammatory cytokines in C6 glioma cells subjected to the effects of LPS (Zheng et al., 2018). Simvastatin regulates the microglia immune response to ALS (Zheng et al., 2018). Inhibition of microglia and development of neuroinflammation by statins leads to a neuroprotective effect by attenuating the development of different neurodegenerative diseases including ALS (Bagheri et al., 2020). Interestingly, administration of atorvastatin 10 mg/kg/day for 4 weeks attenuates the degeneration of motor neurons in mice (Iwamoto et al., 2009). Atorvastatin inhibits denervation atrophy and motor neuron loss by 30% (Iwamoto et al., 2009).

In a clinical setting, a case–control study on 948 ALS patients and matched 1,000 healthy controls revealed that statin use for 3 years before the onset of ALS symptoms was protective against ALS neuropathology (Weisskopf et al., 2022). Numerous studies have indicated the neuroprotective effects of statins against various types of neurodegenerative diseases, including ALS, by inhibiting neurotoxicity (Bösel et al., 2005; Wolozin et al., 2007; Bagheri et al., 2020). A retrospective study on 650 ALS patients and 365 matched healthy controls revealed that 65% of ALS

patients have dyslipidemia, mainly hypercholesterolemia, that is correlated with disease severity (Chełstowska et al., 2021). Therefore, hypercholesterolemia followed by mixed dyslipidemia is an important risk factor in the general population for increased ALS risk, and treating these metabolic disorders with statins may reduce the incidence of ALS. Dyslipidemia with increasing cholesterol and LDL levels augments ALS risk (Mariosa et al., 2017).

A follow-up of dyslipidemic patients for >20 years showed that elevation of one unit of LDL was linked with increased ALS risk (Mariosa et al., 2017). Therefore, alterations in the lipid profile are regarded as biomarkers before the onset of ALS. In addition, hypercholesterolemia induces the development and progression of ALS neuropathology (Chen et al., 2018; Bandres-Ciga et al., 2019; Zeng and Zhou, 2019). Thus, total cholesterol and LDL are potential risk factors involved in the pathogenesis of ALS. A large prospective study on 502,409 ALS patients showed that a high cholesterol/HDL ratio and high LDL and ApoA serum levels were associated with increased ALS risk (Thompson et al., 2022). Herein, the premorbid metabolic status may be involved in the pathogenesis of ALS, and the use of statins may improve the metabolic profile and reduce ALS risk. Furthermore, lipid homeostasis is highly dysregulated in the spinal cord gray matter, mainly in the motor neurons, leading to progressive neuronal injury. An increase in cholesterol ester is linked with the degeneration of motor neurons in ALS patients (Dodge et al., 2020).

A similar finding in the ALS mouse model revealed a significant downregulation of cholesterol biosynthesis in the motor neurons (Dodge et al., 2020). Therefore, dysregulation of lipid metabolism in the spinal cord contributes to the pathogenesis of ALS. Hence, restoration of lipid homeostasis by statins could prevent ALS development. Moreover, the protective effects of statins against ALS risk may be sex-dependent (Nefussy et al., 2011). A retrospective study illustrated that the use of statins reduced ALS risk in women, only signifying the sex-dependent effects of statins (Nefussy et al., 2011). The protective role of statins against ALS is listed in Table 2.

These findings proposed the neuroprotective effects of statins against the development and progression of ALS by regulating dyslipidemia and inflammatory changes, as shown in Figure 6.

TABLE 2 The protective effects of statins against ALS.

Type of the study	Findings	References
Preclinical	Lovastatin 40 mg/kg attenuates ALS risk in mouse models by 28%	Kreple et al., 2023
Preclinical	Simvastatin reduces the activation of astrocytes and microglia and inhibits the release of pro-inflammatory cytokines in C6 glioma cells	Zheng et al., 2018
Preclinical	Administration of atorvastatin 10 mg/kg/day for 4 weeks attenuates the degeneration of motor neurons in mice	Iwamoto et al., 2009
Longitudinal study	Prolonged use of statins >3 years reduces ALS risk	Weisskopf et al., 2022
Clinical studies	Statins have protective effects against neurodegenerative diseases including ALS by inhibiting neurotoxicity	Bösel et al., 2005; Wolozin et al., 2007; Bagheri et al., 2020

5.2 Hazardous effects

It has been observed that statins may adversely affect the incidence and progression of ALS (Gaimari et al., 2022). A population-based study revealed that long-term use of statins is associated with the acceleration of ALS severity (Mariosa et al., 2020). Evidence from previous studies indicated that prolonged use of statins may be associated with the development of ALS-like syndrome (Edwards et al., 2007; Colman et al., 2008). Statins promote the progression of peripheral neuropathy and rhabdomyolysis, though the association of statins with upper motor lesions was disproportionate (Edwards et al., 2007). Data obtained from a retrospective study proposed that statin use increases ALS risk compared to placebo (Colman et al., 2008). A population-based case–control study on 2,475 ALS patients and 12,375 healthy controls illustrated that statins increase ALS risk in women (Mariosa et al., 2020). Small muscle mass and low-statin metabolizing enzymes in women may explain the sex difference in the effect of statins (Group, 2008). The neurotoxic effects of statins may increase ALS risk in women mainly in the first year from the onset of ALS (Skajaa et al., 2021). A recent population-based cohort study revealed that genetic predisposition for statin therapy is linked with augmentation of ALS risk (Wang et al., 2023). Thus, statins may increase ALS, independent of cholesterol-lowering effects, which gives an insight into a new avenue regarding the role of statins in ALS.

It has been illustrated that not all statins produce detrimental effects on motor neurons, though a class-dependent effect was postulated. A previous *in vitro* study demonstrated that 7-day exposure of motor neurons to fluvastatin has less effects on spinal motor neurons in a dose-dependent manner (Murinson et al., 2012). In comparison, much higher concentrations of other statins are required to produce neurotoxic effects. However, this neurotoxic effect was not observed on cortical neurons or Schwann cells (Murinson et al., 2012). However, hydrophilic pravastatin, which has a pharmacokinetic profile distinct from that of lipophilic fluvastatin, produces less toxic effects on the spinal motor neurons (Murinson et al., 2012). Therefore, class-dependent effects of statins by specific mechanisms may be implicated in the pathogenesis of ALS. Lipophilic statins have greater effects on the initiation of ALS neuropathology compared to hydrophilic statins (Golomb et al., 2018). However, statins affect ALS through cholesterol-dependent and cholesterol-independent mechanisms. Inhibition of neuronal cholesterol by statins interferes with the lipid raft, which mediates the neuronal pro-survival pathway (Fracassi et al., 2019).

The cholesterol-independent mechanism of statins is through the reduction of mevalonate, which is essential for neuronal survival (Moutinho et al., 2017). Therefore, statins may attenuate the survival of motor neurons through the suppression of pro-survival signaling. In addition, statins induce the expression of pro-apoptotic pathways such as Bcl-2 and FOXO3a, leading to neuronal apoptosis (Wood et al., 2013). Of note, statins affect inflammatory signaling that distorts G-protein and carnitine palmitoyl transferase

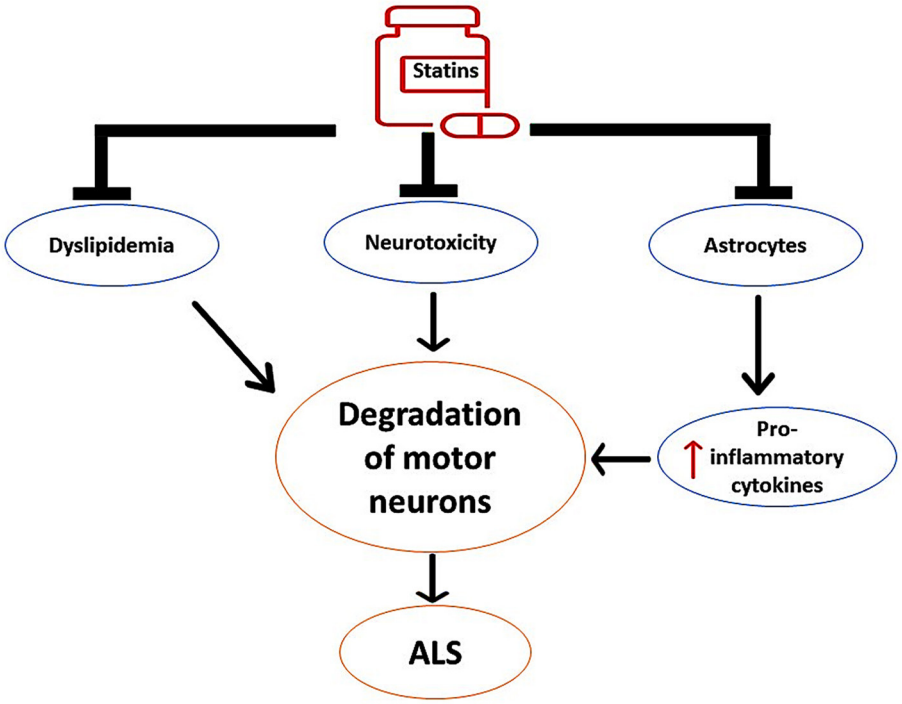


FIGURE 6
The neuroprotective effects of statins against the development of ALS. Statins inhibit the activity of overactivated astrocytes and the release of pro-inflammatory cytokines. Statins attenuate the progression of neurotoxicity, thereby preventing the degeneration of motor neurons. In addition, statins attenuate the development of dyslipidemia, which is implicated in the degeneration of motor neurons.

in the mitochondrial membrane, leading to oxidative stress (Yanae et al., 2011). In addition, statins decrease the binding of Rho and Ras proteins to the cell membrane, which is intricately involved in neuronal endocytosis. In addition, statins induce apoptosis in glioma cell lines through Akt/ERKI/2 signaling (Yanae et al., 2011). In addition, statins that interfere with musculoskeletal metabolism may increase ALS risk (Gaimari et al., 2022). Therefore, ALS could be a potential adverse effect of statin therapy.

Nakamura et al. (2022) observed that high HDL in ALS patients predicts poor prognosis for all patients, though low LDL augments ALS risk in women only. A retrospective study on 78 ALS patients showed that high HDL levels and low LDL levels are correlated with hypermetabolism in ALS patients (Nakamura et al., 2022). High HDL activates the expression of mechanistic target of rapamycin (mTOR) via phosphatidylinositol 3 kinase (PI3K), causing inhibition of autophagy and augmentation of ALS neuropathology (Wang and Peng, 2012). Inhibition of autophagy accelerates the accumulation of TDP-43, increasing the pathogenesis of ALS (Tang et al., 2019). In ALS, muscle metabolism is shifted toward the lipid rather than glycolytic pathway. However, high HDL induces muscle glycolysis and reduces β-oxidation in muscles, thereby producing a protective effect (Ferri et al., 2017). In this state, the lipid-lowering effect of statins by increasing HDL and reducing LDL may be implicated in the pathogenesis of ALS.

The mechanism for induction of ALS neuropathology by statins may be related to the dysregulation of liver X receptor signaling (LXR) signaling in the motor neurons (Beltowski, 2010). Statins suppress the synthesis of endogenous LXR agonist oxysterols and reduce the expression of the LXR gene. Of note, mice lacking the *LXR* gene experience an ALS phenotype. Statin-induced inhibition of *LXR* gene expression promotes circulating sterols, which are neurotoxics (Beltowski, 2010). Therefore, LXR agonists may attenuate statin-induced ALS. In this state, statin therapy might not be safe in ALS patients (Zinman et al., 2008), although an observational study indicated that statin therapy is rarely associated with ALS risk (Golomb et al., 2009).

Moreover, brain cholesterol and even dyslipidemia are considered protective factors against ALS neuropathology (Dupuis et al., 2008; Yoshii et al., 2010). A case–control study on 369 ALS patients and 286 healthy controls observed that dyslipidemia and a high LDL/HDL ratio prolong the survival of ALS patients by 12 months (Dupuis et al., 2008). It has been shown that hypermetabolism is augmented in ALS patients; thus, reduction of cholesterol by statin therapy may reduce the nutritional status of muscles and neurons, leading to the progression of the pathogenesis of ALS (Dupuis et al., 2008). Yoshii et al. proposed that high energy demand in ALS can reduce the LDL/HDL ratio, which correlated with respiratory complications in ALS patients (Yoshii et al., 2010). The hazardous effects of statins are listed in Table 3.

Taken together, statins may accelerate ALS neuropathology by alteration of lipid profile and dysregulation of neuronal inflammatory signaling (Figure 7).

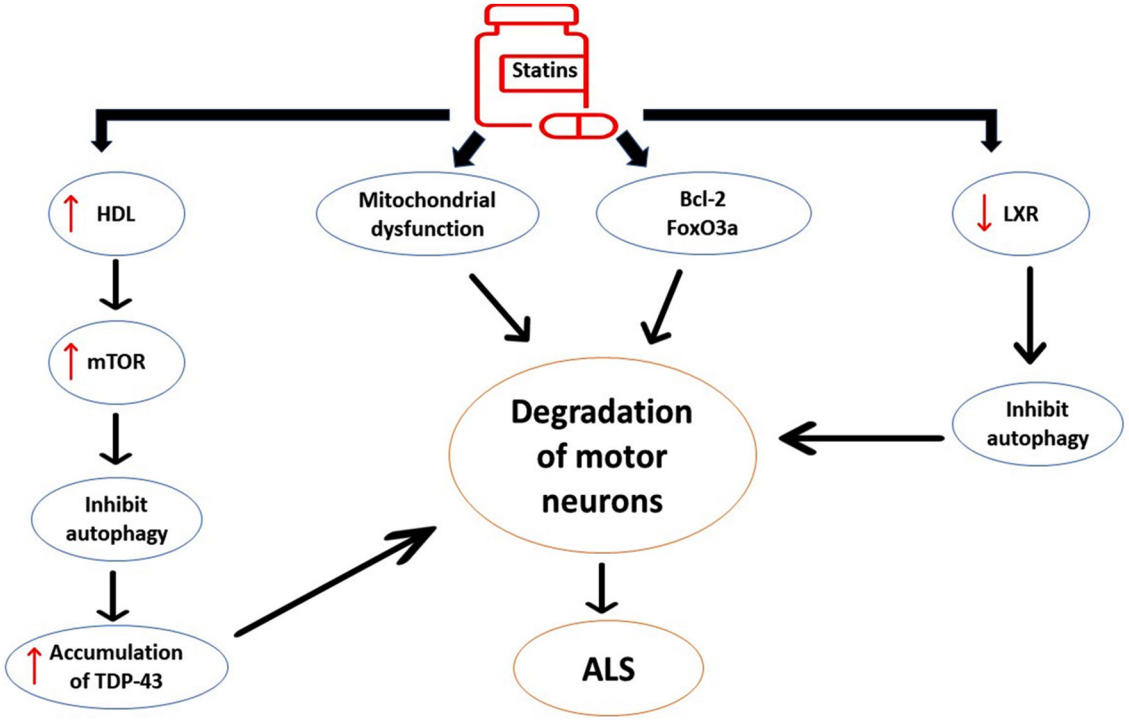


FIGURE 7
The detrimental effects of statins on ALS neuropathology. Statins induce the expression of pro-apoptotic pathways such as Bcl-2 and FOXO3a, leading to neuronal apoptosis. Statins affect inflammatory signaling that distorts G-protein and carnitine palmitoyl transferase in the mitochondrial membrane, leading to oxidative stress and mitochondrial dysfunction. Statin-induced high HDL activates the expression of the mechanistic target of rapamycin (mTOR), causing inhibition of autophagy and augmentation of ALS neuropathology. Statins inhibit the expression of liver X receptor signaling (LXR) signaling in the motor neurons. These changes induced by statin use trigger the degeneration of motor neurons and development of ALS.

5.3 Neutral effects

It has been perceived that metabolic changes such as diabetes and dyslipidemia are common in ALS patients due to a derangement of energy balance and hypermetabolism (Schumacher et al., 2020). A prospective cohort study showed that statin use did not affect the overall survival of ALS patients (Schumacher et al., 2020); thus, statin therapy for the management of dyslipidemia should not be discontinued in ALS patients. A retrospective study included 459 ALS patients, 72 of them were on treatment with statins at the onset of the disease, and there was no significant association between statins and increased ALS risk (Drory et al., 2008). A pooled analysis of observational studies for the association between statin use and ALS risk was inconclusive (Macías Saint-Gerons and Castro, 2019). A systematic meta-analysis found no association between statin use and ALS risk (Chang et al., 2021). A recent meta-analysis and systematic review of 13,890 ALS patients from eight clinical studies revealed no significant association between prolonged use of statins and ALS risk (Nabizadeh et al., 2022). Other systematic reviews and meta-analyses illustrated that prolonged use of statins was not linked with ALS risk (Hu and Ji, 2022). Therefore, most recent studies and meta-analysis reviews indicated that statin use was not associated with disease progression or amelioration of survival in ALS patients.

6 Discussion

Statins as a risk factor for the development of ALS should be explained with caution, as the increasing use of statins has dramatically increased from 5% in 1991 to 40% in 1998 (Toft Sørensen and Lash, 2009). Many adverse effects related to statin medications are reported from uncontrolled clinical trials and non-randomized studies (Cameron et al., 2015). The evidence for statin-induced neurotoxic effects is highly limited (Samant and Gupta, 2021). ALS patients are commonly associated with dyslipidemia, liver steatosis, and other metabolic disorders (Colman et al., 2008; D'Amico et al., 2021). However, it is difficult to verify the causal relationship between ALS and metabolic disorders as most of the reported studies were observational. In 2007, the WHO declared that prolonged use of statins may induce the development of ALS-like syndrome and may increase ALS risk (Edwards et al., 2007), and this was the first report to suggest the potential link between statin use and ALS risk. The WHO database regarding this association is called Vigibase, which contains 4,000,000 subjects who reported the adverse effects of different medications, including statins (Macías Saint-Gerons and Castro, 2019).

Initially, a cohort study involving 172 ALS patients revealed that 25% of ALS neuropathologies is related to long-term use of statins (Edwards et al., 2007). Colman et al. (2008) in 2008 described an identical association between statin use and ALS

TABLE 3 The hazardous effects of statins on ALS.

Type of the study	Findings	References
Clinical	Long-term use of statins is associated with the acceleration of the severity of ALS	Mariosa et al., 2020
Clinical	Prolonged use of statins may be associated with the development of ALS-like syndrome	Edwards et al., 2007
A retrospective study	Statin use increases ALS risk compared to placebo	Colman et al., 2008
A cohort study	Statin use in women may increase ALS risk mainly in the first year from onset of ALS	Skajaa et al., 2021
Preclinical	Fluvastatin reduces effects on spinal motor neurons in a dose-dependent effect	Murinson et al., 2012
Preclinical	Lipophilic statins have greater effects on the initiation of ALS neuropathology compared to hydrophilic statins	Golomb et al., 2018
A retrospective study	High HDL level and low LDL level due to prolonged use of statins are correlated with hypermetabolism in ALS patients	Nakamura et al., 2022
Preclinical	Induction of ALS neuropathology by statins may be related to the dysregulation of LXR signaling in the motor neurons	Beltowski, 2010

risk, depending on the Vigibase database. Despite of this evidence, there is no valid and robust clinical evidence explaining the causal relationship between statin therapy and ALS risk. In fact, the surveillance databases give clues and provide an idea regarding the connection between statin therapy and ALS that should be confirmed by preclinical and clinical studies regarding the re-analysis of databases. In addition, the analysis of databases should be in relation to the incidence and prevalence of ALS in certain regions worldwide regarding the prevalence of statin use. For example, a pooled analysis of clinical trials showed an association between statin use and risk for development of ALS. However, these findings did not provide robust and strong clinical evidence for this association due to improper description of study criteria (Rothman et al., 2008). Moreover, misdiagnosis and misclassification of ALS cases included in clinical trials and observational studies affect the outcomes and validity of different studies (Sørensen et al., 2006). The biased null-hypothesis in some studies could be an important cause for the negative association between statin use and ALS risk (Sørensen et al., 2006). Therefore, systematic reviews and meta-analyses illustrated no association between long-term use of statins and ALS risk (Chang et al., 2021; Hu and Ji, 2022; Nabizadeh et al., 2022). Currently, small incidence of ALS despite the high prevalence of statins use supports a null-hypothesis between long-term use of statins and ALS risk (Colman et al., 2008).

Interestingly, measures of ALS progression should be evaluated in patients with prolonged use of statins. Of note, magnetic resonance tomography (MRI) of the CNS and CSF biomarkers can predict the severity of ALS progression (Spinelli et al., 2020; Dreger et al., 2022). Functional staging of ALS is commonly measured by King's clinical staging and Milano–Torino (MiToS). The MiToS system uses six stages, from 0 to 5, and is based on functional ability, as assessed by the ALS Functional Rating Scale-Revised (ALSFRS-R), with stage 0 being normal function and stage 5 being death. The King's system uses five stages, from 1 to 5, and is based on disease burden, as measured by clinical involvement and significant feeding or respiratory failure, with stage 1 being symptom onset and stage 5 being death (Fang et al., 2017). King's clinical staging has higher resolution in the early stage of ALS; however, MiToS staging has a great resolution for the late stage of ALS (Fang et al., 2017). Therefore, both staging systems are recommended to evaluate the clinical staging of ALS patients.

In addition, the ALS-functional scale can measure clinical motor deficits in ALS patients (Spinelli et al., 2020; Dreger et al., 2022). Despite these measures, there is little agreement as to what measures to use in a given clinical setting in ALS patients since ALS is regarded as a protean disease that may progress rapidly or slowly. In addition, the prognosis of ALS is poor, which should be discussed with patients regarding survival and response to the current treatments (van Eenennaam et al., 2020). The personalized ENCALS survival prediction model dependably estimates the personalized prognosis of ALS patients without destroying hope and anxiety. The communication guide supports physicians in discussing the personalized prognosis for ALS patients and their families (van Eenennaam et al., 2020).

Taken together, these limitations in the explanation of data result in controversial outcomes with opposing mechanisms regarding the association between statin use and ALS neuropathology. The present review had many limitations, such as the limitation of prospective studies, and most of the published studies were subjected to many limiting factors, such as bias and heterogeneity. Therefore, reaching a final conclusion regarding the exact role of statins in ALS remains difficult. Therefore, large-scale prospective studies with proper ALS diagnostic criteria to elucidate the connotation between statins use and ALS are recommended in this regard.

7 Conclusions

ALS is a neurodegenerative disease characterized by muscle weakness, muscle twitching, and muscle wasting due to progressive neurodegeneration of motor neurons located in the brain, motor cortex, and spinal cord. It has been shown that prolonged use of statins may induce the development of ALS-like syndrome and may increase ALS risk. Conversely, results from preclinical and clinical studies highlighted the protective role of statins against ALS neuropathology. Recently, meta-analyses and systematic Reviews showed no association between long-term use of statins and ALS risk. Therefore, there is a strong controversy regarding this association. Statins as a risk factor for the development of ALS should be explained with caution, as the use of statins has significantly increased. At this time, the small incidence of

ALS despite the high prevalence of statins use supports a null-hypothesis between long-term statin use and ALS risk. Collectively, these precincts in the explanation of data result in controversial outcomes with contrasting mechanisms regarding the association between statin use and ALS neuropathology. Consequently, large-scale prospective studies involving patients with appropriate ALS diagnostic criteria to explicate the association between statin use and ALS are recommended in this regard.

Author contributions

HA-k: Supervision, Writing – original draft. MJ: Supervision, Writing – original draft. GS: Project administration, Writing – review & editing. HM: Supervision, Writing – review & editing. AA-G: Writing – original draft, Writing – review & editing. AA: Writing – review & editing. SJ: Writing – original draft, Writing – review & editing. AS: Software, Writing – review & editing. MA: Funding acquisition, Software, Writing – review & editing.

Funding

The author(s) declare that no financial support was received for the research, authorship, and/or publication of this article.

Acknowledgments

The authors are thankful to the Deanship of Graduate Studies and Scientific Research at the University of Bisha for supporting this work through the Fast-Track Research Support Program.

Conflict of interest

The authors declare that the research was conducted in the absence of any commercial or financial relationships that could be construed as a potential conflict of interest.

Publisher's note

All claims expressed in this article are solely those of the authors and do not necessarily represent those of their affiliated organizations, or those of the publisher, the editors and the reviewers. Any product that may be evaluated in this article, or claim that may be made by its manufacturer, is not guaranteed or endorsed by the publisher.

References

Ali, N. H., Al-Kuraishy, H. M., Al-Gareeb, A. I., Alnaaim, S. A., Alexiou, A., Papadakis, M., et al. (2024). Neprilysin inhibitors and risk of Alzheimer's disease: a future perspective. *J. Cell. Mol. Med.* 28:e17993. doi: 10.1111/jcmm.17993

Al-Kuraishy, H. M., Abdulhadi, M. H., Hussien, N. R., Al-Niemi, M. S., Rasheed, H. A., and Al-Gareeb, A. I. (2020a). Involvement of orexinergic system in psychiatric and neurodegenerative disorders: a scoping review. *Brain Circ.* 6, 70–80. doi: 10.4103/bc.bc_42_19

Al-Kuraishy, H. M., and Al-Gareeb, A. I. (2016). Effects of rosuvastatin alone or in combination with omega-3 fatty acid on adiponectin levels and cardiometabolic profile. *J. basic Clin. Pharm.* 8:8. doi: 10.4103/0976-0105.195080

Al-Kuraishy, H. M., and Al-Gareeb, A. I. (2017). Acylation-stimulating protein is a surrogate biomarker for acute myocardial infarction: role of statins. *J. Lab. Physicians* 9, 163–169. doi: 10.4103/0974-2727.208263

Al-Kuraishy, H. M., Al-Gareeb, A. I., and Al-Buhadilly, A. K. (2018a). Rosuvastatin improves vaspin serum levels in obese patients with acute coronary syndrome. *Diseases* 6:9. doi: 10.3390/diseases6010009

Al-Kuraishy, H. M., Al-Gareeb, A. I., Alexiou, A., Papadakis, M., Alsayegh, A. A., Almohmadi, N. H., et al. (2023a). Pros and cons for statins use and risk of Parkinson's disease: an updated perspective. *Pharmacol. Res. Perspect.* 11:e01063. doi: 10.1002/prp2.1063

Al-Kuraishy, H. M., Al-Gareeb, A. I., Alsayegh, A. A., Hakami, Z. H., Khamjan, N. A., Saad, H. M., et al. (2023b). A potential link between visceral obesity and risk of Alzheimer's disease. *Neurochem. Res.* 48, 745–766. doi: 10.1007/s11064-022-03817-4

Al-Kuraishy, H. M., Al-Gareeb, A. I., Hussien, N. R., Al-Naimi, M. S., and Rasheed, H. A. (2019). Statins an oft-prescribed drug is implicated in peripheral neuropathy: the time to know more. *J. Pak. Med. Assoc.* 69, S108–S112.

Al-Kuraishy, H. M., Al-Gareeb, A. I., and Naji, M. T. (2020b). Brain natriuretic peptide in patients with acute ischemic stroke: role of statins. *Biomed. Biotechnol. Res. J.* 4, 239–245. doi: 10.4103/bbrj.bbrj_44_20

Al-Kuraishy, H. M., Al-Gareeb, A. I., and Waheed, H. J. (2018b). Lipoprotein-associated phospholipase A2 is linked with poor cardio-metabolic profile in patients with ischemic stroke: a study of effects of statins. *J. Neurosci. Rural Pract.* 9, 496–503. doi: 10.4103/jnrp.jnrp_97_18

Al-Kuraishy, H. M., Hussian, N. R., Al-Naimi, M. S., and Al-Gareeb, A. I. (2020c). Statins role in vitiligo: a mini-review. *Turk. J. Dermatol.* 14, 1–7. doi: 10.4103/TJD.TJD_38_19

Al-Kuraishy, H. M., Jabir, M. S., Al-Gareeb, A. I., and Albuhadily, A. K. (2023c). The conceivable role of prolactin hormone in Parkinson disease: the same goal but with different ways. *Ageing Res. Rev.* 91:102075. doi: 10.1016/j.arr.2023.102075

Alromi, D., Madani, S., and Seifalian, A. (2021). Emerging application of magnetic nanoparticles for diagnosis and treatment of cancer. *Polymers* 13:4146. doi: 10.3390/polym13234146

Alrouji, M., Al-Kuraishy, H. M., Al-Gareeb, A. I., Ashour, N. A., Jabir, M. S., Negm, W. A., et al. (2024). Metformin role in Parkinson's disease: a double-sword effect. *Mol. Cell. Biochem.* 479, 975–991. doi: 10.1007/s11010-023-04771-7

Al-Rubiay, H. F., Al-Kuraishy, H. M., and Al-Gareeb, A. I. (2021). Intercellular adhesive molecule 1 (ICAM-1) and acute ischaemic stroke: role of statins. *J. Pak. Med. Assoc.* 71, S11–S16.

Alsubaie, N., Al-Kuraishy, H. M., Al-Gareeb, A. I., Alharbi, B., De Waard, M., Sabatier, J.-M., et al. (2022). Statins use in Alzheimer disease: bane or boon from frantic search and narrative review. *Brain Sci.* 12:1290. doi: 10.3390/brainsci12101290

Andrews, J. A., Jackson, C. E., Heiman-Patterson, T. D., Bettica, P., Brooks, B. R., and Pioro, E. P. (2020). Real-world evidence of riluzole effectiveness in treating amyotrophic lateral sclerosis. *Amyotroph. Lateral Scler. Front. Degener.* 21, 509–518. doi: 10.1080/21678421.2020.1771734

Bagheri, H., Ghasemi, F., Barreto, G. E., Sathyapalan, T., Jamialahmadi, T., and Sahebkar, A. (2020). The effects of statins on microglial cells to protect against neurodegenerative disorders: a mechanistic review. *Biofactors* 46, 309–325. doi: 10.1002/biof.1597

Bandres-Ciga, S., Noyce, A. J., Hemani, G., Nicolas, A., Calvo, A., Mora, G., et al. (2019). Shared polygenic risk and causal inferences in amyotrophic lateral sclerosis. *Ann. Neurol.* 85, 470–481. doi: 10.1002/ana.25431

Bede, P., Murad, A., and Hardiman, O. (2021). Pathological neural networks and artificial neural networks in ALS: diagnostic classification based on pathognomonic neuroimaging features. *J. Neurol.* 269, 2440–2452. doi: 10.1007/s00415-021-10801-5

Beltowski, J. (2010). Statins and ALS: the possible role of impaired LXR signaling. *Med. Sci. Monit. Int. Med. J. Exp. Clin. Res.* 16, RA73–RA78.

Bennett, S. A., Tanaz, R., Cobos, S. N., and Torrente, M. P. (2019). Epigenetics in amyotrophic lateral sclerosis: a role for histone post-translational modifications in neurodegenerative disease. *Transl. Res.* 204, 19–30. doi: 10.1016/j.trsl.2018.10.002

Berdyński, M., Miszta, P., Safranow, K., Andersen, P. M., Morita, M., Filipek, S., et al. (2022). SOD1 mutations associated with amyotrophic lateral sclerosis analysis of variant severity. *Sci. Rep.* 12:103. doi: 10.1038/s41598-021-03891-8

Borghero, G., Sechi, M. M., Vasta, R., Pierri, V., Pili, F., Pateri, I., et al. (2023). Spatial clustering of amyotrophic lateral sclerosis in Sardinia, Italy: the contribution of age, sex, and genetic factors. *Muscle Nerve* 68, 323–328. doi: 10.1002/mus.27939

Bösel, J., Gandor, F., Harms, C., Synowitz, M., Harms, U., Djoufack, P. C., et al. (2005). Neuroprotective effects of atorvastatin against glutamate-induced excitotoxicity in primary cortical neurones. *J. Neurochem.* 92, 1386–1398. doi: 10.1111/j.1471-4159.2004.02980.x

Brenner, D., and Freischmidt, A. (2022). Update on genetics of amyotrophic lateral sclerosis. *Curr. Opin. Neurol.* 35, 672–677. doi: 10.1097/WCO.0000000000001093

Cameron, C., Fireman, B., Hutton, B., Clifford, T., Coyle, D., Wells, G., et al. (2015). Network meta-analysis incorporating randomized controlled trials and non-randomized comparative cohort studies for assessing the safety and effectiveness of medical treatments: challenges and opportunities. *Syst. Rev.* 4, 1–8. doi: 10.1186/s13643-015-0133-0

Chang, M. C., Kwak, S. G., Park, J.-S., and Park, D. (2021). Relationship between statins and the risk of amyotrophic lateral sclerosis: a PRISMA-compliant meta-analysis. *Medicine* 100:e26751. doi: 10.1097/MD.0000000000026751

Chełstowska, B., Barańczyk-Kuzma, A., and Kuzma-Kozakiewicz, M. (2021). Dyslipidemia in patients with amyotrophic lateral sclerosis–a case control retrospective study. *Amyotroph. Lateral Scler. Front. Degener.* 22, 195–205. doi: 10.1080/21678421.2020.1832119

Chen, S., Liao, Q., Lu, K., Zhou, J., Huang, C., and Bi, F. (2020). Riluzole exhibits no therapeutic efficacy on a transgenic rat model of amyotrophic lateral sclerosis. *Curr. Neurovasc. Res.* 17, 275–285. doi: 10.2174/1567202617666200409125227

Chen, X., Yazdani, S., Piehl, F., Magnusson, P. K. E., and Fang, F. (2018). Polygenic link between blood lipids and amyotrophic lateral sclerosis. *Neurobiol. Aging* 67, 202.e1. doi: 10.1016/j.neurobiolaging.2018.03.022

Chiò, A., Logroscino, G., Traynor, B. J., Collins, J., Simeone, J. C., Goldstein, L. A., et al. (2013). Global epidemiology of amyotrophic lateral sclerosis: a systematic review of the published literature. *Neuroepidemiology* 41, 118–130. doi: 10.1159/000351153

Cho, H., and Shukla, S. (2020). Role of edaravone as a treatment option for patients with amyotrophic lateral sclerosis. *Pharmaceuticals* 14:29. doi: 10.3390/ph14010029

Climent, E., Benaiges, D., and Pedro-Botet, J. (2021). Hydrophilic or lipophilic statins? *Front. Cardiovasc. Med.* 8:687585. doi: 10.3389/fcvm.2021.687585

Colman, E., Szarfman, A., Wyeth, J., Mosholder, A., Jillapalli, D., Levine, J., et al. (2008). An evaluation of a data mining signal for amyotrophic lateral sclerosis and statins detected in FDA's spontaneous adverse event reporting system. *Pharmacoepidemiol. Drug Saf.* 17, 1068–1076. doi: 10.1002/pds.1643

D'Amico, E., Grosso, G., Nieves, J. W., Zanghì, A., Factor-Litvak, P., and Mitsumoto, H. (2021). Metabolic abnormalities, dietary risk factors and nutritional management in amyotrophic lateral sclerosis. *Nutrients* 13:2273. doi: 10.3390/nu13072273

Davis, S. A., Itaman, S., Khalid-Janney, C. M., Sherard, J. A., Dowell, J. A., Cairns, N. J., et al. (2018). TDP-43 interacts with mitochondrial proteins critical for mitophagy and mitochondrial dynamics. *Neurosci. Lett.* 678, 8–15. doi: 10.1016/j.neulet.2018.04.053

Del Tredici, K., and Braak, H. (2022). Neuropathology and neuroanatomy of TDP-43 amyotrophic lateral sclerosis. *Curr. Opin. Neurol.* 35, 660–671. doi: 10.1097/WCO.0000000000001098

Delpont, B., Beauvais, K., Jacquin-Piques, A., Alavoine, V., Rault, P., Blanc-Labarre, C., et al. (2019). Clinical features of pain in amyotrophic lateral sclerosis: a clinical challenge. *Rev. Neurol.* 175, 11–15. doi: 10.1016/j.neurol.2017.11.009

Deng, F., Tuomi, S.-K., Neuvonen, M., Hirvensalo, P., Kulju, S., Wenzel, C., et al. (2021). Comparative hepatic and intestinal efflux transport of statins. *Drug Metab. Dispos.* 49, 750–759. doi: 10.1124/dmd.121.000430

Diana, A., and Bongioanni, P. (2022). "Glutamate-based treatment for amyotrophic lateral sclerosis/motor neuron disease," in *Glutamate and Neuropsychiatric Disorders: Current and Emerging Treatments*, ed. Z. M. Pavlovic (Cham: Springer), 359–380. doi: 10.1007/978-3-030-87480-3_12

Dodge, J. C., Jensen, E. H., Yu, J., Sardi, S. P., Bialas, A. R., Taksir, T. V., et al. (2020). Neutral lipid cacostasis contributes to disease pathogenesis in amyotrophic lateral sclerosis. *J. Neurosci.* 40, 9137–9147. doi: 10.1523/JNEUROSCI.1388-20.2020

Dreger, M., Steinbach, R., Otto, M., Turner, M. R., and Grosskreutz, J. (2022). Cerebrospinal fluid biomarkers of disease activity and progression in amyotrophic lateral sclerosis. *J. Neurol. Neurosurg. Psychiatry* 93, 422–435. doi: 10.1136/jnnp-2021-327503

Drory, V. E., Bronipolsky, T., Artamonov, I., and Nefussy, B. (2008). Influence of statins treatment on survival in patients with amyotrophic lateral sclerosis. *J. Neurol. Sci.* 273, 81–83. doi: 10.1016/j.jns.2008.06.022

Dupuis, L., Corcia, P., Fergani, A., Gonzalez De Aguilar, J.-L., Bonnefont-Rousselot, D., Bittar, R., et al. (2008). Dyslipidemia is a protective factor in amyotrophic lateral sclerosis. *Neurology* 70, 1004–1009. doi: 10.1212/01.wnl.0000285080.70324.27

Edwards, I. R., Star, K., and Kiuru, A. (2007). Statins, neuromuscular degenerative disease and an amyotrophic lateral sclerosis-like syndrome: an analysis of individual case safety reports from vigibase. *Drug Saf.* 30, 515–525. doi: 10.2165/00002018-200730060-00005

Elfawy, H. A., and Das, B. (2019). Crosstalk between mitochondrial dysfunction, oxidative stress, and age related neurodegenerative disease: etiologies and therapeutic strategies. *Life Sci.* 218, 165–184. doi: 10.1016/j.lfs.2018.12.029

Fang, T., Al Khleifat, A., Stahl, D. R., Lazo La Torre, C., Murphy, C., Young, C., et al. (2017). Comparison of the King's and MiToS staging systems for ALS. *Amyotroph. Lateral Scler. Frontotemporal Degener.* 18, 227–232. doi: 10.1080/21678421.2016.1265565

Farina, S., Esposito, F., Battistoni, M., Biamonti, G., and Francia, S. (2021). Post-translational modifications modulate proteinopathies of TDP-43, FUS and hnRNP-A/B in amyotrophic lateral sclerosis. *Front. Mol. Biosci.* 8:693325. doi: 10.3389/fmolb.2021.693325

Feldman, E. L., Goutman, S. A., Petri, S., Mazzini, L., Savelieff, M. G., Shaw, P. J., et al. (2022). Amyotrophic lateral sclerosis. *Lancet* 400, 1363–1380. doi: 10.1016/S0140-6736(22)01272-7

Ferri, G., Ferreira, F., and Djapic, V. (2017). "Multi-domain robotics competitions: the CMRE experience from SAUC-E to the European robotics league emergency robots," in *Ocean 2017-Aberdeen* (Aberdeen: IEEE), 1–7. doi: 10.1109/OCEANSE.2017.8084767

Filppula, A. M., Hirvensalo, P., Parviainen, H., Ivaska, V. E., Lönnberg, K. I., Deng, F., et al. (2021). Comparative hepatic and intestinal metabolism and pharmacodynamics of statins. *Drug Metab. Dispos.* 49, 658–667. doi: 10.1124/dmd.121.000406

Fontana, I. C., Souza, D. G., Souza, D. O., Gee, A., Zimmer, E. R., and Bongarzone, S. (2023). A medicinal chemistry perspective on excitatory amino acid transporter 2 dysfunction in neurodegenerative diseases. *J. Med. Chem.* 66, 2330–2346. doi: 10.1021/acs.jmedchem.2c01572

Fracassi, A., Marangoni, M., Rosso, P., Pallottini, V., Fioramonti, M., Siteni, S., et al. (2019). Statins and the brain: more than lipid lowering agents? *Curr. Neuropharmacol.* 17, 59–83. doi: 10.2174/1570159X15666170703101816

Gagliardi, D., Comi, G. P., Bresolin, N., and Corti, S. (2019). Micro RNA s as regulators of cell death mechanisms in amyotrophic lateral sclerosis. *J. Cell. Mol. Med.* 23, 1647–1656. doi: 10.1111/jcmm.13976

Gagliardi, S., Pandini, C., Garofalo, M., Bordoni, M., Pansarasa, O., and Cereda, C. (2018a). Long non coding RNAs and ALS: still much to do. *Non-coding RNA Res.* 3, 226–231. doi: 10.1016/j.ncrna.2018.11.004

Gagliardi, S., Zucca, S., Pandini, C., Diamanti, L., Bordoni, M., Sproviero, D., et al. (2018b). Long non-coding and coding RNAs characterization in peripheral blood mononuclear cells and spinal cord from amyotrophic lateral sclerosis patients. *Sci. Rep.* 8:2378. doi: 10.1038/s41598-018-20679-5

Gaimari, A., Fusaroli, M., Raschi, E., Baldin, E., Vignatelli, L., Nonino, F., et al. (2022). Amyotrophic lateral sclerosis as an adverse drug reaction: a disproportionality analysis of the food and drug administration adverse event reporting system. *Drug Saf.* 45, 663–673. doi: 10.1007/s40264-022-01184-1

Golomb, B. A., Kwon, E. K., Koperski, S., and Evans, M. A. (2009). Amyotrophic lateral sclerosis-like conditions in possible association with cholesterol-lowering drugs: an analysis of patient reports to the University of California, San Diego (UCSD) Statin Effects Study. *Drug Saf.* 32, 649–661. doi: 10.2165/00002018-200932080-00004

Golomb, B. A., Verden, A., Messner, A. K., Koslik, H. J., and Hoffman, K. B. (2018). Amyotrophic lateral sclerosis associated with statin use: a disproportionality analysis of the FDA's adverse event reporting system. *Drug Saf.* 41, 403–413. doi: 10.1007/s40264-017-0620-4

Goutman, S. A., Hardiman, O., Al-Chalabi, A., Chió, A., Savelieff, M. G., Kiernan, M. C., et al. (2022). Recent advances in the diagnosis and prognosis of amyotrophic lateral sclerosis. *Lancet Neurol.* 21, 480–493. doi: 10.1016/S1474-4422(21)00465-8

Gregory, J. M., Fagegaltier, D., Phatnani, H., and Harms, M. B. (2020). Genetics of amyotrophic lateral sclerosis. *Curr. Genet. Med. Rep.* 8, 121–131. doi: 10.1007/s40142-020-00194-8

Group, H. P. S. C. (2002). MRC/BHF Heart Protection Study of cholesterol lowering with simvastatin in 20 536 high-risk individuals: a randomised placebocontrolled trial. *Lancet* 360, 7–22. doi: 10.1016/S0140-6736(02)09327-3

Group, S. C. (2008). SLCO1B1 variants and statin-induced myopathy—a genomewide study. *N. Engl. J. Med.* 359, 789–799. doi: 10.1056/NEJMoa0801936

Haag, M. D. M., Hofman, A., Koudstaal, P. J., Stricker, B. H. C., and Breteler, M. M. B. (2009). Statins are associated with a reduced risk of Alzheimer disease regardless of lipophilicity. The Rotterdam Study. *J. Neurol. Neurosurg. Psychiatry* 80, 13–17. doi: 10.1136/jnnp.2008.150433

Hansson, O. (2021). Biomarkers for neurodegenerative diseases. *Nat. Med.* 27, 954–963. doi: 10.1038/s41591-021-01382-x

Hartmann, H., Ho, W. Y., Chang, J., and Ling, S. (2022). Cholesterol dyshomeostasis in amyotrophic lateral sclerosis: cause, consequence, or epiphenomenon? *FEBS J.* 289, 7688–7709. doi: 10.1111/febs.16175

Hirota, T., Fujita, Y., and Ieiri, I. (2020). An updated review of pharmacokinetic drug interactions and pharmacogenetics of statins. *Expert Opin. Drug Metab. Toxicol.* 16, 809–822. doi: 10.1080/17425255.2020.1801634

Hu, N., and Ji, H. (2022). Medications on hypertension, hyperlipidemia, diabetes, and risk of amyotrophic lateral sclerosis: a systematic review and meta-analysis. *Neurol. Sci.* 43, 5189–5199. doi: 10.1007/s10072-022-06131-7

Iwamoto, K., Yoshii, Y., and Ikeda, K. (2009). Atorvastatin treatment attenuates motor neuron degeneration in wobbler mice. *Amyotroph. Lateral Scler.* 10, 405–409. doi: 10.3109/17482960902870993

Jamshidnejad-Tosaramandani, T., Kashanian, S., Al-Sabri, M. H., Kročianová, D., Clemensson, L. E., Gentreau, M., et al. (2022). Statins and cognition: modifying factors and possible underlying mechanisms. *Front. Aging Neurosci.* 14:968039. doi: 10.3389/fnagi.2022.968039

Jeong, S., Jang, W., and Shin, D. W. (2019). Association of statin use with Parkinson's disease: dose–response relationship. *Mov. Disord.* 34, 1014–1021. doi: 10.1002/mds.27681

Kabir, M. T., Uddin, M. S., Abdeen, A., Ashraf, G. M., Perveen, A., Hafeez, A., et al. (2020). Evidence linking protein misfolding to quality control in progressive neurodegenerative diseases. *Curr. Top. Med. Chem.* 20, 2025–2043. doi: 10.2174/1568026620666200618114924

Kadhim, S. S., Al-Windy, S. A., Al-Nami, M. S., Al-kuraishy, H. M., and Al-Gareeb, A. I. (2019). Possible role of statins on the inflammatory biomarkers in patients with periodontal disease: a cross-sectional study. *Dent. Hypotheses* 10, 70–75. doi: 10.4103/denthyp.denthyp_60_19

Kreple, C. J., Searles Nielsen, S., Schoch, K. M., Shen, T., Shabsovich, M., Song, Y., et al. (2023). Protective effects of lovastatin in a population-based ALS study and mouse model. *Ann. Neurol.* 93, 881–892. doi: 10.1002/ana.26600

Lin, F.-C., Chuang, Y.-S., Hsieh, H.-M., Lee, T.-C., Chiu, K.-F., Liu, C.-K., et al. (2015). Early statin use and the progression of Alzheimer disease: a total population-based case-control study. *Medicine* 94:e2143. doi: 10.1097/MD.0000000000002143

Liu, G., Sterling, N. W., Kong, L., Lewis, M. M., Mailman, R. B., Chen, H., et al. (2017). Statins may facilitate Parkinson's disease: insight gained from a large, national claims database. *Mov. Disord.* 32, 913–917. doi: 10.1002/mds.27006

Liu, X. (2019). Transporter-mediated drug-drug interactions and their significance. *Drug Transp. Drug Dispos. Eff. Toxic.* 1141, 241–291.

Macías Saint-Gerons, D., and Castro, J. L. (2019). Amyotrophic lateral sclerosis associated with statins. A disproportionality analysis of the WHO Program for International Drug Monitoring database (VigiBase). *Eur. J. Clin. Pharmacol.* 75, 587–589. doi: 10.1007/s00228-018-2587-1

Mariosa, D., Hammar, N., Malmström, H., Ingre, C., Jungner, I., Ye, W., et al. (2017). Blood biomarkers of carbohydrate, lipid, and apolipoprotein metabolisms and risk of amyotrophic lateral sclerosis: a more than 20-year follow-up of the Swedish AMORIS cohort. *Ann. Neurol.* 81, 718–728. doi: 10.1002/ana.24936

Mariosa, D., Kamel, F., Bellocco, R., Ronnevi, L., Almqvist, C., Larsson, H., et al. (2020). Antidiabetics, statins and the risk of amyotrophic lateral sclerosis. *Eur. J. Neurol.* 27, 1010–1016. doi: 10.1111/ene.14190

Masrori, P., and Van Damme, P. (2020). Amyotrophic lateral sclerosis: a clinical review. *Eur. J. Neurol.* 27, 1918–1929. doi: 10.1111/ene.14393

McGuinness, B., Craig, D., Bullock, R., and Passmore, P. (2009). Statins for the prevention of dementia. *Cochrane Database Syst. Rev.* 15:CD003160. doi: 10.1002/14651858.CD003160.pub2

Mehta, P., Raymond, J., Punjani, R., Larson, T., Han, M., Bove, F., et al. (2022). Incidence of amyotrophic lateral sclerosis in the United States, 2014–2016. *Amyotroph. Lateral Scler. Front. Degener.* 23, 378–382. doi: 10.1080/21678421.2021.2023190

Mori, F., Miki, Y., Kon, T., Tanji, K., and Wakabayashi, K. (2019). Autophagy is a common degradation pathway for Bunina bodies and TDP-43 inclusions in amyotrophic lateral sclerosis. *J. Neuropathol. Exp. Neurol.* 78, 910–921. doi: 10.1093/jnen/nlz072

Motataianu, A., Serban, G., Barcutean, L., and Balasa, R. (2022). Oxidative stress in amyotrophic lateral sclerosis: synergy of genetic and environmental factors. *Int. J. Mol. Sci.* 23:9339. doi: 10.3390/ijms23169339

Moutinho, M., Nunes, M. J., and Rodrigues, E. (2017). The mevalonate pathway in neurons: it's not just about cholesterol. *Exp. Cell Res.* 360, 55–60. doi: 10.1016/j.yexcr.2017.02.034

Murinson, B. B., Haughey, N. J., and Maragakis, N. J. (2012). Selected statins produce rapid spinal motor neuron loss *in vitro*. *BMC Musculoskelet. Disord.* 13, 1–6. doi: 10.1186/1471-2474-13-100

Nabizadeh, F., Balabandian, M., Sharafi, A. M., Ghaderi, A., Rostami, M. R., and Naser Moghadasi, A. (2022). Statins and risk of amyotrophic lateral sclerosis: a systematic review and meta-analysis. *Acta Neurol. Belg.* 122, 979–986. doi: 10.1007/s13760-021-01753-8

Nakamura, R., Kurihara, M., Ogawa, N., Kitamura, A., Yamakawa, I., Bamba, S., et al. (2022). Investigation of the prognostic predictive value of serum lipid profiles in amyotrophic lateral sclerosis: roles of sex and hypermetabolism. *Sci. Rep.* 12:1826. doi: 10.1038/s41598-022-05714-w

Nefussy, B., Hirsch, J., Cudkowicz, M. E., and Drory, V. E. (2011). Gender-based effect of statins on functional decline in amyotrophic lateral sclerosis. *J. Neurol. Sci.* 300, 23–27. doi: 10.1016/j.jns.2010.10.011

Prince, M., Albanese, E., Guerchet, M., and Prina, M. (2014). World Alzheimer Report 2014. *Dementia and Risk Reduction: An analysis of protective and modifiable risk factors.* Alzheimer's Disease International. Available online at: https://unilim.hal.science/hal-03495430/doc

Re, D. B., Le Verche, V., Yu, C., Amoroso, M. W., Politi, K. A., Phani, S., et al. (2014). Necroptosis drives motor neuron death in models of both sporadic and familial ALS. *Neuron* 81, 1001–1008. doi: 10.1016/j.neuron.2014.01.011

Renton, A. E., Chiò, A., and Traynor, B. J. (2014). State of play in amyotrophic lateral sclerosis genetics. *Nat. Neurosci.* 17, 17–23. doi: 10.1038/nn.3584

Rothman, K. J., Greenland, S., and Lash, T. L. (2008). *Modern epidemiology*. Wolters Kluwer Health/Lippincott Williams and Wilkins Philadelphia.

Roy, A., and Pahan, K. (2011). Prospects of statins in Parkinson disease. *Neuroscientist* 17, 244–255. doi: 10.1177/1073858410385006

Samant, N. P., and Gupta, G. L. (2021). Novel therapeutic strategies for Alzheimer's disease targeting brain cholesterol homeostasis. *Eur. J. Neurosci.* 53, 673–686. doi: 10.1111/ejn.14949

Schultz, B. G., Patten, D. K., and Berlau, D. J. (2018). The role of statins in both cognitive impairment and protection against dementia: a tale of two mechanisms. *Transl. Neurodegener.* 7, 1–11. doi: 10.1186/s40035-018-0110-3

Schumacher, J., Peter, R. S., Nagel, G., Rothenbacher, D., Rosenbohm, A., Ludolph, A. C., et al. (2020). Statins, diabetes mellitus and prognosis of amyotrophic lateral sclerosis: data from 501 patients of a population-based registry in southwest Germany. *Eur. J. Neurol.* 27, 1405–1414. doi: 10.1111/ene.14300

Simon, T. G., Duberg, A.-S., Aleman, S., Hagstrom, H., Nguyen, L. H., Khalili, H., et al. (2019). Lipophilic statins and risk for hepatocellular carcinoma and death in patients with chronic viral hepatitis: results from a nationwide Swedish population. *Ann. Intern. Med.* 171, 318–327. doi: 10.7326/M18-2753

Skajaa, N., Bakos, I., Horváth-Puhó, E., Henderson, V. W., Lash, T. L., and Sørensen, H. T. (2021). Statin initiation and risk of amyotrophic lateral sclerosis: a Danish population-based cohort study. *Epidemiology* 32, 756–762. doi: 10.1097/EDE.0000000000001384

Sørensen, H. T., Lash, T. L., and Rothman, K. J. (2006). Beyond randomized controlled trials: a critical comparison of trials with nonrandomized studies. *Hepatology* 44, 1075–1082. doi: 10.1002/hep.21404

Spinelli, E. G., Riva, N., Rancoita, P. M. V., Schito, P., Doretti, A., Poletti, B., et al. (2020). Structural MRI outcomes and predictors of disease progression in amyotrophic lateral sclerosis. *NeuroImage Clin.* 27:102315. doi: 10.1016/j.nicl.2020.102315

Strandberg, T. E., Vanhanen, H., and Tikkanen, M. J. (1999). Effect of statins on C-reactive protein in patients with coronary artery disease. *Lancet* 353, 118–119. doi: 10.1016/S0140-6736(05)76154-7

Strong, M. J. (2010). The evidence for altered RNA metabolism in amyotrophic lateral sclerosis (ALS). *J. Neurol. Sci.* 288, 1–12. doi: 10.1016/j.jns.2009.09.029

Tang, S., Tabet, F., Cochran, B. J., Cuesta Torres, L. F., Wu, B. J., Barter, P. J., et al. (2019). Apolipoprotein AI enhances insulin-dependent and insulin-independent glucose uptake by skeletal muscle. *Sci. Rep.* 9:1350. doi: 10.1038/s41598-018-38014-3

Tedeschi, V., Petrozziello, T., and Secondo, A. (2021). Ca^{2+} dysregulation in the pathogenesis of amyotrophic lateral sclerosis. *Int. Rev. Cell Mol. Biol.* 363, 21–47. doi: 10.1016/bs.ircmb.2021.02.014

Thompson, A. G., Talbot, K., and Turner, M. R. (2022). Higher blood high density lipoprotein and apolipoprotein A1 levels are associated with reduced risk of developing amyotrophic lateral sclerosis. *J. Neurol. Neurosurg. Psychiatry* 93, 75–81. doi: 10.1136/jnnp-2021-327133

Toft Sørensen, H., and Lash, T. L. (2009). Statins and amyotrophic lateral sclerosis–the level of evidence for an association. *J. Intern. Med.* 266, 520–526. doi: 10.1111/j.1365-2796.2009.02173.x

van Eenennaam, R. M., Kruithof, W. J., van Es, M. A., Kruitwagen-van Reenen, E. T., Westeneng, H.-J., Visser-Meily, J. M. A., et al. (2020). Discussing personalized prognosis in amyotrophic lateral sclerosis: development of a communication guide. *BMC Neurol.* 20, 1–11. doi: 10.1186/s12883-020-02004-8

Verber, N. S., Shepheard, S. R., Sassani, M., McDonough, H. E., Moore, S. A., Alix, J. J. P., et al. (2019). Biomarkers in motor neuron disease: a state of the art review. *Front. Neurol.* 10:291. doi: 10.3389/fneur.2019.00291

Vinceti, M., Filippini, T., Malagoli, C., Violi, F., Mandrioli, J., Consonni, D., et al. (2019). Amyotrophic lateral sclerosis incidence following exposure to inorganic selenium in drinking water: a long-term follow-up. *Environ. Res.* 179:108742. doi: 10.1016/j.envres.2019.108742

Vogt, M. A., Ehsaei, Z., Knuckles, P., Higginbottom, A., Helmbrecht, M. S., Kunath, T., et al. (2018). TDP-43 induces p53-mediated cell death of cortical progenitors and immature neurons. *Sci. Rep.* 8:8097. doi: 10.1038/s41598-018-26397-2

Wagstaff, L. R., Mitton, M. W., Arvik, B. M., and Doraiswamy, P. M. (2003). Statin-associated memory loss: analysis of 60 case reports and review of the literature. *Pharmacother. J. Hum. Pharmacol. Drug Ther.* 23, 871–880. doi: 10.1592/phco.23.7.871.32720

Wahner, A. D., Bronstein, J. M., Bordelon, Y. M., and Ritz, B. (2008). Statin use and the risk of Parkinson disease. *Neurology* 70, 1418–1422. doi: 10.1212/01.wnl.0000286942.14552.51

Wang, S., and Peng, D. (2012). Regulation of adipocyte autophagy—The potential anti-obesity mechanism of high density lipoprotein and ApolipoproteinA-I. *Lipids Health Dis.* 11, 1–8. doi: 10.1186/1476-511X-11-131

Wang, W., Wang, L., Lu, J., Siedlak, S. L., Fujioka, H., Liang, J., et al. (2016). The inhibition of TDP-43 mitochondrial localization blocks its neuronal toxicity. *Nat. Med.* 22, 869–878. doi: 10.1038/nm.4130

Wang, W., Zhang, L., Xia, K., Huang, T., and Fan, D. (2023). Mendelian randomization analysis reveals statins potentially increase amyotrophic lateral sclerosis risk independent of peripheral cholesterol-lowering effects. *Biomedicines* 11:1359. doi: 10.3390/biomedicines11051359

Weisskopf, M. G., Levy, J., Dickerson, A. S., Paganoni, S., and Leventer-Roberts, M. (2022). Statin medications and amyotrophic lateral sclerosis incidence and mortality. *Am. J. Epidemiol.* 191, 1248–1257. doi: 10.1093/aje/kwac054

Wolozin, B., Wang, S. W., Li, N.-C., Lee, A., Lee, T. A., and Kazis, L. E. (2007). Simvastatin is associated with a reduced incidence of dementia and Parkinson's disease. *BMC Med.* 5, 1–11. doi: 10.1186/1741-7015-5-20

Wood, W. G., Igbavboa, U., Muller, W. E., and Eckert, G. P. (2013). Statins, Bcl-2, and apoptosis: cell death or cell protection? *Mol. Neurobiol.* 48, 308–314. doi: 10.1007/s12035-013-8496-5

Wright, G. S. A., Antonyuk, S. V., and Hasnain, S. S. (2019). The biophysics of superoxide dismutase-1 and amyotrophic lateral sclerosis. *Q. Rev. Biophys.* 52:e12. doi: 10.1017/S003358351900012X

Yanae, M., Tsubaki, M., Satou, T., Itoh, T., Imano, M., Yamazoe, Y., et al. (2011). Statin-induced apoptosis via the suppression of ERK1/2 and Akt activation by inhibition of the geranylgeranyl-pyrophosphate biosynthesis in glioblastoma. *J. Exp. Clin. Cancer Res.* 30, 1–8. doi: 10.1186/1756-9966-30-74

Yoshii, Y., Hadano, S., Otomo, A., Kawabe, K., Ikeda, K., and Iwasaki, Y. (2010). Lower serum lipid levels are related to respiratory impairment in patients with ALS. *Neurology* 74, 2027–2028. doi: 10.1212/WNL.0b013e3181e03bbe

Zeng, P., and Zhou, X. (2019). Causal effects of blood lipids on amyotrophic lateral sclerosis: a Mendelian randomization study. *Hum. Mol. Genet.* 28, 688–697. doi: 10.1093/hmg/ddy384

Zheng, X., Liao, Y., Wang, J., Hu, S., Rudramurthy, G. R., Swamy, M. K., et al. (2018). The antineuroinflammatory effect of simvastatin on lipopolysaccharide activated microglial cells. *Evid.-Based Complement. Altern. Med.* 2018:9691085. doi: 10.1155/2018/9691085

Zinman, L., Sadeghi, R., Gawel, M., Patton, D., and Kiss, A. (2008). Are statin medications safe in patients with ALS? *Amyotroph. Lateral Scler.* 9, 223–228. doi: 10.1080/17482960802031092

frontiers | Frontiers in Pharmacology

TYPE Original Research
PUBLISHED 29 July 2024
DOI 10.3389/fphar.2024.1449452

Check for updates

OPEN ACCESS

EDITED BY
Pukar Khanal,
Emory University, United States

REVIEWED BY
Zsolt Gall,
George Emil Palade University of Medicine, Pharmacy, Sciences and Technology of Târgu Mureş, Romania
Smita Kumari,
The Ohio State University, United States

*CORRESPONDENCE
Hua Li,
flora@hnucm.edu.cn
Wang-hua Liu,
003439@hnucm.edu.cn

RECEIVED 15 June 2024
ACCEPTED 15 July 2024
PUBLISHED 29 July 2024

CITATION
Zhou C, Qiu S-w, Wang F-m, Liu Y-c, Hu W, Yang M-l, Liu W-h and Li H (2024), Gasdermin D could be lost in the brain parenchyma infarct core and a pyroptosis-autophagy inhibition effect of Jie-Du-Huo-Xue decoction after stroke.
Front. Pharmacol. 15:1449452.
doi: 10.3389/fphar.2024.1449452

COPYRIGHT
© 2024 Zhou, Qiu, Wang, Liu, Hu, Yang, Liu and Li. This is an open-access article distributed under the terms of the Creative Commons Attribution License (CC BY). The use, distribution or reproduction in other forums is permitted, provided the original author(s) and the copyright owner(s) are credited and that the original publication in this journal is cited, in accordance with accepted academic practice. No use, distribution or reproduction is permitted which does not comply with these terms.

Gasdermin D could be lost in the brain parenchyma infarct core and a pyroptosis-autophagy inhibition effect of Jie-Du-Huo-Xue decoction after stroke

Chang Zhou[1,2,3], Shi-wei Qiu[1,2], Feng-ming Wang[1], Yu-chen Liu[1,2], Wei Hu[1], Mei-lan Yang[1], Wang-hua Liu[1,2,4,5]* and Hua Li[1,2]*

[1]Hunan University of Chinese Medicine, Changsha, Hunan, China, [2]Provincial Key Laboratory of TCM Diagnostics, Hunan University of Chinese Medicine, Changsha, Hunan, China, [3]Key Laboratory of Hunan Province for Integrated Traditional Chinese and Western Medicine on Prevention and Treatment of Cardio-Cerebral Diseases, Changsha, Hunan, China, [4]Key Laboratory of TCM Heart and Lung Syndrome Differentiation & Medicated Diet and Dietotherapy, University of Chinese Medicine, Changsha, Hunan, China, [5]Hunan Engineering Technology Research Center for Medicinal and Functional Food, Hunan University of Chinese Medicine, Changsha, Hunan, China

Background: The Chinese ethnic medicine Jie-Du-Huo-Xue Decoction (JDHXD) is used to alleviate neuroinflammation in cerebral ischemia (CI). Our previous studies have confirmed that JDHXD can inhibit microglial pyroptosis in CI. However, the pharmacological mechanism of JDHXD in alleviating neuroinflammation and pyroptosis needs to be further elucidated. New research points out that there is an interaction between autophagy and inflammasome NLRP3, and autophagy can help clear NLRP3. The NLRP3 is a key initiator of pyroptosis and autophagy. The effect of JDHXD promoting autophagy to clear NLRP3 to inhibit pyroptosis on cerebral ischemia-reperfusion inflammatory injury is currently unknown. We speculate that JDHXD can inhibit pyroptosis in CI by promoting autophagy to clear NLRP3.

Methods: Chemical characterization of JDHXD was performed using LC-MS. Model of middle cerebral artery occlusion/reperfusion (MCAO/R) was established in SD rats. Neurological deficits, neuron damage, and cerebral infarct volume were evaluated. Western Blot and immunofluorescence were used to detect neuronal pyroptosis and autophagy.

Results: 30 possible substance metabolites in JDHXD medicated serum were analyzed by LC-MS (Composite Score > 0.98). Furthermore, JDHXD protects rat neurological function and cerebral infarct size after CI. JDHXD inhibited the

Abbreviations: CI, cerebral ischemia; CIRI, cerebral ischemia-reperfusion injury; SMCs, smooth muscle cells; CNS, central nervous system; JDHXD, Jie-Du-Huo-Xue decoction; DAMPs, damage-associated molecular patterns; LC3, lipidation of microtubule-associated light chain 3; ASC, apoptosis-associated speck-like protein containing a card; BBB, blood-brain barrier; ROS, reactive oxygen species; EC, endothelial cell; ECM, extracellular matrix; GSDMD, gasdermin D; ULK1, unc-51-like autophagy activating kinase 1; NLRP3, nucleotide-binding oligomerization domain-like receptor pyrin domain containing 3.

expression of pyroptosis and autophagy after CI. Our western blot and immunofluorescence results showed that JDHXD treatment can reduce the expression of autophagy-related factors ULK1, beclin1, and LC3-II. The expression of NLRP3 protein was lower in the JDHXD group than in the I/R group. Compared with the I/R group, the expressions of pyroptosis-related factors caspase-1 P 10, GSDMD-NT, IL-18, and IL-1β decreased in the JDHXD group. Furthermore, we observed an unexpected result: immunofluorescence demonstrated that Gasdermin D (GSDMD) was significantly absent in the infarct core, and highly expressed in the peri-infarct and contralateral cerebral hemispheres. This finding challenges the prevailing view that GSDMD is elevated in the ischemic cerebral hemisphere.

Conclusion: JDHXD inhibited pyroptosis and autophagy after MCAO/R. JDHXD suppressed pyroptosis and autophagy by inhibiting NLRP3, thereby alleviating CI. In addition, we present a different observation from previous studies that the expression of GSDMD in the infarct core was lower than that in the peri-infarct and contralateral non-ischemic hemispheres on day 3 of CI.

KEYWORDS

stroke, cerebral ischemia-reperfusion injury, pyroptosis, autophagy, NLRP3

Introduction

"To die or not to die, that is the question," as Shakespeare said in *Hamlet*. How neurons die is also a question in stroke research. Stroke stands as the foremost cause of mortality and acquired physical impairment worldwide. The range of available treatments remains limited to recanalization therapies, which include systemic thrombolysis and interventional thrombectomy (Haupt et al., 2023). Recanalizing techniques, however, are restricted to short time frames and a certain imaging profile of stroke. Therefore, the development of neuroprotectants remains important. Multitude potential targets for neuroprotection in the cascade of ischemic stroke have been identified, encompassing neuroinflammation, blood-brain barrier (BBB) permeability, and diverse cell death (Huang et al., 2020). Management remains challenging because the pathophysiology of CI is complex and involves multiple cascades. Until now, numerous potential neuroprotective medications have exhibited encouraging preclinical data. Regrettably, none have successfully transitioned into routine clinical practice (Haupt et al., 2023). However, modulating programmed cell death to rescue penumbra neurons remains important in stroke research. In recent years, the newly discovered crosstalk between cell death has stimulated our strong research interest.

Jie-Du-Huo-Xue decoction (JDHXD), was created by Qing-ren Wang, a renowned physician of the Qing Dynasty and the author of *Correction of Errors in Medical Classics*. JDHXD is a traditional Chinese medicine formula utilized for reducing inflammation in CI, comprising 10 botanical drugs (Table 1), and it is still a classic prescription in botanical medicine today. The above plants are not unique to the Chinese medical system and are used as ethnic medicines in Russia, European countries, and Japan (Fiore et al., 2005; Shikov et al., 2014; Nogami-Hara et al., 2018; Shikov et al., 2021). Our previous study confirmed that JDHXD has a neuroprotective effect on CIRI by inhibiting microglial pyroptosis and promoting microglial M1-M2 phenotype transformation (Zhou et al., 2023). Pyroptosis is triggered by a wide range of infectious and non-infectious stimuli (Vercammen et al., 1998; Bergsbaken et al., 2009; Gou et al., 2021). Upon the onset of CI, the body initiates the pattern signal associated with damage-associated molecular patterns (DAMPs) (Fricker et al., 2018). Subsequently, the intracellular promoter protein nucleotide-binding oligomerization domain-like receptor pyrin domain containing 3 (NLRP3) can recruit pro-caspase-1 (Sun et al., 2020; Yang et al., 2022). When caspase-1 is formed, the active caspase-1 cleaves the protein GSDMD to activate it. Activated GSDMD accumulates in the cell membrane and forms pores (Burdette et al., 2021). Meanwhile, caspase-1 can additionally trigger the maturation of pro-IL-1β and pro-IL-18. Upon maturation, IL-1β and IL-18 are released into the extracellular space, consequently attracting additional inflammasomes (Luan et al., 2020), following the aggregation of inflammasomes, the inflammatory response escalates, exacerbating tissue damage further. For example, IL-1β can damage the BBB by inducing microglia-mediated inflammatory responses (Niu et al., 2023).

Autophagy, an intracellular degradation process essential for cellular homeostasis, occurs extensively in ischemic stroke through autolysosome degradation of damaged or aged organelles and proteins (Shen et al., 2021; Shi et al., 2021). The regulation of autophagy involves damage sensors, often converging on the mechanistic target of rapamycin complex 1 (MTORC1), a primary inhibitor of autophagy (Plaza-Zabala et al., 2017). During classical autophagy, MTORC1 inhibition promotes activation of the autophagy pre-initiation complex comprising the unc-51-like autophagy activating kinase 1 (ULK-1). phosphate, essential for forming the pre-autophagosomal membrane or phagophore (Zhai et al., 2023). The synchronized action of autophagy-related proteins (ATGs) regulates the elongation of this structure, resulting in the development of the autophagosome. Consequently, ATGs lipidate microtubule-associated light chain 3 (LC3), leading to its accumulation in autophagosomal membranes, where it aids in cargo engulfment by binding to autophagic substrates (Hou et al., 2019; Zhang et al., 2020).

Interestingly, the NLRP3-mediated canonical pyroptosis pathway is influenced by autophagy, because autophagy can remove NLRP3, thereby inhibiting pyroptosis (Biasizzo and Kopitar-Jerala, 2020; Liu et al., 2021; Ji et al., 2022). The inhibition of pyroptosis by autophagy is primarily achieved

TABLE 1 Botanicals of Jie-Du-Huo-Xue decoction.

Standard name	English name	Chinese name	Part used	Grammage (g, %)	Cat#
Pueraria edulis Pamp [Fabaceae]	*Pueraria lobata root*	*Gegen*	Root	15 g (13.76%)	CK22082901
Paeonia veitchii Lynch [Paeoniaceae]	*Red peony root*	*Chishao*	Root	15 g (13.76%)	SL22081501
Prunus persica (L.) Batsch [Rosaceae]	*Peach seed*	*Taoren*	Seeds	12 g (11.01%)	2022070201
Anethum graveolens L. [Apiaceae]	*Chinese angelica*	*Danggui*	Root	15 g (13.76%)	TH22091903
Rehmannia glutinosa (Gaertn.) DC. [Orobanchaceae]	*Rehmannia root*	*Dihuang*	Root	15 g (13.76%)	2022090401
Carthamus tinctorius L. [Asteraceae]	*Safflower*	*Honghua*	Flower	10 g (9.17%)	2022080504
Forsythia suspensa (Thunb.) Vahl [Oleaceae]	*Forsythia suspensa*	*Lianqiao*	Gains	15 g (13.76%)	RS22080501
Bupleurum falcatum L. [Apiaceae]	*Chinese thorowax root*	*Chaihu*	Root	10 g (9.17%)	CK22091401
Citrus medica L. [Rutaceae]	*Immature trifoliate-orange fruit*	*Zhiqiao*	Gains	6 g (5.5%)	XZ22083002
Glycyrrhiza glabra L. [Fabaceae]	*Licorice*	*Gancao*	Root	6 g (5.5%)	NG22090503

through three mechanisms. Firstly, autophagy reduces apoptosis-associated speck-like protein containing a card (ASC). Secondly, it phosphorylates NLRP3. Thirdly, autophagy removes reactive oxygen species (ROS) (Zhao S. et al., 2021). NLRP3, ASC, and ROS, which are inhibited by autophagy, are all key initiators of pyroptosis. The accumulation of ROS is one of the most important pathophysiological processes of CIRI, and ROS can promote the palmitoylation of GSDMD and aggravate pyroptosis (Du et al., 2024). The inflammasome complex composed of NLRP3 and ASC is the initiator of the classic NLRP3/caspase-1/GSDMD pyroptosis pathway. Research on the interaction between pyroptosis and autophagy based on the inflammasome NLRP3 has been carried out in cardiovascular and metabolic diseases (Liu et al., 2019; Hu et al., 2022).

The above inspired us to study the mechanism of JDHXD on CIRI further. Based on our previous confirmation that JDHXD can inhibit pyroptosis in rats on the third day of CI, we hypothesized that JDHXD alleviates CI inflammatory damage by promoting autophagy to inhibit NLRP3-mediated classical pyroptosis. Therefore, the present study was conducted to confirm whether JDHXD alleviates inflammatory damage following CI by promoting autophagy to inhibit NLRP3-mediated pyroptosis.

Materials and methods

Composition and quality control for JDHXD

Our earlier research found that JDHXD has a significant applicability value in ischemic stroke. Our previous studies have described the specific composition, preparation method, and HPLC spectrum of JDHXD (Zhou et al., 2023). All botanicals (listed in Table 1) were obtained from the First Affiliated Hospital of Hunan University of Chinese Medicine pharmacies. The purchased drugs were identified in source, properties, physicochemical properties, authenticity, purity, and quality. Samples of the drugs were stored in the Key Laboratory of Chinese Medicine Diagnostics of Hunan Province. The full standard names have been checked through the following website, http://mpns.kew.org/mpns-portal/. The preparation method of JDHXD decoction is as follows: mix the required ten kinds of botanicals, add an appropriate amount of water, soak for 2 h, and decoct in water. Use 6 times the water for the first time and decoct for 1.5 h; use 3 times the water for the second time and decoct for 1.5 h. Mix the two decoctions and concentrate them to a crude drug concentration of 1 g/mL.

Animals

A total of 96 male SD rats were used in this experiment. After excluding 24 rats that failed to establish the model, the remaining 72 rats were included in subsequent experiments. The reason for using male rats in this study is that estrogen can protect against CI (Niu et al., 2023). Efforts were also taken to reduce animal suffering during the trial. The Hunan University of Chinese Medicine Laboratory Animal Research Center provided specific pathogen-free male Sprague-Dawley rats weighing 250–280 g (No: 430727221102014621 and 430727221102520668). The rats were maintained in a standard SPF barrier environment at 23°C with a light-dark cycle of 12:12 h. Three rats were housed in a single cage,

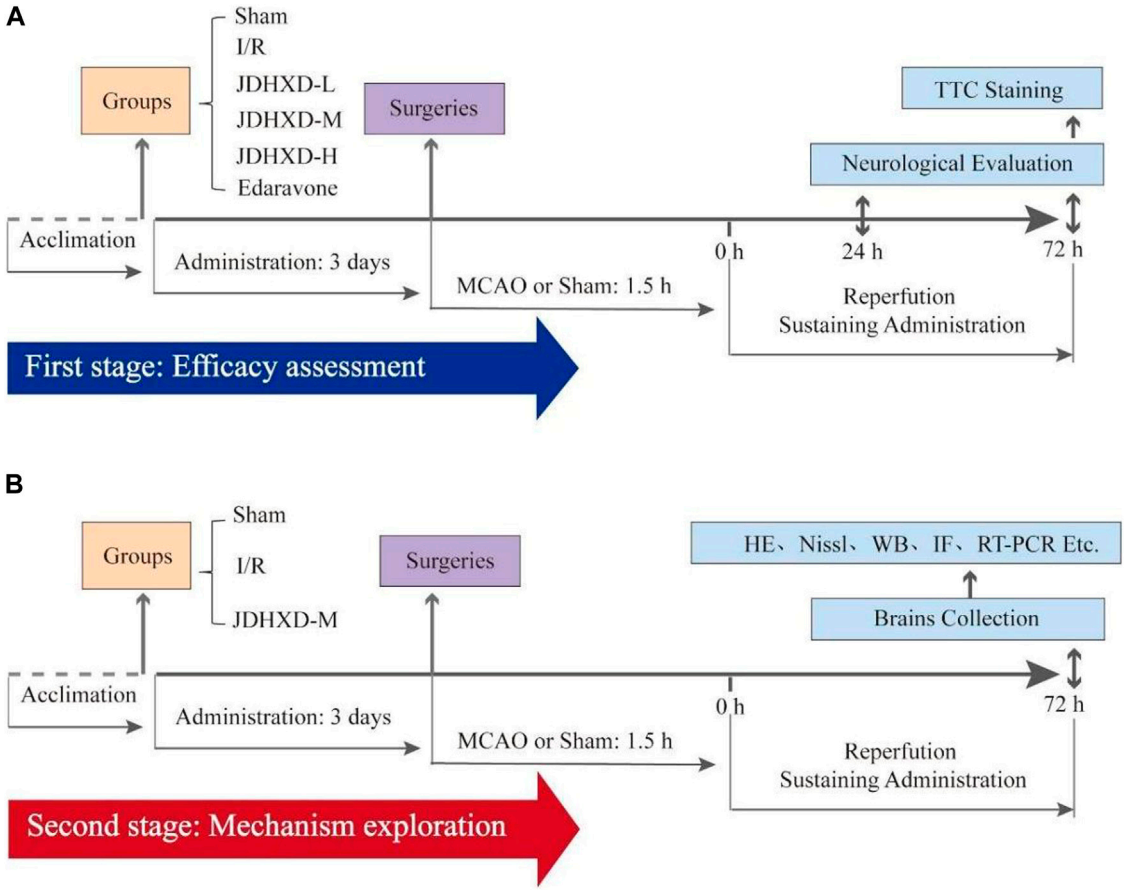


FIGURE 1
This schematic diagram of the present study. **(A)** The first stage evaluates Jie-Du-Huo-Xue decoction's (JDHXD) efficiency against ischemia-reperfusion injury. **(B)** The second phase of this study aimed to investigate the interactive effects of JDHXD on pyroptosis and autophagy.

with the animals permitted to consume food and water at their discretion. Before drug administration or surgery, rats were fed adaptively for 3 days in advance, and feeding was stopped 1 day before surgery, but drinking water was not restricted. If the neurological function injury score of a rat exceeds three points following modeling, or if it is predicted that the animal will not survive until the conclusion of the experiment, such rats will be euthanized by an overdose of anesthesia. Due to the limitations of the MCAO/R model and the rats will be killed for sampling 3 days after modeling, no special postoperative treatment will be performed on rats with CI.

Drug administration and experimental design

Briefly, the equivalent dose for rats is calculated as 10.71 g/kg/day based on the ratio of body surface area between humans and rats. Subsequently, we established the low, medium, and high dosage JDHXD for the current experiment as 5.36, 10.71, and 21.42 g/kg/day respectively. The volume for gavage administration was calculated at 2 mL per 200 g body weight. Preparation of low, medium, and high concentrations of JDHXD was done according to the rat dosages. Edaravone 3.2 mg/kg/day was administered intraperitoneally to rats in the positive drug group.

In the first stage of this study, 36 rats were randomly divided into sham operation group (Sham), ischemia and reperfusion group (I/R), JDHXD low-dosage group (JDHXD-L), JDHXD medium-dosage group (JDHXD-M), JDHXD high-dosage group (JDHXD-H) and Edaravone group by random number table method. The number of rats required in each group was calculated based on three rats for each detection method. The rats in the JDHXD-treated groups were orally administered the corresponding dosage of a concentrated solution of JDHXD, and the other rats were given the same volume of distilled water. The administration of the drug occurred twice daily at 9:00 and 16:00 for 3 days before the surgery and continued for 3 days after the surgery until the animals were sacrificed. Following the assessment of neurological function and the cerebral infarct area, the optimal dosage of JDHXD (JDHXD-M) was chosen for subsequent experiments.

During the second stage of this trial, 36 rats were randomly allocated to one of three groups: the sham group (Sham), the ischemia and reperfusion group (I/R), and the JDHXD medium-dosage group (JDHXD-M). For the JDHXD-M animal, drug administration took place as previously reported 3 days before the surgery and the last 3 days post-reperfusion. The rats were

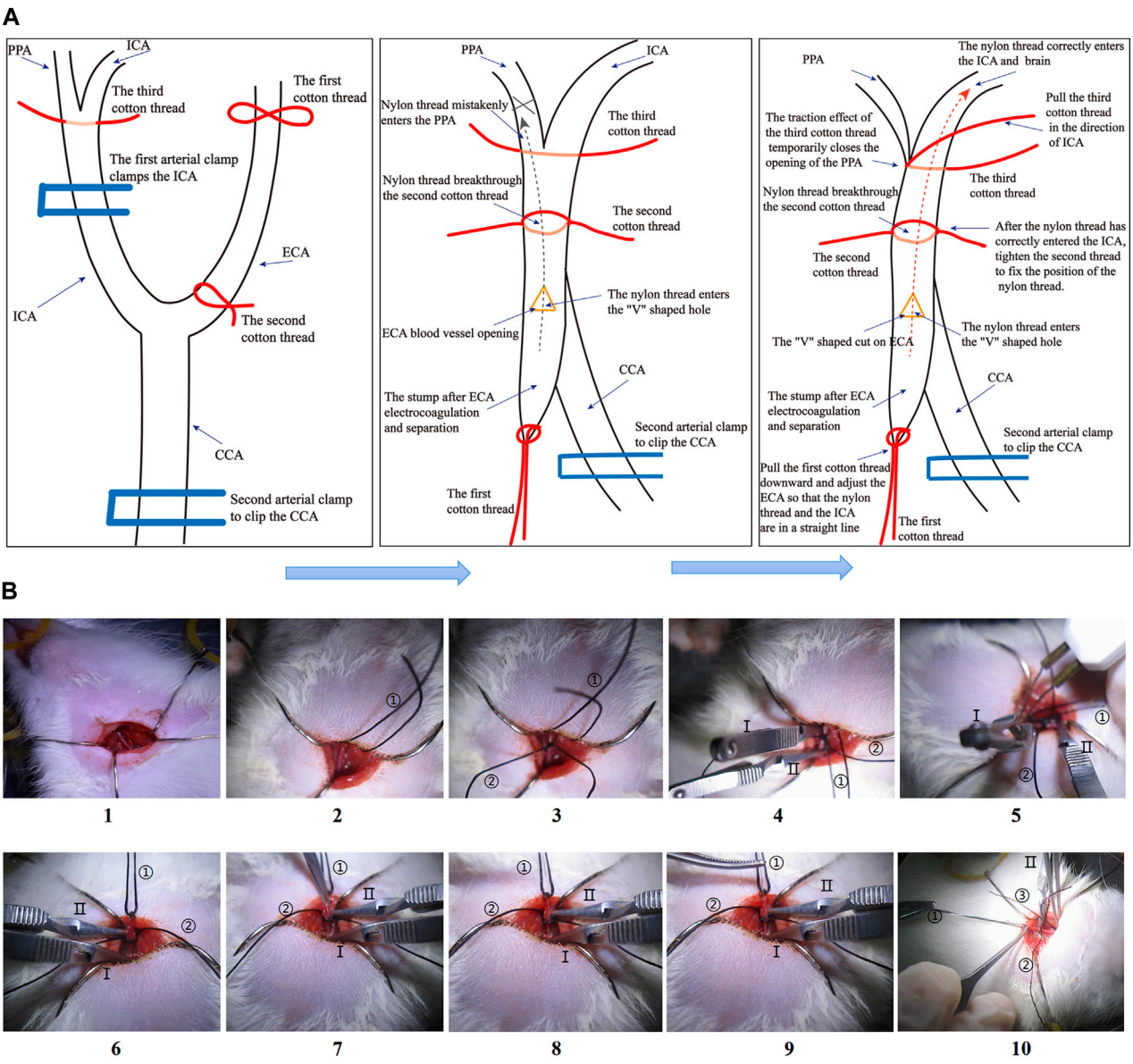


FIGURE 2
(A) Steps diagram of the Middle cerebral artery occlusion model (MCAO) in this study. **(A)** Schematic diagram of the MCAO operation steps. **(B)** The physical diagram of the operation steps of the MCAO. "①" in Figure 1B shows the first cotton thread, "②" shows the second cotton thread, and "③" shows the third cotton thread. "I" in Figure 1B shows the first arterial clip, and "II" shows the second arterial clip.

beheaded 72 h after the surgeries. Figure 1 depicts the theoretical diagram for the research.

Cerebral ischemia-reperfusion injury models

The models of focal CIRI were built with the MCAO method (Lyu et al., 2021; Huang et al., 2022). 4% isoflurane gives respiratory induction rats anesthesia, and 2% isoflurane maintains euthanasia. The left common carotid artery (CCA) was found and seen by dissection from surrounding tissues after skin cleansing and incision. The internal and external carotid arteries were then carefully exposed. After occluding the internal carotid artery with a microvascular clip and securing the distal end, the external carotid artery was transected 1 cm from the site of separation of the external carotid arteries (ECA) and internal carotid arteries (ICA). After removing the microvascular clip, a nylon monofilament (cat# 2636-A4, Beijing Cinontech, China) was introduced via the external carotid artery incision into the internal carotid arteries. Finally, when the monofilament was attached to the external carotid artery stump, resistance was felt. The monofilament was severed after 1.5 h of MCAO to accomplish reperfusion. In the current investigation, rats in the I/R and JDHXD-treated groups received blinded MCAO/R procedures, whereas rats in the sham group experienced simply the identical method without monofilament insertion. Compared with the previous method, we made detailed improvements in the surgical operation this time to shorten the operation time and

improve the stability of the model (Figure 2). In addition, this modeling method is also helpful to avoid mistaken insertion of nylon monofilament into the pterygopalatine artery (PPA).

Neurological function assessment

At 24 h and 72 h following brain infarction, the neurological deficit was measured by the Zea Longa tests. To rule out the effect of surgical failure, rats with MCAO/R but no obvious neurological abnormalities were eliminated. As previously indicated, Zea Longa tests were graded on a five-point scale (Longa et al., 1989). (0 = no deficiency, 1 = failure to extend right forepaw, 2 = right circling, 3 = right falling, 4 = No spontaneous walking with a low level of consciousness.) Before commencing the blinded testing, assessments were carried out without prior knowledge of the group allocation of the rats. Before the blinded testing, the assessments were done without knowing which group the rats were in.

2,3,5-Triphenyltetrazolium Chloride (TTC)

The brains were extracted, sliced into 3-mm-thick coronal sections, arranged on a mold, and then incubated at 37°C for 30 min in a solution comprising 2% TTC (cat# T8877-5G, Sigma, USA). Subsequently, digital photographs of the brain slices were taken (cat# HUAWEI Mate 30, HUAWEI, China), and the infarction percentage was calculated using ImageJ software (National Institutes of Health, USA). To ensure uniformity in the thickness of the slices, the brain was cut into five slices. Photography was conducted under laboratory fluorescent lighting, with no additional light sources or color processing. During the image-taking process, the same distance and lighting conditions were maintained as much as possible.

HE staining

The histological evaluation of exfoliated rat brain tissue is conducted by hematoxylin-eosin (HE) staining. The initial step in this process is the immersion of the tissue in a 4% paraformaldehyde (PFA) solution for approximately 24 h. This is followed by the sectioning of the brain tissue for observation and subsequent dehydration through a graded ethanol series. After this procedure, the embedded brain tissue is then sliced at a thickness of 3 μm. Afterward, the tissue is subjected to dewaxing, which involves the removal of wax from the sections through a series of ethanol solutions. These slices were sequentially stained using hematoxylin and eosin (cat# G1003, Servicebio). The stained samples were examined using an upright optical microscope (NIKON ECLIPSE E100, Nikon, Japan) with an imaging system (NIKON DS-U3, Nikon, Japan).

Nissl staining

Nissl staining was used to measure neuronal damage. Similar to the HE staining procedure, the tissue was initially placed in 4% PFA overnight, after which it was dehydrated with a graded alcohol series. It was then embedded in paraffin. The paraffin-embedded brain tissue was sectioned at a thickness of 3 μm. Subsequently, the tissue was incubated at 30°C for 5 minutes, during which it was stained with 1% toluidine blue (cat# G1032, Servicebio). After incubation in xylene for 10 min, sections were rinsed in a graded ethanol series and mounted. Finally, images of the same brain area were acquired using a light microscope and blinded analysis. The region surrounding the infarct core of the brain was selected as the site for quantifying the extent of neuronal damage. The corresponding hippocampal field, designated as CA-1, was identified for analysis. Efforts were made to maintain consistent section positions across different experimental groups.

LC-MS analysis of JDHXD and Medicinal serum

In our current study, we collected the abdominal aorta blood of rats 30 min after administration of JDHXD and performed non-targeted LC-MS component detection to analyze the drug metabolites. Under a low-temperature environment, extract JDHXD and blank serum samples and JDHXD drug-containing serum samples. There were three groups of rat samples: the blank serum group, the JDHXD group, and the drug-containing serum group. The biological replicates of each group were 3 cases. The metabolite extraction method is as follows: the samples were thawed on ice, after 30 s vortex, the samples were centrifuged at 12000 rpm (RCF = 13800 (×g), R = 8.6 cm) for 15 min at 4 °C. 300 μL of supernatant was transferred to a fresh tube and 1,000 μL of extracted solution containing 10 μg/mL of internal standard was added, then the samples were sonicated for 5 min in ice-water. After placing 1 h in −40°C, the samples were centrifuged at 12000 rpm (RCF = 13800 (×g), R = 8.6 cm) for 15 min at 4°C. The supernatant was carefully filtered through a 0.22 μm microporous membrane, then 200 μL from each sample and pooled as QC samples. Store at −80°C until the UHPLC- MS analysis. 400 μL of plasma samples were added to 40 μL of hydrochloric acid (2 mol/L), then the mixture was vortexed for 1 min and followed by incubation for 15 min at 4°C. The vortex and incubated cycle were repeated for 4 times. Add 1.6 mL acetonitrile, then the mixture was vortexed for 5 min and the samples were centrifuged at 12000 rpm (RCF = 13800 (×g), R = 8.6 cm) for 5 min at 4°C. 1800 μL of supernatant was transferred to a fresh tube and nitrogen dried. The dried samples were reconstituted in 150 μL of 80% methyl alcohol containing 10 μg/mL of internal standard by vortex for 5 min. The constitution was then centrifuged at 12000 rpm (RCF = 13800 (×g), R = 8.6 cm) for 5 min at 4°C, and 120 μL of supernatant was transferred to a fresh glass vial for LC/MS analysis. LC-MS/MS analysis was performed on a UHPLC system (Vanquish, Thermo Fisher Scientific) with a Waters UPLC BEH C18 column (1.7 μm 2.1*100 mm). The sample injection volume was set at 5 μL. The flow rate was set at 0.5 mL/min. The mobile phase consisted of 0.1% formic acid in water (A) and 0.1% formic acid in acetonitrile (B). The multi-step linear elution gradient program was as follows: 0–11 min, 85%–25% A; 11–12 min, 25%–2% A; 12–14 min, 2%–2% A; 14–14.1 min, 2%–85% A; 14.1–15 min, 85%–85% A; 15–16 min, 85%–85% A. A Q Exactive Focus mass spectrometer coupled with Xcalibur software was employed to obtain the MS and MS/MS data based on the IDA acquisition mode. During each acquisition cycle, the mass range was from 100 to 1,500, the top three of every cycle were screened and the corresponding MS/MS data were further acquired. Sheath gas flow rate: 45 Arb, Aux gas flow rate:

15 Arb, Capillary temperature: 400°C, Full ms resolution: 70000, MS/MS resolution: 17500, Collision energy: 15/30/45 in NCE mode, Spray Voltage: 4.0 kV (positive) or −4.0 kV (negative).

Western blot analysis

Based on the BCA protein assay kit (cat# ABW0104, Abiowell, China), the Western blot was used to measure and assess the amount of peri-infarcted protein levels. Briefly, proteins were transferred onto PVDF membranes (cat# IPVH00010, Millipore, USA). After the membranes were blocked with 4% nonfat milk for 2.5 h, the membranes were then incubated for 8 h at 4°C with multiple antibodies. Antibody information: NLRP3 (1:10,000, cat# ET1610-93, HUABIO), ASC (1:10,000, cat# 340097, ZENBIO), Caspase-1 (1:10,000, cat# ET1608-69, HUABIO), Gasdermin D (1:10,000, cat# HA721144, HUABIO), IL-18 (1:5,000, cat# 60070-1-Ig, Proteintech), IL-1β (1:5,000, cat# 511369, ZENBIO), IL-6 (1:5,000, cat# R1412-2, HUABIO), ULK1 (1:10,000, cat# 20986-1-AP, Proteintech), Beclin1 (1:10,000, cat#11306-1-AP, Proteintech), LC3 (I/II) (1:10,000, cat#12741, Cell Signaling), ZO-1 (1:10,000, cat# 21773-1-AP, Proteintech), P62 (1:5000, cat#HA721171, HUABIO), Beta Actin (1:10,000, cat# 20536-1-AP, Proteintech). The membranes were further incubated with horseradish peroxidase (HRP)-linked goat anti-rabbit IgG (1:10, 000, cat# E-AB-1003, Elabscience) or goat anti-mouse IgG secondary antibodies (1:10, 000, cat# E-AB-1001, Elabscience) for 1 h. After ECL photography, wash the membrane with stripping buffer for 20 min, and recycle the membrane. The blocking step should be conducted with 4% nonfat milk for 2.5 h, then incubated with another primary antibody. Repeat the previous steps to detect the expression level of another antibody. The amounts of proteins were detected and assessed using Bio-Rad Laboratories (BIO-RAD, USA). The Western blot images were analyzed by ImageJ software (NIH, USA).

Immunohistochemical Staining

In brief, paraffin-embedded brain tissue was cut into 3 mm thick sections and dewaxed with xylene, then eluted with an ethanol gradient. The sections were placed in a microwave oven and antigen retrieval was conducted using sodium citrate. A blocking agent was then added, and the sections were incubated at 4°C for 30 min with 5% goat serum. The primary antibody, GSDMD (1:500, cat# 20770-1-AP, Proteintech), was applied, and the sections were incubated at 4°C overnight. The secondary antibody was applied at 37°C for 30 min. The DAB/DEC color development solution was applied for a period of five minutes, followed by a 3-minute incubation with hematoxylin staining solution. Hydrochloric acid-ethanol differentiation was conducted for 20 seconds, lithium carbonate solution was used for blueing, and the sections were then dehydrated and mounted. The sections were photographed under a microscope, and Image J software was employed to analyze the intensity of brown-yellow positive expression.

Immunofluorescence

Briefly, the 3-mm-thick sections of brain tissues were blocked for 1 h with 5% goat serum. Thereafter, they were incubated for 24 h at 4°C with multiple primary antibodies. Antibody information: GSDMD (1:500, cat# 20770-1-AP, Proteintech), GSDMD (1:500, cat# 20770-1-AP, Servicebio), NLRP3 (1:200, cat# GB114320-100, Servicebio), caspase-1 (1:600, cat# GB11383-100, Servicebio), LC3 (I/II) (1:2000, cat# GB11124, Servicebio), NLRP3 (1:500, cat# ET1610-93, HUABIO), Caspase-1 (1:100, cat# 22915-1-AP, Proteintech), NeuN (1:1,000, cat# GB11138, Servicebio), DAPI (1:500, cat# G1012, Servicebio). DAPI glows blue by UV excitation wavelength 330–380 nm and emission wavelength 420 nm; FITC glows green by excitation wavelength 465–495 nm and emission wavelength 515–555 nm; CY3 glows red by excitation wavelength 510–560 nm and emission wavelength 590 nm. The figures were taken by fluorescence microscope (Nikon, Japan).

Analytical statistics

Continuous data were presented as mean ± standard deviation (SD) using the GraphPad Prism software, and one-way ANOVA was conducted to ascertain significant differences between groups (GraphPad Prism Software Inc., San Diego, CA, USA). A significance level of $p < 0.05$ was employed to determine statistical significance. Data that significantly deviate from the mean will be eliminated. Outliers are identified through the Grubbs test, and the number of repeated tests is increased for values that deviate from the norm or for different research personnel to verify the results. If a significant deviation is confirmed, outliers are removed.

Results

Metabolites analysis of JDHXD medicated serum

The Supplementary Material showed the untargeted LC-MS positive/negative ion spectrum of JDHXD blood metabolites (Supplementary Material S1). Because LC-MS yields total anion and total cation maps, there is masking of the wave peaks of different substances and does not facilitate direct labeling of the metabolite peak spectra directly in the ion maps, the specific comparison of the blood-entry metabolites is shown in Table 2. Table 2 illustrates the comparison of the metabolites. Table 2 showed 30 possible metabolites with a similarity score of >0.98 in the JDHXD medicated serum component spectrum analyzed by LC-MS. Then based on the ten plant combinations of JDHXD: *Pueraria edulis* Pamp [Fabaceae], *Paeonia veitchii* Lynch [Paeoniaceae], *Prunus persica (L.)* Batsch [Rosaceae], *Anethum graveolens* L. [Apiaceae], *Rehmannia glutinosa (Gaertn.)* DC. [Orobanchaceae], *Carthamus tinctorius* L. [Asteraceae], *Forsythia suspensa (Thunb.)* Vahl [Oleaceae], *Bupleurum falcatum* L. [Apiaceae], *Citrus medica* L. [Rutaceae], *Glycyrrhiza glabra* L. [Fabaceae]). A total of 1,174 possible metabolites derived from the JDHXD-containing serum were selected (Composite Score >0.6). The closer the spectrum similarity score is to 1, the higher the structural similarity. The Table 2 shows the metabolites' name, original plant source, and metabolite spectrum composite score. In addition, the table also showed the assay values for metabolites with a composite score greater than 0.98 in blank serum, JDHXD drug solution, and JDHXD-containing serum. It is important to

TABLE 2 LC-MS/MS analysis of metabolites in JDHXD medicated serum (Composite Score >0.98).

No.	Name	Botanical drugs	Compo-site score	Blank serum 1	Blank serum 2	Blank serum 3	JDHXD1	JDHXD2	JDHXD3	JDHXD serum 1	JDHXD serum 2	JDHXD serum 3
1	2-Octenoic acid	*Bupleurum falcatum* L. [Apiaceae]	1	33526386.99	31918941.05	30366077.07	27679886.45	26047574.2	24637554.42	27034216.46	26327116.06	38194633.09
2	5-HYDROXYMETHYL-2-FURANCARBOXYLIC ACID	*Rehmannia glutinosa (Gaertn.)* DC. [Orobanchaceae]	1	2295488.679	1450542.933	0	47674890.75	46527312.41	45174820.9	0	5855370.021	1755579.779
3	Baicalein	*Carthamus tinctorius* L. [Asteraceae]; *Paeonia veitchii Lynch* [Paeoniaceae]	1	137603888.2	127435055.9	112581544.4	172283.2092	212336.696	156548.459	54268574.01	47023934.24	10016018.54
4	Indole-3-carboxylic acid	*Glycyrrhiza glabra* L. [Fabaceae]	1	13469142.89	13203008.53	1,3942008.28	938468.7319	948294.1136	1071481.947	10427139.83	10232425.35	3633702.402
5	Methylnissolin-3-O-glucoside	*Anethum graveolens* L. [Apiaceae]	1	0	0	0	24772478.77	23077088.44	22967588.59	0	116848.4373	0
6	p-Hydroxybenzaldehyde	*Pueraria edulis* Pamp [Fabaceae]	1	12749816.97	14434648.55	10935133.36	245007095.3	247008477	248652406	9160790.757	12444179.78	9300150.971
7	Quercetin	*Pueraria edulis* Pamp [Fabaceae] *Bupleurum falcatum* L. [Apiaceae]; *Carthamus tinctorius* L. [Asteraceae]	1	0	103208.5123	44908.55502	24938053.79	25916371.08	24771563.58	155264.0965	41445.76569	572401.8785
8	Scutellarein	*Carthamus tinctorius* L. [Asteraceae]	1	24613.20225	44530.70708	36508.43751	39425330.14	44126473.96	42195209.75	895059.6164	1193062.241	1479907.622
9	Genistein	*Pueraria edulis* Pamp [Fabaceae]	0.999999	521618.1842	734657.2362	1015771.452	12448055.45	12604829.35	12234904.15	692576.0342	909797.7863	283964.5742
10	Pyrocatechol	*Carthamus tinctorius* L. [Asteraceae]; *Prunus persica* (L.) Batsch [Rosaceae]	0.999979769	1792675.296	1384688.008	1105512.573	7269450.303	7389564.14	4310365.589	420742.8586	569956.6155	669592.9478
11	Adenine	*Anethum graveolens* L. [Apiaceae]	0.999903462	45080650.33	26234116.14	36324013.37	437433834.8	440172444.8	450436588.3	7527368.949	2353952.37	11944398.68
12	Liquiritigenin	*Pueraria edulis* Pamp [Fabaceae]; *Glycyrrhiza glabra* L. [Fabaceae]	0.997646692	336233.2093	1520972.604	1332806.392	400249.906	347373.701	604859.6631	33012207.55	29884405.33	4889048.021
13	Daidzein	*Pueraria edulis* Pamp [Fabaceae]	0.997220308	2505838.863	2775918.922	2929516.206	1879687960	1892177727	1903152190	8916035.238	9355704.749	2074290.392
14	Xanthotoxol	*Citrus medica* L. [Rutaceae]; *Anethum graveolens* L. [Apiaceae]	0.995398154	36926.79674	46667.67757	67998.31834	7631357.438	7869663.346	8017132.314	33288.52626	23352.52818	0
15	Isorhamnetin	*Glycyrrhiza glabra* L. [Fabaceae]; *Bupleurum falcatum* L. [Apiaceae]	0.995101077	0	0	0	16959827.81	16268316.34	17705896.29	718125.0212	786451.8819	930092.657

(Continued on following page)

10.3389/fphar.2024.1449452

TABLE 2 (*Continued*) LC-MS/MS analysis of metabolites in JDHXD medicated serum (Composite Score >0.98).

No.	Name	Botanical drugs	Compo-site score	Blank serum 1	Blank serum 2	Blank serum 3	JDHXD1	JDHXD2	JDHXD3	JDHXD serum 1	JDHXD serum 2	JDHXD serum 3
16	Scopoletin	*Forsythia suspensa (Thunb.)* Vahl [Oleaceae]; *Anethum graveolens* L. [Apiaceae]; *Glycyrrhiza glabra* L. [Fabaceae]; *Bupleurum falcatum* L. [Apiaceae]	0.994920231	3523516.481	8497248.766	10094242.82	6800668.766	13988634.03	5619104.177	9739483.531	9207170.189	7637459.356
17	(+/−)-Jasmonic acid	*Citrus medica* L. [Rutaceae]	0.993650846	1753070.721	2265081.225	2082550.086	426540.3759	367005.5974	468690.1548	1348686.564	1554043.158	2145586.288
18	Biochanin A	*Pueraria edulis* Pamp [Fabaceae]	0.993143385	440662.2446	160976.2658	146674.3868	100822826.1	94854103.23	97635226.94	973690.2118	1295050.31	716833.6495
19	Methyl hexadecanoate	*Pueraria edulis* Pamp [Fabaceae]; *Paeonia veitchii* Lynch [Paeoniaceae]; *Prunus persica* (L.) Batsch [Rosaceae]	0.992738	7880680.801	8535370.148	8955699.694	34947.47829	11954.25219	31124.7922	13847800.96	13810169.31	4548178.284
20	Wogonin	*Forsythia suspensa* (Thunb.) Vahl [Oleaceae]	0.992622154	46158333.28	46449517.26	51646546.05	158776245.8	162275820.2	161536285.4	376697167.7	376936701	5645137.914
21	7-Hydroxycoumarin	*Citrus medica* L. [Rutaceae]; *Anethum graveolens* L. [Apiaceae]; *Forsythia suspensa* (Thunb.) Vahl [Oleaceae]	0.992348385	1985240.076	1736999.464	1855661.178	396904414.6	419959144.6	423509537.4	1192292.781	1957527.618	2247232.647
22	Genkwanin	*Glycyrrhiza glabra* L. [Fabaceae]	0.991977154	2606722.886	2530362.482	2049485.537	68686232.5	69161039.5	67201769.7	26985912.45	24348705.02	5769563.191
23	magnolol	*Citrus medica* L. [Rutaceae]	0.991036923	116667.3412	54730.46163	27195.76422	12225491.42	10810012.82	11666127.15	145676.0231	388400.8612	149898.6976
24	Kaempferide	*Carthamus tinctorius* L. [Asteraceae]	0.989199846	495096.6106	492660.8302	404650.9711	912147.3486	1114992.206	1188308.663	876900.6075	684449.6833	176742.502
25	alpha-Linolenic acid	*Bupleurum falcatum* L. [Apiaceae]; *Carthamus tinctorius* L. [Asteraceae]; *Prunus persica* (L.) Batsch [Rosaceae]	0.983700692	11457160.96	16259517.7	18252916.84	2128424.436	2185558.256	2164212.649	15802196.7	13628633.97	18885641.98
26	Nicotinic acid	*Anethum graveolens* L. [Apiaceae]	0.983485385	8732229.227	8962208.648	10506670.64	13565913.01	13326116.13	13092406.35	8996147.805	8554744.259	10736957.42
27	2-Ethylphenol	*Anethum graveolens* L. [Apiaceae]	0.982149	3018656.272	2265248.912	2895775.329	7723605.129	8139428.666	7543579.113	3220141.108	2092897.664	3386825.874
28	eriocitrin	*Citrus medica* L. [Rutaceae]	0.980994231	0	0	0	2727903.033	3145598.286	2642769.072	0	0	0
29	Choline [M+]	*Anethum graveolens* L. [Apiaceae]; *Forsythia suspensa* (Thunb.) Vahl [Oleaceae]	0.980813	837414910.2	974847415.3	952590406.2	2371366284	2309712551	2441160317	973100819.5	870448804.8	972883048.3
30	Palmatine	*Pueraria edulis* Pamp [Fabaceae]; *Glycyrrhiza glabra* L. [Fabaceae]	0.980601769	55410.34584	59111.41605	145233.4135	240442449.3	226089832.4	230532979.3	116481.8016	209755.6923	248578.5025

10.3389/fphar.2024.1449452

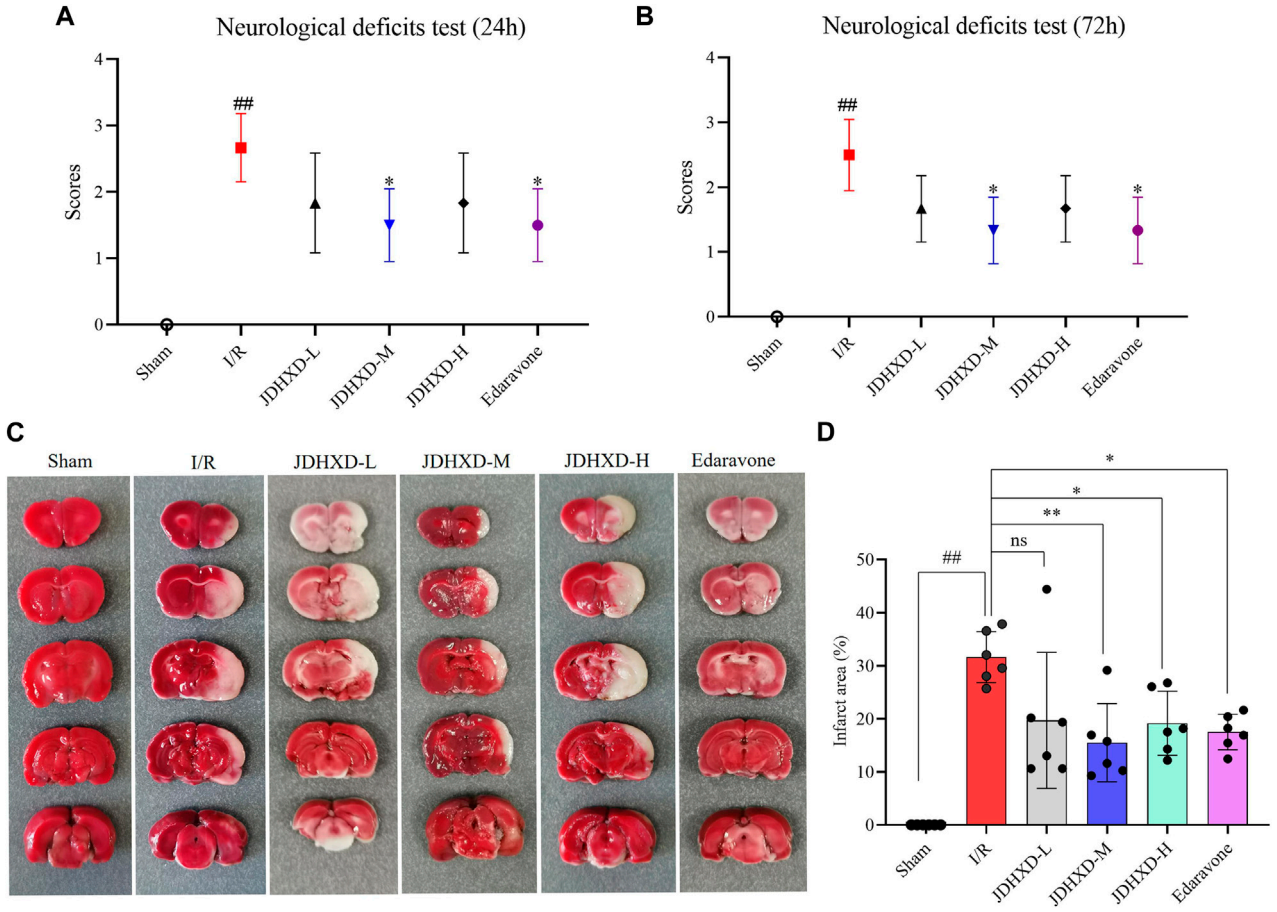


FIGURE 3
JDHXD reduced neurological deficits and cerebral infarction following CIRI. **(A)** Test for neurological impairments 24 h after reperfusion. **(B)** Test for neurological impairments 72 h after reperfusion. Both **(A)** and **(B)** demonstrated that a modest dosage of JDHXD decreased neurological deficits in rats 24 and 72 h after reperfusion, n = 6. **(C)** Typical pictures of TTC staining of rat brain tissue in each group. Non-infarcted tissue is stained red by the TTC solution, while the infarcted area is white. **(D)** Comparison of the brain infarct area to different groups, n = 6. $^{\#\#}p < 0.01$ vs. Sham group; $^{**}p < 0.01$ vs. I/R group. $^{*}p < 0.05$ vs. I/R group. (JDHXD, Jie-Du-Huo-Xue decoction; CIRI, cerebral ischemia-reperfusion injury; TTC, 2,3,5-Triphenyltetrazolium Chloride).

explain that since non-targeted LC-MS will detect a large number of possible substances, only possible substances with a similarity of >0.98 are shown in Table 2. This is why some theoretically important active substances are not shown in Table 2.

JDHXD mitigated neurological impairments and cerebral infarction

Compared with the I/R group, the JDHXD-M treated group showed significantly lower neurological deficit scores at 24 and 72 h after reperfusion ($p < 0.05$). The group administered the positive drug exhibited a similar trend to that observed in the JDHXD-M group. In the current experiment, we optimized the MCAO modeling method, shortened the operation time, and made the model more stable. Figure 3 illustrated that rats in the sham group displayed no cerebral infarction, whereas those in the I/R group showed evident cerebral ischemia ($p < 0.01$). JDHXD-M group revealed significantly less cerebral infarct area than the I/R group ($p < 0.01$). Different from the previous results, the JDHXD-H group also exhibited significant statistical differences ($p < 0.05$). Based on the findings from the initial stage of this study, the subsequent tests selected the suitable dose of JDHXD (JDHXD-M) to assess its potential effects on the interplay between neuroinflammation-related pyroptosis and autophagy.

JDHXD reduced neuronal damage after CIRI in rats

The above results demonstrated that JDHXD could reduce neurological impairment and cerebral infarction induced by CIRI. To further demonstrate the neuroprotective effect of JDHXD, we evaluated the morphological changes of neurons in the central-infarct zone, peri-infarct zone, hippocampus CA-1, and corpus striatum (Figures 4A, B). Compared with the sham group, the cells in the infarct core area were arranged disorderly in the I/R group. Typical cell shrinkage and nuclear pyknosis occur. Vacuoles surrounding cells indicate the presence of tissue edema. As illustrated in Figures 4C, D,

10.3389/fphar.2024.1449452

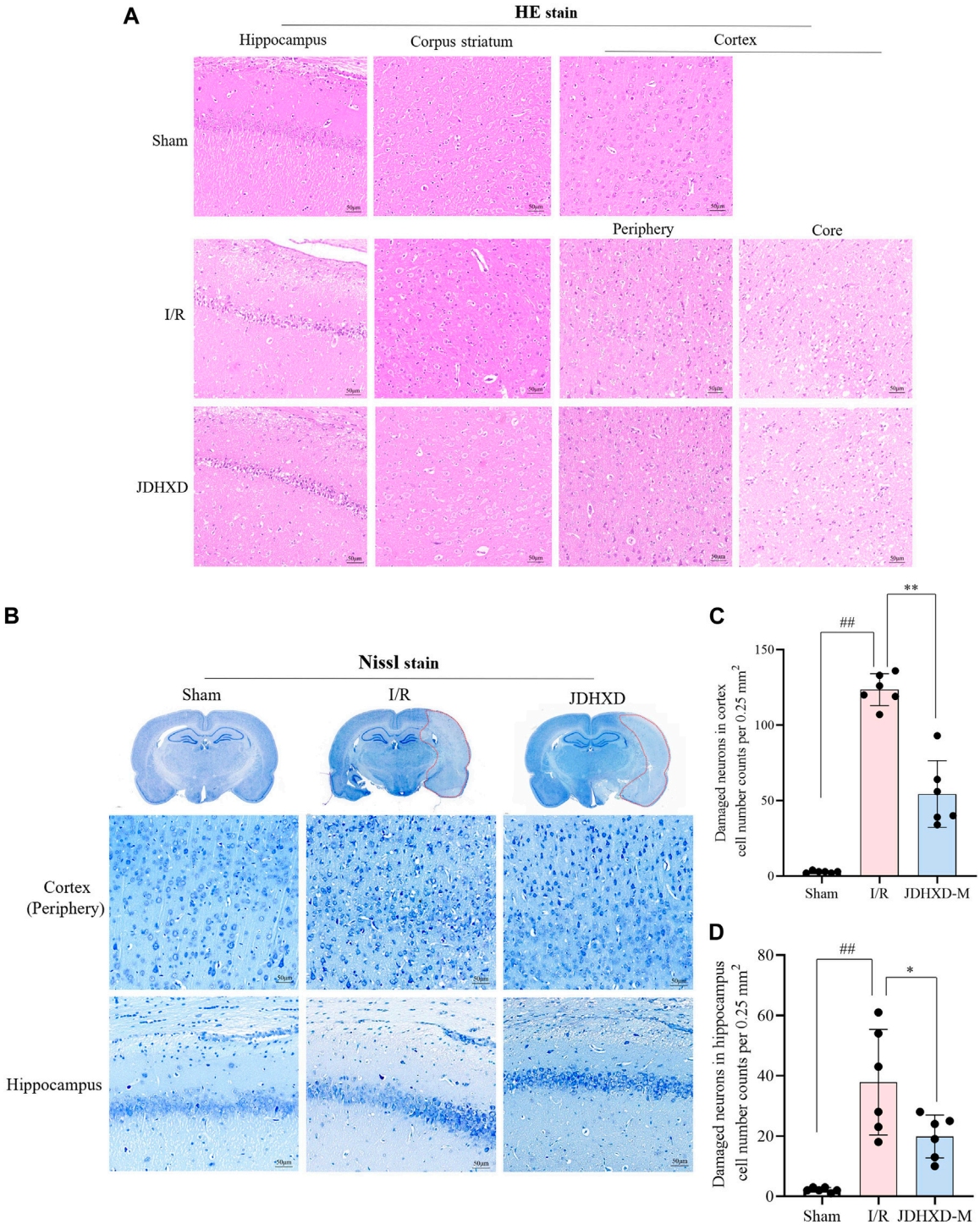


FIGURE 4
JDHXD ameliorated neuronal injury 72 h post-CIRI in rats. **(A)** Representative images of HE staining in the ischemic cortex, hippocampus, and corpus striatum. scale bars = 50 μm, n = 3. **(B)** Panoramic scan with Nissl staining and partial map of cortex and hippocampus-CA1. **(C, D)** Quantitative assessment of neuronal damage in the cortex and hippocampus, n = 6. $^{\#\#}p < 0.01$ vs. Sham group; $^{*}p < 0.05$ vs. I/R group.. (The edge of the infarct core was selected as the observation field for the purpose of counting the number of damaged neurons. This was because, in the infarct core, there was no significant difference in the number of neurons with abnormal morphology between the I/R group and the JDHXD group. The presence of damaged neurons can be identified by the following characteristics: cell shrinkage, reduced synapses, obvious cell morphology collapse, disordered cell arrangement, and widened tissue gaps around cells under Nissl staining.)

JDHXD treatment reduced the number of morphologically abnormal cells in the cortical penumbra compared with the I/R group ($p < 0.01$). Furthermore, JDHXD treatment reduced morphologically abnormal cell numbers in the hippocampal CA-1 compared with the I/R group ($p < 0.05$). However, the protective effect of JDHXD was not reflected in

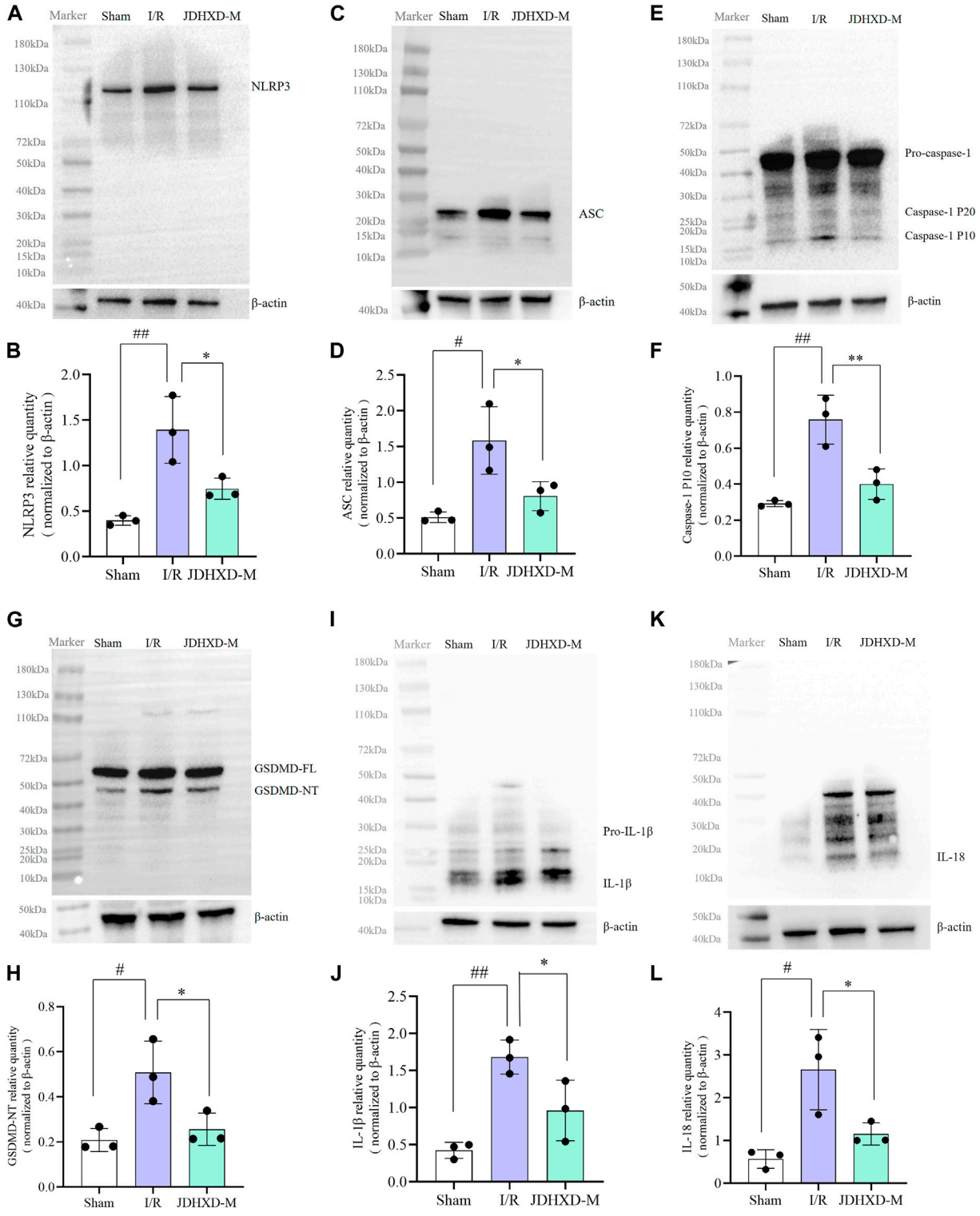


FIGURE 5
Expression of pyroptosis-related molecules in the peri-infarct region following JDHXD-M therapy. **(A, B)** Western blot of the NLRP3, ASC, pro-caspase-1, caspase-1 P10, GSDMD-FL, GSDMD-NT, IL-1β, IL-18 and β-actin proteins in peri-infarct tissues. **(C–L)** Statistical chart of relative expression of NLRP3, ASC, Caspase-1 P10, GSDMD-NT, IL-1β, IL-18. Data are expressed as means ± SD, n = 3, $^{\#\#}p < 0.01$ vs. Sham group; $^{\#}p < 0.05$ vs. Sham group; $^{**}p < 0.01$ vs. I/R group; $^{*}p < 0.05$ vs. I/R group. (GSDMD, gasdermin D; GSDMD-FL, Gasdermin D full length; GSDMD-NT, Gasdermin D N terminal; IL, interleukin; NLRP3, nucleotide-binding oligomerization domain-like receptor pyrin domain containing 3; ASC, apoptosis-associated speck-like protein containing a card; SD, standard deviation).

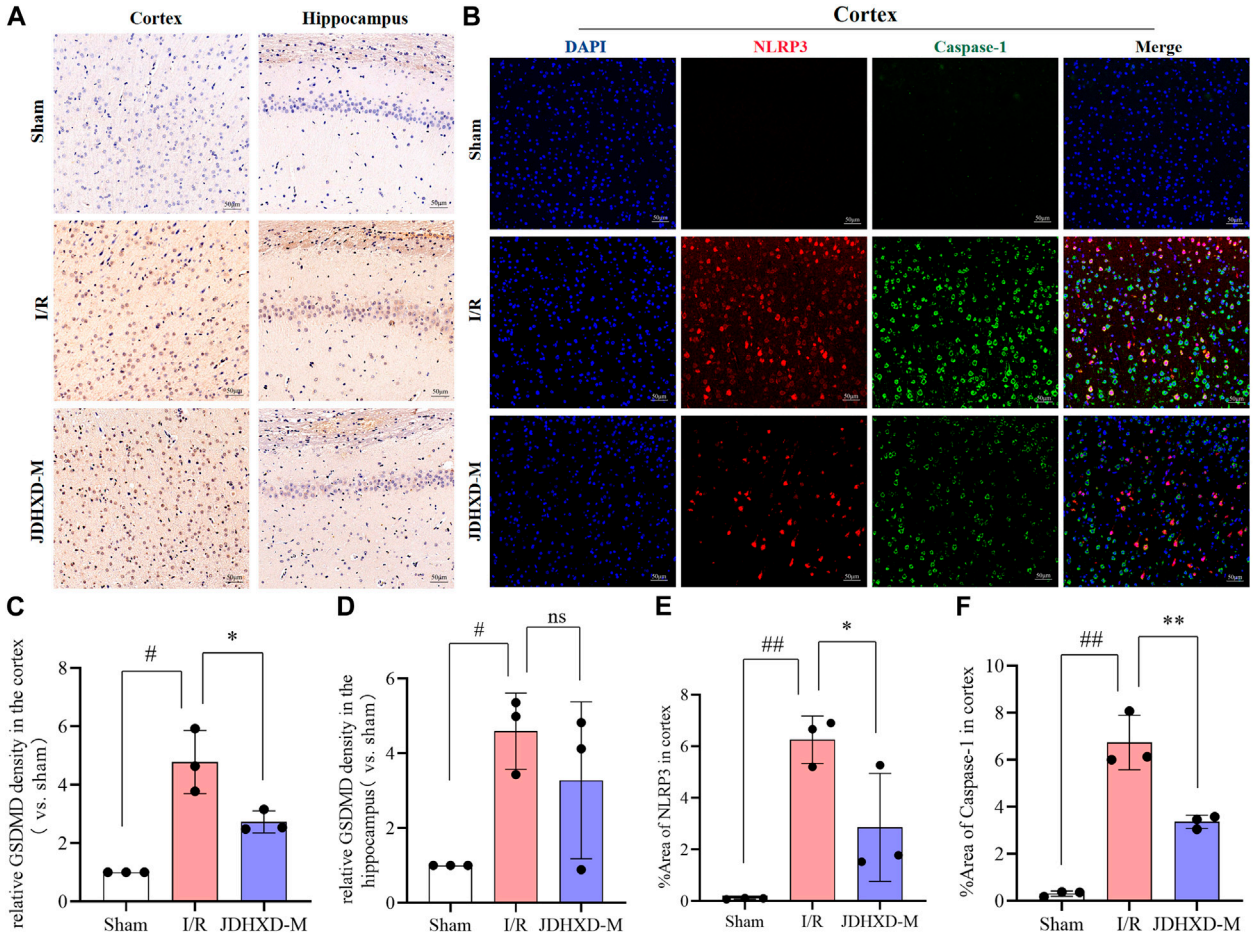


FIGURE 6
Immunohistochemistry and immunofluorescence results of relative expression of pyroptosis-related proteins. **(A)** Immunohistochemistry results of GSDMD in the penumbra on the third day after CI in rats. Brown represents the positive expression of GSDMD, and blue represents the nucleus. **(B)** Immunofluorescence results of NLRP3 and caspase-1 in the penumbra zone on the third day after CI in rats, NLRP3 (red), caspase-1 (green), DAPI (blue). **(C)** Relative expression of GSDMD in the penumbra of ischemic cortex in immunohistochemistry experiment. **(D)** Relative expression of GSDMD in the ischemic hippocampus in immunohistochemistry experiment. **(E)** Expression area % of NLRP3 in ischemic cortical penumbra in immunofluorescence experiment. **(F)** Expression area % of caspase-1 in the ischemic cortical penumbra in immunofluorescence experiment. Data are expressed as means ± SD, n = 3, $^{\#\#}p < 0.01$ vs. Sham group; $^{\#}p < 0.05$ vs. Sham group; $^{**}p < 0.01$ vs. I/R group; $^{*}p < 0.05$ vs. I/R group. (GSDMD, gasdermin D; NLRP3, nucleotide-binding oligomerization domain-like receptor pyrin domain containing 3; DAPI, 4′,6-diamidino-2-phenylindole).

the infarct center. There was no significant difference in the infarct core between the I/R and JDHXD groups ($p > 0.05$). These results are consistent with the indicative significance of neurological function assessment and cerebral infarct area measurement.

JDHXD reduces the neuronal pyroptosis in the penumbra 3 Days following CI

To better represent the expression of pyroptosis-related proteins, we showed the Western blot image of the entire PVDF membrane. As shown in Figures 5A–D, JDHXD-M inhibited the expression of NLRP3 and ASC around the infarct on the third day after CI in rats ($p < 0.05$). This indicates that JDHXD inhibits the expression of inflammasomes that induce pyroptosis. Consistent with previous findings, JDHXD-M markedly reduced the expression levels of caspase-1 P10 ($p < 0.01$), and GSDMD-NT ($p < 0.05$) (Figures 5E–G). GSDMD-NT can oligomerize to form holes on the cell membrane and is the direct executor of pyroptosis. Caspase-1 P10 is one of the effector fragments after caspase-1 cleavage, which is upstream of GSDMD and can cleave GSDMD-FL into GSDMD-NT. This indicates that JDHXD-M inhibits the classical pathway pyroptosis around the infarct on the third day after CI in rats. Similar results have been observed with downstream signaling molecules of pyroptosis, including IL-18 and IL-1β (Figure 5I–L). Compared with the IR group, the expression of IL-18 and IL-1β in the JDHXD-M group was significantly reduced ($p < 0.05$). IL-1β and IL-18 are downstream inflammatory factors released by pyroptotic GSDMD pores, causing inflammatory damage to brain tissue.

We further examined the localization of pyroptosis markers such as NLRP3, caspase-1, and GSDMD by immunofluorescence and immunohistochemistry. The immunohistochemistry showed that brown-yellow GSDMD positive expression can be observed around

10.3389/fphar.2024.1449452

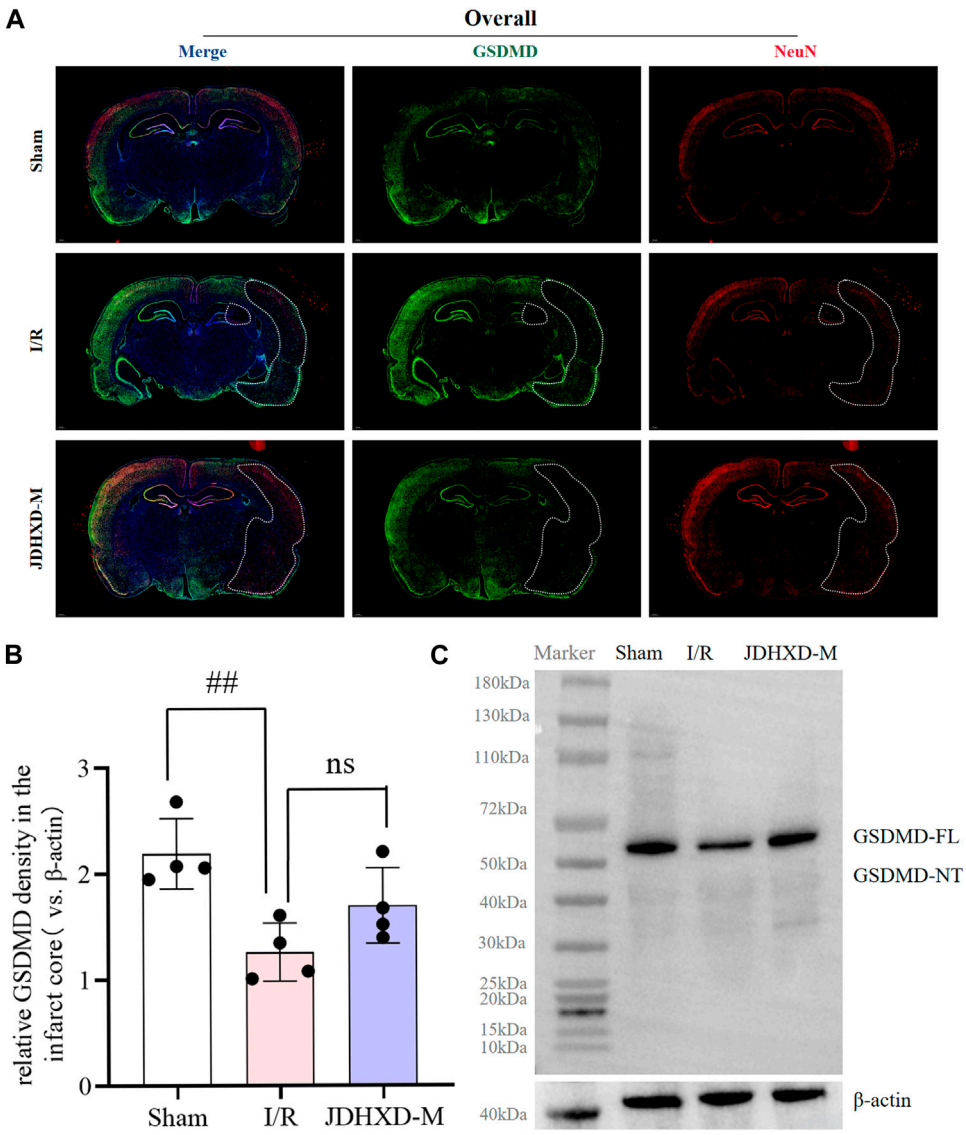


FIGURE 7
The key pyroptosis execution protein GSDMD is lost in the infarct core area on the third day after CI in rats. **(A)** Immunofluorescence panoramic scan of GSDMD and NeuN. GSDMD (green), NeuN (red), DAPI (blue). The white dotted line is the core area of infarction. **(B)** Relative expression of GSDMD protein in the infarct core. n = 4, scale bar = 50 μm $^{\#}p < 0.05$ vs. Sham group; $^{*}p < 0.05$ vs. I/R group. **(C)** Typical Western blot image of GSDMD protein in the infarct core area. (GSDMD, gasdermin D; DAPI, 4′,6-diamidino-2-phenylindole; JDHXD, Jie-Du-Huo-Xue decoction; CIRI, cerebral ischemia-reperfusion injury; NeuN, neuron-specific nuclear protein).

the infarction in the ischemic hemisphere (Figure 6A). We discovered that the expression of NLRP3 and caspase-1 increased in the infarcted hemisphere in I/R and JDHXD-M groups (Figure 6B). Three days after CI in rats, NLRP3 could be observed in the infarct core, while the expression of caspase-1 and GSDMD was mainly in the peri-infarct penumbra. These findings align with our prior investigations and those of other research teams. Compared with the I/R group, the relative density of GSDMD in the ischemic hemisphere of the JDHXD-M group was significantly reduced. (Figure 6C, D, $p < 0.05$). Compared with the IR group, the fluorescence area percentage of NLRP3 and caspase-1 in the ischemic hemisphere of the JDHXD-M group was significantly reduced (Figure 6E, F, $p < 0.05$). In summary, JDHXD inhibits the expression of pyroptosis.

Loss of pyroptotic GSDMD protein May contribute to adverse outcomes of CIRI

During performing GSDMD fluorescence staining, we observed an intriguing phenomenon that, to the best of our knowledge, has not been previously reported. In this preliminary report, we present our observations on this phenomenon. Our findings indicate that the green GSDMD fluorescence is distributed symmetrically in the left and right cerebral hemispheres. In contrast, the green GSDMD fluorescence is absent in the infarct core of the I/R group and JDHXD-M group (Figure 7A). It is crucial to highlight that previous studies have described this phenomenon as a high expression of GSDMD in the penumbra. However, the results of our panoramic

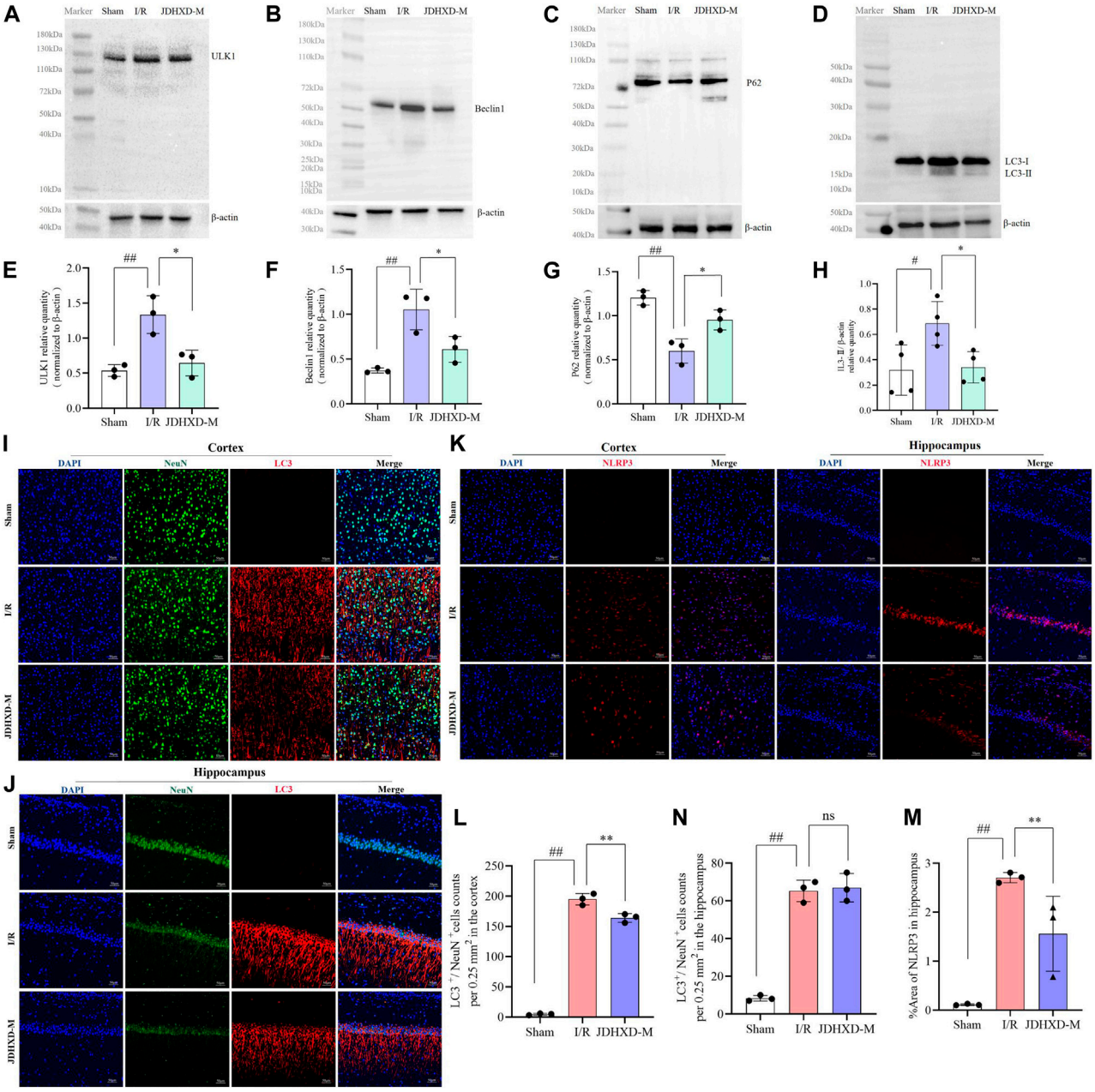


FIGURE 8
Expression levels of autophagy-related molecules in the peri-infarct region following treatment with JDHXD-M. **(A)** Western blot of the ULK-1. **(B)** Western blot of beclin1. **(C)** Western blot of P62. **(D)** Western blot of LC3-I/II. **(E–H)** Relative expression of ULK1, beclin1, P62, LC3-I/II in the infarct core. Data are expressed as means ± SD, n = 3, scale bar = 50 μm $^{\#\#}p < 0.01$ vs. Sham group; $^{**}p < 0.01$ vs. I/R group, $^{*}p < 0.05$ vs. I/R group. **(I)** Double immunofluorescence staining of the cortex with NeuN (green) and LC3 (red) on day 3 after MCAO. **(J)** Double immunofluorescence staining of the hippocampus with NeuN (green) and LC3 (red) on day 3 after MCAO. **(L)** The histogram quantified the $LC3^{+}/NeuN^{+}$ cells of the cortex. **(M)** The histogram quantified the $LC3^{+}/NeuN^{+}$ cells of the hippocampus. **(K)** Immunofluorescence results of NLRP3 in the penumbra on the third day after CIRI in rats, NLRP3 (red) and DAPI (blue). **(N)** Expression area % of NLRP3 in immunofluorescence experiment. Data are expressed as means ± SD, n = 3, scale bar = 50 μm $^{\#\#}p < 0.01$ vs. Sham group; $^{**}p < 0.01$ vs. I/R group; $^{ns}p > 0.05$. (LC3, lipidation of microtubule-associated light chain 3; ULK1, unc-51-like autophagy activating kinase 1; NLRP3, nucleotide-binding oligomerization domain-like receptor pyrin domain containing 3; CIRI, cerebral ischemia-reperfusion injury; NeuN, neuron-specific nuclear protein; JDHXD-M, Jie-Du-Huo-Xue decoction-medium dose).

scan demonstrate that the expression intensity of GSDMD fluorescence in the non-infarcted hemisphere and penumbra is nearly identical, and is significantly higher than that observed in the infarct core area. To ensure the accuracy and reproducibility of the results, we replaced the GSDMD antibodies with different species antibodies and performed the procedures by different personnel. The results remained consistent with those previously described. Furthermore, western blot analysis of brain tissue from the core of the infarction revealed a significant reduction in GSDMD-FL expression in the I/R group ($p < 0.05$). However, the protein bands of GSDMD-NT in the infarct core of the sham operation group, I/R group, and JDHXD group were not visible

(Figures 7B, C). The results of Western blotting were aligned with those of double immunofluorescence, thereby providing a basis for proposing a phenomenon that was inconsistent with previous findings. This may indicate that the loss of pyroptotic GSDMD protein after CI may also contribute to the adverse outcomes of CI. It is possible that excessive activation of GSDMD around the infarct and massive loss of the infarct core may result in damage after CI. Although further investigation is required to elucidate the underlying mechanism, we have elected to present this valuable finding for consideration.

JDHXD inhibited the expression of NLRP3 protein of pyroptosis not by promoting autophagy

Similar to pyroptosis, autophagy can also regulate cellular inflammatory responses through the inflammasome (Wang et al., 2020). Autophagy is a double-edged sword. Moderate autophagy during CI is conducive to maintaining cell function under the low energy supply state of ischemia and hypoxia (Wei et al., 2012). Insufficient autophagy is not conducive to the clearance of inflammatory products and stress in the early stage of ischemia, but excessive autophagy can cause tissue damage (Wang et al., 2018). The state of autophagy in CI is both an enemy and a friend, so there is no conclusion on whether autophagy is good or bad in CI(Nabavi et al., 2019; Orellana-Urzúa et al., 2020). Major studies suggested that autophagy is enhanced after CI, and appropriate inhibition of autophagy can reduce ischemia-reperfusion injury. Our study also supported the above view. To explore the intervention effect of JDHXD on neuronal autophagy during the initial phase of CIRI, we assessed the expression of autophagy-related proteins. Our findings revealed that on the third day following CI in rats, the level of autophagy was higher than the normal level. Compared to the sham group, the expression of the autophagy-initiating factor ULK1 was found to be significantly elevated in the IR group ($p < 0.01$). Furthermore, the expression of beclin1 demonstrated a significant upregulation following CI ($p < 0.01$). Similarly, the level of LC3-II, a marker of autophagy, was elevated in the ischemic hemisphere ($p < 0.05$). JDHXD downregulated the ULK1, beclin1, and LC3-Ⅱ in rats with CIRI, which indicates that JDHXD inhibited autophagy in the ischemic hemisphere (Figures 8A-H, $p < 0.05$).

We used immunofluorescence to label the autophagy protein LC3 and NeuN to observe the level of neuronal autophagy, and the results supported the above conclusions (Figure 8I, L, $p < 0.01$). Interestingly, the expression of LC3 in the hippocampus was not different between the IR and the JDHXD-M groups (Figure 8J, N, $p > 0.05$). At the same time, the expression level of NLRP3 did not increase due to the decrease in autophagy levels (Figure 8K, M, $p < 0.01$). The above results suggest that JDHXD suppressed the excessively increased autophagy level after CI.

Discussion

Timely and reliable national stroke surveillance remains a significant challenge (Ziaeian et al., 2022). Due to the strict window period of treatment and the inpatient system to be improved, acute ischemic stroke continues to be the primary cause of mortality and disability (Mosconi and Paciaroni, 2022; Ziaeian et al., 2022). The pathological mechanism of CI is very complex, involving multiple disease stages such as the early and recovery stages. Different cell death modes such as apoptosis, autophagy, and pyroptosis crosstalk each other (Zhao S. et al., 2021). Oxidative stress, immunity, inflammation, thrombosis, and many other links are also involved (Yingze et al., 2022; Maïer et al., 2023; Wang et al., 2023). Above all, developing drugs to treat CI became much harder. New research confirms that inflammatory response is the main thread during all stages of stroke (Maïer et al., 2023). Emerging studies have shown that traditional medicine plays an important role in attenuating the inflammatory damage caused by CI, which undoubtedly suggests the importance of further searching for ethnic medicine alternative therapies for CI.

In this work, we observed the regulatory effect of JDXHD on programmed death in the acute phase of CI based on the previous confirmation that JDHXD inhibits microglial pyroptosis in the acute phase of CI. Before studying the mechanism of JDHXD's protective effect on CI, we detected the blood metabolites of JDHXD by LC-MS. We detected and analyzed 30 possible metabolites (Composite Score > 0.98). Previous studies have given some evidence that JDHXD metabolites inhibit programmed cell death. For example, Pueraria lobata root can dilate cerebral blood vessels, enhance cerebral blood flow, ameliorate cerebral circulation, and stabilize cerebral vascular function, thereby improving blood and oxygen supply to brain tissue and cells, and reducing the occurrence of neurological dysfunction (Hongyun et al., 2017). Chinese thorowax root may enhance depression-like behavior and decrease hippocampus neuron death following CI, probably by boosting the expression of BDNF, p-CREB, and Bcl-2 while reducing the levels of Bax and Caspase-3 (Wang A. R. et al., 2021). Licorice can promote cell proliferation, migration, and angiogenesis, and reduce mitochondrial membrane potential damage and apoptosis. Simultaneously, liquiritigenin can decrease the expression of associated adhesion molecules and mitigate the generation of reactive oxygen species. Mechanistically, liquiritigenin can activate the Keap1/Nrf2 antioxidant pathway, thereby preserving the integrity of the BBB (Li et al., 2021). Ferulic acid, for example, has been shown to encourage the development of new blood vessels *in vivo*. Ferulic acid boosted the expression of VEGF and platelet-derived growth factor (PDGF) (Lin et al., 2010). Rehmannia glutinosa can improve the post-ischemic repair signaling pathway (Fu et al., 2022). This investigation demonstrated that JDHXD exerts an inhibitory effect on neuronal pyroptosis and autophagy following CI in rats. JDHXD reduces the expression of NLRP3, caspase-1 P10, GSDMD-NT, IL-1β, and IL-18. JDHXD also inhibited the expression of autophagy-related factors, such as ULK1, beclin1, and LC3-II on the third day after CI (Figure 9).

Pyroptosis and autophagy are both forms of programmed cell death (Adhami et al., 2007; Xue et al., 2019). Among them, pyroptosis is a pro-inflammatory cell death mode. The traditional view is that autophagy has nothing to do with inflammatory response, but the latest research shows that autophagy is also involved in the regulation of inflammatory response (Su et al., 2016). The conventional and the non-canonical pathways are the two primary pathways of pyroptosis. In CI, pyroptosis is primarily the conventional pathway (Yu et al., 2021). Pyroptosis signals in the

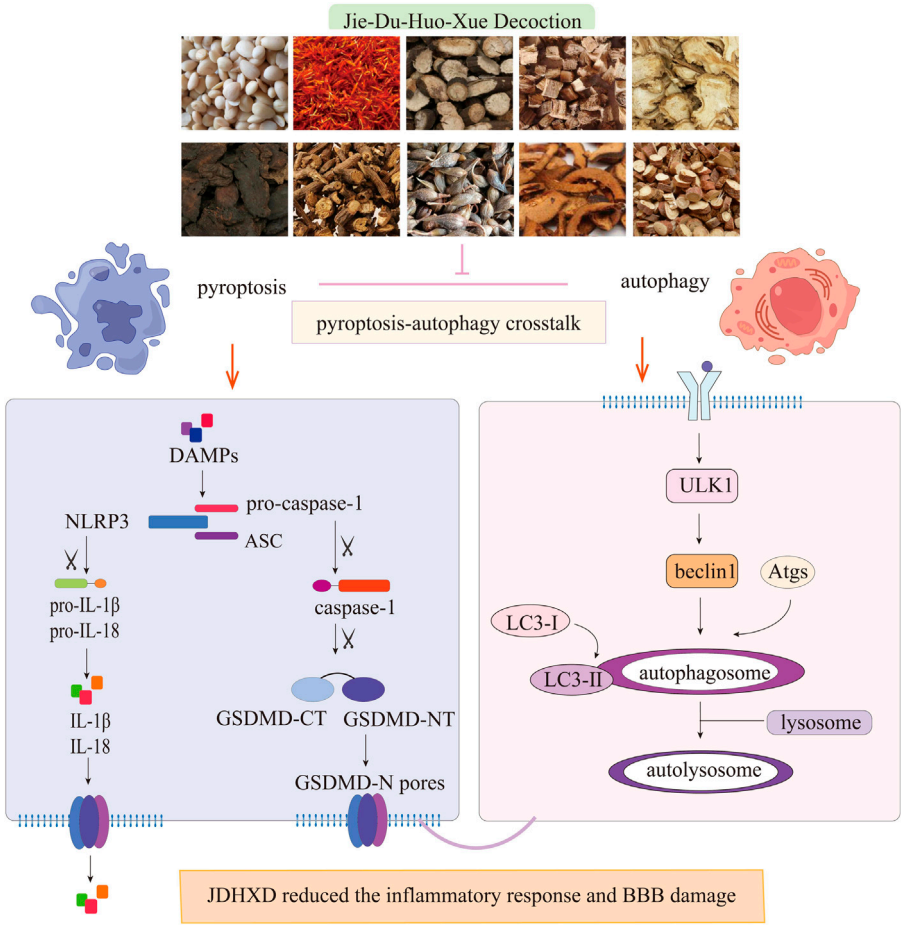


FIGURE 9
JDHXD against CIRI in rats. JDHXD reduced pyroptosis and autophagy. JDHXD consists of 10 botanical drugs (*Pueraria edulis* Pamp [Fabaceae], *Paeonia veitchii* Lynch [Paeoniaceae], *Prunus persica* (L.) Batsch [Rosaceae], *Anethum graveolens* L. [Apiaceae], *Rehmannia glutinosa (Gaertn.)* DC. [Orobanchaceae], *Carthamus tinctorius* L. [Asteraceae], *Forsythia suspensa (Thunb.)* Vahl [Oleaceae], *Bupleurum falcatum* L. [Apiaceae], *Citrus medica* L. [Rutaceae], *Glycyrrhiza glabra* L. [Fabaceae]). Our results showed that JDHXD inhibited both focal death and autophagy. On the one hand, JDHXD inhibited the classical pyroptosis pathway, suppressed the expression of NLRP3/caspase-1/GSDMD, and reduced the production of IL-1β and IL-18. On the other hand, JDHXD also inhibited the expression of ULK1/beclin1/LC3-II on the autophagy pathway. NLRP3 serves as a nexus linking focal death and autophagy, and JDHXD inhibition of NLRP3 does not work by promoting autophagy. (LC3, lipidation of microtubule-associated light chain 3; ULK1, unc-51-like autophagy activating kinase 1; NLRP3, nucleotide-binding oligomerization domain-like receptor pyrin domain containing 3; GSDMD-CT, gasdermin D C terminal; GSDMD-NT, Gasdermin D N terminal; IL, interleukin).

canonical pathways activate several cytoplasmic sensor proteins and encourage the formation of various inflammasomes (Gou et al., 2021). CI causes a strong neuroinflammatory response in a strict temporal and spatial order (Gelderblom et al., 2009). During the first 24 h of CIRI, the inflammation is mainly confined to the intravascular compartment (Stoll et al., 2022). This may be driven by local platelet and leukocyte-derived DAMPs and chemokines (Kollikowski et al., 2022). During pyroptosis, the NLRP3 inflammasome is activated by DAMPs produced in CIRI (Chang et al., 2020). And then NLRP3 cleaves pro-caspase-1 into activated caspase-1. Activated caspase-1 promotes the maturation of IL-18 and IL-1β and activates GSDMD. GSDMD is one of the gasdermin protein family (McKenzie et al., 2018; Van Opdenbosch and Lamkanfi, 2019). It has an autoinhibitory domain. When caspase-1 is cleaved, the active N-terminal is exposed, and the N-terminal gathers on the cell membrane to form a ring-shaped membrane hole, causing the cell to collapse (Burdette et al., 2021; Wang J. et al., 2021). Small inflammatory molecules such as IL-18 and IL-1β can be released from the pores of GSDMD, and then recruit more pro-inflammatory factors to gather, induce an inflammatory cascade reaction, and aggravate cerebral ischemic injury (Schneider et al., 2017; Evavold et al., 2018; Luan et al., 2020). Our study proved that JDHXD can inhibit many links of pyroptosis in the classical pathway in the rat MCAO model. It can not only inhibit NLRP3 but also inhibit the active structure of caspase-1 P10 and GSDMD-N terminal, as well as the downstream inflammatory factors of pyroptosis. Inhibition of neuronal pyroptosis by JDHXD can help relieve neuroinflammation in the acute phase of CIRI, protect the brain parenchyma, and reduce neurological impairment and cognitive impairment after CIRI. JDHXD inhibits pyroptosis of the NLRP3/caspase-1/GSDMD pathway, which is of great value in inhibiting CI. Because studies have shown that preventive inhibition of NLRP3 inflammasome can maintain its early therapeutic effect into the subacute phase,

inhibition of NLRP3 inflammasome in the acute phase of CI directly affects inflammation in the ischemic penumbra after stroke (Bellut et al., 2023). Early treatment effects tend to have long-term immunomodulatory effects, ultimately leading to better neurological outcomes. In addition, inhibition of NLRP3 can reduce secondary infarct growth in small and medium-sized CI (Bellut et al., 2023). Therefore, JDHXD may have a delayed immunomodulatory effect by inhibiting NLRP3 during the acute phase of CI, but further studies are needed. In addition, JDHXD has an important protective effect on the prognosis of stroke by inhibiting IL-1β and IL-18 produced downstream of pyroptosis. IL-18 has been shown in multiple clinical studies to be a potent proinflammatory cytokine with atherogenic properties (Goldstein et al., 2006). In addition, higher plasma IL-1β levels are associated with the most severe damage in patients with ischemic stroke (Tirandi et al., 2023). JDHXD's inhibition of IL-1β and IL-18 may reduce the diffusion of interleukins through the damaged BBB.

Interestingly, our study proposes a hypothesis that is different from previous studies. The loss of the pyroptosis execution protein GSDMD protein in the ischemic core area may lead to adverse consequences of CI. Although many previous studies have shown that GSDMD is lowly expressed in the core of cerebral ischemic infarction and highly expressed in the periphery of the infarction (Luo et al., 2022), to our knowledge, we are the first to show that GSDMD is also highly expressed in the healthy brain contralateral to the ischemic brain. Our panoramic scanning results show that the expression intensity of GSDMD fluorescence in the non-infarcted hemisphere and penumbra is almost the same, and is much higher than that in the infarct core area. Different GSDMD antibodies were used and staining operations were performed by different personnel, and the same results were obtained. In addition, Western blot results also support the low expression of GSDMD-FL in the core area of infarction. We are very excited about this finding, which is contrary to previous findings. At the same time, our previous results on microglial pyroptosis also support the enhanced expression of GSDMD in the infarct penumbra. We speculate that pyroptosis GSDMD may have a double-edged sword effect like autophagy. Just like "Yin" and "Yang" in philosophy are opposite and unified with each other. Excessive activation of GSDMD at the infarct edge will aggravate post-ischemic brain injury, and the loss of GSDMD protein in the core area of infarction after cerebral ischemia may also lead to adverse outcomes of CIRI. We do not rule out the possibility that the following bias may occur: the fluorescent antibody cannot label GSDMD-NT very accurately but instead displays GSDMD-FL. To eliminate the interference of the above factors, we used antibodies of different species produced by two different formulas in immunofluorescence. If our hypothesis that GSDMD is lost in the infarct core is confirmed in subsequent studies, it may provide new clues to the role of pyroptosis in CI. Pyroptosis may not be entirely a pro-inflammatory injury during CIRI, and GSDMD may also have a potential protective mechanism against CI. Although we have not yet studied the mechanism of this phenomenon in depth, we chose to report this valuable finding.

In comparison to pro-inflammatory pyroptosis, the regulation of inflammation by autophagy and its role in CI is more confusing. There has been debate over whether autophagy has a protective or harmful effect (Plaza-Zabala et al., 2017). By far the most prevalent description is that autophagy is a double-edged sword (Wei et al., 2012). Both positive and negative autophagy regulation can improve neuroprotection *in vivo* models of CI (Wang et al., 2022; Zheng et al., 2022; Zhai et al., 2023). Autophagy is a self-protective catabolic mechanism in cells. Some misfolded proteins and damaged organelles are destroyed and recycled via this mechanism to preserve cellular equilibrium (Adhami et al., 2007). The activation or inhibition of autophagy under ischemia and hypoxia is still controversial, and there is no shortage of contrary research results. Autophagy is commonly thought to be triggered in reaction to nutrient deprivation or metabolic stress, aiming to sustain tissue equilibrium by recycling dysfunctional proteins and organelles (Zhao J. et al., 2021; Ji et al., 2022). Briefly, autolysosomes arise as a result of the sequestration of cytoplasmic material into autophagosomes and fusion with lysosomes. Under nutritional shortage, AMPK is activated, inactivating mTORC1 or phosphorylating different serine residues of ULK1 (Zhai et al., 2023). However, some studies have also proved that autophagy is inhibited under nutrient deprivation (Zheng et al., 2022). Our research results indicate that neuronal autophagy is triggered by CI and it can be inhibited by JDHXD. JDHXD suppressed the expression of the autophagy promoter ULK1, as well as beclin1 and LC3-II. In our current study, on day 3 after CI in rats, autophagy in neurons in the cerebral ischemic penumbra was higher than normal, suggesting that ischemia and hypoxia lead to excessive autophagy, which causes excessive neuronal death. JDHXD-M intervention can promote neuronal autophagy and reduce neuroinflammation.

Updated research changes the old view that autophagy is not involved in inflammatory responses. Emerging research suggests that autophagy may protect against inflammation (Wang et al., 2020). The mechanisms by which autophagy inactivates the inflammasome are diverse, including clearance of ASC and IL-1β, and selective targeting of ROS to lysosomes for clearance by mitophagy (Li et al., 2015; Shibutani et al., 2015). However, our findings do not support the above view because autophagy promoted the inflammatory damage of CI in our study. The concurrent activation of LC3-II and beclin-1 proteins, along with NLRP3, IL-1β, and caspase-1, is functionally implicated in the progression and pathogenesis of CIRI, characterized by concurrent activation of autophagy, pyroptosis, and inflammation. These three processes are often triggered in a sequential and interconnected order. Both pyroptosis and autophagy are active in the cortical area of the ischemic penumbra. On the one hand, NLRP3 is involved in the initiation of pyroptosis, and on the other hand, NLRP3 is activated by the acute and subacute injury signals after CI in rats, and NLRP3 subsequently cleaves caspase-1 and GSDMD to induce pyroptosis. At this time, the level of autophagy was activated due to ischemia and hypoxia, and the activated autophagy did not inhibit the phosphorylation of NLRP3 and ASC. This promotes the inflammatory response following CI. The intervention of JDHXD suppressed the expression of autophagy markers ULK1, Beclin1, and LC3-II. On the third day after CI, the activation of autophagy did not reduce NLRP3, and activated NLRP3 could activate pro-inflammatory programmed cell death.

Our results support the widely accepted view that autophagy is overactivated after CI and that inhibition of NLRP3 can suppress the

expression of pyroptosis and autophagy (Liu et al., 2021). Interestingly, some studies have suggested that enhancing mitochondrial autophagy and reducing NLRP3 inflammasome activation has a neuroprotective effect on rats after CI (Ji et al., 2022). In addition, some reports promoting autophagy can inhibit pyroptosis in myocardial ischemia (Zhang et al., 2023). The inconsistency of pathophysiological mechanisms of the same cell death pattern in different tissues has considerable research prospects. It is postulated that this phenomenon may be attributed to the specific effects of NLRP3 in diverse tissues, degrees of ischemia, and cell types. The clearance ability of autophagy on NLRP3 may be different in different tissues, organs, and cells, thus affecting the interaction between autophagy and pyroptosis. Although JDHXD did not activate autophagy and inhibit pyroptosis as we speculated, it inhibited pyroptosis and autophagy at the same time, indicating that JDHXD inhibits pyroptosis possibly by directly inhibiting the cleavage of NLRP3 and GSDMD-NT.

Our study confirmed that JDHXD inhibits pyroptosis and autophagy and alleviates inflammatory damage. However, there are some deficiencies and limitations in the experimental design. First, in the western blot experiment, the housekeeping protein we chose was β-actin. New studies suggested that in neurological diseases, housekeeping proteins such as β-actin and GAPDH may be changed after injury or in neuropathological states (Li and Shen, 2013). Our current experiments have not verified that the expression of β-actin is constant in all samples of the CI model, so the possible experimental bias caused by β-actin cannot be ruled out. Secondly, due to the limitations of experimental conditions, our experiments could not directly observe the pores formed by GSDMD oligomerization but only observed the expression of GSDMD by western blot and immunofluorescence. Future research can improve the experimental design from the above perspectives.

Conclusion

In conclusion, our study demonstrated that JDHXD inhibited the expression of pyroptosis and autophagy on the third day of CI. Furthermore, JDHXD exhibited an anti-CI effect. Our findings also indicated that the inhibitory effect of JDHXD on pyroptosis was not mediated by the promotion of autophagy. In a surprising twist, our findings revealed that GSDMD expression was low in the infarct core but high in the peri-infarct and healthy brain regions, a result that challenges previous assumptions.

Data availability statement

The raw data supporting the conclusions of this article will be made available by the authors, without undue reservation.

Ethics statement

The animal study was approved by the Hunan University of Chinese Medicine Ethics Committee followed all applicable rules and laws (Approval number: LL2022101801). The study was conducted in accordance with the local legislation and institutional requirements.

Author contributions

CZ: Writing–original draft, Resources, Investigation, Data curation. S-wQ: Data curation, Writing–original draft. F-mW: Writing–original draft. Y-cL: Writing–original draft. WH: Writing–original draft. M-lY: Writing–original draft. W-hL: Writing–review and editing, Supervision, Project administration, Funding acquisition. HL: Writing–review and editing, Supervision, Project administration, Funding acquisition, Data curation.

Funding

The author(s) declare that financial support was received for the research, authorship, and/or publication of this article. This study was supported by the Natural Science Foundation of Hunan Province (2023JJ30451); The Key Items of the Research Program of Chinese Medicine in Hunan Province (2021013, A2023038); Key Project of Scientific Research Project of Hunan Provincial Department of Education (23A0308); Hunan University of Chinese medicine Postgraduate Innovation Project (2022CX52, 2022CX53, and 2022CX58).

Acknowledgments

We thank Company Servicebio and Biotree for their excellent technical assistance.

Conflict of interest

The authors declare that the research was conducted in the absence of any commercial or financial relationships that could be construed as a potential conflict of interest.

Publisher's note

All claims expressed in this article are solely those of the authors and do not necessarily represent those of their affiliated organizations, or those of the publisher, the editors and the reviewers. Any product that may be evaluated in this article, or claim that may be made by its manufacturer, is not guaranteed or endorsed by the publisher.

Supplementary material

The Supplementary Material for this article can be found online at: https://www.frontiersin.org/articles/10.3389/fphar.2024.1449452/full#supplementary-material

References

Adhami, F., Schloemer, A., and Kuan, C. Y. (2007). The roles of autophagy in cerebral ischemia. *Autophagy* 3, 42–44. doi:10.4161/auto.3412

Bellut, M., Bieber, M., Kraft, P., Weber, A. N. R., Stoll, G., and Schuhmann, M. K. (2023). Delayed NLRP3 inflammasome inhibition ameliorates subacute stroke progression in mice. *J. Neuroinflammation* 20, 4. doi:10.1186/s12974-022-02674-w

Bergsbaken, T., Fink, S. L., and Cookson, B. T. (2009). Pyroptosis: host cell death and inflammation. *Nat. Rev. Microbiol.* 7, 99–109. doi:10.1038/nrmicro2070

Biasizzo, M., and Kopitar-Jerala, N. (2020). Interplay between NLRP3 inflammasome and autophagy. *Front. Immunol.* 11, 591803. doi:10.3389/fimmu.2020.591803

Burdette, B. E., Esparza, A. N., Zhu, H., and Wang, S. (2021). Gasdermin D in pyroptosis. *Acta Pharm. Sin. B* 11, 2768–2782. doi:10.1016/j.apsb.2021.02.006

Chang, Y., Zhu, J., Wang, D., Li, H., He, Y., Liu, K., et al. (2020). NLRP3 inflammasome-mediated microglial pyroptosis is critically involved in the development of post-cardiac arrest brain injury. *J. Neuroinflammation* 17, 219. doi:10.1186/s12974-020-01879-1

Du, G., Healy, L. B., David, L., Walker, C., El-Baba, T. J., Lutomski, C. A., et al. (2024). ROS-dependent S-palmitoylation activates cleaved and intact gasdermin D. *Nature* 630, 437–446. doi:10.1038/s41586-024-07373-5

Evavold, C. L., Ruan, J., Tan, Y., Xia, S., Wu, H., and Kagan, J. C. (2018). The pore-forming protein gasdermin D regulates interleukin-1 secretion from living macrophages. *Immunity* 48, 35–44. doi:10.1016/j.immuni.2017.11.013

Fiore, C., Eisenhut, M., Ragazzi, E., Zanchin, G., and Armanini, D. (2005). A history of the therapeutic use of liquorice in Europe. *J. Ethnopharmacol.* 99, 317–324. doi:10.1016/j.jep.2005.04.015

Fricker, M., Tolkovsky, A. M., Borutaite, V., Coleman, M., and Brown, G. C. (2018). Neuronal cell death. *Physiol. Rev.* 98, 813–880. doi:10.1152/physrev.00011.2017

Fu, C., Wu, Y., Liu, S., Luo, C., Lu, Y., Liu, M., et al. (2022). Rehmannioside A improves cognitive impairment and alleviates ferroptosis via activating PI3K/AKT/Nrf2 and SLC7A11/GPX4 signaling pathway after ischemia. *J. Ethnopharmacol.* 289, 115021. doi:10.1016/j.jep.2022.115021

Gelderblom, M., Leypoldt, F., Steinbach, K., Behrens, D., Choe, C. U., Siler, D. A., et al. (2009). Temporal and spatial dynamics of cerebral immune cell accumulation in stroke. *Stroke* 40, 1849–1857. doi:10.1161/STROKEAHA.108.534503

Goldstein, L. B., Adams, R., Alberts, M. J., Appel, L. J., Brass, L. M., Bushnell, C. D., et al. (2006). Primary prevention of ischemic stroke: a guideline from the American heart association/American stroke association stroke council: cosponsored by the atherosclerotic peripheral vascular disease interdisciplinary working group; cardiovascular nursing council; clinical cardiology council; nutrition, physical activity, and metabolism council; and the quality of care and outcomes research interdisciplinary working group: the American academy of neurology affirms the value of this guideline. *Stroke* 37, 1583–1633. doi:10.1161/01.STR.0000223048.70103.F1

Gou, X., Xu, D., Li, F., Hou, K., Fang, W., and Li, Y. (2021). Pyroptosis in stroke-new insights into disease mechanisms and therapeutic strategies. *J. Physiol. Biochem.* 77, 511–529. doi:10.1007/s13105-021-00817-w

Haupt, M., Gerner, S. T., Bähr, M., and Doeppner, T. R. (2023). Neuroprotective strategies for ischemic stroke-future perspectives. *Int. J. Mol. Sci.* 24, 4334. doi:10.3390/ijms24054334

Hongyun, H., Tao, G., Pengyue, Z., Liqiang, Y., and Yihao, D. (2017). Puerarin provides a neuroprotection against transient cerebral ischemia by attenuating autophagy at the ischemic penumbra in neurons but not in astrocytes. *Neurosci. Lett.* 643, 45–51. doi:10.1016/j.neulet.2017.02.009

Hou, K., Xu, D., Li, F., Chen, S., and Li, Y. (2019). The progress of neuronal autophagy in cerebral ischemia stroke: mechanisms, roles and research methods. *J. Neurol. Sci.* 400, 72–82. doi:10.1016/j.jns.2019.03.015

Hu, Y., Shi, Y., Chen, H., Tao, M., Zhou, X., Li, J., et al. (2022). Blockade of autophagy prevents the progression of hyperuricemic nephropathy through inhibiting NLRP3 inflammasome-mediated pyroptosis. *Front. Immunol.* 13, 858494. doi:10.3389/fimmu.2022.858494

Huang, S. S., Su, H. H., Chien, S. Y., Chung, H. Y., Luo, S. T., Chu, Y. T., et al. (2022). Activation of peripheral TRPM8 mitigates ischemic stroke by topically applied menthol. *J. Neuroinflammation* 19, 192. doi:10.1186/s12974-022-02553-4

Huang, Y., Chen, S., Luo, Y., and Han, Z. (2020). Crosstalk between inflammation and the BBB in stroke. *Curr. Neuropharmacol.* 18, 1227–1236. doi:10.2174/1570159X18666200620230321

Ji, Z. J., Shi, Y., Li, X., Hou, R., Yang, Y., Liu, Z. Q., et al. (2022). Neuroprotective effect of taohong siwu decoction on cerebral ischemia/reperfusion injury via mitophagy-NLRP3 inflammasome pathway. *Front. Pharmacol.* 13, 910217. doi:10.3389/fphar.2022.910217

Kilkenny, C., Browne, W., Cuthill, I. C., Emerson, M., Altman, D. G., and National Centre for the Replacement, Refinement and Reduction of Amimals in Research (2011). Animal research: reporting *in vivo* experiments--the ARRIVE guidelines. *J. Cereb. Blood Flow. Metab.* 31, 991–993. doi:10.1038/jcbfm.2010.220

Kollikowski, A. M., Pham, M., Marz, A. G., Papp, L., Nieswandt, B., Stoll, G., et al. (2022). Platelet activation and chemokine release are related to local neutrophil-dominant inflammation during hyperacute human stroke. *Transl. Stroke Res.* 13, 364–369. doi:10.1007/s12975-021-00938-w

Li, L., Tan, J., Miao, Y., Lei, P., and Zhang, Q. (2015). ROS and Autophagy: interactions and molecular regulatory mechanisms. *Cell Mol. Neurobiol.* 35, 615–621. doi:10.1007/s10571-015-0166-x

Li, M., Ke, J., Deng, Y., Chen, C., Huang, Y., Bian, Y., et al. (2021). The protective effect of liquiritin in hypoxia/reoxygenation-induced disruption on blood brain barrier. *Front. Pharmacol.* 12, 671783. doi:10.3389/fphar.2021.671783

Li, R., and Shen, Y. (2013). An old method facing a new challenge: re-visiting housekeeping proteins as internal reference control for neuroscience research. *Life Sci.* 92, 747–751. doi:10.1016/j.lfs.2013.02.014

Lin, C. M., Chiu, J. H., Wu, I. H., Wang, B. W., Pan, C. M., and Chen, Y. H. (2010). Ferulic acid augments angiogenesis via VEGF, PDGF and HIF-1 alpha. *J. Nutr. Biochem.* 21, 627–633. doi:10.1016/j.jnutbio.2009.04.001

Liu, H., Zhao, Z., Wu, T., Zhang, Q., Lu, F., Gu, J., et al. (2021). Inhibition of autophagy-dependent pyroptosis attenuates cerebral ischaemia/reperfusion injury. *J. Cell Mol. Med.* 25, 5060–5069. doi:10.1111/jcmm.16483

Liu, X., Feng, Z., Du, L., Huang, Y., Ge, J., Deng, Y., et al. (2019). The potential role of microRNA-124 in cerebral ischemia injury. *Int. J. Mol. Sci.* 21, 120. doi:10.3390/ijms21010120

Longa, E. Z., Weinstein, P. R., Carlson, S., and Cummins, R. (1989). Reversible middle cerebral artery occlusion without craniectomy in rats. *Stroke* 20, 84–91. doi:10.1161/01.str.20.1.84

Luan, J., Chen, W., Fan, J., Wang, S., Zhang, X., Zai, W., et al. (2020). GSDMD membrane pore is critical for IL-1β release and antagonizing IL-1β by hepatocyte-specific nanobiologics is a promising therapeutics for murine alcoholic steatohepatitis. *Biomaterials* 227, 119570. doi:10.1016/j.biomaterials.2019.119570

Luo, L., Liu, M., Fan, Y., Zhang, J., Liu, L., Li, Y., et al. (2022). Intermittent theta-burst stimulation improves motor function by inhibiting neuronal pyroptosis and regulating microglial polarization via TLR4/NFκB/NLRP3 signaling pathway in cerebral ischemic mice. *J. Neuroinflammation* 19, 141. doi:10.1186/s12974-022-02501-2

Lyu, Z., Li, Q., Yu, Z., Chan, Y., Fu, L., Li, Y., et al. (2021). Yi-zhi-fang-dai formula exerts neuroprotective effects against pyroptosis and blood-brain barrier-glymphatic dysfunctions to prevent amyloid-beta acute accumulation after cerebral ischemia and reperfusion in rats. *Front. Pharmacol.* 12, 791059. doi:10.3389/fphar.2021.791059

Maïer, B., Tsai, A. S., Einhaus, J. F., Desilles, J. P., Ho-Tin-Noé, B., Gory, B., et al. (2023). Neuroimaging is the new "spatial omic": multi-omic approaches to neuro-inflammation and immuno-thrombosis in acute ischemic stroke. *Semin. Immunopathol.* 45, 125–143. doi:10.1007/s00281-023-00984-6

Mckenzie, B. A., Mamik, M. K., Saito, L. B., Boghozian, R., Monaco, M. C., Major, E. O., et al. (2018). Caspase-1 inhibition prevents glial inflammasome activation and pyroptosis in models of multiple sclerosis. *Proc. Natl. Acad. Sci. U. S. A.* 115, E6065–E6074. doi:10.1073/pnas.1722041115

Mosconi, M. G., and Paciaroni, M. (2022). Treatments in ischemic stroke: current and future. *Eur. Neurol.* 85, 349–366. doi:10.1159/000525822

Nabavi, S. F., Sureda, A., Sanches-Silva, A., Pandima Devi, K., Ahmed, T., Shahid, M., et al. (2019). Novel therapeutic strategies for stroke: the role of autophagy. *Crit. Rev. Clin. Lab. Sci.* 56, 182–199. doi:10.1080/10408363.2019.1575333

Niu, P., Li, L., Zhang, Y., Su, Z., Wang, B., Liu, H., et al. (2023). Immune regulation based on sex differences in ischemic stroke pathology. *Front. Immunol.* 14, 1087815. doi:10.3389/fimmu.2023.1087815

Nogami-Hara, A., Nagao, M., Takasaki, K., Egashira, N., Fujikawa, R., Kubota, K., et al. (2018). The Japanese Angelica acutiloba root and yokukansan increase hippocampal acetylcholine level, prevent apoptosis and improve memory in a rat model of repeated cerebral ischemia. *J. Ethnopharmacol.* 214, 190–196. doi:10.1016/j.jep.2017.12.025

Orellana-Urzúa, S., Rojas, I., Líbano, L., and Rodrigo, R. (2020). Pathophysiology of ischemic stroke: role of oxidative stress. *Curr. Pharm. Des.* 26, 4246–4260. doi:10.2174/1381612826666200708133912

Plaza-Zabala, A., Sierra-Torre, V., and Sierra, A. (2017). Autophagy and microglia: novel partners in neurodegeneration and aging. *Int. J. Mol. Sci.* 18, 598. doi:10.3390/ijms18030598

Schneider, K. S., Groß, C. J., Dreier, R. F., Saller, B. S., Mishra, R., Gorka, O., et al. (2017). The inflammasome drives GSDMD-independent secondary pyroptosis and IL-1 release in the absence of caspase-1 protease activity. *Cell Rep.* 21, 3846–3859. doi:10.1016/j.celrep.2017.12.018

Shen, L., Gan, Q., Yang, Y., Reis, C., Zhang, Z., Xu, S., et al. (2021). Mitophagy in cerebral ischemia and ischemia/reperfusion injury. *Front. Aging Neurosci.* 13, 687246. doi:10.3389/fnagi.2021.687246

Shi, Q., Cheng, Q., and Chen, C. (2021). The role of autophagy in the pathogenesis of ischemic stroke. *Curr. Neuropharmacol.* 19, 629–640. doi:10.2174/1570159X18666200729101913

Shibutani, S. T., Saitoh, T., Nowag, H., Munz, C., and Yoshimori, T. (2015). Autophagy and autophagy-related proteins in the immune system. *Nat. Immunol.* 16, 1014–1024. doi:10.1038/ni.3273

Shikov, A. N., Narkevich, I. A., Flisyuk, E. V., Luzhanin, V. G., and Pozharitskaya, O. N. (2021). Medicinal plants from the 14(th) edition of the Russian Pharmacopoeia, recent updates. *J. Ethnopharmacol.* 268, 113685. doi:10.1016/j.jep.2020.113685

Shikov, A. N., Pozharitskaya, O. N., Makarov, V. G., Wagner, H., Verpoorte, R., and Heinrich, M. (2014). Medicinal plants of the Russian Pharmacopoeia; their history and applications. *J. Ethnopharmacol.* 154, 481–536. doi:10.1016/j.jep.2014.04.007

Stoll, G., Schuhmann, M. K., Nieswandt, B., Kollikowski, A. M., and Pham, M. (2022). An intravascular perspective on hyper-acute neutrophil, T-cell and platelet responses: similarities between human and experimental stroke. *J. Cereb. Blood Flow. Metab.* 42, 1561–1567. doi:10.1177/0271678X221105764

Su, P., Zhang, J., Wang, D., Zhao, F., Cao, Z., Aschner, M., et al. (2016). The role of autophagy in modulation of neuroinflammation in microglia. *Neuroscience* 319, 155–167. doi:10.1016/j.neuroscience.2016.01.035

Sun, R., Peng, M., Xu, P., Huang, F., Xie, Y., Li, J., et al. (2020). Low-density lipoprotein receptor (LDLR) regulates NLRP3-mediated neuronal pyroptosis following cerebral ischemia/reperfusion injury. *J. Neuroinflammation* 17, 330. doi:10.1186/s12974-020-01988-x

Tirandi, A., Sgura, C., Carbone, F., Montecucco, F., and Liberale, L. (2023). Inflammatory biomarkers of ischemic stroke. *Intern Emerg. Med.* 18, 723–732. doi:10.1007/s11739-023-03201-2

Van Opdenbosch, N., and Lamkanfi, M. (2019). Caspases in cell death, inflammation, and disease. *Immunity* 50, 1352–1364. doi:10.1016/j.immuni.2019.05.020

Vercammen, D., Beyaert, R., Denecker, G., Goossens, V., Van Loo, G., Declercq, W., et al. (1998). Inhibition of caspases increases the sensitivity of L929 cells to necrosis mediated by tumor necrosis factor. *J. Exp. Med.* 187, 1477–1485. doi:10.1084/jem.187.9.1477

Wang, A. R., Mi, L. F., Zhang, Z. L., Hu, M. Z., Zhao, Z. Y., Liu, B., et al. (2021a). Saikosaponin A improved depression-like behavior and inhibited hippocampal neuronal apoptosis after cerebral ischemia through p-CREB/BDNF pathway. *Behav. Brain Res.* 403, 113138. doi:10.1016/j.bbr.2021.113138

Wang, J., Yao, J., Liu, Y., and Huang, L. (2021b). Targeting the gasdermin D as a strategy for ischemic stroke therapy. *Biochem. Pharmacol.* 188, 114585. doi:10.1016/j.bcp.2021.114585

Wang, L., Dai, M., Ge, Y., Chen, J., Wang, C., Yao, C., et al. (2022). EGCG protects the mouse brain against cerebral ischemia/reperfusion injury by suppressing autophagy via the AKT/AMPK/mTOR phosphorylation pathway. *Front. Pharmacol.* 13, 921394. doi:10.3389/fphar.2022.921394

Wang, P., Shao, B. Z., Deng, Z., Chen, S., Yue, Z., and Miao, C. Y. (2018). Autophagy in ischemic stroke. *Prog. Neurobiol.* 163-164, 98–117. doi:10.1016/j.pneurobio.2018.01.001

Wang, X. X., Zhang, B., Xia, R., and Jia, Q. Y. (2020). Inflammation, apoptosis and autophagy as critical players in vascular dementia. *Eur. Rev. Med. Pharmacol. Sci.* 24, 9601–9614. doi:10.26355/eurrev_202009_23048

Wang, Y. R., Cui, W. Q., Wu, H. Y., Xu, X. D., and Xu, X. Q. (2023). The role of T cells in acute ischemic stroke. *Brain Res. Bull.* 196, 20–33. doi:10.1016/j.brainresbull.2023.03.005

Wei, K., Wang, P., and Miao, C. Y. (2012). A double-edged sword with therapeutic potential: an updated role of autophagy in ischemic cerebral injury. *CNS Neurosci. Ther.* 18, 879–886. doi:10.1111/cns.12005

Xue, Y., Enosi Tuipulotu, D., Tan, W. H., Kay, C., and Man, S. M. (2019). Emerging activators and regulators of inflammasomes and pyroptosis. *Trends Immunol.* 40, 1035–1052. doi:10.1016/j.it.2019.09.005

Yang, K., Bao, T., Zeng, J., Wang, S., Yuan, X., Xiang, W., et al. (2022). Research progress on pyroptosis-mediated immune-inflammatory response in ischemic stroke and the role of natural plant components as regulator of pyroptosis: a review. *Biomed. Pharmacother.* 157, 113999. doi:10.1016/j.biopha.2022.113999

Yingze, Y., Zhihong, J., Tong, J., Yina, L., Zhi, Z., Xu, Z., et al. (2022). NOX2-mediated reactive oxygen species are double-edged swords in focal cerebral ischemia in mice. *J. Neuroinflammation* 19, 184. doi:10.1186/s12974-022-02551-6

Yu, P., Zhang, X., Liu, N., Tang, L., Peng, C., and Chen, X. (2021). Pyroptosis: mechanisms and diseases. *Signal Transduct. Target Ther.* 6, 128. doi:10.1038/s41392-021-00507-5

Zhai, J., Li, N., Zhang, X., Li, Y., Ma, K., Wang, R., et al. (2023). Isoflurane enhances autophagy by activating AMPK/ULK1, inhibits NLRP3, and reduces cognitive impairment after cerebral ischemia-reperfusion injury in rats. *J. Mol. Neurosci.* 73, 549–562. doi:10.1007/s12031-023-02135-w

Zhang, X., Wang, Z., Li, X., Chen, J., Yu, Z., Li, X., et al. (2023). Polydatin protects against atherosclerosis by activating autophagy and inhibiting pyroptosis mediated by the NLRP3 inflammasome. *J. Ethnopharmacol.* 309, 116304. doi:10.1016/j.jep.2023.116304

Zhang, Y., Cao, Y., and Liu, C. (2020). Autophagy and ischemic stroke. *Adv. Exp. Med. Biol.* 1207, 111–134. doi:10.1007/978-981-15-4272-5_7

Zhao, J., Dong, Y., Chen, X., Xiao, X., Tan, B., Chen, G., et al. (2021a). p53 inhibition protects against neuronal ischemia/reperfusion injury by the p53/PRAS40/mTOR pathway. *Oxid. Med. Cell Longev.* 2021, 4729465. doi:10.1155/2021/4729465

Zhao, S., Li, X., Wang, J., and Wang, H. (2021b). The role of the effects of autophagy on NLRP3 inflammasome in inflammatory nervous system diseases. *Front. Cell Dev. Biol.* 9, 657478. doi:10.3389/fcell.2021.657478

Zheng, Y., Hu, Y., Han, Z., Yan, F., Zhang, S., Yang, Z., et al. (2022). Lomitapide ameliorates middle cerebral artery occlusion-induced cerebral ischemia/reperfusion injury by promoting neuronal autophagy and inhibiting microglial migration. *CNS Neurosci. Ther.* 28, 2183–2194. doi:10.1111/cns.13961

Zhou, C., Li, J. X., Zheng, C. X., Zhou, X. Q., Chen, C., Qiu, S. W., et al. (2023). Neuroprotective effects of Jie-du-huo-xue decoction on microglia pyroptosis after cerebral ischemia and Reperfusion--From the perspective of glial-vascular unit. *J. Ethnopharmacol.* 318, 116990. doi:10.1016/j.jep.2023.116990

Ziaeian, B., Xu, H., Matsouaka, R. A., Xian, Y., Khan, Y., Schwamm, L. S., et al. (2022). US surveillance of acute ischemic stroke patient characteristics, care quality, and outcomes for 2019. *Stroke* 53, 3386–3393. doi:10.1161/STROKEAHA.122.039098

frontiers | Frontiers in Pharmacology

TYPE Original Research
PUBLISHED 29 July 2024
DOI 10.3389/fphar.2024.1447757

Check for updates

OPEN ACCESS

EDITED BY
Pukar Khanal,
Emory University, United States

REVIEWED BY
Nikita Kanbarkar,
KLE University, India
Santosh Basavaraj Patil,
KLE College of Pharmacy, India
Laxmi Pattanashetti,
KLE College of Pharmacy Hubli, India

*CORRESPONDENCE
Zsolt Gáll,
zsolt.gall@umfst.ro

RECEIVED 12 June 2024
ACCEPTED 15 July 2024
PUBLISHED 29 July 2024

CITATION
Gáll Z, Boros B, Kelemen K, Urkon M, Zolcseak I, Márton K and Kolcsar M (2024), Melatonin improves cognitive dysfunction and decreases gliosis in the streptozotocin-induced rat model of sporadic Alzheimer's disease.
Front. Pharmacol. 15:1447757.
doi: 10.3389/fphar.2024.1447757

COPYRIGHT
© 2024 Gáll, Boros, Kelemen, Urkon, Zolcseak, Márton and Kolcsar. This is an open-access article distributed under the terms of the Creative Commons Attribution License (CC BY). The use, distribution or reproduction in other forums is permitted, provided the original author(s) and the copyright owner(s) are credited and that the original publication in this journal is cited, in accordance with accepted academic practice. No use, distribution or reproduction is permitted which does not comply with these terms.

Melatonin improves cognitive dysfunction and decreases gliosis in the streptozotocin-induced rat model of sporadic Alzheimer's disease

Zsolt Gáll[1]*, Bernadett Boros[2], Krisztina Kelemen[3], Melinda Urkon[1], István Zolcseak[2], Kincső Márton[4] and Melinda Kolcsar[1]

[1]Department of Pharmacology and Clinical Pharmacy, George Emil Palade University of Medicine, Pharmacy, Science, and Technology of Targu Mures, Târgu Mures, Romania, [2]Faculty of Pharmacy, George Emil Palade University of Medicine, Pharmacy, Science, and Technology of Targu Mures, Târgu Mures, Romania, [3]Department of Physiology, George Emil Palade University of Medicine, Pharmacy, Science, and Technology of Targu Mures, Târgu Mures, Romania, [4]Faculty of Medicine, George Emil Palade University of Medicine, Pharmacy, Science, and Technology of Targu Mures, Târgu Mures, Romania

Introduction: Alzheimer's disease (AD) and other forms of dementia have a devastating effect on the community and healthcare system, as neurodegenerative diseases are causing disability and dependency in older population. Pharmacological treatment options are limited to symptomatic alleviation of cholinergic deficit and accelerated clearance of β-amyloid aggregates, but accessible disease-modifying interventions are needed especially in the early phase of AD. Melatonin was previously demonstrated to improve cognitive function in clinical setting and experimental studies also.

Methods: In this study, the influence of melatonin supplementation was studied on behavioral parameters and morphological aspects of the hippocampus and amygdala of rats. Streptozotocin (STZ) was injected intracerebroventricularly to induce AD-like symptoms in male adult Wistar rats (n = 18) which were compared to age-matched, sham-operated animals (n = 16). Melatonin was administered once daily in a dose of 20 mg/kg body weight by oral route. Behavioral analysis included open-field, novel object recognition, and radial-arm maze tests. TNF-α and MMP-9 levels were determined from blood samples to assess the anti-inflammatory and neuroprotective effects of melatonin. Immunohistological staining of brain sections was performed using anti-NeuN, anti-IBA-1, and anti-GFAP primary antibodies to evaluate the cellular reorganization of hippocampus.

Results and Discussion: The results show that after 40 days of treatment, melatonin improved the cognitive performance of STZ-induced rats and reduced the activation of microglia in both CA1 and CA3 regions of the hippocampus. STZ-injected animals had higher levels of GFAP-labeled astrocytes in the CA1 region, but melatonin treatment reduced this to that of the control group. In conclusion, melatonin may be a potential therapeutic option for treating AD-like cognitive decline and neuroinflammation.

KEYWORDS

melatonin, Alzheimer's disease, animal model, cognitive dysfunction, neuroinflammation

1 Introduction

Alzheimer's disease (AD) is an age-related neurodegenerative pathology, the most common type of dementia which affects around 50 million people worldwide and the exact cause remains unknown (Livingston et al., 2017). Several hypotheses attempt to explain the main features of AD, such as progressive cholinergic decline, β-amyloid accumulation, and a series of metabolic alterations leading to neurofibrillary tangle formation and insulin resistance in the brain (Estrada and Contreras, 2019; Kang et al., 2020). Most drugs developed to reduce amyloid synthesis failed to show clinically relevant improvement and despite the vast amount of resources invested in development and research only two new treatment options have been registered for AD patients in the last decade (Decourt et al., 2022; Cummings et al., 2024). Overall, there is an obvious β-amyloid peptide accumulation in the nerve cells that leads to early axonopathy, synaptic loss, neuronal destruction (Rosales-Corral et al., 2012) and the phenomenon predominantly affects the signaling pathways of memory-related molecular signatures (Kaushik et al., 2022). Hippocampal dysfunction is a commonly observed feature of Alzheimer's disease, which can involve metabolic disturbances (i.e., hypometabolism) and morphological reorganization (Small et al., 2011; Klyubin et al., 2012; Padurariu et al., 2012). The main symptom (i.e., memory disturbances) is primarily caused by the destruction of cholinergic neurons, but β-amyloid accumulation and oxidative stress can also reduce acetylcholine synthesis by reducing choline acetyl transferase activity or increasing acetylcholinesterase (AChE) activity (Rosales-Corral et al., 2012).

Due to the progressive character of AD, prevention and early diagnosis can be effective options in the symptomatic treatment of the disease. Several risk factors, such as systemic inflammation (i.e., autoimmune diseases), obesity, diabetes, and hypertension were identified but effective and tolerable interventions are sparse. Even though neuronal damage characterized by the accumulation of toxic proteins, inflammation, and atrophy can be slowed down by certain drugs, the efficacy of immune-modulatory, anti-inflammatory, or neuroprotective agents depends on early diagnosis (Munafò et al., 2020; Pais et al., 2020). As a recent meta-analysis demonstrated, regular physical activity was the only protective factor against dementia and Alzheimer's disease that all adults could benefit from (Iso-Markku et al., 2022). It has also been shown that sleep disorders can cause cognitive impairment, and impaired melatonin synthesis has been found in Alzheimer's patients (Cardinali D et al., 2010). In addition, melatonin secretion might increase after moderate-intensity exercises (Kaylee et al., 2020). Moreover, longer sleep duration leads to reduced β-amyloid levels in older cognitively unimpaired adults (Insel et al., 2021). Consequently, melatonin might be the key mediator of the beneficial effects of sleep on the clearance of β-amyloid from the brain (Li et al., 2020).

Melatonin (N-acetyl-5-methoxytryptamine) is the primary secretory product of the pineal gland, but it is also produced in the gastrointestinal tract, respiratory epithelium, pancreas, adrenal glands, thyroid gland, thymus, urogenital tract, placenta and even in non-endocrine cells (Kvetnoy et al., 2022). Indeed, it regulates biorhythm and controls sleep, but at molecular levels it is involved in the metabolism of free radicals due to its antioxidant capacity. It modulates immune responses, cell proliferation and differentiation, and also has neuroprotective effects in several preclinical models (Rosales-Corral et al., 2012; Miranda-Riestra et al., 2022; Tozihi et al., 2023). On the other hand, decreased levels of melatonin were observed in the cerebrospinal fluid of elderly subjects with early AD-like neuropathological changes (Rosales-Corral et al., 2012). Interestingly, pinealectomy causes pyramidal cell loss in the cornu Ammonis 1 (CA1) and cornu Ammonis 3 (CA3) regions of rats, which can be reversed by melatonin supplementation (De Butte and Pappas, 2007).

This study aimed to investigate whether melatonin treatment would reverse the neuroinflammation and cellular reorganization in the sporadic model of Alzheimer's disease in rats induced by intracerebroventricular (ICV) injection of streptozotocine (STZ). Behavioral, biochemical, and histopathological tests were conducted to assess the effect of subchronic melatonin treatment on cognitive performance and neuronal damage, respectively.

2 Materials and methods

2.1 Drugs and administration

STZ was purchased from Cayman Chemicals. Rats in the STZ group received an ICV injection of STZ (3 mg/kg body weight) dissolved in 8 μL citrate buffer (0.05 M, pH = 4.5), and the rats in the control (CTRL) group received an equal volume of vehicle. Melatonin (Cayman Chemicals, Ann Arbor, MI, United States) was dissolved in ethyl alcohol (50 mg/mL) and incorporated in food pellets, followed by solvent evaporation. The pellets were freshly prepared before drug administration, and the amount of melatonin was calculated for each animal using a 20 mg/kg body weight dose per day.

2.2 Animals and experimental groups

The experiment was carried out on 5–6-month-old male Wistar rats (350–450 g). They were kept in a polypropylene cage (1291H Eurostandard Type III H, 425 mm × 266 mm × 185 mm, Techniplast, Milan, Italy) and maintained under standard housing conditions (temperature 20°C ± 2°C and humidity 60% ± 10%) with a 12-h light-dark cycle. Animals were housed singly 7 days prior to the start of the experiments. No environmental enrichment, including hiding spaces, was provided. Dry food pellets (Cantacuzino Institute, Bucharest, Romania) and water were available *ad libitum*. The rats were procured from the Biobase of UMFST George Emil Palade of Targu Mures, Romania. The experimental protocol was approved by the Ethics Committee of George Emil Palade University of Medicine, Pharmacy, Science, and Technology of Targu Mures (approval no. 366/2018) and the National Authority (no. 123/2018).

Thirty-four rats were randomly divided into four groups, from which two groups consisted of sham-operated animals (CTRL and CTRL + MEL) and the other two received ICV-STZ injections (STZ and STZ + MEL). The first group of animals (CTRL) was injected with citrate buffer ICV and administered orally with pellets containing vehicle used for melatonin dosing (n = 8); the second

group (CTRL + MEL) was injected with citrate buffer ICV and administered with pellets containing melatonin (n = 8); the third group (STZ) was injected ICV with STZ and received vehicle containing pellets (n = 9); the fourth group (STZ + MEL) was injected ICV with STZ and received melatonin containing pellets (n = 9). Melatonin (20 mg/kg) was administered daily, beginning on the sixth day of the experiment until the end of the study. Total treatment duration was 30 days, which corresponds to a subchronic treatment regimen.

Briefly, animals were anesthetized with a mixture of ketamine (100 mg/kg body weight) and xylazine (10 mg/kg body weight) through intraperitoneal administration. Rats were then placed into a stereotactic apparatus (Digital Stereotaxic with Manual Fine Drive, Leica Biosystems, Buffalo Grove, IL, United States) and injected bilaterally with STZ at a sub-diabetogenic total dose of 3 mg/kg (dissolved in 0.05 M citrate buffer, pH 4.5, in one single dose on day one) using a 10 μL Hamilton syringe (Hamilton® glass syringe 700 series RN, Hamilton syringe Hamilton syringe (Hamilton® glass syringe 700 series RN), Hamilton, Bonaduz, Switzerland) with a 26-G needle into each ventricle (4 μL/ventricle). The sham-operated animals received an equal volume of vehicle (0.05 M citrate buffer, pH 4.5) by the same procedure. Stereotactic coordinates relative to bregma, dura mater and inter-hemispheric scissure: antero-posterior: −0.7 mm; ventral: −3.6 mm; lateral: ±1.5 mm. The injection speed was set to 0.4 μL/min using a motorized programmable stereotaxic injector (Stoelting QSI Model 5311, Stoelting Co., Wood Dale, IL, United States), and the injection needle remained for at least 2 min in place, to prevent backflow of the administered solution (Kraska et al., 2012; Knezovic et al., 2015; Homolak et al., 2021). Postoperatively, animals were hydrated intraperitoneally with 6 mL saline solution and monitored for signs of pain.

After the ICV injection, animals were allowed a 5-day recovery period during which they were kept in individual home cages and their body weight, food, and water intake were monitored daily. Although STZ exhibit specific pancreatic β-cell toxicity when injected intraperitoneally, the STZ-ICV injection did not affect peripheral blood glucose levels and body weight as demonstrated previously (Song et al., 2018). Immediately after recovery, all animals were randomly assigned to a control or treatment group. Due to mortality observed in the STZ-injected groups (5 animals died shortly after ICV injection) that could be associated with STZ acute toxicity as described earlier (Chen et al., 2014; Guardia de Souza e Silva et al., 2020; Gáspár et al., 2022), 29 animals were included in the behavioral, biochemical, and histological analysis. The number of animals/group at the end of the experiment was as follows: CTRL n = 8, CTRL + MEL n = 8, STZ n = 7, STZ + MEL n = 6. In exceptional situations, where biological samples obtained were not validated due to sampling procedure errors, the number of samples used for those analyses was specified.

2.3 Behavioral studies

On the 20th day of the experiment counted from the day of STZ injection, behavioral testing began with an open field test, followed by novel object recognition and radial arm maze tests. The timeline of the experiment is shown in Figure 1.

2.3.1 Open field test

To assess the exploratory and locomotor activity of the animals, the first behavioral test implemented was an open field test on day 20. The open field apparatus consisted of a black floor (60 × 60 cm) and transparent walls (60 cm). The intensity of the illumination was controlled for and set to an average light intensity of 150 ± 10 lux. The rats were placed in the center of the box and left undisturbed to explore the apparatus for 5 min. The activity of rats was monitored and recorded with a CMOS video camera (30 fps) and behavior analysis software (Ethovision XT, version 11.5, Noldus IT, Wageningen, Netherlands). The detection options were optimized for each trial. Automatic analysis was used to detect the rat at three points (head, body, tail) and record the distance moved, the number of entries and the time spent in different zones of the apparatus. In addition, rearing and grooming were measured by semi-automatic analysis performed by two blinded observers.

2.3.2 Novel object recognition test

There is a wide range of uses for the NOR test, including the assessment of memory deficits, anxiety, attention, novel object preferences, exploratory patterns, and pharmacological therapy (Antunes and Biala, 2012). The apparatus consisted of an open box made of Plexiglas (60 × 60 cm) and transparent walls (60 cm) positioned on the floor. The light intensity was set to 80 ± 10 lux.

The objects to be explored were made of plastic, glass, or wood. The height of the objects was approximately the same (5 ± 2 cm), and they were fixed to the base of the apparatus to prevent displacement by animals. Objects were positioned 10 cm away from the box walls, allowing animals to move along the walls undisturbed. After each trial, 70% alcohol was used to clean the box and the objects, removing olfactory cues. The familiar and novel objects were counterbalanced in the left and right positions, to prevent bias towards a particular location. Object exploration was quantified by Ethovision XT 11.5 software using the nose point of the rats (touching or no more than 0.5 cm away from the object) but activities such as leaning against, turning around, standing, or sitting on the objects were excluded.

Two inter-trial intervals were used to determine the short- or long-term memory of the rats, and all rats were subjected to three trials: one acquisition trial and two retention trials. The first was the acquisition trial, performed using two identical wood cuboid objects. Second, an intertrial period of 2 h was followed by the first retention trial, where one familiar object was replaced by a cylindrical transparent glass. The third trial was another retention trial completed after a 24-h inter-trial period. In this trial, the previously novel object was replaced with a black, round plastic object. In every phase, the animals had 5 min to explore the environment and the objects (Mathiasen and DiCamillo, 2010). Consequently, short-term memory was evaluated 2 h after the presentation of identical objects, while long-term memory was assessed 24 h after the acquisition trial. The main parameter of this test was the discrimination index (DI), calculated using the time spent with the novel (TN) and the familiar object (TF) as Eq. 1 shows:

$$DI = (TN - TF) / (TN + TF) \quad (1)$$

The DI is a number between −1 and +1. If it is near −1, the animal prefers the familiar object, if it is near +1, they prefer the novel one.

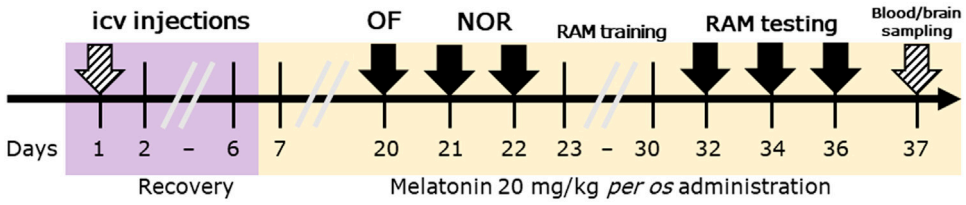


FIGURE 1
Timeline of the study design. Legend: OF, open field test; NOR, novel object recognition test; RAM, radial arm maze test; ICV, intracerebroventricular. Solid arrows represent behavioral tests, while striped arrows represent surgical interventions.

2.3.3 Radial arm maze test

The cognitive functions of the animals, such as spatial learning and memory, were tested with the radial arm maze test (RAM). The RAM test is an 8-arm radial maze used to observe visuospatial learning ability and memory. The apparatus used for testing was initially described by Olton and Samuelson (1976) and was constructed in-house according to standard specifications: an octagonal center platform surrounded by eight wooden arms (50 cm long and 10 cm wide) with 20 cm high walls; at the end of each arm there was a hole, which contained food that was not visible from the central platform. To test both working and reference memory of rats, two out of the eight arms did not contain food pellets (the unbaited arm). The position of the baited and unbaited arms was the same across all trials. Various environmental marks and objects (pictures, doors, tables, windows) were available to assist with spatial orientation.

After 2 days of acclimatization to testing conditions (apparatus, laboratory conditions with controlled visual cues) and to food restriction (5 days of food deprivation until reaching 80%–85% of their *ad libitum* body weight) to ensure their motivation for task completion, animals underwent a training phase that comprised one daily test and lasted for 7 days. The diet restriction was necessary to motivate the animals to explore the labyrinth.

The test phase was comprised of four trials conducted every other day. All trials were terminated after 10 min or after all pellets were found (Fole et al., 2017). Each animal was placed on the center platform of the apparatus in random order and their activity was observed and recorded with a camera (CMOS, 30 frame/sec) mounted above the apparatus. Researchers observed the experiment in the next room. The behavioral parameters were recorded offline using Ethovision XT software (Noldus IT, Netherlands). The following parameters were automatically measured: the number of baits collected or target visits, the total number of errors, which included the reentry into a previously visited baited or unbaited arm (working memory error), the first entry into an unbaited arm (reference memory error). To standardize the olfactory background, a disinfectant solution containing ethanol and isopropanol was used for cleaning before the first and after each test.

2.4 Biochemistry

Based on serum samples obtained by cardiac puncture and followed by centrifugation, TNF-α and MMP-9 levels were determined using commercial test kits (St John's Laboratory, London, United Kingdom, catalog numbers STJ150174 and STJ150078, respectively). Quantitation was performed using optical density measurement on Luminex 200 instrument (Luminex Corp., Austin, TX, United States). The results were expressed as ng/mL.

2.5 Immunohistochemical procedures

2.5.1 Sample collection

Rats were transcardially perfused with ice-cold saline for 1.5 min followed by an ice-cold fixative solution containing 4% paraformaldehyde (Sigma Aldrich, St. Louis, MO, United States) and 0.25% picric acid (Sigma Aldrich, St. Louis, MO, United States) in phosphate buffer (pH = 7.4) for 20 min under anesthesia with ketamine hydrochloride (100 mg/kg) and xylazine (10 mg/kg) injected intraperitoneally on the 37th day after STZ injection. We collected blood and brain samples. Blood was collected via cardiac puncture before perfusion. After perfusion, the brain was carefully removed, placed in fixative solution and after 48 h, placed into 0.1 M phosphate buffer solution. 60 µm-thick coronal sections were cut with a microtome (VT 1000S, Leica, Nussloch, Germany) and stored at 4°C until immunohistochemistry was performed.

2.5.2 Fluorescent immunohistochemistry

Triple immunofluorescent staining was used to identify neurons, astrocytes, and microglia (Gáll et al., 2022). Sections were washed in 0.1 M phosphate buffer (PB, pH 7.4, Sigma Aldrich, St. Louis, MO, United States) and transferred to a 24-well tissue culture plate (TPP, Trasadingen, Switzerland). The plates were placed on an orbital shaker (Heidolph, Germany) and incubated at 37°C for 10 min for antigen retrieval. All samples were stained in a free-floating manner in 24-well tissue culture plates in 500 µL volume on an orbital shaker. After being washed 3 times for 10 min in 0.1 M PB, sections were washed in tris buffered-saline (TBS) (3 times 10 min), then incubated in a blocking solution of TBS, containing 10% normal goat serum (NGS) (Vectro Laboratories, Inc., Burlingame CA, United States, 94010), followed by incubation with a mixture of primary guinea pig polyclonal anti-NeuN antibody (guinea pig raised-polyclonal, dilution 1:500; product no: 266004, Synaptics Systems GmbH, Goettingen, Germany), primary rabbit polyclonal anti-IBA-1 antibody (rabbit raised-polyclonal, dilution 1:500; product no: HS234013, Synaptics Systems GmbH, Goettingen, Germany), and

primary mouse monoclonal anti-GFAP antibody (mouse raised-monoclonal dilution 1:500; product no: 173211, Synaptics Systems GmbH, Goettingen, Germany) diluted in TBS containing 2% NGS and 0.1% Triton X-100 (Sigma Aldrich) for 24 h at room temperature. Sections were washed three times in TBS, then secondary antibodies made up in TBS, containing 2% NGS at room temperature for 2 h were applied to label the NeuN immunostaining with Alexa488-conjugated donkey anti-guinea pig (1:500, Jackson ImmunoResearch Laboratories, West Grove, PA, United States), the IBA1 immunostaining with Alexa594-conjugated donkey anti-rabbit (1:500, Jackson ImmunoResearch Laboratories, West Grove, PA, United States), and the GFAP immunostaining with Alexa647-conjugated donkey anti-mouse (1:500, Jackson ImmunoResearch Laboratories, West Grove, PA, United States). The stained sections were washed 3 × 10 min in TBS followed by 3 × 5 min in 0.1 PB, then mounted on slides and coverslipped with mounting medium containing 4′,6-diamidino-2-phenylindole (DAPI) for cell nuclei labeling (Vectashield with DAPI, Vector Laboratories, Burlingame, CA, United States) and sealed with nail polish. A negative control was prepared for all immunostaining by omitting the primary antibodies.

The sections were analyzed using 3DHISTECH Pannoramic MIDI II slide scanner collaborating with the Institute of Experimental Medicine (Budapest, Hungary). Fluorescent images were obtained with Zeiss, Plan-Apochromat ×20 dry objectives, Cy3.5 SB, Cy5-Q, LED-FITC and DAPI-Q filters. Digitized images were processed with ImageJ Fiji (v.1.5.3t with Java 1.8.0_322) and Ilastik (v.1.4.0) softwares. In the first step, the supervised machine learning process was facilitated by manually annotating the signal and the background pixels. Then, the pixel classification workflow was implemented as described by Berg et al. (2019). The resulting images were used for quantitative analysis. The total cell count and percent labelled area were determined using the "analyze particles" command that counts and measures objects in threshold images in ImageJ Fiji. Hippocampal regions and layers were differentiated based on cell density and relative location using DAPI staining. CA1 and CA3 regions of the hippocampus were quantified individually in four hippocampal sections per animal. The final value of each measurement presented is its group average (± standard deviation, SD).

2.6 Statistical analysis

All data was checked for normal distribution and was treated accordingly. The normality of raw data was ruled by Kolmogorov-Smirnov test using GraphPad Prism eight software (GraphPad Software, United States), the same software being used for figure generation. Data with a normal distribution were presented as mean ± SEM. A two-way ANOVA analysis was employed to examine the main effects of ICV-STZ injection and melatonin treatment. In the case of some parameters where repeated measurements were performed (NOR and RAM tests) a three-way ANOVA analysis was used. The *post hoc* Tukey's test was then performed for multiple comparisons. Where the sample sizes were different, Sidak's multiple comparison test was implemented. Nonparametric distributed data were analyzed by a Kruskal-Wallis test followed by Dunn's *post hoc* test to detect the significant differences between groups $p < 0.05$ was considered statistically significant.

3 Results

3.1 Effects of melatonin supplementation on behavior

3.1.1 Open-field test

All animals showed unaltered locomotor activity and neophobia-induced anxiety when placed in the apparatus. Analyzing the activity of rats during a 5-min testing session, two-way ANOVA tests showed significant interaction between STZ injection and melatonin treatment [$F(1, 25) = 7.552$, $p = 0.0110$] for the distance travelled in the testing box. Post-hoc Tukey's multiple comparison test revealed significant increase in the CTRL + MEL group compared to CTRL and STZ + MEL groups (Figure 2A). Accordingly, the freezing time of CTRL + MEL group was significantly reduced (Figure 2B). The number of entries and the time spent in the center zone of the apparatus were increased by the ICV-STZ injection, the intervention showing a significant main effect in the two-way ANOVA test ($F(1, 24) = 4.947$, $p = 0.0358$; $F(1, 24) = 22.00$, $p < 0.0001$). Interestingly, melatonin treatment did not influence these parameters (Figure 2C). Conversely, the vertical exploratory activity expressed as the number of rearing was increased by melatonin treatment [$F(1, 25) = 10.73$, $p = 0.0031$; Figure 2D], the CTRL + MEL group showed significant increase compared to CTRL and STZ + MEL groups. The self-grooming activity of the animals was also studied, but no effect of ICV-STZ injection or melatonin treatment was observed.

3.1.2 NOR test

In the familiarization phase, the two-way ANOVA analysis revealed no significant effect of ICV-STZ injection or melatonin treatment on the exploration of identical objects in the acquisition trial [$F(1, 22) = 1.344$, $p = 0.2587$; $F(1, 22) = 1.577$, $p = 0.2223$]. This means that there was no external influence on object preference. The first retention trial was performed after a 2-h intertrial interval, when a novel object replaced one of the familiar objects. One-way ANOVA revealed no significant differences for the DI values (Figure 3A) [$F(3, 21) = 1.649$, $p = 0.21$]. However, a high dispersion of the data was observed, so it was not possible to estimate the effect of melatonin treatment correctly. However, there was a significant effect of melatonin treatment on DI values observed during the second retention trial [$F(3, 24) = 6.44$, $P = 0.002$]. Post hoc Tukey's multiple comparison test showed a significant decrease in DI following STZ injection ($p = 0.005$) when compared to the CTRL group. The other significant finding is that melatonin treatment administered after STZ injection increased the DI values significantly compared to the STZ group, up to the level of the CTRL group (Figure 3B).

3.1.3 RAM test

For the evaluation of spatial learning and memory functions animals were tested on RAM. A high level of variability was observed, especially in the animals injected with ICV -STZ, during the 7-day learning period. Concerning the target visits,

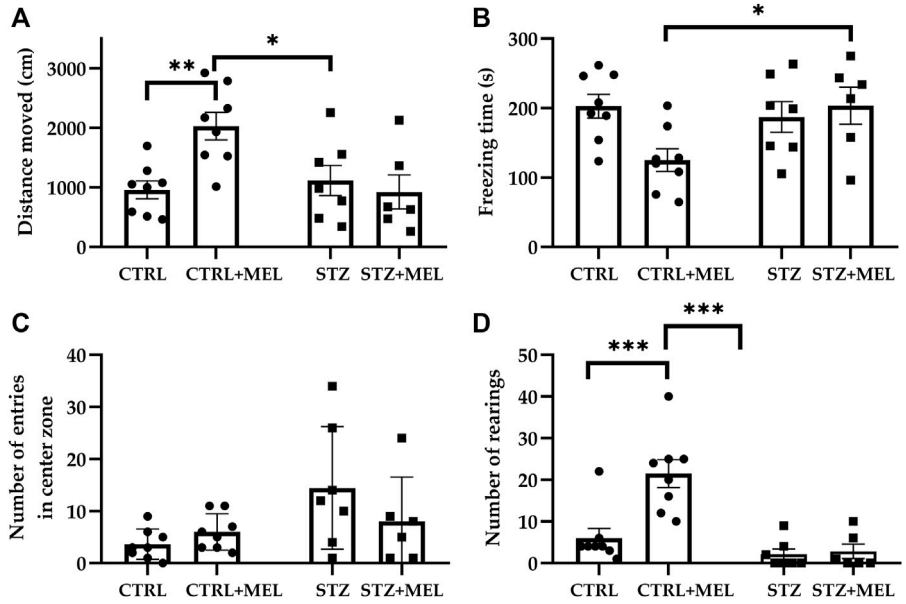


FIGURE 2
Open field test performance of melatonin treated rats underwent ICV-STZ injection. Quantified parameters: distance moved **(A)**, freezing time **(B)**, number of entries in the center zone **(C)**, and the number of rearings **(D)**. Legend: *$p < 0.05$, **$p < 0.01$, ***$p < 0.001$, CTRL−control group icv injected with buffer and treated with vehicle (n = 8), CTRL + MEL−group icv injected with buffer and treated with melatonin (n = 8), STZ−group icv injected with streptozotocin and treated with vehicle (n = 7), STZ + MEL−group icv injected with streptozotocin and treated with melatonin (n = 6).

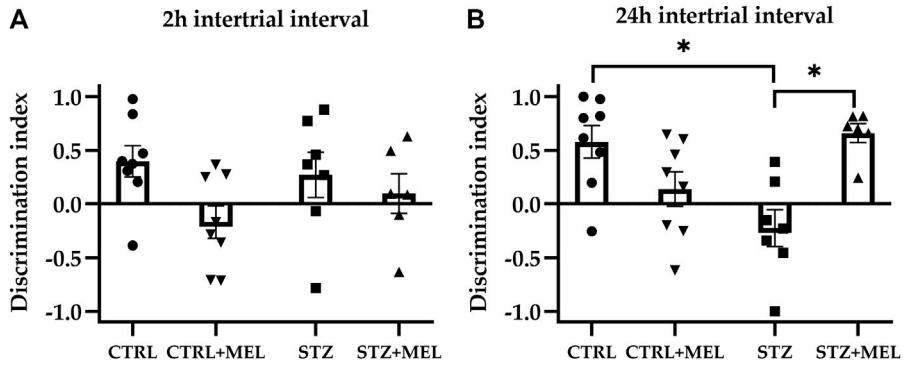


FIGURE 3
The discrimination index derived from novel object recognition task as a measure of recognition memory. Two intertrial intervals were tested: **(A)** 2-hrs and **(B)** 24-hrs. Data is expressed as mean ± SEM. Legend: *$p < 0.05$, CTRL−control group icv injected with buffer and treated with vehicle (n = 8), CTRL + MEL−group icv injected with buffer and treated with melatonin (n = 8), STZ−group icv injected with streptozotocin and treated with vehicle (n = 7), STZ + MEL−group icv injected with streptozotocin and treated with melatonin (n = 6).

all groups performed similarly during the four test trials that comprised the test phase. This confirmed that all animals were capable of learning to complete the task and no differences were observed between the control and treated groups regarding the time needed to complete the task ($p > 0.05$). To evaluate the reference and working memory a three-way ANOVA analysis was performed using ICV-STZ injection, melatonin treatment, and trial number as main factors. The main effects of ICV-STZ injection and melatonin treatment were significant in the case of total errors [F (1, 92) = 3.954, $p = 0.0497$; F (1, 92) = 5.981, $p = 0.0164$, respectively] and working memory errors [F (1, 92) = 4.017, $p = 0.0480$; F (1, 92) = 4.952, $p = 0.0285$, respectively]. Moreover, an ICV-STZ × melatonin treatment interaction was also observed in the case of both parameters [F (1, 92) = 15.75, $p = 0.0001$; F (1, 92) = 13.59, $p = 0.0004$]. Interestingly, reference memory errors were significantly influenced by melatonin treatment [F (1, 92) = 5.027, $p = 0.0274$] only, but the interaction between ICV-STZ injection and melatonin treatment was also significant [F (1, 92) = 11.66, $p = 0.0010$]. The main effect of the trials and all interactions with the trials were not significant. So, the data was analyzed further using Tukey's multiple comparison *post hoc* tests to find significant differences between the groups. As shown in Figure 4, the total number of errors [F (3, 23) = 7.290, $p = 0.0013$), Figure 4B], the

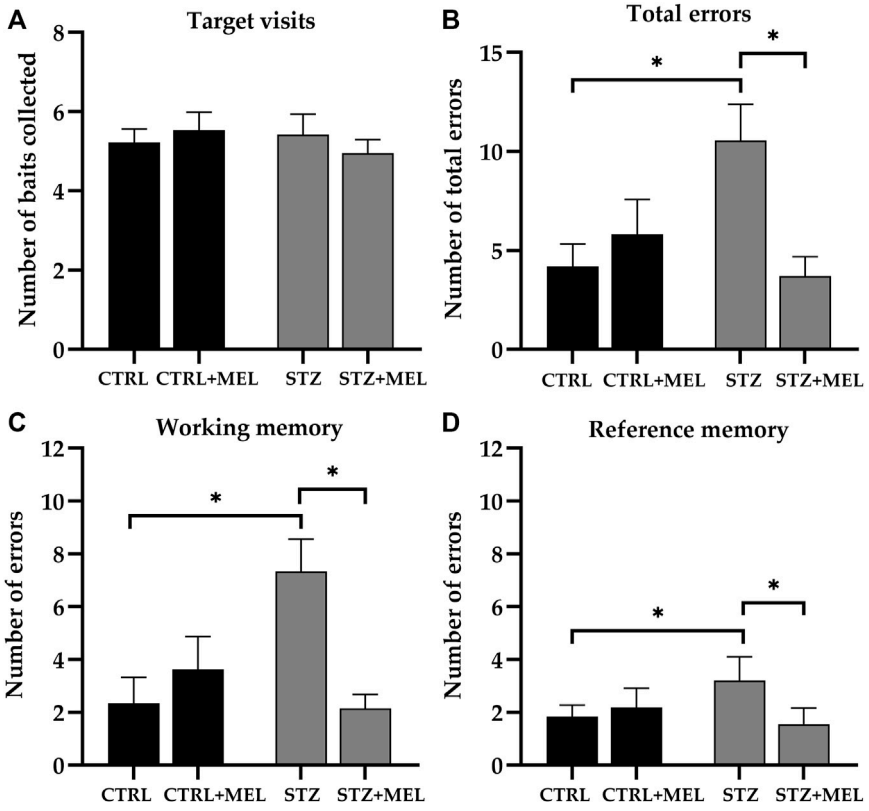


FIGURE 4
Radial arm maze test performance of melatonin treated rats underwent ICV-STZ injec-tion. Quantified parameters: target visits **(A)**, total errors **(B)**, working **(C)**, and reference memory errors **(D)**. Legend: *$p < 0.05$, CTRL−control group icv injected with buffer and treated with ve-hicle (n = 8), CTRL + MEL−group icv injected with buffer and treated with melatonin (n = 8), STZ−group icv injected with streptozotocin and treated with vehicle (n = 7), STZ + MEL−group icv in-jected with streptozotocin and treated with melatonin (n = 6).

number of reference memory errors [F (3, 23) = 6.543, p = 0.0023; Figure 4C], and the number of working memory errors [F (3, 23) = 5.381, p = 0.0059; Figure 4D] were significantly influenced by melatonin treatment. An increase in the number of errors in the case of the ICV-STZ group was observed, whereas melatonin treatment significantly decreased the STZ-induced alteration in cognitive performance.

3.2 Effects of melatonin supplementation on serum levels of TNF-α and MMP-9

In this study, the MMP-9 levels were determined using rat serum collected at the end of the experiment. Overall, melatonin treatment significantly influenced the MMP-9 levels as confirmed by the one-way ANOVA test [F (1, 21) = 4.706, p = 0.0417; Figure 5A). Post-hoc tests revealed that MMP-9 levels were reduced by melatonin treatment in the sham-operated control group, only a slight decrease being observed in the STZ-injected group. Similarly, TNF-α levels were significantly lower in melatonin-treated sham-operated animals than in sham-operated controls and STZ-injected animals [F (1, 21) = 5.385, p = 0.031]. The *post hoc* analysis with Sidak's multiple comparisons tests revealed significant differences between groups (Figure 5B).

3.3 Effects of melatonin supplementation on cellular reorganization of the hippocampus

3.3.1 NeuN immunoreactive cells

Neuronal reorganization following STZ injection and melatonin treatment was examined in the hippocampus via neuronal nuclei antigen (NeuN) immunohistochemistry. NeuN-positive cells were observed in the pyramidal layer of the CA1 and CA3 hippocampal regions and the dentate gyrus's granule cell layer. For STZ-injected animals, the pyramidal layer of the hippocampus showed a loose layout compared to those not injected with STZ (Figures 6A–D). Because of the limitations of the automated cell counting method used in this study (i.e., superposed cells or compact layers of cells could not be recognized and counted), the absolute number of NeuN cells could not be determined automatically. Instead, the percentage area% of the NeuN signal was evaluated in each CA1 and CA3 region. There were no differences between the groups in response to melatonin treatment (Figures 6E, F). However, STZ-injected groups showed decreased percentage area% of the NeuN signal in both CA1 and CA3 regions of the hippocampus [F (3, 54) = 15.95, $p < 0.0001$ and F (3, 54) = 25.46, $p < 0.0001$, respectively].

3.3.2 GFAP immunoreactive cells

Astrogliosis associated with STZ induced neuroinflammation was studied in the hippocampus by glial fibrillary acidic protein (GFAP) immunohistochemistry (Figures 7A–D). The number of astrocytes was

10.3389/fphar.2024.1447757

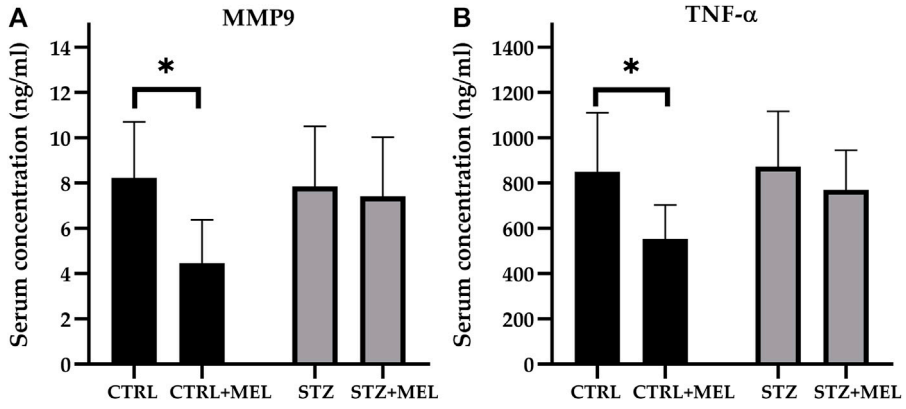


FIGURE 5
Serum levels of **(A)** MMP-9 and **(B)** TNF-α after melatonin treatment in ICV-STZ model of Alzheimer's disease. Legend: *$p < 0.05$, CTRL−control group icv injected with buffer and treated with vehicle (n = 7), CTRL + MEL−group icv injected with buffer and treated with melatonin (n = 8), STZ−group icv injected with streptozotocin and treated with vehicle (n = 5), STZ + MEL−group icv injected with streptozotocin and treated with melatonin (n = 6).

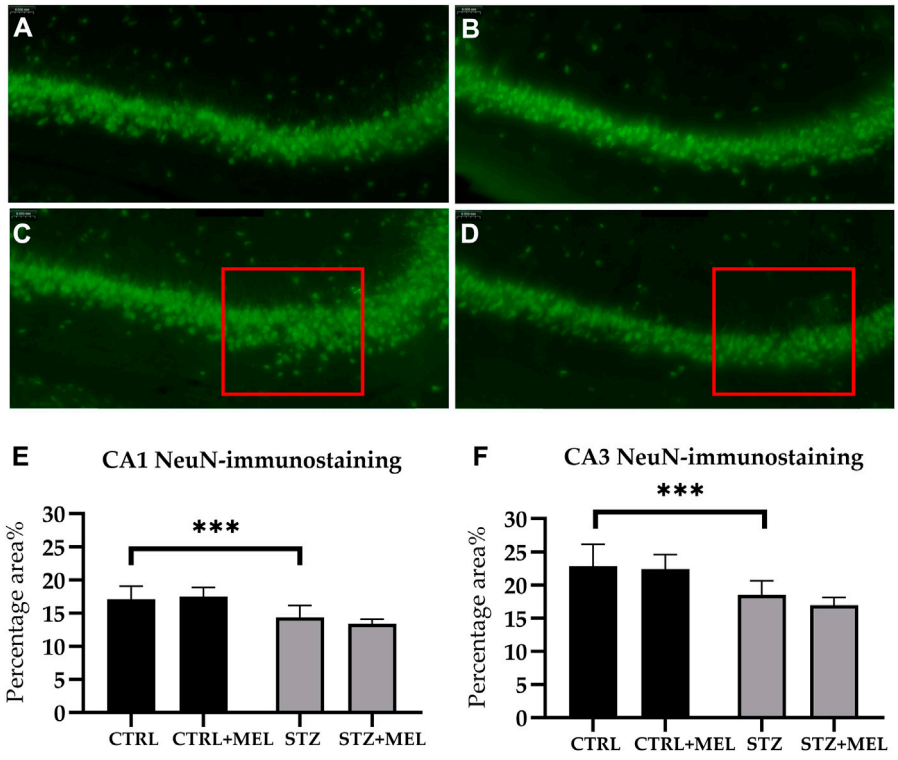


FIGURE 6
Effects of chronic melatonin (20 mg/kg body weight) treatment on the hippocampal re-organization induced by ICV-STZ in rats. Representative confocal microscopy images of the cornu Ammonis 3 (CA3) region **(A)** in the control group injected ICV with citrate buffer; **(B)** in the control group treated with melatonin; **(C)** in the ICV-STZ injected group; **(D)** in the ICV-STZ injected and melatonin treated group. The percentage area of neuron specific nuclear protein (NeuN) immunostaining (expressed as percentage of the area covered by positive signal compared to the total area of a region) revealed no effect of the melatonin treatment on STZ-induced cell loss in the **(E)** CA1 region and **(F)** CA3 region of the hippocampus. The magnification was ×20. The scale bar indicates 50 μm. Legend: ***$p < 0.001$, CTRL−control group icv injected with buffer and treated with vehicle (n = 10 hippocampi from n = 5 animals), CTRL + MEL−group icv injected with buffer and treated with melatonin (n = 16 hippocampi from n = 8 animals), STZ−group icv injected with streptozotocin and treated with vehicle (n = 20 hippocampi from n = 7 animals), STZ + MEL−group icv injected with streptozotocin and treated with melatonin (n = 12 hippocampi from n = 6 animals). The red rectangle indicates the region where significant modifications were observed.

counted in the CA1 and CA3 regions of the hippocampus and the cell density was calculated. On the other hand, the mean astrocyte cell size was determined. STZ-injected animals showed no difference in the density and cell surface of GFAP-labeled astrocytes compared to CTRL group. However, melatonin treatment significantly reduced the cell density in the CA3, and the cell surface in the CA1 region (Figures 7E–H).

10.3389/fphar.2024.1447757

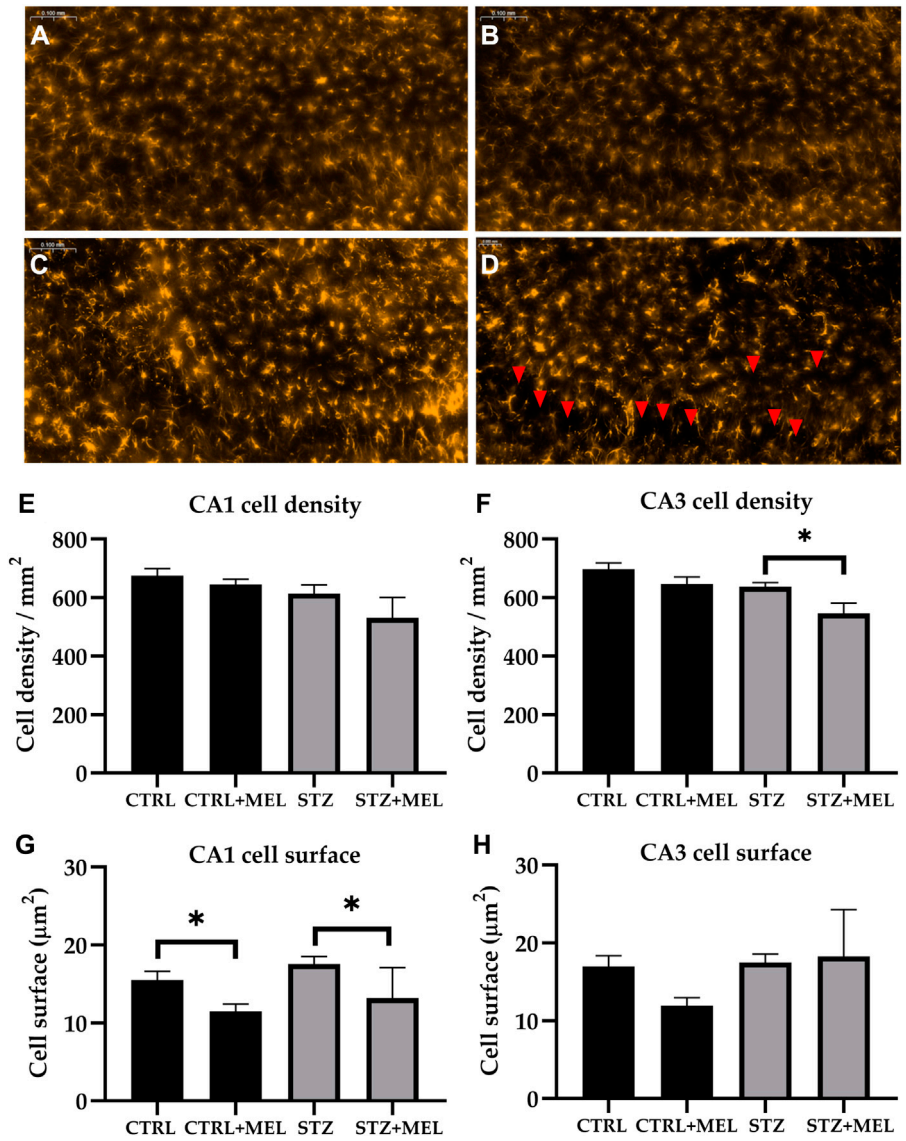


FIGURE 7
Effects of chronic melatonin (20 mg/kg body weight) treatment on the GFAP-positive astrocytes in the ICV-STZ sporadic model of Alzheimer's disease in rats. Representative confocal microscopy images of the cornu Ammonis 3 (CA3) region **(A)** in the control group injected ICV with citrate buffer; **(B)** in the control group treated with melatonin; **(C)** in the ICV-STZ injected group; **(D)** in the ICV-STZ injected and melatonin treated group. The magnification was ×20. The scale bar indicates 50 µm. The astrocyte density (expressed as cell/mm^2) revealed no effect of the melatonin treatment in the CA1 region **(E)** but it did reduce astrocyte density in the CA3 region **(F)** of the hippocampus. The astrocyte dimension (expressed as mean cell surface in µm^2) showed significant decrease in both melatonin treated groups in the CA1 region **(G)**, however, the modifications did not reach the limit of significance in the CA3 region **(H)**. Data in column graphs are expressed as mean ± SEM (n = 5–8).; Legend: *$p < 0.05$, CTRL–control group icv injected with buffer and treated with vehicle (n = 10 hippocampi from n = 5 animals), CTRL + MEL–group icv injected with buffer and treated with melatonin (n = 16 hippocampi from n = 8 animals), STZ–group icv injected with streptozotocin and treated with vehicle (n = 20 hippocampi from n = 7 animals), STZ + MEL–group icv injected with streptozotocin and treated with melatonin (n = 12 hippocampi from n = 6 animals). Red arrowheads indicate the regions where significant differences were observed.

3.3.3 IBA-1 immunoreactive cells

Alterations involving microglia were studied in the CA1 and CA3 regions of the hippocampus by ionized calcium-binding adapter molecule 1 (IBA-1) immunohistochemistry. Microglia cell density was significantly different between treatment groups (Figures 8A–D). STZ injection increased the number of IBA-1 positive microglia compared to controls both in the CA1 (440.8 ± 20.8 vs. 376.1 ± 15 cell/mm^2) and CA3 subregions (446 ± 18.4 vs. 400.1 ± 15.8 cell/mm^2). However, melatonin treatment reduced it in the CA1 (373.5 ± 16.6 cell/mm^2) and CA3 (404.2 ± 16.5 cell/mm^2) regions of the hippocampus to a comparable level to controls ($p < 0.05$, Figures 8E, F).

4 Discussion

Alzheimer's disease and dementia are associated with a decrease in melatonin production (Bubenik and Konturek, 2011;

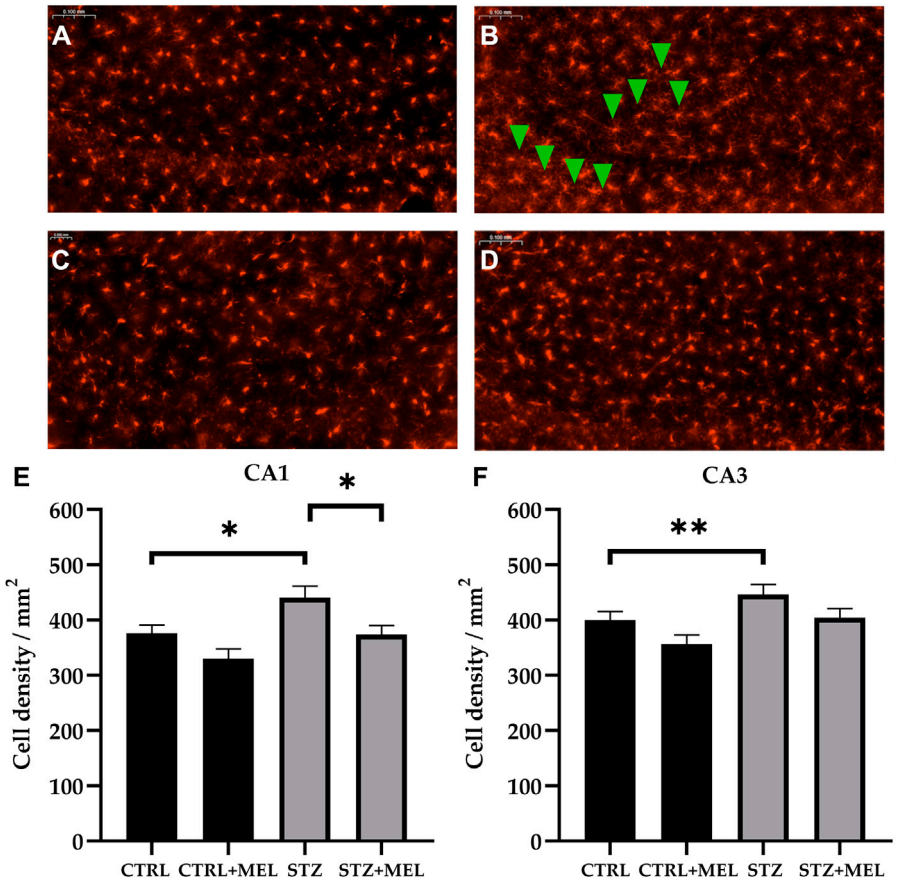


FIGURE 8
Effects of chronic melatonin (20 mg/kg body weight) treatment on the IBA-1-positive microglia in the ICV-STZ sporadic model of Alzheimer's disease in rats. Representative confocal microscopy images of the cornu Ammonis 3 (CA3) region **(A)** in the control group injected ICV with citrate buffer; **(B)** in the control group treated with melatonin; **(C)** in the ICV-STZ injected group; **(D)** in the ICV-STZ injected and melatonin treated group. The magnification was ×20. The scale bar indicates 50 μm. The microglia density (expressed as cell/mm^2) showed significant increase due to ICV-STZ injection in both CA1 and CA3 regions and melatonin treatment reduced this increase in the CA1 region **(E)**, however it did not reach significance limit in the CA3 region **(F)** of the hippocampus. Data in column graphs are expressed as mean ± SEM (n = 5–8).; Legend: *$p < 0.05$, **$p < 0.01$, CTRL–control group icv injected with buffer and treated with vehicle (n = 10 hippocampi from n = 5 animals), CTRL + MEL–group icv injected with buffer and treated with melatonin (n = 16 hippocampi from n = 8 animals), STZ–group icv injected with streptozotocin and treated with vehicle (n = 20 hippocampi from n = 7 animals), STZ + MEL–group icv injected with streptozotocin and treated with melatonin (n = 12 hippocampi from n = 6 animals). Green arrowheads indicate the regions where significant differences were observed.

Nous et al., 2021) and an age-dependent decline of melatonin production was also demonstrated in rat models of AD, however, supplementation can restore the normal levels in serum and pineal gland (Rudnitskaya et al., 2015). During the last few years, melatonin has been recognized as a promising tool for treating conditions with inflammatory origins (Favero et al., 2017). It has also been recognized as a neuroprotective agent (Tozihi et al., 2023). Melatonin's beneficial effects have already been reported in other AD models (Cheng et al., 2006) and traumatic brain injury (Ikram et al., 2021). Melatonin exerted antiapoptotic activity (Wang, 2009), decreased tau hyperphosphorylation (Das et al., 2020), stimulated neurotrophic factors (Miranda-Riestra et al., 2022), and reduced neuroinflammation by affecting microglia and astrocytes (Hardeland et al., 2015; Hardeland, 2021; Zhou et al., 2021). This study was conducted to investigate the potential efficacy of subchronic melatonin treatment in alleviating the cognitive decline and neurodegeneration induced by ICV injected STZ. The results presented here showed that melatonin treatment improved cognitive performance of rats in both the novel object recognition and radial arm maze tests, reduced the levels of TNF-α and MMP-9 in the serum, and led to a reduction in astrogliosis and microglia cell density in the hippocampus.

The progression of AD has previously been linked to neuroinflammation, free radical formation and mitochondrial dysfunction with consequent neuronal loss, as well as to increased glutamatergic signaling (Rosales-Corral et al., 2012). Based on this hypothesis, several animal models were used to elucidate the pathophysiological features and behavioral manifestation of neurodegeneration. STZ, a glucosamine-nitrosourea derivative, causes diabetes by targeting GLUT-2 transporters in the pancreas when administered intraperitoneally. But injected intracerebroventricularly STZ induces lesions that resemble human AD including metabolic, neuropathological, and behavioral disturbances (Grieb, 2016; Kamat et al., 2016; Ravelli et al., 2017). Although the exact mechanisms are not known, this animal model became popular in the last decade because it can provide an insight into

the temporal dynamics and the nature of the pathophysiological processes (Homolak et al., 2021). Injection of STZ into the brain results in neuroinflammation, oxidative stress, impaired orientation and memory, reduced insulin receptor function, excitotoxicity, increased tau phosphorylation, amyloid accumulation, and synaptotoxicity. The presence of neuroinflammation was detected 1 week after the administration of 3 mg/kg of STZ, and information processing, episodic, working, and reference memory problems were noted (Kraska et al., 2012). Furthermore, this model can be used to identify and observe cellular reorganization of key brain regions, since activation of microglia and astrocytes is affected by inflammatory cytokines, as well as oxidative stress (Mishra et al., 2018). In this study, STZ-injected rats showed an increased number of microglia and astrocytes in both CA1 and CA3 regions. Melatonin treatment reduced the number of microglia and the surface area of astrocytes.

Cognitive impairment is a common feature of several pathological conditions, including Alzheimer's disease and traumatic brain injury. Melatonin is an endogenous hormone that plays a role in circadian rhythm regulation, sleep-wake cycles, and neuroprotection. Recent studies have also suggested that melatonin may have cognitive enhancing effects, although the underlying mechanisms are not fully understood. Recently, Andrade et al. (2023) found that long-term melatonin treatment reversed the cognitive impairment in the Y-maze induced by ICV-STZ; however, it did not influence the performance of rats in the object location test. These differences could be associated with the different effects of melatonin on the involved brain regions. Or melatonin may have a dose-dependent effect on different learning tasks. For example, Madhu et al. (2021) conducted a dose-response study assessing the cognitive improvement caused by melatonin in a persistent cognitive and mood dysfunction model in rats. Based on their findings, melatonin's effects on cognition were dose-dependent—in low doses, recognition memory is affected, while in higher doses, more complex cognitive functions are improved. The novel object recognition and radial arm maze tests are widely used behavioral paradigms to evaluate cognitive function in rodents (Antunes and Biala, 2012). The novel object recognition test assesses recognition memory, while the radial arm maze test evaluates spatial memory and learning. Our results demonstrate that melatonin treatment improves performance in both tests. As a possible explanation for cognitive enhancement, it should be noted that melatonin increased cholinergic transmission by inhibiting AChE in the neocortex and hippocampal regions (Rosales-Corral et al., 2012). This could be a similar mechanism to the existing AChE inhibiting drugs, such as rivastigmine, galantamine or donepezil. Nonetheless, this study provides further evidence for a potential therapeutic application of melatonin in the treatment of cognitive impairment.

TNF-α and MMP-9 are pro-inflammatory cytokines and proteases, respectively, which have been implicated in the pathophysiology of cognitive impairment. Elevated levels of these biomarkers have been observed in various pathological conditions, including Alzheimer's disease and traumatic brain injury. The role of TNF -α in Alzheimer's disease has been recently reviewed by Plantone et al. (2023). In astrocyte cell culture TNF-α induced amyloidogenic processes including Aβ production (Zhao et al., 2011). In clinical setting, it has been demonstrated that peripheral TNF-α elevation enhances brain pro-inflammatory cytokine expression and Alzheimer's disease patients exhibit high level of serum TNF-α concentrations (Culjak et al., 2021). Moreover, some evidence suggests that serum TNF-α concentrations are negatively correlated with cognitive function (Kim et al., 2017). Thus, any intervention that decreases serum TNF-α levels might be protective for brain health and cognitive status (Park et al., 2019; Li et al., 2022). On the other hand, an elevated MMP-9 level has also been reported in Alzheimer's disease and a variety of neurological and inflammatory diseases (Hernandes-Alejandro et al., 2020). However, Ringland et al. (2021) showed that MMP-9 inhibition alone did not improve spatial learning and memory in mice, as measured by the radial arm water maze. As described earlier, TNF-α levels increase to a maximum level after 6 h following STZ-injection and remain elevated for a 1-week period (Souza et al., 2017). This is in line with the results obtained by Rai et al. (2014), suggesting that neuroinflammation and glial activation induced by STZ-injection occur earlier (7–9 days after STZ-injection) than cognitive impairment, which takes 14–16 days to become visible. However, there is no evidence whether the chronic stage is characterized by elevated TNF-α and MMP-9 levels. In the current work, no difference was observed between sham-operated and STZ-injected animals at the end of the experiment, 37-days after STZ-injection. On the other hand, melatonin treatment significantly reduced the levels of TNF-α and MMP-9 in the serum of sham-operated animals. However, the reduction did not achieve statistical significance in STZ-injected animals Further experiments with additional treatment groups are needed to clarify the effects of melatonin treatment on TNF-α and MMP-9 levels in the chronic phase.

Astrogliosis, a hallmark of Alzheimer's disease, refers to the hypertrophy and hyperplasia of astrocytes in response to various insults, including neuroinflammation. Astrocytes play a key role in the maintenance of the central nervous system and are involved in a variety of physiological and pathological processes. However, excessive astrogliosis can lead to the formation of a glial scar, which can impede axonal regeneration and functional recovery following injury. STZ injection was demonstrated to increase astrocyte density in some brain regions, but not in the hippocampus (Humphrey et al., 2023). This is in accordance with the results of the current study, where no increase was observed due to STZ-injection. On the other hand, the current work showed that melatonin decreased astrocyte density in the CA3 at a dose of 20 mg/kg and reduced the astrocyte surface in the CA1 (i.e., reducing astrocyte ramifications without decreasing their number). Although, Andrade et al. found no influence of melatonin treatment on the GFAP protein expression in the hippocampus at a dose of 10 mg/kg melatonin (Andrade et al., 2023), it might exert direct inhibition on cell proliferation at higher doses (Estaras et al., 2023).

Similarly, microglia, the resident immune cells of the brain, play an important role in the regulation of neuroinflammation. In response to injury or infection, microglia become activated and release pro-inflammatory cytokines and chemokines. While this response is necessary for the clearance of pathogens and damaged cells, excessive microglial activation can lead to chronic inflammation and damage to healthy tissue. As microglia play a critical role in β-amyloid induced synapse loss and cognitive decline in AD, they might represent a potential therapeutic approach in AD treatment (Miao et al., 2023). Melatonin was shown to reduce microglial activation both in the scopolamine induced amnesia rodent model (Muhammad et al., 2019) and the kainic-acid model of hippocampal neurodegeneration and oxidative stress (Chung and Han, 2003). Nasiri et al. (2019) described that melatonin pretreated stem cells therapy significantly reduced

IBA-1 positive glial cells number in a rat model of AD. The results of this study provide further support that melatonin treatment may reduce microglia cell numbers and activation in the injured brain. Recently, one of the possible mechanisms by which melatonin could ameliorate hippocampal damage, namely the inhibition of the Cathepsin B/nucleotide-binding oligomerization domain-like receptor pyrin domain-containing 3 (NLRP3) signaling pathway, was revealed (Gao et al., 2024). To note, β-amyloid plaques and tau aggregates stimulate microglia and astrocytes, which trigger the chronic neuroinflammatory response, neuronal death and pyroptosis through the activation of the intracellular NLRP3 inflammasome (Liang et al., 2022). Therefore, the potential inhibitory effect of melatonin on inflammatory cytokines, astrogliosis and microglial function along with its cognitive enhancing activity might confer an crucial role for melatonin in treating AD.

Finally, the current study has some limitations which should be acknowledged (Livingston et al., 2017): the experiment was performed using male animals only, whereas AD affects more women than men and sex differences could be found in disease progression and phenotype (Estrada and Contreras, 2019); the effects of melatonin described here were not supported by mechanistic investigations, the association between improved cognitive performance and decreased activation of microglia needs further investigations.

5 Conclusion

Melatonin treatment improved the cognitive performance of rats and reduced the activation of microglia in both CA1 and CA3 regions of the hippocampus. These findings support the existing evidence for melatonin as a potential therapeutic option in neurodegenerative diseases, such as Alzheimer's disease. Further research is needed to confirm these findings and probe the underlying mechanisms.

Data availability statement

The raw data supporting the conclusions of this article will be made available by the authors, without undue reservation.

Ethics statement

The animal study was approved by the Ethics Committee of George Emil Palade University of Medicine, Pharmacy, Science, and Technology of Targu Mures. The study was conducted in accordance with the local legislation and institutional requirements.

Author contributions

ZG: Conceptualization, Funding acquisition, Methodology, Project administration, Resources, Software, Visualization, Writing–original draft, Writing–review and editing. BB: Conceptualization, Investigation, Methodology, Software, Writing–review and editing. KK: Methodology, Supervision, Validation, Writing–review and editing. MU: Investigation, Supervision, Validation, Writing–review and editing. IZ: Investigation, Methodology, Software, Writing–review and editing. KM: Investigation, Software, Visualization, Writing–review and editing. MK: Funding acquisition, Methodology, Project administration, Validation, Writing–review and editing.

Funding

The author(s) declare that financial support was received for the research, authorship, and/or publication of this article. This study was funded by a joint grant from Studium Prospero Foundation and the Hungarian Academy of Sciences (contract no. 137/26.01.2017). The funders played no role in the study design, the collection, analysis or interpretation of data, the writing of this paper, or the decision to submit it for publication.

Acknowledgments

The authors would like to thank Dr. Kovács Béla for the technical assistance provided for the determination of serum inflammatory markers.

Conflict of interest

The authors declare that the research was conducted in the absence of any commercial or financial relationships that could be construed as a potential conflict of interest.

Publisher's note

All claims expressed in this article are solely those of the authors and do not necessarily represent those of their affiliated organizations, or those of the publisher, the editors and the reviewers. Any product that may be evaluated in this article, or claim that may be made by its manufacturer, is not guaranteed or endorsed by the publisher.

References

Andrade, M. K., Souza, L. C., Azevedo, E. M., Bail, E. L., Zanata, S. M., Andreatini, R., et al. (2023). Melatonin reduces β-amyloid accumulation and improves short-term memory in streptozotocin-induced sporadic Alzheimer's disease model. *IBRO Neurosci. Rep.* 14, 264–272. doi:10.1016/j.ibneur.2023.01.005

Antunes, M., and Biala, G. (2012). The novel object recognition memory: neurobiology, test procedure, and its modifications. *Cogn. Process* 13 (2), 93–110. doi:10.1007/s10339-011-0430-z

Berg, S., Kutra, D., Kroeger, T., Straehle, C. N., Kausler, B. X., Haubold, C., et al. (2019). ilastik: interactive machine learning for (bio)image analysis. *Nat. Methods* 16 (12), 1226–1232. doi:10.1038/s41592-019-0582-9

Bubenik, G. A., and Konturek, S. J. (2011). Melatonin and aging: prospects for human treatment. *J. Physiol. Pharmacol.* 62 (1), 13–19.

Cardinali D, P., Furio A, M., and Brusco L, I. (2010). Clinical aspects of melatonin intervention in Alzheimers disease progression. *Curr. Neuropharmacol.* 8 (3), 218–227. doi:10.2174/157015910792246209

Chen, Y., Liang, Z., Tian, Z., Blanchard, J., Dai, C., Chalbot, S., et al. (2014). Intracerebroventricular streptozotocin exacerbates Alzheimer-like changes of 3xTg-AD mice. *Mol. Neurobiol.* 49 (1), 547–562. doi:10.1007/s12035-013-8539-y

Cheng, Y., Feng, Z., Zhang, Q., and Zhang, J. (2006). Beneficial effects of melatonin in experimental models of Alzheimer disease. *Acta Pharmacol. Sin.* 27 (2), 129–139. doi:10.1111/j.1745-7254.2006.00267.x

Chung, S.-Y., and Han, S.-H. (2003). Melatonin attenuates kainic acid-induced hippocampal neurodegeneration and oxidative stress through microglial inhibition. *J. Pineal Res.* 34 (2), 95–102. doi:10.1034/j.1600-079x.2003.00010.x

Culjak, M., Perkovic, M. N., Uzun, S., Strac, D. S., Erjavec, G. N., Leko, M. B., et al. (2021). The association between TNF-alpha, IL-1 alpha and IL-10 with Alzheimer's disease. *Curr. Alzheimer Res.* 17 (11), 972–984. doi:10.2174/1567205017666201130092427

Cummings, J., Osse, A. M. L., Cammann, D., Powell, J., and Chen, J. (2024). Anti-amyloid monoclonal antibodies for the treatment of Alzheimer's disease. *BioDrugs* 38 (1), 5–22. doi:10.1007/s40259-023-00633-2

Das, R., Balmik, A. A., and Chinnathambi, S. (2020). Melatonin reduces GSK3β-mediated tau phosphorylation, enhances Nrf2 nuclear translocation and anti-inflammation. *ASN Neuro* 12, 175909142098120. doi:10.1177/1759091420981204

De Butte, M., and Pappas, B. A. (2007). Pinealectomy causes hippocampal CA1 and CA3 cell loss: reversal by melatonin supplementation. *Neurobiol. Aging* 28 (2), 306–313. doi:10.1016/j.neurobiolaging.2005.12.004

Decourt, B., Noorda, K., Noorda, K., Shi, J., and Sabbagh, M. N. (2022). Review of advanced drug trials focusing on the reduction of brain beta-amyloid to prevent and treat dementia. *J. Exp. Pharmacol.* 14, 331–352. doi:10.2147/JEP.S265626

Estaras, M., Ortiz-Placin, C., Castillejo-Rufo, A., Fernandez-Bermejo, M., Blanco, G., Mateos, J. M., et al. (2023). Melatonin controls cell proliferation and modulates mitochondrial physiology in pancreatic stellate cells. *J. Physiol. Biochem.* 79 (1), 235–249. doi:10.1007/s13105-022-00930-4

Estrada, J. A., and Contreras, I. (2019). Nutritional modulation of immune and central nervous system homeostasis: the role of diet in development of neuroinflammation and neurological disease. *Nutrients* 11 (5), 1076. doi:10.3390/nu11051076

Favero, G., Franceschetti, L., Bonomini, F., Rodella, L. F., and Rezzani, R. (2017). Melatonin as an anti-inflammatory agent modulating inflammasome activation. *Int. J. Endocrinol.* 2017, 1835195–1835213. doi:10.1155/2017/1835195

Fole, A., Miguéns, M., Morales, L., González-Martín, C., Ambrosio, E., and Del Olmo, N. (2017). Lewis and Fischer 344 rats as a model for genetic differences in spatial learning and memory: cocaine effects. *Prog. Neuro-Psychopharmacology Biol. Psychiatry* 76, 49–57. doi:10.1016/j.pnpbp.2017.02.024

Gáll, Z., Kelemen, K., Tolokán, A., Zolcseak, I., Sável, I., Bod, R., et al. (2022). Anticonvulsant action and long-term effects of chronic cannabidiol treatment in the rat pentylenetetrazole-kindling model of epilepsy. *Biomedicines* 10 (8), 1811. doi:10.3390/biomedicines10081811

Gao, Z., Luo, K., Hu, Y., Niu, Y., Zhu, X., Li, S., et al. (2024). Melatonin alleviates chronic stress-induced hippocampal microglia pyroptosis and subsequent depression-like behaviors by inhibiting Cathepsin B/NLRP3 signaling pathway in rats. *Transl. Psychiatry* 14 (1), 166. doi:10.1038/s41398-024-02887-y

Gáspár, A., Hutka, B., Ernyey, A. J., Tajti, B. T., Varga, B. T., Zádori, Z. S., et al. (2022). Performance of the intracerebroventricularly injected streptozotocin Alzheimer's disease model in a translationally relevant, aged and experienced rat population. *Sci. Rep.* 12 (1), 20247. doi:10.1038/s41598-022-24292-5

Grieb, P. (2016). Intracerebroventricular streptozotocin injections as a model of Alzheimer's disease: in search of a relevant mechanism. *Mol. Neurobiol.* 53 (3), 1741–1752. doi:10.1007/s12035-015-9132-3

Guardia de Souza e Silva, T., do Val de Paulo, M. E. F., da Silva, J. R. M., da Silva Alves, A., Britto, L. R. G., Xavier, G. F., et al. (2020). Oral treatment with royal jelly improves memory and presents neuroprotective effects on icv-STZ rat model of sporadic Alzheimer's disease. *Heliyon* 6 (2), e03281. doi:10.1016/j.heliyon.2020.e03281

Hardeland, R. (2021). Melatonin and microglia. *Int. J. Mol. Sci.* 22 (15), 8296. doi:10.3390/ijms22158296

Hardeland, R., Cardinali, D. P., Brown, G. M., and Pandi-Perumal, S. R. (2015). Melatonin and brain inflammaging. *Prog. Neurobiol.* 127–128, 46–63. doi:10.1016/j.pneurobio.2015.02.001

Hernandes-Alejandro, M., Montaño, S., Harrington, C. R., Wischik, C. M., Salas-Casas, A., Cortes-Reynosa, P., et al. (2020). Analysis of the relationship between metalloprotease-9 and tau protein in Alzheimer's disease. *J. Alzheimer's Dis.* 76 (2), 553–569. doi:10.3233/JAD-200146

Homolak, J., Perhoc, A. B., Knezovic, A., Osmanovic Barilar, J., and Salkovic-Petrisic, M. (2021). Additional methodological considerations regarding optimization of the dose of intracerebroventricular streptozotocin A response to: "Optimization of intracerebroventricular streptozotocin dose for the induction of neuroinflammation and memory impairments". *Metab. Brain Dis.* 36 (1), 97–102. doi:10.1007/s11011-020-00637-9

Humphrey, C. M., Hooker, J. W., Thapa, M., Wilcox, M. J., Ostrowski, D., and Ostrowski, T. D. (2023). Synaptic loss and gliosis in the nucleus tractus solitarii with streptozotocin-induced Alzheimer's disease. *Brain Res.* 1801, 148202. doi:10.1016/j.brainres.2022.148202

Ikram, M., Park, H. Y., Ali, T., and Kim, M. O. (2021). Melatonin as a potential regulator of oxidative stress, and neuroinflammation: mechanisms and implications for the management of brain injury-induced neurodegeneration. *J. Inflamm. Res.* 14, 6251–6264. doi:10.2147/JIR.S334423

Insel, P. S., Mohlenhoff, B. S., Neylan, T. C., Krystal, A. D., and Mackin, R. S. (2021). Association of sleep and β-amyloid pathology among older cognitively unimpaired adults. *JAMA Netw. Open* 4 (7), e2117573. doi:10.1001/jamanetworkopen.2021.17573

Iso-Markku, P., Kujala, U. M., Knittle, K., Polet, J., Vuoksimaa, E., and Waller, K. (2022). Physical activity as a protective factor for dementia and Alzheimer's disease: systematic review, meta-analysis and quality assessment of cohort and case–control studies. *Br. J. Sports Med.* 56 (12), 701–709. doi:10.1136/bjsports-2021-104981

Kamat, P. K., Kalani, A., Rai, S., Tota, S. K., Kumar, A., and Ahmad, A. S. (2016). Streptozotocin intracerebroventricular-induced neurotoxicity and brain insulin resistance: a therapeutic intervention for treatment of sporadic Alzheimer's disease (sAD)-Like pathology. *Mol. Neurobiol.* 53 (7), 4548–4562. doi:10.1007/s12035-015-9384-y

Kang, Y. J., Diep, Y. N., Tran, M., and Cho, H. (2020). Therapeutic targeting strategies for early-to late-staged Alzheimer's disease. *Int. J. Mol. Sci.* 21 (24), 9591. doi:10.3390/ijms21249591

Kaushik, M., Kaushik, P., and Parvez, S. (2022). Memory related molecular signatures: the pivots for memory consolidation and Alzheimer's related memory decline. *Ageing Res. Rev.* 76, 101577. doi:10.1016/j.arr.2022.101577

Kaylee, M. P., Seth, A., Von, R., Abigail, J. L., Amber, N. D., and Elizabeth, S. E. (2020). Influence of aerobic exercise on sleep and salivary melatonin in men. *Int. J. Sport Exerc Med.* 6 (2). doi:10.23937/2469-5718/1510161

Kim, Y. S., Lee, K. J., and Kim, H. (2017). Serum tumour necrosis factor-α and interleukin-6 levels in Alzheimer's disease and mild cognitive impairment. *Psychogeriatrics* 17 (4), 224–230. doi:10.1111/psyg.12218

Klyubin, I., Cullen, W. K., Hu, N.-W., and Rowan, M. J. (2012). Alzheimer's disease Aβ assemblies mediating rapid disruption of synaptic plasticity and memory. *Mol. Brain* 5 (1), 25. doi:10.1186/1756-6606-5-25

Knezovic, A., Osmanovic-Barilar, J., Curlin, M., Hof, P. R., Simic, G., Riederer, P., et al. (2015). Staging of cognitive deficits and neuropathological and ultrastructural changes in streptozotocin-induced rat model of Alzheimer's disease. *J. Neural Transm.* 122, 577–592. doi:10.1007/s00702-015-1394-4

Kraska, A., Santin, M. D., Dorieux, O., Joseph-Mathurin, N., Bourrin, E., Petit, F., et al. (2012). *In vivo* cross-sectional characterization of cerebral alterations induced by intracerebroventricular administration of streptozotocin. *PLoS One* 7 (9), e46196. doi:10.1371/journal.pone.0046196

Kvetnoy, I., Ivanov, D., Mironova, E., Evsyukova, I., Nasyrov, R., Kvetnaia, T., et al. (2022). Melatonin as the cornerstone of neuroimmunoendocrinology. *Int. J. Mol. Sci.* 23 (3), 1835. doi:10.3390/ijms23031835

Li, Y., Fan, H., Ni, M., Zhang, W., Fang, F., Sun, J., et al. (2022). Etanercept reduces neuron injury and neuroinflammation via inactivating c-Jun N-terminal kinase and nuclear factor-κB pathways in Alzheimer's disease: an *in vitro* and *in vivo* investigation. *Neuroscience* 484, 140–150. doi:10.1016/j.neuroscience.2021.11.001

Li, Y., Zhang, J., Wan, J., Liu, A., and Sun, J. (2020). Melatonin regulates Aβ production/clearance balance and Aβ neurotoxicity: a potential therapeutic molecule for Alzheimer's disease. *Biomed. Pharmacother.* 132, 110887. doi:10.1016/j.biopha.2020.110887

Liang, T., Zhang, Y., Wu, S., Chen, Q., and Wang, L. (2022). The role of NLRP3 inflammasome in Alzheimer's disease and potential therapeutic targets. *Front. Pharmacol.* 13, 845185. doi:10.3389/fphar.2022.845185

Livingston, G., Sommerlad, A., Orgeta, V., Costafreda, S. G., Huntley, J., Ames, D., et al. (2017). Dementia prevention, intervention, and care. *Lancet* 390 (10113), 2673–2734. doi:10.1016/S0140-6736(17)31363-6

Madhu, L. N., Kodali, M., Attaluri, S., Shuai, B., Melissari, L., Rao, X., et al. (2021). Melatonin improves brain function in a model of chronic Gulf War illness with modulation of oxidative stress, NLRP3 inflammasomes, and BDNF-ERK-CREB pathway in the hippocampus. *Redox Biol.* 43, 101973. doi:10.1016/j.redox.2021.101973

Mathiasen, J. R., and DiCamillo, A. (2010). Novel object recognition in the rat: a facile assay for cognitive function. *Curr. Protoc. Pharmacol.* 49 (1). doi:10.1002/0471141755.ph0559s49

Miao, J., Ma, H., Yang, Y., Liao, Y., Lin, C., Zheng, J., et al. (2023). Microglia in Alzheimer's disease: pathogenesis, mechanisms, and therapeutic potentials. *Front. Aging Neurosci.* 15, 1201982. doi:10.3389/fnagi.2023.1201982

Miranda-Riestra, A., Estrada-Reyes, R., Torres-Sanchez, E. D., Carreño-García, S., Ortiz, G. G., and Benítez-King, G. (2022). Melatonin: a neurotrophic factor? *Molecules* 27 (22), 7742. doi:10.3390/molecules27227742

Mishra, S. K., Singh, S., Shukla, S., and Shukla, R. (2018). Intracerebroventricular streptozotocin impairs adult neurogenesis and cognitive functions via regulating neuroinflammation and insulin signaling in adult rats. *Neurochem. Int.* 113, 56–68. doi:10.1016/j.neuint.2017.11.012

Muhammad, T., Ali, T., Ikram, M., Khan, A., Alam, S. I., and Kim, M. O. (2019). Melatonin rescue oxidative stress-mediated neuroinflammation/neurodegeneration and memory impairment in scopolamine-induced amnesia mice model. *J. Neuroimmune Pharmacol.* 14 (2), 278–294. doi:10.1007/s11481-018-9824-3

Munafò, A., Burgaletto, C., Di Benedetto, G., Di Mauro, M., Di Mauro, R., Bernardini, R., et al. (2020). Repositioning of immunomodulators: a ray of hope for Alzheimer's disease? *Front. Neurosci.* 14, 14. doi:10.3389/fnins.2020.614643

Nasiri, E., Alizadeh, A., Roushandeh, A. M., Gazor, R., Hashemi-Firouzi, N., and Golipoor, Z. (2019). Melatonin-pretreated adipose-derived mesenchymal stem cells efficeintly improved learning, memory, and cognition in an animal model of Alzheimer's disease. *Metab. Brain Dis.* 34 (4), 1131–1143. doi:10.1007/s11011-019-00421-4

Nous, A., Engelborghs, S., and Smolders, I. (2021). Melatonin levels in the Alzheimer's disease continuum: a systematic review. *Alzheimers Res. Ther.* 13 (1), 52. doi:10.1186/s13195-021-00788-6

Olton, D. S., and Samuelson, R. J. (1976). Remembrance of places passed: spatial memory in rats. *J. Exp. Psychol. Anim. Behav. Process* 2 (2), 97–116. doi:10.1037/0097-7403.2.2.97

Padurariu, M., Ciobica, A., Mavroudis, I., Fotiou, D., and Baloyannis, S. (2012). Hippocampal neuronal loss in the CA1 and CA3 areas of Alzheimer's disease patients. *Psychiatr. Danub* 24 (2), 152–158.

Pais, M., Martinez, L., Ribeiro, O., Loureiro, J., Fernandez, R., Valiengo, L., et al. (2020). Early diagnosis and treatment of Alzheimer's disease: new definitions and challenges. *Braz. J. Psychiatry* 42 (4), 431–441. doi:10.1590/1516-4446-2019-0735

Park, J., Lee, S.-Y., Shon, J., Kim, K., Lee, H. J., Kim, K. A., et al. (2019). Adalimumab improves cognitive impairment, exerts neuroprotective effects and attenuates neuroinflammation in an Aβ1-40-injected mouse model of Alzheimer's disease. *Cytotherapy* 21 (6), 671–682. doi:10.1016/j.jcyt.2019.04.054

Plantone, D., Pardini, M., Righi, D., Manco, C., Colombo, B. M., and De Stefano, N. (2023). The role of TNF-α in Alzheimer's disease: a narrative review. *Cells* 13 (1), 54. doi:10.3390/cells13010054

Rai, S., Kamat, P. K., Nath, C., and Shukla, R. (2014). Glial activation and post-synaptic neurotoxicity: The key events in Streptozotocin (ICV) induced memory impairment in rats. *Pharmacology Biochemistry and Behavior* 117, 104–117. doi:10.1016/j.pbb.2013.11.035

Ravelli, K. G., Rosário, B., dos, A., Camarini, R., Hernandes, M. S., and Britto, L. R. (2017). Intracerebroventricular streptozotocin as a model of Alzheimer's disease: neurochemical and behavioral characterization in mice. *Neurotox. Res.* 31 (3), 327–333. doi:10.1007/s12640-016-9684-7

Ringland, C., Schweig, J. E., Eisenbaum, M., Paris, D., Ait-Ghezala, G., Mullan, M., et al. (2021). MMP9 modulation improves specific neurobehavioral deficits in a mouse model of Alzheimer's disease. *BMC Neurosci.* 22 (1), 39. doi:10.1186/s12868-021-00643-2

Rosales-Corral, S. A., Acuña-Castroviejo, D., Coto-Montes, A., Boga, J. A., Manchester, L. C., Fuentes-Broto, L., et al. (2012). Alzheimer's disease: pathological mechanisms and the beneficial role of melatonin. *J. Pineal Res.* 52 (2), 167–202. doi:10.1111/j.1600-079X.2011.00937.x

Rudnitskaya, E. A., Maksimova, K. Y., Muraleva, N. A., Logvinov, S. V., Yanshole, L. V., Kolosova, N. G., et al. (2015). Beneficial effects of melatonin in a rat model of sporadic Alzheimer's disease. *Biogerontology* 16 (3), 303–316. doi:10.1007/s10522-014-9547-7

Small, S. A., Schobel, S. A., Buxton, R. B., Witter, M. P., and Barnes, C. A. (2011). A pathophysiological framework of hippocampal dysfunction in ageing and disease. *Nat. Rev. Neurosci.* 12 (10), 585–601. doi:10.1038/nrn3085

Song, J.-Z., Cui, S.-Y., Cui, X.-Y., Hu, X., Ma, Y.-N., Ding, H., et al. (2018). Dysfunction of GABAergic neurons in the parafacial zone mediates sleep disturbances in a streptozotocin-induced rat model of sporadic Alzheimer's disease. *Metab. Brain Dis.* 33 (1), 127–137. doi:10.1007/s11011-017-0125-y

Souza, L. C., Jesse, C. R., de Gomes, M. G., Viana, C. E., Mattos, E., Silva, N. C., et al. (2017). Intracerebroventricular administration of streptozotocin as an experimental approach to depression: evidence for the involvement of proinflammatory cytokines and indoleamine-2,3-dioxygenase. *Neurotox. Res.* 31 (4), 464–477. doi:10.1007/s12640-016-9691-8

Tozihi, M., Shademan, B., Yousefi, H., Avci, C. B., Nourazarian, A., and Dehghan, G. (2023). Melatonin: a promising neuroprotective agent for cerebral ischemia-reperfusion injury. *Front. Aging Neurosci.* 15, 1227513. doi:10.3389/fnagi.2023.1227513

Wang, X. (2009). The antiapoptotic activity of melatonin in neurodegenerative diseases. *CNS Neurosci. Ther.* 15 (4), 345–357. doi:10.1111/j.1755-5949.2009.00105.x

Zhao, J., O'Connor, T., and Vassar, R. (2011). The contribution of activated astrocytes to Aβ production: implications for Alzheimer's disease pathogenesis. *J. Neuroinflammation* 8 (1), 150. doi:10.1186/1742-2094-8-150

Zhou, Q., Lin, L., Li, H., Wang, H., Jiang, S., Huang, P., et al. (2021). Melatonin reduces neuroinflammation and improves axonal hypomyelination by modulating M1/M2 microglia polarization via JAK2-STAT3-telomerase pathway in postnatal rats exposed to lipopolysaccharide. *Mol. Neurobiol.* 58 (12), 6552–6576. doi:10.1007/s12035-021-02568-7

frontiers | Frontiers in Pharmacology

TYPE Systematic Review
PUBLISHED 31 July 2024
DOI 10.3389/fphar.2024.1434512

Check for updates

OPEN ACCESS

EDITED BY
Pukar Khanal,
Emory University, United States

REVIEWED BY
Sharad Chand,
MIT World Peace University, India
Geetanjali Salimath,
KLE College of Pharmacy, India
Uday Venkat Mateti,
Nitte (Deemed to be University), India
Raushan Kumar Chaudhary,
Nitte Gulabi Shetty Memorial Institute of Pharmaceutical Sciences, India

*CORRESPONDENCE
Mostafa M. Bahaa,
mostafabahaamnf@gmail.com
mbahaa@horus.edu.eg

RECEIVED 17 May 2024
ACCEPTED 10 July 2024
PUBLISHED 31 July 2024

CITATION
Badawoud AM, Ali LS, Abdallah MS, El Sabaa RM, Bahaa MM, Elmasry TA, Wahsh E, Yasser M, Eltantawy N, Eldesoqui M and Hamouda MA (2024), The relation between Parkinson's disease and non-steroidal anti-inflammatories; a systematic review and meta-analysis. *Front. Pharmacol.* 15:1434512. doi: 10.3389/fphar.2024.1434512

COPYRIGHT
© 2024 Badawoud, Ali, Abdallah, El Sabaa, Bahaa, Elmasry, Wahsh, Yasser, Eltantawy, Eldesoqui and Hamouda. This is an open-access article distributed under the terms of the Creative Commons Attribution License (CC BY). The use, distribution or reproduction in other forums is permitted, provided the original author(s) and the copyright owner(s) are credited and that the original publication in this journal is cited, in accordance with accepted academic practice. No use, distribution or reproduction is permitted which does not comply with these terms.

The relation between Parkinson's disease and non-steroidal anti-inflammatories; a systematic review and meta-analysis

Amal Mohammad Badawoud[1], Lashin Saad Ali[2,3], Mahmoud S. Abdallah[4,5], Ramy M. El Sabaa[6], Mostafa M. Bahaa[7]*, Thanaa A. Elmasry[8], Eman Wahsh[9], Mohamed Yasser[10,11], Nashwa Eltantawy[12], Mamdouh Eldesoqui[13,14] and Manal A. Hamouda[6]

[1]Department of Pharmacy Practice, College of Pharmacy, Princess Nourah Bint Abdulrahman University, Riyadh, Saudi Arabia, [2]Department of Basic Medical Science, Faculty of Dentistry, Al-Ahliyya Amman University, Amman, Jordan, [3]Physiology Department, Faculty of Medicine, Mansoura University, Mansoura, Egypt, [4]Department of Clinical Pharmacy, Faculty of Pharmacy, University of Sadat City (USC), Sadat City, Egypt, [5]Department of PharmD, Faculty of Pharmacy, Jadara University, Irbid, Jordan, [6]Clinical Pharmacy Department, Faculty of Pharmacy, Menuofia University, Shibin Al Kawm, Egypt, [7]Pharmacy Practice Department, Faculty of Pharmacy, Horus University, New Damietta, Egypt, [8]Pharmacology and Toxicology Department, Faculty of Pharmacy, Tanta University, Tanta, Egypt, [9]Pharmacology and Toxicology Department, Faculty of Pharmacy, Sinai University, Arish, Egypt, [10]Department of Pharmaceutics, Faculty of Pharmacy, Port Said University, Port Said, Egypt, [11]Department of Pharmaceutics and Industrial Pharmacy, Faculty of Pharmacy, Horus University, New Damietta, Egypt, [12]Pharmacy Practice Department, Faculty of Pharmacy, Heliopolis University, Cairo, Egypt, [13]Department of Basic Medical Sciences, College of Medicine, AlMaarefa University, Riyadh, Saudi Arabia, [14]Department of Anatomy and Embryology, Faculty of Medicine, Mansoura University, Mansoura, Egypt

Background: Parkinson's disease (PD) is a neurological condition that typically shows up with aging. It is characterized by generalized slowness of movement, resting tremor or stiffness, and bradykinesia. PD patients' brains mostly exhibit an increase in inflammatory mediators and microglial response. Nevertheless, a variety of non-steroidal anti-inflammatory medications (NSAIDS) offered neuroprotection in animal models and preclinical trials.

Aim: The current systematic review and meta-analysis were designed to try to resolve the debate over the association of NSAID use with the development of PD because the results of several studies were somehow contradictory.

Methods: An intense search was performed on Scopus, PubMed, and Web of Science databases for articles relating the incidence of PD to the use of NSAIDs. Statistical analysis of the included studies was carried out using Review Manager version 5.4.1 by random effect model. The outcome was identified as the development of PD in patients who were on NSAIDs, ibuprofen only, aspirin only, and non-aspirin NSAIDs. This was analyzed using pooled analysis of odds ratio (OR) at a significance level of ≤0.05 and a confidence level of 95%. A statistically significant decreased risk of PD was observed in patients taking NSAIDs, Ibuprofen, and non-aspirin NSAIDs.

Results: The ORs of PD occurrence in patients who took NSAIDs, Ibuprofen, and non-aspirin NSAIDs were 0.88 [95% CI (0.8–0.97), p = 0.01], 0.73 [95% CI (0.53–1), p = 0.05] and 0.85 [95% CI (0.75–0.97), p = 0.01]. Meanwhile, the risk of PD in patients who took aspirin was not statistically significant.

Conclusion: In conclusion, Ibuprofen, non-aspirin NSAIDs, and other types of NSAIDs could be associated with a reduction in PD risk. However, there was no association between aspirin intake and the development of PD.

KEYWORDS

NSAIDs (non-steroidal anti-inflammatory drugs), Parkinson's disease, aspirin, ibuprofen, neuroprotecion

1 Introduction

Parkinson's disease (PD) is a neurological condition that typically shows up with aging or longevity. In addition to generalized slowness of movement (bradykinesia), there are at least two other symptoms of resting tremor or stiffness. Other signs include loss of smell, difficulty sleeping, mood swings, excessive salivation, constipation, and irregular, frequent limb movements during sleep (REM behavior disorder). The prevalence of PD among those aged 60 years and older is 1%. The disease is associated with the presence of Lewy bodies and the degeneration of dopaminergic neurons in the substantia nigra. Most of these diseases are idiopathic. Only 10% of cases especially in children have a genetic component (Alexoudi et al., 2018; Kabra et al., 2018; Mirpour et al., 2018; Zafar and Yaddanapudi, 2022).

Inflammation may play a role in the development of PD, as was earlier mentioned, according to a considerable body of evidence from both human samples and animal models. However, the precise cause of this reaction is still unknown. It's possible that continuing neuronal cell death in PD leads to inflammation, but it's also possible that misfolded—synuclein (Syn) has a direct impact. Peripheral inflammation and genes linked to PD risk suggest a crucial role in the chronic inflammatory response at the onset of this neurodegenerative condition, in addition to the well-known microgliosis and astrogliosis in PD brains (Pajares et al., 2020).

Nonsteroidal anti-inflammatory medicines (NSAIDs) are commonly used to alleviate pain, reduce swelling, relieve stiffness, and treat inflammation in the limbs (Driver et al., 2011). These drugs have extensive clinical usage. Besides their anti-inflammatory properties, NSAIDs have also garnered interest for their potential in preventing and treating Parkinson's disease (Bornebroek et al., 2007). The usage of NSAIDs is associated with Parkinson's disease and can be explained from a biological perspective. Neuroinflammation has been found to be associated with the development of Parkinson's disease, and NSAIDs have been shown to offer neuroprotection in animal models (Herna et al., 2006). In animal models, a variety of NSAIDS offer neuroprotection, while PD patients' brains exhibit an increase in inflammatory mediators and microglial response. The relationship between NSAID use and the risk of PD has gotten very little attention in observational research, despite a plethora of epidemiological evidence supporting their protective benefits in the development of Alzheimer's disease. A reduction in the risk of PD has been linked by the majority of these studies to the use of non-aspirin NSAIDs. However, studies on animal models have demonstrated that mice can be protected from MPTP-induced striatal dopamine depletion by taking acetylsalicylic acid (aspirin) (Herna et al., 2006; Ton et al., 2006; Bornebroek et al., 2007; Driver et al., 2011; Manthripragada et al., 2011).

Contradictory findings were observed regarding the association between NSAIDs and PD disease development. For example, Gagne and Power (2010) showed that there was an association between the use of non-aspirin NSAIDs and the reduction of PD risk. This study also showed that there was no association between aspirin use and PD development. On the other hand, a study was conducted by Samii et al. (2009) on 11 observational studies and showed no effect of NSAIDs on developing PD. Due to the conflicting literature and the gap of knowledge, this systematic review/meta-analysis was designed to try to resolve the debate over the association of NSAID use with the development of PD as the results of several studies were somehow contradictory.

2 Materials and methods

2.1 Search strategy

Scopus, PubMed, and Web of Science databases were employed to search for articles relating to the risk of PD to the use of NSAIDs from inception till February 2024. The search strategy was by title, abstract, and keywords as follows: (non-steroidal anti-inflammatory OR NSAIDS OR Aspirin OR Ibuprofen OR Naproxen OR Diclofenac AND Parkinson*)

2.2 Eligibility criteria and screening

All studies describing the risk between NSAIDS and PD were included. Randomized controlled trials, case-control, and cohort studies were included in this study. We identified the PICO of the study. We included a population of any age and any follow-up time taking any NSAID as an intervention. We didn't put a restriction on the duration of aspirin intake, types of NSAIDs, or language of the study. The comparison group was the group who didn't take any NSAID, and the outcome was the incidence of PD. We excluded case reports, case series, narrative or systematic reviews, and meta-analyses. In addition, we excluded conference abstracts and unpublished manuscripts to prevent the bias of results. We also excluded studies describing the risk of neurodegenerative disease other than PD or describing the risk of PD in drugs other than NSAIDs because they didn't fit into the outcome of interest. Screening was done by 2 authors independently and any difference between them was referred to a third author. Title and abstract screening were done first, and eligible articles were screened by full text thereafter.

TABLE 1 Newcastle-Ottawa scale for quality assessment of case-control studies.

Study ID	Is the case definition adequate?	Representativeness of the cases	Selection of the controls	Definition of controls	Comparability of cases and controls	Ascertainment of exposure	Same method of ascertainment for cases and controls	Nonresponse rate
Wahner 2007 (Wahner et al., 2007)	★	★	★	—	★★	★	—	★
Starhof 2019 (Starhof et al., 2020)	★	★	★	—	★★	—	—	—
Powers 2008 (Powers et al., 2008)	★	★	★	★	★	—	—	—
Manthripragada 2011 (Manthripragada et al., 2011)	★	★	★	★	★★	—	—	★
Hernan 2006 (Herna et al., 2006)	★	★	★	★	★★	★	—	—
Etminan and Suissa 2006 (Etminan and Suissa, 2008)	★	★	★	—	★	★	—	—
Driver 2010 (Driver et al., 2011)	★	★	★	—	★★	—	—	—
Ton 2006 (Ton et al., 2006)	★	★	★	—	—	★	★	★
Sung 2016 (Sung et al., 2016)	★	★	★	★	★	★	★	★
Hancock 2007 (Hancock et al., 2007)	★	★	★	★	★★	—	—	★
Becker 2011 (Becker et al., 2011)	★	★	★	★	★	—	—	—

10.3389/fphar.2024.1434512

10.3389/fphar.2024.1434512

TABLE 2 New-Castle Ottawa scale for cohort studies.

Study ID	Representative-ness of the exposed cohort	Selection of the non-exposed cohort	Ascertainment of exposure	Demonstration that outcome of interest was not present at start of study	Comparability	Assessment of outcome	Was follow-up long enough for outcomes to occur	Adequ-acy of follow up
Etminan 2008 (Etminan et al., 2008)	★	–	★	–	★★	★	★	★
Chen 2003 (Chen et al., 2003)	★	★	★	★	–	★	★	★
Chen 2005 (Chen et al., 2005)	★	★	★	–	★	★	–	–

2.3 Data extraction

Two authors carried out data extraction independently using Excel sheets and any difference was resolved by a third author. We extracted main baseline data as study design, sample size, age and gender of cases and controls, duration of NSAID use, duration of PD, type of NSAID, and effect sizes whether odds ratio or risk ratio.

2.4 Quality assessment

Quality assessment of the included studies was done independently by 2 authors as well with a third author to revise it. We carried out the process using the Newcastle-Ottawa Scale for case-control, and cohort studies. It is a tool made of 8 questions as presented in Tables 1, 2, each of them can take a star except one question of comparability that can take 2 stars, so the maximum score is 9. A score of 0–3 means low quality, 4–6 means moderate quality and 7–9 means high quality.

2.5 Statistical analysis

We carried out statistical analysis of the included studies using Review Manager version 5.4.1 by random effect model. The outcome was the PD onset in patients taking NSAIDs, ibuprofen only, aspirin only, and non-aspirin NSAIDs. This was analyzed using pooled analysis of odds ratio at a significance level of 0.05 and confidence level of 95%. We assessed the heterogeneity using the I^2 value and Q statistics with the *p*-value assessing the significance of present heterogeneity at 0.05.

2.6 Publication bias assessment

The publication bias assessment was checked for pooled studies according to Egger et al. (1997) Funnel plots were constructed to present the relationship between effect size and standard error.

3 Results

3.1 Database searching and screening

Our search methodology resulted in 287 articles from the searched databases. After the removal of duplicates, 197 articles entered the screening process. By title and abstract screening, 23 articles were eligible for full-text screening which resulted in 14 articles entering our systematic review and meta-analysis (Figure 1).

3.2 Quality assessment

Of the 14 included studies, 11 were case-control, and 3 were cohort studies. Five case controls were of high quality and 6 were of moderate quality. Regarding cohort studies, 2 studies were of high quality and 1 was of moderate quality. This is shown in Tables 1, 2.

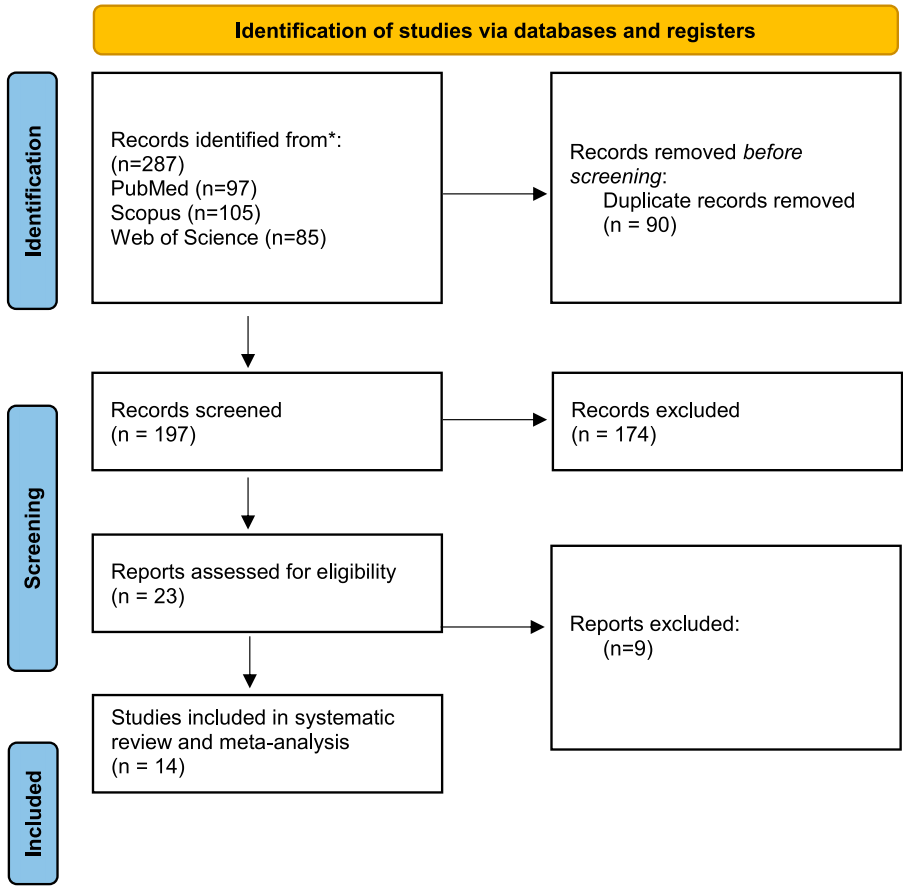


FIGURE 1
PRISMA flow diagram of database searching and screening.

3.3 Baseline characteristics

Baseline data related to the included studies are summarized in the Table 3. We reported the adjustment done when calculating the odds ratio of PD occurrence and the lag time between NSAID and PD occurrence. We also reported the frequency of NSAID intake if mentioned.

3.4 Statistical analysis

Statistical tests were classified into 4 categories: NSAIDs, ibuprofen, Aspirin, and Non-aspirin NSAIDs. We calculated the odds ratio of PD occurrence in each case using the random effect model. Regarding NSAID use, the odds ratio of PD occurrence in patients who took NSAIDs was 0.89 (95% CI: 0.82–0.97, $p = 0.005$) (Figure 2). This shows a statistically significant decreased risk of PD in patients taking NSAIDs.

Regarding the use of ibuprofen, it is shown in Figure 3 that there was no statistically significant association between ibuprofen intake and risk of PD [OR 0.9, 95% CI (0.7–1.17), $p = 0.44$] with heterogeneity measured by $I^2 = 45\%$, $p = 0.16$.

Non-aspirin NSAIDs were associated with a lower risk of PD. [OR 0.83, 95% CI (0.72–0.94), $p = 0.005$] Heterogeneity was of $I^2 = 58\%$, $p = 0.01$ (Figure 4). Sensitivity analysis by leave one out method was done and heterogeneity became insignificant ($I^2 = 47\%$, $p = 0.07$) after removing Becker et al. (2011). Odds ratio became 0.77, 95% CI [0.66–0.91], $p = 0.001$ (Figure 5).

The association between aspirin and PD risk was null as shown in the Figure 6.

3.5 Risk of publication bias assessment using Egger's test and funnel plots

Regarding the risk of publication bias assessed by Egger's test and funnel plots, it is seen to be low in NSAIDs and aspirin while it is moderate in non-aspirin NSAIDs and ibuprofen. A low risk of bias in NSAIDs and aspirin is associated with low heterogeneity in both, while a moderate risk of bias in non-aspirin NSAIDs is associated with moderate heterogeneity, however, the funnel plot isn't extremely accurate in the ibuprofen analysis due to a low number of included studies (Figures 7–10).

4 Discussion

Several studies including observational or systematic reviews and meta-analyses addressed the association between NSAIDs

TABLE 3 Baseline Characteristics of the included studies.

Study ID	Design	Sample Size, N		Age, mean (SD)		Gender (M/F)		Lag time, years	NSAID duration	Adjustment	Type of NSAID	Follow up
		Cases	Controls	Cases	Controls	Cases	Controls					
Wahner 2007 (Wahner et al., 2007)	Case-control	293	286	70.0 (10.7)	69.0 (12.9)	157/136	146/140	5	Regularly	Age at diagnosis, sex, race, geographical location, smoking, education	Aspirin, non-aspirin NSAIDs	—
Starhof 2019 (Starhof et al., 2020)	Case-control	155	7750	63.8 (9.3)	63.8 (9.3)	77/78	3850/3900	5	>2 prescriptions	Age, sex, place of residency, and COPD status	Non-aspirin NSAIDs	—
Powers 2008 (Powers et al., 2008)	Case-control	1,186	928	69.6 (30–97)	67.7 (25–94)	790/396	374/554	—	Ever	Age, race, sex and geographical location	NSAIDS	—
Manthripragada 2011 (Manthripragada et al., 2011)	Case control	1,931	9,651	72.2 (10.5)	72.2 (10.5)	1,121/810	5603/4048	5	Ever	Age, sex, comorbidities, COPD	Aspirin, non-aspirin NSAIDs	—
Hernan 2006 (Herna et al., 2006)	Case-control	1,258	6,638	70.7	68.7	765/493	3923/2715	—	Ever	Age, sex, treatment start date, clinic, smoking status, MI, arthritis	Aspirin, Non aspirin NSAIDs	—
Etminan and Suissa 2006 (Etminan and Suissa, 2008)	Case-control	1,259	12,590	73.9 (10.3)	73.9 (10.3)	692/567	5665/6925	1	Ever	Age, sex, antipsychotics, anti-RA medications	NSAIDs	—
Etminan 2008 (Etminan et al., 2008)	Cohort	5,010	692,068	—	—	—	—	—	Ever	age, sex, comorbidity (and use of antipsychotic medications	NSAIDs	6 years
Driver 2010 (Driver et al., 2011)	Case-control	565	2458	58.57 (40.1–85.0)	58.55 (40.0–85.0)	—	—	5	ever	Smoking, alcohol, BMI, exercise to sweat	Aspirin, Non aspirin NSAIDs	—
Chen 2003 (Chen et al., 2003)	Cohort	142,902		—	—	—	—	2	Ever	Age, smoking, caffeine and alcohol intake	Aspirin, Non aspirin NSAIDs	18 years
Ton 2006 (Ton et al., 2006)	Case-control	206	383	69.2 (9.0)	69.4 (8.6)	121/105	239/144	5	Ever	Age, sex, smoking, duration of enrolment, clinic	Aspirin, non aspirin NSAIDs, Ibuprofen	—
Sung 2016 (Sung et al., 2016)	Case-control	—	—	—	—	—	—	—	Ever	sex, age, and comorbidities, and NSAID use	NSAIDs	—
Chen 2005 (Chen et al., 2005)	Cohort	—	—	—	—	—	—	—	≥1/day	Age, sex, smoking, vitamin use, coffee, arthritis, other analgesics	Aspirin., ibuprofen, other NSAIDs	9 years
Hancock 2007 (Hancock et al., 2007)	Case-control	356	317	66.1 (10.7)	58.1(11.6)	235/121	139/178	—	Ever	Age at examination, sex	NSAIDs	—
Becker 2011 (Becker et al., 2011)	Case-control	4,026	15,969	60–80	60–80	2364/1662	9362/6607	—	Ever	BMI, smoking and comorbidities	Aspirin, Non aspirin NSAIDs, Ibuprofen, other NSAIDs	—

10.3389/fphar.2024.1434512

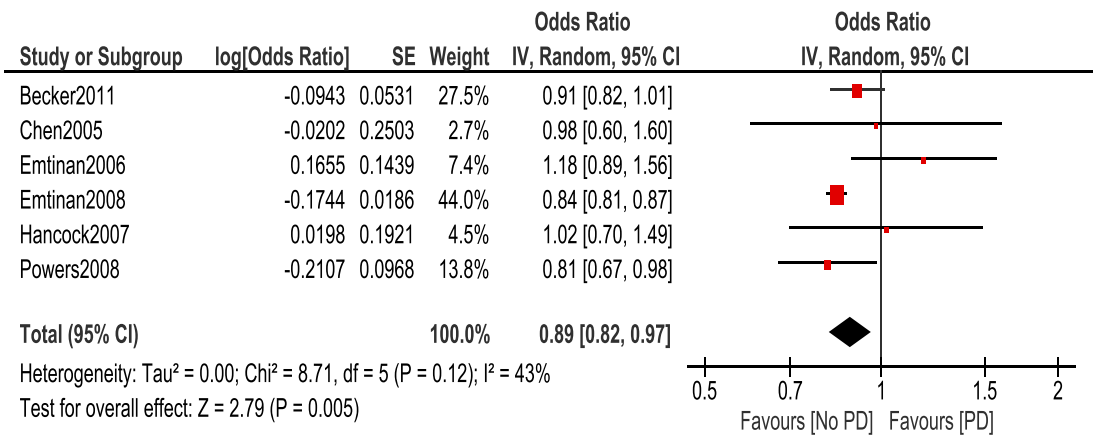


FIGURE 2
Forest plot of PD risk in patients who took NSAIDs.

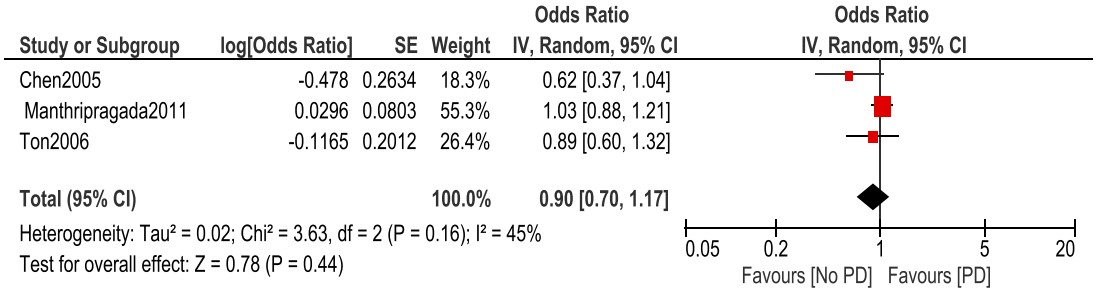


FIGURE 3
Forest plot of PD risk in patients who took Ibuprofen.

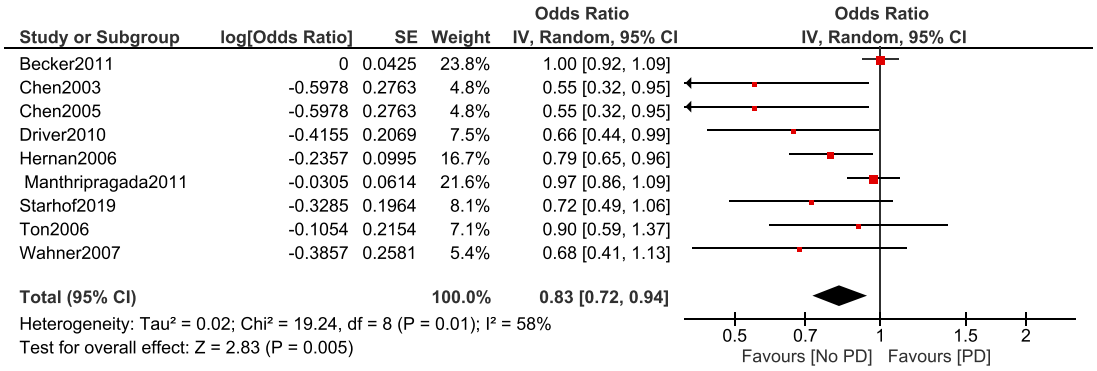


FIGURE 4
Forest plot of PD risk in patients who took Non-aspirin NSAIDs.

and the development of PD. Our study is considered among the most comprehensive since we targeted all available recent evidence and because of the categories we made. Our study included 17 studies which will be published until January 2024.

Our findings showed that there is a statistically significant reduction of PD risk in patients taking non-aspirin NSAIDs, and NSAIDS other than aspirin and ibuprofen. However, there was no statistically significant association between aspirin, and ibuprofen and the development of PD. Our findings are consistent with a meta-analysis conducted by Gagne and Power (2010) which showed the association between the use of non-aspirin NSAIDs and the reduction

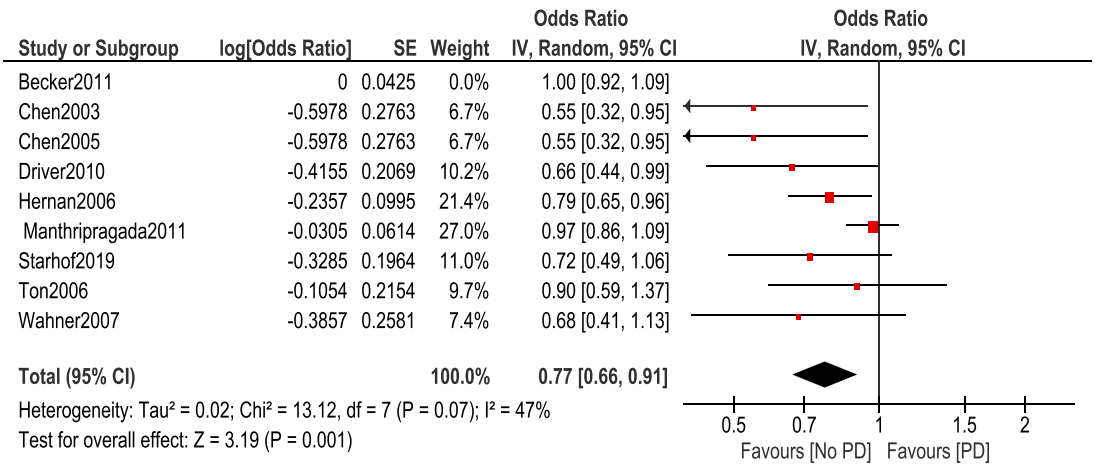


FIGURE 5
Leave one out, a meta-analysis of PD risk in Non-aspirin NSAIDs use.

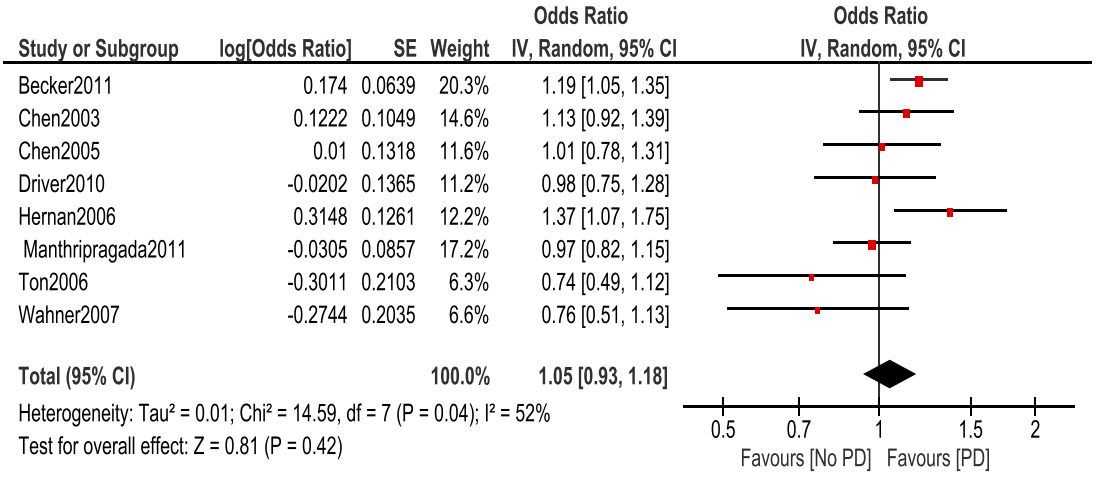


FIGURE 6
Forest plot of PD risk in patients who took Aspirin.

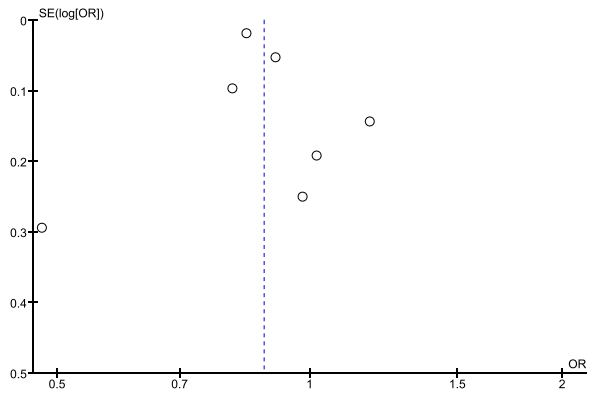


FIGURE 7
Funnel plot for risk of bias in NSAID users.

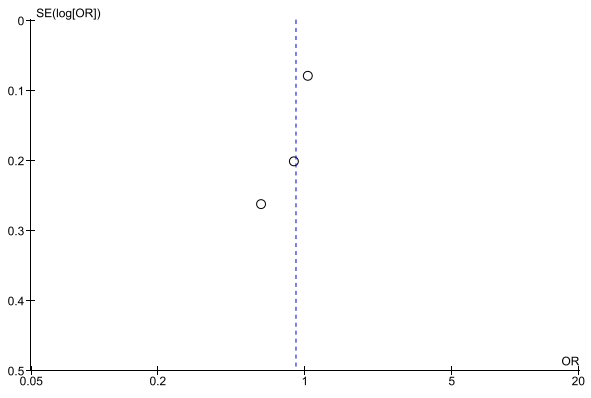


FIGURE 8
Funnel plot for risk of bias in ibuprofen users.

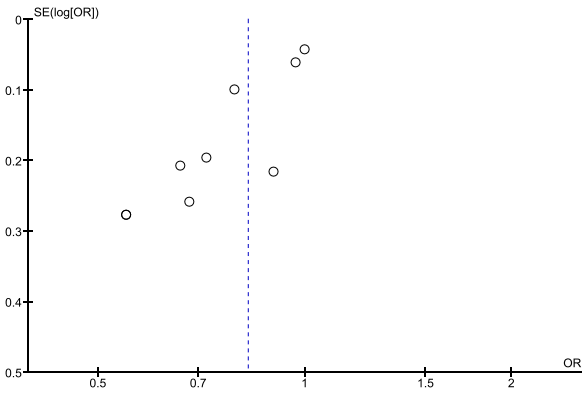


FIGURE 9
Funnel plot for risk of bias in non-aspirin-NSAIDs users.

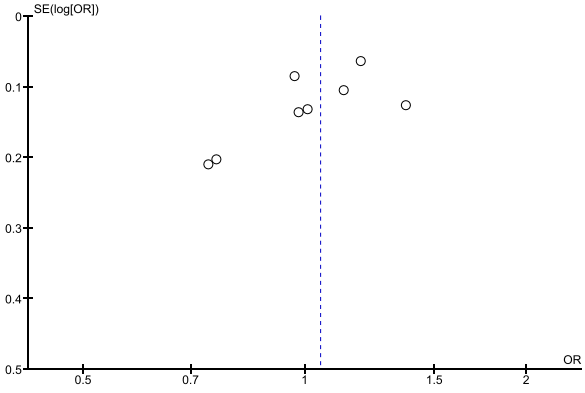


FIGURE 10
Funnel plot for risk of bias in aspirin users.

of PD risk. This study also showed that there is no association between aspirin use and PD development as shown by our findings. This study was conducted on 6 observational studies, so our study included more studies and in contrast to our analysis method by odds ratio, it was conducted using risk ratio. A similar inclusion of studies that observed the occurrence of PD some years after NSAID use was applied in this study as our inclusion criteria. This was done since it is improbable that exposures discovered within a year of PD diagnosis have an impact on disease incidence because PD initiation likely occurs long before the onset of symptoms (Rathore et al., 2009).

Another study done by Samii et al. (2009) on 11 observational studies showed that no effect of NSAIDs on developing PD which is inconsistent with our studies. It was also shown by 4 studies that risk reduction of PD had been observed in 4 studies in men compared to women, however, this is not enough to produce an evident protective role of NSAIDs from PD. This study also showed that ibuprofen is associated with a reduction of PD risk with a pooled risk ratio of 0.76 (95% CI 0.65, 0.89) through data from 3 studies. This study also showed that there was no statistically significant association between aspirin use and the development of PD through pooled analysis of six studies with a risk ratio of 1.08 (95% CI 0.93, 1.26) (Samii et al., 2009). This shows similar findings to our study as we found no statistically significant association between aspirin use and the development of PD. [OR 1.05. 95% CI (0.93–1.18)], $p = 0.42$.

Another systematic review by Alharbi et al. (2020) was conducted using 5 observational studies. It compared PD risk in aspirin users and non-users in addition to a comparison between PD risk in NSAID users and non-users. Findings regarding aspirin were different from our findings and those of other mentioned studies. A statistically significant rise in PD prevalence was observed among aspirin users compared to aspirin non-users with OR = 5.98 (95% CI = 1.743–20.547), $p = 0.004$. This is inconsistent with our study which showed no association between aspirin use and risk of PD. This study used the same effect estimate used by us (odds ratio), however the difference in results can be attributed to a greater number of studies involved in our systematic review and meta-analysis as we used a total of 10 studies to determine the relation between aspirin and PD while Alharbi et al. (2020) used only 5 studies so we provide more comprehensive and more up to date evidence. Alharbi et al. (2020) observed no statistically significant association between NSAID use and the development of PD using 5 studies as well with OR = 1.18 (95% CI = 0.580–2.436), $p > 0.05$ (Alharbi et al., 2020). This is inconsistent with our findings as we observed a statistically significant association between the use of NSAIDs and non-aspirin NSAIDs and the development of PD with an odds ratio of 0.89 (95 CI: 0.82–0.97, $p = 0.005$) and OR 0.83, 95% CI [0.72–0.94], $p = 0.005$ respectively.

The previous three meta-analyses had various limitations that should be addressed, and this supports the need for a further meta-analysis. Gagne and Power (2010) and Samii et al. (2009) were published in 2010 and 2009, respectively so they included a limited number of studies. Due to the recently published articles, a new meta-analysis should be done to include further findings.

Alharbi et al. (2020) showed an increased risk of PD in people taking aspirin however, many limitations exist in this meta-analysis such as incorrect OR estimates in addition to missing the inclusion of many studies investigating the risk of PD in people taking aspirin such as Chen et al. (2005), Driver et al. (2011), Wahner et al. (2007), Manthripragada et al. (2011), and Ton et al. (2006).

A study done by Poly et al. (2019) on 17 observational studies found that no statistically significant association exists between the use of NSAIDs and the development of PD with a risk ratio of 0.95 (95% CI 0.860–1.048), $p = 0.304$. This is inconsistent with our findings, and this can be attributed to various reasons. Firstly, in our analysis, we included studies that used adjusted effect estimates to lessen the risk of confounding bias associated with various factors in the primary studies such as age, gender, other comorbidities, disease duration, duration of NSAID use, etc. Secondly, in the part of NSAIDs analysis, we included studies that mentioned NSAIDs as a whole without the

inclusion of studies investigating aspirin alone, ibuprofen alone, or non-aspirin NSAIDs alone. Thirdly, there is a major limitation in Poly et al. (2019)'s analysis as they included the hazard ratio and odds ratio in the same meta-analysis to produce risk ratio which is not appropriate statistically and could produce inaccurate results. Moreover, this study is entitled with elderly population, however, it included patients older than 18 years of age which is another major limitation. Furthermore, there exist other factors that may cause differences in results such as the difference in the used effect estimate as they used risk ratio not odds ratio. In addition to this, the risk ratio is less than 1 and the upper interval approaches 1 (Poly et al., 2019).

This study also showed that aspirin use is slightly associated with an increased risk of PD with RR 1.10, 95% CI 1.004–1.218, $p = 0.04$ which is inconsistent with our findings (no association) but consistent with the findings of Alharbi et al. (2020); Poly et al. (2019). Different from Poly et al. (2019), our study included a subgroup of non-aspirin NSAIDs which was observed to be associated with a decreased risk of PD exposure. Moreover, we included aspirin as a subgroup and the association was null. However, Poly et al. (2019) found an increased risk. Although the two studies included ten studies, we did n't include Bower et al. (2006) as we excluded conference abstracts to include the high-quality peer-reviewed papers which increases the quality of the meta-analysis as well as that the full-text of the abstract wasn't accessible. Moreover, there exist other factors that lead to differences in findings between us and Poly et al. (2019) as mentioned earlier.

Our results come in agreement with *in vitro* and *in vivo* studies. Several animal studies reported the efficacy of NSAIDs' ability to reduce the risk of PD (Sánchez-pernaute et al., 2004; Wang et al., 2005; Parepally et al., 2006). The mechanism of NSAIDs regarding PD risk is not obvious till now. NSAIDs are frequently employed as the initial therapy option for inflammatory conditions and pain management. Recent research has demonstrated that the pharmacological benefits of NSAIDs are attributed to the inhibition of COX, and these medications have positive impacts in managing several neurological conditions (Sánchez-pernaute et al., 2004). Indomethacin removes nitric oxide free radicals, fenamate NSAIDs enhance GABA-A receptor function, and acetylsalicylic acid prevents the movement of NF-kB. Microglia, being a significant producer of prostaglandins (PGs), are thus seen as a suitable focus for neurological processes in the central nervous system (Terzi et al., 2018). The activation of PGE2 takes place during inflammation. Inflammatory activation by tumor necrosis factor (TNF)-α and interleukin (IL)-1β induces the production of COX-2 and membrane-associated PGES-1. Furthermore, cytosolic PGES is consistently linked with COX-1 (Terzi et al., 2018). COX-2 is the main factor responsible for the synthesis of PG in both acute and chronic inflammation. Selective COX-2 inhibitors are frequently employed to inhibit the production of PGE2 in microglial cells. Furthermore, COX-2 is stimulated in excitatory forebrain neurons within the brain. However, it is primarily increased in microglial cells both in laboratory settings (*in vitro*) and in living organisms (*in vivo*), and it is also influenced by the expression of mPGES-1 by microglia. Peroxisome proliferator-activated receptor-gamma (PPAR-γ) belongs to a set of nuclear receptors that can be activated by synthetic agonists, including NSAIDs such as indomethacin, ibuprofen, and diclofenac (Parepally et al., 2006). PPAR-γ synthetic agonists regulate brain inflammation and the viability of other neural cells. Additionally, they are involved in many pathways related to microglia, peripheral macrophages, and lymphocytes. Research indicates that NSAIDs have neuroprotective properties via inhibiting microglia in brain illnesses through a PPAR-γ-dependent mechanism (Terzi et al., 2018).

Our study provides comprehensive evidence with a large number of participants from different observational studies. Adjustment to different factors such as age, gender, smoking, and comorbidities was done so confounding is controlled with a large percentage. We defined NSAIDs into different categories including aspirin, ibuprofen, and non-aspirin NSAIDs.

Some limitations include the use of observational studies and the absence of experimental ones due to limited available data. Some studies reported a lag time of 5 years and some of less years between PD and NSAID use so this can result in bias. Moreover, PD can develop through a variety of mechanisms. But the focus of this study is solely on the inflammation-related mechanism.

We recommend future experimental studies defining the period between drug intake, its dose, and its type. Population should also be defined to explain the main risk.

5 Conclusion

Ibuprofen, non-aspirin NSAIDs, and other types of NSAIDs are associated with a reduction in PD risk, however, there was no association between aspirin intake and the development of PD.

Data availability statement

The raw data supporting the conclusions of this article will be made available by the authors, without undue reservation.

Author contributions

AB: Funding acquisition, Software, Validation, Writing–original draft, Writing–review and editing. LS: Data curation, Funding acquisition, Methodology, Writing–review and editing. MA: Data curation, Formal Analysis, Funding acquisition, Investigation, Methodology, Validation, Writing–original draft, Writing–review and editing. RE: Conceptualization, Writing–original draft. MB: Project administration, Writing–original draft, Writing–review and editing. TE: Methodology, Project administration, Writing–original draft, Writing–review and editing. EW: Investigation, Software, Writing–original draft, Writing–review and editing. MY: Data curation, Resources, Validation, Writing–original draft, Writing–review and editing. NE: Conceptualization, Formal Analysis, Software, Writing–original draft, Writing–review and editing. ME: Formal analysis, Funding acquisition, Supervision, Software, Writing–review and editing. MH: Conceptualization, Formal Analysis, Investigation, Writing–original draft, Writing–review and editing.

Funding

The author(s) declare that financial support was received for the research, authorship, and/or publication of this article. Thanks to AlMaarefa University, Researchers Supporting Project number (MHIRSP2024009), Almaarefa University, Riyadh, Saudi Arabia, for supporting this research.

Acknowledgments

Thanks to AlMaarefa University, Researchers Supporting Project number (MHIRSP2024009), Almaarefa University, Riyadh, Saudi Arabia, for supporting this research.

Conflict of interest

The authors declare that the research was conducted in the absence of any commercial or financial relationships that could be construed as a potential conflict of interest.

Publisher's note

All claims expressed in this article are solely those of the authors and do not necessarily represent those of their affiliated organizations, or those of the publisher, the editors and the reviewers. Any product that may be evaluated in this article, or claim that may be made by its manufacturer, is not guaranteed or endorsed by the publisher.

References

Alexoudi, A., Alexoudi, I., and Gatzonis, S. (2018). Parkinson's disease pathogenesis, evolution and alternative pathways: a review. *Rev. Neurol. Paris.* 174 (10), 699–704. doi:10.1016/J.NEUROL.2017.12.003

Alharbi, B. A., et al. (2020). Non-steroidal anti-inflammatory drugs and Parkinson's disease: a systematic review and meta-analysis. *Ann. Med. Health Sci. Res.* 10 (5), 1023–1028.

Becker, C., Jick, S. S., and Meier, C. R. (2011). NSAID use and risk of Parkinson disease: a population-based case-control study. *Eur. J. Neurol.* 18 (11), 1336–1342. doi:10.1111/j.1468-1331.2011.03399.x

Bornebroek, M., de Lau, L. M. L., Haag, M. D. M., Koudstaal, P. J., Hofman, A., Stricker, B. H. C., et al. (2007). Nonsteroidal anti-inflammatory drugs and the risk of Parkinson disease. *Neuroepidemiology* 28 (4), 193–196. doi:10.1159/000108110

Bower, J. H., Maraganore, D. M., Peterson, B. J., et al. (2006). Immunologic diseases, anti-inflammatory drugs, and Parkinson disease: a case-control study. *Neurology*. 67 (7109), 494–496.

Chen, H., Jacobs, E., Schwarzschild, M. A., McCullough, M. L., Calle, E. E., Thun, M. J., et al. (2005). Nonsteroidal antiinflammatory drug use and the risk for Parkinson's disease. *Ann. Neurol.* 58 (6), 963–967. doi:10.1002/ana.20682

Chen, Z. F., Shi, S. M., Hu, R. X., Zhang, M., Liang, H., Zhou, Z. Y., et al. (2003). Nonsteroidal anti-inflammatory drugs and the risk of Parkinson disease. *Arch. Neurol.* 60 (8), 1059–1064. doi:10.1001/ARCHNEUR.60.8.1059

Driver, J. A., Logroscino, G., Lu, L., Gaziano, J. M., and Kurth, T. (2011). Use of non-steroidal anti-inflammatory drugs and risk of Parkinson's disease: nested case-control study. *BMJ* 342, d198. doi:10.1136/bmj.d198

Egger, M., Smith, G. D., Schneider, M., and Minder, C. (1997). Bias in meta-analysis detected by a simple, graphical test. *bmj*. 315 (7109), 629–634.

Etminan, M., Carleton, B. C., and Samii, A. (2008). Non-steroidal anti-inflammatory drug use and the risk of Parkinson disease: a retrospective cohort study. *J. Clin. Neurosci. Off. J. Neurosurg. Soc. Australas.* 15 (5), 576–577. doi:10.1016/j.jocn.2007.02.095

Etminan, M., and Suissa, S. (2008). NSAID use and the risk of Parkinsons disease. *Curr. Drug Saf.* 1 (3), 223–225. doi:10.2174/157488606777934404

Gagne, J. J., and Power, M. C. (2010). Anti-inflammatory drugs and risk of Parkinson disease: a meta-analysis. *Neurology* 74 (12), 995–1002. doi:10.1212/WNL.0b013e3181d5a4a3

Hancock, D. B., Martin, E. R., Stajich, J. M., Jewett, R., Stacy, M. A., Scott, B. L., et al. (2007). Smoking, caffeine, and nonsteroidal anti-inflammatory drugs in families with Parkinson disease. *Arch. Neurol.* 64 (4), 576–580. doi:10.1001/archneur.64.4.576

Herna, M. A., Logroscino, G., and Garcı, L. A. (2006). Inflammatory drugs and the incidence of Parkinson disease. *Neurology* 34, 1097–1099.

Kabra, A., Sharma, R., Kabra, R., and Baghel, U. S. (2018). Emerging and alternative therapies for Parkinson disease: an updated review. *Curr. Pharm. Des.* 24 (22), 2573–2582. doi:10.2174/1381612824666180820150150

Manthripragada, A. D., Schernhammer, E. S., Qiu, J., Friis, S., Wermuth, L., Olsen, J. H., et al. (2011). Non-steroidal anti-inflammatory drug use and the risk of Parkinson's disease. *Neuroepidemiology* 36 (3), 155–161. doi:10.1159/000325653

Mirpour, S., Turkbey, E. B., Marashdeh, W., El Khouli, R., and Subramaniam, R. M. (2018). Impact of DAT-SPECT on management of patients suspected of parkinsonism. *Clin. Nucl. Med.* 43 (10), 710–714. doi:10.1097/RLU.0000000000002240

Pajares, M., I Rojo, A., Manda, G., Boscá, L., and Cuadrado, A. (2020). Inflammation in Parkinson's disease: mechanisms and therapeutic implications. *Cells* 9 (7), 1687. doi:10.3390/CELLS9071687

Parepally, J. M. R., Mandula, H., and Smith, Q. R. (2006). Brain uptake of nonsteroidal anti-inflammatory drugs: ibuprofen, flurbiprofen, and indomethacin. *Pharm. Res.* 23 (5), 873–881. doi:10.1007/s11095-006-9905-5

Poly, T. N., Islam, M. M. R., Yang, H.-C., and Li, Y.-C. J. (2019). Non-steroidal anti-inflammatory drugs and risk of Parkinson's disease in the elderly population: a meta-analysis. *Eur. J. Clin. Pharmacol.* 75 (1), 99–108. doi:10.1007/s00228-018-2561-y

Powers, K. M., Kay, D. M., Factor, S. A., Zabetian, C. P., Higgins, D. S., Samii, A., et al. (2008). Combined effects of smoking, coffee, and NSAIDs on Parkinson's disease risk. *Mov. Disord.* 23 (1), 88–95. doi:10.1002/mds.21782

Rathore, C., Radhakrishnan, A., Nayak, S. D., and Radhakrishnan, K. (2009). Use of antihypertensives and the risk of Parkinson disease. *Neurology* 72 (6), 578–579. doi:10.1212/01.WNL.0000344171.22760.24

Samii, A., Etminan, M., Wiens, M. O., and Jafari, S. (2009). NSAID use and the risk of Parkinson ' s disease systematic review and meta-analysis of observational studies. *Drugs Aging* 26 (9), 769–779. doi:10.2165/11316780-000000000-00000

Sánchez-pernaute, R., Ferree, A., Cooper, O., Yu, M., Brownell, A., and Isacson, O. (2004) Selective COX-2 inhibition prevents progressive dopamine neuron degeneration in a rat model of Parkinson ' s disease, 11, 1–11.

Starhof, C., Hejl, A.-M., Korbo, L., Winge, K., and Friis, S. (2020). Risk of multiple system atrophy and the use of anti-inflammatory drugs: a Danish register-based case-control study. *Neuroepidemiology* 54 (1), 58–63. doi:10.1159/000503003

Sung, Y. F., Liu, F. C., Lee, J. T., Yang, F. C., Chou, Y. C., et al. (2016). Reduced risk of Parkinson disease in patients with rheumatoid arthritis: a nationwide population-based study. *Mayo Clin. Proc.* 91 (10), 1346–1353. doi:10.1016/j.mayocp.2016.06.023

Terzi, M., Altun, G., Şen, S., Kocaman, A., Kaplan, A. A., Yurt, K. K., et al. (2018). The use of non-steroidal anti-inflammatory drugs in neurological diseases. *J. Chem. Neuroanat.* 87, 12–24. doi:10.1016/j.jchemneu.2017.03.003

Ton, T. G., Heckbert, S. R., Longstreth, W. T., Rossing, M. A., Kukull, W. A., Franklin, G. M., et al. (2006). Nonsteroidal anti-inflammatory drugs and risk of Parkinson's disease. *Mov. Disord.* 21 (7), 964–969. doi:10.1002/mds.20856

Wahner, A. D., Bronstein, J. M., Bordelon, Y. M., and Ritz, B. (2007). Nonsteroidal anti-inflammatory drugs may protect against Parkinson disease. *Neurology* 69 (19), 1836–1842. doi:10.1212/01.wnl.0000279519.99344.ad

Wang, T., Pei, Z., Zhang, W., Liu, B., Langenbach, R., Lee, C., et al. (2005). "MPP + -induced COX-2 activation and subsequent dopaminergic neurodegeneration," vol. 18, pp. 1134–1136. doi:10.1096/fj.04-2457fje

Zafar, S., and Yaddanapudi, S. S. (2022). Parkinson disease. *StatPearls* 8, 1–13.

frontiers | Frontiers in Pharmacology

TYPE Original Research
PUBLISHED 13 August 2024
DOI 10.3389/fphar.2024.1452989

Check for updates

OPEN ACCESS

EDITED BY
Rupesh V. Chikhale,
University of Cambridge, United Kingdom

REVIEWED BY
Stefano Pieretti,
National Institute of Health (ISS), Italy
Smita Kumari,
The Ohio State University, United States

*CORRESPONDENCE
Sajad Fakhri,
pharmacy.sajad@yahoo.com
Javier Echeverría,
javier.echeverriam@usach.cl

†These authors have contributed equally to this work and share first authorship

RECEIVED 21 June 2024
ACCEPTED 31 July 2024
PUBLISHED 13 August 2024

CITATION
Bagheri Bavandpouri FS, Azizi A, Abbaszadeh F, Kiani A, Farzaei MH, Mohammadi-Noori E, Fakhri S and Echeverría J (2024) Polydatin attenuated neuropathic pain and motor dysfunction following spinal cord injury in rats by employing its anti-inflammatory and antioxidant effects.
Front. Pharmacol. 15:1452989.
doi: 10.3389/fphar.2024.1452989

COPYRIGHT
© 2024 Bagheri Bavandpouri, Azizi, Abbaszadeh, Kiani, Farzaei, Mohammadi-Noori, Fakhri and Echeverría. This is an open-access article distributed under the terms of the Creative Commons Attribution License (CC BY). The use, distribution or reproduction in other forums is permitted, provided the original author(s) and the copyright owner(s) are credited and that the original publication in this journal is cited, in accordance with accepted academic practice. No use, distribution or reproduction is permitted which does not comply with these terms.

Polydatin attenuated neuropathic pain and motor dysfunction following spinal cord injury in rats by employing its anti-inflammatory and antioxidant effects

Faezeh Sadat Bagheri Bavandpouri[1†], Atefeh Azizi[1†], Fatemeh Abbaszadeh[2], Amir Kiani[3,4], Mohammad Hosein Farzaei[3], Ehsan Mohammadi-Noori[3], Sajad Fakhri[3*] and Javier Echeverría[5*]

[1]Student Research Committee, Kermanshah University of Medical Sciences, Kermanshah, Iran, [2]Neurobiology Research Center, Shahid Beheshti University of Medical Sciences, Tehran, Iran, [3]Pharmaceutical Sciences Research Center, Health Institute, Kermanshah University of Medical Sciences, Kermanshah, Iran, [4]Regenerative Medicine Research Center (RMRC), Kermanshah University of Medical Sciences, Kermanshah, Iran, [5]Departamento de Ciencias del Ambiente, Facultad de Química y Biología, Universidad de Santiago de Chile, Santiago, Chile

Background: Considering the complex pathological mechanisms behind spinal cord injury (SCI) and the adverse effects of present non-approved drugs against SCI, new studies are needed to introduce novel multi-target active ingredients with higher efficacy and lower side effects. Polydatin (PLD) is a naturally occurring stilbenoid glucoside recognized for its antioxidative and anti-inflammatory properties. This study aimed to assess the effects of PLD on sensory-motor function following SCI in rats.

Methods: Following laminectomy and clip compression injury at the thoracic 8 (T8)-T9 level of the spinal cord, rats were randomly assigned to five groups: Sham, SCI, and three groups receiving different doses of PLD treatment (1, 2, and 3 mg/kg). Over 4 weeks, behavioral tests were done such as von Frey, acetone drop, hot plate, Basso-Beattie-Bresnahan, and inclined plane test. At the end of the study, changes in catalase and glutathione activity, nitrite level, activity of matrix metalloproteinase 2 (MMP2) and MMP9 as well as spinal tissue remyelination/neurogenesis, were evaluated.

Results: The results revealed that PLD treatment significantly improved the behavioral performance of the animals starting from the first week after SCI. Additionally, PLD increased catalase, and glutathione levels, and MMP2 activity

Abbreviations: ANOVA, analysis of variance; BBB, Basso-Beattie-Bresnahan; DTNB, 5,5′-dithio-bis(2 nitrobenzoic acid); H&E, hematoxylin and eosin; HO-1, heme oxygenase 1; iNOS, Inducible nitric oxide synthase; ip, intraperitoneal; MMP2, matrix metalloproteinase-2; MMP9, matrix metalloproteinase-9; NEDD, naphthyl ethylenediamine dihydrochloride; NIH, National Institutes of Health; NO, nitric oxide; Nrf2, nuclear factor erythroid 2-related factor 2; OD, optical density; PBS, phosphate-buffered saline; PFA, paraformaldehyde; PLD, Polydatin; PWL, paw withdrawal latency; RNS, Reactive nitrogen species; ROS, reactive oxygen species; SCI, Spinal cord injury; SEM, standard error of the mean.

while reduced serum nitrite levels and MMP9. These positive effects were accompanied by a reduction in the size of the lesion and preservation of neuronal count.

Conclusion: In conclusion, PLD showed neuroprotective effects in SCI rats by employing anti-inflammatory and antioxidant effects, through which improve sensory and motor function.

KEYWORDS

spinal cord injury, polydatin, oxidative stress, inflammation, motor activity, neuropathic pain

1 Introduction

Spinal cord injury (SCI) is a complex and multifaceted process that involves both primary and secondary damage to the spinal cord. Secondary injury refers to a series of biochemical and cellular processes that occur after the initial injury, and further worsening the harm to the spinal cord. Amongst those mechanisms, inflammation, oxidative stress, apoptosis, excitotoxicity, demyelination, and glial scar formation play critical roles (Anjum et al., 2020). In this regard, oxidative stress plays a significant role in causing neurological injuries. This occurs through the excessive production of reactive oxygen species (ROS), including free radicals and lipid peroxides. Several studies have demonstrated that levels of oxidative stress increase after SCI, leading to a decrease in the antioxidant defense potential, including activities of glutathione and catalase (Jia et al., 2012; Stewart et al., 2022a). Furthermore, SCI-induced oxidative stress also leads to the modification of signaling pathways. Studies have revealed that an increase in inducible nitric oxide synthase (iNOS), the crucial enzyme responsible for the synthesis of nitric oxide (NO), increased following SCI (Conti et al., 2007). NO has been found to inhibit the expression of matrix metalloproteinase-2 (MMP2) (Chen and Wang, 2004). Hence, employing pharmacological intervention to protect against these effects could be a promising therapeutic strategy. Researchers have increasingly focused on exploring the pharmacological effects of natural products on various diseases due to their wide range of beneficial activities and minimal side effects.

Polydatin (PLD), 3,4,5-Trihydroxystilbene-3-beta-monoglucoside or piceid, is a naturally occurring stilbenoid glucoside and glycosided form of resveratrol. PLD is the main bioactive ingredient extracted from the roots of the *Reynoutria japonica* Houtt (Polygonaceae), bark of *Picea sitchensis* (Bong.) Carrière (Pinaceae). In addition, PLD also can be found in significant amounts in common botanical sources, as grapes, hop cones, peanuts, and red wines. PLD is used as chemomarker to characterize the quality of *Reynoutria japonica* in the Pharmacopoeia of the People's Republic of China where is traditionally used for treatment of hyperlipemia, inflammation, infection and cancer. PLD exhibits a range of beneficial properties, including anti-inflammatory, immunoregulatory, antioxidant, and anti-tumor activities (Karami et al., 2022). In a comparative study, it was found that PLD has superior and higher activity in inhibiting hydroxyl radicals than resveratrol (Wang et al., 2015). As a potent stilbenoid polyphenol, PLD has the ability to modulate crucial signaling pathways associated with inflammation, oxidative stress, and apoptosis, thereby exhibiting potential biological activities (Fakhri et al., 2021a). Additionally, PLD exhibited greater antioxidant (Şöhretoğlu et al., 2018) and anti-inflammatory (Lanzilli et al., 2012) effects compared to its glycoside derivative, resveratrol. As well, PLD possesses superior biodistribution and antioxidant activity. Moreover, PLD demonstrates higher intestinal absorption due to the presence of its sugar groups (Wang et al., 2015), distinguishing it from resveratrol. Overall, considering the critical role of inflammation, oxidative stress and apoptosis behind neurodegeneration and the aforementioned multi-targeting potential of PD with more bioavailability in the regulation of multiple dysregulated pathways, in the present study, we examined the neuroprotective benefits of intrathecal (i.t.) administration of PLD after SCI.

2 Materials and methods

2.1 Chemical and reagents

Polydatin and cefazolin was purchased from Sigma–Aldrich (Sigma Chemical Co., St. Louis, MO, United States) and Exir company (Exir company, Iran, i.p.), respectively. All the other chemicals and reagents were of analytical reagent grade purchased from commercial sources.

2.2 Experimental animals

In total, 35 male Wistar rats, aged 8–9 weeks, were obtained and kept in controlled conditions with equal light/darkness (12 h) at the animal house of Kermanshah University of Medical Sciences (temperature 24°C ± 2°C, with fresh water and food *ad libitum*, 10 days prior to the beginning of study). The study was conducted under the guidelines of this university's animal care committee (IR.KUMS.REC. 1400.388, **Supplementary material**). The male rats were allocated into the following groups: Sham, SCI groups that received distilled water as a solvent, and three treatment groups that received doses of 1, 2, and 3 mg/kg of PLD, respectively. Male rats included in ours research, since they have more consistent hormonal levels in comparison to females, which could be influenced by their estrous cycle specially in rat behavior (Zeng et al., 2023).

2.3 Spinal cord injury

At the start of surgery, rats were anesthetized with ketamine and xylazine (80/10 mg/kg, intraperitoneal (i.p.). The thoracic vertebrae

(T8-T9) were removed using a micro rongeur (Fine Science Tools, United States. To create a compression model of SCI, rats in the SCI and PLD groups were subjected to a force of 90 g for 1 min using an aneurysm clip (Aesculap, Tuttlingen, Germany). The muscles and skin were sutured after the surgery. 30 min after SCI, rats received 10 μL of doses of 1, 2, and 3 mg/kg PLD or distilled water intrathecally. 40 mg/kg of cefazolin (i.p.) (Exir company, Iran, i.p.) and 2 mL of normal saline (subcutaneous) and manual bladder massage were performed as post-surgery care until the return of normal bladder function (Fakhri et al., 2018; Fakhri et al., 2019).

2.4 Behavioral test

Behavioral tests were conducted on all animals before surgery (day 0) and weekly after surgery on days 7, 14, 21, and 28.

2.4.1 Cold allodynia

To assess cold sensitivity in rats, a few drops of acetone (100 μL) were sprayed onto the soles of the animals from a distance of 200 mm. The response of the hind paw was observed and scored as follows: no paw withdrawal (scored as 0), startle response without paw withdrawal (scored as 1), partial withdrawal of the paw, 5–30 s (scored as 2), prolonged withdrawal of the paw, >30 s (scored as 3), and licking and jumping (scored as 4) (Kauppila, 2000; Fakhri et al., 2018).

2.4.2 Heat hyperalgesia

To measure hyperalgesia, each animal was placed in a plexiglass chamber on a hot plate device (Harvard device, United States, 50°C ± 2°C). The delay time for paw withdrawal, indicated by licking or jumping, was recorded as paw withdrawal latency (PWL). To prevent tissue damage, a cut-off time of 1 min was considered (Fakhri et al., 2022b).

2.4.3 Mechanical allodynia

The assessment of mechanical allodynia was carried out by using von Frey filaments. Both lateral plantar areas of the paw were tested with a series of von Frey strings (10, 15, 26, 60, and 100 g). Each strand was applied five times. 3 positive answers (leg dragging) out of 5 tests were considered as the allodynia threshold (Fakhri et al., 2019).

2.4.4 Inclined plane test

The inclined plane test was used to evaluate the motor function of rats after SCI. In this experiment, the rats were placed on an inclined plane with a variable angle between 0 and 60. The maximum angle at which the animal kept its balance for at least 5 s was taken as the response (Fakhri et al., 2018).

2.4.5 Basso-Beattie-Bresnahan (BBB) scores

The Basso-Beattie-Bresnahan (BBB) score test was another locomotor test used to evaluate the motor function of rats. The test involved observing the rat's hind limb movements for 4 min and assigning a score based on the degree of movement and coordination. The score ranges from 0 (no movement) to 21 (normal movement). The average score of both paws was considered as the final response (Fakhri et al., 2021b).

2.5 Biochemical test

At the end of the behavioral evaluation (day 28), the rats were sacrificed and their serum samples were used for biochemical studies.

2.5.1 Nitrite assay

Nitric oxide levels in serum samples are assessed by the Griess assay. Therefore, this test provides an indirect indication of NO levels. Griess reagent was prepared from a solution of sulfonamide (dissolved in 5% phosphoric acid) and naphthyl ethylenediamine dihydrochloride (NEDD). In each of the wells of the plate, a mixture of serum sample and sulfonamide solution was poured. After minutes, 50 mL of NEDD solution was added. After a 5-minute incubation, the optical density (OD) was measured at 540 nm. The standard curve was plotted simultaneously using different concentrations of sodium nitrite (Sun et al., 2003).

2.5.2 Glutathione/catalase assay

Changes in glutathione and catalase levels were evaluated to determine antioxidant levels. For the evaluation of glutathione, we employed Ellman's reagent. To perform the test, we mixed 50 μL of phosphate-buffered saline (PBS), 40 μL of the serum sample, and 100 μL of 5,5'-dithio-bis(2-nitrobenzoic acid) (DTNB). This mixture was incubated for 10 min. Finally, we measured the optical density (OD) of each well at 412 nm using a plate reader (Eyer and Podhradský, 1986).

The catalase activity was measured with the Aebi method (Aebi, 1984). First, the combination of serum samples and hydrogen peroxide (65 mM) was incubated in the plate well for 4 min at 25°C. In order to stop the reaction, 100 μL ammonium molybdate (32.4 mM) was then added. Finally, an optical density reader was used to measure OD at 405 nm (Fakhri et al., 2022b).

The percentage difference in concentration between the sham group and other groups can be calculated as: (C_sham − C_samp)/C_sham) × 100.

2.6 The activity of MMP2 and MMP9

To assess the activity of MMP-2 and MMP-9 gelatin zymography was performed. Following doing Bradford protein assay, serum protein was loaded at 100 μg per sample and electrophoresis was used with a voltage of 150 V. Gels were washed in a renaturation buffer (Triton™ X-100 in Tris-HCl, pH 7.5) on the shaker. In following, the gels were incubated for 18 h at 37°C in an incubation buffer consisting of NaN_3, NaCl, and $CaCl_2$ in Tris-HCl. Then, gels were stained with Coomassie blue and destained in an acetic acid and methanol solution. Image j software was used to evaluate the bands area and intensity (Fakhri et al., 2021b).

2.7 Histological analysis

Rats were perfused transcardially with approximately 250 mL of PBS (pH 7.3) and 300 mL of 4% paraformaldehyde (PFA) on days 7, 21, and 28. The tissue from the injury site of the spinal cord was collected and prepared using a tissue processor. Subsequently, it was

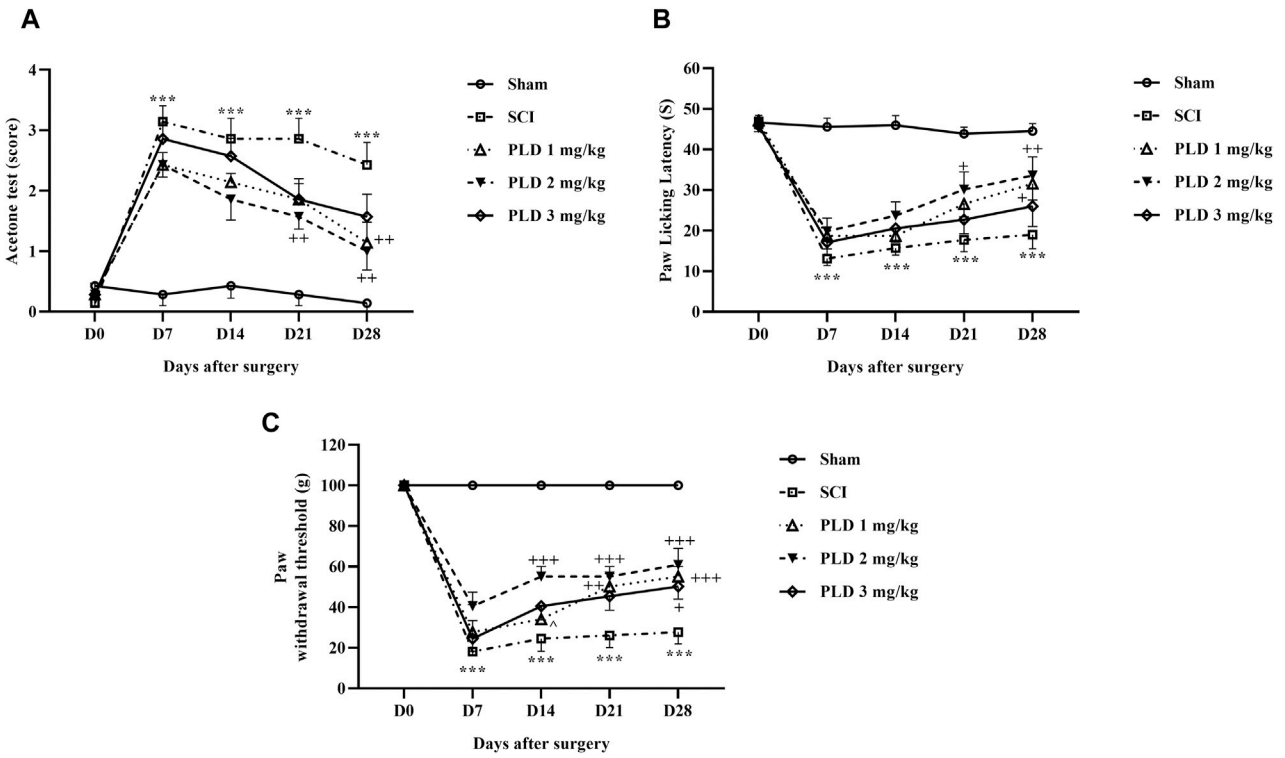


FIGURE 1
The impact of PLD on behaviors related to pain after SCI. The paw response threshold to cold **(A)**, thermal **(B)**, and mechanical **(C)** stimuli were measured and the data is presented as the mean ± SEM (n = 7). The statistical analysis was done using a two-way ANOVA. ***p < 0.001 vs. sham group; ^{+}p < 0.05, ^{++}p < 0.01, ^{+++}p < 0.001 vs. SCI group; $^{\wedge}p$ < 0.05 vs. PLD 2 mg/kg group.

embedded in paraffin. The paraffinized tissue was then cut into sequential sections and stained with hematoxylin and eosin (H&E). These stained sections were observed under a light microscope at both 10× and 40× magnification. To analyze the injury site, as well as the number of neurons in the dorsal and ventral horns, Image J software developed by National Institutes of Health (NIH) was utilized for quantification (Fakhri et al., 2018; Fakhri et al., 2019; Fakhri et al.,2021b).

2.8 Statistical analysis

The data has been presented in the form of mean ± standard error of the mean (SEM), and it has been analyzed using GraphPad Prism software (version 8.4.3). One-way and two-way analysis of variance (ANOVA) have been applied, followed by Tukey's and Bonferroni's *post hoc* analyses. A statistically significant difference has been considered at $p < 0.05$.

3 Results

3.1 Behavioral result

3.1.1 Cold allodynia

Cold pain response threshold data were subjected to two-way ANOVA analysis. It was found that during the 4-week follow-up, rats in the sham group continued to have normal sensitivity to cold on all the investigated days. However, rats in the SCI group showed significant hypersensitivity to cold compared to the sham group ($p <$ 0.001). Furthermore, animals treated with different doses of PLD compared to the SCI group had a higher response threshold to cold stimulation and the best results were obtained after 2 mg/kg treatment ($p < 0.01$) (Figure 1A).

3.1.2 Heat hyperalgesia

The results of the threshold for responding to a thermal pain stimulus are displayed in the Figure 1B. The findings indicate that the paw-licking latency was consistently similar on all test days for the control group (sham). However, the animals in the SCI group became highly sensitive to the thermal pain stimulus. Administration of PLD increased the response threshold to heat stimulus in injured animals, and intrathecal injection of 2 mg/kg PLD was more effective than the other two doses ($p <$ 0.01). (Figure 1B).

3.1.3 Mechanical allodynia

The paw withdrawal responses to mechanical stimulation were almost the same in the sham group after 4 weeks. However, SCI caused a significant and sustained reduction in the paw withdrawal threshold ($p < 0.001$), indicating the presence of mechanical allodynia. Importantly, treatment with PLD, particularly at a dose of 2 mg/kg, effectively reduced the symptoms induced by SCI from day 7 onwards ($p < 0.001$) (Figure 1C).

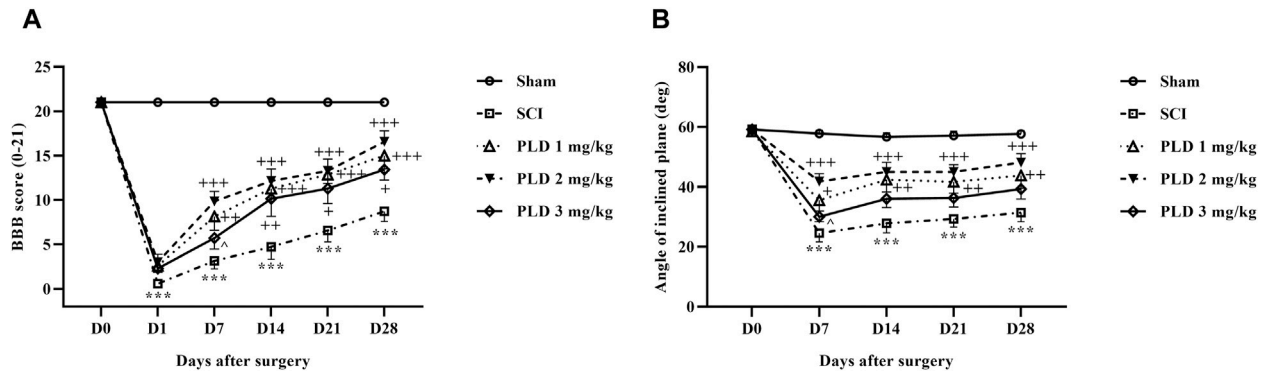


FIGURE 2
The impact of PLD on motor ability after SCI. The BBB score **(A)**, and inclined-plane **(B)** test were measured and the data is presented as the mean ± SEM (n = 7). The statistical analysis was done using a two-way ANOVA. ***$p < 0.001$ vs. sham group; $^{+}p < 0.05$, $^{++}p < 0.01$, $^{+++}p < 0.001$ vs. SCI group; $^{\wedge}p < 0.05$ vs. PLD 2 mg/kg group.

3.1.4 Motor activity

The motor behavior of rats following SCI was evaluated using the BBB scale and inclined plane test. The sham group had a stable score of 21, indicating that the laminectomy surgical did not cause any functional impairments. In contrast, the SCI rats showed significantly lower scores of 0 and 2 on the first day after the injury, and this reduction in motor performance persisted until day 28 post-SCI ($p < 0.001$). Interestingly, the administration of various doses of PLD effectively improved the motor function of the SCI rats, starting from day 1, when compared to the SCI group ($p < 0.001$) (Figure 2A).

The sham group maintained a consistent ability to stand and balance on the ramp over 4 weeks, averaging at approximately 60°C. However, the group with SCI experienced a significant decline in average balance angle, compared to the sham group ($p < 0.001$). Rats treated with various doses of PLD, especially the dose of 2 mg/kg showed substantial improvement from the first week ($p < 0.001$) (Figure 2B).

3.2 Biochemical result

3.2.1 Nitrite assay

In comparison to the sham group, the SCI group showed a significant increase in serum nitrite levels ($p < 0.05$). While treatment with PLD 2 mg/kg resulted in a decrease in the serum nitrite level ($p < 0.05$) in comparison to the SCI group ($p < 0.05$). Although the other doses of PLD (1 mg/g and 3 mg/kg) also decreased serum levels of nitrite, it was not significant (Figure 3A)

3.2.2 Catalase and glutathione assay

According to the results, the SCI group showed a significant reduction in the serum levels of catalase and glutathione compared to the sham group ($p < 0.001$). However, treatment with PLD, particularly at a dose of 2 mg/kg, was able to effectively compensate for this decrease ($p < 0.01$). Figures 3B, C presents that the administration of PLD 2 mg/kg decreased the differences between the group and sham group (see formula in Section 2.5.2). Other doses of PLD (1 and 3 mg/kg) also decreased the differences between groups and sham group, however those was not significant (Figures 3B, C).

3.3 MMP2 and MMP9 activity

In day 28, the SCI group showed an elevation in MMP-9 activity while a reduction in MMP-2 in comparison to the sham group ($p < 0.001$). However, with PLD treatment, those changes reversed. The results showed that PLD 2 mg/kg potentially elevated anti-inflammatory MMP2 ($p < 0.05$). However, PLD made a non-significant reduction in the activity of MMP9 (Figures 4A, B).

3.4 Histological analysis

The histopathological analysis revealed that in the SCI group, there was a notable increase in the lesion size (Figures 5A, B) and a significant decrease in the number of neurons in both the dorsal (Figures 6A, B) and ventral (Figures 6C, D) horns of the spinal cord, as compared to the sham group ($p < 0.001$). On the contrary, in the groups treated with PLD, there was a remarkable decrease in the size of the lesion during 1 month. This reduction in the size of the lesion was accompanied by an increase in the number of neurons in both horns of the spinal cord ($p < 0.001$).

4 Discussion

The results of this study showed that treatment with PLD can significantly improve sensory and motor function and increase the number of dorsal-ventral spinal cord neurons and lesion size. In addition, PLD increased the level of catalase and glutathione, as well as MMP2 activity while reducing nitrite levels and MMP9 activity to protect the spinal cord tissue from secondary damages caused by oxidative stress.

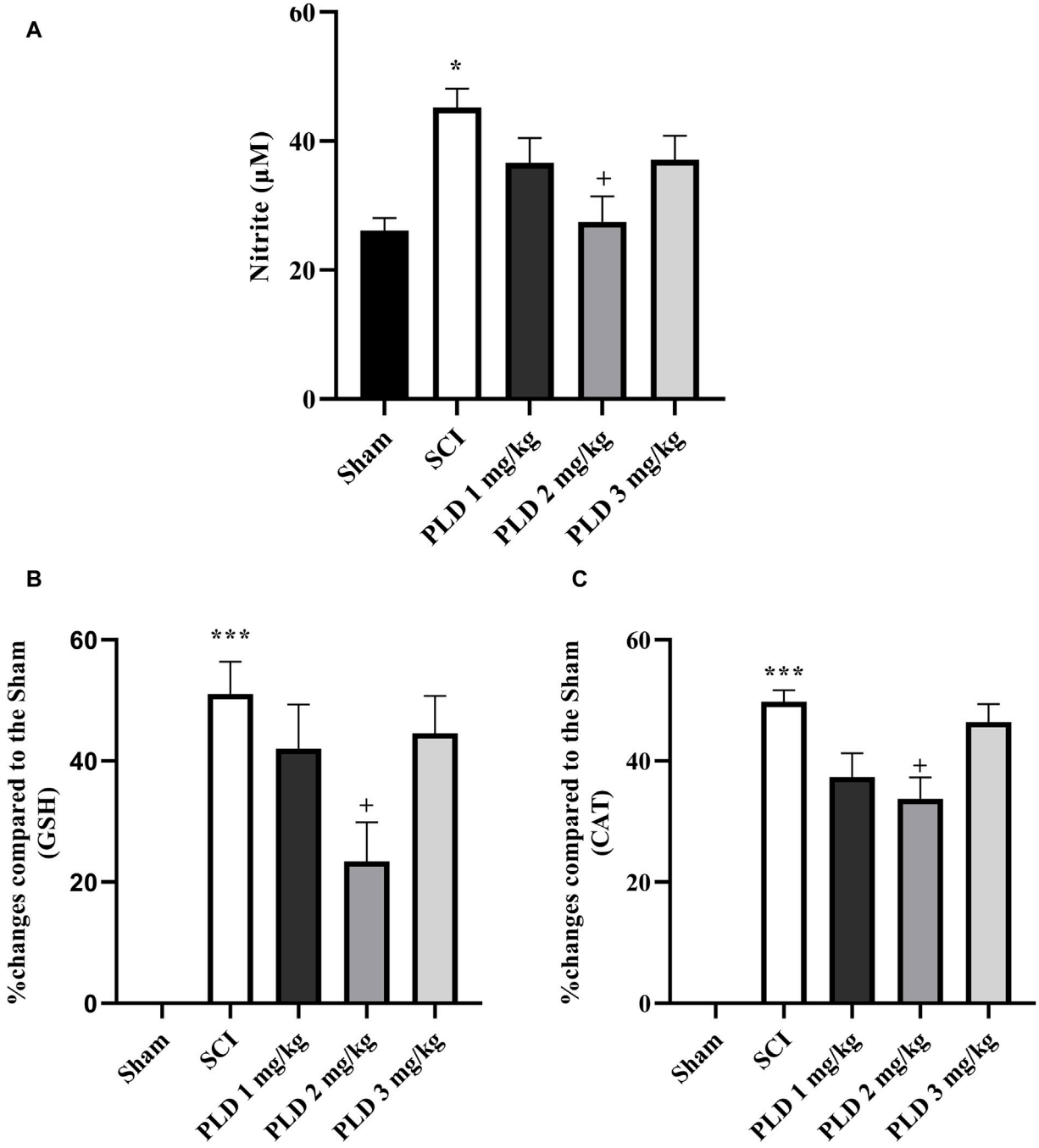


FIGURE 3
Effect of PLD on changes of oxidative stress. The level of nitrite **(A)**, and percentage of activity changes of glutathione **(B)** and catalase **(C)** were measured and the data is presented as the mean ± SEM (n = 3). The statistical analysis was done using a one-way ANOVA. *$p < 0.05$ and ***$p < 0.001$ vs. sham group; $^{+}p < 0.05$ vs. SCI group.

SCI can be divided into two primary components: mechanical damage from temporary spinal cord compression and the development of early post-injury lesions. Subsequently, a series of additional damages can worsen nerve dysfunction and result in irreversible harm (Hu et al., 2023). The inflammatory response and apoptosis in the affected tissue are triggered by oxidative stress (Chandra et al., 2000; Zhang et al., 2012). Actually, after SCI, oxidative stress has been linked to the development of neuropathic pain through its ability to promote inflammation, nerve damage, and increased sensitivity to pain. Reactive oxygen and nitrogen species (ROS and RNS) can cause harm to DNA, lipids, and proteins, resulting in inflammation and disruption of cellular and tissue function (Hassler et al., 2014; Carrasco et al., 2018).

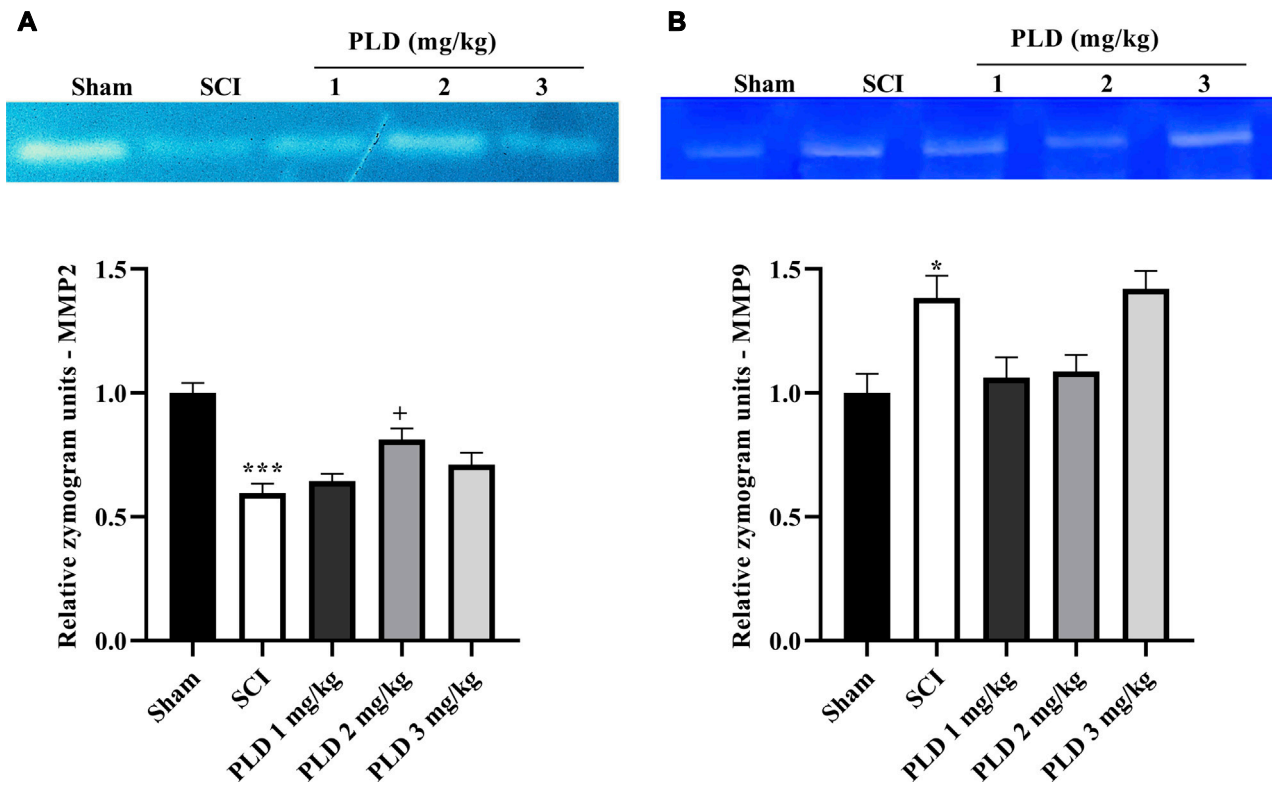


FIGURE 4
The impact of PLD on MMP-2 **(A)** and MMP-9 **(B)** activity after compression SCI. Data presented as mean ± SEM. *$p < 0.05$, ***$p < 0.001$ vs. sham, $^{+}p < 0.05$ vs. SCI group.

Research has been conducted on PLD to explore its potential health advantages, such as its antioxidant and anti-inflammatory properties (Chen et al., 2021). PLD is a resveratrol derivative (glucoside of resveratrol) with improved bioavailability. PLD has been compared to resveratrol in several studies, and it has been found to have a higher activity of scavenging hydroxyl radicals than resveratrol (Wang et al., 2015). Research has shown that PLD can modulate nitric oxide levels, and improve catalase and glutathione activity, thereby contributing to its antioxidant and anti-inflammatory effects (Karami et al., 2022). Our findings also confirmed these results (Increasing the level of catalase and glutathione and decreasing the level of nitrite).

Arriving at the most effective dose is a critical key point in combating neurodegeneration; though, this process would be challenging considering interindividual variation affected by age, gender, genetics, exercise, diet, and health status. Hormesis is a biphasic dose-response relationship known by high-dose inhibition and low-dose stimulation of biological responses, characterized by either graphical J/U-shaped or an inverted U-shaped dose-response curve. Hormetic responses are affected by several stimuli, including chemical exposures, dietary restriction, thermal/light/electricity extremes, hypoxia, ionizing radiation, and physical stress (Fakhri et al., 2022a). Based on the hormesis dose-response relationship, our study showed a better neuroprotective effect for PLD 2 mg/kg than 1 and 3 mg/kg in the regulation of motor dysfunction and neuropathic pain by combating inflammation and oxidative stress, as well as improving neuronal survival and spinal tissue repair.

PLD has been found to inhibit the production of pro-inflammatory molecules, such as cytokines and prostaglandins, which are involved in the signaling of pain. By reducing inflammation, PLD may help to alleviate pain associated with inflammatory conditions, such as arthritis or muscle strain (Karami et al., 2022; Zhang et al., 2024). Additionally, PLD has been shown to have antioxidant properties, which can help to reduce oxidative stress and damage in the body (Chen et al., 2015). Oxidative stress has been linked to the development and maintenance of chronic pain conditions, and by neutralizing free radicals and reducing oxidative damage, PLD may help to alleviate pain (Luo et al., 2022). Xi et al. reported that PLD attenuated vincristine-induced neuropathic pain in rats by suppressing the activation of inflammatory factors and inhibiting oxidative stress (Xi et al., 2022). Another study demonstrated that PLD attenuated experimental diabetic neuropathy in rats by suppressing the activation of inflammatory factors and inhibiting oxidative stress (Bheereddy et al., 2021). On the other hand, the reduction of pain was linked to improved motor performance. Lv et al. found that when rats were given intraperitoneal PLD, their locomotor activity improved. This has been attributed to the suppression of oxidative stress and apoptosis through the nuclear factor erythroid 2-related factor 2 (Nrf2)/heme oxygenase 1 (HO-1) pathway (Lv et al., 2019b). The mediators of oxidative stress has been found to inhibit the expression of MMP2 and elevate the activity of MMP9 (Chen and

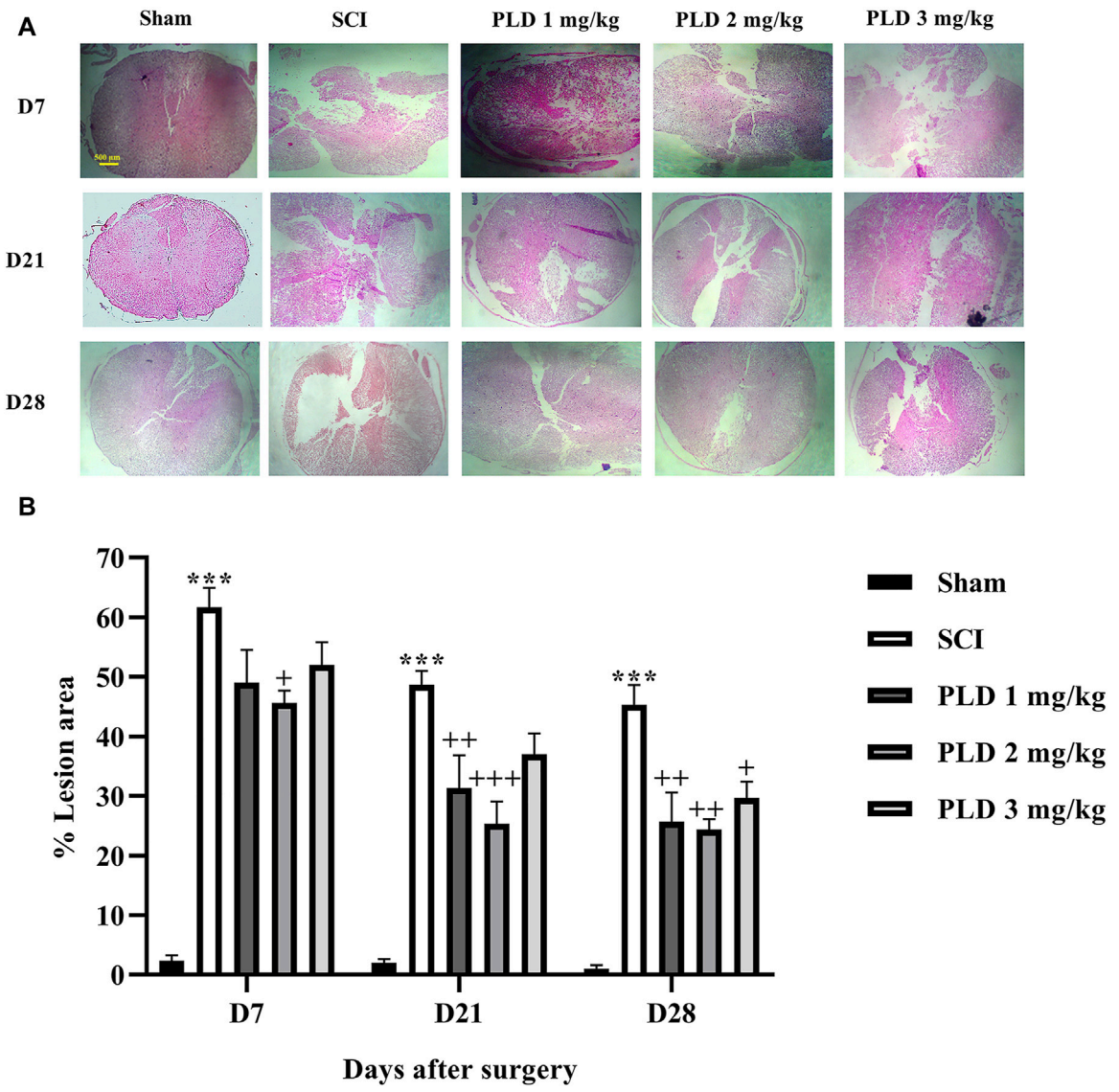


FIGURE 5
The impact of PLD on the lesion size after SCI **(A)** and associate analysis **(B)**. The data is presented as the mean ± SEM (n = 3). The statistical analysis was done using a two-way ANOVA. ***$p < 0.001$ vs. sham group;+$p < 0.05$, $^{++}p < 0.01$, $^{+++}p < 0.001$ vs. SCI group; $^{\dagger}p < 0.05$ vs. PLD 2 mg/kg group. The scale bar (yellow line) shows 500 μm.

Wang, 2004). In our study, SCI made an increase in nitrite level, while decreased in catalase and glutathione, thereby increased the activity of MMP9 and decreased those of MMP2. These biochemical and zymography results made increased lesion size and suppressed numbers of sensory/motor neurons in rats. In terms of histology, studies have shown that PLD can promote axonal regeneration, improve histological damage, inhibit apoptosis levels, and reduce tissue damage after SCI (Lv et al., 2019a; Zhan et al., 2022). In the current study, PLD was also able to reduce the size of the lesion after SCI and preserve the dorsal and ventral horn neurons.

We also found that SCI decreased the survival rate of sensory/motor neurons in the ventral/dorsal horns of spinal cord, respectively. These changes were reverted following PLD administration, which were in line with the behavioral results. Consistent with these results, we also found that PLD increased the response to cold, heat, and mechanical stimuli as well as maintaining limb movement following SCI by regulating inflammation/oxidative stress and histological protection (Figure 7).

Amongst SCI experimental models regarding examining the therapeutic effect and neuroprotective study following SCI, the compression model is a better experimental choice. Moreover, compression SCI is useful to evaluate the minimal loss of neurons after SCI. Compression SCI is also beneficial to study the secondary mechanisms and cell transplantation therapies (Sun et al., 2017). On the other hand, some experimental models of SCI possess minor limitations, however we used compression SCI which is more suitable for translational research and similar to those in SCI patients (Cregg et al., 2014). Regarding possible experimental limitations in SCI research protocols, pre-clinical SCI models commonly use young adult animals, while clinical models

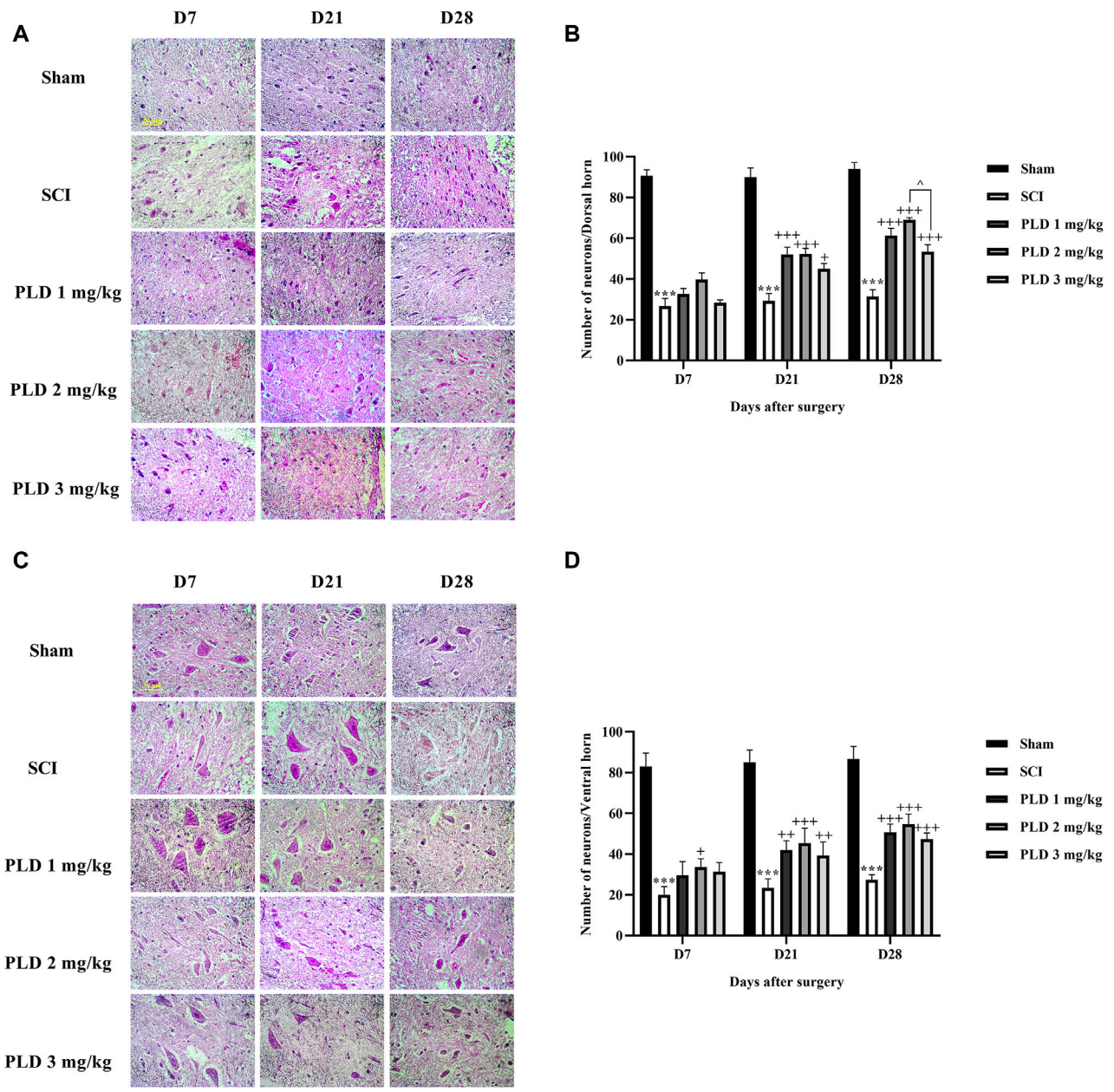


FIGURE 6
The impact of PLD on the number of neurons in both horns of the spinal cord after SCI. The dorsal **(A, B)** and ventral **(C, D)** horns of the spinal cord were measured and the data is presented as the mean ± SEM (n = 3). The statistical analysis was done using a two-way ANOVA. *** $p < 0.001$ vs. sham group; $^{+}p < 0.05$, $^{++}$ $p < 0.01$, $^{+++}$ $p < 0.001$ vs. SCI group; $^{\wedge}p < 0.05$ vs. PLD 2 mg/kg group. The scale bar (yellow line) shows 50 μm.

engages human subjects with wide age ranges (Stewart et al., 2022b). Other limitations include the inability to directly apply long-distance axon regeneration, which is required in humans to treat spinal injuries, to animal models. Larger volumes of reinnervation-needed gray matter in humans makes slower recovery and reduces spontaneous recovery in human after SCI (Kjell and Olson, 2016). Another important limitation of the compression method is that after SCI some neural tracts may not be well damaged leading to undesired results in regeneration research. Furthermore, about 4–6 weeks post-injury, tissue sparing may increase, presenting that the late subacute and early intermediate stages of the secondary injury are related to limited neuroanatomical recovery (Ahmed et al., 2019).

5 Conclusion

Our findings suggest that PLD can improve sensory-motor dysfunction caused by SCI in rats. This is due to the effective antioxidative properties of PLD, which reduced nitrite levels, enhanced catalase, and glutathione activity, ultimately leading to a reduction in histological damages. These results indicated that

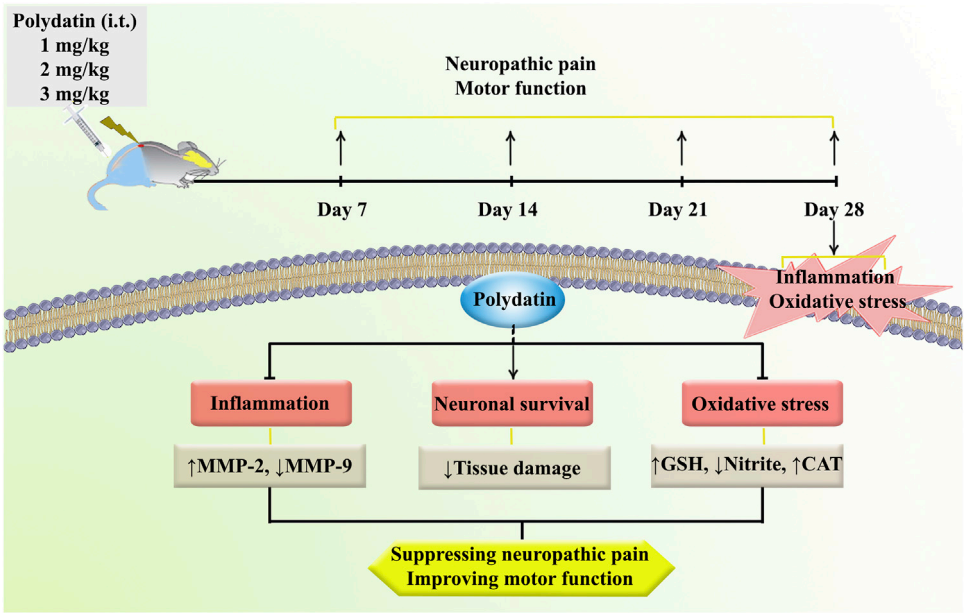


FIGURE 7
A description of the research methodologies and the regulatory role of PLD in the treatment of neuropathic pain and motor dysfunction via anti-inflammatory and antioxidant mechanisms.

PLD has therapeutic potential for individuals experiencing SCI-related dysfunction.

Data availability statement

The raw data supporting the conclusions of this article will be made available by the corresponding author upon request.

Ethics statement

The animal study was approved by Dr. Mahmoodreza Moradi/Kermanshah University of Medical Sciences Dr. Reza Khodarahmi/Kermanshah University of Medical Sciences. The study was conducted in accordance with the local legislation and institutional requirements.

Author contributions

FB: Investigation, Writing–original draft. AA: Investigation, Writing–original draft. FA: Data curation, Investigation, Formal analysis, Writing–original draft. AK: Investigation, Writing–original draft. MF: Writing–original draft, Investigation, Writing–review and editing. EM-N: Investigation, Writing–original draft. SF: Writing–original draft, Writing–review and editing, Data curation, Investigation, Methodology. JE: Writing–original draft, Writing–review and editing, Investigation.

Funding

The author(s) declare that financial support was received for the research, authorship, and/or publication of this article. This research was supported by the Kermanshah University of Medical Sciences (Grant no. 4000831), Kermanshah, Iran and Dirección de Investigación Científica y Tecnológica - Universidad de Santiago de Chile (DICYT-USACH) project 022341EM_Ayudante, Chile.

Conflict of interest

The authors declare that the research was conducted in the absence of any commercial or financial relationships that could be construed as a potential conflict of interest.

The author(s) declared that they were an editorial board member of Frontiers, at the time of submission. This had no impact on the peer review process and the final decision.

Publisher's note

All claims expressed in this article are solely those of the authors and do not necessarily represent those of their affiliated organizations, or those of the publisher, the editors and the reviewers. Any product that may be evaluated in this article, or claim that may be made by its manufacturer, is not guaranteed or endorsed by the publisher.

References

Aebi, H. (1984). Catalase *in vitro*. *Methods Enzym.* 105, 121–126. doi:10.1016/S0076-6879(84)05016-3

Ahmed, R. U., Alam, M., and Zheng, Y.-P. (2019). Experimental spinal cord injury and behavioral tests in laboratory rats. *Heliyon* 5, e01324. doi:10.1016/j.heliyon.2019.e01324

Anjum, A., Yazid, M. D., Fauzi Daud, M., Idris, J., Ng, A. M. H., Selvi Naicker, A., et al. (2020). Spinal cord injury: pathophysiology, multimolecular interactions, and underlying recovery mechanisms. *Int. J. Mol. Sci.* 21, 7533. doi:10.3390/ijms21207533

Bheereddy, P., Yerra, V. G., Kalvala, A. K., Sherkhane, B., and Kumar, A. (2021). SIRT1 activation by polydatin alleviates oxidative damage and elevates mitochondrial biogenesis in experimental diabetic neuropathy. *Cell. Mol. Neurobiol.* 41, 1563–1577. doi:10.1007/s10571-020-00923-1

Carrasco, C., Naziroğlu, M., Rodríguez, A. B., and Pariente, J. A. (2018). Neuropathic pain: delving into the oxidative origin and the possible implication of transient receptor potential channels. *Front. Physiol.* 9, 95. doi:10.3389/fphys.2018.00095

Chandra, J., Samali, A., and Orrenius, S. (2000). Triggering and modulation of apoptosis by oxidative stress. *Free Radic. Biol. Med.* 29, 323–333. doi:10.1016/S0891-5849(00)00302-6

Chen, G., Yang, Z., Wen, D., Guo, J., Xiong, Q., Li, P., et al. (2021). Polydatin has anti-inflammatory and antioxidant effects in LPS-induced macrophages and improves DSS-induced mice colitis. *Immun. Inflamm. Dis.* 9, 959–970. doi:10.1002/iid3.455

Chen, H.-H., and Wang, D. L. (2004). Nitric oxide inhibits matrix metalloproteinase-2 expression via the induction of activating transcription factor 3 in endothelial cells. *Mol. Pharmacol.* 65, 1130–1140. doi:10.1124/mol.65.5.1130

Chen, Y., Zhang, D., Liao, Z., Wang, B., Gong, S., Wang, C., et al. (2015). Anti-oxidant polydatin (piceid) protects against substantia nigral motor degeneration in multiple rodent models of Parkinson's disease. *Mol. Neurodegener.* 10, 4. doi:10.1186/1750-1326-10-4

Conti, A., Miscusi, M., Cardali, S., Germanò, A., Suzuki, H., Cuzzocrea, S., et al. (2007). Nitric oxide in the injured spinal cord: synthases cross-talk, oxidative stress and inflammation. *Brain Res. Rev.* 54, 205–218. doi:10.1016/j.brainresrev.2007.01.013

Cregg, J. M., DePaul, M. A., Filous, A. R., Lang, B. T., Tran, A., and Silver, J. (2014). Functional regeneration beyond the glial scar. *Exp. Neurol.* 253, 197–207. doi:10.1016/j.expneurol.2013.12.024

Eyer, P., and Podhradský, D. (1986). Evaluation of the micromethod for determination of glutathione using enzymatic cycling and Ellman's reagent. *Anal. Biochem.* 153, 57–66. doi:10.1016/0003-2697(86)90061-8

Fakhri, S., Dargahi, L., Abbaszadeh, F., and Jorjani, M. (2018). Astaxanthin attenuates neuroinflammation contributed to the neuropathic pain and motor dysfunction following compression spinal cord injury. *Brain Res. Bull.* 143, 217–224. doi:10.1016/j.brainresbull.2018.09.011

Fakhri, S., Dargahi, L., Abbaszadeh, F., and Jorjani, M. (2019). Effects of astaxanthin on sensory-motor function in a compression model of spinal cord injury: involvement of ERK and AKT signalling pathway. *Eur. J. Pain* 23, 750–764. doi:10.1002/ejp.1342

Fakhri, S., Gravandi, M. M., Abdian, S., Akkol, E. K., Farzaei, M. H., and Sobarzo-Sánchez, E. (2021a). The neuroprotective role of polydatin: neuropharmacological mechanisms, molecular targets, therapeutic potentials, and clinical perspective. *Molecules* 26, 5985. doi:10.3390/molecules26195985

Fakhri, S., Kiani, A., Jalili, C., Abbaszadeh, F., Piri, S., Farzaei, M. H., et al. (2021b). Intrathecal administration of melatonin ameliorates the neuroinflammation- mediated sensory and motor dysfunction in A rat model of compression spinal cord injury. *Curr. Mol. Pharmacol.* 14, 646–657. doi:10.2174/1874467213666201230101811

Fakhri, S., Piri, S., Moradi, S. Z., and Khan, H. (2022a). Phytochemicals targeting oxidative stress, interconnected neuroinflammatory, and neuroapoptotic pathways following radiation. *Curr. Neuropharmacol.* 20, 836–856. doi:10.2174/1570159X19666210809103346

Fakhri, S., Sabouri, S., Kiani, A., Farzaei, M. H., Rashidi, K., Mohammadi-Farani, A., et al. (2022b). Intrathecal administration of naringenin improves motor dysfunction and neuropathic pain following compression spinal cord injury in rats: relevance to its antioxidant and anti-inflammatory activities. *Korean J. Pain* 35, 291–302. doi:10.3344/kjp.2022.35.3.291

Hassler, S. N., Johnson, K. M., and Hulsebosch, C. E. (2014). Reactive oxygen species and lipid peroxidation inhibitors reduce mechanical sensitivity in a chronic neuropathic pain model of spinal cord injury in rats. *J. Neurochem.* 131, 413–417. doi:10.1111/jnc.12830

Hu, X., Xu, W., Ren, Y., Wang, Z., He, X., Huang, R., et al. (2023). Spinal cord injury: molecular mechanisms and therapeutic interventions. *Signal Transduct. Target. Ther.* 8, 245. doi:10.1038/s41392-023-01477-6

Jia, Z., Zhu, H., Li, J., Wang, X., Misra, H., and Li, Y. (2012). Oxidative stress in spinal cord injury and antioxidant-based intervention. *Spinal Cord.* 50, 264–274. doi:10.1038/sc.2011.111

Karami, A., Fakhri, S., Kooshki, L., and Khan, H. (2022). Polydatin: pharmacological mechanisms, therapeutic targets, biological activities, and health benefits. *Molecules* 27, 6474. doi:10.3390/molecules27196474

Kauppila, T. (2000). Cold exposure enhances tactile allodynia transiently in mononeuropathic rats. *Exp. Neurol.* 161, 740–744. doi:10.1006/exnr.1999.7287

Kjell, J., and Olson, L. (2016). Rat models of spinal cord injury: from pathology to potential therapies. *Dis. Model. Mech.* 9, 1125–1137. doi:10.1242/dmm.025833

Lanzilli, G., Cottarelli, A., Nicotera, G., Guida, S., Ravagnan, G., and Fuggetta, M. P. (2012). Anti-inflammatory effect of resveratrol and polydatin by *in vitro* IL-17 modulation. *Inflammation* 35, 240–248. doi:10.1007/s10753-011-9310-z

Luo, J., Chen, S., Wang, L., Zhao, X., and Piao, C. (2022). Pharmacological effects of polydatin in the treatment of metabolic diseases: a review. *Phytomedicine* 102, 154161. doi:10.1016/j.phymed.2022.154161

Lv, R., Du, L., Liu, X., Zhou, F., Zhang, Z., and Zhang, L. (2019a). Polydatin alleviates traumatic spinal cord injury by reducing microglial inflammation via regulation of iNOS and NLRP3 inflammasome pathway. *Int. Immunopharmacol.* 70, 28–36. doi:10.1016/j.intimp.2019.02.006

Lv, R., Du, L., Zhang, L., and Zhang, Z. (2019b). Polydatin attenuates spinal cord injury in rats by inhibiting oxidative stress and microglia apoptosis via Nrf2/HO-1 pathway. *Life Sci.* 217, 119–127. doi:10.1016/j.lfs.2018.11.053

Şöhretoğlu, D., Baran, M. Y., Arroo, R., and Kuruüzüm-Uz, A. (2018). Recent advances in chemistry, therapeutic properties and sources of polydatin. *Phytochem. Rev.* 17, 973–1005. doi:10.1007/s11101-018-9574-0

Stewart, A. N., Glaser, E. P., Mott, C. A., Bailey, W. M., Sullivan, P. G., Patel, S. P., et al. (2022a). Advanced age and neurotrauma diminish glutathione and impair antioxidant defense after spinal cord injury. *J. Neurotrauma* 39, 1075–1089. doi:10.1089/neu.2022.0010

Stewart, A. N., Jones, L. A. T., and Gensel, J. C. (2022b). Improving translatability of spinal cord injury research by including age as a demographic variable. *Front. Cell. Neurosci.* 16, 1017153. doi:10.3389/fncel.2022.1017153

Sun, G., Chen, Y., Zhou, Z., Yang, S., Zhong, C., and Li, Z. (2017). A progressive compression model of thoracic spinal cord injury in mice: function assessment and pathological changes in spinal cord. *Neural Regen. Res.* 12, 1365–1374. doi:10.4103/1673-5374.213693

Sun, J., Zhang, X., Broderick, M., and Fein, H. (2003). Measurement of nitric oxide production in biological systems by using griess reaction assay. *Sensors* 3, 276–284. doi:10.3390/s30800276

Wang, H.-L., Gao, J.-P., Han, Y.-L., Xu, X., Wu, R., Gao, Y., et al. (2015). Comparative studies of polydatin and resveratrol on mutual transformation and antioxidative effect *in vivo*. *Phytomedicine* 22, 553–559. doi:10.1016/j.phymed.2015.03.014

Xi, P., Mao, R., Wu, S., Liu, L., Cai, C., Lu, L., et al. (2022). Using network pharmacology and animal experiment to investigate the therapeutic mechanisms of polydatin against vincristine-induced neuropathic pain. *Mediat. Inflamm.* 2022, 6010952–6011013. doi:10.1155/2022/6010952

Zeng, P.-Y., Tsai, Y.-H., Lee, C.-L., Ma, Y.-K., and Kuo, T.-H. (2023). Minimal influence of estrous cycle on studies of female mouse behaviors. *Front. Mol. Neurosci.* 16, 1146109. doi:10.3389/fnmol.2023.1146109

Zhan, J., Luo, D., Zhao, B., Chen, S., Luan, J., Luo, J., et al. (2022). Polydatin administration attenuates the severe sublesional bone loss in mice with chronic spinal cord injury. *Aging (Albany. NY)* 14, 8856–8875. doi:10.18632/aging.204382

Zhang, N., Yin, Y., Xu, S.-J., Wu, Y.-P., and Chen, W.-S. (2012). Inflammation and apoptosis in spinal cord injury. *Indian J. Med. Res.* 135, 287–296. Available at: http://www.ncbi.nlm.nih.gov/pubmed/22561613.

Zhang, Z., Sun, Z., Jia, R., Jiang, D., Xu, Z., Zhang, Y., et al. (2024). Protective effects of polydatin against bone and joint disorders: the *in vitro* and *in vivo* evidence so far. *Nutr. Res. Rev.* 37, 96–107. doi:10.1017/S0954422423000082

frontiers | Frontiers in Pharmacology

TYPE Original Research
PUBLISHED 25 September 2024
DOI 10.3389/fphar.2024.1469602

Check for updates

OPEN ACCESS

EDITED BY
Pukar Khanal,
Emory University, United States

REVIEWED BY
Smita Kumari,
The Ohio State University, United States
Kunal Bhattacharya,
Pratiksha Institute of Pharmaceutical Sciences (PIPS), India
Zsolt Gall,
George Emil Palade University of Medicine, Pharmacy, Sciences and Technology of Târgu Mureş, Romania

*CORRESPONDENCE
Chin-Yi Cheng,
c5398@ms22.hinet.net

RECEIVED 24 July 2024
ACCEPTED 16 September 2024
PUBLISHED 25 September 2024

CITATION
Huang S-C, Huang H-C, Liao W-L, Kao S-T and Cheng C-Y (2024) Neuroprotective effects of *Gastrodia elata* Blume on promoting M2 microglial polarization by inhibiting JNK/TLR4/T3JAM/NF-κB signaling after transient ischemic stroke in rats.
Front. Pharmacol. 15:1469602.
doi: 10.3389/fphar.2024.1469602

COPYRIGHT
© 2024 Huang, Huang, Liao, Kao and Cheng. This is an open-access article distributed under the terms of the Creative Commons Attribution License (CC BY). The use, distribution or reproduction in other forums is permitted, provided the original author(s) and the copyright owner(s) are credited and that the original publication in this journal is cited, in accordance with accepted academic practice. No use, distribution or reproduction is permitted which does not comply with these terms.

Neuroprotective effects of *Gastrodia elata* Blume on promoting M2 microglial polarization by inhibiting JNK/TLR4/T3JAM/NF-κB signaling after transient ischemic stroke in rats

Shang-Chih Huang[1], Hui-Chi Huang[2], Wen-Ling Liao[3], Shung-Te Kao[2] and Chin-Yi Cheng[4,5]*

[1]Department of Neurology, China Medical University Hospital, Taichung, Taiwan, [2]School of Chinese Medicine, College of Chinese Medicine, China Medical University, Taichung, Taiwan, [3]Graduate Institute of Integrated Medicine, College of Chinese Medicine, China Medical University, Taichung, Taiwan, [4]School of Post-Baccalaureate Chinese Medicine, College of Chinese Medicine, China Medical University, Taichung, Taiwan, [5]Department of Chinese Medicine, Hui-Sheng Hospital, Taichung, Taiwan

Background: *Gastrodia elata* Blume, also called Tian Ma (TM), has been used to treat stroke for centuries. However, its effects on inflammation in acute cerebral ischemic injury and underlying mechanisms involved in microglial polarization remain unknown. The present study explored the effects of the TM extract on the modulation of microglial M1/M2 polarization 2 days after transient cerebral ischemia.

Methods: Male Sprague Dawley rats were intracerebroventricularly administered with 1% dimethyl sulfoxide 25 min before cerebral ischemia and subsequently intraperitoneally administered 0.25 g/kg (DO + TM-0.25 g), 0.5 g/kg (DO + TM-0.5 g), or 1 g/kg (DO + TM-1 g) of the TM extract after cerebral ischemia onset.

Results: DO + TM-0.5 g and DO + TM-1 g treatments downregulated the following: phospho-c-Jun N-terminal kinase (p-JNK)/JNK, tumor necrosis factor (TNF) receptor-associated factor 3 (TRAF3), TRAF3-interacting JNK-activating modulator (T3JAM), p-nuclear factor-kappa B p65 (p-NF-κB p65)/NF-κB p65, ionized calcium-binding adapter molecule 1 (Iba1), CD86, TNF-α, interleukin (IL)-1β, and IL-6 expression and toll-like receptor 4 (TLR4)/Iba1, CD86/Iba1, and p-NF-κB p65/Iba1 coexpression. These treatments also upregulated IL-10, nerve growth factor, and vascular endothelial growth factor A expression and YM-1/2/Iba1 and IL-10/neuronal nuclei coexpression in the cortical ischemic rim. The JNK inhibitor SP600125 exerted similar treatment effects as the DO + TM-0.5 g and DO + TM-1 g treatments.

Conclusion: DO + TM-0.5 g and DO + TM-1 g/kg treatments attenuate cerebral infarction by inhibiting JNK-mediated signaling. TM likely exerts the

neuroprotective effects of promoting M1 to M2 microglial polarization by inhibiting JNK/TLR4/T3JAM/NF-κB-mediated signaling in the cortical ischemic rim 2 days after transient cerebral ischemia.

KEYWORDS

Gastrodia elata Blume, cerebral ischemia, C-Jun N-terminal kinase, toll-like receptor 4, TRAF3-interacting JNK-activating modulator

Introduction

In acute cerebral ischemia, the major pathological mechanism underlying neurological injury is the inflammatory response and the involvement of resident microglia (Xiang et al., 2018; Song et al., 2021). The neuroinflammation and immune reactions that occur after cerebral ischemia/reperfusion (I/R) injury can exacerbate cerebral infarction (Gan et al., 2020). Toll-like receptors (TLRs), one of the transmembrane pattern recognition receptor families, expressed on antigen-presenting cells, including microglia and macrophages, can respond to damage-associated molecular patterns (DAMPs), inducing inflammatory reaction (Ashayeri et al., 2021). TLR4 triggers downstream inflammatory cascades through myeloid differentiation primary response protein 88 (MyD88)/tumor necrosis factor (TNF) receptor-associated factor (TRAF) 6- and TRAF3/TRAF3-interacting c-Jun N-terminal kinase (JNK)-activating modulator (T3JAM)-mediated nuclear factor-kappa B (NF-κB) activation. Studies reported that the TRAF3/T3JAM signaling pathway is closely related to the activation of JNK- and TLR4/NF-κB-mediated signaling (Dadgostar et al., 2003; Li et al., 2019). Furthermore, TLR4-mediated signaling pathways activate the downstream targets JNK and p38 mitogen-activated protein kinase (MAPK), which in turn induce TLR4 upregulation, amplifying TLR4/NF-κB-mediated signaling and exacerbating infarct expansion in the acute stage of ischemic stroke (Cheng et al., 2021; Dong et al., 2021). Thus, the interaction between JNK (p38 MAPK) and TLR4 plays a crucial role in TLR4/T3JAM/NF-κB-associated inflammatory cascades (Cheng et al., 2021). NF-κB, a proinflammatory transcription factor, is expressed in glial cells as a heterodimer of RelA (p65) and p50 subunits; it binds to its endogenous inhibitor IκB in the inactive state. The interaction of TLR4 with DAMPs triggers the activation of IκB kinase, phosphorylating and degrading IκB and resulting in the nuclear translocation of NF-κB and the production of inflammation-related genes in cerebral ischemia (Jover-Mengual et al., 2021). Moreover, the phosphorylation of NF-κB p65 (S536) results in its decreased affinity for IκBα, causing excessive activation and nuclear translocation of NF-κB p65 (Christian et al., 2016). In response to cerebral ischemia, the cytosolic multiprotein complexes of inflammasomes are formed, leading to the secretion of proinflammatory mediators (de Zoete et al., 2014). Among inflammasomes, nucleotide-binding oligomerization domain and leucine-rich repeat (NLR) family pyrin domain containing 3 (NLRP3) is one of the best characterized components of the NLR family that mediates caspase-1 activation and subsequently induces the secretion of proinflammatory factors, such as interleukin-1β (IL-1β) and IL-18, thereby initiating inflammatory cascades (Kelley et al., 2019). By contrast, inhibition of inflammasome components, such as NLRP3 and caspase-1, can alleviate cerebral infarct expansion in acute ischemic stroke (Luo et al., 2022).

The TLR4/JNK (p38 MAPK)/NF-κB-mediated inflammatory signaling pathway is positively correlated with glial NLRP3 inflammasome activity and plays a vital role in microglial activation and polarization (Dong et al., 2021; Jover-Mengual et al., 2021). Microglia are involved in both central nervous system injury and recovery, and these functions are linked to their ability for polarization into the proinflammatory (M1) or anti-inflammatory (M2) phenotype after activation (Ye et al., 2019). In the early stage of cerebral ischemic insults, TLR4-induced microglia are rapidly activated and polarized into M1 and M2 phenotypes in response to the inflammatory cascade and M1 and M2 microglia are characterized by the markers CD86 and YM-1/2, respectively (Wen et al., 2018; Wang et al., 2020; Dong et al., 2021). Within 24 h after cerebral ischemia onset, activated microglia that migrate or infiltrate into the ischemic area are mainly polarized into the M2 phenotype, and they release neurotrophic factors and anti-inflammatory mediators, promoting myelin regeneration, debris clearance, and nerve repair in the ischemic core. Subsequently, the activated microglia are polarized into the proinflammatory M1 phenotype, initiating the release of proinflammatory factors in the peri-infarct area, thereby aggravating ischemic stroke (Xiang et al., 2018; Yusuying et al., 2022). Thus, the increased M1 to M2 ratio is closely related to ischemic injury during transient focal cerebral ischemia, whereas pharmacological interventions for promoting M2 microglia protect against ischemic brain damage (Dong et al., 2021; Wang et al., 2022).

Gastrodia elata Blume (also called Tian Ma [TM]), a well-known traditional Chinese herbal medicine, has long been used for treating convulsions, dizziness, headache, limb numbness, and stroke (Wang et al., 2019). TM reduces cerebral infarct partly by inhibiting TNF-α expression in the cortical ischemic rim in acute ischemic stroke (Seok et al., 2019). Gastrodin and parishin C are the biologically active compounds isolated from TM (Lin et al., 2021). Gastrodin ameliorates ischemic stroke by downregulating TNF-α and IL-1β expression in the ischemic area in the acute (Peng et al., 2015) and subacute (Liu et al., 2016) stages of transient middle cerebral artery (MCA) occlusion. Its anti-inflammatory effects are partly due to the activation of nuclear factor erythroid 2-related factor 2-mediated signaling in the ischemic region after transient MCA occlusion (Peng et al., 2015). Parishin C exerts neuroprotective effects partly by suppressing TNF-α, IL-1β, and IL-6 expression in the cortical ischemic rim in the acute stage of transient MCA occlusion (Wang et al., 2021). Anisalcohol derived from TM has been reported to exert anti-neuroinflammatory effects by inhibiting M1 polarization and promoting M2 polarization in lipopolysaccharide-stimulated BV2 microglial cells (Xiang et al., 2018). Taken together, these findings indicate that TM and its main ingredients might provide

TABLE 1 Primary antibodies used in the present study.

Host	Primary antibody	Western blot (Dilution)	IF (Dilution)	Supplier/catalog No.
Rab	p-JNK	1:1000		CST/#9251
Rab	JNK	1:1000		CST/#9252
Rab	p-p38 MAPK	1:1000		CST/#9211
Rab	p38 MAPK	1:1000		CST/#9212
Rab	TRAF6	1:1000		abcam/ab40675
Rab	TRAF3	1:500		abcam/ab36988
Rab	T3JAM	1:500		Merck/SAB4503206
Rab	p-NF-κB p65	1:1000	1:200	CST/#3033
Rab	NF-κB p65	1:1000		abcam/ab16502
Rab	NLRP3	1:1000		abcam/ab263899
Rab	Iba1	1:1000	1:100	abcam/ab178846
Rab	Nrf2	1:1000		abcam/ab92946
Rab	VEGF-A	1:1000		Proteintech/#19003-1-AP
Mou	CD86	1:1000	1:100	abcam/ab220188
Rab	TNF-α	1:1000		abcam/ab205587
Mou	IL-6	1:2000		abcam/ab9324
Rab	YM-1/2	1:10000	1:100	abcam/ab192029
Rab	IL-10	1:1000		abcam/ab192271
Rab	NGF	1:1000		abcam/ab6199
Mou	Actin (loading control)	1:5000		Novus Biologicals/NB600-501
Mou	TLR4		1:100	abcam/ab22048
Mou	Iba1		1:100	abcam/ab283319
Rab	Il-10		1:100	abcam/ab9969
Mou	NeuN		1:100	Merck Millipore/MAB377

Rab, Rabbit; Mou, Mouse; CST, cell signaling technology; VEGF-A, vascular endothelial growth factor A; NGF, nerve growth factor; NeuN, neuronal nuclei.

beneficial effects against ischemic stroke by inhibiting proinflammatory factor expression during cerebral ischemia. However, the detailed pathway involved in the modulation of microglial polarization of the TM extract in acute ischemic stroke remains unclear. In this study, we explored the anti-inflammatory effects of the TM extract on microglia M1 and M2 polarization in the cortical ischemic rim 2 days after transient MCA occlusion.

Materials and methods

TM extract preparation

TM extract powder (Batch Number A0418102) was obtained from Kaohsiung Chuang Song Zong (KCSZ) Pharmaceutical Co., Ltd. (Taiwan). The dried rhizomes of TM were imported from Sichuan Province, China, and their quality was evaluated in KCSZ Ligang Laboratory (Taiwan). The data and voucher specimens from KCSZ Ligang Laboratory were confirmed by Professor Jin-Pin Lin (China Medical University, Taiwan) based on the Chinese Pharmacopoeia (11th Edition). TM extract powder was produced as follows: TM dry rhizomes were boiled in boiling water for 1.5 h, and the aqueous extract of TM was obtained. The aqueous extract and corn starch as an excipient were granulated and dried in a fluidized bed dryer. Each gram of the TM extract powder comprised 0.5 g each of the TM extract and corn starch. The TM extract solution was made by dissolving 2 g TM extract powder in 8 mL of normal saline and then centrifuging at 1,000 g at 4°C for 10 min. The supernatant fraction of the TM extract solution (0.125 g/mL) was used for TM treatment.

Ultra-performance liquid chromatography analysis of the TM extract marker

Gastrodin (>98% purity; Sunhank Technology, Tainan, Taiwan) was dissolved in methanol (10 mg/mL) and used to make six standard solutions (concentration ranging from 1.0 to

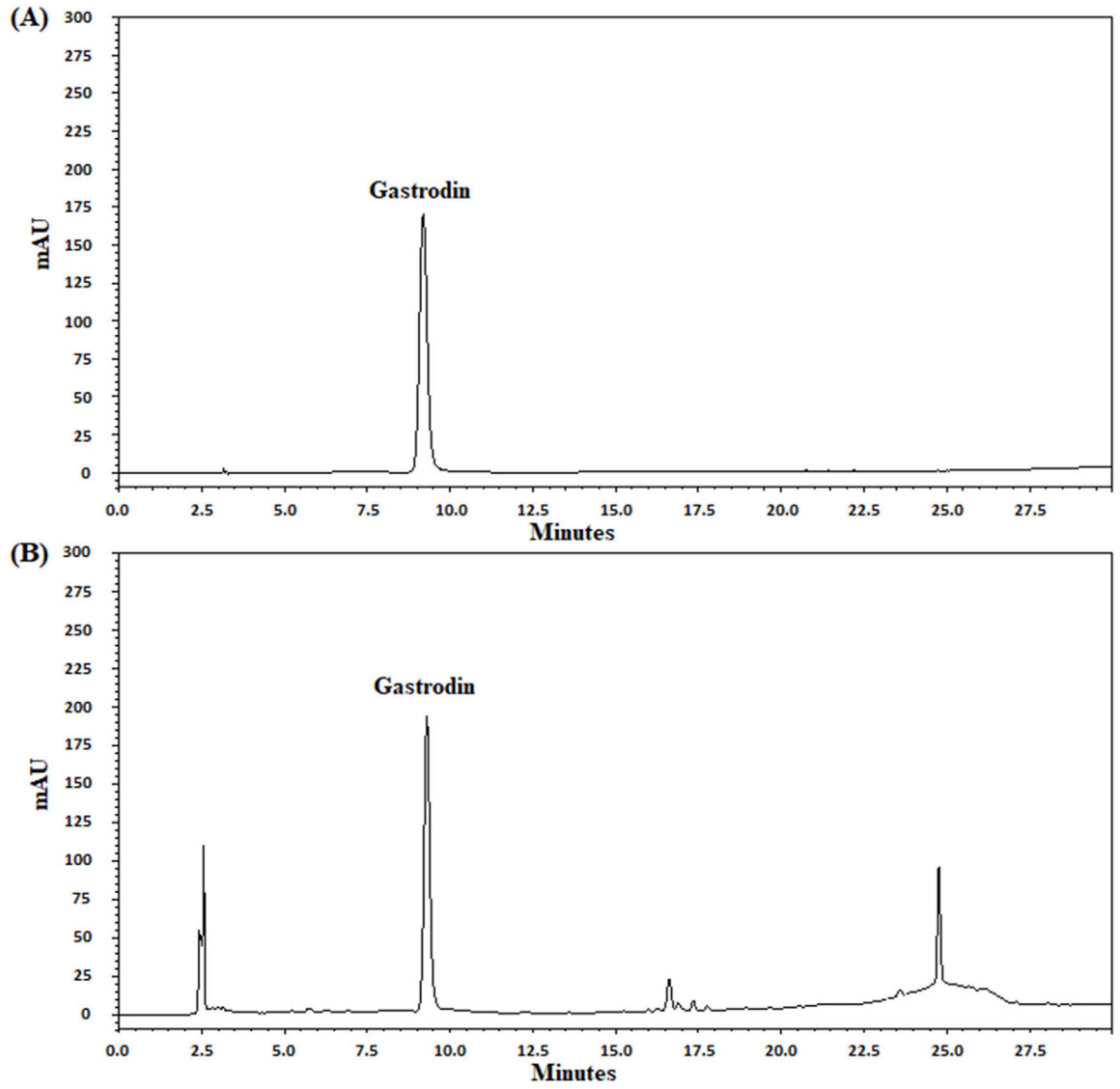


FIGURE 1
UPLC chromatograms of gastrodin in the TM extract. UPLC chromatograms **(A, B)** indicate the standard (gastrodin) and TM extract solutions, respectively. mAU, milli-absorbance unit.

0.01562 mg/mL) for ultra-performance liquid chromatography (UPLC). The sample solution of the TM extract was prepared by dissolving it in methanol. A Shimadzu LC-2060C 3D UPLC system (Kyoto, Japan) equipped with a Fortis C18 column (250 × 4.6 mm, 5 μm; maintained at 30°C) was used to screen and identify the chemical marker. Next, 5 μL of a gastrodin standard or TM extract solution was injected using a mobile phase of water (solvent A) and methanol (solvent B) (v/v). The UPLC was programmed as follows: 0–10 min, 10% B; 10–30 min, 10% B to 70% B. The flow rate (1.0 mL/min) and the photodiode array detector (220 nm) were set.

Animals and transient MCA occlusion

Male Sprague Dawley rats (300–320 g) were purchased from Bio-LASCO (Taipei, Taiwan). The rats used in this study were housed under standard laboratory conditions (room temperature [RT]: 22°C ± 2°C; relative humidity: 55% ± 10%; light/dark cycle: 12/12 h) with free access to water and food. The sample size used in this study was determined based on our previous studies (Cheng et al., 2021; Tsai et al., 2022) and that could offer sufficient statistical power. All the animal experiments were conducted strictly in line with the guidelines of the Institutional Animal Care and Use Committee of China Medical University (No. CMUIACUC-2021-318). The rat model of MCA occlusion was established as previously described (Tsai et al., 2022). In brief, the rats were initially anesthetized with 5% isoflurane and fixed to the stereotaxic frame by the ear bars. Their skulls were exposed by cutting the scalp skins transversely. A small hole was made in the skull (right side, 1.5 mm posterior to the bregma and lateral to the midline). A nylon monofilament (0.2 mm in diameter) was introduced into the internal carotid artery for interrupting the blood flow to the MCA,

10.3389/fphar.2024.1469602

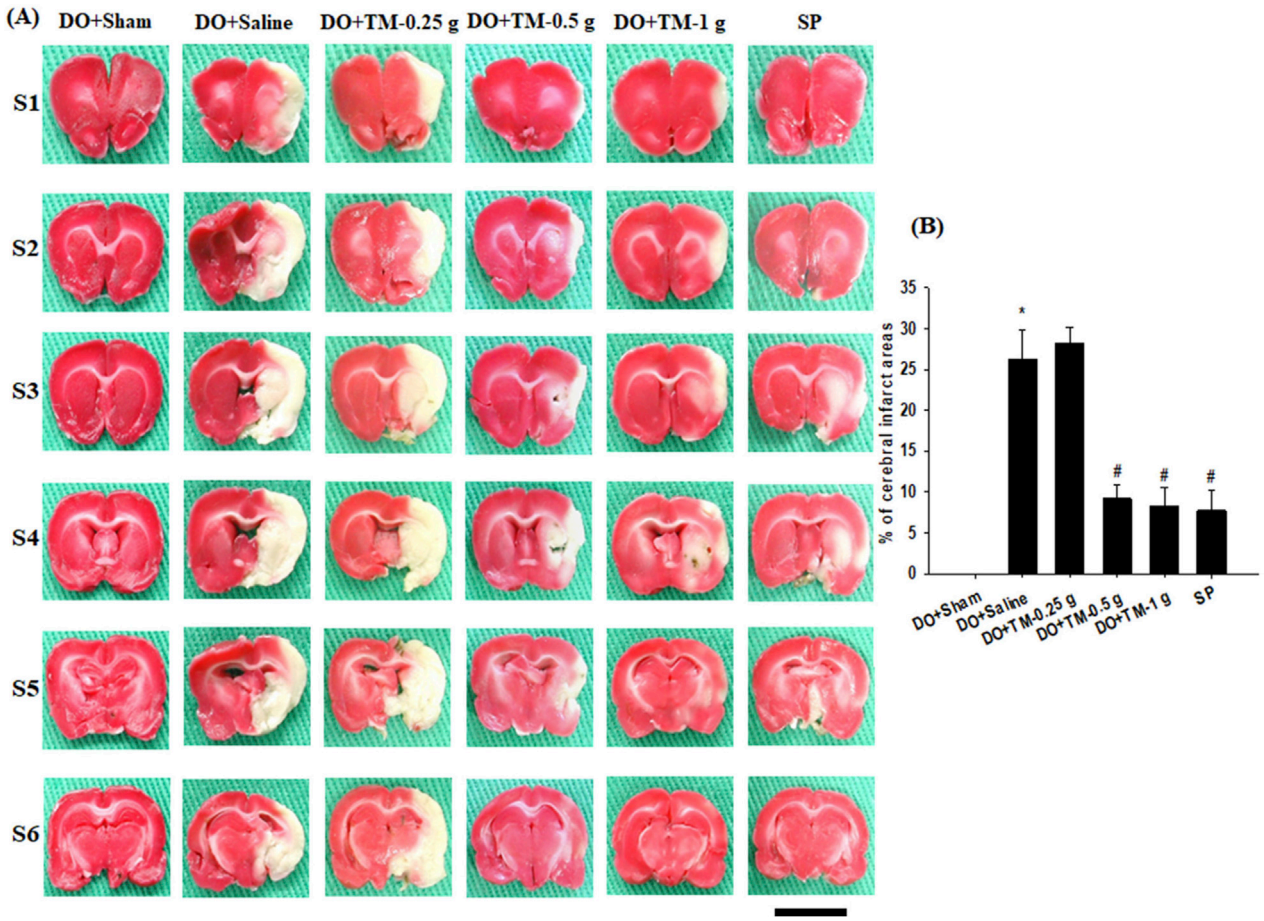


FIGURE 2
Effects of DO + TM-0.5 g and DO + TM-1 g treatments on cerebral infarct. **(A)** Selected TTC-stained brain slices (S1–S6) of the DO + Sham, DO + Saline, DO + TM-0.25 g, DO + TM-0.5 g, DO + TM-1 g, and SP groups (n = 6) reveal infarct areas (pale white) and normal tissues (dark red). **(B)** The bar graph shows the infarct percentages in the experimental groups 2 days after reperfusion. $^{*}P < 0.05$ vs. DO + Sham; $^{\#}P < 0.05$ vs. DO + Saline. Scale bar indicates 1 cm.

TABLE 2 The NFSs in the experimental groups (n = 16).

Group	DO + Sham	DO + Saline	DO + TM-025 g	DO + TM-0.5 g	DO + TM-1 g	SP
Day 1	0.0 (0–0)	8.0 (7–9)*	8.0 (7–10)	4.5 (4–6)#	5.0 (3–6)#	5.0 (3–6)#
Day 2	0.0 (0–0)	8.0 (7–11)*	8.0 (7–11)	4.0 (3–6)#	4.0 (2–6)#	4.0 (3–5)#

Each value was expressed as median (range). NFSs, neurological function scores; $^{*}P < 0.05$ vs. DO + Sham; $^{\#}P < 0.05$ vs. DO + Saline.

causing MCA occlusion. After 2 h of MCA occlusion, the nylon monofilament was carefully withdrawn to allow MCA reperfusion. The establishment of the MCA occlusion model was verified through changes in the MCA blood flow, which were monitored using a laser Doppler blood flowmeter (DRT4; Moor Instruments, Wilmington, DE, United States). Successful establishment of the MCA occlusion model was defined as a reduction in the MCA blood flow to 10%–20% of baseline during the ischemia period and an increase in the MCA blood flow to 70% of baseline during the reperfusion period. In the ischemia period, the rats were awake and subjected to modified neurological severity score (mNSS) tests to assess neurological function. Except in the DO + Sham group, the rats with neurological function scores (NFSs) less than 7 revealed incomplete MCA occlusion and were excluded from the study. All the experimental animals were administered intramuscularly with ketorolac, a non-steroidal anti-inflammatory drug, at 1 mg/kg after surgery to reduce pain, suffering and distress.

Neurological evaluation

The rats were subjected to mNSS tests to evaluate neurological function at 1 and 2 days after reperfusion for motor (muscle strength and walking ability), sensory (placing and proprioception), balance, and reflex (pinna reflex, corneal reflex, and startle reflex) testing, as previously described (Cheng et al., 2021). NFSs were determined

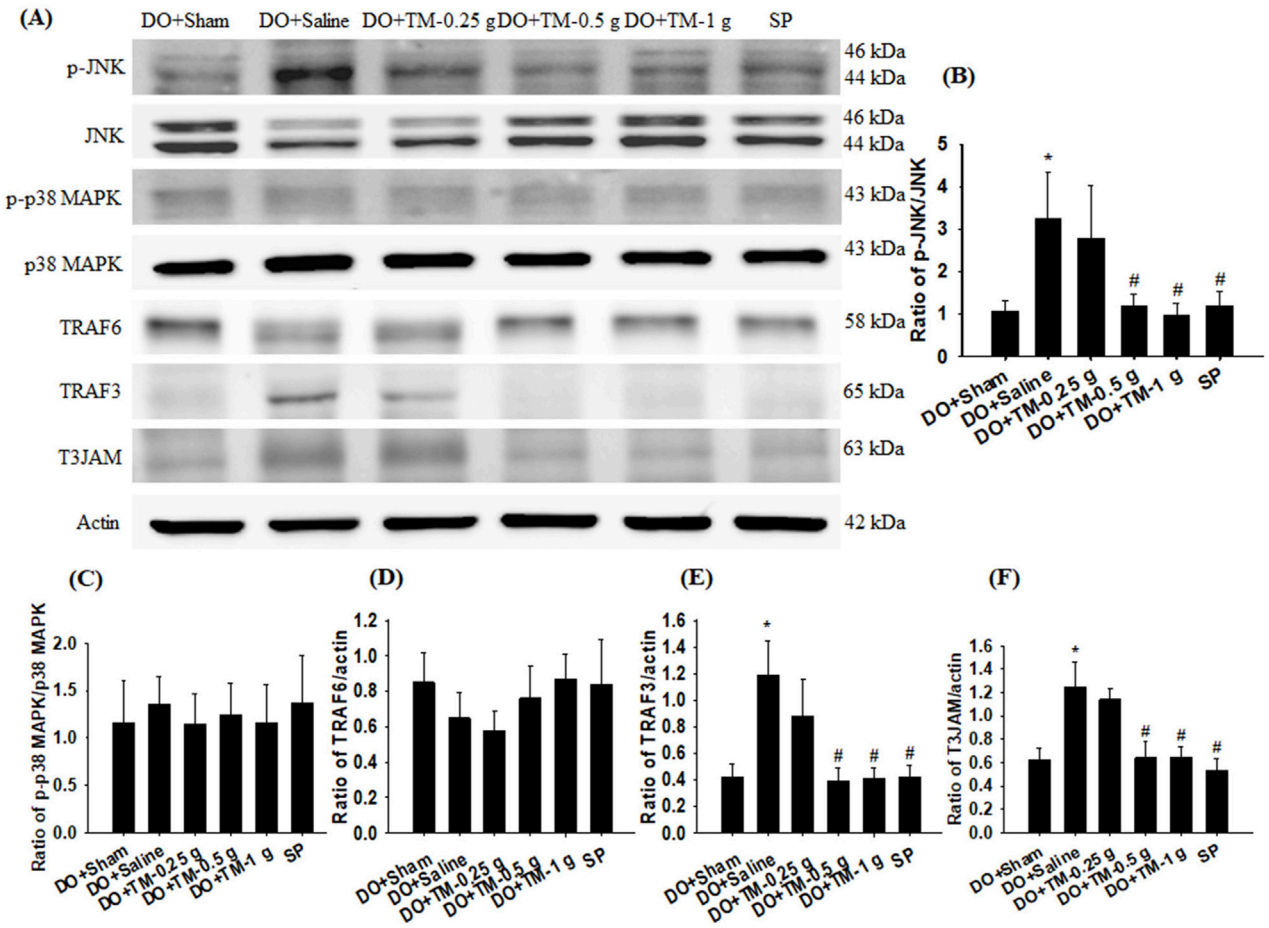


FIGURE 3
Protein expression of MAPKs, TRAF6, TRAF3, and T3JAM in the cortical ischemic rim. **(A)** Selected Western blot images reveal p-JNK, JNK, p-p38 MAPK, p38 MAPK, TRAF6, TRAF3, T3JAM, and actin expression in the cortical ischemic rim in the DO + Sham, DO + Saline, DO + TM-0.25 g, DO + TM-0.5 g, DO + TM-1 g, and SP groups (n = 5) 2 days after reperfusion. Quantification of the ratios of **(B)** p-JNK to JNK, **(C)** p-p38 MAPK to p38 MAPK, **(D)** TRAF6 to actin, **(E)** TRAF3 to actin, and **(F)** T3JAM to actin was performed in the experimental groups. *$P < 0.05$ vs. DO + Sham; #$P < 0.05$ vs. DO + Saline.

based on the neurological examination results, which range from 0 (normal) to 18 (maximal neurological deficit). In this study, the neurological evaluation and cell identification and counting were performed by an experienced laboratory assistant who was blinded to the grouping state.

Experiment A

Grouping

Thirty-six rats were randomly assigned to six groups (n = 6 each): DO + Sham, DO + Saline, DO + TM-0.25 g, DO + TM-0.5 g, DO + TM-1 g, and SP groups. The doses of the TM extract administered in the TM treatment groups were determined through preliminary experiments. The TM treatment groups were administered intracerebroventricularly with 1% dimethyl sulfoxide (DMSO) 25 min before MCA occlusion; after MCA occlusion onset, the rats were injected intraperitoneally with the TM extract at 0.25 g/kg for the DO + TM-0.25 g group, 0.5 g/kg for the DO + TM-0.5 g group, and 1 g/kg for the DO + TM-1 g group. After 2 days of reperfusion, the rats were subjected to neurological evaluation; they were then killed through CO_2 inhalation (flow rate: 5.5 L/min), and their brains were harvested. The DO + Saline group was treated in the same protocols as the DO + TM-1 g group, except normal saline was administered instead of the TM extract. The DO + Sham group was treated in the same protocols as the DO + Saline group; however, the MCA was not blocked. The SP group was treated in the same protocols as the DO + Saline group; however, the rats were administered intracerebroventricularly with SP600125, a JNK inhibitor, instead of 1% DMSO.

Intracerebroventricular administration of 1% DMSO or SP600125

Twenty-five minutes before MCA occlusion, the rats were administered intracerebroventricularly with 10 μL of 1% DMSO or 10 μL of SP600125 solution (2 mM in 1% DMSO, ab120065, Abcam, Waltham, MA, United States) through a burr hole in the right side of the skull using a microsyringe (10 μL, Hamilton Company, Reno, NV, United States), as previously described (Cheng et al., 2021).

TABLE 3 The ratios of target proteins in Western blot analysis in the experimental groups (n = 5).

Group	DO + Sham	DO + Saline	DO + TM-0.25 g	DO + TM-0.5 g	DO + TM-1 g	SP
p-JNK/JNK	1.07 ± 0.23	3.24 ± 1.08*	2.79 ± 1.23	1.19 ± 0.28#	0.97 ± 0.28#	1.19 ± 0.34#
p-p38/p38	1.16 ± 0.44	1.35 ± 0.30	1.14 ± 0.33	1.24 ± 0.34	1.16 ± 0.40	1.37 ± 0.50
TRAF6/actin	0.85 ± 0.17	0.65 ± 0.14	0.58 ± 0.11	0.76 ± 0.18	0.87 ± 0.14	0.84 ± 0.25
TRAF3/actin	0.42 ± 0.10	1.19 ± 0.26*	0.88 ± 0.28	0.39 ± 0.10#	0.41 ± 0.08#	0.42 ± 0.09#
T3JAM/actin	0.62 ± 0.10	1.25 ± 0.21*	1.14 ± 0.10	0.64 ± 0.14#	0.65 ± 0.09#	0.53 ± 0.10#
p-NF-κB/NF-κB	0.47 ± 0.05	1.77 ± 0.48*	1.52 ± 0.23	0.47 ± 0.07#	0.42 ± 0.05#	0.49 ± 0.06#
NLRP3/actin	0.65 ± 0.05	1.49 ± 0.21*	1.51 ± 0.24	0.64 ± 0.05#	0.70 ± 0.12#	0.63 ± 0.08#
Iba1/actin	0.79 ± 0.09	1.27 ± 0.16*	1.25 ± 0.10	0.80 ± 0.06#	0.72 ± 0.13#	0.75 ± 0.12#
VEGF-A/actin	1.42 ± 0.19	0.55 ± 0.18*	0.47 ± 0.11	0.95 ± 0.20#	1.35 ± 0.14#	1.02 ± 0.21#
CD86/actin	0.52 ± 0.03	1.08 ± 0.19*	1.01 ± 0.09	0.58 ± 0.07#	0.57 ± 0.09#	0.55 ± 0.06#
TNF-α/actin	0.37 ± 0.05	1.07 ± 0.04*	0.97 ± 0.12	0.40 ± 0.07#	0.41 ± 0.05#	0.42 ± 0.09#
IL-1β/actin	0.40 ± 0.03	0.72 ± 0.11*	0.72 ± 0.09	0.43 ± 0.04#	0.43 ± 0.05#	0.37 ± 0.06#
IL-6/actin	0.33 ± 0.07	0.67 ± 0.09*	0.65 ± 0.06	0.33 ± 0.04#	0.34 ± 0.05#	0.31 ± 0.03#
YM-1/2/actin	0.93 ± 0.14	0.29 ± 0.12*	0.28 ± 0.12	0.73 ± 0.09#	1.06 ± 0.28#	0.83 ± 0.17#
IL-10/actin	0.62 ± 0.04	0.46 ± 0.06*	0.53 ± 0.06	0.65 ± 0.04#	0.68 ± 0.05#	0.67 ± 0.09#
NGF/actin	0.82 ± 0.07	0.41 ± 0.03*	0.42 ± 0.06	0.74 ± 0.10#	0.92 ± 0.12#	0.74 ± 0.15#

Each value was expressed as mean ± standard deviation. p-p38/p38, p-p38 MAPK/p38 MAPK; p-NF-κB/NF-κB, p-NF-κB p65/NF-κB p65. *$P < 0.05$ vs. DO + Sham; #$P < 0.05$ vs. DO + Saline.

Cerebral infarction assessment

The harvested rat brains were cut into six 2-mm-thick sections for cerebral infarct assessment, as previously described (Cheng et al., 2021). In brief, the sections were stained using 2% 2,3,5-triphenyltetrazolium chloride (TTC; Merck, St. Louis, MO, United States) at 37°C for 5 min. Quantification of the percentage of cerebral infarct areas (divided by the total coronal sectional area) was performed using ImageJ (NIH, Bethesda, MD, United States).

Experiment B

Grouping

Thirty rats were randomly assigned to six groups (n = 5 each)—DO + Sham, DO + Saline, DO + TM-0.25 g, DO + TM-0.5 g, DO + TM-1 g, and SP groups—with the same procedures and protocols as those described for Experiment A.

Western blot analysis

In the harvested rat brains, The MCA territory was separated and removed. The right cortical ischemic rims (between 3 and 9 mm from the ischemic core) that were cut from the separated ischemic cortices were collected for Western blot analysis, as previously described (Cheng et al., 2017). The homogenized protein samples were separated based on size through sodium dodecyl sulfate–polyacrylamide gel (10%) electrophoresis. After electrophoresis, the separated proteins were transferred from the gel onto a nitrocellulose (NC) membrane (Hybond-c Extra, Amersham Biosciences, United Kingdom) in transfer buffer. The NC membrane was incubated in 5% skim milk containing 0.1% Tween 20 at RT for 60 min to block nonspecific binding. The target proteins on NC membranes were incubated with primary antibodies diluted in phosphate buffered saline (PBS) containing 5% bovine serum albumin (BSA) (Table 1) at 4°C overnight and then with goat anti-rabbit (1:5000 in PBS/5% BSA, AB_2313567, Jackson, PA, United States) or goat anti-mouse (1:5000 in PBS/5% BSA, AB_10015289, Jackson, PA, United States) IgG secondary antibody at RT for 1 h. Finally, the NC membranes were incubated with an enhanced chemiluminescence reagent (ECL-plus GE Healthcare) and then detected using the FUJIFILM luminescent image analyzer (LAS-3000, Tokyo, Japan). Densitometric analysis of Western blots was performed using ImageJ software.

Experiment C

Grouping

Thirty rats were randomly assigned to six groups (n = 5 each)—DO + Sham, DO + Saline, DO + TM-0.25 g, DO + TM-0.5 g, DO + TM-1 g, and SP groups—with the same procedures and protocols as those described for Experiment A.

Double immunofluorescence staining

The harvested rat brains were embedded in tissue freezing medium, frozen, and cut into 15-μm thick slices, which were used for double immunofluorescence (IF) staining, as previously described (Cheng et al., 2020). The brain slices were postfixed with 4% paraformaldehyde at RT for 15 min, stained with primary

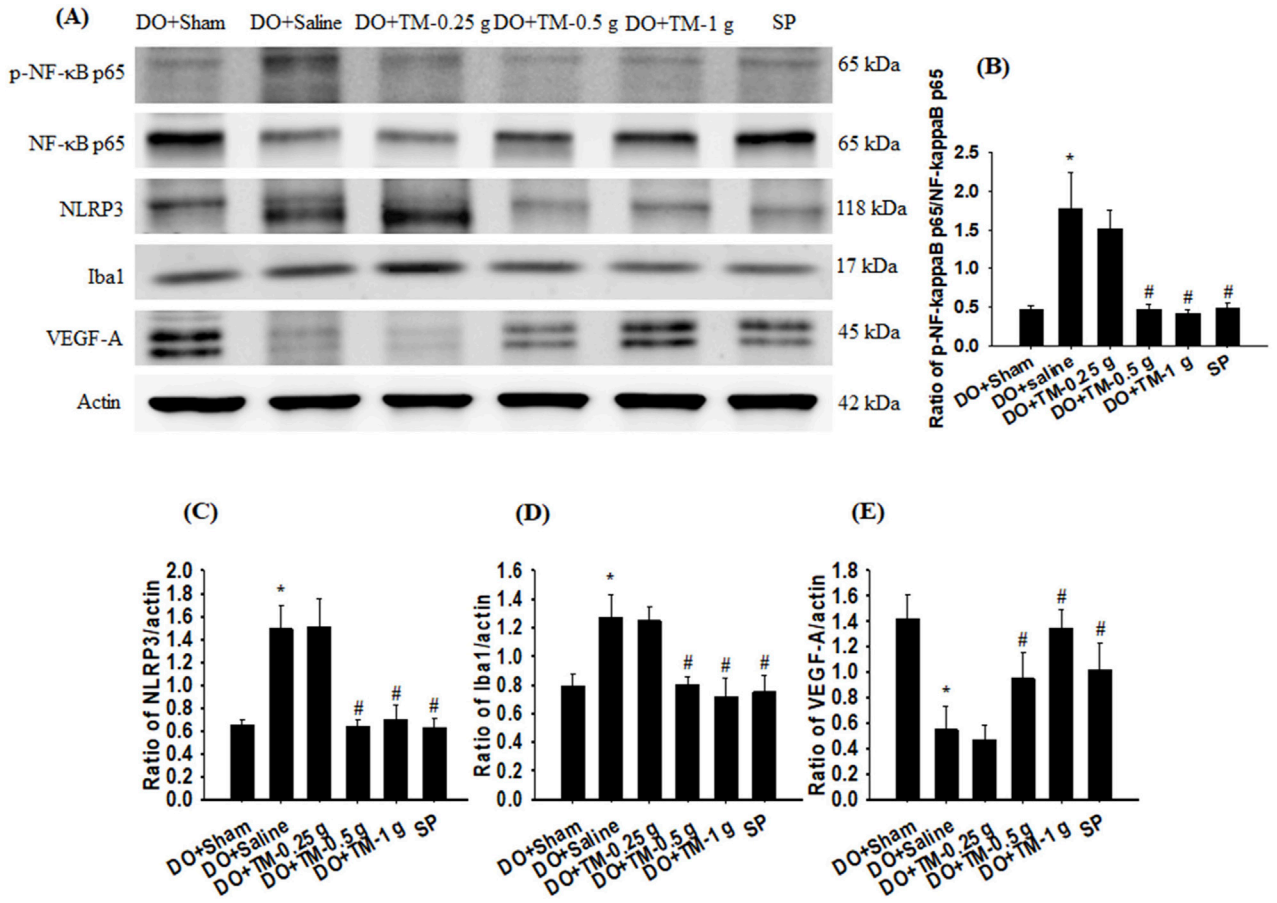


FIGURE 4
Protein expression of p-NF-κB p65, NF-κB p65, NLRP3, Iba1, Nrf2, and VEGF-A in the cortical ischemic rim. **(A)** Selected Western blot images reveal p-NF-κB p65, NF-κB p65, NLRP3, Iba1, Nrf2, VEGF-A, and actin expression in the cortical ischemic rim in the DO + Sham, DO + Saline, DO + TM-0.25 g, DO + TM-0.5 g, DO + TM-1 g, and SP groups (n = 5) 2 days after reperfusion. Quantification of the ratios of **(B)** p-NF-κB p65 to NF-κB p65, **(C)** NLRP3 to actin, **(D)** Iba1 to actin, and **(E)** VEGF-A to actin was performed in the experimental groups. *$P < 0.05$ vs. DO + Sham; #$P < 0.05$ vs. DO + Saline.

antibodies diluted in PBS/5% BSA (revealed in Table 1) at 4°C overnight, and simultaneously stained with DyLight 594-conjugated AffiniPure goat anti-mouse (red, 1:100 in PBS/5% BSA, AB_2338871, Jackson, PA, United States) and DyLight 488-conjugated AffiniPure goat anti-rabbit (green, 1:100 in PBS/5% BSA, AB_2338046, Jackson, PA, United States) IgG secondary antibodies at 37°C for 1.5 h. The colocalization of IF signals of two markers more than or equal to 50% in a cell was defined as double-labeled positive. Immunopositive cells in the selected cortical ischemic rim were counted in nine fields of view at 400 × magnification using fluorescence microscopic methods (CKX53; Olympus, Tokyo, Japan). The double-labeled TLR4/Iba1, CD86/Iba1, p-NF-κB p65/Iba1, YM-1/2/Iba1, and IL-10/NeuN cells were counted and expressed as percentage of immunopositive cells in the selected cortical ischemic rim.

Statistical analysis

All the experimental data, except the neurological examination, were investigated using one-way ANOVA with *post hoc* Bonferroni test and are presented as mean ± standard deviation. The data obtained from the neurological examination were investigated using one-way ANOVA with Mann-Whitney U test and are presented as median (range). In these tests, p values <0.05 were deemed statistically significant.

Results

UPLC analysis of the marker of the TM extract

In UPLC analysis, gastrodin retention times from the standard and TM extract solutions were 9.21 and 9.30 min, respectively. Moreover, the gastrodin content in the TM extract was 0.21 mg/mL (Figures 1A, B).

Effects of TM treatments on brain infarcts

TTC staining of coronal sections after 2 days of reperfusion revealed no infarct area in the DO + Sham group. By contrast, the infarct areas of the brain coronal sections were significantly higher in

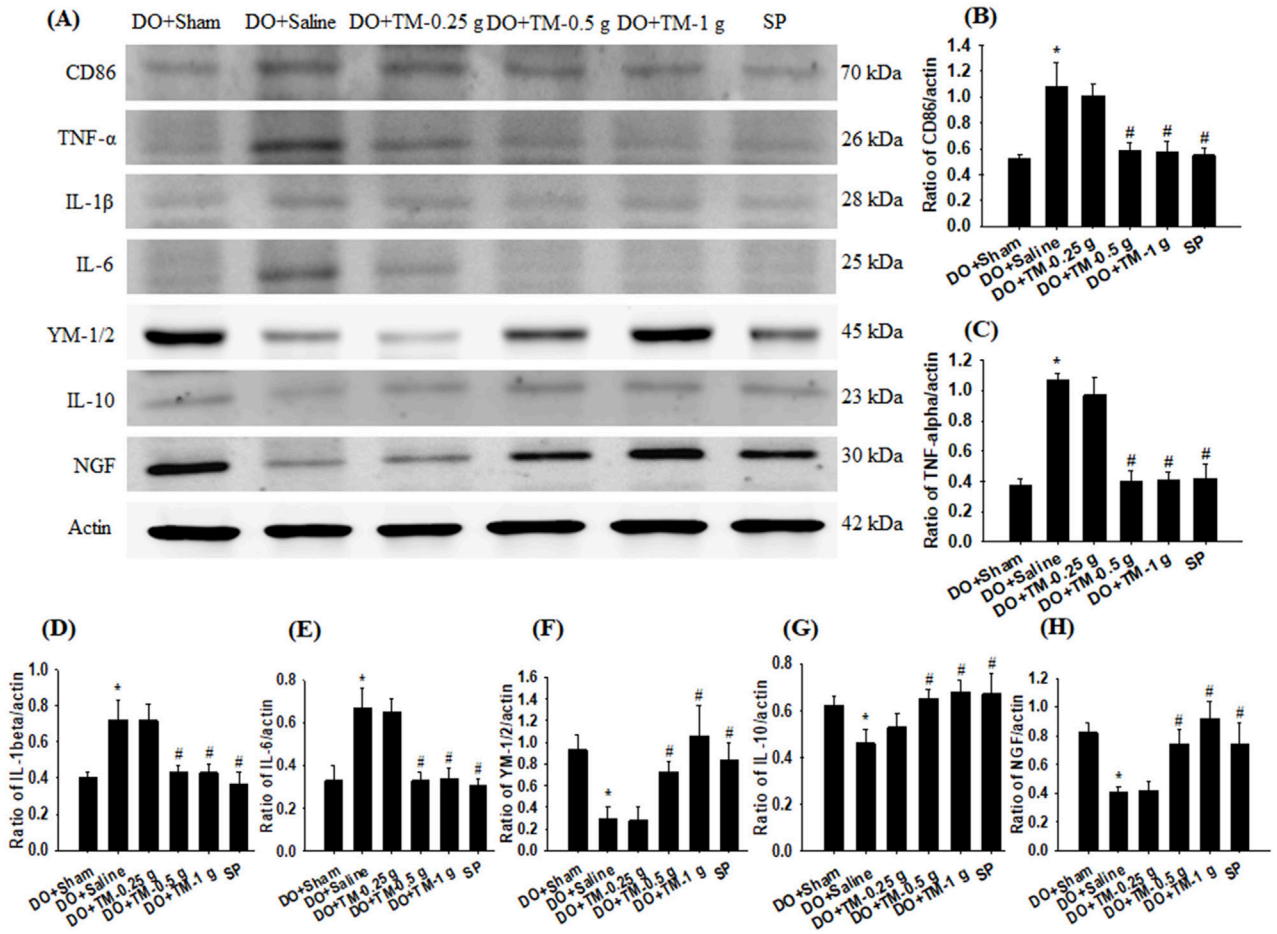


FIGURE 5
Protein expression of CD86, TNF-α, IL-1β, IL-6, YM-1/2, IL-10, and NGF in the cortical ischemic rim. **(A)** Selected Western blot images reveal CD86, TNF-α, IL-1β, IL-6, YM-1/2, IL-10, NGF, and actin expression in the cortical ischemic rim in the DO + Sham, DO + Saline, DO + TM-0.25 g, DO + TM-0.5 g, DO + TM-1 g, and SP groups (n = 5) 2 days after reperfusion. Quantification of the ratios of **(B)** CD86 to actin, **(C)** TNF-α to actin, **(D)** IL-1β to actin, **(E)** IL-6 to actin, **(F)** YM-1/2 to actin, **(G)** IL-10 to actin, and **(H)** NGF to actin was performed in the experimental groups. *$P < 0.05$ vs. DO + Sham; #$P < 0.05$ vs. DO + Saline.

the DO + Saline group than in the DO + Sham group ($P < 0.05$) and were significantly lower in the DO + TM-0.5 g, DO + TM-1 g, and SP groups than in the DO + Saline group (all $P < 0.05$; Figures 2A, B).

Effects of TM treatments on neurological deficits

The NFSs were markedly greater in the DO + Saline group compared to those in the DO + Sham group ($P < 0.05$). In addition, compared with the DO + Saline group, the NFSs were significantly lower in the DO + TM-0.5 g, DO + TM-1 g, and SP groups (all $P < 0.05$; Table 2) at 1 and 2 days after ischemic stroke.

Effects of TM treatments on the levels of MAPKs, TRAF6, TRAF3, and T3JAM

The ratios of p-JNK to JNK, TRAF3 to actin, and T3JAM to actin in the cortical ischemic rim were significantly higher in the DO + Saline group than in the DO + Sham group (all $P < 0.05$). In addition, there were significantly lower in the ratios of the aforementioned proteins in the DO + TM-0.5 g, DO + TM-1 g, and SP groups than in the DO + Saline group 2 days after reperfusion (all $P < 0.05$; Figures 3A, B, E, F and Table 3). The ratios of p-p38 MAPK to p38 MAPK and TRAF6 to actin in the cortical ischemic rim were not significantly different in the experimental groups ($P > 0.05$; Figures 3A, C, D and Table 3).

Effects of TM treatments on the levels of p-NF-κB p65, NF-κB p65, NLRP3, ionized calcium-binding adapter molecule 1, and vascular endothelial growth factor A

The ratios of p-NF-κB p65 to NF-κB p65, NLRP3 to actin, and ionized calcium-binding adapter molecule 1 (Iba1) to actin in the cortical ischemic rim were significantly higher in the DO + Saline group than in the DO + Sham group (all $P < 0.05$). In addition, the ratios of the aforementioned proteins were significantly lower in the

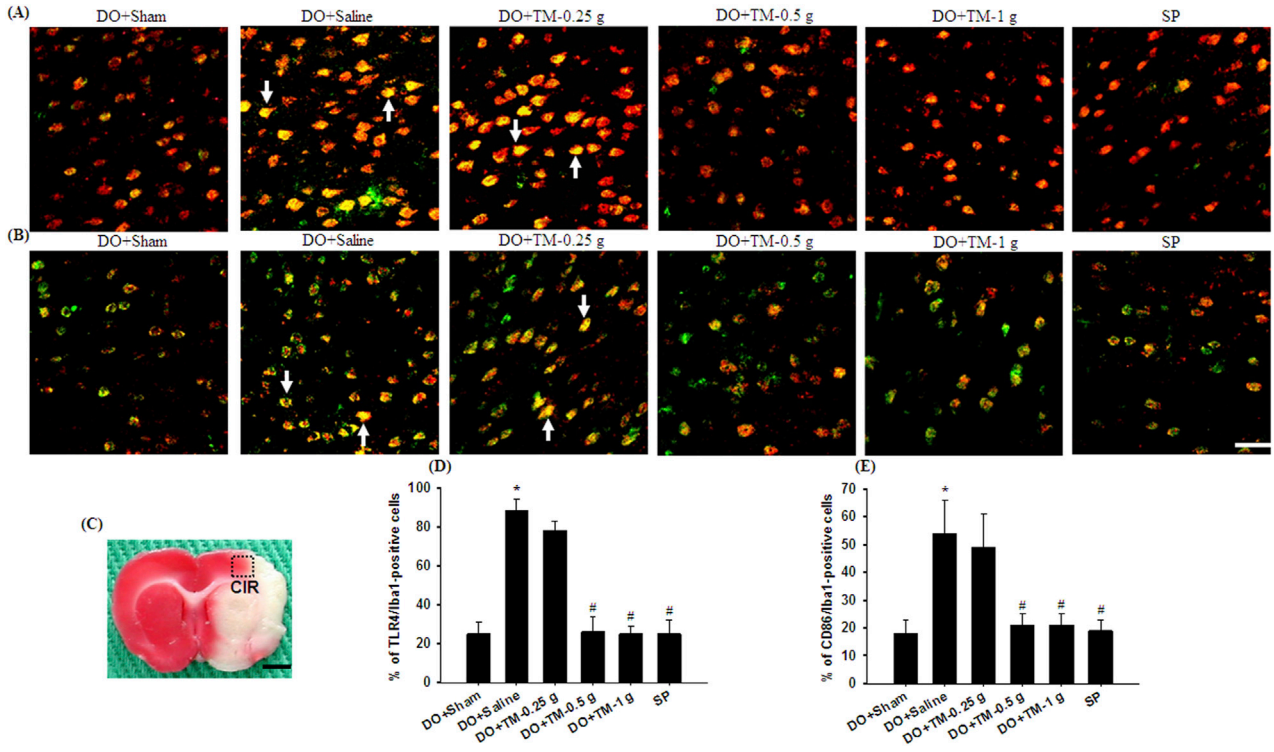


FIGURE 6
The percentages of TLR4/Iba1-and CD86/Iba1-positive cells in the cortical ischemic rim. Representative IF images reveal **(A)** TLR4 (red)/Iba1 (green) and **(B)** CD86 (red)/Iba1 (green) expression in the cortical ischemic rim in the DO + Sham, DO + Saline, DO + TM-0.25 g, DO + TM-0.5 g, DO + TM-1 g, and SP groups (n = 5) 2 days after reperfusion. Arrows in **(A, B)** point to TLR4/Iba1 (yellow)- and CD86/Iba1 (yellow)-positive cells, respectively. **(C)** The dashed line square in a representative coronal section shows the region where immunopositive cells were detected. CIR, cortical ischemic rim. Dashed line square equals 1 mm^2. Scale bar indicates **(B)** 50 μm and **(C)** 2 mm. Quantification of the percentages of **(D)** TLR4/Iba1-and **(E)** CD86/Iba1-positive cells was performed in the experimental groups. *P < 0.05 vs. DO + Sham; #P < 0.05 vs. DO + Saline.

DO + TM-0.5 g, DO + TM-1 g, and SP groups compared to those in the DO + Saline group 2 days after reperfusion (all P < 0.05; Figures 4A–D and Table 3). By contrast, the ratio of vascular endothelial growth factor A (VEGF-A) to actin in the cortical ischemic rim was significantly lower in the DO + Saline group than in the DO + Sham group (P < 0.05) and was significantly higher in the DO + TM-0.5 g, DO + TM-1 g, and SP groups than in the DO + Saline group (P < 0.05; Figures 4A, E and Table 3).

Effects of TM treatments on the levels of CD86, TNF-α, IL-1β, IL-6, YM-1/2, IL-10, and nerve growth factor

The ratios of CD86 to actin, TNF-α to actin, IL-1β to actin, and IL-6 to actin in the cortical ischemic rim were significantly higher in the DO + Saline group than in the DO + Sham group (all P < 0.05) and were significantly lower in the DO + TM-0.5 g, DO + TM-1 g, and SP groups than in the DO + Saline group 2 days after reperfusion (all P < 0.05; Figures 5A–E and Table 3). By contrast, the ratios of YM-1/2 to actin, IL-10 to actin, and nerve growth factor (NGF) to actin in the cortical ischemic rim were significantly lower in the DO + Saline group than in the DO + Sham group (all P < 0.05) and were significantly higher in the DO + TM-0.5 g, DO + TM-1 g, and SP groups than in the DO + Saline group (all P < 0.05; Figures 5A, F–H and Table 3).

Effects of TM treatments on the levels of TLR4/Iba1-, CD86/Iba1-, p-NF-κB p65/Iba1-, YM-1/2/Iba1-, and IL-10/neuronal nuclei-positive cells

TLR4-, $CD86^-$, p-NF-κB p65-, and partial YM-1/2-positive cells were colocalized with Iba1 in the cortical ischemic rim (Figures 6A, B, 7A, B-1–B-3, 8A). In addition, p-NF-κB p65/Iba1 double-labeled cells were examined in the nucleus (Figures 7B-4, B-5) and IL-10-positive cells were colocalized with neuronal nuclei (NeuN) in the cortical ischemic rim (Figure 8B). All the above-mentioned double-labeled cells were examined in the selected cortical ischemic rim (Figure 6C). The percentages of TLR4/Iba1-, CD86/Iba1-, and p-NF-κB p65/Iba1-positive cells in the cortical ischemic rim were significantly greater in the DO + Saline group compared to those in the DO + Sham group. In addition, the percentages of above-mentioned positive cells were significantly lower in the DO + TM-0.5 g, DO + TM-1 g, and SP groups than in the DO + Saline group 2 days after reperfusion (all P < 0.05; Figures 6A, B, D, E, 7A, C). By contrast, the percentages of YM-1/2/Iba1-and IL-10/NeuN-positive cells in the cortical ischemic rim were significantly lower in the DO + Saline group compared to those in the DO + Sham group and were significantly greater in the DO + TM-0.5 g, DO + TM-1 g, and SP groups compared to those in the DO + Saline group (all P < 0.05; Figures 8A–D).

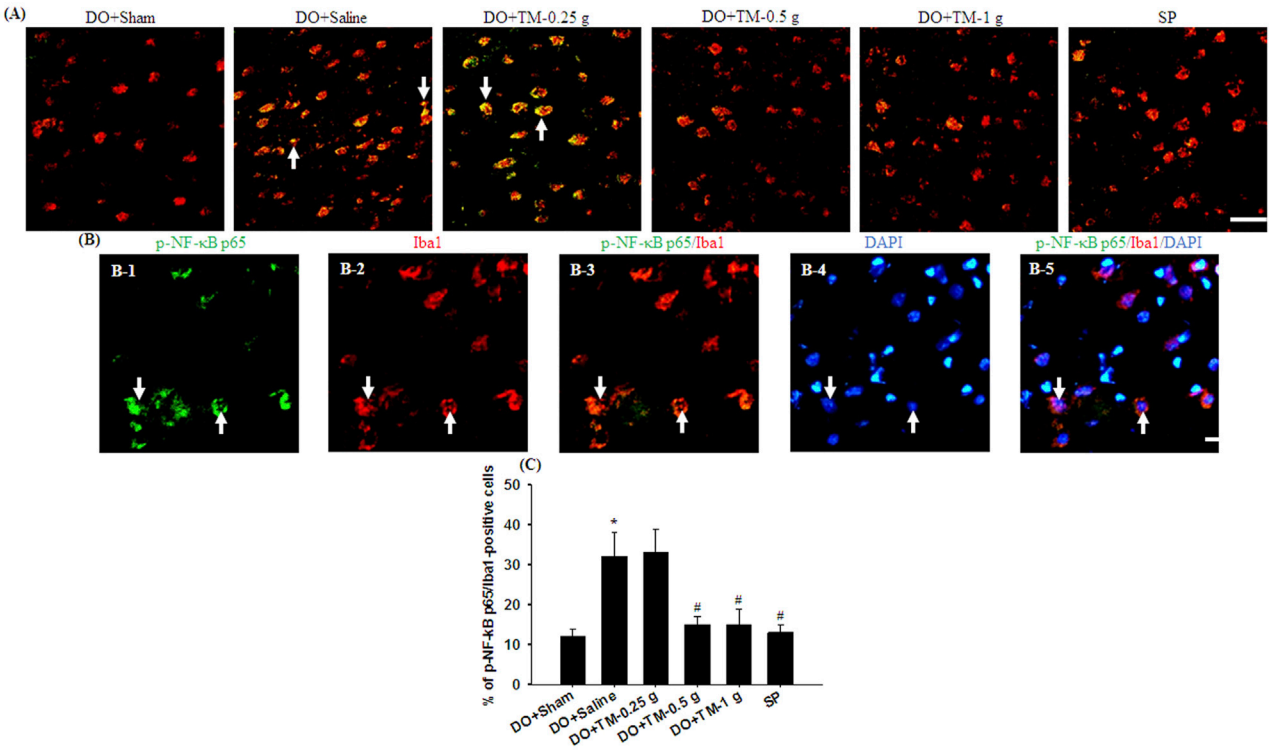


FIGURE 7
The percentage of p-NF-κB p65/Iba1-positive cells in the cortical ischemic rim. **(A)** Representative IF images reveal p-NF-κB p65 (green)/Iba1 (red) expression in the cortical ischemic rim in the DO + Sham, DO + Saline, DO + TM-0.25 g, DO + TM-0.5 g, DO + TM-1 g, and SP groups (n = 5) 2 days after reperfusion. Arrows in **(A)**, **(B-1)**, **(B-2)**, **(B-3)**, **(B-4)**, and **(B-5)** point to p-NF-κB p65/Iba1 (yellow)-, p-NF-κB p65 (green)-, Iba1 (red)-, p-NF-κB p65/Iba1 (yellow)-, DAPI (blue)-, and p-NF-κB p65/Iba1/DAPI (light pink)-positive cells, respectively. Scale bar indicates **(A)** 50 μm and **(B)** 10 μm. Quantification of the percentage of **(C)** p-NF-κB p65/Iba1-positive cells was performed in the experimental groups. DAPI, 4′,6-diamidino-2-phenylindole (used as a nuclear counterstain). $^{*}P < 0.05$ vs. DO + Sham; $^{\#}P < 0.05$ vs. DO + Saline.

Discussion

Post-ischemic inflammation plays a vital role in cerebral infarction in the acute stage of transient cerebral ischemia (Zhang et al., 2021). Furthermore, the interaction between TLR4- and JNK (p38 MAPK)-mediated inflammatory signaling pathways induces the downstream activation of the NF-κB pathway, amplifying microglial activation and exacerbating I/R injury in acute ischemic stroke (Cheng et al., 2021; Zhang et al., 2021). UPLC analysis revealed that gastrodin (a marker of the TM extract) contents were 0.42, 0.84, and 1.68 mg in 0.25, 0.5, and 1 g/kg of the TM extract solutions, respectively. Moreover, our results revealed that cerebral infarction and neurological deficits were predominantly created 2 days after transient MCA occlusion. However, 0.5 and 1 g/kg, but not 0.25 g/kg, of the TM extract significantly reduced infarct areas and promoted neurological function recovery. Moreover, Western blotting and double IF staining revealed that the levels of p-JNK/JNK and TLR4/Iba1 (microglia marker), but not of p-p38 MAPK/p38 MAPK, were markedly increased in the cortical ischemic rim. However, 0.5 and 1 g/kg TM restored these levels of p-JNK and TLR4 in the cortical ischemic rim, reducing the interaction between JNK- and TLR4-mediated inflammatory cascades in microglia in the acute stage after transient cerebral ischemia. Overall, the findings imply that TM treatments protect against cerebral infarction at least partly by suppressing the interaction between JNK and TLR4 in microglia in the cortical ischemic rim 2 days after transient MCA occlusion.

TLR4 expressed on activated microglia recognizes DAMPs and then triggers MyD88/TRAF6- and TRAF3/T3JAM-mediated inflammatory signaling pathways (Wang et al., 2011; Cheng et al., 2021). TLR4 expression plays a vital role in innate immunity. Moreover, TLR4-induced neuroinflammation through downstream NF-κB signaling activation is positively correlated with ischemic stroke severity (Wang et al., 2015). The results of the current study indicated that the expression of TRAF3, but not of TRAF6, was markedly upregulated in the cortical ischemic rim, whereas TM treatments reversed the increased expression of TRAF3 and T3JAM in the acute stage of transient MCA occlusion. TRAF3 is a central regulator of ischemic signaling pathways, and it participates in apoptosis, inflammation, and oxidative stress events in acute ischemic stroke (Gong et al., 2015). T3JAM, a coiled-coil membrane protein, is predominantly expressed in the immune system and interacts with TRAF3 (Li et al., 2019). Their interaction in the cytosol amplifies JNK activation (Dadgostar et al., 2003) and causes TLR4-induced nuclear translocation of the NF-κB p65 subunit in acute cerebral ischemia (Gong et al., 2015; Cheng et al., 2021). The NF-κB family comprises five members: p50, P52, p65, c-Rel, and Rel-B. In cerebral I/R injury, p65 phosphorylation enhances the stability of the NF-κB complex, which is translocated to the nucleus for

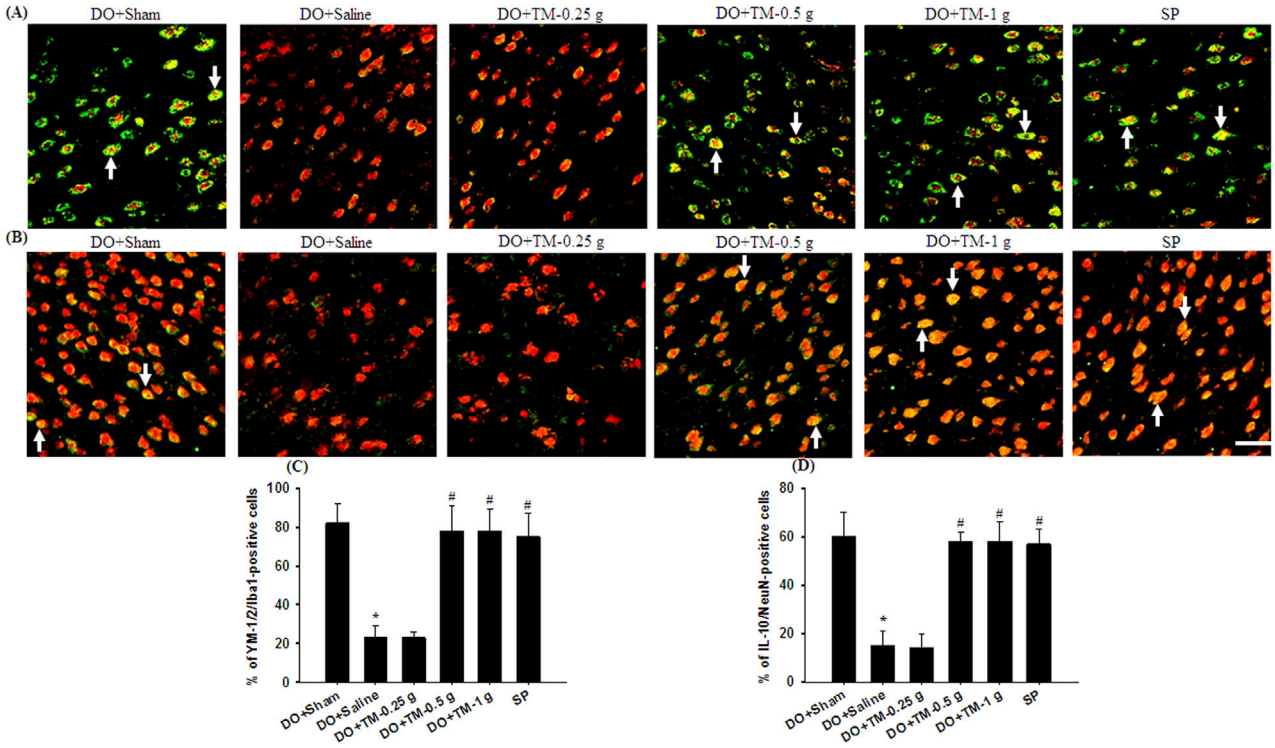


FIGURE 8
The percentages of YM-1/2/Iba1-and IL-10/NeuN-positive cells in the cortical ischemic rim. Representative IF images reveal **(A)** YM-1/2 (green)/Iba1 (red) and **(B)** IL-10 (green)/NeuN (red) expression in the cortical ischemic rim in the DO + Sham, DO + Saline, DO + TM-0.25 g, DO + TM-0.5 g, DO + TM-1 g, and SP groups (n = 5) 2 days after reperfusion. Arrows in **(A)** and **(B)** point to YM-1/2/Iba1 (yellow)- and IL-10/NeuN (yellow)-positive cells, respectively. Scale bar indicates 50 μm. Quantification of the percentages of **(C)** YM-1/2/Iba1-and **(D)** IL-10/NeuN-positive cells was performed in the experimental groups. $^{*}P < 0.05$ vs. DO + Sham; $^{\#}P < 0.05$ vs. DO + Saline.

inducing the expression of genes encoding proinflammatory factors. Thus, p-NF-κB p65 is considered as an indicator of NF-κB activation (Wang et al., 2018). NF-κB p65, an essential transcriptional regulator, binds to IκB in the inactive state under normal conditions, whereas the NF-κB p65/IκB complex is dissociated through IκB degradation following cerebral I/R stimulation; the free NF-κB p65 complex is translocated to the nucleus in the activation (phosphorylation) state (Stephenson et al., 2000; Gong et al., 2023). In addition, p65 phosphorylation is essential for the nuclear translocation of NF-κB p65 and the transcription of its inflammatory mediators, which induces microglial activation and polarization toward the M1 phenotype, aggravating cerebral I/R injury (Yang et al., 2021). NF-κB p65 translocation also promotes polarization toward the M1 phenotype and inhibits conversion into the M2 phenotype in activated microglia (Li et al., 2022). The NLRP3 inflammasome, a critical component in the innate immune system, participates the progression of microglial polarization in the ischemic area in the acute stage of cerebral ischemia (Bian et al., 2021). The NLRP3 inflammasome mainly localized in the microglia is generated by the activation of the NF-κB signaling pathway; it then upregulates IL-1β and IL-18 expression, promoting M1 microglial polarization after MCA occlusion (Bian et al., 2021; Xue et al., 2023). By contrast, the inhibition of NLRP3 inflammasome activity suppresses microglial activation and M1 polarization, thereby downregulating the inflammatory response in the penumbra and reducing the infarct size in the early stages of cerebral ischemia (Xue et al., 2023). Thus, the pharmacological modulation of the NF-κB p65/NLRP3-mediated pathway and subsequent promotion of M1 to M2 polarization can reduce neurological deficits and cerebral infarct and is a promising therapeutic strategy in the acute stage of transient cerebral ischemia (Song et al., 2021; Li et al., 2022). Furthermore, studies have shown that the promotion of the microglial polarization shift from M1 to M2 phenotype in the ischemic area in the acute phase of cerebral ischemia is critical for long-term neurological function recovery (Gelosa et al., 2019; Suofu et al., 2023). In the present study, p-NF-κB p65-positive cells were colocalized with Iba1 in the nuclei, and these p-NF-κB p65/Iba1 double-labeled cells were predominantly detected in the cortical ischemic rim. Western blotting results further revealed markedly increased levels of p-NF-κB p65/NF-κB p65, NLRP3, and Iba1 in the cortical ischemic rim. Elevated Iba1 levels are commonly used as a marker of microglial activation (Jurga et al., 2020). Taken together, these results revealed that p-NF-κB p65 was translocated to the nucleus and induced the transcription of the downstream target NLRP3, thereby upregulating NF-κB p65/NLRP3 signaling in activated microglia. However, TM treatments restored the increased levels of the aforementioned proteins in the cortical ischemic rim 2 days after transient MCA occlusion. According to these findings, we suggest that TM treatments ameliorate cerebral infarction possibly by downregulating JNK/TLR4/T3JAM-mediated signaling in activated microglia. Furthermore, TM treatments exert

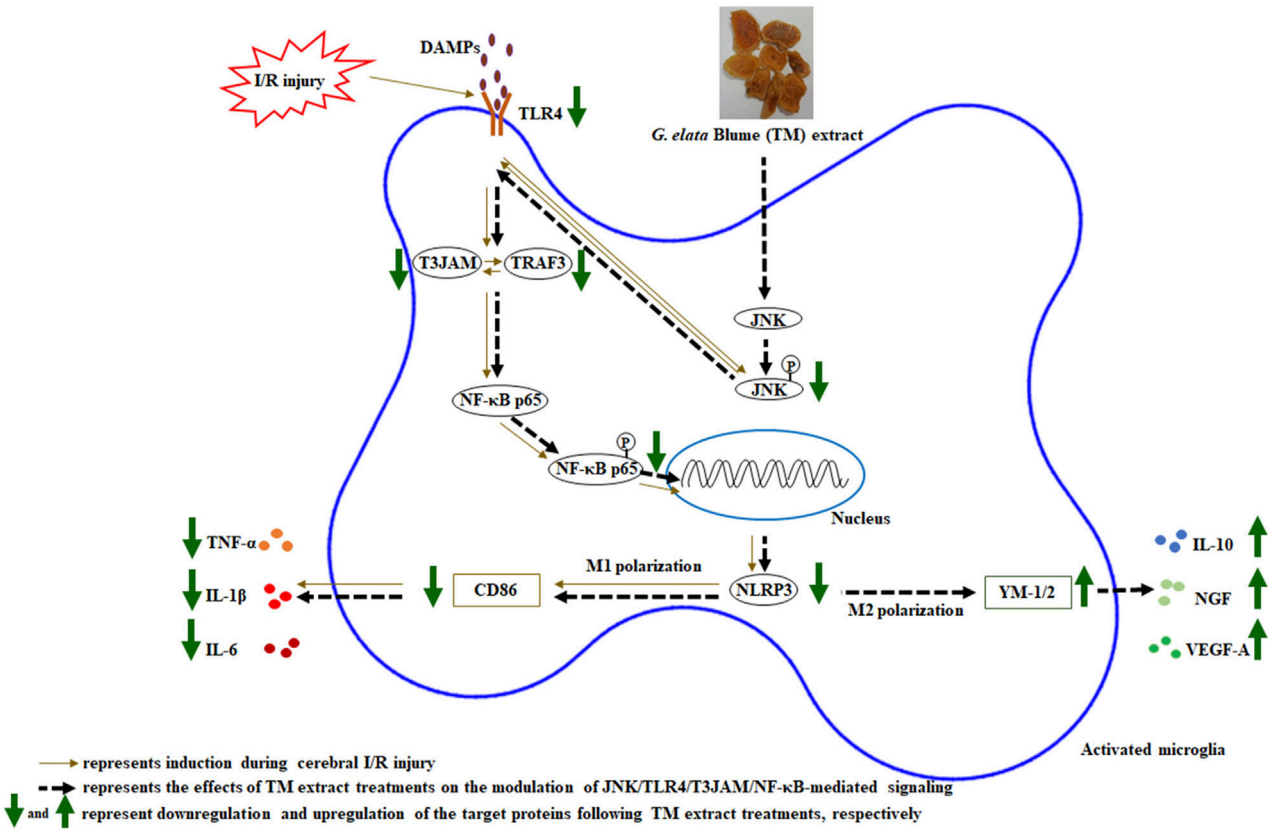


FIGURE 9
Schematic representation of the possible mechanisms of the TM extract on promoting microglia M2 polarization by inhibiting JNK/TLR4/T3JAM/NF-κB-mediated signaling after transient MCA occlusion. P, phosphorylated.

TABLE 4 Effects of the TM extract on neurological deficits in MCA occlusion models.

MCA occlusion models	Treatments	Neurological function tests	NFSs	References
2 h of ischemia followed by 24 h of reperfusion	Pretreatment with the TM extract at 11.4 and 102.6 mg/kg	Bederson's improving method including forelimb flexion, floor walking, response to vibrissae touch, and body rotation tests	NFSs ↓	(Duan et al., 2015)
2 h of ischemia followed by 24 h of reperfusion	Pretreatment with the TM extract at 200 mg/kg	Longa's scoring	NFSs ↓	(Wang et al., 2019)
1 h of ischemia followed by 24 h of reperfusion	Pretreatment with the TM extract at 10 g/kg	Corner test Adhesive removal test	NFSs ↓	(Seok et al., 2019)

neuroprotective effects by suppressing M1 microglial polarization at least partly by downregulating JNK/TLR4/T3JAM-mediated NF-κB p65/NLRP3 signaling in the cortical ischemic rim in the acute stage of transient MCA occlusion.

Activated microglia are highly plastic cells and undergo morphological transformation into either the proinflammatory M1 or anti-inflammatory M2 phenotype (Jover-Mengual et al., 2021). Microglia undergo polarization toward the M2 phenotype at 1–3 days after cerebral ischemia but gradually shift to the M1 phenotype 3–14 days after ischemia (Zhao et al., 2019; Ran et al., 2021). M1 microglia (with TNF-α or CD86 as markers) generate pro-inflammatory factors, such as TNF-α, IL-1β, IL-6, and interferon-γ, which promote inflammation and exacerbate I/R injury and cerebral infarction. By contrast, M2 microglia (with CD206 or YM-1/2 as markers) generate anti-inflammatory factors, such as transforming growth factor-β, IL-4, and IL-10, and neurotrophic factors, such as NGF and VEGF, which promote neuronal proliferation, differentiation, and survival and restoration of the blood–brain barrier, thereby promoting tissue recovery (Wijaya et al., 2021; Guo et al., 2022; Li et al., 2022; Wan et al., 2022). In our study, Western blotting and IF revealed that in the cortical ischemic rim, CD86, CD86/Iba1, TNF-α, IL-1β, and IL-6 levels were markedly upregulated, whereas YM-1/2, YM-1/2/Iba1, IL-10, IL-10/NeuN (mature neuron marker), and NGF levels were significantly downregulated. The level of VEGF-A, a member of the VEGF family, also markedly reduced in the acute stage of transient MCA occlusion. However, TM treatments reversed all these changes

2 days after reperfusion. Accordingly, we infer that TM treatments protect against M1 microglia-induced inflammation, possibly by downregulating TNF-α, IL-1β, and IL-6 expression and upregulating IL-10, NGF, and VEGF-A expression in the cortical ischemic rim. Furthermore, the neuroprotective effects of TM treatments on promoting the microglial polarization shift from M1 to M2 may be partly due to the downregulation of JNK/TLR4/T3JAM/NF-κB-mediated signaling in the cortical ischemic rim 2 days after reperfusion.

To identify the detailed reaction mechanisms underlying the anti-infarct effects of TM treatments on the modulation of JNK-related TLR4/T3JAM/NF-κB-mediated signaling 2 days after transient MCA occlusion, we pretreated SP600125 in the SP group. SP600125, a JNK inhibitor, effectively blocks JNK activation in the acute stage of cerebral ischemia (Cheng et al., 2021). TTC staining, Western blotting, and IF assays revealed that the effects of SP treatment on the aforementioned proteins are similar to those of TM treatments and those subsequently reduced cerebral infarct areas and NFSs 2 days after reperfusion. Thus, TM treatments ameliorate cerebral infarction and neurological deficits by inhibiting the JNK signaling pathway in the peri-infarct cortex. Moreover, the neuroprotective effects of TM treatments on promoting microglial M1 to M2 polarization are due to the inhibition of JNK/TLR4/T3JAM/NF-κB-mediated signaling in the cortical ischemic rim 2 days after reperfusion (Figure 9). Previous research showed that TM pretreatments attenuate neurological deficits in the acute phase of transient MCA occlusion (Duan et al., 2015; Seok et al., 2019; Wang et al., 2019) (Table 4). In the present study, TM treatments at the onset of cerebral ischemia can also improve neurological function recovery in the acute phase of transient cerebral ischemia. Furthermore, other studies reported that the bioactive ingredients of the TM extract include gastrodin, 4-hydroxybenzyl alcohol, parishin, and 3,4-dihydroxybenzaldehyde, which exert anti-inflammatory effects by modulating MAPK and NF-κB activation *in vitro* and *in vivo* models (Kim et al., 2012; Xiang et al., 2018; Li et al., 2020; Lin et al., 2021; Ma et al., 2024). In addition, the TM extract and its bioactive ingredients exert anti-inflammatory effects by downregulating a variety of proinflammatory mediators, such as TNF-α, IL-1β, and nitric oxide, in various models of ischemia-induced injury (Li et al., 2018; Seok et al., 2019; Wang et al., 2019; Kim et al., 2020). Thus, we reasonably assume that gastrodin (0.84–1.68 mg/kg) in the TM extract possibly interacts with other bioactive ingredients and subsequently provides neuroprotective effects through modulation of JNK-mediated NF-κB signaling during cerebral ischemic injury. However, further investigation is warranted. In the present study, we further provided evidence that the TM extract protects against cerebral I/R-induced inflammatory responses by inhibiting the JNK-related TLR4/T3JAM/NF-κB signaling pathway. To the best of our knowledge, this is the first study to show that the TM extract promotes microglial M2 polarization by inhibiting JNK-mediated TLR4/T3JAM/NF-κB signaling in acute ischemic stroke.

In conclusion, our findings revealed that the 0.5 and 1 g/kg TM extract reduced the cerebral infarct area and attenuated neurological dysfunction in the acute stage of MCA occlusion. Furthermore, TM treatments protected against cerebral infarction by inhibiting the JNK signaling pathway in the cortical ischemic rim. The neuroprotective effects of TM treatments on promoting M2 microglial polarization are attributed to the inhibition of the JNK/TLR4/T3JAM/NF-κB signaling pathway in the cortical ischemic rim 2 days after reperfusion. Thus, these findings suggest that *G. elata* Blume extract treatment is a potential therapeutic strategy for reducing cerebral infarction by downregulating the inflammatory response in the acute stage of cerebral ischemia. However, there are still some limitations in this study. First, we should do more exploration to find the better time point of TM administration following cerebral I/R injury. Second, we mainly focused on the anti-inflammatory effects of TM treatments on inhibition of JNK-mediated TLR4/T3JAM/ NF-κB signaling in acute ischemic stroke, but we could not exclude the possibility of the interaction with other signaling pathways, such as chemokine-mediated signaling. Third, the potential effects of the TM extract on MCA occlusion in rodents may not adequately simulate clinical stroke, which is influenced by a variety of factors, including age, gender, and body conditions. Fourth, the observation time point was short only 48 h and the findings of the present study could not reflect the long-term effects of the TM extract during cerebral ischemia. In addition, Paolicelli et al. reported that microglia are often coexpressing M1 and M2 markers and exist in dynamic and multidimensional states depending on environmental stimuli. Thus, reactive microglia should be focused on the specialized functions instead of simply dividing into the dichotomous M1/M2 polarization paradigm (Paolicelli et al., 2022). Thus, future studies should identify the effects and detailed reaction mechanisms of *G. elata* Blume extract on microglial functions in the subacute stage of transient cerebral ischemia.

Data availability statement

The original contributions presented in the study are included in the article/Supplementary Material, further inquiries can be directed to the corresponding author.

Ethics statement

The animal study was approved by the Institutional Animal Care and Use Committee of China Medical University (No. CMUIACUC-2021-318). The study was conducted in accordance with the local legislation and institutional requirements.

Author contributions

S-CH: Writing–review and editing. H-CH: Writing–review and editing. W-LL: Writing–review and editing. S-TK: Writing–review and editing. C-YC: Writing–original draft.

Funding

The author(s) declare that financial support was received for the research, authorship, and/or publication of this article. This research was funded by China Medical University Hospital (DMR-111-127 and DMR-113-209), Taichung, Taiwan.

Conflict of interest

The authors declare that the research was conducted in the absence of any commercial or financial relationships that could be construed as a potential conflict of interest.

Publisher's note

All claims expressed in this article are solely those of the authors and do not necessarily represent those of their affiliated organizations, or those of the publisher, the editors and the reviewers. Any product that may be evaluated in this article, or claim that may be made by its manufacturer, is not guaranteed or endorsed by the publisher.

Supplementary material

The Supplementary Material for this article can be found online at: https://www.frontiersin.org/articles/10.3389/fphar.2024.1469602/full#supplementary-material

References

Ashayeri, A. R., Mirzaasgari, Z., Gorji, A., and Khaleghi Ghadiri, M. (2021). Toll-like receptor signaling pathways: novel therapeutic targets for cerebrovascular disorders. *Int. J. Mol. Sci.* 22 (11), 6153. doi:10.3390/ijms22116153

Bian, H. J., Xu, S. Y., Li, H. Q., Jia, J. Q., Ye, L., Shu, S., et al. (2021). JLX001 ameliorates cerebral ischemia injury by modulating microglial polarization and compromising NLRP3 inflammasome activation via the NF-κB signaling pathway. *Int. Immunopharmacol.* 101 (Pt A), 108325. doi:10.1016/j.intimp.2021.108325

Cheng, C. Y., Chiang, S. Y., Kao, S. T., and Huang, S. C. (2021). Alpinia oxyphylla Miq extract reduces cerebral infarction by downregulating JNK-mediated TLR4/T3JAM- and ASK1-related inflammatory signaling in the acute phase of transient focal cerebral ischemia in rats. *Chin. Med.* 16 (1), 82. doi:10.1186/s13020-021-00495-2

Cheng, C. Y., Ho, T. Y., Hsiang, C. Y., Tang, N. Y., Hsieh, C. L., Kao, S. T., et al. (2017). Angelica sinensis exerts angiogenic and anti-apoptotic effects against cerebral ischemia-reperfusion injury by activating p38MAPK/HIF-1[Formula: see text]/VEGF-A signaling in rats. *Am. J. Chin. Med.* 45 (8), 1683–1708. doi:10.1142/S0192415X17500914

Cheng, C. Y., Kao, S. T., and Lee, Y. C. (2020). Angelica sinensis extract protects against ischemia-reperfusion injury in the hippocampus by activating p38 MAPK-mediated p90RSK/p-Bad and p90RSK/CREB/BDNF signaling after transient global cerebral ischemia in rats. *J. Ethnopharmacol.* 252, 112612. doi:10.1016/j.jep.2020.112612

Christian, F., Smith, E. L., and Carmody, R. J. (2016). The regulation of NF-κB subunits by phosphorylation. *Cells* 5 (1), 12. doi:10.3390/cells5010012

Dadgostar, H., Doyle, S. E., Shahangian, A., Garcia, D. E., and Cheng, G. (2003). T3JAM, a novel protein that specifically interacts with TRAF3 and promotes the activation of JNK(1). *FEBS Lett.* 553 (3), 403–407. doi:10.1016/s0014-5793(03)01072-x

de Zoete, M. R., Palm, N. W., Zhu, S., and Flavell, R. A. (2014). Inflammasomes. *Cold Spring Harb. Perspect. Biol.* 6 (12), a016287. doi:10.1101/cshperspect.a016287

Dong, R., Huang, R., Wang, J., Liu, H., and Xu, Z. (2021). Effects of microglial activation and polarization on brain injury after stroke. *Front. Neurol.* 12, 620948. doi:10.3389/fneur.2021.620948

Duan, X., Wang, W., Liu, X., Yan, H., Dai, R., and Lin, Q. (2015). Neuroprotective effect of ethyl acetate extract from gastrodia elata against transient focal cerebral ischemia in rats induced by middle cerebral artery occlusion. *J. Tradit. Chin. Med.* 35 (6), 671–678. doi:10.1016/s0254-6272(15)30158-8

Gan, Y. M., Liu, D. L., Chen, C., Duan, W., Yang, Y. X., and Du, J. R. (2020). Phthalide derivative CD21 alleviates cerebral ischemia-induced neuroinflammation: involvement of microglial M2 polarization via AMPK activation. *Eur. J. Pharmacol.* 886, 173552. doi:10.1016/j.ejphar.2020.173552

Gelosa, P., Bonfanti, E., Castiglioni, L., Delgado-Garcia, J. M., Gruart, A., Fontana, L., et al. (2019). Improvement of fiber connectivity and functional recovery after stroke by montelukast, an available and safe anti-asthmatic drug. *Pharmacol. Res.* 142, 223–236. doi:10.1016/j.phrs.2019.02.025

Gong, J., Li, Z. Z., Guo, S., Zhang, X. J., Zhang, P., Zhao, G. N., et al. (2015). Neuron-specific tumor necrosis factor receptor-associated factor 3 is a central regulator of neuronal death in acute ischemic stroke. *Hypertension* 66 (3), 604–616. doi:10.1161/HYPERTENSIONAHA.115.05430

Gong, P., Jia, H. Y., Li, R., Ma, Z., Si, M., Qian, C., et al. (2023). Downregulation of Nogo-B ameliorates cerebral ischemia/reperfusion injury in mice through regulating microglia polarization via TLR4/NF-kappaB pathway. *Neurochem. Int.* 167, 105553. doi:10.1016/j.neuint.2023.105553

Guo, S., Wang, H., and Yin, Y. (2022). Microglia polarization from M1 to M2 in neurodegenerative diseases. *Front. Aging Neurosci.* 14, 815347. doi:10.3389/fnagi.2022.815347

Jover-Mengual, T., Hwang, J. Y., Byun, H. R., Court-Vazquez, B. L., Centeno, J. M., Burguete, M. C., et al. (2021). The role of NF-κB triggered inflammation in cerebral ischemia. *Front. Cell. Neurosci.* 15, 633610. doi:10.3389/fncel.2021.633610

Jurga, A. M., Paleczna, M., and Kuter, K. Z. (2020). Overview of general and discriminating markers of differential microglia phenotypes. *Front. Cell. Neurosci.* 14, 198. doi:10.3389/fncel.2020.00198

Kelley, N., Jeltema, D., Duan, Y., and He, Y. (2019). The NLRP3 inflammasome: an overview of mechanisms of activation and regulation. *Int. J. Mol. Sci.* 20 (3), 3328. doi:10.3390/ijms20133328

Kim, B. W., Koppula, S., Kim, J. W., Lim, H. W., Hwang, J. W., Kim, I. S., et al. (2012). Modulation of LPS-stimulated neuroinflammation in BV-2 microglia by Gastrodia elata: 4-hydroxybenzyl alcohol is the bioactive candidate. *J. Ethnopharmacol.* 139 (2), 549–557. doi:10.1016/j.jep.2011.11.048

Kim, H. M., Kwon, J., Lee, K., Lee, J. W., Jang, D. S., and Kwon, H. C. (2020). Constituents of gastrodia elata and their neuroprotective effects in HT22 hippocampal neuronal, R28 retinal cells, and BV2 microglial cells. *Plants (Basel)* 9 (8), 1051. doi:10.3390/plants9081051

Li, J. J., Liu, S. J., Liu, X. Y., and Ling, E. A. (2018). Herbal compounds with special reference to gastrodin as potential therapeutic agents for microglia mediated neuroinflammation. *Curr. Med. Chem.* 25 (42), 5958–5974. doi:10.2174/0929867325666180214123929

Li, R., Zhou, Y., Zhang, S., Li, J., Zheng, Y., and Fan, X. (2022). The natural (poly) phenols as modulators of microglia polarization via TLR4/NF-κB pathway exert anti-inflammatory activity in ischemic stroke. *Eur. J. Pharmacol.* 914, 174660. doi:10.1016/j.ejphar.2021.174660

Li, X., Xiang, B., Shen, T., Xiao, C., Dai, R., He, F., et al. (2020). Anti-neuroinflammatory effect of 3,4-dihydroxybenzaldehyde in ischemic stroke. *Int. Immunopharmacol.* 82, 106353. doi:10.1016/j.intimp.2020.106353

Li, Y., Guan, J., Wang, W., Hou, C., Zhou, L., Ma, J., et al. (2019). TRAF3-interacting JNK-activating modulator promotes inflammation by stimulating translocation of Toll-like receptor 4 to lipid rafts. *J. Biol. Chem.* 294 (8), 2744–2756. doi:10.1074/jbc.RA118.003137

Lin, B., Chen, R., Wang, Q., Li, Z., Yang, S., and Feng, Y. (2021). Transcriptomic and metabolomic profiling reveals the protective effect of acanthopanax senticosus (rupr. and maxim.) harms combined with gastrodia elata Blume on cerebral ischemia-reperfusion injury. *Front. Pharmacol.* 12, 619076. doi:10.3389/fphar.2021.619076

Liu, B., Li, F., Shi, J., Yang, D., Deng, Y., and Gong, Q. (2016). Gastrodin ameliorates subacute phase cerebral ischemia-reperfusion injury by inhibiting inflammation and apoptosis in rats. *Mol. Med. Rep.* 14 (5), 4144–4152. doi:10.3892/mmr.2016.5785

Luo, L., Liu, M., Fan, Y., Zhang, J., Liu, L., Li, Y., et al. (2022). Intermittent theta-burst stimulation improves motor function by inhibiting neuronal pyroptosis and regulating microglial polarization via TLR4/NFκB/NLRP3 signaling pathway in cerebral ischemic mice. *J. Neuroinflammation* 19 (1), 141. doi:10.1186/s12974-022-02501-2

Ma, T., Chen, P., Dong, H., and Wang, X. (2024). Identification of key anti-neuroinflammatory components in Gastrodiae Rhizoma based on spectrum-effect relationships and its mechanism exploration. *J. Pharm. Biomed. Anal.* 248, 116266. doi:10.1016/j.jpba.2024.116266

Paolicelli, R. C., Sierra, A., Stevens, B., Tremblay, M. E., Aguzzi, A., Aiami, B., et al. (2022). Microglia states and nomenclature: a field at its crossroads. *Neuron* 110 (21), 3458–3483. doi:10.1016/j.neuron.2022.10.020

Peng, Z., Wang, S., Chen, G., Cai, M., Liu, R., Deng, J., et al. (2015). Gastrodin alleviates cerebral ischemic damage in mice by improving anti-oxidant and anti-inflammation activities and inhibiting apoptosis pathway. *Neurochem. Res.* 40 (4), 661–673. doi:10.1007/s11064-015-1513-5

Ran, Y., Qie, S., Gao, F., Ding, Z., Yang, S., Tian, G., et al. (2021). Baicalein ameliorates ischemic brain damage through suppressing proinflammatory microglia polarization via inhibiting the TLR4/NF-κB and STAT1 pathway. *Brain Res.* 1770, 147626. doi:10.1016/j.brainres.2021.147626

Seok, P. R., Oh, S. J., Choi, J. W., Lim, C. R., Choi, J. R., Kim, J. H., et al. (2019). The protective effects of Gastrodia elata Blume extracts on middle cerebral artery occlusion in rats. *Food Sci. Biotechnol.* 28 (3), 857–864. doi:10.1007/s10068-018-0516-9

Song, Z., Feng, J., Zhang, Q., Deng, S., Yu, D., Zhang, Y., et al. (2021). Tanshinone IIA protects against cerebral ischemia reperfusion injury by regulating microglial activation and polarization *via* NF-κB pathway. *Front. Pharmacol.* 12, 641848. doi:10.3389/fphar.2021.641848

Stephenson, D., Yin, T., Smalstig, E. B., Hsu, M. A., Panetta, J., Little, S., et al. (2000). Transcription factor nuclear factor-kappa B is activated in neurons after focal cerebral ischemia. *J. Cereb. Blood Flow. Metab.* 20 (3), 592–603. doi:10.1097/00004647-200003000-00017

Suofu, Y., Jauhari, A., Nirmala, E. S., Mullins, W. A., Wang, X., Li, F., et al. (2023). Neuronal melatonin type 1 receptor overexpression promotes M2 microglia polarization in cerebral ischemia/reperfusion-induced injury. *Neurosci. Lett.* 795, 137043. doi:10.1016/j.neulet.2022.137043

Tsai, Y. T., Huang, H. C., Kao, S. T., Chang, T. T., and Cheng, C. Y. (2022). Neuroprotective effects of alpinia oxyphylla miq against mitochondria-related apoptosis by the interactions between upregulated p38 MAPK signaling and downregulated JNK signaling in the subacute phase of cerebral ischemia-reperfusion in rats. *Am. J. Chin. Med.* 50 (8), 2057–2083. doi:10.1142/S0192415X22500884

Wan, T., Huang, Y., Gao, X., Wu, W., and Guo, W. (2022). Microglia polarization: a novel target of exosome for stroke treatment. *Front. Cell Dev. Biol.* 10, 842320. doi:10.3389/fcell.2022.842320

Wang, D., Wang, Q., Chen, R., Yang, S., Li, Z., and Feng, Y. (2019). Exploring the effects of Gastrodia elata Blume on the treatment of cerebral ischemia-reperfusion injury using UPLC-Q/TOF-MS-based plasma metabolomics. *Food Funct.* 10 (11), 7204–7215. doi:10.1039/c9fo01729a

Wang, P. F., Xiong, X. Y., Chen, J., Wang, Y. C., Duan, W., and Yang, Q. W. (2015). Function and mechanism of toll-like receptors in cerebral ischemic tolerance: from preconditioning to treatment. *J. Neuroinflammation* 12, 80. doi:10.1186/s12974-015-0301-0

Wang, Q., Lv, C., Sun, Y., Han, X., Wang, S., Mao, Z., et al. (2018). The role of alpha-lipoic acid in the pathomechanism of acute ischemic stroke. *Cell. Physiol. biochem.* 48 (1), 42–53. doi:10.1159/000491661

Wang, S., Liang, R., and Liu, H. (2022). Phoenixin-20 ameliorates brain infarction by promoting microglia M2 polarization in an ischemic stroke model. *Metab. Brain Dis.* 37 (5), 1517–1526. doi:10.1007/s11011-022-00950-5

Wang, T., Chen, H., Xia, S., Chen, X., Sun, H., and Xu, Z. (2021). Ameliorative effect of parishin C against cerebral ischemia-induced brain tissue injury by reducing oxidative stress and inflammatory responses in rat model. *Neuropsychiatr. Dis. Treat.* 17, 1811–1823. doi:10.2147/NDT.S309065

Wang, T., Zhao, N., Peng, L., Li, Y., Huang, X., Zhu, J., et al. (2020). DJ-1 regulates microglial polarization through P62-mediated TRAF6/IRF5 signaling in cerebral ischemia-reperfusion. *Front. Cell Dev. Biol.* 8, 593890. doi:10.3389/fcell.2020.593890

Wang, Y. C., Lin, S., and Yang, Q. W. (2011). Toll-like receptors in cerebral ischemic inflammatory injury. *J. Neuroinflammation* 8, 134. doi:10.1186/1742-2094-8-134

Wen, M., Ye, J., Han, Y., Huang, L., Yang, H., Jiang, W., et al. (2018). Hypertonic saline regulates microglial M2 polarization via miR-200b/KLF4 in cerebral edema treatment. *Biochem. Biophys. Res. Commun.* 499 (2), 345–353. doi:10.1016/j.bbrc.2018.03.161

Wijaya, A. R., Surudarma, I. W., Wihandani, D. M., and Putra, I. (2021). Polymorphisms of vascular endothelial growth factor-2578C/A rs699947 are risk factors for diabetic retinopathy in type-2 diabetes mellitus patients in Bali, Indonesia. *Biomed. (Taipei)* 11 (2), 11–17. doi:10.37796/2211-8039.1170

Xiang, B., Xiao, C., Shen, T., and Li, X. (2018). Anti-inflammatory effects of anisalcohol on lipopolysaccharide-stimulated BV2 microglia via selective modulation of microglia polarization and down-regulation of NF-κB p65 and JNK activation. *Mol. Immunol.* 95, 39–46. doi:10.1016/j.molimm.2018.01.011

Xue, K., Qi, M., She, T., Jiang, Z., Zhang, Y., Wang, X., et al. (2023). Argon mitigates post-stroke neuroinflammation by regulating M1/M2 polarization and inhibiting NF-κB/NLRP3 inflammasome signaling. *J. Mol. Cell Biol.* 14 (12), mjac077. doi:10.1093/jmcb/mjac077

Yang, C., Gong, S., Chen, X., Wang, M., Zhang, L., Hu, C., et al. (2021). Analgecine regulates microglia polarization in ischemic stroke by inhibiting NF-κB through the TLR4 MyD88 pathway. *Int. Immunopharmacol.* 99, 107930. doi:10.1016/j.intimp.2021.107930

Ye, Y., Jin, T., Zhang, X., Zeng, Z., Ye, B., Wang, J., et al. (2019). Meisoindigo protects against focal cerebral ischemia-reperfusion injury by inhibiting NLRP3 inflammasome activation and regulating microglia/macrophage polarization via TLR4/NF-κB signaling pathway. *Front. Cell. Neurosci.* 13, 553. doi:10.3389/fncel.2019.00553

Yusuying, S., Yusuyin, S., and Cheng, X. (2022). Translocator protein regulate polarization phenotype transformation of microglia after cerebral ischemia-reperfusion injury. *Neuroscience* 480, 203–216. doi:10.1016/j.neuroscience.2021.09.024

Zhang, X., Zhang, Q., Huang, L., Liu, M., Cheng, Z., Zheng, Y., et al. (2021). *Pien-Tze-Huang* attenuates neuroinflammation in cerebral ischaemia-reperfusion injury in rats through the TLR4/NF-κB/MAPK pathway. *Pharm. Biol.* 59 (1), 828–839. doi:10.1080/13880209.2021.1942926

Zhao, R., Ying, M., Gu, S., Yin, W., Li, Y., Yuan, H., et al. (2019). Cysteinyl leukotriene receptor 2 is involved in inflammation and neuronal damage by mediating microglia M1/M2 polarization through NF-κB pathway. *Neuroscience* 422, 99–118. doi:10.1016/j.neuroscience.2019.10.048

frontiers | Frontiers in Pharmacology

TYPE Original Research
PUBLISHED 02 October 2024
DOI 10.3389/fphar.2024.1395014

Check for updates

OPEN ACCESS

EDITED BY
Pukar Khanal,
Emory University, United States

REVIEWED BY
Bijendra Mandar,
Sopan Pharmaceutical Pvt Ltd., Nepal
Kunal Bhattacharya,
Pratiksha Institute of Pharmaceutical Sciences (PIPS), India

*CORRESPONDENCE
Mohd Saeed,
mo.saeed@uoh.edu.sa

RECEIVED 02 March 2024
ACCEPTED 31 May 2024
PUBLISHED 02 October 2024

CITATION
Saeed M, Haque A, Shoaib A and Danish Rizvi SM (2024), Exploring novel natural compound-based therapies for Duchenne muscular dystrophy management: insights from network pharmacology, QSAR modeling, molecular dynamics, and free energy calculations. *Front. Pharmacol.* 15:1395014. doi: 10.3389/fphar.2024.1395014

COPYRIGHT
© 2024 Saeed, Haque, Shoaib and Danish Rizvi. This is an open-access article distributed under the terms of the Creative Commons Attribution License (CC BY). The use, distribution or reproduction in other forums is permitted, provided the original author(s) and the copyright owner(s) are credited and that the original publication in this journal is cited, in accordance with accepted academic practice. No use, distribution or reproduction is permitted which does not comply with these terms.

Exploring novel natural compound-based therapies for Duchenne muscular dystrophy management: insights from network pharmacology, QSAR modeling, molecular dynamics, and free energy calculations

Mohd Saeed[1]*, Ashanul Haque[2], Ambreen Shoaib[3] and Syed Mohd Danish Rizvi[4]

[1]Department of Biology, College of Sciences, University of Ha'il, Ha'il, Saudi Arabia, [2]Department of Chemistry, College of Sciences, University of Ha'il, Ha'il, Saudi Arabia, [3]Department of Clinical Pharmacy, College of Pharmacy, Jazan University, Jazan, Saudi Arabia, [4]Department of Pharmaceutics, College of Pharmacy, University of Ha'il, Ha'il, Saudi Arabia

Muscular dystrophies encompass a heterogeneous group of rare neuromuscular diseases characterized by progressive muscle degeneration and weakness. Among these, Duchenne muscular dystrophy (DMD) stands out as one of the most severe forms. The present study employs an integrative approach combining network pharmacology, quantitative structure-activity relationship (QSAR) modeling, molecular dynamics (MD) simulations, and free energy calculations to identify potential therapeutic targets and natural compounds for DMD. Upon analyzing the GSE38417 dataset, it was found that individuals with DMD exhibited 290 upregulated differentially expressed genes (DEGs) compared to healthy controls. By utilizing gene ontology (GO) and protein-protein interaction (PPI) network analysis, this study provides insights into the functional roles of the identified DEGs, identifying ten hub genes that play a critical role in the pathology of DMD. These key genes include DMD, TTN, PLEC, DTNA, PKP2, SLC24A, FBXO32, SNTA1, SMAD3, and NOS1. Furthermore, through the use of ligand-based pharmacophore modeling and virtual screening, three natural compounds were identified as potential inhibitors. Among these, compounds 3874518 and 12314417 have demonstrated significant promise as an inhibitor of the SMAD3 protein, a crucial factor in the fibrotic and inflammatory mechanisms associated with DMD. The therapeutic potential of the compounds was further supported by molecular dynamics simulation and Molecular Mechanics/Generalized Born Surface Area (MM/GBSA) analysis. These findings suggest that the compounds are viable candidates for experimental validation against DMD.

KEYWORDS

Duchenne muscular dystrophy, network pharmacology, computational drug discovery, pharmacophore modeling, molecular dynamics simulation, QSAR

1 Introduction

Muscular dystrophies (MD) refer to a variety of inherited conditions that cause progressive weakening and degeneration of skeletal muscles. This group of disorders is known for its genetic and clinical diversity, with symptoms appearing from birth to late adulthood depending on the specific type. The most diverse forms of MD include limb-girdle, facioscapulohumeral, oculopharyngeal, emery-Dreifuss, distal, and Duchenne and Becker muscular dystrophies (Angelini, 2010). MD encompass a range of genetic disorders that can be X-linked, autosomal recessive, or autosomal dominant. These conditions manifest as muscular discomfort, weakness, and degeneration. Mutations in proteins within the sarcomere, nucleus, basement, or outer membrane of muscle cells and nonstructural enzymatic proteins are implicated in the pathogenesis of MD (Amato and Griggs, 2011). Different genetic deletions or mutations can lead to enzymatic or metabolic disorders, resulting in a variety of MDs (Gao and McNally, 2015; Allen et al., 2016). Variation in the X-lined gene DMD, where dystrophin is mutated frequently, causes Duchenne muscular dystrophy (DMD), which is the most severe form (Brinkmeyer-Langford and Kornegay, 2013). This condition affects around 1 in every 3,500 to 5,000 male infants born globally (Hoffman et al., 1987). Downregulation of protein expression during DMD or BMD is an outcome of mutations associated with Dytrophin gene (Le Rumeur, 2015). Limb-girdle muscular dystrophy (LGMD) is a progressive muscle weakness affecting the pelvic and shoulder girdles, primarily caused by mutations in proteins like myotilin, lamin, caveolin-3, calpain-3, dysferlin, γ-sarcoglycan, TCAP, TRIM32, FKRP, and titin. These mutations cause various subtypes of LGMD and are associated with other forms of muscular dystrophies, including distal and congenital dystrophies (Lovering et al., 2005).

Genetic profiling has revealed significant changes in gene expression in DMD. These changes offer insights into the disease's molecular basis and highlight potential therapeutic targets. Altered gene expression contributes to characteristic features of the disease. These altered gene expression leads to inflammation, fibrosis, and muscle degeneration. Studies have identified multiple genes associated with these biological processes, suggesting potential therapeutic interventions. Wang et al. (2013) found several hub genes associated with DMD, including C3AR1, TLR7, IRF8, and CD33, which are linked to immune and inflammation responses. Wang et al. (2021) identified proteins acting as hubs for DMD and BMD, finding 1,281 genes overexpressed and 189 downregulated. The informational evolution underscores the complexity of DMD and the need for ongoing research to understand its molecular intricacies.

Based on the immunomodulators of DMD pathology, various drug targets were used in phase I and preclinical trials (Malik et al., 2012; Tripodi et al., 2021). Inhibiting the SMAD3 signaling pathway to help reduce inflammation and fibrosis in DMD patients. SMAD3 is a protein with two domains, MH1 and MH2, crucial for TGF-β-induced transcriptional activation. The MH2 domain interacts with transcriptional cofactors and the type I TGF-β receptor. It binds to various proteins without a common sequence motif, making it essential for activating TGF-β signals, as demonstrated by studies the domain of SMAD3 in transforming growth factor-β signaling (Imoto et al., 2005a).

Halofuginone was tested in the mouse model to inhibit SMAD3 signaling, and it was observed that the inhibition of SMAD3 reduced fibrosis and improved muscle function (Tripodi et al., 2021). Osseni et al. (2022) found that tubastatin A can inhibit HDAC6, thereby enabling the acetylation of SMAD3. It also prevents nuclear translocation and Smad2/3 phosphorylation, reducing muscle atrophy and fibrosis by downregulating TGF-β signaling through Smad3 acetylation. Overall, both studies showed that inhibiting SMAD3 restricts the progression of fibrosis improves muscle movement.

This study aims to focus on the SMAD3 gene, which is a key mediator in the TGF-β signaling pathway in DMD. The gene expression data from the GEO database was used to identify differentially expressed genes and to construct a Protein-Protein Interaction network. Molecular docking was used to screen 2,569 natural compounds against SMAD3's MH2 domain, selecting three compounds with strong binding affinities. The study validated these compounds' potential as therapeutic agents through molecular dynamics simulations, principal component analysis (PCA), free energy landscape analysis (FEL analysis), and MM/GBSA calculations. This approach addresses a gap in current management strategies for DMD and sets the stage for developing more targeted and effective therapeutic options. The study's integrative approach combines high-throughput gene expression analysis, network-based bioinformatics, and advanced computational docking and simulation methods.

2 Methodology

2.1 Data collection, preprocessing and differential gene expression analysis

In order to find the gene expression data, a search was performed in the Gene Expression Omnibus (GEO) database using the keyword "muscular dystrophy" (Clough and Barrett, 2016). The data was filtered specifically for the species "*Homo sapiens*." The microarray dataset with the accession number GSE38417 was selected for further examination based on the data processing. The selected dataset contains the microarray datasets of healthy (control) and active MD patients. The microarray gene expression data from the selected groups were analysed using the GEO2R tool to determine the DEGs (Rezaei and Jabbari, 2022). The GEO2R software was used to obtain the *p*-value and false discovery rate (FDR) using the *T*-test and the Benjamini and Hochberg technique (Aubert et al., 2004). DEGs were selected by using a cut-off value of an absolute value of the log(fold change) $| > 2$ and a significance threshold of $p < 0.05$. DEGs were classified as upregulated or downregulated according to logFC ≥ 2 and logFC ≤ -2, respectively.

2.2 Protein-protein interaction network analysis, gene ontology and pathway analysis

This study integrated GEO for expression data, STRING for building interaction networks, and Cytoscape for network

visualization (Menche et al., 2015). In order to examine the protein-protein interaction (PPI) network of DEGs, the search Tool for the Retrieval of Interacting Genes' (STRING, version 12.0) (Szklarczyk et al., 2021) was utilised. The PPI network was visualised using the web-based software Cytoscope. The next step was to locate the hub genes in Cytoscape (Shannon et al., 2003) by using the MCC method and the CytoHubba plugin (Chin et al., 2014). Further, gene ontology was employed to evaluate the roles of the genes.

Here, the GO approach was used to analyze the molecular function of the gene. To perform GO analysis, the g:Profiler server (Reimand et al., 2007) was used, and the GOST tool was used to define the advanced parameters. Over-representation analysis (ORA), also known as gene set enrichment analysis, functional enrichment analysis, and other similar analyses, are all services provided by the GOST programme (Raudvere et al., 2019). This analysis is carried out on a list of input genes. Annotated genes were the primary ones chosen in this case under the advanced option. After that, g:SCS was selected as a significance threshold and set the user threshold to 0.5. When determining the *p*-values, the default parameter was used as the starting point, and a false discovery rate (FDR) threshold of $p < 0.05$ was implemented in order to analyze the data. A statistically significant *p*-value of less than 0.05 was achieved by using the ShinyGO 0.80 programme to carry out the route analysis (Ge et al., 2020). The pathway database known as the Kyoto Encyclopaedia of Genes and Genomes (KEGG) was used by this algorithm in order to discover the genes that were implicated (Kanehisa and Goto, 2000). The KEGG pathway representation predominantly focuses the intricate relationship of gene products, primarily proteins, while additionally includes functional RNAs (Kanehisa and Goto, 2000). The FDR cut-off in the KEGG pathway has been set as 0.05. Consequently, relevant genes were acquired, and among them, additional selection was conducted based on the enrichment score (0.05).

2.3 Target preparation

The top hub genes were identified using information from the literature to analyze their functions. Based on this data, a possible target gene was selected. This selected gene was then queried in the Uniprot database (UniProt Consortium, 2015), and the results were refined by applying a filter for humans (*H. sapiens*). The data was then examined and further analyzed based on family and domain information. As a result, a specific domain was selected as the target protein for further investigation.

2.4 Molecular docking

2.4.1 Protein preparation

The target protein SMAD3 (PDB: 1MJS) was downloaded from the protein data bank (PDB) (UniProt Consortium, 2015). CASTp server (Tian et al., 2018) was used to identify the residues, and the CASTp server (Tian et al., 2018) was used associated with binding sites. The protein was prepared using the Autodock tool. The grid box with the following dimensions, 18 Å × 22 Å × 26 Å, was generated to cover the binding site residues. The centre of the grid box was situated at 28.39 Å × 5.22 Å × 4.37 Å along the x, y, and z-axes Hydrogen atoms and Gasteiger charges are added, while water molecules and heteroatoms are removed before docking.

2.4.2 Ligand preparation

The compound library preparation process began with a search of the Selleckchem database for the desired natural substance. (https://www.selleckchem.com/screening/natural-product-library.html). The retrieved compounds were later converted into SMILES for PubChem (Kim et al., 2023) CID using the "PubChem Identifier Exchange Service." By removing duplicate entries from both conversion processes, distinct CIDs were obtained. Then, the CIDs corresponding to the 3D-SDF structures were acquired using the PubChem API. The other 2D-SDF structures were Collected and converted retrieved and converted to 3D-SDF. After that, the 3D-SDF files were optimized in size using the MMFF94 force field, and Open-babel was used to convert these to PDBQT (O'Boyle et al., 2011). Ligand was converted to PDB from SDF using an open-babel tool. Similarly, open- Babel was used to convert the PDB file to a PDBQT file. The addition of hydrogen was also done by the open-Babel programme.

2.4.3 Ligand-protein docking

The AutoDock 4.2 software (Morris et al., 2009) and AutoDock Vina 1.2.0 (Eberhardt et al., 2021) were used in order to carry out the protein-ligand docking process. AutoDock Vina is a validated and robust molecular docking tool favoured for its advanced scoring function, efficient optimization algorithms, and multithreading capabilities (Trott and Olson, 2010). These features enhance the accuracy and speed of docking simulations, which is crucial for the reliable prediction of binding energies and modes in protein-ligand interactions. The tool's development focuses on both empirical and knowledge-based potentials, which ensures improved prediction accuracy compared to its predecessors (Forli et al., 2016). Additionally, in the process of conducting docking-based virtual screening, the following characteristics were taken into consideration: twenty binding modes, ten exhaustiveness, and a maximum energy difference of four (kcal/mol).

2.4.4 Molecular dynamics (MD) simulation

The protein-ligand complex has been simulated employing the poses were used for a 100 ns molecular dynamics simulation using Gromacs 2022.4 (2022) (Bauer et al., 2022) (MD). The CHARMM36 force field parameter was used to establish the molecular topology (Huang and MacKerell, 2013). The CGneFF server was used to build topologies and force-field parameters for both the hit molecule and the control inhibitor (Vanommeslaeghe et al., 2010). The Ewald particle mesh method was used to determine the electrostatic force across a specific distance. The system was hydrated using the TIP3P model after being placed into a solvation box (cubic) with a distance of 1.0 nm from the wall (Harrach and Drossel, 2014). The neutralisation process was then carried out using Na^+ and Cl^- ions. After fifty thousand cycles of the steepest descent (SD) method, the system was able to get rid of steric conflicts. Afterwards, the LINCS approach was employed to attain system stability and restrict the bonds (Hess et al., 1997). Furthermore, during a 100 ps simulation period in the NVT ensemble, the system's temperature was raised to 310 K using a 2 fs timestep. Furthermore, the system was exposed to continuous

pressure (NPT ensemble) at 310 K and 1 atmosphere for 1 ns. The simulation was run for 100 ns. The velocity-rescaling technique (Hess et al., 1997) was used to include temperature coupling, while the Parrinello-Rahman pressure method (Hess et al., 1997) was used to provide constant pressure was employed to maintain constant pressure. Hydrogen bonding, root mean square fluctuation (RMSF), and root mean square deviation (RMSD) were evaluated with the use of the GROMACS internal tool during a subsequent post-MD examination.

2.4.5 Principal component analysis (PCA)

Prior to principal component analysis, the trajectory was cleaned by eliminating the periodic boundary condition. For computing the covariance matrix, the Gmx covar tool that is included in the GROMACS package was used. It is possible to utilise the covariance matrix in order to characterise the connection that exists between the atomic variations that are present in the protein-ligand complex. The eigenvalues and eigenvectors of the covariance matrix were obtained via the gmx anaeig function. The following step utilized the GROMACS software, specifically the "gmx anaproj" function, to obtain the PC coordinates for each frame.

2.5 Free energy landscape (FEL)

The processes of biomolecule recognition, aggregation, and folding are some of the processes that can be better understood by examining the steady state, which is represented by the minima of the Free Energy Landscape (FEL), and the transient state, which is represented by the barriers of the FEL, in biological systems (Papaleo et al., 2009). The FEL was calculated by calculating the energy distribution according to Eq. 1a:

$$\Delta G(X) = -kBTln\,P(X) \tag{1a}$$

The variables X, G, kB, T, and P(X) represent the reaction coordinate, Gibbs free energy, Boltzmann constant, absolute temperature, and probability distribution of the system along the reaction coordinate, respectively.

2.6 Binding-free energy

When estimating the binding free energy of the protein-ligand complex, the GROMACS add-on tool gmx MM/PBSA was used as the information source (Valdes-Tresanco et al., 2021). The equations applied to compute the MM/GBSA are shown in Eqs 1–6.

$$\Delta G = G_{complex} - \left[G_{receptor} + G_{ligand} \right] \tag{1b}$$

$$\Delta G_{binding} = \Delta H - T\Delta S \tag{2}$$

$$\Delta H = \Delta G_{GAS} + \Delta G_{SOLV} \tag{3}$$

$$\Delta G_{GAS} = \Delta E_{EL} + \Delta E_{VDWAALS} \tag{4}$$

$$\Delta G_{SOLV} = \Delta E_{GB} + \Delta E_{SURF} \tag{5}$$

$$\Delta E_{SURF} = \gamma.SASA \tag{6}$$

Here, ΔG is defined as the variation in the protein-ligand formation's Gibbs free energy in Eq. 1b. In the solvent, $G_{complex}$, $G_{receptor}$, and G_{ligand} denote the total free energies of the protein-ligand complex, free enzyme, and ligand, respectively. $\Delta G_{binding}$ signifies the modification in the Gibbs free energy corresponding to the protein-ligand binding interaction, while ΔH stands for the modification in enthalpy that incorporates both the gas-phase energy (ΔG_{GAS}) and the total solvation free energy (ΔG_{SOLV}). The binding free energy, shown as TΔS, is the cumulative sum of the change in entropy. ΔE_{EL} represents a change in electrostatic energy, while $\Delta E_{VDWAALS}$ signifies the change in van der Waals energy. These two components combine to yield ΔG_{GAS}. Moreover, ΔE_{GB} indicates the change in polar solvation energy brought on by polar group interaction, while Δ,E_{-SURF}. denotes a change in solvation-free energy brought on by the non-polar interaction. A variation of the solvent-accessible surface area (SASA) was made using the solvent surface tension parameter (γ) in order to compute the solvent-accessible surface area (SURF) of the solvent.

3 Results

3.1 Healthy vs. active comparison for Duchenne muscular dystrophy (DMD)

Using microarray datasets from healthy persons and those with active DMD, the current research tried to discover the genes that are expressed differently between the two groups of people. The GSE38417 dataset was derived from the GEO database, which served as its primary source. The GEO2R approach was used to find DEGs in the dataset. A volcano plot is used to show the differential gene expression analysis results (Figure 1A). The x-axis displays the log2 fold change between healthy and DMD conditions; each gene's expression level varies from condition to condition. The importance of the expression change is shown by negative log10 of the *p*-value, displayed along the y-axis. The genes thought to be more differently expressed are those with greater and further to the left or right points. Following the requirements of an adjusted *p*-value (P.adj) less than 0.05 and a logarithmic function (logFC) more than 2, genes that are substantially upregulated are represented by red dots, while genes that are significantly downregulated are represented by blue points. Here, we observed 290 upregulated and 977 downregulated DEGs. Figure 1B) illustrates a mean difference (MA) plot for gene expression data from DMD versus control samples. The y-axis shows the log2FC, log2 Fold change and the x-axis shows the log2Exp, log2 expression. The genes with red dots show a highly differentially expressed gene set, whereas genes with blue points may have modest expression levels but large fold changes.

Figure 1C shows the box plot that compares the distribution of gene expression levels between the healthy (green boxes) and the active DMD (blue boxes) for a series of samples on a logarithmic scale. The centre line in each box shows the median expression level, while the height of the box shows the interquartile range (the middle 50% of data points). There were 1,267 genes found to have differential expression between healthy and active DMD conditions, out of a total of 53,408, with an adjusted *p*-value less than 0.05. These plots were used to analyse and visualise the microarray dataset data and understand the biological significance of gene expression changes in diseases like Duchenne

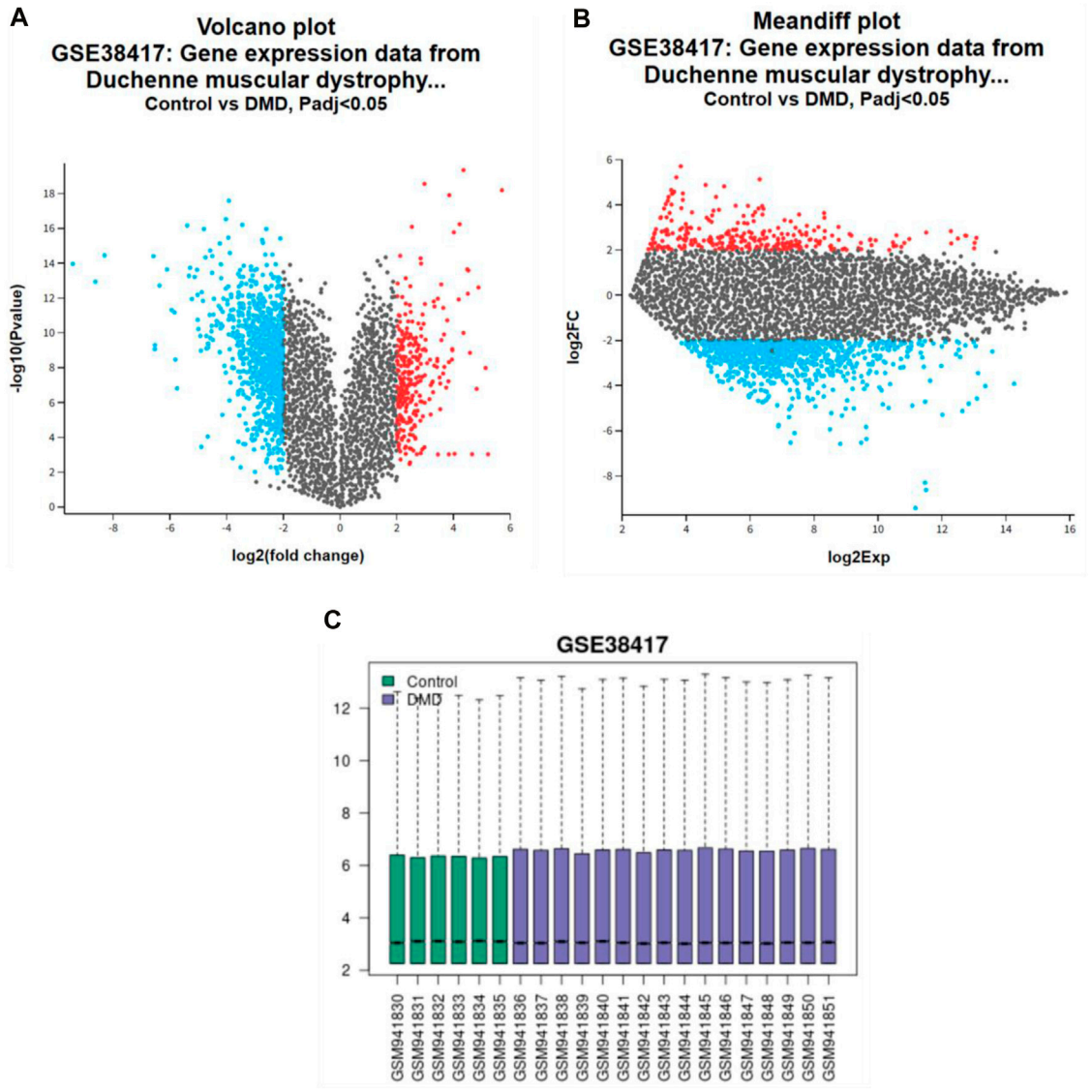


FIGURE 1
Gene expression analysis in DMD: **(A)** volcano plot, **(B)** MA plots highlighting differential expression between control and DMD cases, with **(C)** Sample distribution bar graphs.

muscular dystrophy. There is a chance that the genes that are elevated (290 DEGs) are responsible for the production of proteins that play an important part in the development of DMD disease. Therefore, the purpose of the research was to examine the dataset GSE38417 in order to identify the DEGs that were elevated.

3.2 Protein-protein interaction

Using the STRING platform, the upregulated differentially expressed genes (DEGs) were analysed for protein-protein interactions (PPIs). The medium confidence level was set at 0.90, which is the lowest needed interaction score. Figure 2 illustrates the PPI, which represents the interaction network between DEGs. Disconnected nodes were ignored in the analysis as shown in the Figure 2. Multiple significant nodes and links were among the 290 upregulated DEGs identified from GSE38417. TTN had the highest node degree, with a value of 11. The genes DMD and SLC2A4 exhibited a node degree of 10, which was the second highest among all genes. PLEC and SMAD3 followed this, which was 8 node degree. FBXO32 and MAPT exhibited significant node degree, with a value of 7. The genes were subjected to additional analysis using the Cytohubba plugin of Cytoscape. Cytoscape employed a colour gradient that spanned from red to yellow in order to represent the hubs, thereby signifying their varied degrees of importance within the network. Through this study, the most notable hubs are identified, which are subsequently used in constructing a PPI network. Figure 3 displayed the protein-protein interaction (PPI) network of the top 10 hubs, and Table 1 presented a ranking of the genes based on their scores. Both of these figures were shown in the same document. Figure 3 shows the use of Maximal Clique Centrality (MCC) values to

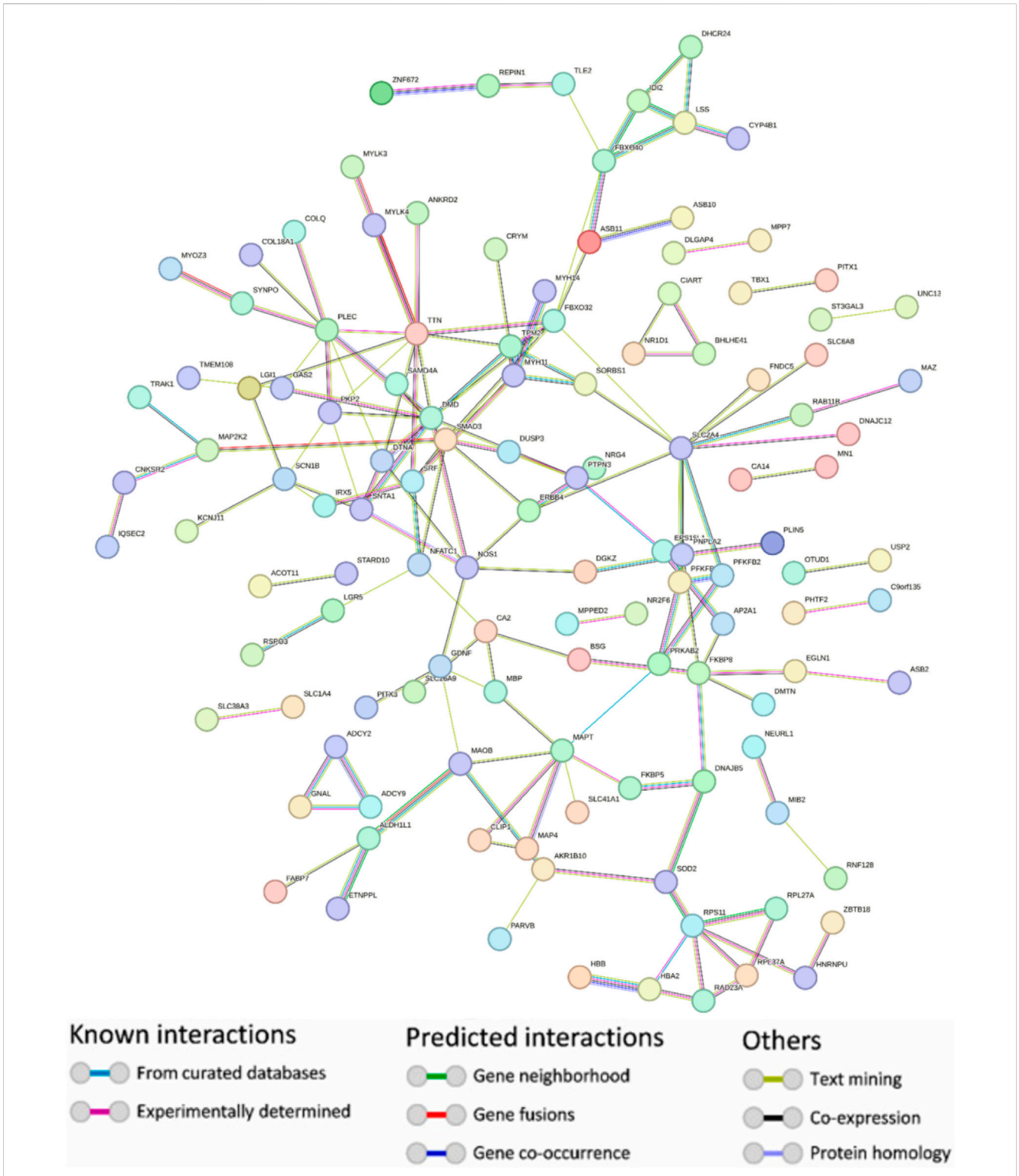


FIGURE 2
Protein-protein interaction network depicting upregulated genes with hidden disconnected nodes. Node colours indicate different entity classifications, while edge colors represent the nature and source of interactions—ranging from experimentally determined (red) to predicted connections (green) and associations identified through text mining (blue) and co-expression (purple).

display the gene gradient. The top 10 hubs found by PPI network analysis were DMD, TTN, PLEC, DTNA, PKP2, SLC24A, FBXO32, SNTA1, SMAD3, and NOS1. The DMD gene exhibited the highest MMC score of 29, while the TTN gene scored 23. These two genes, DMD and TTN, are the most significant differentially expressed genes (DEGs) that contribute to the development of muscular dystrophy. The PLEC gene scored 17, the DTNA gene exhibited a score of 12, and the PKP2, SLC24A,

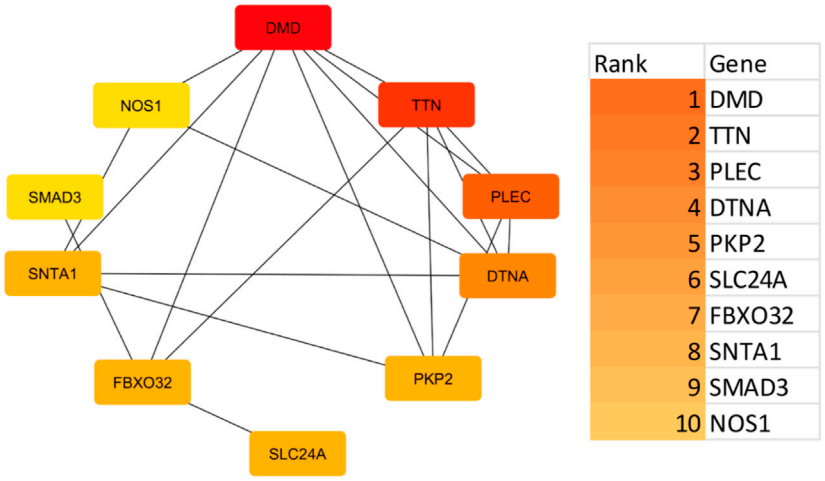


FIGURE 3
A key regulatory protein interaction network highlights central hub proteins as identified by cytohubba analysis. Gene interaction network with a gradient scale indicating Maximal Clique Centrality (MCC) values for each gene. The gradient bar on the right, ranging from dark orange to light yellow, visually represents the MCC values from highest to lowest, facilitating an understanding of the hierarchical importance of these genes in the network.

TABLE 1 Top 10 hub proteins in network STRING network ranked by MCC method.

Rank	Name	Score	Gene symbol
1	ENSP00000354923	29	DMD
2	ENSP00000467141	23	TTN
3	ENSP00000323856	17	PLEC
4	ENSP00000470152	12	DTNA
5	ENSP00000070846	10	PKP2
5	ENSP00000320935	10	SLC24A
5	ENSP00000428205	10	FBXO32
5	ENSP00000217381	10	SNTA1
9	ENSP00000332973	9	SMAD3
9	ENSP00000477999	9	NOS1

FBXO32, and SNTA1 genes exhibited scores of 10. SMAD3 and NOS1 exhibited an MCC score of 9. The top 10 hubs were subsequently used for a literature analysis to examine the association between these genes and muscular dystrophy.

3.3 Gene ontology

Studies on the enrichment of pathways using Gene Ontology (GO) and the Kyoto Encyclopaedia of Genes and Genomes (KEGG) were carried out with the assistance of the g: Profiler tool. These efforts enhanced the understanding of the biological significance of the upregulated DEGs in the GSE38417 dataset. Examining the functional and route links between these DEGs helped researchers better understand their potential roles in biological systems. The user's threshold was set to 0.5 in this case, which used the g:SCS threshold. The cellular components (CC), biological processes (BP), and molecular functions (MF) domains were the primary areas of concentration for the GO analysis as shown in Figure 4. Sodium channel regulator activity, PDZ (PSD-95/Dlg/ZO-1) domain binding, dystroglycan binding, nitric-oxide synthase binding, and structural components of muscle were among the molecular processes linked to the DEGs. It was shown that the top ten hub proteins are linked to several biological processes, including those involving the cardiovascular system, striated muscle contraction, blood circulation, and cardiac muscle contraction. The top 10 hub proteins were shown to be connected with several cellular components, including the sarcolemma, Z disc, I band, syntrophin complex, and sarcomere. Duchenne muscular dystrophy (DMD) disrupts a complicated network of interactions and activities, as shown by the association between DEGs and these biological processes and cellular components. Hub proteins have recently been identified, which raises the possibility that they are therapeutic treatment targets due to their potential importance in disease progression. Gaining insight into these connections aids in understanding the underlying pathological processes of DMD and has the potential to identify efficient therapies.

3.4 Pathway analysis

Further, pathway enrichment analysis using the top 10 hub genes was performed. Figure 5 shows that each pathway has a horizontal line ending in a dot, with the dot's position indicating the fold enrichment. The colour of the dot, which is a statistical metric that is used when testing several hypotheses, correlates to the -log10 of the false discovery rate (FDR). In terms of statistical significance, a deeper shade indicates a greater enrichment than a lighter shade does. The size of the dot is a representation of the number of genes that are involved in the pathway; bigger dots will indicate that there are more genes involved. The arrhythmogenic right ventricular cardiomyopathy and dilated cardiomyopathy pathways exhibit the highest fold enrichment, accompanied by a

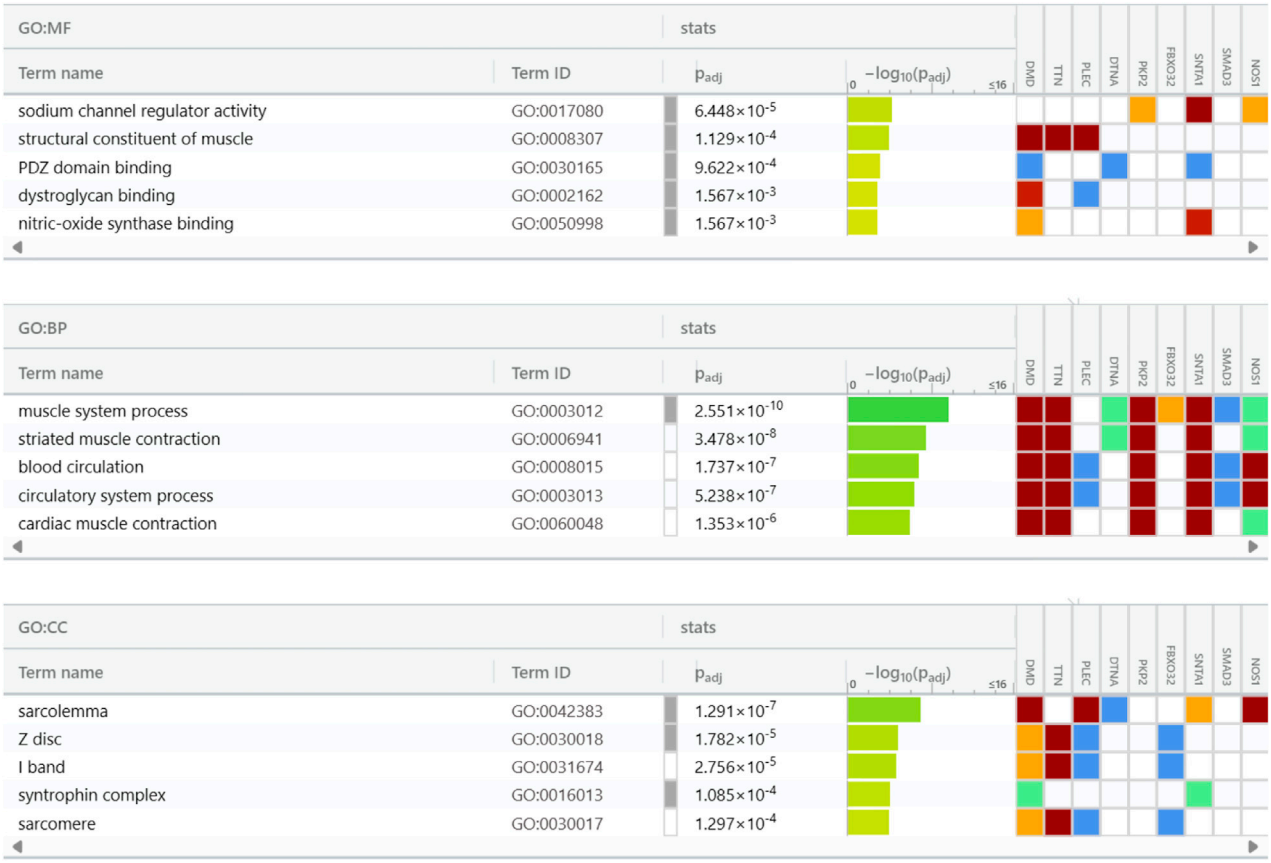


FIGURE 4
Gene Ontology insights into cellular components (CC), biological processes (BP), and molecular functions (MF) of the top 10 hub genes.

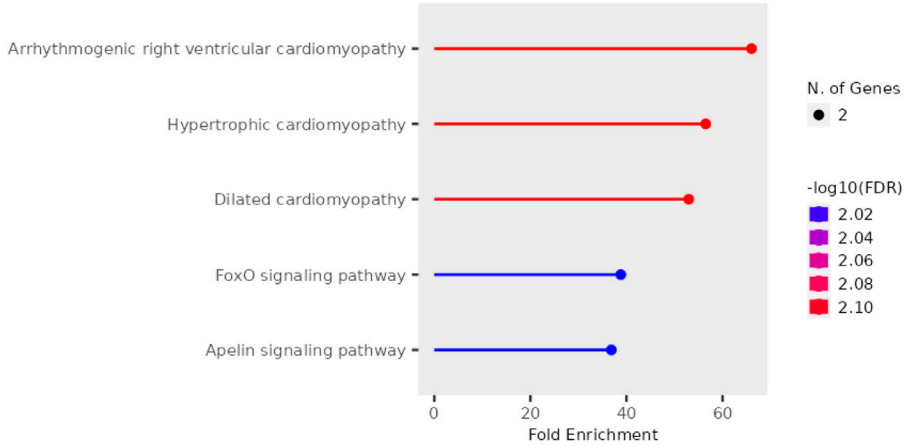


FIGURE 5
Pathway enrichment analysis of top hub genes identified from the PPI network analysis.

highly significant FDR (indicated by the red colour). Hypertrophic cardiomyopathy shows a slightly lower fold enrichment but still maintains a significant FDR. On the other hand, the FoxO signaling pathway and Apelin signaling pathway display lower fold enrichments and less significant FDRs (indicated by the blue colour). The enrichment scores and the genes involved in the pathway are listed in Table 2. It was observed that DMD, TTN, and SMAD3 were involved in most of the pathways.

TABLE 2 Enrichment scores of key signalling pathways and their related genes.

Enrichment FDR	Fold enrichment	Pathway	Genes
0.007792883	66.03463203	Arrhythmogenic right ventricular cardiomyopathy	DMD, PKP2
0.007792883	56.4962963	Hypertrophic cardiomyopathy	DMD, TTN
0.007792883	52.96527778	Dilated cardiomyopathy	DMD, TTN
0.009610153	38.81424936	FoxO signalling pathway	FBXO32, SMAD3
0.009610153	36.84541063	Apelin signalling pathway	SMAD3, NOS1

3.5 SMAD3 a key target in Duchenne muscular dystrophy

The target identified by reviewing various literatures, the upregulation of specific genes in muscular dystrophies, including DMD, might involve intricate interactions between compensatory mechanisms, cellular stress responses, and pathogenic processes. The therapeutic genes involved in DMD were discussed here. The Dystrophin gene is generally not excessively expressed in DMD. However, mutations result in a lack or substantial decrease of dystrophin protein (Duan et al., 2021). Titin (TTN) could potentially be up-regulated as a compensatory mechanism in response to muscle injury. The function of titin in preserving muscle flexibility and structural integrity is critical. In order to preserve the structure and functionality of the muscles, the body may respond to damage to the muscle fibers by up-regulating TTN expression (Loescher et al., 2022). Plectin, or PLEC, serves as a link between the cell membrane and the cytoskeleton, especially in muscle cells. The overexpression of this gene may occur as a reaction to heightened mechanical strain and cellular instability in dystrophic muscles. The overexpression of DTNA may be a way for the dystrophin-associated protein complex to compensate for dystrophin's loss or malfunction by stabilising the membrane of the muscle cell (Wiche, 1998). The PKP2 gene, also known as Plakophilin 2, has a role in cell adhesion and may be upregulated in muscular dystrophies as a protective reaction to cellular stress and damage, in an effort to preserve cellular integrity (Papaleo et al., 2009). The SLC24A gene family is responsible for encoding sodium/potassium/calcium exchangers. Overexpression may be associated with disrupted ion homeostasis in dystrophic muscles, a prevalent characteristic in muscular diseases.

The FBXO32 gene, also known as Atrogin-1, plays a role in the development of muscular atrophy. Overexpression of this gene in muscular dystrophy may serve as an indicator of continuous muscle loss and atrophy, which are characteristic features of these disorders (Ghasemi et al., 2022). The SNTA1 gene, also known as Syntrophin Alpha 1, is a constituent of the dystrophin complex. Overexpression may arise as a compensatory strategy to stabilise the muscular membrane when functional dystrophin is lacking (Jimenez-Vazquez et al., 2022). NOS1, also known as Nitric Oxide Synthase 1, plays a role in the synthesis of nitric oxide, which serves as a signaling molecule. The overexpression of this gene may be associated with changes in blood circulation or inflammation in muscles affected by dystrophy (Buchwalow et al., 2006). SMAD3 overexpression, which is implicated in TGF-beta signaling, may be associated with fibrosis, a prevalent consequence in muscular dystrophies (Liu et al., 1997). The upregulation of these genes is frequently a reaction to the underlying muscle dysfunction and not a primary instigator of the disease itself. These alterations can be involved in intricate feedback loops where the body endeavors to counterbalance or react to muscle injury, but they can also contribute to the advancement of disease in certain instances. Comprehending these alterations in gene expression is crucial for the development of precise treatments for muscle dystrophies.

SMAD3 overexpression has been associated with muscular dystrophies, according to research. The significance of this discovery lies in the fact that SMAD3 is an essential component of the TGF-β signaling pathway, which plays a role in the processes of tissue remodeling, inflammation, and fibrosis. There are a total of two domains that make up SMAD3. The N-terminus is the location of one of the two, whereas the C-terminus is the location of the other. Because the MH2 domain engages in interactions with a multitude of transcriptional cofactors and the type I TGF-β receptor (TβR-I), it is essential for the activation of transcription by TGF-β. One of the earlier studies indicated that the four particular lysine residues that make up the SMAD3 MH2 domain—Lys333, Lys341, Lys378, and Lys409—were essential to the operation of the domain (Imoto et al., 2005b). Therefore, the goal of targeting the MH2 domain of SMAD3 was to impede the fibrosis process associated with Duchenne muscular dystrophy (DMD).

The SMAD3 gene plays a critical role in DMD, primarily through its involvement in the TGF-β signaling pathway, which is instrumental in processes such as tissue remodeling, inflammation, and fibrosis. These processes are central to the pathology of DMD, where progressive muscle degeneration is compounded by excessive fibrosis and chronic inflammation. The activation of SMAD3 in TGF-β signaling leads to the upregulation of extracellular matrix proteins, contributing significantly to the muscle stiffness and fibrosis seen in DMD patients (Bernasconi et al., 1999; Qin et al., 2011). By modulating SMAD3 activity, there is potential to alter the course of tissue remodeling and inflammatory responses that exacerbate muscle damage (Roberts et al., 2003). Furthermore, the role of SMAD3 in DMD shares mechanistic similarities with its function in cancer metastasis, where it regulates cellular proliferation, migration, and invasion—processes similarly detrimental in DMD albeit through different pathological outcomes (Ismaeel et al., 2019). This crossover highlights SMAD3 as a versatile target in both oncological and muscular pathologies, underpinning its importance across different disease contexts. Targeting the TGF-β/SMAD3 pathway in DMD could therefore mitigate fibrotic tissue development and reduce

TABLE 3 Average and top binding scores of the ligands, along with the number of hydrogen bonds (selected compounds are shown in Bold).

Ligands	Average binding energy (kcal/mol)	Top binding energy	Hydrogen bonds
5,281,600	−8.43	**−9.6**	**5**
72,950,887	−7.64	−9.6	1
3,874,518	−7.97	**−9.5**	**9**
12,314,417	−7.84	**−9.5**	**6**
4,485,132	−7.38	−9.4	4
4,463,283	−7.96	−9.3	6
437,080	−7.82	−9.3	6
5,281,847	−8.15	−9.2	3
4,441	−8.08	−9.2	6
328,441	−7.99	−9.2	0

inflammation, potentially preserving muscle function and improving patient outcomes (Flanders, 2004). Given this pivotal role, targeting SMAD3 presents a promising therapeutic strategy for managing DMD, as evidenced by research models showing reduced fibrosis and improved muscle functions upon modulation of this pathway (Zhou and Lu, 2010). These studies collectively advocate for further exploration of SMAD3 inhibitors as potential therapeutic agents in DMD treatment regimens.

3.6 Virtual screening

The MH2 domain of SMAD3 was tested against 2,569 natural compounds. The binding site residues of the MH2 domain of SMAD3 were GLN315, PRO317, ASN320, ALA328, ARG367, THR370, ILE371 and ARG372, as predicted by CASTp server. Top three hits were selected that showed a top binding energy > −9 kcal/mol (Table 3). The three compounds were 12,314,417 (Ojv-VI), 3,874,518 (Hederacoside C), and 5,281,600 (Amentoflavone). These compounds had binding values of −9.6 kcal/mol, −9.5 kcal/mol, and −9.5 kcal/mol, respectively.

Figure 6 shows the best-docked complexes had protein-ligand interactions. It was observed that 5,281,600 forms five hydrogen bonds with residues Pro87, Gln85, Glu152, Tyr153, and Thr136 (Figure 6A). 3,874,518 forms nine hydrogen bonds with the residues Tyr7, Glu166, Gln85, Arg154, Glu152, Gln91, Pro87, Ala98, and Arg142, (Figure 6B). 12,314,417 forms six hydrogen bonds with the residues Arg142, Thr140, Glu166, His168, Tyr133, and Thr136. The stability of interactions between proteins and ligands is dependent on hydrogen bonds. The identification of the individual residues involved in these interactions can offer valuable insights about the binding mechanism of the compound to the protein and its impact on the protein's function (Salentin et al., 2014). Therefore, in order to facilitate molecular-dynamic simulation, these three compounds were selected.

The 2D structure of the identified compounds are shown in the Supplementary Figure S1 The Tanimoto similarity of compounds 12,314,417, 3,874,518, and 5,281,600 with SIS3, the known inhibitor of SMAD3 phosphorylation, compared to study the fundamental differences in their mechanisms of action. The values in Supplementary Table S1 suggest that 5,281,600 has low to moderate structural resemblance to SIS3, while 3,874,518 and 12,314,417 show very little similarity. The Tanimoto scores indicate considerable structural differences from SIS3, suggesting that similar biological effects can be achieved through entirely different chemical structures and binding mechanisms.

3.7 Molecular dynamics simulation

The post-dynamics simulation study provides critical insights into the flexibility of protein-ligand complexes. During the 100 ns production run, only the best-docked complexes were analyzed. The Root Mean Square Deviation (RMSD) of both the protein and ligand, as shown in Figure 7, highlights the stability and conformational changes over time. These RMSD values indicate how closely the system maintains its initial structure, offering valuable information about the dynamic behavior and potential binding efficacy of the ligand within the active site of the protein.

3.7.1 RMSD

The RMSD is a statistical measure that evaluates the degree toward which protein complexes deviate from their initial structure. This allows for the determination of the overall stability of the complexes. As can be seen in Figure 7A, the magnitude of the protein varied from 0.2 nm to 0.37 nm. The protein in the 3,874,518 complex first showed a variance of between 0.2 and 0.3 nm. After that, the more significant fluctuation rose to a range of 0.32–0.36 nm. With the exception of a single, more notable deviation at 45 ps by 0.3 nm, the protein molecule in the 5,281,600-ligand complex changed consistently between 0.2 nm and 0.25 nm. A stable conformation between 0.25 and 0.24 nm was also observed in the protein combination with 12,314,417. In general, the prediction of a stable conformation in the simulation was supported by the protein RMSD. Figure 7B displays the ligand's Root Mean Square Deviation (RMSD). At the initial stage, the ligand 3,874,518 exhibited significant fluctuation and reached 0.7 nm, followed by a subsequent period of consistent configuration. Similarly, during the early phase, 12,314,417 exhibited fluctuations with variations reached 0.7 nm and 1.2 nm. On the other side, after 70 ps, it arrived at a stable conformation with a

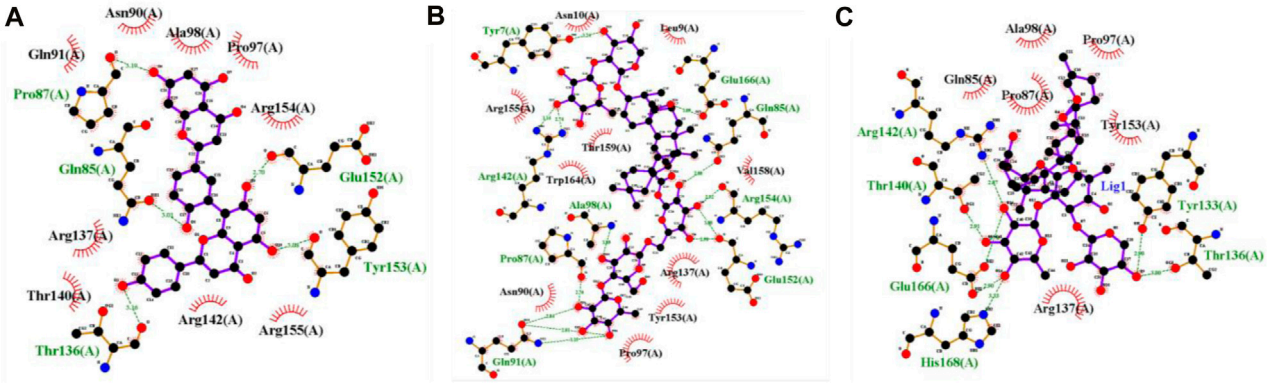


FIGURE 6
2D interaction representation of the top three docked complex **(A)** 5,281,600 **(B)** 3,874,518 **(C)** 12,314,417 (Green lines with residues indicate hydrogen bonds).

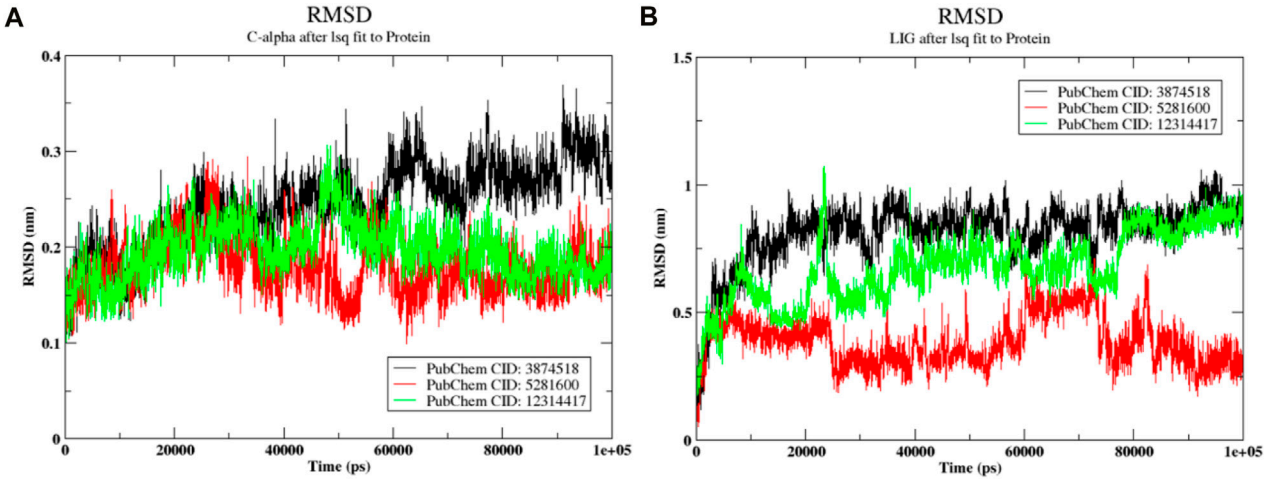


FIGURE 7
Conformational analysis over the 100 ns molecular dynamics simulation **(A)** RMSD of the Protein (SMAD3) **(B)** RMSD of the ligands.

difference of 77 nm regarding the original docked stance. Meanwhile, the 5,281,600 showed deviation ranging from 0.5 nm to 0.4 nm and stability in the last 20 ps. Overall, in the last 20 ps all ligands showed stability.

3.7.2 Conformation analysis

Figures 8A,B,C show the positions of the compounds at 0, 90, and 100 ns during the molecular dynamics simulation, respectively. It was noted that the 3,874,518 showed a deviation from its starting state at 90 ns. However, from 90 to 100 ns, it maintained a similar conformation. Similarly, compounds 5,281,600 and 12,314,417 pose at 0, 90, and 100 ns, as shown in Figures 8D–J, showing a deviation from their starting states at 90 ns. However, from 90 to 100 ns, it maintained a stable conformation.

Despite some early spatial configurational deviations, all three compounds were able to achieve stable conformations by the conclusion of the simulation duration, as seen above. This suggests that, during the course of 100 ns, these compounds' molecular motions go through an adaptation phase and then enter a stable state.

3.7.3 RMSF and SASA studies

Figure 9A displays the protein's root mean square fluctuation. In this case, it was shown that complexed protein residues with compound 3,874,518 showed larger fluctuations of 0.3 nm than residues with ASP31, PRO32, SER33, ASN34, and SER35. Protein in the complex of compound 5,281,600 showed a higher fluctuation of 0.3 nm, which appears in the residues VAL46 and ASN467. Similarly, protein complexed with compound 12,314,417 showed the maximum fluctuation of 0.3 nm that occurred in the residue HIS96 and PRO97. In general, the complexed form did not exhibit significant changes in protein residues. The SASA plot of SMAD3 is shown in Figure 9B when it is coupled to the ligands 3,874,518, 5,281,600, and 12,314,417. The 3,874,518 complex was shown to have a stable conformation at first, but in the last 20 ns, it diverged, suggesting changes in the solvent-exposed surface area. Similarly, in

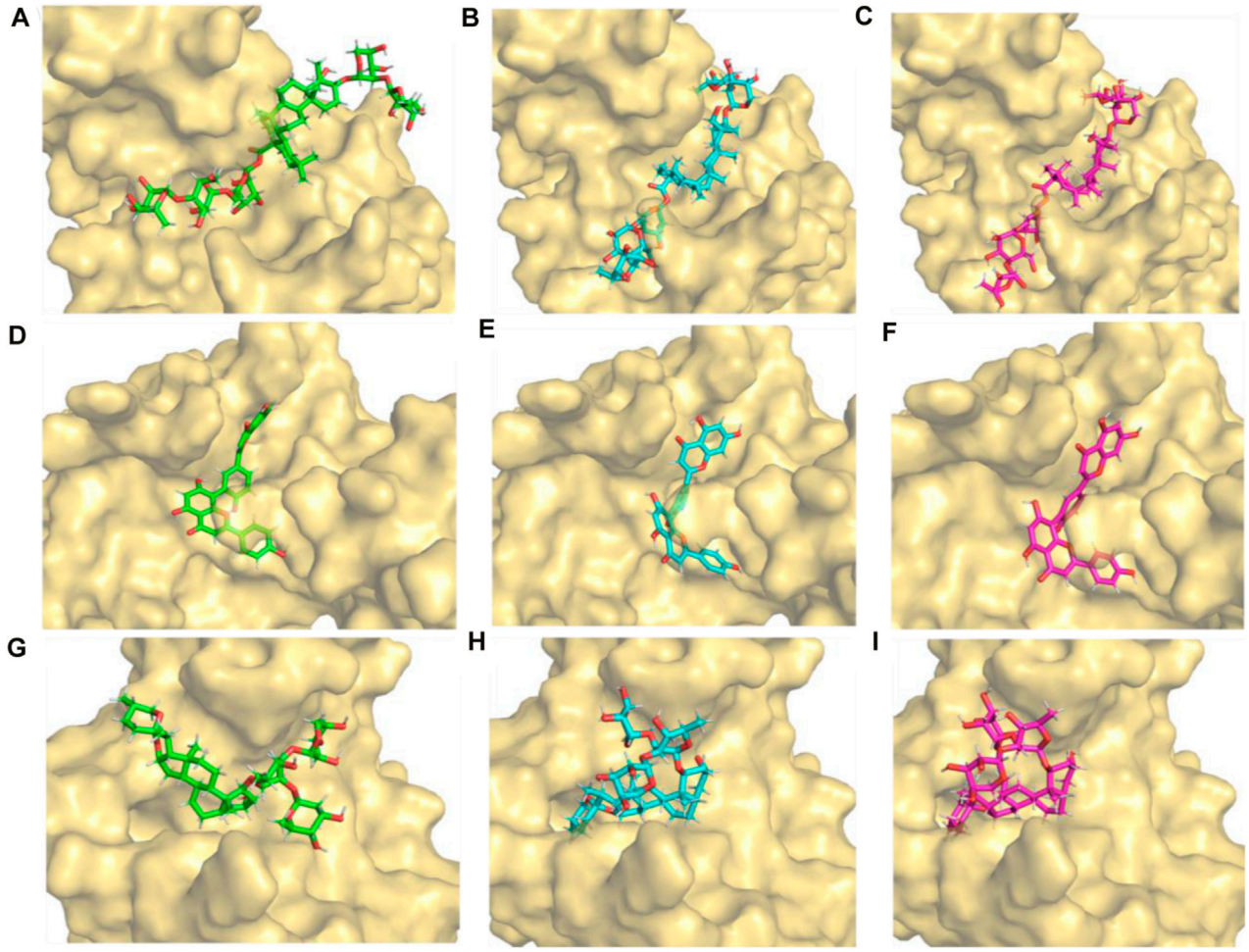


FIGURE 8
Initial (0 ns), stable (90 ns), and final (100 ns) conformation of the protein-ligand complexes extracted from 100 ns molecular dynamics simulation **(A–C)** 3,874,518 **(D–F)** 5,281,600 and **(G–I)** 12,314,417.

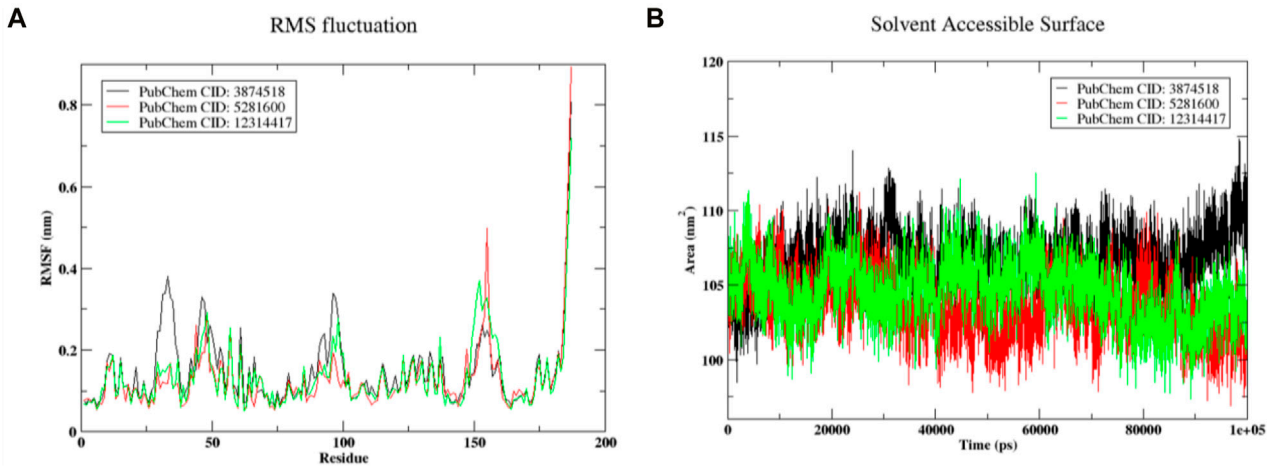


FIGURE 9
(A) RMSF of the complex **(B)** The SASA plot showed change in exposed surface area (on y-axis) with simulation time in picosecond (on x-axis).

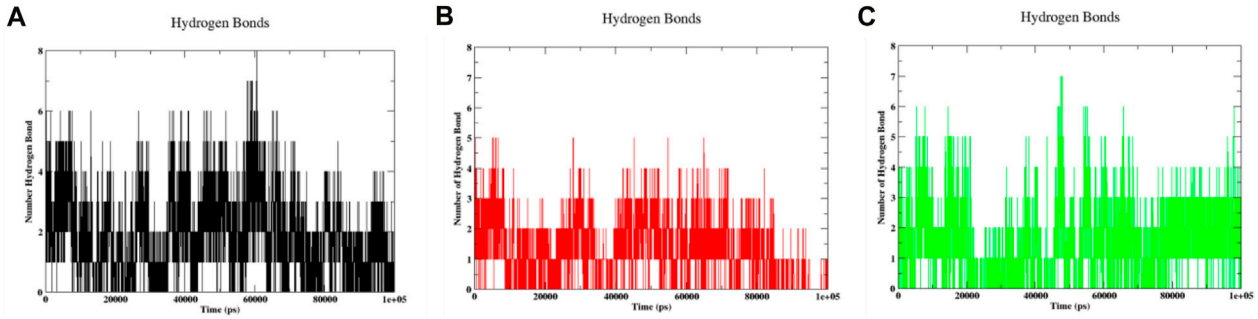


FIGURE 10
Hydrogen bonds formed during the MD run of 100 ns for **(A)** 3,874,518 **(B)** 5,281,600 **(C)** 12,314,417.

the initial phase, 5,281,600 showed stable conformation, but at the last 20 ns, it deviated downward from 105 nm^2 to 110 nm^2 which indicated the extension of the molecule in the solvent. Additionally, 12,314,417 shows relatively stable SASA, suggesting a stable structure in the solvent during the simulation period. Change in SASA showed the conformational change, however, this change was in the acceptable range.

3.7.4 Hydrogen bonds analysis

Hydrogen bonds are crucial in molecular dynamics simulations as they significantly impact the structure, function, and interactions of biomolecules within a simulated environment. This facilitates the understanding of their behaviour within actual biological systems (Salo-Ahen et al., 2020). Within the context of the actual case, an estimation of the formation of hydrogen bonds was carried out during the molecular dynamics simulation of the protein-ligand pair. As the ligand 3,874,518 is attached to the protein, Figure 10A shows that it forms 6–8 hydrogen bonds during the 20–60 ns simulation and then progressively reduces to 3–6 hydrogen bonds after 60 ns until 100 ns. Figure 10B depicts the formation of a hydrogen bond when ligand 5,281,600 binds to the protein. It was found that the compound 5,281,600 produced 4–5 bonds within the first 70 ns, however, after that time period, the number of bonds rapidly decreased from 4 to 2. Figure 10C shows the synthesis of hydrogen resulting from the binding of the compound 12,314,417 to the protein. During the initial period of 20 ns, there was a downward trend of sloping down in the formation of hydrogen bonds. However, the value shifted from 20 to 40 ns to 2 to 5. At a time interval of 45 ns, it established a total of 7 hydrogen bonds. The bond formation steadily dropped from 45 ns to of the range of 6 to 4. Throughout the simulation, the amount of hydrogen bonds fluctuated, creating an uneven pattern. However, it is noticeable that detection of H-bonds is highly sensitive to the interatomic distance. These interatomic distances changed marginally during the simulation that can affect the detection of H-bonds. Moreover, the positive side of the observation shown in Figure 10 is that compounds always shown presence of minimum one hydrogen bond.

3.7.5 Principal component analysis (PCA) and free energy landscape (FEL)

A scatter plot is used to display the trajectory that was generated by the MD simulation. The Principal Component Analysis is used to provide this plot (PCA). Figure 11A showed the formation of four distinct clusters by molecule 3,874,518 during the MD run, illustrating its transition from its initial to final state. Similarly, the 12,314,417 formed three distinct clusters, but these clusters exhibited a higher level of interconnection as shown inFigure 11C. This suggests that for this compound complex, there was a lower degree of transition compared to the 3,874,518. The 5,281,600 complex formed two closely grouped clusters as shown in Figure 11B, suggesting a higher level of stability compared to other molecules. Additionally, the free energy landscape (FEL) of the 3,874,518, 5,281,600, and 12,314,417, respectively, is shown in Figures 11(D–F). Figures 11(D–F) demonstrates the energy distribution across the conformational landscape. The plot shows regions of low free energy basin in blue, which correspond to more stable conformations or states that the protein-ligand complex frequently occupies. The surrounding areas in orange and yellow represent higher free energy states. The plots represented the stability states of several conformations for the aforementioned system that developed throughout the simulation run. The x-axis showed PC1, while the y-axis plotted PC2. These principal components served as reaction coordinates to show various conformations and their corresponding free energy. Here, in Figure 11C, the plot of 3,874,518 showed four energy basins with multiple energy barriers that suggested an stable conformations of the system separated in the space by barriers. Similarly, Figure 11E 12,314,417 showed three energy basins with multiple energy barriers this suggested unstable system conformation during simulation. However, the FEL of 5,281,600 showed two energy basins with a single energy barrier, as observed in Figure 11D, which indicated stable conformation of the system. Overall, PCA and FEL results indicated that the 5,281,600 could be a strong binder of SMAD3. Overall, complex 5,281,600 and 12,314,417 showed more stable characteristics than 3,874,518 where the conformations are distributed in wider space with few minimas. The total portion occupied by the blue color in the plots were larger for 5,281,600 and 12,314,417 that also suggests larger for 5,281,600 and 12,314,417, suggesting its higher chance of reaching minima.

3.7.6 Binding free energy

Several different energetic components were used to determine the binding-free energy of the protein-ligand combination.

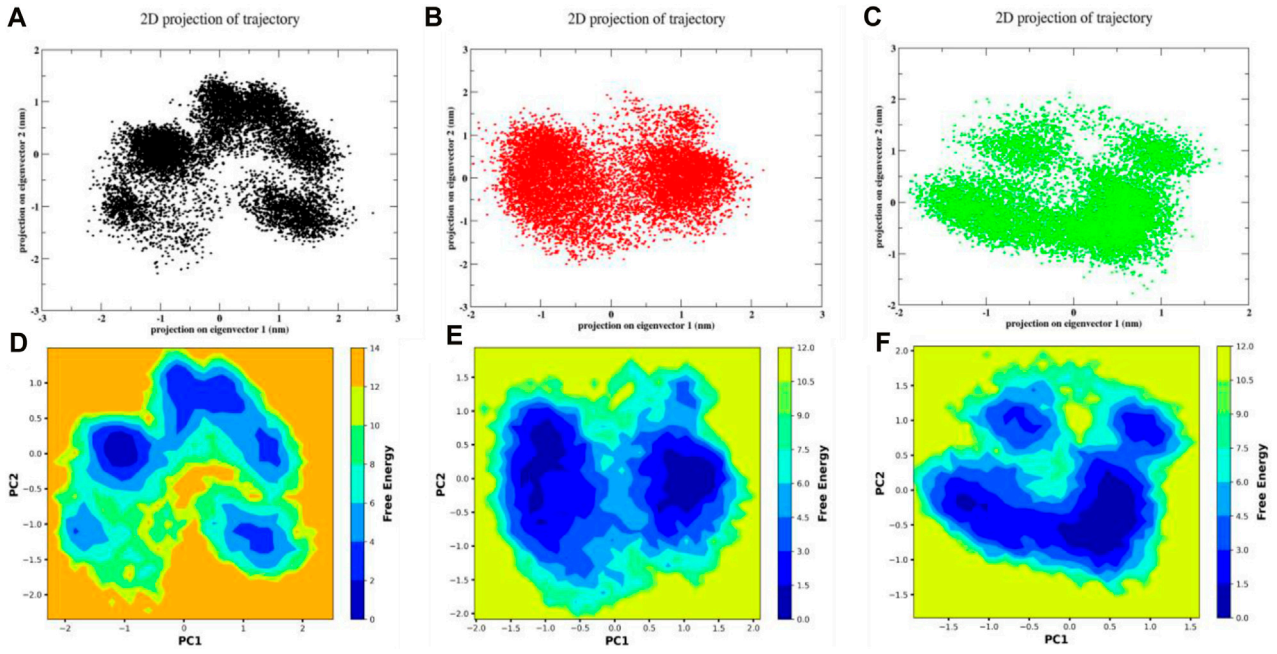


FIGURE 11
The scatter plot representation of PCA for **(A)** 3,874,518 **(B)** 5,281,600 **(C)** 12,314,417 and FEL of **(D)** 3,874,518 **(E)** 5,281,600 **(F)** 12,314,417.

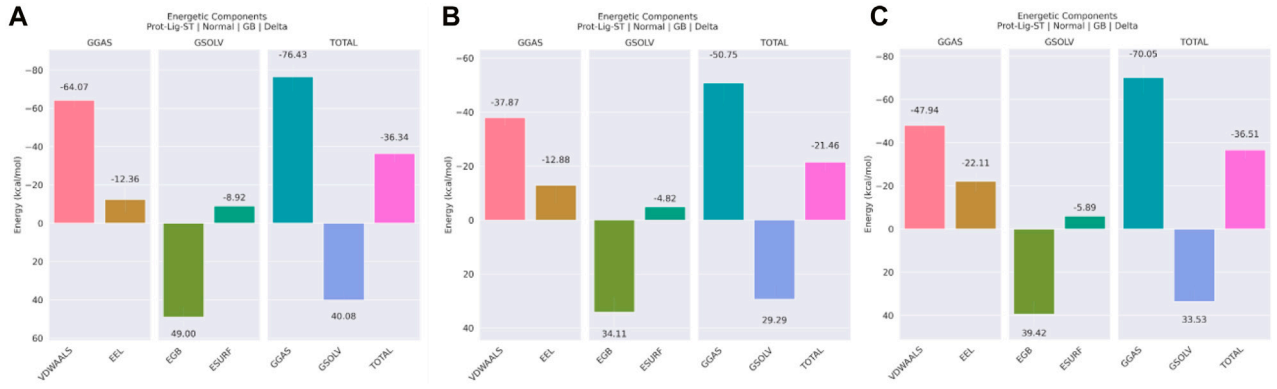


FIGURE 12
Binding Free Energy using MMGBSA technique representation for the complex of compound **(A)** 3,874,518 **(B)** 5,281,600 **(C)** 12,314,417.

According to the data shown in Figure 12A, the 3,874,518 complex, which is composed of the GGAS and GSOLV, has a total binding energy of −36.34 kcal/mol overall. Moreover, in Figure 12B, total binding free energy was observed as −21.46 kcal/mole for the 5,281,600 complex, and in Figure 12C, total binding energy of the 12,314,417 complex observed as −36.51 kcal/mole. This suggested that the 12,314,417 complex showed strongest binding affinity with the protein molecule. Later, close observation on the different energetic components were made, van der Waals contributed most negatively (−64.07, −37.87, and −47.94 kcal/mol) in all three complexes. This showed that steric clashes were perfectly removed in all the complexes. Electrostatic interaction was also favorable for all the three complexes, in the 12,314,417 complex the electrostatic interaction was best. The complex 3,874,518 and 12,314,417 showed very similar binding energy and emerged as the best ligand to bind with the target protein.

Additionally, the binding free energy of the compounds were calculated using the MM/PBSA technique. Supplementary Figure S2 showed the binding free energy of the complexes. 12,314,417 had the lowest binding free energy was 29.38 kcal/mol 3,874,518 also showed similar binding free energy with 27.81 kcal/mole 5,281,600 had binding free energy of 17.09 kcal/mol. The binding free energy trend was similar in both MM/GBSA and MM/PBSA technique. Morever, binding free energy was calculated for comparative analysis of the three compounds. Among the three compounds, both 3,874,518 and 12,314,417 better binding free energy than 5,281,600.

3.8 Discussion

Recent studies on DMD have highlighted gene-targeted medicines, including exon skipping and gene editing, as effective methods to slow down the disease's advancement. The main goal of these therapies is to repair or substitute the function of the faulty dystrophin gene, which plays a crucial role in DMD pathogenesis (Chung Liang et al., 2022; Moorwood et al., 2011). Advancements in comprehending the interaction between the immune system and skeletal muscles have revealed new possibilities for therapeutic targeting. Studies have emphasised the significance of T-Cell profiling and transcriptome analysis of circulating immune cells in DMD, indicating their potential as new biomarkers or therapeutic targets. This immunological analysis could assist in identifying specific groups of cells that either worsen or can reduce muscle damage, allowing for a more customised therapeutic approach (Molinaro et al., 2024). Research on gene therapy and cell transplantation is ongoing. The procedures entail directly introducing accurate copies of the dystrophin gene or transplanting genetically repaired muscle stem cells into patients. Although these technologies show promise, they also pose notable technological and ethical obstacles such as delivery mechanisms, lasting effectiveness, and possible unintended consequences (Sun et al., 2020).

DMD is characterised by abnormal gene expression, and this work comprehensively evaluates those genes. The gene expression patterns of healthy individuals, as well as those with active DMD, are compared to achieve this. Specifically, the GSE38417 dataset from the Gene Expression Omnibus is used for the study (GEO). In a prior study, Lombardo et al. (2021) and Wu et al. (2022) used a dataset that was quite similar to GSE38417 in order to explore gene modules and their relationships with DMD. Additionally, 290 differentially expressed genes (DEGs) that were upregulated were discovered in the first analysis, demonstrating that substantial gene expression changes connected with DMD. The upregulation genes directly impact the diseased condition. Controlling these upregulated genes would bring down the physiopathology for a given disease, the investigation by Moorwood et al. (2011) revealed that utrophin gene upregulation may be used as a treatment strategy for DMD. Additionally, Kemaladewi et al. (2019) demonstrated that in pre-symptomatic MDC1A mice, up-regulating Lama1 via the CRISPR/dCas9-based approach averted muscle fibrosis and hindlimb paralysis when started early. According to Kemaladewi et al. (2019), it partially reversed the course of the illness and reduced dystrophic features when administered to symptomatic mice with muscle fibrosis and hind limb paralysis that were already evident. The enhanced DEGs were then constructed for PPI networks by using the STRING database and a stringent interaction confidence score threshold of 0.90. This was done in order to guarantee optimal analytical accuracy. It was recognised that the expression of particular genes in DMD might represent a compensatory response to cellular stress or a manifestation of pathogenic processes. Hence, a thorough literature study was used to identify gene targets strategically. The DMD gene typically exhibits low expression in DMD due to mutations that result in a marked reduction of dystrophin protein. Conversely, genes such as TTN, SMAD3 and PLEC may be upregulated in response to muscle injury or cellular instability. However, on the basis of enrichment scores, SMAD3 is identified as the most connected gene. Likewise, Multiple studies have demonstrated that TGFβ1/SMAD3 directly interact with the muscular membrane and inhibits the progression of muscle weakening (Goodman et al., 2013; Zhang et al., 2019). Moreover, Pathway enrichment studies offer a valuable understanding of the functional and pathway connections of these genes that are expressed differently (DEGs), highlighting their involvement in immune-related activities. Consequently, it becomes clear that it might be a great target for the therapy of muscular dystrophy, especially Duchenne muscular dystrophy. It was then tested against a library of naturally occurring chemicals. Natural compound PGC-1 α have shown effective results in DMD conditions by targeting PPARγ (Suntar et al., 2020). Another study demonstrated that Isolecanoric acid (ILA), a natural product, was used to explore its anti-inflammatory effect in DMD conditions (Matias-Valiente et al., 2024). Three compounds in the presented study were identified as the most promising candidates for targeting SMAD3 and its desired domain. The protein molecule in the complex state showed a minimum deviation from its native state, and RMSD was under 0.3 nm during the complete simulation. Studies have shown that under 0.3 nm, RMSD could be considered as minimum and acceptable deviation (Sharma et al., 2021). This confirmed that the binding of the ligand brought some change in the protein conformation, but these were considered stable. However, the RMSD of the ligand molecule was higher than that of the protein molecule. The deviation in the ligand molecule in the protein-bound state is acceptable at the early stage of the simulation, which also underline the limitation of the rigid docking algorithm.

The molecular interactions between molecules 3,874,518, 5,281,600, and 12,314,417, which target the MH2 domain of SMAD3, are essential for influencing the TGF-β signaling pathway implicated in conditions such as DMD, which is distinguished by an excessive accumulation of fibrosis (Chen et al., 2014). These molecules exhibit a strong affinity for the MH2 domain and a low free energy of binding, indicating that they establish stable and energetically advantageous interactions. The stability of these compounds is of the utmost importance for their potential as therapeutic agents, as it indicates that they can consistently and effectively disrupt the normal functioning of SMAD3 within the TGF-β pathway, which is well-known for its substantial contribution to the promotion of fibrosis (Budi et al., 2021). Based on the interaction between these molecules and critical residues in the MH2 domain, it is possible that they could alter the activity of SMAD3 by impeding its normal signaling functions. This could involve impeding essential phosphorylation processes that are required for the activation of genes associated with fibrosis. Consequently, these molecules may reduce the pathological signaling responsible for fibrotic tissue formation, a primary component of DMD pathology, by inhibiting SMAD3. This activity corresponds to the therapeutic objectives of managing and alleviating fibrosis in muscular dystrophies, presenting a potentially fruitful pathway for advancing treatments. Extensive research has been conducted previously on the role of the TGF-β/SMAD signaling pathway in fibrosis across various diseases, underlining the therapeutic potential of modulating this pathway (Bujak and Frangogiannis, 2007; Schiro et al., 2011; Piersma et al., 2015).

The suggested chemical interactions of these drugs with SMAD3 present a potential therapeutic approach for treating disorders marked by excessive fibrosis, such as DMD. Additional empirical research, including thorough biochemical testing and clinical studies, is necessary to validate these results and guarantee the safety and effectiveness of these compounds for human usage. The future applications of targeting the SMAD3 pathway in fibrotic diseases such as DMD are promising and diverse. Precision medicine initiatives could leverage genetic

insights to tailor SMAD3 inhibitors to the unique genetic makeup of individual patients, potentially enhancing treatment efficacy and reducing side effects. Insights like these are crucial for creating specific treatments that can control these pathways. The study's discussion on prospective treatment strategies, like using natural chemicals that target specific genes or pathways critical in DMD, emphasises the study's translational potential. This component shows promise by indicating potential pathways for translating the findings of this study into clinical therapies. This thorough method improves the comprehension of DMD on a molecular scale and paves the way for future therapeutic advancements focused on more efficient treatment or control of the condition.

4 Conclusion

The present study was performed to identify hit molecules targeting the MH2 domain of SMAD3 that is involved in DMD. SMAD3 upregulation showed a significant impact on DMD. Screening of natural compounds found three most promising hit compounds: (a) 3,874,518 (b) 5,281,600 (c) 12,314,417. In the molecular dynamic study, 3,874,518 and 12,314,417 showed stable conformation after initial conformational jump. Combined, these two compounds a protein-ligand complex with a greater binding free energy. The fact that these chemicals remain stable at the protein's binding site suggests that they may impose some kind of inhibitory mechanism on the protein. Further, experimental assays are required to validate the computational findings.

Data availability statement

The raw data supporting the conclusion of this article will be made available by the authors, without undue reservation.

Author contributions

MS: Supervision, Writing–original draft, Conceptualization, Funding acquisition, Project administration, Writing–review and editing. AH: Supervision, Writing–original draft, Data curation, Validation, Visualization. AS: Conceptualization, Methodology, Project administration, Visualization, Writing–review and editing. SD: Investigation, Methodology, Validation, Visualization, Writing–original draft.

Funding

The author(s) declare that financial support was received for the research, authorship, and/or publication of this article.

Acknowledgments

The authors extend their appreciation to the King Salman center For Disability Research for funding this work through Research Group no KSRG-2023-422.

Conflict of interest

The authors declare that the research was conducted in the absence of any commercial or financial relationships that could be construed as a potential conflict of interest.

Publisher's note

All claims expressed in this article are solely those of the authors and do not necessarily represent those of their affiliated organizations, or those of the publisher, the editors and the reviewers. Any product that may be evaluated in this article, or claim that may be made by its manufacturer, is not guaranteed or endorsed by the publisher.

Supplementary material

The Supplementary Material for this article can be found online at: https://www.frontiersin.org/articles/10.3389/fphar.2024.1395014/full#supplementary-material

References

Allen, D. G., Whitehead, N. P., and Froehner, S. C. (2016). Absence of dystrophin disrupts skeletal muscle signaling: roles of Ca2+, reactive oxygen species, and nitric oxide in the development of muscular dystrophy. *Physiol. Rev.* 96 (1), 253–305. doi:10.1152/physrev.00007.2015

Amato, A. A., and Griggs, R. C. (2011). Overview of the muscular dystrophies. *Handb. Clin. Neurol.* 101, 1–9. doi:10.1016/B978-0-08-045031-5.00001-3

Angelini, C. (2010). Chapter 31: muscular dystrophy. *Handb. Clin. Neurol.* 95, 477–488. doi:10.1016/S0072-9752(08)02131-3

Aubert, J., Bar-Hen, A., Daudin, J. J., and Robin, S. (2004). Determination of the differentially expressed genes in microarray experiments using local FDR. *BMC Bioinforma.* 5, 125. doi:10.1186/1471-2105-5-125

Bauer, P., Hess, B., and Lindahl, E. (2022). *GROMACS 2022.1 manual*. doi:10.5281/ZENODO.2022.6103568

Bernasconi, P., Di Blasi, C., Mora, M., Morandi, L., Galbiati, S., Confalonieri, P., et al. (1999). Transforming growth factor-beta1 and fibrosis in congenital muscular dystrophies. *Neuromuscul. Disord.* 9 (1), 28–33. doi:10.1016/s0960-8966(98)00093-5

Brinkmeyer-Langford, C., and Kornegay, J. N. (2013). Comparative genomics of X-linked muscular dystrophies: the golden retriever model. *Curr. Genomics* 14 (5), 330–342. doi:10.2174/13892029113149990004

Buchwalow, I. B., Minin, E. A., Müller, F. U., Lewin, G., Samoilova, V. E., Schmitz, W., et al. (2006). Nitric oxide synthase in muscular dystrophies: a re-evaluation. *Acta Neuropathol.* 111 (6), 579–588. doi:10.1007/s00401-006-0069-5

Budi, E. H., Schaub, J. R., Decaris, M., Turner, S., and Derynck, R. (2021). TGF-β as a driver of fibrosis: physiological roles and therapeutic opportunities. *J. Pathol.* 254 (4), 358–373. doi:10.1002/path.5680

Bujak, M., and Frangogiannis, N. G. (2007). The role of TGF-beta signaling in myocardial infarction and cardiac remodeling. *Cardiovasc Res.* 74 (2), 184–195. doi:10.1016/j.cardiores.2006.10.002

Chen, J., Xia, Y., Lin, X., Feng, X. H., and Wang, Y. (2014). Smad3 signaling activates bone marrow-derived fibroblasts in renal fibrosis. *Lab. Invest.* 94 (5), 545–556. doi:10.1038/labinvest.2014.43

Chin, C. H., Chen, S. H., Wu, H. H., Ho, C. W., Ko, M. T., and Lin, C. Y. (2014). cytoHubba: identifying hub objects and sub-networks from complex

interactome. *BMC Syst. Biol.* 8 (Suppl. 4), S11. doi:10.1186/1752-0509-8-S4-S11

Chung Liang, L., Sulaiman, N., and Yazid, M. D. (2022). A decade of progress in gene targeted therapeutic strategies in Duchenne muscular dystrophy: a systematic review. *Front. Bioeng. Biotechnol.* 10, 833833. doi:10.3389/fbioe.2022.833833

Clough, E., and Barrett, T. (2016). The gene expression Omnibus database. *Methods Mol. Biol.* 1418, 93–110. doi:10.1007/978-1-4939-3578-9_5

Duan, D., Goemans, N., Takeda, S., Mercuri, E., and Aartsma-Rus, A. (2021). Duchenne muscular dystrophy. *Nat. Rev. Dis. Prim.* 7 (1), 13. doi:10.1038/s41572-021-00248-3

Eberhardt, J., Santos-Martins, D., Tillack, A. F., and Forli, S. (2021). AutoDock Vina 1.2.0: new docking methods, expanded force field, and Python bindings. *J. Chem. Inf. Model* 61 (8), 3891–3898. doi:10.1021/acs.jcim.1c00203

Flanders, K. C. (2004). Smad3 as a mediator of the fibrotic response. *Int. J. Exp. Pathol.* 85 (2), 47–64. doi:10.1111/j.0959-9673.2004.00377.x

Forli, S., Huey, R., Pique, M. E., Sanner, M. F., Goodsell, D. S., and Olson, A. J. (2016). Computational protein-ligand docking and virtual drug screening with the AutoDock suite. *Nat. Protoc.* 11 (5), 905–919. doi:10.1038/nprot.2016.051

Gao, Q. Q., and McNally, E. M. (2015). The dystrophin complex: structure, function, and implications for therapy. *Compr. Physiol.* 5 (3), 1223–1239. doi:10.1002/cphy.c140048

Ge, S. X., Jung, D., and Yao, R. (2020). ShinyGO: a graphical gene-set enrichment tool for animals and plants. *Bioinformatics* 36 (8), 2628–2629. doi:10.1093/bioinformatics/btz931

Ghasemi, S., Mahdavi, M., Maleki, M., Salahshourifar, I., and Kalayinia, S. (2022). A novel likely pathogenic variant in the FBXO32 gene associated with dilated cardiomyopathy according to whole-exome sequencing. *BMC Med. Genomics* 15 (1), 234. doi:10.1186/s12920-022-01388-5

Goodman, C. A., McNally, R. M., Hoffmann, F. M., and Hornberger, T. A. (2013). Smad3 induces atrogin-1, inhibits mTOR and protein synthesis, and promotes muscle atrophy *in vivo*. *Mol. Endocrinol.* 27 (11), 1946–1957. doi:10.1210/me.2013-1194

Harrach, M. F., and Drossel, B. (2014). Structure and dynamics of TIP3P, TIP4P, and TIP5P water near smooth and atomistic walls of different hydroaffinity. *J. Chem. Phys.* 140 (17), 174501. doi:10.1063/1.4872239

Hess, B., Bekker, H., Berendsen, H. J. C., and Fraaije, J. G. E. M. (1997). LINCS: a linear constraint solver for molecular simulations. *J. Comput. Chem.* 18 (12), 1463–1472. doi:10.1002/(sici)1096-987x(199709)18:12<1463::aid-jcc4>3.3.co;2-l

Hoffman, E. P., Brown, R. H., Jr., and Kunkel, L. M. (1987). Dystrophin: the protein product of the Duchenne muscular dystrophy locus. *Cell* 51 (6), 919–928. doi:10.1016/0092-8674(87)90579-4

Huang, J., and MacKerell, A. D., Jr. (2013). CHARMM36 all-atom additive protein force field: validation based on comparison to NMR data. *J. Comput. Chem.* 34 (25), 2135–2145. doi:10.1002/jcc.23354

Imoto, S., Sugiyama, K., Sekine, Y., and Matsuda, T. (2005a). Roles for lysine residues of the MH2 domain of Smad3 in transforming growth factor-beta signaling. *FEBS Lett.* 579 (13), 2853–2862. doi:10.1016/j.febslet.2005.04.023

Imoto, S., Sugiyama, K., Sekine, Y., and Matsuda, T. (2005b). Roles for lysine residues of the MH2 domain of Smad3 in transforming growth factor-beta signaling. *FEBS Lett.* 579 (13), 2853–2862. doi:10.1016/j.febslet.2005.04.023

Ismaeel, A., Kim, J. S., Kirk, J. S., Smith, R. S., Bohannon, W. T., and Koutakis, P. (2019). Role of transforming growth factor-β in skeletal muscle fibrosis: a review. *Int. J. Mol. Sci.* 20 (10), 2446. doi:10.3390/ijms20102446

Jimenez-Vazquez, E. N., Arad, M., Macías, Á., Vera-Pedrosa, M. L., Cruz, F. M., Gutierrez, L. K., et al. (2022). SNTA1 gene rescues ion channel function and is antiarrhythmic in cardiomyocytes derived from induced pluripotent stem cells from muscular dystrophy patients. *Elife* 11, e76576. doi:10.7554/eLife.76576

Kanehisa, M., and Goto, S. (2000). KEGG: kyoto encyclopedia of genes and genomes. *Nucleic Acids Res.* 28 (1), 27–30. doi:10.1093/nar/28.1.27

Kemaladewi, D. U., Bassi, P. S., Erwood, S., Al-Basha, D., Gawlik, K. I., Lindsay, K., et al. (2019). A mutation-independent approach for muscular dystrophy via upregulation of a modifier gene. *Nature* 572 (7767), 125–130. doi:10.1038/s41586-019-1430-x

Kim, S., Chen, J., Cheng, T., Gindulyte, A., He, J., He, S., et al. (2023). PubChem 2023 update. *Nucleic Acids Res.* 51 (D1), D1373–D1380. doi:10.1093/nar/gkac956

Le Rumeur, E. (2015). Dystrophin and the two related genetic diseases, Duchenne and Becker muscular dystrophies. *Bosn. J. Basic Med. Sci.* 15 (3), 14–20. doi:10.17305/bjbms.2015.636

Liu, X., Sun, Y., Constantinescu, S. N., Karam, E., Weinberg, R. A., and Lodish, H. F. (1997). Transforming growth factor beta-induced phosphorylation of Smad3 is required for growth inhibition and transcriptional induction in epithelial cells. *Proc. Natl. Acad. Sci. U. S. A.* 94 (20), 10669–10674. doi:10.1073/pnas.94.20.10669

Loescher, C. M., Hobbach, A. J., and Linke, W. A. (2022). Titin (TTN): from molecule to modifications, mechanics, and medical significance. *Cardiovasc Res.* 118 (14), 2903–2918. doi:10.1093/cvr/cvab328

Lombardo, S. D., Basile, M. S., Ciurleo, R., Bramanti, A., Arcidiacono, A., Mangano, K., et al. (2021). A network medicine approach for drug repurposing in Duchenne muscular dystrophy. *Genes (Basel)* 12 (4), 543. doi:10.3390/genes12040543

Lovering, R. M., Porter, N. C., and Bloch, R. J. (2005). The muscular dystrophies: from genes to therapies. *Phys. Ther.* 85 (12), 1372–1388. doi:10.1093/ptj/85.12.1372

Malik, V., Rodino-Klapac, L. R., and Mendell, J. R. (2012). Emerging drugs for Duchenne muscular dystrophy. *Expert Opin. Emerg. drugs* 17 (2), 261–277. doi:10.1517/14728214.2012.691965

Martonak, R., Laio, A., and Parrinello, M. (2003). Predicting crystal structures: the Parrinello-Rahman method revisited. *Phys. Rev. Lett.* 90 (7), 075503. doi:10.1103/PhysRevLett.90.075503

Matias-Valiente, L., Sanchez-Fernandez, C., Rodriguez-Outeiriño, L., Ramos, M. C., Díaz, C., Crespo, G., et al. (2024). Evaluation of pro-regenerative and anti-inflammatory effects of isolecanoric acid in the muscle: potential treatment of Duchenne Muscular Dystrophy. *Biomed. Pharmacother.* 170, 116056. doi:10.1016/j.biopha.2023.116056

Menche, J., Sharma, A., Kitsak, M., Ghiassian, S. D., Vidal, M., Loscalzo, J., et al. (2015). Disease networks. Uncovering disease-disease relationships through the incomplete interactome. *Science* 347 (6224), 1257601. doi:10.1126/science.1257601

Molinaro, M., Torrente, Y., Villa, C., and Farini, A. (2024). Advancing biomarker discovery and therapeutic targets in Duchenne muscular dystrophy: a comprehensive review. *Int. J. Mol. Sci.* 25 (1), 631. doi:10.3390/ijms25010631

Moorwood, C., Lozynska, O., Suri, N., Napper, A. D., Diamond, S. L., and Khurana, T. S. (2011). Drug discovery for Duchenne muscular dystrophy via utrophin promoter activation screening. *PLoS One* 6 (10), e26169. doi:10.1371/journal.pone.0026169

Morris, G. M., Huey, R., Lindstrom, W., Sanner, M. F., Belew, R. K., Goodsell, D. S., et al. (2009). AutoDock4 and AutoDockTools4: automated docking with selective receptor flexibility. *J. Comput. Chem.* 30 (16), 2785–2791. doi:10.1002/jcc.21256

O'Boyle, N. M., Banck, M., James, C. A., Morley, C., Vandermeersch, T., and Hutchison, G. R. (2011). Open Babel: an open chemical toolbox. *J. Cheminform* 3, 33. doi:10.1186/1758-2946-3-33

Osseni, A., Ravel-Chapuis, A., Belotti, E., Scionti, I., Gangloff, Y. G., Moncollin, V., et al. (2022). Pharmacological inhibition of HDAC6 improves muscle phenotypes in dystrophin-deficient mice by downregulating TGF-β via Smad3 acetylation. *Nat. Commun.* 13 (1), 7108. doi:10.1038/s41467-022-34831-3

Papaleo, E., Mereghetti, P., Fantucci, P., Grandori, R., and De Gioia, L. (2009). Free-energy landscape, principal component analysis, and structural clustering to identify representative conformations from molecular dynamics simulations: the myoglobin case. *J. Mol. Graph Model* 27 (8), 889–899. doi:10.1016/j.jmgm.2009.01.006

Piersma, B., Bank, R. A., and Boersema, M. (2015). Signaling in fibrosis: TGF-β, WNT, and YAP/TAZ converge. *Front. Med. (Lausanne)* 2, 59. doi:10.3389/fmed.2015.00059

Qin, W., Chung, A. C. K., Huang, X. R., Meng, X. M., Hui, D. S. C., Yu, C. M., et al. (2011). TGF-β/Smad3 signaling promotes renal fibrosis by inhibiting miR-29. *J. Am. Soc. Nephrol.* 22 (8), 1462–1474. doi:10.1681/ASN.2010121308

Raudvere, U., Kolberg, L., Kuzmin, I., Arak, T., Adler, P., Peterson, H., et al. (2019). g:Profiler: a web server for functional enrichment analysis and conversions of gene lists (2019 update). *Nucleic Acids Res.* 47 (W1), W191–W198. doi:10.1093/nar/gkz369

Reimand, J., Kull, M., Peterson, H., Hansen, J., and Vilo, J. (2007). g:Profiler--a web-based toolset for functional profiling of gene lists from large-scale experiments. *Nucleic Acids Res.* 35 (Web Server issue), W193–W200. doi:10.1093/nar/gkm226

Rezaei, N., and Jabbari, P. (2022). *Immunoinformatics of cancers: practical machine learning approaches using R*. Academic Press.

Roberts, A. B., Russo, A., Felici, A., and Flanders, K. C. (2003). Smad3: a key player in pathogenetic mechanisms dependent on TGF-beta. *Ann. N. Y. Acad. Sci.* 995, 1–10. doi:10.1111/j.1749-6632.2003.tb03205.x

Salentin, S., Haupt, V. J., Daminelli, S., and Schroeder, M. (2014). Polypharmacology rescored: protein-ligand interaction profiles for remote binding site similarity assessment. *Prog. Biophys. Mol. Biol.* 116 (2-3), 174–186. doi:10.1016/j.pbiomolbio.2014.05.006

Salo-Ahen, O. M., Alanko, I., Bhadane, R., Bonvin, A. M. J. J., Honorato, R. V., Hossain, S., et al. (2020). Molecular dynamics simulations in drug discovery and pharmaceutical development. *Processes* 9 (1), 71. doi:10.3390/pr9010071

Schiro, M. M., Stauber, S. E., Peterson, T. L., Krueger, C., Darnell, S. J., Satyshur, K. A., et al. (2011). Mutations in protein-binding hot-spots on the hub protein Smad3 differentially affect its protein interactions and Smad3-regulated gene expression. *PLoS One* 6 (9), e25021. doi:10.1371/journal.pone.0025021

Shannon, P., Markiel, A., Ozier, O., Baliga, N. S., Wang, J. T., Ramage, D., et al. (2003). Cytoscape: a software environment for integrated models of biomolecular interaction networks. *Genome Res.* 13 (11), 2498–2504. doi:10.1101/gr.1239303

Sharma, P., Joshi, T., Joshi, T., Chandra, S., and Tamta, S. (2021). Molecular dynamics simulation for screening phytochemicals as α-amylase inhibitors from medicinal plants. *J. Biomol. Struct. Dyn.* 39 (17), 6524–6538. doi:10.1080/07391102.2020.1801507

Sun, C., Shen, L., Zhang, Z., and Xie, X. (2020). Therapeutic strategies for Duchenne muscular dystrophy: an update. *GenesGenes (Basel)* 11 (8), 837. doi:10.3390/genes11080837

Suntar, I., Sureda, A., Belwal, T., Sanches Silva, A., Vacca, R. A., Tewari, D., et al. (2020). Natural products, PGC-1 α, and Duchenne muscular dystrophy. *Acta Pharm. Sin. B* 10 (5), 734–745. doi:10.1016/j.apsb.2020.01.001

Szklarczyk, D., Gable, A. L., Nastou, K. C., Lyon, D., Kirsch, R., Pyysalo, S., et al. (2021). The STRING database in 2021: customizable protein-protein networks, and functional characterization of user-uploaded gene/measurement sets. *Nucleic Acids Res.* 49 (D1), D605–D612. doi:10.1093/nar/gkaa1074

Tian, W., Chen, C., Lei, X., Zhao, J., and Liang, J. (2018). CASTp 3.0: computed atlas of surface topography of proteins. *Nucleic Acids Res.* 46 (W1), W363–W367. doi:10.1093/nar/gky473

Tripodi, L., Villa, C., Molinaro, D., Torrente, Y., and Farini, A. (2021). The immune system in Duchenne muscular dystrophy pathogenesis. *Biomedicines* 9 (10), 1447. doi:10.3390/biomedicines9101447

Trott, O., and Olson, A. J. (2010). AutoDock Vina: improving the speed and accuracy of docking with a new scoring function, efficient optimization, and multithreading. *J. Comput. Chem.* 31 (2), 455–461. doi:10.1002/jcc.21334

UniProt Consortium, (2015). UniProt: a hub for protein information. *Nucl. Acids Res.* 43 (Database issue), D204–D212. doi:10.1093/nar/gku989

Valdes-Tresanco, M. S., Valiente, P. A., and Moreno, E. (2021). gmx_MMPBSA: a new tool to perform end-state free energy calculations with GROMACS. *J. Chem. Theory Comput.* 17 (10), 6281–6291. doi:10.1021/acs.jctc.1c00645

Vanommeslaeghe, K., Hatcher, E., Acharya, C., Kundu, S., Zhong, S., Shim, J., et al. (2010). CHARMM general force field: a force field for drug-like molecules compatible with the CHARMM all-atom additive biological force fields. *J. Comput. Chem.* 31 (4), 671–690. doi:10.1002/jcc.21367

Wang, D., Wang, Z. J., Song, X. X., Pu, L. H., Li, X., and Wang, Y. (2013). Analysis of differentially expressed genes in various stages of Duchenne muscular dystrophy by using a network view. *Genet. Mol. Res.* 12 (4), 4480–4488. doi:10.4238/2013.October.10.13

Wang, J., Fan, Q., Yu, T., and Zhang, Y. (2021). Identifying the hub genes for Duchenne muscular dystrophy and Becker muscular dystrophy by weighted correlation network analysis. *BMC Genom Data* 22 (1), 57. doi:10.1186/s12863-021-01014-w

Wiche, G. (1998). Role of plectin in cytoskeleton organization and dynamics. *J. Cell Sci.* 111 (Pt 17), 2477–2486. doi:10.1242/jcs.111.17.2477

Wu, X., Dong, N., Yu, L., Liu, M., Jiang, J., Tang, T., et al. (2022). Identification of immune-related features involved in Duchenne muscular dystrophy: a bidirectional transcriptome and proteome-driven analysis. *Front. Immunol.* 13, 1017423. doi:10.3389/fimmu.2022.1017423

ww, P. D. B. c. (2019). Protein Data Bank: the single global archive for 3D macromolecular structure data. *Nucleic Acids Res.* 47 (D1), D520–D528. doi:10.1093/nar/gky949

Zhang, P., He, J., Wang, F., Gong, J., Wang, L., Wu, Q., et al. (2019). Hemojuvelin is a novel suppressor for Duchenne muscular dystrophy and age-related muscle wasting. *J. Cachexia Sarcopenia Muscle* 10 (3), 557–573. doi:10.1002/jcsm.12414

Zhou, L., and Lu, H. (2010). Targeting fibrosis in Duchenne muscular dystrophy. *J. Neuropathol. Exp. Neurol.* 69 (8), 771–776. doi:10.1097/NEN.0b013e3181e9a34b

frontiers | Frontiers in Pharmacology

TYPE Original Research
PUBLISHED 31 October 2024
DOI 10.3389/fphar.2024.1492237

Check for updates

OPEN ACCESS

EDITED BY
Pukar Khanal,
Emory University, United States

REVIEWED BY
Smita Kumari,
The Ohio State University, United States
Laxmi Pattanashetti,
KLE College of Pharmacy Hubli, India
Priyanka Patil,
KLE College of Pharmacy, India

*CORRESPONDENCE
Qiang Xue,
ygzxq3@sina.com
Xiaoyu Xu,
xuxiaoyu@swu.edu.cn

RECEIVED 10 September 2024
ACCEPTED 21 October 2024
PUBLISHED 31 October 2024

CITATION
Ren H, Tang L, Yuan Z, Liu Y, Zhou X, Xiao X, Wu X, Chen W, Chen Y, Wang H, Xue Q and Xu X (2024) Combined administration of catalpol, puerarin, gastrodin, and borneol modulates the Tlr4/Myd88/NF-κB signaling pathway and alleviates microglia inflammation in Alzheimer's disease.
Front. Pharmacol. 15:1492237.
doi: 10.3389/fphar.2024.1492237

COPYRIGHT
© 2024 Ren, Tang, Yuan, Liu, Zhou, Xiao, Wu, Chen, Chen, Wang, Xue and Xu. This is an open-access article distributed under the terms of the Creative Commons Attribution License (CC BY). The use, distribution or reproduction in other forums is permitted, provided the original author(s) and the copyright owner(s) are credited and that the original publication in this journal is cited, in accordance with accepted academic practice. No use, distribution or reproduction is permitted which does not comply with these terms.

Combined administration of catalpol, puerarin, gastrodin, and borneol modulates the Tlr4/Myd88/NF-κB signaling pathway and alleviates microglia inflammation in Alzheimer's disease

Huijing Ren[1,2], Ling Tang[3], Zhiying Yuan[1], Yang Liu[1], Xuejiao Zhou[1], Xiao Xiao[1], Xingyu Wu[1], Weihai Chen[4], Yi Chen[1], Hongjin Wang[1], Qiang Xue[5]* and Xiaoyu Xu[1,6,7,8]*

[1]College of Pharmaceutical Sciences and Chinese Medicine, Southwest University, Chongqing, China, [2]Tongren Polytechnic College, Tongren, Guizhou, China, [3]Shapingba District People's Hospital of Chongqing, Chongqing, China, [4]Faculty of Psychology, Southwest University, Chongqing, China, [5]Chongqing Medical and Pharmaceutical College, Chongqing, China, [6]Southwest University Hospital, Chongqing, China, [7]Chongqing Key Laboratory of New Drug Screening form Traditional Chinese Medicine, Chongqing, China, [8]Key Disciplines of Traditional Chinese Medicine of Chongqing City, Rehabilitation Medicine of Southwest University, Chongqing, China

Alzheimer's Disease (AD) is a progressive neurodegenerative disorder affecting millions of people worldwide, with no effective treatment currently available. In recent decades, various traditional Chinese medicines (TCMs) and their active ingredients have shown the potential to attenuate the pathogenesis of AD in cellular and animal models. However, the effects of TCM formulas, which are typically administered in practice, have been less studied. This study aims to investigate the therapeutic effects of several formulas consisting of 4 components herbal components: catalpol, puerarin, gastrodin, and borneol, on streptozotocin (STZ)-induced AD models in cells and rats. The new object recognition (NOR), elevated plus maze (EMP), and Morris water maze (MWM) tests were used to evaluate the cognitive functions of rats. Golgi staining, Haematoxylin and Eosin (HE) staining, and Nissl staining analyses were employed assess the physiology of hippocampal tissues. Gene expression profiles were analyzed used transcriptomics and reverse transcription quantitative polymerase chain reaction analysis, while protein expression levels were determined using immunoblotting, immunohistochemical, and immunofluorescence. The production of cytokines was evaluated with enzyme-linked immunosorbent assay. The results demonstrated that the combined administration of these 4 components (CPGB) had superior mitigating effects on AD cell model, as evidenced by the reduced pro-inflammatory cytokine production and decreased deposition of Aβ protein. Further *in vivo* and *in vitro* experiments confirmed that varying doses of CPGB formula effectively ameliorated STZ-induced cognitive deficits, as shown by NOR, MWM, and EMP tests, as well as pathological changes in hippocampal tissues and a 3-dimensional brain neurovascular unit (3D-NVU) model, including

decreased deposition of Aβ protein and formation of plaques. Transcriptome sequencing and analysis identified 35 genes with significantly altered expression levels due to STZ and CPGB treatment in hippocampal tissues, which were enriched in the Tlr4/Myd88/NF-κB signaling pathway. Interference with this pathway significantly influenced the therapeutic effects of CPGB in the 3D-NVU model. Collectively, these findings suggest that the combined administration of catalpol, puerarin, gastrodin, and borneol offers superior therapeutic effects on AD by modulating the Tlr4/Myd88/NF-κB signaling pathway. This study strengthens the theoretical foundation for using TCMs to treat AD, proving new insights and references for alleviating and treating AD.

KEYWORDS

AD, TCM, 3D-NUV, TLR4/MyD88/NF-κB, transcriptome

Introduction

Alzheimer's disease (AD) is a progressive neurological disorder characterized by dementia, and it is considered one of the most expensive, lethal, and burdensome diseases of this century (Scheltens et al., 2021). According to Alzheimer Disease International, the majority of the 10 million new cases of dementia each year are attributed to AD (Prince et al., 2015). Cohort studies have also reported that the median survival time after an AD dementia diagnosis is less than 6 years (Mayeda et al., 2017; Rhodius-Meester et al., 2019). In recent decades, significant advancements have been made in understanding the pathology of AD, including amyloid beta (Aβ) deposition and plaque (Depp et al., 2023), neurofibrillary tangles of abnormally phosphorylated Tau protein (Wegmann et al., 2021), neuroinflammation, oxidative stress, neuronal loss, synaptic dysfunction (Jack et al., 2024; Scheltens et al., 2021). At the cellular level, alterations in neurons, microglia, and astroglia have been observed to drive the gradual progression of AD before cognitive impairment becomes apparent (De Strooper and Karran, 2016). For example, neuroinflammation in microglia, a group of highly motile phagocytes in the central nervous system frequently found near Aβ deposits in AD patients (Merighi et al., 2022), is recognized as a major component of AD pathology, contributing to disease progression and neurodegeneration (Venegas et al., 2017; Xie et al., 2022). This makes it a popular therapeutic target for AD treatment (Lewcock et al., 2020; Venegas et al., 2017). Specifically, Aβ binds to several innate immune receptors in microglia, including toll-like receptor 2 (TLR2), TLR4, and TLR6, activating the microglia (Liu et al., 2012). Activated microglia then produce elevated levels of pro-inflammatory cytokines such as tumor necrosis factor (TNF)-α, interleukin (IL)-1β, IL-6, nitric oxide (NO), and reactive oxygen species (ROS) (Rani et al., 2023; Thakur et al., 2023), leading to neuroinflammation and AD progression.

Traditional Chinese medicine, including Chinese herbs and their extracts, has been frequently used in the treatment of dementia due to their multi-target and multi-pathway mechanisms, offering promising therapeutical for complex diseases like AD (Chen et al., 2020). Various active ingredients extracted from Chinese herbs have shown beneficial effects on AD through diverse mechanisms. For instance, catalpol, an active compound from *Rehmannia glutinos*, has been reported to slow AD progression by enhancing the expression of neural stem cell exosome-released miR-138-5p (Chen et al., 2022; Meng et al., 2023). Similarly, puerarin, derived from *Puerariae Lobatae Radix*, demonstrates neuroprotective effects by targeting the PI3K/Akt signaling pathway (Wang et al., 2022). Gastrodin, from *Gastrodia elata*, reduces neuro-inflammation in AD models by inhibiting the NF-κB signaling pathway (Yin et al., 2024). Lastly, borneol, extracted from *Blumea balsamifera DC* or *Cinnamomum camphora* (L.) *Presl*, has been found to effectively relieves AD-like symptoms in mice by clearing Aβ aggregates (Ye et al., 2024). These studies highlight the potential of individual herbal ingredients in targeting different aspects of AD pathology.

However, most of these ingredients were administered as single compounds, whereas combination therapies have been shown to produce enhanced therapeutic effects in complex diseases like AD (Cummings et al., 2024; Cummings et al., 2019). Given that TCM traditionally involves the use of multi-ingredient formulations and that AD is a multifactorial disease (Scheltens et al., 2021), it is hypothesized that combining these plant-derived ingredients may offer superior benefits in mitigating AD progression.

We hypothesize that the combined administration of catalpol, puerarin, gastrodin, and borneol will demonstrate improved mitigative effects on AD progression compared to their individual use. To validate our hypothesis, we will formulate these 4 ingredients into different combinations and evaluate their therapeutic effects on AD progression in models. Subsequently, we will further explore the underlying mechanisms of the formulation with the most potent therapeutic effects. Our research aims to further refine the theoretical foundation of using traditional Chinese medicine to treat AD, providing new insights and references for alleviating and treating the disease.

Materials and methods

Formulation preparation

In this study, we utilized 4 plant-derived compounds: catalpol (CAS: 2415-24-9), puerarin (CAS: 3681-99-0), gastrodin (CAS: 62499-27-8) and borneol (CAS: 124-76-5). Catalpol, puerarin, and gastrodin were sourced from Dierg Pharmaceutical Technology Co., Ltd., Nanjing, China, while borneol was obtained from Tongrentang, Chongqing, China. Supplementary

Figure S1 presents the chemical structure diagrams of these compounds. In our previous research, we discovered that a combination of catalpol, puerarin, and borneol in a 1:4:2 ratio maximized brain absorption and exhibited neuroprotection effects in an ischemic model (Qiang et al., 2016; Tang et al., 2016). Building on these findings, we incorporated gastrodin into the formulation, using a 1:4:2:2 ratio for CPGB, which yielded significantly improved results in AD models compared to other ratios (data not shown). For this optimized ratio, we prepared 15 formulations: catalpol alone (C), puerarin alone (P), gastrodin (G), borneol (B), catalpol + puerarin (CP), catalpol + gastrodin (CG), catalpol +borneol (CB), puerarin +gastrodin (PG), puerarin + borneol (PB), gastrodin + borneol (GB), catalpol + puerarin + gastrodin (CPG), puerarin + gastrodin + borneol (PGB), catalpol + gastrodin + borneol (CGB), catalpol + puerarin + borneol (CPB), catalpol + puerarin + gastrodin + borneol (CPGB). These formulations were prepared using a 35% hydroxypropyl-beta-cyclodextrin solution (Merck, Kenilworth, NJ, United States), which was commonly used to solubilize poorly soluble drugs due to its ability to form inclusion complexes with hydrophobic molecules (Wang and Brusseau, 1993). Specifically, 800 mg of puerarin and 400 mg of borneol were dissolved in 50 mL of the solution, followed by the addition of 200 mg of catalpol and 400 mg of gastrodin to create the high-dose CPGB solution (360 mg/kg). The solution was subsequently diluted to obtain mild (180 mg/kg) and low (90 mg/kg) doses. All these formulations were freshly prepared and used immediately, and no changes in the physical appearance of the solution were observed during the preparation or usage process. As a result, a stability study on these formulations was not conducted in this study. Additionally, we used donepezil hydrochloride tablets (DPN; Zein Bio, Nanjing, China) as a positive control to evaluate the therapeutic effects of these formulations.

Cell culture and treatment

The pheochromocytoma cell line (PC12) and the BV2 microglial cell line (BV2) used in this study were kindly provided by Prof. Hongyi Qi from the College of Pharmacy, Southwest University, Chongqing, China. These cell lines were cultured in a complete medium composed of 89% Dulbecco's Modified Eagle Medium: Nutrient Mixture F-12 (DMEM/F12; Gibco, Waltham, MA, United States), 10% fetal bovine serum (FBS; Gibco, Waltham, MA, United States), and 1% penicillin-streptomycin (PS; Gibco, Waltham, MA, United States) maintained at 37%°C in an incubator with 5% CO_2. Once the cells reached 90% confluence, they were detached, collected, and resuspended in a complete medium for subsequent experiments.

AD cell model establishment and treatment

Referencing previous studies (Gupta et al., 2018; Kamat, 2015; Li et al., 2020), we established an AD cell model by treating PC12 and BV2 cells with 0.5 mol/mL STZ. Briefly, PC12/BV2 cells were evenly seeded into 6-well plates (ThermoFisher, Shanghai, China) at a density of 2×10^5 cells each well. After 24 h of proliferation, the supernatant was discarded, and a fresh complete medium containing either no additives, 0.5 mol/mL streptozotocin (STZ; Solarbio, Beijing, China) or 0.5 mol/mL STZ plus various formulations was added for further culture. Each treatment was performed with 3 replicates. Following cultivation, the supernatant was collected for subsequent enzyme-linked immunosorbent assay (ELISA) experiments, while cells from each well were collected for total RNA or total protein extraction.

Alternatively, PC12/BV2 cells were seeded onto sterile coverslips in 24-well plates (ThermoFisher, Shanghai, China) at a density of 5×10^4 cells/mL, with 1 mL of cell suspension added to each well. After 24 h of proliferation, the supernatant was discarded, and a fresh complete medium containing either no additives, 0.5 mol/L STZ, or 0.5 mol/L STZ plus various formulations was added for further culture. Each treatment was performed with 3 replicates. After cultivation, the coverslips were collected for subsequent immunofluorescence analyses.

Three-dimensional brain neurovascular unit (3D-NVU) model establishment and treatment

To establish the 3D-NVU model, hippocampal neural stem cells (NSCs) and brain microvascular endothelial cells (BMECS) were harvested according to previous established methods (Liu et al., 2013; Wang et al., 2021). Briefly, NSCs were isolated from the hippocampi of 24-h-old SD rat pups. After anesthesia and decapitation, the brains were quickly removed under sterile conditions and placed in cold D-Hanks solution (Solarbio, Beijing, China). The hippocampal region was dissected, minced, and centrifuged at 800 rpm for 5 min. The resulting tissue was digested with accutase (ThermoFisher, Shanghai, China) for 5 min at 37°C. The cell suspension was filtered and centrifuged. The pellet was resuspended in DMEM/F12 medium containing 20 ng/mL epidermal growth factor (EGF), 10 ng/mL basic fibroblast growth factor (bFGF), 2% B27, and 0.0002% heparin, then cultured at 37°C with 5% CO2. Cells were passaged or used for experiments after 6-7 days. BMECs were isolated from the cortex of 10-day-old SD rats. After decapitation and removal of the brain, the cortex was dissected, and large blood vessels and meninges were removed. The tissue was homogenized, followed by centrifugation at 1,200 rpm for 5 min. The homogenate was treated with 25% BSA and centrifuged at 2,500 rpm to collect the microvascular fragments. The fragments were digested with 0.1% type II collagenase for 5 min, then centrifuged and resuspended in complete medium with 20% FBS. Cells were seeded into collagen-coated flasks and cultured at 37°C with 5% CO2. Media were changed every 2-3 days, and cells were used when 90% confluence was reached.

NSCs and BMECs were mixed with Matrigel (Corning, Corning, NY, United States) at a 1:10 density ratio. The mixture was resuspended, and 150 μL of the cell/Matrigel mixture was evenly distributed at the bottom of a laser confocal dish and incubated to solidify. After 20 min of incubation, an additional 50 μL of the cell/Matrigel mixture was spread over the surface of the solidified layer and returned to the incubator for another 20 min before adding the medium. The NSC/BMEC co-

culture medium consisted of DMEM/F12 and Neurobasal (ThermoFisher, Shanghai, China) in a 1:1 ratio, supplemented with 2% B27, 20 ng/mL recombinant human EGF (rhEGF), and 10 mg/mL recombinant human basic fibroblast growth factor (rhbFGF). On the 3rd day, the B27 supplement was switched to a formulation containing vitamin A. After 7 days of culture, the 3D-NVU model was successfully replicated, as confirmed by the positive expression of β-tubulin3, glial fibrillary acidic protein (GFAP), and CD31 marker proteins (Wang et al., 2021). After confirming the successful establishment of the 3D-NVU model, a medium containing either no additives, 0.5 mol/L STZ, 0.5 mol/L STZ plus various formulations, or 0.5 mol/L STZ + various formulations + inhibitors were added for further culture. Each treatment was performed with 3 replicates. Following cultivation, the supernatant was collected for subsequent ELISA experiments, while cells from each well were collected for total RNA or total protein extraction.

BV2 conditioned medium collection and treatment

Referencing a previous study (Qureshi et al., 2022), a conditioned medium of microglia was employed to induce cellular damage. Briefly, BV2 cells were evenly seeded into 6-well plates at a density of 2×10^5 cells per well. After 24 h of culture, the medium in each well was replaced with a fresh complete medium containing either no additives, 0.5 mol/L STZ, or 0.5 mol/L STZ plus various formulations. Following another 24 h of culture, the medium was discarded, and the cells were washed 3 times. Subsequently, 1 mL of completing medium was added to each well for an additional 24 h of culture. The medium in each well was then collected as a conditioned medium. Additionally, PC12 cells were seeded into 96-well plates at the density of 2×10^3 per well. After 24 h of culture, the medium was discarded, and the collected conditioned medium from BV2 cells was added to the wells for an additional 24 h of culture. The viability of the PC12 cells was then assessed using the Cell Count Kit-8 (CCK8) assay. Briefly, the supernatant was discarded, and 100 μL of fresh complete medium containing 10% CCK-8 solution (Solarbio, Beijing, China) was added. After 2 h of incubation, the optical density at 450 nm (OD450) was measured using a microplate reader (ThermoFisher, Shanghai, China).

Animal housing and management

The rats used in this study were male Sprague-Dawley rats of specific pathogen-free grade, aged 3–4 months with weights ranging from 350 to 380 g. They were purchased from Liaoning Changsheng Biotechnology Co., Ltd. (Shenyang, China). The rats were maintained at the Experimental Animal Center of the College of Pharmacy, Southwest University. They were housed in standard cages at 22°C ± 2°C, on a 12-h light/dark cycle, with a humidity level of 40%–60%. Throughout the experimental period, all rats had free access to water and food, and the bedding was refreshed every 2 days.

AD rat model establishment

Following a previous study (Moreira-Silva et al., 2018), an AD rat model was established through intracerebroventricular (ICV) injection of STZ. Briefly, after 1 week of adaptive feeding and a subsequent 12-h fasting period, the rats were anesthetized with 5% isoflurane. Their heads were then secured in a stereotaxic apparatus, and anesthesia was maintained with 2% isoflurane. The fur on the scalp was trimmed, and the skin was disinfected with iodine and alcohol. A midline incision approximately 1.5 cm in length was made along the sagittal suture to expose the skull. The periosteum was washed with 3% hydrogen peroxide (Solarbio, Beijing, China) and pushed aside to fully expose the cranial bone. Bilateral burr holes were drilled based on coordinates referenced from the bregma: −0.8 mm anteroposterior, ± 1.4 mm mediolateral, and −3.6 mm dorsoventral, according to the rat brain atlas by Paxinos and Watson (Paxinos and Watson, 2006). Small burr holes were carefully drilled using a dental drill, thinning the skull without penetrating it. A microsyringe (Hamilton, Reno, NV, United States) was then carefully inserted vertically to a depth of 3.8 mm. Afterward, both STZ and arachidonoylethanolamide (AEA; Sigma-Aldrich, St. Louis, MO, United States) were prepared in citrate buffer (Merck, Kenilworth, NJ, United States) and administered using an automated microinjection system (Insight Equipment LTDA, São Paulo, Brazil). This system included a polyethylene microtube connected to an injection needle and the inserted microsyringe coupled with an infusion pump. Each rat received 2 ICV bilateral injections of 2 μL at a rate of 1 μL/min. The first injection consisted of either citrate buffer (for sham procedure; 0.05 M) or AEA (100 ng). Five minutes later, a second injection of either citrate buffer or STZ (2 mg/kg) was administered. To prevent reflux, the injection needle was left in place for at least 2 min following each infusion. Post-surgery, the rats received an intraperitoneal injection of ceftriaxone sodium (100 mg/kg; Merck, Kenilworth, NJ, United States) once daily for 3 days to prevent infection, along with analgesic carprofen (5 mg/kg; Merck, Kenilworth, NJ, United States). Additionally, 2 mL of saline was administered subcutaneously for rehydration. The rats were then kept on thermal blankets with controlled temperature until full recovery.

Treatment of rats and sample collection

On the day following surgery, rats in both the sham and model groups were orally administered a 35% hydroxypropyl β-cyclodextrin solution. Meanwhile, those in the treatment groups received DPN and CPGB at doses of 90, 180, and 360 mg/kg for low, medium, and high doses, respectively, via gavage at a rate of 1 mL/kg. Each group consisted of 16 rats. The treatment was administered daily for 42 consecutive days. The doses of CPGB were determined referencing to our previous research (Tang et al., 2016). An earlier acute toxicity study confirmed that these doses did not produce any observable toxic effects on the major organs of the rats. In summary, rats administered 5.12 g/kg of CPGB exhibited no abnormal reactions compared to normal rats. In contrast, rats given 6.4 g/kg of CPGB exhibited mild symptoms, such as reduced activity and partial paralysis, which resolved within 24 h. Furthermore, a 14-days treatment with CPGB at doses of 5.12 g/kg or lower did not

result in any signs of toxicity, mortality, or significant changes in behavior, body weight, or organ function. Behavioral assessments were performed using the Novel Objective Recognition (NOR) test from days 31–33, the Elevated Plus Maze (EPM) test from days 34–35, and the Morris Water Maze (MWM) test from days 46 to 36. Upon completing the MWM test on the 42nd day, 3 rats from each group were euthanized to collect hippocampal electrical signals. The remaining rats were anesthetized and euthanized by cervical dislocation, after which their brains were collected for further experiments.

New object recognition

To evaluate the hippocampus-dependent non-emotional memory in rats, the NOR test was conducted from days 31–33, as referenced in a previous study (Leger et al., 2013). The experimental setup consisted of a cylindrical enclosure made of black Plexiglas plastic, measuring 50 cm in both diameter and height. To minimize anxiety due to unfamiliarity, rats were allowed to acclimate to the environment by being placed in the apparatus for 5 min, 24 h before the test. During the familiarization phase, 2 identical objects, labeled A1 and A2, were positioned at opposite corners of the enclosure, each 5 cm from the corner. Each rat was gently placed in the enclosure and allowed to explore the objects for 5 min. After a 24-h interval, object A2 was replaced with a new object for the test session, and the rat was reintroduced to the enclosure to explore the objects for another 5 min. Exploratory behavior was defined as orienting the nose towards an object at a distance of less than 2 cm or making physical contact with the object using the nose. The exploration time for each object during both the familiarization and test sessions was recorded. The Discrimination Index (DI) was calculated using the following formula: DI = Time spent in exploring the novel object/(Time spent in exploring old object + Time spent in exploring the novel object).

Elevated plus maze

To investigate anxiety-related behavior in rats, the EMP test was conducted, referencing a previous study (Walf and Frye, 2007). The maze consisted of 1 open arm and 1 closed arm. On the 34th after surgery, each rat was placed facing outwards on the open arm for free exploration. The time taken for the rat transition from the open arm to its initial entry into the closed arm was recorded by a camera and noted as the initial escape latency (EL1). If this time exceeded 90 s, it was recorded as 90 s. On the 35th day, the same test method was used to obtain the ultimate escape latency (EL2). The relative escape latency (REL) was calculated using the following formula: REL = EL2/EL1 × 100%.

Morris water maze test

The spatial learning and memory abilities of rats were assessed using the Morris Water Maze (MWM) experiment (Vorhees and Williams, 2006). The procedure involved a series of acquisition trials conducted over 5 consecutive days. Each day, the rats underwent 4 trials with a minimum inter-trial interval of 15 s. In each trial, rats were released from a randomly selected starting point and given up to 120 s to locate the platform. Upon finding the platform, they were allowed to remain on it for 5 s. If a rat failed to find the platform independently, it was manually guided to the platform and held there for 15 s. The latency times for all trials were recorded. On the 6th day, a probe trial was conducted to evaluate spatial memory without the platform. During this trial, the frequency of platform crossings, as well as the duration and distance traveled within the target quadrant, were measured. The EthoVisionXT 8.5 software (Noldus, Wageningen, Netherlands) was used to analyze the frequency of each rat passing through the location of the original platform, the swimming distance within the quadrant, and the time spent in the platform area. More crossings and longer routes indicated better learning and memory retention, as did longer durations spent in the quadrant containing the original platform.

Hippocampal electrical signal acquisition test

After the MWM test, 3 randomly selected rats were anesthesia with 5% isoflurane, and their heads were secured on a brain stereotaxic instrument (Insight Equipment LTDA, São Paulo, Brazil). Recordings were made using a NeurLynx 32-channel electrophysiological recorder. An 8-channel recording electrode was implanted with coordinates relative to the brain Bregma point as the zero point: dorsoventral at −3.6 mm and lateral ventricle at 2.5 mm. Following a 30-min baseline recording, the spike peak potential was recorded for an additional 30-min.

ELISA

ELISA was employed to determine the concentrations of Aβ1-42, TNF-α, IL-1β, and IL-6 in the hippocampal tissue homogenate or collected supernatant using commercialized ELISA kits (Nanjing Jiancheng, Nanjing, China) according to their instructions. In brief, 100 μL of supernatant was added to each well of the reaction plate, which was then sealed with a membrane and incubated at room temperature for 2 h. Subsequently, biotinylated antibody, horseradish peroxidase-labeled streptavidin, and tetramethylbenzidine solution were added to each well. The plate was incubated overnight at room temperature in the dark. Finally, 50 μL of stop solution was added to terminate the reaction, and the OD450 was measured using a microplate reader.

RNA extraction and reverse transcription quantitative polymerase chain reaction (TR-qPCR) analysis

Total RNA from collected hippocampal tissue and cells was extracted using Trizol Reagent (TransGen, Beijing, China) following the manufacturer's protocol. The concentration and purity of extracted RNA were measured using a NanoDrop ND-2000 spectrophotometer (Thermo Fisher Scientific, Wilmington, NC, United States), and its integrity was confirmed through 1%

agarose gel electrophoresis. Following this, the total RNA samples were reverse transcribed to complementary DNA (cDNA) using the RevertAid First Strand cDNA Synthesis Kit (ThermoFisher, Shanghai, China) following the manufacturer's instructions. RT-qPCR was then conducted under the following conditions: initial denaturation at 95°C for 30 s, followed by 40 cycles of denaturation at 95°C for 5 s, and annealing and extension at 60°C for 30 s. The primer sequences used in this study are listed in Supplementary Table S1, and the data was analyzed using the $2^{\Delta\Delta C}$ method in Excel.

Total protein extraction and immunoblotting analysis

Proteins were extracted from collected hippocampal tissue and cells using RIPA lysis buffer (Solarbio, Beijing). The protein concentrations were determined with a BCA kit (Beyond, Shanghai, China). Subsequently, the proteins were denatured at 100°C for 10 min. And 30 μg of the extracted total protein from each sample were loaded onto a 12% sodium dodecyl sulfate-polyacrylamide for electrophoresis. After electrophoresis, the proteins were transferred onto a polyvinylidene fluoride membrane. The membrane was blocked with 5% skim milk in TBST for 2 h. Following blocking, the membranes were incubated overnight at 4°C with primary antibodies. On the following day, the membranes were treated with a secondary antibody and enhanced chemiluminescent reagents to visualize the protein bands. The antibodies used in this study are listed in Supplementary Table S2. The intensity of the protein bands was analyzed using ImageJ software.

Histological analysis

For Golgi staining, a Golgi staining kit (Servicebio, Chengdu, China) was employed. Briefly, the brain tissues collected were first washed and fixed with 4% paraformaldehyde (Life iLab Bio, Shanghai, China) at −20°C for 24 h. Following fixation, the tissues were immersed in a dark A + B mixture at room temperature for 14 days, then soaked in C solution for an additional 5 days. The tissues were subsequently sectioned using a freezing microtome set to a thickness of 180 μm. These sections were stained with D solution and observed under a microscope for imaging.

The remaining freshly collected brain tissues were fixed in 4% paraformaldehyde for 48 h. After fixation, the tissues were rinsed several times with tap water, dehydrated through a gradient alcohol series, soaked in paraffin, and then embedded. For Haematoxylin and Eosin (HE) staining analysis, the paraffin sections (5 μm thick) were incubated at 80°C for 20 min, de-paraffinized, and then soaked in haematoxylin solution (Solarbio, Beijing, China) for 15 min. The sections were rinsed with tap water for re-bluing, stained in eosin, hydrated through a gradient alcohol series, cleared with xylene, and mounted with neutral resin before being air-dried, observed, and photographed under a microscope.

For Nissl staining, a Nissl staining kit (Beyotime, Shanghai, China) was employed. Briefly, brain sections were dewaxed, stained with methylene blue solution for 10 min, differentiated for 1 min, treated with ammonium molybdate solution for 5 min, and sealed using a neutral gum. The Nissl bodies were then visualized and imaged using a fluorescence microscope (Olympus, Tokyo, Japan) and quantified with ImageJ software.

For Immunohistochemical staining, the sections were dewaxed, washed 3 times, immersed with 3% H_2O_2 at room temperature for 10 min, and incubated with antigen retrieval solution at 37°C for 20 min. The sections were blocked with 5% bovine serum albumin (ThermoFisher, Shanghai, China) at room temperature for 2 h. Following blocking, sections were incubated with primary antibody at 4°C for 16 h, followed by 3 times washes. The sections were then incubated with a secondary antibody at 37°C for 30 min. DAB coloration was applied, and the nucleus was counterstained with hematoxylin. After dehydration, sections were sealed with neutral resin. The antibodies used in this study are listed in Supplementary Table S2. The Aβ-16 was visualized and imaged using a fluorescence microscope and quantified with ImageJ software.

Immunofluorescence

The collected brain tissues and cell slices were dewaxed and fixed with 4% paraformaldehyde at −20°C for 10 min. Following fixation, the tissues and cells were permeabilized with 0.1% Triton X-100 (Solarbio, Beijing, China) at room temperature for 10 min. They were then blocked with 10 g/L bovine serum albumin (Solarbio, Beijing, China) for another 10 min and incubated overnight at 4°C with primary antibodies. After 3 washing, the secondary antibody was applied and incubated at room temperature for 4 h. The antibodies used in this study are listed in Supplementary Table S2. The cell nuclei were stained with 4′,6-diamidino-2-phenylindole (DAPI; Solarbio, Beijing, China) for 5 min at room temperature. Finally, the brain tissues and cells were observed and digitally captured using a fluorescence microscope.

Transcriptome sequencing and analysis

Total RNA was extracted from the collected hippocampus tissues using Trizol Reagent, following the standard phenol/chloroform phase separation method. The RNA concentration and integrity were measured with a NanoDrop ND-2000 spectrophotometer and an Agilent Bioanalyzer 2100 (Agilent Technologies; Santa Clara, CA, United States). Only samples with an RNA integrity number (RIN) above 0.8 were selected for subsequent sequencing. Complementary DNA libraries were constructed using the Illumina TruSeq RNA Sample Prep Kit (Illumina; San Diego, CA, United States), resulting in an average fragment size of 150 bp, excluding adaptors. The quality and integrity of these libraries were assessed with an Agilent 2100 Bioanalyzer and an ABI StepOnePlus Real-Time PCR System (Thermo Fisher Scientific; Waltham, MA, United States). The RNA-Seq FASTQ files were aligned to the rat genome using the Hisat2 algorithm (Kim et al., 2019), referencing data from the Ensembl Rat Genome Database (https://ftp.ensembl.org/pub/release-112/fasta/rattus_norvegicus/). Cufflinks (Trapnell et al., 2012) were used to process the resulting binary alignment/map (BAM) files to evaluate transcript abundance and identify potential

10.3389/fphar.2024.1492237

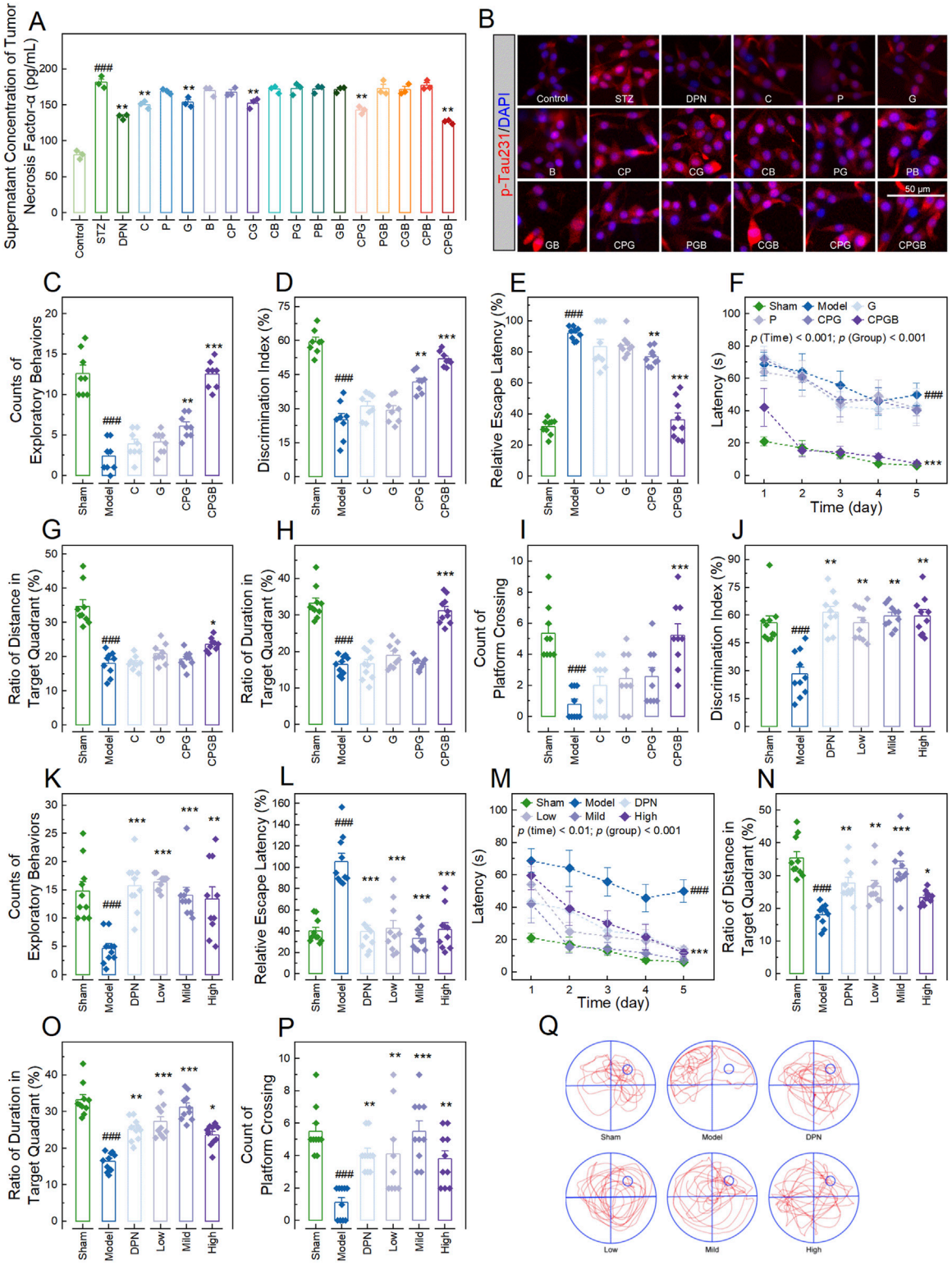


FIGURE 1
Evaluation of formulations for optimal therapeutic effects and their impact on cognitive behaviors in Alzheimer's disease rats. **(A)**: Bar chart with dots showing the concentration of tumor necrosis factor-α in the supernatant of PC12 cells treated with various additives (n = 3); **(B)**: Representative microscopy images showing the p-Tau231in PC12 cells treated with various additives (n = 3); **(C, D, J, K)**: Bar charts with dots illustrating the counts of exploratory behaviors ((**C, K**); n = 8) and discrimination indexes ((**D, J**); n = 8–10) of rats in the new object recognition test; **(E, L)**: Bar charts with dots of the relative escape latency of rats (n = 10); **(F, M)**: Dot-line plots presenting the latencies of rats over the 5 days of Morris water maze tests (n = 10); **(G–I, N–P)**: Bar charts with dots representing the ratios of distance ((**G, N**); n = 10) and duration ((**H, O**); n = 10) of rats in the target quadrant, along with the platform crossing counts of rats ((**I, P**); n = 10) in the Morris water maze tests; and **(Q)**: Swim paths illustrating the representative trajectories of rats in the Morris water maze test. In **(A, C–P)**, data are expressed as mean ± standard error. Statistical analyses were performed using one-way analysis of variance
(*Continued*)

FIGURE 1 (Continued)
(A, D, E, G, H, J, L, N–P), the Kruskal-Wallis test **(C, I, K)**, and repeated measures one-way analysis of variance **(F, M)**: ###, $p < 0.001$ compared to the Control/Sham group; *, $p < 0.05$, **, $p < 0.01$, ***, $p < 0.001$ compared to the STZ/Model group. STZ, streptozotocin; DPN, donepezil hydrochloride tablets; p-Tua231, phosphorylated Tau protein at threonine 231; DAPI, 6-diamidino-2-phenylindole.

mRNA isoforms. Additionally, StringTie (v1.3.3b) (Pertea et al., 2015) was used to assemble the mapped reads from each sample using a reference-based approach. Transcript expression levels were quantified in terms of fragments per kilobase million (FPKM), and Principal Component Analysis (PCA) was conducted based on these FPKM values. The Kyoto Encyclopedia of Genes and Genomes (KEGG) and gene ontology (GO) enrichment analyses of differentially expressed genes (DEGs) were performed using DESeq2 software (Love et al., 2014) and the ClusterProfiler R package (Wu et al., 2021). The Benjamini-Hochberg method was applied to control the false discovery rate.

Statistical analysis

Unless specified otherwise, all data were expressed as mean ± standard error and analyzed statistically using SPSS and RStudio software. Initially, continuous variables were tested for normal distribution and variance homogeneity. If the data satisfied both conditions, an independent samples analysis of variance (ANOVA) was employed for preliminary hypothesis testing, followed by the LSD method for *post hoc* analysis. For data not meeting these criteria, the Kruskal-Wallis test was used, with the Tukey method for *post hoc* testing. For repeated-measures data (e.g., escape latency), a repeated measures ANOVA method was applied to assess differences across groups and time points. A P value less than 0.05 was considered indicative of statistical significance in all hypothesis tests. In transcriptomics analysis, the similarity of gene expression profiles among different groups was evaluated using the permutational multivariate analysis of variance (PERMANOVA) method. In differential expression analysis, genes with $|\text{Log2 (FoldChange)}| \geq 1$ and p-value < 0.05 were deemed significantly differentially expressed genes (DEGs). In KEGG and GO enrichment analysis signaling pathways with p values < 0.05 were considered significantly enriched. Data plots were created using OriginPro software (v2024), while all schematic diagrams and microscope images were illustrated or enhanced using Adobe Illustrator and Adobe Photoshop unless otherwise noted.

Results

Evaluation of formulations for optimal therapeutic effects

To investigate the therapeutic effects of the 15 formulations on AD, we first measured concentrations of proinflammatory cytokines in the supernatant of PC12 cells treated with STZ and various formulations. The results indicated that STZ treatment significantly elevated the levels of TNF-α, IL-1β, IL-6, and Aβ1-42 ($p < 0.001$; Figure 1A; Supplementary Figures S2A–C) in the supernatant, as well as the expression of p-Tau231 ($p < 0.001$; Figure 1B; Supplementary Figure S2D) in PC12 cells. These increases were significantly mitigated by the positive drug DPN and 4 formulations: C, G, CPG, and CPGB ($p < 0.01$), while other treatments did not show significant effects ($p > 0.05$) (Figures 1A, B; Supplementary Figures S2A–D).

Next, we examined the therapeutic effects of these 4 formulations in an AD rat model. Rats in each group exhibited similar probe times and exploration speeds in the test phase of the NOR test and swimming speeds in the MWM test ($p > 0.05$; Supplementary Figures S2E–G). However, AD rats demonstrated significant reductions in exploratory behavior counts and discrimination index in the NOR test, as well as in the ratios of distance and duration of swimming in the target quadrant, and platform crossing counts in the MWM test ($p < 0.001$; Figures 1C, D, G–I). They also showed significant increases in relative escape latency in the EMP test and latency in the MWM test ($p < 0.001$; Figures 1E, F). These changes were significantly ameliorated by CPGB treatment ($p < 0.05$), but not by C or G treatments ($p > 0.05$; Figures 1C–I). Although CPG treatment exhibited some mitigating effects, its therapeutic impact was notably less than that of CPGB treatment ($p < 0.05$; Figures 1C–I). Hence, we chose CPGB as our formulation in the following experiments.

CPGB mitigated STZ-induced AD-related cognitive behaviors in rats

After confirming that CPGB exhibits greater therapeutic effects on AD rats, we further explored the impacts of low (90 mg/kg), mild (180 mg/kg), and high (360 mg/kg) doses of CPGB on the cognitive behaviors of AD rats. In the familiarization phase of the NOR test and MWM test, rats across all groups displayed similar exploratory behavior counts, probe times, and swimming speeds ($p > 0.05$; Supplementary Figures S1H–J). However, during the test phase of the NOR test, DPN and all 3 doses of CPGB significantly improved the STZ-induced reductions in exploratory behavior counts and discrimination index, independent of dose ($p < 0.01$; Figures 1J, K). STZ treatment significantly increased the relative escape latency and latency in EMP and MWM tests ($p < 0.001$; Figures 1L, M). Both DPN and CPGB treatments significantly reduced these increases ($p < 0.01$), with the mild dose of CPGB resulting in significantly lower relative escape latency and latency compared to the low or high doses ($p < 0.05$; Figures 1L, M). In the MWM test, DPN and CPGB treatments also significantly mitigated the STZ-induced reductions in the ratios of distance and duration of swimming in the target quadrant, as well as in platform crossing counts ($p < 0.05$; Figures 1N–P). Rats treated with the mild dose of CPGB showed significantly higher ratios of distance and duration of swimming in

10.3389/fphar.2024.1492237

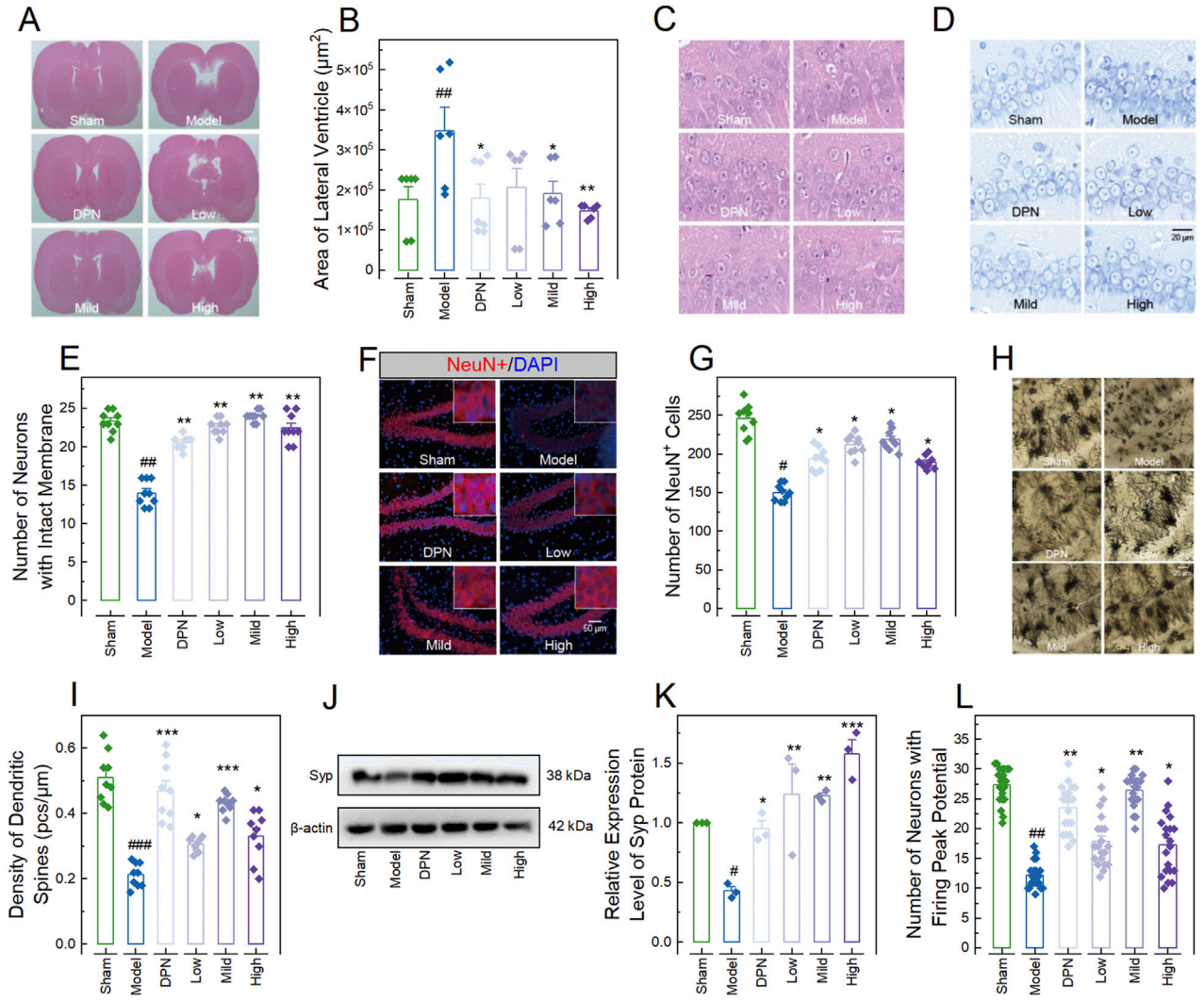


FIGURE 2
CPGB attenuated streptozotocin-induced pathological changes in rats. **(A, C, D, F, H)**: Representative microscopy images of hematoxylin and eosin-stained brain sections **(A)** and hippocampal tissue sections **(C)**, Nissl-stained bodies in hippocampal tissue sections **(D)**, NeuN staining in hippocampal tissue section **(F)**, and Golgi staining in hippocampal tissue sections **(H)**; **(B, E, G, I, K, L)**: Bar charts with dots representing the areas of lateral ventricles (n = 6–7; **(B)**), number of neurons with intact membranes (n = 9; **(E)**), number of NeuN⁺ cells (n = 9; **(G)**), density of dendritic spines (n = 9; **(I)**), relative gray values of Spy protein (n = 3; **(K)**), and number of neurons with firing peak potential (n = 21; **(L)**) in rats across different groups; and **(J)**: Representative gel images showing the expression level of Syp protein. In **(B, E, G, I, K, L)**, data are expressed as mean ± standard error. Statistical analyses were conducted using one-way analysis of variance **(B, I, K)** and the Kruskal-Wallis test **(E, G, L)**: $^{\#}$, $p < 0.05$, $^{\#\#}$, $p < 0.01$, $^{\#\#\#}$, $p < 0.001$ compared to the Sham group; *, $p < 0.05$, **, $p < 0.01$, ***, $p < 0.001$ compared to the Model group. DPN, donepezil hydrochloride tablets; DAPI, 6-diamidino-2-phenylindole.

the target quadrant and platform crossing counts compared to those treated with low or high doses ($p < 0.05$; Figures 1N–P). Detailed trajectories of rats in the MWM test are visualized in Figure 1Q.

CPGB ameliorated STZ-induced AD-related pathological changes in rats

To further validate the therapeutic effects of CPGB on AD in rats, we evaluated the pathological changes in the lateral ventricle and hippocampus, as well as the electrophysiological dysfunction of hippocampal neurons. HE staining results showed that STZ treatment significantly enlarged the lateral ventricles in rats ($p < 0.01$). This enlargement was significantly reduced by treatments with mild and high doses of CPGB, as well as DPN ($p < 0.05$), but not by a low dose of CPGB ($p > 0.05$) (Figures 2A, B). Additionally, most hippocampal neurons in the Model group were degenerated, displaying blurred cell contours, ruptured cell bodies, and irregular arrangements compared to the Sham group. In contrast, neurons in rats treated with DPN or CPGB were intact and well-organized with clear outlines (Figure 2C). Nissl staining and immunofluorescence results indicated that the nuclear structure in the hippocampus of the Model group was unclear, with indistinct surrounding Nissl bodies. The number of neurons with intact membranes and NeuN⁺ cells in the hippocampus was significantly decreased in the Model group compared to the Sham group ($p < 0.05$). Rats treated with DPN and CPGB exhibited distinct Nissl bodies around the nucleus and a significantly increased number of neurons with intact membrane and

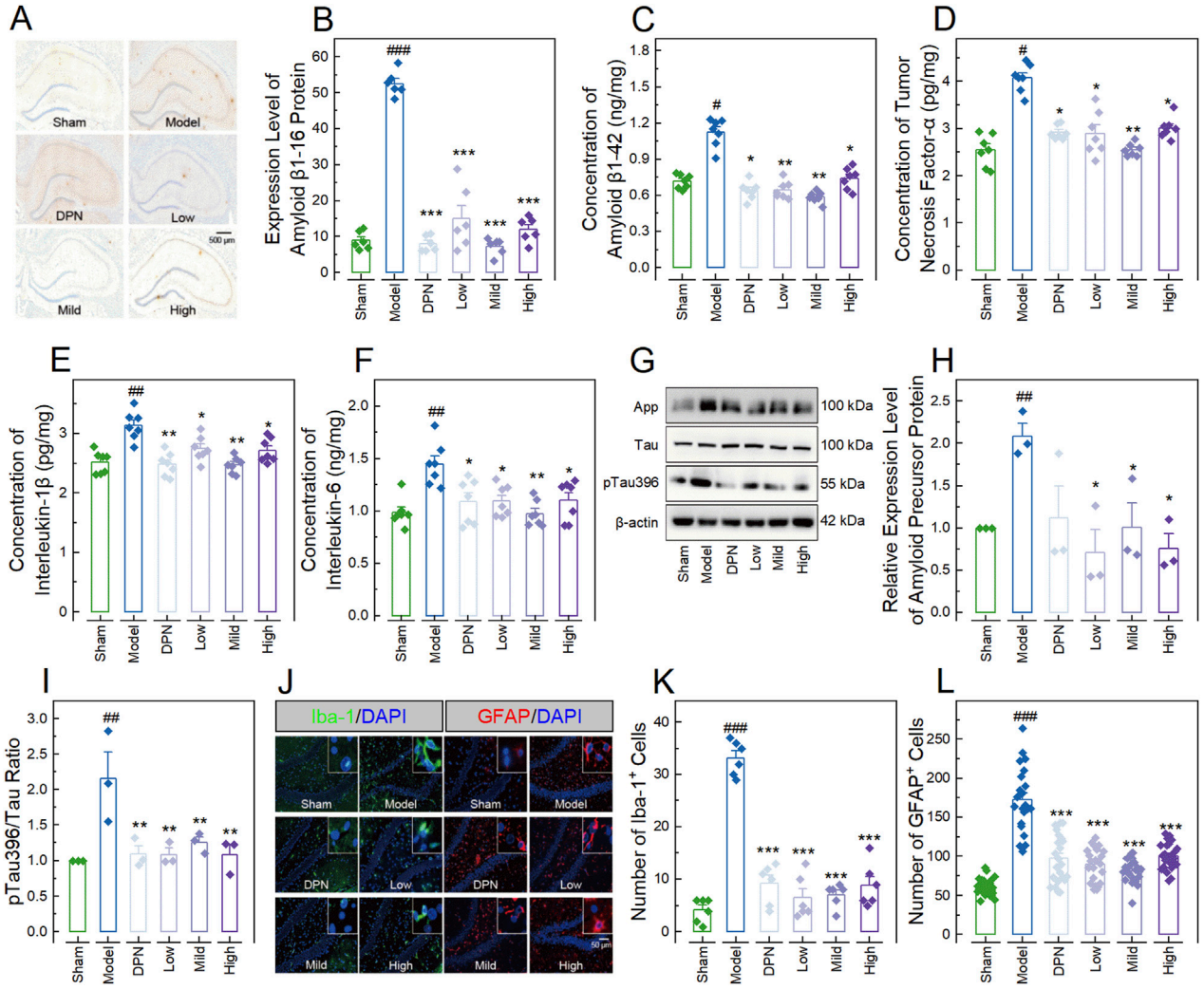


FIGURE 3
CPGB Mitigated increases in Alzheimer's disease-related markers induced by streptozotocin in rats. **(A, J)**: Representative microscopy images showing stained amyloid β1-16 protein **(A)**, Iba-1, and GFAP **(J)** in hippocampal tissue sections; **(B–F, H, I, K, L)**: Bar charts with dots representing the expression level of amyloid β1-16 protein (n = 6; **(B)**), concentrations of amyloid β1-42 (n = 7; **(C)**), tumor necrosis factor-α (n = 7; **(D)**), interlukin-1β (n = 7; **(E)**), and interlukin-6 (n = 7; **(F)**), the relative expression level of App (n = 3; **(H)**), the ratio of pTau396 to Tau (n = 3; **(I)**), as well as the numbers of cells expressing Iba-1 (n = 6; **(K)**) and GFAP (n = 20; **(L)**); and **(G)** Representative gel images showing the expression levels of App, Tau, and pTau396, in the hippocampus of rats. In **(B–F, H, I, K, L)**, data are expressed as mean ± standard error. Statistical analyses were conducted using one-way analysis of variance **(B–F, H, I)** and the Kruskal-Wallis test **(K, L)**: $^{\#}$, $p < 0.05$, $^{\#\#}$, $p < 0.01$, $^{\#\#\#}$, $p < 0.001$ compared to the Sham group; *, $p < 0.05$, **, $p < 0.01$, ***, $p < 0.001$ compared to the Model group. DPN, donepezil hydrochloride tablets; DAPI, 6-diamidino-2-phenylindole; App, amyloid precursor protein; Iba-1, ionized calcium-binding adaptor molecule 1; GFAP, glial fibrillary acidic protein.

NeuN^{+} cells compared to the Model group ($p < 0.05$) (Figures 2D–G). Golgi staining results demonstrated that the density, branch number, and total length of dendritic spines in hippocampal neurons were significantly lower in the Model group compared to the Sham group ($p < 0.001$). Treatments with DPN and CPGB significantly mitigated these decreases ($p < 0.01$), with a mild dose of CPGB exhibiting a better mitigative effect than the low and high doses ($p < 0.05$) (Figures 2H, I). Immunoblotting results showed that DPN and CPGB treatments significantly reversed the STZ-induced downregulation of Syp protein in hippocampal neurons ($p < 0.05$) (Figures 2J, K). Finally, the electrophysiological test identified a significantly decreased number of neurons with firing peak potentials in the hippocampal of the Model group ($p < 0.01$), which was significantly lower than in those treated with DPN and CPGB ($p < 0.05$) (Figure 2L).

CPGB attenuated STZ-induced increases of AD-related markers in rats

In the meanwhile, we also investigated the effects of CPGB on AD-related markers in rats, including Aβ protein deposition, Tau protein hyperphosphorylation, hippocampal glial cell activation, and pro-inflammatory cytokine production. Immunohistochemistry results demonstrated a significantly higher level of Aβ1-16 in the Model group compared to the Sham group ($p < 0.001$). This increase was significantly inhibited by treatments with DPN and CPGB ($p < 0.001$), with the mild dose of CPGB resulting in a lower Aβ1-16 level compared to the low and high doses ($p < 0.05$) (Figures 3A, B). ELISA results indicated that treatments with DPN and CPGB significantly

10.3389/fphar.2024.1492237

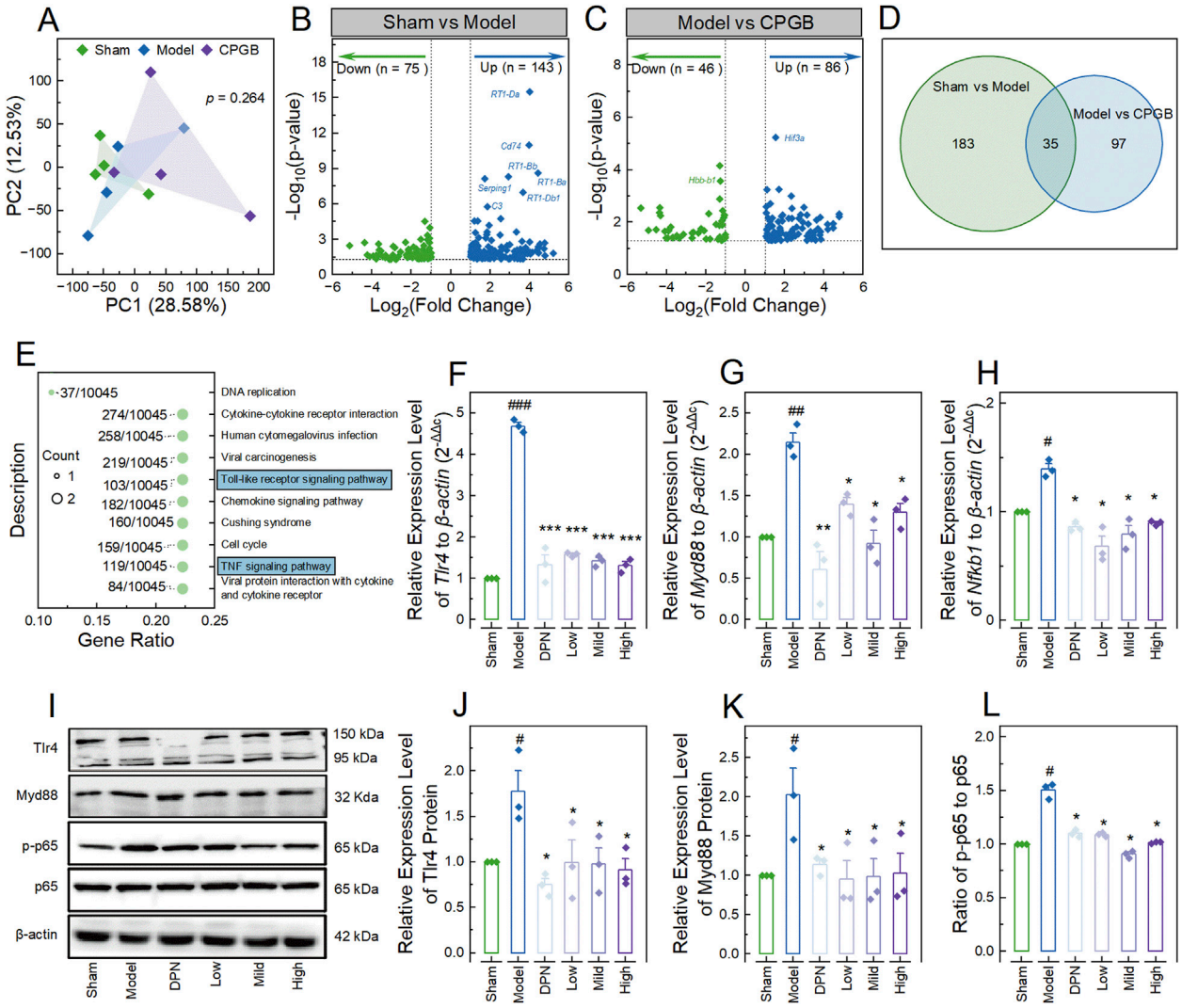


FIGURE 4
Investigating the underlying mechanisms behind the therapeutic effects of CPGB on Alzheimer's disease in rats. **(A)**: Principal coordinate analysis plot based on unweighted unifrac distances, showing the variance in gene expression profiles among groups (n = 4); **(B, C)**: Volcano plots representing the differentially expressed genes (DEGs) between the Sham and Model groups **(B)** and between the Model and CPGB groups **(C)**; **(D)**: Venn diagram illustrating the shared and unique DEGs between the 2 comparisons; **(E)**: Bubble chart showing the significantly enriched KEGG pathways by the shared DEGs in **(D)**; **(F–H, J–L)**: Bar charts with dot showing the relative expression levels of mRNA *Tlr4* **(F)**, *Myd88* **(G)**, as well as *Nfkb1* **(H)**, proteins Tlr4 **(J)** and Myd88 **(K)**,and the ratio of p-p65 to p65 **(L)** (n = 3); and **(I)**: Representative gel images showing the expression levels of Tlr4, Myd88, p-p65, and p65, in the hippocampus of rats. In A, a permutational multivariate analysis of variance algorithm was used to calculate the similarity of gene expression profiles among groups. In **(E)**, the size of bubbles indicates the count of genes enriched into that KEGG pathway; "Gene Ratio" represents the ratio of the count of enriched genes to the total number of genes; the label alongside each bubble indicates the counts of genes in that KEGG pathway relative to total number of genes in the category. In **(F–H, J–L)**, data are expressed as mean ± standard error. Statistical analyses were conducted using one-way analysis of variance: $^{\#}$, $p < 0.05$, $^{\#\#}$, $p < 0.01$, $^{\#\#\#}$, $p < 0.001$ compared to the Sham group; *, $p < 0.05$, **, $p < 0.01$, ***, $p < 0.001$ compared to the Model group. DPN, donepezil hydrochloride tablets.

reversed the STZ-induced increases of Aβ1-42, TNF-α, IL-1β, and IL-6 concentrations in the Model group ($p < 0.05$; Figures 3C–F). Immunoblotting analysis revealed a significantly higher relative expression of amyloid precursor protein (App) and a higher pTau396 to Tau ratio ($p < 0.01$), both of which were significantly inhibited by CPGB treatments ($p < 0.05$) (Figures 3G–I). Finally, immunofluorescence analysis showed a significant increase in the number of microglia expressing ionized calcium-binding adaptor molecule 1 (Iba-1) and astrocytes expressing GFAP in the Model group compared to the Sham group ($p < 0.001$). These increases were also significantly ameliorated by treatments with DPN and CPGB ($p < 0.001$) (Figures 3J–L).

Investigating the underlying mechanism behind the therapeutic effects of CPGB on AD in rats

To uncover the underlying mechanisms of CPGB's therapeutic effects on AD rats, we randomly collected hippocampus samples from the 3 groups of rats: Sham (n = 4), Model (n = 4), and Mild (n =

4) groups. Then, we analyzed their mRNA expression profiles using transcriptome sequencing. This process generated a total of 141.93 Gbp of raw bases and 946.16 million raw reads, averaging 11.83 Gbp raw bases and 78.85 million raw reads per sample (Supplementary Table S3). After quality control and assembly, we annotated and quantified 20057 genes across the 12 hippocampal samples (Supplementary Table S4). PCA and PERMANOVA demonstrated no significant differences in gene expression profiles among groups (p = 0.264; Figure 4A). In the model group, compared to the Sham group, we identified 75 down-regulated and 143 up-regulated DEGs (Figure 4B; Supplementary Table S5). Similarly, in the CPGB group, compared to the Model group, there were 46 down-regulated and 86 up-regulated DEGs (Figure 4C; Supplementary Table S5). We further identified 35 DEGs common to both comparisons, including *Pkib*, *Hif3a*, *SNORD115*, *AABR07049688.1*, *Clec3a*, *LOC690082*, *AABR07036007.1*, *Ccr3*, *Ros1*, *Fndc9*, *AABR07053635.2*, *Wnt10b*, *Nod2*, *AABR07037487.1*, *U4*, *Tmem71*, *LOC100363125*, *Cdk1*, *Phex*, *PVR*, *AABR07047576.1*, *Ramp3*, *Cyp11b2*, *Spats1*, *Clec12b*, *AABR07043510.1*, *Aspg*, *AABR07019663.1*, *C7*, *Ccl5*, *Fam110d*, *Mcm3*, *AABR07028036.1*, *Vsig8*, and *Metazoa_SRP* (Figure 4D). These genes were enriched in 40 GO terms, primarily related to immune-inflammatory response regulation (Supplementary Table S6), and in 10 KEGG signaling pathways, including Viral protein interaction with cytokine and cytokine receptor, TNF signaling pathway, Cell cycle, Cushing syndrome, Chemokine signaling pathway, Toll-like receptor signaling pathway, Viral carcinogenesis, Human cytomegalovirus infection, Cytokine-cytokine receptor interaction, and DNA replication (Supplementary Table S6; Figure 4E).

Given the elevated pro-inflammatory responses in the hippocampus and the critical roles of the TLR and NF-κB pathways in neural inflammatory regulation (Squillace and Salvemini, 2022), we hypothesized that CPGB exerts its therapeutic effects on AD in rats by modulating the TLR4/Myd88/NF-κB signaling pathway. To test this hypothesis, we measured the relative expression levels of the *Tlr4*, *Myd88*, and *Nfkb1* genes compared to the housekeeping gene *β-actin* using the RT-qPCR method. The results showed significantly higher relative expression levels of *Tlr4*, *Myd88*, and *Nfkb1* in the Model group compared to the Sham group ($p < 0.01$). These increases were significantly reduced by treatments with DPN and CPGB ($p < 0.05$) (Figures 4F–H). Similarly, immunoblotting analysis also revealed significant increases in the relative express levels of Tlr4 and Myd88 proteins, as well as an increased ratio of p-p65 to p65 ($p < 0.05$). These increases were also significantly mitigated by DPN and CPGB treatments ($p < 0.05$) (Figures 4I–L).

CPGB down-regulated the TLR4/Myd88/NF-κB signaling pathway and inhibited STZ-induced microglia neurotoxicity

To confirm the involvement of the TLR4/Myd88/NF-κB signaling pathway in the mitigating effects of CPGB on AD, we assessed pro-inflammatory responses and the activity of this signaling pathway in BV2 cells treated with STZ and 90 μg/mL (Low), 180 μg/mL (Mild), and 360 μg/mL (High) doses of CPGB. It was observed that the STZ challenge significantly increased the concentrations of pro-inflammatory cytokines TNF-α, IL-1β, and IL-6 in the supernatant of BV2 cells ($p < 0.05$; Figures 5A–C), as well as the expression levels Tlr4, Myd88 ($p < 0.01$; Figures 5D–F), and Iba-1 proteins, and the ratio of p-p65 to p65 ($p < 0.01$; Figures 5G, H) in BV cells. All these increases were significantly reduced by treatments with DPN and CPGB ($p < 0.05$; Figures 5A–H).

Additionally, PC12 cells treated with conditioned medium from BV2 cells in the STZ group demonstrated significantly lower viability compared to those treated with conditioned medium from BV2 in the Control group ($p < 0.05$; Figure 5I). In contrast, PC12 cells treated with conditioned medium from BV2 in the DPN and CPGB groups demonstrated significantly higher viability compared to those treated with conditioned medium from BV2 cells in the STZ group ($p < 0.05$; Figure 5I).

CPGB attenuated STZ-induced pathogenesis of AD in a 3D-NVU model by inhibiting the TLR4/Myd88/NF-κB signaling pathway

We also developed a 3D-NVU AD model, representing the core structure of AD pathological damage (Hongjin et al., 2020), and treated this model STZ and varying doses of CPGB: 90 μg/mL (Low), 180 μg/mL (Mild), and 360 μg/mL (High). We then assessed indicators related to AD and inflammatory response. As shown in Figures 6A–D, STZ treatment significantly increases the concentrations of TNF-α, IL-1β, IL-6, and Aβ1-42 in the supernatant ($p < 0.01$). These increases were significantly inhibited by treatments with DPN and CPGB ($p < 0.05$). Immunoblotting analysis confirmed that STZ treatment significantly elevated the relative expression level of APP and the ratio of p-Tau396 to Tau ($p < 0.01$). These elevations were also significantly reduced by treatments with DPN and CPGB ($p < 0.05$; Figures 6E–G). Additionally, immunofluorescence analysis showed that DPN and CPGB treatments reduced the expression level of GFAP in the model (Figure 6H). As expected, STZ treatment significantly increased the relative expression levels of Tlr4 and Myd88 proteins and the ratio of p-p65 to p65 ($p < 0.01$). These increases were significantly mitigated by treatments with DPN and CPGB ($p < 0.05$; Figures 6I–L).

To confirm the necessity of the TLR4/Myd88/NF-κB signaling pathway, we interfered with this pathway by inhibiting the Tlr4 protein using Tak242 (MilloporeSigma, Burlington, MA, United States) and activating the NF-κB complex with phorbol 12-myristate 13-acetate (PMA; MilloporeSigma, Burlington, MA, United States) in the 3D-NVU model treated with STZ and 180 mg/mL of CPGB. As shown in Figures 6M–O, Tak242 treatment did not enhance the inhibitory effects of CPGB on the STZ-induced increases in the relative expression level of App or the ratio of pTau396 to Tau ($p > 0.05$). In contrast, PMA treatment significantly blocked these increases ($p < 0.05$). Similarly, Tak242 treatment did not enhance the inhibitory effects of CPGB on the STZ-induced increases in the concentrations of TNF-α, IL-1β, IL-6, and Aβ1-42 ($p > 0.05$), whereas PMA treatment significantly blocked these increases ($p < 0.05$) (Figures 6P–S).

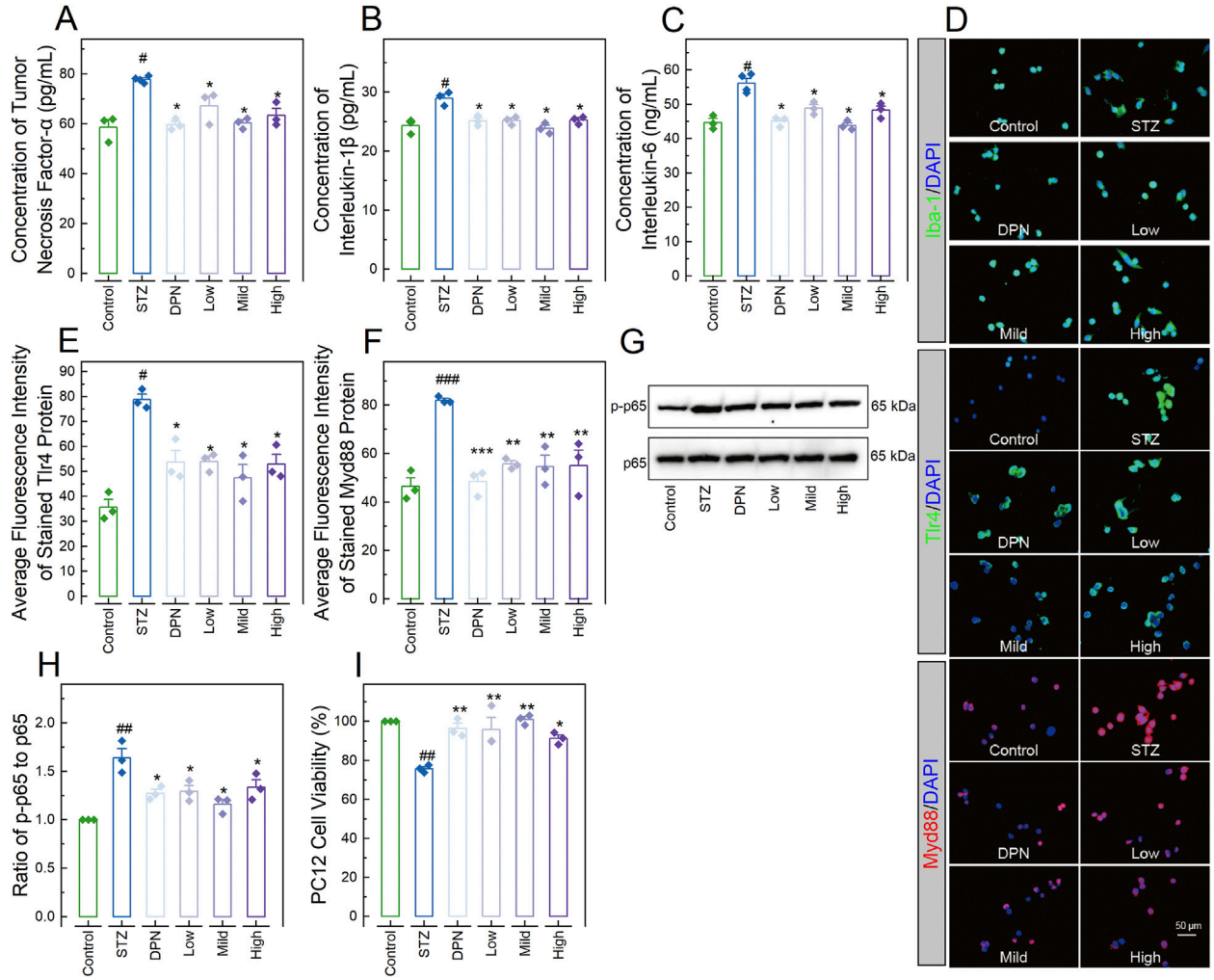


FIGURE 5
CPGB downregulated the TLR4/Myd88/NF-κB signaling pathway and inhibited STZ-induced microglia neurotoxicity. **(A–C, E, F)**: Bar charts with dots presenting the concentrations of pro-inflammatory cytokines tumor necrosis factor-α (n = 3; **(A)**), interleukin-1β (n = 3; **(B)**), and interleukin-6 (n = 3; **(C)**) in the supernatant of BV2 cells, as well as the average fluorescence intensity of stained Tlr4 (n = 3; **(E)**) and Myd88 (n = 3; **(F)**) proteins expressed in BV2 cells; **(D)**: Representative microscopy images showing the stained Iba-1, Tlr4, and Myd88 proteins expressed in BV2 cells; **(G)**: Representative gel images showing the expression levels of p-p65 and p65 proteins expressed in BV2 cells; **(H)**: Bar chart showing the relative gray values of pp65 and p65 proteins expressed in BV2 cells (n = 3); and **(I)**: Bar chart showing illustrating the viabilities of PC12 cells treated with conditioned medium from BV2 cells in each group (n = 3). In **(A–C, E, F, H, I)**: data are expressed as mean ± standard error. Statistical analyses were conducted using one-way analysis of variance: $^{\#}$, $p < 0.05$, $^{\#\#}$, $p < 0.01$, $^{\#\#\#}$, $p < 0.001$ compared to the Control group; *, $p < 0.05$, **, $p < 0.01$, ***, $p < 0.001$ compared to the STZ group. STZ, streptozotocin; DPN, donepezil hydrochloride tablets; DAPI, 6-diamidino-2-phenylindole; Iba-1, ionized calcium-binding adaptor molecule 1.

Discussion

AD is one of the most expensive, lethal, and burdensome diseases of this century, affecting millions of people worldwide (Prince et al., 2015; Scheltens et al., 2021; Selkoe, 2021). In recent decades, multiple Chinese herbs and their extracts have been shown to attenuate the pathogenesis of AD (Han et al., 2020; Li et al., 2021). However, few studies have reported the therapeutic effects of a compound prescription in Chinese medicine. In this study, we investigated the therapeutic effects of CPGB, a formulation comprising 4 ingredients extracted from 4 different Chinese herbs, on AD employing cellular, organoid, and animal models.

Several models are available for studying AD, each with distinct advantages and limitations. Transgenic AD models, while accurately mimicking key features like Aβ deposition and Tau hyperphosphorylation, have significant drawbacks, including a long latency for the appearance of pathology (6–9 months) and complex, time-consuming breeding processes. Additionally, the limited number of animals with consistent pathological and cognitive symptoms further complicates their use in large-scale studies. Aβ or Tau protein injection models, which involve direct brain injections, often result in localized damage due to poor diffusion of the proteins, leading to inconsistent cognitive deficits. These models primarily simulate specific aspects of AD pathology but fail to represent the broader, multifactorial nature of the disease. The aluminum-induced model is another simple and cost-effective approach, but it only reproduces single pathological features, typically focusing on cognitive deficits rather than the full

10.3389/fphar.2024.1492237

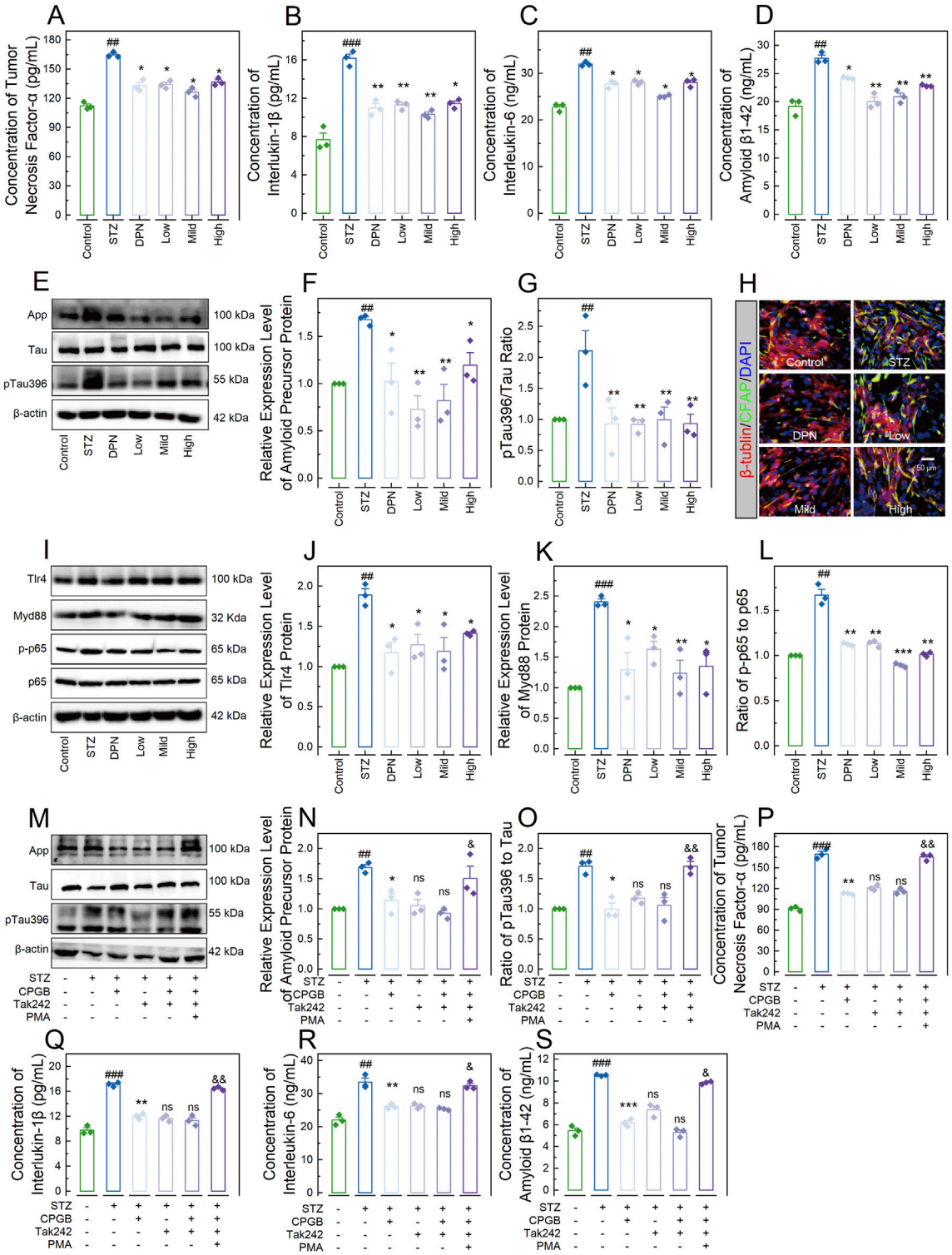


FIGURE 6
CPGB attenuated STZ-induced pathogenesis of Alzheimer's disease in a 3-dimensional brain neurovascular unit model. **(A–D, P–S)**: Bar charts with dots representing the concentrations of tumor necrosis factor-α **(A, P)**, interleukin-1β **(B, Q)**, interleukin-6 **(C, R)**, and amyloid β1-42 protein **(D, S)** in the supernatant across different groups (n = 3); **(F, G, J–L, N, O)**: Bar charts showing the relative expression levels of App **(F, N)**, Tlr4 **(J)**, and Myd88 **(K)** proteins, as well as the ratio of pTau396 to Tau **(G, O)** and p-p65 to p65 **(L)** across different groups (n = 3); **(E, I, M)**: Representative gel images showing the expression levels of App, pTau396, and Tau proteins **(E, M)**, as well as Tlr4, Myd88, p-p65, and p65 proteins **(I)** across different groups; and **(H)**: Representative microscopy images showing the stained β-tubulin and CFAP across groups. In **(A–D, F, G, J–L, N–P)**, data are expressed as mean ± standard error. Statistical analyses were conducted using one-way analysis of variance: $^{\#}$, $p < 0.05$, $^{\#\#}$, $p < 0.01$, $^{\#\#\#}$, $p < 0.001$ compared to the Control group; *, $p < 0.05$, **, $p < 0.01$, ***, $p < 0.001$ compared to the STZ group; ns: non-significant, $^{\&}$, $p < 0.05$, $^{\&\&}$, $p < 0.01$. STZ, streptozotocin; DPN, donepezil hydrochloride tablets; DAPI, 6-diamidino-2-phenylindole; App, amyloid precursor protein; GFAP, glial fibrillary acidic protein; PMA, phorbol 12-myristate 13-acetate.

spectrum of AD-related pathology. Aging models, though relevant to AD pathogenesis, require long experimental periods and are often too expensive for routine use. Moreover, neuroinflammation models, such as those induced by lipopolysaccharide (LPS), can mimic inflammation-related cognitive deficits but lack the hallmark pathologies of AD, including Aβ accumulation. In contrast, the STZ-induced AD model offers several advantages. It reproduces a wide range of AD-like features, including ventricular enlargement, neuroinflammation, Aβ deposition, Tau hyperphosphorylation, oxidative stress, and synaptic dysfunction. Additionally, the STZ model is economically feasible and allows for rapid induction of AD-like pathology, making it well-suited for studies requiring timely results. Given its ability to mimic the complex, multifactorial nature of AD, particularly the sporadic form, it provides a robust model for investigating therapeutic interventions like CPGB (Drummond and Wisniewski, 2017; Yokoyama et al., 2022). Hence, we chose this model to explore the therapeutic effects of CPGB on AD.

Firstly, we selected 4 active ingredients, namely catalpol, puerarin, gastrodin, and borneol (Supplementary Figure S1), and developed 15 formulations through permutations and combinations. To identify a formulation with optimal therapeutic effects on AD, we established an AD cell model according to previous studies (Gupta et al., 2018; Kamat, 2015; Li et al., 2020), and evaluated the mitigative effects of these 15 formulations. The results showed that 4 formulations, including catalpol, gastrodin, CPG, and CPGB, significantly reduced concentrations of pro-inflammatory cytokines TNF-α, IL-1β, and IL-6 in the supernatant, as well as Aβ1-42 and the pTua231/Tau ratio (Figures 1A, B; Supplementary Figures S2A–D), which are considered AD-related indicators in cellular models (Lista et al., 2014). Subsequently, referencing our previous studies, we further evaluated the therapeutic effects of these formulations on AD using an STZ-induced AD rat model. The results demonstrated that CPGB produced greater improvements in STZ-induced Aβ protein deposition, pTua231 plaque formation, and cognitive deficits in the NOR and MWM tests, which are commonly used in AD rat models (Leger et al., 2013; Vorhees and Williams, 2006) (Figures 1C–I, 2). All these findings confirmed that CPGB was more effective in treating STZ-induced AD than other formulations, especially these monotherapy, suggesting that the great potential of CPGB in treating AD compared (Moreira-Silva et al., 2018).

Afterwards, we examined the therapeutic effects of low, mild, and high doses of CPGB, which were confirmed to show no significant toxicities on rats in our previous studies, on the behavioral, pathological, and molecular alterations induced by STZ. As anticipated, all doses of CPGB significantly alleviated STZ-induced cognitive deficits, AD-related pathological progressions, and molecular depositions in the hippocampus of rats (Figures 2, 3). The hippocampus, a core structure affected by AD, is composed of blood vessels (including endothelial cells, pericytes, and basement membrane), neurons, a variety of glial cells, and the extracellular matrix. Hence, to further explore CPGB's effects, we established a 3D-NVU model, which reflects the dynamic integrity of brain structure and functions (Bhalerao et al., 2020; Caffrey et al., 2021), and validated the therapeutic effects of CPGB on AD at the organoid level. Similarly, CPGB significantly mitigated STZ-induced AD-related pathological progression and molecular deposition in this model (Figure 5). Together, these findings further confirm the efficacy of CPGB in preventing the pathogenesis of AD. Notably, we observed no significant differences in the AD-preventing efficacy of CPGB across different doses (Figures 2, 3, 5), suggesting a dose-independent therapeutic effect. However, this observation requires validation over a wider range of concentrations.

After confirming the effects, we further explored the underlying mechanisms. Through transcriptome sequencing and analysis, we identified 35 genes affected by both STZ and CPGB in the hippocampal tissues (Figures 4A–D). These genes were significantly enriched into 10 KEGG pathways (Figure 4E). Notably, the Toll-like receptor signaling pathway and NF-κB signaling pathway have been previously proven to play crucial roles in the pathogenesis of AD by regulating microglia-derived proinflammatory responses (Jha et al., 2019; Su et al., 2016). Therefore, we examined the activity of the Tlr4/Myd88/NF-κB signaling pathway by assessing the expression levels of its checkpoints in cellular and organoid models. As anticipated, CPGB significantly ameliorated STZ-induced increases in the relative expression levels of Tlr4, Myd88, and p65 proteins (Figures 4F–L, 5, 6A–L). Furthermore, inhibiting the Tlr4 protein did not enhance the therapeutic effects of CPGB, whereas activating the Myd88 protein significantly blocked these effects (Figures 6M–S). These findings suggest that the Tlr4/Myd88/NF-κB signaling pathway is essential for CPGB to exert its therapeutic effects on AD. It should be noted that we identified approximately 200 DEGs in each comparison, whereas a previous transcriptomic study identified thousands of DEGs (Mathys et al., 2019). This discrepancy suggests that other cells in the tissue, unaffected by STZ, might have influenced our transcriptome analysis results, explaining the lack of significant difference in gene expression profiles across groups (Figure 4A). Consequently, conducting a single-cell sequencing on rat hippocampal tissue or transcriptome sequencing on PC12 cells may reveal more DEGs and enrich additional signaling pathways, thus providing a broader understanding of potential mechanisms behind CPGB's therapeutic effects on AD.

Our study is the first to combine 4 known bioactive compounds from TCMs with therapeutic potential for AD, demonstrating that this combination therapy is more effective than single-agent treatments. We have also preliminarily identified the molecular mechanisms by which this formulation affects microglial cells. Future experiments could further explore the pharmacological properties of this combination to provide theoretical support for its clinical application. However, our research has certain limitations. Notably, we did not investigate the compatibility of these 4 compounds or whether they interact with each other in ways that could impact the polypharmacological effect of this formulation, potentially influencing its therapeutic outcomes. This aspect warrants further investigation in future studies.

Conclusion

In summary, our study demonstrated that the CPGB formula has superior mitigating effects on STZ-induced production of pro-inflammatory cytokines, as well as the deposition of Aβ proteins and hyperphosphorylated Tau proteins in PC12 cells. It also showed

improvements in cognitive deficits in an AD rat model, compared to its components or other formulas. We further confirmed that varying doses of CPGB effectively prevented STZ-induced pathogenesis of AD, including cognitive deficits in rats, pathological changes in hippocampal tissues, and the production and deposition of AD-related markers in hippocampal tissues, 3D-NVU model, and BV2 cells. Additionally, our findings revealed that the Tlr4/Myd88/NF-κB signaling pathway is essential for the therapeutic effects of CPGB on AD pathogenesis. Our study enhances the theoretical foundation for using traditional Chinese medicine to treat AD, providing new insights and references for alleviating and treating AD.

Data availability statement

The raw data generated in the transcriptome sequencing have been uploaded to the NCBI (BioProject) database, accession number PRJNA1149930. All data and materials can be accessed from the corresponding author once requested.

Ethics statement

The animal study was approved by Ethics Committee of Southwest University. The study was conducted in accordance with the local legislation and institutional requirements.

Author contributions

HR: Writing–review and editing, Writing–original draft, Visualization, Methodology, Investigation, Formal Analysis, Data curation, Conceptualization. LT: Writing–review and editing. ZY: Investigation, Methodology, Validation, Visualization, Writing–review and editing. YL: Writing–review and editing, Visualization, Investigation. XZ: Writing–review and editing, Investigation. XXi: Investigation, Writing–review and editing. XW: Investigation, Writing–review and editing. WC: Methodology, Writing–review and editing. YC: Writing–review and editing. HW: Methodology, Writing–review and editing. QX: Project administration, Supervision, Writing–review and editing. XXu: Project administration, Resources, Supervision, Writing–review and editing.

Funding

The author(s) declare that financial support was received for the research, authorship, and/or publication of this article. This study was financially supported by the National Natural Science Foundation of China (No. 81473549).

Acknowledgments

The authors thank Yu Yang from the Faculty of Psychology, Southwest University, Chongqing, China, for providing technical assistance, Taoren Ruan from Chongqing Hospital of Traditional Chinese Medicine, Chongqing, China, for supplying Donepezil Hydrochloride, as well as other members in the laboratory led by Xiaoyu Xu for their valuable contributions and insightful conversations.

Conflict of interest

The authors declare that the research was conducted in the absence of any commercial or financial relationships that could be construed as a potential conflict of interest.

Publisher's note

All claims expressed in this article are solely those of the authors and do not necessarily represent those of their affiliated organizations, or those of the publisher, the editors and the reviewers. Any product that may be evaluated in this article, or claim that may be made by its manufacturer, is not guaranteed or endorsed by the publisher.

Supplementary material

The Supplementary Material for this article can be found online at: https://www.frontiersin.org/articles/10.3389/fphar.2024.1492237/full#supplementary-material

SUPPLEMENTARY TABLE S1
Sequences of primers used in transcription-quantitative polymerase chain reaction analysis.

SUPPLEMENTARY TABLE S2
Detailed information about antibodies used in immunofluorescence, immunoblotting, and immunohistochemical experiments.

SUPPLEMENTARY TABLE S3
Detailed information about the generated raw data in transcriptome sequencing. Note: Q20 indicates the percentage of bases with a Phred quality score >20, signifying the reliability of base identification in the sequencing data.

SUPPLEMENTARY TABLE S4
Detailed information about the annotated and quantified genes for the generated data.

SUPPLEMENTARY TABLE S5
Detailed statistical information about the genes with p-value < 0.05.

SUPPLEMENTARY TABLE S6
Detailed results of gene ontology and kyoto encyclopedia of genes and genomes (KEGG) enrichment analyses.

SUPPLEMENTARY FIGURE S1
Chemical structure diagrams of the 4 plant-extracted compounds we used in this study.

SUPPLEMENTARY FIGURE S2
Evaluation of formulations for optimal therapeutic effects and their impact on cognitive behaviors in Alzheimer's disease rats. **(A–C)**: Bar charts with dots depicting the concentrations of interleukin-1β, interleukin-6, and amyloid β1-42 in the supernatant of PC12 cell treated with various additives (n = 3); **(D)**: Bar chart with dot showing the average fluorescence intensity of the stained p-Tua231 protein in the PC12 cells treated with various additives (n = 3); **(E, F, H, I)**: Bar charts with dots illustrating the probe time **(E)**, exploration speed **(F, I)**, and exploratory behavior counts **(H)** of rats

(n = 8–10) in the new object recognition tests; and **(G, J)**: Bar charts with dot representing the swimming speed of rats in the Morris water maze tests (n = 8–10). Data are expressed as mean ± standard error. Statistical analyses were performed using one-way analysis of variance **(A–G, I, J)** and the Kruskal-Wallis test **(H)**: ###, $p < 0.001$ compared to the Control/Sham group; *, $p < 0.05$, **, $p < 0.01$ compared to the STZ/Model group. STZ, streptozotocin; DPN, donepezil hydrochloride tablets; p-Tua231, phosphorylated Tau protein at threonine 231.

References

Bhalerao, A., Sivandzade, F., Archie, S. R., Chowdhury, E. A., Noorani, B., and Cucullo, L. (2020). *In vitro* modeling of the neurovascular unit: advances in the field. *Fluids Barriers CNS* 17, 22–20. doi:10.1186/s12987-020-00183-7

Caffrey, T. M., Button, E. B., and Robert, J. (2021). Toward three-dimensional *in vitro* models to study neurovascular unit functions in health and disease. *Neural Regen. Res.* 16, 2132–2140. doi:10.4103/1673-5374.310671

Chen, H., Deng, C., Meng, Z., and Meng, S. (2022). Effects of catalpol on alzheimer's disease and its mechanisms. *Evid. Based Complement. Altern. Med.* 2022, 2794243. doi:10.1155/2022/2794243

Chen, S.-Y., Gao, Y., Sun, J.-Y., Meng, X.-L., Yang, D., Fan, L.-H., et al. (2020). Traditional Chinese medicine: role in reducing β-amyloid, apoptosis, autophagy, neuroinflammation, oxidative stress, and mitochondrial dysfunction of alzheimer's disease. *Front. Pharmacol.* 11, 497. doi:10.3389/fphar.2020.00497

Cummings, J. L., Osse, A. M. L., Kinney, J. W., Cammann, D., and Chen, J. (2024). Alzheimer's disease: combination therapies and clinical trials for combination therapy development. *CNS Drugs* 38, 613–624. doi:10.1007/s40263-024-01103-1

Cummings, J. L., Tong, G., and Ballard, C. (2019). Treatment combinations for alzheimer's disease: current and future pharmacotherapy options. *J. Alzheimers Dis.* 67, 779–794. doi:10.3233/JAD-180766

Depp, C., Sun, T., Sasmita, A. O., Spieth, L., Berghoff, S. A., Nazarenko, T., et al. (2023). Myelin dysfunction drives amyloid-β deposition in models of alzheimer's disease. *Nature* 618, 349–357. doi:10.1038/s41586-023-06120-6

De Strooper, B., and Karran, E. (2016). The cellular phase of alzheimer's disease. *Cell* 164, 603–615. doi:10.1016/j.cell.2015.12.056

Drummond, E., and Wisniewski, T. (2017). Alzheimer's disease: experimental models and reality. *Acta neuropathol.* 133, 155–175. doi:10.1007/s00401-016-1662-x

Gupta, S., Yadav, K., Mantri, S. S., Singhal, N. K., Ganesh, S., and Sandhir, R. (2018). Evidence for compromised insulin signaling and neuronal vulnerability in experimental model of sporadic alzheimer's disease. *Mol. Neurobiol.* 55, 8916–8935. doi:10.1007/s12035-018-0985-0

Han, Y., Sun, H., Zhang, A., Yan, G., and Wang, X.-j. (2020). Chinmedomics, a new strategy for evaluating the therapeutic efficacy of herbal medicines. *Pharmacol. Ther.* 216, 107680. doi:10.1016/j.pharmthera.2020.107680

Hongjin, W., Han, C., Baoxiang, J., Shiqi, Y., and Xiaoyu, X. (2020). Reconstituting neurovascular unit based on the close relations between neural stem cells and endothelial cells: an effective method to explore neurogenesis and angiogenesis. *Rev. Neurosci.* 31, 143–159. doi:10.1515/revneuro-2019-0023

Jack, C. R., Andrews, S. J., Beach, T. G., Buracchio, T., Dunn, B., Graf, A., et al. (2024). Revised criteria for the diagnosis and staging of alzheimer's disease. *Alzheimers Dement.* 20, 5143–5169. doi:10.1002/alz.13859

Jha, N. K., Jha, S. K., Kar, R., Nand, P., Swati, K., and Goswami, V. K. (2019). Nuclear factor-kappa β as a therapeutic target for alzheimer's disease. *J. Neurochem.* 150, 113–137. doi:10.1111/jnc.14687

Kamat, P. K. (2015). Streptozotocin induced alzheimer's disease like changes and the underlying neural degeneration and regeneration mechanism. *Neural Regen. Res.* 10, 1050–1052. doi:10.4103/1673-5374.160076

Kim, D., Paggi, J. M., Park, C., Bennett, C., and Salzberg, S. L. (2019). Graph-based genome alignment and genotyping with HISAT2 and HISAT-genotype. *Nat. Biotechnol.* 37, 907–915. doi:10.1038/s41587-019-0201-4

Leger, M., Quiedeville, A., Bouet, V., Haelewyn, B., Boulouard, M., Schumann-Bard, P., et al. (2013). Object recognition test in mice. *Nat. Protoc.* 8, 2531–2537. doi:10.1038/nprot.2013.155

Lewcock, J. W., Schlepckow, K., Di Paolo, G., Tahirovic, S., Monroe, K. M., and Haass, C. (2020). Emerging microglia biology defines novel therapeutic approaches for alzheimer's disease. *Neuron* 108, 801–821. doi:10.1016/j.neuron.2020.09.029

Li, S., Wu, Z., and Le, W. (2021). Traditional Chinese medicine for dementia. *Alzheimers Dement.* 17, 1066–1071. doi:10.1002/alz.12258

Li, Y., Xu, P., Shan, J., Sun, W., Ji, X., Chi, T., et al. (2020). Interaction between hyperphosphorylated tau and pyroptosis in forskolin and streptozotocin induced AD models. *Biomed. & Pharmacother.* 121, 109618. doi:10.1016/j.biopha.2019.109618

Lista, S., Garaci, F. G., Ewers, M., Teipel, S., Zetterberg, H., Blennow, K., et al. (2014). CSF Aβ1-42 combined with neuroimaging biomarkers in the early detection, diagnosis and prediction of alzheimer's disease. *Alzheimers Dement.* 10, 381–392. doi:10.1016/j.jalz.2013.04.506

Liu, S., Liu, Y., Hao, W., Wolf, L., Kiliaan, A. J., Penke, B., et al. (2012). TLR2 is a primary receptor for alzheimer's amyloid β peptide to trigger neuroinflammatory activation. *J. Immunol.* 188, 1098–1107. doi:10.4049/jimmunol.1101121

Liu, Y., Xue, Q., Tang, Q., Hou, M., Qi, H., Chen, G., et al. (2013). A simple method for isolating and culturing the rat brain microvascular endothelial cells. *Microvasc. Res.* 90, 199–205. doi:10.1016/j.mvr.2013.08.004

Love, M. I., Huber, W., and Anders, S. (2014). Moderated estimation of fold change and dispersion for RNA-seq data with DESeq2. *Genome Biol.* 15, 550–621. doi:10.1186/s13059-014-0550-8

Mathys, H., Davila-Velderrain, J., Peng, Z., Gao, F., Mohammadi, S., Young, J. Z., et al. (2019). Single-cell transcriptomic analysis of alzheimer's disease. *Nature* 570, 332–337. doi:10.1038/s41586-019-1195-2

Mayeda, E. R., Glymour, M. M., Quesenberry, C. P., Johnson, J. K., Pérez-Stable, E. J., and Whitmer, R. A. (2017). Survival after dementia diagnosis in five racial/ethnic groups. *Alzheimers Dement.* 13, 761–769. doi:10.1016/j.jalz.2016.12.008

Meng, S., Chen, H., Deng, C., and Meng, Z. (2023). Catalpol mitigates alzheimer's disease progression by promoting the expression of neural stem cell exosomes released miR-138-5p. *Neurotox. Res.* 41, 41–56. doi:10.1007/s12640-022-00626-z

Merighi, S., Nigro, M., Travagli, A., and Gessi, S. (2022). Microglia and alzheimer's disease. *Int. J. Mol. Sci.* 23, 12990. doi:10.3390/ijms232112990

Moreira-Silva, D., Carrettiero, D. C., Oliveira, A. S. A., Rodrigues, S., Dos Santos-Lopes, J., Canas, P. M., et al. (2018). Anandamide effects in a streptozotocin-induced alzheimer's disease-like sporadic dementia in rats. *Front. Neurosci.* 12, 653. doi:10.3389/fnins.2018.00653

Paxinos, G., and Watson, C. (2006). *The rat brain in stereotaxic coordinates: hard cover edition*. Amsterdam, Netherlands: Elsevier.

Pertea, M., Pertea, G. M., Antonescu, C. M., Chang, T.-C., Mendell, J. T., and Salzberg, S. L. (2015). StringTie enables improved reconstruction of a transcriptome from RNA-seq reads. *Nat. Biotechnol.* 33, 290–295. doi:10.1038/nbt.3122

Prince, M., Wimo, A., Guerchet, M., Ali, G.-C., Wu, Y.-T., and Prina, M. (2015). World alzheimer report 2015. The global impact of dementia: an analysis of prevalence, incidence, cost and trends. *Alzheimer's Dis. Int.*

Qiang, X., Yang, L., Ran, H., Sheng, Y., Jie, T., Xu, L., et al. (2016). Lyophilized powder of catalpol and puerarin protects neurovascular unit from stroke. *Int. J. Biol. Sci.* 12, 367–380. doi:10.7150/ijbs.14059

Qureshi, S., Ali, G., Muhammad, T., Idrees, M., Ullah, S., Khan, S. A., et al. (2022). Thiadiazine-thione derivatives ameliorate STZ-induced diabetic neuropathy by regulating insulin and neuroinflammatory signaling. *Int. Immunopharmacol.* 113, 109421. doi:10.1016/j.intimp.2022.109421

Rani, V., Verma, R., Kumar, K., and Chawla, R. (2023). Role of pro-inflammatory cytokines in alzheimer's disease and neuroprotective effects of pegylated self-assembled nanoscaffolds. *Curr. Res. Pharmacol. Drug Discov.* 4, 100149. doi:10.1016/j.crphar.2022.100149

Rhodius-Meester, H. F. M., Tijms, B. M., Lemstra, A. W., Prins, N. D., Pijnenburg, Y. A., Bouwman, F., et al. (2019). Survival in memory clinic cohort is short, even in young-onset dementia. *J. Neurol. Neurosurg. Psychiatry* 90, 726–728. doi:10.1136/jnnp-2018-318820

Scheltens, P., De Strooper, B., Kivipelto, M., Holstege, H., Chételat, G., Teunissen, C. E., et al. (2021). Alzheimer's disease. *Lancet* 397, 1577–1590. doi:10.1016/S0140-6736(20)32205-4

Selkoe, D. J. (2021). Treatments for alzheimer's disease emerge. *Science* 373, 624–626. doi:10.1126/science.abi6401

Squillace, S., and Salvemini, D. (2022). Toll-like receptor-mediated neuroinflammation: relevance for cognitive dysfunctions. *Trends Pharmacol. Sci.* 43, 726–739. doi:10.1016/j.tips.2022.05.004

Su, F., Bai, F., Zhou, H., and Zhang, Z. (2016). Microglial toll-like receptors and alzheimer's disease. *Brain, Behav. Immun.* 52, 187–198. doi:10.1016/j.bbi.2015.10.010

Tang, D. D., Zhang, J., Wang, J. R., Zhang, J. F., and Xu, X. Y. (2016). Borneol promotes oral absorption and penetration into brain of puerarin and catalpol. *Zhongguo Zhong Yao Za Zhi* 41, 2720–2726. doi:10.4268/cjcmm20161425

Thakur, S., Dhapola, R., Sarma, P., Medhi, B., and Reddy, D. H. (2023). Neuroinflammation in alzheimer's disease: current progress in molecular signaling and therapeutics. *Inflammation* 46, 1–17. doi:10.1007/s10753-022-01721-1

Trapnell, C., Roberts, A., Goff, L., Pertea, G., Kim, D., Kelley, D. R., et al. (2012). Differential gene and transcript expression analysis of RNA-seq experiments with TopHat and cufflinks. *Nat. Protoc.* 7, 562–578. doi:10.1038/nprot.2012.016

Venegas, C., Kumar, S., Franklin, B. S., Dierkes, T., Brinkschulte, R., Tejera, D., et al. (2017). Microglia-derived ASC specks cross-seed amyloid-β in alzheimer's disease. *Nature* 552, 355–361. doi:10.1038/nature25158

Vorhees, C. V., and Williams, M. T. (2006). Morris water maze: procedures for assessing spatial and related forms of learning and memory. *Nat. Protoc.* 1, 848–858. doi:10.1038/nprot.2006.116

Walf, A. A., and Frye, C. A. (2007). The use of the elevated plus maze as an assay of anxiety-related behavior in rodents. *Nat. Protoc.* 2, 322–328. doi:10.1038/nprot.2007.44

Wang, H., Yang, H., Shi, Y., Xiao, Y., Yin, Y., Jiang, B., et al. (2021). Reconstituting neurovascular unit with primary neural stem cells and brain microvascular endothelial cells in three-dimensional matrix. *Brain Pathol.* 31, e12940. doi:10.1111/bpa.12940

Wang, Q., Shen, Z.-N., Zhang, S.-J., Sun, Y., Zheng, F.-J., and Li, Y.-H. (2022). Protective effects and mechanism of puerarin targeting PI3K/Akt signal pathway on neurological diseases. *Front. Pharmacol.* 13, 1022053. doi:10.3389/fphar.2022.1022053

Wang, X., and Brusseau, M. L. (1993). Solubilization of some low-polarity organic compounds by hydroxypropyl-. beta.-cyclodextrin. *Environ. Sci. & Technol.* 27, 2821–2825. doi:10.1021/es00049a023

Wegmann, S., Biernat, J., and Mandelkow, E. (2021). A current view on Tau protein phosphorylation in alzheimer's disease. *Curr. Opin. Neurobiol.* 69, 131–138. doi:10.1016/j.conb.2021.03.003

Wu, T., Hu, E., Xu, S., Chen, M., Guo, P., Dai, Z., et al. (2021). clusterProfiler 4.0: a universal enrichment tool for interpreting omics data. *Innov* 2, 100141. doi:10.1016/j.xinn.2021.100141

Xie, J., Van Hoecke, L., and Vandenbroucke, R. E. (2022). The impact of systemic inflammation on alzheimer's disease pathology. *Front. Immunol.* 12, 796867. doi:10.3389/fimmu.2021.796867

Ye, T., Yan, X., Bai, H., Wu, Y., Liu, J., Zhang, X., et al. (2024). Borneol regulates meningeal lymphatic valve plasticity to clear Aβ aggregates in the prevention of AD-like symptoms. *Phytomedicine* 130, 155753. doi:10.1016/j.phymed.2024.155753

Yin, H., Liu, R., and Bie, L. (2024). Gastrodin ameliorates neuroinflammation in alzheimer's disease mice by inhibiting NF-κB signaling activation via PPARγ stimulation. *Aging (Albany NY)* 16, 8657–8666. doi:10.18632/aging.205831

Yokoyama, M., Kobayashi, H., Tatsumi, L., and Tomita, T. (2022). Mouse models of alzheimer's disease. *Front. Mol. Neurosci.* 15, 912995. doi:10.3389/fnmol.2022.912995

Glossary

AD	Alzheimer's Disease
3D-NVU	3-dimensional brain neurovascular unit
AEA	arachidonoylethanolamide
ANOVA	analysis of variance
App	amyloid precursor protein
Aβ	amyloid beta
BMSCs	brain microvascular endothelial cells
DAPI	4′,6-diamidino-2-phenylindole
DI	Discrimination index
DMEM/F12	Dulbecco's modified eagle medium: Nutrient mixture F-12
DPN	donepezil hydrochloride tablets
ELISA	enzyme-linked immunosorbent assay
EMP	elevated plus maze
FBS	fetal bovine serum
FPKM	fragments per kilobase million
GFAP	glial fibrillary acidic protein
GO	gene ontology
HE	Haematoxylin and Eosin
ICV	intracerebroventricular
IL	interleukin
Iba-1	adaptor molecule 1
KEGG	Kyoto Encyclopedia of Genes and Genomes
MWM	Morris water maze
NO	nitric oxide
NOR	new object recognition
NSCs	neural stem cells
PC12	pheochromocytoma cell line
PCA	principal component analysis
PERMANOVA	permutational multivariate analysis of variance
PS	penicillin-streptomycin
ROS	reactive oxygen species
RT-qPCR	reverse transcription quantitative polymerase chain reaction
STZ	streptozotocin
TCMs	traditional Chinese medicine
TLR	toll-like receptor
TNF-α	tumor necrosis factor-α
cDNA	complementary DNA
rhEGF	recombinant human epidermal growth factor
rhbFGF	recombinant human basic fibroblast growth factor

frontiers | Frontiers in Neuroscience

TYPE Original Research
PUBLISHED 13 November 2024
DOI 10.3389/fnins.2024.1497102

Check for updates

OPEN ACCESS

EDITED BY
Pukar Khanal,
Emory University, United States

REVIEWED BY
Yadu Nandan Dey,
Dr. B.C. Roy College of Pharmacy and Allied Health Sciences, India
Pramod Nagaraju,
Case Western Reserve University, United States
Amita Kumari,
Emory University, United States

*CORRESPONDENCE
Guofang Xue
xueguofangty@163.com
Zhaojun Wang
wzhaojun1025@126.com

RECEIVED 16 September 2024
ACCEPTED 23 October 2024
PUBLISHED 13 November 2024

CITATION
Li S, Adamu A, Ye Y, Gao F, Mi R, Xue G and Wang Z (2024) (+)-Borneol inhibits neuroinflammation and M1 phenotype polarization of microglia in epileptogenesis through the TLR4-NFκB signaling pathway. *Front. Neurosci.* 18:1497102. doi: 10.3389/fnins.2024.1497102

COPYRIGHT
© 2024 Li, Adamu, Ye, Gao, Mi, Xue and Wang. This is an open-access article distributed under the terms of the Creative Commons Attribution License (CC BY). The use, distribution or reproduction in other forums is permitted, provided the original author(s) and the copyright owner(s) are credited and that the original publication in this journal is cited, in accordance with accepted academic practice. No use, distribution or reproduction is permitted which does not comply with these terms.

(+)-Borneol inhibits neuroinflammation and M1 phenotype polarization of microglia in epileptogenesis through the TLR4-NFκB signaling pathway

Shuo Li[1], Alhamdu Adamu[1], Yucai Ye[2], Fankai Gao[3], Rulin Mi[3], Guofang Xue[3]* and Zhaojun Wang[2]*

[1]Second Clinical Medical School, Shanxi Medical University, Taiyuan, China, [2]Department of Physiology, Shanxi Medical University, Taiyuan, China, [3]Department of Neurology, Second Hospital of Shanxi Medical University, Taiyuan, China

Objective: To investigate the effect of (+)-borneol on neuroinflammation and microglia phenotype polarization in epileptogenesis and its possible mechanism.

Methods: Based on mouse models of status epilepticus (SE) induced by pilocarpine, and treated with 15 mg/kg (+)-borneol, western-blot was used to detect the expressions of NeuN, Iba-1, TLR4, p65 and p-p65 in the hippocampus. Immunofluorescence was used to detect the expression of apoptosis-related proteins Bax and Bcl-2. To explore the effect of (+)-borneol on microglia *in vitro*, we used the kainic acid-induced microglia model and the concentration of (+)-borneol was 25 μM according to CCK-8 results. The levels of tumor necrosis factor-α (TNF-α), interleukin-1β (IL-1β) and interleukin-10 (IL-10) in the supernatant of each group was detected by ELISA. The nitric oxide (NO) content in the supernatant was detected by Griess method. The expressions of Iba-1 and TLR4-NFκB signaling pathway-related proteins (TLR4, p65, p-p65) were detected by Western-Blot. Immunofluorescence was used to detect microglia's M1 and M2 phenotype polarization and the expression of Iba-1 and TLR4.

Results: (+)-borneol reduced hippocampal neuronal injury, apoptosis, and microglia activation by inhibiting the TLR-NFκB signaling pathway in SE mice. TLR4 agonist LPS partially reversed the neuroprotective effect of (+)-borneol. In the KA-induced microglia model, (+)-borneol inhibited microglia activation, M1 phenotype polarization, and secretion of pro-inflammatory cytokines through the TLR4-NFκB signaling pathway. LPS treatment inhibited the therapeutic effects of (+)-borneol.

Conclusion: (+)-borneol inhibits microglial neuroinflammation and M1 phenotype polarization through TLR4-NFκB signaling pathway and reduces neuronal damage and apoptosis in SE mice. Therefore, (+)-borneol may be a potential drug for epilepsy modification therapy.

KEYWORDS

epileptogenesis, (+)-borneol, microglia, neuroinflammation, TLR4-NFκB

1 Introduction

Epilepsy is a chronic brain disease characterized by recurrent seizures (Beghi, 2020). The causes of the epilepsy mainly include malformtion of cortical development, cerebrovascular diseases, brain tumors, traumatic brain injury, and central nervous system infection (Pitkänen et al., 2015). At present, epilepsy has become the second most common disease of the nervous system, affecting about 70 million people around the world (Thijs et al., 2019). Comorbidities such as anxiety, depression and stigma bring great pressure on patients and a heavy burden to families and society (Trinka et al., 2019; Beghi, 2020). Antiseizure medications (ASMs) are currently the main means of controlling seizures, such as sodiumvalproate, lamotrigine, levetiracetam, carbamazepine (Manford, 2017). However, they can only reduce the frequency and/or severity of seizures, cannot interfere with the process of the disease or change the prognosis and one-third of patients are resistant to existing drugs (Thijs et al., 2019).

Disease-modifying therapy (DMT) is a treatment that modifies the course of disease through medical intervention, which has been widely used in various neurological diseases (Chiò et al., 2020; Liu et al., 2021a; Tabrizi et al., 2022). In the existing studies on epilepsy modifying therapy, the frequency and duration of hippocampal paroxysmal discharges in epileptic mice can be reduced by inhibiting neuroinflammation (Gong et al., 2022), or the comorbidities such as learning and memory deficits of rats post-status epilepticus (SE) can be improved (Casillas-Espinosa et al., 2023). Both of them can achieve the purpose of disease modification. It has become the main research direction of epilepsy to search for new therapeutic targets and more effective drugs to delay the development of epilepsy, improve the pathological damage after seizures, and achieve the purpose of epilepsy modification therapy (Galanopoulou et al., 2021).

Epileptogenesis refers to the chronic process of the formation of epileptic pathological foci (Pitkänen et al., 2015).In other words, the brain undergoes molecular cellular changes caused by epileptogenic factors, then the excitability of neurons increases and leads to spontaneous recurrent seizures (SRS) (Pitkänen et al., 2007). The whole process is called epileptogenesis, which is the main target of epilepsy modification therapy. In this process, a series of pathophysiological changes occur, including abnormal neuroinflammation, excessive activation of glia, massive secretion of inflammatory factors, active plasticity of abnormal neuronal networks and dendritic spines, dysregulation of voltage-gated ion channels, neuronal damage, apoptosis, blood–brain barrier damage, and infiltration of peripheral immune cells into the brain (Li et al., 2023; Jean et al., 2023; Issa et al., 2023). Recent studies have shown that neuroinflammation and its coupled activation of glia and release of inflammatory factors are the initiating factors of epilepsy and run through the whole process (Mukhtar, 2020; Soltani Khaboushan et al., 2022).Neuroinflammation and its related pathways have become important targets for drug development, and drugs targeting neuroinflammation are also considered promising drugs and put into basic or clinical research (Clossen and Reddy, 2017).

Microglia are the resident immune cells in the nervous system, which are involved in maintaining the homeostasis of the central nervous system (Borst et al., 2021). According to the different proinflammatory or anti-inflammatory functions, microglia are generally divided into M1 phenotype (neurotoxic) and M2 phenotype (neuroprotective), and the two phenotypes can transform into each other (Kwon and Koh, 2020). In the early stage of epilepsy, microglia can be activated and respond to neuroinflammation first (Sano et al., 2021). and the M1 phenotype is significantly increased, accompanied by a large number of inflammatory factors (Benson et al., 2015). Activated microglia are involved in subsequent astrocyte activation and can contribute to astrocyte dysfunction and acute seizures (Henning et al., 2023). A variety of drugs can inhibit neuroinflammation by regulating the phenotype polarization of microglia (Yang et al., 2017; Zhang et al., 2019; Liu et al., 2021b). In addition to participating in neuroinflammation to increase neuronal excitability, microglia can also cause non-inflammatory changes through enhanced mTOR signaling, which disrupts central nervous system homeostasis and eventually leads to SRS (Zhao et al., 2018). The inhibition of microglia after SE reduced the frequency of SRS, the duration and severity of seizures (Wang et al., 2015). Therefore, microglia play an important role in epileptogenesis and may be a potential target for epilepsy modification therapy.

(+)-Borneol (C10H18O) is the main component of natural borneol. It is believed to have the functions of "medicinal guide" (Ren et al., 2024) and "clearing heat" (Zou et al., 2017; Zhong et al., 2023) in traditional Chinese medicine, so it is widely used in prescriptions for the treatment of mental disorders. Recent studies have shown that (+)-borneol can inhibit oxidative stress (Hua et al., 2021; Chen et al., 2022), neuroinflammation (Liu et al., 2011) and apoptosis (Liu et al., 2011), and it can cross the blood–brain barrier (Liu et al., 2021) to play a neuroprotective role in a variety of nervous system diseases (Wang et al., 2019; Xie et al., 2022; Ma et al., 2023). Our previous studies have shown that (+)-borneol can inhibit neuroinflammation and apoptosis in the hippocampus of rats with status epilepticus (SE) (Gao et al., 2023). However, the effects of (+)-borneol on neuroinflammation and phenotype polarization of microglia in epilepsy are still unclear. In the present study, we examined the expression of inflammatory cytokines, microglia phenotypic markers, neuronal markers, apoptosis-related proteins and TLR4-NFκB signaling pathway-related proteins to evaluate whether (+)-borneol could play a neuroprotective role by regulating microglial neuroinflammation and phenotypic polarization *in vitro* and *in vivo* through TLR4-NFκB signaling pathway.

2 Methods

2.1 Chemicals

(+)-Borneol was gifted to Simcere Pharmaceuticals. LPS was purchased from Beijing Solarbio Science & Technology Co., Ltd. (Cat No:L8880). Lithium chloride was purchased from Sigam (United States). Atropine and Pilocarpine was purchased from Shanghai Aladdin Biochemical Technology Co., Ltd. Diazepam was purchased from Jinyao Pharmaceutical. KA was purchased from Yuanye (Shanghai, China, Cat No:S30773).

2.2 Animals

C57BL/6 male mice, aged 8 weeks, 18-22 g, were purchased from the Animal Center of Shanxi Medical University and raised in the tertiary SPF animal facility of the Animal Experimental Center of Shanxi Medical University. The average room temperature was

20–25°C, the relative humidity was 30–50%, and the light and dark cycles were alternating for 12 h. They had free access to water and food. After 1 week of acclimatization, the mice were randomly divided into 4 groups: normal Control group (Control group), epilepsy model group (SE group), (+)-borneol group (SE + Borneol group), and TLR4 agonist group (SE + Borneol+LPS group), with 12 mice in each group. All experimental protocols were in accordance with NIH guidelines and have been reviewed by the Ethics Committee of the Second Hospital of Shanxi Medical University. The ethics record number was DW2023018.

2.3 Preparation of (+)-borneol solution

(+)-Borneol was dissolved in dimethyl sulfoxide (DMSO) in 100 mg/mL, diluted to 2 mg/mL in normal saline for intraperitoneal injection *in vivo*, or diluted to 1 mM solution in PBS for cell experiments.

2.4 Animal model preparation and grouping treatment

The mice in the SE group, SE + Borneol group and SE + Borneol+LPS group were intraperitoneally injected with lithium chloride (127 mg/kg) for pretreatment and were intraperitoneally injected with atropine (1 mg/kg) 20 h later. Pilocarpine (200 mg/kg) was injected intraperitoneally 30 min later. About 20–30 min later, seizures were observed. Thirty minutes after successful modeling, diazepam (10 mg/kg) was injected intraperitoneally to terminate the seizure. The mice in the Control group were intraperitoneally injected with the same volume of normal saline. Animal behavior was assessed according to the Racine grade (Racine, 1972). The criteria for successful modeling were Racine grade IV (generalized tonic–clonic standing on the hind limbs) or grade V (generalized tonic–clonic standing even unable to maintain balance) lasting more than 30 min, or failure to restore normal behavior between seizures.

The mice in the SE + Borneol group were intraperitoneally injected with (+)-borneol solution (15 mg/kg) daily for 7 days, and those in the SE + Borneol+LPS group were intraperitoneally injected with LPS solution (0.5 mg/kg) 6 h before (+)-borneol injection. The other groups were injected with the same volume of solvent at the same time point.

2.5 Immunofluorescence

After 7 days of drug administration, brains were removed by heart perfusion, fixed and dehydrated, snap-frozen in liquid nitrogen, and stored in a cryogenic refrigerator at −80°C. Frozen sections were 20 μm brain slices. After 1 h of equilibrium at room temperature, the surrounding embedding agent was washed off with PBS and fixed with 4% paraformaldehyde. Brain slices were fixed with 4% paraformaldehyde for 30 min at room temperature, incubated with 0.5%TritonX-100 for 15 min at room temperature, blocked with BSA for 1 h, and incubated with the next primary antibody drop at 4°C overnight: Bax (1:50, Bioworld, USA), Bcl-2 (1:50, Bioworld, USA). The next day, after rewarming at room temperature for 1 h, fluorescent secondary antibody (1:150, Bioss, China) was incubated in the dark for 1 h, and DAPI was incubated in the dark for 10 min after washing. Anti-fluorescence quencher was added to seal the slides, and the slides were observed under the fluorescence microscope (Olympus, BX51, Japan) and photographed under 10x objective lens with the same parameters as the control group. Finally, Image-J was used for analysis.

2.6 Cell culture

The BV2 microglia cell line was purchased from Wuhan Pricella Biotechnology Co., LTD.

BV2 microglia cells were cultured in the complete medium (DMEM/F12, 10% fetal bovine serum, 1% penicillin–streptomycin solution) at 37°C and 5%CO2 incubator (Thermo, Germany). The culture medium was discarded, washed twice with phosphate-buffered saline (PBS), and digested with 0.25% trypsin in the incubator for 5 min. The digestion was terminated with 2 times the amount of trypsin in complete medium, centrifuged at 1000 rpm for 5 min, and the supernatant was discarded and the complete medium was resuspended and passaged at a ratio of 1:3.

2.7 CCK-8

Cells in the logarithmic phase were collected and seeded in 96-well plates at 50000 /mL cell concentration and 100 μL per well. The cells were treated with 600 μM KA (Source, Shanghai, China). After 12 h, (+)-borneol solution of 6 μM, 12.5 μM, 25 μM, 50 μM, 100 μM and 200 μM was added, respectively. After 12 h, the culture medium was discarded, and the culture medium containing 10 μL CCK-8 solution was added to each well. After incubation at 37°C for 1 h, the absorbance was measured by the microplate reader (Bio-Tek, United States) at 450 nm. Cell survival rate = [(experimental well-blank well)/ (control well-blank well)] × 100%. The CCK-8 kit was purchased from Boster, China (Cat No:AR1160).

2.8 Groups and treatment of cells

Microglia were seeded in 6-well or 12-well plates at a density of 50,000 cells /ml. The cells were divided into 4 groups: Control group (Control group), model group (KA group), (+)-borneol group (KA + Borneol group), and TLR4 agonist group (KA + Borneol+LPS group). After 24 h, the cells adhered to the culture dishes, the medium of each group was discarded and the cells were washed twice with PBS. The complete medium containing 600 μM KA was added in the KA group, KA + Borneol group and KA + Borneol+LPS group. In the KA + Borneol group and KA + TLR4 agonist group, (+)-borneol solution with a final concentration of 25 μM was added after 12 h of KA treatment. In the KA + Borneol+LPS group, LPS solution with a final concentration of 50 ng/mL was added 1 h before (+)-borneol was added.

2.9 Elisa

After the cells were grouped and cultured, the cell culture supernatant of each group was collected and centrifuged at 1000 rpm for 5 min, and the supernatant was removed and placed at −20°C for

later use, which were tested within 1 week of collection According to the instructions of ELISA, the absorbance was measured at 450 nm using a microplate reader and the contents of TNF-α (Boster, China), IL-1β (Boster, China) and IL-10 (Bioswamp, China) in the cell supernatant of each group were calculated.

2.10 Griess

Using Griess kit (Beyotime, S0021S, China), Griess Reagent I and II reagents in the kit were equilibrated to room temperature. According to the instructions, the complete medium same as the cell culture was used to dilute standards (0, 1, 2, 5, 10, 20, 40, 60, 100 μM). In a 96-well plate, 50 μL of standard or cell supernatant from each group was added to each well. 50 μL of Griess Reagent I and II reagents that had equilibrated to room temperature were successively added to each well. Stir gently and mix well. The absorbance was measured at 540 nm using a microplate reader. The concentration of nitric oxide in the supernatant of each group was calculated by drawing a standard curve based on the results of the standard.

2.11 Western blot

After 7 days of drug administration, the animals were sacrificed by neck removal, and the hippocampus was removed from the whole brain, weighed, cut into pieces on ice, and thoroughly blown after adding precooled RIPA (the ratio of tissue weight and RIPA was 1 g:10 mL) and 1% protease inhibitors. The tissues were crushed by an ultrasonic morcellator (QSONICA, United States) for 2 s ultrasound and 2 s intervals. The time of morcellation was determined according to the situation of the tissue. Then the tissue was centrifuged at 13000 rpm for 25 min at 4°C, and the protein concentration was determined by BCA method and quantified to 35 μg/10 μL. The appropriate concentration of separation gel was selected according to the molecular weight, and the proteins were separated by electrophoresis and transferred to the PVDF membrane. The protein was blocked with protein-free rapid blocking solution (Boster, China) at room temperature for 15 min, and incubated in the following primary antibody solution at 4°C overnight: NeuN (1:500, Abclonal, China), Iba-1 (1:1000, Bioworld, United States), TLR4 (1:1000, Proteintech, China), p65 (1:2000, Bioss, China), p-p65 (1:1000, Bioss, China), GAPDH (1:1000, Bioworld, United States), β-actin (1:1000, Bioworld, China). Secondary antibody (1:10000, Servicebio, China) incubation and exposure were performed the next day. Finally, the grayscale was analyzed by Image- J.

The cells were grouped and treated as described in section 2.8. The cells in each group were added with precooled RIPA and protease inhibitors, then the cells were fully lysed, centrifuged at 12000 rpm for 20 min at 4°C, and the protein concentration was determined by BCA method and quantified to 15 μg/10 μL. The latter steps were the same as above.

2.12 Cell immunofluorescence

Cells were uniformly seeded in 12-well plates with cell-specific slides placed in advance, and cells were grouped and treated as described in section 2.8. The cells were fixed with 4% paraformaldehyde for 30 min at room temperature and then incubated with 0.25%TritonX-100 for 10 min (membrane proteins) or 15 min (nuclear and cytoplasmic proteins) at room temperature. After that, the cells were blocked with BSA for 1 h, and the cells were covered with the next primary antibody solution and incubated at 4°C overnight: Iba-1 (1:100, Proteintech, China), CD86 (1:50, Boster, China), CD206 (1:400, Proteintech, China), TLR4 (1:50, Abclonal, China), p65 (1:100, Bioss, China), p-p65 (1:100, Bioss, China). The next day, the fluorescent secondary antibody (1:150, Bioss, China) was incubated in the dark for 1 h after rewarming at room temperature, and DAPI was incubated in the dark for 10 min after washing. Anti-fluorescence quencher was added to seal the slides, and the slides were observed under the fluorescence microscope and photographed under 20x objective lens with the same parameters as the control group. Finally, Image-J was used for analysis.

2.13 Statistical analysis

The results were compared using GraphPad Prism V8.0.2. The experimental data were represented as mean ± SEM. The data were analyzed by one-way ANOVA followed by Tukey's post-hoc tests for multiple comparisons. $p < 0.05$ was considered statistically significant.

3 Results

3.1 (+)-Borneol reduced hippocampal neuronal damage and apoptosis in SE mice

The expression of neuronal marker NeuN, pro-apoptotic protein Bax and anti-apoptotic protein Bcl-2 were examined in the hippocampus of SE mice.

The results of Western Blot showed that the expression of NeuN in the SE group was significantly lower than that in the Control group ($p < 0.001$). (+)-Borneol treatment reduced hippocampal neuronal damage after SE ($p < 0.01$) and TLR4 activated by LPS partially reversed the effect ($p < 0.05$; Figures 1A,B).

The results of immunofluorescence of Bax (Figure 2) and Bcl-2 (Figure 3) showed that the expression of Bax was increased ($p < 0.001$) and the expression of Bcl-2 was decreased ($p < 0.001$) in each brain region in the SE group compared with the Control group. Treatment with (+)-borneol reduced the expression of Bax ($p < 0.001$) and increased Bcl-2 (CA1, $p < 0.01$, CA3, DG $p < 0.001$). Activation of TLR4 reversed the anti-apoptosis effect of (+)-borneol (Bax, CA1 $p < 0.001$, CA3 $p < 0.05$, DG $p < 0.01$ and Bcl-2, CA1, CA3 $p < 0.05$, DG $p < 0.01$).

3.2 (+)-Borneol reduced microglia activation in the hippocampus of SE mice

The expression of microglia marker Iba-1 in the hippocampus of epileptic mice was detected.

The results of Western Blot showed that the expression of Iba-1 in the SE group has a higher level than that in the Control group ($p < 0.001$). (+)-Borneol treatment reduced Iba-1 expression ($p < 0.01$) and TLR4 agonist LPS increased the Iba-1 expression compared with the SE + Borneol group ($p < 0.05$) (Figures 4A,B).

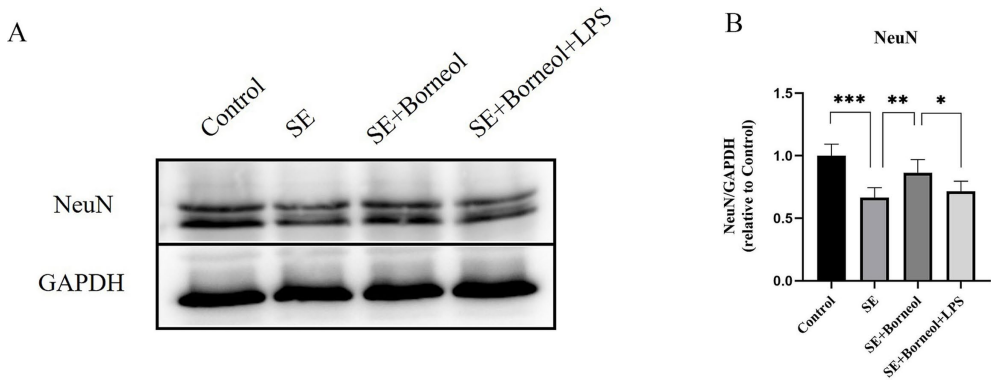


FIGURE 1
Effect of (+)-borneol on the NeuN expression in SE mice hippocampus. **(A)** Western-Blot representative diagrams of NeuN in each group of mice. **(B)** Analysis and statistics of Western-Blot results. ***$p < 0.001$; **$p < 0.01$; *$p < 0.05$; $n = 6$.

3.3 (+)-Borneol inhibited the activation of TLR4-NFκB signaling pathway in the hippocampus of SE mice

The expression of TLR4, p65/NFκB and p-p65/NFκB in the hippocampus of SE mice was detected.

Western Blot results showed that the expression of TLR4 and p-p65/p65 in the hippocampus of the SE group was significantly higher than that of the Control group ($p < 0.001$). After the treatment of (+)-borneol, the expression of TLR4 and pp65/p65 was decreased ($p < 0.01$). Compared with the SE + Borneol group, the SE + Borneol+LPS group had significant increases in the expression of TLR4 and p-p65/p65 ($p < 0.05$) (Figures 5A–C).

3.4 The optimal concentration of (+)-borneol in KA-induced BV2 microglia was 25 μM

To determine the optimal concentration of (+)-borneol on KA-induced microglia, microglia were treated with different concentrations of (+)-borneol after 12 h of KA-induced, then co-cultured with KA for another 12 h. Cell viability was detected by CCK-8 (Figure 6). The results showed that treatment with 600 μM KA significantly decreased the viability of microglia ($p < 0.001$). The toxic effect of KA was counteracted by treatment with 25 μM (+)-borneol ($p < 0.01$).When the concentration increased to 200 μM, (+)-borneol produced toxic effects ($p < 0.05$). The concentration of (+)-borneol, which can antagonize the toxicity of KA and has high cell activity, was selected as the optimal concentration in this experiment, so it was determined to be 25 μM. (+)-Borneol inhibited KA-induced pro-inflammatory cytokines secretion in BV2 microglia.

3.5 (+)-Borneol inhibited KA-induced pro-inflammatory cytokines secretion in BV2 microglia

The levels of proinflammatory cytokines TNFα, IL-1β and anti-inflammatory cytokine IL-10 in the culture supernatant of BV2 microglia were detected by ELISA. The level of NO in the culture supernatant was detected by the Griess method.

Compared with the Control group, the secretion of three pro-inflammatory cytokines (TNFα, IL-1β and NO) was increased, and the secretion of anti-inflammatory cytokine (IL-10) was decreased in the KA group ($p < 0.001$). Compared with the KA group, the secretion of proinflammatory cytokines in the KA + Borneol group decreased ($p < 0.001$), and there was no significant difference in the secretion of anti-inflammatory cytokines ($p > 0.05$). Compared with the KA + Borneol group, the KA + Borneol+LPS group showed increased secretion of pro-inflammatory cytokines (TNFα $p < 0.01$, IL-1β and NO $p < 0.05$), but no significant difference in anti-inflammatory cytokines ($p > 0.05$) (Figure 7).

3.6 (+)-Borneol inhibited KA-induced activation of BV2 microglia and inhibited microglial polarization to M1 phenotype

Western Blot was used to detect the expression of Iba-1 in BV2 microglia. Immunofluorescence assay was used to detect the expression of Iba-1, M1 marker CD86 and M2 marker CD206 in BV2 microglia.

The expression of Iba-1 was detected by Western Blot (Figures 8A,B). Compared with the Control group, the expression of Iba-1 in the KA group increased ($p < 0.001$). Compared with the KA group, the KA + Borneol group had a significant reduction in the expression of Iba-1 ($p < 0.001$). Compared with the KA + Borneol group, the KA + Borneol+LPS group had a significant increase in the expression of Iba-1 ($p < 0.05$).

The results of immunofluorescence detection of Iba-1 showed that the average fluorescence intensity of Iba-1 in the KA group was higher than that in the Control group ($p < 0.001$). The average fluorescence intensity of Iba-1 in the KA + Borneol group was lower than that in the KA group ($p < 0.001$). Compared with the KA+ Borneol group, the KA + Borneol+LPS group had a significantly increased mean fluorescence intensity of Iba-1 ($p < 0.05$). The immunofluorescence results were identical to Western-Blot's (Figures 8C,D).

The results of immunofluorescence detection of CD86 and CD206 showed that, compared with the Control group, the average fluorescence intensity of CD86 in the KA group was increased ($p < 0.001$), and the average fluorescence intensity of CD206 was decreased ($p < 0.001$). Compared with the KA group, the average fluorescence intensity of CD86 in the KA + Borneol

10.3389/fnins.2024.1497102

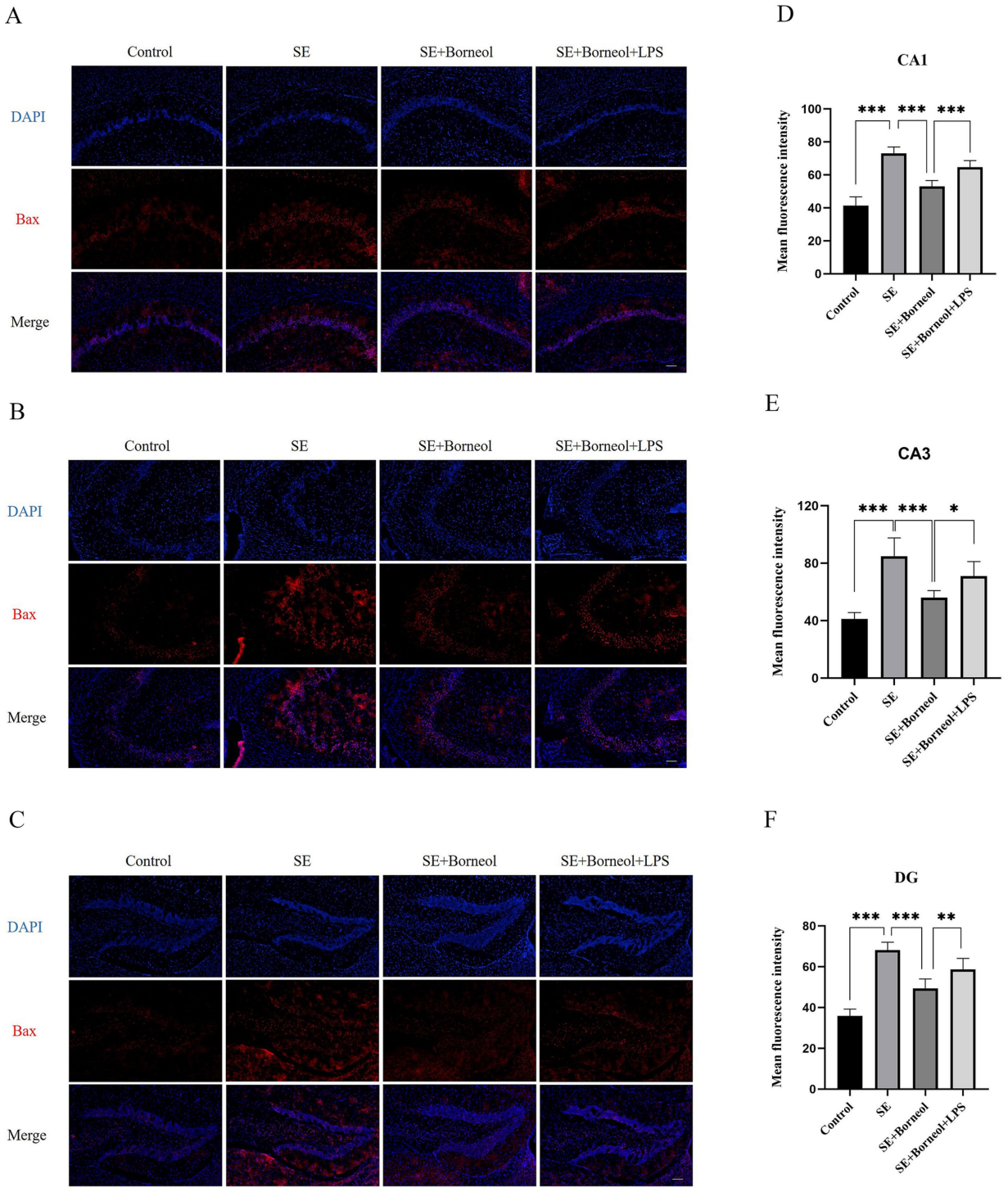


FIGURE 2
Effect of (+)-borneol on the Bax expression in SE mice hippocampus. **(A–C)** Immunofluorescence representative diagrams of Bax in CA1 **(A)**, CA3 **(B)**, and DG **(C)** region. **(D–F)** Analysis and statistics of immunofluorescence in each region. Bar = 200 μm. ***$p < 0.001$; **$p < 0.01$; *$p < 0.05$; $n = 6$.

group was decreased ($p < 0.001$), and there was no significant difference in the average fluorescence intensity of CD206 ($p > 0.05$). Compared with the KA + Borneol group, the mean fluorescence intensity of CD86 was increased in the KA + Borneol+LPS group ($p < 0.05$), but there was no significant difference in CD206 (Figures 9A–D).

3.7 (+)-Borneol inhibited KA-induced activation of TLR4-NFκB signaling pathway in BV2 microglia

The expression of TLR4, p65/NFκB and p-p65/NFκB in each group were detected.

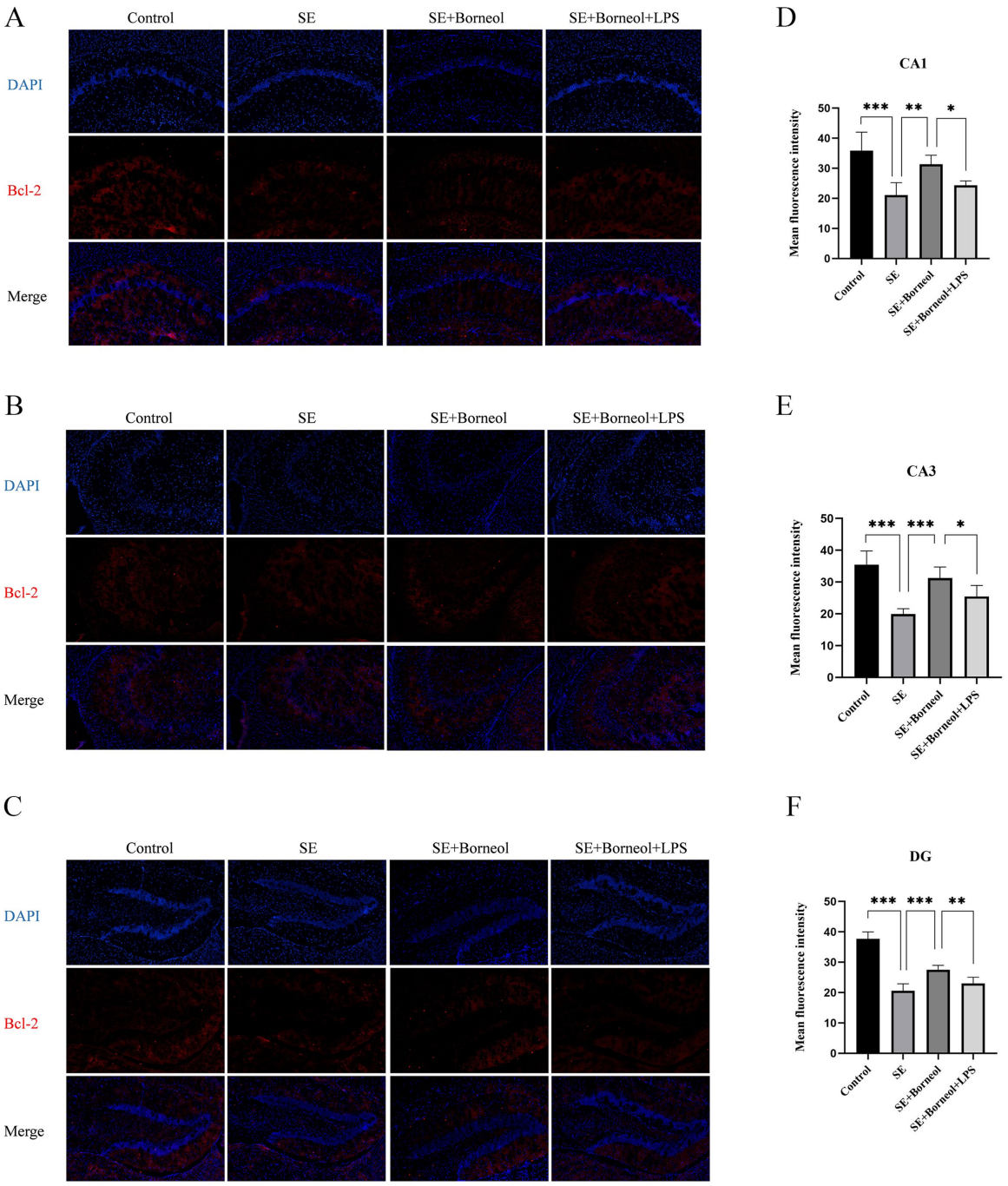


FIGURE 3
Effect of (+)-borneol on the Bcl-2 expression in SE mice hippocampus. **(A–C)**, Immunofluorescence representative diagrams of Bcl-2 in CA1 **(A)**, CA3 **(B)**, and DG **(C)** region. **(D–F)** Analysis and statistics of immunofluorescence in each region. Bar = 200 μm. ***$p < 0.001$; **$p < 0.01$; *$p < 0.05$; $n = 6$.

Western Blot results showed that the expression of TLR4 and p-p65/p65 in the KA group was significantly higher than that in the Control group ($p < 0.001$). The expression of TLR4 and pp65/p65 in KA + Borneol group decreased (TLR4 $p < 0.05$, p-p65/p65 $p < 0.001$). Compared with the KA + Borneol group, the KA + Borneol+LPS group had significantly increased expressions of TLR4 and p-p65/p65 ($p < 0.05$) (Figures 10A–C).

The results of TLR4 immunofluorescence showed that the mean fluorescence intensity of TLR4 in the KA group was increased compared with the Control group ($p < 0.001$). Compared with the KA group, the average fluorescence intensity of TLR4 in the KA + Borneol group was decreased ($p < 0.001$). Compared with the KA+ Borneol group, the KA + Borneol+LPS group had a significantly increased mean fluorescence intensity of TLR4 ($p < 0.05$). The immunofluorescence results were identical to those of Western Blot (Figures 10D,E).

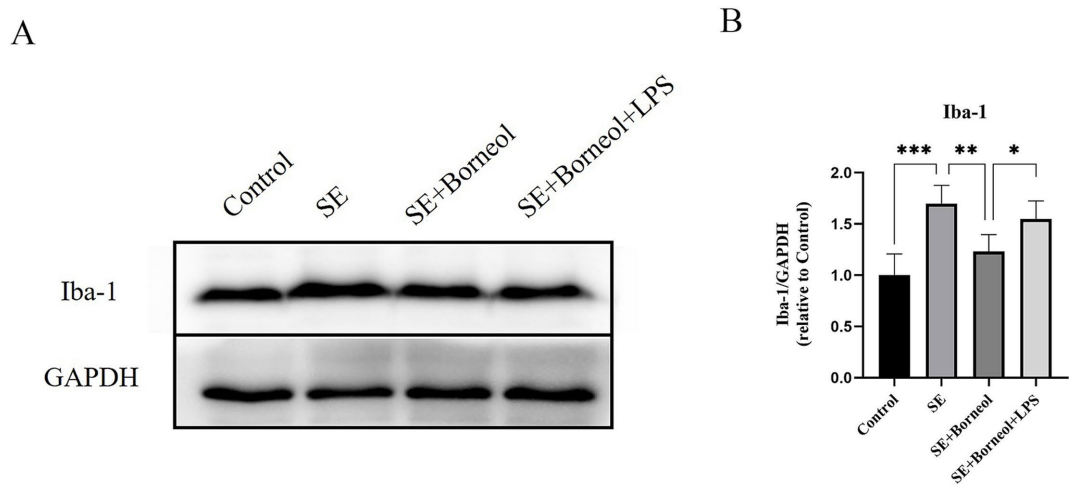


FIGURE 4
Effect of (+)-borneol on the Iba-1 expression in SE mice hippocampus. **(A)** Western-Blot representative diagrams of Iba-1 in each group of mice. **(B)** Analysis and statistics of Western-Blot results. ***$p < 0.001$; **$p < 0.01$; *$p < 0.05$; $n = 6$.

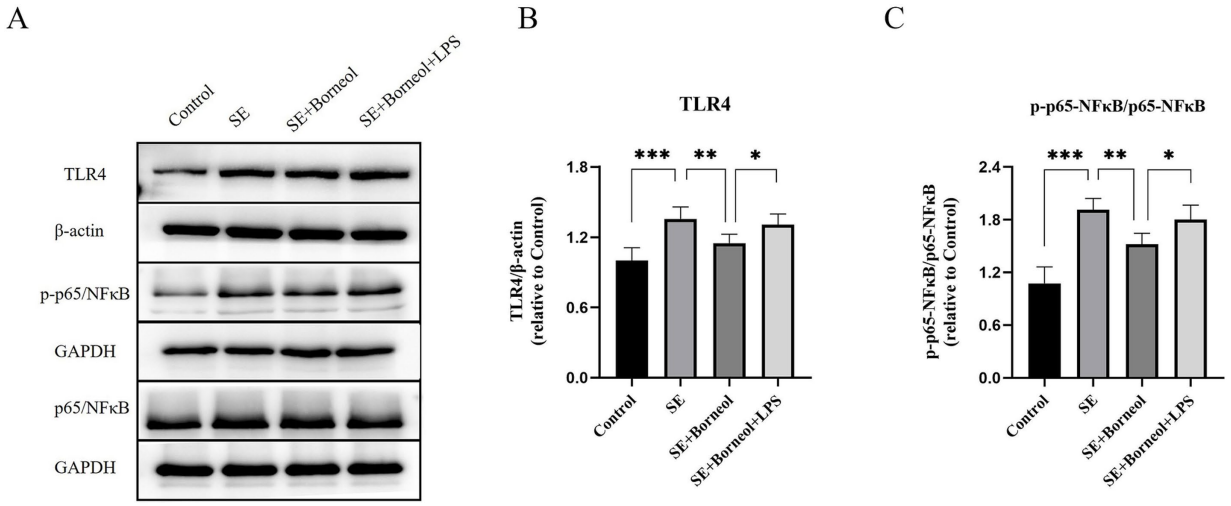


FIGURE 5
Effect of (+)-borneol on the TLR4, p65 and p-p65 expression in SE mice hippocampus. **(A)** Western-Blot representative diagrams of TLR4, p65 and p-p65 in each group of mice. **(B)** Analysis and statistics of TLR4 Western-Blot results. **(C)** Analysis and statistics of p-p65/p65 Western-Blot results. ***$p < 0.001$; **$p < 0.01$; *$p < 0.05$; $n = 6$.

4 Discussion

Our study demonstrated that (+)-borneol was neuroprotective in a pilocarpine-induced status epilepticus (SE) mouse model and inhibited KA-induced BV2 microglial neuroinflammation and M1 phenotype polarization.

According to the results, administration of (+)-borneol after SE reduced hippocampal neuronal damage and apoptosis, and inhibited microglial activation. TLR4 activation reversed the neuroprotective effects of (+)-borneol. In the microglia model induced by KA, (+)-borneol treatment reduced the secretion of pro-inflammatory cytokines, inhibited microglial activation and M1 phenotype polarization, and TLR4 agonist inhibited the anti-inflammatory effects of (+)-borneol. Moreover, (+)-borneol inhibited the activation of the TLR4-NFκB signaling pathway both *in vitro* and *in vivo*.

Currently, the most common clinically drug-resistant epilepsy to existing ASMs is mesial temporal lobe epilepsy (MTLE), which is also the most common type of focal epilepsy in adults (Vega-García et al., 2022; Panina et al., 2023). Studies on the mechanism of MTLE are based on animal models, and the pilocarpine-induced SE model is the most commonly used of these, which can produce similar pathological changes to human MTLE (Lévesque et al., 2021).

KA is an excitatory neurotransmitter glutamate analog that acts on α-amino3-hydroxy-5-methyl-4-isoxazolepropionic acid (AMPA) receptors to cause excessive Ca^{2+} influx. It can cause

intracellular calcium overload and neuronal damage, resulting in epileptogenic effects (Zhang and Zhu, 2011). By acting on microglia, KA can simulate the epilepsy microenvironment, induce the proliferation and activation of microglia, and produce pro-inflammatory cytokines. Our previous experiment explored that the optimal injury concentration of KA on BV2 microglia was 600 μM, which was used as the model concentration for BV2 cells in this study.

Pathological changes such as abnormal increase of neuronal excitability in seizures and SE, neuroinflammation, oxidative stress, and mitochondrial dysfunction in epilepsy can lead to neuronal damage (Madireddy and Madireddy, 2023). The hippocampal neuron loss is the most obvious, which may develop into hippocampal damage, atrophy and sclerosis (Thompson, 2023). The loss of neurons and the resulting brain damage can lead to serious long-term consequences, such as impaired learning and memory, cognitive function, or the development of chronic epilepsy (Chepurnov et al., 2012).

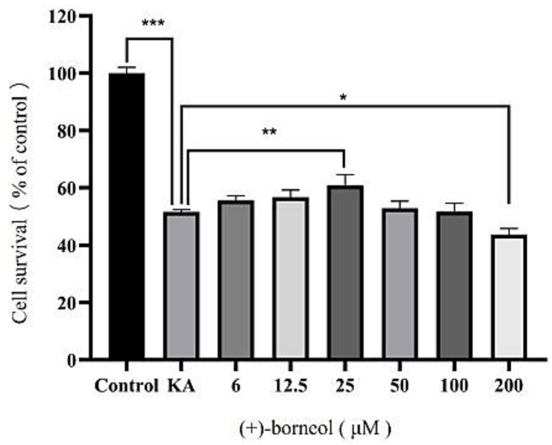


FIGURE 6
Different (+)-borneol concentration and microglia activity. ***$p < 0.001$; **$p < 0.01$; *$p < 0.05$; $n = 3$.

Apoptosis is a form of programmed cell death which is closely related to neuronal damage in epilepsy (Henshall and Simon, 2005). Seizures can also activate the intrinsic apoptotic pathway of cells (Henshall, 2007). Bcl-2 family proteins regulate pro- and anti-apoptotic intracellular signals and are an important class of proteins that regulate apoptosis (Ashkenazi et al., 2017). Among them, anti-apoptotic protein Bcl-2 and pro-apoptotic protein Bax are important members. The anti-apoptotic and pro-apoptotic proteins of the Bcl-2 family maintain a dynamic balance under physiological effects, and promoting the positive or negative balance of apoptosis may become a new opportunity to intervene in diseases (Singh et al., 2019). In the present study, we also observed that (+)-borneol treatment increased the expression of NeuN and Bcl-2 and decreased the expression of Bax in the hippocampus. (+)-Borneol treatment reduced neuronal damage and apoptosis after SE, and TLR4 activation partially reversed the therapeutic effects of (+)-borneol.

Neuroinflammation mainly includes excessive activation of glia and excessive secretion of pro-inflammatory cytokines. Microglia can be activated in the early stage of epilepsy, phagocytose apoptotic cells, secrete appropriate amounts of inflammatory factors, and play a neuroprotective role (Hiragi et al., 2018). Subsequently, microglia secrete a large number of inflammatory cytokines, and excessive neuroinflammation induces astrocyte activation and dysfunction, reduces the seizure threshold, and mediates neuronal damage (Patel et al., 2019; Shen et al., 2023; Henning et al., 2023). Seizures further aggravate neuroinflammation, forming a vicious cycle and accelerating the process of epilepsy (Pracucci et al., 2021).

Our previous study has shown that microglia and astrocytes are rapidly activated and the secretion of inflammatory cytokines is increased after SE in rats (Gao et al., 2023; Tian et al., 2019). (+)-Borneol reduces the secretion of pro-inflammatory cytokines in the hippocampus of rats with SE. However, the effect of (+)-borneol on the secretion of pro-inflammatory and anti-inflammatory cytokines in microglia has not been investigated *in vitro*. Our results suggest that (+)-borneol inhibits microglia overactivation both *in vivo* and *in vitro*. *In vitro*, (+)-borneol

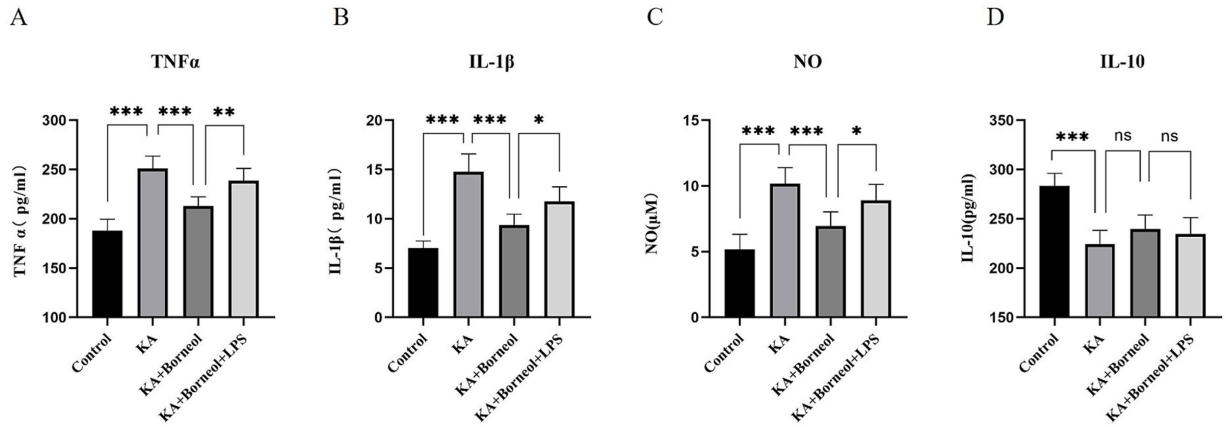


FIGURE 7
Effect of (+)-borneol on KA-induced inflammatory cytokine secretion in BV2 microglia. Statistical results of TNF-α **(A)**, IL-1β **(B)**, NO **(C)**, and IL-10 **(D)** of BV2 microglia supernatant in each group. ***$p<0.001$; **$p < 0.01$; *$p < 0.05$; ns $p > 0.05$; $n = 6$.

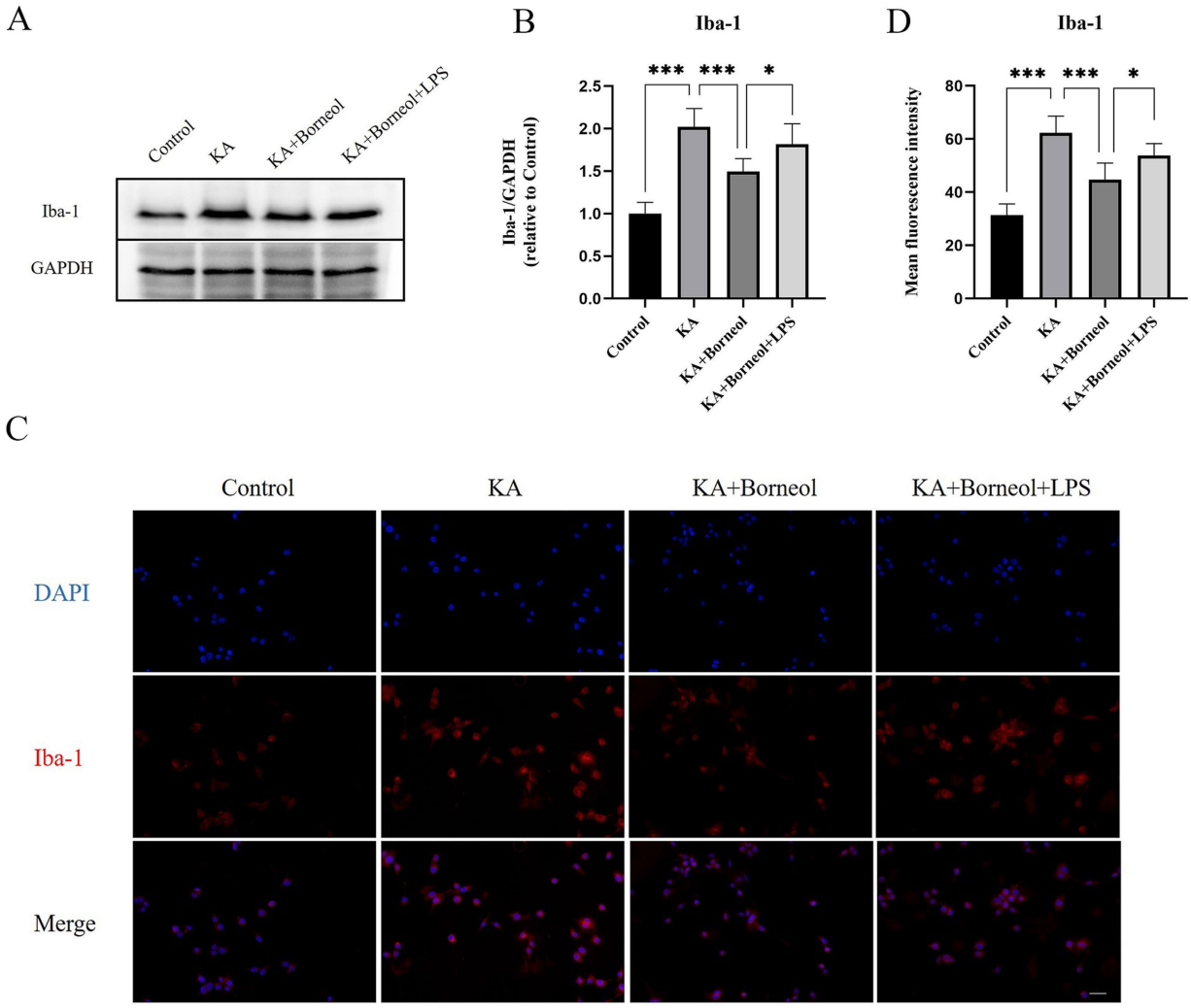


FIGURE 8
Effect of (+)-borneol on Iba-1 in KA-induced BV2 microglia. **(A)** Western-Blot representative diagrams of Iba-1 in each group of BV2 microglia. **(B)** Analysis and statistics of Western-Blot results. **(C)** Immunofluorescence representative diagrams of Iba-1 in each group of BV2 microglia. **(D)** Analysis and statistics of immunofluorescence results. Bar = 100 μm. ***$p<0.001$; **$p < 0.01$; *$p < 0.05$; ns $p > 0.05$; $n = 6$.

treatment reduced KA-induced secretion of pro-inflammatory cytokines but had no significant effect on anti-inflammatory cytokines in BV2 microglia. TLR4 agonist treatment could partially reverse the anti-inflammatory effects of (+)-borneol. In addition, (+)-borneol has been reported to ameliorate epileptic seizures by inhibiting the excitability of glutamatergic synaptic transmission. These results suggest that (+)-borneol, as an anti-inflammatory agent, may have a therapeutic effect on epilepsy modification.

In recent years, microglia have been divided into two phenotypes according to their functions: the pro-inflammatory neurotoxic M1 and the anti-inflammatory neuroprotective M2. These two phenotypes are in dynamic changes and can be transformed into each other (Kwon and Koh, 2020). The regulation of M1 and M2 phenotype polarization has become an effective target for a variety of drugs to inhibit neuroinflammation and a potential direction for the treatment of nervous system diseases (Zhang et al., 2019; Jiang et al., 2021; Long et al., 2024). Previous studies have reported that targeting microglial phenotype polarization in epilepsy can reduce neuronal damage (Peng et al., 2019), and activation of M1 microglia can promote SE-induced neuroinflammation (Liang et al., 2023). The results of our study showed that (+)-borneol inhibited KA-induced M1 but not M2 polarization of BV2 microglia, suggesting that (+)-borneol inhibits the proinflammatory phenotype of microglia polarization.

TLR4 is a transmembrane protein that recognizes exogenous ligand LPS and endogenous ligands produced by stress and cell injury (Paudel et al., 2020). After binding to the ligand, it can activate the downstream NF-κB signaling pathway, secrete and release inflammatory factors, and activate the inflammatory cascade (Shi et al., 2018). TLR4 inhibitors can effectively improve the symptoms of epilepsy in mice (Dong et al., 2022).

NF-κB is a widely expressed transcription factor that is associated with biological processes of neuroinflammation and apoptosis (Dresselhaus and Meffert, 2019; Shih et al., 2015). P65

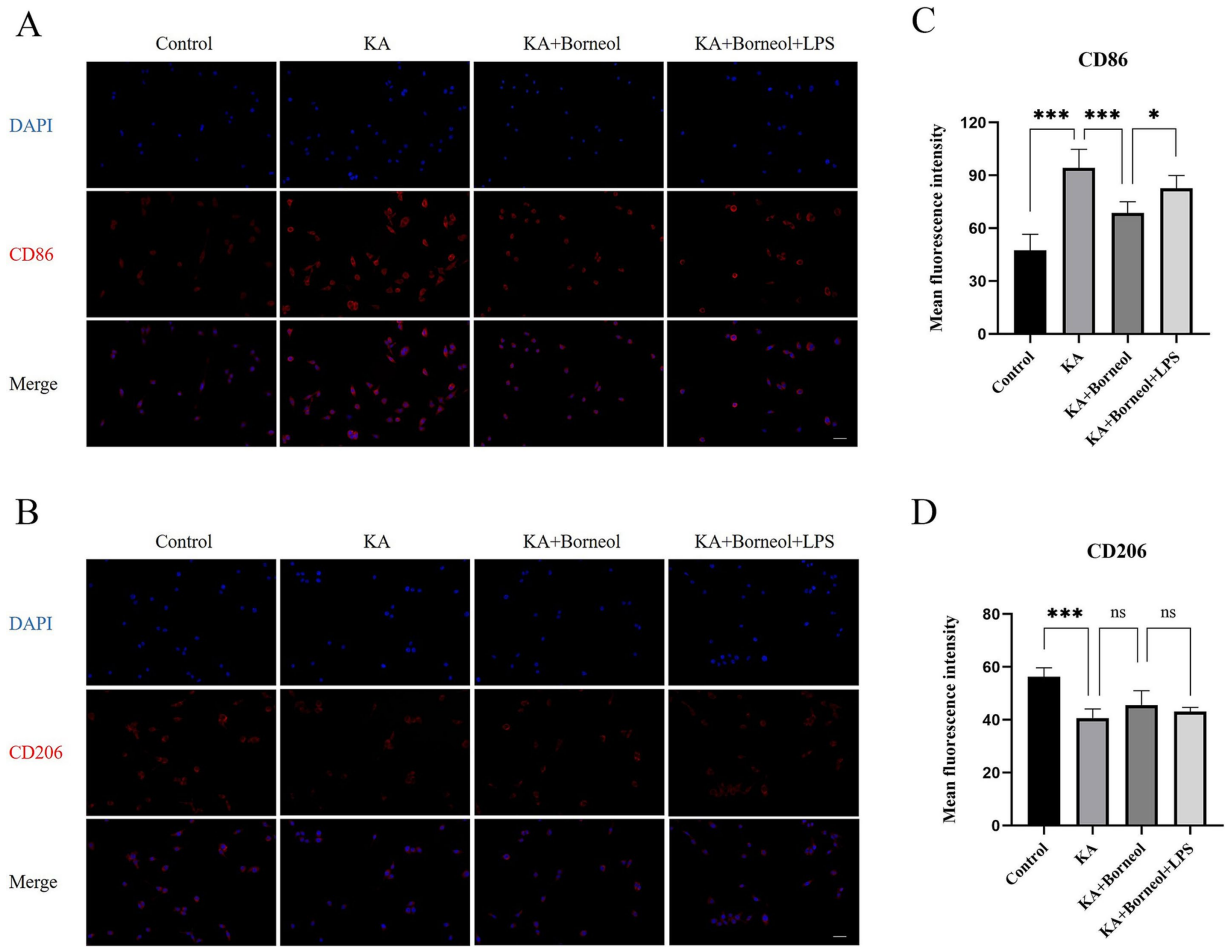


FIGURE 9
Effect of (+)-borneol on CD86 and CD206 in KA-induced BV2 microglia. **(A,B)** Immunofluorescence representative diagrams of CD86 **(A)** and CD206 **(B)** in each group of BV2 microglia. **(C,D)** Analysis and statistics of immunofluorescence results. Bar = 100 μm; ***$p<0.001$; **$p < 0.01$; *$p < 0.05$; ns $p > 0.05$; $n = 6$.

(Rel A) is a member of the NF-κB family. Under physiological conditions, p65 is mainly distributed in the cytoplasm in the form of p50-p65 heterodimers, which bind to IκB inhibitory proteins. Under pathological stimulation, IκB undergoes phosphorylation and degradation, releasing p65 into the nucleus. The phosphorylation of P65 can promote the binding of p65 to the nucleus, initiate the transcription of inflammation-related genes, and promote the occurrence of neuroinflammation (Aloor et al., 2015).

After binding to ligands, TLR4 distributed on the membrane of microglia can activate the downstream NF-κB, promote its nuclear translocation, promote the polarization of microglia to M1 phenotype, and secrete a large number of proinflammatory cytokines (Li et al., 2022; Younger et al., 2019). Previous studies have shown that (+)-borneol inhibits the activation of the NF-κB signaling pathway in mice with sepsis and in microglia and ischemic stroke models (Wang et al., 2019; Chang et al., 2017), but the effect of (+)-borneol on its upstream TLR4 has not been investigated. The present study found that (+)-borneol reduced TLR4 expression and p-p65/p65 ratio in the hippocampus of SE mice and KA-induced BV2 microglia. The effect of (+)-borneol was partially reversed by administration of TLR4 agonist LPS, suggesting that the effects of (+)-borneol on microglia neuroinflammation and phenotype polarization may be mediated by targeting TLR4 and inhibiting TLR4-NFκB signaling pathway.

The results of this study suggest that (+)-borneol can inhibit neuroinflammation in epilepsy and may be used as a potential anti-epileptogenesis drug for epilepsy modifying therapy, delaying the progression of epilepsy and improving the long-term prognosis of epilepsy.

However, the present study only investigated the pathophysiological changes of (+)-borneol in SE mice within 7 days and the possible mechanisms, but not the role of (+)-borneol in chronic epilepsy. Further studies are needed to investigate the electrophysiological effects of (+)-borneol on SE by monitoring the frequency and duration of chronic and recurrent seizures with electroencephalogram. It should be mentioned that as the data of this study represents the results in male mice only, conclusions are limited to males.

Overall, data from our study suggests that (+)-borneol alleviates neuroinflammation and inhibits microglia M1 phenotype polarization during epilepsy both *in vitro* and *in vivo*.

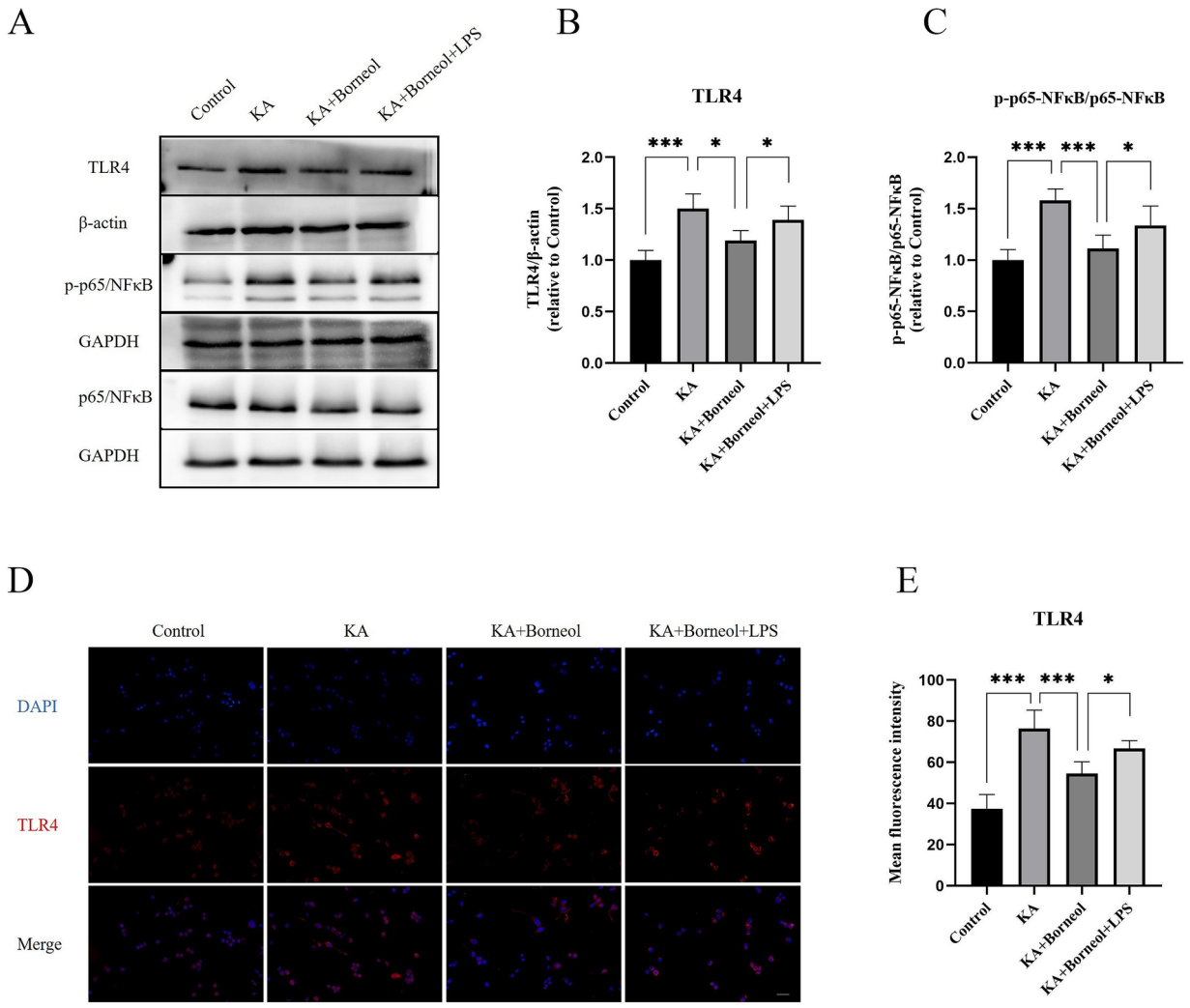


FIGURE 10
Effect of (+)-borneol on the TLR4, p65 and p-p65 expression KA-induced BV2 microglia. **(A)** Western-Blot representative diagrams of TLR4, p65 and p-p65 in each group of mice. **(B)** Analysis and statistics of TLR4 Western-Blot results. **(C)** Analysis and statistics of p-p65/p65 Western-Blot results. **(D)** Immunofluorescence representative diagrams of TLR4. **(E)** Analysis and statistics of immunofluorescence results. Bar=100 μm. ***$p<0.001$, **$p<0.01$, *$p<0.05$, n =6.

Data availability statement

The raw data supporting the conclusions of this article will be made available by the authors, without undue reservation.

Ethics statement

The animal study was approved by the Ethics Committee of the Second Hospital of Shanxi Medical University. The ethics record number was DW2023018. The study was conducted in accordance with the local legislation and institutional requirements.

Author contributions

SL: Conceptualization, Formal analysis, Investigation, Methodology, Visualization, Writing – original draft, Writing – review & editing. AA: Visualization, Writing – review & editing. YY: Conceptualization, Investigation, Methodology, Writing – review & editing. FG: Supervision, Visualization, Writing – review & editing. RM: Project administration, Writing – review & editing. GX: Conceptualization, Funding acquisition, Methodology, Project administration, Resources, Supervision, Writing – review & editing. ZW: Conceptualization, Methodology, Project administration, Resources, Supervision, Writing – review & editing.

Funding

The author(s) declare that financial support was received for the research, authorship, and/or publication of this article. This work was supported by the Scientific research project of Shanxi Traditional Chinese Medicine Administration (Grant: 2023ZYYC2035) and Research Project Supported by Shanxi Scholarship Council of China (Grant: 2024–150).

Conflict of interest

The authors declare that the research was conducted in the absence of any commercial or financial relationships that could be construed as a potential conflict of interest.

Publisher's note

All claims expressed in this article are solely those of the authors and do not necessarily represent those of their affiliated organizations, or those of the publisher, the editors and the reviewers. Any product that may be evaluated in this article, or claim that may be made by its manufacturer, is not guaranteed or endorsed by the publisher.

Supplementary material

The Supplementary material for this article can be found online at: https://www.frontiersin.org/articles/10.3389/fnins.2024.1497102/full#supplementary-material

References

Aloor, R., Zhang, C., Bandyopadhyay, M., and Dasgupta, S. (2015). Impact of nuclear factor-κB on restoration of neuron growth and differentiation in hippocampus of degenerative brain. *J. Neurosci. Res.* 93, 1471–1475. doi: 10.1002/jnr.23547

Ashkenazi, A., Fairbrother, W. J., Leverson, J. D., and Souers, A. J. (2017). From basic apoptosis discoveries to advanced selective BCL-2 family inhibitors. *Nat. Rev. Drug Discov.* 16, 273–284. doi: 10.1038/nrd.2016.253

Beghi, E. (2020). The epidemiology of epilepsy. *Neuroepidemiology* 54, 185–191. doi: 10.1159/000503831

Benson, M. J., Manzanero, S., and Borges, K. (2015). Complex alterations in microglial M1/M2 markers during the development of epilepsy in two mouse models. *Epilepsia* 56, 895–905. doi: 10.1111/epi.12960

Borst, K., Dumas, A. A., and Prinz, M. (2021). Microglia: immune and non-immune functions. *Immunity* 54, 2194–2208. doi: 10.1016/j.immuni.2021.09.014

Casillas-Espinosa, P. M., Anderson, A., Harutyunyan, A., Li, C., Lee, J., Braine, E. L., et al. (2023). Disease-modifying effects of sodium selenate in a model of drug-resistant, temporal lobe epilepsy. *eLife* 12:e78877. doi: 10.7554/eLife.78877

Chang, L., Yin, C. Y., Wu, H. Y., Tian, B. B., Zhu, Y., Luo, C. X., et al. (2017). (+)-Borneol is neuroprotective against permanent cerebral ischemia in rats by suppressing production of proinflammatory cytokines. *J. Biomed. Res.* 31, 306–314. doi: 10.7555/JBR.31.20160138

Chen, H., Xu, X., Tang, Q., Ni, L., Cao, S., Hao, Y., et al. (2022). (+)-Borneol inhibits the generation of reactive oxygen species and neutrophil extracellular traps induced by phorbol-12-myristate-13-acetate. *Front. Pharmacol.* 13:1023450. doi: 10.3389/fphar.2022.1023450

Chepurnov, S. A., Suleĭmanova, E. M., Guliaev, M. V., Abbasova, K. R., Pirogov, I. A., and Chepurnova, N. E. (2012). Neuroprotection in epilepsy. *Usp. Fiziol. Nauk* 43, 55–71

Chiò, A., Mazzini, L., and Mora, G. (2020). Disease-modifying therapies in amyotrophic lateral sclerosis. *Neuropharmacology* 167:107986. doi: 10.1016/j.neuropharm.2020.107986

Clossen, B. L., and Reddy, D. S. (2017). Novel therapeutic approaches for disease-modification of epileptogenesis for curing epilepsy. *Biochim. Biophys. Acta Mol. basis Dis.* 1863, 1519–1538. doi: 10.1016/j.bbadis.2017.02.003

Dong, J., Liao, Y., and Wu, B. (2022). TAK-242 ameliorates epileptic symptoms in mice by inhibiting the TLR4/NF-κB signaling pathway. *Ann. Transl. Med.* 10:795. doi: 10.21037/atm-22-2707

Dresselhaus, E. C., and Meffert, M. K. (2019). Cellular specificity of NF-κB function in the nervous system. *Front. Immunol.* 10:1043. doi: 10.3389/fimmu.2019.01043

Galanopoulou, A. S., Löscher, W., Lubbers, L., O'Brien, T. J., Staley, K., Vezzani, A., et al. (2021). Antiepileptogenesis and disease modification: Progress, challenges, and the path forward-report of the preclinical working group of the 2018 NINDS-sponsored antiepileptogenesis and disease modification workshop. *Epilepsia Open* 6, 276–296. doi: 10.1002/epi4.12490

Gao, F., Chen, R., Li, S., Li, A., Bai, B., Mi, R., et al. (2023). (+)-Borneol exerts neuroprotective effects via suppressing the NF-κB pathway in the pilocarpine-induced epileptogenesis rat model. *Brain Res.* 1810:148382. doi: 10.1016/j.brainres.2023.148382

Gong, L., Zhu, T., Chen, C., Xia, N., Yao, Y., Ding, J., et al. (2022). Miconazole exerts disease-modifying effects during epilepsy by suppressing neuroinflammation via NF-κB pathway and iNOS production. *Neurobiol. Dis.* 172:105823. doi: 10.1016/j.nbd.2022.105823

Henning, L., Antony, H., Breuer, A., Müller, J., Seifert, G., Audinat, E., et al. (2023). Reactive microglia are the major source of tumor necrosis factor alpha and contribute to astrocyte dysfunction and acute seizures in experimental temporal lobe epilepsy. *Glia* 71, 168–186. doi: 10.1002/glia.24265

Henshall, D. C. (2007). Apoptosis signalling pathways in seizure-induced neuronal death and epilepsy. *Biochem. Soc. Trans.* 35, 421–423. doi: 10.1042/BST0350421

Henshall, D. C., and Simon, R. P. (2005). Epilepsy and apoptosis pathways. *J. Cereb. Blood Flow Metab.* 25, 1557–1572. doi: 10.1038/sj.jcbfm.9600149

Hiragi, T., Ikegaya, Y., and Koyama, R. (2018). Microglia after seizures and in epilepsy. *Cells* 7:26. doi: 10.3390/cells7040026

Hua, Y., Zhou, L., Yang, W., An, W., Kou, X., Ren, J., et al. (2021). Y-2 reduces oxidative stress and inflammation and improves neurological function of collagenase-induced intracerebral hemorrhage rats. *Eur. J. Pharmacol.* 910:174507. doi: 10.1016/j.ejphar.2021.174507

Issa, N. P., Nunn, K. C., Wu, S., Haider, H. A., and Tao, J. X. (2023). Putative roles for homeostatic plasticity in epileptogenesis. *Epilepsia* 64, 539–552. doi: 10.1111/epi.17500

Jean, G., Carton, J., Haq, K., and Musto, A. E. (2023). The role of dendritic spines in epileptogenesis. *Front. Cell. Neurosci.* 17:1173694. doi: 10.3389/fncel.2023.1173694

Jiang, Q., Wei, D., He, X., Gan, C., Long, X., and Zhang, H. (2021). Phillyrin prevents Neuroinflammation-induced blood-brain barrier damage following traumatic brain injury via altering microglial polarization. *Front. Pharmacol.* 12:719823. doi: 10.3389/fphar.2021.719823

Kwon, H. S., and Koh, S. H. (2020). Neuroinflammation in neurodegenerative disorders: the roles of microglia and astrocytes. *Transl. Neurodegener* 9:42. doi: 10.1186/s40035-020-00221-2

Lévesque, M., Biagini, G., de Curtis, M., Gnatkovsky, V., Pitsch, J., Wang, S., et al. (2021). The pilocarpine model of mesial temporal lobe epilepsy: over one decade later, with more rodent species and new investigative approaches. *Neurosci. Biobehav. Rev.* 130, 274–291. doi: 10.1016/j.neubiorev.2021.08.020

Li, W., Wu, J., Zeng, Y., and Zheng, W. (2023). Neuroinflammation in epileptogenesis: from pathophysiology to therapeutic strategies. *Front. Immunol.* 14:1269241. doi: 10.3389/fimmu.2023.1269241

Li, R., Zhou, Y., Zhang, S., Li, J., Zheng, Y., and Fan, X. (2022). The natural (poly) phenols as modulators of microglia polarization via TLR4/NF-κB pathway exert anti-inflammatory activity in ischemic stroke. *Eur. J. Pharmacol.* 914:174660. doi: 10.1016/j.ejphar.2021.174660

Liang, X. S., Qian, T. L., Xiong, Y. F., Liang, X. T., Ding, Y. W., Zhu, X. Y., et al. (2023). IRAK-M ablation promotes status epilepticus-induced Neuroinflammation via activating M1 microglia and impairing excitatory synaptic function. *Mol. Neurobiol.* 60, 5199–5213. doi: 10.1007/s12035-023-03407-7

Liu, Z., Liao, Q., Wen, H., and Zhang, Y. (2021b). Disease modifying therapies in relapsing-remitting multiple sclerosis: A systematic review and network meta-analysis. *Autoimmun. Rev.* 20:102826. doi: 10.1016/j.autrev.2021.102826

Liu, S., Long, Y., Yu, S., Zhang, D., Yang, Q., Ci, Z., et al. (2021). Borneol in cardio-cerebrovascular diseases: pharmacological actions, mechanisms, and therapeutics. *Pharmacol. Res.* 169:105627. doi: 10.1016/j.phrs.2021.105627

Liu, X., Ma, J., Ding, G., Gong, Q., Wang, Y., Yu, H., et al. (2021a). Microglia Polarization from M1 toward M2 phenotype is promoted by Astragalus polysaccharides mediated through inhibition of miR-155 in experimental autoimmune encephalomyelitis. *Oxidative Med. Cell. Longev.* 2021:5753452. doi: 10.1155/2021/5753452

Liu, R., Zhang, L., Lan, X., Li, L., Zhang, T. T., Sun, J. H., et al. (2011). Protection by borneol on cortical neurons against oxygen-glucose deprivation/reperfusion: involvement of anti-oxidation and anti-inflammation through nuclear transcription factor κappaB signaling pathway. *Neuroscience* 176, 408–419. doi: 10.1016/j.neuroscience.2010.11.029

Long, Y., Li, X. Q., Deng, J., Ye, Q. B., Li, D., Ma, Y., et al. (2024). Modulating the polarization phenotype of microglia - A valuable strategy for central nervous system diseases. *Ageing Res. Rev.* 93:102160. doi: 10.1016/j.arr.2023.102160

Ma, R., Lu, D., Xie, Q., Yuan, J., Ren, M., Li, Y., et al. (2023). L-Borneol and d-Borneol promote transdifferentiation of astrocytes into neurons in rats by regulating Wnt/notch

pathway to exert neuroprotective effect during recovery from cerebral ischaemia. *Phytomedicine* 109:154583. doi: 10.1016/j.phymed.2022.154583

Madireddy, S., and Madireddy, S. (2023). Therapeutic strategies to ameliorate neuronal damage in epilepsy by regulating oxidative stress, mitochondrial dysfunction, and Neuroinflammation. *Brain Sci.* 13:784. doi: 10.3390/brainsci13050784

Manford, M. (2017). Recent advances in epilepsy. *J. Neurol.* 264, 1811–1824. doi: 10.1007/s00415-017-8394-2

Mukhtar, I. (2020). Inflammatory and immune mechanisms underlying epileptogenesis and epilepsy: from pathogenesis to treatment target. *Seizure* 82, 65–79. doi: 10.1016/j.seizure.2020.09.015

Panina, Y. S., Timechko, E. E., Usoltseva, A. A., Yakovleva, K. D., Kantimirova, E. A., and Dmitrenko, D. V. (2023). Biomarkers of drug resistance in temporal lobe epilepsy in adults. *Meta* 13:83. doi: 10.3390/metabo13010083

Patel, D. C., Tewari, B. P., Chaunsali, L., and Sontheimer, H. (2019). Neuron-glia interactions in the pathophysiology of epilepsy. *Nat. Rev. Neurosci.* 20, 282–297. doi: 10.1038/s41583-019-0126-4

Paudel, Y. N., Angelopoulou, E., Akyuz, E., Piperi, C., Othman, I., and Shaikh, M. F. (2020). Role of innate immune receptor TLR4 and its endogenous ligands in epileptogenesis. *Pharmacol. Res.* 160:105172. doi: 10.1016/j.phrs.2020.105172

Peng, J., Wang, K., Xiang, W., Li, Y., Hao, Y., and Guan, Y. (2019). Rosiglitazone polarizes microglia and protects against pilocarpine-induced status epilepticus. *CNS Neurosci. Ther.* 25, 1363–1372. doi: 10.1111/cns.13265

Pitkänen, A., Kharatishvili, I., Karhunen, H., Lukasiuk, K., Immonen, R., Nairismägi, J., et al. (2007). Epileptogenesis in experimental models. *Epilepsia* 48, 13–20. doi: 10.1111/j.1528-1167.2007.01063.x

Pitkänen, A., Lukasiuk, K., Dudek, F. E., and Staley, K. J. (2015). Epileptogenesis. *Cold Spring Harb. Perspect. Med.* 5:a022822. doi: 10.1101/cshperspect.a022822

Pracucci, E., Pillai, V., Lamers, D., Parra, R., and Landi, S. (2021). Neuroinflammation: A signature or a cause of epilepsy? *Int. J. Mol. Sci.* 22:6981. doi: 10.3390/ijms22136981

Racine, R. J. (1972). Modification of seizure activity by electrical stimulation. II. Motor seizure. *Electroencephalogr. Clin. Neurophysiol.* 32, 281–294. doi: 10.1016/0013-4694(72)90177-0

Ren, J., Zhang, X., Zhou, L., Cao, W., Zhang, L., Chen, X., et al. (2024). Comprehensive evaluation of Dragon's blood in combination with borneol in ameliorating ischemic/reperfusion brain injury using RNA sequencing, metabolomics, and 16S rRNA sequencing. *Front. Pharmacol.* 15:1372449. doi: 10.3389/fphar.2024.1372449

Sano, F., Shigetomi, E., Shinozaki, Y., Tsuzukiyama, H., Saito, K., Mikoshiba, K., et al. (2021). Reactive astrocyte-driven epileptogenesis is induced by microglia initially activated following status epilepticus. *JCI Insight* 6:e135391. doi: 10.1172/jci.insight.135391

Shen, W., Pristov, J. B., Nobili, P., and Nikolić, L. (2023). Can glial cells save neurons in epilepsy? *Neural Regen. Res.* 18, 1417–1422. doi: 10.4103/1673-5374.360281

Shi, Y., Zhang, L., Teng, J., and Miao, W. (2018). HMGB1 mediates microglia activation via the TLR4/NF-κB pathway in coriaria lactone induced epilepsy. *Mol. Med. Rep.* 17, 5125–5131. doi: 10.3892/mmr.2018.8485

Shih, R. H., Wang, C. Y., and Yang, C. M. (2015). NF-kappaB signaling pathways in neurological inflammation: A Mini review. *Front. Mol. Neurosci.* 8:77. doi: 10.3389/fnmol.2015.00077

Singh, R., Letai, A., and Sarosiek, K. (2019). Regulation of apoptosis in health and disease: the balancing act of BCL-2 family proteins. *Nat. Rev. Mol. Cell Biol.* 20, 175–193. doi: 10.1038/s41580-018-0089-8

Soltani Khaboushan, A., Yazdanpanah, N., and Rezaei, N. (2022). Neuroinflammation and Proinflammatory cytokines in Epileptogenesis. *Mol. Neurobiol.* 59, 1724–1743. doi: 10.1007/s12035-022-02725-6

Tabrizi, S. J., Estevez-Fraga, C., van Roon-Mom, W. M. C., Flower, M. D., Scahill, R. I., Wild, E. J., et al. (2022). Potential disease-modifying therapies for Huntington's disease: lessons learned and future opportunities. *Lancet Neurol.* 21, 645–658. doi: 10.1016/S1474-4422(22)00121-1

Thijs, R. D., Surges, R., O'Brien, T. J., and Sander, J. W. (2019). Epilepsy in adults. *Lancet* 393, 689–701. doi: 10.1016/S0140-6736(18)32596-0

Thompson, K. (2023). Status epilepticus and early development: neuronal injury, neurodegeneration, and their consequences. *Epilepsia Open* 8, S110–s116. doi: 10.1002/epi4.12601

Tian, M. J., Wang, R. F., Hölscher, C., Mi, R. L., Yuan, Z. Y., Li, D. F., et al. (2019). The novel GLP-1/GIP dual receptor agonist DA3-CH is neuroprotective in the pilocarpine-induced epileptogenesis rat model. *Epilepsy Res.* 154, 97–106. doi: 10.1016/j.eplepsyres.2019.05.008

Trinka, E., Kwan, P., Lee, B., and Dash, A. (2019). Epilepsy in Asia: disease burden, management barriers, and challenges. *Epilepsia* 60, 7–21. doi: 10.1111/epi.14458

Vega-García, A., Guevara-Guzmán, R., García-Gómez, O., Feria-Romero, I., Fernández-Valverde, F., Alonso-Vanegas, M., et al. (2022). Aberrant connection formation and glia involvement in the progression of Pharmacoresistant mesial temporal lobe epilepsy. *Curr. Pharm. Des.* 28, 2283–2297. doi: 10.2174/1381612828666220616162739

Wang, L., Liang, Q., Lin, A., Wu, Y., Min, H., Song, S., et al. (2019). Borneol alleviates brain injury in sepsis mice by blocking neuronal effect of endotoxin. *Life Sci.* 232:116647. doi: 10.1016/j.lfs.2019.116647

Wang, N., Mi, X., Gao, B., Gu, J., Wang, W., Zhang, Y., et al. (2015). Minocycline inhibits brain inflammation and attenuates spontaneous recurrent seizures following pilocarpine-induced status epilepticus. *Neuroscience* 287, 144–156. doi: 10.1016/j.neuroscience.2014.12.021

Xie, Q., Li, J., Dong, T., Yuan, J., Lu, D., Ma, R., et al. (2022). Neuroprotective effects of synthetic borneol and natural borneol based on the neurovascular unit against cerebral ischaemic injury. *J. Pharm. Pharmacol.* 74, 236–249. doi: 10.1093/jpp/rgab167

Yang, X., Xu, S., Qian, Y., and Xiao, Q. (2017). Resveratrol regulates microglia M1/M2 polarization via PGC-1α in conditions of neuroinflammatory injury. *Brain Behav. Immun.* 64, 162–172. doi: 10.1016/j.bbi.2017.03.003

Younger, D., Murugan, M., Rama Rao, K. V., Wu, L. J., and Chandra, N. (2019). Microglia receptors in animal models of traumatic brain injury. *Mol. Neurobiol.* 56, 5202–5228. doi: 10.1007/s12035-018-1428-7

Zhang, J., Zheng, Y., Luo, Y., Du, Y., Zhang, X., and Fu, J. (2019). Curcumin inhibits LPS-induced neuroinflammation by promoting microglial M2 polarization via TREM2/TLR4/ NF-κB pathways in BV2 cells. *Mol. Immunol.* 116, 29–37. doi: 10.1016/j.molimm.2019.09.020

Zhang, X. M., and Zhu, J. (2011). Kainic acid-induced neurotoxicity: targeting glial responses and glia-derived cytokines. *Curr. Neuropharmacol.* 9, 388–398. doi: 10.2174/157015911795596540

Zhao, X., Liao, Y., Morgan, S., Mathur, R., Feustel, P., Mazurkiewicz, J., et al. (2018). Noninflammatory changes of microglia are sufficient to cause epilepsy. *Cell Rep.* 22, 2080–2093. doi: 10.1016/j.celrep.2018.02.004

Zhong, Y., Qi, Y., Jiang, Z., Hu, Y., Zhang, X., Wu, C., et al. (2023). Analysis of medication rules and application characteristics of Chinese patent medicine containing borneol based on data mining. *Heliyon* 9:e21232. doi: 10.1016/j.heliyon.2023.e21232

Zou, L., Zhang, Y., Li, W., Zhang, J., Wang, D., Fu, J., et al. (2017). Comparison of chemical profiles, anti-inflammatory activity, and UPLC-Q-TOF/MS-based metabolomics in Endotoxic fever rats between synthetic Borneol and natural Borneol. *Molecules* 22:1446. doi: 10.3390/molecules22091446

frontiers | Frontiers in Pharmacology

TYPE Original Research
PUBLISHED 06 January 2025
DOI 10.3389/fphar.2024.1508726

Check for updates

OPEN ACCESS

EDITED BY
Pukar Khanal,
Emory University, United States

REVIEWED BY
Smita Kumari,
The Ohio State University, United States
Pramod Nagaraju,
Case Western Reserve University, United States

*CORRESPONDENCE
Yongchang Diwu,
diwu66@sntcm.edu.cn

†These authors share first authorship

RECEIVED 09 October 2024
ACCEPTED 05 December 2024
PUBLISHED 06 January 2025

CITATION
Yang C, Zhao E, Zhang H, Duan L, Han X, Ding H, Cheng Y, Wang D, Lei X and Diwu Y (2025) Xixin Decoction's novel mechanism for alleviating Alzheimer's disease cognitive dysfunction by modulating amyloid-β transport across the blood–brain barrier to reduce neuroinflammation.
Front. Pharmacol. 15:1508726.
doi: 10.3389/fphar.2024.1508726

COPYRIGHT
© 2025 Yang, Zhao, Zhang, Duan, Han, Ding, Cheng, Wang, Lei and Diwu. This is an open-access article distributed under the terms of the Creative Commons Attribution License (CC BY). The use, distribution or reproduction in other forums is permitted, provided the original author(s) and the copyright owner(s) are credited and that the original publication in this journal is cited, in accordance with accepted academic practice. No use, distribution or reproduction is permitted which does not comply with these terms.

Xixin Decoction's novel mechanism for alleviating Alzheimer's disease cognitive dysfunction by modulating amyloid-β transport across the blood–brain barrier to reduce neuroinflammation

Chaokai Yang[1†], Enlong Zhao[1], Hu Zhang[1], Liqi Duan[1], Xinyue Han[1], Hongli Ding[1], Yan Cheng[1], Dengkun Wang[1,2,3], Xiaojing Lei[2,3,4] and Yongchang Diwu[2,3,4*†]

[1]The First Clinical Medical College of Shaanxi University of Chinese Medicine, Xianyang, China, [2]Key Research Laboratory for Prevention and Treatment of Cerebrospinal diseases, Shaanxi Provincial Administration of Traditional Chinese Medicine, Xianyang, China, [3]Discipline Innovation Team for Neurodegenerative Diseases of Shaanxi University of Chinese Medicine, Xianyang, China, [4]College of Basic Medicine, Shaanxi University of Chinese Medicine, Xianyang, China

Purpose: Xixin Decoction (XXD) is a classical formula that has been used to effectively treat dementia for over 300 years. Modern clinical studies have demonstrated its significant therapeutic effects in treating Alzheimer's disease (AD) without notable adverse reactions. Nevertheless, the specific mechanisms underlying its efficacy remain to be elucidated. This investigation sought to elucidate XXD's impact on various aspects of AD pathology, including blood-brain barrier (BBB) impairment, neuroinflammatory processes, and amyloid-β (Aβ) deposition, as well as the molecular pathways involved in these effects.

Methods: *In vitro* experiments were conducted using hCMEC/D3 and HBVP cell coculture to establish an *in vitro* blood-brain barrier (BBB) model. BBB damage was induced in this model by 24-h exposure to 1 μg/mL lipopolysaccharide (LPS). After 24, 48, and 72 h of treatment with 10% XXD-medicated serum, the effects of XXD were assessed through Western blotting, RT-PCR, and immunofluorescence techniques. *In vivo*, SAMP8 mice were administered various doses of XXD via gavage for 8 weeks, including high-dose XXD group (H-XXD) at 5.07 g kg^{-1}·d^{-1}, medium-dose XXD group (M-XXD) at 2.535 g kg^{-1}·d^{-1}, and low-dose XXD group (L-XXD) at 1.2675 g kg^{-1}·d^{-1}. Cognitive function was subsequently evaluated using the Morris water maze test. BBB integrity was evaluated using Evans blue staining, and protein expression levels were analyzed via ELISA, Western blotting, and immunofluorescence.

Results: *In vitro* experiments revealed that XXD-containing serum, when cultured for 24, 48, and 72 h, could upregulate the expression of P-gp mRNA and protein, downregulate CB1 protein expression, and upregulate CB2 and Mfsd2a protein expression. *In vivo* studies demonstrated that XXD improved spatial learning and memory abilities in SAMP8 mice, reduced the amount of Evans blue extravasation in brain tissues, modulated the BBB-associated P-gp/ECS axis, RAGE/

LRP1 receptor system, as well as MRP2 and Mfsd2a proteins, and decreased the accumulation of Aβ in the brains of SAMP8 mice. Additionally, XXD upregulated the expression of TREM2, downregulated IBA1, TLR1, TLR2, and CMPK2 expression, and reduced the levels of pro-inflammatory factors NLRP3, NF-κB p65, COX-2, TNF-α, and IL-1β in the hippocampal tissues.

Conclusion: XXD may exert its effects by regulating the P-gp/ECS axis, the RAGE/LRP1 receptor system, and the expression of MRP2 and Mfsd2a proteins, thereby modulating the transport function of the BBB to expedite the clearance of Aβ, reduce cerebral Aβ accumulation, and consequently inhibit the activation of microglia induced by Aβ aggregation. This process may suppress the activation of the CMPK2/NLRP3 and TLRs/NF-κB pathways, diminish the production of inflammatory cytokines and chemokines, alleviate neuroinflammation associated with microglia in the brain of AD, and ultimately improve AD pathology.

KEYWORDS

Alzheimer's disease, Xixin Decoction, blood-brain barrier, amyloid-beta, neuroinflammation

1 Introduction

Alzheimer's disease (AD) is the primary type of dementia among the elderly and ranks as the fifth most common cause of death globally, impacting an estimated 50 million individuals around the world. Owing to the acceleration of population aging, the prevalence of AD is projected to double by the year 2050 (Dumurgier and Sabia, 2020). The blood-brain barrier (BBB) is a complex vascular structure composed of multiple cell types. It isolates the central nervous system (CNS) from the peripheral bloodstream, tightly controlling the movement of molecules and ions to protect the brain from toxins and pathogens and maintain an environment conducive to normal neuronal function (Peng et al., 2021). Currently, the amyloid-β (Aβ) plaque deposition and neurofibrillary tangles resulting from tau protein hyperphosphorylation are considered typical pathological features of AD. The BBB is integral to the clearance of cerebral metabolic waste and is crucial in facilitating Aβ transport across the brain. The typical movement of Aβ across the blood-brain barrier is facilitated by numerous transporters, including LRP1, RAGE, and P-gp (Van Gool et al., 2019; Kim and Priefer, 2020; Vulin et al., 2023; Xing et al., 2023). As Alzheimer's disease progresses, these transporters show dysregulation in expression and function, resulting in aberrant Aβ transport and deposition (Hanafy et al., 2023; Wang et al., 2021). Neuroinflammation is an inflammatory response in the central nervous system (CNS) triggered by pathological damage in either the periphery or the CNS, leading to the production of proinflammatory cytokines such as interleukin-1beta (IL-1β), IL-6, IL-8, and tumor necrosis factor (TNF), as well as chemokines, complement proteins, and various small molecule messengers, including prostaglandins, nitric oxide (NO), and reactive oxygen species (ROS) (Leng and Edison, 2021). Microglia, the central nervous system's equivalent of macrophages, are crucial for maintaining CNS homeostasis and are widely regarded as the primary drivers of neuroinflammation in AD (Eshraghi et al., 2021; Chen et al., 2021). In the early stages of AD, activated by Aβ plaque accumulation, microglia produce inflammatory mediators such as cytokines and chemokines, facilitating Aβ clearance and further microglial recruitment (Wang et al., 2023). However, as the disease advances, excessive Aβ accumulation can result in overactivation of microglia, leading to the production of excessive proinflammatory cytokines such as IL-1β, IL-6, and TNF-α. This leads to chronic and sustained neuroinflammation, causing increased neuronal cell death (Huang et al., 2022). Consequently, a vicious cycle is established among Aβ accumulation, activated microglia, and proinflammatory factors (Wei et al., 2022). Simultaneously, neuroinflammation driven by microglial activation further disrupts BBB integrity and transport function (Hussain et al., 2021; Lai et al., 2021; Chaves et al., 2017; Barabási et al., 2023) (Figure 1). Thus, regulating and repairing BBB integrity and transport dysfunction, reducing pathological brain Aβ accumulation, inhibiting microglial activation, and alleviating neuroinflammation may be important approaches to improving AD development.

Presently, five drugs approved by the US Food and Drug Administration (FDA) for treating Alzheimer's disease include memantine, aducanumab, and three acetylcholinesterase inhibitors (Argueta et al., 2022). These medications only temporarily treat Alzheimer's symptoms, but fail to control or reverse its underlying pathology (Long et al., 2021). Traditional Chinese medicine (TCM), known for its multi-component, multi-pathway, and multi-target effects, provides unique advantages and significant potential for the prevention and treatment of Alzheimer's disease (Ding et al., 2022; Chiu et al., 2021; Liu et al., 2024). Based on long-term clinical practice and research of ancient and modern literature, Professor Yongchang Diwu from our research team has innovatively proposed that "marrow deficiency and turbid phlegm" is the pathological foundation for the development of AD, and the traditional famous formula "Xixin Decoction" is chosen for clinical treatment (Diwu, 2016).

Xixin decoction (XXD) originates from the "*Syndrome Differentiation Records*" by Chen Shiduo, a famous Chinese physician in the Qing Dynasty. The seminal work was written circa 1,687, over three centuries ago. XXD has the efficacy of benefiting qi, producing sperm, nourishing marrow, dissipating phlegm for resuscitation, and enhancing intelligence (Wang and Yan, 2009). It is a well-established prescription for dementia that has been clinically verified many times (Xiong et al., 2017; Zeng and

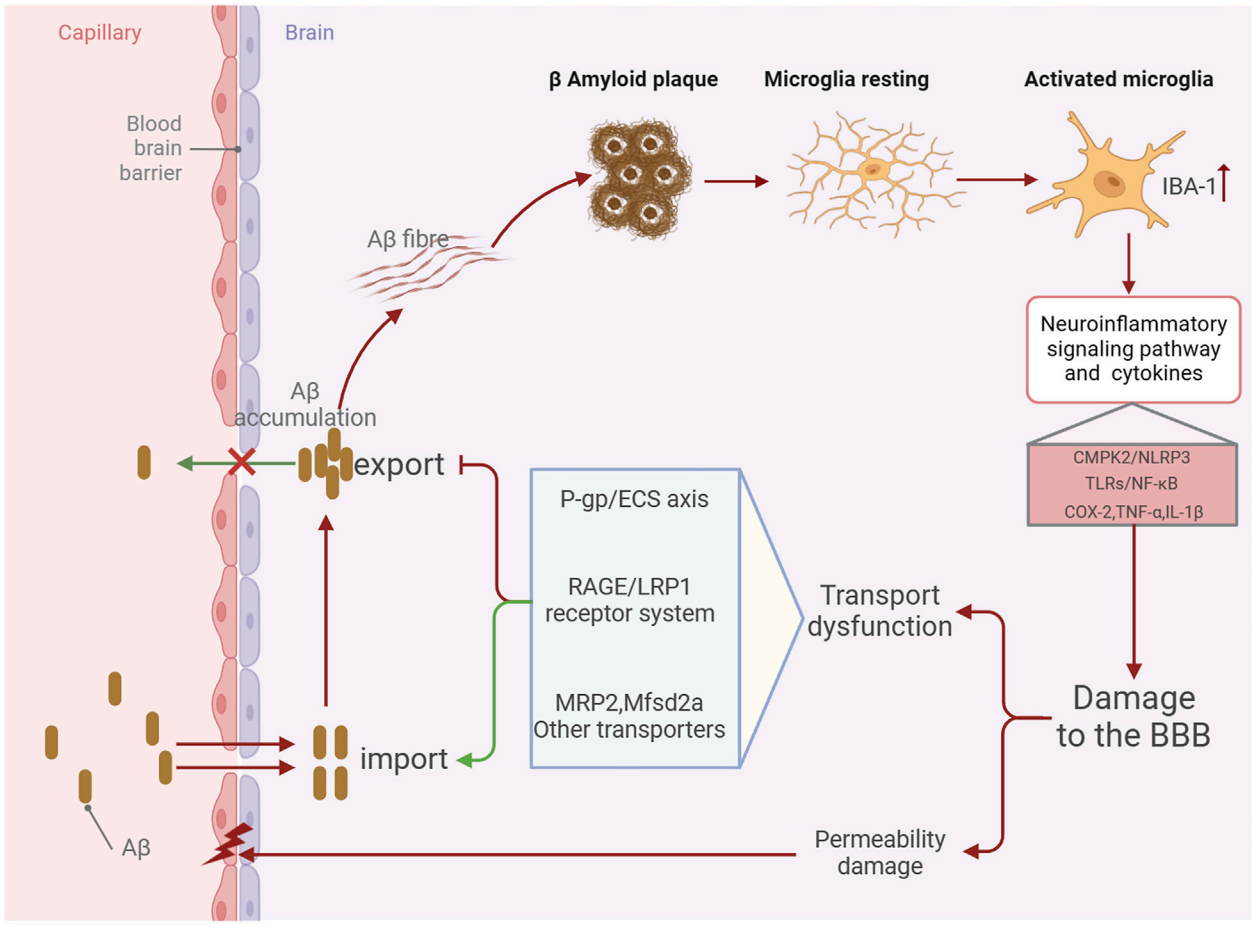


FIGURE 1
Schematic diagram of the mechanism by which BBB damage in the AD brain aggravates Aβ accumulation and promotes neuroinflammation.

Zhou, 2018), and it is also a representative formula for the treatment of dementia with marrow deficiency and turbid phlegm in traditional Chinese medicine (Wang and Yan, 2009). Pharmacological research indicates that XXD and its active metabolites exert anti-AD effects (Yang et al., 2017; Wu et al., 2022; Wang et al., 2022; Hajialyani et al., 2019; Kong et al., 2017).

Furthermore, previous research has found that XXD can affect mouse hippocampal synaptic ultrastructure, protect synaptic integrity (Gao et al., 2018), influence the levels of synaptic function-related proteins, reduce neuronal and synaptic damage, and participate in synaptic plasticity (Lei et al., 2020; Qu et al., 2019). Additionally, evidence indicates that XXD can lower toxic Aβ levels in the brain and promote cholinergic nerve repair (Chen et al., 2020). However, the specific pathways through which XXD affects pathological brain Aβ accumulation and inflammatory toxicity require further research.

Therefore, this study utilized *in vitro* BBB models (hCMEC/D3 and HBVP cell coculture) and SAMP8 mouse models to demonstrate the key role of BBB damage in AD, conduct an in-depth investigation of the relationship between BBB transport dysfunction, neuroinflammation, and pathological brain Aβ accumulation in AD, and reveal the possible pathways involved. Furthermore, XXD-medicated serum and granules were used to intervene in both the *in vitro* BBB models and the animal models to detect relevant indicators to verify whether XXD can regulate and repair BBB integrity and transport dysfunction, reduce pathological brain Aβ accumulation, and inhibit microglia-related neuroinflammation, thereby improving AD. The findings are expected to provide a scientific foundation for the clinical application of XXD.

2 Materials and methods

2.1 Cells and animals

Immortalized human brain microvascular endothelial cells (hCMEC/D3) and immortalized human brain pericytes (HBVP) were obtained from Shanghai Zhongqiao Xinzhou Biotechnology Co., Ltd. (Shanghai, China).

Male SAMP8 mice (60, SPF grade) and male SAMR1 mice (12, SPF grade), 14 weeks old, weighing (30 ± 5) g, were purchased from Zhishan (Beijing) Health and Medical Research Institute Co., Ltd. (Beijing, China), with animal production license number SCXK (Beijing) 2016-0010. Additionally, 20 male SPF-grade SD rats, 6 weeks old, weighing (200 ± 20) g, were obtained from

Chengdu Dashuo Biotechnology Co., Ltd. (Chengdu, China), license number SCXK (Sichuan) 2020-030. All animals were housed in the SPF-grade facility of the Shaanxi Collaborative Innovation Center of Chinese Medicinal Resources Industrialization. They were maintained in individually ventilated cages (IVC) under controlled environmental conditions: 12-h light/dark cycle, ambient temperature of 20°C–25°C, relative humidity of 45%–55%, and noise levels ≤60 dB. Standard laboratory chow and water were provided *ad libitum*. This study was conducted in accordance with the guidelines of the Animal Experimental Ethics Committee of Shaanxi University of Chinese Medicine. All experimental protocols were approved by the university's Animal Ethics Committee (approval numbers: SUCMDL20220110001 and SUCMDL20211001001).

2.2 Antibodies and reagents

Fetal bovine serum (FBS, FBS00321-1) was purchased from AusGeneX (Australia). Sodium pentobarbital (Lot No. 3G223G27) was obtained from Shengxing Biotechnology Co., Ltd. (China). Antibodies against cannabinoid receptor 1 (CB1, AI10227475) and P-glycoprotein (P-gp, BA07303498) were purchased from Bioss (Beijing, China). The antibody against cannabinoid receptor 2 (CB2, 218402) was purchased from Lifespan Biosciences (United States). Rat IL-1β ELISA Kit (Lot No. 20220714-20174A), Rat COX-2 ELISA Kit (Lot No. 20220714-20359A), Rat $A\beta_{1\text{-}42}$ ELISA Kit (Lot No. 20220714-20127A), Rat NF-κBp65 ELISA Kit (Lot No. 20220714-21622A), Rat NLRP3 ELISA Kit (Lot No. 20220714-20810A), and Rat TNF-α ELISA Kit (Lot No. 20220714-20852A) were purchased from Enzyme-linked Biotechnology Co., Ltd. (Shanghai, China). Anti-TLR1 antibody (AA07135689), Anti-TLR2 antibody (BA06081077), and Anti-TREM2 antibody (BA08065558) were purchased from Bioss (Beijing, China). The antibody against IBA1 (8525-1904) was purchased from Cell Signaling Technology (CST, United States). Anti-CMPK2 antibody (8525-1904) was purchased from Arigo Biolaboratories Corporation (Taiwan, China). Antibodies against AGER (GR3402053-12) and TLR2 (GR3359428-10) were purchased from Abcam (UK). BCA Protein Assay Kit (P0010) was obtained from Beyotime Biotechnology (Shanghai, China). Anti-Mfsd2a (724A041) and Anti-LRP1 (722A022) antibodies were purchased from Absin Bioscience (Shanghai, China). Anti-MRP2 antibody (BA02187624) was purchased from Bioss (Beijing, China). Anti-GAPDH antibody (AB-PR-001) was obtained from Xianzhi Bioscience (Hangzhou, China). HRP-conjugated goat anti-rabbit IgG secondary antibody (A0208) and anti-fluorescence quenching mounting medium (G1401) were purchased from Beyotime Biotechnology (Shanghai, China). Cy3-conjugated goat anti-rabbit IgG (GB21303) and DAPI (G1012) were purchased from Servicebio (Wuhan, China).

2.3 Composition and quantitative analysis of the major metabolites of XXD

The XXD was composed of Panax ginseng C. A. Mey. [Araliaceae; Ginseng Radix et Rhizoma] 30 g, Poria cocos (Schw.) Wolf [Polyporaceae; Poria cocos sclerotium] 30 g, Ziziphus jujuba Mill. [Rhamnaceae; Semen Ziziphi Spinosae] 30 g, Pinellia ternata (Thunb.) Makino [Araceae; Pinelliae ternatae rhizoma] 15 g, Citrus reticulata Blanco [Rutaceae; Citri reticulatae pericarpium] 9 g, Massa Medicata Fermentata [Fungi; Massae Medicatae Fermentatae] 9 g, Aconitum carmichaelii Debx. [Ranunculaceae; Radix Aconiti Lateralis Preparata] 3 g, Acorus tatarinowii Schott [Acoraceae; Rhizoma Acori Tatarinowii] 3 g, and Glycyrrhiza uralensis Fisch. ex DC. [Fabaceae; Radix Glycyrrhizae Preparata] 3 g.

Ten batches of botanical drug decoction were purchased from Beijing Tong Ren Tang Pharmaceutical (Table 1). They were soaked in water at a ratio of 1:10 for 1 h, decocted for an additional hour, and filtered through gauze. Subsequently, the residue was decocted again with eight times the amount of water for 30 min and filtered through gauze. The two filtrates were combined, concentrated to 400 mL, and then freeze-dried into powder.

Liquiritin (Lot: Z07J12X136344), spinosin (Lot: N10GB167286), hesperidin (Lot: K09S11L123847), ginsenoside Rg1 (Lot: C27N11Q132589), ginsenoside Re (Lot: J25GB152733), β-asarone (Lot: J23GB155719), ginsenoside Rb1 (Lot: O16GB158610), and ammonium glycyrrhizinate (Lot: M04GB140062) (all were provided by Shanghai yuanye Bio-Technology Co., Ltd., with a mass fraction ≥98%) were used as reference substances for the quantitative determination of the XXD freeze-dried powder. The ginsenosides Rg1, Re, and Rb1 were derived from Radix Ginseng, the hesperidin from Pericarpium Citri Reticulatae, the liquiritin and ammonium glycyrrhizinate from Radix et Rhizoma Glycyrrhizae, the β-asarone from Rhizoma Acori Tatarinowii, and the spinosin from Semen Ziziphi Spinosae. Following precision weighing of the reference substances, they were dissolved in 70% methanol to prepare the solutions. Each solution was injected into an HPLC system with a precisely measured volume of 10 μL. The regression equations were obtained using the reference substance concentration ($\mu g \cdot mL^{-1}$) as the independent variable and the peak area as the dependent variable (Table 2).

The XXD freeze-dried powder (1 g) was placed in a stoppered Erlenmeyer flask. Subsequently, 10 mL of 70% methanol was added to the flask, which was then sealed and weighed. The solution was ultrasonically extracted (250 W, 40 kHz) for 50 min, cooled, reweighed, and brought to the original weight with 70% methanol. It was then shaken well and passed through a 0.22 μm membrane, thus obtaining the test solution, which was injected and measured at 0, 8, 16, 24, 32, 40, and 48 h. The relative standard deviation (RSD) of the peak areas of the eight reference substances ranged from 0.31% to 2.06%, indicating good stability of the test solution within 48 h. Precision weighing of known-content XXD freeze-dried powder was followed by the addition of liquiritin (0.21391 mg/mL), spinosin (0.0615 mg/mL), hesperidin (0.21391 mg/mL), ginsenoside Rg1 (1.697227 mg/mL), ginsenoside Re (0.746067 mg/mL), β-asarone (0.026484 mg/mL), ginsenoside Rb1 (0.621261 mg/mL), and ammonium glycyrrhizinate (0.138041 mg/mL). The solution was then injected and measured; and the average sample recovery rates were calculated as 96.69%, 100.14%, 102.73%, 102.97%, 100.06%, 103.15%, 96.33%, and 96.53% for liquiritin, spinosin, hesperidin, ginsenoside Rg1, ginsenoside Re, β-asarone, ginsenoside Rb1, and ammonium glycyrrhizinate, respectively, with RSDs of 0.26%–2.59%, indicating that this method showed good accuracy. The

TABLE 1 Information on 10 batches of Xixin Decoction.

Lot	Panax ginseng	Glycyrrhiza uralensis	Citrus reticulata	Ziziphus jujuba	Acorus tatarinowii	Massa medicata fermentata	Poria cocos	Pinellia ternata	Aconitum carmichaelii
S1	22030201	20201202	200601	S20220201	s20220502	202106001	211201	210305	220401
S2	22030202	20201203	200602	S20220202	s20220503	202106002	211202	210304	220402
S3	22030203	20201204	200603	S20220203	s20220504	202106004	211206	210303	20210301
S4	22030204	20201205	200604	S20220401	200901	202106005	211207	210302	20210302
S5	22030205	20201206	200605	S20220402	200904	202106006	211208	210301	20210303
S6	200501	20201207	2022111019	210301	200906	202106009	2203001	210208	210801
S7	200502	220301	2022111018	210302	s20220505	2012001	2203002	210207	210802
S8	200503	220302	2022111020	210303	s20220506	2012002	2203003	210206	210803
S9	200504	220303	2022111017	210304	s20220507	2012003	201001	210205	210804
S10	200505	220304	2022111019	210305	s20220508	2012004	201002	210204	210805

TABLE 2 Reference product linear relationship and its range.

Metabolite	Linear relationship	R^2	Linear range
Liquiritin	Y = 13560x+41.907	0.9998	0.018671875–0.29875
Spinosin	Y = 13492x+54.248	0.9997	0.42–0.013125
Hesperidin	Y = 10433x+63.481	0.9997	0.013219–0.545
Ginsenoside Rg1	Y = 1,421x+30.341	0.9998	4.72–0.07375
Ginsenoside Re	Y = 1822x+24.366	0.9999	2.57–0.020078125
β-asarone	Y = 58627x+170.54	0.9997	0.003125–0.4
Ginsenoside Rb1	Y = 3571.5x+48.668	0.9996	0.013125–1.68
Ammonium glycyrrhizinate	Y = 3380.8x+22.3	0.9998	0.034063–0.545

TABLE 3 Contents of eight main metabolites in XXD freeze-dried powder (mg/g).

Serial number	Liquiritin	Spinosin	Hesperidin	Ginsenoside Rg1	Ginsenoside Re	β-asarone	Ginsenoside Rb1	Ammonium glycyrrhizinate
S1	0.034091	0.046250694	0.182789	1.263342334	0.785716557	0.018897	0.419318	0.122108
S2	0.03758	0.052251149	0.201823	1.393430542	0.865617764	0.022877	0.491655	0.13529
S3	0.036532	0.060267395	0.229851	1.313783631	0.766150044	0.025839	0.523932	0.132669
S4	0.036783	0.061902926	0.231003	1.323181468	0.855789206	0.025532	0.560824	0.133167
S5	0.052649	0.080738224	0.23488	1.5223532	0.553456418	0.032631	0.468437	0.172148
S6	0.053599	0.079642728	0.267564	1.561168356	0.578036723	0.037313	0.477856	0.172504
S7	0.033923	0.059124637	0.421689	1.48674555	0.588972245	0.027454	0.546249	0.115218
S8	0.037423	0.066186777	0.463668	1.588738722	0.629773721	0.030212	0.594219	0.129175
S9	0.037509	0.065433511	0.46516	1.925405151	0.895773844	0.030199	0.566533	0.127523
S10	0.046577	0.066175291	0.429965	2.084475222	0.752984027	0.028797	0.384752	0.152622

content of the eight metabolites in the samples was calculated (Table 3).

2.4 Medicinal herbs and preparation

This study used concentrated botanical drug granules, and each 1 g of the concentrated botanical drug granules corresponded to the following botanical drug decoction pieces: 3.3 g of Panax ginseng, 10 g of Poria cocos, 10 g of Ziziphus jujuba, 12 g of Pinellia ternata, 12 g of Citrus reticulata, 10 g of Massa Medicata Fermentata, 3 g of Aconitum carmichaelii, 6 g of Acorus tatarinowii, and 3 g of Glycyrrhiza uralensis. The XXD granules were purchased from China Resources Sanjiu Medical and Pharmaceutical Co., Ltd., a manufacturer holding a Good Manufacturing Practice (GMP) certificate, ensuring the stability of the medication. The granules were produced with the following batch numbers: Panax ginseng Lot: 2110005C, Poria cocos Lot: 2109003C, Ziziphus jujuba Lot: 2170003C, Pinellia ternata Lot: 2109003C, Citrus reticulata Lot: 2109002S, Massa Medicata Fermentata Lot: 2104006S, Aconitum carmichaelii Lot: 2109001S, Acorus tatarinowii Lot: 2108002S, Glycyrrhiza uralensis Lot: 2110006C. Each packet contains 19.5 g of granules (equivalent to 132 g of botanical drug). The granules were mixed according to the dosage of the raw herbs, dissolved in 60°C distilled water, heated and stirred constantly, and prepared into a solution with a concentration of 88.725 mg/mL, and stored at 4°C in a sealed container.

Preparation of XXD-Medicated Serum: Following a 7-day acclimation period, 20 rats were randomly divided into two groups (n = 10 each): blank serum group and XXD-medicated serum group. The rat dosage, calculated using the Human-Animal Body Surface Area Conversion Table (Huang et al., 2004), was established at 3.375 g $kg^{-1}·d^{-1}$. Control group animals received an equivalent volume of saline solution. Oral gavage was administered daily for a week. Two hours post-final dose, the rats were anesthetized using intraperitoneal sodium pentobarbital. Blood was then collected aseptically from the abdominal aorta and allowed to coagulate for 2 h. After centrifugation, the serum was pooled by group, heat-inactivated (56°C, 30 min), sterile filtered, and cryopreserved at −80°C for subsequent use.

The probiotic freeze-dried powder, 3 g/bag, was purchased from Weikaihaien (Shandong) Biological Engineering Co., Ltd., Lot: 2022022. It was dissolved in distilled water at room temperature, shaken well, and prepared into a solution with a concentration of 0.0078 mg/mL, and stored at 4°C in a sealed container.

2.5 *In vitro* experimental protocol

2.5.1 Coculture of hCMEC/D3 and HBVP cells

A Transwell coculture system was utilized to construct an *in vitro* BBB model. The hCMEC/D3 and HBVP cells were seeded into the upper and lower chambers, respectively, of a six-well Transwell plate at a 1:1 ratio and cultured until they reached more than 85% confluence. After digestion and counting, the hCMEC/D3 and HBVP cells were added to their respective chambers at a 1:1 volume ratio, and the culture medium was added to the appropriate level. After 48 h of coculture, a 4-h liquid surface leakage test was performed to evaluate the BBB model's establishment. After changing the culture medium, if the liquid surface difference was greater than 0.5 cm, the culture continued for 4 h. If the liquid surface difference remained unchanged, the *in vitro* BBB model was considered to be preliminarily established.

2.5.2 Lipopolysaccharide stimulation of hCMEC/D3 and HBVP cells

Lipopolysaccharide (LPS), a constituent of the outer membrane of Gram-negative bacteria, is commonly used to induce neuroinflammation (Yu et al., 2024). After successfully establishing the *in vitro* BBB model, LPS was used to induce BBB damage. Logarithmically growing hCMEC/D3 and HBVP cells were seeded into 96-well plates. After 8 h of incubation, 100 μL of a diluted LPS solution (initial concentration of 100 mg/mL) was added to each well at final concentrations of 0.5, 1, 1.5, and 2 μg/mL. Cell viability was evaluated at 24, 48, and 72 h to determine the optimal culture time and concentration.

2.5.3 XXD-medicated serum intervention and grouping

The LPS-induced hCMEC/D3 and HBVP cells were treated with 5%, 10%, and 20% XXD-medicated serum, and cell viability was calculated to screen for the optimal concentration. The successfully established *in vitro* BBB models were subdivided into the following groups: control group, LPS group, 24-h XXD-medicated serum group, 48-h XXD-medicated serum group, 72-h XXD-medicated serum group, and blank serum group.

2.5.4 Western blot detection of BBB transport-related protein expression

Logarithmically growing hCMEC/D3 and HBVP cells were modeled, grouped, administered, and incubated as described above. Following this, Western blotting experiments were performed. The cells were collected, centrifuged, lysed, and centrifuged again to collect the supernatant. Protein levels were determined via the BCA assay. Each well was loaded with 20 μg of total protein. Proteins were separated by SDS-PAGE (6% stacking gel at 60 V, 10% separating gel at 90 V), followed by wet transfer at 300 mA for 90 min. Subsequently, the samples were blocked using 5% skim milk on a shaker for 1 h and subsequently incubated with primary antibodies (antibodies against P-glycoprotein [P-gp], cannabinoid receptor types 1 and 2 [CB1 and CB2], and major facilitator superfamily domain-containing protein 2a [Mfsd2a]) at a 1:5000 dilution at 4°C overnight with shaking. Following three washes in TBST, secondary antibodies were applied at room temperature for 90 min. Subsequently, TBST washing was performed three times, ECL reagent was used for darkroom exposure, and band gray values were analyzed using ImageJ software (v 1.8.0).

2.5.5 RT-PCR detection of P-gp mRNA

The *in vitro* BBB model was incubated, then removed, digested, and centrifuged. RNA extraction was performed with TRIzol, followed by cDNA synthesis using a reverse transcription kit. RT-PCR was conducted according to the manufacturer's instructions. The amplified products were separated via 1%

TABLE 4 Rt-PCR primer sequences.

Gene	Primer sequence (5′~3′)	Product length (bp)
P-gp	Forward: GACATGACCAGGTATGCCTATTATT	160
	Reverse: ACCAGCCTATCTCCTGTCGCAT	
GAPDH	Forward: GGAAGCTTGTCATCAATGGAAATC	168
	Reverse: TGATGACCCTTTTGGCTCCC	

agarose gel electrophoresis and imaged using an image analyzer. Expression levels of mRNA were determined using the $2^{-\Delta\Delta CT}$ method. Primer details are provided in Table 4.

2.5.6 Immunofluorescence detection of P-gp expression

The incubated *in vitro* BBB model was extracted post-incubation, PBS-washed, and fixed with 4% paraformaldehyde. Membrane permeabilization was achieved using Triton X-100, followed by BSA blocking (37°C, 1 h). Sequential antibody incubations were performed: primary (overnight) and secondary (1 h). Nuclear counterstaining employed DAPI, and the samples were subsequently imaged using a fluorescence microscope at a magnification of ×20.

2.6 *In vivo* experimental protocol

2.6.1 Animal grouping and drug administration

SAMR1 mice were designated as the control group (Control), while SAMP8 mice were randomly divided into the model group (Model), the probiotics group (Probiotics), the high-dose Xixin Decoction granules group (H-XXD), the medium-dose Xixin Decoction granules group (M-XXD), and the low-dose Xixin Decoction granules group (L-XXD), with eight mice in each group. The dosages were calculated based on the equivalent clinical dosages and the body surface area of the animals (Huang et al., 2004). The probiotics group received a dose of 0.39 $g{\cdot}kg^{-1}{\cdot}d^{-1}$, the M-XXD group received a dose of 2.535 $g{\cdot}kg^{-1}{\cdot}d^{-1}$, the H-XXD group received twice the equivalent clinical dose at 5.07 $g{\cdot}kg^{-1}{\cdot}d^{-1}$, and the L-XXD group received half the equivalent clinical dose at 1.2675 $g{\cdot}kg^{-1}{\cdot}d^{-1}$. The treatment was administered continuously for 8 weeks. The drugs were dissolved in distilled water to prepare solutions of the appropriate concentrations. Each treatment group received the drugs by gavage daily at the designated dose, with a volume of 10 $mL{\cdot}kg^{-1}{\cdot}d^{-1}$. Equivalent volumes of distilled water were administered to both the control and model groups via gavage.

2.6.2 Behavioral testing

The Morris water maze test was performed for six consecutive days after administration. The initial 5 days consisted of place navigation trials. Mice were released into the water pool from four different quadrants each day, facing the wall. The escape latency, defined as the time required to find the submerged platform, was recorded with a limit of 60 s per trial. Upon reaching the platform, mice were permitted a 10-s rest period. If mice were unable to find the platform within the allotted time, they were gently guided to it, allowed a 10-s rest, and assigned a maximum escape latency of 60 s. On the sixth day, a spatial probe test was conducted by removing the hidden platform and releasing mice from the first quadrant, facing the pool wall. They were allowed to swim freely for 60 s. During this trial, the time spent in the target quadrant and frequency of crossing the former platform site were recorded.

2.6.3 BBB permeability testing

Following the final behavioral test, four mice per group were randomly chosen and injected with a 2% Evans blue solution (4 mL/kg) through the tail vein. Specific methods referred to the published literature (Schoch et al., 2014). Upon turning blue in limbs and eyes, the mice were anesthetized via intraperitoneal injection of 0.5% sodium pentobarbital (0.1 mL/g). The specific methods were performed with reference to the literature (Levin-Arama et al., 2016). Cardiac perfusion was performed through the left ventricle with physiological saline until the liver and kidneys turned white and clear fluid flowed from the right atrium. This was followed by rapid perfusion with 4% paraformaldehyde precooled to 4 °C, which was maintained at a slow and steady rate for 10–15 min. The brain tissue was subsequently collected, fixed in 4% paraformaldehyde (4°C, 12 h), embedded in OCT, rapidly frozen at −20°C, and sectioned coronally at 20 μm. Evans blue extravasation was observed under a laser confocal microscope and quantified using ImageJ 1.8.0 software.

2.6.4 ELISA detection of hippocampal $A\beta_{1\text{-}42}$ content and levels of neuroinflammatory factors

Hippocampal tissue was precooled on ice and homogenized in nine times the volume of the PBS solution, and the supernatant was collected. Following the instructions provided with the ELISA kit, the levels of $A\beta_{1\text{-}42}$, NF-κB p65, NLRP3, TNF-α, and IL-1β were measured. Absorbance at 450 nm was assessed using an enzyme-labeled instrument.

2.6.5 Immunofluorescence detection of BBB transport-related protein receptors and microglial activation markers in the hippocampal CA1 region

Anesthesia was administered to the mice via intraperitoneal injection of 0.5% sodium pentobarbital. A thoracic incision exposed the heart, allowing for left ventricular needle insertion and right atrial appendage excision. Perfusion commenced with physiological saline until clear fluid emerged from the oronasal cavities, followed by 4% paraformaldehyde perfusion until complete body rigidity. The intact brain was extracted and underwent a series of preparatory steps: 24-h fixation in 4% paraformaldehyde, ethanol dehydration, xylene clearing, and paraffin embedding. Five-micrometer sections were prepared and subsequently washed thrice with PBS before

blocking with 3% bovine serum albumin (37°C, 30 min). Primary antibody incubation (targeting P-gp, CB1, CB2, RAGE, IBA1, TREM2, TLR1, and TLR2) was conducted overnight at 4°C. Following PBS washing, sections were incubated with fluorescent secondary antibodies (37°C, 1 h). After additional PBS washes, DAPI staining was performed, and sections were mounted using an anti-fluorescence quenching medium. Imaging was performed using confocal microscopy at a magnification of ×40, and relative fluorescence intensity was quantified with ImageJ software (version 1.8.0).

2.6.6 Western blot detection of BBB transport-related protein receptors and neuroinflammatory factors in mouse hippocampal tissue

Hippocampal tissue was extracted, lysed, and homogenized ultrasonically on ice. Post-lysis centrifugation at 12,000 × g for 15 min at 4°C, the supernatant was collected for BCA protein quantification. Each well was loaded with 20 μg of total protein. Proteins underwent SDS-PAGE separation (6% stacking gel, 60V; 10% separating gel, 90V) and wet transfer (300mA, 90min). Membranes were blocked with 5% skim milk (1h, shaking) and incubated overnight with primary antibodies (anti-P-gp, CB1, CB2, RAGE, IBA1, TLR1, TLR2, TREM2, Mfsd2a, MRP2, LRP1, and CMPK2) at 4°C under agitation. After TBST washing, secondary antibody incubation was performed (90min, room temperature). ECL-based chemiluminescence detection was conducted in darkness. Band intensities were analyzed using ImageJ (v1.8.0).

2.7 Data analysis

Statistical analyses were conducted using GraphPad Prism 9.0 software. Data are presented as mean ± SD. Levene's test assessed variance homogeneity. One-way ANOVA was applied for multiple group comparisons, followed by LSD-t tests for data with significant differences. A p-value <0.05 was considered statistically significant.

3 Results

3.1 *In vitro* experimental results

3.1.1 Optimal concentration screening for LPS and XXD-medicated serum

LPS can disrupt the BBB through various pathways, and damage to the BBB can contribute to the progression of a range of diseases, with AD being a notable example (Peng et al., 2021). Therefore, this study utilized LPS to establish a BBB inflammation model. Optimal LPS concentration was determined through cell viability assessment using the MTT assay. The results showed that, after treating hCMEC/D3 and HBVP cells with 0.5–2 μg/mL LPS, cell viability exhibited a notable decline in comparison to the control group and exhibited a negative correlation with the LPS concentration. As high concentrations of LPS could cause irreversible cell damage, 1 μg/mL LPS was selected for subsequent experiments. On comparing the cell viability of hCMEC/D3 and HBVP cells exposed to 1 μg/mL LPS for 24, 48, and 72 h, it was found that cell viability in the 48-h and 72-h groups exhibited no statistically significant difference from that in the 24-h group (Figures 2A, B). Therefore, a 24-h treatment with 1 μg/mL LPS was used as the modeling condition.

After the administration of 1 μg/mL LPS to hCMEC/D3 and HBVP cells for 24 h, different concentrations of XXD-medicated serum were added for co-incubation. The MTT assay results indicated that 1 μg/mL LPS significantly inhibited cell proliferation, while 10% XXD-medicated serum significantly reversed this effect and increased cell viability (Figures 2C, D). Additionally, the 15% concentration of XXD-medicated serum did not show any further improvement in cell viability. This observation suggests that the 15% concentration may have reached a saturation point of the pharmacological effect or potentially introduced additional adverse effects, thereby failing to further enhance cell viability. Therefore, 10% XXD-medicated serum was chosen for subsequent experiments, as it exhibited the best efficacy in restoring cell viability while avoiding the potential drawbacks associated with higher concentrations.

3.1.2 XXD-medicated serum promotes P-gp expression in the *in vitro* BBB model

The BBB can be described as a highly evolved CNS microvascular functional unit, comprising CNS endothelial cells, neural progenitor cells, pericytes, astrocytes, and other neural and immune cells, in addition to various functional protein structures (Obermeier et al., 2013). These components form the neurovascular unit (NVU) that maintains BBB function (Huang et al., 2020). Pericytes envelop the abluminal surface of cerebral vascular walls, including capillaries, precapillary arterioles, and postcapillary venules. The highest pericyte coverage rate is seen in the neural tissue among the capillary beds of different organs (Allt and Lawrenson, 2001). Pericytes are crucial in promoting vascular stability and maintaining BBB integrity (Winkler et al., 2011). Therefore, this study employed hCMEC/D3 and HBVP cells to construct an *in vitro* BBB model.

P-gp, an ABC transporter encoded by the human MDR1 gene, serves as a crucial efflux mechanism in the BBB. It inhibits substrate drug entry into the brain while promoting the elimination of endogenous molecules, including Aβ—a hallmark pathological feature of AD (Pyun et al., 2022). This study revealed that, relative to the control group, LPS treatment significantly downregulated both mRNA and protein expression of P-gp, indicating that P-gp expression is reduced when the BBB is damaged. Relative to the LPS group, the XXD-medicated serum upregulated P-gp mRNA and protein expression after 24, 48, and 72 h of culture, with the most significant effect observed at 48 h (Figure 3), suggesting that XXD can improve BBB transport dysfunction by upregulating P-gp expression.

3.1.3 XXD-medicated serum upregulates CB2 and Mfsd2a expression and downregulates CB1 expression in the in vitro BBB model

Endocannabinoids, originating from dietary omega-3 and omega-6 polyunsaturated fatty acids, are endogenous bioactive lipids. The endocannabinoid system (ECS) is characterized by two primary receptors: CB1 and CB2. CB1 is predominantly

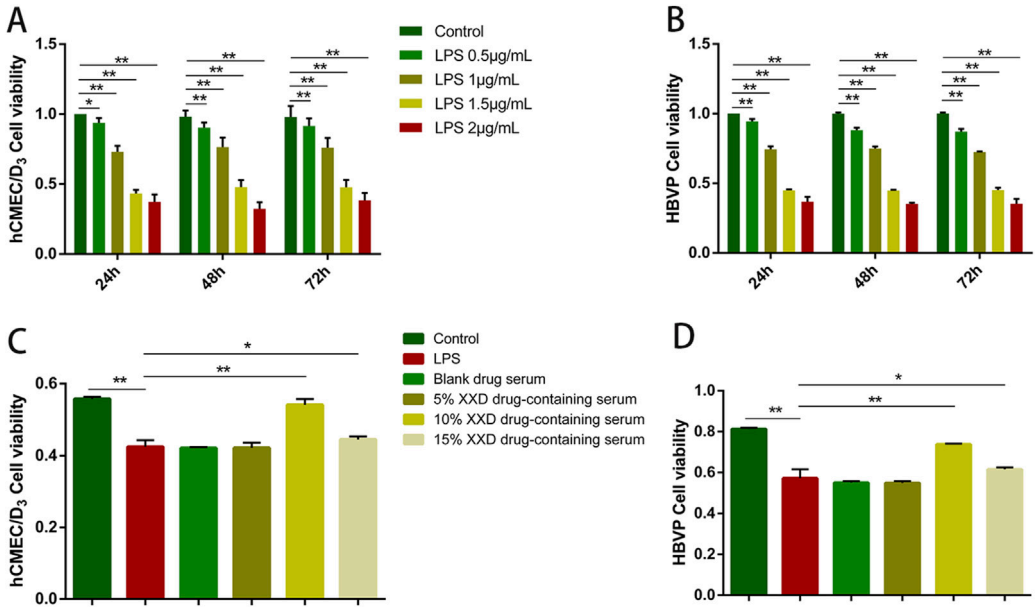


FIGURE 2
Screening of optimal concentrations of LPS and XXD medicated serum. **(A)** Effects of different concentrations of LPS on the viability of hCMEC/D3 cells after 24, 48, and 72 h of incubation; **(B)** Effects of different concentrations of LPS on the viability of HBVP cells after 24, 48, and 72 h of incubation; **(C)** Effects of different concentrations of XXD medicated serum on the viability of LPS-induced hCMEC/D3 cells; **(D)** Effects of different concentrations of XXD medicated serum on the viability of LPS-induced HBVP cells. MTT assay; $^{**}p < 0.01$; $^{*}p < 0.05$.

expressed in CNS presynaptic regions (Zou and Kumar, 2018). It modulates cytokine release both within and outside the CNS and immune cell migration, with expression levels influenced by cell activation and stimulus type (Paul et al., 2012). CB2 is predominantly expressed in peripheral immune cells and brain tissue (Nagarkatti et al., 2009). Primarily serving an immunomodulatory function, it regulates immune cell migration and cytokine release both within and beyond the immune system (Massi et al., 2006). During neuroinflammation or BBB dysfunction, P-gp regulates ECS-related receptor protein expression, thereby influencing the inflammatory process. Regulating the P-gp/ECS axis can alleviate BBB dysfunction and neuroinflammation. Mfsd2a, a member of the major facilitator superfamily (MFS), plays a critical role in BBB integrity and DHA transport. Mfsd2a-deficient mice exhibit significantly lower brain DHA levels, resulting in neuronal loss and cognitive impairment due to DHA's crucial role in brain development and maintenance. Mfsd2a inhibits CNS endothelial cell transport and mitigates BBB damage. Consequently, it has gained prominence in neurological disease research (Huang and Li, 2021).

This study demonstrated that, relative to the control group, LPS treatment upregulated CB1 protein expression while downregulating both CB2 and Mfsd2a expression. indicating that neuroinflammation can lead to an abnormal ECS as well as abnormal Mfsd2a expression, resulting in BBB dysfunction. Compared with the LPS group, XXD-medicated serum downregulated CB1 expression and upregulated CB2 and Mfsd2a expression after incubation for 24, 48, and 72 h (Figure 4), suggesting that XXD can improve BBB dysfunction by modulating the expression of the transport-related protein Mfsd2a and the P-gp/ECS axis.

3.2 *In vivo* experimental results

3.2.1 XXD improves learning and spatial memory abilities and reduces evans blue extravasation in SAMP8 mice

SAMP8 mice serve as an optimal AD model, demonstrating age-associated learning and memory impairments, in addition to exhibiting the majority of pathological characteristics associated with AD pathogenesis, including oxidative stress, inflammation, and Aβ deposition. Therefore, SAMP8 mice aid in visualizing the effects of AD and provide an effective method for finding new therapeutic targets (Liu et al., 2020).

The Morris water maze is a commonly used behavioral test for assessing spatial cognition in rodents (Vorhees and Williams, 2006). This study investigates, compared to SAMR1 controls, SAMP8 mice exhibited significantly prolonged escape latencies over five consecutive days, along with decreased target quadrant dwell time and crossings, indicating marked spatial cognitive impairment. High-dose XXD treatment, relative to untreated SAMP8 mice, significantly reduced escape latencies throughout the 5-day period and increased target quadrant residence time. Medium- and low-dose XXD groups also demonstrated significantly shortened escape latencies (Figures 5A–C). These results suggest XXD's potential to ameliorate spatial cognitive deficits in SAMP8 mice.

Evans blue, a widely utilized azo dye, is often used for tracing and observing BBB integrity. Under normal conditions, Evans blue, which is bound to plasma albumin, is unable to pass through the BBB and thus is incapable of staining the nervous system. However, if the BBB is disrupted, Evans blue is able to penetrate and cause staining (Liu et al., 2018). In this study, Evans blue extravasation was

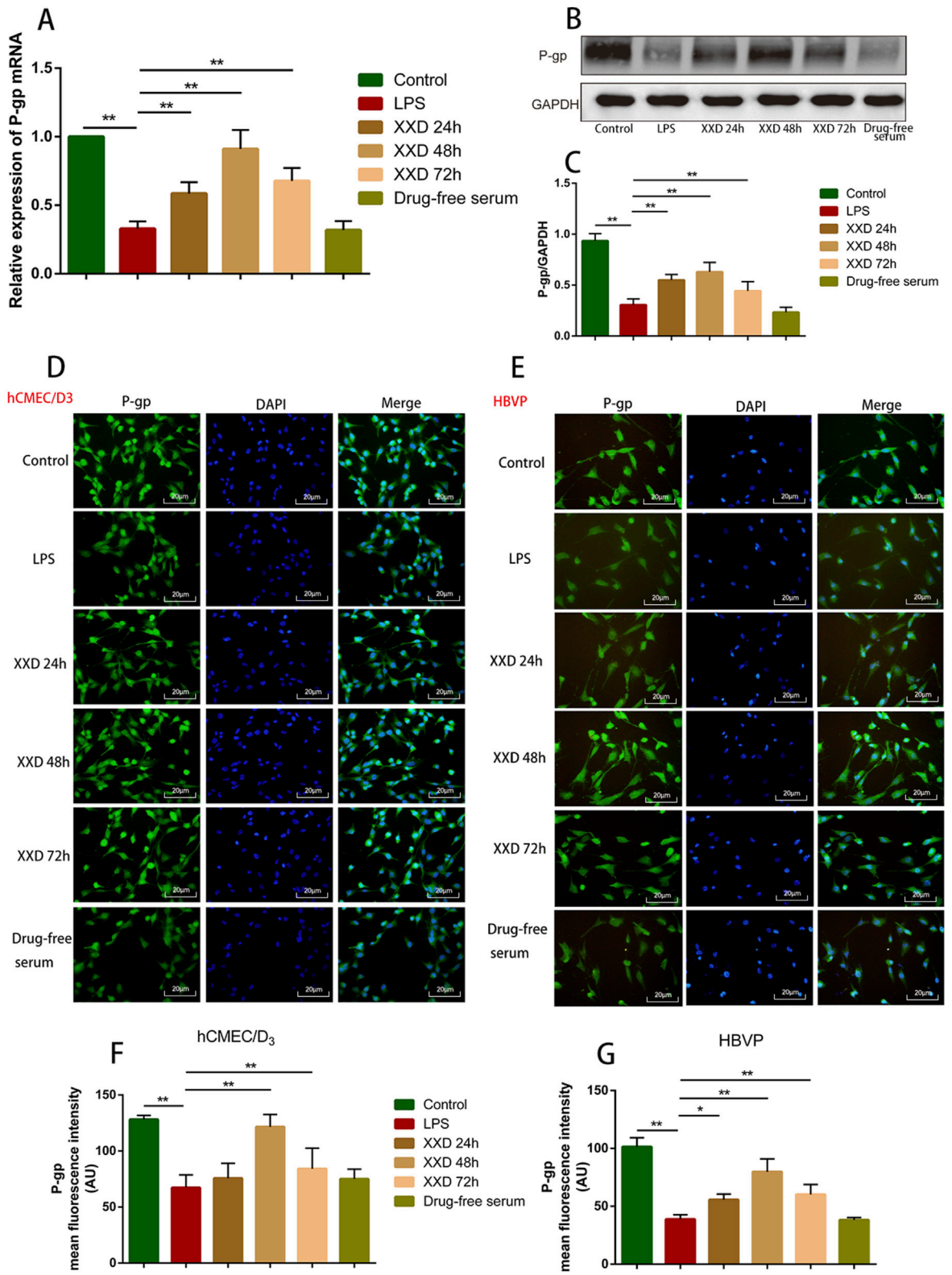


FIGURE 3
XXD medicated serum promotes P-gp expression in the blood-brain barrier cell model. **(A)** Comparison of P-gp mRNA expression; **(B)** and **(C)** Comparison of relative P-gp protein expression; **(D)** and **(F)** Comparison of P-gp protein positive expression in hCMEC/D3 cells; **(E)** and **(G)** Comparison of P-gp protein positive expression in HBVP cells. Scale bar: 20 μm; images at ×200 magnification; $^{**}p < 0.01$, $^{*}p < 0.05$.

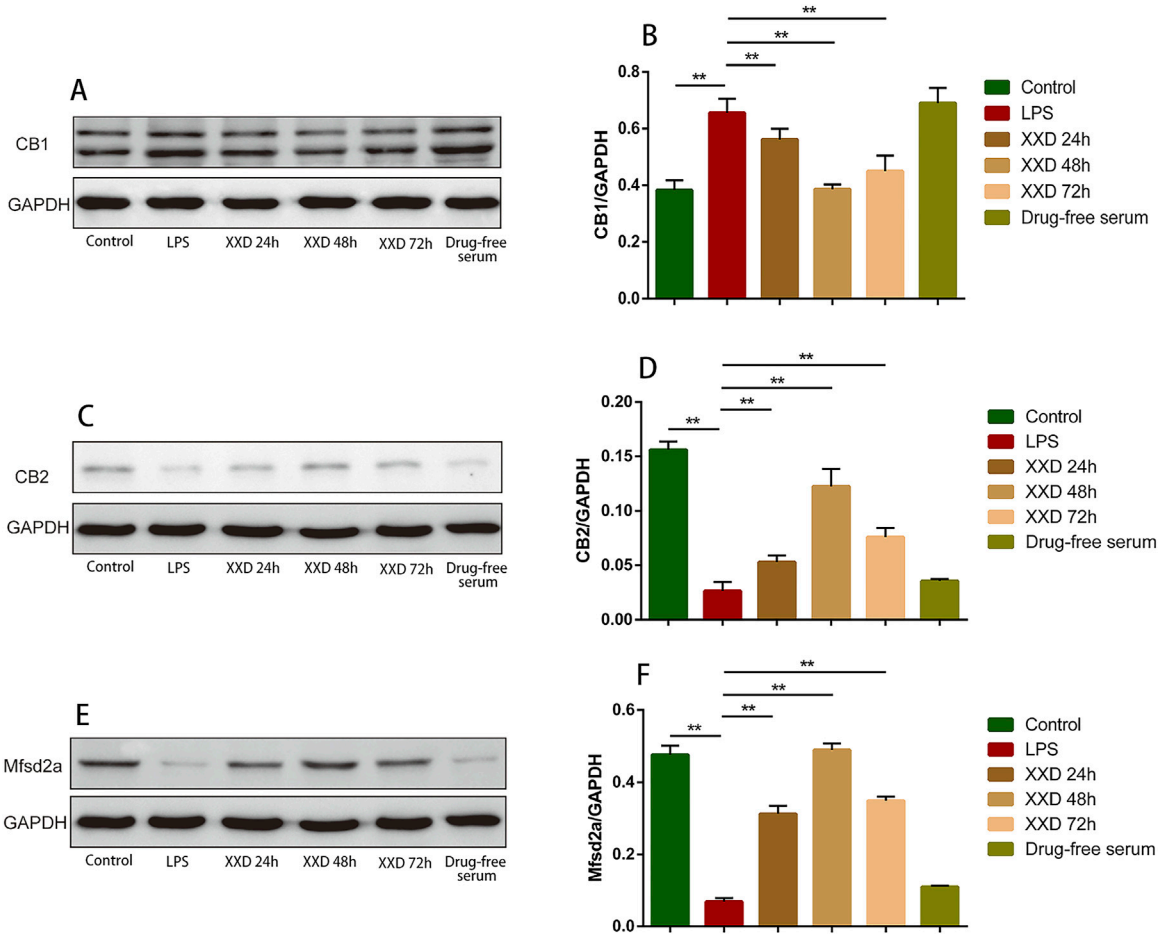


FIGURE 4
XXD medicated serum upregulates CB2 and Mfsd2a expression and downregulates CB1 expression in the blood-brain barrier cell model. **(A)** and **(B)** Comparison of relative CB1 protein expression; **(C)** and **(D)** Comparison of relative CB2 protein expression; **(E)** and **(F)** Comparison of relative Mfsd2a protein expression; $^{**}p < 0.01$, $^{*}p < 0.05$.

markedly increased in the brain tissue of SAMP8 mice, indicating BBB damage and increased permeability. Compared with the SAMP8 group, Evans blue extravasation in the brain tissue of XXD-treated groups significantly decreased (Figures 5D, E). Therefore, XXD may reduce BBB permeability by improving its ultrastructure, although the specific mechanisms require further investigation.

3.2.2 XXD regulates BBB transport-related proteins and promotes $A\beta_{1\text{-}42}$ clearance in SAMP8 mice

3.2.2.1 XXD regulates the P-gp/ECS axis

In a healthy CNS, Aβ production and clearance rates have been observed to be 7.6% and 8.3% per hour (Bateman et al., 2006). P-gp plays a pivotal role in the normal clearance of Aβ through the BBB, with its expression and function negatively related to aging, Aβ deposition, and AD. Hartz and colleagues demonstrated that inhibiting P-gp reduces $A\beta_{42}$ transport across brain capillary lumens (Hartz et al., 2010). The present research demonstrated that P-gp fluorescence intensity and protein expression in the hippocampal CA1 region of SAMP8 mice significantly decreased, while $A\beta_{1\text{-}42}$ content significantly increased, indicating a negative correlation between hippocampal Aβ accumulation and P-gp expression in SAMP8 mice. In comparison to the SAMP8 group, the P-gp fluorescence intensity and protein expression in the hippocampal CA1 region of XXD-treated mice in all dosage groups significantly increased (Figure 6A, B, G, H), while hippocampal $A\beta_{1\text{-}42}$ content significantly decreased (Figure 7F), indicating that XXD can upregulate P-gp expression and reduce Aβ accumulation.

The ECS is a widespread neuroregulatory network that undergoes changes and functional decline in many neurological diseases, potentially serving as a key component in regulating neuroinflammation and the pathogenesis of neurodegenerative diseases (Stella, 2010). The ECS comprises endocannabinoids, cannabinoid receptors CB1 and CB2, and proteins participating in endocannabinoid metabolism. The primary endogenous agonists of CB1 and CB2 are 2-arachidonoylglycerol (2-AG) and N-arachidonoylethanolamine (AEA) (Hillard, 2018). In the hippocampus of patients with AD, 2-AG levels are elevated, which has also been confirmed in rodent models (van der Stelt et al., 2006). Elevated endocannabinoids may boost the neuroprotective effects of CB1 and, via CB2 activation, inhibit microglial inflammation while stimulating Aβ phagocytosis (Papa et al., 2022). P-gp and ECS are closely related. Cannabidiol (CBD)

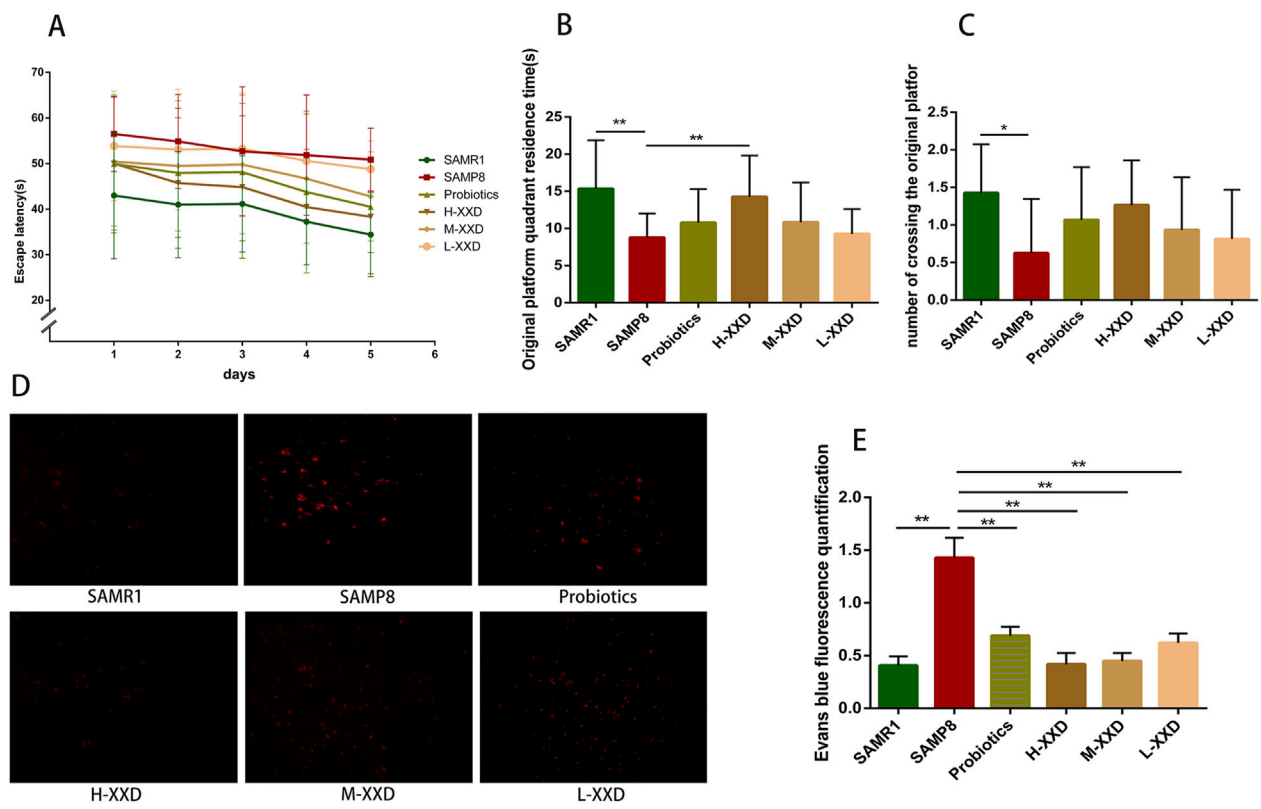


FIGURE 5
XXD improves learning and spatial memory impairments in SAMP8 mice and reduces Evans blue extravasation. **(A)** Escape latency (s) in the place navigation test (n = 8); **(B)** Time spent in the target quadrant (s) in the spatial probe test (n = 8); **(C)** Number of crossings over the platform location in the spatial probe test; **(D)** and **(E)** Comparison of Evans blue extravasation in the brains of different groups of mice (n = 4); images at ×400 magnification; $^{**}p < 0.01$, $^{*}p < 0.05$.

can act through typical endocannabinoid receptors (CB1 and CB2) or various non-typical pathways, exerting an effect that inhibits the P-gp efflux function (Gómez et al., 2021). In intestinal inflammation models, P-gp knockdown or inhibition reduces the secretion of endocannabinoids, and the loss of CB2 exacerbates acute intestinal inflammation (Szabady et al., 2018). Therefore, it can be hypothesized that, in the CNS, P-gp may regulate ECS receptor expression, contributing to neuroinflammation or BBB dysfunction. In this study, the fluorescence intensity and expression of CB1 in the hippocampal CA1 region of SAMP8 mice increased, while the fluorescence intensity and expression of CB2 decreased, indicating a decline in ECS function in AD. Compared with the SAMP8 group, in all XXD-dose groups, the fluorescence intensity and expression of CB1 in the mouse hippocampal CA1 region decreased (Figures 6C, D, I, J), while the fluorescence intensity and expression of CB2 increased (Figures 6E, F, K, L), indicating that XXD has a regulatory effect on the ECS. Therefore, XXD may promote Aβ transport across the BBB and reduce Aβ accumulation in the brain by regulating the P-gp/ECS axis.

3.2.2.2 XXD regulates the RAGE/LRP1 receptor system and MRP2 and Mfsd2a proteins

The transportation of Aβ across the BBB is mainly achieved through the RAGE/LRP1 receptor system. RAGE facilitates Aβ entry into the brain, while LRP1 mediates the removal of Aβfrom the brain. Blocking RAGE can decrease Aβ entry into the brain, inhibit NF-κB signaling and neuronal apoptosis, and improve cognitive function (Wang et al., 2018). LRP1 deficiency leads to reduced plasma Aβ, increased brain Aβ, and spatial memory deficits (Storck et al., 2016). In this study, in the hippocampal CA1 region of SAMP8 mice, the fluorescence intensity and protein expression of RAGE increased, LRP1 expression decreased, and Aβ content increased, suggesting that Aβ accumulation in the AD brain may have a relationship with the dysregulation of the RAGE/LRP1 receptor system in the BBB. Compared with the SAMP8 group, in all XXD-dose groups, RAGE expression decreased (Figure 7A, B, D, E), LRP1 expression increased (Figures 7A, C), and Aβ content decreased in the mouse hippocampal CA1 region (Figure 7F), suggesting that XXD potentially modulates RAGE/LRP1 receptor activity, thereby impeding Aβ influx into the brain while facilitating its efflux and elimination.

The ATP-binding cassette subfamily C member 1 (ABCC1), also known as multidrug resistance-associated protein 1 (MRP1), is a complete transporter exhibiting efflux capabilities. MRP1's export function serves as a crucial pathway for Aβ elimination from cerebral tissue via the blood-brain barrier (BBB). Research has demonstrated that a lack of MRP1 results in elevated Aβ

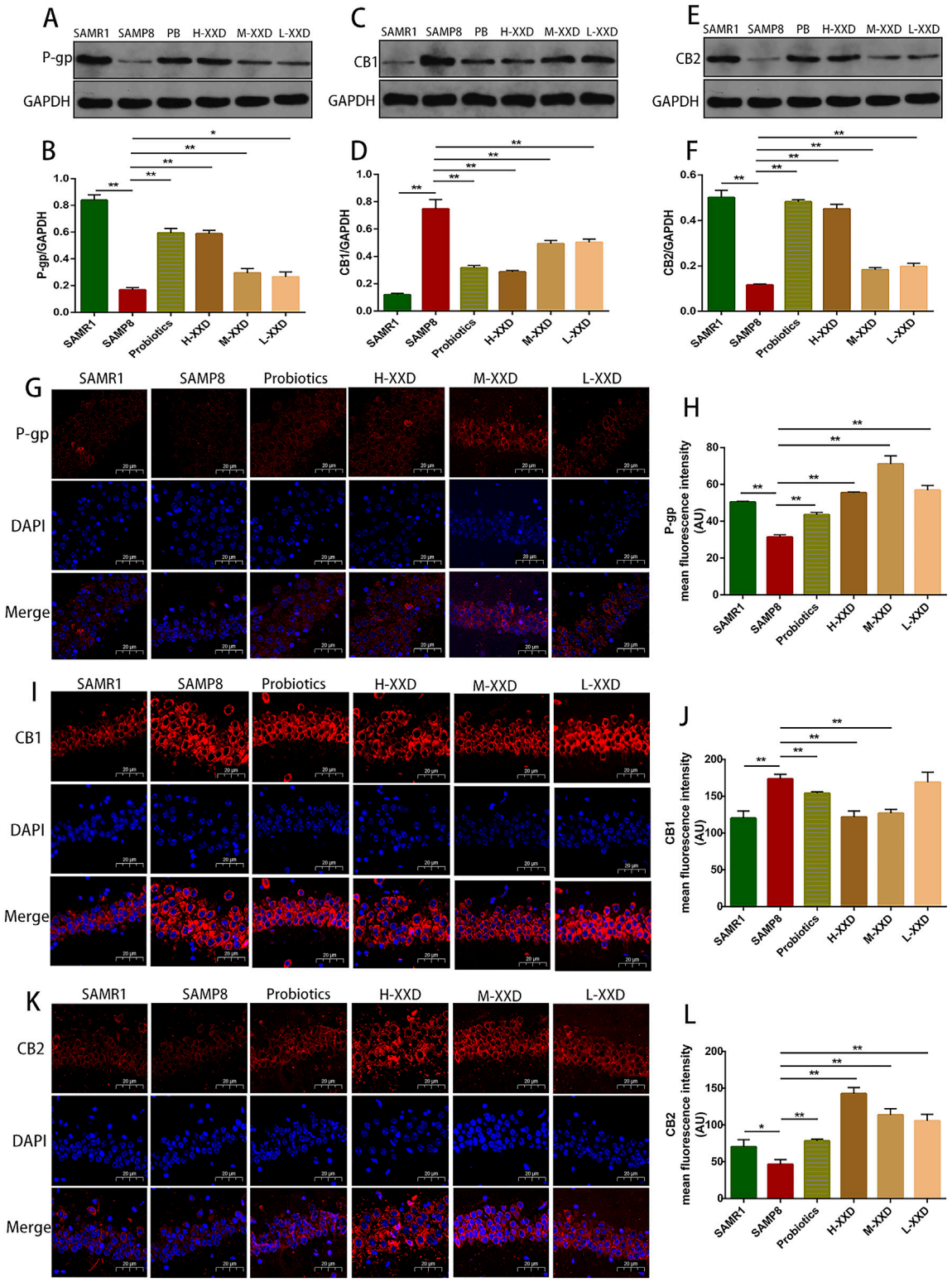


FIGURE 6
XXD Modulates the P-gp/eCBs Axis in the Hippocampal CA1 Region of SAMP8 Mice; **(A)** and **(B)** Comparison of relative P-gp protein expression levels; **(C)** and **(D)** Comparison of relative CB1 protein expression levels; **(E)** and **(F)** Comparison of relative CB2 protein expression levels; **(G)** and **(H)** Immunohistochemical staining for P-gp in the hippocampal CA1 region of mice; **(I)** and **(J)** Immunohistochemical staining for CB1 in the hippocampal CA1 region of mice; **(K)** and **(L)** Immunohistochemical staining for CB2 in the hippocampal CA1 region of mice; (n = 6); scale bar: 20μm; images captured at ×400 magnification; $^{**}p < 0.01$, $^{*}p < 0.05$.

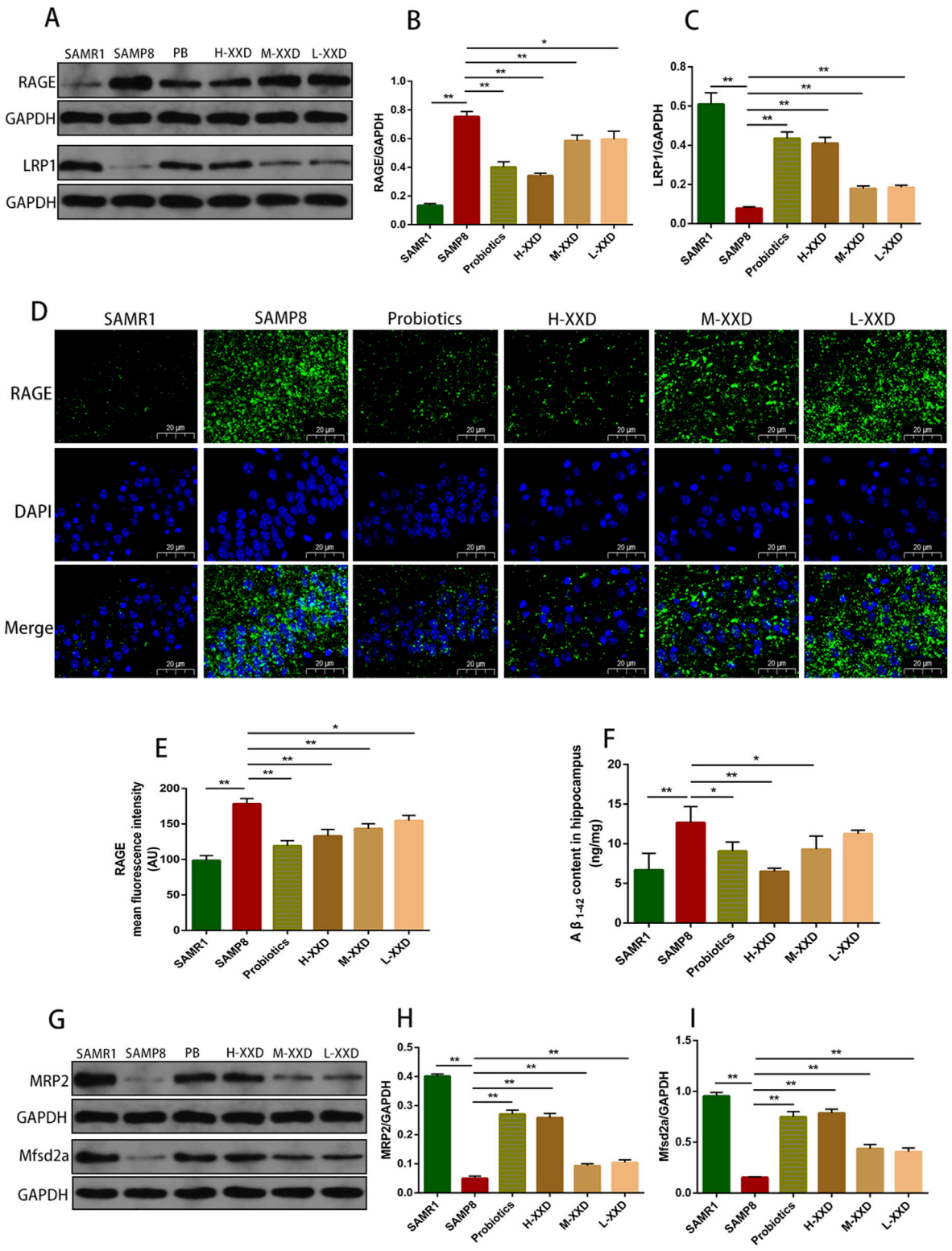


FIGURE 7
XXD Regulates the RAGE/LRP1 Receptor System and MRP2, Mfsd2a Proteins, Accelerating $A\beta_{1-42}$ Clearance in the Brains of SAMP8 Mice; **(A)**, **(B)**, and **(C)** Comparison of relative RAGE and LRP1 protein expression levels; **(D)** and **(E)** Comparison of RAGE protein positive expression in the hippocampal CA1 region; **(F)** Comparison of hippocampal $A\beta_{1-42}$ content; **(G)**, **(H)**, and **(I)** Comparison of relative MRP2 and Mfsd2a protein expression levels; (n = 6); Scale bar: 20μm; images captured at ×400 magnification; $^{**}p < 0.01$, $^{*}p < 0.05$.

concentrations within the murine brain (Aykac and Sehirli, 2021). Similarly, MRP2/ABCC2 serves as an ATP-dependent efflux transporter present in the BBB (Girardin, 2006), potentially contributing to the clearance of Aβ from the brain. In this study, MRP2 expression in the hippocampal region of SAMP8 mice decreased, while Aβ content increased, suggesting that Aβ accumulation in the AD brain may have a correlation with MRP2 deficiency. Mice in the XXD treatment groups exhibited increased MRP2 expression (Figures 7G, H) and decreased Aβ content (Figure 7F), indicating that XXD may promote Aβ efflux by enhancing MRP2 activity.

Mfsd2a is a sodium-dependent lysophosphatidylcholine (LPC) symporter present in BBB endothelial cells (Huang and Li, 2021). Studies have shown that Mfsd2a-knockout mice exhibit increased endocytosis, leading to BBB leakage (Chow and Gu, 2017). Research on rats with chronic cerebral hypoperfusion has demonstrated that Mfsd2a overexpression can reduce BBB damage and cognitive decline (Shang et al., 2019). In this study, Mfsd2a protein expression in the hippocampal region of SAMP8 mice was reduced, whereas BBB permeability increased, indicating that BBB leakage in the AD brain may be linked to the reduced expression of the nutrient transporter Mfsd2a. Compared with the SAMP8 group, in all XXD-dose groups, Mfsd2a expression in the mouse hippocampal region increased (Figures 7G, I)and BBB permeability decreased, indicating that XXD may alleviate BBB damage by increasing Mfsd2a expression.

3.2.3 XXD inhibits microglial activation and alleviates neuroinflammation in SAMP8 mice

As the primary CNS immune cells, microglia are pivotal in Alzheimer's disease (AD). Upon activation, they can adopt either the neurotoxic pro-inflammatory M1 phenotype or the neuroprotective M2 state (Xie et al., 2021). Studies have shown that Aβ stimulation can upregulate the activity marker CD68 and M1 markers TNF-α, IL-1β, and CD86 in primary microglia (Shi et al., 2017). Injection of Aβ into the mouse hippocampus also increases levels of M1 microglia (Xie et al., 2020). IBA1 is a specific calcium-binding protein participating in microglial remodeling, regulating their migration, membrane ruffling, and phagocytosis, and is commonly used to assess microglial activation (Hendrickx et al., 2017).

TREM2 is specifically expressed in microglia and has anti-inflammatory effects (Qin et al., 2021). Suppression of TREM2-mediated signaling in microglial cells enhances the expression of TNF-α and nitric oxide synthase 2 (NOS2) genes. Conversely, elevated TREM2 levels lead to decreased transcription of TNF-α, IL-1β, and NOS2 (Takahashi et al., 2005). TLRs are crucial components of the neuroimmune system, exerting a pivotal influence on microglial activation and polarization. Activation of TLRs leads to NF-κB upregulation, promoting the synthesis of inflammatory mediators including cytokines (TNF-α, IL-1β, IL-6) and enzymes (iNOS, COX2). TLR2 forms a heterodimer with TLR1, enhancing pro-inflammatory cytokine production via the MyD88-dependent pathway and NF-κB activation. Studies show that increased TREM2 expression decreases specific TLRs (2, 4, 6) and pro-inflammatory mediators (IL-1β, TNF-α, IL-6) in microglia, thereby reducing $A\beta_{1-42}$-induced neuroinflammatory responses (Long et al., 2019).

NLRP3 is a core component of the NLRP3 inflammasome, widely distributed in the CNS and highly expressed in microglia. NLRP3 recognizes exogenous or endogenous PAMPs and DAMPs, activates the downstream transcription factor NFκB, phosphorylates and degrades IκBα, facilitates NF-κBp65 nuclear translocation, initiating target gene transcription and upregulating NLRP3, IL-1β, and IL-18 precursor expression. Under PAMP and DAMP stimulation, the NLRP3 inflammasome assembles, releasing mature IL-1β and IL-18 and activating Gasdermin D, which causes microglial membrane rupture and the further release of more inflammatory factors (Hanslik and Ulland, 2020). CMPK2 is a newly discovered upstream factor of the NLRP3 inflammasome. It has been demonstrated that CMPK2 knockdown inhibits NLRP3 inflammasome activation (Chen et al., 2022).

The present research demonstrated that TREM2 expression in the hippocampus of SAMP8 mice was decreased, while IBA1, TLR1, and TLR2 expression significantly increased. Furthermore, the average fluorescence intensity of TMER2 in the mouse hippocampal CA1 region decreased, while the average fluorescence intensities of IBA1, TLR1, and TLR2 increased. Therefore, reduced TMER2 expression in the hippocampal region of SAMP8 mice can upregulate IBA1 expression and promote the overexpression of TLR1 and TLR2, thereby mediating microglia-related neuroinflammation. In addition, CMPK2 protein expression and NLRP3, NF-κB p65, COX-2, TNF-α, and IL-1β levels in hippocampal tissue were significantly increased, suggesting that microglia-related neuroinflammation in the brains of SAMP8 mice may be achieved through the CMPK2/NLRP3 and TLRs/NF-κB pathways. Compared with the SAMP8 group, in all XXD-dose groups, TMER2 expression in the mouse hippocampal region increased (Figure 8D), while IBA1, TLR1, and TLR2 expression significantly decreased (Figures 8A–C). The mean fluorescence intensity of TMER2 in the hippocampal CA1 region increased (Figure 8H), while the average fluorescence intensities of IBA1, TLR1, and TLR2 were reduced (Figures 8E–G). CMPK2 protein expression and NLRP3, NF-κB p65, COX-2, TNF-α, and IL-1β levels in hippocampal tissue were significantly decreased (Figures 9A–G). Thus, XXD may inhibit microglial activation by upregulating TMER2 expression, thereby inhibiting the activation of the CMPK2/NLRP3 and TLRs/NF-κB pathways, ultimately leading to reduced neuroinflammation.

4 Discussion

This study investigated the mechanism by which XXD ameliorates cognitive impairment in Alzheimer's disease (AD). The research revealed that AD pathogenesis is a vicious cycle: BBB dysfunction leads to excessive Aβ accumulation, which triggers neuroinflammatory responses driven by microglial activation. This inflammation further damages the BBB, perpetuating the cycle. XXD may interrupt this harmful cascade by modulating both BBB function and neuroinflammation.

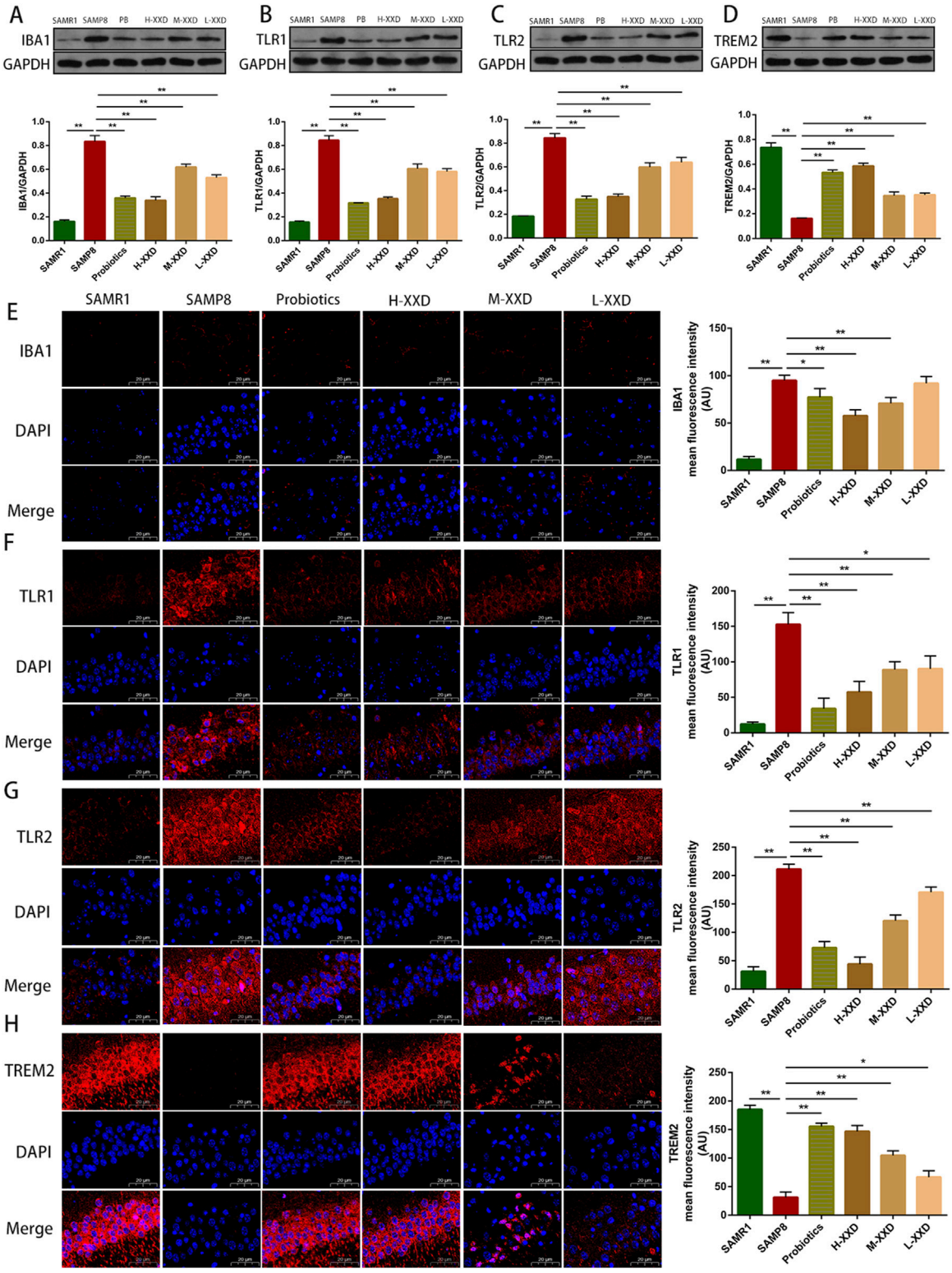


FIGURE 8
XXD Upregulates TREM2 Expression and Downregulates IBA1, TLR1, and TLR2 Expression, Inhibiting Microglial Activation; **(A)** and **(E)** Analysis of relative IBA1 protein expression levels and average fluorescence intensity of IBA1 in the hippocampal CA1 region of mice; **(B)** and **(F)** Analysis of relative TLR1 protein expression levels and average fluorescence intensity of TLR1 in the hippocampal CA1 region of mice; **(C)** and **(G)** Analysis of relative TLR2 protein expression levels and average fluorescence intensity of TLR2 in the hippocampal CA1 region of mice; **(D)** and **(H)** Analysis of relative TREM2 protein expression levels and average fluorescence intensity of TREM2 in the hippocampal CA1 region of mice; (n = 6); Scale bar: 20μm; images captured at ×400 magnification; $^{**}p < 0.01$, $^{*}p < 0.05$.

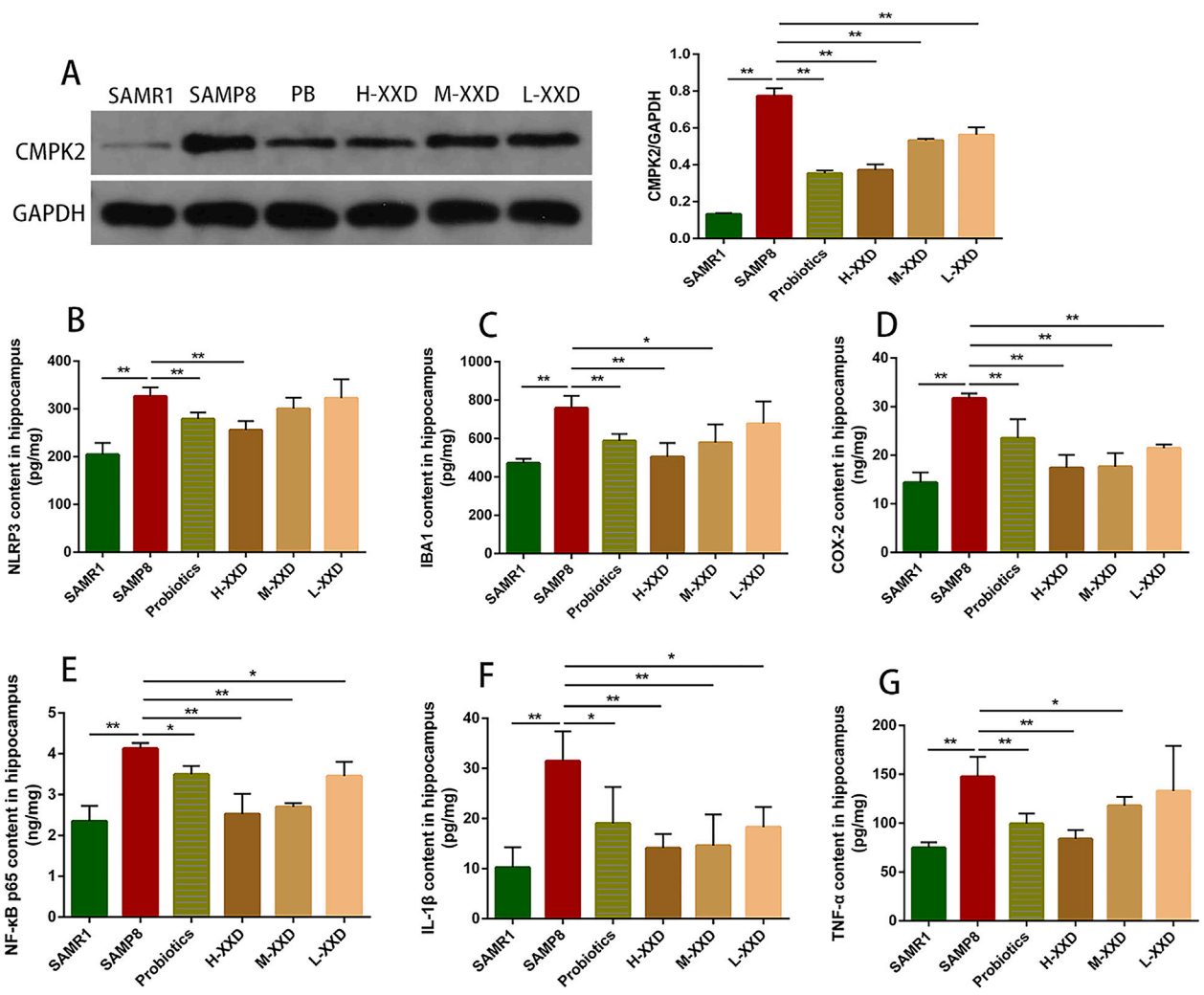


FIGURE 9
XXD reduces the levels of inflammation-related molecules and cytokines in the hippocampus: **(A)** Comparison of relative expression levels of CMPK2 protein in the hippocampus of different groups of mice; **(B)** Comparison of NLRP3 protein levels in the hippocampus of different groups of mice; **(C)** Comparison of IBA1 protein levels in the hippocampus of different groups of mice; **(D)** Comparison of COX-2 protein levels in the hippocampus of different groups of mice; **(E)** Comparison of NF-κB p65 protein levels in the hippocampus of different groups of mice; **(F)** Comparison of IL-1β protein levels in the hippocampus of different groups of mice; **(G)** Comparison of TNF-α protein levels in the hippocampus of different groups of mice. (n = 6); $^{**}p < 0.01$, $^{*}p < 0.05$.

4.1 Abnormal expression of BBB transport-related proteins and receptors promotes excessive Aβ accumulation in the AD brain

The blood-brain barrier (BBB) serves as a selective and semi-permeable boundary, restricting the infiltration of pathogens, neurotoxins, immune factors, and macromolecules from the peripheral blood into the central nervous system (CNS) (Tao et al., 2022). Simultaneously, it selectively allows the passage of essential nutrients necessary for maintaining healthy brain function (Jones and Shusta, 2007). There is substantial evidence suggesting that significant BBB dysfunction in Alzheimer's disease (AD) results in excessive accumulation of β-amyloid (Aβ) (Wang et al., 2021). The excessive deposition of Aβ in AD is a result of an imbalance between its production and clearance. The blood-brain barrier (BBB), a critical structure involved in the clearance of metabolic waste from the brain, includes various transporter proteins such as P-gp, Mfsd2a, RAGE, LRP-1, MRP, CB1, and CB2 (Pyun et al., 2022; Huang and Li, 2021; Stella, 2010; Hillard, 2018; Wang et al., 2018; Ma et al., 2018; Nies et al., 2004), which mediate the transport of Aβ into and out of the brain. *In vitro* studies demonstrated that the LPS-induced BBB damage model exhibited reduced expression of P-gp mRNA and protein, decreased levels of CB2 and Mfsd2a, and increased CB1 protein expression, suggesting aberrations in Aβ transport-related proteins and receptors under BBB damage conditions. To confirm these expression patterns in an *in vivo* AD model, SAMP8 mice were employed. The results showed impaired spatial learning and memory abilities in SAMP8 mice, along with increased Evans blue extravasation in brain tissue, indicating that cognitive deficits are linked to BBB dysfunction.

Additionally, a significant rise in $A\beta_{1-42}$ content in the hippocampus of SAMP8 mice was observed, and abnormalities were noted in the P-gp/ECS axis, the RAGE/LRP1 receptor system, as well as MRP2 and Mfsd2a levels, suggesting that the dysregulation of BBB transport-related proteins and receptors in AD contributes to excessive Aβ accumulation.

4.2 Aβ pathology promotes microglia-related neuroinflammation in the AD brain

Neuroinflammation, a consistent pathological feature throughout the progression of Alzheimer's disease (AD), accelerates the onset and progression of the disease. Studies indicate a potential link between Aβ and neuroinflammation in AD, where pathological Aβ deposition is associated with the activation of macrophages, microglia, and astrocytes, as well as the release of pro-inflammatory cytokines (Ying et al., 2023). Microglia are pivotal in driving neuroinflammation in AD; Aβ aggregation induces sustained microglial activation, resulting in elevated secretion of inflammatory cytokines and chemokines that further exacerbate microglial activity (Huang et al., 2022). Thus, alleviating Aβ accumulation in the brain may be essential for mitigating microglia-mediated neuroinflammation in AD. The results of this study show that reduced TREM2 expression in the hippocampus of SAMP8 mice can upregulate IBA1 expression and enhance the overexpression of TLR1 and TLR2, thereby mediating microglia-related neuroinflammation. Further analysis of downstream inflammatory molecules and cytokines (CMPK2, NLRP3, NF-κB p65, COX-2, TNF-α, and IL-1β) indicated that microglia-related neuroinflammation in the brains of SAMP8 mice might be mediated through the CMPK2/NLRP3 and TLRs/NF-κB pathways. Additionally, a significant increase in the Aβ content in the hippocampus of SAMP8 mice was observed, confirming that microglia-related neuroinflammation and Aβ pathology mutually promote each other.

4.3 Microglial activation-mediated neuroinflammation exacerbates BBB damage in the AD brain

Microglia are brain-resident cells that play a crucial role in immune responses within the brain. In the AD brain, activated microglia are frequently observed surrounding Aβ plaques and release inflammatory cytokines such as IL-1, IL-6, TNF-α, and TGF-β (da Fonseca et al., 2014). These inflammatory cytokines can downregulate the expression of tight junction proteins and disrupt BBB integrity through both direct and indirect pathways, thereby exacerbating BBB leakage (Hussain et al., 2021). In addition, neuroinflammation also exerts detrimental effects on BBB transport function. Studies have shown that neuroinflammation leads to a significant increase in the levels of P-gp and RAGE proteins in rat brain microvessels, both of which are critical for the bidirectional transport of Aβ across the BBB (Lai et al., 2021).

In rat brain capillaries, TNF-α exposure can induce a series of cascade events that lead to the activation of the transcription factor NF-κB, which regulates the expression and activity of P-gp, breast cancer resistance protein (BCRP), and MRP1 (Chaves et al., 2017), thus disrupting BBB transport function. In another study, the pro-inflammatory cytokine IL-6 resulted in a reduction in the immunostaining area fraction of P-gp, zonula occludens-1 (ZO-1), and aquaporin 4 (AQP4) in the brain microvessels of wild-type mice. Treatment with the anti-inflammatory cytokine IL-10 led to an increase in the immunostaining area fraction of AQP4, providing the first evidence that IL-10 can at least partially prevent IL-6-induced BBB damage (Barabási et al., 2023). In summary, neuroinflammation mediated by microglial activation exacerbates BBB integrity and transport dysfunction. Related studies have shown that LPS promotes the secretion of cytokines and chemokines by microglial cells, which are closely associated with the neuroinflammatory process (He et al., 2021). Consequently, in this *in vitro* study, LPS was employed as an inducer for the BBB inflammation damage model.

The findings demonstrated that LPS reduced P-gp mRNA and protein expression, increased CB1 expression, and decreased CB2 and Mfsd2a expression in the *in vitro* BBB model, indicating that LPS-induced neuroinflammation leads to aberrant expression of the P-gp/ECS axis and Mfsd2a, thereby impairing BBB transport function. Additionally, the *in vivo* study revealed that reduced TREM2 expression in the hippocampal tissue of SAMP8 mice upregulated IBA1 expression and promoted overexpression of TLR1 and TLR2, thus mediating microglia-related neuroinflammation. This neuroinflammation may be mediated through the CMPK2/NLRP3 and TLRs/NF-κB pathways. Further investigation showed that Evans blue extravasation in the brain tissue of SAMP8 mice was significantly elevated, while the expression of the P-gp/ECS axis, the RAGE/LRP1 receptor system, MRP2, and Mfsd2a in hippocampal tissue was markedly abnormal, indicating damage to BBB integrity and transport function. Consequently, microglial activation-mediated neuroinflammation in the AD brain exacerbates BBB integrity and transport function impairments, which, in turn, amplifies neuroinflammation, forming a vicious cycle (Takata et al., 2021).

4.4 By modulating the BBB transport function to reduce Aβ accumulation and mitigate neuroinflammation, XXD ameliorates cognitive deficits in AD

This study demonstrates the effectiveness of XXD in mitigating the deleterious cascade reaction involving blood-brain barrier (BBB) transport dysfunction, excessive Aβ accumulation, and neuroinflammation. The results show that XXD can not only regulate and restore BBB integrity and transport function, thereby reducing pathological Aβ accumulation in the brain, but also suppress neuroinflammatory responses induced by Aβ accumulation. *In vitro* results show that XXD drug-containing serum culture for 24, 48, and 72 h can upregulate P-gp mRNA and protein expression, downregulate CB1 protein expression, and upregulate CB2 and Mfsd2a protein expression, indicating that XXD may improve BBB transport dysfunction by regulating the expression of transporter-related proteins Mfsd2a and the P-gp/

ECS system. Subsequent *in vivo* studies revealed that XXD may reduce Aβ accumulation in the brains of SAMP8 mice by regulating the P-gp/ECS axis, the RAGE/LRP1 receptor system, and MRP2 and Mfsd2a proteins, promoting Aβ efflux across the BBB and inhibiting Aβ influx across the BBB. Further investigation found that XXD could upregulate TMER2 expression and downregulate IBA1, TLR1, TLR2, CMPK2 expression, thereby reducing the levels of pro-inflammatory factors NLRP3, NF-κB p65, COX-2, TNF-α, and IL-1β in hippocampal tissue. This suggests that XXD may inhibit microglial activation by upregulating TMER2 expression, thereby inhibiting the activation of the CMPK2/NLRP3 pathway and the TLRs/NF-κB pathway, alleviating neuroinflammation, and improving spatial learning and memory impairments in SAMP8 mice.

Currently, the majority of pharmacological interventions for Alzheimer's disease (AD) target single pathways. However, due to the complex pathophysiology of AD, monotherapeutic approaches often fall short in achieving comprehensive symptom improvement. Consequently, single-target therapies exhibit limitations in both long-term efficacy and disease-modifying potential. In contrast, XXD demonstrates a distinctive advantage by generating multi-target synergistic effects. Research indicates that XXD can modulate blood-brain barrier (BBB) transport function through the regulation of the P-gp/ECS axis, the RAGE/LRP1 receptor system, and the expression profiles of MRP2 and Mfsd2a proteins. This modulation facilitates the efflux of $A\beta_{1-42}$ and reduces Aβ deposition within the cerebral parenchyma. As a result, the activation of microglia triggered by Aβ oligomerization is attenuated, and the activation of the CMPK2/NLRP3 and TLRs/NF-κB pathways is suppressed. This leads to a reduction in the synthesis of pro-inflammatory cytokines and chemokines, alleviating microglia-mediated neuroinflammation in the AD brain and ultimately reducing AD-associated cognitive deficits. This multi-faceted mechanism not only enhances therapeutic efficacy but also potentially mitigates the risk of developing resistance, which is commonly associated with single-target pharmacological interventions.

Although this study has initially elucidated the multi-target mechanism of XXD, the intricate interaction networks and precise regulatory pathways require further investigation. Future research could employ cutting-edge methodologies, such as high-throughput screening, proteomic analysis, and metabolomic profiling, to further elucidate the complex mechanisms underlying XXD's multi-target actions. Such investigations are crucial for unveiling the comprehensive, multi-tiered regulatory framework that underpins XXD's therapeutic efficacy in AD management.

Data availability statement

The original contributions presented in the study are included in the article/supplementary material, further inquiries can be directed to the corresponding author.

Ethics statement

The animal study was approved by The Animal Experimental Ethics Committee of Shaanxi University of Chinese Medicine. The study was conducted in accordance with the local legislation and institutional requirements.

Author contributions

CY: Formal Analysis, Visualization, Writing–original draft. EZ: Data curation, Investigation, Writing–review and editing. HZ: Data curation, Investigation, Writing–review and editing. LD: Data curation, Investigation, Writing–review and editing. XH: Data curation, Investigation, Writing–review and editing. HD: Data curation, Investigation, Writing–review and editing. YC: Data curation, Investigation, Writing–review and editing. DW: Formal Analysis, Visualization, Writing–review and editing. XL: Formal Analysis, Visualization, Writing–review and editing. YD: Conceptualization, Funding acquisition, Methodology, Project administration, Supervision, Writing–review and editing.

Funding

The author(s) declare that financial support was received for the research, authorship, and/or publication of this article. The National Natural Science Foundation of China (No. 82074503), Shaanxi Provincial High-level Talent Special Support Program ([2018] No. 33), and the Discipline Innovation Team Construction Project of Shaanxi University of Chinese Medicine (No. 2019-QN05) contributed funding for this study.

Conflict of interest

The authors declare that the research was conducted in the absence of any commercial or financial relationships that could be construed as a potential conflict of interest.

Generative AI statement

The author(s) declare that no Generative AI was used in the creation of this manuscript.

Publisher's note

All claims expressed in this article are solely those of the authors and do not necessarily represent those of their affiliated organizations, or those of the publisher, the editors and the reviewers. Any product that may be evaluated in this article, or claim that may be made by its manufacturer, is not guaranteed or endorsed by the publisher.

References

Allt, G., and Lawrenson, J. G. (2001). Pericytes: cell biology and pathology. *Cells Tissues Organs* 169 (1), 1–11. doi:10.1159/000047855

Argueta, N., Notari, E., and Szigeti, K. (2022). Role of pharmacogenomics in individualizing treatment for Alzheimer's disease. *CNS Drugs* 36 (4), 365–376. doi:10.1007/s40263-022-00915-3

Aykac, A., and Sehirli, A. Ö. (2021). The function and expression of ATP-binding cassette transporters proteins in the Alzheimer's disease. *Glob. Med. Genet.* 8 (4), 149–155. doi:10.1055/s-0041-1735541

Barabási, B., Barna, L., Santa-Maria, A. R., Harazin, A., Molnár, R., Kincses, A., et al. (2023). Role of interleukin-6 and interleukin-10 in morphological and functional changes of the blood-brain barrier in hypertriglyceridemia. *Fluids Barriers CNS* 20 (1), 15. doi:10.1186/s12987-023-00418-3

Bateman, R. J., Munsell, L. Y., Morris, J. C., Swarm, R., Yarasheski, K. E., and Holtzman, D. M. (2006). Human amyloid-beta synthesis and clearance rates as measured in cerebrospinal fluid *in vivo*. *Nat. Med.* 12 (7), 856–861. doi:10.1038/nm1438

Chaves, C., Remiao, F., Cisternino, S., and Decleves, X. (2017). Opioids and the blood-brain barrier: a dynamic interaction with consequences on drug disposition in brain. *Curr. Neuropharmacol.* 15 (8), 1156–1173. doi:10.2174/1570159X15666170504095823

Chen, L., Diwu, Y. C., Wen, X. Q., Yue, T., Qu, X. X., Lei, X. J., et al. (2020). Effects of tonifying spleen and stomach Yuanqi prescriptions on hippocampal morphology and function and cortical cholinergic system in SAMP8 mice. *Chin. Traditional Herb. Drugs* 51, 5187–5193. doi:10.13192/j.issn.1000-1719.2020.10.052

Chen, Y., Hong, T., Chen, F., Sun, Y., Wang, Y., and Cui, L. (2021). Interplay between microglia and Alzheimer's disease-focus on the most relevant risks: APOE genotype, sex and age. *Front. Aging Neurosci.* 13, 631827. doi:10.3389/fnagi.2021.631827

Chen, Y., Wu, L., Shi, M., Zeng, D., Hu, R., Wu, X., et al. (2022). Electroacupuncture inhibits NLRP3 activation by regulating CMPK2 after spinal cord injury. *Front. Immunol.* 13, 788556. doi:10.3389/fimmu.2022.788556

Chiu, Y. J., Lin, C. H., Lee, M. C., Hsieh-Li, H. M., Chen, C. M., Wu, Y. R., et al. (2021). Formulated Chinese medicine Shaoyao Gancao Tang reduces NLRP1 and NLRP3 in Alzheimer's disease cell and mouse models for neuroprotection and cognitive improvement. *Aging (Albany NY)* 13 (11), 15620–15637. doi:10.18632/aging.203125

Chow, B. W., and Gu, C. (2017). Gradual suppression of transcytosis governs functional blood-retinal barrier formation. *Neuron* 93 (6), 1325–1333. doi:10.1016/j.neuron.2017.02.043

da Fonseca, A. C., Matias, D., Garcia, C., Amaral, R., Geraldo, L. H., Freitas, C., et al. (2014). The impact of microglial activation on blood-brain barrier in brain diseases. *Front. Cell Neurosci.* 8, 362. doi:10.3389/fncel.2014.00362

Ding, M. R., Qu, Y. J., Hu, B., and An, H. M. (2022). Signal pathways in the treatment of Alzheimer's disease with traditional Chinese medicine. *Biomed. Pharmacother.* 152, 113208. doi:10.1016/j.biopha.2022.113208

Diwu, Y. C. (2016). A re-recognition of the pathogenesis and treatment of 'marrow deficiency and turbid phlegm' in senile dementia. *J. Tradit. Chin. Med.* 57 (12), 1075–1077. doi:10.13288/j.11-2166/r.2016.12.023

Dumurgier, J., and Sabia, S. (2020). Epidemiology of Alzheimer's disease: latest trends. *Rev. Prat.* 70 (2), 149–151.

Eshraghi, M., Adlimoghaddam, A., Mahmoodzadeh, A., Sharifzad, F., Yasavoli-Sharahi, H., Lorzadeh, S., et al. (2021). Alzheimer's disease pathogenesis: role of autophagy and mitophagy focusing in microglia. *Int. J. Mol. Sci.* 22 (7), 3330. doi:10.3390/ijms22073330

Gao, Y. B., Diwu, Y. C., Tang, X. C., Gu, Z., Yang, K., Zhai, J. M., et al. (2018). Effects of Xixin Decoction on synaptic function-related proteins and receptors expression in APP/PS1 double transgenic mice. *Chin. J. Integr. Traditional West. Med.* 38, 699–706. doi:10.7661/j.cjim.20180828.242

Girardin, F. (2006). Membrane transporter proteins: a challenge for CNS drug development. *Dialogues Clin. Neurosci.* 8 (3), 311–321. doi:10.31887/DCNS.2006.8.3/fgirardin

Gómez, C. T., Lairion, F., Repetto, M., Ettcheto, M., Merelli, A., Lazarowski, A., et al. (2021). Cannabidiol (CBD) alters the functionality of neutrophils (PMN). Implications in the refractory epilepsy treatment. *Pharm. (Basel)* 14 (3), 220. doi:10.3390/ph14030220

Hajialyani, M., Hosein Farzaei, M., Echeverría, J., Nabavi, S. M., Uriarte, E., and Sobarzo-Sánchez, E. (2019). Hesperidin as a neuroprotective agent: a review of animal and clinical evidence. *Molecules* 24 (3), 648. doi:10.3390/molecules24030648

Hanafy, A. S., Lamprecht, A., and Dietrich, D. (2023). Local perfusion of capillaries reveals disrupted beta-amyloid homeostasis at the blood-brain barrier in Tg2576 murine Alzheimer's model. *Fluids Barriers CNS* 20 (1), 85. doi:10.1186/s12987-023-00492-7

Hanslik, K. L., and Ulland, T. K. (2020). The role of microglia and the Nlrp3 inflammasome in Alzheimer's disease. *Front. Neurol.* 11, 570711. doi:10.3389/fneur.2020.570711

Hartz, A. M., Miller, D. S., and Bauer, B. (2010). Restoring blood-brain barrier P-glycoprotein reduces brain amyloid-beta in a mouse model of Alzheimer's disease. *Mol. Pharmacol.* 77 (5), 715–723. doi:10.1124/mol.109.061754

He, Y., Taylor, N., Yao, X., and Bhattacharya, A. (2021). Mouse primary microglia respond differently to LPS and poly (I:C) *in vitro*. *Sci. Rep.* 11 (1), 10447. doi:10.1038/s41598-021-89777-1

Hendrickx, D. A. E., van Eden, C. G., Schuurman, K. G., Hamann, J., and Huitinga, I. (2017). Staining of HLA-DR, Iba1 and CD68 in human microglia reveals partially overlapping expression depending on cellular morphology and pathology. *J. Neuroimmunol.* 309, 12–22. doi:10.1016/j.jneuroim.2017.04.007

Hillard, C. J. (2018). Circulating endocannabinoids: from whence do they come and where are they going? *Neuropsychopharmacology* 43 (1), 155–172. doi:10.1038/npp.2017.130

Huang, B., and Li, X. (2021). The role of Mfsd2a in nervous system diseases. *Front. Neurosci.* 15, 730534. doi:10.3389/fnins.2021.730534

Huang, C., Li, Z., Qu, W., and Guo, W. (2022). Astaxanthin-folic acid combined treatment potentiates neuronal regeneration and functional recovery after brachial plexus avulsion and reimplantation. *Front. Neurosci.* 16, 923750. doi:10.3389/fnins.2022.923750

Huang, J. H., Huang, X. H., Chen, Z. Y., Zheng, Q. S., and Sun, R. Y. (2004). Equivalent dose conversion between animals and between animals and humans in pharmacological experiments. *Chin. J. Clin. Pharmacol. Ther.* 9, 1069–1072. doi:10.3969/j.issn.1009-2501.2004.09.026

Huang, S. F., Othman, A., Koshkin, A., Fischer, S., Fischer, D., Zamboni, N., et al. (2020). Astrocyte glutathione maintains endothelial barrier stability. *Redox Biol.* 34, 101576. doi:10.1016/j.redox.2020.101576

Hussain, B., Fang, C., and Chang, J. (2021). Blood-brain barrier breakdown: an emerging biomarker of cognitive impairment in normal aging and dementia. *Front. Neurosci.* 15, 688090. doi:10.3389/fnins.2021.688090

Jones, A. R., and Shusta, E. V. (2007). Blood-brain barrier transport of therapeutics via receptor-mediation. *Pharm. Res.* 24 (9), 1759–1771. doi:10.1007/s11095-007-9379-0

Kim, D. E., and Priefer, R. (2020). Therapeutic potential of direct clearance of the amyloid-β in Alzheimer's disease. *Brain Sci.* 10, 93. doi:10.3390/brainsci10020093

Kong, Z. H., Chen, X., Hua, H. P., Liang, L., and Liu, L. J. (2017). The oral pretreatment of glycyrrhizin prevents surgery-induced cognitive impairment in aged mice by reducing neuroinflammation and Alzheimer's-related pathology via HMGB1 inhibition. *J. Mol. Neurosci.* 63 (3-4), 385–395. doi:10.1007/s12031-017-0989-7

Lai, P. H., Wang, T. H., Zhang, N. Y., Wu, K. C., Yao, C. J., and Lin, C. J. (2021). Changes of blood-brain-barrier function and transfer of amyloid beta in rats with collagen-induced arthritis. *J. Neuroinflammation* 18 (1), 35. doi:10.1186/s12974-021-02086-2

Lei, X. J., Diwu, Y. C., Qu, X. X., Wen, X. Q., Yue, T., Chen, L., et al. (2020). Effects of tonifying spleen and stomach Yuanqi prescriptions on the expression of hippocampal synaptic active zone proteins cplx1/2 and stx1 in SAMP8 mice. *China J. Traditional Chin. Med. Pharm.* 35, 5811–5815.

Leng, F., and Edison, P. (2021). Neuroinflammation and microglial activation in Alzheimer disease: where do we go from here? *Nat. Rev. Neurol.* 17 (3), 157–172. doi:10.1038/s41582-020-00435-y

Levin-Arama, M., Abraham, L., Waner, T., Harmelin, A., Steinberg, D. M., Lahav, T., et al. (2016). Subcutaneous compared with intraperitoneal KetamineXylazine for anesthesia of mice. *J. Am. Assoc. Lab. Anim. Sci.* 55 (6), 794–800.

Liu, B., Liu, J., and Shi, J. S. (2020). SAMP8 mice as a model of age-related cognition decline with underlying mechanisms in Alzheimer's disease. *J. Alzheimers Dis.* 75 (2), 385–395. doi:10.3233/JAD-200063

Liu, C., Zhong, L., Tian, X. L., and Han, Y. C. (2018). Protective effects of 8-MOP on blood-brain barrier via the Nrf-2/HO-1 pathway in mice model of cerebral infarction. *Eur. Rev. Med. Pharmacol. Sci.* 22 (13), 4278–4287. doi:10.26355/eurrev_201807_15424

Liu, S., Xu, L., Shen, Y., Wang, L., Lai, X., and Hu, H. (2024). Qingxin Kaiqiao Fang decreases Tau hyperphosphorylation in Alzheimer's disease via the PI3K/Akt/GSK3β pathway *in vitro* and *in vivo*. *J. Ethnopharmacol.* 318 (Pt B), 117031. doi:10.1016/j.jep.2023.117031

Long, H., Zhong, G., Wang, C., Zhang, J., Zhang, Y., Luo, J., et al. (2019). TREM2 attenuates $A\beta_{1-42}$-mediated neuroinflammation in BV-2 cells by downregulating TLR signaling. *Neurochem. Res.* 44 (8), 1830–1839. doi:10.1007/s11064-019-02817-1

Long, Q. H., Wu, Y. G., He, L. L., Ding, L., Tan, A. H., Shi, H. Y., et al. (2021). Suan-Zao-Ren Decoction ameliorates synaptic plasticity through inhibition of the Aβ deposition and JAK2/STAT3 signaling pathway in AD model of APP/PS1 transgenic mice. *Chin. Med.* 16 (1), 14. doi:10.1186/s13020-021-00425-2

Ma, Q., Zhao, Z., Sagare, A. P., Wu, Y., Wang, M., Owens, N. C., et al. (2018). Blood-brain barrier-associated pericytes internalize and clear aggregated amyloid-β42 by LRP1-dependent apolipoprotein E isoform-specific mechanism. *Mol. Neurodegener.* 13 (1), 57. doi:10.1186/s13024-018-0286-0

Massi, P., Vaccani, A., and Parolaro, D. (2006). Cannabinoids, immune system and cytokine network. *Curr. Pharm. Des.* 12 (24), 3135–3146. doi:10.2174/138161206777947425

Nagarkatti, P., Pandey, R., Rieder, S. A., Hegde, V. L., and Nagarkatti, M. (2009). Cannabinoids as novel anti-inflammatory drugs. *Future Med. Chem.* 1 (7), 1333–1349. doi:10.4155/fmc.09.93

Nies, A. T., Jedlitschky, G., König, J., Herold-Mende, C., Steiner, H. H., Schmitt, H. P., et al. (2004). Expression and immunolocalization of the multidrug resistance proteins, MRP1-MRP6 (ABCC1-ABCC6), in human brain. *Hum. brain. Neurosci.* 129 (2), 349–360. doi:10.1016/j.neuroscience.2004.07.051

Obermeier, B., Daneman, R., and Ransohoff, R. M. (2013). Development, maintenance and disruption of the blood-brain barrier. *Nat. Med.* 19 (12), 1584–1596. doi:10.1038/nm.3407

Papa, A., Pasquini, S., Contri, C., Gemma, S., Campiani, G., Butini, S., et al. (2022). Polypharmacological approaches for CNS diseases: focus on endocannabinoid degradation inhibition. *Cells* 11 (3), 471. doi:10.3390/cells11030471

Paul, R. K., Ramamoorthy, A., Scheers, J., Wersto, R. P., Toll, L., Jimenez, L., et al. (2012). Cannabinoid receptor activation correlates with the proapoptotic action of the β2-adrenergic agonist (R,R')-4-methoxy-1-naphthylfenoterol in HepG2 hepatocarcinoma cells. *J. Pharmacol. Exp. Ther.* 343 (1), 157–166. doi:10.1124/jpet.112.195206

Peng, X., Luo, Z., He, S., Zhang, L., and Li, Y. (2021). Blood-brain barrier disruption by lipopolysaccharide and sepsis-associated encephalopathy. *Front. Cell Infect. Microbiol.* 11, 768108. doi:10.3389/fcimb.2021.768108

Pyun, J., McInnes, L. E., Donnelly, P. S., Mawal, C., Bush, A. I., Short, J. L., et al. (2022). Copper bis(thiosemicarbazone) complexes modulate P-glycoprotein expression and function in human brain microvascular endothelial cells. *J. Neurochem.* 162 (3), 226–244. doi:10.1111/jnc.15609

Qin, Q., Teng, Z., Liu, C., Li, Q., Yin, Y., and Tang, Y. (2021). TREM2, microglia, and Alzheimer's disease. *Mech. Ageing Dev.* 195, 111438. doi:10.1016/j.mad.2021.111438

Qu, X. X., Diwu, Y. C., Lei, X. J., Chen, L., Wen, X. Q., and Yue, T. (2019). Effects of tonifying spleen and stomach Yuanqi prescriptions on learning and memory and PKA/ERK/p-CREB signaling pathway in hippocampus of SAMP8 mice. *Chin. Traditional Herb. Drugs* 50, 3389–3395. doi:10.7501/j.issn.0253-2670.2019.14.018

Schoch, A., Thorey, I. S., Engert, J., Winter, G., and Emrich, T. (2014). Comparison of the lateral tail vein and the retro-orbital venous sinus routes of antibody administration in pharmacokinetic studies. *Lab. Anim. (NY)* 43 (3), 95–99. doi:10.1038/laban.481

Shang, J., Yamashita, T., Tian, F., Li, X., Liu, X., Shi, X., et al. (2019). Chronic cerebral hypoperfusion alters amyloid-β transport related proteins in the cortical blood vessels of Alzheimer's disease model mouse. *Brain Res.* 1723, 146379. doi:10.1016/j.brainres.2019.146379

Shi, X., Cai, X., Di, W., Li, J., Xu, X., Zhang, A., et al. (2017). MFG-E8 selectively inhibited aβ-induced microglial M1 polarization via NF-κB and PI3K-akt pathways. *Mol. Neurobiol.* 54 (10), 7777–7788. doi:10.1007/s12035-016-0255-y

Stella, N. (2010). Cannabinoid and cannabinoid-like receptors in microglia, astrocytes, and astrocytomas. *Glia* 58 (9), 1017–1030. doi:10.1002/glia.20983

Storck, S. E., Meister, S., Nahrath, J., Meißner, J. N., Schubert, N., Di Spiezio, A., et al. (2016). Endothelial LRP1 transports amyloid-β(1-42) across the blood-brain barrier. *J. Clin. Invest* 126 (1), 123–136. doi:10.1172/JCI81108

Szabady, R. L., Louissaint, C., Lubben, A., Xie, B., Reeksting, S., Tuohy, C., et al. (2018). Intestinal P-glycoprotein exports endocannabinoids to prevent inflammation and maintain homeostasis. *J. Clin. Invest* 128 (9), 4044–4056. doi:10.1172/JCI96817

Takahashi, K., Rochford, C. D., and Neumann, H. (2005). Clearance of apoptotic neurons without inflammation by microglial triggering receptor expressed on myeloid cells-2. *J. Exp. Med.* 201 (4), 647–657. doi:10.1084/jem.20041611

Takata, F., Nakagawa, S., Matsumoto, J., and Dohgu, S. (2021). Blood-brain barrier dysfunction amplifies the development of neuroinflammation: understanding of cellular events in brain microvascular endothelial cells for prevention and treatment of BBB dysfunction. *Front. Cell Neurosci.* 15, 661838. doi:10.3389/fncel.2021.661838

Tao, Q. Q., Lin, R. R., Chen, Y. H., and Wu, Z. Y. (2022). Discerning the role of blood brain barrier dysfunction in Alzheimer's disease. *Aging Dis.* 13 (5), 1391–1404. doi:10.14336/AD.2022.0130-1

van der Stelt, M., Mazzola, C., Esposito, G., Matias, I., Petrosino, S., De Filippis, D., et al. (2006). Endocannabinoids and beta-amyloid-induced neurotoxicity *in vivo*: effect of pharmacological elevation of endocannabinoid levels. *Cell Mol. Life Sci.* 63 (12), 1410–1424. doi:10.1007/s00018-006-6037-3

Van Gool, B., Storck, S. E., Reekmans, S. M., Lechat, B., Gordts, P., Pradier, L., et al. (2019). LRP1 has a predominant role in production over clearance of Aβ in a mouse model of Alzheimer's disease. *Mol. Neurobiol.* 56, 7234–7245. doi:10.1007/s12035-019-1594-2

Vorhees, C. V., and Williams, M. T. (2006). Morris water maze: procedures for assessing spatial and related forms of learning and memory. *Nat. Protoc.* 1 (2), 848–858. doi:10.1038/nprot.2006.116

Vulin, M., Zhong, Y., Maloney, B. J., Bauer, B., and Hartz, A. M. S. (2023). Proteasome inhibition protects blood-brain barrier P-glycoprotein and lowers Aβ brain levels in an Alzheimer's disease model. *Fluids Barriers CNS* 20, 70. doi:10.1186/s12987-023-00470-z

Wang, D., Chen, F., Han, Z., Yin, Z., Ge, X., and Lei, P. (2021). Relationship between amyloid-β deposition and blood-brain barrier dysfunction in Alzheimer's disease. *Front. Cell Neurosci.* 15, 695479. doi:10.3389/fncel.2021.695479

Wang, D., Ho, C. T., and Bai, N. (2022). Ziziphi Spinosae Semen: an updated review on pharmacological activity, quality control, and application. *J. Food Biochem.* 46 (7), e14153. doi:10.1111/jfbc.14153

Wang, H., Chen, F., Du, Y. F., Long, Y., Reed, M. N., Hu, M., et al. (2018). Targeted inhibition of RAGE reduces amyloid-β influx across the blood-brain barrier and improves cognitive deficits in db/db mice. *Neuropharmacology* 131, 143–153. doi:10.1016/j.neuropharm.2017.12.026

Wang, S., Zhu, T., Ni, W., Zhou, C., Zhou, H., Lin, L., et al. (2023). Early activation of Toll-like receptor-3 reduces the pathological progression of Alzheimer's disease in APP/PS1 mouse. *Alzheimers Res. Ther.* 15 (1), 33. doi:10.1186/s13195-023-01186-w

Wang, Y. Y., and Yan, S. Y. (2009). *Practical Chinese internal medicine*. second ed. Shanghai: Shanghai Scientific and Technical Publishers.

Wei, P. C., Lee-Chen, G. J., Chen, C. M., Chen, Y., Lo, Y. S., and Chang, K. H. (2022). Isorhamnetin attenuated the release of interleukin-6 from β-amyloid-activated microglia and mitigated interleukin-6-mediated neurotoxicity. *Oxid. Med. Cell Longev.* 2022, 3652402. doi:10.1155/2022/3652402

Winkler, E. A., Bell, R. D., and Zlokovic, B. V. (2011). Central nervous system pericytes in health and disease. *Nat. Neurosci.* 14 (11), 1398–1405. doi:10.1038/nn.2946

Wu, J. J., Yang, Y., Wan, Y., Xia, J., Xu, J. F., Zhang, L., et al. (2022). New insights into the role and mechanisms of ginsenoside Rg1 in the management of Alzheimer's disease. *Biomed. Pharmacother.* 152, 113207. doi:10.1016/j.biopha.2022.113207

Xie, L., Liu, Y., Zhang, N., Li, C., Sandhu, A. F., Williams, G., 3rd, et al. (2021). Electroacupuncture improves M2 microglia polarization and glia anti-inflammation of hippocampus in Alzheimer's disease. *Front. Neurosci.* 15, 689629. doi:10.3389/fnins.2021.689629

Xie, L., Zhang, N., Zhang, Q., Li, C., Sandhu, A. F., Iii, G. W., et al. (2020). Inflammatory factors and amyloid β-induced microglial polarization promote inflammatory crosstalk with astrocytes. *Aging (Albany NY)* 12 (22), 22538–22549. doi:10.18632/aging.103663

Xing, Z. K., Du, L. S., Fang, X., Liang, H., Zhang, S. N., Shi, L., et al. (2023). The relationship among amyloid-β deposition, sphingomyelin level, and the expression and function of P-glycoprotein in Alzheimer's disease pathological process. *Neural Regen. Res.* 18, 1300–1307. doi:10.4103/1673-5374.358607

Xiong, Y., Jiang, Y. J., and Zhu, Q. F. (2017). Clinical observation of modified Xixin decoction combined with oxiracetam in treating patients with infarctive vascular dementia. *J. Hunan Univ. Chin. Med.* 33, 50–51. doi:10.16808/j.cnki.issn1003-7705.2017.06.021

Yang, W. T., Zheng, X. W., Chen, S., Shan, C. S., Xu, Q. Q., Zhu, J. Z., et al. (2017). Chinese herbal medicine for Alzheimer's disease: clinical evidence and possible mechanism of neurogenesis. *Biochem. Pharmacol.* 141, 143–155. doi:10.1016/j.bcp.2017.07.002

Ying, C., Kang, P., Binkley, M. M., Ford, A. L., Chen, Y., Hassenstab, J., et al. (2023). Neuroinflammation and amyloid deposition in the progression of mixed Alzheimer and vascular dementia. *Neuroimage Clin.* 38, 103373. doi:10.1016/j.nicl.2023.103373

Yu, Q., Zhang, L., Xu, T., Shao, J., Yuan, F., Yang, Z., et al. (2024). Oligodendroglia-to-pericyte conversion after lipopolysaccharide exposure is gender-dependent. *PLoS One* 19 (8), e0308132. doi:10.1371/journal.pone.0308132

Zeng, Y. M., and Zhou, S. Q. (2018). Treatment of 30 cases of senile dementia with Xixin decoction. *Zhejiang J. Traditional Chin. Med.* 53, 736. doi:10.13633/j.cnki.zjtcm.2018.10.017

Zou, S., and Kumar, U. (2018). Cannabinoid receptors and the endocannabinoid system: signaling and function in the central nervous system. *Int. J. Mol. Sci.* 19 (3), 833. doi:10.3390/ijms19030833

frontiers | Frontiers in Pharmacology

TYPE Review
PUBLISHED 07 January 2025
DOI 10.3389/fphar.2024.1531288

Check for updates

OPEN ACCESS

EDITED BY
Pukar Khanal,
Emory University, United States

REVIEWED BY
Raushan Kumar Chaudhary,
Nitte Gulabi Shetty Memorial Institute of Pharmaceutical Sciences, India
Priyanka Patil,
KLE College of Pharmacy, India
Nikita Kanbarkar,
KLE University, India

*CORRESPONDENCE
Saima Khatoon,
saima.khatoon90@yahoo.com

†These authors have contributed equally to this work

RECEIVED 20 November 2024
ACCEPTED 16 December 2024
PUBLISHED 07 January 2025

CITATION
Khatoon S and Kalam N (2025) Mechanistic insight of curcumin: a potential pharmacological candidate for epilepsy. *Front. Pharmacol.* 15:1531288. doi: 10.3389/fphar.2024.1531288

COPYRIGHT
© 2025 Khatoon and Kalam. This is an open-access article distributed under the terms of the Creative Commons Attribution License (CC BY). The use, distribution or reproduction in other forums is permitted, provided the original author(s) and the copyright owner(s) are credited and that the original publication in this journal is cited, in accordance with accepted academic practice. No use, distribution or reproduction is permitted which does not comply with these terms.

Mechanistic insight of curcumin: a potential pharmacological candidate for epilepsy

Saima Khatoon[1*†] and Nida Kalam[2†]

[1]Department of Obstetrics, Gynecology and Reproductive Sciences, School of Medicine, University of Maryland, Baltimore, MD, United States, [2]Infection and Immunity Research Strength, Jeffrey Cheah School of Medicine and Health Sciences, Monash University, Bandar Sunway, Malaysia

Recurrent spontaneous seizures with an extended epileptic discharge are the hallmarks of epilepsy. At present, there are several available anti-epileptic drugs (AEDs) in the market. Still no adequate treatment for epilepsy treatment is available. The main disadvantages of AEDs are their associated adverse effects. It is a challenge to develop new therapies that can reduce seizures by modulating the underlying mechanisms with no adverse effects. In the last decade, the neuromodulatory potential of phytoconstituents has sparked their usage in the treatment of central nervous system disorders. Curcumin is an active polyphenolic component that interacts at cellular and molecular levels. Curcumin's neuroprotective properties have been discovered in recent preclinical and clinical studies due to its immunomodulatory effects. Curcumin has the propensity to modulate signaling pathways involved in cell survival and manage oxidative stress, apoptosis, and inflammatory mechanisms. Further, curcumin can persuade epigenetic alterations, including histone modifications (acetylation/deacetylation), which are the changes responsible for the altered expression of genes facilitating the process of epileptogenesis. The bioavailability of curcumin in the brain is a concern that needs to be tackled. Therefore, nanonization has emerged as a novel drug delivery system to enhance the pharmacokinetics of curcumin. In the present review, we reviewed curcumin's modulatory effects on potential biomarkers involved in epileptogenesis including dendritic cells, T cell subsets, cytokines, chemokines, apoptosis mediators, antioxidant mechanisms, and cognition impairment. Also, we have discussed the nanocarrier systems for encapsulating curcumin, offering a promising approach to enhance bioavailability of curcumin.

KEYWORDS

curcumin, epilepsy, inflammation, apoptosis, cognition, oxidative stress, epigenetics, nanocarrier systems

1 Introduction

About 70 million people worldwide suffer from epilepsy, a chronic brain disease that is considered to be one of the most common neurological disorders; 80% of those affected live in developing nations (Khatoon et al., 2021). Epilepsy is a disorder of the brain characterized by repeated electrical activity caused by dysregulation of the brain's excitatory and inhibitory mechanisms (Dua et al., 2006). Seizures typically start in confined areas of the brain and can either stay localized known as "focal," or spread to other brain parts, known as "generalized" seizures. For years, this disease was thought to be communicable

and associated with societal stigmas, earning the label "spiritual illness." Even though the blinds were eventually removed, the sickness remains a mystery. It is one of the most prevalent severe neurological illnesses and afflicts nearly 1% of the world's population, necessitating never-ending research to unravel underlying pathomechanisms (Gangar and Bhatt, 2020). According to the studies, epilepsy poses a major burden in the form of seizure-associated disability, fatalities, comorbidities, stigmatization, and major financial costs. Significant advances have been made in the previous decade or two, paving the way for an elaborative understanding of the pathomechanisms that form the basis of disease and contribute to its prognosis (Moshé et al., 2015). Epilepsy still has no definitive cure, making treatment challenging, and almost one-third of persons with epilepsy are resistant to present clinically approved medications. Currently, medications in clinical use focus on symptom alleviation rather than addressing the cause at the cellular and molecular levels. Furthermore, various anti-epileptic drugs (AEDs) developed in the recent 2 decades, with a mixed effect on the percentage of patients who obtained total seizure freedom. AEDs such as phenobarbital, phenytoin, levetiracetam, and lamotrigine have been proven to be P-gp substrates in previous investigations (Luna-Tortós et al., 2008). Furthermore, the upregulation of P-gp has been linked to drug-resistant epilepsy in both epileptic individuals and epileptic animals (Chen et al., 2017). In recent years, explorative studies focused on the molecular signaling pathways, but a shift in the focus from combating pharmacoresistance is required from the exploration for medications that decrease the symptoms (seizures) in favour of a focus on new treatments that target the primary disease.

The linked side effects often cause AEDs treatment failures. They not only cause patients to discontinue therapy early, but they also prevent patients from receiving therapeutic doses and have a detrimental impact on the adherence of patients (Toledano and Gil-Nagel, 2008). Furthermore, anti-epileptic drug side effects may cause associated disabilities, comorbidities, and death (Gilliam et al., 2004). Older medications like primidone, phenobarbital, and benzodiazepines have sedative effects ranging from insignificant drowsiness or exhaustion to profound lethargy. Drowsiness, jerking movements, vertigo, ataxia, gait impairments, vision changes, nystagmus, and tremors are the symptoms of poor coordination. All first-generation AEDs, including phenytoin, carbamazepine, primidone, and benzodiazepines, have a high risk of causing coordination problems. Second-generation anti-epileptic medicines, on the other hand, can cause these side effects (Walia et al., 2004). About 15–20 percent of epilepsy patients who take anti-epileptic medicines experience negative psychological consequences (Chen et al., 2017; Perucca and Gilliam, 2012). These side effects include irritation, aggressiveness, agitation, and violent behavior, as well as depression and psychosis (Perucca and Gilliam, 2012).

Idiosyncratic reactions are one of the concerns because they can cause life-threatening side effects and in severe cases of reaction it necessitates therapy termination. Cellular damage caused by the chemical agent or its by-product, drug, or pharmaceutically active ingredient association with unusual interaction with targets present in the host is among the processes that underpin idiosyncratic reactions associated with AEDs therapy (Zaccara et al., 2007). Furthermore, despite the availability of numerous AEDs, individuals with mesial temporal lobe epilepsy do not attain total seizure independence, and therapy with third-generation AEDs does not obviate the need for surgery (Pohlen et al., 2017). Some biologics, such as monoclonal antibodies, have been used to treat epilepsy; however, the mechanisms underlying human epileptogenesis are still unknown, and clinically meaningful targets for therapy development are still hypothetical (Zhao et al., 2017). Pharmacoresistant epilepsy is the most severe issue that requires immediate attention. The term "resistant epilepsy" is described as the "failure of adequate trials of two tolerated and correctly planned AED regimens (whether as single drug therapies or in combination) to attain seizure independence," according to the International League against Epilepsy (Weaver and Pohlmann-Eden, 2013). It is a condition in which almost 30% of epilepsy patients develop frequent seizures the despite treatment and this condition is labelled by three interchangeable phrases, known as "pharmacoresistant epilepsy," medically intractable epilepsy, or refractory epilepsy (Stafstrom and Carmant, 2015). This form of epilepsy is characterized as chronic, irreversible disorder that is also linked to increasing psychosocial and physical morbidity, as well as a high mortality rate (Englot et al., 2017). Though surgery remains a promising therapy option for pharmacoresistant epilepsy, the risk of losing brain functions renders it unsuitable for most patients. Non-pharmacological therapies such as targeted cooling, vagus nerve stimulation, and gamma knife therapy are also becoming more popular (Rocha, 2013). More than half a million patients with neurological problems have had radiosurgery with Gamma Knife, which offers a reliable, noninvasive treatment for intracranial pathology. Ionising radiation, or radiation that may remove electrons from atoms or molecules and cause chemical bonds to break, new bonds to form, or free radicals to be produced, is essential to radiosurgery. Ionising radiation breaks cellular DNA in cases of radiosurgery of the brain. Substantial percentage of individuals experience seizure independence when only patients who got high-dose radiation were studied (Rolston et al., 2011).

As a result, there is a demand for alternative drugs and therapies, which primarily involves medical techniques, change in lifestyle, and the administration of synthetic and natural medicinal moieties.

The two primary and most well-known databases for biomedical literature, PubMed and Google Scholar, were used to prepare the review. Research Gate and PubMed's electronic resources were used to access full-text documents. The most recent findings are included in the review's content, which references recent articles. Immunopathology of epilepsy, epilepsy and oxidative stress, epilepsy and cognitive impairment, curcumin and neurological disorders, curcumin and oxidative stress, curcumin and cognitive impairment, curcumin and epigenetics, and novel drug delivery systems for curcumin were the terms and phrases that were searched for. The chosen research and review articles were picked because they were closely related to the selected topic.

2 Current treatment strategy for epilepsy

With the advent of several novel anti-epileptic treatments as well as better formulations of older treatments, epilepsy pharmacotherapy has made tremendous strides in the past few

years. Since 1851, many first-generation AEDs have been developed for the treatment of epilepsy. Some of the examples of first-generation AEDs including, primidone, carbamazepine, sodium valproate, phenobarbitone, phenytoin, ethosuximide, and phenobarbitone. Later, second-generation AEDs have been developed, and some the examples, including, lacosamide, gabapentin, lamotrigine, oxcarbazepine, levetiracetam, topiramate, and zonisamide. In recent decades, novel AEDs with distinctive modes of action, including perampanel, retigabine, and brivaracetam, have been released on the market. The multiple processes by which these approved AEDs for the treatment of epilepsy function primarily involve the modulation of voltage-dependent ion channels, activation of GABA, and inhibition of glutamate receptors. Even in patients who react well to treatment, current anti-epileptic drugs have no impact on the inherent natural history or progression of the condition. Additionally, there are not any drugs on the market right now that can stop epilepsy from arising from following a head injury. It is projected that the rapid advancement of understanding of cellular, molecular, and genetic causes of epilepsy will result in more potent and prominent treatments, and preventative measures, and might cures various forms of epilepsy. Managing the condition through patient care and developing various therapeutic strategies is one of the key coping mechanisms. Numerous studies and research findings indicate that combining multiple medications can help control the disease. Different dosages of the same medications have been observed to benefit various individuals. Lamotrigine and sodium valproate has been shown to help treat partial-onset and generalized seizures in several animal models. Other commonly advised combinations include lamotrigine and topiramate for treating a variety of seizures and valproate with ethosuximide for managing absence seizures (Kwan et al., 2011; Brodie and Yuen, 1997).

Surgery is a treatment option for patients with DRE (drug-refractory epilepsy), particularly if they have a condition that can be treated surgically, such as unilateral hippocampal sclerosis or other treatable abnormalities. Therefore, after considering additional anti-epileptic drug trials, various surgical procedures can be carried out based on the indication to manage and treat seizures (Spencer and Huh, 2008). The ketogenic diet is employed as a treatment technique in children with DRE. They are also offered as newborn ketogenic diets based on formula (Kwan et al., 2011). Many different forms of seizures appear to be easier to manage with a ketogenic diet. A ketogenic diet is recognized for controlling gene expression via the epigenetic process. It has been discovered that dietary methyl donor consumption, such as choline, can significantly impact the DNA methylation process. Children with refractory seizures are often treated with ketogenic diets high in fat and low in carbohydrates (Boison and Rho, 2020).

Moreover, studies on micronutrient deficiencies, such as vitamin B12 deficiency, suggest that they may be involved in the pathway and may be helpful in future therapeutic approaches (Sinha et al., 2014). A device known as the vagus nerve stimulator has been authorized for use in adults and adolescents with partial-onset seizures refractory to anti-epileptic medications (Neal et al., 2008). The patient has a vagus nerve stimulator inserted in the chest area that produces a pulse and sends an electrical current to the neck's vagus nerve (Milby et al., 2008).

Combinations of anti-inflammatory medications that target many pathways may be expected to be more successful than individual medications alone due to the complexity of the inflammatory processes that are linked to epileptogenesis. According to research in teenage rats, treatment with anakinra plus a COX-2 inhibitor during epileptogenesis reduced chronic seizures and neuronal cell death, but not treatment with either medication alone (Kwon et al., 2013). Similar to this, when given to animals for a short period of time soon after the onset of epilepsy, VX-765 and an experimental TLR4 antagonist effectively halted the disease's progression and reduced 90% of recurrent seizures (Iori et al., 2017). During epileptogenesis, blocking only one inflammatory route imposed non-significant impact (Iori et al., 2013). Additionally, a conjunction of the ketogenic diet and MAGL inhibition in the acute stage of status epilepticus in mice produced more profound benefits than either intervention alone in stopping persistent epileptic hyperactivity (Terrone et al., 2018); additionally, in a mouse experiment, anakinra improved the ability of diazepam to shorten the period of status epilepticus (Xu et al., 2016).

2.1 Disease modifying therapies in epilepsy

Neuroinflammation, neuronal damage, synaptic reorganisation, and genetic abnormalities are some of the factors that frequently lead to epilepsy. In patients who are at risk (such as those who have had a stroke, infection, or traumatic brain damage), DMTs would try to prevent the start of epilepsy or alter the course of the disease to lessen the frequency and intensity of seizures (Kwon et al., 2013). DMTs may include approaches for avoiding neuronal damage or death, which are frequent causes of epilepsy. Examples include substances that target excitotoxicity, mitochondrial malfunction, or oxidative stress (Khatri and Juvekar, 2016). Epileptogenesis, or the development of epilepsy, can result from persistent inflammation in the brain. Anakinra and other cytokine inhibitors are examples of medications that target inflammatory pathways like IL-1β (Dilena et al., 2019). Epilepsy is thought to develop as a result of epigenetic modifications. For instance, inhibitors of histone deacetylase (HDAC) change the expression of genes to stop epileptogenesis (Teafatiller et al., 2022). When it comes to monogenic epilepsies, CRISPR technology or viral vectors can be used to compensate for or correct gene alterations such as SCN1A (Dravet syndrome) (Carpenter and Lignani, 2021). Recent developments in antisense oligonucleotides for hereditary epilepsies are one example (Li et al., 2021a). Some epilepsies are characterised by synaptic reorganisation, such as the emergence of mossy fibre in the hippocampus. In order to stop progression, potential treatments might interfere with maladaptive synaptic alterations (Danzer, 2017). DMTs might concentrate on stopping tumour growth in situations of epilepsy brought on by tumours (such as low-grade gliomas) (Seidel et al., 2022).

In order to target the fundamental causes of epilepsy instead of merely suppressing seizures, potential disease-modifying medicines are being actively investigated. Anti-inflammatory drugs that target neuroinflammation, including COX-2 inhibitors or IL-1 receptor antagonists (like anakinra), are being researched for their potential to prevent post-trauma epilepsy. Neurosteroids may assist stabilise neuronal excitability and provide long-term advantages in modulating the progression of disease. One such neurosteroid is ganaxolone, a synthetic analogue of allopregnanolone.

For epilepsy linked to tuberous sclerosis complex (TSC), mTOR inhibitors, such everolimus, are already authorised and have demonstrated potential in changing the progression of the condition. Levetiracetam and other preventative medications are also being researched for their ability to stop epilepsy after brain trauma. For certain genetic epilepsies, like Dravet syndrome and Angelman syndrome, new gene-targeted treatments, such as antisense oligonucleotides (ASOs), are being developed. These therapies provide a focused approach to disease modification.

2.2 Pharmacoresistance in epilepsy

A pharmacokinetic theory states that the overexpression of drug efflux vectors in peripheral organs results in a decrease in AED levels. This prevents medications with high enough concentrations from entering the brain and reaching the epileptic centre. This hypothesis is supported by clinical observations in which the overexpression of P-glycoprotein (Pgp), multidrug resistance protein 1, or other transporters on the blood-brain barrier and in neurons was unable to account for the decline in ASM concentration (Tang et al., 2017). The transport hypothesis states that drug efflux carrier upregulation in medication-resistant epilepsy takes place directly in the blood-brain barrier rather than in its periphery, which reduces drug absorption by the brain and, thus, causes resistance (Tang et al., 2017). One of the basic mechanisms of cognition, perception, and awareness is the alteration of the neural network. Disturbances in network activity are essential to the pathophysiology of brain disorders. Individual brain models derived from diffuse magnetic resonance imaging of fifteen individuals with drug-resistant epilepsy have been demonstrated to have prognostic power (Proix et al., 2017). Drug-resistant epilepsy is frequently linked to cortical dysplasia (Barkovich et al., 2015). According to the intrinsic severity theory, both medication resistance and the severity of epilepsy are influenced by common neurobiological processes. Hippocampal tissues taken from patients with mesial temporal lobe epilepsy, the most prevalent type of focal epilepsy that affects 40% of adults and is 30% resistant to AEDs, were subjected to a transcriptome study. Three significant gene clusters that are mostly linked to neuroinflammation and innate immunity, synaptic transmission, and neural network regulation were found to have abnormal expression in this investigation (Bazhanova et al., 2021). Different forms of epilepsy have been linked to polymorphisms in genes that encode channels, receptors, transporters, synaptic transmission, etc. Some of these polymorphisms have also been linked to refractory epilepsy (Liu et al., 2016).

2.3 Curcumin

Curcumin is a phenolic compound with enormous benefits and immense potential in treating various pathological conditions. Characteristically, it has a bright coloured lipophilic polyphenolic chemical obtained from the rhizome of the turmeric plant (Curcumin longa), which is a tropical Southeast Asian spice. Turmeric powder, which contains 2%–5% curcumin, has been used as an anti-inflammatory medication in Indian and Chinese traditional medicine for millennia. It coexists with its keto-enol tautomeric forms in a state of equilibrium. It is partially soluble in water and not very stable; however, it degrades more quickly in a basic medium. Curcumin poses multiple benefits, including, antioxidant, anti-cancer, anti-arthritic, anti-microbial, anti-diabetic, and anti-inflammatory activities, which can be used to treat a variety of ailments including tendinitis, liver cirrhosis, Alzheimer's disease, epilepsy, cardiovascular disease, low blood sugar, gastrointestinal issues, worms, inflammation, cancer, epidermis, and ocular infections. Additionally, it has shown tendency to cross the blood-brain barrier and demonstrated its protective efficacy in various neurological diseases (Eghbaliferiz et al., 2020).

The modulatory effect of curcumin on some of the cell signaling pathways responsible for its disease-modifying properties, represents in Figure 1. Curcumin has been found to modulate Toll-like receptors (TLRs) and the nuclear factor-kappa B (NF-κB) pathway, which are both involved in the innate immune response and inflammation. Curcumin interrupts the activation of TLR signaling by downregulating the expression of TLRs and inhibiting its downstream signaling molecules, like MyD88, and IRAK. Downregulation of TLR signaling can lead to reduction of proinflammatory cytokine and chemokine release, thus reduce the inflammatory cascade release.

Curcumin can inhibit the activation of NF-κB by blocking the phosphorylation and degradation of its inhibitor, IκBα, which usually leads to the nuclear translocation of NF-κB and the activation of its target genes. By inhibiting NF-κB activation, curcumin can reduce the expression of pro-inflammatory cytokines, chemokines, and other inflammatory mediators. Curcumin has also been found to modulate the nuclear factor erythroid 2-related factor 2-antioxidant response element (Nrf2-ARE) pathway, which is involved in the regulation of cellular antioxidant and detoxification responses. Curcumin has been found to have complex effects on the apoptosis signaling pathway. In terms of the extrinsic and intrinsic pathways, curcumin has been reported to modulate both pathways.

According to Nutraceutical Bioavailability Classification Scheme curcumin exhibits poor bioaccessibility, but it is fairly soluble in gastrointestinal fluids and unstable to alkaline pH. Due to its diketone moiety, curcumin often occurs in the solid phase and the keto form in acidic and neutral environments. Curcumin has limited stability at pH = 7 and weak solubility in water. Furthermore, curcumin has a low bioavailability. In fact, it is quickly metabolized in the gut, where it undergoes substantial biotransformation before being quickly eliminated (Xie et al., 2011; Nabavi et al., 2018). These variables collectively cause the concentration of this molecule in human plasma to be at nanomolar levels, which restricts its biological functions. The detailed mechanism of action of curcumin in inhibiting the process of epileptogenesis will be discussed in the following sections.

2.4 Effect of curcumin on neurological disorders

Curcumin extensively studied for its potential neuroprotective effects and potential as a therapeutic agent in treating neurological

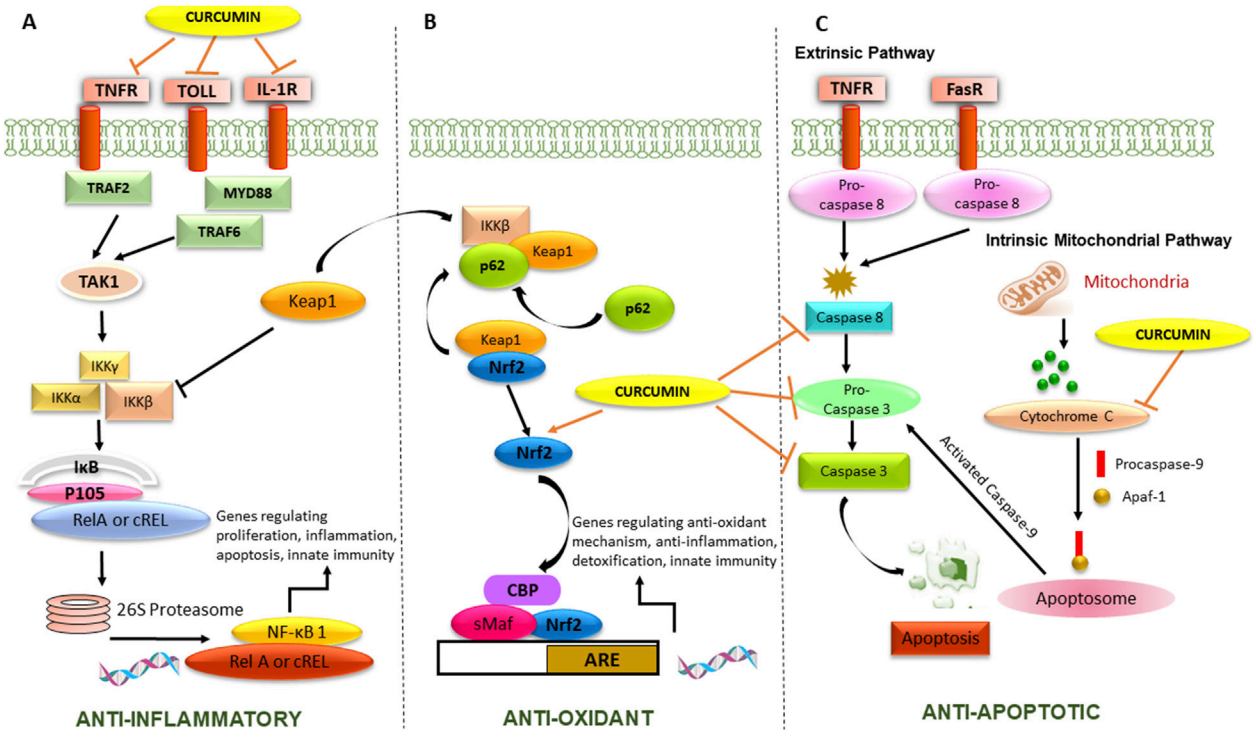


FIGURE 1
Mechanism of action of curcumin responsible for its anti-epileptic activity. The Figure illustrates **(A)** Anti-inflammatory activity by inhibiting cell surface receptors and NF-κB transcription factor, playing a pivotal role in regulating cytokines and chemokines, **(B)** Antioxidant activity by potentiating Nrf2-ARE pathway responsible for transcription of antioxidant genes, **(C)** Anti-apoptotic activity by inhibiting extrinsic and intrinsic mitochondrial pathway.

diseases. One of the most studied neurological diseases with curcumin is Alzheimer's disease (AD). Curcumin has been shown to have various potential neuroprotective effects in AD, including reducing the accumulation of β-amyloid (βA) plaques, decreasing neuroinflammation, and reducing oxidative stress. Studies in animal models of AD have shown that curcumin can improve cognitive function and memory, reducing the disease's pathological features (Lin et al., 2022). Curcumin also aids in preserving mitochondria from the damaging effects of AD; for example, it lessens the oxidative stress brought on by βA in PC12 and the levels of IL-1β and oxidized proteins in the brain of AD mice (Kim et al., 2001; Lim et al., 2001).

Curcumin extensively studied for its potential therapeutic effects in other neurological diseases, including Parkinson's disease (PD), multiple sclerosis (MS), Huntington's disease, and depression.

Treatment with 1-methyl-4-phenyl-1,2,3,6-tetrahydropyridine (MPTP) increased the heat shock protein 90 (HSP90) level in SH-SY5Y dopaminergic cells, but curcumin restored this effect. HSP90's overexpression boosted the effects of curcumin on PD, most likely through the elevation of HSP90. HSP90's silencing considerably reduced the effect caused by curcumin; on the other hand, it enhanced its benefit (Sang et al., 2018). Curcumin reversed motor impairments in the rotenone-PD rat model and boosted the activity of antioxidant enzymes that underpin it is *in-vivo* antioxidant capacity, possibly acting in a neuroprotective way (Khatri and Juvekar, 2016). Moreover, it reversed hippocampal synaptic changes (Darbinyan et al., 2017). Lewis bodies' primary constituent, α-Syn, can bind to curcumin and prevent it from accumulating in neuronal cells (Ahmad and Lapidus, 2012).

The autoimmune encephalomyelitis model for MS (multiple sclerosis) was used as animal models for investigation of effect of curcumin in MS. Reportedly, curcumin inhibited cytokines, IFNγ, IL-17, and IL-12 family members (Kanakasabai et al., 2012). These findings are consistent with those from a related rat model in which curcumin treatment enhanced the degree of myelination, most likely via restoring iNOS mRNA expression and amplifying the Nrf2 cellular defense system against oxidative damage (Mohajeri et al., 2015). Additionally, curcumin increased all the markers for oligodendrocyte progenitors and neural stem cells, including nestin (a marker for NSCs), Olig2, platelet-derived growth factor receptor (PDGFR), and brain-derived neurotrophic factor (BDNF) and nerve growth factor (NGF) (Mohajeri et al., 2015).

Micelle nanoformulation of curcumin with dose of 80 mg/day was investigated in a human clinical studies and demonstrated to decrease Th17 cells population in the peripheral circulation post 6 m months after 6 months, 80 mg/day (Dolati et al., 2018). The study also examined the effect of curcumin Th17 cells because its association with elevated levels of IL-23 and IL-17A as well as increased expression of retinoic acid-related orphan receptor γ (RORγ) in MS patients. This study also reported that treatment with micelle formulation of curcumin treatments significantly decreased RORγ mRNA levels and decreased IL-17 secretion but did not affect the expression profiles and concentration of IL-23 mRNA (Dolati et al., 2018).

NSC-34 cells infected with TDP-43 were used as Amyotrophic lateral sclerosis (ALS) cellular model to evaluate the effect of curcumin treatment in ALS in reversing the impairment caused by the overexpression of TDP-43. It was observed that uncoupling protein-2 levels were significantly reduced due to curcumin produced a beneficial effect on mitochondrial membrane potential (Lu et al., 2012). The initiation and spread of action potentials (APs), facilitated by the overexpression of TDP-43, are also a part of curcumin's protective actions (Dong et al., 2014). Post 1 year of curcumin treatment, an ALS clinical trial utilizing nanocurcumin as an adjunctive therapy to riluzole demonstrated discovered a noticeably higher survival rate (Ahmadi et al., 2018).

The progression of post-ischemic neurodegeneration was seen to be prevented by curcumin treatment utilizing a middle cerebral artery occlusion (MCAO) in a rodent model (Pluta et al., 2015), decreased infarct volume (Zhao et al., 2010; Funk et al., 2013) and oedema of the brain at various times intervals and can achieve improved neurological scores (Zhao et al., 2010; Funk et al., 2013). The reduction of oxidative stress probably brings about these results. Moreover, curcumin decreased neuronal apoptosis by increasing the anti-apoptotic Bcl2 protein and decreasing the translocation of cytochrome-c into the cytoplasm (Zhao et al., 2010; Xia et al., 2017), and reduction of mitochondrial membrane potential (Zhang et al., 2017). Also, it has been demonstrated that curcumin has a protective effect in an intrinsically hypertensive rat model and is stroke-prone, preventing the development of stroke and improving survival rates. The presence of more mitochondrial anion carrier family proteins and the physiological regulation of mitochondrial ROS production caused by curcumin is the most plausible causes of these effects (Lan et al., 2018). These findings were further supported by an *in vitro* cellular model utilizing H_2O_2 to mimic oxidative stress reduced by curcumin therapy (Lan et al., 2018). Therefore, this review will mainly dissect the impact of curcumin on epileptogenic processes.

2.5 Curcumin and its immunomodulatory effect

According to human clinical studies, curcumin is considered to be risk-free if consumed at a se of 10 g/day, and no toxicity is observed in the individuals (Aggarwal et al., 2003; Jurenka, 2009). Curcumin consist of profound activities including, antioxidant, anti-inflammatory, antibacterial, hepatoprotective, neurogenesis-inducing, chemopreventive, and chemotherapeutic action (Aggarwal et al., 2003; Roberts et al., 2017; Asteriou et al., 2018; Bianchi et al., 2018; Kadam et al., 2018; Platania et al., 2018; Sharma et al., 2018; Vucic et al., 2018). Newer research has also presented an intriguing view of curcumin's immunomodulatory potential (Jagetia and Aggarwal, 2007; Momtazi et al., 2016). Curcumin's immune-modulating activities are attributable to its interactions with cells that mediate immunologic reactions, such as B and T-lymphocytes, macrophages, dendritic cells, cytokines, and the transcription factors involved in cell signaling pathways. Curcumin is reported to act by regulating the pleiotropic regulator of inflammation, NF-κB, PPARγ, signal transducer and activator of transcription (STAT), activator protein-1 (AP-1), Nrf2, beta catenin, and their downstream targets in signaling pathways (Han et al., 2002; Shishodia et al., 2007; Gonzales and Orlando, 2008; Soetikno et al., 2011; Ganjali et al., 2014).

The combination of p50/NF-κB1, p52/NF-κB2, p65/RelA, c-Rel, and RelB forms the NF-κB transcription factor dimers family. These transcription factors play a key role in chronic inflammation and are implicated in development, inflammation, and immunological response (Hayden and Ghosh, 2008; Hoesel and Schmid, 2013; Ledoux and Perkins, 2014). In T-lymphocytes, NF-κB plays a vital role in the synthesis of pro-inflammatory molecules such as interleukin (IL)-16, IL-4, IL-2, interferon γ (IFN-γ) and TNF-α (Infantino et al., 2014; Valim et al., 2015; Zhang et al., 2016; Templin et al., 2017). Curcumin exerts pleiotropic effects by impeding NF-κB transcription by inhibiting I kappa B kinase-a (IKK-a) phosphorylation, degrading I kappa B alpha degradation, inhibiting phosphorylation of I kappa B serine 32, and blocking RelA nuclear translocation (Jobin et al., 1999; Grandjean-Laquerriere et al., 2002; Banik et al., 2017). B-lymphocyte stimulator (BLYS) is a cytokine produced mainly by monocytes, dendritic cells, and macrophages in the innate immune system (Nardelli et al., 2001; Bossen and Schneider, 2006). B-cell activating factor (BAFF) plays an immunological role in the immune system's B cell arm and immunoglobulin synthesis that could influence the functioning of B cells eventually (Ng et al., 2004). BLYS and BLYSR protein expression levels are much higher in TLE patients and in tissues of rodent epilepsy models, suggesting that BAFF and BAFFR may play critical roles in regulating immunological and inflammatory responses involved with disease development (Huang et al., 2011; Ma et al., 2017). Curcumin has been suggested as a potential new therapeutic drug for autoimmune illnesses by targeting BLYS. Curcumin's inhibitory action on the expression of BLYS is attributed to its disruption of NF-κB signaling, which decreases p65 nuclear translocation (Huang et al., 2011). Curcumin also suppresses immune function by inhibiting mammalian target of rapamycin (mTOR) pathway and subsequently downregulating cytokine production, such as IL-6 and COX-2. It has a solid ability to block the PI3K/Akt/mTOR pathway in the SH-SY5Y cell line and in the rat model of TLE (Drion et al., 2018; Zhu and Zhu, 2018).

3 Pathogenesis of epilepsy

3.1 Immunopathology of epilepsy

The adaptive immune system after pilocarpine-induced status epilepticus is reflected by a biphasic rise of $CD45^+$ immune cells in the hippocampus brain parenchyma, including innate macrophages and $CD3^+$ T-lymphocytes. The hippocampus macrophages have higher granularity, which indicates that they are activated (Neumann et al., 2017). Microglial cell activation has been reported to increase the expression of IL-6, IL-1β, and TNF-α (Aronica and Gorter, 2007; Aronica and Crino, 2011) and is allied with compromised blood-brain barrier integrity (Lucas et al., 2006).

Elevated CD8-positive T lymphocytes are a hallmark of several CNS disorders involving inflammation (Bernal et al., 2002; Petito et al., 2006) which can eventually cause the precipitation of epileptic seizures. This is supported by research examining the

immunological profile of patients with Rasmussen's encephalitis. Rasmussen's encephalitis is a progressive epileptic disease that causes the affected hemisphere to be destroyed due to unihemispheric lymphocytic infiltrates, microglial nodules, and neuronal death. T-lymphocyte fraction of brain parenchyma was primarily composed of $CD8^+$ cells. $CD4^+$ cells is reported to concentrate in the perivascular region of blood vessels rather than moving into the brain parenchyma. In addition, a cytotoxic T-cell mechanism has been postulated to play a role in neuronal death in human brain disease (Bien et al., 2002a). Assuming infiltrating T lymphocyte density is a criterion for inflammatory processes, disease duration, and neuronal cell death are inversely associated with this attribute. T lymphocyte levels fall as the disease progresses, but neuronal death increases. However, it should be emphasized that the number of T lymphocytes in the blood is still higher than in healthy people (Bien et al., 2002b). These observations corroborate the theory that cytotoxic T-cell reaction against neuronal cells leads to its loss. According to certain studies, these T cells encompass cytotoxic granules and are located near neurons (Bauer and Bien, 2009). This research could indicate that these cells have a role in neuronal cell death. In addition to Th1 and Th2 T cells, anti-inflammatory $CD4^+CD25+Foxp3+$ regulatory T cells (Tregs) and pro-inflammatory T helper 17 (Th17) cells have been discovered. Th17 cells with retinoic acid-related orphan receptor gt (RORgt) play vital roles in generating IL-17, whereas Treg cells expressing the transcription factor, Foxp3, possess anti-inflammatory activity and preserve self-component tolerance (Oukka, 2007; Krasovsky et al., 2009). Th17/Treg balance is crucial for disease progression, and is evident in various studies of different animal models and human autoimmune and inflammatory diseases (Noack and Miossec, 2014). Patients with epilepsy have reduced circulating numbers of total lymphocytes, $CD4^+$ T cells, and natural killer cells, according to studies (Bauer et al., 2008). Th17/Treg imbalance has been identified as a defining hallmark of intractable epilepsy (Ni et al., 2016). Recurrent epileptic activity in the brain can be caused by various inflammatory conditions, such as viral or autoimmune disease, highlighting the importance of inflammation in epilepsy pathogenesis (Vezzani, 2014). Furthermore, prolonged seizure activity stimulates glia and causes endothelial cells to upregulate adhesion molecules, making it easier for leukocytes to extravasate (Librizzi et al., 2007).

3.2 Dendritic cells in epilepsy

Dendritic cells (DCs) are the antigen-presenting cells (APCs) and are the sentinels of the immune system to capture antigens or access self-proteins unusually present in the environment and present them to the surface of T cells to assemble an antigen specific immune response or elicit tolerance, acting as bridge between both the innate and adaptive immune responses. These cells have been linked to a variety of brain disorders, although their exact function is uncertain. It is intended to consider relevant material from the disciplines of immunology and neurology. T lymphocytes' adaptive immune response is dependent on the detection of antigens presented by APCs. Small peptides in extended conformation are seen in these cells, which are produced from antigenic proteins linked to major histocompatibility complex MHC-I and MHC-II molecules. These two are presented differently because they are degraded at two different places inside the APC (Villadangos, 2001). Antigens obtained from external proteins are managed by the endocytic route via lysosomal enzymes and expressed by MHC-II. Presentation via MHC-I molecules, on the other hand, is based on cytosolic antigen recognition in the endoplasmic reticulum, which usually involves endogenous molecules, excluding a specialized condition known as "cross-presentation," which requires the diffusion of exogenous proteins from lysosomal compartment to cytoplasm (Guermonprez et al., 2002).

Effector T-cells can develop from naive T cells that detect peptides linked to MHC molecules. Central and peripheral tolerance mechanisms ensure the eradication of anti-self-reactive T-cells. T-cell anergy, apoptosis, or Tregs ensure tolerance to self-antigen when immature APCs present self-antigen to T cells in the lymph nodes (Starr et al., 2003; Torres-Aguilar et al., 2010). Non-lymphoid peripheral organs may have more peptides released by MHC molecules than lymphoid organs (Clement and Santambrogio, 2013). They might play a role in the onset and development of autoimmune diseases (Collado et al., 2013). The situation of the interactions between T cells and APCs dictates whether naive T cells are primed or tolerated (Steinman, 2003). As a result, APCs play an essential role in tolerance pathomechanisms, and the characteristics of these cells and their surrounding environment influence whether tolerance or immunity is generated. DCs and T-cells interact via CD40:CD40L, resulting in the production of various cytokines and chemokines, including TNF-α, IL-1β, IL-12, type I interferon, and macrophage inflammatory protein-1 (Guermonprez et al., 2002; Banchereau and Steinman, 1998). Furthermore, the transition from immature DCs (iDCs) to mature DCs (mDCs) results in the expression of C-C chemokine receptor type 7 (CCR7) and loss of adhesion to epithelial cells, resulting in relocation towards lymph node T-cell-rich regions (Guermonprez et al., 2002; Winzler et al., 1997).

Recurrent seizures can be caused by several inflammatory conditions, such as viral or autoimmune disease, highlighting the importance of inflammation in epilepsy pathogenesis (Vezzani, 2014). Prolonged electrical activity during seizures stimulates glial cells and causes endothelial cells to upregulate adhesion molecules, allowing leukocytes to extravasate more easily (Librizzi et al., 2007). This reaction is not an associated epiphenomenon of the involved tissue as inhibition of cell infiltration can avert the process of ictogenesis (Fabene et al., 2008). Interestingly, efforts have been made to administer immunomodulatory agents to treat epilepsy (Vezzani, 2015). By secreting cytokines, altering neurotransmitter release or uptake, elevating BBB permeability, and injuring neuronal cells, inflammatory cells increase neuronal excitation and reduce seizure thresholds (Vezzani, 2014). Li et al. (2013) recently demonstrated that DCs might be detected 24 h after the production of seizures in adult rats using Li-pilocarpine-induced status epilepticus model. $CD11^+$ cells were transferred from the periphery and were not derived from microglia, according to negative Iba-1 labelling and radiation experiments. In addition, after kainic acid-induced convulsions, EYFP-expressing cells were identified in the damaged hippocampus of the Cd11c/eyfp Tg animal (Bulloch et al., 2008). FCD (focal cortical dysplasia) is a

disorder in which children develop chronic epilepsy due to spontaneous abnormalities in the cerebral cortex (Rhodes et al., 2007; Iyer et al., 2010).

Along with neurotransmitter imbalance, emerging data suggests that inflammatory mechanisms are involved in non-infectious epilepsy. In the tissue of patients with FCD, stimulation of microglia and macrophages has been observed (Boer et al., 2008). It is unclear if this inflammatory reaction is induced by recurrent episodes of seizures or is an inherent mechanism of FCD. DCs circulates in the blood arteries in chronic epileptic encephalopathy and FCD type II patients' samples, together with perivascular T-lymphocytes (Rhodes et al., 2007; Iyer et al., 2010). PI3K-mTOR pathways are primarily associated with experimental epilepsy and clinical epilepsy studies (Iffland et al., 2022; Nguyen et al., 2022). In addition, through the PI3K/Akt/mTOR signaling pathway, the inflammatory response elicited by IL-1β increases seizure activity and plays a significant role in the pathophysiology of MTLE (Xiao et al., 2015). Also, as evident, the mTOR pathway controls DC's function and maturation (Sathaliyawala et al., 2010). Since autoantibodies have been identified in several kinds of epilepsy, such as Rasmussen encephalitis, this suggests that DCs may be involved in the pathophysiology of epilepsy by preserving a persistent state of inflammation, potentially by triggering autoimmune processes (McNamara et al., 1999). Activation of the mTOR pathway in the CNS can affect neuronal signaling and excitation, axonal and dendritic morphology, the release of neurotransmitters, synaptic plasticity, cognition, and behavior (Bekinschtein et al., 2007; Jaworski et al., 2005; Tang et al., 2002). Axonal and dendritic structure, neurotransmitter production, neuroplasticity, and cognition and behavior are all influenced by mTOR activity in the CNS (Wong, 2013). In animal models of epilepsy and human tissue samples removed from epilepsy patients showed evidence of overactive mTOR signaling pathways in both hereditary and acquired epilepsies. For example, mutations in elements of the mTOR system cause many neurodevelopmental diseases with epileptic symptoms, the most known of which are TSC1/TSC2 and phosphatase and tensin homolog (PTEN) mutations. TSC is an autosomal dominant disorder characterized by cortical abnormalities such as tubers and subependymal giant cell astrocytomas in the brain caused by a heterozygous mutation either in TSC1 or TSC2 (Jülich and Sahin, 2014). TSC1 and TSC2 proteins form a complex that inhibits mTOR activity; therefore, deletion of these proteins causes hyperactive mTOR signaling, intellectual impairment, refractory epilepsy, intellectual impairment, and an autistic-like phenotype (Chu-Shore et al., 2010; Vignoli et al., 2015). PTEN is a tumour suppressor gene that also regulates cellular proliferation and survival while inhibiting mTOR activity (Bonneau and Longy, 2000). Loss of PTEN causes hyperactive mTOR signaling, seizures, and substantial intellectual and behavioral deficits, comparable to mutations in TSC1/TSC2 (Cupolillo et al., 2016).

3.3 Epilepsy and oxidative stress

Calcium signaling is involved in regulating and maintaining neuronal function, encompassing the release of neurotransmitters, neuronal excitation, neurite outgrowth, neuronal plasticity, transcription, and survival of neurons. The mitochondria regulate the free intracellular Ca^{2+} present in cells through various transport mechanisms and preserve Ca^{2+} homeostasis, and work as a Ca^{2+} buffer that regulates the intracellular Ca^{2+} levels; when Ca^{2+} levels get accumulated in the mitochondria, it is released in the matrix, and this progression involves oxidative stress and reduction of adenine nucleotides (Orrenius et al., 2007). Overload of mitochondrial Ca^{2+} ions causes the MPTP opening, eventually leading to necrosis because of ATP depletion or caspase-mediated apoptosis; this explains the multifarious interdependence between Ca^{2+} influx and ROS production (Martinc et al., 2012). Ca^{2+} release in the endoplasmic reticulum and initiation of the caspase-dependent apoptosis cascade through alterations in mitochondrial membrane permeability persuade damage of cells (Harrison et al., 2005; Pinton et al., 2008). Increased activation of glutamate receptors induces oxidative stress, referred to by the excitotoxicity event, and, plays a crucial role in seizure-induced damage (Epstein et al., 1994).

Generalized epilepsy is the chronic form of epilepsy that is distinguished by repeated seizures and causes excessive levels of ROS and RNS in the brain tissue; a series of clinical and preclinical research have documented the association between epileptic seizures and ROS. It is an interesting fact that it is still unclear whether oxidative stress is a basis or result of seizures; it is extensively stated that elevated free radical production can cause persistent seizure activity, which might ultimately result in dysfunction of mitochondria in the limbic structures of the brain that causes neuronal cell damage and loss during epileptogenesis (Chen et al., 2010). However, several preclinical models of epilepsy have shown varying results regarding changes in the redox mechanism. No changes in the levels of GSH in the cortex were observed at 4 h post-SE, signifying that GSH might play an uneven role in the cortex but not in the hippocampus (Gluck et al., 2000), as few studies reported a reduction in hippocampal redox level after SE (Liang and Patel, 2006; Ong et al., 2000). A time-reliant reduction in GSH/glutathione disulfide (GSSG) ratio along with an adequate surge in glutathione peroxidase (GPx) activity and a reduction in glutathione reductase (GR) activity in tissue homogenates and a mitochondrial fraction of hippocampi, subsequent kainic acid-induced SE, have been documented (Liang and Patel, 2006). Increased neuronal injury in the CA3 region occurs between two to 7 days after KA treatment after the onset of reported redox alterations, proposing that oxidative stress might result in seizure-induced apoptosis (Liang et al., 2000; Patel et al., 2001; Mariani et al., 2005). However, studies of oxidative stress or mitochondrial incapacity in the human brain are scarce due to the small tissue accessibility.

LPO has been extensively used as an oxidative stress marker in experimental animals, observations documented that kainic acid-induced seizure susceptibility is accompanying mitochondrial OS due to elevated mitochondrial LPO and disturbed GSH homeostasis in the hippocampus (Shin et al., 2008). Several human studies have reported a reduction of antioxidant levels in the blood of individuals with myoclonic epilepsy and showed that the Cu–Zn–SOD activity in epileptic patients was lesser than in the control individuals (Ben-Menachem et al., 2000). Similarly, a study reported that the GSH, GPx, total antioxidant status, and vitamin-E levels in erythrocytes of the refractory epilepsy group were lower than in the control (Yürekli and Nazıroğlu, 2013).

NF-E2-related factor 2/antioxidant response element (Nrf2/ARE) signaling pathway is a cytoprotective system that occurs endogenously (Xing et al., 2015). The transcription factor

Nrf2 localizes to the cell's nucleus after activation, forming heterodimers with certain other transcription factors like c-Jun before binding to the ARE (Zhang et al., 2019). Several genes involved in cell anti-inflammatory and antioxidant mechanisms, such as NAD(P)H quinone oxidoreductase 1 (NQO1) and heme oxygenase-1 (HO-1), are regulated by Nrf2-ARE binding (Colín-González et al., 2013; Zhong and Tang, 2016). Furthermore, in animal and cell culture models of neurological illnesses such as Parkinson's disease, Alzheimer's disease, and epilepsy, initiation of the Nrf2/ARE pathway plays a crucial role (Calkins et al., 2009; Wang et al., 2014). It has been reported that oxidative stress has a role in the onset and progression of seizures (Sudha et al., 2001). Increased free radicals result in membrane lipid peroxidation and lower glutathione levels in the epileptic brain region (Shi et al., 2018). Furthermore, activation of the Nrf2-ARE pathway in the hippocampus reduced the development of amygdala kindling and improved cognitive impairment and oxidative stress caused by epileptic seizures (Wang et al., 2014; Shi et al., 2015). In conclusion, activating the Nrf2-ARE pathway may significantly protect against seizure-related brain damage.

3.4 Epilepsy and cognition impairment

In epilepsy patients, psychiatric comorbidities are relatively prevalent. Cognitive impairment appears to be one of the main comorbidities allied with chronic epilepsy among these comorbidities (Gaitatzis et al., 2004; Kanner, 2016; Zhu et al., 2017). Despite mounting epidemiological and experimental evidence pointing to a link between epilepsy and neuropsychiatric comorbidities such as memory and cognitive deficiency, the molecular processes underlying this association are unknown.

Extended cytokine-mediated inflammatory signaling activation leads to the dysfunction of neurons culminating in cognitive impairments, which have now been understood better (Cunningham and Sanderson, 2008), and increased activation cytokine signaling in the brain hampers memory and learning (Dantzer et al., 2008). Through cytokine-mediated collaborations among neurons and glia, inflammatory processes inside the CNS contribute to cognitive impairment (Wilson et al., 2002). The activated microglia release inflammatory molecules and free radicals, which cause tissue damage and neurotoxicity through processes such as oxidative stress and synaptic reorganization, all of which are linked to cognitive deficits (d'Avila et al., 2018). Memory retention and hippocampal-dependent learning are both facilitated by neurogenesis (Drapeau et al., 2007). Also, neuroinflammation and redox imbalance coupled with mitochondrial stress and dysfunction can negatively impact cognitive performance, either actively or passively, through decreased hippocampal neurogenesis (Kodali et al., 2018). According to growing evidence, cytokines such as IL-1β, IL-6, and TNF-α have been implicated in the molecular mechanisms involved in learning and memory. Synaptic pruning is considered to be induced by TNF-α and IL-1β production, resulting in decreased synaptic plasticity and morphological brain alterations that have a deleterious impact on memory function (Rosenblat et al., 2014). Cytokines appear early during inflammatory events and promote a more lasting inflammatory reaction. These chain of events could be particularly damaging to the susceptible hippocampus area, creating learning and cognitive impairments (Elderkin-Thompson et al., 2012). These inflammatory cytokines' effects on cognitive functioning can be described as follows: IL-1β may alter neurogenesis and long-term potentiation (LTP); IL-6 influences neural plasticity and neurogenesis; and TNF-α disturbs LTP and synaptic transmission (McAfoose and Baune, 2009). TNF activates two receptors, TNF-p55 (TNFR1) and TNF-p75 (TNFR2), which have a variety of biological consequences. TNF affects synaptic efficiency by increasing surface expression of α-amino-3-hydroxy-5-methyl-4-isoxazolepropionic (AMPA) receptors, which is facilitated by TNFR1 and phosphatidylinositol 3 (PI3) kinase and has the propensity diminish synaptic inhibition via endocytosis of GABA receptor (Stellwagen et al., 2005). TNF's neuromodulatory effects in the brain, as well as its part in synaptic plasticity, were demonstrated by these molecular actions.

Learning and cognitive decline in epileptic patients is attributed to apoptosis during epileptogenesis (Arend et al., 2018). The extrinsic apoptosis pathway is comprised of insults facilitated by death receptors, while in the intrinsic mitochondrial pathway, death signals can either act in a direct or indirect manner on mitochondria, causing cytochrome C release and ultimately forming apoptosome complex (Kajta, 2004; Krantic et al., 2007). Different expressions of several caspases have been studied in brain samples of epileptic patients; the caspases being confined within soma and dendrites of neuronal cells, displaying caspase-mediated damage of proteins (Schindler et al., 2006; Henshall et al., 2012). In surgically resected neocortex tissues from TLE patients, there was a significant increase in the levels of anti-apoptotic mediators Bcl-2 and Bcl-xL compared to the controls. The Bcl-xL has a direct correlation with the frequency of seizures in an epileptic patient. This signifies that the in the pathogenesis of human epilepsy, both pro-apoptotic and anti-apoptotic mechanisms have contributory roles (Henshall et al., 2000).

Similarly, several other studies have revealed gene expression of Bcl-2, procaspase, and caspase in the hippocampus of patients with TLE (Henshall and Engel, 2013). Also, correlative analysis has shown that apoptosis-related gene expression, including p53, Fas, Bax, Bcl-2, and caspase-3, conferring that apoptotic mechanisms get stimulated in TLE patients with mesial temporal sclerosis (Xu et al., 2007). Furthermore, occasional TUNEL-positive cells with apoptotic cells were present in the hippocampus of TLE patients (Henshall and Engel, 2013).

3.5 Epigenetic mechanisms in epilepsy

Epilepsy is a complex disorder that is characterized by alterations in cell functioning which is a cause of complexity. Significant alterations in gene expression and regulation of these gene expressions drive this abnormal cellular function. Recent research has identified epigenetic modulation of gene expression as a significant regulator with rapid and sustained changes. Many elements of cellular physiology are regulated by epigenetic-mediated gene output, including the structure of neurons and release of neurotransmitters, ion channel protein availability, and other essential neuronal activities (Ryley Parrish et al., 2013). Sites for post-translational changes, such as phosphorylation, acetylation, ubiquitination, and methylation, can be found in the N-terminal

tails of histone proteins (Davey et al., 2002). Histone alterations can affect the chromatin organisation and subsequent transcriptional activation on their own or in combination with other epigenome features (176,177). Acetylation of lysine residues on histones' N-terminal tails culminates in a much more transcriptionally favorable situation (Creyghton et al., 2010). Acetylation of histones is regulated by two opposing enzymes histone acetyltransferase (HATs), which is the writer, and the eraser, histone deacetylases (HDACs), which is the eraser (Jagirdar et al., 2015). Acetylation is carried out by HATs, which catalyse the allocation of acetyl moiety to lysine residues, leading to the neutralization of histones' charge and facilitation of the chromatin structure (Carrozza et al., 2003). HDACs eradicate these acetyl moieties from histones, increase their positive charge, and cause chromatin compaction (Jagirdar et al., 2016). Acetylation of histone is known to have an important homeostatic function in plasticity, and synaptogenesis in the brain (Crosio et al., 2003; Farrelly and Maze, 2019). In both experimental and human TLE, studies have found rapid and permanent modifications in the acetylation of lysine at the promoter region of numerous genes, as well as dissimilarities in the activity of HDAC (Huang et al., 2012; Brennan et al., 2016). Following SE induction, there was a reduction in H4 acetylation at the glutamate receptor, GluR2. In the pilocarpine rat model, however, there was an acetylation upsurge at the brain-derived neurotrophic factor (BDNF) promoter after SE (Huang et al., 2002), and induction of c-fos through epileptic processes implies the role of acetylation in controlling mechanisms involved in epilepsy development (Sng et al., 2006). Also, SE causes energy-dependent HDAC Sirtuin 1 (SIRT1) activation, which further leads to the depletion of H4K16ac, implying a connection between epileptogenic events and epigenetic alteration (Hall et al., 2017). In both preclinical animals of epilepsy and human TLE, HDAC2 expression is increased, which could lead to the deregulation of genes associated with the synaptic function (Huang et al., 2012; Huang et al., 2002). Bromodomains (BrDs) are the proteins involved in reading histone tails (Pal et al., 2003). BRD2 is a member of the BrD subfamily, and it is linked to adolescent-onset epilepsy, known as Juvenile Myoclonic Epilepsy (JME) (Pal et al., 2003). Single nucleotide polymorphisms have been discovered at the promoter region of the BRD2 gene, which could contribute to the progression of JME (Cavalleri et al., 2007).

DNA methylation is the epigenomic change that has received the most attention. The addition of a methyl group covalently from S-adenyl methionine (SAM) to the cytosine at the fifth position generates 5-methylcytosine (5 mC). The enzyme family known as DNA methyltransferases (DNMTs) is responsible for this alteration. DNMTs are classified into three families: DNM3b, DNMT1, and DNMT3a (Fatemi et al., 2005; Kinde et al., 2015). DNMT3a and DNMT3b causes the methylation of novel sites on the genome, while DNMT1 keeps pre-existing methylation marks (Song et al., 2012). Depending on the methylation site and the conditions involved, DNA methylation can both stimulate and suppress gene expression (Barrès et al., 2009) even though it is most commonly associated with gene repression (Iguchi-Ariga and Schaffner, 1989; Bird and Wolffe, 1999). The predominance of DNA methylation occurs at CpG dinucleotide and is linked to transcriptional inhibition (Fatemi et al., 2005). CpG islands have a high frequency of promoter regions, which improve availability and stimulate transcription, but methylation of CpG has the reverse effect (Jeziorska et al., 2017). DNA methylation is now known to be dynamic, with methyl groups that can be modified or erased from DNA by eraser enzymes (Ma et al., 2009). DNA methylation is expected in the nervous system and is required for appropriate brain function, especially development and neuronal plasticity (Tsankova et al., 2007; Borrelli et al., 2008; Feng et al., 2010). A variety of illness conditions, including a number of epileptic syndromes, have been associated with abnormal methylation patterns (Kobow et al., 2009; Miller-Delaney et al., 2012; Dębski et al., 2016). Kobow and co-workers demonstrated changes in DNA methylation in rats with chronic epilepsy and hypothesised that DNA methylation might play a pathomechanistic function in the process of epileptogenesis, thus contributing to gene dysregulation (Kobow et al., 2013). Hypermethylation was found to be prevalent in the pilocarpine model of TLE in rats, and it was linked to downregulated gene expression (Kobow et al., 2013). Further research has discovered that epilepsy is caused by a change in the levels of DNA modifying enzymes, namely, DNMT1 and DNMT3a, reportedly elevated in TLE, mainly in neural cells, implying that *de novo* methylation and its regulation has a role to play in human TLE (Zhu et al., 2012). William-Karnesky and colleagues provided important functional insights by showing that inhibiting methylation of DNA in different experimental models of seizures could reduce the genesis of epilepsy. The researchers utilised adenosine increase to reverse the DNA hypermethylation and discovered that it stopped mossy fibre sprouting in the region of the hippocampus and stopped the progression of the disease for 3 months. The relevance of aberrant DNA methylation in the process of epileptogenesis was underlined in this work, with reversal slowing disease development (Williams-Karnesky et al., 2013). Intriguingly, activation of the focal amygdala led to reduced promoter methylation and enhanced gene expression (Dębski et al., 2016). Dębski et al. (2016), experimented with DNA methylation profiles in epilepsy animal models such as pilocarpine, traumatic brain injury, and amygdala stimulation and reported no resemblance in differentially methylated genes. These findings suggest that methylation of DNA is very context-dependent, and epilepsy's aetiology has a significant impact on genetic expression and epigenetic alterations (Dębski et al., 2016). As there were diverse methodologies utilized to collect samples from models of seizures used, this may be possible that factors like anesthetic regimes, rodent strain, etc., influenced the observed methylation patterns (Dębski et al., 2016). In the intra-amygdala KA model of TLE in mice, a genome-wide methylation investigation found substantial differential methylation compared with controls, with hypermethylation being the maximum evident (Miller-Delaney et al., 2012). In human TLE, 146 genes presented changed DNA methylation patterns with hippocampal sclerosis, most of which were hypermethylated. Furthermore, methylation at the promoter regions and start sites of transcription was found to be responsive to several microRNA-encoding genes (Miller-Delaney et al., 2015).

4 Overview of curcumin's effect on epilepsy

4.1 Effect of curcumin on inflammatory mediators

According to a growing body of research, epileptogenesis is supposed to be aided by cellular inflammatory signaling in the brain.

Based on accumulated evidence from clinical and preclinical studies, seizure causes the release of inflammatory mediators at the cellular and molecular level, which has the potential to cause brain excitability and neuronal degeneration (Vezzani et al., 2011). Both clinical and experimental acquired epilepsies demonstrated relationship between seizures and inflammatory mediators (Friedman and Dingledine, 2011; de Vries et al., 2012; Devinsky et al., 2013; Aronica et al., 2017), whereas the involvement of inflammation in hereditary epilepsies is a relatively recent area of study for scientists (Shandra et al., 2017).

In surgically isolated brain tissues from drug-resistant epilepsy patients showed the presence of the inflammatory cascade from drug-resistant epilepsy patients, with reactive gliosis and upregulation of chemokines and cytokines. Chemical or electrical seizures in experimental models of epilepsy cause fast growth of an inflammatory process in the brain (Vezzani et al., 2013) and other areas of the CNS. Glial cells rapidly release cytokines such as IL-1β, TNF-α, IL-6, and HMGB1 (Vezzani et al., 2011), and the expression of cytokine receptors is increased in neurons, microglia, and astrocytes (Balosso et al., 2005) after seizures. In addition to cytokine production, other types of inflammatory mediators, such as prostaglandins (PG), significantly rise after seizures (Shimada et al., 2014). Following seizures, the enzyme cyclooxygenase-2 (COX-2) is rapidly activated in the brain, which is responsible for PG production (Yoshikawa et al., 2006). Experimental and human TLE are both associated with a substantial activation of the classical complement pathway (Aronica et al., 2007). During epileptic episodes, chemokines and associated receptors are also produced (Foresti et al., 2009; Cerri et al., 2016). Cytokines interact with their receptors and activate signaling pathways that cause the production of chemokines, cytokines, enzymes, and receptors, resulting in an inflammatory response. For example, IL-1β and HMGB1 bind to IL-1R1 and TLR-4, respectively, activating intracellular pathways that lead to the NF-κB. The transcription factor NF-κB regulates the expression of several genes involved in neuroinflammation, synaptic plasticity, and cell death/survival and is a common molecule triggered by inflammatory ligands (O'Neill and Kaltschmidt, 1997). As evidenced by the current literature, neuroinflammatory pathways play a critical role in seizure initiation and progression (Balosso et al., 2005; Maroso et al., 2010). By mediating increased calcium influx through NMDA receptors, IL-1β, for example, exerts powerful pro-convulsant effects (Vezzani et al., 2013). Chemokines directly impact neuronal excitability by interacting with receptors expressed at both the presynaptic and postsynaptic levels (Rostène et al., 2007). In cerebellar neurons, for example, CCL2 can modify electrophysiological properties and calcium signaling (van Gassen et al., 2005), inhibits inhibitory responses in neurons in the spinal cord (Gosselin et al., 2005), and in the Schaffer collateral circuit of the hippocampus, potentiates excitatory postsynaptic currents (Zhou et al., 2011). The p38 MAP kinase pathway is critical for mediating the effects of chemokines (Cho and Gruol, 2008). Chemokines are overexpressed in epileptic patients, according to several studies. CCL2 has also been discovered to be substantially expressed in surgically removed brain tissues (Choi et al., 2009), and CCL3 and CCL4 levels have been found to be elevated in MTLE patients (van Gassen et al., 2008). Furthermore, in MTLE models, the CC chemokine receptor 5 (CCR5) is upregulated in the brain vasculature (Louboutin and Strayer, 2013).

According to studies, curcumin can modify these inflammatory pathways linked to neurological diseases. Hyperactivity of cyclin-dependent kinase 5 (Cdk5)/p25 is linked to the production of amyloid and tau pathology in Alzheimer's disease (AD). Curcumin inhibited p25-mediated glial activation and the generation of pro-inflammatory chemokines/cytokines in an animal model (Sundaram et al., 2017). Curcumin's anti-inflammatory activity was further shown in a recent study by reducing TNF-α and IL-6 in the brain areas of a middle cerebral artery blockage stroke model (Zhang et al., 2017). Curcumin has been shown to suppress astrocyte activation by inhibiting the NF-κB signaling pathway, which resulted in decreased astrocyte release of the chemokines MCP-1, RANTES, and CXCL10, as well as decreased macrophage and T-cell infiltration, reducing inflammation in the glial scar in the spinal cord injury (Yuan et al., 2017). Curcumin inhibited the expression of T-cell co-stimulatory molecules (CD80 and CD86) and MHC class II, decreased the levels of pro-inflammatory cytokines (IL-17, IFN-γ, and TNF-α), increased the levels of anti-inflammatory cytokine IL-10, and increased the number of NKR-P1 (+) cells (natural killer cell receptor protein 1 positive cells) in an animal model of myasthenia gravis (Wang et al., 2016). Huang et al. (2018), have discovered that curcumin protects neurons by inhibiting autophagic activity via the PI3K/Akt/mTOR pathway, as well as suppressing inflammatory mediators via the TLR4/p38/MAPK signaling. Curcumin was reported to be efficient in reducing glial activation in the PTZ kindling epilepsy model. In the brains of kindled rodents, mRNA and protein levels of pro-inflammatory cytokines (IL-1β, IL-6, TNF-α), and chemokines (MCP-1) were elevated, which was decreased by curcumin administration (Kaur et al., 2015) (Figure 2). The effect of curcumin on inflammatory mediators induced during epilepsy, is shown in Table 1.

4.2 Effect of curcumin on dendritic cells

Curcumin suppresses the maturation and activity of murine bone marrow-derived DCs (BMDCs) by lowering the expression of CD86, CD80, and MHC-II molecules (Kim et al., 2005). The secretion of IL-12 and other inflammatory cytokines was found to be decreased in curcumin-treated BMDCs, resulting in a suppression of Th1-mediated immune responses. Curcumin was discovered to retain DCs in an immature stage in addition to its inhibitory effects on BMDCs (Kim et al., 2005). The effects of curcumin and hydroethanolic extracts of turmeric were tested on human DCs in *in-vitro* conditions. Decreased expression of co-stimulatory molecules (CD86, CD80, and CD83), lower production of cytokines, as well as reduction of $CD4^+$ proliferation were all discovered in the study (Krasovsky et al., 2009; Shirley et al., 2008). Additionally, when DCs were treated with curcumin, both chemokine release and cell movement were inhibited, resulting in less communication between DCs and T-cells (Shirley et al., 2008). Curcumin-treated DCs have phenotypic characteristics that are comparable to iDCs, and T-cells interacting with these DCs possess tolerogenic functions (Shirley et al., 2008). Curcumin has been demonstrated to reduce the expression of MHC-II molecules, co-stimulatory molecules (CD80, CD40, CD86, CD252, CD205, CD54, and CD256), and inflammatory cytokines in $CD8^+$ DCs, hence slowing their

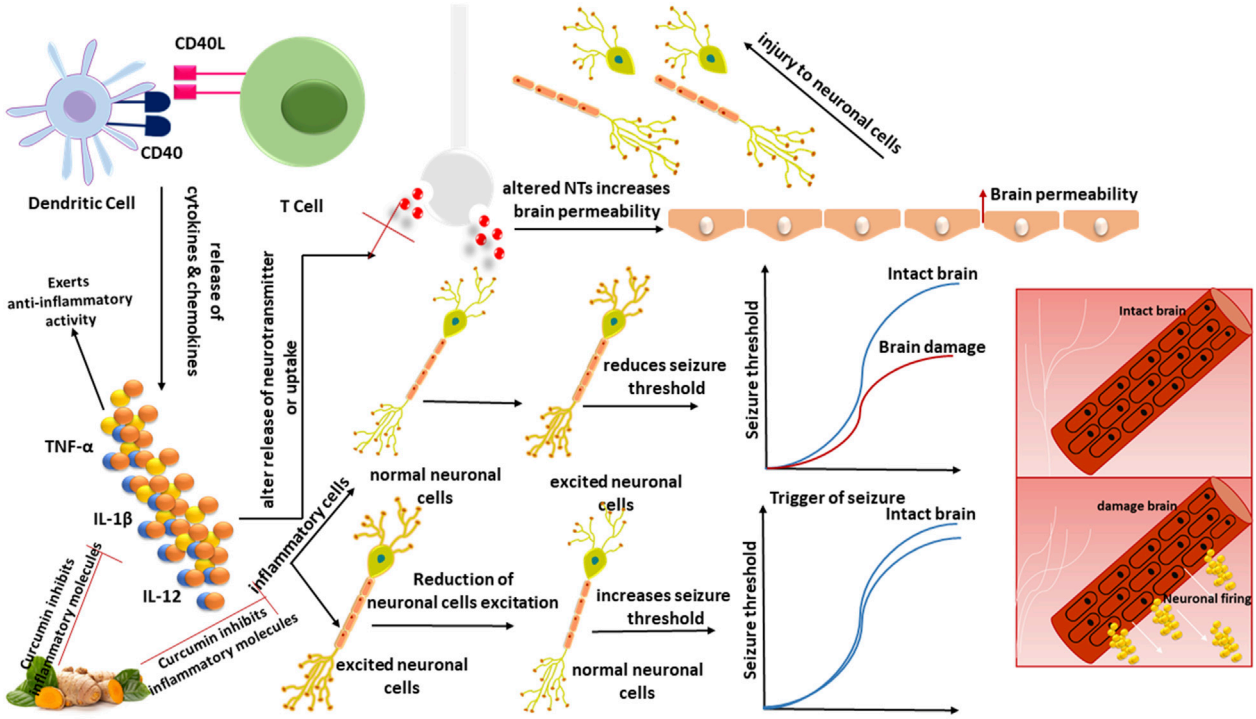


FIGURE 2
TNF-α, IL-1β, and IL-12 are among the cytokines and chemokines produced due to the interaction between DCs and T-cells via CD40:CD40L. Inflammatory cells raise BBB permeability, modify neurotransmitter release or uptake, damage neuronal cells, and secrete cytokines, raising neuronal excitement and lowering the seizure threshold. Reducing inflammatory mediators in the brain regions demonstrates curcumin's anti-inflammatory effect.

maturation and eventual Th1 response (Zhao et al., 2016a; Zhao et al., 2016b). The iDCs were discovered to be incapable of competently triggering the T-cell responses, resulting in an upsurge in the frequency of Tregs in gut-associated lymphoid tissue, providing a "recovery effect" (Zhao et al., 2016a). Similarly, it has been observed that injecting curcumin-treated DCs in BALB/c mice causes $CD4^{+}CD25+FoxP3+$ Treg cells to proliferate (Rogers et al., 2010). Curcumin inhibited STAT1 activation in bone marrow-derived DCs by impeding Janus-activated kinase 1/2 and protein kinase C delta phosphorylation, preventing STAT1 translocation and attaching to the GAS component of the IRF-1 promoter (Jeong et al., 2009). Curcumin has immunomodulatory effects on the AP1 and NF-κB pathways (activator protein) pathways (Ruzicka et al., 2018). Curcumin can also inhibit DC stimulation and maturation by modulating the Janus Kinase (JAK)/STAT pathway (Zhao et al., 2016b). Curcumin derivatives have also been shown to inhibit NF-κB and MAPK pathways by downregulating the downstream targets of the IKK/IκB/NF-κB and c-Raf/MEK/ERK inflammatory cascades (Razali et al., 2018). Curcumin alleviated asthma symptoms in a mouse model by stimulating the Wnt/β-catenin signaling pathway in DCs, which caused decreased expression of co-stimulatory markers (CD86, CD40, and CD11c), as well as decreased $CD4^{+}$ T-cells activation and proliferation (Yang et al., 2017). Curcumin, owing to its anti-inflammatory activities, appears to alter several immune-mediated responses, and so can be a probable therapeutic compound for the management and treatment of seizures, according to accumulating experimental evidence.

4.3 Effect of curcumin on oxidative stress

Curcumin appeared to provide neuroprotection against oxidative stress, according to a growing body of research, by modulating oxidative stress-induced brain injury and a cascade of inflammation and apoptotic signaling (Tiwari and Chopra, 2012). Curcumin increases cell survival in the hippocampus by reducing oxidative stress, as seen by reduced malondialdehyde and glutathione levels (Keskin-Aktan et al., 2018).

Nrf2 is a widely distributed protein in the central nervous system that has been considered a significant regulator of brain inflammation and oxidative stress. Curcumin enone compounds can activate Nrf2, a transcription factor that regulates phase II detoxification and antioxidant genes (Deck et al., 2018). Benzodiazepines (BZDs) are a class of medications used as anxiolytics, sedatives, and, most significantly, anticonvulsants (Griffin et al., 2013). They are more recognized for clinical concerns like cognition and neuropsychomotor deficiency and their role in long-term memory impairment (Buffett-Jerrott and Stewart, 2002). Curcumin reduced the levels of oxidative stress in the blood and the hippocampus and decreased the extracellular signal-regulated kinase (ERK 1/2)/nuclear transcription factor-NF-κB/pNF-κB pathway in a diazepam-induced cognition impairment model, according to a recent study (Sevastre-Berghian et al., 2017). Curcumin can also prevent early brain injury by reducing oxidative stress caused by subarachnoid hemorrhage by inhibiting NF-κB activation (Cai et al., 2017). With the systemic injection of

TABLE 1 Effect of curcumin administration on neuroinflammation induced during epilepsy.

S.No.	Experimental model of epilepsy	Species used	Dose of curcumin	Route of administration	Duration of intervention	Findings	Reference
1	KA-induced SE	Wistar rats	100 mg/kg	Intraperitoneal	14 days	Attenuation of astrocytes activation in the hippocampus, reduction of IL-1β and TNF-α levels in the hippocampus	Jiang et al. (2015)
2	PTZ-induced kindling	Wistar rats	100 mg/kg	Oral	30 days	Significant lowering of cytokines (IL-6, IL-1β, TNF-α) and chemokine (MCP-1) activation in kindled rats (in both hippocampus and cortex). Upregulated expression of Iba-1 and GFAP in curcumin-treated experimental animals. Moreover, a significant lowering of activated glial cell number was observed upon administration of curcumin	Kaur et al. (2015)
3	Organotypic hippocampal-entorhinal cortex slice culture	Sprague Dawley rats	Concentration in medium: 0.05%	NA	21 days	Lowering of pS6 expression at one phosphorylation site. Downregulation of mRNA expression of IL-1β, IL-6 and TGF-β	Drion et al. (2019)
4	KA-induced epilepsy	Sprague Dawley rats	100 mg/kg	Oral	7 days	IL-1β and NLRP3 expression were reduced upon curcumin administration. Curcumin repressed the NLPR3/ inflammasome activation and decreased neuronal loss in the hippocampus region	He et al. (2018)
5	*In vitro*: Astrocyte cell culture *In vivo*: electrically induced SE	Human fetal brain tissue, Sprague Dolly rats	*In vitro*: 10 μM, *In vivo*: 2 μL of 2 mM curcumin solution	Intracerebral ventricle	7 days	Curcumin suppressed the MAPK pathway in cultured astrocytes; curcumin decreased the expression of IL-6 and COX-2 in cultured astrocytes. In electrically induced SE, curcumin administration did not suppress the inflammatory markers	Drion et al. (2018)

Abbreviations: KA, Kainic acid; **SE**, Status epilepticus; **IL-1β**, Interleukin-1 beta; **TNF-α,** Tumour necrosis factor-alpha; **IL-6**, Interleukin-6; **MCP-1**, Monocyte chemoattractant protein -1; **GFAP**, Glial fibrillary ancillary protein; **TGF-β**, transforming growth factor-β; **NLRP3,** NLR family pyrin domain containing 3; **SE**, Status epilepticus; **MAPK**, mitogen-activated protein kinase; **COX-2**, Cyclooxygenase-2.

kainate, curcumin can prevent hippocampus cell loss and lessen seizures in mice (Shin et al., 2007). In a kainic acid epilepsy model, curcumin drastically reduced MDA levels and improved glutathione levels, which are oxidative stress markers (Gupta et al., 2009). Curcumin pre-treatment reduced oxidative stress indicators in a comparable model in another investigation (Kiasalari et al., 2013). PTZ-kindling is a type of persistent epilepsy marked by a steady rise in seizure susceptibility. PTZ kindling promotes molecular and cellular changes in the hippocampus, which are accountable for generated free radicals and neurodegeneration (Zhu et al., 2017). In the rat brain, PTZ kindling raised MDA levels and decreased GSH levels, indicating cellular oxidative stress, while curcumin reduced both (Mehla et al., 2010). In PTZ rodents supplemented with curcumin, considerable antioxidant activity was obvious from levels of lipid peroxidation and protein carbonyls, which is consistent with earlier research (Kaur et al., 2014). In one of the most ground-breaking studies, it was discovered that combining curcumin with well-known AEDs like phenobarbitone, phenytoin, and carbamazepine in sub-therapeutic doses prevented learning and memory impairment caused by seizures, whereas sub-therapeutic administered doses of AEDs alone had no effect. Curcumin also reduces the oxidative imbalance caused by seizures (Reeta et al., 2011). The iron-induced epilepsy model is a well-known human posttraumatic epilepsy model (Willmore et al., 1978). Free iron in the brain causes cellular-thiol processes to be disrupted, as well as the formation of free radicals generated. Curcumin reduced protein

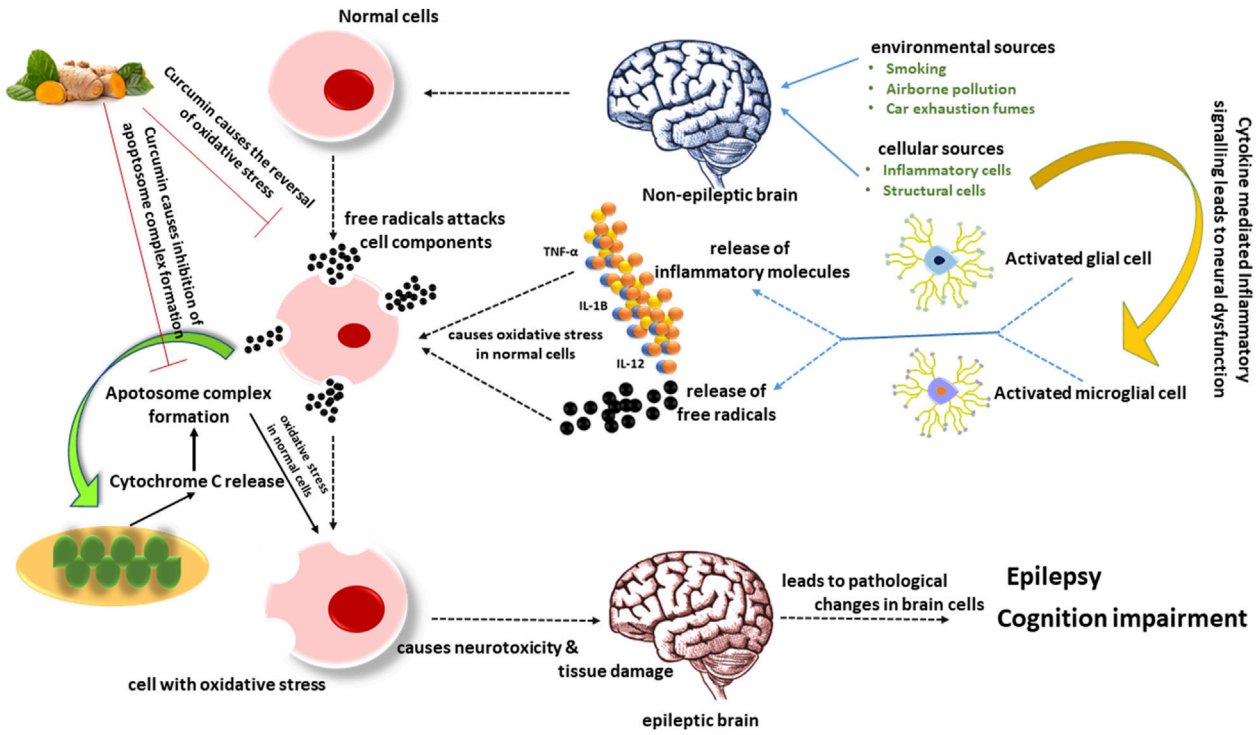


FIGURE 3
Activated microglia generate inflammatory chemicals and free radicals that damage tissue and cause neurotoxicity through synaptic rearrangement, oxidative stress, and other mechanisms associated with cognitive problems. The extrinsic pathway for apoptosis is composed of insults that death receptors facilitate. In contrast, the intrinsic mitochondrial pathway is composed of death signals that can act directly or indirectly on mitochondria, causing the release of cytochrome C and ultimately forming an apoptosome complex. The existing evidence unequivocally demonstrates that neuronal hyperactivity is associated with increased free radical generation, notably in brain tissue. According to reports, curcumin prevents the production of free radicals.

oxidation by a large amount, which may be due to its capacity to pass the blood–brain barrier (Wang et al., 2014) and bind with freely available Fe^{2+}/Fe^{3+} ions (Baum and Ng, 2004). In epileptic models, membrane fluidity is impeded, and curcumin's antioxidant properties may help to reduce the damage. Curcumin also inhibits PKC-mediated excitotoxicity by preventing oxidative modification of the protein kinase C (PKC) regulatory component, which restricts the activation of cytosol PKC activity (Jyoti et al., 2009). SE is a neurological disorder in which recurrent generalized convulsions last more than 30 min and result in significant neuronal damage. The available research clearly shows that neuronal hyperactivity has been linked to increased production of free radicals, particularly in brain tissue (Freitas et al., 2005). In the hippocampus and striatum parts of the brain, a study found a large increase in lipid peroxidation and a considerable drop in GSH, indicating oxidative stress, in agreement with previous research. Curcumin pre-treatment reduced the disruption of oxidative stress-related enzymes in a dose-dependent way (Ahmad, 2013) (Figure 3). The effect of curcumin on oxidative stress, represents in Table 2.

4.4 Effect of curcumin on cognition impairment

The hippocampus region is important for memory and is frequently the site of epileptic episodes. As one of the maximum electrically excited regions of the brain, hippocampal sclerosis is the most commonly diagnosed substrate in mesial temporal lobe epilepsy in both kindling models and TLE patients (Altintaş et al., 2017; Becker, 2018). Epileptic seizures cause neurodegenerative alterations, leading to cognitive impairment (Tai et al., 2018). Long-term TLE is well-documented, with cognitive impairment as a comorbidity (Allone et al., 2017; Rzezak et al., 2017). Multiple epileptogenic and neurogenic alterations also play a role in the evolution of status epilepticus-induced damage and learning and memory problems (Castro et al., 2017). However, current research suggests that neurotransmitter imbalance and changes in neuronal structure due to seizures may play a key role in neurobehavioral changes (Ahmad, 2013; Kubová et al., 2004). Patients with epilepsy frequently experience cognitive deficits (Rodríguez-Cruces et al., 2018). Furthermore, the parahippocampal cortex is linked to memory impairment in patients with mesial TLE and hippocampal sclerosis (Colnaghi et al., 2017). Nearly 30% of epilepsy patients treated with AEDs experience cognitive impairment as a side effect (Hernández et al., 2005; Dalic and Cook, 2016); with higher doses of AEDs, the risk of cognitive impairment increases (Jokeit et al., 2005).

In the kindling model of epilepsy, polyphenolic substances like epigallocatechin gallate are beneficial as a prophylactic agent for cognition impairment (Xie et al., 2012). In a Parkinson's disease mouse model, nanoparticles containing curcumin and piperine dramatically restored the neurobehavioral impairments and

TABLE 2 Effect of curcumin administration on oxidative stress associated with seizures.

S.No.	Experimental model of epilepsy	Species used	Dose of curcumin	Route of administration	Duration of intervention	Findings	Reference
1	PTZ and MES-induced seizures	Wistar rats	Curcumin in the dose 300 mg/kg co-administered with phenytoin, valproate, phenobarbitone and carbamazepine (sub-therapeutic dose)	Oral	Once	Valproate and curcumin + valproate treatments significantly decreased the level of MDA and increased the GSH level in the whole brain tissue when compared with the disease group	Reeta et al. (2011)
2	PTZ-induced kindling	Wistar rats	100, 200 and 300 mg/kg	Oral	35 days	Curcumin administration reduced MDA levels and increased GSH levels in the whole brain dose-dependently	Mehla et al. (2010)
3	PTZ-induced kindling	BALB/c nude mice	60 mg/kg	NA	NA	Curcumin administration led to the upregulation of cysteine, which is a critical reductive biothiol, and oxidative stress in the brain	Li et al. (2020)
4	PTZ-induced kindling	Wistar rats	100 mg/kg	Oral	30 days	Mitochondrial swelling was reduced (by two folds), increased cytochrome c oxidase activity, protein carbonyl levels relatively increased, and restoration of GSH levels in the hippocampus and cortex. Reversal of morphological deficits of mitochondria, restoration of neuronal loss	Kaur et al. (2014)
5	Kainate-induced model of TLE	Wistar rats	100 mg/kg	Oral	7 days	Reduction in levels of MDA, nitrite, and nitrates. Amelioration of neuronal damage in CA1, CA3, and hilar regions, reduction of MFS	Kiasalari et al. (2013)
6	Lithium-pilocarpine model of SE	Sprague–Dawley rats	50, 100 and 200 mg/kg	Oral	3 days	Reduction in levels of TBARS, dose-dependently in the hippocampus and striatum, increase in levels of GSH in the hippocampus and striatum	Ahmad (2013)

Abbreviations: PTZ, Pentylenetetrazole; **MES,** Maximal electroshock seizures; **MDA,** Malondialdehyde; **GSH,** Glutathione; **TLE,** Temporal lobe epilepsy; **MFS,** Mossy fiber sprouting; **CA,** Cornu Ammonis; **TBARS,** Thiobarbituric acid reactive substances.

neuronal degeneration caused in the substantia nigra (Kundu et al., 2016). In mice, functionalized polymerosomes containing curcumin reached the brain and reversed cognitive impairment caused by amyloid-$\beta_{1\text{-}42}$ (Jia et al., 2016). Furthermore, demethoxycurcumin, a natural derivative of curcumin, can alleviate memory impairments caused by scopolamine treatment via changing hippocampus

choline acetyltransferase expression (Lim et al., 2016). In cadmium-induced memory impairment, inhibition of AChE and adenosine deaminase activities, as well as an increase in the antioxidant quality of curcumin, provided improved cognitive qualities (Akinyemi et al., 2017). Curcumin administration has been proven to improve cognitive skills by lowering lipid peroxidation in the brain tissue of elderly female rats, according to a study (Belviranlı et al., 2013). Other studies also found curcumin reverses cognitive impairment dose-dependently (Mehla et al., 2010; Jyoti et al., 2009). Another study supports the neuroprotective efficacy of curcumin, where curcumin administration significantly attenuated cognitive decline associated with the experimental model of chronic epilepsy (Kaur et al., 2015). Reeta et al. (2011) found that when curcumin was combined with subtherapeutic doses of AEDs such as valproate, phenobarbitone, phenytoin, and carbamazepine, cognitive abilities were improved. Because of its potential to alter the central monoaminergic cascade, curcumin ameliorates depression-like behavior and memory loss in PTZ-treated mice (Choudhary et al., 2013). In non-demented persons, a highly absorbable curcumin formulation showed improvement in the memory and attention. Curcumin appears to be an adjuvant therapy for older people with AD and mild cognitive impairment, preventing progressive loss of cognitive abilities by stabilizing the disease course (Dost et al., 2021). As discussed, curcumin has inhibitory potential on inflammatory mediators, such as NF-κB and COX-2, involved in the controlling expression of anti-apoptotic genes like Bcl-2 (Mortezaee et al., 2019).

A study reported curcumin alleviates cerebral hypoperfusion-induced cognitive impairment in rats through suppression of apoptosis (Zheng et al., 2021). In another study, curcumin stimulated the AMPK-JNK pathway, which caused inhibition of mTOR and upregulation of Bcl-2, subsequently enhancing autophagy, suppressing apoptosis, and enhancing cognitive behavior (Yi et al., 2020). Curcumin encapsulated in solid lipid nanoparticles (SLNs) showed better anti-epileptic efficacy and behavior performance in mice (Huang et al., 2020). Interestingly, a study demonstrated curcumin supplementation in rats treated with gentamicin and sodium salicylates reduced caspase-3 levels, which is the pathological mechanism responsible for its improved locomotor and memory function (Abd-Elhakim et al., 2021). Xiang et al. (2021) reported that curcumin treatment in copper-induced neurotoxicity lessened the reduction in mitochondrial membrane potential and translocation of cytochrome c to the nuclear region. The levels of procaspase 3 and procaspase 9 were upregulated upon curcumin administration. In the colistin-induced peripheral neurotoxicity model of mice, curcumin supplementation at 200 mg/kg body weight downregulated the mRNA expression of Bax, caspase-3, and caspase-9. Subsequent decreased levels of caspase-3 and caspase-9. Table 3 lists the cognition-enhancing property of curcumin in epilepsy.

4.5 Effect of curcumin on epigenetic mechanisms

The HDACs inhibition using various substances is considered an epilepsy therapeutic approach because of their ability to regulate several cellular processes (Citraro et al., 2017; Reddy et al., 2018). Curcumin has been reported to be the most powerful inhibitor of HDACs/HATs due to its potential impact on their activity (Hassan et al., 2019). Curcumin has also been shown to be more effective than valproic acid and sodium butyrate, which are established HDAC inhibitors. Also, curcumin drastically lowered the levels of class I HDACs, increasing acetylation (Liu et al., 2005; Chen et al., 2007).

It is reported that curcumin increased SOCS1 and SOCS3 expression, which are suppressors of cytokine signaling, by initiating histone acetylation in SOCS1 and SOCS3 promoter regions in HEL cells. As an inhibitor of HDACs, curcumin suppressed the HDAC enzyme activity and reduced the HDAC1, 3, and 8 levels. Further, curcumin efficiently inhibited HDAC activity and lowered levels of HDAC8 in primary myeloproliferative neoplasms cells (Chen et al., 2013). A study reported that intranasal administration of curcumin inhibited asthma symptoms by disturbing HDAC1 activity leading to NF-κB inhibition in a rodent model of allergic asthma (Islam et al., 2022). Also, curcumin treatment showed elevated expression of acetylated histone H4 and downregulated expression of class I HDAC in the human B lymphoblastoid cell line (Liu et al., 2005). Inhibition of HDAC4s transcription, causing reduction of HDAC expression, has been shown with curcumin treatment in the medulloblastoma cells (Lee et al., 2011). These studies have proposed curcumin as a strong suppressor of HDAC activity.

Curcumin's effects on DNA methylation have been reported in numerous studies. Curcumin has been demonstrated to suppress the action of DNMTs, resulting in significant changes in DNA methylation patterns in various tumour cells (Liu et al., 2009; Parashar et al., 2012). As per molecular docking studies, curcumin covalently inhibits the catalytic thiolate of DNMT1, culminating in hypomethylation (Liu et al., 2009). In global DNA methylation experiments, curcumin caused reversed DNA methylation in Leukemia cells, similar to decitabine (a powerful hypo-methylating drug). It also caused demethylation and Neurog1 expression in LNCaP prostate cancer cells (Shu et al., 2011). Curcumin did not affect global hypo-methylation of DNA in human colon cancer cells, and it did not change the methylation pattern of long interspersed nuclear elements-1. However, it diminished the methylation of genes involved in the NF-κB pathway. Curcumin's hypo-methylating effect was found to be correlated with the intensity of methylation because of the selective demethylation of partially methylated CpG sites rather than completely methylated genes (Link et al., 2013). Furthermore, curcumin administration resulted in the reactivation of silent tumour suppressor genes by causing the demethylation of their promoters, resulting in significant tumour suppression (Jha et al., 2010; Yu et al., 2013). It also caused the methylation of the Nrf2 promoter to be reversed in prostate cancer cells (Khor et al., 2011).

5 Newer delivery systems for enhanced curcumin's bioavailability

A nanocarrier system is a drug delivery system that uses tiny particles (nanoparticles) to transport drugs to targeted sites in the body. These particles can be made from various materials, including

TABLE 3 Effect of curcumin administration on cognition impairment associated with epilepsy.

S.No.	Experimental model of epilepsy	Species used	Dose of curcumin	Route of administration	Duration of intervention	Findings	Reference
1	PTZ-induced kindling	Wistar rats	100 mg/kg	Oral	30 days	Decreased escape latency in MWM suggestive of improved cognitive functions	Kaur et al. (2015)
2	KA-induced status epilepticus	Wistar rats	100 mg/kg	Intraperitoneal	14 days	Decreased neuronal loss in DH and CA3 region, reduced severity of MFS, a significant reduction in escape latency in MWM	Jiang et al. (2015)
3	PTZ-induced kindling	Swiss Albino mice	50, 100 and 200 mg/kg	Intraperitoneal	15 days	Ameliorative effect on depressive behavior and cognitive dysfunction, monoaminergic modulation, inhibition of nitrosative stress, and acetylcholinesterase activity	Choudhary et al. (2013)
4	PTZ and MES-induced seizures	Wistar rats	Curcumin (300 mg/kg) co-administered with phenytoin, valproate, phenobarbitone and carbamazepine (sub-therapeutic dose)	Oral	1 day	Curcumin co-administration with clinically approved AEDs in sub-therapeutic levels avoided learning and memory deficits	Reeta et al. (2011)
5	PTZ-induced kindling	Wistar rats	100, 200, and 300 mg/kg, orally	Oral	35 days	Cognitive impairment ameliorated after curcumin pre-treatment in a dose-dependent manner	Mehla et al. (2010)
6	KA-induced epilepsy	Sprague Dawley rats	100 mg/kg	Oral	7 days	Improvement of recognition efficiency	He et al. (2018)
7	PTZ-induced kindling	Wistar rats	100 mg/kg	Oral	30 days	Curcumin-treated rats performed better in consolidated and long-term memory assessment	Kaur et al. (2014)

Abbreviations: PTZ, Pentylenetetrazole; **MWM,** Morris water maze; **KA,** Kainic acid; **DH,** Dentate hilus; **CA3,** Cornu Ammonis; **MFS,** Mossy fiber sprouting; **MES,** Maximal electroshock seizures; **AEDs,** Anti-epileptic drugs.

lipids, polymers, and metals. The nanocarriers can protect the drugs from degradation in the body, increase their solubility, and provide controlled release, enhancing their therapeutic efficacy and reducing potential side effects. Different types of nanocarrier systems for drug delivery exist, such as liposomes, polymeric nanoparticles, dendrimers, and metallic nanoparticles. Liposomes are spherical vesicles made of lipid bilayers that can encapsulate hydrophobic and hydrophilic drugs. Polymeric nanoparticles are biocompatible polymers that can entrap drugs within the particles or conjugate the drugs to the particle surface. Dendrimers are highly branched, spherical molecules that can encapsulate drugs within their cavities or conjugate drugs to their surface. Metallic nanoparticles, such as gold and silver, can also be used for drug delivery and imaging.

Nanocarrier systems have several advantages over conventional drug delivery methods, including improved drug bioavailability and efficacy, reduced toxicity, targeted drug delivery, and prolonged drug release. However, there are also some challenges associated with the development and use of nanocarrier systems, such as their potential toxicity, stability, and manufacturing scalability. Curcumin's therapeutic applicability is hampered by its poor solubility, physicochemical instabilities, less bioavailability, quick metabolism, and poor pharmacokinetics, despite its vast neuroprotective and disease-modifying properties (308). However, these issues can be addressed by inventing effective delivery systems, and the nanonization concept has offered a platform for overcoming all the barriers to effective curcumin delivery (309). Overall, nanocarrier systems have the potential to revolutionize drug delivery by enabling more effective and targeted therapies for a range of diseases, including cancer, cardiovascular disease, and neurological disorders. There are several different types of nanocarrier systems for drug delivery, each with its unique properties and advantages. Following are the examples of nanocarrier systems.

5.1 Solid nanoparticles

One approach to improve the therapeutic efficacy of curcumin is to formulate it as solid nanoparticles. Solid nanoparticles can enhance the solubility and bioavailability of curcumin, as well as

provide sustained release, targeted delivery, and protection from degradation (Khairnar et al., 2022). There are several methods for preparing curcumin solid nanoparticles, including (i) Precipitation method: Curcumin is dissolved in an organic solvent and then rapidly added to an aqueous solution containing a surfactant. The resulting nanoparticle suspension is then dried and collected. (ii) Emulsion solvent evaporation method: Curcumin is dissolved in an organic solvent, and then the organic phase is emulsified in an aqueous solution containing a surfactant. The organic solvent is then evaporated, resulting in the formation of solid curcumin nanoparticles. (iii) Supercritical fluid technology: Curcumin is dissolved in a supercritical fluid (e.g., carbon dioxide), and then the supercritical fluid is rapidly expanded to form nanoparticles. (iv) Antisolvent precipitation method: Curcumin is dissolved in a solvent, and then an antisolvent (e.g., water) is rapidly added to the solution, causing the curcumin to precipitate and form nanoparticles.

5.2 Biodegradable lipid nanoparticles

BLNPs are a type of drug delivery system that can be used to encapsulate and deliver therapeutic agents, such as drugs or nucleic acids, to target cells or tissues. BLNPs are composed of a biocompatible lipid bilayer that surrounds the cargo that is designed to be biodegradable, meaning that they can break down into harmless components once they have released their payload (Akbari et al., 2022). There are several advantages to using BLNPs for drug delivery. First, the lipid bilayer can protect the cargo from degradation or clearance by the immune system, allowing for more efficient delivery to the target site. Second, because BLNPs can be designed to be biodegradable, they can be cleared from the body without causing toxicity or other adverse effects. BLNPs can be prepared using various methods, including solvent evaporation, solvent injection, and microemulsion techniques. BLNPs have been studied as a potential delivery system for curcumin to enhance its bioavailability and therapeutic efficacy. Several studies have investigated the use of BLNPs for curcumin delivery. For example, one study reported the preparation of curcumin-loaded BLNPs using a solvent evaporation method. The resulting nanoparticles were found to have a high encapsulation efficiency and a sustained release of curcumin over time, suggesting they could be a promising delivery system for curcumin (Li et al., 2021b).

5.3 Carbon complex nanoparticles

Carbon complex nanoparticles (CCNPs) are a type of carbon-based nanoparticle that has been developed for various applications, including drug delivery, imaging, and sensing. CCNPs are typically composed of a core of carbon material, such as carbon nanotubes or graphene, which is coated with a layer of organic or inorganic molecules to improve their properties and functionality (Foldvari and Bagonluri, 2008). One potential application of CCNPs is in drug delivery. CCNPs can be designed to encapsulate various drugs, such as anticancer agents, and can be targeted to specific cells or tissues using surface modifications. The carbon core of the nanoparticle also provides a unique platform for controlled drug release, as the drug can be released in response to changes in temperature, pH, or other environmental factors.

5.4 Chitosan-alginate nanoparticles

Chitosan-alginate nanoparticles are a type of biodegradable nanoparticle that can be used for drug delivery, tissue engineering, and other biomedical applications. Chitosan and alginate are both biocompatible and biodegradable polymers that have been widely studied for their potential use in drug delivery and tissue engineering. Chitosan is a natural polymer derived from chitin, a component of crustacean shells, and has been shown to have antimicrobial and immunomodulatory properties. Alginate is a biocompatible polysaccharide derived from brown seaweed that can form hydrogels in the presence of calcium ions. The combination of chitosan and alginate can form nanoparticles with improved stability and drug encapsulation efficiency. One method for producing chitosan-alginate nanoparticles involves ionic gelation, in which the addition of calcium ions cross-links the polymers. Chitosan-alginate nanoparticles can be designed to be mucoadhesive, allowing them to bind to mucosal surfaces and improve drug delivery to the gastrointestinal tract. They can also be modified to target specific cells or tissues, such as tumor cells, by attaching ligands or antibodies to the nanoparticle surface (Li et al., 2022).

5.5 Niosomes

Niosomes are a type of lipid nanoparticle that can be used for drug delivery. They are composed of non-ionic surfactants, such as Span and Tween, that form a bilayer structure similar to cell membranes. Niosomes can encapsulate various drugs, including hydrophilic and hydrophobic compounds, and protect the drugs from degradation and clearance by the immune system. Niosomes have several advantages over other drug delivery systems. They are biocompatible, biodegradable, and non-toxic, making them suitable for pharmaceutical and cosmetic applications. They can also be modified to target specific cells or tissues, such as cancer cells, by attaching ligands or antibodies to the noisome surface. Another advantage of niosomes is their ability to improve the bioavailability and pharmacokinetics of drugs (Moghassemi and Hadjizadeh, 2014). The lipid bilayer structure of niosomes allows for the sustained release of drugs over time and can also protect the drugs from degradation in the stomach's acidic environment.

5.6 Silk fibroin nanoparticles

Silk fibroin nanoparticles are biodegradable and biocompatible nanoparticles that can be used for drug delivery, tissue engineering, and other biomedical applications. Silk fibroin is a protein derived from the silkworm cocoon and has been widely studied for its potential use in biomedical applications. Silk fibroin nanoparticles can be produced using various methods, including nanoprecipitation, emulsion/solvent evaporation, and electrospinning. The size, morphology, and surface properties of

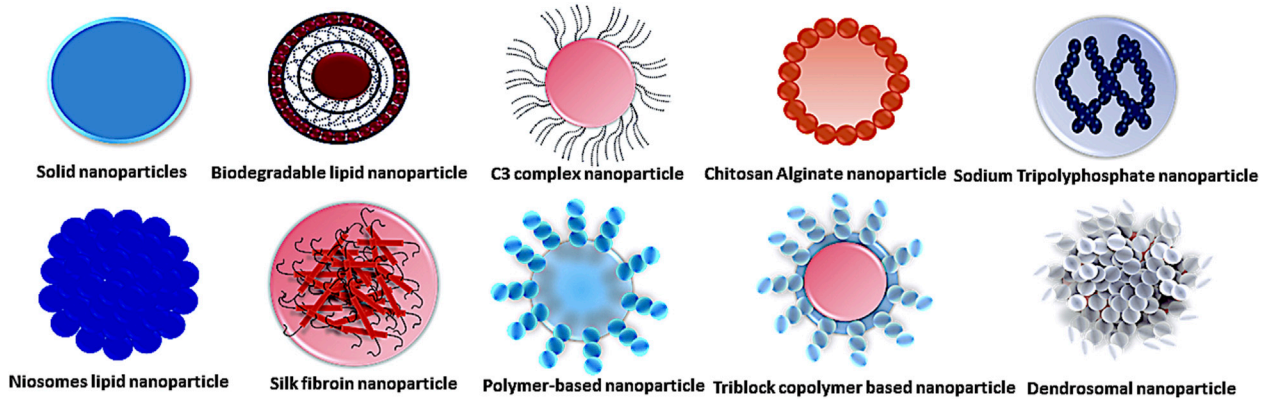


FIGURE 4
Representing different types of nanoparticle carrier systems carries active pharmaceutical ingredients that have been used in several diseases.

the nanoparticles can be controlled by adjusting the production parameters. Silk fibroin nanoparticles have several advantages for drug delivery (Mottaghitalab et al., 2015). They are biocompatible and biodegradable and can be designed to release drugs over a sustained period of time. They can also be modified to target specific cells or tissues, such as cancer cells, by attaching ligands or antibodies to the nanoparticle surface.

5.7 Polymer-based nanoparticles

Polymer-based nanoparticles are a type of nanoparticle that is composed of synthetic or natural polymers, such as poly (lactic-co-glycolic acid) (PLGA), polyethylene glycol (PEG), chitosan, and polyvinyl alcohol (PVA). These nanoparticles are typically between 10 and 1,000 nm in size and can be used for drug delivery, imaging, and tissue engineering applications. Polymer-based nanoparticles can be synthesized using various methods, including emulsion/solvent evaporation, nanoprecipitation, and electrospinning. The choice of method will depend on the specific polymer used and the desired properties of the nanoparticles. One advantage of polymer-based nanoparticles is their biocompatibility and biodegradability. Polymers such as PLGA and chitosan are approved by regulatory agencies for use in medical devices and drug delivery systems. Polymer-based nanoparticles can be designed to release drugs over a sustained period of time, improving their therapeutic efficacy and reducing side effects (Ayub and Wettig, 2022).

5.8 Triblock copolymer-based nanoparticles

Triblock copolymer-based nanoparticles are a type of nanoparticle composed of three blocks of polymers arranged in a linear chain, typically consisting of a hydrophilic block flanked by two hydrophobic blocks. These nanoparticles can be used for drug delivery, imaging, and other biomedical applications. Triblock copolymer-based nanoparticles can be synthesized using various methods, including emulsion/solvent evaporation, nanoprecipitation, and self-assembly. The choice of method will depend on the specific polymer used and the desired properties of the nanoparticles. One advantage of triblock copolymer-based nanoparticles is their ability to self-assemble into well-defined nanostructures. The hydrophobic blocks of the polymer form a core, while the hydrophilic block forms a corona, resulting in a stable and biocompatible nanoparticle. Triblock copolymer-based nanoparticles can be designed to release drugs over a sustained period of time, improving their therapeutic efficacy and reducing side effects. They can also be used to improve the solubility and bioavailability of poorly soluble drugs (Singh et al., 2022).

5.9 Dendrosomal nanoparticles

Dendrosomal nanoparticles are a type of nano-carrier composed of dendrimers, which are highly branched, monodisperse macromolecules with a central core and successive layers of branching that can be functionalized with various chemical groups. Dendrimers can be synthesized with a wide range of sizes and surface chemistries, which makes them ideal for designing nanoparticles with precise sizes, shapes, and functionalization for biomedical applications. Dendrosomal nanoparticles are typically prepared by coating the dendrimer with a lipid bilayer or other amphiphilic materials. The resulting nanoparticles are typically between 50 and 200 nm in diameter and can be loaded with drugs, imaging agents, or other payloads for targeted delivery to specific cells or tissues. One advantage of dendrosomal nanoparticles is their biocompatibility and low toxicity, as dendrimers are often composed of natural or biodegradable polymers. Dendrosomal nanoparticles have been shown to have excellent drug loading and release properties and can be modified with targeting ligands to improve their specificity for specific cells or tissues (dos Santos et al., 2022).

Researchers have been intrigued by several categories of nano-carriers, including micelles, nanoparticles, nanoemulsions, nanocrystals, and nanoliposomes, in order to solve issues associated with curcumin's low bioavailability and pharmacokinetics. In recent years, research has been conducted to determine the efficacy of nanoformulations for improved therapeutic action. Joseph et al., experimented with the diffusion and distribution of curcumin-loaded PLGA-PEG nanoparticles in

TABLE 4 Studies showing the neuroprotective activity of curcumin nanoformulations in different experimental models.

S.No.	Nanoformulation	Size	Experimental model	Proposed mechanism	Reference
1	Biodegradable lipid-based discoidal NPs	10–25 nm	Spinal cord injury in rats	Encapsulated curcumin caused downregulation of the IL-11 and IL-1β, insignificant downregulation of TNF-α, IFN-γ, IL-6, and RANTES, suppression of reactive astrocytes activation, upregulation of IL-10 and IL-13 (anti-inflammatory cytokines), a higher quantity of newly sprouted axons	Krupa et al. (2019)
2	Solid lipid NPs	NA	Epileptic mice	Curcumin-encapsulated NPs improved behavioral performance, more NeuN in the hippocampus, and reduced neuronal apoptosis via Bcl2 and P38 MAPK signaling	Huang et al. (2020)
3	C3 complex NPs	NA	PTZ-induced seizures in mice	Nanocurcumin treatment increased the seizure threshold and downregulated NO.	Aminirad et al. (2017)
4	Chitosan-Alginate- Sodium tripolyphosphate NPs	NA	PTZ-induced kindling in mice	Curcumin-loaded NPs alleviated neuronal cell death, upregulated the EPO and Klotho levels, reduction of mRNA expression of TNF-α in the hippocampus	Mansoor et al. (2018)
5	Chitosan-Alginate- Sodium tripolyphosphate NPs	NA	PTZ-induced kindling in mice	Curcumin NPs showed anticonvulsant activity, prevented cognition impairment, and reduced glial activation and cell death	Hashemian et al. (2017)
6	Niosomes NPs	60 nm	Traumatic brain injury in rats	hNS/PCs + Curcumin-loaded NPs showed improved locomotor activity, improved brain edema, decreased astrogliosis, and decreased TLR4, NF-κB-, and TNF-α- positive cells	Narouiepour et al. (2022)
7	NH_2-PEO-PCL NPs	99.5 + 7.3 nm	Parkinson's disease (Vero and PC12 cells)	Cells treated with varied concentrations of L-DOPA and curcumin-loaded NP for up to 72 h retained a high percentage of vitality	Mogharbel et al. (2022)
8	Silk fibroin NPs	150 nm	Friedrich's ataxia in mice	Removed iron from the heart, reduced oxidative stress, potentiated iron-sulfur cluster biogenesis, improved morphology and function of mitochondria, improved behavior scores	Xu et al. (2022)
9	Polymer (PEG)-based NPs	127.31 ± 2.73 nm	Intracerebral hemorrhage model in C57BL/6 mice	Attenuation of neuronal damage, suppression of iron deposition in the brain tissue around the site of hematoma, elevated perihematomal GPX4 expression by regulating HMOX1 (HO-1) and NFE2L2 (NRF2) expression	Yang et al. (2021)
10	Triblock copolymer nano micelles	96.67 ± 11.94 nm	BCCAO stroke model in rats	Higher bioavailability in plasma, heart, brain, and kidneys, downregulated expressions of IL-1β, NF-κB, IL-6, and TNF-α, and a significant reduction in lipid peroxidation	Li et al. (2021c)
11	Dendrosomal NPs	NA	Cuprizone-induced demyelination in mice	Inhibited accumulation of microglia and astrocytes and in the corpus callosum, a higher index of myelin basic protein intensity in the corpus callosum (indicative of myelin content)	Motavaf et al. (2020)
12	Pluronic F127 NPs	~11 nm	*In vitro*: BBB model *In vivo*: Healthy mice	Encapsulated NPs showed more vigorous fluorescent intensity (6.5 folds) in the brain as compared with pure curcumin. Encapsulated curcumin kept its capacity to bind with Aβ plaques and presented better antiapoptotic activity and improved redox balancing mechanism as compared to pure curcumin	Singh et al. (2020)

Abbreviations: PTZ, Pentylenetetrazole; **NPs,** Nanoparticles; **IL-11,** Interleukin-11; **IL-1β,** Interleukin-1β; **TNF-α,** Tumour necrosis factor-α; **IL-6,** Interleukin-6; **IFN-γ,** Interferon-γ; **RANTES,** Regulated on activation, normal T cell expressed and secreted; **IL-10,** Interleukin-10; **IL-13,** Interleukin-13; **Bcl-2,** B-cell lymphoma 2; **MAPK,** Mitogen-activated protein kinase; **NO,** Nitric oxide; EPO, erythropoietin; **hNS/PCs,** human neural stem/progenitor cells; **TLR4,** Toll-like receptor 4; **NF-κB,** Nuclear factor-κB; PEO, Poly (ethylene oxide); **PCL,** Poly (ε-caprolactone); **PEG,** Polyethylene glycol; **BCCAO,** Bilateral common carotid artery occlusion.

the brain of newborn rats. Injured areas of the neonate rats demonstrated neuroprotection against a compromised blood–brain barrier. The brain parenchyma allows these nanoparticles to spread effectively (Joseph et al., 2018). Zhang et al. (2018) developed curcumin-loaded polysorbate 80 modified cerasome nanoparticles and used ultrasound-targeted microbubble disruption of the BBB to deliver them to MPTP-induced Parkinson's disease in rats. This study found that nanoformulations of curcumin had superior stability, longer duration of action, and higher absorption than free curcumin.

Furthermore, after the administration of created NPs (15 mg curcumin/kg), they reported improved behavior as well as dopamine reduction in experimental animals (Zhang et al., 2018). Polymeric NPs encapsulating curcumin were found to be more effective in

shielding neurons from oxidative insults in both *in-vitro* and *in-vivo* investigations. Human SK-N-SH cells were protected from H_2O_2-mediated free radicals assaults by nano curcumin therapy. In athymic mice, intraperitoneal administration of nano curcumin (25 mg/kg, twice daily) resulted in considerable curcumin levels in the brain, as well as lower levels of H_2O_2 and caspase activity and higher glutathione concentrations (Ray et al., 2011). Curcumin-encapsulated PLGA NPs were found to have an improved effect on the proliferation and differentiation of neural stem cells *in-vitro* and *in-vivo* than pure curcumin in a study. In the hippocampus area, the encapsulated NPs greatly increased the gene expression associated with proliferation and neural development. In the rat model of Aβ-induced AD, NPs administration showed an improved effect on reversing the altered learning and memory characteristics. These NPs stimulated neurogenesis via the canonical Wnt/β-catenin pathway, according to *in silico* molecular docking studies (Tiwari et al., 2014). Mathew et al. (2012) developed PLGA-coated curcumin NPs that were water soluble and combined with Tet-1 peptide, a peptide with increased affinity for neurons. They discovered that curcumin-encapsulated NPs effectively eliminated amyloid aggregates and had antioxidant and non-cytotoxic properties (Mathew et al., 2012). Some of the nanoparticulate systems used for encapsulating curcumin, are shown in Figure 4, and the list of the nanoformulations of curcumin in several neurological disorders, is presented in Table 4.

6 Conclusion

The current review mainly dissected modulatory effects of curcumin on epileptic pathophysiology. Curcumin impose multiple immunomodulatory effects by modulating immune molecules, including T- and B-lymphocytes, macrophages, cytokines, chemokines, DCs, and transcription factors, thus elicits anti-inflammatory mechanism. Curcumin acts by inhibiting NF-κB transcription, which is responsible for the production of cytokines such as IL-6, IL-12, and TNF-α. It is also suppressing NF-κB signaling by imposing an inhibitory action on BLYS, which is an important innate inflammatory response in epilepsy patients. Additionally, curcumin downregulates mTOR signaling which eventually causes a reduction in the levels of cytokines such as COX-2, and IL-6 which are upregulated in epileptic subjects. Curcumin administration suppresses glial activation, a common finding in epileptic patients, by suppressing the levels of cytokines (IL-6, IL-1β, and, TNF-α) and chemokines (MCP-1). Also, curcumin administration reduces the expression of MHC-II and co-stimulatory molecules like CD80, CD40, and CD205. Curcumin activates Nrf2, a regulator for mitigating oxidative stress, and reduces oxidative damage by inhibiting the activation of NF-κB. Curcumin reduces the markers of lipid peroxidation and increases the levels of antioxidant molecules like GSH in epileptic brains. Curcumin prevents the release of cytochrome C from mitochondria and inhibits the formation of apoptosomes and the activity of caspases. The antiapoptotic, antioxidant, and immune modifying abilities of curcumin are the reported mechanisms responsible for enhancing cognition, memory processes, and neurobehavior. Curcumin is a potent HDAC inhibitor, and HDAC inhibition is an emerging therapeutic approach for epilepsy. Also, curcumin increases the activation of histone H4.

Epigenetic associated hypermethylation in TLE patients reversed upon curcumin administration. To overcome the poor bioavailability and physic-chemical properties of curcumin, nanonization has emerged as a promising strategy in several neurological disorders. Several studies have reported better pharmacological efficacy and molecular interactions than pure curcumin. The current literature supports curcumin administration as an adjuvant therapy to the conventional AEDs for treating epilepsy. More combinatorial studies are warranted to understand the synergistic effect imposed by the curcumin. Still many preclinical are in the waiting list to reach the human clinical trials. Therefore, the findings from the reported preclinical research results are essential and may be the scaffold for evaluation of curcumin-based nanoformulation and its pure form for their anti-epileptic potential in clinical studies.

Author contributions

SK: Conceptualization, Data curation, Writing–original draft, Writing–review and editing. NK: Investigation, Writing–original draft, Writing–review and editing.

Funding

The author(s) declare that no financial support was received for the research, authorship, and/or publication of this article.

Conflict of interest

The authors declare that the research was conducted in the absence of any commercial or financial relationships that could be construed as a potential conflict of interest.

Generative AI statement

The author(s) declare that no Generative AI was used in the creation of this manuscript.

Publisher's note

All claims expressed in this article are solely those of the authors and do not necessarily represent those of their affiliated organizations, or those of the publisher, the editors and the reviewers. Any product that may be evaluated in this article, or claim that may be made by its manufacturer, is not guaranteed or endorsed by the publisher.

References

Abd-Elhakim, Y. M., Abdel-Motal, S. M., Malhat, S. M., Mostafa, H. I., Moselhy, A. A. A., Beheiry, R. R., et al. (2021). Curcumin mitigates neurotoxic and neurobehavioral changes of gentamicin and sodium salicylate in rats by adjusting oxidative stress and apoptosis. *Life Sci.* 265, 118824. doi:10.1016/j.lfs.2020.118824

Aggarwal, B. B., Kumar, A., and Bharti, A. C. (2003). Anticancer potential of curcumin: preclinical and clinical studies. *Anticancer Res.* 23, 363–398.

Ahmad, B., and Lapidus, L. J. (2012). Curcumin prevents aggregation in α-synuclein by increasing reconfiguration rate. *J. Biol. Chem.* 287, 9193–9199. doi:10.1074/jbc.M111.325548

Ahmad, M. (2013). Protective effects of curcumin against lithium-pilocarpine induced status epilepticus, cognitive dysfunction and oxidative stress in young rats. *Saudi J. Biol. Sci.* 20, 155–162. doi:10.1016/j.sjbs.2013.01.002

Ahmadi, M., Agah, E., Nafissi, S., Jaafari, M. R., Harirchian, M. H., Sarraf, P., et al. (2018). Safety and efficacy of nanocurcumin as add-on therapy to riluzole in patients with amyotrophic lateral sclerosis: a pilot randomized clinical trial. *Neurother. J. Am. Soc. Exp. Neurother.* 15, 430–438. doi:10.1007/s13311-018-0606-7

Akbari, J., Saeedi, M., Ahmadi, F., Hashemi, S. M. H., Babaei, A., Yaddollahi, S., et al. (2022). Solid lipid nanoparticles and nanostructured lipid carriers: a review of the methods of manufacture and routes of administration. *Pharm. Dev. Technol.* 27, 525–544. doi:10.1080/10837450.2022.2084554

Akinyemi, A. J., Okonkwo, P. K., Faboya, O. A., Onikanni, S. A., Fadaka, A., Olayide, I., et al. (2017). Curcumin improves episodic memory in cadmium induced memory impairment through inhibition of acetylcholinesterase and adenosine deaminase activities in a rat model. *Metab. Brain Dis.* 32, 87–95. doi:10.1007/s11011-016-9887-x

Allone, C., Lo Buono, V., Corallo, F., Pisani, L. R., Pollicino, P., Bramanti, P., et al. (2017). Neuroimaging and cognitive functions in temporal lobe epilepsy: a review of the literature. *J. Neurol. Sci.* 381, 7–15. doi:10.1016/j.jns.2017.08.007

Altintaş, A., Özkara, Ç., Sohtaoğlu, S. M., Uzan, M., Kekik Çinar, Ç., Uysal, Ö., et al. (2017). Cytokine polymorphism and HLA genotyping in patients with temporal lobe epilepsy related to hippocampal sclerosis. *Noro Psikiyatri Arsivi* 54, 350–353. doi:10.5152/npa.2016.12678

Aminirad, A., Mousavi, S. E., Fakhraei, N., and Rezayat, S. M. (2017). The role of nitric oxide in anticonvulsant effect of nanocurcumine on pentylenetetrazole-induced seizure in mice. *Neurosci. Lett.* 651, 226–231. doi:10.1016/j.neulet.2017.05.018

Arend, J., Kegler, A., Caprara, A. L. F., Almeida, C., Gabbi, P., Pascotini, E. T., et al. (2018). Depressive, inflammatory, and metabolic factors associated with cognitive impairment in patients with epilepsy. *Epilepsy Behav. EB* 86, 49–57. doi:10.1016/j.yebeh.2018.07.007

Aronica, E., Bauer, S., Bozzi, Y., Caleo, M., Dingledine, R., Gorter, J. A., et al. (2017). Neuroinflammatory targets and treatments for epilepsy validated in experimental models. *Epilepsia* 58 (Suppl. 3), 27–38. doi:10.1111/epi.13783

Aronica, E., Boer, K., van Vliet, E. A., Redeker, S., Baayen, J. C., Spliet, W. G. M., et al. (2007). Complement activation in experimental and human temporal lobe epilepsy. *Neurobiol. Dis.* 26, 497–511. doi:10.1016/j.nbd.2007.01.015

Aronica, E., and Crino, P. B. (2011). Inflammation in epilepsy: clinical observations. *Epilepsia* 52 (Suppl. 3), 26–32. doi:10.1111/j.1528-1167.2011.03033.x

Aronica, E., and Gorter, J. A. (2007). Gene expression profile in temporal lobe epilepsy. *Neurosci. Rev. J. Bringing Neurobiol. Neurol. Psychiatry* 13, 100–108. doi:10.1177/1073858406295832

Asteriou, E., Gkoutzourelas, A., Mavropoulos, A., Katsiari, C., Sakkas, L. I., and Bogdanos, D. P. (2018). Curcumin for the management of periodontitis and early ACPA-positive rheumatoid arthritis: killing two birds with one stone. *Nutrients* 10, E908. doi:10.3390/nu10070908

Ayub, A., and Wettig, S. (2022). An overview of nanotechnologies for drug delivery to the brain. *Pharmaceutics* 14, 224. doi:10.3390/pharmaceutics14020224

Balosso, S., Ravizza, T., Perego, C., Peschon, J., Campbell, I. L., De Simoni, M. G., et al. (2005). Tumor necrosis factor-alpha inhibits seizures in mice via p75 receptors. *Ann. Neurol.* 57, 804–812. doi:10.1002/ana.20480

Banchereau, J., and Steinman, R. M. (1998). Dendritic cells and the control of immunity. *Nature* 392, 245–252. doi:10.1038/32588

Banik, U., Parasuraman, S., Adhikary, A. K., and Othman, N. H. (2017). Curcumin: the spicy modulator of breast carcinogenesis. *J. Exp. Clin. Cancer Res. CR* 36, 98. doi:10.1186/s13046-017-0566-5

Barkovich, A. J., Dobyns, W. B., and Guerrini, R. (2015). Malformations of cortical development and epilepsy. *Cold Spring Harb. Perspect. Med.* 5, a022392. doi:10.1101/cshperspect.a022392

Barrès, R., Osler, M. E., Yan, J., Rune, A., Fritz, T., Caidahl, K., et al. (2009). Non-CpG methylation of the PGC-1alpha promoter through DNMT3B controls mitochondrial density. *Cell Metab.* 10, 189–198. doi:10.1016/j.cmet.2009.07.011

Bauer, J., and Bien, C. G. (2009). Encephalitis and epilepsy. *Semin. Immunopathol.* 31, 537–544. doi:10.1007/s00281-009-0176-1

Bauer, S., Köller, M., Cepok, S., Todorova-Rudolph, A., Nowak, M., Nockher, W. A., et al. (2008). NK and CD4+ T cell changes in blood after seizures in temporal lobe epilepsy. *Exp. Neurol.* 211, 370–377. doi:10.1016/j.expneurol.2008.01.017

Baum, L., and Ng, A. (2004). Curcumin interaction with copper and iron suggests one possible mechanism of action in Alzheimer's disease animal models. *J. Alzheimers Dis. Jad.* 6, 367–377. doi:10.3233/jad-2004-6403

Bazhanova, E. D., Kozlov, A. A., and Litovchenko, A. V. (2021). Mechanisms of drug resistance in the pathogenesis of epilepsy: role of neuroinflammation. A literature review. *Brain Sci.* 11, 663. doi:10.3390/brainsci11050663

Becker, A. J. (2018). Review: animal models of acquired epilepsy: insights into mechanisms of human epileptogenesis. *Neuropathol. Appl. Neurobiol.* 44, 112–129. doi:10.1111/nan.12451

Bekinschtein, P., Katche, C., Slipczuk, L. N., Igaz, L. M., Cammarota, M., Izquierdo, I., et al. (2007). mTOR signaling in the hippocampus is necessary for memory formation. *Neurobiol. Learn Mem.* 87, 303–307. doi:10.1016/j.nlm.2006.08.007

Belviranlı, M., Okudan, N., Atalık, K. E. N., and Öz, M. (2013). Curcumin improves spatial memory and decreases oxidative damage in aged female rats. *Biogerontology* 14, 187–196. doi:10.1007/s10522-013-9422-y

Ben-Menachem, E., Kyllerman, M., and Marklund, S. (2000). Superoxide dismutase and glutathione peroxidase function in progressive myoclonus epilepsies. *Epilepsy Res.* 40, 33–39. doi:10.1016/s0920-1211(00)00096-6

Bernal, F., Graus, F., Pifarré, A., Saiz, A., Benyahia, B., and Ribalta, T. (2002). Immunohistochemical analysis of anti-Hu-associated paraneoplastic encephalomyelitis. *Acta Neuropathol. Berl.* 103, 509–515. doi:10.1007/s00401-001-0498-0

Bianchi, G., Ravera, S., Traverso, C., Amaro, A., Piaggio, F., Emionite, L., et al. (2018). Curcumin induces a fatal energetic impairment in tumor cells *in vitro* and *in vivo* by inhibiting ATP-synthase activity. *Carcinogenesis* 39, 1141–1150. doi:10.1093/carcin/bgy076

Bien, C. G., Bauer, J., Deckwerth, T. L., Wiendl, H., Deckert, M., Wiestler, O. D., et al. (2002a). Destruction of neurons by cytotoxic T cells: a new pathogenic mechanism in Rasmussen's encephalitis. *Ann. Neurol.* 51, 311–318. doi:10.1002/ana.10100

Bien, C. G., Urbach, H., Deckert, M., Schramm, J., Wiestler, O. D., Lassmann, H., et al. (2002b). Diagnosis and staging of Rasmussen's encephalitis by serial MRI and histopathology. *Neurology* 58, 250–257. doi:10.1212/wnl.58.2.250

Bird, A. P., and Wolffe, A. P. (1999). Methylation-induced repression-belts, braces, and chromatin. *Cell* 99, 451–454. doi:10.1016/s0092-8674(00)81532-9

Boer, K., Troost, D., Jansen, F., Nellist, M., van den Ouweland, A. M. W., Geurts, J. J. G., et al. (2008). Clinicopathological and immunohistochemical findings in an autopsy case of tuberous sclerosis complex. *Neuropathol. Off. J. Jpn. Soc. Neuropathol.* 28, 577–590. doi:10.1111/j.1440-1789.2008.00920.x

Boison, D., and Rho, J. M. (2020). Epigenetics and epilepsy prevention: the therapeutic potential of adenosine and metabolic therapies. *Neuropharmacology* 167, 107741. doi:10.1016/j.neuropharm.2019.107741

Bonneau, D., and Longy, M. (2000). Mutations of the human PTEN gene. *Hum. Mutat.* 16, 109–122. doi:10.1002/1098-1004(200008)16:2<109::AID-HUMU3>3.0.CO;2-0

Borrelli, E., Nestler, E. J., Allis, C. D., and Sassone-Corsi, P. (2008). Decoding the epigenetic language of neuronal plasticity. *Neuron* 60, 961–974. doi:10.1016/j.neuron.2008.10.012

Bossen, C., and Schneider, P. (2006). BAFF, APRIL and their receptors: structure, function and signaling. *Semin. Immunol.* 18, 263–275. doi:10.1016/j.smim.2006.04.006

Brennan, G. P., Dey, D., Chen, Y., Patterson, K. P., Magnetta, E. J., Hall, A. M., et al. (2016). Dual and opposing roles of MicroRNA-124 in epilepsy are mediated through inflammatory and NRSF-dependent gene networks. *Cell Rep.* 14, 2402–2412. doi:10.1016/j.celrep.2016.02.042

Brodie, M. J., and Yuen, A. W. C. (1997). Lamotrigine substitution study: evidence for synergism with sodium valproate? *Epilepsy Res.* 26, 423–432. doi:10.1016/S0920-1211(96)01007-8

Buffett-Jerrott, S. E., and Stewart, S. H. (2002). Cognitive and sedative effects of benzodiazepine use. *Curr. Pharm. Des.* 8, 45–58. doi:10.2174/1381612023396654

Bulloch, K., Miller, M. M., Gal-Toth, J., Milner, T. A., Gottfried-Blackmore, A., Waters, E. M., et al. (2008). CD11c/EYFP transgene illuminates a discrete network of dendritic cells within the embryonic, neonatal, adult, and injured mouse brain. *J. Comp. Neurol.* 508, 687–710. doi:10.1002/cne.21668

Cai, J., Xu, D., Bai, X., Pan, R., Wang, B., Sun, S., et al. (2017). Curcumin mitigates cerebral vasospasm and early brain injury following subarachnoid hemorrhage via inhibiting cerebral inflammation. *Brain Behav.* 7, e00790. doi:10.1002/brb3.790

Calkins, M. J., Johnson, D. A., Townsend, J. A., Vargas, M. R., Dowell, J. A., Williamson, T. P., et al. (2009). The Nrf2/ARE pathway as a potential therapeutic target in neurodegenerative disease. *Antioxid. Redox Signal* 11, 497–508. doi:10.1089/ars.2008.2242

Carpenter, J. C., and Lignani, G. (2021). Gene editing and modulation: the holy grail for the genetic epilepsies? *Neurother. J. Am. Soc. Exp. Neurother.* 18, 1515–1523. doi:10.1007/s13311-021-01081-y

Carrozza, M. J., Utley, R. T., Workman, J. L., and Côté, J. (2003). The diverse functions of histone acetyltransferase complexes. *Trends Genet. TIG* 19, 321–329. doi:10.1016/S0168-9525(03)00115-X

Castro, O. W., Upadhya, D., Kodali, M., and Shetty, A. K. (2017). Resveratrol for easing status epilepticus induced brain injury, inflammation, epileptogenesis, and cognitive and memory dysfunction-are we there yet? *Front. Neurol.* 8, 603. doi:10.3389/fneur.2017.00603

Cavalleri, G. L., Walley, N. M., Soranzo, N., Mulley, J., Doherty, C. P., Kapoor, A., et al. (2007). A multicenter study of BRD2 as a risk factor for juvenile myoclonic epilepsy. *Epilepsia* 48, 706–712. doi:10.1111/j.1528-1167.2007.00977.x

Cerri, C., Genovesi, S., Allegra, M., Pistillo, F., Püntener, U., Guglielmotti, A., et al. (2016). The chemokine CCL2 mediates the seizure-enhancing effects of systemic inflammation. *J. Neurosci. Off. J. Soc. Neurosci.* 36, 3777–3788. doi:10.1523/JNEUROSCI.0451-15.2016

Chen, B., Choi, H., Hirsch, L. J., Katz, A., Legge, A., Buchsbaum, R., et al. (2017). Psychiatric and behavioral side effects of antiepileptic drugs in adults with epilepsy. *Epilepsy Behav. EB* 76, 24–31. doi:10.1016/j.yebeh.2017.08.039

Chen, C., Yu, K., Yan, Q., Xing, C. y., Chen, Y., Yan, Z., et al. (2013). Pure curcumin increases the expression of SOCS1 and SOCS3 in myeloproliferative neoplasms through suppressing class I histone deacetylases. *Carcinogenesis* 34, 1442–1449. doi:10.1093/carcin/bgt070

Chen, S.-D., Yw Chang, A., and Chuang, Y.-C. (2010). The potential role of mitochondrial dysfunction in seizure-associated cell death in the hippocampus and epileptogenesis. *J. Bioenerg. Biomembr.* 42, 461–465. doi:10.1007/s10863-010-9321-8

Chen, Y., Shu, W., Chen, W., Wu, Q., Liu, H., and Cui, G. (2007). Curcumin, both histone deacetylase and p300/CBP-specific inhibitor, represses the activity of nuclear factor kappa B and notch 1 in raji cells. *Basic Clin. Pharmacol. Toxicol.* 101, 427–433. doi:10.1111/j.1742-7843.2007.00142.x

Cho, J., and Gruol, D. L. (2008). The chemokine CCL2 activates p38 mitogen-activated protein kinase pathway in cultured rat hippocampal cells. *J. Neuroimmunol.* 199, 94–103. doi:10.1016/j.jneuroim.2008.05.011

Choi, J., Nordli, D. R., Alden, T. D., DiPatri, A., Laux, L., Kelley, K., et al. (2009). Cellular injury and neuroinflammation in children with chronic intractable epilepsy. *J. Neuroinflammation* 6, 38. doi:10.1186/1742-2094-6-38

Choudhary, K. M., Mishra, A., Poroikov, V. V., and Goel, R. K. (2013). Ameliorative effect of Curcumin on seizure severity, depression like behavior, learning and memory deficit in post-pentylenetetrazole-kindled mice. *Eur. J. Pharmacol.* 704, 33–40. doi:10.1016/j.ejphar.2013.02.012

Chu-Shore, C. J., Major, P., Camposano, S., Muzykewicz, D., and Thiele, E. A. (2010). The natural history of epilepsy in tuberous sclerosis complex. *Epilepsia* 51, 1236–1241. doi:10.1111/j.1528-1167.2009.02474.x

Citraro, R., Leo, A., Santoro, M., D'agostino, G., Constanti, A., and Russo, E. (2017). Role of histone deacetylases (HDACs) in epilepsy and epileptogenesis. *Curr. Pharm. Des.* 23, 5546–5562. doi:10.2174/1381612823666171024130001

Clement, C. C., and Santambrogio, L. (2013). The lymph self-antigen repertoire. *Front. Immunol.* 4, 424. doi:10.3389/fimmu.2013.00424

Colín-González, A. L., Orozco-Ibarra, M., Chánez-Cárdenas, M. E., Rangel-López, E., Santamaría, A., Pedraza-Chaverri, J., et al. (2013). Heme oxygenase-1 (HO-1) upregulation delays morphological and oxidative damage induced in an excitotoxic/pro-oxidant model in the rat striatum. *Neuroscience* 231, 91–101. doi:10.1016/j.neuroscience.2012.11.031

Collado, J. A., Guitart, C., Ciudad, M. T., Alvarez, I., and Jaraquemada, D. (2013). The repertoires of peptides presented by MHC-II in the thymus and in peripheral tissue: a clue for autoimmunity? *Front. Immunol.* 4, 442. doi:10.3389/fimmu.2013.00442

Colnaghi, S., Beltrami, G., Poloni, G., Pichiecchio, A., Bastianello, S., Galimberti, C. A., et al. (2017). Parahippocampal involvement in mesial temporal lobe epilepsy with hippocampal sclerosis: a proof of concept from memory-guided saccades. *Front. Neurol.* 8, 595. doi:10.3389/fneur.2017.00595

Creyghton, M. P., Cheng, A. W., Welstead, G. G., Kooistra, T., Carey, B. W., Steine, E. J., et al. (2010). Histone H3K27ac separates active from poised enhancers and predicts developmental state. *Proc. Natl. Acad. Sci. U. S. A.* 107, 21931–21936. doi:10.1073/pnas.1016071107

Crosio, C., Heitz, E., Allis, C. D., Borrelli, E., and Sassone-Corsi, P. (2003). Chromatin remodeling and neuronal response: multiple signaling pathways induce specific histone H3 modifications and early gene expression in hippocampal neurons. *J. Cell Sci.* 116, 4905–4914. doi:10.1242/jcs.00804

Cunningham, C., and Sanderson, D. J. (2008). Malaise in the water maze: untangling the effects of LPS and IL-1beta on learning and memory. *Brain Behav. Immun.* 22, 1117–1127. doi:10.1016/j.bbi.2008.05.007

Cupolillo, D., Hoxha, E., Faralli, A., De Luca, A., Rossi, F., Tempia, F., et al. (2016). Autistic-like traits and cerebellar dysfunction in purkinje cell PTEN knock-out mice. *Neuropsychopharmacol. Off. Publ. Am. Coll. Neuropsychopharmacol.* 41, 1457–1466. doi:10.1038/npp.2015.339

Dalic, L., and Cook, M. J. (2016). Managing drug-resistant epilepsy: challenges and solutions. *Neuropsychiatr. Dis. Treat.* 12, 2605–2616. doi:10.2147/NDT.S84852

Dantzer, R., O'Connor, J. C., Freund, G. G., Johnson, R. W., and Kelley, K. W. (2008). From inflammation to sickness and depression: when the immune system subjugates the brain. *Nat. Rev. Neurosci.* 9, 46–56. doi:10.1038/nrn2297

Danzer, S. (2017). Mossy fiber sprouting in the epileptic brain: taking on the lernaean Hydra. *Epilepsy Curr.* 17, 50–51. doi:10.5698/1535-7511-17.1.50

Darbinyan, L. V., Hambardzumyan, L. E., Simonyan, K. V., Chavushyan, V. A., Manukyan, L. P., Badalyan, S. A., et al. (2017). Protective effects of curcumin against rotenone-induced rat model of Parkinson's disease: *in vivo* electrophysiological and behavioral study. *Metab. Brain Dis.* 32, 1791–1803. doi:10.1007/s11011-017-0060-y

Davey, C. A., Sargent, D. F., Luger, K., Maeder, A. W., and Richmond, T. J. (2002). Solvent mediated interactions in the structure of the nucleosome core particle at 1.9 a resolution. *J. Mol. Biol.* 319, 1097–1113. doi:10.1016/S0022-2836(02)00386-8

d'Avila, J. C., Siqueira, L. D., Mazeraud, A., Azevedo, E. P., Foguel, D., Castro-Faria-Neto, H. C., et al. (2018). Age-related cognitive impairment is associated with long-term neuroinflammation and oxidative stress in a mouse model of episodic systemic inflammation. *J. Neuroinflammation* 15, 28. doi:10.1186/s12974-018-1059-y

Dębski, K. J., Pitkanen, A., Puhakka, N., Bot, A. M., Khurana, I., Harikrishnan, K. N., et al. (2016). Etiology matters - genomic DNA methylation patterns in three rat models of acquired epilepsy. *Sci. Rep.* 6, 25668. doi:10.1038/srep25668

Deck, L. M., Hunsaker, L. A., Vander Jagt, T. A., Whalen, L. J., Royer, R. E., and Vander Jagt, D. L. (2018). Activation of anti-oxidant Nrf2 signaling by enone analogues of curcumin. *Eur. J. Med. Chem.* 143, 854–865. doi:10.1016/j.ejmech.2017.11.048

Devinsky, O., Vezzani, A., Najjar, S., De Lanerolle, N. C., and Rogawski, M. A. (2013). Glia and epilepsy: excitability and inflammation. *Trends Neurosci.* 36, 174–184. doi:10.1016/j.tins.2012.11.008

de Vries, H. E., Kooij, G., Frenkel, D., Georgopoulos, S., Monsonego, A., and Janigro, D. (2012). Inflammatory events at blood-brain barrier in neuroinflammatory and neurodegenerative disorders: implications for clinical disease. *Epilepsia* 53 (Suppl. 6), 45–52. doi:10.1111/j.1528-1167.2012.03702.x

Dilena, R., Mauri, E., Aronica, E., Bernasconi, P., Bana, C., Cappelletti, C., et al. (2019). Therapeutic effect of Anakinra in the relapsing chronic phase of febrile infection–related epilepsy syndrome. *Epilepsia Open* 4, 344–350. doi:10.1002/epi4.12317

Dolati, S., Marofi, F., Babaloo, Z., Aghebati-Maleki, L., Roshangar, L., Ahmadi, M., et al. (2018). Dysregulated network of miRNAs involved in the pathogenesis of multiple sclerosis. *Biomed. Pharmacother. Biomedecine Pharmacother.* 104, 280–290. doi:10.1016/j.biopha.2018.05.050

Dong, H., Xu, L., Wu, L., Wang, X., Duan, W., Li, H., et al. (2014). Curcumin abolishes mutant TDP-43 induced excitability in a motoneuron-like cellular model of ALS. *Neuroscience* 272, 141–153. doi:10.1016/j.neuroscience.2014.04.032

dos Santos, M. G., Prestes, J. P., and Pranke, P. (2022). Nanopolymers: powerful tools in neuroprotection and neuroregeneration. *Curr. Nanosci.* 18, 668–674. doi:10.2174/1573413718666211217123809

Dost, F. S., Kaya, D., Ontan, M. S., Erken, N., Bulut, E. A., Aydin, A. E., et al. (2021). Theracurmin supplementation may be a therapeutic option for older patients with alzheimer's disease: a 6-month retrospective follow-up study. *Curr. Alzheimer Res.* 18, 1087–1092. doi:10.2174/1567205019666211221125255

Drapeau, E., Montaron, M.-F., Aguerre, S., and Abrous, D. N. (2007). Learning-induced survival of new neurons depends on the cognitive status of aged rats. *J. Neurosci. Off. J. Soc. Neurosci.* 27, 6037–6044. doi:10.1523/JNEUROSCI.1031-07.2007

Drion, C. M., Kooijman, L., Aronica, E., van Vliet, E. A., Wadman, W. J., Chameau, P., et al. (2019). Curcumin reduces development of seizurelike events in the hippocampal-entorhinal cortex slice culture model for epileptogenesis. *Epilepsia* 60, 605–614. doi:10.1111/epi.14667

Drion, C. M., van Scheppingen, J., Arena, A., Geijtenbeek, K. W., Kooijman, L., van Vliet, E. A., et al. (2018). Effects of rapamycin and curcumin on inflammation and oxidative stress *in vitro* and *in vivo* - in search of potential anti-epileptogenic strategies for temporal lobe epilepsy. *J. Neuroinflammation* 15, 212. doi:10.1186/s12974-018-1247-9

Dua, T., de Boer, H. M., Prilipko, L. L., and Saxena, S. (2006). Epilepsy care in the world: results of an ILAE/IBE/WHO global campaign against epilepsy survey. *Epilepsia* 47, 1225–1231. doi:10.1111/j.1528-1167.2006.00595.x

Eghbaliferiz, S., Farhadi, F., Barreto, G. E., Majeed, M., and Sahebkar, A. (2020). Effects of curcumin on neurological diseases: focus on astrocytes. *Pharmacol. Rep. P. R.* 72, 769–782. doi:10.1007/s43440-020-00112-3

Elderkin-Thompson, V., Irwin, M. R., Hellemann, G., and Kumar, A. (2012). Interleukin-6 and memory functions of encoding and recall in healthy and depressed elderly adults. *Am. J. Geriatr. Psychiatry Off. J. Am. Assoc. Geriatr. Psychiatry* 20, 753–763. doi:10.1097/JGP.0b013e31825d08d6

Englot, D. J., Birk, H., and Chang, E. F. (2017). Seizure outcomes in nonresective epilepsy surgery: an update. *Neurosurg. Rev.* 40, 181–194. doi:10.1007/s10143-016-0725-8

Epstein, F. H., Lipton, S. A., and Rosenberg, P. A. (1994). Excitatory amino acids as a final common pathway for neurologic disorders. *N. Engl. J. Med.* 330, 613–622. doi:10.1056/NEJM199403033300907

Fabene, P. F., Navarro Mora, G., Martinello, M., Rossi, B., Merigo, F., Ottoboni, L., et al. (2008). A role for leukocyte-endothelial adhesion mechanisms in epilepsy. *Nat. Med.* 14, 1377–1383. doi:10.1038/nm.1878

Farrelly, L. A., and Maze, I. (2019). An emerging perspective on "histone code" mediated regulation of neural plasticity and disease. *Curr. Opin. Neurobiol.* 59, 157–163. doi:10.1016/j.conb.2019.07.001

Fatemi, M., Pao, M. M., Jeong, S., Gal-Yam, E. N., Egger, G., Weisenberger, D. J., et al. (2005). Footprinting of mammalian promoters: use of a CpG DNA methyltransferase revealing nucleosome positions at a single molecule level. *Nucleic Acids Res.* 33, e176. doi:10.1093/nar/gni180

Feng, J., Zhou, Y., Campbell, S. L., Li, E., Sweatt, J. D., et al. (2010). Dnmt1 and Dnmt3a maintain DNA methylation and regulate synaptic function in adult forebrain neurons. *Nat. Neurosci.* 13, 423–430. doi:10.1038/nn.2514

Foldvari, M., and Bagonluri, M. (2008). Carbon nanotubes as functional excipients for nanomedicines: II. Drug delivery and biocompatibility issues. *Nanomedicine Nanotechnol. Biol. Med.* 4, 183–200. doi:10.1016/j.nano.2008.04.003

Foresti, M. L., Arisi, G. M., Katki, K., Montañez, A., Sanchez, R. M., and Shapiro, L. A. (2009). Chemokine CCL2 and its receptor CCR2 are increased in the hippocampus following pilocarpine-induced status epilepticus. *J. Neuroinflammation* 6, 40. doi:10.1186/1742-2094-6-40

Freitas, R. M., Vasconcelos, S. M. M., Souza, F. C. F., Viana, G. S. B., and Fonteles, M. M. F. (2005). Oxidative stress in the hippocampus after pilocarpine-induced status epilepticus in Wistar rats. *FEBS J.* 272, 1307–1312. doi:10.1111/j.1742-4658.2004.04537.x

Friedman, A., and Dingledine, R. (2011). Molecular cascades that mediate the influence of inflammation on epilepsy. *Epilepsia* 52 (Suppl. 3), 33–39. doi:10.1111/j.1528-1167.2011.03034.x

Funk, J. L., Frye, J. B., Davis-Gorman, G., Spera, A. L., Bernas, M. J., Witte, M. H., et al. (2013). Curcuminoids limit neutrophil-mediated reperfusion injury in experimental stroke by targeting the endothelium. *Microcirc. N. Y. N.* 20, 544–554. doi:10.1111/micc.12054

Gaitatzis, A., Carroll, K., Majeed, A., and W Sander, J. (2004). The epidemiology of the comorbidity of epilepsy in the general population. *Epilepsia* 45, 1613–1622. doi:10.1111/j.0013-9580.2004.17504.x

Gangar, K., and Bhatt, L. K. (2020). Therapeutic targets for the treatment of comorbidities associated with epilepsy. *Curr. Mol. Pharmacol.* 13, 85–93. doi:10.2174/1874467212666191203101606

Ganjali, S., Sahebkar, A., Mahdipour, E., Jamialahmadi, K., Torabi, S., Akhlaghi, S., et al. (2014). Investigation of the effects of curcumin on serum cytokines in obese individuals: a randomized controlled trial. *ScientificWorldJournal* 2014, 898361. doi:10.1155/2014/898361

Gilliam, F., Carter, J., and Vahle, V. (2004). Tolerability of antiseizure medications: implications for health outcomes. *Neurology* 63, S9-S12–S12. doi:10.1212/wnl.63.10_suppl_4.s9

Gluck, M. R., Jayatilleke, E., Shaw, S., Rowan, A. J., and Haroutunian, V. (2000). CNS oxidative stress associated with the kainic acid rodent model of experimental epilepsy. *Epilepsy Res.* 39, 63–71. doi:10.1016/s0920-1211(99)00111-4

Gonzales, A. M., and Orlando, R. A. (2008). Curcumin and resveratrol inhibit nuclear factor-kappaB-mediated cytokine expression in adipocytes. *Nutr. Metab.* 5, 17. doi:10.1186/1743-7075-5-17

Gosselin, R. D., Varela, C., Banisadr, G., Mechighel, P., Rostene, W., Kitabgi, P., et al. (2005). Constitutive expression of CCR2 chemokine receptor and inhibition by MCP-1/CCL2 of GABA-induced currents in spinal cord neurones. *J. Neurochem.* 95, 1023–1034. doi:10.1111/j.1471-4159.2005.03431.x

Grandjean-Laquerriere, A., Gangloff, S. C., Le Naour, R., Trentesaux, C., Hornebeck, W., and Guenounou, M. (2002). Relative contribution of NF-kappaB and AP-1 in the modulation by curcumin and pyrrolidine dithiocarbamate of the UVB-induced cytokine expression by keratinocytes. *Cytokine* 18, 168–177. doi:10.1006/cyto.2002.0888

Griffin, C. E., Kaye, A. M., Bueno, F. R., and Kaye, A. D. (2013). Benzodiazepine pharmacology and central nervous system-mediated effects. *Ochsner J.* 13, 214–223.

Guermonprez, P., Valladeau, J., Zitvogel, L., Théry, C., and Amigorena, S. (2002). Antigen presentation and T cell stimulation by dendritic cells. *Annu. Rev. Immunol.* 20, 621–667. doi:10.1146/annurev.immunol.20.100301.064828

Gupta, Y. K., Briyal, S., and Sharma, M. (2009). Protective effect of curcumin against kainic acid induced seizures and oxidative stress in rats. *Indian J. Physiol. Pharmacol.* 53, 39–46.

Hall, A. M., Brennan, G. P., Nguyen, T. M., Singh-Taylor, A., Mun, H. S., Sargious, M. J., et al. (2017). The role of Sirt1 in epileptogenesis. *eNeuro* 4, 0301–0316.2017. doi:10.1523/ENEURO.0301-16.2017

Han, S.-S., Keum, Y.-S., Seo, H.-J., and Surh, Y.-J. (2002). Curcumin suppresses activation of NF-kappaB and AP-1 induced by phorbol ester in cultured human promyelocytic leukemia cells. *J. Biochem. Mol. Biol.* 35, 337–342. doi:10.5483/bmbrep.2002.35.3.337

Harrison, J. F., Hollensworth, S. B., Spitz, D. R., Copeland, W. C., Wilson, G. L., and LeDoux, S. P. (2005). Oxidative stress-induced apoptosis in neurons correlates with mitochondrial DNA base excision repair pathway imbalance. *Nucleic Acids Res.* 33, 4660–4671. doi:10.1093/nar/gki759

Hashemian, M., Anissian, D., Ghasemi-Kasman, M., Akbari, A., Khalili-Fomeshi, M., Ghasemi, S., et al. (2017). Curcumin-loaded chitosan-alginate-STPP nanoparticles ameliorate memory deficits and reduce glial activation in pentylenetetrazol-induced kindling model of epilepsy. *Prog. Neuropsychopharmacol. Biol. Psychiatry* 79, 462–471. doi:10.1016/j.pnpbp.2017.07.025

Hassan, F.-U., Rehman, M. S.-U., Khan, M. S., Ali, M. A., Javed, A., Nawaz, A., et al. (2019). Curcumin as an alternative epigenetic modulator: mechanism of action and potential effects. *Front. Genet.* 10, 514. doi:10.3389/fgene.2019.00514

Hayden, M. S., and Ghosh, S. (2008). Shared principles in NF-kappaB signaling. *Cell* 132, 344–362. doi:10.1016/j.cell.2008.01.020

He, Q., Jiang, L., Man, S., Wu, L., Hu, Y., and Chen, W. (2018). Curcumin reduces neuronal loss and inhibits the NLRP3 inflammasome activation in an epileptic rat model. *Curr. Neurovasc Res.* 15, 186–192. doi:10.2174/1567202615666180731100224

Henshall, D. C., Clark, R. S., Adelson, P. D., Chen, M., Watkins, S. C., and Simon, R. P. (2000). Alterations in bcl-2 and caspase gene family protein expression in human temporal lobe epilepsy. *Neurology* 55, 250–257. doi:10.1212/wnl.55.2.250

Henshall, D. C., and Engel, T. (2013). Contribution of apoptosis-associated signaling pathways to epileptogenesis: lessons from Bcl-2 family knockouts. *Front. Cell Neurosci.* 7, 110. doi:10.3389/fncel.2013.00110

Henshall, D. C., and Meldrum, B. S. (2012). "Cell death and survival mechanisms after single and repeated brief seizures," in *Jasper's basic mechanisms of the epilepsies* J. Noebels, M. Avoli, and M. Rogawski (Oxford University Press), 362–376.

Hernández, R., Fernández, M., de los, A., Miranda, G., and Suástegui, R. (2005). Decrease of folic acid and cognitive alterations in patients with epilepsy treated with phenytoin or carbamazepine, pilot study. *Rev. Investig. Clin. Organo Hosp. Enfermedades Nutr.* 57, 522–531.

Hoesel, B., and Schmid, J. A. (2013). The complexity of NF-κB signaling in inflammation and cancer. *Mol. Cancer* 12, 86. doi:10.1186/1476-4598-12-86

Huang, G., Yang, Y., Xu, Z., Zhou, P., Gong, W., Li, Y., et al. (2011). Downregulation of B lymphocyte stimulator expression by curcumin in B lymphocyte via suppressing nuclear translocation of NF-κB. *Eur. J. Pharmacol.* 650, 451–457. doi:10.1016/j.ejphar.2010.09.065

Huang, L., Chen, C., Zhang, X., Li, X., Chen, Z., Yang, C., et al. (2018). Neuroprotective effect of curcumin against cerebral ischemia-reperfusion via mediating autophagy and inflammation. *J. Mol. Neurosci. MN* 64, 129–139. doi:10.1007/s12031-017-1006-x

Huang, R., Zhu, Y., Lin, L., Song, S., and Cheng, L. (2020). Solid lipid nanoparticles enhanced the neuroprotective role of curcumin against epilepsy through activation of bcl-2 family and P38 MAPK pathways. *ACS Chem. Neurosci.* 11, 1985–1995. doi:10.1021/acschemneuro.0c00242

Huang, Y., Doherty, J. J., and Dingledine, R. (2002). Altered histone acetylation at glutamate receptor 2 and brain-derived neurotrophic factor genes is an early event triggered by status epilepticus. *J. Neurosci. Off. J. Soc. Neurosci.* 22, 8422–8428. doi:10.1523/JNEUROSCI.22-19-08422.2002

Huang, Y., Zhao, F., Wang, L., Yin, H., Zhou, C., and Wang, X. (2012). Increased expression of histone deacetylases 2 in temporal lobe epilepsy: a study of epileptic patients and rat models. *Synap. N. Y. N.* 66, 151–159. doi:10.1002/syn.20995

Iffland, P. H., Everett, M. E., Cobb-Pitstick, K. M., Bowser, L. E., Barnes, A. E., Babus, J. K., et al. (2022). NPRL3 loss alters neuronal morphology, mTOR localization, cortical lamination, and seizure threshold. *Brain J. Neurol.* awac044, 3872–3885. doi:10.1093/brain/awac044

Iguchi-Ariga, S. M., and Schaffner, W. (1989). CpG methylation of the cAMP-responsive enhancer/promoter sequence TGACGTCA abolishes specific factor binding as well as transcriptional activation. *Genes Dev.* 3, 612–619. doi:10.1101/gad.3.5.612

Infantino, V., Iacobazzi, V., Menga, A., Avantaggiati, M. L., and Palmieri, F. (2014). A key role of the mitochondrial citrate carrier (SLC25A1) in TNFα- and IFNγ-triggered inflammation. *Biochim. Biophys. Acta* 1839, 1217–1225. doi:10.1016/j.bbagrm.2014.07.013

Iori, V., Iyer, A. M., Ravizza, T., Beltrame, L., Paracchini, L., Marchini, S., et al. (2017). Blockade of the IL-1R1/TLR4 pathway mediates disease-modification therapeutic effects in a model of acquired epilepsy. *Neurobiol. Dis.* 99, 12–23. doi:10.1016/j.nbd.2016.12.007

Iori, V., Maroso, M., Rizzi, M., Iyer, A. M., Vertemara, R., Carli, M., et al. (2013). Receptor for Advanced Glycation Endproducts is upregulated in temporal lobe epilepsy and contributes to experimental seizures. *Neurobiol. Dis.* 58, 102–114. doi:10.1016/j.nbd.2013.03.006

Islam, R., Dash, D., and Singh, R. (2022). Intranasal curcumin and sodium butyrate modulates airway inflammation and fibrosis via HDAC inhibition in allergic asthma. *Cytokine* 149, 155720. doi:10.1016/j.cyto.2021.155720

Iyer, A., Zurolo, E., Spliet, W. G. M., van Rijen, P. C., Baayen, J. C., Gorter, J. A., et al. (2010). Evaluation of the innate and adaptive immunity in type I and type II focal cortical dysplasias: innate and Adaptive Immunity in FCD I and FCD II. *Epilepsia* 51, 1763–1773. doi:10.1111/j.1528-1167.2010.02547.x

Jagetia, G. C., and Aggarwal, B. B. (2007). "Spicing up" of the immune system by curcumin. *J. Clin. Immunol.* 27, 19–35. doi:10.1007/s10875-006-9066-7

Jagirdar, R., Drexel, M., Bukovac, A., Tasan, R. O., and Sperk, G. (2016). Expression of class II histone deacetylases in two mouse models of temporal lobe epilepsy. *J. Neurochem.* 136, 717–730. doi:10.1111/jnc.13440

Jagirdar, R., Drexel, M., Kirchmair, E., Tasan, R. O., and Sperk, G. (2015). Rapid changes in expression of class I and IV histone deacetylases during epileptogenesis in mouse models of temporal lobe epilepsy. *Exp. Neurol.* 273, 92–104. doi:10.1016/j.expneurol.2015.07.026

Jaworski, J., Spangler, S., Seeburg, D. P., Hoogenraad, C. C., and Sheng, M. (2005). Control of dendritic arborization by the phosphoinositide-3'-kinase-Akt-mammalian target of rapamycin pathway. *J. Neurosci. Off. J. Soc. Neurosci.* 25, 11300–11312. doi:10.1523/JNEUROSCI.2270-05.2005

Jeong, Y.-I., Kim, S. W., Jung, I. D., Lee, J. S., Chang, J. H., Lee, C. M., et al. (2009). Curcumin suppresses the induction of indoleamine 2,3-dioxygenase by blocking the Janus-activated kinase-protein kinase Cdelta-STAT1 signaling pathway in interferon-gamma-stimulated murine dendritic cells. *J. Biol. Chem.* 284, 3700–3708. doi:10.1074/jbc.M807328200

Jeziorska, D. M., Murray, R. J. S., De, G. M., Gaentzsch, R., Garrick, D., Ayyub, H., et al. (2017). DNA methylation of intragenic CpG islands depends on their transcriptional activity during differentiation and disease. *Proc. Natl. Acad. Sci. U. S. A.* 114, E7526–E7535. doi:10.1073/pnas.1703087114

Jha, A. K., Nikbakht, M., Parashar, G., Shrivastava, A., Capalash, N., and Kaur, J. (2010). Reversal of hypermethylation and reactivation of the RARβ2 gene by natural compounds in cervical cancer cell lines. *Folia Biol. (Praha)* 56, 195–200. doi:10.14712/fb2010056050195

Jia, T., Sun, Z., Lu, Y., Gao, J., Zou, H., Xie, F., et al. (2016). A dual brain-targeting curcumin-loaded polymersomes ameliorated cognitive dysfunction in intrahippocampal amyloid-β1-42-injected mice. *Int. J. Nanomedicine* 11, 3765–3775. doi:10.2147/IJN.S94622

Jiang, Z., Guo, M., Shi, C., Wang, H., Yao, L., Liu, L., et al. (2015). Protection against cognitive impairment and modification of epileptogenesis with curcumin in a post-status epilepticus model of temporal lobe epilepsy. *Neuroscience* 310, 362–371. doi:10.1016/j.neuroscience.2015.09.058

Jobin, C., Bradham, C. A., Russo, M. P., Juma, B., Narula, A. S., Brenner, D. A., et al. (1999). Curcumin blocks cytokine-mediated NF-kappa B activation and proinflammatory gene expression by inhibiting inhibitory factor I-kappa B kinase activity. *J. Immunol. Balt. Md* 163, 3474–3483. doi:10.4049/jimmunol.163.6.3474

Jokeit, H., Krämer, G., and Ebner, A. (2005). Do antiepileptic drugs accelerate forgetting? *Epilepsy Behav. EB* 6, 430–432. doi:10.1016/j.yebeh.2004.12.012

Joseph, A., Wood, T., Chen, C.-C., Corry, K., Snyder, J. M., Juul, S. E., et al. (2018). Curcumin-loaded polymeric nanoparticles for neuroprotection in neonatal rats with hypoxic-ischemic encephalopathy. *Nano Res.* 11, 5670–5688. doi:10.1007/s12274-018-2104-y

Jülich, K., and Sahin, M. (2014). Mechanism-based treatment in tuberous sclerosis complex. *Pediatr. Neurol.* 50, 290–296. doi:10.1016/j.pediatrneurol.2013.12.002

Jurenka, J. S. (2009). Anti-inflammatory properties of curcumin, a major constituent of Curcuma longa: a review of preclinical and clinical research. *Altern. Med. Rev. J. Clin. Ther.* 14, 141–153.

Jyoti, A., Sethi, P., and Sharma, D. (2009). Curcumin protects against electrobehavioral progression of seizures in the iron-induced experimental model of epileptogenesis. *Epilepsy Behav. EB* 14, 300–308. doi:10.1016/j.yebeh.2008.11.011

Kadam, S., Kanitkar, M., Dixit, K., Deshpande, R., Seshadri, V., and Kale, V. (2018). Curcumin reverses diabetes-induced endothelial progenitor cell dysfunction by enhancing MnSOD expression and activity *in vitro* and *in vivo*. *J. Tissue Eng. Regen. Med.* 12, 1594–1607. doi:10.1002/term.2684

Kajta, M. (2004). Apoptosis in the central nervous system: mechanisms and protective strategies. *Pol. J. Pharmacol.* 56, 689–700.

Kanakasabai, S., Casalini, E., Walline, C. C., Mo, C., Chearwae, W., and Bright, J. J. (2012). Differential regulation of CD4(+) T helper cell responses by curcumin in experimental autoimmune encephalomyelitis. *J. Nutr. Biochem.* 23, 1498–1507. doi:10.1016/j.jnutbio.2011.10.002

Kanner, A. M. (2016). Management of psychiatric and neurological comorbidities in epilepsy. *Nat. Rev. Neurol.* 12, 106–116. doi:10.1038/nrneurol.2015.243

Kaur, H., Bal, A., and Sandhir, R. (2014). Curcumin supplementation improves mitochondrial and behavioral deficits in experimental model of chronic epilepsy. *Pharmacol. Biochem. Behav.* 125, 55–64. doi:10.1016/j.pbb.2014.08.001

Kaur, H., Patro, I., Tikoo, K., and Sandhir, R. (2015). Curcumin attenuates inflammatory response and cognitive deficits in experimental model of chronic epilepsy. *Neurochem. Int.* 89, 40–50. doi:10.1016/j.neuint.2015.07.009

Keskin-Aktan, A., Akbulut, K. G., Yazici-Mutlu, Ç., Sonugur, G., Ocal, M., and Akbulut, H. (2018). The effects of melatonin and curcumin on the expression of SIRT2, Bcl-2 and Bax in the hippocampus of adult rats. *Brain Res. Bull.* 137, 306–310. doi:10.1016/j.brainresbull.2018.01.006

Khairnar, S. V., Pagare, P., Thakre, A., Nambiar, A. R., Junnuthula, V., Abraham, M. C., et al. (2022). Review on the scale-up methods for the preparation of solid lipid nanoparticles. *Pharmaceutics* 14, 1886. doi:10.3390/pharmaceutics14091886

Khatoon, S., Agarwal, N. B., Samim, M., and Alam, O. (2021). Neuroprotective effect of fisetin through suppression of IL-1R/TLR Axis and apoptosis in pentylenetetrazole-induced kindling in mice. *Front. Neurol.* 12, 689069. doi:10.3389/fneur.2021.689069

Khatri, D. K., and Juvekar, A. R. (2016). Neuroprotective effect of curcumin as evinced by abrogation of rotenone-induced motor deficits, oxidative and mitochondrial dysfunctions in mouse model of Parkinson's disease. *Pharmacol. Biochem. Behav.* 150–151, 39–47. doi:10.1016/j.pbb.2016.09.002

Khor, T. O., Huang, Y., Wu, T.-Y., Shu, L., Lee, J., and Kong, A. N. T. (2011). Pharmacodynamics of curcumin as DNA hypomethylation agent in restoring the expression of Nrf2 via promoter CpGs demethylation. *Biochem. Pharmacol.* 82, 1073–1078. doi:10.1016/j.bcp.2011.07.065

Kiasalari, Z., Roghani, M., Khalili, M., Rahmati, B., and Baluchnejadmojarad, T. (2013). Antiepileptogenic effect of curcumin on kainate-induced model of temporal lobe epilepsy. *Pharm. Biol.* 51, 1572–1578. doi:10.3109/13880209.2013.803128

Kim, D. S., Park, S. Y., and Kim, J. K. (2001). Curcuminoids from Curcuma longa L. (Zingiberaceae) that protect PC12 rat pheochromocytoma and normal human umbilical vein endothelial cells from betaA(1-42) insult. *Neurosci. Lett.* 303, 57–61. doi:10.1016/s0304-3940(01)01677-9

Kim, G.-Y., Kim, K.-H., Lee, S.-H., Yoon, M. S., Moon, D. O., et al. (2005). Curcumin inhibits immunostimulatory function of dendritic cells: MAPKs and translocation of NF-kappa B as potential targets. *J. Immunol. Balt. Md* 174, 8116–8124. doi:10.4049/jimmunol.174.12.8116

Kinde, B., Gabel, H. W., Gilbert, C. S., Griffith, E. C., and Greenberg, M. E. (2015). Reading the unique DNA methylation landscape of the brain: non-CpG methylation, hydroxymethylation, and MeCP2. *Proc. Natl. Acad. Sci. U. S. A.* 112, 6800–6806. doi:10.1073/pnas.1411269112

Kobow, K., Jeske, I., Hildebrandt, M., Hauke, J., Hahnen, E., Buslei, R., et al. (2009). Increased reelin promoter methylation is associated with granule cell dispersion in human temporal lobe epilepsy. *J. Neuropathol. Exp. Neurol.* 68, 356–364. doi:10.1097/NEN.0b013e31819ba737

Kobow, K., Kaspi, A., Harikrishnan, K. N., Kiese, K., Ziemann, M., Khurana, I., et al. (2013). Deep sequencing reveals increased DNA methylation in chronic rat epilepsy. *Acta Neuropathol. Berl.* 126, 741–756. doi:10.1007/s00401-013-1168-8

Kodali, M., Hattiangady, B., Shetty, G. A., Bates, A., Shuai, B., and Shetty, A. K. (2018). Curcumin treatment leads to better cognitive and mood function in a model of Gulf War Illness with enhanced neurogenesis, and alleviation of inflammation and mitochondrial dysfunction in the hippocampus. *Brain Behav. Immun.* 69, 499–514. doi:10.1016/j.bbi.2018.01.009

Krantic, S., Mechawar, N., Reix, S., and Quirion, R. (2007). Apoptosis-inducing factor: a matter of neuron life and death. *Prog. Neurobiol.* 81, 179–196. doi:10.1016/j.pneurobio.2006.12.002

Krasovsky, J., Chang, D. H., Deng, G., Yeung, S., Lee, M., Leung, P. C., et al. (2009). Inhibition of human dendritic cell activation by hydroethanolic but not lipophilic extracts of turmeric (Curcuma longa). *Planta Med.* 75, 312–315. doi:10.1055/s-0028-1088367

Krupa, P., Svobodova, B., Dubisova, J., Kubinova, S., Jendelova, P., and Machova Urdzikova, L. (2019). Nano-formulated curcumin (Lipodisq™) modulates the local inflammatory response, reduces glial scar and preserves the white matter after spinal cord injury in rats. *Neuropharmacology* 155, 54–64. doi:10.1016/j.neuropharm.2019.05.018

Kubová, H., Mares, P., Suchomelová, L., Brozek, G., Druga, R., and Pitkänen, A. (2004). Status epilepticus in immature rats leads to behavioural and cognitive impairment and epileptogenesis. *Eur. J. Neurosci.* 19, 3255–3265. doi:10.1111/j.0953-816X.2004.03410.x

Kundu, P., Das, M., Tripathy, K., and Sahoo, S. K. (2016). Delivery of dual drug loaded lipid based nanoparticles across the blood-brain barrier impart enhanced neuroprotection in a rotenone induced mouse model of Parkinson's disease. *ACS Chem. Neurosci.* 7, 1658–1670. doi:10.1021/acschemneuro.6b00207

Kwan, P., Schachter, S. C., and Brodie, M. J. (2011). Drug-resistant epilepsy. *N. Engl. J. Med.* 365, 919–926. doi:10.1056/NEJMra1004418

Kwon, Y. S., Pineda, E., Auvin, S., Shin, D., Mazarati, A., and Sankar, R. (2013). Neuroprotective and antiepileptogenic effects of combination of anti-inflammatory drugs in the immature brain. *J. Neuroinflammation* 10, 30. doi:10.1186/1742-2094-10-30

Lan, C., Chen, X., Zhang, Y., Wang, W., Wang, W. E., Liu, Y., et al. (2018). Curcumin prevents strokes in stroke-prone spontaneously hypertensive rats by improving vascular endothelial function. *BMC Cardiovasc Disord.* 18, 43. doi:10.1186/s12872-018-0768-6

Ledoux, A. C., and Perkins, N. D. (2014). NF-κB and the cell cycle. *Biochem. Soc. Trans.* 42, 76–81. doi:10.1042/BST20130156

Lee, S. J., Krauthauser, C., Maduskuie, V., Fawcett, P. T., Olson, J. M., and Rajasekaran, S. A. (2011). Curcumin-induced HDAC inhibition and attenuation of medulloblastoma growth *in vitro* and *in vivo*. *BMC Cancer* 11, 144. doi:10.1186/1471-2407-11-144

Li, F., Xu, Y., Li, X., Wang, X., Yang, Z., Li, W., et al. (2021c). Triblock copolymer nanomicelles loaded with curcumin attenuates inflammation via inhibiting the NF-κB pathway in the rat model of cerebral ischemia. *Int. J. Nanomedicine* 16, 3173–3183. doi:10.2147/IJN.S300379

Li, M., Jancovski, N., Jafar-Nejad, P., Burbano, L. E., Rollo, B., Richards, K., et al. (2021a). Antisense oligonucleotide therapy reduces seizures and extends life span in an SCN2A gain-of-function epilepsy model. *J. Clin. Invest* 131, e152079. doi:10.1172/JCI152079

Li, N., Li, X., Cheng, P., Yang, P., Shi, P., Kong, L., et al. (2021b). Preparation of curcumin solid lipid nanoparticles loaded with flower-shaped lactose for lung inhalation and preliminary evaluation of cytotoxicity *in vitro*. *Evid-Based Complement. Altern. Med. ECAM* 2021, 4828169. doi:10.1155/2021/4828169

Li, S., Song, D., Huang, W., Li, Z., and Liu, Z. (2020). *In situ* imaging of cysteine in the brains of mice with epilepsy by a near-infrared emissive fluorescent probe. *Anal. Chem.* 92, 2802–2808. doi:10.1021/acs.analchem.9b05211

Li, S., Zhang, H., Chen, K., Jin, M., Vu, S. H., Jung, S., et al. (2022). Application of chitosan/alginate nanoparticle in oral drug delivery systems: prospects and challenges. *Drug Deliv.* 29, 1142–1149. doi:10.1080/10717544.2022.2058646

Li, X.-W., Yang, F., Wang, Y.-G., Wang, J. C., Ma, L., and Jiang, W. (2013). Brain recruitment of dendritic cells following Li-pilocarpine induced status epilepticus in adult rats. *Brain Res. Bull.* 91, 8–13. doi:10.1016/j.brainresbull.2012.11.007

Liang, L. P., Ho, Y. S., and Patel, M. (2000). Mitochondrial superoxide production in kainate-induced hippocampal damage. *Neuroscience* 101, 563–570. doi:10.1016/s0306-4522(00)00397-3

Liang, L.-P., and Patel, M. (2006). Seizure-induced changes in mitochondrial redox status. *Free Radic. Biol. Med.* 40, 316–322. doi:10.1016/j.freeradbiomed.2005.08.026

Librizzi, L., Regondi, M. C., Pastori, C., Frigerio, S., Frassoni, C., and de Curtis, M. (2007). Expression of adhesion factors induced by epileptiform activity in the endothelium of the isolated Guinea pig brain *in vitro*. *Epilepsia* 48, 743–751. doi:10.1111/j.1528-1167.2007.01047.x

Lim, D. W., Son, H. J., Um, M. Y., Kim, I. H., Han, D., Cho, S., et al. (2016). Enhanced cognitive effects of demethoxycurcumin, a natural derivative of curcumin on scopolamine-induced memory impairment in mice. *Mol. Basel Switz.* 21, E1022. doi:10.3390/molecules21081022

Lim, G. P., Chu, T., Yang, F., Beech, W., Frautschy, S. A., and Cole, G. M. (2001). The curry spice curcumin reduces oxidative damage and amyloid pathology in an Alzheimer transgenic mouse. *J. Neurosci. Off. J. Soc. Neurosci.* 21, 8370–8377. doi:10.1523/JNEUROSCI.21-21-08370.2001

Lin, Y.-W., Fang, C.-H., Yang, C.-Y., Liang, Y. J., and Lin, F. H. (2022). Investigating a curcumin-loaded PLGA-PEG-PLGA thermo-sensitive hydrogel for the prevention of alzheimer's disease. *Antioxid. Basel Switz.* 11, 727. doi:10.3390/antiox11040727

Link, A., Balaguer, F., Shen, Y., Lozano, J. J., Leung, H. C. E., Boland, C. R., et al. (2013). Curcumin modulates DNA methylation in colorectal cancer cells. *PloS One* 8, e57709. doi:10.1371/journal.pone.0057709

Liu, H., Chen, Y., Cui, G., and Zhou, J. (2005). Curcumin, a potent anti-tumor reagent, is a novel histone deacetylase inhibitor regulating B-NHL cell line Raji proliferation. *Acta Pharmacol. Sin.* 26, 603–609. doi:10.1111/j.1745-7254.2005.00081.x

Liu, X., Ou, S., Xu, T., Liu, S., Yuan, J., Huang, H., et al. (2016). New differentially expressed genes and differential DNA methylation underlying refractory epilepsy. *Oncotarget* 7, 87402–87416. doi:10.18632/oncotarget.13642

Liu, Z., Xie, Z., Jones, W., Pavlovicz, R. E., Liu, S., Yu, J., et al. (2009). Curcumin is a potent DNA hypomethylation agent. *Bioorg Med. Chem. Lett.* 19, 706–709. doi:10.1016/j.bmcl.2008.12.041

Louboutin, J.-P., and Strayer, D. S. (2013). Relationship between the chemokine receptor CCR5 and microglia in neurological disorders: consequences of targeting CCR5 on neuroinflammation, neuronal death and regeneration in a model of epilepsy. *CNS Neurol. Disord. Drug Targets* 12, 815–829. doi:10.2174/18715273113126660173

Lu, J., Duan, W., Guo, Y., Jiang, H., Li, Z., Huang, J., et al. (2012). Mitochondrial dysfunction in human TDP-43 transfected NSC34 cell lines and the protective effect of dimethoxy curcumin. *Brain Res. Bull.* 89, 185–190. doi:10.1016/j.brainresbull.2012.09.005

Lucas, S.-M., Rothwell, N. J., and Gibson, R. M. (2006). The role of inflammation in CNS injury and disease. *Br. J. Pharmacol.* 147 (Suppl. 1), S232–S240. doi:10.1038/sj.bjp.0706400

Luna-Tortós, C., Fedrowitz, M., and Löscher, W. (2008). Several major antiepileptic drugs are substrates for human P-glycoprotein. *Neuropharmacology* 55, 1364–1375. doi:10.1016/j.neuropharm.2008.08.032

Ma, D. K., Jang, M.-H., Guo, J. U., Kitabatake, Y., Chang, M. L., Pow-Anpongkul, N., et al. (2009). Neuronal activity-induced Gadd45b promotes epigenetic DNA demethylation and adult neurogenesis. *Science* 323, 1074–1077. doi:10.1126/science.1166859

Ma, L., Li, R., Huang, H., Yuan, J., Ou, S., Xu, T., et al. (2017). Up-regulated BAFF and BAFF receptor expression in patients with intractable temporal lobe epilepsy and a pilocarpine-induced epilepsy rat model. *Seizure* 48, 79–88. doi:10.1016/j.seizure.2017.03.016

Mansoor, S. R., Hashemian, M., Khalili-Fomeshi, M., Ashrafpour, M., Moghadamnia, A. A., and Ghasemi-Kasman, M. (2018). Upregulation of klotho and erythropoietin contributes to the neuroprotection induced by curcumin-loaded nanoparticles in experimental model of chronic epilepsy. *Brain Res. Bull.* 142, 281–288. doi:10.1016/j.brainresbull.2018.08.010

Mariani, E., Polidori, M. C., Cherubini, A., and Mecocci, P. (2005). Oxidative stress in brain aging, neurodegenerative and vascular diseases: an overview. *J. Chromatogr. B* 827, 65–75. doi:10.1016/j.jchromb.2005.04.023

Maroso, M., Balosso, S., Ravizza, T., Liu, J., Aronica, E., Iyer, A. M., et al. (2010). Toll-like receptor 4 and high-mobility group box-1 are involved in ictogenesis and can be targeted to reduce seizures. *Nat. Med.* 16, 413–419. doi:10.1038/nm.2127

Martinc, B., Grabnar, I., and Vovk, T. (2012). The role of reactive species in epileptogenesis and influence of antiepileptic drug therapy on oxidative stress. *Curr. Neuropharmacol.* 10, 328–343. doi:10.2174/157015912804143504

Mathew, A., Fukuda, T., Nagaoka, Y., Hasumura, T., Morimoto, H., Yoshida, Y., et al. (2012). Curcumin loaded-PLGA nanoparticles conjugated with Tet-1 peptide for potential use in Alzheimer's disease. *PloS One* 7, e32616. doi:10.1371/journal.pone.0032616

McAfoose, J., and Baune, B. T. (2009). Evidence for a cytokine model of cognitive function. *Neurosci. Biobehav Rev.* 33, 355–366. doi:10.1016/j.neubiorev.2008.10.005

McNamara, J. O., Whitney, K. D., Andrews, P. I., He, X. P., Janumpalli, S., and Patel, M. N. (1999). Evidence for glutamate receptor autoimmunity in the pathogenesis of Rasmussen encephalitis. *Adv. Neurol.* 79, 543–550.

Mehla, J., Reeta, K. H., Gupta, P., and Gupta, Y. K. (2010). Protective effect of curcumin against seizures and cognitive impairment in a pentylenetetrazole-kindled epileptic rat model. *Life Sci.* 87, 596–603. doi:10.1016/j.lfs.2010.09.006

Milby, A. H., Halpern, C. H., and Baltuch, G. H. (2008). Vagus nerve stimulation for epilepsy and depression. *Neurother. J. Am. Soc. Exp. Neurother.* 5, 75–85. doi:10.1016/j.nurt.2007.10.071

Miller-Delaney, S. F. C., Bryan, K., Das, S., McKiernan, R. C., Bray, I. M., Reynolds, J. P., et al. (2015). Differential DNA methylation profiles of coding and non-coding genes define hippocampal sclerosis in human temporal lobe epilepsy. *Brain J. Neurol.* 138, 616–631. doi:10.1093/brain/awu373

Miller-Delaney, S. F. C., Das, S., Sano, T., Jimenez-Mateos, E. M., Bryan, K., Buckley, P. G., et al. (2012). Differential DNA methylation patterns define status epilepticus and epileptic tolerance. *J. Neurosci. Off. J. Soc. Neurosci.* 32, 1577–1588. doi:10.1523/JNEUROSCI.5180-11.2012

Mogharbel, B. F., Cardoso, M. A., Irioda, A. C., Stricker, P. E. F., Slompo, R. C., Appel, J. M., et al. (2022). Biodegradable nanoparticles loaded with levodopa and curcumin for treatment of Parkinson's disease. *Mol. Basel Switz.* 27, 2811. doi:10.3390/molecules27092811

Moghassemi, S., and Hadjizadeh, A. (2014). Nano-niosomes as nanoscale drug delivery systems: an illustrated review. *J. Control. Release* 185, 22–36. doi:10.1016/j.jconrel.2014.04.015

Mohajeri, M., Sadeghizadeh, M., Najafi, F., and Javan, M. (2015). Polymerized nano-curcumin attenuates neurological symptoms in EAE model of multiple sclerosis through down regulation of inflammatory and oxidative processes and enhancing neuroprotection and myelin repair. *Neuropharmacology* 99, 156–167. doi:10.1016/j.neuropharm.2015.07.013

Momtazi, A. A., Shahabipour, F., Khatibi, S., Johnston, T. P., Pirro, M., and Sahebkar, A. (2016). Curcumin as a MicroRNA regulator in cancer: a review. *Rev. Physiol. Biochem. Pharmacol.* 171, 1–38. doi:10.1007/112_2016_3

Mortezaee, K., Salehi, E., Mirtavoos-Mahyari, H., Motevaseli, E., Najafi, M., Farhood, B., et al. (2019). Mechanisms of apoptosis modulation by curcumin: implications for cancer therapy. *J. Cell Physiol.* 234, 12537–12550. doi:10.1002/jcp.28122

Moshé, S. L., Perucca, E., Ryvlin, P., and Tomson, T. (2015). Epilepsy: new advances. *Lancet Lond Engl.* 385, 884–898. doi:10.1016/S0140-6736(14)60456-6

Motavaf, M., Sadeghizadeh, M., Babashah, S., Zare, L., and Javan, M. (2020). Protective effects of a nano-formulation of curcumin against cuprizone-induced demyelination in the mouse corpus callosum. *Iran. J. Pharm. Res. IJPR* 19, 310–320. doi:10.22037/ijpr.2020.112952.14033

Mottaghitalab, F., Farokhi, M., Shokrgozar, M. A., Atyabi, F., and Hosseinkhani, H. (2015). Silk fibroin nanoparticle as a novel drug delivery system. *J. Control. Release* 206, 161–176. doi:10.1016/j.jconrel.2015.03.020

Nabavi, S. M., Russo, G. L., Tedesco, I., Daglia, M., Orhan, I. E., et al. (2018). Curcumin and melanoma: from chemistry to medicine. *Nutr. Cancer* 70, 164–175. doi:10.1080/01635581.2018.1412485

Nardelli, B., Belvedere, O., Roschke, V., Moore, P. A., Olsen, H. S., Migone, T. S., et al. (2001). Synthesis and release of B-lymphocyte stimulator from myeloid cells. *Blood* 97, 198–204. doi:10.1182/blood.v97.1.198

Narouiepour, A., Ebrahimzadeh-Bideskan, A., Rajabzadeh, G., Gorji, A., and Negah, S. S. (2022). Neural stem cell therapy in conjunction with curcumin loaded in niosomal nanoparticles enhanced recovery from traumatic brain injury. *Sci. Rep.* 12, 3572. doi:10.1038/s41598-022-07367-1

Neal, E. G., Chaffe, H., Schwartz, R. H., Lawson, M. S., Edwards, N., Fitzsimmons, G., et al. (2008). The ketogenic diet for the treatment of childhood epilepsy: a randomised controlled trial. *Lancet Neurol.* 7, 500–506. doi:10.1016/S1474-4422(08)70092-9

Neumann, A.-M., Abele, J., Kirschstein, T., Engelmann, R., Sellmann, T., Köhling, R., et al. (2017). Mycophenolate mofetil prevents the delayed T cell response after pilocarpine-induced status epilepticus in mice. *PloS One* 12, e0187330. doi:10.1371/journal.pone.0187330

Ng, L. G., Sutherland, A. P. R., Newton, R., Qian, F., Cachero, T. G., Scott, M. L., et al. (2004). B cell-activating factor belonging to the TNF family (BAFF)-R is the principal BAFF receptor facilitating BAFF costimulation of circulating T and B cells. *J. Immunol. Balt. Md* 173, 807–817. doi:10.4049/jimmunol.173.2.807

Nguyen, L. H., Leiser, S. C., Song, D., Brunner, D., Roberds, S. L., Wong, M., et al. (2022). Inhibition of MEK-ERK signaling reduces seizures in two mouse models of tuberous sclerosis complex. *Epilepsy Res.* 181, 106890. doi:10.1016/j.eplepsyres.2022.106890

Ni, F.-F., Li, C.-R., Liao, J.-X., Wang, G. B., Lin, S. F., Xia, Y., et al. (2016). The effects of ketogenic diet on the Th17/Treg cells imbalance in patients with intractable childhood epilepsy. *Seizure* 38, 17–22. doi:10.1016/j.seizure.2016.03.006

Noack, M., and Miossec, P. (2014). Th17 and regulatory T cell balance in autoimmune and inflammatory diseases. *Autoimmun. Rev.* 13, 668–677. doi:10.1016/j.autrev.2013.12.004

O'Neill, L. A., and Kaltschmidt, C. (1997). NF-kappa B: a crucial transcription factor for glial and neuronal cell function. *Trends Neurosci.* 20, 252–258. doi:10.1016/s0166-2236(96)01035-1

Ong, W. Y., Hu, C. Y., Hjelle, O. P., Ottersen, O. P., and Halliwell, B. (2000). Changes in glutathione in the hippocampus of rats injected with kainate: depletion in neurons and upregulation in glia. *Exp. Brain Res.* 132, 510–516. doi:10.1007/s002210000347

Orrenius, S., Gogvadze, V., and Zhivotovsky, B. (2007). Mitochondrial oxidative stress: implications for cell death. *Annu. Rev. Pharmacol. Toxicol.* 47, 143–183. doi:10.1146/annurev.pharmtox.47.120505.105122

Oukka, M. (2007). Interplay between pathogenic Th17 and regulatory T cells. *Ann. Rheum. Dis.* 66 (Suppl. 3), iii87–90. doi:10.1136/ard.2007.078527

Pal, D. K., Evgrafov, O. V., Tabares, P., Zhang, F., Durner, M., and Greenberg, D. A. (2003). BRD2 (RING3) is a probable major susceptibility gene for common juvenile myoclonic epilepsy. *Am. J. Hum. Genet.* 73, 261–270. doi:10.1086/377006

Parashar, G., Parashar, N. C., and Capalash, N. (2012). Curcumin causes promoter hypomethylation and increased expression of FANCF gene in SiHa cell line. *Mol. Cell Biochem.* 365, 29–35. doi:10.1007/s11010-012-1240-z

Patel, M., Liang, L. P., and Roberts, L. J. (2001). Enhanced hippocampal F2-isoprostane formation following kainate-induced seizures. *J. Neurochem.* 79, 1065–1069. doi:10.1046/j.1471-4159.2001.00659.x

Perucca, P., and Gilliam, F. G. (2012). Adverse effects of antiepileptic drugs. *Lancet Neurol.* 11, 792–802. doi:10.1016/S1474-4422(12)70153-9

Petito, C. K., Torres-Muñoz, J. E., Zielger, F., and McCarthy, M. (2006). Brain CD8+ and cytotoxic T lymphocytes are associated with, and may be specific for, human immunodeficiency virus type 1 encephalitis in patients with acquired immunodeficiency syndrome. *J. Neurovirol* 12, 272–283. doi:10.1080/13550280600879204

Pinton, P., Giorgi, C., Siviero, R., Zecchini, E., and Rizzuto, R. (2008). Calcium and apoptosis: ER-mitochondria Ca2+ transfer in the control of apoptosis. *Oncogene* 27, 6407–6418. doi:10.1038/onc.2008.308

Platania, C. B. M., Fidilio, A., Lazzara, F., Piazza, C., Geraci, F., Giurdanella, G., et al. (2018). Retinal protection and distribution of curcumin *in vitro* and *in vivo*. *Front. Pharmacol.* 9, 670. doi:10.3389/fphar.2018.00670

Pluta, R., Bogucka-Kocka, A., Ułamek-Kozioł, M., Furmaga-Jabłońska, W., Januszewski, S., Brzozowska, J., et al. (2015). Neurogenesis and neuroprotection in postischemic brain neurodegeneration with Alzheimer phenotype: is there a role for curcumin? *Folia Neuropathol.* 53, 89–99. doi:10.5114/fn.2015.52405

Pohlen, M. S., Jin, J., Tobias, R. S., and Maheshwari, A. (2017). Pharmacoresistance with newer anti-epileptic drugs in mesial temporal lobe epilepsy with hippocampal sclerosis. *Epilepsy Res.* 137, 56–60. doi:10.1016/j.eplepsyres.2017.09.012

Proix, T., Bartolomei, F., Guye, M., and Jirsa, V. K. (2017). Individual brain structure and modelling predict seizure propagation. *Brain J. Neurol.* 140, 641–654. doi:10.1093/brain/awx004

Ray, B., Bisht, S., Maitra, A., and Lahiri, D. K. (2011). Neuroprotective and neurorescue effects of a novel polymeric nanoparticle formulation of curcumin (NanoCurc™) in the neuronal cell culture and animal model: implications for Alzheimer's disease. *J. Alzheimers Dis. Jad.* 23, 61–77. doi:10.3233/JAD-2010-101374

Razali, N. A., Nazarudin, N. A., Lai, K. S., Abas, F., and Ahmad, S. (2018). Curcumin derivative, 2,6-bis(2-fluorobenzylidene)cyclohexanone (MS65) inhibits interleukin-6 production through suppression of NF-κB and MAPK pathways in histamine-induced human keratinocytes cell (HaCaT). *BMC Complement. Altern. Med.* 18, 217. doi:10.1186/s12906-018-2223-8

Reddy, S. D., Clossen, B. L., and Reddy, D. S. (2018). Epigenetic histone deacetylation inhibition prevents the development and persistence of temporal lobe epilepsy. *J. Pharmacol. Exp. Ther.* 364, 97–109. doi:10.1124/jpet.117.244939

Reeta, K. H., Mehla, J., Pahuja, M., and Gupta, Y. K. (2011). Pharmacokinetic and pharmacodynamic interactions of valproate, phenytoin, phenobarbitone and carbamazepine with curcumin in experimental models of epilepsy in rats. *Pharmacol. Biochem. Behav.* 99, 399–407. doi:10.1016/j.pbb.2011.05.011

Rhodes, R. H., Lehman, R. M., Wu, B. Y., and Roychowdhury, S. (2007). Focal chronic inflammatory epileptic encephalopathy in a patient with malformations of cortical development, with a review of the spectrum of chronic inflammatory epileptic encephalopathy. *Epilepsia* 48, 1184–1202. doi:10.1111/j.1528-1167.2007.01034.x

Roberts, J. L., Poklepovic, A., and Booth, L. (2017). Curcumin interacts with sildenafil to kill GI tumor cells via endoplasmic reticulum stress and reactive oxygen/nitrogen species. *Oncotarget* 8, 99451–99469. doi:10.18632/oncotarget.19807

Rocha, L. (2013). Interaction between electrical modulation of the brain and pharmacotherapy to control pharmacoresistant epilepsy. *Pharmacol. Ther.* 138, 211–228. doi:10.1016/j.pharmthera.2013.01.009

Rodríguez-Cruces, R., Velázquez-Pérez, L., Rodríguez-Leyva, I., Velasco, A. L., Trejo-Martínez, D., Barragán-Campos, H. M., et al. (2018). Association of white matter diffusion characteristics and cognitive deficits in temporal lobe epilepsy. *Epilepsy Behav. EB* 79, 138–145. doi:10.1016/j.yebeh.2017.11.040

Rogers, N. M., Kireta, S., and Coates, P. T. H. (2010). Curcumin induces maturation-arrested dendritic cells that expand regulatory T cells *in vitro* and *in vivo*. *Clin. Exp. Immunol.* 162, 460–473. doi:10.1111/j.1365-2249.2010.04232.x

Rolston, J. D., Quigg, M., and Barbaro, N. M. (2011). Gamma knife radiosurgery for mesial temporal lobe epilepsy. *Epilepsy Res. Treat.* 2011, 840616. doi:10.1155/2011/840616

Rosenblat, J. D., Cha, D. S., Mansur, R. B., and McIntyre, R. S. (2014). Inflamed moods: a review of the interactions between inflammation and mood disorders. *Prog. Neuropsychopharmacol. Biol. Psychiatry* 53, 23–34. doi:10.1016/j.pnpbp.2014.01.013

Rostène, W., Kitabgi, P., and Parsadaniantz, S. M. (2007). Chemokines: a new class of neuromodulator? *Nat. Rev. Neurosci.* 8, 895–903. doi:10.1038/nrn2255

Ruzicka, J., Urdzikova, L. M., Svobodova, B., Amin, A. G., Karova, K., Dubisova, J., et al. (2018). Does combined therapy of curcumin and epigallocatechin gallate have a synergistic neuroprotective effect against spinal cord injury? *Neural Regen. Res.* 13, 119–127. doi:10.4103/1673-5374.224379

Ryley Parrish, R., Albertson, A. J., Buckingham, S. C., Hablitz, J. J., Mascia, K. L., Davis Haselden, W., et al. (2013). Status epilepticus triggers early and late alterations in brain-derived neurotrophic factor and NMDA glutamate receptor Grin2b DNA methylation levels in the hippocampus. *Neuroscience* 248, 602–619. doi:10.1016/j.neuroscience.2013.06.029

Rzezak, P., Lima, E. M., Gargaro, A. C., Coimbra, E., de Vincentiis, S., Velasco, T. R., et al. (2017). Everyday memory impairment in patients with temporal lobe epilepsy caused by hippocampal sclerosis. *Epilepsy Behav. EB* 69, 31–36. doi:10.1016/j.yebeh.2017.01.008

Sang, Q., Liu, X., Wang, L., Qi, L., Sun, W., Wang, W., et al. (2018). Curcumin protects an SH-SY5Y cell model of Parkinson's disease against toxic injury by regulating HSP90. *Cell Physiol. Biochem. Int. J. Exp. Cell Physiol. Biochem. Pharmacol.* 51, 681–691. doi:10.1159/000495326

Sathaliyawala, T., O'Gorman, W. E., Greter, M., Bogunovic, M., Konjufca, V., Hou, Z. E., et al. (2010). Mammalian target of rapamycin controls dendritic cell development downstream of Flt3 ligand signaling. *Immunity* 33, 597–606. doi:10.1016/j.immuni.2010.09.012

Schindler, C. K., Pearson, E. G., Bonner, H. P., Simon, R. P., Prehn, J. H. M., et al. (2006). Caspase-3 cleavage and nuclear localization of caspase-activated DNase in human temporal lobe epilepsy. *J. Cereb. Blood Flow. Metab.* 26, 583–589. doi:10.1038/sj.jcbfm.9600219

Seidel, S., Wehner, T., Miller, D., Wellmer, J., Schlegel, U., and Grönheit, W. (2022). Brain tumor related epilepsy: pathophysiological approaches and rational management of antiseizure medication. *Neurol. Res. Pract.* 4, 45. doi:10.1186/s42466-022-00205-9

Sevastre-Berghian, A. C., Făgărăsan, V., Toma, V. A., Bâldea, I., Olteanu, D., Moldovan, R., et al. (2017). Curcumin reverses the diazepam-induced cognitive impairment by modulation of oxidative stress and ERK 1/2/NF-κB pathway in brain. *Oxid. Med. Cell Longev.* 2017, 3037876. doi:10.1155/2017/3037876

Shandra, O., Moshé, S. L., and Galanopoulou, A. S. (2017). Inflammation in epileptic encephalopathies. *Adv. Protein Chem. Struct. Biol.* 108, 59–84. doi:10.1016/bs.apcsb.2017.01.005

Sharma, C., Suhalka, P., and Bhatnagar, M. (2018). Curcumin and resveratrol rescue cortical-hippocampal system from chronic fluoride-induced neurodegeneration and enhance memory retrieval. *Int. J. Neurosci.* 128, 1007–1021. doi:10.1080/00207454.2018.1458727

Shi, L., Wu, L., Chen, Z., Yang, J., Chen, X., Yu, F., et al. (2015). MiR-141 activates nrf2-dependent antioxidant pathway via down-regulating the expression of Keap1 conferring the resistance of hepatocellular carcinoma cells to 5-fluorouracil. *Cell Physiol. Biochem. Int. J. Exp. Cell Physiol. Biochem. Pharmacol.* 35, 2333–2348. doi:10.1159/000374036

Shi, Y., Miao, W., Teng, J., and Zhang, L. (2018). Ginsenoside Rb1 protects the brain from damage induced by epileptic seizure via Nrf2/ARE signaling. *Cell Physiol. Biochem. Int. J. Exp. Cell Physiol. Biochem. Pharmacol.* 45, 212–225. doi:10.1159/000486768

Shimada, T., Takemiya, T., Sugiura, H., and Yamagata, K. (2014). Role of inflammatory mediators in the pathogenesis of epilepsy. *Mediat. Inflamm.* 2014, 901902. doi:10.1155/2014/901902

Shin, E.-J., Jeong, J. H., Bing, G., Park, E. S., Chae, J. S., Yen, T. P. H., et al. (2008). Kainate-induced mitochondrial oxidative stress contributes to hippocampal

degeneration in senescence-accelerated mice. *Cell Signal* 20, 645–658. doi:10.1016/j.cellsig.2007.11.014

Shin, H. J., Lee, J. Y., Son, E., Lee, D. H., Kim, H. J., Kang, S. S., et al. (2007). Curcumin attenuates the kainic acid-induced hippocampal cell death in the mice. *Neurosci. Lett.* 416, 49–54. doi:10.1016/j.neulet.2007.01.060

Shirley, S. A., Montpetit, A. J., Lockey, R. F., and Mohapatra, S. S. (2008). Curcumin prevents human dendritic cell response to immune stimulants. *Biochem. Biophys. Res. Commun.* 374, 431–436. doi:10.1016/j.bbrc.2008.07.051

Shishodia, S., Singh, T., and Chaturvedi, M. M. (2007). Modulation of transcription factors by curcumin. *Adv. Exp. Med. Biol.* 595, 127–148. doi:10.1007/978-0-387-46401-5_4

Shu, L., Khor, T. O., Lee, J.-H., Boyanapalli, S. S. S., Huang, Y., Wu, T. Y., et al. (2011). Epigenetic CpG demethylation of the promoter and reactivation of the expression of Neurog1 by curcumin in prostate LNCaP cells. *AAPS J.* 13, 606–614. doi:10.1208/s12248-011-9300-y

Singh, A., Mahajan, S. D., Kutscher, H. L., Kim, S., and Prasad, P. N. (2020). Curcumin-pluronic nanoparticles: a theranostic nanoformulation for alzheimer's disease. *Crit. Rev. Biomed. Eng.* 48, 153–168. doi:10.1615/CritRevBiomedEng.2020034302

Singh, V., Eljaaly, K., Md, S., Alhakamy, N. A., and Kesharwani, P. (2022). Triblock copolymeric drug delivery as an emerging nanocarrier for treatment of infectious diseases. *J. Drug Deliv. Sci. Technol.* 75, 103691. doi:10.1016/j.jddst.2022.103691

Sinha, J. K., Ghosh, S., Swain, U., Giridharan, N. V., and Raghunath, M. (2014). Increased macromolecular damage due to oxidative stress in the neocortex and hippocampus of WNIN/Ob, a novel rat model of premature aging. *Neuroscience* 269, 256–264. doi:10.1016/j.neuroscience.2014.03.040

Sng, J. C. G., Taniura, H., and Yoneda, Y. (2006). Histone modifications in kainate-induced status epilepticus. *Eur. J. Neurosci.* 23, 1269–1282. doi:10.1111/j.1460-9568.2006.04641.x

Soetikno, V., Sari, F. R., Veeraveedu, P. T., Thandavarayan, R. A., Harima, M., Sukumaran, V., et al. (2011). Curcumin ameliorates macrophage infiltration by inhibiting NF-κB activation and proinflammatory cytokines in streptozotocin induced-diabetic nephropathy. *Nutr. Metab.* 8, 35. doi:10.1186/1743-7075-8-35

Song, J., Teplova, M., Ishibe-Murakami, S., and Patel, D. J. (2012). Structure-based mechanistic insights into DNMT1-mediated maintenance DNA methylation. *Science* 335, 709–712. doi:10.1126/science.1214453

Spencer, S., and Huh, L. (2008). Outcomes of epilepsy surgery in adults and children. *Lancet Neurol.* 7, 525–537. doi:10.1016/S1474-4422(08)70109-1

Stafstrom, C. E., and Carmant, L. (2015). Seizures and epilepsy: an overview for neuroscientists. *Cold Spring Harb. Perspect. Med.* 5, a022426. doi:10.1101/cshperspect.a022426

Starr, T. K., Jameson, S. C., and Hogquist, K. A. (2003). Positive and negative selection of T cells. *Annu. Rev. Immunol.* 21, 139–176. doi:10.1146/annurev.immunol.21.120601.141107

Steinman, R. M. (2003). The control of immunity and tolerance by dendritic cell. *Pathol. Biol. Paris.* 51, 59–60. doi:10.1016/s0369-8114(03)00096-8

Stellwagen, D., Beattie, E. C., Seo, J. Y., and Malenka, R. C. (2005). Differential regulation of AMPA receptor and GABA receptor trafficking by tumor necrosis factor-alpha. *J. Neurosci. Off. J. Soc. Neurosci.* 25, 3219–3228. doi:10.1523/JNEUROSCI.4486-04.2005

Sudha, K., Rao, A. V., and Rao, A. (2001). Oxidative stress and antioxidants in epilepsy. *Clin. Chim. Acta* 303, 19–24. doi:10.1016/S0009-8981(00)00337-5

Sundaram, J. R., Poore, C. P., Sulaimee, N. H. B., Pareek, T., Cheong, W. F., Wenk, M. R., et al. (2017). Curcumin ameliorates neuroinflammation, neurodegeneration, and memory deficits in p25 transgenic mouse model that bears hallmarks of alzheimer's disease. *J. Alzheimers Dis. Jad.* 60, 1429–1442. doi:10.3233/JAD-170093

Tai, X. Y., Bernhardt, B., Thom, M., Thompson, P., Baxendale, S., Koepp, M., et al. (2018). Review: neurodegenerative processes in temporal lobe epilepsy with hippocampal sclerosis: clinical, pathological and neuroimaging evidence. *Neuropathol. Appl. Neurobiol.* 44, 70–90. doi:10.1111/nan.12458

Tang, F., Hartz, A. M. S., and Bauer, B. (2017). Drug-resistant epilepsy: multiple hypotheses, few answers. *Front. Neurol.* 8, 301. doi:10.3389/fneur.2017.00301

Tang, S. J., Reis, G., Kang, H., Gingras, A. C., Sonenberg, N., and Schuman, E. M. (2002). A rapamycin-sensitive signaling pathway contributes to long-term synaptic plasticity in the hippocampus. *Proc. Natl. Acad. Sci.* 99, 467–472. doi:10.1073/pnas.012605299

Teafatiller, T., Subramanian, S., Marquez, F. E., Kitazawa, M., and Subramanian, V. S. (2022). Valproic acid upregulates sodium-dependent vitamin C transporter-2 functional expression in neuronal cells. *Life Sci.* 308, 120944. doi:10.1016/j.lfs.2022.120944

Templin, J., Atanackovic, D., Hasche, D., Radhakrishnan, S. V., and Luetkens, T. (2017). Oscillating expression of interleukin-16 in multiple myeloma is associated with proliferation, clonogenic growth, and PI3K/NFKB/MAPK activation. *Oncotarget* 8, 49253–49263. doi:10.18632/oncotarget.17534

Terrone, G., Pauletti, A., Salamone, A., Rizzi, M., Villa, B. R., Porcu, L., et al. (2018). Inhibition of monoacylglycerol lipase terminates diazepam-resistant status epilepticus in mice and its effects are potentiated by a ketogenic diet. *Epilepsia* 59, 79–91. doi:10.1111/epi.13950

Tiwari, S. K., Agarwal, S., Seth, B., Yadav, A., Nair, S., Bhatnagar, P., et al. (2014). Curcumin-loaded nanoparticles potently induce adult neurogenesis and reverse cognitive deficits in Alzheimer's disease model via canonical Wnt/β-catenin pathway. *ACS Nano* 8, 76–103. doi:10.1021/nn405077y

Tiwari, V., and Chopra, K. (2012). Attenuation of oxidative stress, neuroinflammation, and apoptosis by curcumin prevents cognitive deficits in rats postnatally exposed to ethanol. *Psychopharmacol. Berl.* 224, 519–535. doi:10.1007/s00213-012-2779-9

Toledano, R., and Gil-Nagel, A. (2008). Adverse effects of antiepileptic drugs. *Semin. Neurol.* 28, 317–327. doi:10.1055/s-2008-1079336

Torres-Aguilar, H., Aguilar-Ruiz, S. R., González-Pérez, G., Munguía, R., Bajaña, S., Meraz-Ríos, M. A., et al. (2010). Tolerogenic dendritic cells generated with different immunosuppressive cytokines induce antigen-specific anergy and regulatory properties in memory CD4+ T cells. *J. Immunol. Balt. Md* 184, 1765–1775. doi:10.4049/jimmunol.0902133

Tsankova, N., Renthal, W., Kumar, A., and Nestler, E. J. (2007). Epigenetic regulation in psychiatric disorders. *Nat. Rev. Neurosci.* 8, 355–367. doi:10.1038/nrn2132

Valim, C. X. R., da Silva, E. Z. M., Assis, M. A., Fernandes, F. F., Coelho, P. S. R., Oliver, C., et al. (2015). rPbPga1 from paracoccidioides brasiliensis activates mast cells and macrophages via NFkB. *PLoS Negl. Trop. Dis.* 9, e0004032. doi:10.1371/journal.pntd.0004032

van Gassen, K. L. I., de Wit, M., Koerkamp, MJAG, Rensen, M. G. A., van Rijen, P. C., Holstege, F. C. P., et al. (2008). Possible role of the innate immunity in temporal lobe epilepsy. *Epilepsia* 49, 1055–1065. doi:10.1111/j.1528-1167.2007.01470.x

van Gassen, K. L. I., Netzeband, J. G., de Graan, P. N. E., and Gruol, D. L. (2005). The chemokine CCL2 modulates Ca2+ dynamics and electrophysiological properties of cultured cerebellar Purkinje neurons. *Eur. J. Neurosci.* 21, 2949–2957. doi:10.1111/j.1460-9568.2005.04113.x

Vezzani, A. (2014). Epilepsy and inflammation in the brain: overview and pathophysiology. *Epilepsy Curr.* 14, 3–7. doi:10.5698/1535-7511-14.s2.3

Vezzani, A. (2015). Anti-inflammatory drugs in epilepsy: does it impact epileptogenesis? *Expert Opin. Drug Saf.* 14, 583–592. doi:10.1517/14740338.2015.1010508

Vezzani, A., Aronica, E., Mazarati, A., and Pittman, Q. J. (2013). Epilepsy and brain inflammation. *Exp. Neurol.* 244, 11–21. doi:10.1016/j.expneurol.2011.09.033

Vezzani, A., French, J., Bartfai, T., and Baram, T. Z. (2011). The role of inflammation in epilepsy. *Nat. Rev. Neurol.* 7, 31–40. doi:10.1038/nrneurol.2010.178

Vignoli, A., La Briola, F., Peron, A., Turner, K., Vannicola, C., Saccani, M., et al. (2015). Autism spectrum disorder in tuberous sclerosis complex: searching for risk markers. *Orphanet J. Rare Dis.* 10, 154. doi:10.1186/s13023-015-0371-1

Villadangos, J. A. (2001). Presentation of antigens by MHC class II molecules: getting the most out of them. *Mol. Immunol.* 38, 329–346. doi:10.1016/s0161-5890(01)00069-4

Vucic, M., Cojbasic, I., Vucic, J., and Pavlovic, V. (2018). The effect of curcumin and PI3K/Akt inhibitor on monosodium glutamate-induced rat thymocytes toxicity. *Gen. Physiol. Biophys.* 37, 329–336. doi:10.4149/gpb_2017050

Walia, K. S., Khan, E. A., Ko, D. H., Raza, S. S., and Khan, Y. N. (2004). Side effects of antiepileptics-a review. *Pain Pract. Off. J. World Inst. Pain* 4, 194–203. doi:10.1111/j.1533-2500.2004.04304.x

Wang, S., Li, H., Zhang, M., Yue, L. T., Wang, C. C., Zhang, P., et al. (2016). Curcumin ameliorates experimental autoimmune myasthenia gravis by diverse immune cells. *Neurosci. Lett.* 626, 25–34. doi:10.1016/j.neulet.2016.05.020

Wang, W., Wu, Y., Zhang, G., Fang, H., Wang, H., Zang, H., et al. (2014). Activation of Nrf2-ARE signal pathway protects the brain from damage induced by epileptic seizure. *Brain Res.* 1544, 54–61. doi:10.1016/j.brainres.2013.12.004

Weaver, D. F., and Pohlmann-Eden, B. (2013). Pharmacoresistant epilepsy: unmet needs in solving the puzzle(s). *Epilepsia* 54, 80–85. doi:10.1111/epi.12191

Williams-Karnesky, R. L., Sandau, U. S., Lusardi, T. A., Lytle, N. K., Farrell, J. M., Pritchard, E. M., et al. (2013). Epigenetic changes induced by adenosine augmentation therapy prevent epileptogenesis. *J. Clin. Invest* 123, 3552–3563. doi:10.1172/JCI65636

Willmore, L. J., Sypert, G. W., and Munson, J. B. (1978). Recurrent seizures induced by cortical iron injection: a model of posttraumatic epilepsy. *Ann. Neurol.* 4, 329–336. doi:10.1002/ana.410040408

Wilson, C. J., Finch, C. E., and Cohen, H. J. (2002). Cytokines and cognition-the case for a head-to-toe inflammatory paradigm. *J. Am. Geriatr. Soc.* 50, 2041–2056. doi:10.1046/j.1532-5415.2002.50619.x

Winzler, C., Rovere, P., Rescigno, M., Granucci, F., Penna, G., Adorini, L., et al. (1997). Maturation stages of mouse dendritic cells in growth factor-dependent long-term cultures. *J. Exp. Med.* 185, 317–328. doi:10.1084/jem.185.2.317

Wong, M. (2013). A critical review of mTOR inhibitors and epilepsy: from basic science to clinical trials. *Expert Rev. Neurother.* 13, 657–669. doi:10.1586/ern.13.48

Xia, M., Ye, Z., Shi, Y., Zhou, L., and Hua, Y. (2017). Curcumin improves diabetes mellitus-associated cerebral infarction by increasing the expression of GLUT1 and GLUT3. *Mol. Med. Rep.* 17, 1963–1969. doi:10.3892/mmr.2017.8085

Xiang, B., Li, D., Chen, Y., Zhang, Y., Sun, T., et al. (2021). Curcumin ameliorates copper-induced neurotoxicity through inhibiting oxidative stress and mitochondrial apoptosis in SH-SY5Y cells. *Neurochem. Res.* 46, 367–378. doi:10.1007/s11064-020-03173-1

Xiao, Z., Peng, J., Yang, L., Kong, H., and Yin, F. (2015). Interleukin-1β plays a role in the pathogenesis of mesial temporal lobe epilepsy through the PI3K/Akt/mTOR signaling pathway in hippocampal neurons. *J. Neuroimmunol.* 282, 110–117. doi:10.1016/j.jneuroim.2015.04.003

Xie, T., Wang, W., Mao, Z., Qu, Z. z., Luan, S. q., Jia, L. j., et al. (2012). Effects of epigallocatechin-3-gallate on pentylenetetrazole-induced kindling, cognitive impairment and oxidative stress in rats. *Neurosci. Lett.* 516, 237–241. doi:10.1016/j.neulet.2012.04.001

Xie, X., Tao, Q., Zou, Y., Zhang, F., Guo, M., Wang, Y., et al. (2011). PLGA nanoparticles improve the oral bioavailability of curcumin in rats: characterizations and mechanisms. *J. Agric. Food Chem.* 59, 9280–9289. doi:10.1021/jf202135j

Xing, H.-Y., Cai, Y.-Q., Wang, X.-F., Wang, L. L., Li, P., Wang, G. Y., et al. (2015). The cytoprotective effect of hyperoside against oxidative stress is mediated by the nrf2-ARE signaling pathway through GSK-3β inactivation. *PloS One* 10, e0145183. doi:10.1371/journal.pone.0145183

Xu, L., Sun, Z., Xing, Z., Liu, Y., Zhao, H., Tang, Z., et al. (2022). Cur@SF NPs alleviate Friedreich's ataxia in a mouse model through synergistic iron chelation and antioxidation. *J. Nanobiotechnology* 20, 118. doi:10.1186/s12951-022-01333-9

Xu, S., Pang, Q., Liu, Y., Shang, W., Zhai, G., and Ge, M. (2007). Neuronal apoptosis in the resected sclerotic hippocampus in patients with mesial temporal lobe epilepsy. *J. Clin. Neurosci.* 14, 835–840. doi:10.1016/j.jocn.2006.08.002

Xu, Z.-H., Wang, Y., Tao, A.-F., Yu, J., Wang, X. Y., Zu, Y. Y., et al. (2016). Interleukin-1 receptor is a target for adjunctive control of diazepam-refractory status epilepticus in mice. *Neuroscience* 328, 22–29. doi:10.1016/j.neuroscience.2016.04.036

Yang, C., Han, M., Li, R., Zhou, L., Zhang, Y., Duan, L., et al. (2021). Curcumin nanoparticles inhibiting ferroptosis for the enhanced treatment of intracerebral hemorrhage. *Int. J. Nanomedicine* 16, 8049–8065. doi:10.2147/IJN.S334965

Yang, X., Lv, J.-N., Li, H., Jiao, B., Zhang, Q. H., Zhang, Y., et al. (2017). Curcumin reduces lung inflammation via Wnt/β-catenin signaling in mouse model of asthma. *J. Asthma Off. J. Assoc. Care Asthma* 54, 335–340. doi:10.1080/02770903.2016.1218018

Yi, L.-T., Dong, S.-Q., Wang, S.-S., Chen, M., Li, C. F., Geng, D., et al. (2020). Curcumin attenuates cognitive impairment by enhancing autophagy in chemotherapy. *Neurobiol. Dis.* 136, 104715. doi:10.1016/j.nbd.2019.104715

Yoshikawa, K., Kita, Y., Kishimoto, K., and Shimizu, T. (2006). Profiling of eicosanoid production in the rat hippocampus during kainic acid-induced seizure: dual phase regulation and differential involvement of COX-1 and COX-2. *J. Biol. Chem.* 281, 14663–14669. doi:10.1074/jbc.M511089200

Yu, J., Peng, Y., Wu, L.-C., Xie, Z., Deng, Y., Hughes, T., et al. (2013). Curcumin down-regulates DNA methyltransferase 1 and plays an anti-leukemic role in acute myeloid leukemia. *PloS One* 8, e55934. doi:10.1371/journal.pone.0055934

Yuan, J., Liu, W., Zhu, H., Chen, Y., Zhang, X., Li, L., et al. (2017). Curcumin inhibits glial scar formation by suppressing astrocyte-induced inflammation and fibrosis *in vitro* and *in vivo*. *Brain Res.* 1655, 90–103. doi:10.1016/j.brainres.2016.11.002

Yürekli, V. A., and Nazıroğlu, M. (2013). Selenium and topiramate attenuates blood oxidative toxicity in patients with epilepsy: a clinical pilot study. *Biol. Trace Elem. Res.* 152, 180–186. doi:10.1007/s12011-013-9616-9

Zaccara, G., Franciotta, D., and Perucca, E. (2007). Idiosyncratic adverse reactions to antiepileptic drugs. *Epilepsia* 48, 1223–1244. doi:10.1111/j.1528-1167.2007.01041.x

Zhang, H., Zheng, W., Feng, X., Yang, F., Qin, H., Wu, S., et al. (2019). Nrf2–ARE signaling acts as master pathway for the cellular antioxidant activity of fisetin. *Molecules* 24, 708. doi:10.3390/molecules24040708

Zhang, N., Yan, F., Liang, X., Wu, M., Shen, Y., Chen, M., et al. (2018). Localized delivery of curcumin into brain with polysorbate 80-modified cerasomes by ultrasound-targeted microbubble destruction for improved Parkinson's disease therapy. *Theranostics* 8, 2264–2277. doi:10.7150/thno.23734

Zhang, X., Zhou, X., Li, L., Sun, M., Gao, Q., Zhang, P., et al. (2016). Chronic hypoxia in pregnancy affects thymus development in Balb/c mouse offspring via IL2 Signaling. *Mol. Reprod. Dev.* 83, 337–346. doi:10.1002/mrd.22630

Zhang, Y., Yan, Y., Cao, Y., Yang, Y., Zhao, Q., Jing, R., et al. (2017). Potential therapeutic and protective effect of curcumin against stroke in the male albino stroke-induced model rats. *Life Sci.* 183, 45–49. doi:10.1016/j.lfs.2017.06.023

Zhao, H.-M., Xu, R., Huang, X.-Y., Cheng, S. M., Huang, M. F., Yue, H. Y., et al. (2016a). Curcumin improves regulatory T cells in gut-associated lymphoid tissue of colitis mice. *World J. Gastroenterol.* 22, 5374–5383. doi:10.3748/wjg.v22.i23.5374

Zhao, H.-M., Xu, R., Huang, X.-Y., Cheng, S. M., Huang, M. F., Yue, H. Y., et al. (2016b). Curcumin suppressed activation of dendritic cells via JAK/STAT/SOCS signal in mice with experimental colitis. *Front. Pharmacol.* 7, 455. doi:10.3389/fphar.2016.00455

Zhao, J., Wang, Y., Xu, C., Liu, K., Chen, L., et al. (2017). Therapeutic potential of an anti-high mobility group box-1 monoclonal antibody in epilepsy. *Brain Behav. Immun.* 64, 308–319. doi:10.1016/j.bbi.2017.02.002

Zhao, J., Yu, S., Zheng, W., Feng, G., Luo, G., Wang, L., et al. (2010). Curcumin improves outcomes and attenuates focal cerebral ischemic injury via antiapoptotic mechanisms in rats. *Neurochem. Res.* 35, 374–379. doi:10.1007/s11064-009-0065-y

Zheng, Y., Zhang, J., Zhao, Y., Zhang, X., Guan, J., et al. (2021). Curcumin protects against cognitive impairments in a rat model of chronic cerebral hypoperfusion combined with diabetes mellitus by suppressing neuroinflammation, apoptosis, and pyroptosis. *Int. Immunopharmacol.* 93, 107422. doi:10.1016/j.intimp.2021.107422

Zhong, Z.-Y., and Tang, Y. (2016). Upregulation of periostin prevents high glucose-induced mitochondrial apoptosis in human umbilical vein endothelial cells via activation of Nrf2/HO-1 signaling. *Cell Physiol. Biochem. Int. J. Exp. Cell Physiol. Biochem. Pharmacol.* 39, 71–80. doi:10.1159/000445606

Zhou, Y., Tang, H., Liu, J., Dong, J., and Xiong, H. (2011). Chemokine CCL2 modulation of neuronal excitability and synaptic transmission in rat hippocampal slices. *J. Neurochem.* 116, 406–414. doi:10.1111/j.1471-4159.2010.07121.x

Zhu, Q., Wang, L., Zhang, Y., Zhao, F. h., Luo, J., Xiao, Z., et al. (2012). Increased expression of DNA methyltransferase 1 and 3a in human temporal lobe epilepsy. *J. Mol. Neurosci. MN* 46, 420–426. doi:10.1007/s12031-011-9602-7

Zhu, X., Dong, J., Han, B., Huang, R., Zhang, A., Xia, Z., et al. (2017). Neuronal nitric oxide synthase contributes to PTZ kindling-induced cognitive impairment and depressive-like behavior. *Front. Behav. Neurosci.* 11, 203. doi:10.3389/fnbeh.2017.00203

Zhu, X., and Zhu, R. (2018). Curcumin suppresses the progression of laryngeal squamous cell carcinoma through the upregulation of miR-145 and inhibition of the PI3K/Akt/mTOR pathway. *OncoTargets Ther.* 11, 3521–3531. doi:10.2147/OTT.S159236

frontiers | Frontiers in Pharmacology

TYPE Original Research
PUBLISHED 22 January 2025
DOI 10.3389/fphar.2024.1528032

Check for updates

OPEN ACCESS

EDITED BY
Pukar Khanal,
Emory University, United States

REVIEWED BY
Jagdish Chand,
JSS Academy of Higher Education and Research, India
Moumita Dhara,
Nitte College of Pharmaceutical Science, India

*CORRESPONDENCE
Nidhi,
nidhiagarwal@jamiahamdard.ac.in

RECEIVED 14 November 2024
ACCEPTED 30 December 2024
PUBLISHED 22 January 2025

CITATION
Dahalia M, Gupta S, Majid H, Vohora D and Nidhi (2025) Pirfenidone regulates seizures through the HMGB1/TLR4 axis to improve cognitive functions and modulate oxidative stress and neurotransmitters in PTZ-induced kindling in mice.
Front. Pharmacol. 15:1528032.
doi: 10.3389/fphar.2024.1528032

COPYRIGHT
© 2025 Dahalia, Gupta, Majid, Vohora and Nidhi. This is an open-access article distributed under the terms of the Creative Commons Attribution License (CC BY). The use, distribution or reproduction in other forums is permitted, provided the original author(s) and the copyright owner(s) are credited and that the original publication in this journal is cited, in accordance with accepted academic practice. No use, distribution or reproduction is permitted which does not comply with these terms.

Pirfenidone regulates seizures through the HMGB1/TLR4 axis to improve cognitive functions and modulate oxidative stress and neurotransmitters in PTZ-induced kindling in mice

Mansi Dahalia [1], Sparsh Gupta[2], Haya Majid [3], Divya Vohora [1] and Nidhi [3]*

[1]Department of Pharmacology, School of Pharmaceutical Education and Research, Jamia Hamdard, New Delhi, India, [2]Department of Pharmacology, Vardhman Mahavir Medical College, New Delhi, India, [3]Department of Translational and Clinical Research, School of Chemical and Life Sciences, Jamia Hamdard, New Delhi, India

Background: Epilepsy is a neurological disorder characterized by recurrent seizures due to abnormal electrical activity in the brain. Pirfenidone, an antifibrotic drug, has shown anti-inflammatory and antioxidant properties in various disease models, including neurological conditions. However, its potential anticonvulsant effects have not been thoroughly explored. This study aims to evaluate the anticonvulsant potential of pirfenidone in a pentylenetetrazol-induced kindling model of epilepsy, focusing on its effect on seizure activity, cognition, antioxidant profiles, inflammatory markers, neurotransmitter balance, liver enzyme levels, and histopathological changes.

Methods: Healthy male Swiss albino mice were subjected to an acute Increasing Current Electroshock test and chronic pentylenetetrazol-kindling model. Pirfenidone was administered at doses of 100, 200, and 300 mg/kg, orally, with sodium valproate as a standard drug. Seizure severity and cognitive function were assessed in the pentylenetetrazol-kindling model, along with biochemical assays that evaluated antioxidant enzymes, inflammatory markers, neurotransmitter levels, and liver enzyme levels. Histopathological changes were also assessed in the hippocampus and cortex of experimental mice.

Results: Pirfenidone at 200 mg/kg and 300 mg/kg significantly increased Seizure Threshold Current in the Increasing Current Electroshock test, indicating a protective effect against seizures. In the pentylenetetrazol-kindling model, pirfenidone delayed seizure onset and reduced severity, with the 300 mg/kg dose showing the strongest impact. Pirfenidone also demonstrated significant improvements in cognitive function, as evidenced by enhanced performance in passive avoidance and elevated plus maze tests. Antioxidant profiles showed increased levels of superoxide dismutase, catalase, and reduced glutathione, with a corresponding reduction in malondialdehyde and acetylcholinesterase levels. Pirfenidone significantly reduced pro-inflammatory cytokines including interleukin-6, interleukin-1β, transforming growth factor-β, tumor necrosis factor- α, high-mobility group box-1, and toll-like receptor-4, elevated gamma-aminobutyric acid, decreased glutamate levels, modulated aspartate

aminotransferase and alanine aminotransferase levels. Histopathological analysis revealed that pirfenidone ameliorated cellular disintegration and neuronal damage in the hippocampus and cortex.

Conclusion: Pirfenidone shows potential as an anticonvulsant, anti-inflammatory, hepatoprotective, and neuroprotective agent, with additional benefits in improving cognition and oxidative stress profiles in epilepsy treatment. Further studies are required to explore its long-term safety and efficacy.

KEYWORDS

anticonvulsant, cognition, epilepsy, neuroinflammation, neurotransmitters, pentylenetetrazole, pirfenidone

Highlights

- PFD significantly reduced key neuroinflammatory cytokines (IL-6, IL-1β, TGF-β, TNF-α, HMGB1, TLR-4) and ameliorated neuronal damage in the hippocampus and cortex, preserving structural integrity.
- PFD restored the balance between GABA and glutamate, improving inhibitory and excitatory neurotransmission, and enhanced cognitive function in PTZ-kindled mice.
- PFD increased SOD, catalase, and GSH levels while reducing MDA levels, demonstrating strong antioxidant effects and hepatoprotection by normalizing AST and ALT levels.
- PFD exhibited dose-dependent anticonvulsant effects in PTZ-kindled mice, comparable to sodium valproate (SVP), highlighting its therapeutic potential in epilepsy management.

1 Introduction

Epilepsy is a chronic neurological disorder affecting approximately 51 million people worldwide, with nearly 40% experiencing drug resistance (Ghaith et al., 2024; Waris et al., 2024). Beyond seizures, cognitive deficits such as memory loss and learning difficulties are common due to seizure activity, neuroinflammation, and hippocampal and cortical damage (Liu et al., 2023). Factors like seizure severity, brain damage, and side effects of anti-seizure medications worsen these impairments (Pinto et al., 2024). While older medications, including barbiturates and valproate, often impair cognition, even newer drugs like topiramate can cause long-term cognitive deficits, sometimes leading to treatment discontinuation (Tombini et al., 2023). Current anti-seizure medications (ASMs) offer symptomatic relief but fail to address the root causes of epilepsy, such as neuroinflammation, oxidative stress, and neurotransmitter imbalances (Tombini et al., 2023; Pinto et al., 2024). Their cognitive and behavioral side effects further limit long-term use, highlighting the need for therapies that not only control seizures but also target these underlying mechanisms (Pinto et al., 2024). Innovative treatments focusing on reducing neuroinflammation, mitigating oxidative stress, and restoring neurotransmitter balance are essential to improve cognitive outcomes and enhance patients' quality of life (Khan et al., 2024; Waris et al., 2024).

Oxidative stress and impaired antioxidant defenses contribute to neuronal damage in epilepsy, characterized by increased reactive oxygen species (ROS) and lipid peroxidation (MDA), alongside decreased superoxide dismutase (SOD), catalase, and reduced glutathione (GSH) (Alam et al., 2023). Long-term antiepileptic drug use, such as valproic acid, can exacerbate oxidative stress and lipid peroxidation (Madireddy and Madireddy, 2023). Chronic oxidative damage is linked to neuronal degeneration, structural abnormalities, and cognitive impairments (Tombini et al., 2023; Khan et al., 2024; Stasenko et al., 2024). Elevated acetylcholinesterase (AChE) activity further disrupts cholinergic signaling, increasing neuronal excitability and cognitive deficits, while reducing its activity improves synaptic transmission and cognition (Akyüz et al., 2020; Komali et al., 2021; Alyami et al., 2022).

Neuroinflammation drives seizure onset and progression through astrocyte and microglial activation, releasing cytokines such as IL-6, IL-1β, and TNF-α, and disrupting the blood-brain barrier (Tavakoli et al., 2023; Tyagi et al., 2023). Key mediators of neuroinflammation include TGF-β, which regulates immune responses, and HMGB1, which activates TLR4, promoting pro-inflammatory cytokine release and neuronal hyperexcitability (Vezzani et al., 2008; Kamali et al., 2020). Imbalance of neurotransmitters, particularly gamma-aminobutyric acid (GABA) and glutamate, plays a key role in seizures. GABA, the brain's primary inhibitory neurotransmitter, reduces neuronal excitability, while excessive glutamate release during seizures causes excitotoxicity and neuronal damage (Ivens et al., 2007; Tian et al., 2016; Nodirahon et al., 2024). Despite various ASMs targeting sodium and calcium channels, GABAergic pathways, and glutamate inhibition, many patients remain treatment-resistant, highlighting the need for novel therapeutic strategies (Imran et al., 2023; Mir et al., 2023; Löscher et al., 2020).

Pirfenidone (PFD), a pyridone-derivative compound (5-methyl-1-phenyl-2-[1H]-pyridone), is an orally administered drug approved for idiopathic pulmonary fibrosis (IPF) due to its established efficacy (Nakamura et al., 2023). Beyond fibrosis, PFD shows potential in neurological conditions like neurofibromatosis, secondary progressive multiple sclerosis, and limbic seizures (Babovic-Vuksanovic et al., 2004). Its therapeutic effects stem from modulating cytokines and growth factors such as TGF-β, TNF-α, and IL-6, reducing inflammation and immune responses (Aimo et al., 2022). PFD also inhibits lipid peroxidation in experimental models, offering protection against tissue damage (Misra and Rabideau, 2000; Salazar-Montes et al., 2008). Neuroprotective effects have been demonstrated through reduced oxidative stress and neuronal loss in seizure-related brain injuries, including kainic acid-induced excitotoxicity and traumatic brain

injury models (Castro-Torres et al., 2014; 2015; Bozkurt et al., 2022). However, its direct anticonvulsant effects remain unexplored. Given its anti-inflammatory, antioxidant, and neuroprotective properties, this study aims to evaluate PFD's anticonvulsant potential in a pentylenetetrazole (PTZ) -kindling model, focusing on oxidative stress, neuroinflammatory pathways, and key neurotransmitter systems involved in seizure development.

2 Material and methods

2.1 Animals

Healthy male Swiss albino mice weighing 25 g–30 g, were procured from the Central Animal House Facility of Jamia Hamdard, New Delhi, India. The mice were kept in polypropylene cages (43 cm × 28.6 cm × 15.5 cm) with unrestricted access to *ad libitum* water and a pellet diet. Animal care procedures adhered to the guidelines set by the Committee for Control and Supervision of Experiments on Animals (CCSEA), India, as well as the protocols established by the Institutional Animal Ethics Committee of Jamia Hamdard, New Delhi, India (173/GO/Re/2000/CPCSEA, 28 January 2000) under an approved protocol (Protocol no. 1906).

2.2 Materials

PFD 200 mg tablets (Pirfenex 400, Cipla Pvt. Ltd., India) and Sodium Valproate (SVP) 200 mg tablets (Valprol-CR 200, INTAS Pharmaceuticals Ltd., India) were purchased. Pentylenetetrazole (PTZ) was obtained from Sigma-Aldrich, United States. All other chemicals utilized were of analytical grade quality.

3 Methodology

3.1 Acute study: increasing current electroshock test

The mice were randomly assigned to six groups (n = 6). Group I functioned as the control, and Group II, the positive control for the ICES test, was given SVP at 200 mg/kg *p.o.*, while Groups III, IV, and V received PFD at doses of 100, 200, and 300 mg/kg *p.o.*, respectively. Group VI received a combination of PFD (300 mg/kg *p.o.*) and SVP (200 mg/kg p.o.). All treatments were administered 1 h before the ICES test, except Group VI, which received PFD 1 h before SVP; the ICES test was conducted 1 h after SVP. Using an electro-convulsiometer, each mouse was administered an electric shock via ear electrodes, starting with an initial current of 2 mA delivered as a single train of pulses for 0.2 s. The intensity of the current was gradually increased at a rate of 2 mA every 2 s. The seizure threshold current (STC) was determined as the current level that triggered tonic hind limb extension (HLE). If tonic HLE was not observed up to the maximum current of 30 mA, no further increase in current was applied, and this maximum value was recorded for subsequent calculations (Agarwal et al., 2013).

3.2 Chronic study

The experimental design involved randomly assigning animals into seven distinct groups, each comprising nine mice. The seizure scores were evaluated using a sample size of nine animals per group. Additionally, behavioral and biochemical assessments were conducted with six animals per group, while histopathological analysis was carried out using three animals per group.

The sample size was calculated using G* Power software, version 3.1. The groups were as follows:

- Group I (Control): 1% carboxymethylcellulose (CMC) administered orally and normal saline administered intraperitoneally.
- Group II: 1% CMC administered orally along with PTZ (25 mg/kg, *i.p.*) administered every other day.
- Group III (Standard): SVP at 200 mg/kg *p.o* administered orally in addition to PTZ (25 mg/kg, *i.p.*) (Kumar et al., 2016)
- Group IV: PFD at 100 mg/kg *p.o* administered orally and PTZ (25 mg/kg, *i.p.*) (Castro-Torres et al., 2014)
- Group V: PFD at 200 mg/kg *p.o* administered orally along with PTZ (25 mg/kg, *i.p.*) (Liu et al., 2024)
- Group VI: PFD at 300 mg/kg *p.o* administered orally along with PTZ (25 mg/kg, i.p.) (Liu and Shi, 2019)
- Group VII: Combination of PFD (300 mg/kg *p.o*) and SVP (200 mg/kg *p.o*) along with PTZ (25 mg/kg, *i.p.*).

3.3 Drug administration protocol

PFD and SVP were weighed and suspended in 1% carboxymethyl cellulose (CMC) prepared with double-distilled water. PTZ was dissolved in normal saline (0.9% sodium chloride solution) and administered on alternate days. Control animals were given a suspension of 1% CMC in double-distilled water, administered orally once daily. The doses selected for PFD were 100, 200, and 300 mg/kg *p.o.* and were administered daily, while SVP was administered at a dose of 200 mg/kg *p.o.* Daily, 1 h before PTZ administration for 42 days. In the PTZ-kindling model, a sub-convulsant dose of PTZ (25 mg/kg, *i.p.*) was administered on alternate days, whereas treatments PFD and SVP were administered daily for 42 days. All drugs were administered in a volume of 10 mL/kg.

3.4 Pentylenetetrazol-kindling in mice

Following PTZ administration, the animals were monitored for 30 min to assess seizure intensity using the Racine score (Sehar et al., 2015; Khatoon et al., 2021). Seizure severity was evaluated with the following scoring system: Stage 0: no response; Stage 1: ear and facial twitches; Stage 2: myoclonic body jerks without an upright position; Stage 3: myoclonic jerks with an upright posture and bilateral forelimb clonus; Stage 4: tonic-clonic seizures; Stage 5: generalized tonic-clonic seizures with loss of postural control. Mice were deemed fully kindled after displaying a seizure score of four during three consecutive PTZ injections. The cumulative seizure score for each group was calculated at the end of the 1st, 2nd,

3rd, 4th, 5th, and 6th week. The animals remained drug-free for 3 days after the development of kindling, and then on 4th day animals were subjected to behavioral assessment followed by sacrificing them using CO_2 chamber (Zhao et al., 2022) for biochemical estimations on 8th day.

3.5 Behavioral assessment

3.5.1 Step down latency on passive avoidance response apparatus

The Step-Down Latency (SDL) test was conducted using a passive avoidance response apparatus to evaluate the effects of PFD on cognition. In the center of the apparatus's grid floor, a glass Petri dish was placed upside down, creating a shock-free zone. Each mouse was positioned in this shock-free zone, and upon stepping down, it received a mild electric shock of 20 V through the grid floor. This training session lasted 1 min. After training, the time it took for the mouse to step down was recorded, with no shock administered, and this time was termed acquisition latency. The same procedure was repeated 24 h later, with the recorded time termed retention latency. Mice that did not step down within 600 s were assigned this cut-off time (Khatoon et al., 2023).

3.5.2 Transfer latency on elevated plus maze apparatus

The elevated plus maze test was conducted to assess the impact of PFD on spatial learning and memory. The maze consists of four arms, two open and two closed, each measuring 16 cm in length and 5 cm in width. The closed arms are 15 cm high, extending from a central platform (5 cm × 5 cm), with the entire setup elevated 25 cm above the ground. Each mouse was initially placed at the end of an open arm. Transfer latency (TL) was defined as the time it took for a mouse to move from the open arm to one of the closed arms with all four limbs. The TL measured on the first day for each mouse was recorded as acquisition latency. If a mouse did not enter any closed arm, it was gently guided to one, and a TL of 90 s was assigned. After this, each mouse was allowed to explore the maze for an additional 2 min before being returned to its cage. Retention latency was evaluated 24 h later to assess memory retention of the task (Sehar et al., 2015).

3.6 Biochemical estimations

3.6.1 Tissue preparation and biochemical analysis

The animals were euthanized after neurobehavioral assessment, for tissue preparation and biochemical analysis. Blood was drawn from the tail vein before euthanizing the animals, and serum was separated and preserved for measuring aspartate aminotransferase (AST) and alanine aminotransferase (ALT) levels. The separated serum was aliquoted to avoid repeated freeze-thaw cycles and stored at −80°C for further analysis. After sacrificing, the whole brain was isolated and rinsed with cold 0.9% saline, then the brain tissues hippocampus, and cerebral cortex, were excised and weighed. The tissues were snap-frozen in liquid nitrogen and stored at −80°C until biochemical and histological analyses were performed. The tissues were homogenized in 0.1 M Phosphate Buffered Saline (PBS, pH 7.4) to create a 10% homogenate while maintaining the sample on ice. The homogenates were then centrifuged at 10,000 rpm for 20 min at 4°C, and the resulting post-mitochondrial supernatant was used for the estimation of inflammatory cytokines (IL-6, IL-1β, TGF-β, TNF-α, HMGB-1, and TLR-4), neurotransmitters (GABA and glutamate), and liver enzyme levels (AST and ALT) using ELISA kits and also for the estimation of reduced GSH (Jollow et al., 1974), and antioxidant enzymes like SOD (Misra and Fridovich, 1972) and catalase (Greenwald, 2018) and AChE (Ellman et al., 1961) and MDA (Ohkawa et al., 1979). Protein estimation in hippocampus and cortex homogenates was determined by the method of Lowry et al. (1951) using bovine serum albumin as standard.

3.7 Estimation of oxidative stress parameters

3.7.1 Estimation of lipid peroxidation

MDA, a byproduct of lipid peroxidation, was measured to assess the extent of lipid peroxidation in cortex and hippocampal tissue homogenates. This colorimetric assay relies on the reaction between thiobarbituric acid and lipid peroxides, forming a pink chromogen that can be quantified spectrophotometrically at a wavelength of 535 nm. In brief, 100 µg of cortex and hippocampal homogenate protein was mixed with 1 mL of 20% trichloroacetic acid (adjusted to pH 3.5), 1 mL of 0.67% thiobarbituric acid, and 0.1 mL of 8% sodium dodecyl sulfate (SDS). The reaction mixture was then heated in a water bath at 95°C for 1 h. After heating, the pink chromogen was extracted using a 10: 1 solution of butanol and pyridine, and absorbance was measured at 535 nm against a blank. The results were calculated as nmol MDA per hour per mg protein using a molar extinction coefficient of (1.56 × 10 5 M^{-1} cm^{-1}) (Ohkawa et al., 1979).

3.7.2 Estimation of superoxide dismutase activity

The reaction mixture was prepared by combining 1.8 mL of glycine buffer (50 mM, pH 10.4) with 0.2 mL of phenazine methosulfate. The reaction was initiated by adding (−) epinephrine. Superoxide dismutase enzyme activity was assessed by monitoring the autoxidation of (−) epinephrine at 480 nm over a period of 3 min. Enzyme activity was expressed as nanomoles of (−) epinephrine protected from oxidation per minute per mg of protein, using a molar extinction coefficient of 4.02 × 103 M^{-1} cm^{-1} (Misra and Fridovich, 1972).

3.7.3 Estimation of catalase activity

A reaction mixture of 3 mL was prepared, consisting of 2.0 mL of PBS (0.1 M, pH 7.4), 0.95 mL of hydrogen peroxide (0.019 M), and 0.05 mL of 10% phenazine methosulfate. Enzyme activity was determined by measuring the change in absorbance at 240 nm. Catalase activity was calculated as micromoles of hydrogen peroxide decomposed per minute per milligram of protein, using a molar extinction coefficient of 40 M^{-1} cm^{-1} (Greenwald, 2018).

3.7.4 Estimation of reduced glutathione

Phenazine methosulphate was precipitated by mixing with 4% sulfosalicylic acid in a 1:1 ratio. The samples were then stored at 4°C for 1 h, followed by centrifugation at 4,000 rpm (5,600 g) for 15 min at 4°C. The assay mixture, totaling 3 mL, consisted of 0.4 mL of the resulting supernatant, 2.2 mL of 0.1 M sodium phosphate buffer (pH 7.4), and 0.4 mL of 5,5′-dithio-bis-2-nitrobenzoic acid (DTNB). The absorbance of the reaction product was measured at 412 nm using a spectrophotometer. The concentration of reduced glutathione (GSH) was calculated as micromoles of GSH per

milligram of tissue, employing a molar extinction coefficient of $1.36 \times 104\ M^{-1}\ cm^{-1}$ (Jollow et al., 1974).

3.8 Estimation of acetylcholinesterase activity

The reaction mixture consisted of 0.2 mL of acetylthiocholine iodide (75 mM), 0.1 mL of buffered Ellman's reagent DTNB (10 mM in 15 mM $NaHCO_3$), and 3 mL of PBS (25 mM, pH 7.4). This mixture was incubated at room temperature for 10 min. After incubation, 0.2 mL of tissue homogenate was added. The optical density (OD) was then measured at 412 nm within 5 min using a spectrophotometer to determine the rate of substrate hydrolysis, expressed as micromoles of substrate hydrolyzed per minute per milligram of protein (Ellman et al., 1961).

3.9 Estimation of neuroinflammatory markers, neurotransmitters, and liver enzymes via enzyme-linked immunosorbent assay

The levels of IL-6, IL-1β, TGF-β, TNF-α, HMGB-1, TLR-4, GABA, and glutamate in the hippocampus and cortex tissues of the experimental mice were quantitatively assessed. Additionally, serum samples were analyzed to measure AST and ALT levels. All the estimations were done using ELISA kits from KRISHGEN BioSystems, following the manufacturer's guidelines. All assays were performed according to the manufacturer's protocols.

3.10 Histopathological studies

The mice from each group were sacrificed and brains were extracted and fixed in 4% paraformaldehyde at 4°C for 4 h, then embedded in paraffin wax. Coronal and hippocampal sections (4 μm thick) were prepared and mounted on polylysine-coated slides. The Nissl Staining was performed using paraffin sections which were deparaffinized and rehydrated through a sequence of washes: two 10-min washes in xylene, two 5-min washes in 100% ethanol, a 5-min wash in 95% ethanol, a 5-min wash in 90% ethanol, a 3-min wash in 80% ethanol, a 3-min wash in 70% ethanol, and a final 5-min rinse in distilled water. Sections were then stained with 0.1% cresyl violet solution (prepared in 0.01% glacial acetic acid) at 37°C for 10 min, rinsed briefly in distilled water, and differentiated in 95% ethanol for 30 s. Neuronal damage was evaluated under a 400x microscope (Wu et al., 2021).

3.11 Statistical analysis

The experimental findings are presented as Mean ± Standard Error of the Mean (SEM). Data were analyzed using one-way ANOVA, followed by Tukey's multiple comparison test except seizure score which was analyzed using two-way ANOVA, followed by Tukey's multiple comparison test. All statistical analyses were conducted with GraphPad Prism 9 software, and a p-value of less than 0.05 was regarded as statistically significant.

4 Results

4.1 Effect of pirfenidone administration on the increasing current electroshock test in mice

In the ICES test, PFD 100 mg/kg *p.o.*, did not significantly increase the STC compared to the control group. Group II, which received 200 mg/kg *p.o.* of SVP orally (acting as the positive control), demonstrated a highly significant increase in STC ($p < 0.001$) compared to the control group. Similarly, Groups IV and V, treated with PFD at doses of 200 mg/kg *p.o* and 300 mg/kg *p.o* respectively, showed a statistically significant increase in STC ($p < 0.05$ and $p < 0.001$, respectively) compared to the control group. This suggests that PFD at doses of 200 mg/kg *p.o* and 300 mg/kg offers protection against hind limb extension (HLE) comparable to that of SVP. Moreover, the combination treatment in Group VI (SVP + PFD 300 mg/kg) also led to a significant increase in STC compared to the control group suggesting a potential enhancement in efficacy of the combination of PFD and SVP, as shown in Table 1.

4.2 Effect of pirfenidone administration on pentylenetetrazol -induced kindling model in mice

Mean seizure scores were calculated by the end of each week over 6 weeks. The group treated with Vehicle + PTZ developed stage 4 seizures by the 5th week, indicating the onset of generalized tonic-clonic seizures. In the first week, all groups started from a relatively similar baseline, with the Control group showing stable, low values throughout the study period. By the second week, the PTZ + Vehicle group began to deviate significantly from the Control group ($p < 0.001$), showing a sharp upward trend, indicating the detrimental effect of PTZ treatment. In contrast, treatment groups demonstrated varying degrees of reduction in the measured parameter compared to the PTZ + Vehicle group ($p < 0.001$).

By the third week, the differences became more pronounced, with PFD 200 mg/kg and PFD 300 mg/kg and combination treatments showing a substantial reduction ($p < 0.001$). The groups receiving PFD 300 + SVP + PTZ demonstrated the most effective reduction, suggesting a possible dose-response relationship and synergistic effect. During the fourth, fifth and sixth weeks, the treatment groups maintained their respective trajectories ($p < 0.001$) (Figure 1).

4.3 Effect of pirfenidone administration on transfer latency in pentylenetetrazol-induced kindling model in mice

In the elevated plus maze experiment, the vehicle + PTZ group showed an increased exploration time in the closed arms compared to the control group, indicated by a significant rise in acquisition latency ($p < 0.05$) and retention latency ($p < 0.001$). In contrast, a notable decrease in retention latency was observed in the PFD 200 + PTZ ($p < 0.05$), PFD 300 + PTZ ($p < 0.001$), and PFD 300 + SVP + PTZ ($p < 0.001$) groups compared to the vehicle + PTZ group. Additionally, only the PFD 300 + PTZ group demonstrated a significant reduction in acquisition latency ($p < 0.05$) (Figure 2).

10.3389/fphar.2024.1528032

TABLE 1 Effect of Pirfenidone Administration on the Increasing Current Electroshock Test in mice.

Group	No. of animals	STC (mA)
CONTROL	6	17.33 ± 0.71
SVP	6	27.5 ± 1.02[a]
100 PFD	6	18.5 ± 1.78
200 PFD	6	23.66 ± 1.72[b]
300 PFD	6	26.5 ± 0.92[c]
300 PFD + SVP	6	28.66 ± 0.80[d]

Data were analyzed by one-way ANOVA followed by Tukey's multiple comparison test (n = 6) and expressed as mean ± SEM., Results were considered significant with p-value ≤ 0.05 and F (5,30) = 15.

[a]P < 0.001 Control vs. SVP.

[b]P < 0.05 Control vs. PFD 200 mg/kg.

[c]P < 0.001 Control vs. PFD 300 mg/kg.

[d]P < 0.001 Control vs. SVP + PFD 300 mg/kg.

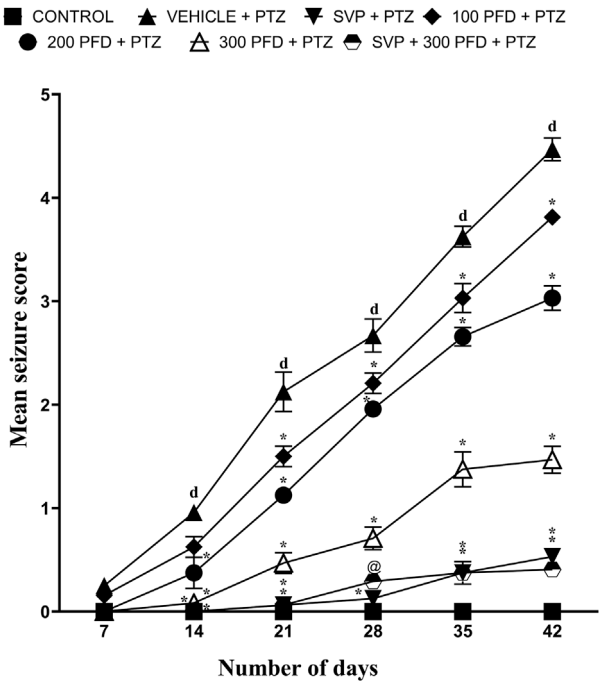


FIGURE 1
The effect of Pirfenidone administration on mean seizure scores in PTZ-induced kindling in mice. Data were analyzed by two-way ANOVA followed by Tukey's multiple comparison test and expressed as mean ± SEM (n = 9). Results were considered significant with p-value ≤ 0.05 and F values F (30,294) = 57.8, F (5,294) = 523 and F (6,294) = 712; dp < 0.001 Control vs. PTZ + vehicle, *p < 0.001 PTZ + vehicle vs. SVP + PTZ; PFD 100 + PTZ, PFD 200 + PTZ, PFD 300 + PTZ, PFD 300 + SVP + PTZ, and @p < 0.01 PTZ + vehicle vs. SVP + PFD 300 + PTZ.

4.4 Effect of pirfenidone administration on the step-down latency in pentylenetetrazol-induced kindling model in mice

In the passive avoidance response test, the vehicle + PTZ group exhibited a significant reduction (p < 0.01) in both acquisition and retention latency compared to the control group, indicating impaired cognition. Similarly, the VPA + PTZ, PFD 100 + PTZ, and PFD 300 + VPA + PTZ groups also demonstrated a significant decrease (p < 0.05) in acquisition latency, with the VPA + PTZ and PFD 100 + PTZ groups also showing a significant reduction (p < 0.01) in retention latency, further suggesting cognitive impairment. However, in the PFD 300 + PTZ group, there was a significant improvement (p < 0.05) in memory function, as evidenced by a notable increase in both acquisition and retention latency compared to the vehicle + PTZ group. Mice treated with PFD displayed preserved memory function, as indicated by their increased latency to step down from the platform (Figure 3).

4.5 Effect of pirfenidone administration on lipid peroxidation level in pentylenetetrazol-induced kindling model in mice

The MDA level was significantly elevated (p < 0.001) in the vehicle + PTZ group compared to the control group in both hippocampus and cortex. PFD 100 + PTZ (p < 0.01), PFD 200 + PTZ (p < 0.001), and PFD 300 + PTZ (p < 0.001) showed significant reduction MDA levels in cortex, similarly, all groups PFD 100 + PTZ (p < 0.001), PFD 200 + PTZ (p < 0.001), PFD 300 + PTZ (p < 0.001) and also PFD 300 + SVP + PTZ showed significant reduction MDA levels in Hippocampus (Figure 4).

4.6 Effect of pirfenidone administration on antioxidant profile in pentylenetetrazol-induced kindling model in mice

The antioxidant enzymes SOD, Catalase, and GSH levels were significantly reduced (p < 0.001) in the Vehicle + PTZ group compared to the control group in the hippocampus and cortex, with the Vehicle + PTZ group also showing significant reduction (p < 0.01) in reduced GSH levels compared to the control group in the hippocampus. SOD levels were significantly improved by PFD 100 + PTZ (p < 0.05), PFD 200 + PTZ (p < 0.01), PFD 300 + PTZ (p < 0.001) and PFD 300 + SVP + PTZ (p < 0.01) in cortex, whereas in hippocampus groups PFD 200 + PTZ (p < 0.05), PFD 300 + PTZ (p < 0.01) and PFD 300 + SVP + PTZ (p < 0.05) showed significant increase in SOD levels. The catalase

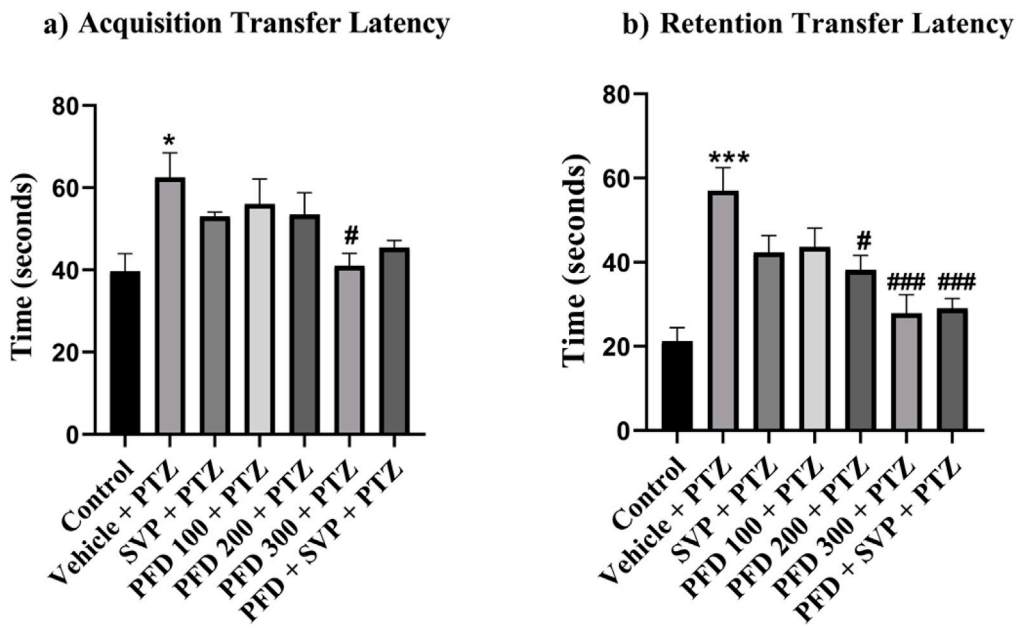


FIGURE 2
Effect of Pirfenidone administration on the transfer latency of the PTZ-induced kindling in mice. Data were analyzed by one-way ANOVA followed by Tukey's multiple comparison tests (n = 6) and expressed as mean ± SEM, **(A)** Acquisition Transfer Latency F (6,35) = 3.75, **(B)** Retention Transfer latency F (6,35) = 9.01 *p < 0.05 Control vs. PTZ + vehicle, ***p < 0.001 Control vs. PTZ + vehicle, #p < 0.05 PTZ + vehicle vs. PFD200 + PTZ, PFD 300 + PTZ, ###p < 0.001 PTZ + vehicle vs. PFD300, PFD300 + SVP + PTZ.

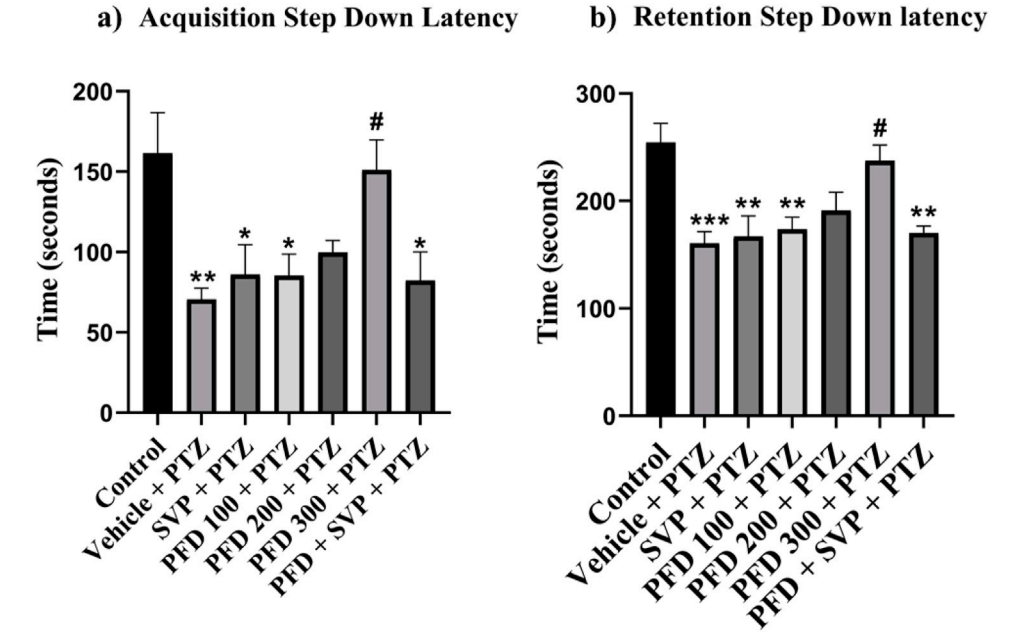


FIGURE 3
Effect of Pirfenidone administration on the step-down latency of the PTZ-induced kindling in mice. Data were analyzed by one-way ANOVA followed by Tukey's multiple comparison tests (n = 6) and expressed as mean ± SEM, **(A)** Acquisition Step Down Latency F (6,35) = 4.72, **(B)** Retention step down latency F (6,35) = 6.71 **p < 0.01 Control vs. PTZ + vehicle, **p < 0.05 Control vs. PTZ + vehicle, PFD 100 + PTZ, SVP + PTZ, PFD300 + SVP + PTZ, ***p < 0.001 Control vs. PTZ + vehicle, #p < 0.05 PTZ + vehicle vs. PFD 300 + PTZ.

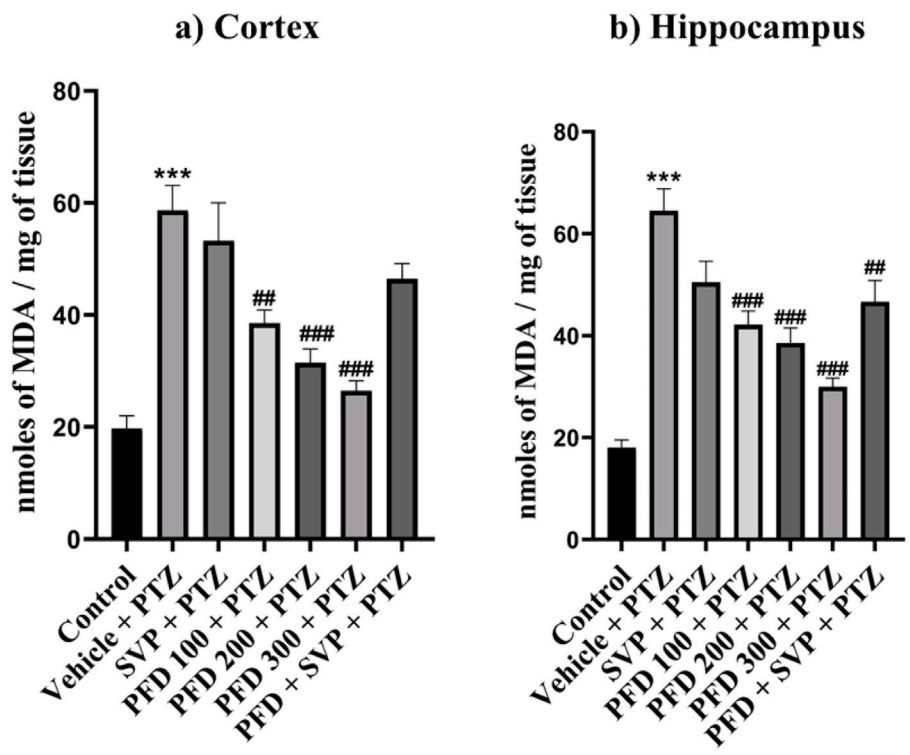


FIGURE 4
Effect of PFD administration on Malondialdehyde levels of the PTZ-induced kindling in mice. Data were analyzed by one-way ANOVA followed by Tukey's multiple comparison tests (n = 6) and expressed as mean ± SEM, MDA levels in **(A)** Cortex F (6,35) = 15.5 and **(B)** Hippocampus F (6,35) = 20.9, ***p < 0.001 Control vs. PTZ + vehicle, ##p < 0.01 PTZ + vehicle vs. PFD 100 + PTZ, PFD300 + SVP + PTZ, ###p < 0.001 PTZ + vehicle vs. PFD 100 + PTZ, PFD200 + PTZ, PFD 300 + PTZ.

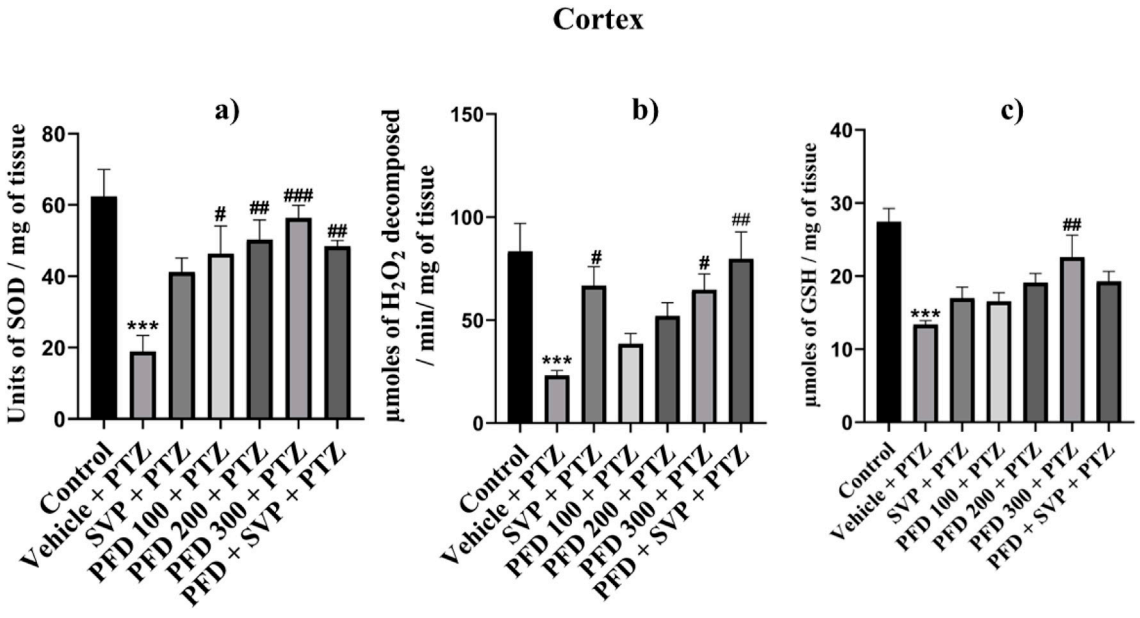


FIGURE 5
Effect of Pirfenidone administration on Superoxide dismutase, Catalase, and reduced Glutathione levels cortex in PTZ-induced kindling in mice. Data were analyzed by one-way ANOVA followed by Tukey's multiple comparison tests (n = 6) and expressed as mean ± SEM, **(A)** SOD levels in Cortex F (6,35) = 6.80, ***p < 0.001 Control vs. PTZ + vehicle, #p < 0.05 PTZ + vehicle vs. PFD100 + PTZ, ##p < 0.05 PTZ + vehicle vs. PFD200 + PTZ, PFD 300 + SVP + PTZ, ###p < 0.001 PTZ + vehicle vs. PFD300 + PTZ. **(B)** Catalase levels in Cortex F (6,35) = 5.89, ***p < 0.001 Control vs. PTZ + vehicle, #p < 0.05 PTZ + vehicle vs. SVP + PTZ, PFD300 + PTZ, ##p < 0.05 PTZ + vehicle vs. PFD 300 + SVP + PTZ. **(C)** GSH levels in Cortex F (6,35) = 7.41, ***p < 0.001 Control vs. PTZ + vehicle, ##p < 0.01 PTZ + vehicle vs. PFD300 + PTZ.

10.3389/fphar.2024.1528032

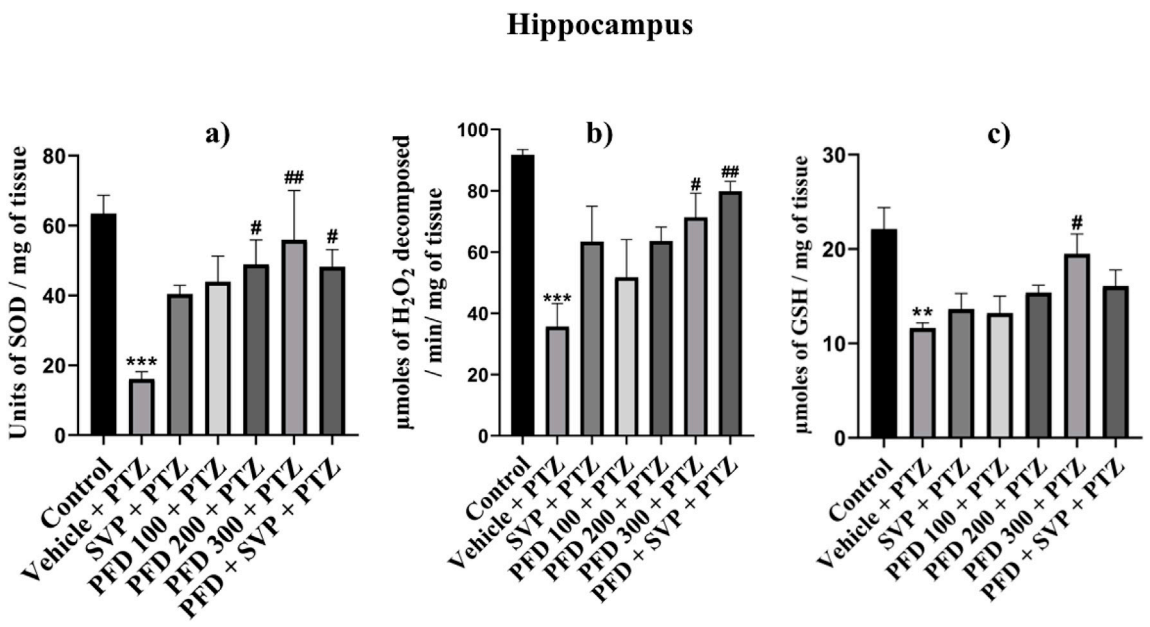


FIGURE 6
Effect of Pirfenidone administration on Superoxide dismutase, Catalase, and reduced Glutathione levels in hippocampus PTZ-induced kindling in mice. Data were analyzed by one-way ANOVA followed by Tukey's multiple comparison tests (n = 6) and expressed as mean ± SEM, **(A)** SOD levels in Hippocampus F (6,35) = 4.30,***p < 0.001 Control vs. PTZ + vehicle, #p < 0.05 PTZ + vehicle vs. PFD200 + PTZ, PFD 300 + SVP + PTZ, ##p < 0.05 PTZ + vehicle vs. PFD300 + PTZ, **(B)** Catalase levels in Hippocampus F (6,35) = 5.37, ***p < 0.001 Control vs. PTZ + vehicle, #p < 0.05 PTZ + vehicle vs. PFD300 + PTZ, ##p < 0.05 PTZ + vehicle vs. PFD 300 + SVP + PTZ. **(C)** GSH levels in Hippocampus F (6,35) = 4.95, **p < 0.01 Control vs. PTZ + vehicle, #p < 0.05 PTZ + vehicle vs. PFD300 + PTZ.

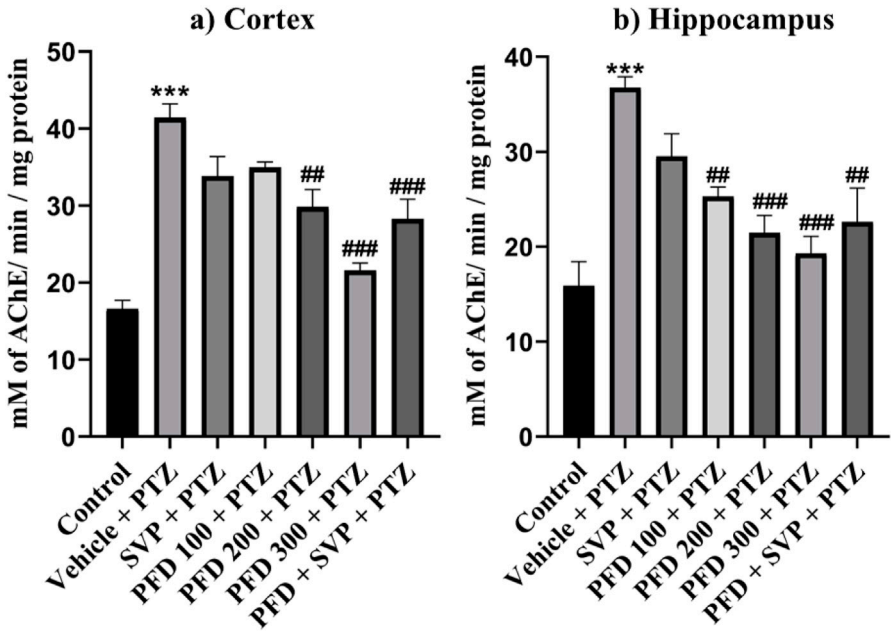


FIGURE 7
Effect of Pirfenidone on Acetylcholine estrase levels in PTZ-induced kindled mice. Data were analyzed by one-way ANOVA followed by Tukey's multiple comparison tests (n = 6) and expressed as mean ± SEM, AChE levels in **(A)** Cortex F (6,35) = 20.6 and **(B)** Hippocampus F (6,35) = 10.1, ***p < 0.001 Control vs. PTZ + vehicle, #p < 0.05 PTZ + vehicle vs. PFD100 + PTZ, ##p < 0.05 PTZ + vehicle vs. PFD200 + PTZ, PFD 300 + SVP + PTZ, ###p < 0.001 PTZ + vehicle vs. PFD200 + PTZ, PFD 300 + PTZ, PFD 300 + SVP + PTZ.

10.3389/fphar.2024.1528032

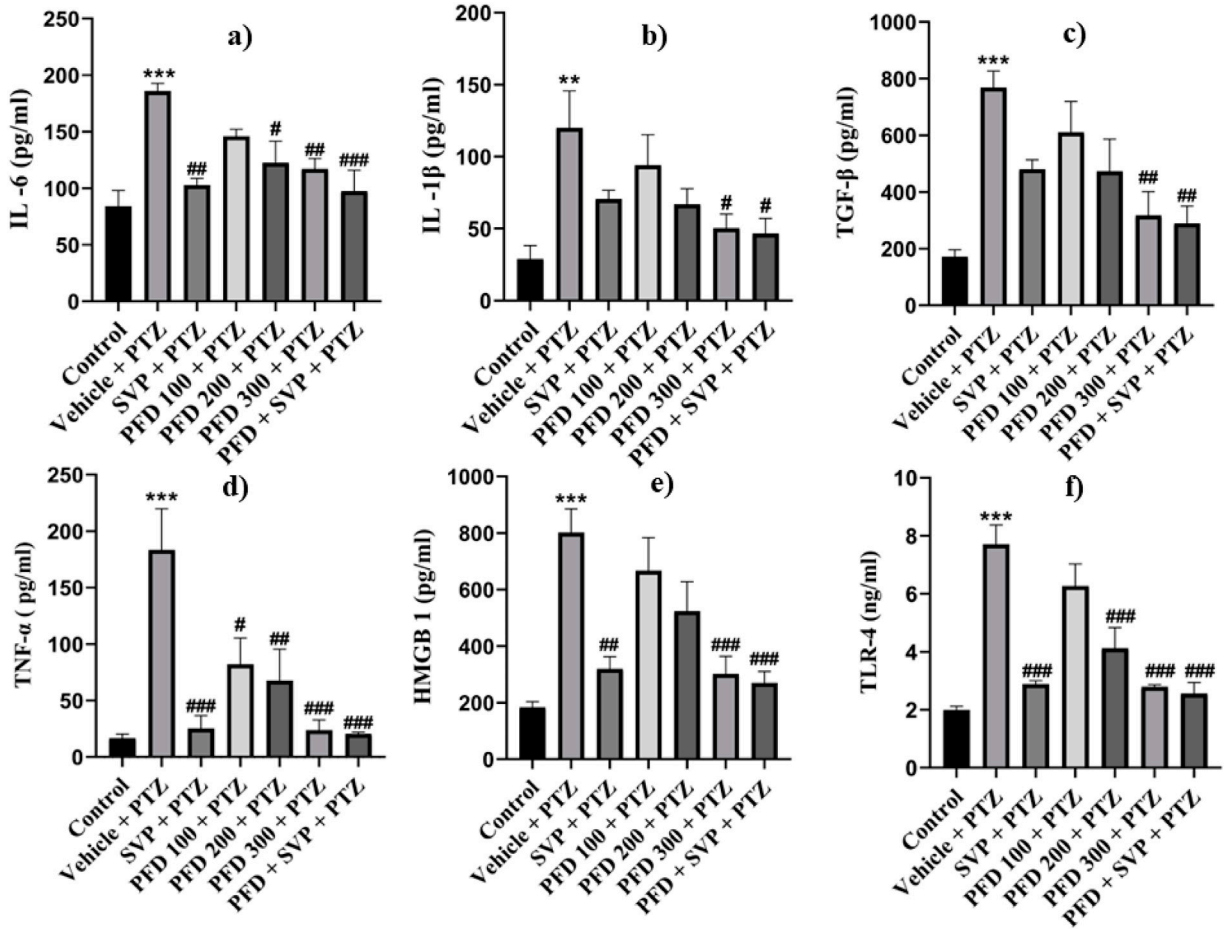


FIGURE 8
Effect of PFD on levels of IL-6, IL-1β, TNF-α, TGF-β, HMGB-1, and TLR-4 in the Cortex of the PTZ-induced kindled mice. Data were analyzed by one-way ANOVA followed by Tukey's multiple comparison tests (n = 6) and expressed as mean ± SEM, In cortex **(A)** IL-6 F (6,35) = 7.34 ***p < 0.001 Control vs. PTZ + vehicle, #p < 0.05 PTZ + vehicle vs. PFD200 + PTZ, ##p < 0.01 PTZ + vehicle vs. SVP + PTZ, PFD300 + PTZ, ###p < 0.001 PTZ + vehicle vs. PFD 300 + SVP + PTZ. **(B)** IL-1β F (6,35) = 4.27, **p < 0.01 Control vs. PTZ + vehicle, #p < 0.05 PTZ + vehicle vs. PFD100 + PTZ, PFD 300 + SVP + PTZ, **(C)** TNF-ά F (6,35) = 8.87, ***p < 0.001 Control vs. PTZ + vehicle, #p < 0.05 PTZ + vehicle vs. PFD100 + PTZ, ##p < 0.01 PTZ + vehicle vs. PFD 200 + PTZ and ###p < 0.001 PTZ + vehicle vs. SVP + PTZ, PFD300 + PTZ, PFD 300 + SVP + PTZ. **(D)** TGF-β, F (6,35) = 7.15, ***p < 0.001 Control vs. PTZ + vehicle, ##p < 0.01 PTZ + vehicle vs. PFD300 + PTZ, PFD 300 + SVP + PTZ. **(E)** HMGB1, F (6,35) = 9.39, ***p < 0.001 Control vs. PTZ + vehicle, ##p < 0.01 PTZ + vehicle vs. SVP + PTZ, ###p < 0.001 PTZ + vehicle vs. PFD300 + PTZ, PFD 300 + SVP + PTZ. **(F)** TLR4, F (6,35) = 18.9, ***p < 0.001 Control vs. PTZ + vehicle, ###p < 0.001 PTZ + vehicle vs. SVP + PTZ, PFD 200+ PTZ, PFD 300 + PTZ, PFD300 +SVP + PTZ.

activity by PFD 300 + PTZ ($p < 0.05$) and PFD 300 + SVP + PTZ ($p < 0.01$) compared to vehicle + PTZ group in both hippocampus and cortex, but in cortex SVP + PTZ ($p < 0.05$) group also showed significant rise compared to Vehicle + PTZ group. The GSH levels were significantly raised by the PFD 300 + PTZ group compared to the Vehicle + PTZ group in the cortex ($p < 0.01$) and hippocampus ($p < 0.05$) (Figures 5, 6).

4.7 Effect of pirfenidone administration on acetylcholine esterase activity in pentylenetetrazol-induced kindling model in mice

The acetylcholine esterase enzyme level was significantly increased ($p < 0.001$) in the vehicle + PTZ group compared to the control group in both hippocampus and cortex. In the hippocampus, all the groups PFD 100 + PTZ ($p < 0.05$), PFD 200 + PTZ ($p < 0.001$), PFD 300 + PTZ ($p < 0.001$), and PFD 300 + SVP + PTZ ($p < 0.01$) showed significant decrease in AChE levels compared to vehicle + PTZ group. In the cortex, PFD 200 + PTZ ($p < 0.01$), PFD 300 + PTZ ($p < 0.001$), and PFD 300 + SVP + PTZ ($p < 0.001$) showed a significant decrease in AChE levels compared to vehicle + PTZ group (Figure 7).

4.8 Effect of pirfenidone administration on neuroinflammatory markers in the hippocampus and cortex of pentylenetetrazol-induced kindling model in mice

The concentrations of inflammatory cytokines in the hippocampus and cortex of the experimental animals were

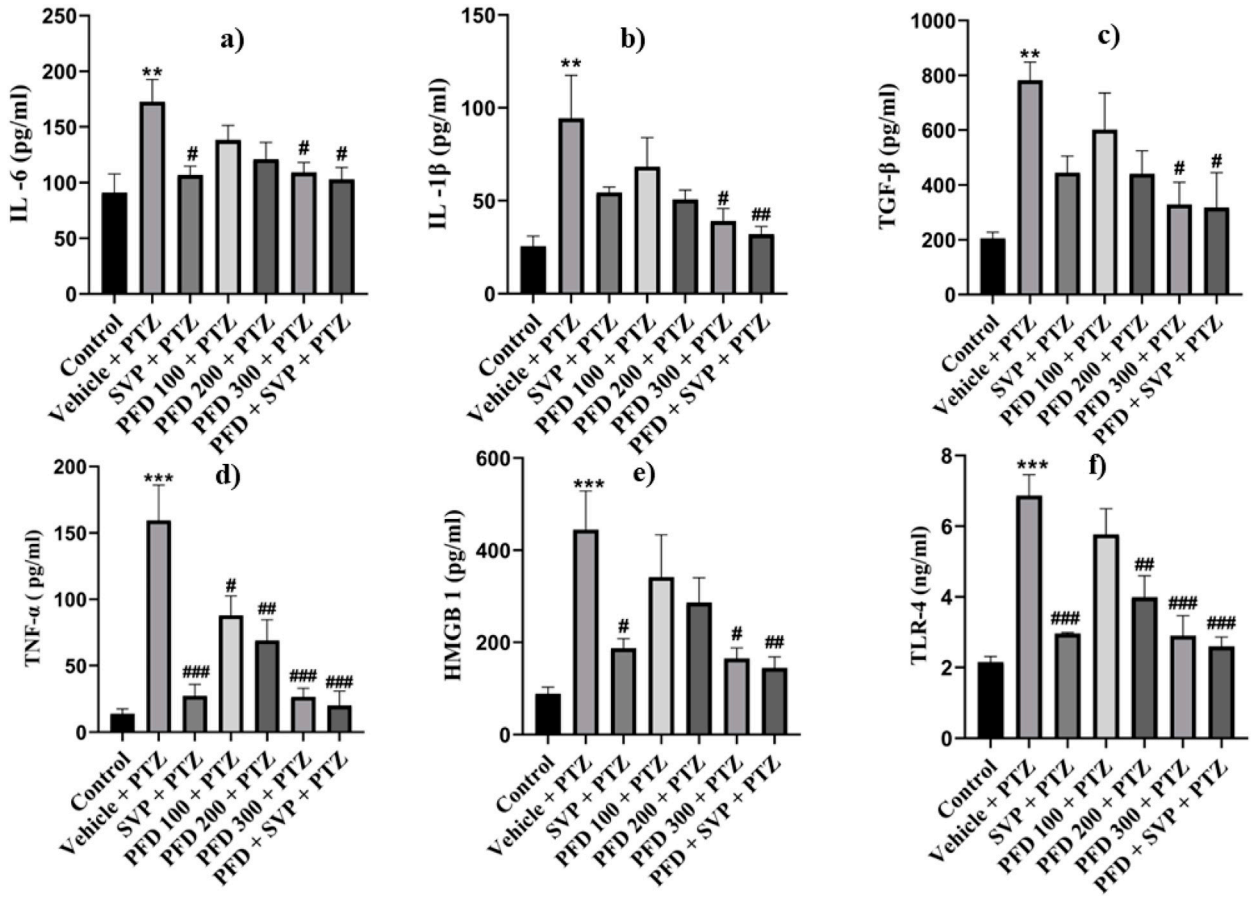


FIGURE 9
Effect of PFD on levels of IL-6, IL-1β, TNF-α,TGF-β, HMGB-1, and TLR-4 in the Hippocampus of the PTZ-induced kindled mice.Data were analyzed by one-way ANOVA followed by Tukey's multiple comparison tests (n = 6) and expressed as mean ± SEM, In Hippocampus **(A)** IL-6, F (6,35) = 3.96 **p < 0.01 Control vs. PTZ + vehicle #p < 0.05 PTZ + vehicle vs. SVP + PTZ, PFD 300 + PTZ, PFD 300 + SVP + PTZ, **(B)** IL-1β F (6,35) = 4.29 **p < 0.01 Control vs. PTZ + vehicle, #p < 0.05 PTZ + vehicle vs. PFD300 + PTZ, ##p < 0.01 PTZ + vehicle vs. PFD 300 + SVP + PTZ. **(C)** TNF-&aacgr; F (6,35) = 13.8, ***p < 0.001 Control vs. PTZ + vehicle, #p < 0.05 PTZ + vehicle vs. PFD100 + PTZ, ##p < 0.01 PTZ + vehicle vs. PFD200 + PTZ, ###p < 0.001 PTZ + vehicle vs. SVP + PTZ, PFD 300 + PTZ, PFD 300 + SVP + PTZ. **(D)** TGF-β, F (6,35) = 4.70 **p < 0.01 Control vs. PTZ + vehicle, #p < 0.05 PTZ + vehicle vs. PFD300 + PTZ, SVP + PTZ, PFD 300 + SVP + PTZ. **(E)** HMGB1, F (6,35) = 5.47, ***p < 0.001 Control vs. PTZ + vehicle, #p < 0.05 PTZ + vehicle vs. PFD300 + PTZ, SVP + PTZ, ##p < 0.01 PTZ + vehicle vs. PFD 300 + SVP + PTZ. **(F)** TLR4, F (6,35) = 13.2, ##p < 0.01 PTZ + vehicle vs. PFD 200+ PTZ, ###p < 0.001 PTZ + vehicle vs. SVP + PTZ, PFD 300 + PTZ, PFD300 +SVP + PTZ.

evaluated using ELISA kits. In the Vehicle + PTZ group, there was a significant increase in the concentrations of IL-6 ($p < 0.01$), IL-1β ($p < 0.01$), TGF-β ($p < 0.01$), TNF-α ($p < 0.001$), HMGB1 ($p < 0.001$), and TLR-4 ($p < 0.001$) in both the hippocampus and cortex as compared to the control group. The PTZ-treated group did not show a significant reduction in the levels of IL-6, IL-1β, TGF-β, HMGB1, and TLR-4 in the hippocampus and cortex, except for TNF-α, which was significantly reduced ($p < 0.05$) in both regions. In contrast, all the mentioned cytokine levels were significantly reduced in the hippocampus and cortex tissues of the PFD 300 mg/kg + PTZ and PFD + SVP + PTZ groups compared to the Vehicle + PTZ group. In the PFD 200 mg/kg + PTZ group, the levels of TNF-α and TLR-4 were significantly decreased in both the hippocampus ($p < 0.01$) and cortex ($p < 0.01$, $p < 0.001$, respectively) of kindled mice when compared with the Vehicle + PTZ group. However, IL-1β levels were not significantly decreased in the hippocampus and cortex of the SVP + PTZ group compared to the Vehicle + PTZ group. Nevertheless, the concentrations of IL-6 ($p < 0.05$, $p < 0.01$), TNF-α ($p < 0.001$), HMGB1 ($p < 0.05$, $p < 0.01$), and TLR-4 ($p < 0.001$) were significantly decreased in the hippocampus and cortex of the SVP + PTZ group (Figures 8, 9).

4.9 Effects of pirfenidone administration on neurotransmitters levels in pentylenetetrazol-induced kindling in mice

The levels of GABA were significantly reduced in the Vehicle + PTZ group ($p < 0.001$) compared to the control group. However, the GABA concentration in the hippocampus significantly increased in the PFD 200 mg/kg *p.o* + PTZ ($p < 0.05$) and PFD 300 mg/kg + PTZ ($p < 0.001$) groups compared to the Vehicle + PTZ group. In the cortex, the PFD 300 mg/kg *p.o* + PTZ group ($p < 0.001$) also exhibited a significant increase in GABA levels compared to the

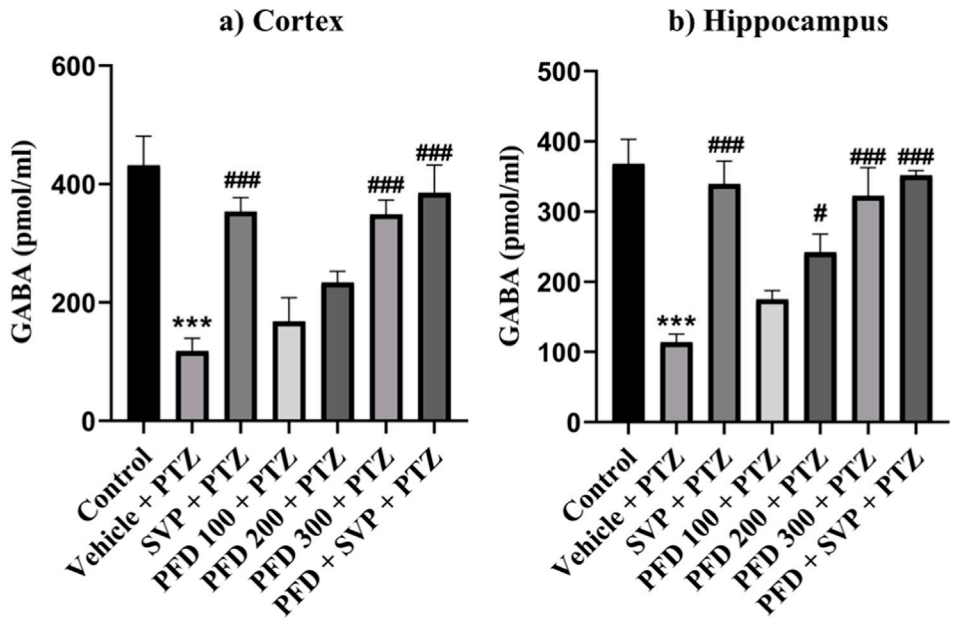


FIGURE 10
Effect PFD on Levels of GABA in the Hippocampus and Cortex of the PTZ-induced kindled mice. Data were analyzed by one-way ANOVA followed by Tukey's multiple comparison tests (n = 6) and expressed as mean ± SEM, **(A)** GABA levels in Cortex F (6,35) = 12.1; ***p < 0.001 Control vs. PTZ + vehicle, ###p < 0.001 PTZ + vehicle vs. SVP + PTZ, PFD 300 + PTZ, PFD300 + SVP Q20 + PTZ, and **(B)** GABA levels in Hippocampus F (6,35) = 13.9, ***p < 0.001 Control vs. PTZ + vehicle, #p < 0.05 PTZ + vehicle vs. SVP + PTZ, ###p < 0.001 PTZ + vehicle vs. SVP + PTZ, PFD 300 + PTZ, PFD300 + SVP Q20 + PTZ.

Vehicle + PTZ group. Both the SVP + PTZ and PFD 300 mg/kg + SVP + PTZ groups showed a significant increase in GABA levels ($p < 0.001$) in the hippocampus and cortex of kindled mice compared to the Vehicle + PTZ group. Furthermore, glutamate levels in the hippocampus and cortex were significantly increased in the Vehicle + PTZ group ($p < 0.001$) compared to the control group. However, the PFD 300 mg/kg + PTZ group demonstrated a significant decrease in glutamate levels ($p < 0.05$) in both the hippocampus and cortex compared to the Vehicle + PTZ group. Additionally, the SVP + PTZ ($p < 0.05$) and PFD 300 mg/kg + SVP + PTZ ($p < 0.01$) groups also showed significant decreases in glutamate levels compared to the Vehicle + PTZ group (Figures 10, 11).

4.10 Effects of pirfenidone administration on liver enzyme levels in pentylenetetrazol-induced kindling in mice

The levels of AST ($p < 0.001$) and ALT ($p < 0.01$) enzymes were significantly increased in the Vehicle + PTZ group in comparison to the control group. On the other hand, administration of SVP + PTZ ($p < 0.01$), PFD 300 + PTZ ($p < 0.01$), and SVP + PFD 300 + PTZ ($p < 0.01$) significantly decreased the level of AST in kindled mice. On the other hand, SVP + PTZ ($p < 0.01$), PFD 100 + PTZ ($p < 0.05$), PFD 200 + PTZ ($p < 0.05$), PFD 300 + PTZ ($p < 0.01$) and SVP + PFD 300 + PTZ ($p < 0.01$) groups significantly decreased the levels of the ALT of kindled mice in comparison to the vehicle + PTZ group (Figure 12).

4.11 Effects of pirfenidone histopathological analysis of pentylenetetrazol-induced kindling in mice

The control group displayed normal histological features in the CA1 region of the hippocampus and cortex, with no signs of pyknosis, cellular disintegration, vacuolations, or apoptotic changes, as observed with CV staining at ×400 magnification. In contrast, the vehicle + PTZ group exhibited severe damage in the CA1 region and cortex, characterized by significant cellular disintegration, marked pyknosis, and degenerative changes (red arrow). The PFD 100 + PTZ and PFD 200 + PTZ groups showed moderate damage, with visible cellular disintegration and pyknosis, though numerous healthy neurons (black arrow) were present. In the PFD 300 + PTZ and SVP + PTZ groups, damage was mild, with reduced cellular disintegration and pyknosis. The PFD 300 + SVP + PTZ group demonstrated minimal damage, indicating the protective effects of the combined treatment (Figures 13, 14).

5 Discussion

The study investigated the effects of PFD on seizure activity, cognition, oxidative stress, inflammatory markers, neurotransmitter levels, and liver enzyme levels, in a PTZ-induced kindling model of epilepsy. It was observed that higher doses of PFD (200 mg/kg and 300 mg/kg) increased the seizure threshold current (STC) significantly during the ICES test, indicating a protective effect

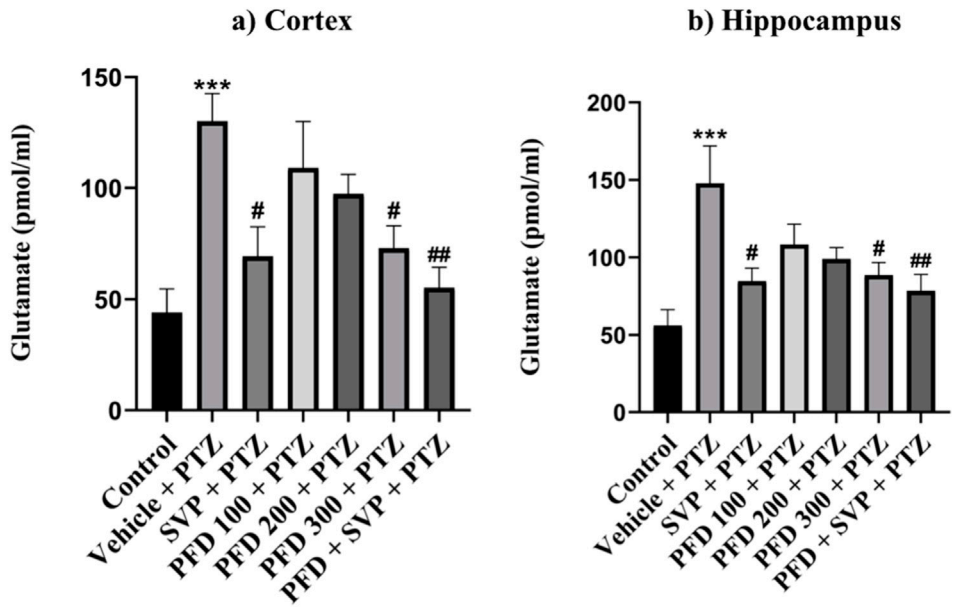


FIGURE 11
Effect PFD on Levels of Glutamate in the Hippocampus and Cortex of the PTZ-induced kindled mice. Data were analyzed by one-way ANOVA followed by Tukey's multiple comparison tests (n = 6) and expressed as mean ± SEM, **(A)** Glutamate levels in Cortex F (6,35) = 5.83; ***p < 0.001 Control vs. PTZ + vehicle, #p < 0.05 PTZ + vehicle vs. SVP + PTZ, PFD 300 + PTZ, ##p < 0.01 PTZ + vehicle vs. PFD300 + SVP + PTZ and **(B)** Glutamate levels in Hippocampus F (6,35) = 4.93 ***p < 0.001 Control vs. PTZ + vehicle, #p < 0.05 PTZ + vehicle vs. SVP + PTZ, PFD 300 + PTZ, ##p < 0.01 PTZ + vehicle vs. PFD300 + SVP + PTZ.

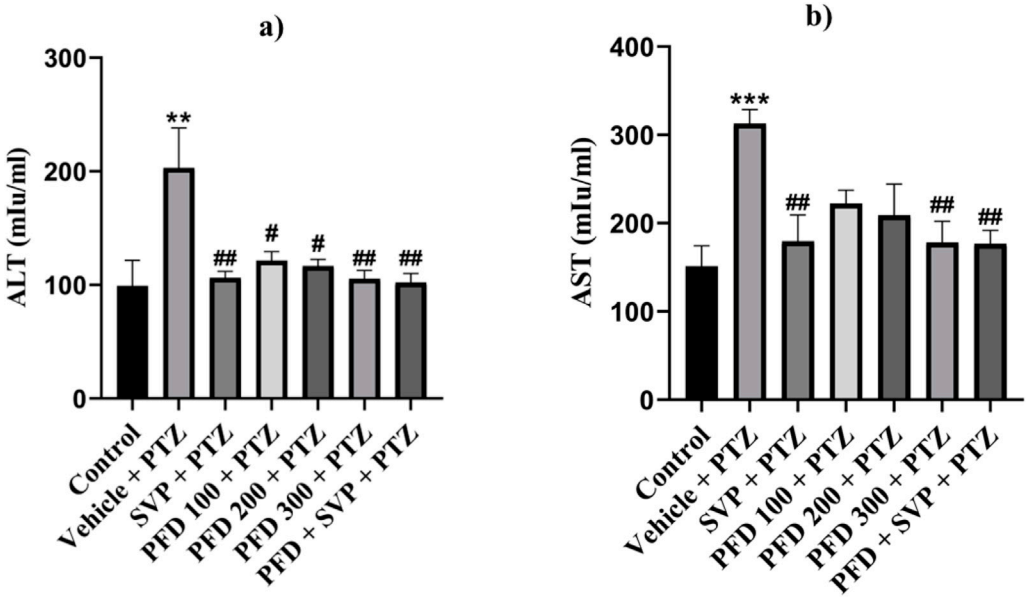


FIGURE 12
The effect of Pirfenidone administration on levels of ALT and AST enzymes in PTZ-induced kindled mice. Data were analyzed by one-way ANOVA followed by Tukey's multiple comparison test (n = 6) and expressed as mean ± SEM. Results were considered significant with p-value ≤ 0.05. **(A)** presents ALT levels, F (6,35) = 4.70 **p < 0.01 Control vs. PTZ + vehicle; #p < 0.05 PTZ + vehicle vs. PFD 100 + PTZ, PFD 200 + PTZ; ##p < 0.01 PTZ + vehicle vs. SVP + PTZ, PFD 300 + PTZ, PFD 300 + SVP + PTZ. **(B)** presents AST levels, F (6,35) = 5.05 ***p < 0.001 Control vs. PTZ + vehicle; ##p < 0.01 PTZ + vehicle vs. SVP + PTZ; PFD300 + PTZ; PFD300 + SVP + PTZ.

against seizures. This protection may be attributed to findings from an *in vivo* study, where a single dose of PFD (325 mg/kg) administered 90 min after KA (kainic acid) injection significantly reduced neuronal loss specifically in the CA1 and CA3 areas of the hippocampus. These results suggest that PFD may protect neurons from excitotoxic damage associated with seizures (Castro-Torres

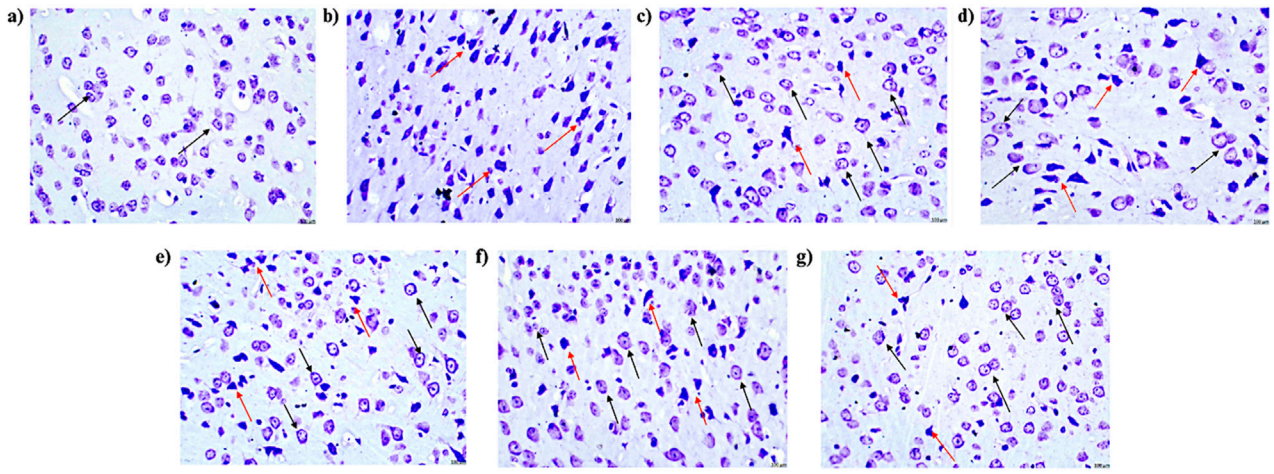


FIGURE 13
Microscopic examination of the cortical tissue samples using ×400 magnification using cresyl violet dye indicating neuronal damage (n = 3) **(A)** Control **(B)** PTZ + Vehicle **(C)** SVP + Vehicle **(D)** PFD 100 + PTZ **(E)** PFD 200 + PTZ **(F)** PFD 300 + PTZ **(G)** PFD 300 + SVP + PTZ. **(A)** Control: Black arrows indicate a normal histological appearance of the CA1 region of the cortex, with no signs of pyknosis, cellular disintegration, vacuolations, or apoptotic changes observed. **(B)** Vehicle + PTZ: The section shows a severely damaged CA1 region of the cortex with extensive cellular disintegration, marked pyknosis, and degenerative changes (red arrow), indicating significant neuronal damage. **(C)** SVP (200 mg/kg) + PTZ: The section reveals a minimally damaged CA1 region of the cortex with minimal cellular disintegration, mild pyknosis, and degenerative changes (red arrow). Numerous healthy neurons (black arrow) are still visible, indicating partial neuroprotection by SVP. **(D)** PFD (100 mg/kg) + PTZ: The section displays a moderately damaged CA1 region of the cortex with moderate cellular disintegration, marked pyknosis, and degenerative changes (red arrow). However, numerous healthy neurons (black arrow) are also present, indicating limited neuroprotection at this dose. **(E)** PFD (200 mg/kg) + PTZ: The section shows mildly damaged CA1 region of the cortex, similar to the 100 mg/kg dose, with moderate cellular disintegration, marked pyknosis, and degenerative changes (red arrow). Numerous healthy neurons (black arrow) are still visible. **(F)** PFD (300 mg/kg) + PTZ: The section shows minimally damaged CA1 region of the cortex, with mild cellular disintegration, pyknosis, and degenerative changes (red arrow). Numerous healthy neurons (black arrow) are present, suggesting significant neuroprotection at this higher dose. **(G)** PFD (300 mg/kg) + SVP (200 mg/kg) + PTZ: The section shows a minimally damaged CA1 region of the cortex, with minimal cellular disintegration, mild pyknosis, and degenerative changes (red arrow). Numerous healthy neurons (black arrow) are observed, indicating a synergistic neuroprotective effect when PFD (300 mg/kg) is combined with SVP (200 mg/kg).

et al., 2014). Seizures often lead to mitochondrial dysfunction, which exacerbates neuronal damage and lowers seizure thresholds. PFD may protect mitochondrial function by preventing oxidative damage, thus preserving cellular energy balance and contributing to an increased STC (Castro-Torres et al., 2015; Bozkurt et al., 2022).

The PTZ-induced kindling model is extensively used to investigate the mechanisms of epilepsy and to evaluate the efficacy of anticonvulsant drugs as it is favored for exploring long-term neurochemical and structural changes in the brain (Khatoon et al., 2021). Repetitive administration of a sub-convulsive dose of PTZ (25 mg/kg, *i.p.*) led to chemical kindling, resulting in the emergence of seizures resembling generalized tonic-clonic seizures (Aleshin et al., 2023). SVP is among the most widely used antiepileptic drugs and is proven to show anticonvulsant effects in the PTZ model (Wang et al., 2020). In this study, PFD administration reduced seizure severity significantly compared to the PTZ + vehicle group. The exact mechanisms behind this increase in STC and reduction in seizure severity may include the reduction of inflammation and oxidative stress in the brain, which are key contributors to seizure activity. PFD may induce protection against seizures by increasing the brain's resistance to seizure-inducing stimuli, thereby making it more difficult for seizures to be triggered (Bozkurt et al., 2022).

Oxidative stress, characterized by increased reactive oxygen species (ROS) and lipid peroxidation, contributes significantly to neuronal damage in epilepsy (Madireddy and Madireddy, 2023). Elevated malondialdehyde (MDA) levels and reduced antioxidant enzyme activity (SOD, catalase, and GSH) in the Vehicle + PTZ group indicate increased oxidative stress. PFD treatment, particularly at 300 mg/kg, effectively restored antioxidant profiles, reducing MDA levels and enhancing antioxidant enzyme activities. These findings are supported by studies demonstrating PFD's antioxidant properties in mitigating oxidative damage in various models of neuroinflammation and tissue injury (Salazar-Montes et al., 2008; Dutta et al., 2017; Aimo et al., 2022; Bozkurt et al., 2022). By enhancing antioxidant defenses, PFD may prevent ROS-induced excitotoxicity and protect against mitochondrial dysfunction, thereby preserving neuronal function (Dutta et al., 2017).

Acetylcholinesterase (AChE) plays a critical role in regulating cholinergic transmission, which is essential for neuronal excitability and cognitive function (Komali et al., 2021). Elevated AChE activity, often observed in epilepsy, disrupts cholinergic signaling by accelerating acetylcholine hydrolysis, leading to increased neuronal excitability and cognitive impairments such as memory and learning deficits (Alyami et al., 2022). In this study, PFD significantly reduced AChE activity in the hippocampus and cortex, thereby preserving acetylcholine levels and improving cognitive outcomes, as evidenced by enhanced performance in behavioral tasks like passive avoidance and elevated plus maze tests. Additionally, PFD's antioxidant properties may contribute to this effect by mitigating oxidative stress, a known contributor to cholinergic dysfunction in epilepsy (Evani et al., 2020). Oxidative stress can impair cholinergic neurons, further increasing AChE activity and aggravating cognitive deficits (Madireddy and

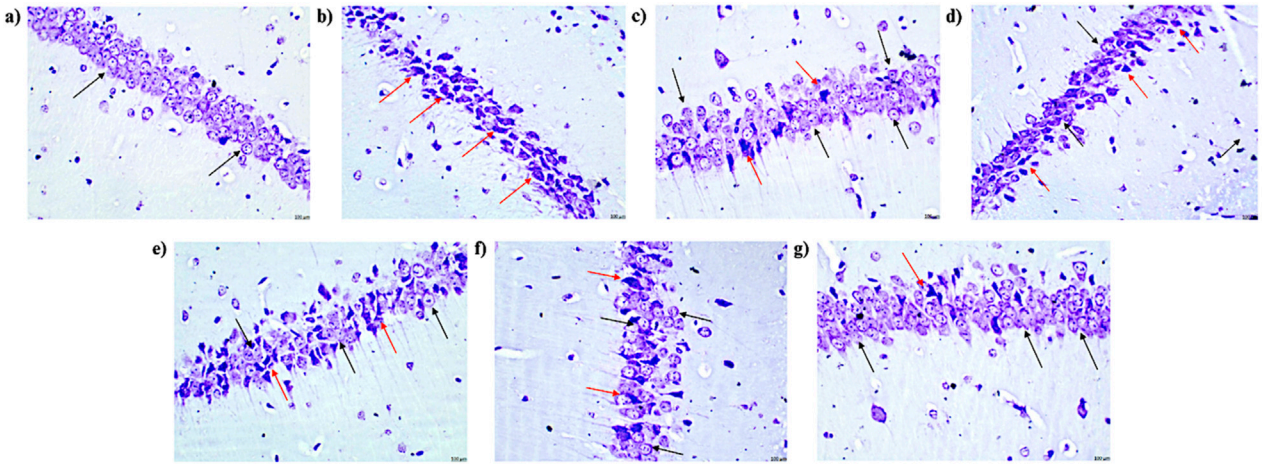


FIGURE 14
Microscopic examination of the hippocampal tissue samples using ×400 magnification using cresyl violet dye indicating neuronal damage (n = 3) **(A)** Control **(B)** PTZ + Vehicle **(C)** SVP + Vehicle **(D)** PFD 100 + PTZ **(E)** PFD 200 + PTZ **(F)** PFD 300 + PTZ **(G)** PFD 300 + SVP + PTZ. **(A)** Control: Black arrows indicate a normal histological appearance of the CA1 region of the hippocampus, with no signs of pyknosis, cellular disintegration, vacuolations, or apoptotic changes observed. **(B)** Vehicle + PTZ: The section shows a severely damaged CA1 region of the hippocampus with extensive cellular disintegration, marked pyknosis, and degenerative changes (red arrow), indicating significant neuronal damage. **(C)** SVP (200 mg/kg) + PTZ: The section reveals a minimally damaged CA1 region of the hippocampus with minimal cellular disintegration, mild pyknosis, and degenerative changes (red arrow). Numerous healthy neurons (black arrow) are still visible, indicating partial neuroprotection by SVP. **(D)** PFD (100 mg/kg) + PTZ: The section displays a moderately damaged CA1 region of the hippocampus with moderate cellular disintegration, marked pyknosis, and degenerative changes (red arrow). However, numerous healthy neurons (black arrow) are also present, indicating limited neuroprotection at this dose. **(E)** PFD (200 mg/kg) + PTZ: The section shows a mildly damaged CA1 region of the hippocampus, similar to the 100 mg/kg dose, with moderate cellular disintegration, marked pyknosis, and degenerative changes (red arrow). Numerous healthy neurons (black arrow) are still visible. **(F)** PFD (300 mg/kg) + PTZ: The section shows minimally damaged CA1 region of the hippocampus, with mild cellular disintegration, pyknosis, and degenerative changes (red arrow). Numerous healthy neurons (black arrow) are present, suggesting significant neuroprotection at this higher dose. **(G)** PFD (300 mg/kg) + SVP (200 mg/kg) + PTZ: The section shows a minimally damaged CA1 region of the hippocampus, with minimal cellular disintegration, mild pyknosis, and degenerative changes (red arrow). Numerous healthy neurons (black arrow) are observed, indicating a synergistic neuroprotective effect when PFD (300 mg/kg) is combined with SVP (200 mg/kg).

Madireddy, 2023). Previous studies have shown that reducing AChE activity not only improves cognitive performance but also stabilizes neuronal excitability, thereby offering neuroprotective effects in epilepsy (Komali et al., 2021; Alyami et al., 2022).

Epilepsy is often accompanied by cognitive deficits, primarily due to hippocampal dysfunction and neuroinflammation (Novak et al., 2022). Behavioral tests such as transfer latency in the elevated plus maze and step-down latency in the passive avoidance test demonstrated that PFD, particularly at 300 mg/kg, significantly improved both acquisition and retention latency. This suggests enhanced memory retention and preserves cognitive function. Such improvements align with reductions in pro-inflammatory cytokines (IL-6, TNF-α, IL-1β, and HMGB1) and oxidative markers observed in this study.

Neuroinflammation disrupts hippocampal plasticity, impairing spatial learning and memory (Suleymanova, 2021). PFD's ability to reduce cytokines like HMGB1 and TLR-4 likely stabilized the neuronal microenvironment, supporting hippocampal function. Furthermore, the restoration of GABA and reduction of glutamate levels in the hippocampus and cortex may have alleviated cognitive impairments, consistent with prior research linking GABAergic dysfunction and glutamate excitotoxicity to cognitive decline in epilepsy on mice model of cognitive dysfunction (Zhu et al., 2020; Zhou et al., 2022).

PFD administration significantly reduced pro-inflammatory cytokines such as IL-1β, IL-6, and TNF-α, in the hippocampus and cortex, likely due to its ability to inhibit the release of these pro-inflammatory cytokines, which are known to enhance neuronal excitability and promote seizures, while simultaneously enhancing the production of anti-inflammatory cytokines like IL-10 (Soltani Khaboushan et al., 2022). Although data on PFD treatment for neurological disorders is limited, there is evidence from other studies that PFD has demonstrated protective effects against silica-induced lung injury, where it reduced the release of pro-inflammatory cytokines such as TNF-α, IL-1β, and IL-6 in mice (Cao et al., 2022) Additionally, PFD reduced levels of IL-1β and IL-18 in animal models of pulmonary hypertension by suppressing the NOD-like pyrin domain-containing protein 3 (NLRP3) inflammasome (Brunet et al., 2022). This mechanism is especially pertinent to neurological disorders, where the activation of the NLRP3 inflammasome, along with pro-IL-1β, can trigger TLR4 activation. This, in turn, initiates NF-κB signaling, which drives the transcription of NF-κB-dependent genes in the nucleus evident in epilepsy animal models (Liu et al., 2017; Sharawy and Serrya, 2020; Cai and Lin, 2022).

In recent studies, PFD has been identified as a significant modulator of the HMGB1/TLR4 signaling axis, which is crucial in regulating neuroinflammation and neuronal plasticity (Zhao et al., 2014). In murine models of acute pancreatitis, PFD treatment resulted in reduced serum levels of HMGB1 and C-reactive protein (Palathingal Bava et al., 2022), two

inflammatory markers that have been linked to poor outcomes in clinical studies of epilepsy (Zhong et al., 2019; Chen et al., 2023a). Similarly, in this study, the PFD administration effectively suppressed the levels of HMGB1 and TLR-4 in the hippocampus and cortex in a dose-dependent manner in comparison to the control group. This suppression is particularly important because HMGB1, when released extracellularly, binds to TLR4 and activates downstream pro-inflammatory pathways, including MAPK. These pathways subsequently lead to the increased production of growth factors such as TGF-β, which are known to exacerbate neuroinflammatory responses, disrupt the BBB, and contribute to the onset of seizures (Zhang et al., 2017). The ability of PFD to modulate TGF-β and other cytokines involved in inflammation, as observed in this study, suggests that it can stabilize the neuronal environment by reducing excitatory conditions that might lead to seizures. By inhibiting the activity of TGF-β and reducing its levels, PFD potentially diminishes the inflammatory response, thereby mitigating the harmful effects associated with epilepsy. This effect could be attributed to the reduction of HMGB1/TLR4 signaling, which dampens the inflammatory response and leads to a lower production of TGF-β (Zhang et al., 2017). Simultaneously, the HMGB1/TLR4 axis can influence the Smad signaling pathway, which is required for the downstream effects of TGF-β. Inhibiting HMGB1/TLR4 signaling may reduce the phosphorylation and activation of Smad2/3, thereby decreasing TGF-β signaling and its associated effects. This inhibition may help to stabilize the neuronal environment, reduce the likelihood of seizures, and protect against seizure-induced neuronal damage (Song et al., 2021; Chen et al., 2023b).

The GABAergic system, responsible for inhibitory neurotransmission, is also adversely affected by the activation of TLR4 signaling. Activation of TLR4 by HMGB1 leads to a decrease in GABA synthesis and postsynaptic GABA receptor activity, contributing to the imbalance between excitation and inhibition in the brain. This imbalance promotes neuroinflammation and neurodegeneration, both of which are critical factors in the development and exacerbation of epilepsy (Yan et al., 2015). Elevated extracellular glutamate levels can lead to hyperexcitability of neurons, which is a key factor in the initiation and propagation of seizures. Studies have shown that during seizures, there is often a significant increase in extracellular glutamate concentrations, which can reach neurotoxic levels, further exacerbating the excitatory environment in the brain (During and Spencer, 1993). A reduction in GABA levels can lower the threshold for seizure generation, as the inhibitory control over neuronal firing is diminished. This decrease in GABAergic inhibition is a critical factor in seizure development, especially when combined with elevated glutamate levels (Ueda et al., 2001). It was observed that PFD administration significantly increased GABA levels and decreased glutamate levels compared to the control group. Additionally, under pathological conditions, excessive glutamate release and impaired clearance can lead to excitotoxicity, a key contributor to neuronal damage and seizure activity. HMGB1 release in response to glutamate-induced excitotoxicity further activates TLR4, amplifying the inflammatory response and neuronal damage, creating a vicious cycle of neuroinflammation and excitotoxicity. PFD's role in reducing HMGB1 and TLR4 levels may interrupt this cycle, reducing glutamate levels and protecting neurons from excitotoxic damage. This reduction in extracellular glutamate, coupled with the preservation of GABA levels, is crucial for lowering the threshold for seizure generation and maintaining neuronal stability. The ability of PFD to reduce HMGB1 and TLR4 levels could help preserve GABAergic transmission, thereby restoring the balance between excitatory and inhibitory neurotransmission, which is essential for controlling seizure activity (Zou and Crews, 2015).

Certain AEDs are known to cause hepatotoxicity, which can range from mild, transient elevations in liver enzymes to severe liver injury leading to acute liver failure. Among these, phenytoin, SVP, and carbamazepine are particularly associated with liver toxicity. These ASMs undergo extensive hepatic metabolism, which can result in the formation of toxic metabolites that contribute to liver injury (Vidaurre et al., 2017). In this study, it was observed that PFD effectively reduced elevated AST and ALT levels, suggesting a protective effect on liver function. In an investigation into the effects of PFD on D-galactosamine and lipopolysaccharide-induced acute hepatotoxicity in rats, PFD significantly reduced the elevated ALT and AST levels (Wang et al., 2008). Similarly, in a study on liver fibrosis induced by carbon tetrachloride (CCl4) in mice, PFD treatment resulted in a marked decrease in ALT and AST levels, highlighting its effectiveness in mitigating liver damage associated with fibrosis (Xiao et al., 2016). Further supporting these findings, a study on experimental liver cirrhosis demonstrated that PFD treatment significantly reduced ALT and AST levels in cirrhotic rats, along with a decrease in other markers of liver damage (García et al., 2002). Additionally, in patients with chronic hepatitis C, long-term treatment with PFD was associated with a trend toward normalization of ALT and AST levels and improvements in other liver function indicators (Flores-Contreras et al., 2014).

Histopathological analysis confirmed PFD's neuroprotective effects. In the vehicle + PTZ group, severe neuronal damage was observed in both the hippocampus and cortex, characterized by pronounced pyknosis, cellular disintegration, and degenerative changes. Severe neuronal damage, including pyknosis and cellular disintegration, observed in the Vehicle + PTZ group was significantly alleviated in PFD-treated groups, particularly at 300 mg/kg. These findings are consistent with studies demonstrating PFD's ability to preserve neuronal architecture in models of neuroinflammation and excitotoxicity (Dutta et al., 2017; Bozkurt et al., 2022). PFD treatment, particularly at the 300 mg/kg dose, significantly alleviated these histopathological abnormalities. The hippocampus and cortex of PFD-treated animals exhibited a reduction in pyknosis and cellular disintegration, with more preserved neuronal architecture compared to the vehicle + PTZ group. This protective effect was most pronounced in the PFD 300 mg/kg + SVP combination group, which showed minimal neuronal damage, suggesting a potential synergistic effect between PFD and SVP. The preservation of hippocampal and cortical neurons likely contributed to improved cognitive outcomes and reduced seizure severity. Additionally, the combination of PFD with SVP showed minimized neuronal damage, indicating potential combinatory benefits in epilepsy treatment. The histopathological findings corroborate the biochemical and behavioral results of this study. Additionally, by

reducing pro-inflammatory cytokines and modulating antioxidant enzyme activity, PFD likely stabilizes the neuronal microenvironment, preserving structural integrity in the hippocampus and cortex.

Due to these properties, PFD has also shown possible benefits during the secondary phase of Traumatic brain injury, where neuroinflammation causes worsening neurological outcomes. It was observed that PFD reduced neuroinflammation by decreasing levels of neuron-specific enolase (NSE) and S100B (biomarkers of brain injury) and improved neurological outcomes in the Garcia test (Bozkurt et al., 2022). Similarly, administration of PFD in patients with secondary progressive multiple sclerosis (SPMS) has been shown to stabilize or even improve neurological functions over up to 2 years. Patients treated with PFD had fewer relapses and showed improvement in bladder function, another common symptom of epilepsy where loss of bladder control is observed (Walker et al., 2005). This suggests that PFD may reduce cognitive and physical dysfunction and slow the progression of neurological disabilities by mitigating inflammation and oxidative stress (Walker et al., 2005). Relatively, similar results where PFD's anti-inflammatory activity has been assessed in various organ systems, including the heart (Aimo et al., 2022) kidneys (Bai et al., 2021) liver (Escutia-Gutiérrez et al., 2021) and lungs (Ruwanpura et al., 2020).

While the present study demonstrates the anticonvulsant, neuroprotective, and cognitive-enhancing effects of pirfenidone (PFD) in a PTZ-induced kindling model of epilepsy, it is important to acknowledge the limitation of not evaluating the long-term effects of PFD treatment. Chronic epilepsy management requires sustained efficacy and safety over extended durations, particularly concerning cognitive outcomes and seizure control. The current findings provide critical insights into the acute and sub-chronic effects of PFD; however, further investigations are necessary to determine its potential as a chronic therapeutic agent.

This study provides evidence of PFD anticonvulsant and neuroprotective effects in the PTZ-induced kindling model of epilepsy The 6-week treatment period was sufficient to demonstrate significant improvements in seizure control, cognitive performance, and biochemical modulation, establishing a strong foundation for PFD's therapeutic potential. The study also observed the modulation of the HMGB1/TLR4 pathway as a key mechanism of PFD's effects, supported by reductions in pro-inflammatory markers. Additionally, the evaluation of three doses (100, 200, and 300 mg/kg) demonstrated that 300 mg/kg was the most effective, suggesting a strong dose-response relationship.

However, this study did not explore the long-term effects of PFD, which are essential for chronic conditions like epilepsy. Investigating its sustained efficacy, safety, and cognitive benefits over extended durations remains a vital next step. Future studies should focus on assessing the long-term impact of PFD through chronic treatment regimens in animal models, incorporating neurobehavioral assessments, biochemical analyses, and histopathological evaluations over extended timeframes. Additionally, studies exploring the molecular mechanisms underlying the sustained modulation of neuroinflammation, oxidative stress, and neurotransmitter balance by PFD would provide a deeper understanding of its therapeutic potential. Simultaneously, expanding the dose range and use of placebo in future studies could further refine the therapeutic index and optimize clinical translation. Lastly, while male mice were used to reduce variability and focus on establishing baseline efficacy, future studies should include both sexes to evaluate potential gender-specific responses to PFD.

6 Conclusion

PFD exhibited significant anti-inflammatory, anticonvulsant, and neuroprotective effects in a PTZ-induced kindling model of epilepsy. It effectively reduced seizure severity, enhanced cognitive performance, and modulated oxidative stress by decreasing malondialdehyde (MDA) levels and boosting antioxidant enzymes (SOD, catalase, GSH). Additionally, PFD's ability to reduce pro-inflammatory cytokines and modulate neurotransmitter levels suggests a protective role in mitigating neuroinflammation and excitotoxicity, both of which are critical in the pathogenesis of epilepsy. Furthermore, PFD displayed hepatoprotective properties by reducing elevated liver enzyme levels, indicating its potential safety in long-term use. Histopathological analysis confirmed its neuroprotective role, preserving hippocampal and cortical integrity. These findings indicate that PFD holds potential as an adjunct therapy for epilepsy. However, additional research is necessary to investigate its long-term effectiveness, safety, and applicability across various epilepsy models and its potential for clinical use.

Data availability statement

The original contributions presented in the study are included in the article/supplementary material, further inquiries can be directed to the corresponding author.

Ethics statement

The animal study was approved by The Institutional Animal Ethics Committee of Jamia Hamdard, New Delhi, India. The study was conducted in accordance with the local legislation and institutional requirements.

Author contributions

MD: Data curation, Formal Analysis, Funding acquisition, Investigation, Methodology, Resources, Software, Writing–original draft, Writing–review and editing. SG: Formal Analysis, Resources, Validation, Visualization, Writing–review and editing. HM: Formal Analysis, Methodology, Writing–review and editing. DV: Data curation, Formal Analysis, Investigation, Resources, Supervision, Visualization, Writing–review and editing. N: Conceptualization, Data curation, Formal Analysis, Funding acquisition, Methodology, Supervision, Validation, Visualization, Writing–review and editing.

Funding

The author(s) declare that no financial support was received for the research, authorship, and/or publication of this article.

Conflict of interest

The authors declare that the research was conducted in the absence of any commercial or financial relationships that could be construed as a potential conflict of interest.

The author(s) declared that they were an editorial board member of Frontiers, at the time of submission. This had no impact on the peer review process and the final decision.

Generative AI statement

The author(s) declare that no Generative AI was used in the creation of this manuscript.

Publisher's note

All claims expressed in this article are solely those of the authors and do not necessarily represent those of their affiliated organizations, or those of the publisher, the editors and the reviewers. Any product that may be evaluated in this article, or claim that may be made by its manufacturer, is not guaranteed or endorsed by the publisher.

References

Agarwal, N. B., Jain, S., Nagpal, D., Agarwal, N. K., Mediratta, P. K., and Sharma, K. K. (2013). Liposomal formulation of curcumin attenuates seizures in different experimental models of epilepsy in mice. *Fundam. Clin. Pharmacol.* 27, 169–172. doi:10.1111/j.1472-8206.2011.01002.x

Aimo, A., Spitaleri, G., Panichella, G., Lupón, J., Emdin, M., and Bayes-Genis, A. (2022). Pirfenidone as a novel cardiac protective treatment. *Heart Fail Rev.* 27, 525–532. doi:10.1007/s10741-021-10175-w

Akyüz, E., Doğanyiğit, Z., Paudel, Y. N., Kaymak, E., Yilmaz, S., Uner, A., et al. (2020). Increased ACh-associated immunoreactivity in autonomic centers in PTZ kindling model of epilepsy. *Biomedicines* 8, 113. doi:10.3390/biomedicines8050113

Alam, Md. N., Singh, L., Khan, N. A., Asiri, Y. I., Hassan, M. Z., Afzal, O., et al. (2023). Ameliorative effect of ethanolic extract of moringa oleifera leaves in combination with curcumin against PTZ-induced kindled epilepsy in rats: *in vivo* and *in silico*. *Pharmaceuticals* 16, 1223. doi:10.3390/ph16091223

Aleshin, V. A., Graf, A. V., Artiukhov, A. V., Ksenofontov, A. L., Zavileyskiy, L. G., Maslova, M. V., et al. (2023). Pentylenetetrazole-induced seizures are increased after kindling, exhibiting vitamin-responsive correlations to the post-seizures behavior, amino acids metabolism and key metabolic regulators in the rat brain. *Int. J. Mol. Sci.* 24, 12405. doi:10.3390/ijms241512405

Alyami, N. M., Abdi, S., Alyami, H. M., and Almeer, R. (2022). Proanthocyanidins alleviate pentylenetetrazole-induced epileptic seizures in mice via the antioxidant activity. *Neurochem. Res.* 47, 3012–3023. doi:10.1007/s11064-022-03647-4

Babovic-Vuksanovic, D., Petrovic, L., Knudsen, B. E., Plummer, T. B., Parisi, J. E., Babovic, S., et al. (2004). Survival of human neurofibroma in immunodeficient mice and initial results of therapy with pirfenidone. *Biomed. Res. Int.* 2004, 79–85. doi:10.1155/S1110724304308107

Bai, X., Nie, P., Lou, Y., Zhu, Y., Jiang, S., Li, B., et al. (2021). Pirfenidone is a renal protective drug: mechanisms, signalling pathways, and preclinical evidence. *Eur. J. Pharmacol.* 911, 174503. doi:10.1016/j.ejphar.2021.174503

Bozkurt, I., Ozturk, Y., Guney, G., Arslan, B., Gulbahar, O., Guvenc, Y., et al. (2022). Effects of pirfenidone on experimental head injury in rats. *Int. J. Clin. Exp. Pathol.* 15, 20–28.

Brunet, D., Van, S. D., Masson, B., Antigny, F., Haddad, F., Kloeckner, M., et al. (2022). Left ventricular diastolic dysfunction in chronic thromboembolic pulmonary hypertension. *J. Heart Lung Transplant.* 41, S26–S27. doi:10.1016/j.healun.2022.01.057

Cai, M., and Lin, W. (2022). The function of NF-kappa B during epilepsy, a potential therapeutic target. *Front. Neurosci.* 16, 851394. doi:10.3389/fnins.2022.851394

Cao, Z., Liu, Y., Zhang, Z., Yang, P., Li, Z., Song, M., et al. (2022). Pirfenidone ameliorates silica-induced lung inflammation and fibrosis in mice by inhibiting the secretion of interleukin-17A. *Acta Pharmacol. Sin.* 43, 908–918. doi:10.1038/s41401-021-00706-4

Castro-Torres, R. D., Chaparro-Huerta, V., Flores-Soto, M. E., Bañuelos-Pineda, J., Camins, A., Orozco-Suárez, S. A., et al. (2014). A single dose of pirfenidone attenuates neuronal loss and reduces lipid peroxidation after kainic acid-induced excitotoxicity in the pubescent rat Hippocampus. *J. Mol. Neurosci.* 52, 193–201. doi:10.1007/s12031-013-0121-6

Castro-Torres, R. D., Chaparro-Huerta, V., Flores-Soto, M. E., Jave-Suárez, L., Camins, A., Armendáriz-Borunda, J., et al. (2015). Pirfenidone attenuates microglial reactivity and reduces inducible nitric oxide synthase mRNA expression after kainic acid-mediated excitotoxicity in pubescent rat Hippocampus. *J. Mol. Neurosci.* 56, 245–254. doi:10.1007/s12031-015-0509-6

Chen, Y., Chen, X., and Liang, Y. (2023a). Meta-analysis of HMGB1 levels in the cerebrospinal fluid and serum of patients with epilepsy. *Neurol. Sci.* 44, 2329–2337. doi:10.1007/s10072-023-06720-0

Chen, Y., Nagib, M. M., Yasmen, N., Sluter, M. N., Littlejohn, T. L., Yu, Y., et al. (2023b). Neuroinflammatory mediators in acquired epilepsy: an update. *Inflamm. Res.* 72, 683–701. doi:10.1007/s00011-023-01700-8

During, M. J., and Spencer, D. D. (1993). Extracellular hippocampal glutamate and spontaneous seizure in the conscious human brain. *Lancet* 341, 1607–1610. doi:10.1016/0140-6736(93)90754-5

Dutta, D., Kumar, S. L. H., and Grewal, A. K. (2017). Neuroprotective effect of pirfenidone on scopolamine induced cognitive impairment and oxidative stress. *Indian J. Physiology Pharmacol.* 61, 416–429.

Ellman, G. L., Courtney, K. D., Andres, V., and Featherstone, R. M. (1961). A new and rapid colorimetric determination of acetylcholinesterase activity. *Biochem. Pharmacol.* 7, 88–95. doi:10.1016/0006-2952(61)90145-9

Escutia-Gutiérrez, R., Rodríguez-Sanabria, J. S., Monraz-Méndez, C. A., García-Bañuelos, J., Santos-García, A., Sandoval-Rodríguez, A., et al. (2021). Pirfenidone modifies hepatic miRNAs expression in a model of MAFLD/NASH. *Sci. Rep.* 11, 11709. doi:10.1038/s41598-021-91187-2

Evani, S. J., Karna, S. L. R., Seshu, J., and Leung, K. P. (2020). Pirfenidone regulates LPS mediated activation of neutrophils. *Sci. Rep.* 10, 19936. doi:10.1038/s41598-020-76271-3

Flores-Contreras, L., Sandoval-Rodríguez, A. S., Mena-Enriquez, M. G., Lucano-Landeros, S., Arellano-Olivera, I., Álvarez-Álvarez, A., et al. (2014). Treatment with pirfenidone for two years decreases fibrosis, cytokine levels and enhances CB2 gene expression in patients with chronic hepatitis C. *BMC Gastroenterol.* 14, 131. doi:10.1186/1471-230X-14-131

García, L., Hernández, I., Sandoval, A., Salazar, A., Garcia, J., Vera, J., et al. (2002). Pirfenidone effectively reverses experimental liver fibrosis. *J. Hepatol.* 37, 797–805. doi:10.1016/S0168-8278(02)00272-6

Ghaith, A. K., El-Hajj, V. G., Sanchez-Garavito, J. E., Zamanian, C., Ghanem, M., Bon-Nieves, A., et al. (2024). Trends in the utilization of surgical modalities for the treatment of drug-resistant epilepsy: a comprehensive 10-year analysis using the national inpatient sample. *Neurosurgery*. doi:10.1227/neu.0000000000002811

Greenwald, R. A. (2018). *Handbook methods for oxygen radical research*. Boca Raton, London, New York: CRC Press web Taylor and Francis group.

Imran, M., Riaz, T., Majid, H., and Maqsood, S. (2023). Identification of botanicals using molecular biotechnology. *Polym. Med.* 53, 69–79. doi:10.17219/PIM/163119

Ivens, S., Kaufer, D., Flores, L. P., Bechmann, I., Zumsteg, D., Tomkins, O., et al. (2007). TGF-beta receptor-mediated albumin uptake into astrocytes is involved in neocortical epileptogenesis. *Brain* 130 (Pt 2), 535–547. doi:10.1093/BRAIN/AWL317

Jollow, D. J., Mitchell, J. R., Zampaglione, N., and Gillette, J. R. (1974). Bromobenzene-induced liver necrosis. Protective role of glutathione and evidence for 3,4-bromobenzene oxide as the hepatotoxic metabolite. *Pharmacology* 11, 151–169. doi:10.1159/000136485

Kamali, A. N., Zian, Z., Bautista, J. M., Hamedifar, H., Hossein-Khannazer, N., Hosseinzadeh, R., et al. (2020). The potential role of pro-inflammatory and anti-inflammatory cytokines in epilepsy pathogenesis. *Endocr. Metab. Immune Disord. Drug Targets* 21, 1760–1774. doi:10.2174/1871530320999201116200940

Khan, W. U., Salman, M., Ali, M., Majid, H., Yar, M. S., Akhtar, M., et al. (2024). Neuroprotective effects of sulforaphane in a rat model of alzheimer's disease induced by aβ (1-42) peptides. *Neurochem. Int.* 179, 105839. doi:10.1016/J.NEUINT.2024.105839

Khatoon, S., Agarwal, N. B., Samim, M., and Alam, O. (2021). Neuroprotective effect of fisetin through suppression of IL-1R/TLR Axis and apoptosis in pentylenetetrazole-induced kindling in mice. *Front. Neurol.* 12, 689069. doi:10.3389/fneur.2021.689069

Khatoon, S., Samim, M., Dahalia, M., and Nidhi (2023). Fisetin provides neuroprotection in pentylenetetrazole-induced cognition impairment by upregulating CREB/BDNF. *Eur. J. Pharmacol.* 944, 175583. doi:10.1016/j.ejphar.2023.175583

Komali, E., Venkataramaiah, C., and Rajendra, W. (2021). Antiepileptic potential of Bacopa monnieri in the rat brain during PTZ-induced epilepsy with reference to cholinergic system and ATPases. *J. Tradit. Complement. Med.* 11, 137–143. doi:10.1016/j.jtcme.2020.02.011

Kumar, V., Sharma, S. K., Nagarajan, K., and Dixit, P. K. (2016). Effects of lycopene and sodium valproate on pentylenetetrazol-induced kindling in mice. *Iran. J. Med. Sci.* 41, 430–436.

Liu, J., and Shi, G. (2019). Pirfenidone activates cannabinoid receptor 2 in a mouse model of bleomycin-induced pulmonary fibrosis. *Exp. Ther. Med.* 18, 4241–4248. doi:10.3892/etm.2019.8045

Liu, J., Zhang, P., Zou, Q., Liang, J., Chen, Y., Cai, Y., et al. (2023). Status of epilepsy in the tropics: an overlooked perspective. *Epilepsia Open* 8, 32–45. doi:10.1002/EPI4.12686

Liu, N., Song, Y., Liu, T., Wang, H., Yu, N., and Ma, H. (2024). Metformin enhanced the effect of pirfenidone on pulmonary fibrosis in mice. *Clin. Respir. J.* 18, e13731. doi:10.1111/crj.13731

Liu, T., Zhang, L., Joo, D., and Sun, S.-C. (2017). NF-κB signaling in inflammation. *Signal Transduct. Target Ther.* 2, 17023. doi:10.1038/sigtrans.2017.23

Löscher, W., Potschka, H., Sisodiya, S. M., and Vezzani, A. (2020). Drug resistance in epilepsy: clinical impact, potential mechanisms, and new innovative treatment options. *Pharmacol. Rev.* 72, 606–638. doi:10.1124/pr.120.019539

Lowry, O. H., Rosebrough, N. J., Farr, A. L., and Randall, R. J. (1951). Protein measurement with the Folin phenol reagent. *J. Biol. Chem.* 1, 265–275. doi:10.1016/s0021-9258(19)52451-6

Madireddy, S., and Madireddy, S. (2023). Therapeutic strategies to ameliorate neuronal damage in epilepsy by regulating oxidative stress, mitochondrial dysfunction, and neuroinflammation. *Brain Sci.* 13, 784. doi:10.3390/brainsci13050784

Mir, M. A., Malik, A. B., Zulfkar, D., and Dar, M. A. (2023). Adverse reactions caused by antiepileptic medications in real-world medical settings. *Int. J. Curr. Res. Physiology Pharmacol.*, 25–35.

Misra, H. P., and Fridovich, I. (1972). The role of superoxide anion in the autoxidation of epinephrine and a simple assay for superoxide dismutase. *J. Biol. Chem.* 247, 3170–3175. doi:10.1016/s0021-9258(19)45228-9

Misra, H. P., and Rabideau, C. (2000). Pirfenidone inhibits NADPH-dependent microsomal lipid peroxidation and scavenges hydroxyl radicals. *Mol. Cell Biochem.* 204, 119–126. doi:10.1023/A:1007023532508

Nakamura, Y., Shimizu, Y., Fujimaki-Shiraishi, M., Uchida, N., Takemasa, A., and Niho, S. (2023). A protective effect of pirfenidone in lung fibroblast–endothelial cell network via inhibition of rho-kinase activity. *Biomedicines* 11, 2259. doi:10.3390/biomedicines11082259

Nodirahon, A., Majid, H., Waghdhare, S., Vohora, D., and Nidhi (2024). The effect of sodium glucose Co-transport 2 inhibitors on cognitive impairment and depression in type 2 diabetes mellitus patients. *Clin. Epidemiol. Glob. Health* 26, 101555. doi:10.1016/J.CEGH.2024.101555

Novak, A., Vizjak, K., and Rakusa, M. (2022). Cognitive impairment in people with epilepsy. *J. Clin. Med.* 11, 267. doi:10.3390/jcm11010267

Ohkawa, H., Ohishi, N., and Yagi, K. (1979). Assay for lipid peroxides in animal tissues by thiobarbituric acid reaction. *Anal. Biochem.* 95, 351–358. doi:10.1016/0003-2697(79)90738-3

Palathingal Bava, E., George, J., Tarique, M., Iyer, S., Sahay, P., Gomez Aguilar, B., et al. (2022). Pirfenidone increases IL-10 and improves acute pancreatitis in multiple clinically relevant murine models. *JCI Insight* 7, e141108. doi:10.1172/jci.insight.141108

Pinto, L. F., Silva, L. S., João, R. B., Boldrini, V., Cendes, F., and Yasuda, C. L. (2024). Practices in the prescription of antiseizure medications: is it time to change? *Arq. Neuropsiquiatr.* 82, 001–010. doi:10.1055/s-0043-1777806

Ruwanpura, S. M., Thomas, B. J., and Bardin, P. G. (2020). Pirfenidone: molecular mechanisms and potential clinical applications in lung disease. *Am. J. Respir. Cell Mol. Biol.* 62, 413–422. doi:10.1165/rcmb.2019-0328TR

Salazar-Montes, A., Ruiz-Corro, L., López-Reyes, A., Castrejón-Gómez, E., and Armendáriz-Borunda, J. (2008). Potent antioxidant role of Pirfenidone in experimental cirrhosis. *Eur. J. Pharmacol.* 595, 69–77. doi:10.1016/j.ejphar.2008.06.110

Sehar, N., Agarwal, N. B., Vohora, D., and Raisuddin, S. (2015). Atorvastatin prevents development of kindling by modulating hippocampal levels of dopamine, glutamate, and GABA in mice. *Epilepsy and Behav.* 42, 48–53. doi:10.1016/j.yebeh.2014.11.011

Sharawy, M. H., and Serrya, M. S. (2020). Pirfenidone attenuates gentamicin-induced acute kidney injury by inhibiting inflammasome-dependent NLRP3 pathway in rats. *Life Sci.* 260, 118454. doi:10.1016/j.lfs.2020.118454

Soltani Khaboushan, A., Yazdanpanah, N., and Rezaei, N. (2022). Neuroinflammation and proinflammatory cytokines in epileptogenesis. *Mol. Neurobiol.* 59, 1724–1743. doi:10.1007/s12035-022-02725-6

Song, Z., Wu, T., Sun, J., Wang, H., Hua, F., Nicolas, Y. S. M., et al. (2021). Metformin attenuates post-epidural fibrosis by inhibiting the TGF-β1/Smad3 and HMGB1/TLR4 signaling pathways. *J. Cell Mol. Med.* 25, 3272–3283. doi:10.1111/jcmm.16398

Stasenko, A., Lin, C., Bonilha, L., Bernhardt, B. C., and McDonald, C. R. (2024). Neurobehavioral and clinical comorbidities in epilepsy: the role of white matter network disruption. *Neurosci.* 30, 105–131. doi:10.1177/10738584221076133

Suleymanova, E. M. (2021). Behavioral comorbidities of epilepsy and neuroinflammation: evidence from experimental and clinical studies. *Epilepsy and Behav.* 117, 107869. doi:10.1016/j.yebeh.2021.107869

Tavakoli, Z., Tahmasebi Dehkordi, H., Lorigooini, Z., Rahimi-Madiseh, M., Korani, M. S., and Amini-Khoei, H. (2023). Anticonvulsant effect of quercetin in pentylenetetrazole (PTZ)-induced seizures in male mice: the role of anti-neuroinflammatory and anti-oxidative stress. *Int. Immunopharmacol.* 116, 109772. doi:10.1016/j.intimp.2023.109772

Tian, Q., Xiao, Q., Yu, W., Gu, M., Zhao, N., and Lü, Y. (2016). The inhibition of transforming growth factor beta-activated kinase 1 contributed to neuroprotection via inflammatory reaction in pilocarpine-induced rats with epilepsy. *Neuroscience* 325, 111–123. doi:10.1016/J.NEUROSCIENCE.2016.03.045

Tombini, M., Boscarino, M., and Di Lazzaro, V. (2023). Tackling seizures in patients with Alzheimer's disease. *Expert Rev. Neurother.* 23, 1131–1145. doi:10.1080/14737175.2023.2278487

Tyagi, K., Masoom, M., Majid, H., Garg, A., Bhurani, D., Agarwal, N. B., et al. (2023). Role of cytokines in chemotherapy-related cognitive impairment of breast cancer patients: a systematic review. *Curr. Rev. Clin. Exp. Pharmacol.* 18, 110–119. doi:10.2174/2772432817666220304212456

Ueda, Y., Doi, T., Tokumaru, J., Yokoyama, H., Nakajima, A., Mitsuyama, Y., et al. (2001). Collapse of extracellular glutamate regulation during epileptogenesis: down-regulation and functional failure of glutamate transporter function in rats with chronic seizures induced by kainic acid. *J. Neurochem.* 76, 892–900. doi:10.1046/j.1471-4159.2001.00087.x

Vezzani, A., Balosso, S., and Ravizza, T. (2008). The role of cytokines in the pathophysiology of epilepsy. *Brain Behav. Immun.* 22, 797–803. doi:10.1016/J.BBI.2008.03.009

Vidaurre, J., Gedela, S., and Yarosz, S. (2017). Antiepileptic drugs and liver disease. *Pediatr. Neurol.* 77, 23–36. doi:10.1016/J.PEDIATRNEUROL.2017.09.013

Walker, J. E., Giri, S. N., and Margolin, S. B. (2005). A double-blind, randomized, controlled study of oral pirfenidone for treatment of secondary progressive multiple sclerosis. *Multiple Scler. J.* 11, 149–158. doi:10.1191/1352458505ms1134oa

Wang, F., Wen, T., Chen, X. Y., and Wu, H. (2008). Protective effects of pirfenidone on D-galactosamine and lipopolysaccharide-induced acute hepatotoxicity in rats. *Inflamm. Res.* 57, 183–188. doi:10.1007/S00011-007-7153-8

Wang, Y., Wang, G., Tao, J., Li, X., Hu, L., Li, Q., et al. (2020). Autophagy associated with the efficacy of valproic acid in PTZ-induced epileptic rats. *Brain Res.* 1745, 146923. doi:10.1016/j.brainres.2020.146923

Waris, A., Siraj, M., Khan, A., Lin, J., Asim, M., and Alhumaydh, F. A. (2024). A comprehensive overview of the current status and advancements in various treatment strategies against epilepsy. *ACS Pharmacol. Transl. Sci.* 7, 3729–3757. doi:10.1021/acsptsci.4c00494

Wu, J., Cai, Y., Wu, X., Ying, Y., Tai, Y., and He, M. (2021). Transcardiac perfusion of the mouse for brain tissue dissection and fixation. *Bio Protoc.* 11, e3988. doi:10.21769/BioProtoc.3988

Xiao, M., Qu, X. H., Lv, J. P., Shi, Y., Li, C. X., and Xie, K. J. (2016). Effects of pirfenidone on hepatic fibrosis in mice induced by carbon tetrachloride. *Zhongguo Ying Yong Sheng Li Xue Za Zhi* 32 (4), 378–382. doi:10.13459/J.CNKI.CJAP.2016.04.023

Yan, X., Jiang, E., and Weng, H.-R. (2015). Activation of toll like receptor 4 attenuates GABA synthesis and postsynaptic GABA receptor activities in the spinal dorsal horn via releasing interleukin-1 beta. *J. Neuroinflammation* 12, 222. doi:10.1186/s12974-014-0222-3

Zhang, H., Zhang, R., Chen, J., Shi, M., Li, W., and Zhang, X. (2017). High mobility group Box1 inhibitor glycyrrhizic acid attenuates kidney injury in streptozotocin-induced diabetic rats. *Kidney Blood Press Res.* 42, 894–904. doi:10.1159/000485045

Zhao, M., Zhou, A., Xu, L., and Zhang, X. (2014). The role of TLR4-mediated PTEN/PI3K/AKT/NF-κB signaling pathway in neuroinflammation in hippocampal neurons. *Neuroscience* 269, 93–101. doi:10.1016/J.NEUROSCIENCE.2014.03.039

Zhao, X., Cheng, P., Xu, R., Meng, K., Liao, S., Jia, P., et al. (2022). Insights into the development of pentylenetetrazole-induced epileptic seizures from dynamic metabolomic changes. *Metab. Brain Dis.* 37, 2441–2455. doi:10.1007/s11011-022-01018-0

Zhong, R., Chen, Q., Li, M., Zhang, X., and Lin, W. (2019). Elevated blood C-reactive protein levels in patients with epilepsy: a systematic review and meta-analysis. *Front. Neurol.* 10, 974. doi:10.3389/fneur.2019.00974

Zhou, X., Zhang, C., Wang, L., and Jin, S. (2022). Remimazolam induced cognitive dysfunction in mice via glutamate excitotoxicity. *Transl. Neurosci.* 13, 104–115. doi:10.1515/tnsci-2022-0220

Zhu, L., Chen, L., Xu, P., Lu, D., Dai, S., Zhong, L., et al. (2020). Genetic and molecular basis of epilepsy-related cognitive dysfunction. *Epilepsy and Behav.* 104, 106848. doi:10.1016/j.yebeh.2019.106848

Zou, J., and Crews, F. T. (2015). Glutamate/NMDA excitotoxicity and HMGB1/TLR4 neuroimmune toxicity converge as components of neurodegeneration. *AIMS Mol. Sci.* 2, 77–100. doi:10.3934/molsci.2015.2.77

frontiers | Frontiers in Pharmacology

TYPE Original Research
PUBLISHED 27 January 2025
DOI 10.3389/fphar.2024.1519649

Check for updates

OPEN ACCESS

EDITED BY
Rupesh V. Chikhale,
University of Cambridge, United Kingdom

REVIEWED BY
Namde Jadhav,
Krishna Institute of Medical Sciences Deemed University, India
Kumaraswamy Gandla,
Chaitanya (Deemed to be University), India
Jayadev Hiremath,
BVVS Hanagal Shri Kumareshwar College of Pharmacy, India

*CORRESPONDENCE
Archana S. Patil,
archupharma@gmail.com

†These authors have contributed equally to this work

RECEIVED 30 October 2024
ACCEPTED 18 December 2024
PUBLISHED 27 January 2025

CITATION
Revankar AA, Patil AS, Karishetti R, Chougule KR, Patil P and Salokhe A (2025) Enhanced bioavailability of Quercetin-loaded niosomal in situ gel for the management of Parkinson's disease.
Front. Pharmacol. 15:1519649.
doi: 10.3389/fphar.2024.1519649

COPYRIGHT
© 2025 Revankar, Patil, Karishetti, Chougule, Patil and Salokhe. This is an open-access article distributed under the terms of the Creative Commons Attribution License (CC BY). The use, distribution or reproduction in other forums is permitted, provided the original author(s) and the copyright owner(s) are credited and that the original publication in this journal is cited, in accordance with accepted academic practice. No use, distribution or reproduction is permitted which does not comply with these terms.

Enhanced bioavailability of Quercetin-loaded niosomal in situ gel for the management of Parkinson's disease

Abhishek A. Revankar[1†], Archana S. Patil[1*†], Reshma Karishetti[2†], Krutuja R. Chougule[1†], Priyanka Patil[3†] and Abhijit Salokhe[1†]

[1]Department of Pharmaceutics, KLE College of Pharmacy, KLE Academy of Higher Education and Research, Belagavi, Karnataka, India, [2]Department of pathology, Jawaharlal Nehru Medical College, KLE Academy of Higher Education and Research, Belagavi, Karnataka, India, [3]Department of Pharmacology, KLE College of Pharmacy, KLE Academy of Higher Education and Research, Belagavi, Karnataka, India

Background: Parkinson's disease (PD) is the second most prevalent neurological disorder, characterized by motor symptoms such as tremor and rigidity due to the degeneration of dopaminergic neurons in the substantia nigra. This study investigates the formulation of quercetin, a natural bioflavonoid with potent antioxidant and anti-inflammatory properties, as niosomes for intranasal delivery to enhance its bioavailability and therapeutic potential for PD.

Methods: The niosomal formulation was optimized for critical parameters including particle size, entrapment efficiency, and zeta potential. Male Wistar rats were utilized to assess the effects of quercetin-loaded niosomes on motor function, dopaminergic neuron protection, and oxidative stress alleviation.

Results: The optimized niosomal formulation exhibited a particle size of 195 nm, a polydispersity index (PDI) of 0.29, a zeta potential (ZP) of −30.63 mV, and an entrapment efficiency (EE) of 82.77%. *In vivo* evaluations conducted using the haloperidol-induced PD model revealed significant enhancements in behavioural, biochemical, and histopathological outcomes when compared to both disease controls and the standard treatment group. Additionally, short-term stability tests confirmed the robustness of the formulation.

Conclusion: The findings suggest that the quercetin-loaded niosomal formulation offers improved drug delivery and efficacy, indicating its potential as a superior treatment option for PD compared to conventional dosage forms. This approach may pave the way for enhanced therapeutic strategies targeting the neurodegenerative processes underlying Parkinson's disease.

KEYWORDS

biochemical assay, intranasal, niosomes, Parkinson disease, quercetin

1 Introduction

Parkinson's disease (PD) ranks as the second most common neurodegenerative disorder, primarily manifesting through hallmark motor symptoms such as tremor, bradykinesia, postural instability, and rigidity, with non-motor symptoms including sleep disturbances, olfactory deficits, cognitive impairments, and depression often predating the motor manifestations (Madiha et al., 2021). The neuropathological underpinnings of PD involve progressive

degeneration of dopaminergic neurons within the substantia nigra pars compacta, culminating in a marked dopamine (DA) deficit in the striatum. This dopaminergic depletion, coupled with alterations in other monoamines (e.g., serotonin, norepinephrine), drives the symptomatic profile of PD, both motor and non-motor (Madiha et al., 2021). Although PD's etiology remains largely enigmatic, evidence implicates genetic mutations, environmental toxins, oxidative stress, mitochondrial impairment, and neuroinflammation in its pathogenesis (Madiha et al., 2021). Current therapeutic strategies are primarily symptomatic, leveraging dopaminergic agents like levodopa, whose efficacy, however, wanes over time and is often accompanied by adverse effects (Jiang et al., 2023; Mitsuboshi et al., 2022).

Quercetin, a polyphenolic bioflavonoid widely distributed in fruits and vegetables, exhibits potent antioxidant and anti-inflammatory properties, offering a promising neuroprotective potential for PD management (Wrobel-Biedrawa et al., 2022; Grewal et al., 2021). It is known to neutralize reactive oxygen species (ROS), bolster endogenous antioxidant defenses, and modulate inflammatory cascades, presenting an ideal candidate for neuroprotection (Wrobel-Biedrawa et al., 2022). Additionally, quercetin has shown efficacy in curbing α-synuclein aggregation, a pathological hallmark associated with neurodegeneration in PD (Grewal et al., 2021). However, quercetin is categorized in a Biopharmaceutical Classification System (BCS) as Class IV (Sirvi et al., 2022) compound, indicating poor solubility and permeability. These limitations significantly impede its therapeutic potential, necessitating innovative formulation strategies to enhance its bioavailability. Niosomal encapsulation offers a promising approach, as it can improve Quercetin's solubility and permeability, thus optimizing its delivery and bioefficacy in PD models (Madiha et al., 2021; Nirmal et al., 2010). Preclinical studies corroborate quercetin's ability to ameliorate motor function, preserve dopaminergic neurons, and mitigate oxidative stress in PD animal models (Grewal et al., 2021). However, transitioning these findings into clinical settings demands further research, particularly in optimizing delivery methods to improve quercetin's therapeutic viability (Nirmal et al., 2010).

Niosomes, composed of a nonionic surfactant shell and an aqueous core, exhibit enhanced chemical and physical stability over liposomes, making them suitable for diverse drug delivery applications (Rajoria and Gupta, 2012). Given their versatility, niosomes are particularly advantageous for nasal delivery, boasting compatibility with both hydrophilic and lipophilic drugs, high biocompatibility, low toxicity, and enhanced permeability across biological membranes. These attributes render niosomes an appealing carrier for quercetin, enhancing its stability and membrane penetration capabilities, particularly when incorporated into an intranasal delivery system (Elkomy et al., 2023). The intranasal delivery of quercetin-loaded niosomal *in situ* gel offers direct central nervous system (CNS) access via the olfactory and trigeminal pathways, minimizing systemic side effects (Gastrointestinal Irritation, Hepatotoxicity, Renal Stress) while enhancing bioavailability. Moreover, an *in situ* mucoadhesive gel can facilitate prolonged nasal residence time, thereby augmenting drug absorption and therapeutic outcomes (Hu et al., 2022; Teaima et al., 2022).

Previous attempts to utilize quercetin in Parkinson's disease treatment have involved various formulations; (Acıkara et al., 2022; Tamtaji et al., 2020); however, these have often been limited by low oral bioavailability and a lack of targeted brain delivery. In this study, we have developed an intranasal *in situ* gel formulation of quercetin that is designed to bypass these limitations, offering direct brain targeting and enhanced bioavailability. This approach leverages the intranasal route to facilitate efficient drug delivery to the central nervous system, potentially improving therapeutic outcomes for Parkinson's patients.

2 Materials and methods

A pure sample of Quercetin was sourced from Kemphasol, Mumbai, India with haloperidol provided as a gift sample by Vamsi Labs Ltd., and L-dopa procured from Otto Chemicals, India. Cholesterol was obtained from Loba Chemie, while dialysis membranes (molecular weight cutoff range 12,000–14,000 g/mole) and dialysis tubing were sourced from Hi-Media Laboratories, Mumbai, India. Poloxamer 407 (P407) and benzalkonium chloride were procured from Sigma Aldrich Pvt. Ltd., Mumbai, India.

2.1 Preparation of niosomes

Niosomes were formulated via the ethanol injection method. A fixed amount of Quercetin, along with varying ratios of Span (Sp) and cholesterol (CH) as shown in Table 1, was dissolved in 10 mL of ethanol. The organic solution was subsequently injected into 10 mL of Type 1 Millipore water using a 22-gauge needle attached to an injection pump, maintaining a constant flow rate of 20 drops per minute. The resultant mixture was stirred magnetically at 65°C on a hotplate magnetic stirrer (MS-H550-Pro, Medfuture Biotech Co., Jinan, China) for 1 hour, ensuring complete ethanol evaporation, leading to niosome formation. To achieve smaller particle sizes, the dispersion underwent ultrasonic probe sonication for 5 min at a 30% pulse rate (Glascock et al., 2011).

2.2 Experimental design

The Design Expert® software (version 13, Stat-Ease Inc., Minneapolis, MN, United States) was employed to create a three-factor, three-level (3^3) Box-Behnken Design (BBD) with five center points, resulting in 17 experimental runs as depicted in Table 1. This design, favored for its efficiency in generating higher-order response surfaces with fewer runs, was used to optimize Quercetin -loaded niosomes with Span 60 (X1), Cholesterol (X2), and Sonication time (X3) as independent variables. The response variables included particle size (Y1), entrapment efficiency (Y2), and zeta potential (Y3) (Eid et al., 2022). Optimization utilized constraints aimed at maximizing nasal membrane permeation, minimizing particle size, and enhancing entrapment efficiency to increase payload capacity. The batch with the highest desirability was selected as the optimized formulation. Factor levels were selected by preliminary studies to maximize entrapment efficiency in niosomal dispersions (Elkomy et al., 2022; Elkomy et al., 2017).

2.3 Characterization of quercetin-loaded niosomal dispersion

2.3.1 Determination of PS, ZP, and PDI

Particle size, PDI and Zeta potential values of Quercetin loaded niosomes were measured physicochemically using the dynamic light

TABLE 1 Formulation design parameters for the optimization of Quercetin-loaded niosomes using box-behnken design.

Independent variables			
Span 60 (mg)	30	45	60
Cholesterol (mg)	20	30	10
Sonication time (Mins)	5	10	15
Dependent variables			
Particle size	Minimum		
%Entrapment efficiency	Maximum		
Zeta potential	In range		

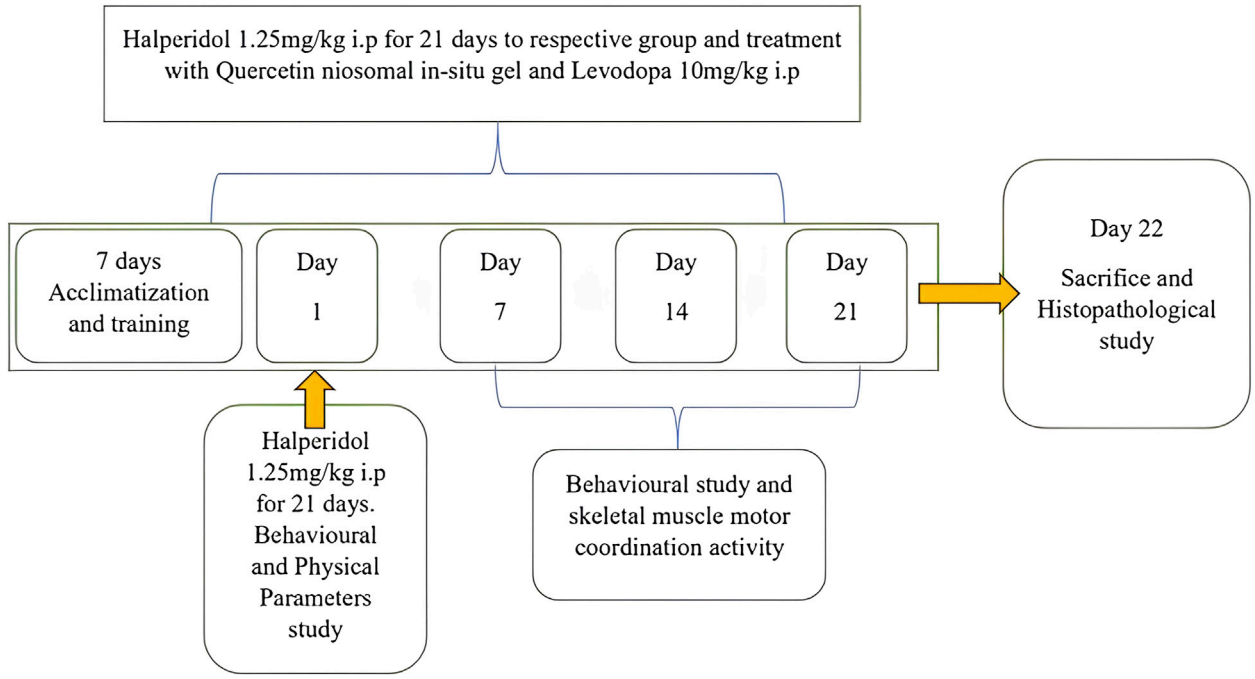


FIGURE 1
Schematic description of the experimental plan.

scattering technique in accordance with standard protocols. The Nano ZSU3100 (Malvern Instruments, United Kingdom) was the instrument used for this assessment. The niosomes suspensions were combined with Millipore water type 1 (1:10), The assessment was carried out at room temperature, which was 25°C ± 0.5°C (Teaima et al., 2022). The triplicate mean ± SD was used to report the results.

2.3.2 Determination of entrapment efficiency

The EE% of QUE-loaded niosomes was determined indirectly by calculating the difference between the total amount of quercetin incorporated into formulation and the amount that remained in the supernatant after separating the prepared vesicles by centrifugation at 15,000 rpm for 1 h at 4 °C using cooling centrifuge. The concentration of free quercetin was measured spectrophotometrically by measuring the ultraviolet (UV) absorbance, at λ max 256 nm (Shilakari Asthana et al., 2016). Drug EE% was calculated according to the following equation.

$$EE = \frac{\text{Total amount of drug added} - \text{Amount of drug in supernant}}{\text{Total amount amount of drug added}} \times 100$$

2.3.3 Morphological analysis by transmission electron microscopy (TEM)

To perform Transmission Electron Microscopy (TEM) analysis using the TECNAI G2 SPIRIT BIOTWIN, dilute 0.5 µL of the sample with 4.0 mL of distilled water. Pipette 0.2 µL of the diluted sample onto a 200-mesh copper-carbon grid. Stain the grid with 2% Phosphotungstic Acid (PTA) and let it dry at room temperature. Place the dried grid into the TEM sample holder. Use the Tecnai Imaging and Analysis software to capture images and perform measurements.

TABLE 2 Experimental design for formulations based on the box-behnken design (3^3).

Run	Factor 1 A: Span 60 in mg	Factor 2 B: Cholesterol in mg	Factor 3 C:Sonication time	Response 1 PS (nm)	Response 2 EE (%)	Response 3 ZP (mV)
1	30	20	10	155	68	−22
2	30	30	15	165	75	−26.8
3	30	40	10	220	84	−35
4	30	30	5	220	84.2	−22
5	45	30	10	170	76	−23
6	45	30	10	220	78	−26.49
7	45	30	10	195	81	−24.7
8	45	30	10	220	80	−29.4
9	45	40	15	210	81.7	−28.9
10	45	20	15	142	60	−34
11	45	20	5	170	68.9	−19.4
12	45	30	10	201	83	−18
13	45	40	5	276	81.8	−29.4
14	60	30	5	215	70.36	−33
15	60	40	10	180	83	−39
16	60	30	15	200	70.4	−25.8
17	60	20	10	128	71	−17.8

2.3.4 *In vitro* release study

In vitro release of niosomes suspension was carried out by dialysis bag method. A dialysis sac was washed and soaked in distilled water. Vesicle suspension was pipetted into a bag made up of tubing and sealed followed by placing the dialysis bag into a beaker containing 90 mL of PBS pH. The vessel was placed over magnetic stirrer (50 rpm) and the temperature was maintained at 37°C ± 0.5°C. Samples were withdrawn at predetermined time intervals and immediately replaced with the fresh medium to maintain the sink condition throughout experiment. Samples were diluted and analyzed for drug content by using UV/visible spectrophotometer at 256 nm (Schmolka, 2014).

2.3.5 Stability studies of optimized formulation

To determine the stability of the optimized niosomes, short term stability studies were conducted in compliance with ICH GCP guidelines. The prepared formulation was stored in glass vials within a humidity-controlled oven maintained at a temperature of 25 ± 2°C and relative humidity of 65% ± 5%. Additionally, it was refrigerated at 4 ± 2°C with relative humidity of 65% ± 5%. At regular intervals 0, 30 and 90 days, a sample was taken for analysis.

2.3.6 Formulation of *in situ* nasal gel of quercetin loaded niosomes

To enhance the formulation, optimized niosomes were incorporated into an *in situ* gel to extend nasal residence time, improve physical stability, and increase patient acceptability. The thermosensitive *in situ* gel was prepared using a modified cold method, where the gelling agent poloxamer 407 was dispersed within the optimized niosomal dispersion. The formulation was stored at 4°C for further study. The *in situ* gel's characteristics were assessed, including flowability, pH, viscosity, transparency, gelation temperature, gelation time, and *in vitro* drug diffusion properties (Galgatte et al., 2014).

2.4 Evaluation of niosomal *in situ* gel

2.4.1 Determination of pH

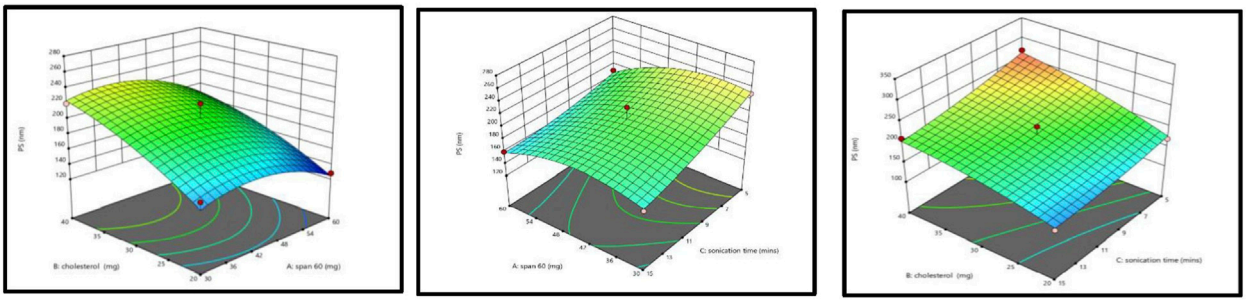
The pH of niosomal *in situ* gel was determined by digital pH meter. 1 gm of gel was placed in distilled water (25 mL) and the pH was measured using pH meter.

2.4.2 Determination of flowability of niosomal *in situ* gel

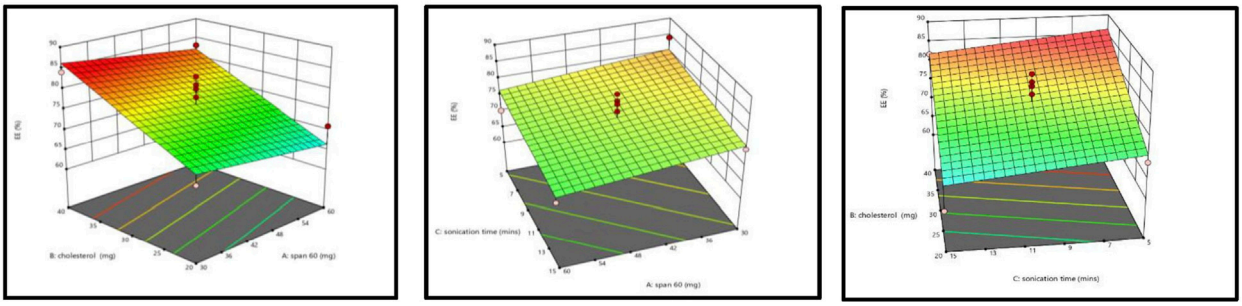
Test tube inversion method was used to determine the Transition of sol to gel of the niosomal *in situ* gel (NIG). NIG (2 mL) was transferred to a test tube, covered with paraffin and then inverted. It was maintained at 32°C in the water bath at a steady temperature and the flowability of the sample was analysed (Afreen et al., 2022).

2.4.3 Determination of viscosity

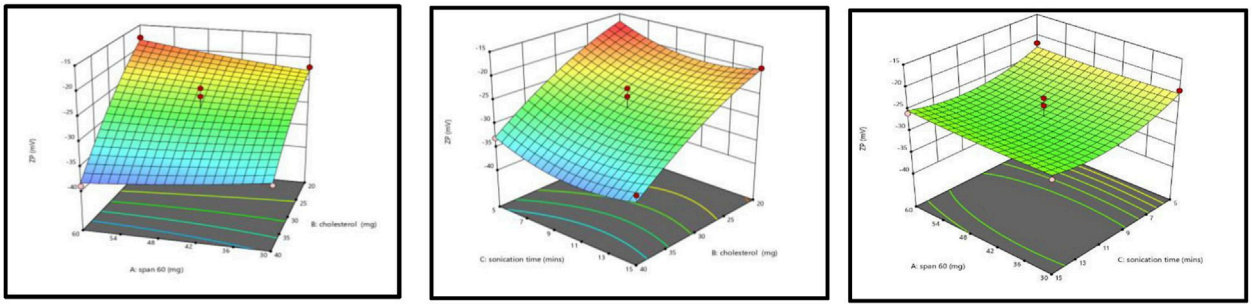
The viscosity of the prepared gel formulations was assessed using a Brookfield DV-II Pro Plus viscometer equipped with a



(A) Response surface plot showing the effect of concentration of span 60 (a), Cholesterol (b) and Sonication time (c) on Particle Size



(B) Contour and Response surface plot showing the effect of concentration of Span 60 (a), Cholesterol (b) and Sonication time (c) on entrapment efficiency



(C) Contour and Response surface plot showing the effect of concentration of Span 60 (a), Cholesterol (b) and Sonication time (c) on Zeta Potential

FIGURE 2
(A) Response surface plot depicting the effect of span 60 concentration (a), cholesterol (b), and sonication time (c) on particle size. **(B)** Contour and response surface plot showing the influence of span 60 concentration (a), cholesterol (b), and sonication time (c) on entrapment efficiency. **(C)** Contour and response surface plot depicting the effect of span 60 concentration (a), cholesterol (b), and sonication time (c) on zeta potential.

T-bar spindle. Viscosity measurements were performed across various temperatures and shear rates. To examine temperature-dependent behavior, the formulation was subjected to a constant shear rate within a temperature range of 25°C–40°C. The viscosity of the sol state was measured at room temperature (25°C) using spindle L2, while gel state measurements were conducted at nasal temperature (34°C) using spindle L3, due to the observed increase in viscosity. Viscosity values were calculated as the mean of three replicates to ensure accuracy (Afreen et al., 2022).

2.4.4 *In vitro* drug diffusion study

The Franz diffusion system was used to measure the drug release from a gel using a cellophane dialysis membrane. Before beginning the experiment, cellophane membrane fragments were placed and soaked in a receptor medium of phosphate buffer at pH 6.4 for 2 hours. The cellophane membranes, with effective permeation areas of 2 × 2 cm^2, were then stationed onto the Franz diffusion cells. The donor compartment was filled with 2.5 mg (200 µL) of quercetin-loaded niosomal gel, while the receptor compartment was filled with 12 mL of PBS at pH 6.4. The experiment was carried out at a

TABLE 3 Statistical analysis of model fit for particle size, entrapment efficiency, and zeta potential.

Source	Standard deviation	R^2	Adjusted R^2	Predicted R^2	Press	
Particle size						
Linear	19.88	0.7559	0.6996	0.5978	8462.51	Suggested*
2FI	21.29	0.7847	0.6555	0.3457	13769.29	
Quadratic	17.36	0.8997	0.7708	0.5745	8953.63	Suggested*
Cubic	20.73	0.9183	0.6733			
Entrapment efficiency						
Linear	4.25	0.7064	0.6387	0.4883	409.14	Suggested*
2FI	4.36	0.7627	0.6203	0.2081	633.19	
Quadratic	3.53	0.8910	0.7508	−0.2173	973.27	
Cubic	2.70	0.9635	0.8539			
Zeta potential						
Linear	2.80	0.8375	0.799	0.7186	176.31	Suggested*
2FI	2.91	0.8646	0.7834	0.5491	282.55	
Quadratic	2.52	0.9293	0.8385	0.70798	183.10	Suggested*
Cubic	3.02	0.9419	0.7677			

*Equation models suggested by the Design of Expert Software.

temperature of 34°C ± 1°C with constant stirring. An aliquot of 0.5 mL was taken from the receptor compartment at different time intervals: 0.5, 1, 2, 4, 6, 8, 12, and 24 h. The samples were appropriately diluted and analyzed at 256 nm using UV-Visible spectroscopy. The *in vitro* release experiments were analyzed kinetically using different mathematical models, including Zero order, First order, Korsmeyer–Peppas, Higuchi and Hixson Crowell, to determine the goodness of fit in terms of R^2 values (Saleem et al., 2021).

2.4.5 *In vivo* pharmacodynamic study design

The study protocol was reviewed and approved by the Institutional Animal Ethical Committee of KLE COP, Belagavi (accession number: 221/Po/Re/S/2000/CPCSEA) Male Wistar rats weighing 150–200 g were used in the experiment and were categorized into 4 groups having 6 animals in each group. The rats were divided into four groups, each consisting of six rats.

1. Normal group: Received food and water only.
2. Control group: Administered Haloperidol at 1.25 mg/kg via intraperitoneal injection (i.p.) for 21 days.
3. Standard group: Given Haloperidol at 1.25 mg/kg (i.p.) in combination with L-dopa at 10 mg/kg for 21 days.
4. Niosomal *In situ* gel group: Treated with Haloperidol at 1.25 mg/kg (i.p.) for 21 days along with Quercetin (niosomes *in situ* gel) intranasally (0.5 mL) for 21 days.

Quercetin niosomal *in situ* gel was administered intranasally at a dose of 10 mg/kg. L-dopa (standard) was administered intraperitoneally (I.P.) at a dose of 10 mg/kg. The animals were trained using the rotarod, actophotometer, balance beam, and catalepsy tests for acquisition. After administering the test agents, changes in latency were examined on the 7th (first dose), 14th, and 21st days. Twenty-five days after the last dose, the normal, control, standard, and treatment groups were euthanized, and their brains were removed for further histopathological and biochemical estimations, including reduced GSH, MDA, and SOD (Shrivastava et al., 2013). Experimental plan is displayed in Figure 1.

2.4.6 *In vivo* screening models for Parkinson disease

2.4.6.1 Behavioral testing

Behavioral tests like Rotarod, Balance Beam, and Actophotometer are used in Parkinson's disease research to measure motor coordination, balance, and activity levels in animal models, providing insights into disease progression and evaluating potential therapies (Hira et al., 2020).

2.4.6.1.1 Rotarod analysis. The rotarod device was used to assess the grip strength. In order to evaluate "minimal cognitive deficits" like balance and motor control, this tool is widely used. Before starting therapy, each rat underwent a training session to become acclimated to the apparatus. The animal was fastened to a rotating rod with a 7 cm diameter and 25 revolutions per minute. After being given Quercetin and Haloperidol, each rat was put on a rotating rod with a 180-second cutoff time. There was an expression for the latency time before the data started to fall (Hira et al., 2020).

2.4.6.1.2 Balance beam analysis. A balance beam device was used to evaluate dyskinetic gait abnormalities. The apparatus consists of a start and finish box-equipped 1-meter-long and 1-cm-wide runway. Foam padding was positioned 50–60 cm above the ground beneath the beam to safeguard the animals. Before the test,

TABLE 4 Response results for particle size, entrapment efficiency, and zeta potential.

Result of ANOVA	Particle size	Entrapment efficiency	Zeta potential
Sum of square	18932.51	564.83	582.30
Degree of freedom	9	3	9
Mean square	2103.6	188.8	64.70
F-value	6.98	10.43	10.23
P-value	0.0090	0.0009	0.0059
Inference	Significant	Significant	Significant

TABLE 5 Validation results of the optimized formulation.

	Independent variable			Responses			Desirability
	Span 60 in mg	Cholesterol in mg	Sonication time (in mins)	VS(nm)	EE(%)	ZP(mV)	
Solution (Predicated values)	60	35.34	8.433	187.10	79.08	−31.810	0.821
Practically performed	60	35.34	8.433	195.9	82.77	−30.63	

the animals were trained, and at the conclusion of the walk, they were given food pellets as a reward. Every 7 days, tests were carried out, and the amount of time it took to get to the end box was measured and recorded in seconds (Kondawar et al., 2011).

2.4.6.1.3 Actophotometer analysis. Animals are forced to move from one location to another by a physical process known as locomotion. Using an actophotometer, this skill can be easily evaluated (activity cage). It's a device made up of photoelectric cells. When an animal in a cage interrupts the light beam falling on the photocell, a count of the animal's movements is displayed on the screen. Every animal was trained for the test 1 day prior to it, and it was conducted every 7 days. The results were expressed in counts/5 min and the cutoff time was 5 min (Ranpariya et al., 2011).

2.4.6.2 Preparation tissue homogenate

Brains were separated and thoroughly cleaned after animals were sacrificed. One gram of brain was homogenized with Tris-buffer (pH 7.4) using a homogenizer. After that, it was centrifuged for 15 min at 7,000 rpm in cold centrifugation. For additional estimation, the supernatant was obtained and kept in sterile Eppendorf tubes. The supernatant obtained was used to estimate Malondialdehyde (MDA) (Hira et al., 2019), superoxide dismutase (SOD) (Ellman, 1959), glutathione (GSH) (Bhangale and Acharya, 2016; Abdelbary and Abd-Elsalam, 2019).

2.4.6.3 Statistical analysis

The data for the Rotarod, Actophotometer, and Balance Beam tests, as well as the biochemical assays (GSH, MDA, SOD), are presented as mean ± SEM (n = 6). All data were analyzed using appropriate statistical methods. Specifically, two-way ANOVA with Tukey's multiple comparisons test was applied for the behavioral assessments (Rotarod, Actophotometer, and Balance Beam tests), and one-way ANOVA with Dunnett's multiple comparisons test was used for the biochemical assays (GSH, MDA, SOD). The *p*-values for all the behavioral results were less than 0.001, indicating highly significant differences between the disease group and the treatment groups.

3 Results

3.1 Formulation of quercetin-loaded niosome using a Box-Behnken experimental design

Quercetin-loaded niosomes were successfully prepared utilizing a modified ethanol injection technique. A total of 17 formulations were developed using Span 60, cholesterol, and varying sonication times. The formulations were optimized through a Box-Behnken experimental design, as detailed in Table 2.

3.2 Response surface analysis

3.2.1 Response surface plot showing the effect of concentration of span 60 (A), cholestrol (B) and sonication time (C) on particle size (PS)

For effective brain targeting, it is critical to maintain the particle size (PS) of niosomes within the range of 100–300 nm. The PS values produced for niosomes were analyzed using a polynomial quadratic model, demonstrating adequate precision (10.52) and a reasonable difference between the predicted R^2 (0.5745) and the adjusted R^2 (0.7708), with a discrepancy of less than 0.2. Observed particle sizes ranged from 128 nm to 270 nm. The final equation for PS analysis, expressed in terms of coded factors, highlighted the influences of Span 60 (A), Cholesterol (B), and Sonication time (C).

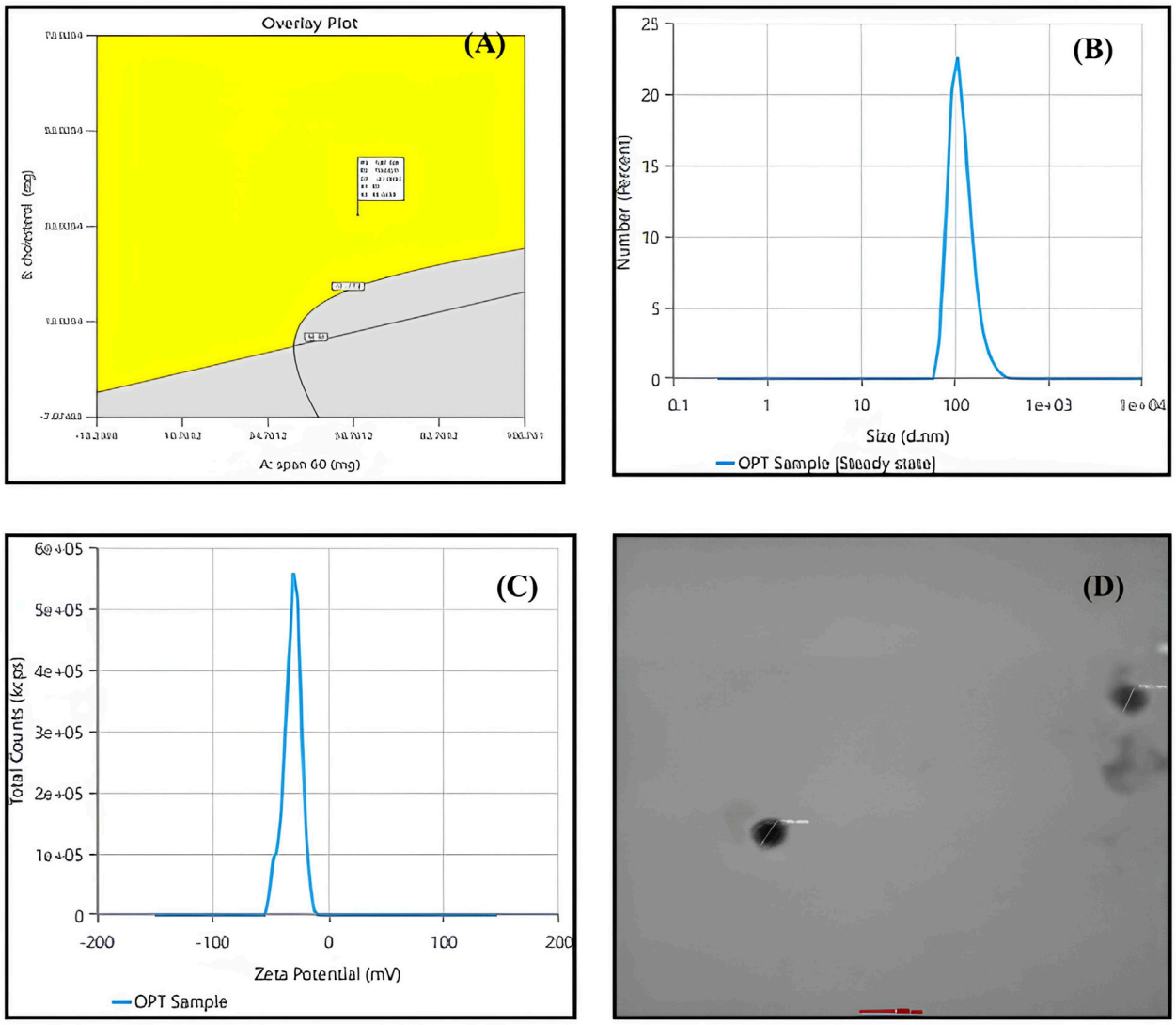


FIGURE 3
(A) overlay plot indicating the optimized box-behnken experimental design conditions marked within the design space. **(B)** Particle size peak report from zetasizer indicating 195.9 nm for the optimized niosomes dispersion. **(C)** Zeta potential peak report from zetasizer indicating −30.63 mV for the optimized niosomes dispersion. **(D)** transmission electron microscopy (TEM) image of optimized quercetin-loaded niosomes.

Cholesterol significantly influences niosomal size by increasing vesicle rigidity and stability. As the cholesterol concentration rises, it competes with the drug for space within the bilayer, leading to a larger hydrodynamic diameter and increased particle size due to strengthened bilayer structure (Shah et al., 2020). Additionally, cholesterol's mechanism includes increasing chain order in liquid-state bilayers while reducing it in gel-state bilayers, transforming the gel phase gradually into a liquid-ordered state. This shift favours encapsulation efficiency for hydrophilic drugs and decreases the release rate of the entrapped drug by enhancing membrane stability (Uchegbu and Vyas, 1998).

In contrast, increasing Span 60 concentration and sonication time reduces particle size. Span 60, with its long alkyl chain (C18), lowers surface tension, facilitating smaller vesicle formation, while also contributing to bilayer rigidity, thus stabilizing smaller, uniform particles (Essa, 2010; Owodeha-Ashaka et al., 2010). Sonication, by applying ultrasound waves, induces cavitation, breaking larger vesicles into smaller, more uniform ones (Khallaf et al., 2020). This combination of Span 60 and sonication supports the creation of optimized niosomes with suitable PS for brain delivery (Abdelkader et al., 2014; Shah et al., 2020; Nasr et al., 2020). Response surface plot showing the effect of concentration of Span 60 (A), Cholestrol (B) and Sonication time (C) on particle size (PS) is depicted in Figure 2.

$$PS = +201.20 - 14A + 35.63B - 22.88C - 3.25AB + 8.75AC - 8BC - 21.10A^2 - 9.3.5B^2 + 6.15C^2$$

3.2.2 Response surface plot showing the effect of concentration of span 60 (A), cholesterol(B) and sonication time (C) on entrapment efficiency (EE%)

Entrapment efficiency (EE%) is a critical measure indicating the proportion of a drug successfully encapsulated within nanocarriers,

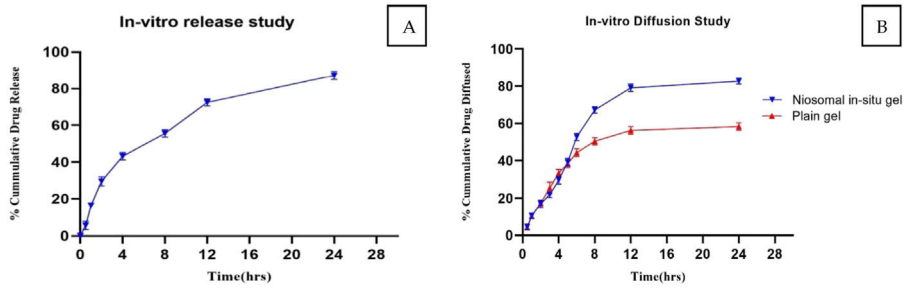


FIGURE 4
(A) *In Vitro* Release Profile of Quercetin-Loaded Niosomes for the Optimized Batch. **(B)** Comparative diffusion study of niosomal *in situ* gel and plain gel.

TABLE 6 Kinetic analysis of niosomal formulations.

Kinetic model	R^2
Zero order	0.9158
First order	0.9164
Higuchi	0.982
Kors-peppas	0.7705
Hixson	0.9071

ensuring more of the drug is available to exert its therapeutic effects at the target site. In this study, the EE% ranged from 60% to 84.2%. The EE% values of the generated niosomes were analyzed using a linear model with an adequate precision of 9.7. The difference between the predicted R^2 (0.4883) and the adjusted R^2 (0.6387) was less than 0.2, indicating a reasonable model fit.

An increase in cholesterol concentration positively influences encapsulation efficiency (EE%) due to Cholesterol's significant role in enhancing drug encapsulation within the vesicle membranes. A higher percentage of Cholesterol correlates with an increased EE%, as Cholesterol modulates the mechanical strength, cohesion, and permeability of lipid bilayers in niosomes. Specifically, Cholesterol reduces the fluidity of niosomes, thereby imparting rigidity to the vesicles, which results in less permeable niosomes—a critical attribute under high-stress conditions (Moghassemi and Hadjizadeh, 2014). Conversely, an increase in Span 60, coupled with increased sonication, adversely affects entrapment efficiency. This phenomenon arises from the interaction between Cholesterol and Span 60 within the bilayer of the vesicles, primarily due to hydrogen bonding (Moghassemi and Hadjizadeh, 2014). Span 60, characterized by its long alkyl chain (C18) and low water solubility, facilitates tight packing within the niosomal bilayer (Uchegbu and Vyas, 1998). While this tight packing aids in reducing overall vesicle size, it may also restrict the volume of drug that can be encapsulated (Masjedi and Montahaei, 2021). Cholesterol effectively cements the leakage pathways within the bilayer membranes, resulting in a firmer membrane structure as the surfactants become more densely packed during the filling process (38). Response surface plot showing the effect of concentration of span 60 (A), Cholestrol (B) and Sonication time (C) on Encapsulation Effeciency (%EE) is depicted in Figure 2.

$$EE = +79.60 - 2.06A + 7.83B - 2.26C$$

3.2.3 Response surface plot showing the effect of concentration of span 60 (A), cholesterol (B) and sonication time (C) on zeta potential (ZP)

The zeta potential (ZP) of the developed niosomal dispersion was analyzed to elucidate the surface charge characteristics, which are pivotal for predicting the colloidal stability of the dispersion. Elevated absolute ZP values provide adequate electrostatic repulsion to mitigate particle aggregation. The analysis revealed that quercetin-loaded niosomes exhibited a negative surface charge, with average values ranging from −39 mV to −17.8 mV. This assessment was conducted using a polynomial quadratic model, which demonstrated an adequate precision of 11.2 and a reasonable disparity between the predicted R^2 (0.7078) and the adjusted R^2 (0.6387), with the difference being less than 0.2. The inclusion of cholesterol enhances the magnitude of the negative surface charge on the niosomes. This effect arises from cholesterol's capacity to interact with the charged head groups of surfactants, such as dicetylphosphate, thereby contributing to the negative zeta potential (Junyaprasert et al., 2008; Zolghadri et al., 2023). The type of surfactant, the presence of charged species, and storage conditions are significant formulation parameters that influence the zeta potential of niosomes (Durán-Lobato et al., 2022). An increase in the amount of Span 60 within niosomes typically correlates with a decrease in the magnitude of the zeta potential. This decrease can be attributed to the hydrophobic nature of the surfactant, which diminishes the electrostatic repulsion among the niosomes, leading to reduced stability and an increased propensity for aggregation (Shah et al., 2012). However, sonication time may not be a major determinant compared to these other parameters. Further targeted research is warranted to conclusively elucidate the impact of sonication time on zeta potential. The quadratic equation of factors affecting ZP is shown below. Response surface plot showing the effect of concentration of span 60 (A), Cholestrol (B) and Sonication time (C) on zeta potential (ZP) is depicted in Figure 2.

TABLE 7 Characterization of optimized niosomal dispersion at 0 Months and after 3 Months of storage at room temperature.

	Vesicle size (nm)	% Entrapment efficiency	Zeta potential (mV)	% Drug release	Polydispersity index
0 months	187	79.08	−31.08	0.223	86.7
3 months	210	76.2	−29.3	0.25	82.3

TABLE 8 Determination of flowability through gelation time.

Concentration of poloxamer 407	Time required in seconds
17%	No gelation
19%	45
21%	58
23%	63

$$ZP = -27.08 + 0.1750A - 7.98B - 1.40C - 2.05AB + 0.2AC + 0.1000BC + 0.3150A^2 - 1.69B^2 + 2.66C^2$$

3.3 Analysis of ANOVA of calculated response

Analysis of variance of calculated Responses and summary of the results of responses of particle size, entrapment efficiency, and Zeta potential are depicted in Table 3, 4 respectively.

3.4 Formulation optimization

The Design expert® software provided a range of suggestions that optimally satisfied the set constraints. The selected formula had a desirability value of 0.821. Table 5 displays the values of experimental, predicted value for the response variables of the optimized Quercetin loaded niosomes formula. These findings demonstrated the validity of the final models. Overlay plot showing optimized box Behnken experimental design conditions as a flag within the design space is illustrated in Figure 3. Peak report depicting particle size and zeta potential for the optimized niosomes dispersion is displayed in Figure 3.

3.5 Morphological analysis by transmission electron microscopy (TEM)

Niosomal morphological analysis was conducted using Transmission Electron Microscopy (TEM), as illustrated in Figure 3. The resulting images clearly demonstrate that the Quercetin-loaded niosomes exhibit a spherical morphology with a homogeneous size distribution, indicative of the stability of the prepared niosomes. The niosomes displayed a well-defined spherical shape characterized by a distinct wall structure. The stability of the multiple bilayers, along with their rigidity, is primarily governed by the hydrogen bonding interactions between the ester groups of Span 60 and the hydroxyl groups of cholesterol (Syed et al., 2021; El-Diasty et al., 2020).

3.6 *In Vitro* release and kinetic analysis of quercetin loaded niosomes

The *in vitro* release profile of quercetin from the optimized niosomal formulation displayed a marked biphasic pattern across the 24-hour assessment period. The release commenced with a rapid "burst" phase within the first 2 hours, during which approximately 29.56% of quercetin was discharged from the niosomes. This initial release surge is likely due to quercetin molecules adsorbed on or proximate to the niosomal surface, which diffuse swiftly into the surrounding medium owing to their superficial positioning. Such an immediate release phase could prove beneficial in clinical applications, potentially facilitating a more rapid onset of therapeutic action.

Subsequently, the release profile transitioned into a sustained release phase, characterized by a gradual release of quercetin, culminating in an overall cumulative release of 87.16% by the end of the 24-hour period, as presented in Figure 4. This prolonged release phase is attributed to the gradual diffusion of quercetin encapsulated within the lipid bilayers, which mediates a controlled release and may extend therapeutic effects over an extended period.

To elucidate the underlying kinetics of quercetin release from the niosomal structure, various mathematical models were employed. Curve-fitting analyses revealed that the release process predominantly adhered to first-order kinetics, demonstrated by a strong regression coefficient ($R^2 = 0.968$), indicating that the release rate is directly proportional to the concentration of quercetin within the formulation.

Further analysis of the release data using the Higuchi model—a model that describes release as a diffusion-controlled mechanism from a homogenous matrix—indicated a linear fit, as shown in Table 6 and corresponding figure, suggesting that the quercetin release was diffusion-driven. The alignment of the release profile with both first-order and Higuchi kinetics supports a mechanism whereby an initial rapid release is succeeded by a sustained, diffusion-driven phase, aligning with the anticipated properties of niosomal drug delivery systems.

The observed biphasic release pattern, encompassing an initial rapid phase followed by extended release, highlights the potential of quercetin-loaded niosomes to offer a prompt therapeutic dose, succeeded by continuous release. This characteristic is particularly advantageous in enhancing quercetin's bioavailability and therapeutic efficacy in the treatment of Parkinson's disease. These findings underscore the promise of this formulation as a feasible intranasal drug delivery approach, advancing

TABLE 9 pH, Gelation temperature, Viscosity for sol and gel value of the *in situ* gel.

Trails	pH	Gelation temperature	Viscosity for sol (Cps)	Viscosity for gel (Cps)
1	6.8	34	42.08	1980
2	6.5	31.5	50.7	1937
3	6.6	33.5	79.8	1895
Average	6.63	34.13	57.52	1937.33
SD	±0.21	±0.21	16.13	34.7

Mean ± SD (N = 3).

neuroprotective treatment modalities. Additionally, the release pattern conformed to the Higuchi model as shown in Table 6 and Figure (Supplementary File) (Syed et al., 2021; El-Diasty et al., 2020; Hong et al., 2020).

3.7 Stability study

The stability of the optimized quercetin-loaded niosomal formulation was meticulously evaluated over a 3-month period to assess its robustness and shelf-life under standard storage conditions. The formulation was stored at room temperature (25°C ± 2°C) and monitored at regular intervals to determine any variations in key characteristics, namely particle size, entrapment efficiency, and polydispersity index (PDI) as shown in Table 7. These parameters are critical indicators of the physical stability of the niosomal system, as fluctuations in size, drug retention, or homogeneity could impact the formulation's efficacy, bioavailability, and suitability for therapeutic use.

Particle Size: Particle size stability is crucial, as it directly influences the delivery and release profile of the formulation. Consistency in particle size indicates that the niosomes maintain structural integrity without aggregation or degradation of vesicles over time. Throughout the 3-month storage period, particle size measurements were conducted at defined intervals to observe any potential increase due to vesicle fusion or particle aggregation.

Entrapment Efficiency (EE): Entrapment efficiency is a measure of the percentage of quercetin encapsulated within the niosomal vesicles relative to the initial amount. Stability in EE over time indicates that the formulation retains quercetin effectively without significant leakage or degradation.

3.8 Evaluation of *in situ* gel

The flowability of the formulation, represented by the gelation time required for phase transition from sol to gel, was recorded in Table 8. The optimized *in situ* gel formulation demonstrated a drug content of 94% w/v, while its pH was slightly alkaline at 6.8, as shown in Table 9. Determining the gelation temperature, a critical step in the development of thermoreversible *in situ* gels, revealed that using 19% w/v Poloxamer 407 yielded optimal results with a transition temperature of 32°C–33°C; this temperature varied with polymer concentrations between 17% and 23% (Syed et al., 2021; El-Diasty et al., 2020). The optimized niosomal *in situ* gel exhibited excellent rheological properties, with a sol viscosity of 57.52 cP and a gel viscosity of 1937.33 cP (Syed et al., 2021), as detailed in Table 9. *In vitro* diffusion studies compared the quercetin release profiles of a quercetin-loaded niosomal *in situ* gel and a plain gel over 24 h. The plain gel, with unencapsulated quercetin, displayed a slower diffusion profile, achieving only a 58.27% cumulative release, limited by its lack of niosomal encapsulation. Conversely, the niosomal *in situ* gel demonstrated a biphasic release pattern, with an initial burst release of 39.23% in the first 5 h, followed by sustained release, reaching 82.74% by 24 h. This enhanced permeation is due to niosomes encapsulating quercetin within lipid bilayers, which increase solubility and facilitate membrane interaction, allowing for controlled, prolonged drug release, which is beneficial for applications requiring consistent bioavailability.

3.9 *In Vivo* characterization

3.9.1 Behavioural parameter

Behavioural parameters like rotarod, actophotometer, and balance beam are assessed in Parkinson's disease to evaluate motor coordination, activity levels, and balance, which are commonly impaired in the condition and the scores of each parameter is depicted in Figure 5 (Hong et al., 2020).

3.9.2 Rotarod analysis

On day 0, no significant differences in rotarod performance were observed across the groups, establishing a baseline for motor coordination. By day 14, however, the disease group exhibited a substantial decline in performance compared to the normal group, reflecting the motor impairments characteristic of Parkinson's disease. In contrast, both the standard treatment and experimental treatment groups showed marked improvements in performance relative to the disease group, indicating that the treatments effectively enhance motor coordination and balance, potentially mitigating Parkinsonian motor deficits. By day 21, the disease group continued to demonstrate significantly impaired performance, highlighting persistent motor dysfunction. Both treatment groups maintained their enhanced performance, underscoring the therapeutic potential of these interventions in alleviating Parkinson's symptoms, particularly bradykinesia (Jamwal et al., 2017).

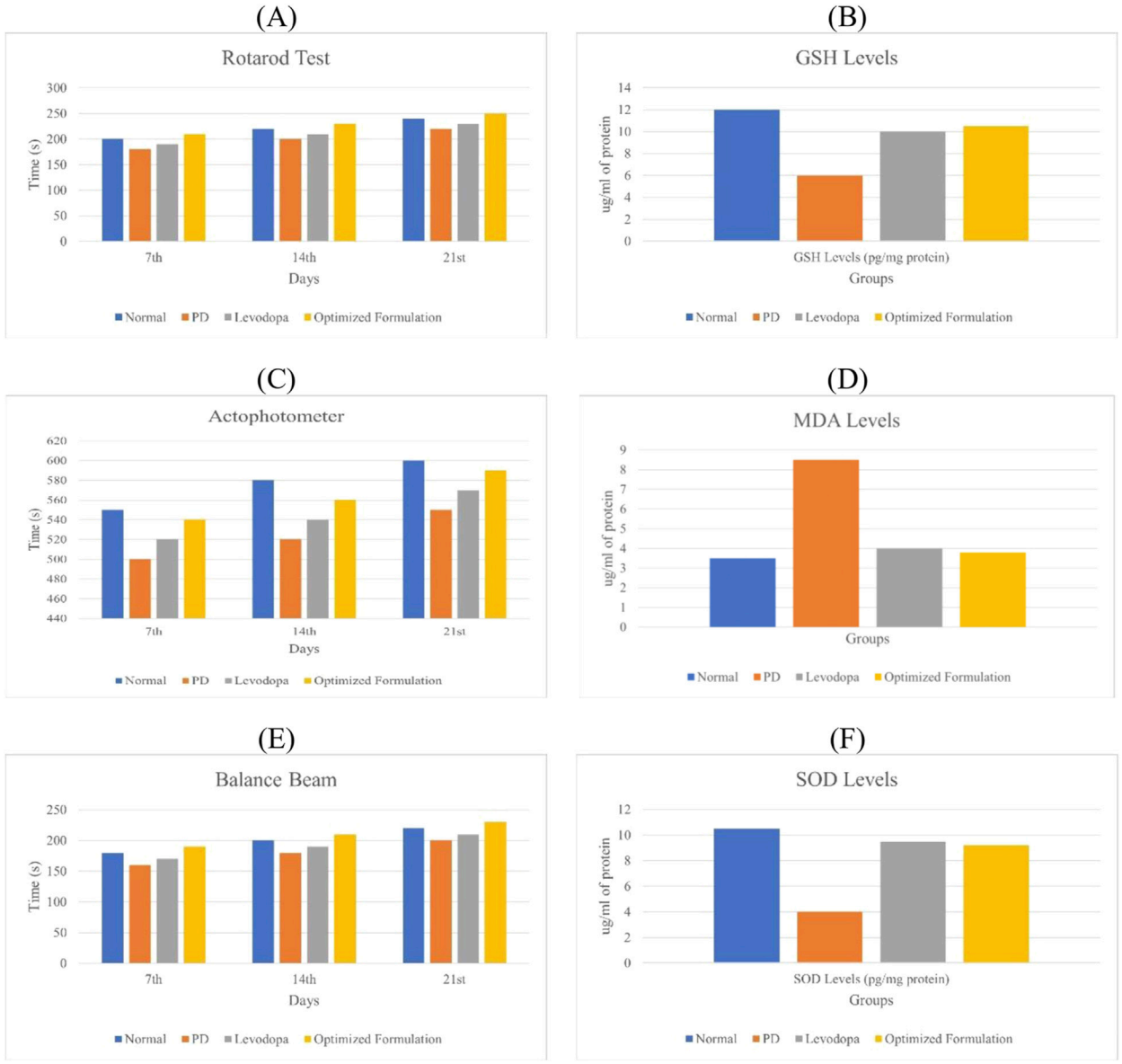


FIGURE 5
(A) Rotarod performance of different animal groups. **(C)** Effect of quercetin-loaded niosomes on actophotometer scores in rats. **(E)** Effect of quercetin-loaded niosomes on balance beam performance in rats. **(B)** Glutathione (GSH) estimation in the rat brain. **(D)** Malondialdehyde (MDA) estimation in the rat brain. **(F)** Superoxide dismutase (SOD) estimation in the rat brain.

3.9.3 Actophotometer analysis

On day 7, there were no significant differences in actophotometer activity counts across the groups, indicating comparable baseline activity levels. By day 14, the disease group showed a significant reduction in activity counts compared to the normal group, which aligns with the motor deficits observed in Parkinson's disease. Both the standard and treatment groups exhibited significant improvements in activity counts, reflecting positive effects on motor activity and coordination. On day 21, the disease group continued to show significantly lower activity counts compared to the normal group, reaffirming the persistence of Parkinson's symptoms in the absence of intervention. However, both treatment groups maintained elevated activity counts, reflecting sustained therapeutic benefits in improving motor dysfunctions, as shown in Figure 5 (Jaiswal et al., 2016).

3.9.4 Balance beam test

On day 7, there were no significant differences in balance beam traversal times across the groups, indicating no early variations in motor performance. By day 14, the disease group exhibited a significant increase in traversal time compared to the normal group, suggesting the balance and coordination deficits typical of Parkinson's pathology. Both the standard and treatment groups showed significantly reduced traversal times relative to the disease group, indicating improvements in balance and motor function. By

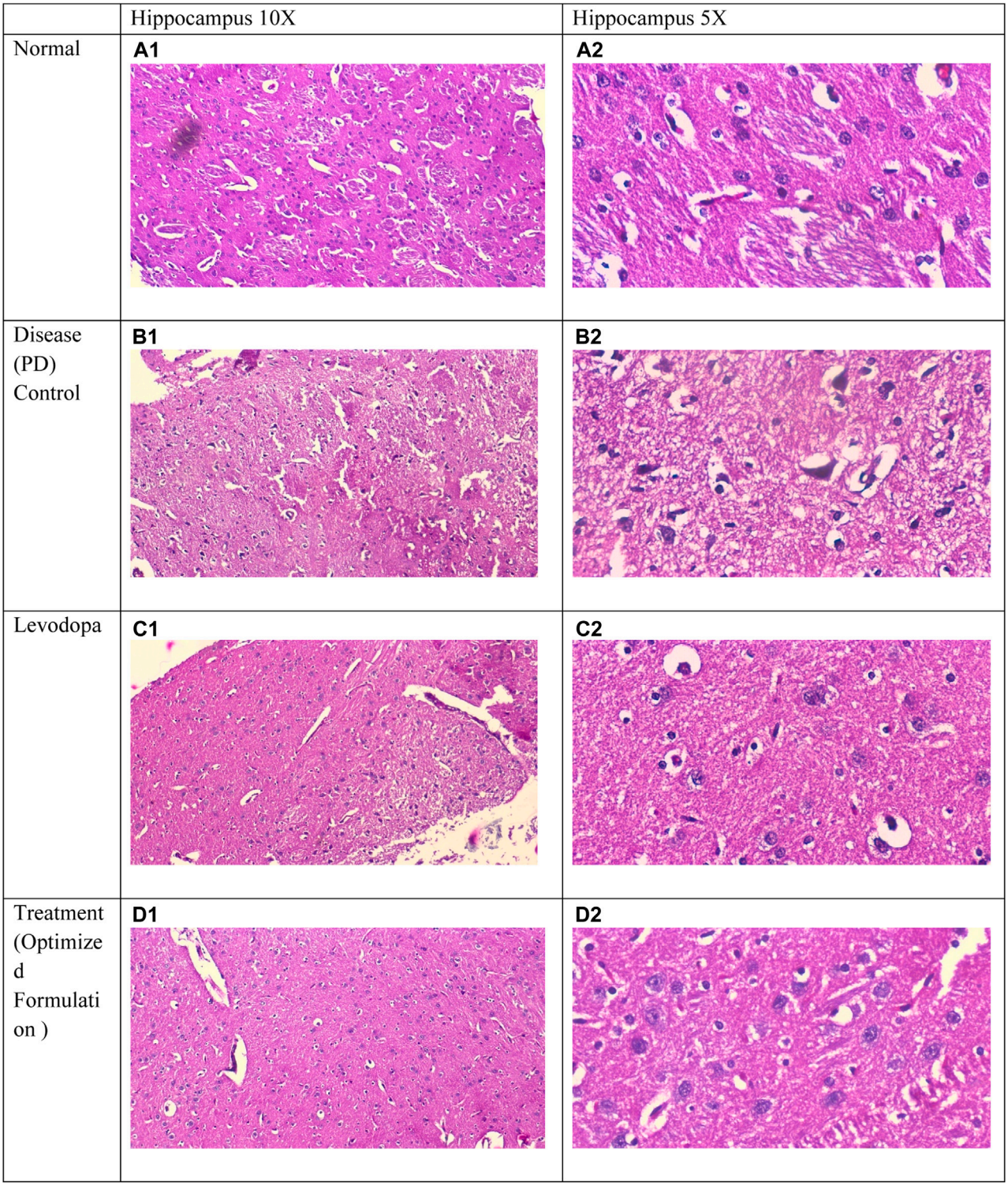


FIGURE 6
Comparative Histological Analysis of Cerebral Tissue Across Study Groups : **(A1, A2)** depict normal parenchyma with intact morphology and no pathological changes. **(B1, B2)** indicate severe gliosis, edema, neuronal loss, and vessel congestion in the positive control group. **(C1, C2)** display reduced gliosis and edema in the standard group. **(D1, D2)** from the treatment group demonstrate further improvement, with minimal gliosis and no vascular congestion.

day 21, the disease group continued to demonstrate prolonged traversal times, while both treatment groups maintained improved traversal times, demonstrating the efficacy of the treatments in alleviating Parkinson's disease symptoms, particularly issues related to balance and coordination (Jamwal et al., 2017).

3.9.5 Estimation of glutathione (GSH)

The disease group exhibited a significant decrease in GSH levels compared to the normal group. Both the standard and treatment groups showed elevated GSH levels, indicating a neuroprotective effect. The increase in GSH levels was highly significant for both the standard and treatment groups when compared to the disease group, as illustrated in Figure 5A (Jaiswal et al., 2016).

3.9.6 Estimation of malondialdehyde (MDA)

The disease group displayed significantly elevated levels of MDA compared to the normal group. In contrast, both the standard and treatment groups exhibited reduced MDA levels compared to the disease group, indicating a neuroprotective effect. The reduction in MDA levels was significant in both the standard and treatment groups when compared to the disease group, as shown in Figure 5B (Jaiswal et al., 2016).

3.9.7 Estimation of superoxide dismutase (SOD)

The disease group demonstrated significantly reduced SOD levels compared to the normal group. Both the standard and treatment groups exhibited increased SOD levels relative to the disease group, suggesting a neuroprotective effect. The increase in SOD levels was significant for both the standard and treatment groups compared to the disease group, as depicted in Figure 5C (Jaiswal et al., 2016).

3.10 Statistical analysis

The *p*-values for all the behavioral and biochemical assay results were less than 0.001, highlighting significant differences between the disease group and the treatment groups. These results underscore the efficacy of the treatments in mitigating Parkinson's disease-related impairments and neurodegeneration.

3.11 Histopathology of hippocampus of rat brain

The examination of a section of the cerebral cortex stained with hematoxylin and eosin (H&E) reveals several critical observations: (A) Cortical neurons (↑) characterized by rounded vesicular nuclei (yellow ↑) display sharply demarcated nuclear contours, while blood vessels (v) are accompanied by a narrow perivascular space indicative of degenerated and shrunken neurons. Notably, the disease group exhibits a significantly elevated histological score in comparison to the normal group, reflecting an increase in cortical neurons with rounded vesicular nuclei and neuropil exhibiting sharply demarcated nuclei or signs of meningeal involvement (Syed et al., 2021; Jaiswal et al., 2016).

Figure 6 (A1) and (A2) depict the normal parenchyma morphology, featuring oval-shaped cells with prominent nucleoli and pale basophilic cytoplasm, devoid of significant gliosis, edema, neuronal loss, or congestion of meningeal vessels. In stark contrast, Figure 6 (B1) and (B2), representative of the positive control group, reveal cerebral tissue marked by pronounced gliosis, edema, and congestion of meningeal vessels, along with observable neuronal loss and occasional neutrophilic infiltration. Figure 6 (C2) and (C3), corresponding to the standard group, illustrate a slight reduction in both gliosis and edema, with an absence of neutrophils or meningeal vessel congestion. Likewise, Figure 6 (D1) and (D2), belonging to the treatment 1 group, demonstrate diminished gliosis and edema, also lacking neutrophils and meningeal vessel congestion (Hong et al., 2020; Jamwal et al., 2017; Jaiswal et al., 2016).

4 Discussion

Parkinson's disease (PD) stands as the second most prevalent neurodegenerative disorder, predominantly characterized by motor symptoms such as tremors, bradykinesia, postural instability, and rigidity. These motor manifestations are often preceded by a range of non-motor symptoms, including sleep disturbances, olfactory deficits, cognitive impairments, and depression, which can significantly impact patients' quality of life (Madiha et al., 2021). Quercetin, a polyphenolic bioflavonoid found abundantly in fruits and vegetables, possesses powerful antioxidant and anti-inflammatory properties, presenting a promising neuroprotective candidate for PD treatment (Wrobel-Biedrawa et al., 2022; Grewal et al., 2021). Quercetin effectively neutralizes reactive oxygen species (ROS), enhances endogenous antioxidant defences, and modulates inflammatory pathways, which are crucial in slowing neurodegeneration (Wrobel-Biedrawa et al., 2022). Additionally, it has demonstrated efficacy in inhibiting α-synuclein aggregation, a pathological hallmark of PD, further underscoring its potential role in neuroprotection (Grewal et al., 2021).

However, quercetin's therapeutic application is challenged by its classification as a Biopharmaceutical Classification System (BCS) Class IV compound, signifying poor solubility and permeability, which limits its bioavailability and clinical effectiveness (Sirvi et al., 2022). To overcome these limitations, innovative formulation strategies, such as niosomal encapsulation, offer a viable approach by enhancing quercetin's solubility and permeability, thereby improving its bioefficacy in PD models (Madiha et al., 2021; Nirmal et al., 2010). In this study, we developed an intranasal *in situ* gel formulation of quercetin aimed at overcoming these delivery challenges. This formulation capitalizes on the intranasal route, which enables direct brain targeting and improved bioavailability, potentially offering more effective therapeutic outcomes for PD patients by ensuring efficient central nervous system drug delivery.

The formulation of niosomes was achieved through the ethanol injection method, incorporating a fixed amount of Quercetin along with varied ratios of Span (Sp) and cholesterol (CH). Using Design Expert® software (version 13, Stat-Ease Inc., Minneapolis, MN, United States), a three-factor, three-level (3^3) Box-Behnken Design (BBD). Increased cholesterol concentration competes with the drug for bilayer space, resulting in a larger hydrodynamic diameter due to a more structured bilayer (Shah et al., 2020). Cholesterol stabilizes bilayers by ordering lipid chains, thus enhancing encapsulation efficiency for hydrophilic drugs and decreasing drug release rates by reinforcing membrane stability (Uchegbu and Vyas, 1998). Conversely, increased Span 60 concentration and sonication time effectively reduced particle size. Span 60, with its long alkyl chain (C18), lowers surface tension, aiding in smaller vesicle formation and providing bilayer rigidity for more stable particles (Essa, 2010; Owodeha-Ashaka et al., 2010). The

ultrasound waves applied during sonication break larger vesicles into smaller, uniform ones through cavitation (Khallaf et al., 2020). This combination of Span 60 and sonication yielded optimized niosomes with suitable particle size for brain delivery (Abdelkader et al., 2014; Shah et al., 2020; Nasr et al., 2020).

Cholesterol concentration was also positively correlated with encapsulation efficiency (EE%), due to its impact on enhancing the mechanical strength, cohesion, and permeability of lipid bilayers in niosomes. Elevated cholesterol levels reduce vesicle fluidity, thus imparting rigidity and lowering permeability—an advantage under high-stress conditions (Moghassemi and Hadjizadeh, 2014). Conversely, an increase in Span 60 and sonication adversely influenced EE, likely due to hydrogen bonding interactions between cholesterol and Span 60 within the bilayer, restricting drug encapsulation volume despite reduced vesicle size (Moghassemi and Hadjizadeh, 2014). Span 60, characterized by its long C18 chain and low water solubility, promotes tight packing in the bilayer, but this also limits the drug volume encapsulated (Masjedi and Montahaei, 2021). Cholesterol helps seal potential leakage pathways within bilayer membranes, creating a more robust structure as surfactants densely pack during formulation (Junyaprasert et al., 2008; Zolghadri et al., 2023).

The type of surfactant, charged species presence, and storage conditions notably impact niosome zeta potential (Durán-Lobato et al., 2022). With an increase in Span 60, zeta potential magnitude decreases, attributable to the surfactant's hydrophobic nature, which weakens electrostatic repulsion and encourages aggregation (Shah et al., 2012). While sonication time has less impact on zeta potential, further studies are warranted to clarify its effects. Images of the Quercetin-loaded niosomes showed a spherical morphology with a uniform size distribution, signifying niosomal stability, well-defined structure, and rigid bilayer. Stability is driven by hydrogen bonding interactions between Span 60 ester groups and cholesterol hydroxyl groups (Syed et al., 2021; El-Diasty et al., 2020). The formulation, stored at room temperature (25°C ± 2°C), was regularly evaluated for particle size, entrapment efficiency, and polydispersity index (PDI) to ensure physical stability, as these parameters affect therapeutic efficacy, bioavailability, and formulation suitability.

Particle size stability is essential as it affects the formulation's delivery and release profile. Consistent particle size indicates preserved vesicle integrity without fusion or aggregation over time. Entrapment efficiency (EE%) stability suggests effective retention of quercetin without significant leakage, with all evaluations indicating a sustained capacity for drug encapsulation and a robust, physically stable formulation.

Behavioral assessments, including the rotarod, actophotometer, and balance beam tests, are pivotal tools for evaluating motor coordination, activity, and balance deficits in Parkinson's disease models, as these impairments are central features of the condition. The rotarod test, in particular, serves as a robust indicator of motor dysfunction, often revealing characteristic symptoms such as balance disturbances and motor incoordination in untreated Parkinson's models. Such impairments align with the hallmark symptoms of bradykinesia and muscle rigidity that arise from dopaminergic neurodegeneration. Enhanced rotarod performance in groups receiving either standard or experimental treatments suggests that these interventions may alleviate motor symptoms, thereby reinforcing their clinical potential in the therapeutic management of Parkinson's disease (Hong et al., 2020; Jamwal et al., 2017).

The actophotometer test complements this analysis by measuring overall activity levels, which often decline in Parkinson's disease, reflecting motor inactivity and fatigue typical of the condition. Lower activity counts in untreated groups highlight the motor impairment intrinsic to Parkinson's pathology, mirroring the apathy and reduced physical engagement observed clinically. Conversely, elevated activity levels in treatment groups suggest that these interventions may effectively restore normal motor activity, thus underscoring their importance in managing the disease's debilitating motor symptoms (Jaiswal et al., 2016).

The balance beam test further elucidates motor coordination deficits, with traversal time serving as a metric for postural and balance impairments. In untreated models, prolonged traversal times reflect significant coordination difficulties, comparable to the postural instability seen in Parkinson's patients, where such balance issues substantially impact patient safety and quality of life. Improved traversal times in treatment groups indicate that these therapies may help mitigate balance issues, reducing fall risk and improving patient outcomes (Jamwal et al., 2017).

Oxidative stress, a critical component of Parkinson's pathology, was evaluated through biochemical assays of markers such as glutathione (GSH), malondialdehyde (MDA), and superoxide dismutase (SOD). Lower levels of GSH and SOD in untreated groups correlate with weakened antioxidant defenses typical of neurodegenerative conditions. An increase in these antioxidant markers in treatment groups points to a neuroprotective effect, suggesting that these interventions bolster antioxidant capacity. Conversely, elevated MDA levels in untreated models signal increased lipid peroxidation, a sign of oxidative damage. Treatments that reduce MDA levels may offer neuroprotection by lessening oxidative stress, a factor crucial for slowing disease progression (Jaiswal et al., 2016).

Histopathological analysis of the hippocampus corroborates neurodegeneration in Parkinson's disease models, with untreated groups displaying markers such as gliosis, edema, and cortical neuron degeneration. These pathological changes reflect inflammatory processes and neuronal loss characteristic of Parkinsonian neurodegeneration. Reduced gliosis and edema in treated groups suggest that neuroprotective agents may counteract neuroinflammatory processes, thereby mitigating cellular damage in affected brain regions. The observed absence of gliosis and inflammation in these groups highlights the potential of these therapies to curb pathological changes central to Parkinson's progression (Syed et al., 2021; Jaiswal et al., 2016; Hong et al., 2020).

Parkinson's disease (PD), marked by motor and non-motor symptoms, severely impacts patients' quality of life. Quercetin, with antioxidant and anti-inflammatory properties, shows neuroprotective potential for PD by mitigating oxidative stress and inhibiting α-synuclein aggregation. Its therapeutic application benefits from intranasal delivery using niosomes, which enhance bioavailability and stability, improving quercetin's efficacy in PD models.

5 Conclusion

In summary, the study successfully formulated and characterized quercetin-loaded niosomes with desirable properties such as optimal particle size, high entrapment efficiency, and stable zeta potential. The *in vitro* and *in vivo* results indicate that these niosomes can significantly enhance the bioavailability and therapeutic efficacy of quercetin. The study confirms that quercetin-loaded niosomes are a promising delivery system for neuroprotection in Parkinson's disease. Future research should focus on further optimizing the formulation for large-scale production and exploring the detailed mechanisms underlying the observed pharmacodynamic effects. Additionally, long-term stability studies and clinical trials are necessary to validate the efficacy and safety of quercetin-loaded niosomes in human subjects.

Data availability statement

The original contributions presented in the study are included in the article/supplementary material, further inquiries can be directed to the corresponding author.

Ethics statement

The animal study was approved by Institutional Animal Ethical Committee (accession number: 221/Po/Re/S/2000/CPCSEA). The study was conducted in accordance with the local legislation and institutional requirements.

Author contributions

AR: Conceptualization, Formal Analysis, Investigation, Methodology, Validation, Visualization, Writing–original draft. AP: Conceptualization, Data curation, Formal Analysis, Funding acquisition, Investigation, Methodology, Supervision, Validation, Visualization, Writing–original draft, Writing–review and editing. RK: Formal Analysis, Writing–review and editing. KC: Formal Analysis, Writing–review and editing. PP: Formal Analysis, Writing–review and editing. AS: Writing–review and editing.

Funding

The author(s) declare that financial support was received for the research, authorship, and/or publication of this article. This research was funded by the KAHER grant and Ref. No. KAHER/ RD/23-24/ D-29092316.

Acknowledgments

The authors like the extend their gratitude to Kemphasol, Mumbai for providing the drug (Quercetin). We are also thankful to Loba chemicals for cholesterol and also otto chemicals for Levo-dopa. Our heartfelt appreciation goes to the KLE Academy of Higher Education and Research, Belagavi, the department of Pharmaceutics, KLE College of Pharmacy, Belagavi, Karnataka and the KAHER Prabhakar Kore Basic Research Center, Nehru Nagar, Belagavi, and also department of pathology, KAHER JNMC, Belagavi for histopathological evaluation for their invaluable support and facilities.

Conflict of interest

The authors declare that the research was conducted in the absence of any commercial or financial relationships that could be construed as a potential conflict of interest.

Generative AI statement

The authors declare that no Generative AI was used in the creation of this manuscript.

Publisher's note

All claims expressed in this article are solely those of the authors and do not necessarily represent those of their affiliated organizations, or those of the publisher, the editors and the reviewers. Any product that may be evaluated in this article, or claim that may be made by its manufacturer, is not guaranteed or endorsed by the publisher.

References

Abdelbary, A. A., and Abd-Elsalam, W. H. (2019). New peceol™/span™ 60 niosomes coated with chitosan for candesartan cilexetil: perspective increase in absolute bioavailability in rats. *J. Biomed. Nanotechnol.* 15 (8), 1761–1772. doi:10.2147/IJN.S324171

Abdelkader, H., Farghaly, U., and Moharram, H. (2014). Effects of surfactant type and cholesterol level on niosomes physical properties and *in vivo* ocular performance using timolol maleate as a model drug. *J. Pharm. Investig.* 44, 329–337. doi:10.1007/s40005-014-0121-8

Acıkara, O. B., Karatoprak, G. S., Yucel, C., Akkol, E. K., Sobarzo-Sanchez, E., Khayatkashani, M., et al. (2022). A critical analysis of quercetin as the attractive target for the treatment of Parkinson's disease. *CNS Neurol. Disord. Drug Targets* 21 (9), 795–817. doi:10.2174/1871527320666211206122407

Afreen, U., Fahelelbom, K. M., Shah, S. N. H., Ashames, A., Almas, U., Khan, S. A., et al. (2022). Formulation and evaluation of niosomes-based chlorpheniramine gel for the treatment of mild to moderate skin allergy. *J. Exp. Nanosci.* 17 (1), 467–495. doi:10.1080/17458080.2022.2094915

Bhangale, J. O., and Acharya, S. R. (2016). Anti-Parkinson activity of petroleum ether extract of Ficus religiosa (L.) leaves. *Adv. Pharmacol. Pharm. Sci.* 1 (1), 9436106–9436109. doi:10.1155/2016/9436106

Durán-Lobato, M., Díaz-Montes, E., Castro-Muñoz, R., Diban, N., Bolton, F. J., Bongiorno, M., et al. (2022). Microalgae as sources of bioactive compounds: potential applications and challenges. *Algal Res.* 63, 102705.

Eid, H. M., Ali, A. A., Ali, A. M., Eissa, E. M., Hassan, R. M., Abo El-Ela, F. I., et al. (2022). Potential use of tailored citicoline chitosan-coated liposomes for effective wound healing in diabetic rat model. *Int. J. Nanomedicine* 10, 555–575. doi:10.2147/IJN.S342504

El-Diasty, E. M., Elkomy, M. H., Eid, H. M., Mostafa, M., Mady, F. M., and Fahmy, A. M. (2020). Development and evaluation of nanostructured lipid carriers for controlled delivery of cetirizine hydrochloride. *J. Adv. Res.* 23, 51–60.

Elkomy, M. H., Alruwaili, N. K., Elmowafy, M., Shalaby, K., Zafar, A., Ahmad, N., et al. (2022). Surface-modified bilosomes nanogel bearing a natural plant alkaloid for

safe management of rheumatoid arthritis inflammation. *Pharmaceutics* 14 (3), 563. doi:10.3390/pharmaceutics14030563

Elkomy, M. H., El Menshawe, S. F., Eid, H. M., and Ali, A. M. (2017). Development of a nanogel formulation for transdermal delivery of tenoxicam: a pharmacokinetic–pharmacodynamic modeling approach for quantitative prediction of skin absorption. *Drug Dev. Ind. Pharm.* 43 (4), 531–544. doi:10.1080/03639045.2016.1268153

Elkomy, M. H., Zaki, R. M., Alsaidan, O. A., Elmowafy, M., Zafar, A., Shalaby, K., et al. (2023). Intranasal nanotransferosomal gel for quercetin brain targeting: I. Optimization, characterization, brain localization, and cytotoxic studies. *Pharmaceutics* 15 (7), 1805. doi:10.3390/pharmaceutics15071805

Ellman, G. L. (1959). Tissue sulfhydryl groups. *Arch. Biochem. Biophys.* 82, 70–77. doi:10.1016/0003-9861(59)90090-6

Essa, E. A. (2010). Effect of formulation and processing variables on the particle size of sorbitan monopalmitate niosomes. *Asian J. Pharm.* 4 (4), 227–280. doi:10.4103/0973-8398.76752

Galgatte, U. C., Kumbhar, A. B., and Chaudhari, P. D. (2014). Development of *in situ* gel for nasal delivery: design, optimization, *in vitro* and *in vivo* evaluation. *Drug Deliv.* 21 (1), 62–73. doi:10.3109/10717544.2013.849778

Glascock, J. J., Osman, E. Y., Coady, T. H., Rose, F. F., Shababi, M., and Lorson, C. L. (2011). Delivery of therapeutic agents through intracerebroventricular (ICV) and intravenous (IV) injection in mice. *JoVE* 56, 2968–2976. doi:10.3791/2968

Grewal, A. K., Singh, T. G., Sharma, D., Sharma, V., Singh, M., Rahman, M. H., et al. (2021). Mechanistic insights and perspectives involved in neuroprotective action of quercetin. *Biomed. Pharmacother.* 140, 111729. doi:10.1016/j.biopha.2021.111729

Hira, S., Saleem, U., Anwar, F., Raza, Z., Rehman, A. U., and Ahmad, B. (2020). *In silico* study and pharmacological evaluation of eplerinone as an anti-Alzheimer's drug in STZ-Induced Alzheimer's disease model. *ACS Omega* 5, 13973–13983. doi:10.1021/acsomega.0c01381

Hira, S., Saleem, U., Anwar, F., Sohail, M. F., Raza, Z., and Ahmad, B. (2019). β-Carotene: a natural compound improves cognitive impairment and oxidative stress in a mouse model of streptozotocin-induced alzheimer's disease. *Biomolecules* 9 (9), 441. doi:10.3390/biom9090441

Hong, S., Wang, M., Roth, S., Coppola, J. M., Manfra, D. J., and Zhang, Z. (2020). Intranasal drug delivery for brain cancer treatment: current progress and future prospects. *J. Control. Release.* 327, 347–359.

Hu, C., Napolitano, J. G., Ma, S., Hrovat, F., Ragains, M., Russell, D., et al. (2022). Precipitation behavior of highly soluble amphiphilic drugs in solution: physical instability of drugs in solution. *Pharm. Sci.* 111 (8), 2172–2179. doi:10.1016/j.xphs.2022.05.019

Jaiswal, S. K., Sharma, A., Gupta, V. K., Singh, R. K., and Sharma, B. (2016). Curcumin mediated attenuation of carbofuran induced oxidative stress in rat brain. *Biochem. Res. Int.* 6 (1), 7637931. doi:10.1155/2016/7637931

Jamwal, S., Singh, S., and Bansal, P. K. (2017). Behavioral tests for rodent models. *AMND* 8, 315–341. doi:10.1007/978-981-10-5981-0_21

Jiang, Y., Xie, G., Alimujiang, A., Xie, H., Yang, W., Yin, F., et al. (2023). Protective effects of querectin against MPP+-induced dopaminergic neurons injury via the Nrf2 signaling pathway. *FBL* 28 (3), 42. doi:10.31083/j.fbl2803042

Junyaprasert, V. B., Teeranachaideekul, V., and Supaperm, T. (2008). Effect of charged and non-ionic membrane additives on physicochemical properties and stability of niosomes. *AAPS PharmSciTech* 9, 851–859. doi:10.1208/s12249-008-9121-1

Khallaf, R. A., Aboud, H. M., and Sayed, O. M. (2020). Surface modified niosomes of olanzapine for brain targeting via nasal route: preparation, optimization, and *in vivo* evaluation. *J. Liposome Res.* 30, 163–173. doi:10.1080/08982104.2019.1610435

Kondawar, M., Kamble, K., Khandare, M., Maharshi, K., and Awale, V. (2011). Evaluation of the locomotor and diuretic activities of ethanolic extract of leaves of Capparis divaricata Lam (Capparidaceae). *Int. J. Pharm. Sci.* 3 (4), 265–267.

Madiha, S., Batool, Z., Tabassum, S., Liaquat, L., Sadir, S., Shahzad, S., et al. (2021). Quercetin exhibits potent antioxidant activity, restores motor and non-motor deficits induced by rotenone toxicity. *PLoS One* 16 (11), 0258928. doi:10.1371/journal.pone.0258928

Masjedi, M., and Montahaei, T. (2021). An illustrated review on nonionic surfactant vesicles (niosomes) as an approach in modern drug delivery: fabrication, characterization, pharmaceutical, and cosmetic applications. *J. Drug Deliv. Sci. Technol.* 61, 102234. doi:10.1016/j.jddst.2020.102234

Mitsuboshi, S., Niimura, T., Aizawa, F., Goda, M., Zamami, Y., and Ishizawa, K. (2022). Atenolol and mortality events in patients with chronic kidney disease: analysis of data from the Japanese Adverse Drug Event Report database. *BCPT* 130 (4), 553–556. doi:10.1111/bcpt.13717

Moghassemi, S., and Hadjizadeh, A. (2014). Nano-niosomes as nanoscale drug delivery systems: an illustrated review. *J. Control. Release.* 185, 22–36. doi:10.1016/j.jconrel.2014.04.015

Nasr, A. M., Qushawy, M. K., Elkhoudary, M. M., Gawish, A. Y., Elhady, S. S., and Swidan, S. A. (2020). Quality by design for the development and analysis of enhanced *in situ* forming vesicles for the improvement of the bioavailability of fexofenadine HCl *in vitro* and *in vivo*. *Pharmaceutics* 12 (5), 409. doi:10.3390/pharmaceutics12050409

Nirmal, N., Bakliwal, S., and Pawar, S. (2010). *In situ* gel: new trends in controlled and sustained drug delivery system. *Int. J. Pharmtech Res.* 10 (2), 1398–1408.

Owodeha-Ashaka, K., Ilomuanya, M. O., and Iyire, A. (2021). Evaluation of sonication on stability-indicating properties of optimized pilocarpine hydrochloride-loaded niosomes in ocular drug delivery. *Prog. Biomater.* 10, 207–220. doi:10.1007/s40204-021-00164-5

Rajoria, G., and Gupta, A. (2012). *In situ* gelling system: a novel approach for ocular drug delivery. *AJPTR* 2, 24–53.

Ranpariya, V. L., Parmar, S. K., Sheth, N. R., and Chandrashekhar, V. M. (2011). Neuroprotective activity of Matricaria recutita against fluoride-induced stress in rats. *Pharm. Biol.* 49, 696–701. doi:10.3109/13880209.2010.540249

Saleem, U., Gull, Z., Saleem, A., Shah, M. A., Akhtar, M. F., Anwar, F., et al. (2021). Appraisal of anti-Parkinson activity of rhinacanthin-C in haloperidol-induced parkinsonism in mice: a mechanistic approach. *J. Food Biochem.* 45 (4), 13677. doi:10.1111/jfbc.13677

Schmolka, I. R. (2014). Artificial skin I. Preparation and properties of pluronic F-127 gels for treatment of burns. *J. Biomed. Mater. Res.* 6 (6), 571–582. doi:10.1002/jbm.820060609

Shah, P., Bhalodia, D., Shelat, P., Shukla, A., Balaji, B., and Prajapati, B. (2012). Nanoemulsions for delivery of anticancer drug: a novel approach. *Curr. Drug Deliv.* 9, 469–479.

Shah, P., Goodyear, B., Haq, A., Puri, V., and Michniak-Kohn, B. (2020). Evaluations of quality by design (QbD) elements impact for developing niosomes as a promising topical drug delivery platform. *Pharmaceutics* 12 (9), 246. doi:10.3390/pharmaceutics12030246

Shilakari Asthana, G., Sharma, P. K., and Asthana, A. (2016). *In vitro* and *in vivo* evaluation of niosomal formulation for controlled delivery of clarithromycin. *Scientifica* 2016 (1), 6492953. doi:10.1155/2016/6492953

Shrivastava, P., Vaibhav, K., Tabassum, R., Khan, A., Ishrat, T., Khan, M. M., et al. (2013). Antiapoptotic and antiinflammatory effect of Piperine on 6-OHDA induced Parkinson's rat model. *J. Neurochem.* 24, 680–687. doi:10.1016/j.jnutbio.2012.03.018

Sirvi, A., Kuche, K., Chaudhari, D., Ghadi, R., Date, T., Katiyar, S. S., et al. (2022). Supersaturable self-emulsifying drug delivery system: a strategy for improving the loading and oral bioavailability of quercetin. *Sci. Technol.* 71, 103289. doi:10.1016/j.jddst.2022.103289

Syed, A., Ameen, F., Ahmed, M. A., Elgorban, A. M., Shams, Q., and Khan, M. S. (2021). Chitosan-based nanocomposites as drug delivery vehicles in modern pharmacotherapy. *Nanomaterials* 11, 791.

Tamtaji, O. R., Hadinezhad, T., Fallah, M., Shahmirzadi, A. R., Taghizadeh, M., Behnam, M., et al. (2020). The therapeutic potential of quercetin in Parkinson's disease: insights into its molecular and cellular regulation. *Curr. Drug Targets* 21 (5), 509–518. doi:10.2174/1389450120666191112155654

Teaima, M. H., Helal, D. A., Alsofany, J. M., El-Nabarawi, M. A., and Yasser, M. (2022). Ion-triggered *in situ* gelling intranasal spray of dronedarone hydrochloride nanocarriers: *in vitro* optimization and *in vivo* pharmacokinetic appraisal. *Pharmaceutics* 14 (11), 2405. doi:10.3390/pharmaceutics14112405

Uchegbu, I. F., and Vyas, S. P. (1998). Non-ionic surfactant based vesicles (niosomes) in drug delivery. *Int. J. Pharm.* 172, 33–70. doi:10.1016/s0378-5173(98)00169-0

Wrobel-Biedrawa, D., Grabowska, K., Galanty, A., Sobolewska, D., and Podolak, I. (2022). A flavonoid on the brain: quercetin as a potential therapeutic agent in central nervous system disorders. *Life* 12 (4), 591. doi:10.3390/life12040591

Zolghadri, S., Asad, A. G., Farzi, F., Ghajarzadeh, F., Habibi, Z., Rahban, M., et al. (2023). Span 60/cholesterol niosomal formulation as a suitable vehicle for gallic acid delivery with potent *in vitro* antibacterial, antimelanoma, and anti-tyrosinase activity. *Pharmaceutics* 16, 1680. doi:10.3390/ph16121680

frontiers | Frontiers in Pharmacology

TYPE Original Research
PUBLISHED 26 February 2025
DOI 10.3389/fphar.2025.1520988

Check for updates

OPEN ACCESS

EDITED BY
Pukar Khanal,
Emory University, United States

REVIEWED BY
Shinichiro Ochi,
Ehime University, Japan
Sui-yi Xu,
First Hospital of Shanxi Medical University, China

*CORRESPONDENCE
Lehua Yu,
300895@cqmu.edu.cn
Hui Xue,
15147244996@163.com

RECEIVED 04 November 2024
ACCEPTED 04 February 2025
PUBLISHED 26 February 2025

CITATION
Meng T, Zhang X, Zhao J, Xue H and Yu L (2025) Acetate and propionate vs. iTBS as a novel method for cognitive dysfunction and anxiety symptoms in delayed encephalopathy after acute carbon monoxide poisoning rat. *Front. Pharmacol.* 16:1520988. doi: 10.3389/fphar.2025.1520988

COPYRIGHT
© 2025 Meng, Zhang, Zhao, Xue and Yu. This is an open-access article distributed under the terms of the Creative Commons Attribution License (CC BY). The use, distribution or reproduction in other forums is permitted, provided the original author(s) and the copyright owner(s) are credited and that the original publication in this journal is cited, in accordance with accepted academic practice. No use, distribution or reproduction is permitted which does not comply with these terms.

Acetate and propionate vs. iTBS as a novel method for cognitive dysfunction and anxiety symptoms in delayed encephalopathy after acute carbon monoxide poisoning rat

Tianyu Meng[1], Xin Zhang[2], Jili Zhao[2], Hui Xue[2]* and Lehua Yu[1]*

[1]Department of Rehabilitation Medicine, The Second Affiliated Hospital of Chongqing Medical University, Chongqing, China, [2]Department of Neurology, Baotou Central Hospital, Baotou, Inner Mongolia, China

Background: The optimal treatment methods for delayed encephalopathy after acute carbon monoxide (CO) poisoning (DEACMP) were not identified. Thus, this study was conducted to compare the efficacies of intermittent theta burst stimulation (iTBS) and short-chain fatty acids (SCFAs) in treating cognitive dysfunction and anxiety symptoms of DEACMP rat.

Methods: In phase I, a DEACMP rat model was built to assess the inflammation levels in the hippocampus and levels of SCFAs in the serum of DEACMP rats. In phase II, DEACMP rats were randomly assigned into four groups: DEACMP + placebo, DEACMP + SCFAs, DEACMP + sham iTBS, and DEACMP + iTBS. The intervention was continued for 2 weeks. A Morris water maze and open field tests were used to assess cognitive function and anxiety symptoms, respectively.

Results: The levels of three inflammatory factors (IL-1β, IL-6, and TNF-α) and two SCFAs (acetate and propionate) were significantly increased and decreased, respectively, in DEACMP rats. After treatment, cognitive dysfunction and anxiety symptoms were significantly improved in the DEACMP + iTBS group and the DEACMP + SCFAs (consisting of acetate and propionate) group. Both SCFAs and iTBS could significantly improve the increased levels of IL-1β, IL-6, and TNF-α in the hippocampus, and SCFAs could also improve the decreased levels of GPR41, GPR43, dopamine, and norepinephrine in the hippocampus of DEACMP rats.

Conclusion: These results indicate that both iTBS and SCFA solutions consisting of acetate and propionate produced good effects on DEACMP rats by regulating inflammation levels in the hippocampus, and acetate/propionate–GPR41/GPR43–IL-1β/IL-6/TNF-α–dopamine/norepinephrine may be a potential pathway in SCFAs for the treatment of DEACMP.

KEYWORDS

DEACMP, iTBS, SCFAs, inflammation, neurotransmitter

Introduction

Carbon monoxide (CO) is a difficult-to-detect colorless and odorless gas. It can cause multiple organ dysfunctions, mainly characterized by central nervous system (CNS) damage (Chen et al., 2021; Kinoshita et al., 2020). Delayed encephalopathy after acute CO poisoning (DEACMP) is a common and serious complication after CO poisoning (Xu et al., 2019). Approximately 10%–30% of patients develop DEACMP after CO poisoning, resulting in a great economic burden for individuals and society (Wang et al., 2016). Using a DEACMP rat model, we found that the microglial activation regulated by ATP through the P2Y12 receptor pathway may be closely related to the onset of DEACMP (Xiang et al., 2021), and that inflammation may have an important role in the onset of DEACMP (Xiang et al., 2014). Currently, the pathogenesis of DEACMP is still not fully understood. Patients with DEACMP always experience several severe clinical symptoms, such as dementia and cognitive dysfunction (Harper and Croft-Baker, 2004). Our previous studies reported that the combined application of hyperbaric oxygen and medications, such as dexamethasone (Xiang et al., 2017a) and N-butylphthalide (Xiang et al., 2017b), could be potential new methods to improve cognitive dysfunction in DEACMP patients. However, the optimal treatment methods for DEACMP are still not available. Therefore, it is necessary to further explore novel treatment methods for this disease.

Theta burst stimulation (TBS) is a paradigm of repetitive transcranial magnetic stimulation (rTMS). It can enhance synaptic transmission by mimicking cortical theta rhythms, thus enhancing cortical excitability. Intermittent TBS (iTBS) is one of the two main types of TBS used in clinical research. As a non-invasive brain stimulation method, previous research found that iTBS could be used to treat neuropsychiatric disorders, such as depression and stroke (Scho et al., 2024; Han et al., 2024). More recently, iTBS has emerged as a potential intervention for cognitive dysfunction. Stanojevic et al. found that iTBS could mitigate the cognitive impairment in the streptozotocin-induced model of Alzheimer's disease (Stanojevic et al., 2022). A recent meta-analysis showed that patients with cognitive dysfunction improved their cognitive function after receiving iTBS (Zheng et al., 2024). These findings indicate that iTBS may be effective in the treatment of DEACMP, although few studies have focused on the efficacy of iTBS DEACMP.

Short-chain fatty acids (SCFAs) are the main products of the gut microbiota and have wide-ranging effects locally and throughout the body. The three major SCFAs are acetate, propionate, and butyrate. They can affect CNS functions by modulating different pathways to the brain, such as the vagus nerve (O'Riordan et al., 2022). SCFAs are now considered to be major communication links between the gut and the brain. Dysfunction of SCFAs is closely linked to many neuropsychiatric disorders, such as depression (Cheng et al., 2024). More and more researchers now use SCFAs as a novel method for the treatment of diseases, such as propionate for multiple sclerosis disease (Duscha et al., 2020). Li et al. reported that SCFAs could significantly improve cognitive dysfunction in mice (Tian et al., 2024). During the processes by which SCFAs exert beneficial effects on host health, two G-protein-coupled receptors (GPRs), GPR41 and GPR43, play important roles and have received increasing attention. GPRs are a diverse class of cell surface receptors that are closely related to many physiological functions, such as the inflammatory response, and GPR41 and GPR43 are the receptors of SCFAs (Kimura et al., 2014). Therefore, we conducted this study to assess whether SCFAs could yield good efficacy in the treatment of DEACMP, and then preliminarily investigate the underlying mechanism of action. Meanwhile, we assessed the efficacy of iTBS on DEACMP and compared its efficacy with that of SCFAs. Our findings can be helpful in exploring the optimal treatment methods for DEACMP.

Materials and methods

DEACMP model

Sprague–Dawley rats (6–8 weeks, 180–230 g) were provided by SiPeiFu (Beijing) Biotechnology Co. Ltd. (China) and housed under standard conditions. After 1 week of acclimation, the rats were randomly assigned to either an experimental group or a control group. To build the DEACMP model, according to our previous studies (Xiang et al., 2021; Xiang et al., 2014), the rats in the experimental group received CO (static inhalation, 1,000 ppm/40 min and 3,000 ppm/20 min), and the rats in the control group received the same amount of air. The whole procedure was conducted according to the National Institutes of Health guidelines for animal research (*Guide for the Care and Use of Laboratory Animals*, NIH Publication No.8023, revised 1996). Our study was approved by the Ethics Committee of Baotou Central Hospital.

Behavioral experiments

In this study, the escape latency in the Morris water maze (MWM) test was used to assess cognitive function, and the center distance as a percentage of total distance (center distance (%)) in the open field test (OFT) was used to assess anxiety symptoms in the rats. These two behavioral experiments were performed exactly according to our previous studies (Xiang et al., 2021; Xiang et al., 2014) to ensure that the control and experimental groups had similar escape latency and center distance (%). In phase I, after 21 days of CO poisoning, these two behavioral experiments were conducted to assess whether the DEACMP model had been successfully built, and then the rats were sacrificed. The hippocampus and serum of the rats were collected to assess the levels of inflammation and the levels of SCFAs, respectively. In phase II, these two behavioral experiments were conducted after 21 days of CO poisoning, after 1 week of treatment, and after 2 weeks of treatment, and then the rats were sacrificed. The hippocampus of the rats was collected to assess inflammation levels and neurotransmitter levels.

Detection methods

Liquid chromatography-mass spectrometry (LC-MS) was used to detect neurotransmitters in the hippocampus. Briefly,

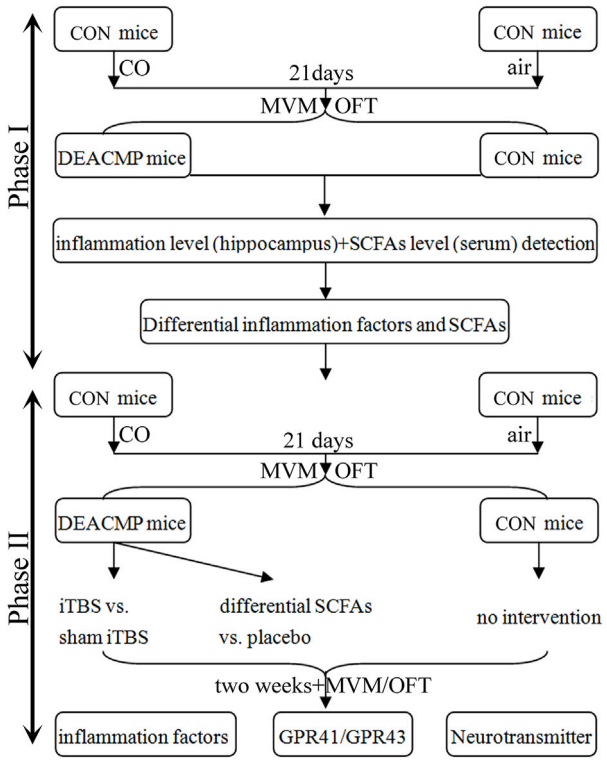


FIGURE 1
Study design. This study consisted of two phases. Phase I was conducted to identify the differential inflammatory factors in the hippocampus and SCFAs in serum, and phase II explored the efficacy of differential SCFAs in the treatment of DEACMP. iTBS was used as a positive control. CON, control; DEACMP, delayed encephalopathy after acute carbon monoxide poisoning; iTBS, intermittent theta burst stimulation; SCFAs, short-chain fatty acids; MWM, Morris water maze; OFT, open field test; GPR41, G protein-coupled receptor 41; GPR43, G protein-coupled receptor 43.

we first weighed the sample and prepared the supernatant (400 μL mixture of methanol-water (4/1, v/v); 2-chloro-l-phenylalanine (75 ng/mL) dissolved in methanol as an internal standard; homogenization at low temperature for 10 min; ultrasonic extraction in an ice water bath for 10 min; centrifugation at 14,000 rpm for 10 min, 4 °C). Then, 300 μL of supernatant and 200 μL of a mixture of methanol-water (4/1, v/v) were transferred to an Eppendorf tube. After vortexing for 30 s, ultrasonic extraction for 5 min, and centrifugation at 14,000 rpm for 10 min at 4 °C, 200 μL of supernatant was transferred to a new Eppendorf tube. In the third step, methanol-water (4/1, v/v) was added to the powder, which was obtained in a freeze-concentration centrifugal dryer. Then, 150 μL of the supernatant obtained after centrifugation (10 min, 14,000 rpm, 4 °C) was transferred to the injection vial for later LC-MS analysis. The quantification of neurotransmitters was conducted on a Waters Acquity UPLC system. In addition, enzyme-linked immunosorbent assay kits (Jianglai Industry Co., Ltd., Shanghai, China) were used to detect interleukin-6 (IL-6), interleukin-1 beta (IL-1β), tumor necrosis factor-α (TNF-α), GPR41, and GPR43. The detection process was according to the manufacturer's instructions.

Intervention modalities

In phase II, after the DEACMP model was successfully built, the DEACMP rats in the experimental group were randomly assigned into four groups: DEACMP + SCFAs group, DEACMP + placebo group, DEACMP + iTBS group, and DEACMP + sham iTBS group. The SCFA solution consisted of sodium acetate (67.5 mmol/L) and sodium propionate (25.9 mmol/L) in a 3: 1 ratio (Tian et al., 2024), and normal saline was used as a placebo. The SCFAs (500 mg/kg per day) and an equal amount of normal saline were given intragastrically (Tian et al., 2024). The iTBS block consisted of twenty trains of ten bursts (three pulses at a frequency of 50 Hz), repeated at 5 Hz (lasting 192 s with 10 s intervals between trains) (Dragic et al., 2020). The MagStim Rapid2 was used to conduct iTBS. The stimulation intensity was set to 30% of the maximum stimulator output, just below the motor threshold. The motor threshold was defined as the stimulation intensity that could cause the minimum visible contraction of the upper limbs (Dragic et al., 2020). In sham iTBS, the coil was rotated 90° around its vertical midline axis to ensure no brain stimulation (Dragic et al., 2020). The intervention was continued for 2 weeks. The setup is described in Figure 1.

Statistical analysis

SPSS 21.0 and R software 4.2 were used for all the statistical analyses. Student's t-test was used to find the differences between the two groups. A paired t-test was used here to determine whether the changes between two-time points in one group were significantly different. However, when the data did not meet the prerequisite assumption of normal distribution, non-parametric methods were used to explore the differences between the two groups. Meanwhile, one-way analysis of variance (ANOVA) was used to find the differences among the three groups; if a significant difference was found in this test, Tamhane's T2 or Bonferroni post-hoc test was then performed to determine which two groups significantly differed according to the equal variance criterion. Spearman's correlation analysis was used to determine the potential correlations between differential factors. A heat map was used to show the changes in neurotransmitters in the different groups. All tests were two-sided, and $p < 0.05$ was considered statistically significant.

Results

Cognitive dysfunction in DEACMP rats

After 21 days of CO poisoning, a DEACMP rat mode was built. To find out whether DEACMP rats had cognitive dysfunction, the Morris water maze test was used. At baseline, the two groups had similar escape latency ($p = 0.850$), but DEACMP rats had a significantly higher escape latency than control rats ($p = 0.0005$, Figure 2A). These results indicate that DEACMP rats had cognitive dysfunction. Meanwhile, to explore whether DEACMP rats had anxiety symptoms, an open-field test was used. At baseline, the two groups had similar center distance (%) ($p = 0.920$), but DEACMP rats eventually had a significantly higher center distance (%) than

10.3389/fphar.2025.1520988

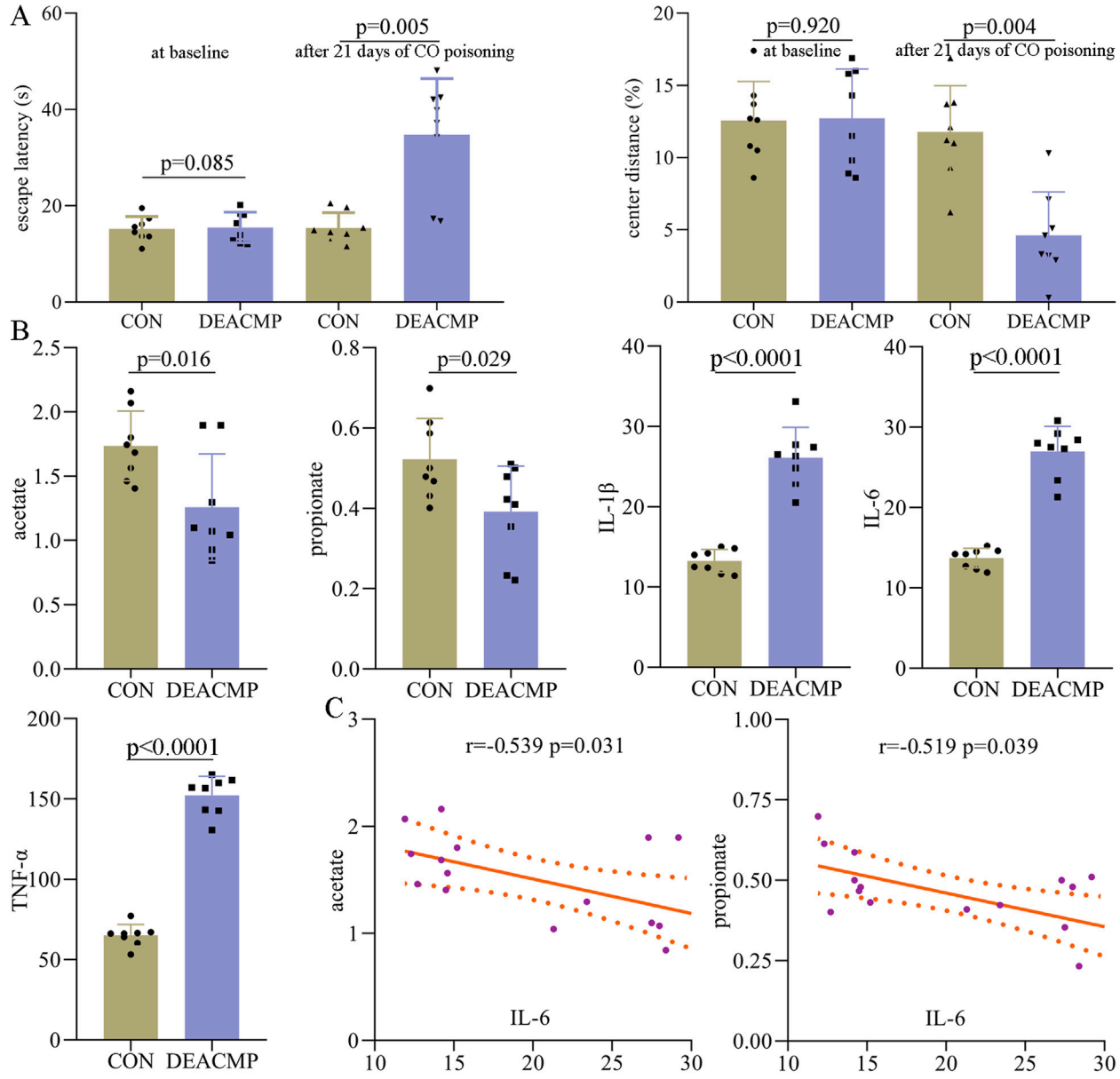


FIGURE 2
Abnormal behaviors and molecules in DEACMP rats. **(A)** After 21 days of CO poisoning, DEACMP rats showed significantly higher escape latency and lower center distance (%) than control rat. **(B)** Two SCFAs (acetate and propionate) in serum and three inflammatory factors (IL-1β, IL-6, and TNF-α) in the hippocampus were significantly changed in DEACMP rats. **(C)** There were significant negative correlations between IL-6 and these two SCFAs (acetate and propionate). CON, control; DEACMP, delayed encephalopathy after acute carbon monoxide poisoning.

the control rats ($p = 0.0004$, Figure 2A). These results show that DEACMP rats had anxiety symptoms.

After being sacrificed, the serum and hippocampus of the rats were collected and stored for later experiments. In this study, eight SCFAs were successfully identified in rat serum: valerate, propionate, isohexanate, isobutyrate, butyrate, acetate, isovalerate, and hexanate. Compared to control rats, DEACMP rats had significantly lower levels of acetate ($p = 0.016$) and propionate ($p = 0.029$, Figure 2B). The levels of the other six SCFAs were similar between the two groups: valerate ($p = 0.570$), isohexanate ($p = 0.239$), isobutyrate ($p = 0.211$), butyrate ($p = 0.862$), isovalerate ($p = 0.129$), and hexanate ($p = 0.644$). In addition, we also assessed the inflammation levels in the hippocampus of DEACMP rats. The results showed that compared to control rats, DEACMP rats had significantly higher levels of IL-1β ($p < 0.0001$), IL-6 ($p < 0.0001$), and TNF-α ($p < 0.0001$, Figure 2B). Spearman's correlation analysis showed that IL-6 was significantly correlated with acetate ($r = -0.539$, $p = 0.031$) and propionate ($r = -0.519$, $p = 0.039$, Figure 2C). These phase I results demonstrate that DEACMP rats had increased inflammation levels in the hippocampus and decreased levels of SCFAs in serum.

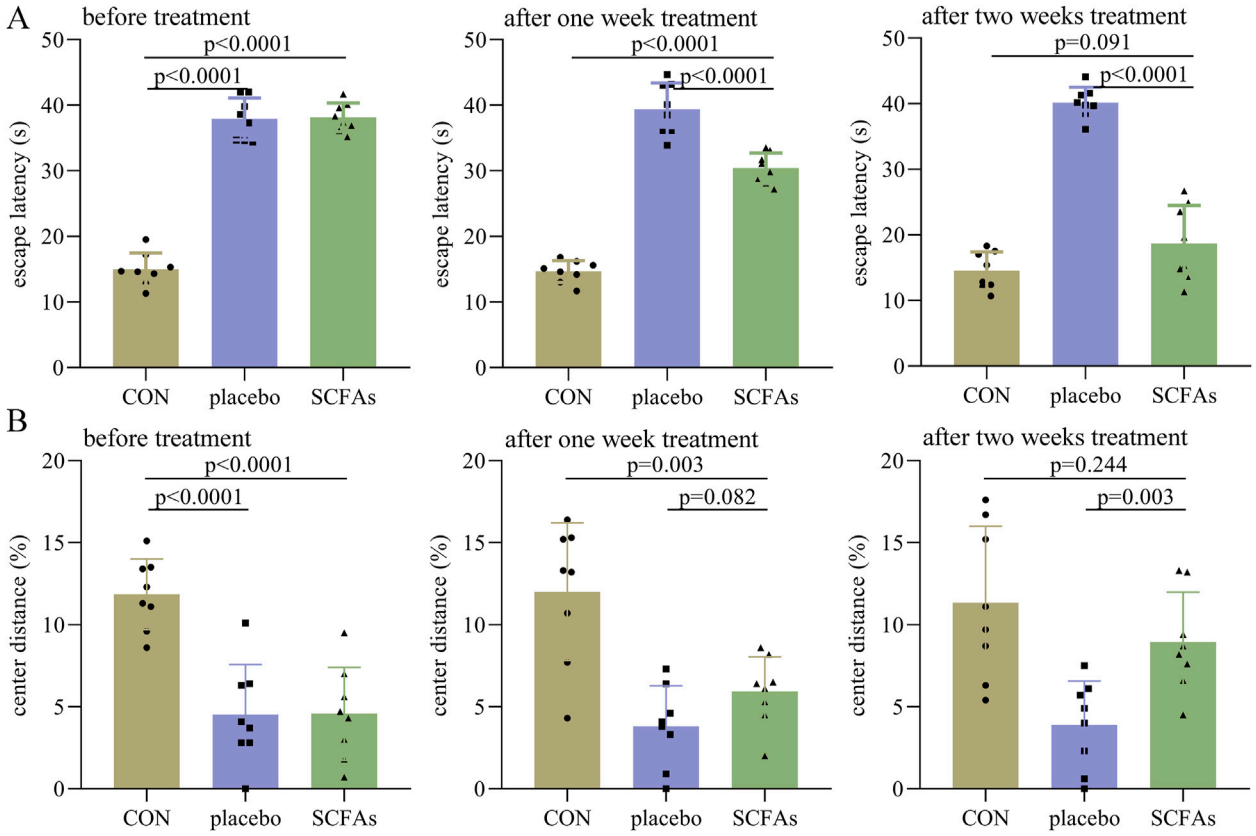


FIGURE 3
Efficacy of SCFAs on cognitive function and anxiety symptoms in DEACMP rats. **(A)** Before treatment, the DEACMP + placebo group and the DEACMP + SCFAs group had similar escape latency. After treatment, the DEACMP + SCFAs group had a significantly lower escape latency than the DEACMP + placebo group. **(B)** Before treatment, the DEACMP + placebo group and the DEACMP + SCFAs group had a similar center distance (%). After 1 week of treatment, the DEACMP + SCFAs group had a non-significantly higher center distance (%) than the DEACMP + placebo group; after 2 weeks of treatment, the DEACMP + SCFAs group had a significantly higher center distance (%) than the DEACMP + placebo group. CON, control; DEACMP, delayed encephalopathy after acute carbon monoxide poisoning; SCFAs, short-chain fatty acids.

Efficacy of SCFAs in the treatment of DEACMP rats

In phase II, before treatment, the control group had a significantly lower escape latency than both the DEACMP + placebo group ($p < 0.0001$) and the DEACAMP + SCFAs group ($p < 0.0001$, Figure 3A). After 1 week of treatment, the escape latency in the DEACAMP + SCFAs group was significantly lower than that of the DEACMP + placebo group ($p < 0.0001$), but still significantly higher than the control group ($p < 0.0001$, Figure 3A). After 2-weeks of treatment, the escape latency in the DEACMP + SCFAs group was significantly lower than that in the DEACMP + placebo group ($p < 0.0001$) and similar to that in the control group ($p = 0.091$, Figure 3A). Meanwhile, we found that, in the DEACMP + SCFAs group, the escape latency after 2 weeks of treatment was significantly lower than the escape latency after 1 week of treatment ($p = 0.0001$), and the latter was significantly lower than the escape latency after 21 days of CO poisoning ($p < 0.0001$). Similar results were found for the center distance (%) after SCFA treatment (Figure 3B). These results indicate that SCFAs could significantly improve cognitive dysfunction and anxiety symptoms in DEACMP rats.

Efficacy of iTBS in the treatment of DEACMP rats

In phase II, before treatment, the control group had a significantly lower escape latency than both the sham iTBS ($p < 0.0001$) and iTBS ($p < 0.0001$) groups (Figure 4A). After 1 week of treatment, the escape latency in the iTBS group was significantly lower than in the sham iTBS group ($p < 0.0001$), but still significantly higher than in the control group ($p < 0.0001$, Figure 4A). After 2 weeks of treatment, the escape latency in the iTBS group was significantly lower than that in the sham iTBS group ($p < 0.0001$), and similar to that in the control group ($p = 0.160$, Figure 4A). Meanwhile, we found that in the iTBS group, the escape latency after 2 weeks of treatment was significantly lower than the escape latency after 1 week of treatment ($p = 0.001$). Similar results were found for the center distance (%) after iTBS treatment (Figure 4B). Meanwhile, at the end of the intervention, we found that the levels of IL-1β ($p < 0.0001$), IL-6 ($p < 0.0001$), and TNF-α ($p < 0.0001$) were significantly lower in the iTBS group than in the sham iTBS group, but the levels of these inflammatory factors were similar between the control and iTBS groups (Figure 4C). These results indicate that iTBS could significantly improve cognitive

10.3389/fphar.2025.1520988

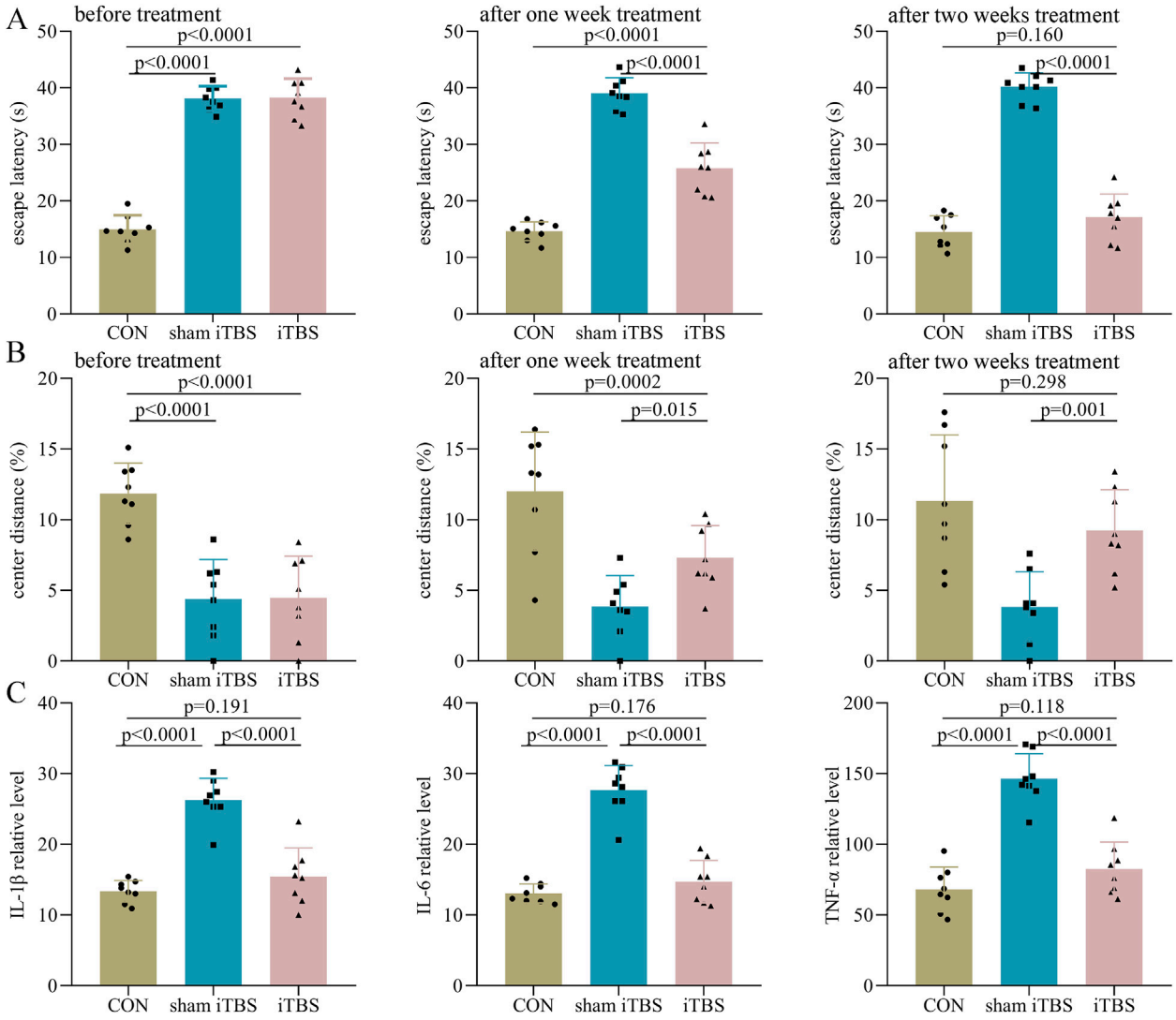


FIGURE 4
Efficacy of iTBS on cognitive function and anxiety symptoms in DEACMP rats. **(A)** Before treatment, the DEACMP + sham iTBS group and the DEACMP + iTBS group had similar escape latency. After treatment, the DEACMP + iTBS group had a significantly lower escape latency than the DEACMP + sham iTBS group. **(B)** Before treatment, the DEACMP + sham iTBS group and DEACMP + iTBS groups had similar escape latency. After treatment, the DEACMP + iTBS group had a significantly higher center distance (%) than the DEACMP + sham iTBS group. **(C)** After 2 weeks of treatment, IL-1β, IL-6, and TNF-α levels were significantly lower in the DEACMP + iTBS group than in the DEACMP + sham iTBS group, but their levels were similar between the CON and the DEACMP + iTBS groups. CON, control; DEACMP, delayed encephalopathy after acute carbon monoxide poisoning; iTBS, intermittent theta burst stimulation.

dysfunction and anxiety symptoms in DEACMP rats and restore the increased inflammation levels in the hippocampus of DEACMP rats.

SCFAs vs. iTBS in the treatment of DEACMP rats

To explore whether these two different treatment methods have different effects in the treatment of DEACMP rats, the escape latency and center distance (%) between the DEACMP + SCFAs and the iTBS groups were compared. As shown in Figure 5A, the two groups had a similar escape latency before treatment ($p = 0.952$). After 1 week of treatment, the reduction in escape latency was significantly higher in the iTBS group than in the SCFA group ($p = 0.0001$); however, after 2 weeks of treatment, the two groups had a similar reduction in escape latency ($p = 0.408$) (Figure 5A). As shown in Figure 5B, the two groups had similar center distance (%) before treatment ($p = 0.993$). After 1 week of treatment, the increase in center distance (%) was significantly higher in the iTBS group than in the SCFAs group ($p = 0.046$), but after 2 weeks of treatment, the two groups had a similar reduction in escape latency ($p = 0.673$) (Figure 5B). These results suggest that iTBS may work faster in the treatment of cognitive dysfunction and anxiety symptoms in DEACMP rats.

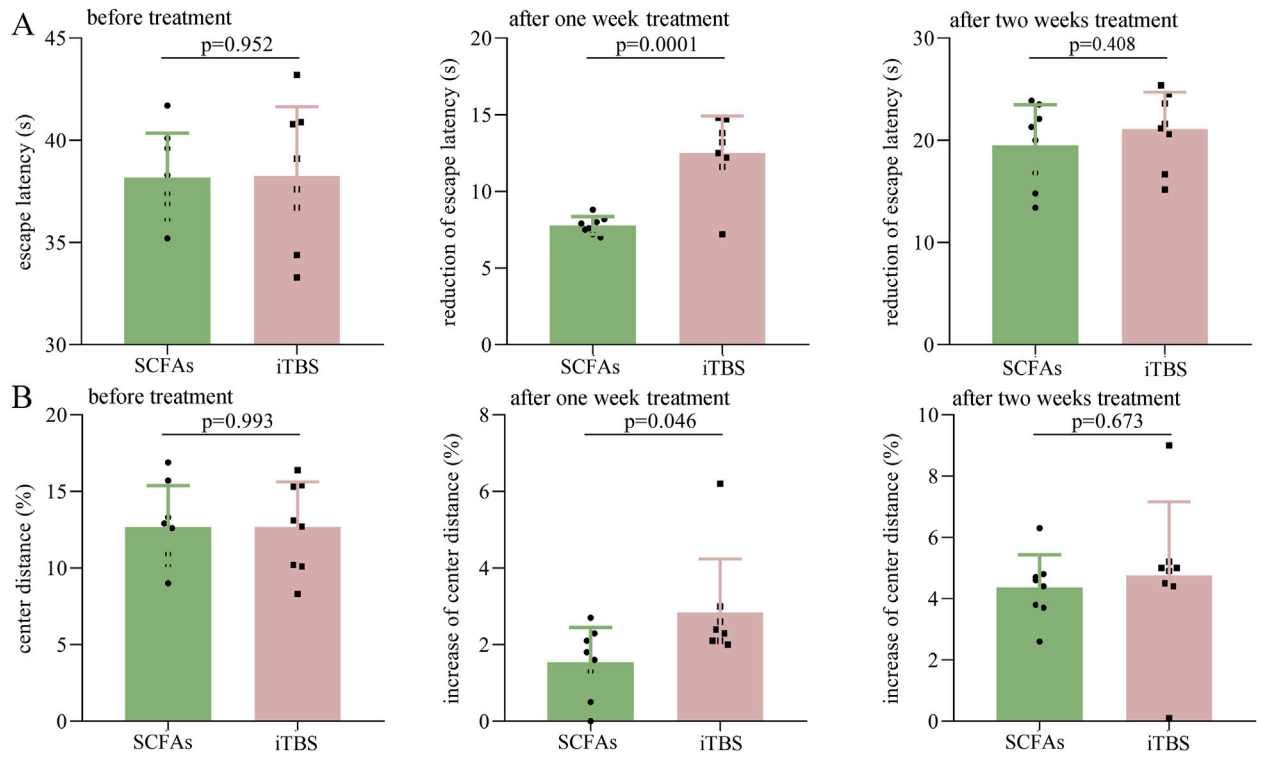


FIGURE 5
Efficacy of SCFAs versus iTBS in the treatment of DEACMP rats. **(A)** Before treatment, the DEACMP + SCFAs and DEACMP + iTBS groups had similar escape latency. The reduction in escape latency was significantly higher in the DEACMP + iTBS group than in the DEACMP + SCFAs group after 1 week of treatment but was similar between the two groups after 2 weeks of treatment. **(B)** Before treatment, the two groups had similar center distance (%). The increase in center distance (%) was significantly higher in the DEACMP + iTBS group than in the DEACMP + SCFAs group after 1 week of treatment but was similar between the two groups after 2 weeks of treatment. DEACMP, delayed encephalopathy after acute carbon monoxide poisoning; SCFAs, short-chain fatty acids; iTBS, intermittent theta burst stimulation.

Inflammatory levels after SCFA treatment

At the end of the intervention (Figure 6A), compared to the control, the DEACMP + placebo group had significantly higher levels of IL-1β ($p < 0.0001$), IL-6 ($p < 0.0001$), and TNF-α ($p < 0.0001$). However, we found that the levels of IL-1β ($p = 0.175$), IL-6 ($p = 0.124$), and TNF-α ($p = 0.104$) were similar between the control and the DEACMP + SCFA groups; the levels of IL-1β ($p = 0.0001$), IL-6 ($p < 0.0001$), and TNF-α ($p < 0.0001$) were significantly lower in the DEACMP + SCFA group than in DEACMP + placebo group. These results showed that SCFAs could significantly relieve inflammation levels in the hippocampus of DEACMP rats.

Both GPR41 and GPR43 levels were found to be significantly lower in the DEACMP + placebo group than in both the control ($p = 0.009$, $p = 0.006$) and DEACMP + SCFAs groups ($p = 0.010$, $p = 0.017$, Figure 6B). The control and DEACMP + SCFAs groups had similar GPR41 ($p = 0.560$) and GPR43 ($p = 0.502$) levels (Figure 6B). Spearman's correlation analysis was used to determine the potential correlations between IL-1β/IL-6/TNF-α and GPR41/GPR43. The results showed that GPR41 was significantly correlated with IL-1β ($r = -0.626$, $p = 0.001$), IL-6 ($r = -0.620$, $p = 0.001$), and TNF-α ($r = -0.538$, $p = 0.007$), and GPR43 was significantly correlated with IL-1β ($r = -0.416$, $p = 0.043$) and TNF-α ($r = -0.422$, $p = 0.040$, Figure 6C). These results show that SCFAs may regulate inflammation levels through their receptors, such as GPR41 and GPR43.

Neurotransmitter levels after SCFA treatment

Neurotransmitters in the catecholamine pathway were detected in this study, and eight neurotransmitters in the hippocampus were successfully identified: dopamine, L-phenylalanine, vanillylmandelic acid, phenylethylamine, tyramine, 3,4-dihydroxyphenylacetic acid, L-tyrosine, and norepinephrine (Figure 7A). Compared to the control group, the DEACMP + placebo group had significantly lower levels of dopamine ($p = 0.008$) and norepinephrine ($p = 0.003$). However, compared to the control group, the DEACMP + SCFAs group had similar levels of dopamine ($p = 0.861$) and norepinephrine ($p = 0.589$). The DEACMP + SCFAs group had significantly higher levels of dopamine ($p = 0.002$) and norepinephrine ($p = 0.004$) than the DEACMP + placebo group. These results indicate that SCFAs could effectively improve dopamine and norepinephrine dysregulations.

Spearman's correlation analysis was used to investigate the potential correlations between differential neurotransmitters and inflammatory factors. The results revealed close relationships between the differential neurotransmitters and inflammatory factors: dopamine vs. IL-6 ($r = -0.454$, $p = 0.026$) and TNF-α ($r = -0.568$, $p = 0.004$); norepinephrine vs. IL-1β ($r = -0.513$, $p = 0.010$), IL-6 ($r = -0.633$, $p = 0.0010$), and TNF-α ($r = -0.600$, $p = 0.002$, Figure 7B). We found that the escape latency was significantly

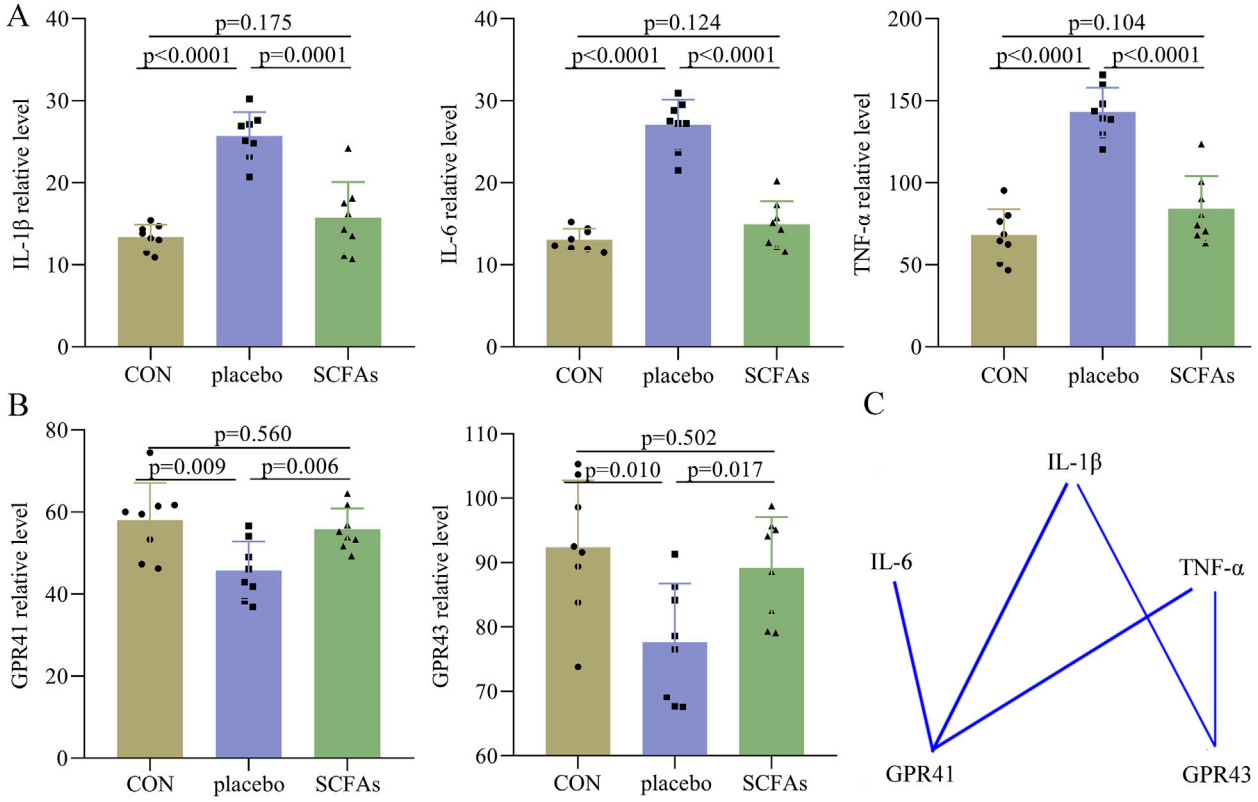


FIGURE 6
Effects of SCFAs on inflammatory factors and SCFA receptors. **(A)** At the end of treatment, we found that the DEACMP + placebo group had significantly higher levels of IL-1β, IL-6, and TNF-α than the control group, but the levels of these inflammatory factors were similar between the control group and DEACMP + SCFA group. **(B)** At the end of treatment, we found that the DEACMP + placebo group had significantly lower levels of GPR41 and GPR43 than the control group, but the levels of these inflammatory factors were similar between the control group and the DEACMP + SCFAs group. **(C)** There were significant correlations between IL-1β/IL-6/TNF-α and GPR41/GPR43. The blue line indicates a negative correlation. CON, control; DEACMP, delayed encephalopathy after acute carbon monoxide poisoning; iTBS, intermittent theta burst stimulation; GPR41, G protein-coupled receptor 41; GPR43, G protein-coupled receptor 43.

correlated with dopamine ($r = -0.410$, $p = 0.046$) and norepinephrine ($r = -0.733$, $p < 0.0001$), and center distance (%) was significantly correlated with norepinephrine ($r = 0.603$, $p = 0.002$, Figure 7B)). These results indicate that these two differential neurotransmitters may play important roles in inflammation levels and behavior in DEACMP rats.

Discussion

In phase I of this study, we found that DEACMP rats had significant cognitive dysfunction and anxiety symptoms compared to control rats. The significantly increased levels of three inflammatory factors (IL-1β, IL-6, and TNF-α) in the hippocampus and decreased levels of two SCFAs (acetate and propionate) in the serum were found in the DEACMP rats. In phase II of this study, we found that both SCFA solution (acetate and propionate) and iTBS could effectively relieve cognitive dysfunction and anxiety symptoms in DEACMP rats. After 2 weeks of treatment, the decreased SCFA receptors (GPR41 and GPR43), increased inflammatory factors (IL-1β, IL-6, and TNF-α), and decreased neurotransmitters (dopamine and norepinephrine) were significantly improved in DEACMP + SCFAs rats. These results suggested that the cognitive dysfunction and anxiety symptoms may be closely related to the inflammation or neurotransmitter levels in the hippocampus of DEACMP rats, and the combination of acetate and propionate may be an effective method for DEACMP. Acetate/propionate–GPR41/GPR43–IL-1β/IL-6/TNF-α–dopamine/norepinephrine may be a potential pathway in SCFA treatment for DEACMP.

rTMS can have neuroprotective effects. Compared to rTMS, iTBS—as a new model of rTMS—needs a shorter time and can produce more long-lasting effects (Chung et al., 2015). However, the neuroprotective mechanisms of iTBS are still unknown. Current evidence suggests that the mechanism of action of this method is mainly related to the regulation of neuronal excitability (Pabst et al., 2022). Shen et al. (2024) reported that iTBS played a neuroprotective role in cerebral ischemia/reperfusion injury by inhibiting endoplasmic reticulum stress and ferroptosis. Considering the close interactions between the nervous and immune systems (Yoo and Mazmanian, 2017), we speculated that iTBS could reduce neuronal death by affecting the immune system and then exerting neuroprotective effects. Interestingly, our study found that iTBS could significantly improve cognitive dysfunction and inflammation levels in DEACMP rats. However, due to the lack of direct evidence, this speculation must be explored in future studies.

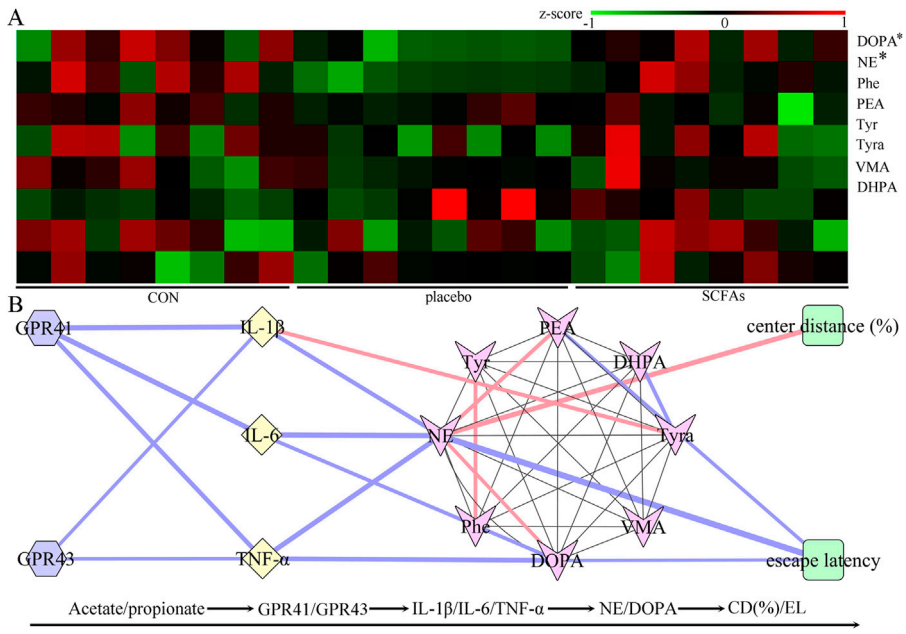


FIGURE 7
Potential pathway of SCFAs in the treatment of DEACMP. **(A)** After 2 weeks of SCFA treatment, the decreased levels of dopamine and norepinephrine in DEACMP rats were significantly increased. **(B)** There were significant correlations between the differential inflammatory factors and catecholamine neurotransmitters (mainly dopamine and norepinephrine), and escape latency and center distance (%) were also mainly correlated with dopamine and norepinephrine. Considering the relationships between SCFA receptors (GPR41 and GPR43) and inflammatory factors, these results suggest that Acetate/propionate–GPR41/GPR43–IL-1β/IL-6/TNF-α–dopamine/norepinephrine may be a potential SCFA pathway in the treatment of DEACMP. Blue and pink lines indicate negative and positive correlations, respectively; the thicker the line, the greater the correlation coefficient. The * indicates the p-value of the DEACMP + SCFA group vs. the DEACMP + placebo group (DOPA, $p = 0.002$; NE, $p = 0.004$). CON, control; DEACMP, delayed encephalopathy after acute carbon monoxide poisoning; SCFAs, short-chain fatty acids; Phe, L-phenylalanine; PEA, phenylethylamine; Tyr, L-tyrosine; Trya, tyramine; DOPA, dopamine; NE, norepinephrine; DHPA, 3,4-dihydroxyphenylacetic acid; VMA, vanillylmandelic acid; GPR41, G protein-coupled receptor 41; GPR43, G protein-coupled receptor 43.

SCFAs have a crucial role in maintaining immune functions, host metabolism, and the gut barrier (Kim, 2023). As a two-carbon SCFA, acetate not only serves as an important energy source but also has an anti-inflammatory function. Previous research found that acetate could regulate the nucleotide-binding oligomerization domain-like receptor protein 3 (NLRP3) inflammasome via GPR43 and Ca2+-dependent mechanisms (Jiang et al., 2019). Propionate, a three-carbon SCFA, can also reduce inflammation levels in the body. Filippone et al. (2020) found that propionate has anti-inflammatory properties and proposed that it could be a potential treatment method for inflammatory diseases. In this study, we found that compared to DECAMP + placebo rats, DECAMP + SCFA rats had significantly lower levels of IL-1β, IL-6, and TNF-α in the hippocampus. Moreover, the levels of GPR41 and GPR43 were significantly increased in DECAMP + SCFAs rats. Considering that GPR41 and GPR43 are the important receptors in microglia (Butovsky and Weiner, 2018), our present results suggest that the combination of acetate and propionate produced anti-inflammatory effects by increasing GPR41 and GPR43 levels to regulate the state of microglia which ultimately improved the cognitive dysfunction and anxiety symptoms in DEACMP rats.

Catecholamines have the closest relationships with many CNS functions, such as cognitive function and motor control (Kobayashi, 2001). Disruptions in the catecholamine pathway are involved in many neuropsychiatric diseases. Currently, dopamine is known to play a crucial role in most cognitive functions, and dopamine dysregulation is viewed as a hallmark of many neuropsychiatric diseases (Costa and Schoenbaum, 2022). Norepinephrine is synthesized from dopamine and has been found to be related to cognitive deficits in maternal mice (Liu et al., 2020). In this study, we found two significantly changed catecholaminergic neurotransmitters (dopamine acid and norepinephrine) in DEACMP rats, and their levels were significantly restored after SCFA intervention. In addition, increased inflammation levels in the brain may disrupt the neurotransmitters there (Gorji, 2022; Oshaghi et al., 2023). Therefore, the results of our study indicated that SCFAs might regulate the catecholamine pathway by modulating the inflammation levels in the hippocampus to ultimately produce good effects in DEACMP rats.

Additionally, previous research has reported a close relationship between SCFAs and neurogenesis (Vicentini et al., 2021; Agnihotri and Mohajeri, 2022). Neurogenesis is the process of brain cell growth and repair. Vicentini et al. (2021) found that SCFA could regulate enteric neuronal survival and also stimulate neurogenesis. Agnihotri and Mohajeri (2022) found that SCFAs had a direct effect on neuronal growth and neurogenesisin the hippocampus. Interestingly, Ochi et al. (2021) reported an association between delayed CO encephalopathy and the impairment of adult neurogenesis. These results indicate that SCFAs may produce effects on DEACMP by regulating neurogenesis. Meanwhile, evidence has shown neurogenesis to be influenced by neurotransmitters (Ojeda and Ávila, 2019; Cameron et al., 1998; Berg et al., 2013). In this study, we found that the dopamine and norepinephrine disruptions in the hippocampus of DEACMP rats were

significantly improved after SCFA treatment. These findings suggest that the efficacy of SCFAs in the treatment of DEACMP may be related to their potential effects on neurogenesis.

Several limitations should be mentioned here. i) The comparative efficacy of iTBS and SCFAs was assessed with 2-week treatment durations. Thus, the long-term efficacy of these two treatment methods was not assessed here. ii) Only one kind of acetate/propionate dose was used in this study. Future studies should be conducted to assess the efficacy of different acetate/propionate doses in the treatment of DEACMP. iii) In phase I, we found that only acetate and propionate were significantly changed in DEACMP rats; thus, in phase II, only these two SCFAs were used to treat DEACMP rats. However, considering that butyrate was also one of the main three SCFAs, future studies should further explore the efficacy of acetate/propionate/butyrate in the treatment of DEACMP.

Conclusion

Our study first investigated the efficacy of iTBS and SCFAs in DEACMP rats. The increased inflammation levels in the hippocampus of DEACMP rats could be restored after iTBS or SCFA treatment, and SCFAs could also improve the decreased levels of dopamine and norepinephrine in the hippocampus of DEACMP rats. We also found that iTBS might work faster in improving cognitive dysfunction than SCFAs; however, considering the potential side effects and tolerability of iTBS, SCFAs might be more appropriate for DEACMP. However, our findings can be used in future studies for validation and support.

Data availability statement

The original contributions presented in the study are included in the article/supplementary material; further inquiries can be directed to the corresponding authors.

Ethics statement

The animal study was approved by the Ethics Committee of Baotou Central Hospital (Approval No. 2024-YJS-001). The study was conducted in accordance with local legislation and institutional requirements.

Author contributions

TM: conceptualization, data curation, formal analysis, methodology, and writing–original draft. XZ: formal analysis, methodology, project administration, and writing–original draft. JZ: data curation, investigation, validation, and writing–original draft. HX: conceptualization, investigation, validation, and writing–original draft. LY: conceptualization, funding acquisition, resources, and writing–review and editing.

Funding

The authors declare that no financial support was received for the research, authorship, and/or publication of this article.

Conflict of interest

The authors declare that the research was conducted in the absence of any commercial or financial relationships that could be construed as a potential conflict of interest.

Generative AI statement

The authors declare that no generative AI was used in the creation of this manuscript.

Publisher's note

All claims expressed in this article are solely those of the authors and do not necessarily represent those of their affiliated organizations, or those of the publisher, the editors and the reviewers. Any product that may be evaluated in this article, or claim that may be made by its manufacturer, is not guaranteed or endorsed by the publisher.

References

Agnihotri, N., and Mohajeri, M. H. (2022). Involvement of intestinal microbiota in adult neurogenesis and the expression of brain-derived neurotrophic factor. *Int. J. Mol. Sci.* 23 (24), 15934. doi:10.3390/ijms232415934

Berg, D. A., Belnoue, L., Song, H., and Simon, A. (2013). Neurotransmitter-mediated control of neurogenesis in the adult vertebrate brain. *Development* 140 (12), 2548–2561. doi:10.1242/dev.088005

Butovsky, O., and Weiner, H. L. (2018). Microglial signatures and their role in health and disease. *Nat. Rev. Neurosci.* 19, 622–635. doi:10.1038/s41583-018-0057-5

Cameron, H. A., Hazel, T. G., and McKay, R. D. (1998). Regulation of neurogenesis by growth factors and neurotransmitters. *J. Neurobiol.* 36 (2), 287–306. doi:10.1002/(sici)1097-4695(199808)36:2<287::aid-neu13>3.0.co;2-b

Chen, R. J., Lee, Y. H., Chen, T. H., Chen, Y. Y., Yeh, Y. L., Chang, C. P., et al. (2021). Carbon monoxide-triggered health effects: the important role of the inflammasome and its possible crosstalk with autophagy and exosomes. *Arch. Toxicol.* 95 (4), 1141–1159. doi:10.1007/s00204-021-02976-7

Cheng, J., Hu, H., Ju, Y., Liu, J., Wang, M., Liu, B., et al. (2024). Gut microbiota-derived short-chain fatty acids and depression: deep insight into biological mechanisms and potential applications. *Gen. Psychiatr.* 37 (1), e101374. doi:10.1136/gpsych-2023-101374

Chung, S. W., Hoy, K. E., and Fitzgerald, P. B. (2015). Theta-burst stimulation: a new form of TMS treatment for depression? *Depress Anxiety* 32 (3), 182–192. doi:10.1002/da.22335

Costa, K. M., and Schoenbaum, G. (2022). Dopamine. *Curr. Biol.* 32 (15), R817–R824. doi:10.1016/j.cub.2022.06.060

Dragic, M., Zeljkovic, M., Stevanovic, I., Ilic, T., Ilic, N., Nedeljkovic, N., et al. (2020). Theta burst stimulation ameliorates symptoms of experimental autoimmune encephalomyelitis and attenuates reactive gliosis. *Brain Res. Bull.* 162, 208–217. doi:10.1016/j.brainresbull.2020.06.013

Duscha, A., Gisevius, B., Hirschberg, S., Yissachar, N., Stangl, G. I., Dawin, E., et al. (2020). Propionic acid shapes the multiple sclerosis disease course by an

immunomodulatory mechanism. *Cell* 180 (6), 1067–1080. doi:10.1016/j.cell.2020.02.035

Filippone, A., Lanza, M., Campolo, M., Casili, G., Paterniti, I., Cuzzocrea, S., et al. (2020). The anti-inflammatory and antioxidant effects of sodium propionate. *Int. J. Mol. Sci.* 21 (8), 3026. doi:10.3390/ijms21083026

Gorji, A. (2022). Neuroinflammation: the pathogenic mechanism of neurological disorders. *Int. J. Mol. Sci.* 23 (10), 5744. doi:10.3390/ijms23105744

Han, D., Cheng, J., Chen, Y., Du, H., Lin, Z., Zhong, R., et al. (2024). Evidence for intermittent theta burst transcranial magnetic stimulation for dysphagia after stroke: a systematic review and meta-analysis. *Dysphagia* 40, 54–65. doi:10.1007/s00455-024-10729-8

Harper, A., and Croft-Baker, J. (2004). Carbon monoxide poisoning: undetected by both patients and their doctors. *Age Ageing* 33, 105–109. doi:10.1093/ageing/afh038

Jiang, Z., Wang, C., Li, N., Bo, L., Zha, Y., Bian, J., et al. (2019). Publisher Correction: acetate attenuates inflammasome activation through GPR43-mediated Ca2+-dependent NLRP3 ubiquitination. *Exp. Mol. Med.* 51 (7), 1–13. doi:10.1038/s12276-019-0296-1

Kim, C. H. (2023). Complex regulatory effects of gut microbial short-chain fatty acids on immune tolerance and autoimmunity. *Cell Mol. Immunol.* 20, 341–350. doi:10.1038/s41423-023-00987-1

Kimura, I., Inoue, D., Hirano, K., and Tsujimoto, G. (2014). The SCFA receptor GPR43 and energy metabolism. *Front. Endocrinol. (Lausanne)* 5, 85. doi:10.3389/fendo.2014.00085

Kinoshita, H., Türkan, H., Vucinic, S., Naqvi, S., Bedair, R., Rezaee, R., et al. (2020). Carbon monoxide poisoning. *Toxicol. Rep.* 7, 169–173. doi:10.1016/j.toxrep.2020.01.005

Kobayashi, K. (2001). Role of catecholamine signaling in brain and nervous system functions: new insights from mouse molecular genetic study. *J. Investig. Dermatol Symp. Proc.* 6 (1), 115–121. doi:10.1046/j.0022-202x.2001.00011.x

Liu, Z., Ma, S., Ye, J., Zhang, H., Li, Y., Sair, A. T., et al. (2020). High-dietary fiber intake alleviates antenatal obesity-induced postpartum depression: roles of gut microbiota and microbial metabolite short-chain fatty acid involved. *J. Agric. Food Chem.* 68 (47), 13697–13710. doi:10.1021/acs.jafc.0c04290

Ochi, S., Sekiya, K., Abe, N., Funahashi, Y., Kumon, H., Yoshino, Y., et al. (2021). Neural precursor cells are decreased in the hippocampus of the delayed carbon monoxide encephalopathy rat model. *Sci. Rep.* 11 (1), 6244. doi:10.1038/s41598-021-85860-9

Ojeda, J., and Ávila, A. (2019). Early actions of neurotransmitters during cortex development and maturation of reprogrammed neurons. *Front. Synaptic Neurosci.* 11, 33. doi:10.3389/fnsyn.2019.00033

O'Riordan, K. J., Collins, M. K., Moloney, G. M., Knox, E. G., Aburto, M. R., Fülling, C., et al. (2022). Short chain fatty acids: microbial metabolites for gut-brain axis signalling. *Mol. Cell Endocrinol.* 546, 111572. doi:10.1016/j.mce.2022.111572

Oshaghi, M., Kourosh-Arami, M., and Roozbehkia, M. (2023). Role of neurotransmitters in immune-mediated inflammatory disorders: a crosstalk between the nervous and immune systems. *Neurol. Sci.* 44 (1), 99–113. doi:10.1007/s10072-022-06413-0

Pabst, A., Proksch, S., Médé, B., Comstock, D. C., Ross, J. M., and Balasubramaniam, R. (2022). A systematic review and meta-analysis of the efficacy of intermittent theta burst stimulation (iTBS) on cognitive enhancement. *Neurosci. Biobehav Rev.* 135, 104587. doi:10.1016/j.neubiorev.2022.104587

Scho, S., Brüchle, W., Schneefeld, J., and Rosenkranz, K. (2024). Enhancing neuroplasticity in major depression: a novel 10 Hz-rTMS protocol is more effective than iTBS. *J. Affect Disord.* 367, 109–117. doi:10.1016/j.jad.2024.08.166

Shen, X. Y., Zhang, X. Y., Han, P. P., Zhao, Y. N., Xu, G. H., and Bi, X. (2024). Mechanisms of intermittent theta-burst stimulation attenuating nerve injury after ischemic reperfusion in rats through endoplasmic reticulum stress and ferroptosis. *Mol. Biol. Rep.* 51 (1), 377. doi:10.1007/s11033-024-09241-x

Stanojevic, J., Dragic, M., Stevanovic, I., Ilic, T., Stojanovic, I., Zeljkovic, M., et al. (2022). Intermittent theta burst stimulation ameliorates cognitive impairment and hippocampal gliosis in the Streptozotocin-induced model of Alzheimer's disease. *Behav. Brain Res.* 433, 113984. doi:10.1016/j.bbr.2022.113984

Tian, Li, Na, X., Jin-feng, Z., Li-sha, Z., Qin, R., Ting-yi, Z., et al. (2024). Effects of short-chain fatty acids on cognitive impairment induced by benzo[a] pyrene in mice. *J. Environ. Hyg.* 14 (3), 218–225. doi:10.13421/j.cnki.hjwsxzz.2024.03.006

Vicentini, F. A., Keenan, C. M., Wallace, L. E., Woods, C., Cavin, J. B., Flockton, A. R., et al. (2021). Intestinal microbiota shapes gut physiology and regulates enteric neurons and glia. *Microbiome* 9 (1), 210. doi:10.1186/s40168-021-01165-z

Wang, H., Li, Y., Wu, Q., Xu, C., and Liu, Q. (2016). Combination of butylphthalide with umbilical mesenchymal stem cells for the treatment of delayed encephalopathy after carbon monoxide poisoning. *Med. Baltim.* 5 (49), e5412. doi:10.1097/MD.0000000000005412

Xiang, W., Xue, H., Wang, B., Li, Y., Zhang, J., Jiang, C., et al. (2017a). Combined application of dexamethasone and hyperbaric oxygen therapy yields better efficacy for patients with delayed encephalopathy after acute carbon monoxide poisoning. *Drug Des. Devel Ther.* 11, 513–519. doi:10.2147/DDDT.S126569

Xiang, W., Xue, H., Wang, B., Li, Y., Zhang, J., Jiang, C., et al. (2017b). Efficacy of N-butylphthalide and hyperbaric oxygen therapy on cognitive dysfunction in patients with delayed encephalopathy after acute carbon monoxide poisoning. *Med. Sci. Monit.* 23, 1501–1506. doi:10.12659/msm.899499

Xiang, W., Yang, Z., Xue, H., Wang, J., Niu, F., Wang, J., et al. (2021). P2Y12 receptor-mediated microglia activation involved in delayed encephalopathy after acute carbon monoxide poisoning. *Aging (Albany NY)* 13 (4), 6134–6143. doi:10.18632/aging.202607

Xiang, W. P., Xue, H., and Wang, B. J. (2014). Delayed encephalopathy of acute carbon monoxide intoxication in rats: potential mechanism and intervention of dexamethasone. *Pak J. Pharm. Sci.* 27 (6 Suppl. l), 2025–2028.

Xu, X. M., Luo, H., Rong, B. B., Zheng, X. M., Wang, F. T., Zhang, S. J., et al. (2019). Management of delayed encephalopathy after CO poisoning: an evidence-based narrative review. *Med. Baltim.* 98 (49), e18199. doi:10.1097/MD.0000000000018199

Yoo, B. B., and Mazmanian, S. K. (2017). The enteric network: interactions between the immune and nervous systems of the gut. *Immunity* 46 (6), 910–926. doi:10.1016/j.immuni.2017.05.011

Zheng, B., Chen, J., Cao, M., Zhang, Y., Chen, S., Yu, H., et al. (2024). The effect of intermittent theta burst stimulation for cognitive dysfunction: a meta-analysis. *Brain Inj.* 38 (9), 675–686. doi:10.1080/02699052.2024.2344087

frontiers | Frontiers in Pharmacology

TYPE Original Research
PUBLISHED 04 April 2025
DOI 10.3389/fphar.2025.1507397

Check for updates

OPEN ACCESS

EDITED BY
Pukar Khanal,
Emory University, United States

REVIEWED BY
Ashutosh Pareek,
Banasthali Vidyapith, India
Archana Patil,
KLE College of Pharmacy, India

*CORRESPONDENCE
Mohammad Hossein Farzaei,
mh.farzaei@gmail.com
Javier Echeverría,
javier.echeverriam@usach.cl

RECEIVED 07 October 2024
ACCEPTED 20 February 2025
PUBLISHED 04 April 2025

CITATION
Amirian R, Mohammadi Pour P, Maleki H, Fakhri S, Asgary S, Farzaei MH and Echeverría J (2025) Evaluating the anti-neuropathic effects of the thymol-loaded nanofibrous scaffold in a rat model of spinal cord injury.
Front. Pharmacol. 16:1507397.
doi: 10.3389/fphar.2025.1507397

COPYRIGHT
© 2025 Amirian, Mohammadi Pour, Maleki, Fakhri, Asgary, Farzaei and Echeverría. This is an open-access article distributed under the terms of the Creative Commons Attribution License (CC BY). The use, distribution or reproduction in other forums is permitted, provided the original author(s) and the copyright owner(s) are credited and that the original publication in this journal is cited, in accordance with accepted academic practice. No use, distribution or reproduction is permitted which does not comply with these terms.

Evaluating the anti-neuropathic effects of the thymol-loaded nanofibrous scaffold in a rat model of spinal cord injury

Roshanak Amirian[1,2,3], Pardis Mohammadi Pour[4], Hassan Maleki[1], Sajad Fakhri[1], Sedigheh Asgary[5], Mohammad Hossein Farzaei[1]* and Javier Echeverría[6]*

[1]Pharmaceutical Sciences Research Center, Health Institute, Kermanshah University of Medical Sciences, Kermanshah, Iran, [2]Student Research Committee, School of Pharmacy, Kermanshah University of Medical Sciences, Kermanshah, Iran, [3]USERN Office, Kermanshah University of Medical Sciences, Kermanshah, Iran, [4]Department of Pharmacognosy, Faculty of Pharmacy, Tehran University of Medical Sciences, Tehran, Iran, [5]Isfahan Cardiovascular Research Center, Cardiovascular Research Institute, Isfahan University of Medical Sciences, Isfahan, Iran, [6]Departamento de Ciencias del Ambiente, Facultad de Química y Biología, Universidad de Santiago de Chile, Santiago, Chile

Background: Spinal cord injury (SCI) is a debilitating condition characterized by partial or complete loss of motor and sensory function caused by mechanical trauma to the spinal cord. Novel therapeutic approaches are continuously explored to enhance spinal cord regeneration and functional recovery.

Purpose: In this study, we investigated the efficacy of the poly(vinyl alcohol) and chitosan (PVA/CS) scaffold loaded with different thymol concentrations (5, 10, and 15 wt%) in a rat compression model for SCI treatment compare to other (e.g., thymol and scaffold) control groups.

Results and discussion: The thymol-loaded scaffold exhibited a smooth surface and a three-dimensional nanofibrous structure with nanoscale diameter. The conducted analyses verified the successful incorporation of thymol into the scaffold and its high water absorption, porosity, and wettability attributes. Behavioral assessment of functional recovery showed improving sensory and locomotor impairment. Furthermore, histopathological examinations indicated the regenerative potential of the thymol-loaded nanofiber scaffold, by neuronal survival.

Conclusion: Therefore, these findings suggest that the thymol-loaded nanofibrous scaffolds have promising pharmacological activities for alleviating neuropathic pain and addressing complications induced by SCI.

KEYWORDS

spinal cord injury, motor activity, neuropathic pain, thymol-scaffold, chitosan, poly(vinyl alcohol)

1 Introduction

Neuropathic pain is a sort of continual ache that occurs when damage or disorder affects the somatosensory nervous system, impacting 7%–10% of the world population (Colloca et al., 2017). Neuropathic pain due to spinal cord injury (SCI), can bring about a lack of sensation, movement, bowel and bladder management, and can range in rigor from mild to

intense (Alizadeh et al., 2019; Joosten and Franken, 2020). Recent investigations have discerned that the modulation of apoptotic gene expression, with potential implications for neuropathic pain, is orchestrated by reactive oxygen species (ROS) and inflammatory factors (Siniscalco et al., 2007). Consequently, ROS assumes a pivotal role in the cascade of events associated with nerve damage, concomitant with processes such as caspase activation, glial activation, and mitochondrial dysfunction (Andersen, 2004). A spectrum of pain medicinal drugs, such as anticonvulsant pills, can also correctly lessen neuropathic pain. Gabapentin is the first line of medication in neuropathic pain (Levendoğlu et al., 2004), and anti-inflammatory drugs such as nonsteroidal anti-inflammatory drugs (NSAIDs) (Colloca et al., 2017; Hayta and Elden, 2018; Terzi et al., 2018; Gurba and Haroutounian, 2022), are effective in reducing neuropathic pain and may be used in combination with other pain medication. Topical treatments containing capsaicin a compound in chili peppers, acts on the transient receptor potential cation channel subfamily V member 1 (TRPV1) receptor to provide analgesic effects by desensitizing pain pathways (Hall et al., 2020; Liau et al., 2020; Zheng et al., 2020; Olusanya et al., 2023).

Herbal medications are sometimes used as complementary or alternative treatments for SCI (Nayak et al., 2001; Boyd et al., 2019). While their therapeutic efficacy has yet to undergo extensive scientific investigation, herbal remedies are garnering increasing attention as a potentially viable alternative owing to their favorable safety profiles in contrast to conventional pharmacological agents. Prominent herbal constituents employed in the context of SCI management encompass curcumin (Indermun et al., 2019; Jin et al., 2021; Li et al., 2021) and ginger (Andrei et al., 2022; Shen C.-L. et al., 2022). Renowned for their anti-inflammatory attributes, these herbs hold promise in mitigating the pain and inflammation typically associated with spinal cord injuries. Furthermore, noteworthy research has indicated that *Ginkgo biloba* L. [Ginkgoaceae] (Kim et al., 2009; Al-Adwani et al., 2019) may augment cerebral and spinal cord blood circulation, accompanied by potential neuroprotective properties that could facilitate the recuperative process following spinal cord injuries. Additionally, thymol (2-isopropyl-5-methylphenol) is the main naturally occurring monoterpene phenol prevalent in thyme essential oils, particularly *Thymus vulgaris* L. [Lamiaceae], and has demonstrated anti-inflammatory and analgesic qualities (Costa et al., 2019; Sheorain et al., 2019; Wang W. et al., 2020; Zheng et al., 2022). This effective agent is appropriate to utilize as an anti-inflammatory activity by inactivating the calcium channels or initiating a corresponding decrease in elastase (Braga et al., 2006), and antioxidant activity was proven by the (2,2-diphenyl-1-picrylhydrazyl) (DPPH) and human red blood cell stabilization methods (Sheorain et al., 2019). However, thymol has a strong irritating/bitter taste and a low aqueous solubility. These physicochemical characteristics lead to the development of pharmaceutical preparation that covers these undesirable characteristics (Nieddu et al., 2014). Besides herbs, the use of scaffolds and thymol in SCI treatment is an area of abiding research in regenerative medicine (Qian et al., 2021; Zheng et al., 2022).

Scaffolds are critical in SCI management, as they provide structural support that closely mimics the natural extracellular matrix (ECM) and thus present a conducive environment for cell adhesion, proliferation, and differentiation, which are key to tissue regeneration (Stokols and Tuszynski, 2004). Nanofibrous scaffolds, often fabricated by the electrospinning process, possess particular advantages due to their nanoscale fibrous architecture, which closely mimics the composition of the ECM. This resemblance increases the scaffold's ability for cell adhesion, migration, and nutrient exchange, which are essential in nerve tissue regeneration (Zhang et al., 2019).

Nanofibrous scaffolds are also effective platforms for localized drug delivery, allowing controlled, sustained release of therapeutic agents directly to the injury site (Faccendini et al., 2017). This localized approach is advantageous for SCI treatment, as it delivers a concentrated dose of bioactive compounds like thymol precisely where needed, reducing systemic side effects (Faccendini et al., 2017).

By combining poly (vinyl alcohol (PVA) and chitosan (CS), two polymers favorable for the fabrication of electrospun nanofibers (NFs), we strengthen the scaffold and make it more stable ensuring it can withstand compression without losing its shape or structural integrity. This is crucial, for creating an environment that promotes tissue regeneration and aids in the recovery of cord function. Additionally, the hydrophilic properties of PVA and CS contribute to the scaffold's functionality. The scaffold's porosity and permeability are vital for infiltration and nutrient exchange. By processing PVA and CS create a scaffold with high porosity allowing for the diffusion of oxygen, nutrients, and waste products. Furthermore, such nanofibrous scaffolds can effectively encapsulate and deliver substances.

In this study, we loaded the nanofibrous scaffold with thymol, a compound with well-reported analgesic anti-inflammatory and antioxidant properties (Yanishlieva et al., 1999; Braga et al., 2006; Ghori et al., 2016) that has also been certified Generally Recognized As Safe (GRAS) by the Food and Drugs Administration (FDA). By incorporating it into the scaffold we achieved controlled and localized delivery, to the injured area, thereby enhancing the effectiveness of the treatment (Zhang et al., 2019). In the realm of SCI, scaffolds serve as a structural foundation, facilitating the growth and regeneration of compromised neural tissue (Koffler et al., 2019; Cheng et al., 2022). A current focus of investigation involves thymol-loaded nanofibrous scaffolds, under scrutiny for their potential to augment tissue regeneration and mitigate pain (Chen et al., 2020; Yue et al., 2021). The underlying principle driving the utilization of thymol-loaded nanofibrous scaffolds revolves around the fusion of thymol's therapeutic advantages with the supportive attributes inherent to nanofibrous scaffolds.

Abbreviations: ANOVA, analysis of variance; BBB, Basso, Beattie, and Bresnahan; CS, chitosan; DSC: Differential scanning calorimetry; DPPH, (2,2-diphenyl-1-picrylhydrazyl); ECM, extracellular matrix; FT-IR, Fourier transform infrared; GRAS, Generally Recognized As Safe; FDA, Food and Drugs Administration; hEnSCs, human endometrial stem cells; IL-1β, interleukin 1 beta; IL-6, interleukin 6; IP, injected intraperitoneal; NMDA, N-methyl-D-aspartate; NSAIDs, nonsteroidal anti-inflammatory drugs; NFs, nanofibers; PBS, phosphate buffered saline; PCL, poly ε-caprolactone; Pox, poly(2-ethyl-2-oxazoline); PVA, poly(vinyl alcohol); ROS, reactive oxygen species; SCI, spinal cord injury; SEM, Scanning electron microscopy; SIPN, semi-interpenetrating polymer network; TNF-α, tumor necrosis factor-alpha; TRPV1, transient receptor potential cation channel subfamily V member 1.

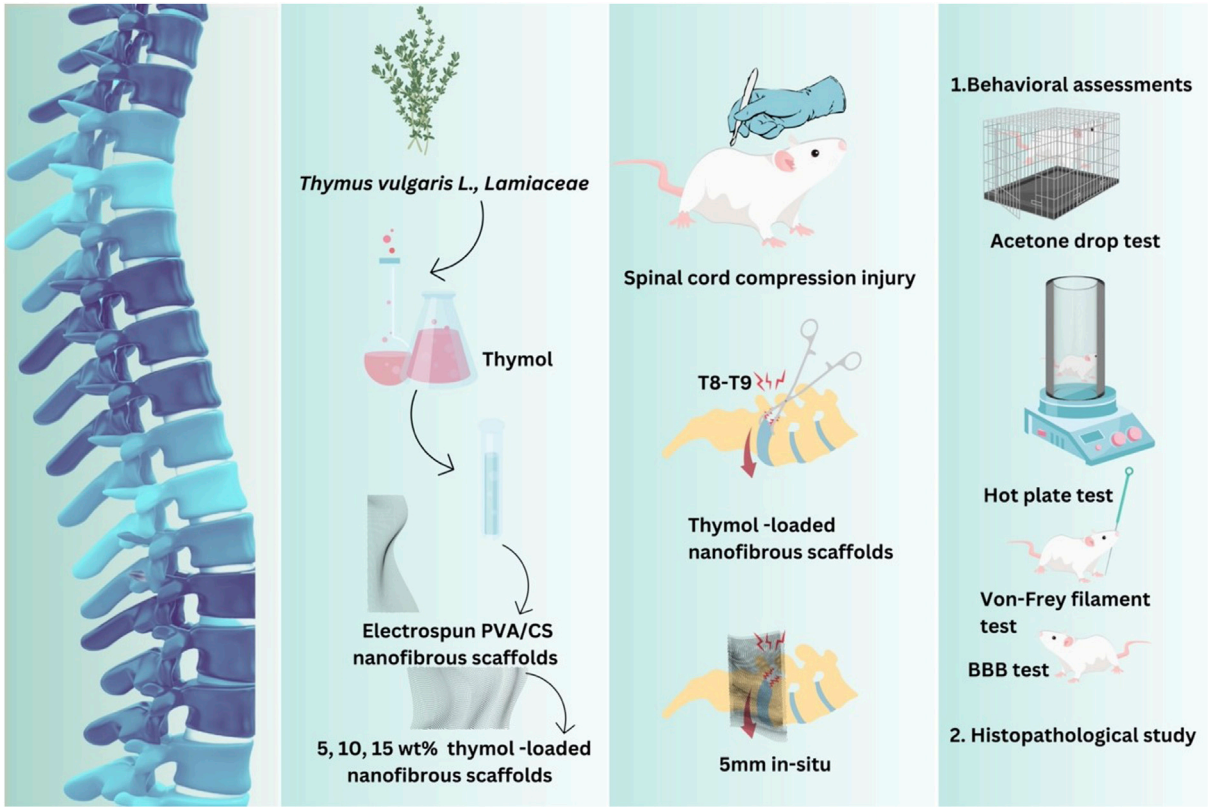


FIGURE 1
Experimental design was conducted using a rat compression model of SCI to evaluate the therapeutic potential of poly(vinyl alcohol)/chitosan (PVA/CS) scaffolds loaded with varying concentrations of thymol (5, 10, and 15 wt%). The timeline of the experiment included scaffold implantation immediately post-injury, followed by behavioral assessments (e.g., locomotor and sensory function) at regular intervals. Histopathological analyses were performed at the endpoint to evaluate overall tissue regeneration. The design aimed to compare the efficacy of thymol-loaded scaffolds against controls in promoting functional recovery and reducing neuropathic pain associated with SCI.

2 Methods and materials

2.1 Materials

Poly (vinyl alcohol) (PVA, Mw: 72 kDa), chitosan (CS, MW: 190–300 kDa, 75%–85% deacetylated), 2,2-diphenyl-1-picrylhydrazyl (DPPH) and thymol (CAS No: 89-83-8) were obtained from Sigma-Aldrich (Steinheim, Germany). Acetic acid and ethanol were bought from Merck Company (Darmstadt, Germany).

2.2 Fabrication of thymol-loaded nanofibrous scaffolds

The blank PVA/CS nanofibrous scaffold and the scaffold containing thymol were fabricated with the electrospinning technique. To prepare the blank scaffold, a mixture of PVA (10% w/v) and CS (2% w/v) was blended at the ratio of 80: 20 v/v. Then, the polymeric mixture was subjected to electrospinning at room temperature (25°C), set at +20 kV applied voltage, flow rate 1 mL/h, and a 15 cm tip-to-collector distance. Likewise, thymol (5–15 wt%) was added to the PVA/CS blended solution and was converted to the electrospun fibers at the same condition. After that, they were removed from the aluminium sheet and stored for further characterizations and examinations.

2.3 Characterization of the scaffolds

Scanning electron microscopy (S-4700, Hitachi Ltd., Tokyo, Japan) at an accelerating voltage of 30.0 kV after a gold plasma sputtering characterized the scaffolds' morphology and diameter distribution. Besides, studying the interactions between the scaffold ingredients and endorsing the incorporation of thymol was conducted using Fourier transform infrared (FT-IR) spectrophotometer (IR Affinity 1S, Shimadzu, Japan) from 400 to 4,000 cm^{-1} at room temperature. The water absorption capacity and the surface wettability of the scaffolds were determined by immersion in water (pH 7.4) at 37°C and water contact angle measurement through the sessile drop technique, respectively (Doostan et al., 2023). Moreover, the antioxidant activity of the prepared scaffolds was performed via DPPH radical scavenging assay as previously described (Mastelić et al., 2008).

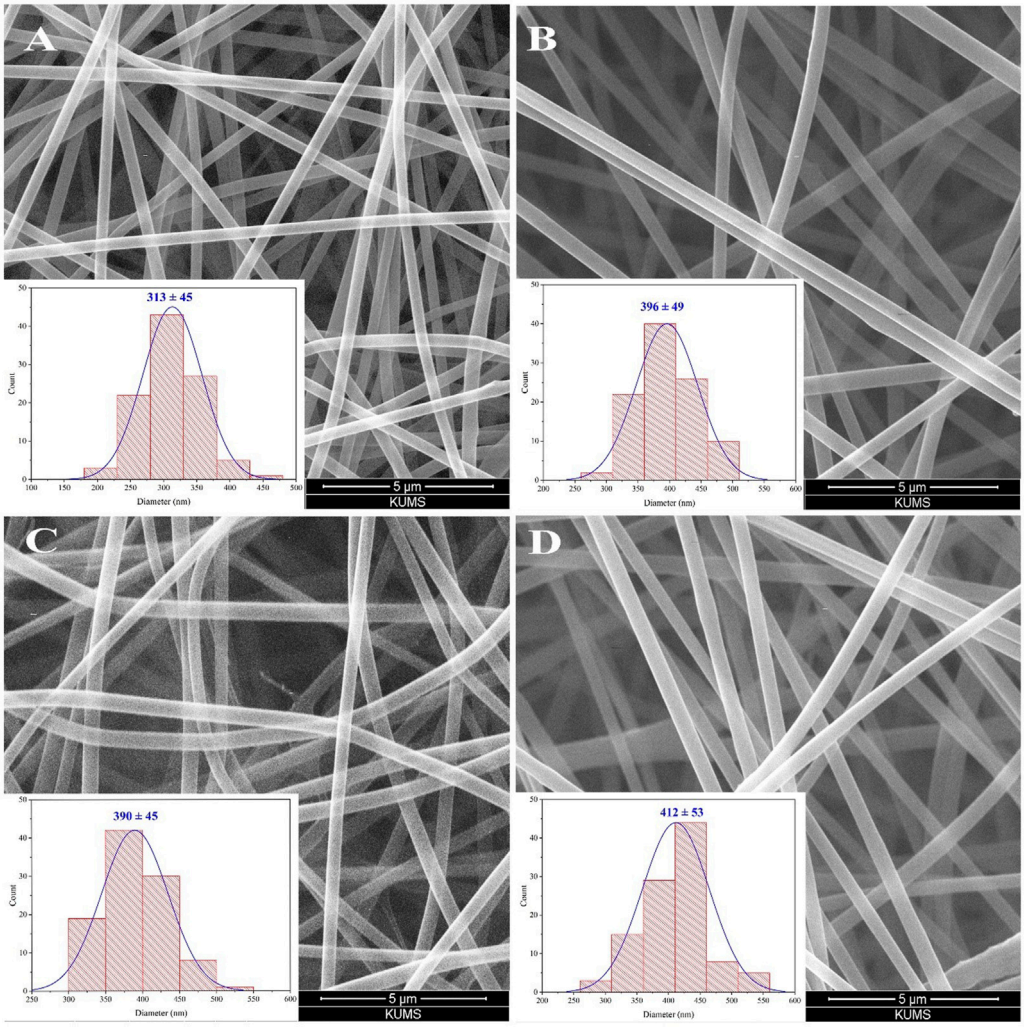


FIGURE 2
SEM image of blank PVA/CS scaffold **(A)** and the scaffold containing 5 wt% **(B)**, 10 wt% **(C)**, and 15 wt% **(D)** thymol with corresponding diameter distribution histograms.

Furthermore, thermal analysis was conducted using Differential Scanning Calorimetry (DSC) to elucidate the thymol-polymer interactions and structural transitions (Zeugolis and Raghunath, 2010). The samples, including pure thymol, blank scaffold, and loaded scaffold, were analyzed with a thermal analyzer (NETZSCH STA 449 F3 Jupiter, Germany) under a nitrogen atmosphere from 25°C to 100°C at a rate of 10°C/min.

2.4 *In vivo* model for spinal cord injury

In the study, 42 adult male Wistar rats weighing (220–260 g) were bought from Aftab Lorestan and held in the central animal house, at Kermanshah University of Medical Sciences. Animals were fed *ad libitum* and kept under standard conditions (light/dark cycle for 12 h in relative humidity of 60% ± 5% and temperature of 24°C ± 2°C). Procedures were performed following the policies for the treatment and care of laboratory animals published by The Iranian National Institute of Health and approved by the Ethics Committee at the Kermanshah University of Medical Sciences (Ethical code: IR.NIMAD.REC.1400.108). All actions were made to relieve mouse distress.

Rats were randomly split into seven groups each six rats as follows: 1) Group 1 (Sham group): received laminectomy without injury and were treated with normal saline; 2) Group 2: received compression injury; 3) Group 3: received compression injury and were treated with thymol (5 mg/kg, intraperitoneally); 4) Group 4: received compression injury and were treated with just the blank scaffold (*in-situ*); 5) Group 5: received compression injury and were treated with the nanofibrous scaffold containing 5 wt% thymol (*in-situ*); 6) Group 6: received compression injury and were treated with the nanofibrous scaffold containing 10 wt% thymol (*in-situ*); 7) Group 7: received compression injury and were treated with the nanofibrous scaffold containing 15 wt% thymol (*in-situ*).

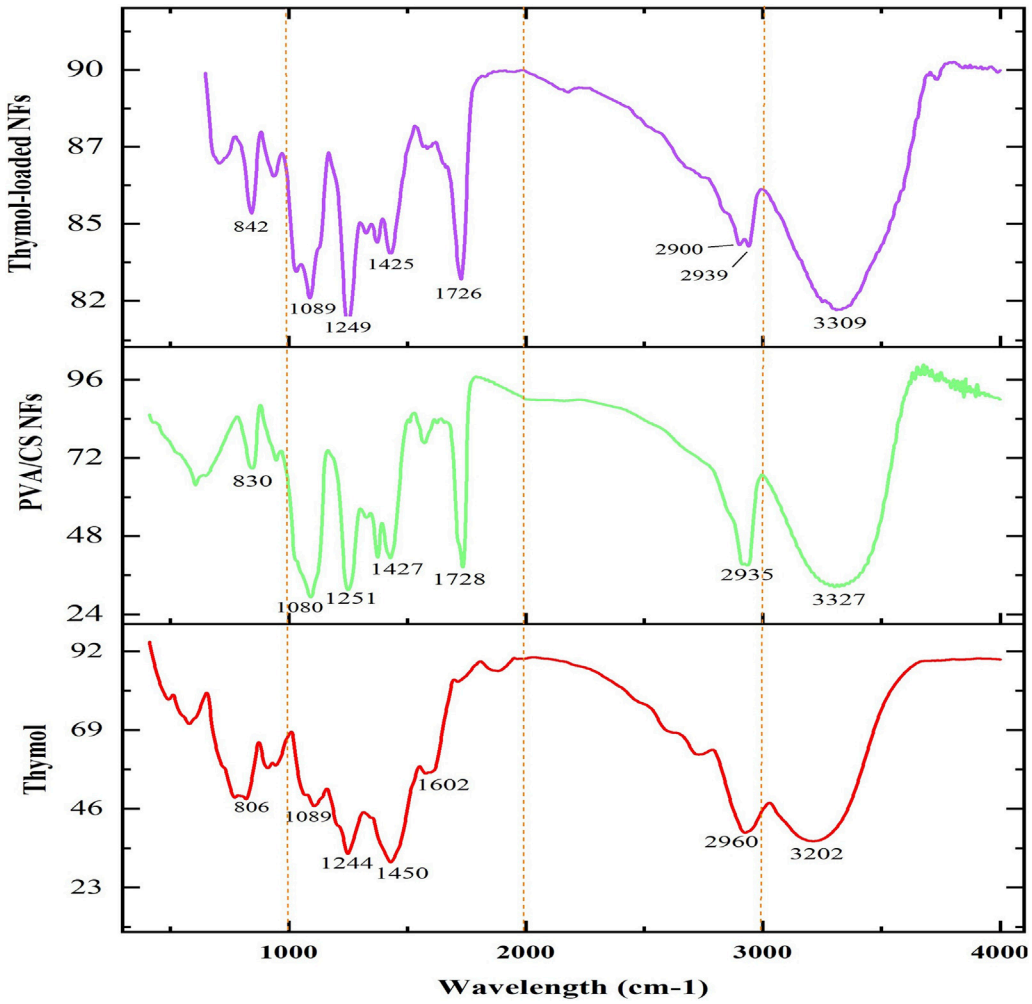


FIGURE 3
FT-IR spectrum of thymol, blank PVA/CS scaffold, and thymol-loaded PVA/CS scaffold.

2.5 Induction of spinal cord injury via compression

Animals were transferred to the laboratory before testing to be adapted to the environment. Anesthesia was induced in rats, by the mixture of ketamine (80 mg/kg) and xylazine (10 mg/kg) injected intraperitoneal (IP). The surgical area was shaved and disinfected with ethanol 70%. Laminectomy was accomplished at the T8-T9 level with a micro rongeur (Fine Science Tools, United States). Henceforward, the extradural clip compression SCI caused damage by closing an aneurysm clip (Aesculap, Tuttlingen, Germany) with a 90 g calibrated closing force, near the spinal cord for 1 min (Poon et al., 2007; Cheriyan et al., 2014; Bagheri Bavandpouri et al., 2024). Then muscles and skin were sutured, and rats were permitted to recover on a 30°C heating pad, and then received saline (2 mL, twice a day, subcutaneously) and cefazoline (40 mg/kg twice on the day of surgery, i.p.) to rehydrate and control urinary tract infections. SCI rendered all animals thoroughly paraplegic. Urinary excretion was manually dragged out two times per day until achieving bladder-emptying reflex comeback.

2.6 Weight change measurement

The rats were weighed at the commencement of experiments and repeated on days 7, 14, 21, and 28. The weight changes in each group were calculated through the directions below:

Weight difference = (Animal's weight on days 7, 14, 21, and 28 – weight on day 0 (before the surgery)).

2.7 Functional recovery assessment using Basso, Beattie, and Bresnahan test

Basso, Beattie, and Bresnahan (BBB) is a locomotor behavior test that is a proper and predictive estimation of locomotor recovery and can also differentiate behavioral developments due to separate injuries (Basso et al., 1995). The approach was based on evaluated behavior before the injury, on the first postoperative day, and then for up to 4 weeks on days 1, 7, 14, 21, and 28. Scoring categories were determined and classified based on the experimental ordering of the Basso, Beattie, and Bresnahan Locomotor Rating Scale.

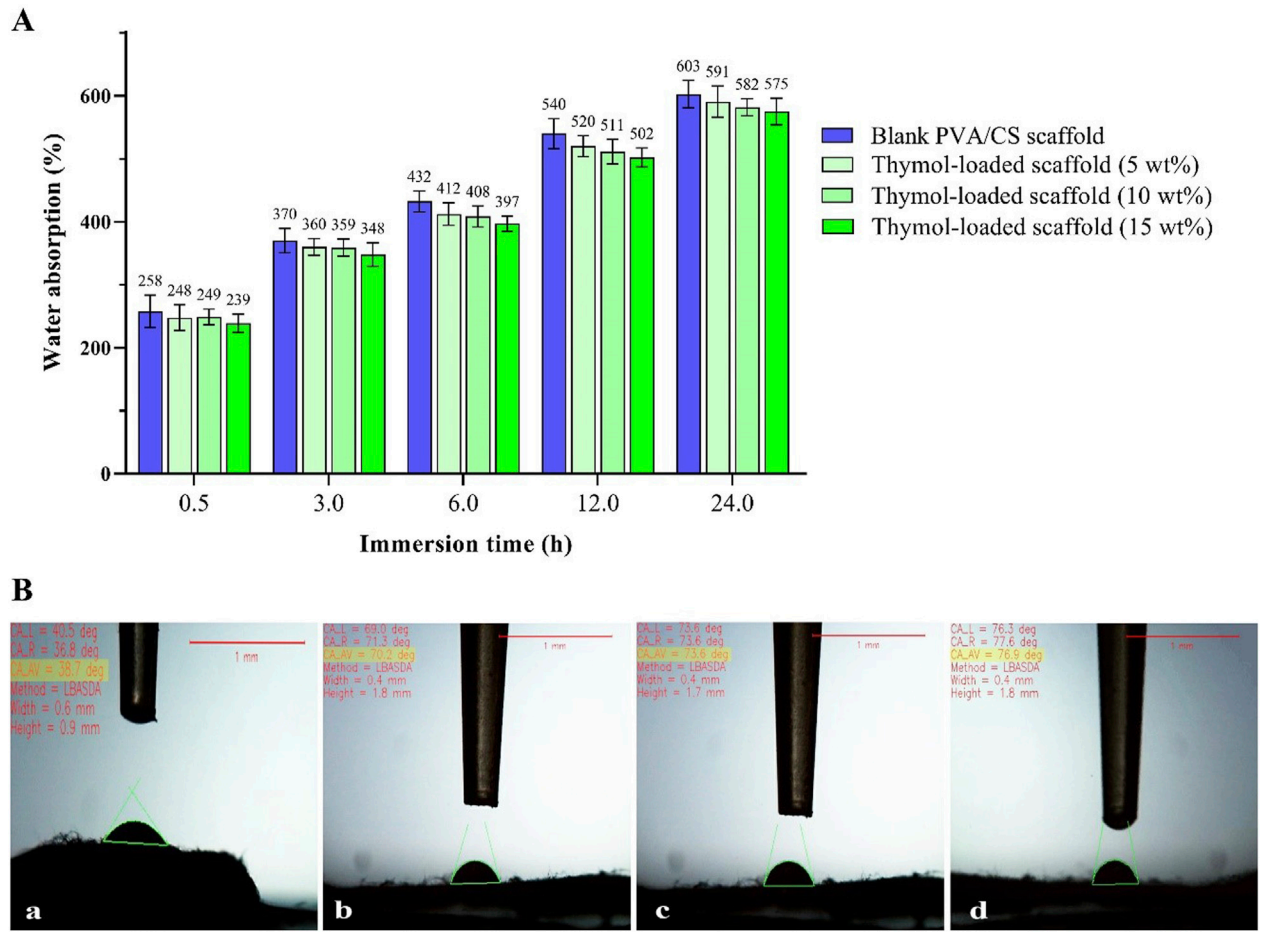


FIGURE 4
(A) The water absorption capacity of the scaffolds at different immersion times, **(B)** The resultant images of the water contact angle of the scaffolds: blank PVA/CS scaffold (a) and the scaffolds containing 5 wt% (b), 10 wt% (c), and 15 wt% (d) thymol with the quantitative values.

2.8 Mechanical sensory testing with von-Frey Filaments

The von Frey test is a gold standard for specifying mechanical thresholds, which were invented by Maximilian von Frey and evaluating mechanical allodynia in mice and rats (Deuis et al., 2017). In this test, a monofilament was used vertically to the plantar surface of the rat's rear paw until its apex, producing a stable pre-determined force (typically 15–180 g for rats) for 2–5 s. When any quick paw withdrawal, licking, or shaking was observed while applying the stimulus, it was considered a positive response. The test was repeated on days 7, 14, 21, and 28.

2.9 Assessing sensory response with acetone drop test

Cold chemical and thermal sensitiveness were estimated by utilizing the acetone drop method (Yoon et al., 1994; Ruan et al., 2018). The technique involved applying (100 μL) of acetone using a micropipette to the rat's hind paw through the wired mesh cage. The rats were placed in the cage and allowed to acclimate for approximately 20 min before acetone application to facilitate exploration of their surroundings. The acetone drop was applied mildly to the rat's rear paws. Rats' reactions such as paw licking, shaking, or rubbing the hind paw and brisk foot withdrawal typically 2–5 s after the acetone administration were documented as positive responses. For each measurement, the paw was sampled three times with an interval of 5 min calculated, which scored 0, 1, 2, 3 and 4, respectively. The test was repeated on days 7, 14, 21, and 28.

2.10 Thermal sensitivity assessment using hot plate test

The hot-plate test scored behavioural for measurements to estimate acute pain sensitivity (Hunskaar et al., 1986). Rats were put, each one separately, on a surface maintained at 50°C–56°C. The rat's movement was restricted by a plexiglass cylinder. The latency to hind paw licking, shaking, or jumping, was recorded by time, and at this point, the animal was instantly released from the hot plate to lessen the suffering. The test was repeated on days 7, 14, 21, and 28.

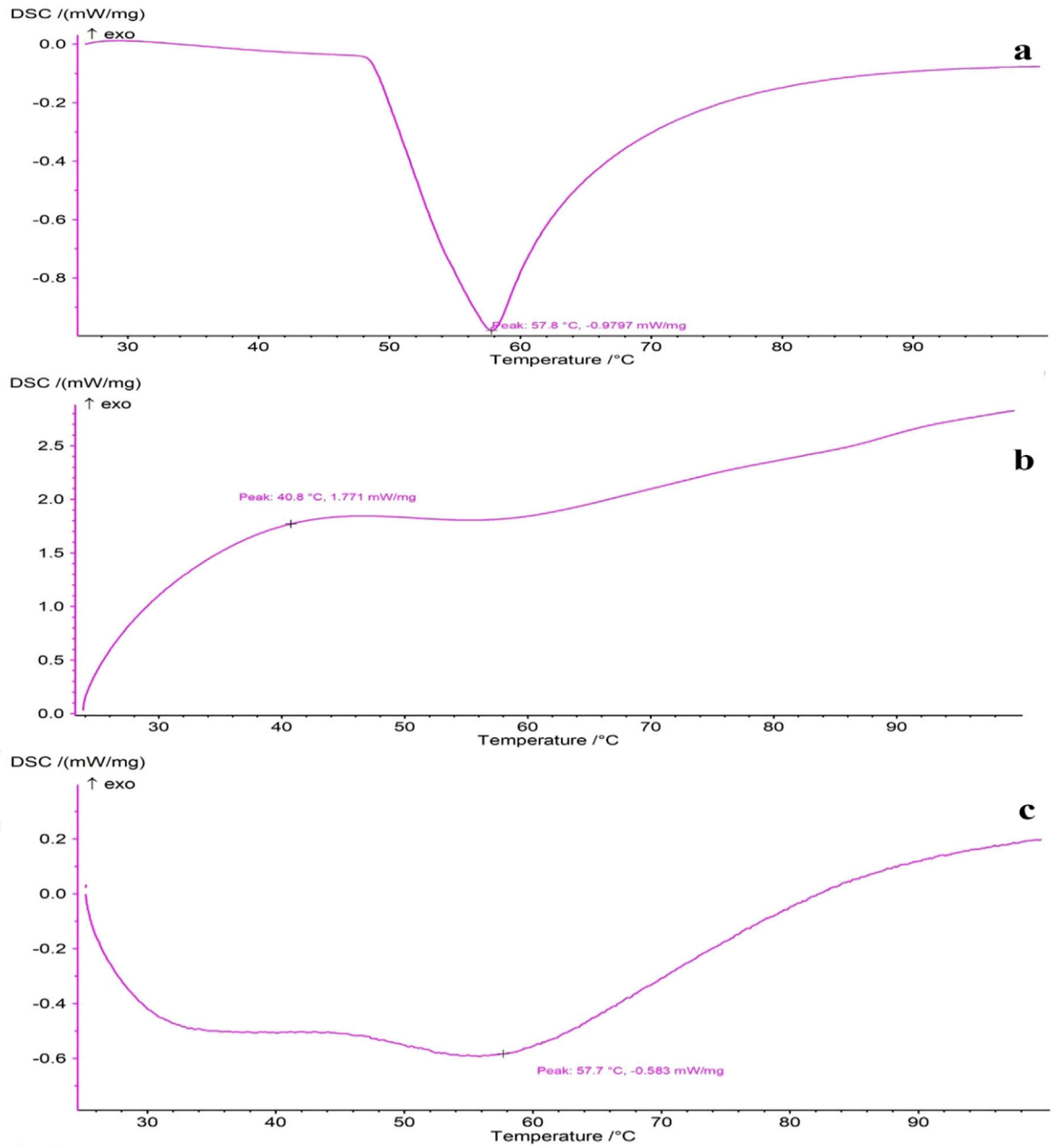


FIGURE 5
DSC thermograms of **(A)** pure thymol, **(B)** blank PVA/CS scaffold, and **(C)** thymol-loaded scaffold.

2.11 Histopathological evaluation of spinal cord injury

All rats were sacrificed (100 mg/kg ketamine + xylazine 20 mg/kg) at the end of day 28 when the behavioral tests were finished. The spinal cord tissue was attentively extracted and then kept in 200 mL of 4% paraformaldehyde and 0.1 M phosphate-buffered saline (PBS). The tissues were then processed (Didban sabz DS2080/H; Iran). The sections of the spinal cord in each rat were stained with H&E. Histopathological alterations were analyzed using a light microscope, and the data was collected at a magnification of 40X.

2.12 Statistical analysis

Statistical analyses were performed using GraphPad Prism software version 6. Results are presented as mean ± standard error of the mean (SEM). One-way or two-way analysis of variance (ANOVA) was conducted, followed by Tukey's or Bonferroni *post hoc* tests, to determine significant differences between groups. A *p*-value of less than 0.05 was considered statistically significant (Fakhri et al., 2018; Bagheri Bavandpouri et al., 2024).

The experimental design is schematized in Figure 1.

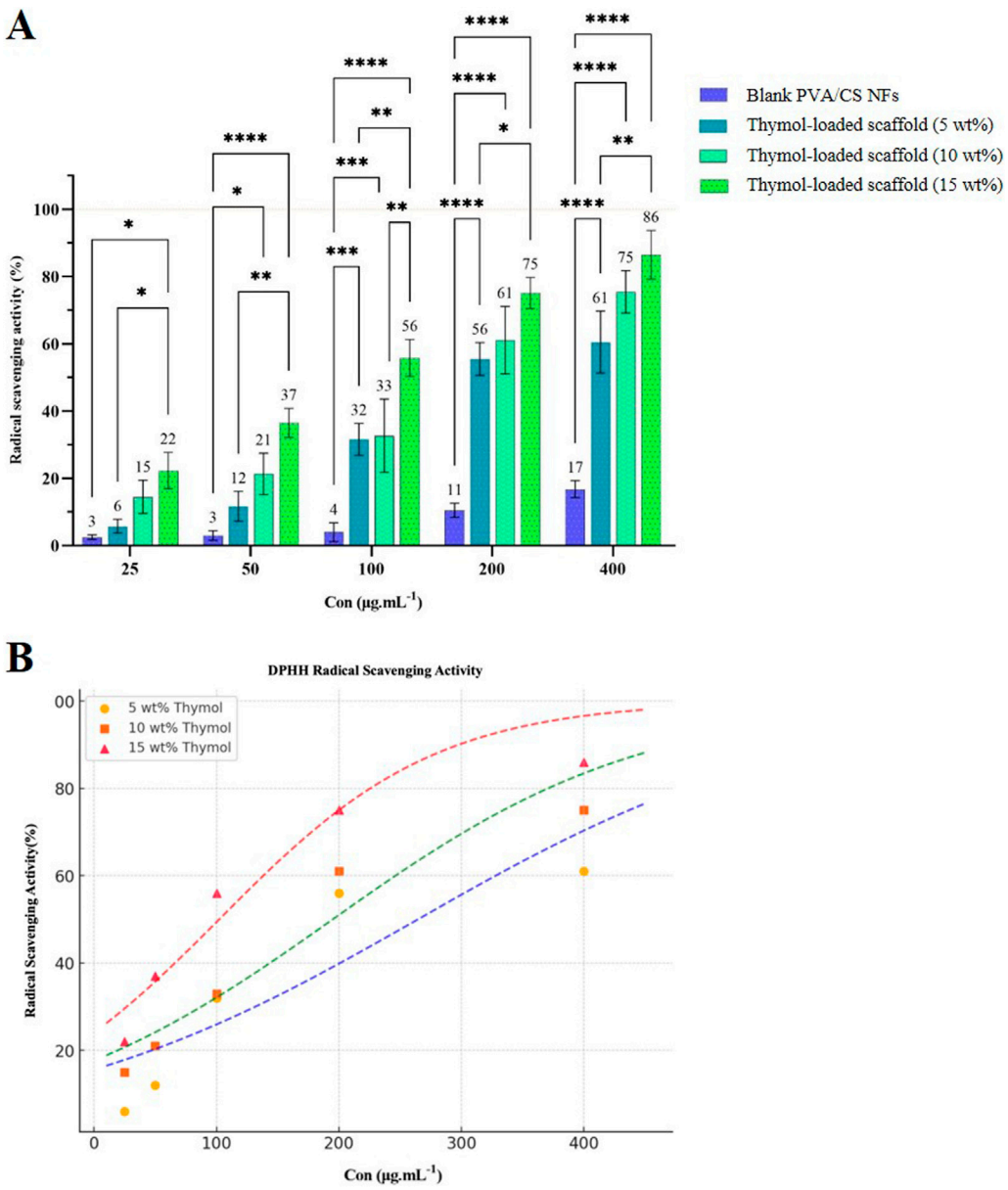


FIGURE 6
(A) Free radical scavenging activity of thymol-loaded and blank PVA/CS scaffolds at different concentrations. **(B)** Determination of IC_{50} values and sigmoidal curve fitting for representing radical scavenging activity of the scaffolds.

3 Results

3.1 Morphological characterization of the scaffolds

The SEM micrographs of blank electrospun PVA/CS scaffold and PVA/CS scaffolds containing 5-15 wt% thymol are depicted in Figure 2. The blank scaffold (without thymol) indicated the diameter distribution 313 ± 45 nm and the uniform morphological structure with the smooth, cylindrical, ribbon-shaped, and bead-free NFs with high porous structure (Figure 2A). Adding 5 wt% thymol in the PVA/CS mixture led to increasing the diameter of NFs to 390 ± 45 nm without any change in the morphology (Figure 2B). Likewise, the uniform and beadless NFs with a diameter distribution of 396 ± 49 nm were formed while the thymol concentration was augmented to 10 wt% (Figure 2C). Whereas, adding 15 wt% thymol resulted in the elevation of the average diameter to 412 ± 53 nm with appropriate morphology (Figure 2D). Further incorporation of thymol (>15 wt%) led to the formation of non-uniform NFs in diameter and morphology that is not desirable and was not used.

3.2 Characterization of scaffold composition via FT-IR

FT-IR spectroscopy was performed to verify the chemical structure of samples and identify the presence of thymol and its interaction with the polymeric matrix. The FT-IR spectra of pure

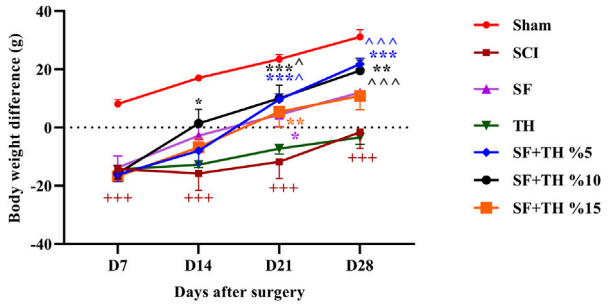


FIGURE 7
Investigating the effect of PVA/CS scaffold loaded with thymol on weight changes following SCI in rats. Data are presented as mean ± SEM (n = 6). (^p < 0.05 and ^^^p < 0.001) vs. TH group, ***p < 0.001, **p < 0.01, *p < 0.05) vs. SCI group and (+++ p < 0.001) vs. Sham group.

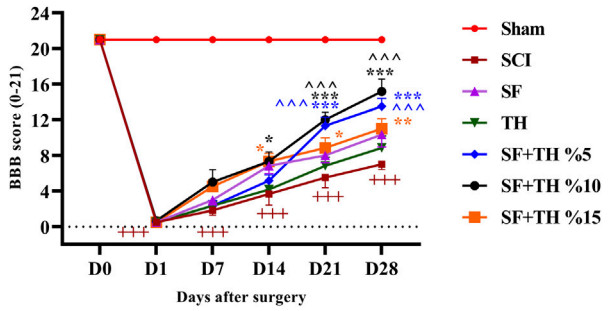


FIGURE 8
Investigating the effect of PVA/CS scaffold loaded with thymol on motor performance in the BBB test following SCI in rats. Data are presented as mean ± SEM (n = 6). (^^^p < 0.001) vs. TH group, (***p < 0.001, **p < 0.01, *p < 0.05) vs. SCI group and (+++p < 0.001) vs Sham group (SF: blank PVA/CS scaffold, TH: free thymol, SF + TH: scaffolds containing thymol).

thymol, the unloaded (blank), and the thymol-loaded scaffolds are presented in Figure 3. The spectrum of thymol indicated the distinguishing peak at 806 cm^{-1} corresponding to out-of-plane C–H wagging vibrations, and peaks at 1,089 cm^{-1}, 1,244 cm^{-1}, 1,450 cm^{-1}, and 1,602 cm^{-1} are attributed to C–O, C–C and C=C stretching vibrations of the phenolic ring of thymol (Wu et al., 2021). In addition, the characteristic peaks occurring at 2,960 cm^{-1} and 3,202 cm^{-1} are assigned to methyl groups (–CH_3) and hydroxyl groups (–OH) of thymol, respectively (Sanchez-Rexach et al., 2016; Michalska-Sionkowska et al., 2017). Besides, the spectrum of blank PVA/CS nanofibrous scaffold exhibited characteristic peaks at 1,080 cm^{-1} and 1,251 cm^{-1} that are associated with C–O–C stretching of ether groups as well as a sharp peak at 1728 cm^{-1} corresponding to the C=O stretching bond of the residual acetyl groups in the CS (Rukmani and Sundrarajan, 2012). Also, the absorption peak at 2,935 cm^{-1} is related to the–CH_2 group, and the broad peak at around 3,327 cm^{-1} is related to the–OH/–NH_2 vibrations of PVA and the primary amines of CS (Rukmani and Sundrarajan, 2012). Furthermore, the spectrum of thymol-loaded PVA/CS NFs elucidated the prominent peaks similar to both thymol and PVA/CS NFs, confirming thymol's presence in the NF structure without any adverse interaction as well as increasing intensity of peaks explicates the efficient loading into the nanofibrous scaffold.

3.3 Contact angle and water absorption capacity

The water absorption capability of the prepared scaffolds is depicted in Figure 4A. In the 30-min immersion, the water holding capacity of the blank PVA/CS scaffold was about 258% and reached 603% after 24 h immersion. The thymol-loaded scaffolds (5, 10, and 15 wt%) were able to absorb nearly 248%, 249%, and 239% reached 591%, 282%, and 575% after 24 h immersion, respectively. After 24 h, no change in the amounts of absorption was observed. These findings signify the high and rapid water absorption ability of the scaffolds, which is probably related to their high porosity. Further, the incorporation of thymol did not significantly alter the PVA/CS scaffold's absorption capability, and there was no significant difference between the scaffolds.

Furthermore, the surface wettability of the scaffolds was evaluated through the water contact angle shown in Figure 4B. The measured contact angle of the blank PVA/CS scaffold was about 38.7°. While these values were 70.2°, 73.6°, and 76.9° for the loaded scaffolds containing 5, 10, and 15 wt% thymol, respectively. These results indicate the prepared scaffolds have a highly hydrophilic and wettable surface, affecting biological response, protein adsorption, and cellular attachment (Doostan et al., 2023).

3.4 Thermal properties of scaffold samples via DSC

The DSC thermograms of pure thymol and the prepared scaffolds are displayed in Figure 5. In the DSC curve of thymol, a sharp endothermic peak appeared around 57°C, corresponding closely to its melting point (Zamani et al., 2015; Giotopoulou et al., 2024). The blank PVA/CS scaffold did not exhibit sharp peaks, indicating the absence of crystalline microstructure. The majority of polymeric chains in the non-crystalline state in the electrospun NFs is likely due to the rapid solidification of stretched polymeric chains during the electrospinning process (Jia et al., 2007; Gholipour, K et al., 2009; Olvera Bernal et al., 2023). Likewise, the DSC thermograph of the thymol-loaded scaffold indicates that the characteristic melting endothermic peak of thymol disappeared upon incorporation into the electrospun NFs. This result implies that thymol converts from crystalline to amorphous form, presumably due to rapid solvent evaporation and restricted molecular mobility caused by intermolecular interactions, e.g., hydrogen bonds, during electrospinning (Chen et al., 2020; Jiffrin et al., 2022). Such conversion, leading to the molecular dispersion of thymol during incorporation into nanofibrous scaffolds, can provide homogeneous distribution and higher drug loading in the nanofiber matrix, ensuring consistent release profiles, which is advantageous for poorly soluble drugs, enhancing solubility,

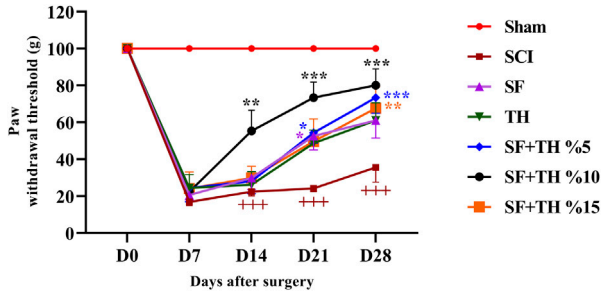


FIGURE 9
Investigating the effect of PVA/CS scaffold loaded with thymol on mechanical pain tolerance threshold following SCI in rats. Data are presented as mean ± SEM (n = 6). ***p < 0.001, **p < 0.01, *p < 0.05) vs. SCI group and (+++ p < 0.001) vs. Sham group (SF: blank PVA/CS scaffold, TH: free thymol, SF + TH: scaffolds containing thymol).

bioavailability, and dissolution rate (Qi and Craig, 2016; Jiffrin et al., 2022).

3.5 DPPH radical scavenging assay

The antioxidant activity of the scaffolds was determined by measuring the DPPH free radical scavenging strength; the results of which are shown in Figure 6A. The blank scaffold showed low antioxidant activity (17%) at high concentrations, possibly owing to the absorption of DDPH molecules by the large surface area of the NFs. The antioxidant activity of the scaffolds was augmented significantly by adding thymol. The activities of the scaffolds rose significantly by adding thymol and further increased in higher quantities. At concentrations of 25–400 μg/mL, the scavenging activities of the scaffolds containing 5, 10, and 15 wt% thymol were found to be from 6%–61%, 15%–75%, and 22%–86%, respectively. The higher loading of thymol resulted in higher antioxidant activity that is due to the presence of thymol in the scaffolds, enabling to donate of hydrogen by hydroxyl groups in the structure and breaking the chain reactions of free radicals (Aziz and Almasi, 2018). Scaffolds exhibited a concentration-dependent activity for radical scavenging, and a rise in thymol content increased antioxidant activity. Blank nanofibrous scaffold of PVA/CS exhibited no radical scavenging activity, but 5, 10, and 15 wt% thymol-loaded scaffolds exhibited significantly increased antioxidant activity at all concentrations (p < 0.05). To further evaluate the antioxidant efficacy, a half-maximal inhibitory concentration (IC_{50}) value was determined with a sigmoidal fitting model Figure 6B. The IC_{50} values, representing a 50% free radical-scavenging activity, were calculated as: 5 wt% thymol-loaded scaffold: 264.52 μg, 10 wt% thymol-loaded scaffold: 194.93 μg, 15 wt% thymol-loaded scaffold: 102.14 μg. These results confirm that the 15 wt% thymol-loaded scaffold exhibited the highest antioxidant activity, with its lowest IC_{50} values. Dose-dependent enhancement in free radical-scavenging activity confirms that thymol is a key player in contributing towards the antioxidant activity of nanofibrous scaffolds, and it can contribute towards minimizing oxidative stress in SCI.

3.6 Weight change measurement

The weight changes of the animals compared to the day before surgery were evaluated and are shown in Figure 7. The obtained results indicate that the sham group showed a normal weight gain pattern over the 4-week period. However, in the injured rats compared to the Sham group, a significant impairment in weight gain was observed during the weeks following the injury (p < 0.001). Treatment with thymol-loaded scaffolds at 10% and 5% resulted in a significant increase in the normal weight of the animals during the 21 days after the injury (p < 0.001), while thymol-loaded scaffolds at 15% led to a notable increase as well (p < 0.01) on day 21. This observed improvement eventually compensated for the weight loss caused by the injury, and no significant differences were observed between the treatment groups.

3.7 Basso, Beattie, and Bresnahan test

Motor performance of rats after SCI was measured by the BBB scale as shown in Figure 8. Examining the movement performance of the sham group indicated no movement disorders after laminectomy, and the rats consistently scored 21 on all examined days. In contrast, the SCI group exhibited complete paralysis on the first day after the injury, with scores of 0 and 1, and throughout the treatment period, they showed a significant decrease in motor performance compared to the sham group animals (p < 0.001). However, the groups treated with 10% and 15% thymol-loaded scaffolds showed an increase in the recovery of movements and joints by day 14 after the injury (p < 0.05), and there was a significant improvement in motor performance for the group treated with 5% and 10% thymol-loaded scaffolds on days 21 and 28 (p < 0.001).

3.8 Von-Frey filament test

Evaluation of mechanical pain was performed by applying the mechanical force of von Frey fibers on the dorsal surface of the rat's hind legs, between the 2nd and 3rd toes (Figure 9). The obtained results show that in the sham group, the mechanical pain tolerance threshold remained consistent during the treatment period after laminectomy. On the other hand, in the SCI group, a significant decrease in the mechanical pain tolerance threshold was observed on day 7, and no significant changes were observed in the following days compared to the sham group (p < 0.001). The group treated with a 10% thymol-loaded scaffold demonstrated an improvement, showing a more pronounced reduction in neuropathic pain caused by foot injury on day 14 (p < 0.01), and continued to exhibit reduced pain levels on days 14, 21, and 28 (p < 0.001). Additionally, the group treated with 5% thymol-loaded scaffolds showed a reduction in neuropathic pain on day 7 (p < 0.05) and sustained the reduction on day 28 (p < 0.001).

3.9 Acetone drop test

The acetone drop test was used to assess the animals' tolerance threshold to the cold pain stimulus and the data are depicted in

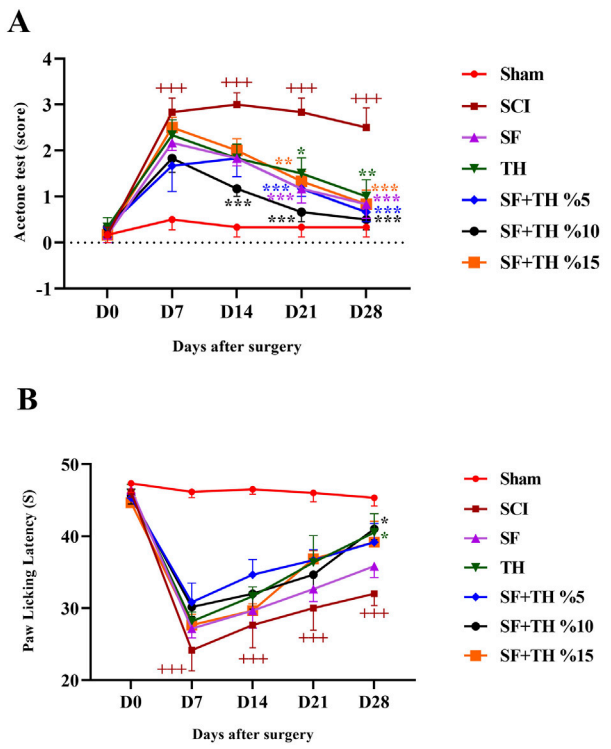


FIGURE 10
Investigating the effect of PVA/CS scaffold loaded with thymol on cold **(A)** and thermal **(B)** pain tolerance threshold following SCI in rats. Data are presented as mean ± SEM (n = 6). (***p < 0.001, **p < 0.01, *p < 0.05) vs SCI group and (+++ p < 0.001) vs Sham group. (SF: blank PVA/CS scaffold, TH: free thymol, SF + TH: scaffolds containing thymol).

Figure 10A. In the sham group, the foot withdrawal reflex in response to the cold stimulus (acetone) remained consistent, and no significant changes were observed in the days following laminectomy. This is despite the fact that the injured animals became highly sensitive to cold and their pain tolerance threshold decreased more clearly, also there is a significant difference in the comparison of the reflexes of this group with the Sham group (p < 0.001). Treatment with a 10% thymol-loaded scaffold increased the tolerance of the response threshold to cold stimulus from day 14 until day 28 after injury (p < 0.001) and also 5% thymol-loaded scaffold and blank scaffold increased the tolerance of the response threshold to the cold stimulus at day 21 (p < 0.001). In contrast, the 15% thymol-loaded scaffold showed a moderate increase at day 21 (p < 0.01).

3.10 Hot plate test

Thermal pain was assessed using the hot plate test, as shown in Figure 10B. The obtained results indicated that the time delay in foot licking, as a measure of pain tolerance threshold due to heat in the sham group, did not change significantly from the first to the 28th days after laminectomy. Compared to the sham group, the SCI group showed a much lower tolerance to thermal pain on days 7 and 14 (p < 0.001) and in the last 2 weeks, the pain tolerance threshold increased slightly in the direction of recovery (p < 0.001). Treatment with a 5 mg/kg dose of thymol and 10% thymol-loaded scaffold was associated with a moderate increase in the tolerance threshold of response to thermal stimuli with a relatively mild slope in the final week after injury (p < 0.05).

3.11 Histopathology analysis

Hematoxylin-eosin staining was used to investigate the extent of tissue damage after SCI, as depicted in Figure 11A. Counting the number of motor neurons (Figure 11B) in the area of the ventral horn of the gray matter of the spinal cord on day 28 after the injury revealed a significant decrease in the number of neurons at the injury site (p < 0.001). Treatment with 10% and 5% thymol-loaded scaffolds demonstrated improved protection of neurons and led to an increase in the number of motor neurons in the ventral region of the spinal cord (p < 0.001). Similarly, 15% thymol-loaded scaffold treatment also showed improvement in the number of motor neurons (p < 0.01).

4 Discussion

SCI is a devastating condition that occurs when the spinal cord suffers damage (McDonald and Sadowsky, 2002). This damage leads to the loss of motor, sensory, and autonomic functions, below the injury site (Anjum et al., 2020). This is a life-altering condition that permanently affects an individual's quality of life and independence (Norrbrink Budh et al., 2006). Unfortunately, there is currently no cure for SCI, and treatment options are limited. The main focus of managing SCI revolves around preventing damage, stabilizing the spine, and providing care to manage complications (Dietrich, 2015). One notable avenue of inquiry pertains to the utilization of stem cell transplantation as a regenerative approach (Nakamura and Okano, 2013; Tahmasebi and Barati, 2022). Within this domain, extensive research is underway, encompassing various stem cell types, including induced pluripotent stem cells (Trawczynski et al., 2019) as well as adult stem cell variants like neural stem cells (Wang J. et al., 2020) and mesenchymal stem cells (Xu and Yang, 2019). Notably, promising outcomes have been observed in studies examining these cell types. Concurrently, another sphere of exploration centers on the deployment of biomaterials in the capacity of scaffolds to facilitate regeneration (Shen H. et al., 2022). These biomaterials, which encompass hydrogels, nanofiber scaffolds, and conductive polymers, serve the pivotal role of providing structural support while creating a conducive environment that fosters cell adhesion, migration, and differentiation (Zhang et al., 2019).

Scaffolding technology has gained significance in tissue engineering, especially in the treatment of SCI (Zhang et al., 2019). This is achieved by supplying a framework that assists in cell building and tissue repair (Shrestha et al., 2014). Extracellular matrices are often not spared in spinal cord injuries, as they are often damaged. This disruption eliminates the matrix that facilitates cell attachment, movement, and change, all of which are key steps in the restoration of nerves. Such aggravated conditions can be overcome

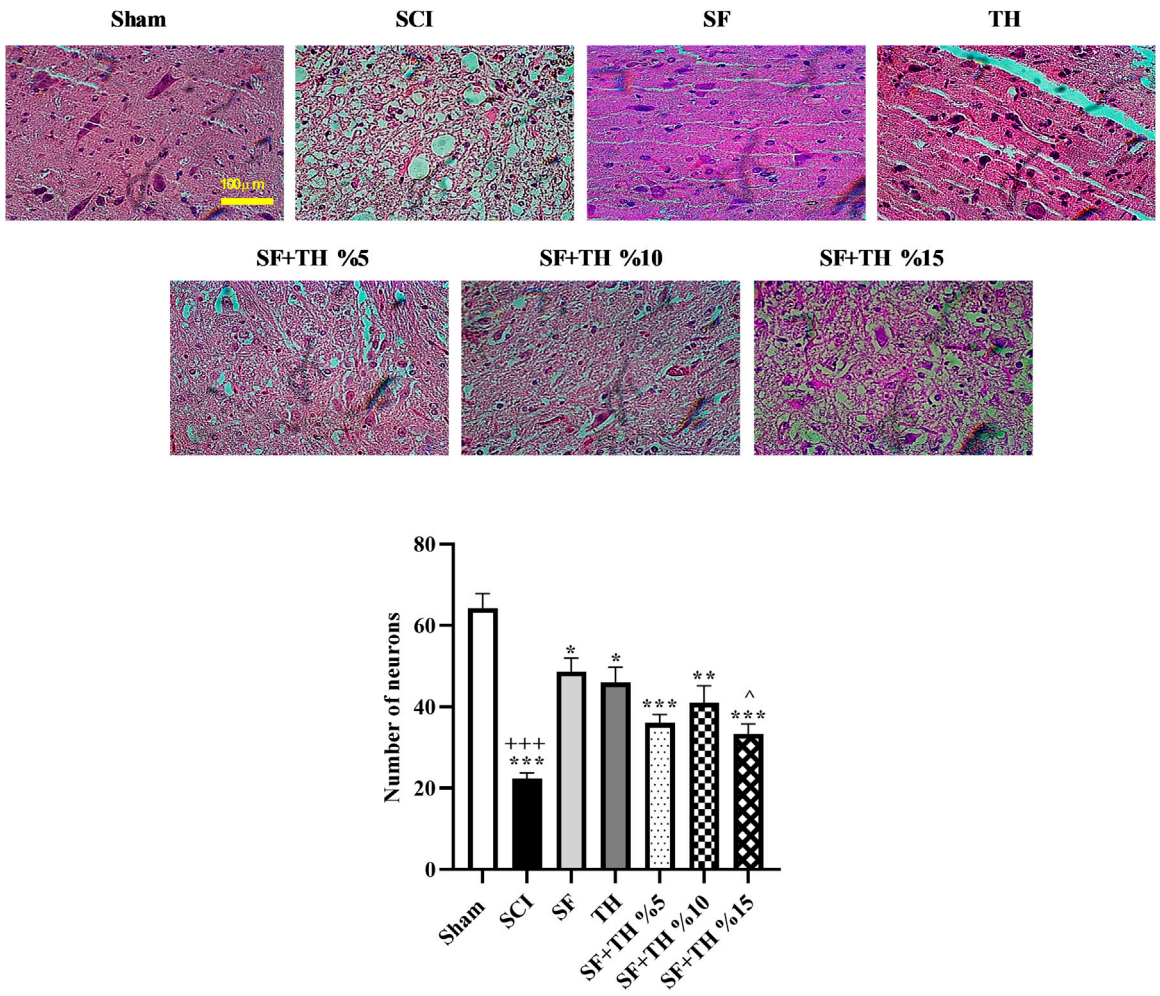


FIGURE 11
(A) Investigating the effect of PVA/CS scaffold loaded with thymol on changes in the number of motor neurons in the ventral horn of the spinal cord in hematoxylin-eosin staining of the transverse sections prepared from the spinal cord with 40x magnification following SCI in rats. **(B)** Data are presented as mean ± SEM (n = 3). (^$p < 0.05$) vs. TH group, (***$p < 0.001$, **$p < 0.01$, *$p < 0.05$) vs. SCI group and (+++ $p < 0.001$) vs. Sham group (SF: blank PVA/CS scaffold, TH: free thymol, SF + TH: scaffolds containing thymol).

by using nanofibrous scaffolds that can restore ECM-like three-dimensional biological structures for the culture of neural tissue (Ma et al., 2021). Due to its high surface area and porosity, the scaffold allows the important nutrients and oxygen to diffuse into the cells, as well as any signaling molecules required for the cells to survive and the tissue to regenerate. This structure is particularly useful in handling situations of SCI where there is a need to localize delivery of treatment, as there is secondary damage that occurs, and there is a need for restoration of function (Snider et al., 2017).

In addition, to their role as a delivery system for molecules and growth factors, biomaterial scaffolds have demonstrated the ability to enhance regeneration and tissue repair, in animal models when combined with cells or growth factors. In this regard, Babaloo et al. designed a scaffold based on poly ε-caprolactone (PCL)/gelatin and seeded by human endometrial stem cells (hEnSCs) were then transplanted into hemisected SCI rats. The results of the study indicated that combination therapy using the differentiated hEnSC seeded on PCL/gelatin scaffolds has the potential to heal the injured spinal cord and limit secondary damage (Babaloo et al., 2019). Investigation led by Fakhri et al., a comprehensive exploration was undertaken, taking into account the pivotal role of glutamate in excitatory toxicity and central sensitization. The primary objective of this study was to assess the impact of ketamine, recognized as an *N*-methyl-D-aspartate (NMDA) receptor antagonist, on sensory-motor functions within a murine model exhibiting SCI. Their robust dataset illuminated compelling findings, revealing a substantial reduction in mechanical allodynia and cold allodynia from the first week through the post-injury within the ketamine-treated group, as compared to the injury group. Their compelling findings collectively underscore the potential therapeutic efficacy of intrathecal ketamine in mitigating sensory-motor dysfunction within a rodent model afflicted by SCI (Fakhri et al., 2020).

Moreover, thymol, an inherent compound found in botanical sources such as thyme, oregano, and basil, emerges as an enticing candidate for multifaceted applications, owing to its well-documented anti-inflammatory, antioxidant, and analgesic properties (Yanishlieva et al., 1999; Braga et al., 2006; Ghori et al., 2016). Thymol displays its inflammatory effects by

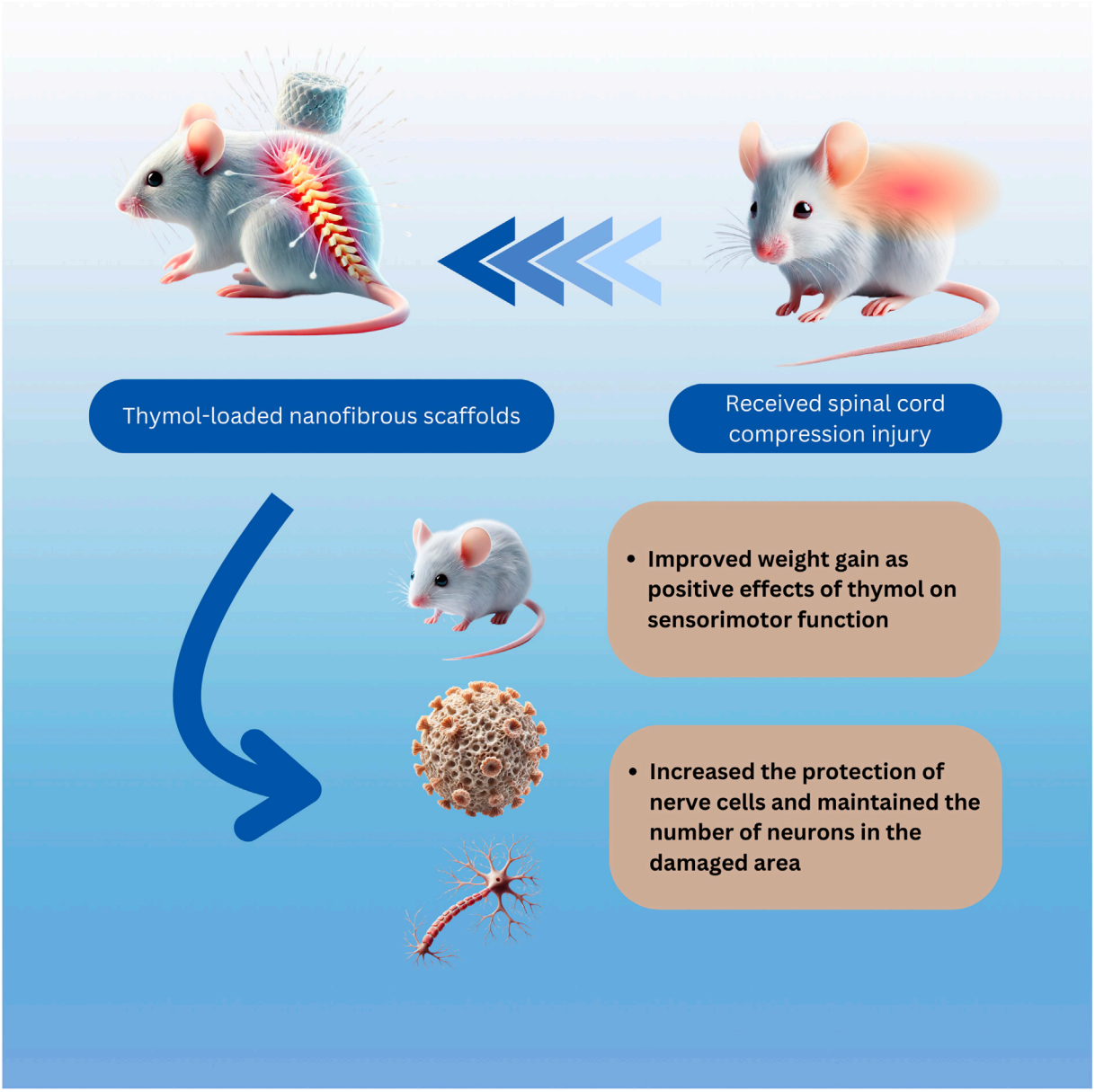


FIGURE 12
Illustration of rat SCI and being treated with thymol-loaded nanofibrous scaffold. The integration of the thymol-loaded PVA/CS nanofibrous scaffold into the injured spinal cord. The scaffold, characterized by its three-dimensional nanofibrous structure and high porosity, is shown to release thymol at the injury site. Thymol exerts anti-inflammatory, antioxidant, and neuroprotective effects, reducing secondary damage and promoting a regenerative microenvironment. Additionally, the sustained release of thymol enhances functional recovery by alleviating neuropathic pain and improving locomotor and sensory functions.

inhibiting signaling pathways and pro-inflammatory mediators. It aids in reducing the production of cytokines like interleukin 1 beta (IL-1β), tumor necrosis factor-alpha (TNF-α), and interleukin 6 (IL-6), ultimately modulating the response (Nagoor Meeran et al., 2015). Thymol also serves as an antioxidant by scavenging radicals and preventing stress. Achieving this ensures the protection of cells and tissues from damage caused by ROS, while also encouraging their regeneration (Yanishlieva et al., 1999). Moreover, thymol exhibits characteristics by diminishing cell death fostering neuronal survival, and enhancing neurite outgrowth (Timalsina et al., 2023a; Timalsina et al., 2023b). Furthermore, the combination of thymol with a nanofiber scaffold for treating SCI offers various benefits. The nanofibrous scaffold serves as a three-dimensional framework that closely mimics the extracellular matrix, promoting cell attachment and movement, including cells within the damaged spinal cord. Thus when examining the potential of thymol and the PVA/CS scaffold, for SCI treatment it is evident that their combination holds promise. Thymol plays a vital role in facilitating cell attachment and spreading, encouraging cell infiltration into the scaffold. This effect was observed in the

Lavanya et al. study, where a drug delivery vehicle using semi-interpenetrating polymer network (SIPN) hydrogels containing sodium alginate and poly (2-ethyl-2-oxazoline) (SA/Pox) loaded with thymol was transplanted into a rat tibial bone defect model system. The study revealed that the incorporation of thymol into SA/Pox/CS hydrogels enhanced bone regeneration. The data demonstrated sustained and prolonged release of thymol from the hydrogels, which promoted osteoblast differentiation *in vitro* and bone formation *in vivo*, indicating its potential application in bone rejuvenation (Lavanya et al., 2023).

In the current study, we plan to examine the chemical properties of the PVA/CS scaffold assess its effectiveness through behavioral tests, and confirm the regenerative results by analyzing tissue samples. By merging, the support offered by the scaffold with the advantages of thymol the goal is to enhance functional recovery and stimulate neural regeneration. The focus of this article revolves around an approach that involves combining a nanofiber scaffold with thymol *in-situ* specifically for treating SCI in rats compression model Figure 12, which can accurately control SCI and provide controlled chronic neuropathic pain and movement disorders (Šedý et al., 2008; Cheriyan et al., 2014).

Through this study, significant advancements in the recovery of rats with SCI were observed following treatment with the nanofiber scaffolds containing thymol, as well as improved weight gain. This effect can be possibly attributed to the positive effects of pelargonidin on sensorimotor function, reducing pain, and addressing other disorders related to the injury. The study also investigated the symptoms of neuropathic pain and movement disorders after the compression model of SCI including thermal, cold, and mechanical pain thresholds, as well as the BBB score in rats. The nanofiber scaffolds loaded with thymol, especially at 10 and 5 wt%, demonstrated significant therapeutic effects in reducing motor defects and increasing the pain tolerance threshold. Additionally, the histological study corroborated these findings, showing consistent trends. Counting the number of motor neurons in the ventral horn revealed that the PVA/CS scaffold loaded with thymol significantly increased number of neurons in the damaged area (Figure 12).

5 Conclusion

In conclusion, the *in-situ* utilization of PVA/CS nanofiber scaffold containing thymol signifies a breakthrough in the realm of SCI treatment. Fabrication of the scaffolds indicated the formation of NFs with appropriate morphology and uniform size. In addition, the relevant analyses exhibited proper loading of thymol as well as high water absorption, porosity, and wettability properties of the scaffolds. The administration of thymol-loaded scaffolds in animal examinations significantly improved the pain threshold compared to the group with SCI-induced pain. Additionally, the scaffolds restored sensory and locomotor activity. Histopathology studies further revealed enhanced neuronal survival. These findings indicate that the thymol-loaded nanofibrous scaffolds possess neuroprotective and analgesic properties, making them a promising therapeutic intervention for treating neuropathic injuries. This innovative therapy potentially enhances recovery and promotes tissue regeneration among individuals with SCI.

Data availability statement

The raw data supporting the conclusions of this article will be made available by the authors, without undue reservation.

Ethics statement

The animal study was approved by Dr. Ehsan Shamsi Gooshki, Committee Secretary, National Institute for Medical Research Development. The study was conducted in accordance with the local legislation and institutional requirements.

Author contributions

RA: Writing–original draft, Investigation, Visualization. PM: Writing–original draft, Investigation. HM: Writing–original draft, Investigation. SF: Writing–original draft, Writing–review and editing, Conceptualization. SA: Writing–original draft, Investigation. MF: Writing–original draft, Writing–review and editing, Conceptualization. JE: Writing–original draft, Writing–review and editing, Conceptualization.

Funding

The author(s) declare that financial support was received for the research, authorship, and/or publication of this article. This work was Elite's Grant; supported by the Ministry of Health and Medical Education of the Islamic Republic of Iran under Grant 4000734.

Conflict of interest

The authors declare that the research was conducted in the absence of any commercial or financial relationships that could be construed as a potential conflict of interest.

The author(s) declared that they were an editorial board member of Frontiers, at the time of submission. This had no impact on the peer review process and the final decision.

Generative AI statement

The authors declare that no Generative AI was used in the creation of this manuscript.

Publisher's note

All claims expressed in this article are solely those of the authors and do not necessarily represent those of their affiliated organizations, or those of the publisher, the editors and the reviewers. Any product that may be evaluated in this article, or claim that may be made by its manufacturer, is not guaranteed or endorsed by the publisher.

References

Al-Adwani, D. G., Renno, W. M., and Orabi, K. Y. (2019). Neurotherapeutic effects of Ginkgo biloba extract and its terpene trilactone, ginkgolide B, on sciatic crush injury model: a new evidence. *PLoS One* 14, e0226626. doi:10.1371/journal.pone.0226626

Alizadeh, A., Dyck, S. M., and Karimi-Abdolrezaee, S. (2019). Traumatic spinal cord injury: an overview of pathophysiology, models and acute injury mechanisms. *Front. Neurol.* 10, 282. doi:10.3389/fneur.2019.00282

Andersen, J. K. (2004). Oxidative stress in neurodegeneration: cause or consequence? *Nat. Med.* 10, S18–S25. doi:10.1038/nrn1434

Andrei, C., Zanfirescu, A., Nițulescu, G. M., and Negreș, S. (2022). Understanding the molecular mechanisms underlying the analgesic effect of ginger. *Nutraceuticals* 2, 384–403. doi:10.3390/nutraceuticals2040029

Anjum, A., Yazid, M. D., Fauzi Daud, M., Idris, J., Ng, A. M. H., Selvi Naicker, A., et al. (2020). Spinal cord injury: pathophysiology, multimolecular interactions, and underlying recovery mechanisms. *Int. J. Mol. Sci.* 21, 7533. doi:10.3390/ijms21207533

Aziz, S. G.-G., and Almasi, H. (2018). Physical characteristics, release properties, and antioxidant and antimicrobial activities of whey protein isolate films incorporated with thyme (Thymus vulgaris L.) extract-loaded nanoliposomes. *Food Bioprocess Technol.* 11, 1552–1565. doi:10.1007/s11947-018-2121-6

Babaloo, H., Ebrahimi-Barough, S., Derakhshan, M. A., Yazdankhah, M., Lotfibakhshaiesh, N., Soleimani, M., et al. (2019). PCL/gelatin nanofibrous scaffolds with human endometrial stem cells/Schwann cells facilitate axon regeneration in spinal cord injury. *J. Cell. Physiol.* 234, 11060–11069. doi:10.1002/jcp.27936

Bagheri Bavandpouri, F. S., Azizi, A., Abbaszadeh, F., Kiani, A., Farzaei, M. H., Mohammadi-Noori, E., et al. (2024). Polydatin attenuated neuropathic pain and motor dysfunction following spinal cord injury in rats by employing its anti-inflammatory and antioxidant effects. *Front. Pharmacol.* 15, 1452989. doi:10.3389/fphar.2024.1452989

Basso, D. M., Beattie, M. S., and Bresnahan, J. C. (1995). A sensitive and reliable locomotor rating scale for open field testing in rats. *J. Neurotrauma* 12, 1–21. doi:10.1089/neu.1995.12.1

Boyd, A., Bleakley, C., Hurley, D. A., Gill, C., Hannon-Fletcher, M., Bell, P., et al. (2019). Herbal medicinal products or preparations for neuropathic pain. *Cochrane Database Syst. Rev.* 2021, CD010528. doi:10.1002/14651858.CD010528.pub4

Braga, P. C., Dal Sasso, M., Culici, M., Bianchi, T., Bordoni, L., and Marabini, L. (2006). Anti-inflammatory activity of thymol: inhibitory effect on the release of human neutrophil elastase. *Pharmacology* 77, 130–136. doi:10.1159/000093790

Chen, Y., Qiu, Y., Chen, W., and Wei, Q. (2020). Electrospun thymol-loaded porous cellulose acetate fibers with potential biomedical applications. *Mater. Sci. Eng. C* 109, 110536. doi:10.1016/j.msec.2019.110536

Cheng, Y., Zhang, Y., and Wu, H. (2022). Polymeric fibers as scaffolds for spinal cord injury: a systematic review. *Front. Bioeng. Biotechnol.* 9, 807533. doi:10.3389/fbioe.2021.807533

Cheriyan, T., Ryan, D. J., Weinreb, J. H., Cheriyan, J., Paul, J. C., Lafage, V., et al. (2014). Spinal cord injury models: a review. *Spinal Cord.* 52, 588–595. doi:10.1038/sc.2014.91

Colloca, L., Ludman, T., Bouhassira, D., Baron, R., Dickenson, A. H., Yarnitsky, D., et al. (2017). Neuropathic pain. *Nat. Rev. Dis. Prim.* 3, 17002. doi:10.1038/nrdp.2017.2

Costa, M. F., Durço, A. O., Rabelo, T. K., Barreto, R. de S. S., and Guimarães, A. G. (2019). Effects of Carvacrol, Thymol and essential oils containing such monoterpenes on wound healing: a systematic review. *J. Pharm. Pharmacol.* 71, 141–155. doi:10.1111/jphp.13054

Deuis, J. R., Dvorakova, L. S., and Vetter, I. (2017). Methods used to evaluate pain behaviors in rodents. *Front. Mol. Neurosci.* 10, 284. doi:10.3389/fnmol.2017.00284

Dietrich, W. (2015). Protection and repair after spinal cord injury: accomplishments and future directions. *Top. Spinal Cord. Inj. Rehabil.* 21, 174–187. doi:10.1310/sci2102-174

Doostan, M., Doostan, M., Mohammadi, P., Khoshnevisan, K., and Maleki, H. (2023). Wound healing promotion by flaxseed extract-loaded polyvinyl alcohol/chitosan nanofibrous scaffolds. *Int. J. Biol. Macromol.* 228, 506–516. doi:10.1016/j.ijbiomac.2022.12.228

Faccendini, A., Vigani, B., Rossi, S., Sandri, G., Bonferoni, M., Caramella, C., et al. (2017). Nanofiber scaffolds as drug delivery systems to bridge spinal cord injury. *Pharmaceuticals* 10, 63. doi:10.3390/ph10030063

Fakhri, S., Abbaszadeh, F., Pouriran, R., and Jorjani, M. (2020). The effects of intrathecal ketamine on improving sensory-motor function in a rat model of compression spinal cord injury. *Physiol. Pharmacol.* 24, 101–110. doi:10.32598/ppj.24.2.20

Fakhri, S., Dargahi, L., Abbaszadeh, F., and Jorjani, M. (2018). Astaxanthin attenuates neuroinflammation contributed to the neuropathic pain and motor dysfunction following compression spinal cord injury. *Brain Res. Bull.* 143, 217–224. doi:10.1016/j.brainresbull.2018.09.011

Gholipour, K. A., Bahrami, S. H., and Nouri, M. (2009). Chitosan-poly(vinyl alcohol) blend nanofibers: morphology, biological and antimicrobial properties. *e-Polymers* 9. doi:10.1515/epoly.2009.9.1.1580

Ghori, S. S., Ahmed, M. I., Arifuddin, M., and Khateeb, M. S. (2016). Evaluation of analgesic and anti-inflammatory activities of formulation containing camphor, menthol and thymol. *Int. J. Pharm. Pharm. Sci.* 8, 271–274.

Giotopoulou, I., Stamatis, H., and Barkoula, N.-M. (2024). Encapsulation of thymol in ethyl cellulose-based microspheres and evaluation of its sustained release for Food applications. *Polym. (Basel)* 16, 3396. doi:10.3390/polym16233396

Gurba, K. N., and Haroutounian, S. (2022). "Antidepressant analgesics in the management of chronic pain," in *Clinical pain management* Wiley, 171–180. doi:10.1002/9781119701170.ch16

Hall, O. M., Broussard, A., Range, T., Carroll Turpin, M. A., Ellis, S., Lim, V. M., et al. (2020). Novel agents in neuropathic pain, the role of capsaicin: pharmacology, efficacy, side effects, different preparations. *Curr. Pain Headache Rep.* 24, 53. doi:10.1007/s11916-020-00886-4

Hayta, E., and Elden, H. (2018). Acute spinal cord injury: a review of pathophysiology and potential of non-steroidal anti-inflammatory drugs for pharmacological intervention. *J. Chem. Neuroanat.* 87, 25–31. doi:10.1016/j.jchemneu.2017.08.001

Hunskaar, S., Berge, O.-G., and Hole, K. (1986). A modified hot-plate test sensitive to mild analgesics. *Behav. Brain Res.* 21, 101–108. doi:10.1016/0166-4328(86)90088-4

Indermun, S., Govender, M., Kumar, P., Choonara, Y. E., and Pillay, V. (2019). "Current and combinative curcumin therapeutics for treating spinal cord injury," in *Curcumin for neurological and psychiatric disorders* (Elsevier), 419–435. doi:10.1016/B978-0-12-815461-8.00023-2

Jia, Y.-T., Gong, J., Gu, X.-H., Kim, H.-Y., Dong, J., and Shen, X.-Y. (2007). Fabrication and characterization of poly (vinyl alcohol)/chitosan blend nanofibers produced by electrospinning method. *Carbohydr. Polym.* 67, 403–409. doi:10.1016/j.carbpol.2006.06.010

Jiffrin, R., Razak, S. I. A., Jamaludin, M. I., Hamzah, A. S. A., Mazian, M. A., Jaya, M. A. T., et al. (2022). Electrospun nanofiber composites for drug delivery: a review on current progresses. *Polym. (Basel)* 14, 3725. doi:10.3390/polym14183725

Jin, W., Botchway, B. O. A., and Liu, X. (2021). Curcumin can activate the Nrf2/HO-1 signaling pathway and scavenge free radicals in spinal cord injury treatment. *Neurorehabil. Neural Repair* 35, 576–584. doi:10.1177/15459683211011232

Joosten, E. A., and Franken, G. (2020). Spinal cord stimulation in chronic neuropathic pain: mechanisms of action, new locations, new paradigms. *Pain* 161, S104–S113. doi:10.1097/j.pain.0000000000001854

Kim, Y. S., Park, H. J., Kim, T. K., Moon, D. E., and Lee, H. J. (2009). The effects of Ginkgo biloba extract EGb 761 on mechanical and cold allodynia in a rat model of neuropathic pain. *Anesth. Analg.* 108, 1958–1963. doi:10.1213/ane.0b013e31819f1972

Koffler, J., Zhu, W., Qu, X., Platoshyn, O., Dulin, J. N., Brock, J., et al. (2019). Biomimetic 3D-printed scaffolds for spinal cord injury repair. *Nat. Med.* 25, 263–269. doi:10.1038/s41591-018-0296-z

Lavanya, K., Balagangadharan, K., Chandran, S. V., and Selvamurugan, N. (2023). Chitosan-coated and thymol-loaded polymeric semi-interpenetrating hydrogels: an effective platform for bioactive molecule delivery and bone regeneration *in vivo*. *Biomater. Adv.* 146, 213305. doi:10.1016/j.bioadv.2023.213305

Levendoğlu, F., Öğün, C. Ö., Özerbil, Ö., Öğün, T. C., and Uğurlu, H. (2004). Gabapentin is a first line drug for the treatment of neuropathic pain in spinal cord injury. *Spine (Phila. pa. 1976)* 29, 743–751. doi:10.1097/01.BRS.0000112068.16108.3A

Li, W., Yao, S., Li, H., Meng, Z., and Sun, X. (2021). Curcumin promotes functional recovery and inhibits neuronal apoptosis after spinal cord injury through the modulation of autophagy. *J. Spinal Cord. Med.* 44, 37–45. doi:10.1080/10790268.2019.1616147

Liau, L. L., Looi, Q. H., Chia, W. C., Subramaniam, T., Ng, M. H., and Law, J. X. (2020). Treatment of spinal cord injury with mesenchymal stem cells. *Cell. Biosci.* 10, 112. doi:10.1186/s13578-020-00475-3

Ma, Y., Shi, H., Wei, Q., Deng, Q., Sun, J., Liu, Z., et al. (2021). Developing a mechanically matched decellularized spinal cord scaffold for the *in situ* matrix-based neural repair of spinal cord injury. *Biomaterials* 279, 121192. doi:10.1016/j.biomaterials.2021.121192

Mastelić, J., Jerković, I., Blazević, I., Poljak-Blazi, M., Borović, S., Ivancić-Baće, I., et al. (2008). Comparative study on the antioxidant and biological activities of carvacrol, thymol, and eugenol derivatives. *J. Agric. Food Chem.* 56, 3989–3996. doi:10.1021/jf073272v

McDonald, J. W., and Sadowsky, C. (2002). Spinal-cord injury. *Lancet* 359, 417–425. doi:10.1016/S0140-6736(02)07603-1

Michalska-Sionkowska, M., Walczak, M., and Sionkowska, A. (2017). Antimicrobial activity of collagen material with thymol addition for potential application as wound dressing. *Polym. Test.* 63, 360–366. doi:10.1016/j.polymertesting.2017.08.036

Nagoor Meeran, M. F., Jagadeesh, G. S., and Selvaraj, P. (2015). Thymol attenuates inflammation in isoproterenol induced myocardial infarcted rats by inhibiting the release of lysosomal enzymes and downregulating the expressions of proinflammatory cytokines. *Eur. J. Pharmacol.* 754, 153–161. doi:10.1016/j.ejphar.2015.02.028

Nakamura, M., and Okano, H. (2013). Cell transplantation therapies for spinal cord injury focusing on induced pluripotent stem cells. *Cell. Res.* 23, 70–80. doi:10.1038/cr.2012.171

Nayak, S., Matheis, R. J., Agostinelli, S., and Shiflett, S. C. (2001). The use of complementary and alternative therapies for chronic pain following spinal cord injury: a pilot survey. *J. Spinal Cord. Med.* 24, 54–62. doi:10.1080/10790268.2001.11753556

Nieddu, M., Rassu, G., Boatto, G., Bosi, P., Trevisi, P., Giunchedi, P., et al. (2014). Improvement of thymol properties by complexation with cyclodextrins: *in vitro* and *in vivo* studies. *Carbohydr. Polym.* 102, 393–399. doi:10.1016/j.carbpol.2013.10.084

Norrbrink Budh, C., Kowalski, J., and Lundeberg, T. (2006). A comprehensive pain management programme comprising educational, cognitive and behavioural interventions for neuropathic pain following spinal cord injury. *J. Rehabil. Med.* 38, 172–180. doi:10.1080/16501970500476258

Olusanya, A., Yearsley, A., Brown, N., Braun, S., Hayes, C., Rose, E., et al. (2023). Capsaicin 8% patch for spinal cord injury focal neuropathic pain, a randomized controlled trial. *Pain Med.* 24, 71–78. doi:10.1093/pm/pnac104

Olvera Bernal, R. A., Olekhnovich, R. O., and Uspenskaya, M. V. (2023). Chitosan/PVA nanofibers as potential material for the development of soft actuators. *Polym. (Basel)* 15, 2037. doi:10.3390/polym15092037

Poon, P. C., Gupta, D., Shoichet, M. S., and Tator, C. H. (2007). Clip compression model is useful for thoracic spinal cord injuries: histologic and functional correlates. *Spine (Phila. pa. 1976)* 32, 2853–2859. doi:10.1097/BRS.0b013e31815b7e6b

Qi, S., and Craig, D. (2016). Recent developments in micro- and nanofabrication techniques for the preparation of amorphous pharmaceutical dosage forms. *Adv. Drug Deliv. Rev.* 100, 67–84. doi:10.1016/j.addr.2016.01.003

Qian, Y., Lin, H., Yan, Z., Shi, J., and Fan, C. (2021). Functional nanomaterials in peripheral nerve regeneration: scaffold design, chemical principles and microenvironmental remodeling. *Mater. Today* 51, 165–187. doi:10.1016/j.mattod.2021.09.014

Ruan, Y., Gu, L., Yan, J., Guo, J., Geng, X., Shi, H., et al. (2018). An effective and concise device for detecting cold allodynia in mice. *Sci. Rep.* 8, 14002. doi:10.1038/s41598-018-31741-7

Rukmani, A., and Sundrarajan, M. (2012). Inclusion of antibacterial agent thymol on β-cyclodextrin-grafted organic cotton. *J. Ind. Text.* 42, 132–144. doi:10.1177/1528083711430244

Sanchez-Rexach, E., Martínez de Arenaza, I., Sarasua, J.-R., and Meaurio, E. (2016). Antimicrobial poly(ε-caprolactone)/thymol blends: phase behavior, interactions and drug release kinetics. *Eur. Polym. J.* 83, 288–299. doi:10.1016/j.eurpolymj.2016.08.029

Šedý, J., Urdzíková, L., Jendelová, P., and Syková, E. (2008). Methods for behavioral testing of spinal cord injured rats. *Neurosci. Biobehav. Rev.* 32, 550–580. doi:10.1016/j.neubiorev.2007.10.001

Shen, C.-L., Wang, R., Ji, G., Elmassry, M. M., Zabet-Moghaddam, M., Vellers, H., et al. (2022a). Dietary supplementation of gingerols- and shogaols-enriched ginger root extract attenuate pain-associated behaviors while modulating gut microbiota and metabolites in rats with spinal nerve ligation. *J. Nutr. Biochem.* 100, 108904. doi:10.1016/j.jnutbio.2021.108904

Shen, H., Fan, C., You, Z., Xiao, Z., Zhao, Y., and Dai, J. (2022b). Advances in biomaterial-based spinal cord injury repair. *Adv. Funct. Mater.* 32, 2110628. doi:10.1002/adfm.202110628

Sheorain, J., Mehra, M., Thakur, R., Grewal, S., and Kumari, S. (2019). *In vitro* anti-inflammatory and antioxidant potential of thymol loaded bipolymeric (tragacanth gum/chitosan) nanocarrier. *Int. J. Biol. Macromol.* 125, 1069–1074. doi:10.1016/j.ijbiomac.2018.12.095

Shrestha, B., Coykendall, K., Li, Y., Moon, A., Priyadarshani, P., and Yao, L. (2014). Repair of injured spinal cord using biomaterial scaffolds and stem cells. *Stem Cell. Res. Ther.* 5, 91. doi:10.1186/scrt480

Siniscalco, D., Fuccio, C., Giordano, C., Ferraccio, F., Palazzo, E., Luongo, L., et al. (2007). Role of reactive oxygen species and spinal cord apoptotic genes in the development of neuropathic pain. *Pharmacol. Res.* 55, 158–166. doi:10.1016/j.phrs.2006.11.009

Snider, S., Cavalli, A., Colombo, F., Gallotti, A. L., Quattrini, A., Salvatore, L., et al. (2017). A novel composite type I collagen scaffold with micropatterned porosity regulates the entrance of phagocytes in a severe model of spinal cord injury. *J. Biomed. Mater. Res. Part B Appl. Biomater.* 105, 1040–1053. doi:10.1002/jbm.b.33645

Stokols, S., and Tuszynski, M. H. (2004). The fabrication and characterization of linearly oriented nerve guidance scaffolds for spinal cord injury. *Biomaterials* 25, 5839–5846. doi:10.1016/j.biomaterials.2004.01.041

Tahmasebi, F., and Barati, S. (2022). Effects of mesenchymal stem cell transplantation on spinal cord injury patients. *Cell. Tissue Res.* 389, 373–384. doi:10.1007/s00441-022-03648-3

Terzi, M., Altun, G., Şen, S., Kocaman, A., Kaplan, A. A., Yurt, K. K., et al. (2018). The use of non-steroidal anti-inflammatory drugs in neurological diseases. *J. Chem. Neuroanat.* 87, 12–24. doi:10.1016/j.jchemneu.2017.03.003

Timalsina, B., Haque, M. N., Choi, H. J., Dash, R., and Moon, I. S. (2023a). Thymol in Trachyspermum ammi seed extract exhibits neuroprotection, learning, and memory enhancement in scopolamine-induced Alzheimer's disease mouse model. *Phyther. Res.* 37, 2811–2826. doi:10.1002/ptr.7777

Timalsina, B., Haque, M. N., Dash, R., Choi, H. J., Ghimire, N., and Moon, I. S. (2023b). Neuronal differentiation and outgrowth effect of thymol in trachyspermum ammi seed extract via BDNF/TrkB signaling pathway in prenatal maternal supplementation and primary hippocampal culture. *Int. J. Mol. Sci.* 24, 8565. doi:10.3390/ijms24108565

Trawczynski, M., Liu, G., David, B. T., and Fessler, R. G. (2019). Restoring motor neurons in spinal cord injury with induced pluripotent stem cells. *Front. Cell. Neurosci.* 13, 369. doi:10.3389/fncel.2019.00369

Wang, J., Chu, R., Ni, N., and Nan, G. (2020a). The effect of Matrigel as scaffold material for neural stem cell transplantation for treating spinal cord injury. *Sci. Rep.* 10, 2576. doi:10.1038/s41598-020-59148-3

Wang, W., Wang, H., Zhao, Z., Huang, X., Xiong, H., and Mei, Z. (2020b). Thymol activates TRPM8-mediated Ca2+ influx for its antipruritic effects and alleviates inflammatory response in Imiquimod-induced mice. *Toxicol. Appl. Pharmacol.* 407, 115247. doi:10.1016/j.taap.2020.115247

Wu, H., Lu, J., Xiao, D., Yan, Z., Li, S., Li, T., et al. (2021). Development and characterization of antimicrobial protein films based on soybean protein isolate incorporating diatomite/thymol complex. *Food Hydrocoll.* 110, 106138. doi:10.1016/j.foodhyd.2020.106138

Xu, P., and Yang, X. (2019). The efficacy and safety of mesenchymal stem cell transplantation for spinal cord injury patients: a meta-analysis and systematic review. *Cell. Transpl.* 28, 36–46. doi:10.1177/0963689718808471

Yanishlieva, N. V., Marinova, E. M., Gordon, M. H., and Raneva, V. G. (1999). Antioxidant activity and mechanism of action of thymol and carvacrol in two lipid systems. *Food Chem.* 64, 59–66. doi:10.1016/S0308-8146(98)00086-7

Yoon, C., Wook, Y. Y., Sik, N. H., Ho, K. S., and Mo, C. J. (1994). Behavioral signs of ongoing pain and cold allodynia in a rat model of neuropathic pain. *Pain* 59, 369–376. doi:10.1016/0304-3959(94)90023-X

Yue, Y., Gong, X., Jiao, W., Li, Y., Yin, X., Si, Y., et al. (2021). *In-situ* electrospinning of thymol-loaded polyurethane fibrous membranes for waterproof, breathable, and antibacterial wound dressing application. *J. Colloid Interface Sci.* 592, 310–318. doi:10.1016/j.jcis.2021.02.048

Zamani, Z., Alipour, D., Moghimi, H. R., Mortazavi, S. A. R., and Saffary, M. (2015). Development and evaluation of thymol microparticles using cellulose derivatives as controlled release dosage form. *Iran. J. Pharm. Res. IJPR* 14, 1031–1040. Available at: http://www.ncbi.nlm.nih.gov/pubmed/26664369.

Zeugolis, D. I., and Raghunath, M. (2010). The physiological relevance of wet versus dry differential scanning calorimetry for biomaterial evaluation: a technical note. *Polym. Int.* 59, 1403–1407. doi:10.1002/pi.2882

Zhang, Q., Shi, B., Ding, J., Yan, L., Thawani, J. P., Fu, C., et al. (2019). Polymer scaffolds facilitate spinal cord injury repair. *Acta Biomater.* 88, 57–77. doi:10.1016/j.actbio.2019.01.056

Zheng, T., Qiu, S., Li, L., Li, B., and Zhang, M. (2022). Polymers containing natural plant phenolic compounds for peripheral nerve injury. *Biomater. Biosens.* 1, 48–61. doi:10.58567/bab01010004

Zheng, Y., Mao, Y.-R., Yuan, T.-F., Xu, D.-S., and Cheng, L.-M. (2020). Multimodal treatment for spinal cord injury: a sword of neuroregeneration upon neuromodulation. *Neural Regen. Res.* 15, 1437–1450. doi:10.4103/1673-5374.274332

Frontiers in Pharmacology

Explores the interactions between chemicals and living beings

The most cited journal in its field, which advances access to pharmacological discoveries to prevent and treat human disease.

Discover the latest Research Topics

See more →



Frontiers

Avenue du Tribunal-Fédéral 34
1005 Lausanne, Switzerland
frontiersin.org

Contact us

+41 (0)21 510 17 00
frontiersin.org/about/contact